

Yu-Qiu Long
Song Cen
Zhi-Fei Long

Advanced Finite Element Method in Structural Engineering



TSINGHUA
UNIVERSITY PRESS



Springer

Yu-Qiu Long
Song Cen
Zhi-Fei Long

**Advanced Finite Element
Method in Structural Engineering**

Yu-Qiu Long
Song Cen
Zhi-Fei Long

Advanced Finite Element Method in Structural Engineering

With 219 figures



AUTHORS:

Yu-Qiu Long

Department of Civil Engineering of
Tsinghua University
100084 Beijing China

Song Cen

School of Aerospace of
Tsinghua University
100084 Beijing China

Zhi-Fei Long

School of Mechanics & Civil Engineering of
China University of Mining & Technology
100083 Beijing China

ISBN 978-7-302-18889-6 Tsinghua University Press, Beijing
ISBN 978-3-642-00315-8 Springer Berlin Heidelberg New York
e ISBN 978-3-642-00316-5 Springer Berlin Heidelberg New York

Library of Congress Control Number: 2009921171

This work is subject to copyright. All rights are reserved, whether the whole or part of the material is concerned, specifically the rights of translation, reprinting, reuse of illustrations, recitation, broadcasting, reproduction on microfilm or in any other way, and storage in data banks. Duplication of this publication or parts thereof is permitted only under the provisions of the German Copyright Law of September 9, 1965, in its current version, and permission for use must always be obtained from Springer-Verlag. Violations are liable to prosecution under the German Copyright Law.

© 2009 Tsinghua University Press, Beijing and Springer-Verlag GmbH Berlin Heidelberg

Co-published by Tsinghua University Press, Beijing and Springer-Verlag GmbH Berlin Heidelberg

Springer is a part of Springer Science+Business Media

springer.com

The use of general descriptive names, registered names, trademarks, etc. in this publication does not imply, even in the absence of a specific statement, that such names are exempt from the relevant protective laws and regulations and therefore free for general use.

Cover design: Frido Steinen-Broo, EStudio Calamar, Spain

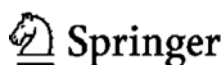
Printed on acid-free paper

Yu-Qiu Long
Song Cen
Zhi-Fei Long

新型有限元论

——结构工程中的高等有限元方法

Advanced Finite Element Method in Structural Engineering



内 容 简 介

本书是在中文专著《新型有限元论》(2004年版)的基础上补充了2004年至2008年期间的新成果所撰写的英文专著,是龙驭球院士、岑松博士和龙志飞教授及其研究组多年来在新型有限元方面研究成果的系统论述。全书分为20章。除首尾两章外,其余18章分为3篇:第1篇是变分原理进展,介绍分区和含参变分原理2项成果;它们为构造新型有限元起到理论指导作用。第2篇是有限元法进展初论,重点介绍广义协调元;这是在协调元与非协调元之间另辟的新路,使协调问题和收敛问题得到合理解决,单元构造方案可以灵活优选,学科内容得到充实更新;广义协调元是新型有限元方面的主要成果,在本书中起核心作用。第3篇是有限元法进展续论,补充介绍4项成果,包括分区混合元法、解析试函数法、第一和第二类四边形面积坐标法和样条函数有限元法,在本书中起锦上添花作用。本书还结合7项成果的论述,介绍了总共108个相关的新单元。

本书可作为高等学校力学、土木、机械等专业研究生和高年级本科生的教材和参考书,也可供相关领域教师和科技人员参考。

版权所有,侵权必究。侵权举报电话:010-62782989 13701121933

图书在版编目(CIP)数据

新型有限元论——结构工程中的高等有限元方法=Advanced Finite Element Method in Structural Engineering: 英文/龙驭球,岑松,龙志飞著. —北京:清华大学出版社,2008.12
ISBN 978-7-302-18889-6

I.新… II.①龙… ②岑… ③龙… III.有限元分析-英文 IV.O241.82

中国版本图书馆CIP数据核字(2008)第175870号

责任编辑:徐晓飞 王海燕

责任校对:王淑云

责任印制:孟凡玉

出版发行:清华大学出版社

<http://www.tup.com.cn>

社总机:010-62770175

投稿与读者服务:010-62776969, c-service@tup.tsinghua.edu.cn

质量反馈:010-62772015, zhiliang@tup.tsinghua.edu.cn

地 址:北京清华大学学研大厦A座

邮 编:100084

邮 购:010-62786544

印 装 者:北京雅昌彩色印刷有限公司

经 销:全国新华书店

开 本:153×235 印张:45 字数:1042千字

版 次:2008年12月第1版 印次:2008年12月第1次印刷

印 数:1~800

定 价:128.00元

本书如存在文字不清、漏印、缺页、倒页、脱页等印装质量问题,请与清华大学出版社出版部联系调换。联系电话:010-62770177 转 3103 产品编号:031557-02



Professor Yu-Qiu Long (1926—) is a Full Professor in the Department of Civil Engineering, Tsinghua University, and also a Member of the Chinese Academy of Engineering since 1995. During the past 60 years, he has been recognized as an expert in the areas of structural mechanics, shell structures, finite element method and variational principle. He was the first President of the Chinese Association of Structural Engineering between 1998 and 2003; Council Member of the Chinese Association of Computational Mechanics from 1957 to 1990; and Editor-in-Chief of a Chinese journal, *Engineering Mechanics*, between 1991 and 1999. He is currently a member of Editorial Boards of many international and Chinese journals, such as *Advances in Structural Engineering* (since 1997), *International Journal of Structural Stability and Dynamics* (since 2001), *Applied Mathematics and Mechanics* (since 1979), and so on. He published his first book on the finite element method in 1978, which is one of the earliest books on this subject in China and has a broad influence on Chinese readers.



Dr. Song Cen (1972—) is serving as an Associate Professor in the Department of Engineering Mechanics, School of Aerospace, Tsinghua University. He is also the deputy secretary-general of Beijing Society of Mechanics; Executive Council Member of the International Chinese Association for Computational Mechanics; Invited Council Member of the Chinese Association of Computational Mechanics. His research interests mainly cover finite element method and computational solid mechanics. Dr. Cen is a recipient of some prestigious Prizes for distinguished young Chinese researchers, including *Xu Zhi-Lun Prize in Mechanics* (2007), *New Academic Prize of Tsinghua University* (2007), *Fok Ying Tung Prize for Young Researchers in Universities* (2006), *the Nationwide (China) Excellent Doctoral Dissertation Award of Year 2002* (supervised by Professor Yu-Qiu Long), and so on.



Professor Zhi-Fei Long (1957—) is a professor in the School of Mechanics & Civil Engineering, China University of Mining & Technology (Beijing). He is an expert in finite element method and structural mechanics, and has published 4 books and more than 90 papers in related fields. He won the Science Award of China Ministry of Education (First Class, 1993), for the studies on the generalized energy principles and new finite element models. The textbook titled by *New Monograph of Finite Element Method* (written by Zhi-Fei Long and Song Cen, published by China Hydraulic and Water-power Press in 2001) has produced a broad influence in Chinese universities.

Preface

The main purpose of this book is to describe some developments in finite element method and related variational principles. Since this book only deals with the areas the authors are familiar with, it is impossible to cover every aspect of these subjects. This book is composed of 20 chapters. Except for *Introduction* (Chap. 1) and *Concluding Remarks* (Chap. 20), in the other 18 chapters, seven theoretical achievements (two achievements in variational principles and five achievements in finite element methods) are introduced, which are subdivided into three Parts.

Part I focuses on advances in the variational principles. Two innovations in this subject are discussed here.

(1) *Sub-region variational principles* (Chap. 2). The concept of *sub-region* is introduced for establishing new variational principles suitable for the developments of the finite element method.

(2) *Variational principles with several adjustable parameters* (Chap. 3). Several adjustable parameters are included in the variational principles so that a broader optimization space is available.

Part II focuses on the main advances in the finite element method—generalized conforming elements (the third innovation). Eight chapters are employed to illustrate this innovation.

(3) *Generalized conforming elements* (Chaps. 4–11). Firstly, from the viewpoint of theory, the generalized conforming element opens a new way between conforming and non-conforming elements, so that the puzzle of the convergence problem for non-conforming elements can be rationally solved. Meanwhile, various new conforming schemes, including point conforming, line conforming, perimeter conforming, SemiLoof conforming, least square conforming and their combination forms, have been successfully proposed. Secondly, from the viewpoint of applications, the successful application of the generalized conforming element method was first realized for thin plate bending problem, in which a series of high performance thin plate element models were presented. Subsequently, the novel technique was successfully generalized to other fields, and a large number of new models, including membrane elements, membrane elements with drilling DOFs, thin-thick plate elements, laminated composite plate elements, flat-shell

elements, curved shell elements, etc., were also successfully constructed.

Part III focuses on the other advances in the finite element method. Eight chapters are employed to discuss four additional subject innovations.

(4) *Sub-region mixed element method* (Chaps. 12–13). It provides a novel solution strategy for fracture problem by complementarity and coupling of displacement-based element and stress-based element.

(5) *Analytical trial function method* (Chaps. 14–15). This method exhibits rewarding cooperation between analytical and discrete methods, and provides effective solution strategy for shear locking, trapezoidal locking, and singular stress problems.

(6) *Quadrilateral area coordinate method* (Chaps. 16–17). This method indicates that the area coordinate method is generalized from the traditional triangular element field to new fields.

(7) *Spline element method* (Chaps. 18–19). This method indicates that the advantages of the spline functions have been adopted by the finite element method.

While introducing above seven theoretical innovations, five new element series with 108 new element models, which were directly derived from the five achievements in FEM, are also discussed in detail or briefly (see Table 20.2). Furthermore, based on these developments, effective solution strategies for five challenging problems (shear-locking problem in thick plate elements, sensitivity problem to mesh distortion, non-convergence problem of non-conforming elements, accuracy loss problem of stress solutions by displacement-based elements, and singular stress problem) have also been found.

To sum up, in the contents of this book, three aspects should be emphasized:

- (1) Seven new achievements in the field of variational principle and FEM;
- (2) five new element series with 108 new element models;
- (3) five sets of novel solution strategies for five challenging problems.

The authors are very grateful to all the colleagues and students who made significant contributions to the contents included in this book. We also thank China Academy of Building Research for compiling our algorithms and finite element models into their FEM software product, SATWE, for designs of high-rise building structures.

Our research activities were financially supported by many foundations and sponsors. We list them below and express our deep gratitude.

- 📖 The National Natural Science Foundation of China (Math85287; 58978341; 59578031; 59878022; 10272063; 10502028; 10872108)
- 📖 The Special Foundation for the Authors of the Nationwide (China) Excellent Doctoral Dissertation (200242)
- 📖 The Program for New Century Excellent Talents in Universities of China (NCET-07-0477)
- 📖 Basic Science Research Foundation of Tsinghua University (JC1999002; JC2002003)
- 📖 China Postdoctoral Science Foundation (12836).
- 📖 The Special Scientific Foundation for Chinese Doctoral Education (97000315; 20020003044)

Contents

Chapter 1 Introduction—The Evolutive Finite Element Method..... 1

- 1.1 Brief Review of the Features of Finite Element Method 1
- 1.2 Finite Element Method and Variational Principles..... 3
- 1.3 Research Areas of FEM 5
- 1.4 Advances in FEM and Outline of This Book 6

References 9

PART I Advances in Variational Principles

Chapter 2 The Sub-Region Variational Principles 15

- 2.1 Introduction 15
- 2.2 The Sub-Region Variational Principle for Elasticity 16
- 2.3 The Sub-Region Variational Principle for Elastic Thin Plate 28
- 2.4 The Sub-Region Variational Principle for Elastic Thick Plate 40
- 2.5 The Sub-Region Variational Principle for Elastic Shallow Shell 51
- 2.6 The Sub-Region Mixed Energy Partial Derivative Theorem 58

References 64

Chapter 3 Variational Principles with Several Adjustable Parameters..... 66

- 3.1 Introduction 66
- 3.2 Several Patterns of Functional Transformation 67
- 3.3 Generalized Variational Principle Involving Several Adjustable Parameters 75
- 3.4 Variable-Substitution-Multiplier Method 83

References 85

PART II Advances in Finite Element Method—Generalized Conforming Elements

Chapter 4 Generalized Conforming Element Theory 89

- 4.1 Introduction 89
- 4.2 Conforming and Nonconforming Elements—Some Consideration about “Conforming” 90
- 4.3 The First Pattern of Generalized Conforming Element—Replacing Nodal Conforming by Line Conforming Conditions..... 91

4.4	The Variational Basis of Generalized Conforming Element—Duality ...	94
4.5	The Synthesis of Energy Method and Weighted Residual Method —Flexibility	97
4.6	The Convergence of Generalized Conforming Element	99
	References.....	99

Chapter 5 Generalized Conforming Thin Plate Element I

—	Introduction	101
5.1	Introduction	101
5.2	The Generalized Conforming Conditions and Their Equivalent Forms for Thin Plate Elements.....	102
5.3	General Formulations of the Generalized Conforming Thin Plate Elements	105
5.4	Several Construction Schemes of the Generalized Conforming Thin Plate Elements.....	107
5.5	A Collection of the Recent Generalized Conforming Thin Plate Elements	111
	References.....	118

Chapter 6 Generalized Conforming Thin Plate Element II

—	Line-Point and SemiLoof Conforming Schemes	120
6.1	Line Conforming Scheme—Elements TGC-9 and TGC-9-1	120
6.2	Line-Point Conforming Scheme—Rectangular Elements	130
6.3	Line-Point Conforming Scheme—Triangular Elements.....	146
6.4	Super-Basis Line-Point Conforming Scheme—Elements GCIII-R12 and GCIII-T9.....	155
6.5	Super-Basis Point Conforming Scheme—Elements MB1-T9 and MB2-T9	164
6.6	SemiLoof Conforming Scheme.....	167
	References.....	174

Chapter 7 Generalized Conforming Thin Plate Element III

—	Perimeter-Point and Least-Square Conforming Schemes	176
7.1	Perimeter-Point Conforming Scheme—Elements LR12-1 and LR12-2.....	176
7.2	The Application of Perimeter Conforming Conditions—Verification for the Convergence of the Element ACM	181
7.3	Super-Basis Perimeter-Point Conforming Scheme—Verification and Improvement of the Element BCIZ.....	187
7.4	Least-square Scheme—Elements LSGC-R12 and LSGC-T9.....	198
	References.....	202

Chapter 8 Generalized Conforming Thick Plate Element	203
8.1 Summary of the Thick Plate Theory	203
8.2 Comparison of the Theories for Thick Plates and Thin Plates	215
8.3 Thick/Thin Beam Element	232
8.4 Review of Displacement-based Thick/Thin Plate Elements	235
8.5 Generalized Conforming Thick/Thin Plate Elements (1) —Starting with Assuming (ψ, γ)	237
8.6 Generalized Conforming Thick/Thin Plate Elements (2) —Starting with Assuming (w, γ)	249
8.7 Generalized Conforming Thin/Thick Plate Elements —From Thin to Thick Plate Elements.....	260
References.....	266
Chapter 9 Generalized Conforming Element for the Analysis of the Laminated Composite Plates	268
9.1 Introduction.....	268
9.2 Fundamental Theory	270
9.3 New Element CTMQ20 for the Analysis of Laminated Composite Plates.....	275
9.4 The Hybrid-Enhanced Post-Processing Procedure for Element Stresses.....	286
9.5 Vibration Analysis of Laminated Composite Plates.....	290
9.6 Numerical Examples	292
References.....	301
Chapter 10 Generalized Conforming Element for the Analysis of Piezoelectric Laminated Composite Plates	304
10.1 Introduction.....	304
10.2 The First-Order Shear Deformation Theory of Piezoelectric Laminated Composite Plate.....	306
10.3 New Piezoelectric Laminated Composite Plate Element CTMQE	309
10.4 The “Partial Hybrid”-Enhanced Post-Processing Procedure for Element Stresses.....	314
10.5 Numerical Examples	318
References.....	323
Chapter 11 Generalized Conforming Membrane and Shell Elements	325
11.1 Introduction	325
11.2 Generalized Conforming Isoparametric Membrane Element.....	326
11.3 Membrane Elements with Drilling Freedoms—Definition of the Drilling Freedom and the Corresponding Rectangular and Quadrilateral Elements	334

11.4	Membrane Elements with Drilling Freedoms—Triangular Elements...	346
11.5	Flat-Shell Elements—Triangular Thick/Thin Shell Element GMST18.....	357
11.6	Shallow Shell Element—Variational Principle and Membrane Locking Problem	370
11.7	Shallow Shell Element—Triangular Element SST21 with Mid-Side Nodes.....	375
11.8	Shell Element for Geometrically Nonlinear Analysis —Triangular Flat-Shell Element GMST18	382
11.9	Shell Element for Geometrically Nonlinear Analysis —Rectangular Shallow Shell Element SSR28	386
	References	398

PART III Other Advances in Finite Element Method

Chapter 12	Sub-Region Mixed Element I—Fundamental Theory and Crack Problem	405
12.1	Review of the Sub-Region Mixed Element Method	405
12.2	Basic Equations of the Sub-Region Mixed Element Method.....	408
12.3	2D Crack Problem.....	411
12.4	Cracked Thick Plate Problem.....	418
12.5	Surface Crack Problem in a 3D Body	426
	References	435
Chapter 13	Sub-Region Mixed Element II—V-Notch Problem	438
13.1	Introduction	438
13.2	Plane V-Notch Problem.....	438
13.3	Plane V-Notch Problem in a Bi-Material	450
13.4	Anti-Plane V-Notch Problem in a Bi-Material	457
13.5	V-Notch Problem in Reissner Plate.....	463
13.6	3D V-Notch Problem.....	481
	References	493
Chapter 14	Analytical Trial Function Method I—Membrane and Plate Bending Elements.....	495
14.1	Recognition of the Analytical Trial Function Method.....	495
14.2	4-Node Membrane Elements Based on the Analytical Trial Function Method	498
14.3	Avoiding Trapezoidal Locking Phenomenon by ATF Elements.....	500
14.4	The Basic Analytical Solutions of the Thick Plate Theory and ATF Elements Free of Shear Locking	504
14.5	Development of Quadrilateral Thin-Thick Plate Element Based on the Analytical Trial Function Method.....	506

14.6 Analytical Trial Function Method for Developing a Triangular Thick Plate Element Based on a Thin Plate Element	510
References	516
Chapter 15 Analytical Trial Function Method II— Singular Elements with Crack and Notch	
15.1 Introduction	518
15.2 The Basic Analytical Solutions of the Plane Crack Problem	519
15.3 Element ATF-MS with Crack Formulated by the Analytical Trial Function Method	523
15.4 Error Analysis of Element ATF-MS with Crack	525
15.5 Analysis of Zero Energy Mode in Element and in Structural System	529
15.6 The Basic Analytical Solutions of the Plane Notch Problem	535
15.7 Element ATF-VN with Notch Formulated by the Analytical Trial Function Method	538
15.8 Error Analysis of Element ATF-VN with Notch	542
References	545
Chapter 16 Quadrilateral Area Coordinate Systems, Part I —Theory and Formulae	
16.1 Introduction	546
16.2 The Isoparametric Coordinate Method and the Area Coordinate Method	547
16.3 Two Shape Characteristic Parameters of a Quadrilateral	549
16.4 The Definition of Quadrilateral Area Coordinates (QACM- I)	553
16.5 Two Identical Relations Among Area Coordinates (QACM- I)	556
16.6 Transformation Relations Between the Area Coordinate System (QACM- I) and the Cartesian or Isoparametric Coordinate System	558
16.7 Differential Formulae (QACM- I)	560
16.8 Integral Formulae (QACM- I)	562
16.9 The Proof of the Basic Formulae (A) and (B) (QACM- I)	565
16.10 The Proof of the Basic Formulae (C) (QACM- I)	569
16.11 The Quadrilateral Area Coordinate System with Only Two Components (QACM- II)	570
References	580
Chapter 17 Quadrilateral Area Coordinate Systems, Part II —New Tools for Constructing Quadrilateral Elements	
17.1 Introduction	582
17.2 Sensitivity Analysis of Isoparametric Elements to Mesh Distortion	583
17.3 Brief Review of the Finite Element Models Formulated by Quadrilateral Area Coordinate Methods	586

17.4	4-Node Quadrilateral Membrane Elements Formulated by the Area Coordinate Method	589
17.5	Geometrically Nonlinear Analysis Using Element AGQ6-I	601
17.6	Quadrilateral Membrane Elements with Drilling Degrees of Freedom Formulated by the Area Coordinate Method	606
17.7	8-Node Quadrilateral Membrane Elements Formulated by the Area Coordinate Method	613
17.8	Quadrilateral Thin Plate Element Formulated by the Area Coordinate Method.....	620
17.9	Quadrilateral Thick Plate Element Formulated by the Area Coordinate Method.....	628
17.10	Quadrilateral Laminated Composite Plate Element Formulated by the Area Coordinate Method	635
	References.....	637
Chapter 18 Spline Element I— Analysis of High-Rise Building Structures		
	18.1 Introduction.....	641
	18.2 Spline Beam Elements	642
	18.3 Spline Plane Membrane Elements.....	646
	18.4 Analysis of Shear Wall Structures by Spline Elements.....	648
	18.5 Analysis of Frame-Tube Structures by Spline Elements.....	655
	References.....	661
Chapter 19 Spline Element II— Analysis of Plate/Shell Structures		
	19.1 Spline Elements for Thin Plate Bending	663
	19.2 Spline Elements for Thick/Thin Beam and Plate	665
	19.3 Spline Elements for Shallow Shell.....	670
	19.4 Spline Elements for Thick/Thin Shell	672
	19.5 Spline Elements for Geometrically Nonlinear Analysis.....	681
	References.....	689
Chapter 20 Concluding Remarks.....		
	20.1 Seven New Achievements in the Finite Element Method	691
	20.2 Five New Element Series with 108 New Element Models	693
	20.3 New Solution Strategies for Five Challenging Problems.....	699
	References.....	700
Appendix		
	A The equivalent equation of the functional stationary condition (2-45)....	703
	B The node conditions derived from the stationary condition (2-77)	704
	C l_{ij} and γ_{ij} in Eq. (13-137).....	705
	D s_{ij} and t_{ij} in Eq. (13-144).....	706

Chapter 1 Introduction—The Evolutive Finite Element Method

Yu-Qiu Long

Department of Civil Engineering, School of Civil Engineering,
Tsinghua University, Beijing, 100084, China

Song Cen

Department of Engineering Mechanics, School of Aerospace,
Tsinghua University, Beijing, 100084, China

Zhi-Fei Long

School of Mechanics & Civil Engineering, China University of
Mining & Technology, Beijing, 100083, China

Abstract This chapter is an opening introduction to the entire book, and also an introduction to the evolutive Finite Element Method (FEM). Firstly, a brief review on the features of FEM is given. Then, a close relationship between FEM and variational principle is discussed according to the development history and categories of FEM. Thirdly, some research areas of FEM of significant interest are listed. Finally, the topics of the book are presented. The purpose of the above arrangement is to explain the background and main idea of this book.

Keywords finite element method, variational principle, research area, advance, outline.

1.1 Brief Review of the Features of Finite Element Method

Computational mechanics is a flourishing subject for science and engineering, in which the physical mechanics problems are solved by cooperation of mechanics, computers and various numerical methods. It has already entered every branch of mechanics, and is being generalized continuously for broader research and application ranges. At the same time, new theories and methods of computational mechanics itself are also being developed gradually.

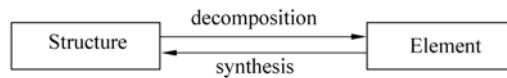
Finite element method is an important branch of computational mechanics. It is a kind of numerical methods in which various mechanics problems are solved

Advanced Finite Element Method in Structural Engineering

by discretizing related continuums. In 1960, R. W. Clough firstly used the name of *Finite Element Method*. Up to date, it has already been one of the most powerful techniques for dealing with problems in mechanics, physics and engineering computations.

1.1.1 Features of FEM from the Viewpoints of Methodology

(1) FEM is an application of both methods of analysis and synthesis: during the procedure, one structure will be firstly decomposed into elements, and then, these elements are synthesized to be the structure again. Solutions for the structure problem can be obtained from such decomposition and synthesis.

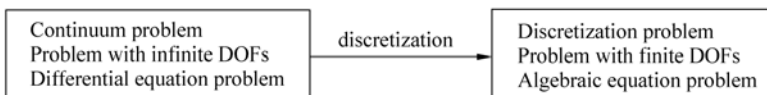


- Decomposition — breaks up the whole into parts, so that difficulties can be transformed into simplicity
- Synthesis — integrates all parts into a whole, so that the prototype can be recovered

(2) From the viewpoint of evolution of mechanics, it can be seen that FEM evolves from the matrix displacement method for frame analysis. Along with the transplantation from frame analysis to elasticity, the matrix displacement method becomes FEM.



(3) From the viewpoint of mathematics, it can be seen that FEM is a discrete approximation for continuum problems. Thus, the original problems with infinite degrees of freedom (DOFs) can be approximately treated as those with finite DOFs. Corresponding differential equations can also be simplified into algebraic ones.



1.1.2 Features of FEM from the Viewpoint of Solution Method Classification

The solution methods for problems in mechanics can be classified into following three categories:

- (1) Analytical methods;

- (2) Numerical methods;
- (3) Semi-analytical methods.

The usual numerical methods are as follows (FEM is one of them—it is not the oldest one but exerts the greatest influence):

(1) Finite difference method—the differential equations are transformed into difference forms so that approximate solutions can be obtained.

(2) Weighted residual method—the differential equations are transformed into weighted integration forms so that approximate solutions can be obtained. In such method, there are five usual schemes: collocation method, sub-domain method, least square method, Galerkin method, and method of moment.

(3) Finite element method—problems related to the differential equations are transformed into those related to stationary values of energy, and sub-region interpolation technique [interpolation is performed in each sub-region (element)] is used, so that approximate solutions can be obtained.

(4) Boundary element method—discretization is performed only at boundaries.

(5) Mesh-free method—its approximate functions are mainly established at discrete points; thus, no mesh is needed.

The usual semi-analytical methods are as follows:

- (1) Kantorovich method;
- (2) Finite strip method;
- (3) Finite element method of line.

1.2 Finite Element Method and Variational Principles

Finite element method has a close relationship with variational principles. Here, this relationship is discussed according to its development history and categories.

1.2.1 Creation of FEM and Variational Principles

It is well recognized in academia that the variational energy principle is the basis of FEM. However, the path to this recognition was not smooth.

Firstly, in the field of applied mathematics, the first paper published on FEM was the report, *Variational methods for the solution of problems of equilibrium and vibration*^[1], delivered by Courant in 1941 and published in 1943. He used the variational principle and sub-region interpolation technique to look for the approximate solutions of torsion problem. In the title of his paper, he named his method, which is called *finite element method* afterwards, as *variational method*. Since computers have not been available at that time, this paper did not attract due attention.

Secondly, in the field of engineering techniques, Turner, Clough, Martin and Toop published the first paper about FEM, entitled *stiffness and deflection analysis of complex structures*^[2], in 1956. They generalized the matrix displacement method of rigid frame to the plane problem in elasticity. In the title of the paper, they named such solution scheme as the *stiffness method for complex structures* (or *direct stiffness method*), and subsequently, Clough denominated it as Finite Element Method^[3]. Like all engineers at that time, these authors did not pay much attention to Courant's paper which had been ignored, and did not pay attention either to the relation between the direct stiffness method and Courant's variational method.

Finally, some related papers began to appear in 1963, including the paper, *Basis for derivation for the Direct Stiffness Method*, by Melosh^[4]. These papers drew an important conclusion that, the basis of the direct stiffness method (i.e. finite element method) is just the variational principle, or, the direct stiffness method is a new Ritz method which is based on the variational principle (new Ritz method using sub-region interpolation technique). In this way, a bridge was successfully built that linked mathematics and engineering. Consequently, FEM is recognized as a numerical method with rigorous theoretical basis and universal application value. Systematical presentation of FEM is given in books and monographs [5–14].

1.2.2 Element Categories and Variational Principles

Different elements are derived from different variational principles. Several element categories and their corresponding variational principles are as follows.

(1) Conforming displacement-based element (its displacement trial functions exactly conform between two adjacent elements)—the minimum potential energy principle.

(2) Non-conforming displacement-based element (its displacement trial functions do not conform exactly between two adjacent elements)—the sub-region potential energy principle.

(3) Generalized conforming displacement-based element (its displacement trial functions are generalized conforming between two adjacent elements)—the degenerated form of sub-region potential energy principle.

(4) Hybrid stress-based element (the stress trial functions satisfying the equilibrium differential equation are used)—the minimum complementary energy principle.

(5) Mixed element (mixed trial functions containing displacements, stresses and strains are used)—generalized variational principle.

(6) Sub-region mixed element (some elements utilize the displacement trial functions, and the other use the stress trial functions)—the sub-region mixed energy principle.

1.3 Research Areas of FEM

During the research history of theories and applications of FEM, the following problems have attracted main attention.

(1) Variational principle and numerical method

In the development of variational principle and FEM, two classical papers should be mentioned: the generalized variational principle proposed by Hu in 1955^[15] which provided a theoretical basis for development of FEM; and the difference formulations based on variational principle proposed by Feng^[16], which is virtually the modern FEM.

New forms of variational principles were proposed in order to satisfy the requirements caused by the development of FEM, such as sub-region potential, complementary and mixed energy principles, the degenerated forms of sub-region variational principles and their applications, variational principles with adjustable parameters and their applications, variational principles for piezoelectric composite structures, variational principles for micromechanics based on the strain gradient theory, and so on. The attention was frequently focused on error estimation, convergence, reliability, self-adaptation and optimization of related numerical methods.

(2) Construction techniques for new elements

The existing construction modes, such as hybrid element, mixed element, quasi-conforming element, strain-based element, spline element, and so on, were extended.

The new construction modes, such as generalized conforming element based on generalized conforming theory, sub-region mixed element based on sub-region mixed variational principle, rational element, new quadrilateral element based on quadrilateral area coordinates, element based on analytical trial functions, were successfully developed.

(3) Challenging problems and their solution strategies

The development of FEM still left some difficult and challenging problems. Some of them have remained unsolved for a long time. Naturally, these unsolved challenging problems became the focus of attention, such as various locking phenomena (shear locking, membrane locking, bulk locking), sensitive problem to mesh distortion, non-convergence problem of some non-conforming elements, spurious zero energy mode, solution oscillation phenomena, accuracy loss problem (stress solutions of displacement-based elements, transverse shear stresses of laminated composite plate), singular stress problem, ill-conditioned phenomena in numerical computations, and so on.

(4) Complicated problems

Complicated problems include finite element analysis of problems with material and geometric nonlinearity, buckling analysis of shell structures, finite element analysis of plastic forming, numerical simulation of impact problem, finite element method based on the strain gradient theory, and so on.

(5) Coupling and interdisciplinary problems

Coupling problems involve fluid-solid coupling, gas-liquid-solid coupling, soil-structure-fluid coupling, force-electricity coupling, etc.

Interdisciplinary problems include numerical simulations and optimization designs in biomechanics, microelectronics, material, and other subjects.

(6) Cooperation with other methods

Cooperation with other methods means the cooperation between FEM and boundary element method, between FEM and line method, between FEM and finite difference method, between FEM and mesh-free method, between numerical and analytical methods, and so on.

(7) Software developments and CAD/CAE techniques

Finite element software was born simultaneously with the birth of finite element theory. The influences brought by them are usually greater than those brought by publications.

Computational mechanics should continuously absorb the state of the art from computer science techniques, and progress together with computer graphics and CAD/CAE techniques.

1.4 Advances in FEM and Outline of This Book

Seven important research areas of FEM are listed in Sect. 1.3. In each area, numerous achievements have been obtained. Here, some examples of advances only in the first two areas, which are also outlined in this book, are given as follows.

1.4.1 Advances in Variational Principles (Two Examples)

In order to satisfy the development requirements of FEM, traditional variational principles need to be reformed. Thus, new variational principles emerge continuously. The following are two examples.

(1) Sub-region variational principles—the variational principles using sub-region interpolation and relaxing continuity conditions at sub-region interfaces^[10,17,18].

One feature of FEM is that the traditional global interpolation is replaced by the sub-region interpolation. The sub-region variational principles are the new variational principles which reflect such feature.

The sub-region variational principles include sub-region potential energy principle, sub-region complementary energy principle, and sub-region mixed energy principle. The generalized conforming element and the sub-region mixed element are the two new element models derived from the sub-region potential energy principle and the sub-region mixed energy principle, respectively.

Detailed discussions will be given in Chap. 2.

(2) Variational principles with adjustable parameters—new variational principles in which energy functionals contain adjustable parameters, first proposed in 1986^[19,20].

For example, the functional Π^* in the following equation is a new functional with one parameter η_1

$$\Pi^* = (1 + \eta_1)\Pi_{\text{HW}} - \eta_1\Pi_{\text{HR}}$$

in which Π_{HW} and Π_{HR} are the functionals of Hu-Washizu variational principle and Hellinger-Reissner variational principle, respectively.

It can be seen that, the functionals Π_{HW} and Π_{HR} of traditional variational principles are the special cases of Π^* . Different functionals can be obtained by assigning different values to parameter η_1 . And by starting from the new functional Π^* , new elements with different performance will be derived. Detailed discussions will be given in Chap. 3.

1.4.2 Advances in Constructions of New Elements (Five Examples)

Among numerous element types, the displacement-based element always occupies the mainstream position. And the numerous displacement-based element models usually can be divided into two types, conforming and non-conforming elements. The main disadvantage of the conforming elements is that they exclude many excellent models, while the main disadvantage of the non-conforming elements is that some of them are not convergent modes. In 1987, the generalized conforming element method was proposed. Based on the generalized conforming theory, it overcomes shortcomings from both conforming and non-conforming elements, and has already been successfully applied in various structure problems. As a result, a large number of new elements with excellent performance have been constructed, which promotes the development of the FEM. Here, five new achievements are given as practical examples to introduce the new advances in the FEM, in which the generalized conforming method is the dominant technique.

(1) Generalized conforming element—non-conforming element which can ensure the convergence

The generalized conforming element opens a new way, limit conforming mode, between conforming and non-conforming elements. From the viewpoint of conforming, it can be seen that, the exact conforming is not required while the necessary fundamental generalized conforming conditions must be satisfied, so that the convergence can be guaranteed in the limit status when the mesh is refined by infinite elements. Since the conforming requirement is appropriate, both convergence and convenience can be achieved.

The first paper on the generalized conforming element was published in 1987^[21], in which the basic concepts and construction method were described by

thin plate bending problem. Subsequently, the generalized conforming theory was successfully generalized to other fields^[22-28], and a large number of new elements, including membrane elements, membrane elements with drilling DOFs, thin-thick plate elements, laminated composite plate elements, flat-shell elements, curved shell elements, etc., were constructed.

Generalized conforming element method is a combination of energy method and weighted residual method. Various new conforming forms, such as line conforming, perimeter conforming, point-line-perimeter conforming and SemiLoof conforming, have been proposed, which reflects the great flexibility of the generalized conforming element method.

Detailed discussions will be given in Chap. 4 to Chap. 11.

(2) Sub-region mixed element method—mixed method convenient for dealing with singular stress problems

The sub-region mixed element method was first proposed in 1982^[29].

The sub-region mixed element method is based on the sub-region mixed energy principle. In such method, a mesh containing two different element types (the conventional displacement-based element and singular stress element) will be used. For singular stress problems (such as crack and notch problems), the singular stress elements (their trial functions contain singular analytical solutions) are collocated in the sub-regions including singular stress points; and the conventional displacement-based elements are collocated in other sub-regions. Since both the singular stress element and the conventional displacement-based element can exhibit each advantage simultaneously in one computation, it provides a novel solution scheme for singular stress problem and is better than the traditional one in which only the displacement-based model is used. Now, it has already been successfully applied in crack problem, notch problem and pipe joint problem of oil platform.

Detailed discussions will be given in Chap. 12 and Chap. 13.

(3) Analytical trial function method—new finite element method in which the analytical solutions are taken as trial functions

A systematic review of the analytical trial function method and its applications was given in the plenary invited paper^[30] at the 11th Nation-wide (China) Conference on Structural Engineering.

In the analytical trial function method, since the analytical solutions are taken as the trial functions of finite elements, analytical and discrete methods can complement each other. As a result, it has been successfully applied in solving some challenging existing problems in FEM. First, for the fracture and notch problems where singular stress point exists, if the analytical solutions containing singular stresses are taken as the trial functions, the computational accuracy of stress intensity factor will be improved dramatically. Thereby, the analytical trial function method has a close relation with the sub-region mixed element method. Secondly, when a mesh is distorted, the precision of many elements will drop rapidly. If the analytical trial function method is employed and cooperates with

the quadrilateral area coordinate method in constructions of new elements, the resulting models will be more insensitive to mesh distortion. Thirdly, in constructions of new thick plate elements, if the analytical solutions of thick plate theory are taken as the trial functions, shear locking phenomenon will be eliminated from the outset. Besides above three points, the analytical trial function method can still be generalized to other fields.

Detailed discussions will be given in Chap. 14 and Chap. 15.

(4) Quadrilateral area coordinate method and its applications—area coordinate method is generalized from the traditional field to new fields

The systematic theory of quadrilateral area coordinate was first established in 1997^[31].

By generalizing the traditional triangular area coordinate method to the quadrilateral or polygonal area coordinate method, the concept and the application scope of the area coordinates are extended. For the past years, the isoparametric coordinate method was almost the unique tool for constructing arbitrary quadrilateral elements. Therefore, the establishment of quadrilateral area coordinate theory provides a new way and a new tool for related jobs. Element models formulated by this new tool are quite insensitive to various mesh distortions, which are much better than those provided by traditional isoparametric coordinate method. At present, some excellent quadrilateral models have been successfully developed by using the new area coordinates, including membrane elements, thin plate elements, thick plate elements, laminated composite plate elements, and shell elements.

Detailed discussions will be given in Chap. 16 and Chap. 17.

(5) Spline elements and their applications—new finite element mode in which the spline functions are taken as the local interpolation functions

The constructions and applications of spline elements have been systematically introduced in two doctoral dissertations^[32,33].

The spline element method combines the high smoothing of spline functions with the high flexibility of finite element method, which overcomes the limitation that the global spline interpolation can only be used in regular domains. Subsequently, 18 spline elements have been developed and successfully applied in various fields, such as plane stress, thin plate, thick plate, thin shell, thick shell, high-rise building structure.

Detailed discussions will be given in Chap. 18 and Chap. 19.

References

- [1] Courant R (1943) Variational methods for the solution of problems of equilibrium and vibration. Bull Am Math Soc 49: 1 – 23
- [2] Turner MJ, Clough RW, Martin HC, Toop LC (1956) Stiffness and deflection analysis of complex structures. J Aeronaut Sci 23(9): 805 – 823

Advanced Finite Element Method in Structural Engineering

- [3] Clough RW (1960) The finite element method in plane stress analysis. In: Proc 2nd Conference on Electronic Computation. Pittsburgh: ASCE, pp345 – 377
- [4] Melosh RJ (1963) Basis for derivation for the direct stiffness method. AIAA Journal 1(7): 1631 – 1637
- [5] Zienkiewicz OC, Taylor RL (2000) The finite element method, 5th edn. Oxford: Butterworth-Heinemann
- [6] Cook RD, Malkus DS, Plesha ME (1989) Concepts and applications of finite element analysis, 3rd edn. John Wiley & Sons Inc, New York
- [7] Huebner KH, Thornton EA, Byrom TG (1995) The finite element method for engineers. John Wiley & Sons Inc, New York
- [8] Bathe KJ (1996) Finite element procedures. Prentice-Hall Inc, New Jersey
- [9] Belytschko T, Liu WK, Moran B (2000) Nonlinear finite elements for continua and structures. Wiley, Chichester
- [10] Chien WZ (1980) Calculus of variations and finite elements (Vol. I). Science Press, Beijing (in Chinese)
- [11] Hu HC (1984) Variational principles of theory of elasticity with applications. Science Press, Beijing
- [12] Long YQ (1978, 1991) Introduction to finite element method. 1st edn, 2nd edn. Higher Education Press, Beijing (in Chinese)
- [13] Long YQ (1992) Introduction to new finite element method. Tsinghua University Press, Beijing (in Chinese)
- [14] Long ZF, Cen S (2001) New monograph of finite element method: principle, programming, developments. China Hydraulic and Water-power Press, Beijing (in Chinese)
- [15] Hu HC (1955) On some variational principles in the theory of elasticity and the theory of plasticity. Scientia Sinica 49(1): 33 – 42
- [16] Feng K (1965) Difference scheme based on variational principle. Chinese Journal of Applied Mathematics and Computational Mathematics 2(4): 238 – 262 (in Chinese)
- [17] Washizu K (1968, 1975, 1982) Variational Methods in Elasticity and Plasticity, 1st edn, 2nd edn, 3rd edn. Pergamon Press
- [18] Long YQ (1981) Piecewise generalized variational principles in elasticity. Shanghai Mechanics 2(2): 1 – 9 (in Chinese)
- [19] Long YQ (1986) Several patterns of functional transformation and generalized variational principles with several arbitrary parameters. International Journal of Solids and Structures 22(10): 1059 – 1069
- [20] Long YQ (1987) Generalized variational principles with several arbitrary parameters and the variable substitution and multiplier method. Applied Mathematics and Mechanics (English Edition) 8(7): 617 – 629
- [21] Long YQ, Xin KG (1987) Generalized conforming element. Tumu Gongcheng Xuebao/China Civil Engineering Journal 20(1): 1 – 14 (in Chinese)
- [22] Long YQ, Xin KG (1989) Generalized conforming element for bending and buckling analysis of plates. Finite Elements in Analysis and Design 5: 15 – 30
- [23] Long YQ, Long ZF, Xu Y (1997) The generalized conforming element (GCE) theory and applications. Advances in Structural Engineering 1(1): 63 – 70

Chapter 1 Introduction—The Evolutive Finite Element Method

- [24] Shi ZC (1990) On the accuracy of the quasi-conforming and generalized conforming finite elements. *Chinese Annals of Mathematics Series B* 11(2): 148 – 155
- [25] Long YQ, Bu XM, Long ZF, Xu Y (1995) Generalized conforming plate bending elements using point and line compatibility conditions. *Computers & Structures* 54(4): 717 – 723
- [26] Long ZF (1992) Triangular and rectangular plate elements based on generalized compatibility conditions. *Computational Mechanics* 10(3/4): 281 – 288
- [27] Long ZF (1993) Two generalized conforming plate elements based on SemiLoof constraints. *Computers & Structures* 47(2): 299 – 304
- [28] Long YQ, Xi F (1992) A universal method for including shear deformation in the thin plate elements. *International Journal for Numerical Methods in Engineering* 34: 171 – 177
- [29] Long YQ, Zhi BC, Kuang WQ, Shan J (1982) Sub-region mixed finite element method for the calculation of stress intensity factor. In: He GQ et al. (eds) *Proceedings of International Conference on FEM*. Science Press, Shanghai, pp738 – 740
- [30] Long YQ, Fu XR (2002) Generalized conforming elements based on analytical trial functions. In: *Proceedings of the Eleventh National Conference on Structural Engineering (Vol. I)*, plenary lecture. China, Changsha, pp28 – 39 (in Chinese)
- [31] Long YQ, Li JX, Long ZF, Cen S (1997) Area-coordinate theory for quadrilateral elements. *Gong Cheng Li Xue / Engineering Mechanics* 14(3): 1 – 11 (in Chinese)
- [32] Yuan S (1984) *Spline elements in stress analysis [Doctoral Dissertation]*. Tsinghua University, Beijing
- [33] Fan Z (1988) *Applications of spline elements and sub-region mixed elements in structural engineering [Doctoral Dissertation]*. Tsinghua University, Beijing (in Chinese)

PART I

Advances in Variational Principles

Chapter 2 The Sub-Region Variational Principles

Chapter 3 Variational Principles with Several Adjustable Parameters

Chapter 2 The Sub-Region Variational Principles

Yu-Qiu Long

Department of Civil Engineering, School of Civil Engineering,
Tsinghua University, Beijing, 100084, China

Zhi-Fei Long

School of Mechanics & Civil Engineering, China University of
Mining & Technology, Beijing, 100083, China

Song Cen

Department of Engineering Mechanics, School of Aerospace,
Tsinghua University, Beijing, 100084, China

Abstract This chapter focuses on the developments of the variational principles which are usually considered as the theoretical basis for the finite element method. In this chapter, we will discuss the *sub-region variational principles* which are the results by the combination of the variational principles and the concept of sub-region interpolation. Following the introduction, the sub-region variational principles for various structural forms, i.e., 3D elastic body, thin plate, thick plate and shallow shell, are presented respectively. Finally, a *sub-region mixed energy partial derivative theorem* is also given.

Keywords variational principle, sub-region variational principle, sub-region mixed energy partial derivative theorem.

2.1 Introduction

Variational principles are usually considered as the theoretical basis for the finite element method. References [1-3] present systematical discussions on some of these variational principles. And, some advances and reviews on this field can be found in the references [4-8].

The sub-region variational principles for elasticity and structural mechanics have been proposed in the references [2, 9]. In the third edition of the reference [1] (1982), the contents of modified variational principles were supplemented. Though the expressions are different, they indeed have a close relationship with the sub-region variational principles.

The studies on the sub-region variational principles were promoted by the advances in the finite element method, and especially by the development of the incompatible element, the generalized conforming element, the hybrid element and the sub-region mixed element approaches. The sub-region generalized variational principles for 3D elasticity was proposed and extended to multi-region mixed energy principle in [2] and [9]. And, the sub-layer variational principle was also discussed in [10]. A review of the sub-region variational principles and their applications in the finite element method was given in [11]. For the elastic thin plate, its sub-region potential principle and sub-region complementary principle were presented in [2], and its sub-region mixed energy principle was given in [12]. For the thick plate and the shallow shell, their sub-region variational principles were proposed in [13] and [14], respectively. And, the reference [15] provided the *sub-region mixed energy partial derivative theorem*, a generalization of the famous *Castigliano first and second energy partial derivative theorems*.

From the viewpoint of structure forms, it can be seen that there are four types, 3D elasticity, thin plate, thick plate and shallow shell, as listed above. The sub-region variational principles of these structures and their energy functional expressions will be introduced in the following four sections, respectively.

From the viewpoint of independent field variables assumed in each sub-region, it can be found that three cases of regions are existing here: ① three-field-region (displacement field, strain field and stress field), ② two-field-region (displacement field and stress field), and ③ single-field-region (displacement field or stress field).

From the viewpoint of energy types, it can be seen that each sub-region can be assumed as either potential or complementary energy region. If all the regions are assumed as potential (or complementary) energy regions, the sub-region potential (or complementary) energy principle will be obtained. If some regions are assumed as potential energy regions, and the others are assumed as complementary energy regions, the sub-region mixed energy variational principle will be obtained.

The sub-region variational principle provides the theoretical basis for developing new finite element methods. For example, the generalized conforming element method described in Part II of this book is based on the sub-region potential energy principle; and the sub-region mixed element method given in Part III is based on the sub-region mixed energy principle.

2.2 The Sub-Region Variational Principle for Elasticity

This section will discuss the various forms^[9,10] of the sub-region generalized variational principle used in elasticity problems. Firstly, let an elastic body be divided into two sub-regions, a and b , then the sub-region three-field generalized mixed, potential and complementary energy variational principles are discussed, respectively. Secondly, two special cases, the sub-region two-field and single-field

generalized variational principles, are discussed. Finally, a general form of the multi-region variational principle is established.

2.2.1 The Sub-Region Three-Field Generalized Mixed Variational Principle for Elasticity

Let an elastic body be divided into two sub-regions a and b ; V_a and V_b be the volumes of the regions a and b , respectively; S_a and S_b be the surfaces of a and b , respectively. Thus, both the surfaces S_a and S_b are composed of three parts:

$$\begin{aligned} S_a &= S_{\sigma a} + S_{ua} + S_{ab} \\ S_b &= S_{\sigma b} + S_{ub} + S_{ab} \end{aligned}$$

Where S_{ab} is the interface between a and b ; $S_{\sigma a}$ and $S_{\sigma b}$ are the boundaries with given tractions $\bar{T}_i (i=1,2,3)$; S_{ua} and S_{ub} are the boundaries with given displacements $\bar{u}_i (i=1,2,3)$. (see Fig. 2.1)

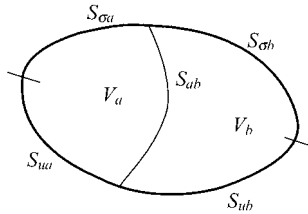


Figure 2.1 An elastic body divided into two sub-regions

In the sub-region three-field generalized mixed variational principle, the displacements, strains and stresses

$$u_i^{(a)}, \varepsilon_{ij}^{(a)}, \sigma_{ij}^{(a)}; \quad u_i^{(b)}, \varepsilon_{ij}^{(b)}, \sigma_{ij}^{(b)} \quad (i, j=1,2,3)$$

in the regions a and b are all field variables. Then the corresponding functional Π_3 can be defined by

$$\Pi_3 = \Pi_{3p}^{(a)} - \Pi_{3c}^{(b)} + H_{pc} \tag{2-1}$$

where $\Pi_{3p}^{(a)}$ is named as the three-field generalized potential energy of the sub-region a (excluding the interface S_{ab}):

$$\Pi_{3p}^{(a)} = \iiint_{V_a} \left[\tilde{U}(\varepsilon_{ij}) - \sigma_{ij} \left(\varepsilon_{ij} - \frac{1}{2} u_{i,j} - \frac{1}{2} u_{j,i} \right) - \bar{F}_i u_i \right] dV - \iint_{S_{\sigma a}} \bar{T}_i u_i dS - \iint_{S_{ua}} T_i (u_i - \bar{u}_i) dS \tag{2-2}$$

in which $\tilde{U}(\varepsilon_{ij})$ denotes the strain energy density; \bar{F}_i denotes the given body force; $u_{i,j}$ denotes the partial derivative of u_i with respect to x_j . $\Pi_{3c}^{(b)}$ is named as the three-field generalized complementary energy of the sub-region b (also excluding the interface S_{ab}):

$$\Pi_{3c}^{(b)} = \iiint_{V_b} [\sigma_{ij}\varepsilon_{ij} - \tilde{U}(\varepsilon_{ij}) + (\sigma_{ij,j} + \bar{F}_i)u_i] dV - \iint_{S_{\sigma b}} (T_i - \bar{T}_i)u_i dS - \iint_{S_{ab}} T_i \bar{u}_i dS \quad (2-3)$$

H_{pc} is the mixed energy at the interface S_{ab} , and given by

$$H_{pc} = \iint_{S_{ab}} T_i^{(b)} u_i^{(a)} dS \quad (2-4)$$

in which $T_i^{(b)}$ denotes the traction of the complementary energy region (sub-region b) at the interface S_{ab} :

$$T_i^{(b)} = \sigma_{ij}^{(b)} n_j^{(b)}$$

$n_j^{(b)}$ is the direction cosine of the outer normal of the region b at the interface S_{ab} ; $u_i^{(a)}$ denotes the displacement of the potential energy region (sub-region a) at the interface S_{ab} .

The sub-region three-field generalized mixed variational principle can be described as follows.

The functional stationary condition

$$\delta \Pi_3 = \delta \Pi_{3p}^{(a)} - \delta \Pi_{3c}^{(b)} + \delta H_{pc} = 0 \quad (2-5)$$

is equivalent to the whole system of equations of the elastic body with sub-regions, including equilibrium differential equation:

$$\sigma_{ij,j} + \bar{F}_i = 0 \quad (\text{in } V) \quad (2-6)$$

strain-displacement relations (geometrical equation)

$$\varepsilon_{ij} = \frac{1}{2}(u_{i,j} + u_{j,i}) \quad (\text{in } V) \quad (2-7)$$

stress-strain relations (constitutive equation)

$$\sigma_{ij} = \frac{\partial \tilde{U}}{\partial \varepsilon_{ij}} \quad (\text{in } V) \quad (2-8)$$

boundary conditions of tractions

$$T_i = \sigma_{ij} n_j = \bar{T}_i \quad (\text{on } S_{\sigma}) \quad (2-9)$$

boundary conditions of displacements

$$u_i = \bar{u}_i \quad (\text{on } S_u) \quad (2-10)$$

and continuous conditions at the interface

$$T_i^{(a)} = -T_i^{(b)} \quad (\text{on } S_{ab}) \quad (2-11)$$

$$u_i^{(a)} = u_i^{(b)} \quad (\text{on } S_{ab}) \quad (2-12)$$

In order to demonstrate the equivalency between the functional stationary condition (2-5) and the Eqs. (2-6) – (2-12), the variation $\delta I_{3p}^{(a)}$ of Eq. (2-2) is firstly developed:

$$\begin{aligned} \delta I_{3p}^{(a)} = & \iiint_{V_a} \left[\left(\frac{\partial \tilde{U}}{\partial \varepsilon_{ij}} - \sigma_{ij} \right) \delta \varepsilon_{ij} - \left(\varepsilon_{ij} - \frac{1}{2} u_{i,j} - \frac{1}{2} u_{j,i} \right) \delta \sigma_{ij} + \sigma_{ij} \delta u_{i,j} - \bar{F}_i \delta u_i \right] dV \\ & - \iint_{S_{\sigma a}} \bar{T}_i \delta u_i dS - \iint_{S_{ua}} [T_i \delta u_i + (u_i - \bar{u}_i) \delta T_i] dS \end{aligned}$$

Since

$$\iiint_{V_a} \sigma_{ij} \delta u_{i,j} dV = \iint_{S_a = S_{\sigma a} + S_{ua} + S_{ab}} T_i \delta u_i dS - \iiint_{V_a} \sigma_{ij,j} \delta u_i dV$$

we have

$$\begin{aligned} \delta I_{3p}^{(a)} = & \iiint_{V_a} \left[\left(\frac{\partial \tilde{U}}{\partial \varepsilon_{ij}} - \sigma_{ij} \right) \delta \varepsilon_{ij} - \left(\varepsilon_{ij} - \frac{1}{2} u_{i,j} - \frac{1}{2} u_{j,i} \right) \delta \sigma_{ij} - (\sigma_{ij,j} + \bar{F}_i) \delta u_i \right] dV \\ & + \iint_{S_{\sigma a}} (T_i - \bar{T}_i) \delta u_i dS - \iint_{S_{ua}} (u_i - \bar{u}_i) \delta T_i dS + \iint_{S_{ab}} T_i^{(a)} \delta u_i^{(a)} dS \end{aligned} \quad (2-13)$$

Secondly, the variation $\delta I_{3c}^{(b)}$ of Eq. (2-3) can be written as:

$$\begin{aligned} \delta I_{3c}^{(b)} = & \iiint_{V_b} \left[\left(\sigma_{ij} - \frac{\partial \tilde{U}}{\partial \varepsilon_{ij}} \right) \delta \varepsilon_{ij} + (\sigma_{ij,j} + \bar{F}_i) \delta u_i + \varepsilon_{ij} \delta \sigma_{ij} + u_i \delta \sigma_{ij,j} \right] dV \\ & - \iint_{S_{\sigma b}} [(T_i - \bar{T}_i) \delta u_i + u_i \delta T_i] dS - \iint_{S_{ub}} \bar{u}_i \delta T_i dS \end{aligned}$$

Since

$$\iiint_{V_b} u_i \delta \sigma_{ij,j} dV = \iint_{S_b = S_{\sigma b} + S_{ub} + S_{ab}} u_i \delta T_i dS - \iiint_{V_b} \frac{1}{2} (u_{i,j} + u_{j,i}) \delta \sigma_{ij} dV$$

we have

$$\begin{aligned} \delta \Pi_{3c}^{(b)} = & \iiint_{V_b} \left[\left(\sigma_{ij} - \frac{\partial \tilde{U}}{\partial \varepsilon_{ij}} \right) \delta \varepsilon_{ij} + (\sigma_{ij,j} + \bar{F}_i) \delta u_i + \left(\varepsilon_{ij} - \frac{1}{2} u_{i,j} - \frac{1}{2} u_{j,i} \right) \delta \sigma_{ij} \right] dV \\ & - \iint_{S_{\sigma b}} (T_i - \bar{T}_i) \delta u_i dS + \iint_{S_{ab}} (u_i - \bar{u}_i) \delta T_i dS + \iint_{S_{ab}} u_i^{(b)} \delta T_i^{(b)} dS \end{aligned} \quad (2-14)$$

Thirdly, the variation δH_{pc} of Eq. (2-4) is

$$\delta H_{pc} = \iint_{S_{ab}} (T_i^{(b)} \delta u_i^{(a)} + u_i^{(a)} \delta T_i^{(b)}) dS \quad (2-15)$$

Finally, the substitution of Eqs. (2-13), (2-14) and (2-15) into (2-5) yields

$$\begin{aligned} \delta \Pi_3 = & \iiint_V \left[\left(\frac{\partial \tilde{U}}{\partial \varepsilon_{ij}} - \sigma_{ij} \right) \delta \varepsilon_{ij} - \left(\varepsilon_{ij} - \frac{1}{2} u_{i,j} - \frac{1}{2} u_{j,i} \right) \delta \sigma_{ij} - (\sigma_{ij,j} + \bar{F}_i) \delta u_i \right] dV \\ & + \iint_{S_{\sigma}} (T_i - \bar{T}_i) \delta u_i dS - \iint_{S_u} (u_i - \bar{u}_i) \delta T_i dS + \iint_{S_{ab}} [(T_i^{(a)} + T_i^{(b)}) \delta u_i^{(a)} \\ & + (u_i^{(a)} - u_i^{(b)}) \delta T_i^{(b)}] dS = 0 \end{aligned} \quad (2-16)$$

Equations (2-6)–(2-12) can be derived from the functional stationary condition (2-16), and vice versa. Thus, the equivalency is proved.

It should be pointed out that, in the expression (2-4) for the mixed energy H_{pc} at the interface S_{ab} , T_i is indicated as belonging to the sub-region b (complementary energy region), and u_i as belonging to the sub-region a (potential energy region). If H_{pc} is defined as

$$\iint_{S_{ab}} T_i^{(a)} u_i^{(b)} dS \quad \text{or} \quad \iint_{S_{ab}} T_i^{(a)} u_i^{(a)} dS \quad \text{or} \quad \iint_{S_{ab}} T_i^{(b)} u_i^{(b)} dS,$$

incorrect results will appear. The reason is that the field variables of the sub-regions a and b are all independent variables, they do not previously satisfy the continuous conditions (2-11) and (2-12) at the interface.

The variational principle discussed above is a kind of unconditioned variational principle. “Unconditioned” has two meanings: ① Firstly, the three variables u_i , ε_{ij} , and σ_{ij} within each sub-region are all independent and have no relation with each other; ② Secondly, at the interface S_{ab} , the variables from the two regions are also independent, they are not required in advance to satisfy the continuous conditions (2-11) and (2-12).

2.2.2 The Transformation Between $\Pi_{3p}^{(a)}$ and $\Pi_{3c}^{(a)}$

In Fig. 2.1, the three-field generalized potential energy $\Pi_{3p}^{(a)}$ and the three-field

generalized complementary energy $\Pi_{3c}^{(a)}$ of the sub-region a (excluding the interface S_{ab}) have the following transformation relationship:

$$\Pi_{3p}^{(a)} + \Pi_{3c}^{(a)} = \iint_{S_{ab}} T_i^{(a)} u_i^{(a)} dS \quad (2-17)$$

The sub-region three-field generalized variational principle has three forms: sub-region mixed energy, sub-region potential energy and sub-region complementary energy. One form can be easily transformed to the other two by using the relation (2-17).

Following is the demonstration of Eq. (2-17). Firstly, the expression of $\Pi_{3c}^{(a)}$ can be written as:

$$\Pi_{3c}^{(a)} = \iiint_{V_a} [\sigma_{ij} \varepsilon_{ij} - \tilde{U}(\varepsilon_{ij}) + (\sigma_{ij,j} + \bar{F}_i) u_i] dV - \iint_{S_{\sigma a}} (T_i - \bar{T}_i) u_i dS - \iint_{S_{ua}} T_i \bar{u}_i dS \quad (2-18)$$

Then, the sum of Eqs. (2-2) and (2-18) can be obtained:

$$\Pi_{3p}^{(a)} + \Pi_{3c}^{(a)} = \iiint_{V_a} \left[\frac{1}{2} \sigma_{ij} (u_{i,j} + u_{j,i}) + \sigma_{ij,j} u_i \right] dV - \iint_{S_{\sigma a} + S_{ua}} T_i u_i dS$$

Since

$$\iiint_{V_a} \left[\frac{1}{2} \sigma_{ij} (u_{i,j} + u_{j,i}) + \sigma_{ij,j} u_i \right] dV = \iiint_{V_a} (\sigma_{ij} u_i)_{,j} dV = \iint_{S_a = S_{\sigma a} + S_{ua} + S_{ab}} T_i u_i dS$$

The substitution of this equation into the previous one will yield Eq. (2-17).

Two special cases can be derived from Eq. (2-17):

Special case 1: when there are no sub-regions in the whole body, $S_{ab} = 0$. Then we have

$$\Pi_{3p} + \Pi_{3c} = 0 \quad (2-19a)$$

Special case 2: when the sub-region a is surrounded by other regions, $S_{\sigma a} = 0$, $S_{ua} = 0$, $S_a = S_{ab}$. Then we have

$$\Pi_{3p}^{(a)} + \Pi_{3c}^{(a)} = \iint_{S_a} T_i^{(a)} u_i^{(a)} dS \quad (2-19b)$$

2.2.3 The Sub-Region Three-Field Generalized Potential and Complementary Energy Principles for Elasticity

Now, by using Eq. (2-17), the functional of the sub-region three-field generalized potential and complementary principles can be derived from the functional of the

sub-region three-field generalized mixed variational principle.

1. The sub-region three-field generalized potential energy principle

In the expression (2-1) of the sub-region three-field generalized mixed variational principle, the sub-region a is represented by the generalized potential energy while the sub-region b is represented by the generalized complementary energy. Here, we require the sub-region b given by the generalized potential energy, too. Then, from Eq. (2-17), we have

$$\Pi_{3c}^{(b)} = -\Pi_{3p}^{(b)} + \iint_{S_{ab}} T_i^{(b)} u_i^{(b)} dS$$

Substitution of this equation into (2-1) yields

$$\Pi_3 = \Pi_{3p}^{(a)} + \Pi_{3p}^{(b)} + H_{pp} \quad (2-20)$$

where H_{pp} is the additional term of the potential energy at the interface S_{ab} :

$$H_{pp} = \iint_{S_{ab}} T_i^{(b)} (u_i^{(a)} - u_i^{(b)}) dS \quad (2-21a)$$

Equations (2-20) and (2-21a) are the functional expressions of the sub-region three-field generalized potential energy principle. It can be shown that the stationary condition $\delta\Pi_3 = 0$ of this functional is equivalent to all equations, boundary conditions and interface continuous conditions of the elastic body with sub-regions. Another expression of H_{pp} can also be obtained by interchanging a and b in Eq. (2-21a):

$$H_{pp} = \iint_{S_{ab}} T_i^{(a)} (u_i^{(b)} - u_i^{(a)}) dS \quad (2-21b)$$

If the continuous condition (2-12) at the interface S_{ab} is satisfied in advance, $H_{pp} = 0$.

2. The sub-region three-field generalized complementary energy principle

In Eq. (2-1), if we require that the sub-region a is given by the generalized complementary energy, the substitution of (2-17) into (2-1) will yield

$$\Pi_3 = -\Pi_{3c}^{(a)} - \Pi_{3c}^{(b)} + H_{cc} \quad (2-22)$$

where H_{cc} is the additional term of the complementary energy at the interface S_{ab} :

$$H_{cc} = \iint_{S_{ab}} (T_i^{(a)} + T_i^{(b)}) u_i^{(a)} dS \quad (2-23a)$$

Equations (2-22) and (2-23a) are the functional expressions of the sub-region

three-field generalized complementary energy principle. Another expression of H_{cc} can also be obtained by interchanging a and b in Eq. (2-23a):

$$H_{cc} = \iint_{S_{ab}} (T_i^{(a)} + T_i^{(b)}) u_i^{(b)} dS \quad (2-23b)$$

If the continuous condition (2-11) at the interface S_{ab} is satisfied in advance, $H_{cc} = 0$.

2.2.4 The Sub-Region Two-Field and Single-Field Variational Principle for Elasticity

The functional expression for the three forms of the sub-region three-field generalized variational principle have been given by Eqs. (2-1), (2-20) and (2-22), respectively. Now, we discuss two special cases.

1. The sub-region two-field generalized variational principle

By employing the relationship

$$\tilde{V}(\sigma_{ij}) = \sigma_{ij} \varepsilon_{ij} - \tilde{U}(\varepsilon_{ij}) \quad (2-24)$$

between the strain energy density $\tilde{U}(\varepsilon_{ij})$ and the strain complementary energy density $\tilde{V}(\sigma_{ij})$, the variable ε_{ij} in the three-field generalized potential energy $\Pi_{3p}^{(a)}$ and the three-field generalized complementary energy $\Pi_{3c}^{(a)}$ of the sub-region a (excluding the interface S_{ab}) can be eliminated. Thus, the two-field (displacement u_i , stress σ_{ij}) generalized potential energy $\Pi_{2p}^{(a)}$ and the two-field generalized complementary energy $\Pi_{2c}^{(a)}$ can be obtained:

$$\Pi_{2p}^{(a)} = \iiint_{V_a} \left[\frac{1}{2} (u_{i,j} + u_{j,i}) \sigma_{ij} - \tilde{V}(\sigma_{ij}) - \bar{F}_i u_i \right] dV - \iint_{S_{\sigma a}} \bar{T}_i u_i dS - \iint_{S_{ua}} T_i (u_i - \bar{u}_i) dS \quad (2-25)$$

$$\Pi_{2c}^{(a)} = \iiint_{V_a} \left[\tilde{V}(\sigma_{ij}) + (\sigma_{ij,j} + \bar{F}_i) u_i \right] dV - \iint_{S_{\sigma a}} (T_i - \bar{T}_i) u_i dS - \iint_{S_{ua}} T_i \bar{u}_i dS \quad (2-26)$$

From Eqs. (2-1), (2-20) and (2-22), the functional expressions of the sub-region two-field generalized mixed energy, potential energy and complementary energy principle can be written as follows:

$$\Pi_2 = \Pi_{2p}^{(a)} - \Pi_{2c}^{(b)} + H_{pc} \quad (2-27)$$

$$\Pi_2 = \Pi_{2p}^{(a)} + \Pi_{2p}^{(b)} + H_{pp} \quad (2-28)$$

$$\Pi_2 = -\Pi_{2c}^{(a)} - \Pi_{2c}^{(b)} + H_{cc} \quad (2-29)$$

where H_{pc} , H_{pp} and H_{cc} are still given by Eqs. (2-4), (2-21) and (2-23), respectively.

2. The sub-region single-field generalized variational principle

Now, we discuss the case where each sub-region has only a single independent variable. If the sub-region a is a potential energy region, only the displacement $u_i^{(a)}$ will be taken as the independent variable. Thus, the $\Pi_{3p}^{(a)}$ in Eq. (2-2) and the $\Pi_{2p}^{(a)}$ in Eq. (2-25) will transform to the single-field potential energy $\Pi_{1p}^{(a)}$ of the region a :

$$\Pi_{1p}^{(a)} = \iiint_{V_a} [\tilde{U}(u_i) - \bar{F}_i u_i] dV - \iint_{S_{\sigma a}} \bar{T}_i u_i dS - \iint_{S_{ua}} T_i (u_i - \bar{u}_i) dS \quad (2-30a)$$

If $u_i^{(a)}$ satisfies the displacement boundary condition (2-10) on S_{ua} in advance, then we have

$$\Pi_{1p}^{(a)} = \iiint_{V_a} [\tilde{U}(u_i) - \bar{F}_i u_i] dV - \iint_{S_{\sigma a}} \bar{T}_i u_i dS \quad (2-30b)$$

If the sub-region a is a complementary energy region, only the stress $\sigma_{ij}^{(a)}$ will be taken as the independent variable, and $\sigma_{ij}^{(a)}$ should satisfy the equilibrium differential Eq. (2-6) in advance. Thus, the $\Pi_{3c}^{(a)}$ in Eq. (2-18) and the $\Pi_{2c}^{(a)}$ in Eq. (2-26) will transform to the single-field complementary energy $\Pi_{1c}^{(a)}$ of the region a :

$$\Pi_{1c}^{(a)} = \iiint_{V_a} \tilde{V}(\sigma_{ij}) dV - \iint_{S_{ua}} T_i \bar{u}_i dS - \iint_{S_{\sigma a}} (T_i - \bar{T}_i) u_i dS \quad (2-31a)$$

If $\sigma_{ij}^{(a)}$ satisfies the boundary condition (2-9) on $S_{\sigma a}$ in advance, then we have

$$\Pi_{1c}^{(a)} = \iiint_{V_a} \tilde{V}(\sigma_{ij}) dV - \iint_{S_{ua}} T_i \bar{u}_i dS \quad (2-31b)$$

From Eqs. (2-1), (2-20) and (2-22), or (2-27), (2-28) and (2-29), the functional expressions of the sub-region single-field generalized mixed energy, potential energy and complementary energy principle can be written as follows:

$$\Pi_1 = \Pi_{1p}^{(a)} - \Pi_{1c}^{(b)} + H_{pc} \quad (2-32)$$

$$\Pi_1 = \Pi_{1p}^{(a)} + \Pi_{1p}^{(b)} + H_{pp} \quad (2-33)$$

$$\Pi_1 = -\Pi_{1c}^{(a)} - \Pi_{1c}^{(b)} + H_{cc} \quad (2-34)$$

where H_{pc} , H_{pp} and H_{cc} are still given by Eqs. (2-4), (2-21) and (2-23), respectively. $T_i^{(a)}$ or $T_i^{(b)}$ in Eq. (2-21), and $u_i^{(a)}$ or $u_i^{(b)}$ in Eq. (2-23), can be treated as Lagrange multipliers.

2.2.5 The General Form of the Multi-Region Variational Principle for Elasticity

From the above discussions, a general form of the multi-region variational principle can be obtained.

Let an elastic body be divided into several sub-regions (see Fig. 2.2). Each sub-region can be arbitrarily appointed as potential energy region or complementary energy region, and each region can be three-field region, or two-field region or single-field region. The interfaces between two adjacent regions are of three types, S_{pc} , S_{pp} and S_{cc} : ① one side of S_{pc} is the potential energy region, while the other side is the complementary one; ② both sides of S_{pp} are potential energy regions; and ③ both sides of S_{cc} are complementary energy regions.

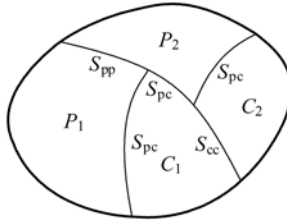


Figure 2.2 An elastic body divided into multi-regions

The general form of the functional for multi-region variational principle can be written as

$$\Pi = \sum_{V_p} \Pi_p - \sum_{V_c} \Pi_c + \sum_{S_{pc}} H_{pc} + \sum_{S_{pp}} H_{pp} + \sum_{S_{cc}} H_{cc} \quad (2-35)$$

The meanings of the terms on the right-side of this equation are as follows:

The first term denotes the sum of the potential (or generalized potential) energy Π_p of each potential energy region V_p , where Π_p can be Π_{1p} or Π_{2p} or Π_{3p} , which is given by Eqs. (2-30), (2-25) and (2-2), respectively.

The second term denotes the sum of the complementary (or generalized complementary) energy Π_c of each complementary energy region V_c , where Π_c can be Π_{1c} or Π_{2c} or Π_{3c} , which is given by Eqs. (2-31), (2-26) and (2-3), respectively.

The third term denotes the sum of the additional term H_{pc} on the interface S_{pc} , in which H_{pc} is given by Eq. (2-4). The fourth term denotes the sum of the additional term H_{pp} on the interface S_{pp} , in which H_{pp} is given by Eq. (2-21). The fifth term denotes the sum of the additional term H_{cc} on the interface S_{cc} , in which H_{cc} is given by Eq. (2-23).

It can be shown that the stationary condition

$$\delta\Pi = 0$$

of the functional Π in Eq. (2-35) is equivalent to all equations, boundary conditions and interface continuous conditions of the elastic body with multi-regions.

If all regions are potential energy regions, the functional of the sub-region potential (or generalized potential) energy principle can be obtained from Eq. (2-35):

$$\Pi = \sum_{V_p} \Pi_p + \sum_{S_{pp}} H_{pp} \quad (2-36)$$

It can be seen that Eqs. (2-20), (2-28) and (2-33) are all special cases of (2-36).

If all regions are complementary energy regions, the functional of the sub-region complementary (or generalized complementary) energy principle can be obtained from Eq. (2-35):

$$\Pi = -\sum_{V_c} \Pi_c + \sum_{S_{cc}} H_{cc} \quad (2-37)$$

It can be seen that Eqs. (2-22), (2-29) and (2-34) are all special cases of (2-37).

Incidentally, the interface S_{ab} can vest in V_a (or V_b), and then, the additional terms H_{pc} , H_{pp} and H_{cc} on S_{ab} will vest in the energy terms $\Pi_p^{(a)}$ and $\Pi_c^{(a)}$ of V_a (or the energy terms $\Pi_p^{(b)}$ and $\Pi_c^{(b)}$ of V_b) as new additional terms. Several cases are discussed as follows:

Firstly, if we assume V_a as potential energy region, when S_{ab} is not included, the potential or generalized potential energy of V_a can be written as

$$\Pi_p^{(a)} = \iiint_{V_a} I_p dV - \iint_{S_{\sigma a}} \bar{T}_i u_i dS - \iint_{S_{ua}} T_i (u_i - \bar{u}_i) dS$$

where I_p denotes the integrand in volume terms of Eqs. (2-30) or (2-25) or (2-2). Now, if S_{ab} vests in V_a , the new additional terms of $\Pi_p^{(a)}$ can be derived as follows:

(1) If the adjacent region V_b is a potential region, S_{ab} can be dealt with in the same manner as S_{ua} . Let $\bar{u}_i = u_i^{(b)}$, so the new additional term in $\Pi_p^{(a)}$ is

$$- \iint_{S_{ab}} T_i^{(a)} (u_i^{(a)} - u_i^{(b)}) dS$$

From Eq. (2-21b), it can be seen that this new additional term is just H_{pp} .

(2) If the adjacent region V_b is a complementary region, S_{ab} can be dealt with in the same manner as $S_{\sigma a}$. Let $\bar{T}_i = -T_i^{(b)}$, so the new additional term in $\Pi_p^{(a)}$ is

$$- \iint_{S_{ab}} (-T_i^{(b)}) u_i^{(a)} dS$$

From Eq. (2-4), it can be seen that this new additional term is just H_{pc} .

Secondly, if we assume V_b as complementary energy region, when S_{ab} is not included, the complementary or generalized complementary energy of V_b can be

written as

$$-II_c^{(b)} = -\iiint_{V_b} I_c dV + \iint_{S_{\sigma b}} (T_i - \bar{T}_i) u_i dS + \iint_{S_{ub}} T_i \bar{u}_i dS$$

where I_c denotes the integrand in volume terms of Eqs. (2-31) or (2-26) or (2-3). Now, if S_{ab} vests in V_b , the new additional terms of $-II_c^{(b)}$ can be derived as follows:

(3) If the adjacent region V_a is a potential region, the new additional term will be $\iint_{S_{ab}} T_i^{(b)} u_i^{(a)} dS$, i.e. H_{pc} .

(4) If the adjacent region V_a is a complementary region, the new additional term will be $\iint_{S_{ab}} (T_i^{(b)} + T_i^{(a)}) u_i^{(b)} dS$, i.e. H_{cc} in Eq. (2-23b).

2.2.6 Some Remarks

The general form of the sub-region generalized variational principle for small displacement elasticity problems is presented in this section, and Eq. (2-35) is its functional expression. Its universality is due to the following reasons:

(1) Each sub-region can be independently specified as potential and complementary energy regions, and the sub-region potential energy, complementary energy and mixed variational principle are three special forms of the general form.

(2) The field variables in each region can be specified independently. The sub-region single-field, two-field, three-field and their mixed forms are all special cases of the general form.

(3) The displacement and traction conditions on each interface can be relaxed partly or completely. It is not necessary to satisfy them in advance.

Various finite element models can all be regarded as the special applications of this principle. For example, the sub-region potential energy principle and its functional (2-36) are the theoretical basis of the generalized conforming elements and the hybrid-displacement elements; the sub-region complementary energy principle and its functional (2-37) are the theoretical basis of the hybrid-stress elements; the sub-region mixed energy principle and its functional (2-1) are the theoretical basis of the sub-region mixed elements.

Besides, there are still some other points worthy of being paid attention to:

(1) By using the relation (2-17), the transformation between the different forms of the variational principle can be performed conveniently.

(2) The general form (2-35) of the functional for the multi-region variational principle establishes a bridge linking the various forms of the variational principle.

2.3 The Sub-Region Variational Principle for Elastic Thin Plate

This section will discuss the sub-region variational principle for elastic thin plate^[2,12,16]. The thin plate variational principle with relaxed continuity requirements has been discussed in [16]. And, the multi-region potential and complementary energy generalized variational principles were given by [2]. Reference [12] proposed the multi-region mixed energy generalized variational principle of thin plate, considered the thin plate multi-region potential and complementary energy generalized variational principles as its special cases, and gave out the transformation relations between generalized potential energy and generalized complementary energy in the sub-regions. By using these relations, transformation between different functionals of the variational principle can be performed conveniently.

The sequence of presentation used in the previous section is adopted again here: firstly, the case with two sub-regions is discussed; secondly, from the three-field principle, the two-field and single-field principles are obtained; finally, the general form of the multi-region variational principle is given.

2.3.1 The Sub-Region Three-Field Generalized Mixed Variational Principle for Thin Plate

1. The description of the sub-regions and the boundaries for thin plate

Let an elastic thin plate be divided into two sub-regions a and b (Fig. 2.3), and Ω_a and Ω_b represent the domains of the regions a and b , respectively. The outer

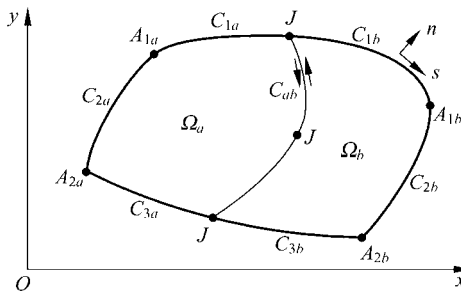


Figure 2.3 A thin plate divided into two sub-regions

boundaries C_a and C_b of the regions a and b are both composed of three parts:

$$C_a = C_{1a} + C_{2a} + C_{3a}$$

$$C_b = C_{1b} + C_{2b} + C_{3b}$$

where C_{1a} and C_{1b} are the fixed boundaries (the deflection \bar{w} and the normal

rotation $\bar{\phi}_n$ on the boundaries are specified); C_{2a} and C_{2b} are the simply-supported boundaries (the deflection \bar{w} and the normal moment \bar{M}_n on the boundaries are specified); and C_{3a} and C_{3b} are the free boundaries (the normal moment \bar{M}_n and the equivalent shear force \bar{V}_n on the boundaries are specified).

The corner points A_a and A_b on the outer boundaries of the regions a and b are composed of two corner point types:

$$A_a = A_{1a} + A_{2a}, \quad A_b = A_{1b} + A_{2b}$$

where A_{1a} and A_{1b} are the corner points where the deflection \bar{w} is specified; A_{2a} and A_{2b} are the corner points where the concentrated force \bar{R} is specified.

The interface of the two regions is C_{ab} , on which the node J is also composed of two node types:

$$J = J_1 + J_2$$

where J_1 is the node where the deflection \bar{w} is specified; J_2 is the node where the concentrated force \bar{R} is specified.

(x, y) are the Cartesian co-ordinates within the mid-surface of the thin plate; n is the outer normal of the boundary; s is the tangent of the boundary, and its positive direction is shown in Fig. 2.3.

2. The key points of the sub-region three-field generalized variational principle

(1) The field variables

Both regions a and b possess three field variables:

Deflections:

$$w(a), \quad w(b)$$

Bending and twisting moments:

$$\mathbf{M}^{(a)} = [M_x \quad M_y \quad M_{xy}]^T{}^{(a)}$$

$$\mathbf{M}^{(b)} = [M_x \quad M_y \quad M_{xy}]^T{}^{(b)}$$

Curvatures:

$$\boldsymbol{\kappa}^{(a)} = [\kappa_x \quad \kappa_y \quad 2\kappa_{xy}]^T{}^{(a)}$$

$$\boldsymbol{\kappa}^{(b)} = [\kappa_x \quad \kappa_y \quad 2\kappa_{xy}]^T{}^{(b)}$$

These field variables are not required to satisfy any conditions in advance within the domain and on the boundaries and interfaces.

(2) Definition of the functional

Let the region a be the potential energy region, and the region b the complementary energy region. Then, the definition of the functional is

$$\Pi_3 = \Pi_{3p}^{(a)} - \Pi_{3c}^{(b)} + H_{pc} + G_{1pc} + G_{2pc} \quad (2-38)$$

where $\Pi_{3p}^{(a)}$ is the three-field generalized potential energy of the region a (excluding the interface C_{ab} and the node J):

$$\begin{aligned} \Pi_{3p}^{(a)} = & \iint_{\Omega_a} \left[\tilde{U}(\boldsymbol{\kappa}) - qw - \left(\frac{\partial^2 w}{\partial x^2} + \kappa_x \right) M_x - \left(\frac{\partial^2 w}{\partial y^2} + \kappa_y \right) M_y - 2 \left(\frac{\partial^2 w}{\partial x \partial y} + \kappa_{xy} \right) M_{xy} \right] dx dy \\ & - \int_{C_{1a} + C_{2a}} \left(Q_n + \frac{\partial M_{ns}}{\partial s} \right) (w - \bar{w}) ds - \int_{C_{3a}} \bar{V}_n w ds + \int_{C_{1a}} M_n \left(\frac{\partial w}{\partial n} - \bar{\psi}_n \right) ds \\ & + \int_{C_{2a} + C_{3a}} \bar{M}_n \frac{\partial w}{\partial n} ds - \sum_{A_{1a}} \Delta M_{ns} (w - \bar{w}) - \sum_{A_{2a}} \bar{R} w \end{aligned} \quad (2-39)$$

Here, q is the density of the normal load; $\tilde{U}(\boldsymbol{\kappa})$ is the density of the strain energy:

$$\tilde{U}(\boldsymbol{\kappa}) = \frac{D}{2} [(\kappa_x + \kappa_y)^2 + 2(1 - \mu)(\kappa_{xy}^2 - \kappa_x \kappa_y)] \quad (2-40)$$

where $D = \frac{Eh^3}{12(1 - \mu^2)}$ is the bending stiffness of the plate; E is the Young's modulus; h is the thickness; μ is the Poisson's ratio; M_n , M_{ns} , and Q_n are the normal bending moment, twisting moment and transverse shear force on the boundary, respectively; ΔM_{ns} is the increment of the twisting moment at two sides of the corner node on the boundary.

$\Pi_{3c}^{(b)}$ is the three-field generalized complementary energy of the region b (excluding the interface C_{ab} and the node J):

$$\begin{aligned} \Pi_{3c}^{(b)} = & \iint_{\Omega_b} \left[M_x \kappa_x + M_y \kappa_y + 2M_{xy} \kappa_{xy} - \tilde{U}(\boldsymbol{\kappa}) + \left(\frac{\partial^2 M_x}{\partial x^2} + \frac{\partial^2 M_y}{\partial y^2} + 2 \frac{\partial^2 M_{xy}}{\partial x \partial y} + q \right) w \right] dx dy \\ & - \int_{C_{1b} + C_{2b}} \left(Q_n + \frac{\partial M_{ns}}{\partial s} \right) \bar{w} ds - \int_{C_{3b}} \left(Q_n + \frac{\partial M_{ns}}{\partial s} - \bar{V}_n \right) w ds + \int_{C_{1b}} M_n \bar{\psi}_n ds \\ & + \int_{C_{2b} + C_{3b}} (M_n - \bar{M}_n) \frac{\partial w}{\partial n} ds - \sum_{A_{1b}} \Delta M_{ns} \bar{w} - \sum_{A_{2b}} (\Delta M_{ns} - \bar{R}) w \end{aligned} \quad (2-41)$$

H_{pc} , G_{1pc} , G_{2pc} are the additional energy terms on the interface C_{ab} and the nodes J_1 and J_2 :

$$H_{pc} = \int_{C_{ab}} \left[M_n^{(b)} \left(\frac{\partial w}{\partial n} \right)^{(a)} + \left(Q_n + \frac{\partial M_{ns}}{\partial s} \right)^{(b)} w^{(a)} \right] ds \quad (2-42)$$

$$G_{1pc} = \sum_{J_1} [-(\Delta M_{ns})^{(a)} (w^{(a)} - \bar{w}) + (\Delta M_{ns})^{(b)} \bar{w}] \quad (2-43)$$

$$G_{2pc} = \sum_{J_2} [(\Delta M_{ns})^{(b)} - \bar{R}] w^{(a)} \quad (2-44)$$

(3) Stationary condition

The stationary condition of the functional is

$$\delta II_3 = \delta II_{3p}^{(a)} - \delta II_{3c}^{(b)} + \delta H_{pc} + \delta G_{1pc} + \delta G_{2pc} = 0 \quad (2-45)$$

which is equivalent to all field equations, boundary conditions, interface conditions, and conditions at the corner points and nodes, including:

The field equations within Ω_a and Ω_b :

$$\left. \begin{aligned} M_x &= D(\kappa_x + \mu\kappa_y), & M_y &= D(\kappa_y + \mu\kappa_x) \\ M_{xy} &= D(1 - \mu)\kappa_{xy} \\ \kappa_x &= -\frac{\partial^2 w}{\partial x^2}, & \kappa_y &= -\frac{\partial^2 w}{\partial y^2}, & \kappa_{xy} &= -\frac{\partial^2 w}{\partial x \partial y} \\ \frac{\partial^2 M_x}{\partial x^2} + \frac{\partial^2 M_y}{\partial y^2} + 2\frac{\partial^2 M_{xy}}{\partial x \partial y} + q &= 0 \end{aligned} \right\} \quad (2-46)$$

The boundary conditions on C_a and C_b :

$$\left. \begin{aligned} Q_n + \frac{\partial M_{ns}}{\partial s} &= \bar{V}_n & (\text{on } C_{3a} + C_{3b}) \\ w &= \bar{w} & (\text{on } C_{1a} + C_{2a} + C_{1b} + C_{2b}) \\ M_n &= \bar{M}_n & (\text{on } C_{2a} + C_{3a} + C_{2b} + C_{3b}) \\ \frac{\partial w}{\partial n} &= \bar{\psi}_n & (\text{on } C_{1a} + C_{1b}) \end{aligned} \right\} \quad (2-47)$$

The interface conditions on C_{ab} :

$$\left. \begin{aligned} M_n^{(a)} &= M_n^{(b)} \\ \left(Q_n + \frac{\partial M_{ns}}{\partial s} \right)^{(a)} &= - \left(Q_n + \frac{\partial M_{ns}}{\partial s} \right)^{(b)} \\ \left(\frac{\partial w}{\partial n} \right)^{(a)} &= - \left(\frac{\partial w}{\partial n} \right)^{(b)} \\ w^{(a)} &= w^{(b)} \end{aligned} \right\} \quad (2-48)$$

The conditions at the corner points:

$$\left. \begin{aligned} w &= \bar{w} & (\text{at } A_{1a} + A_{1b}) \\ \Delta M_{ns} &= \bar{R} & (\text{at } A_{2a} + A_{2b}) \end{aligned} \right\} \quad (2-49)$$

The conditions at the nodes on the interface:

$$\left. \begin{aligned} w^{(a)} &= \bar{w} && \text{(at } J_1) \\ w^{(b)} &= \bar{w} && \text{(at } J_1) \\ w^{(a)} &= w^{(b)} && \text{(at } J_2) \\ (\Delta M_{ns})^{(a)} + (\Delta M_{ns})^{(b)} &= \bar{R} && \text{(at } J_2) \end{aligned} \right\} \quad (2-50)$$

The proof of the above equivalent equations is given in Appendix A.

2.3.2 The Sub-Region Three-Field Generalized Potential and Complementary Energy Principles for Thin Plate

1. The transformation relation between $\Pi_{3p}^{(a)}$ and $\Pi_{3c}^{(a)}$

The three-field generalized potential energy $\Pi_{3p}^{(a)}$ and the three-field generalized complementary energy $\Pi_{3c}^{(a)}$ of the region a (excluding the interface C_{ab} and the node J) have the following transformation relation:

$$\Pi_{3p}^{(a)} + \Pi_{3c}^{(a)} = \int_{C_{ab}} \left[-M_n^{(a)} \left(\frac{\partial w}{\partial n} \right)^{(a)} + \left(Q_n + \frac{\partial M_{ns}}{\partial s} \right)^{(a)} w^{(a)} \right] ds + \sum_{J_1+J_2} w^{(a)} (\Delta M_{ns})^{(a)} \quad (2-51)$$

Proof From Eqs. (2-39) and (2-41), replacing b by a in Eq. (2-41), we have

$$\begin{aligned} \Pi_{3p}^{(a)} + \Pi_{3c}^{(a)} &= \iint_{\Omega_a} \left[- \left(\frac{\partial^2 w}{\partial x^2} M_x + \frac{\partial^2 w}{\partial y^2} M_y + 2 \frac{\partial^2 w}{\partial x \partial y} M_{xy} \right) \right. \\ &\quad \left. + \left(\frac{\partial^2 M_x}{\partial x^2} + \frac{\partial^2 M_y}{\partial y^2} + 2 \frac{\partial^2 M_{xy}}{\partial x \partial y} \right) w \right] dx dy \\ &\quad - \int_{C_{1a}+C_{2a}+C_{3a}} \left[\left(Q_n + \frac{\partial M_{ns}}{\partial s} \right) w - M_n \frac{\partial w}{\partial n} \right] ds - \sum_{A_{1a}+A_{2a}} (\Delta M_{ns}) w \end{aligned} \quad (2-52)$$

By using integration by parts, the following relation can be obtained:

$$\begin{aligned} \iint_{\Omega_a} \left(\frac{\partial^2 M_x}{\partial x^2} + \frac{\partial^2 M_y}{\partial y^2} + 2 \frac{\partial^2 M_{xy}}{\partial x \partial y} \right) w dx dy &= \iint_{\Omega_a} \left(M_x \frac{\partial^2 w}{\partial x^2} + M_y \frac{\partial^2 w}{\partial y^2} + 2 M_{xy} \frac{\partial^2 w}{\partial x \partial y} \right) dx dy \\ &\quad - \int_{C_{1a}+C_{2a}+C_{3a}+C_{ab}} \left[M_n \frac{\partial w}{\partial n} - \left(Q_n + \frac{\partial M_{ns}}{\partial s} \right) w \right] ds + \sum_{A_{1a}+A_{2a}+J_1+J_2} w \Delta M_{ns} \end{aligned} \quad (2-53)$$

Substitution of Eq. (2-53) into Eq. (2-52) yields Eq. (2-51). \square

If the whole domain is not divided into sub-regions, C_{ab} , J_1 and J_2 will no longer exist, so we have

$$\Pi_{3p}^{(a)} + \Pi_{3c}^{(a)} = 0 \quad (2-54)$$

2. The sub-region three-field generalized potential energy principle

In the functional expression (2-38) of the sub-region three-field generalized mixed variational principle, the region a represents the generalized potential energy region, and the region b represents the generalized complementary energy region. Now, if the region b is changed to represent the generalized potential energy region, then from Eq. (2-51), we have

$$\Pi_{3c}^{(b)} = -\Pi_{3p}^{(b)} + \int_{C_{ab}} \left[-M^{(b)} \left(\frac{\partial w}{\partial n} \right)^{(b)} + \left(Q_n + \frac{\partial M_{ns}}{\partial s} \right)^{(b)} w^{(b)} \right] ds + \sum_{J_1+J_2} w^{(b)} (\Delta M_{ns})^{(b)}$$

Substitution of this equation into (2-38) yields

$$\Pi_3 = \Pi_{3p}^{(a)} + \Pi_{3p}^{(b)} + H_{pp} + G_{1pp} + G_{2pp} \quad (2-55)$$

where H_{pp} , G_{1pp} and G_{2pp} are the additional potential energy terms on the interface C_{ab} and the nodes J_1 and J_2 :

$$H_{pp} = \int_{C_{ab}} \left\{ M_n^{(b)} \left[\left(\frac{\partial w}{\partial n} \right)^{(a)} + \left(\frac{\partial w}{\partial n} \right)^{(b)} \right] + \left(Q_n + \frac{\partial M_{ns}}{\partial s} \right)^{(b)} (w^{(a)} - w^{(b)}) \right\} ds \quad (2-56a)$$

$$G_{1pp} = -\sum_{J_1} [(\Delta M_{ns})^{(a)} (w^{(a)} - \bar{w}) + (\Delta M_{ns})^{(b)} (w^{(b)} - \bar{w})] \quad (2-57)$$

$$G_{2pp} = \sum_{J_2} [(\Delta M_{ns})^{(b)} (w^{(a)} - w^{(b)}) - \bar{R} w^{(a)}] \quad (2-58a)$$

Equations (2-55), (2-56a), (2-57) and (2-58a) are the functional expressions of the sub-region three-field generalized potential energy principle. It can be shown that the stationary conditions of this functional is equivalent to all field equations, boundary conditions, interface conditions, corner point and node conditions of the thin plate with sub-regions.

Other expressions of H_{pp} and G_{2pp} can also be obtained by interchanging a and b in Eqs. (2-56a) and (2-58a):

$$H_{pp} = \int_{C_{ab}} \left\{ M_n^{(a)} \left[\left(\frac{\partial w}{\partial n} \right)^{(a)} + \left(\frac{\partial w}{\partial n} \right)^{(b)} \right] + \left(Q_n + \frac{\partial M_{ns}}{\partial s} \right)^{(a)} (w^{(b)} - w^{(a)}) \right\} ds \quad (2-56b)$$

$$G_{2pp} = \sum_{J_2} [(\Delta M_{ns})^{(a)}(w^{(b)} - w^{(a)}) - \bar{R}w^{(b)}] \quad (2-58b)$$

If the displacement continuous conditions on the interface C_{ab} and the nodes J_1 and J_2 are satisfied in advance, then from Eqs. (2-56), (2-57) and (2-58), we can obtain

$$\begin{aligned} H_{pp} &= 0 \\ G_{1pp} &= 0 \\ G_{2pp} &= -\sum_{J_2} \bar{R}w^{(a)} \quad \text{or} \quad G_{2pp} = -\sum_{J_2} \bar{R}w^{(b)} \end{aligned}$$

3. The sub-region three-field generalized complementary energy principle

In Eq. (2-38), if we require that the sub-region a is given by the generalized complementary energy, the substitution of (2-51) into (2-38) will yield

$$\Pi_3 = -\Pi_{3c}^{(a)} - \Pi_{3c}^{(b)} + H_{cc} + G_{1cc} + G_{2cc} \quad (2-59)$$

where H_{cc} , G_{1cc} and G_{2cc} are the additional complementary energy terms on the interface C_{ab} and the nodes J_1 and J_2 :

$$H_{cc} = \int_{C_{ab}} \left\{ (M_n^{(b)} - M_n^{(a)}) \left(\frac{\partial w}{\partial n} \right)^{(a)} + \left[\left(Q_n + \frac{\partial M_{ns}}{\partial s} \right)^{(b)} + \left(Q_n + \frac{\partial M_{ns}}{\partial s} \right)^{(a)} \right] w^{(a)} \right\} ds \quad (2-60a)$$

$$G_{1cc} = \sum_{J_1} [(\Delta M_{ns})^{(b)} + (\Delta M_{ns})^{(a)}] \bar{w} \quad (2-61)$$

$$G_{2cc} = \sum_{J_2} \{ [(\Delta M_{ns})^{(b)} + (\Delta M_{ns})^{(a)} - \bar{R}] w^{(a)} \} \quad (2-62a)$$

Equations (2-59), (2-60a), (2-61) and (2-62a) are the functional expressions of the sub-region three-field generalized complementary energy principle. Other expressions of H_{cc} and G_{2cc} can also be obtained by interchanging a and b in Eqs. (2-60a) and (2-62a):

$$H_{cc} = \int_{C_{ab}} \left\{ (M_n^{(a)} - M_n^{(b)}) \left(\frac{\partial w}{\partial n} \right)^{(b)} + \left[\left(Q_n + \frac{\partial M_{ns}}{\partial s} \right)^{(a)} + \left(Q_n + \frac{\partial M_{ns}}{\partial s} \right)^{(b)} \right] w^{(b)} \right\} ds \quad (2-60b)$$

$$G_{2cc} = \sum_{J_2} \{ [(\Delta M_{ns})^{(b)} + (\Delta M_{ns})^{(a)} - \bar{R}] w^{(b)} \} \quad (2-62b)$$

If the traction conditions on the interface C_{ab} and the node J_2 are satisfied in

advance, then from Eqs. (2-60) and (2-62), we can obtain:

$$H_{cc} = 0, \quad G_{2cc} = 0$$

2.3.3 The Sub-Region Two-Field and Single-Field Variational Principle for Thin Plate

1. The sub-region two-field generalized variational principle

By using the relation between the strain energy density $\tilde{U}(\boldsymbol{\kappa})$ and the strain complementary energy density $\tilde{V}(\mathbf{M})$:

$$\tilde{V}(\mathbf{M}) = M_x \kappa_x + M_y \kappa_y + 2M_{xy} \kappa_{xy} - \tilde{U}(\boldsymbol{\kappa}) \quad (2-63)$$

the variable $\boldsymbol{\kappa}$ in the three-field generalized potential energy $\Pi_{3p}^{(a)}$ and generalized complementary energy $\Pi_{3c}^{(a)}$ of the region a (excluding the interface C_{ab} and the nodes J_1 and J_2) can be eliminated. Thereby, the two-field (displacement field w and internal moment field \mathbf{M}) generalized potential energy $\Pi_{2p}^{(a)}$ and generalized complementary energy $\Pi_{2c}^{(a)}$ can be written as follows:

$$\begin{aligned} \Pi_{2p}^{(a)} = & \iint_{\Omega_a} \left[- \left(\frac{\partial^2 w}{\partial x^2} M_x + \frac{\partial^2 w}{\partial y^2} M_y + 2 \frac{\partial^2 w}{\partial x \partial y} M_{xy} \right) - \tilde{V}(\mathbf{M}) - qw \right] dx dy \\ & - \int_{C_{1a} + C_{2a}} \left(Q_n + \frac{\partial M_{ns}}{\partial s} \right) (w - \bar{w}) ds - \int_{C_{3a}} \bar{V}_n w ds + \int_{C_{1a}} M_n \left(\frac{\partial w}{\partial n} - \bar{\psi}_n \right) ds \\ & + \int_{C_{2a} + C_{3a}} \bar{M}_n \frac{\partial w}{\partial n} ds - \sum_{A_{1a}} \Delta M_{ns} (w - \bar{w}) - \sum_{A_{2a}} \bar{R} w \end{aligned} \quad (2-64)$$

$$\begin{aligned} \Pi_{2c}^{(a)} = & \iint_{\Omega_a} \left[\tilde{V}(\mathbf{M}) + \left(\frac{\partial^2 M_x}{\partial x^2} + \frac{\partial^2 M_y}{\partial y^2} + 2 \frac{\partial^2 M_{xy}}{\partial x \partial y} + q \right) w \right] dx dy \\ & - \int_{C_{1a} + C_{2a}} \left(Q_n + \frac{\partial M_{ns}}{\partial s} \right) \bar{w} ds - \int_{C_{3a}} \left(Q_n + \frac{\partial M_{ns}}{\partial s} - \bar{V}_n \right) w ds + \int_{C_{1a}} M_n \bar{\psi}_n ds \\ & + \int_{C_{2a} + C_{3a}} (M_n - \bar{M}_n) \frac{\partial w}{\partial n} ds - \sum_{A_{1a}} \Delta M_{ns} \bar{w} - \sum_{A_{2a}} (\Delta M_{ns} - \bar{R}) w \end{aligned} \quad (2-65)$$

From Eqs. (2-38), (2-55) and (2-59), the functional expressions of the sub-region two-field generalized mixed energy, potential energy and complementary energy principle can be obtained:

$$\Pi_2 = \Pi_{2p}^{(a)} - \Pi_{2c}^{(b)} + H_{pc} + G_{1pc} + G_{2pc} \quad (2-66)$$

$$\Pi_2 = \Pi_{2p}^{(a)} + \Pi_{2p}^{(b)} + H_{pp} + G_{1pp} + G_{2pp} \quad (2-67)$$

$$\Pi_2 = -\Pi_{2c}^{(a)} - \Pi_{2c}^{(b)} + H_{cc} + G_{1cc} + G_{2cc} \quad (2-68)$$

where H_{pc} , H_{pp} and H_{cc} are still given by Eqs. (2-42), (2-56) and (2-60), respectively; G_{1pc} , G_{2pc} , G_{1pp} , G_{2pp} , G_{1cc} and G_{2cc} are still given by Eqs. (2-43), (2-44), (2-57), (2-58), (2-61) and (2-62), respectively.

2. The sub-region single-field variational principle

Now we consider the case where each sub-region is a single-field region. If the region a is a potential energy region, only the displacement w will be taken as the field variable. Thus, the $\Pi_{3p}^{(a)}$ in Eq. (2-39) or the $\Pi_{2p}^{(a)}$ in Eq. (2-64) will transform to the single-field potential energy $\Pi_{1p}^{(a)}$ of the region a :

$$\begin{aligned} \Pi_{1p}^{(a)} = & \iint_{\Omega_a} [\tilde{U}(w) - qw] dx dy - \int_{C_{1a}+C_{2a}} \left(\frac{\partial M_{ns}}{\partial s} + Q_n \right) (w - \bar{w}) ds \\ & - \int_{C_{3a}} \bar{V}_n w ds + \int_{C_{1a}} M_n \left(\frac{\partial w}{\partial n} - \bar{\psi}_n \right) ds + \int_{C_{2a}+C_{3a}} \bar{M}_n \frac{\partial w}{\partial n} ds \\ & - \sum_{A_{1a}} \Delta M_{ns} (w - \bar{w}) - \sum_{A_{2a}} \bar{R} w \end{aligned} \quad (2-69a)$$

where $Q_n + \frac{\partial M_{ns}}{\partial s}$, M_n and ΔM_{ns} can be expressed as the functions of the displacement w , or looked upon as the Lagrange multipliers on the boundaries and their corner points; $\tilde{U}(w)$ is the strain energy density in terms of the displacement w :

$$\tilde{U}(w) = \frac{D}{2} \left\{ \left(\frac{\partial^2 w}{\partial x^2} + \frac{\partial^2 w}{\partial y^2} \right)^2 + 2(1 - \mu) \left[\left(\frac{\partial^2 w}{\partial x \partial y} \right)^2 - \frac{\partial^2 w}{\partial x^2} \frac{\partial^2 w}{\partial y^2} \right] \right\}$$

If the displacement w satisfies the geometrical boundary and corner point conditions in advance, then

$$\Pi_{1p}^{(a)} = \iint_{\Omega_a} [\tilde{U}(w) - qw] dx dy - \int_{C_{3a}} \bar{V}_n w ds + \int_{C_{2a}+C_{3a}} \bar{M}_n \frac{\partial w}{\partial n} ds - \sum_{A_{2a}} \bar{R} w \quad (2-69b)$$

If the sub-region a is a complementary energy region, only the internal moment \mathbf{M} will be taken as the field variable, and \mathbf{M} should satisfy the equilibrium differential equation in advance.

$$\frac{\partial^2 M_x}{\partial x^2} + \frac{\partial^2 M_y}{\partial y^2} + 2 \frac{\partial^2 M_{xy}}{\partial x \partial y} + q = 0$$

Thus, the $\Pi_{3c}^{(a)}$ in Eq. (2-41) or the $\Pi_{2c}^{(a)}$ in Eq. (2-65) will transform to the single-field complementary energy $\Pi_{1c}^{(a)}$:

$$\begin{aligned} \Pi_{1c}^{(a)} = & \iint_{\Omega_a} \tilde{V}(\mathbf{M}) dx dy - \int_{C_{1a}+C_{2a}} \left(Q_n + \frac{\partial M_{ns}}{\partial S} \right) \bar{w} ds - \int_{C_{3a}} \left(Q_n + \frac{\partial M_{ns}}{\partial S} - \bar{V}_n \right) w ds \\ & + \int_{C_{1a}} M_n \bar{\psi}_n ds + \int_{C_{2a}+C_{3a}} (M_n - \bar{M}_n) \frac{\partial w}{\partial n} ds - \sum_{A_{1a}} \Delta M_{ns} \bar{w} - \sum_{A_{2a}} (\Delta M_{ns} - \bar{R}) w \end{aligned} \quad (2-70a)$$

where w and $\frac{\partial w}{\partial n}$ can be looked upon as the Lagrange multipliers on the boundaries and their corner points.

If \mathbf{M} satisfies the traction boundary and corner point conditions in advance, then

$$\Pi_{1c}^{(a)} = \iint_{\Omega_a} \tilde{V}(\mathbf{M}) dx dy - \int_{C_{1a}+C_{2a}} \left(Q_n + \frac{\partial M_{ns}}{\partial S} \right) \bar{w} ds + \int_{C_{1a}} M_n \bar{\psi}_n ds - \sum_{A_{1a}} \Delta M_{ns} \bar{w} \quad (2-70b)$$

From Eqs. (2-38), (2-55), (2-59), or (2-66), (2-67), (2-68), the functional expressions of the sub-region single-field mixed energy principle, potential energy principle and complementary energy principle can be obtained:

$$\Pi_1 = \Pi_{1p}^{(a)} - \Pi_{1c}^{(b)} + H_{pc} + G_{1pc} + G_{2pc} \quad (2-71)$$

$$\Pi_1 = \Pi_{1p}^{(a)} + \Pi_{1p}^{(b)} + H_{pp} + G_{1pp} + G_{2pp} \quad (2-72)$$

$$\Pi_1 = -\Pi_{1c}^{(a)} - \Pi_{1c}^{(b)} + H_{cc} + G_{1cc} + G_{2cc} \quad (2-73)$$

where H_{pc} , G_{1pc} , G_{2pc} , H_{pp} , G_{1pp} , G_{2pp} , H_{cc} , G_{1cc} and G_{2cc} are the same as those in Eqs. (2-66) to (2-68).

2.3.4 The General Form of the Sub-Region Generalized Variational Principle for Thin Plate

From the above discussions, a general form of the sub-region generalized variational principle can be obtained.

Let an elastic thin plate be divided into several sub-regions. Each sub-region can be arbitrarily appointed as single-field, two-field and three-field potential energy regions (such as the regions Ω_{p1} , Ω_{p2} , Ω_{p3} in Fig. 2.4) or complementary energy regions (such as the regions Ω_{c1} , Ω_{c2} , Ω_{c3} in Fig. 2.4).

The interfaces between two adjacent sub-regions are of three types, C_{pc} , C_{pp} and C_{cc} : ① one side of C_{pc} is the potential energy region, while the other side is the

complementary one; ② both sides of C_{pp} are potential energy regions; and ③ both sides of C_{cc} are complementary energy regions.

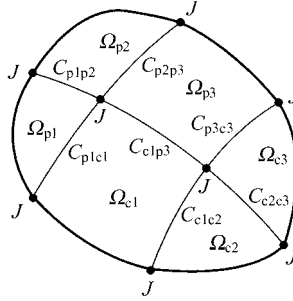


Figure 2.4 A thin plate divided into multi-regions

The node J of the adjacent sub-regions are of two types, J_1 and J_2 : J_1 is the node where the displacement \bar{w} is specified; J_2 is the node where the concentrated force \bar{R} is specified. There are r_p potential energy elements e_p and r_c complementary energy element e_c around the node J .

The general form for the functional of the sub-region variational principle can be written as

$$\Pi = \sum_{\Omega_p} \Pi_p - \sum_{\Omega_c} \Pi_c + \sum_{C_{pc}} H_{pc} + \sum_{C_{pp}} H_{pp} + \sum_{C_{cc}} H_{cc} + \sum_{J_1} G_1 + \sum_{J_2} G_2 \quad (2-74)$$

The meanings of the terms on the right-side of this equation are as follows:

The first term denotes the sum of the potential (or generalized potential) energy Π_p of each potential energy region Ω_p , where Π_p can be Π_{1p} or Π_{2p} or Π_{3p} , which is given by Eqs. (2-69), (2-64) and (2-39), respectively;

The second term denotes the sum of the complementary (or generalized complementary) energy Π_c of each complementary energy region Ω_c , where Π_c can be Π_{1c} or Π_{2c} or Π_{3c} , which is given by Eqs. (2-70), (2-65) and (2-41), respectively;

The third term denotes the sum of the additional mixed energy term H_{pc} on the interface C_{pc} , in which H_{pc} is given by Eq. (2-42);

The fourth term denotes the sum of the additional potential energy term H_{pp} on the interface C_{pp} , in which H_{pp} is given by Eq. (2-56);

The fifth term denotes the sum of the additional complementary energy term H_{cc} on the interface C_{cc} , in which H_{cc} is given by Eq. (2-60).

The sixth term denotes the sum of the additional energy term G_1 at the node J_1 (where the displacement is specified) of the adjacent sub-regions, in which

$$G_1 = - \sum_{e_p} (\Delta M_{ns})^{(e_p)} (w^{(e_p)} - \bar{w}) + \sum_{e_c} (\Delta M_{ns})^{(e_c)} \bar{w} \quad (2-75)$$

The first term on the right side of the above equation means the sum of all the potential elements e_p around the node; the second term means the sum of all the complementary energy elements e_c around the node.

The seventh term denotes the sum of the additional energy term G_2 at the node J_2 (where the concentrated force is specified) of the adjacent sub-regions, in which

$$G_2 = \left[\sum_e (\Delta M_{ns})^{(e)} - \bar{R} \right] w^{(a)} - \sum_{e_p} (\Delta M_{ns})^{(e_p)} w^{(e_p)} \quad (2-76)$$

The \sum_e in the first term on the right side of the above equation denotes the sum of all the elements e (including all e_p and e_c) around the node; $w^{(a)}$ is the displacement of any element a around the node; The \sum_{e_p} in the second term on the right side of the above equation denotes the sum of all the potential elements e_p around the node.

G_{1pc} in (2-43), G_{1pp} in (2-57), and G_{1cc} in (2-61) are all special cases of G_1 in (2-75). G_{2pc} in (2-44), G_{2pp} in (2-58), and G_{2cc} in (2-62) are all special cases of G_2 in (2-76).

It can be shown that the stationary condition

$$\delta II = 0 \quad (2-77)$$

of the functional II in Eq. (2-74) is equivalent to all field equations, boundary conditions, interface conditions, corner point and node conditions of the thin plate system with multi-regions.

The procedure for deriving the node conditions of the node J from the stationary condition (2-77) is given in Appendix B.

If all the sub-regions are potential energy regions, the functional of the sub-region potential (or generalized potential) energy principle can be obtained from Eq. (2-74):

$$II = \sum_{\Omega_p} II_p + \sum_{C_{pp}} H_{pp} + \sum_{J_1} G_{1pp} + \sum_{J_2} G_{2pp} \quad (2-78)$$

where G_{1pp} and G_{2pp} can be obtained from Eqs. (2-75) and (2-76):

$$G_{1pp} = - \sum_{e_p} (\Delta M_{ns})^{(e_p)} (w^{(e_p)} - \bar{w}) \quad (2-79)$$

$$\begin{aligned} G_{2pp} &= \left[\sum_{e_p} (\Delta M_{ns})^{(e_p)} - \bar{R} \right] w^{(a)} - \sum_{e_p} (\Delta M_{ns})^{(e_p)} w^{(e_p)} \\ &= - \sum_{e_p} (\Delta M_{ns})^{(e_p)} (w^{(e_p)} - w^{(a)}) - \bar{R} w^{(a)} \end{aligned} \quad (2-80)$$

Equations (2-55), (2-67) and (2-72) are all the special cases of (2-78). One of the

special cases of the sub-region potential energy principle is that each sub-region is appointed as a single-field potential energy region. At this time, Π_p in Eq. (2-78) will be replaced by Π_{1p} in Eq. (2-69a):

$$\Pi = \sum_{\Omega_p} \Pi_{1p} + \sum_{C_{pp}} H_{pp} + \sum_{J_1} G_{1pp} + \sum_{J_2} G_{2pp} \quad (2-81)$$

If all the sub-regions are complementary energy regions, the functional of the sub-region complementary (or generalized complementary) energy principle can be obtained from Eq. (2-74):

$$\Pi = -\sum_{\Omega_c} \Pi_c + \sum_{C_{cc}} H_{cc} + \sum_{J_1} G_{1cc} + \sum_{J_2} G_{2cc} \quad (2-82)$$

where

$$G_{1cc} = \sum_{e_c} (\Delta M_{ns})^{(e_c)} \bar{w} \quad (2-83)$$

$$G_{2cc} = [\sum_{e_c} (\Delta M_{ns})^{(e_c)} - \bar{R}] w^{(a)} \quad (2-84)$$

Equations (2-59), (2-68) and (2-73) are all the special cases of (2-82). One of the special cases of sub-region complementary energy principle is that each sub-region is appointed as a two-field complementary energy region. At this time, Π_c in Eq. (2-82) will be replaced by Π_{2c} in Eq. (2-65):

$$\Pi = -\sum_{\Omega_c} \Pi_{2c} + \sum_{C_{cc}} H_{cc} + \sum_{J_1} G_{1cc} + \sum_{J_2} G_{2cc} \quad (2-85)$$

2.4 The Sub-Region Variational Principle for Elastic Thick Plate

In the previous section, the sub-region variational principle for thin plate is discussed. This section will consider the thick plate case.

Compared with the thin plate theory, the characteristics of the thick plate theory are as follows: the influences of the transverse shear strain γ_x and γ_y (abbreviations of γ_{xz} and γ_{yz}) are considered; the rotations ψ_x and ψ_y are not dependent on the deflection w , thereby, w , ψ_x and ψ_y are three independent displacements; Besides the normal load \bar{q} , there still are couple loads \bar{m}_x and \bar{m}_y ; the transverse shear forces Q_x and Q_y are not dependent on the bending and twisting moments M_x , M_y and M_{xy} .

The sub-region variational principle for elastic thick plate was proposed in [13].

For comparison, the arrangement of this section is the same as that of the previous one, which can make it easy to understand the similarities and differences of the two principles.

2.4.1 The Sub-Region Three-Field Generalized Mixed Variational Principle for Thick Plate

Here we consider an elastic plate with moderate thickness, i.e. an elastic thick plate. A Cartesian co-ordinate system is established on the mid-surface of the plate (see Fig. 2.5), and the positive direction of the z -axis is downward. n and s denote the directions of the outer normal and the tangent along the boundary, respectively. And, the positive direction of s is shown in Fig. 2.5.

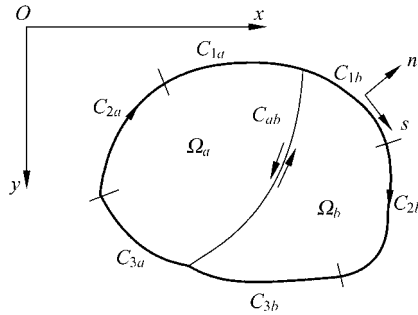


Figure 2.5 A thick plate divided into two sub-regions

Let a thick plate be divided into two sub-regions a and b , and Ω_a and Ω_b represent the domains of the regions a and b , respectively. The outer boundaries C_a and C_b of the regions a and b are both composed of three parts:

$$C_a = C_{1a} + C_{2a} + C_{3a}, \quad C_b = C_{1b} + C_{2b} + C_{3b}$$

where C_{1a} and C_{1b} are the fixed boundaries (the deflection w , the normal rotation ψ_n and the tangent rotation ψ_s of the mid-surface normal line are specified by \bar{w} , $\bar{\psi}_n$ and $\bar{\psi}_s$, respectively); C_{2a} and C_{2b} are the simply-supported boundaries (the deflection w , the tangent rotation ψ_s of the mid-surface normal line and the normal bending moment M_n are specified by \bar{w} , $\bar{\psi}_s$ and \bar{M}_n , respectively); C_{3a} and C_{3b} are the free boundaries (the normal bending moment M_n , the twisting moment M_{ns} and the transverse shear force Q_n are specified by \bar{M}_n , \bar{M}_{ns} and \bar{Q}_n , respectively). The interface of the two regions is denoted by C_{ab} . The positive deflection w is downward; the positive normal rotation ψ_n rotates from n to z ; the positive tangent rotation ψ_s rotates from s to z ; the normal bending moment M_n is positive when the bottom of the plate is under tension; the twisting moment M_{ns}

is positive when it produces positive shear stress τ_{ns} along the positive direction of s at the bottom of the plate; and the positive transverse shear force Q_n is also downward.

The key points of the sub-region generalized mixed variational principle can be listed as follows.

1. The field variables

Both regions a and b possess three field variables:

$$\text{Displacements } \mathbf{d}^{(a)} = [w \ \psi_x \ \psi_y]^T, \quad \mathbf{d}^{(b)} = [w \ \psi_x \ \psi_y]^T$$

$$\text{Internal forces } \mathbf{S}^{(a)} = [M_x \ M_y \ M_{xy} \ Q_x \ Q_y]^T$$

$$\mathbf{S}^{(b)} = [M_x \ M_y \ M_{xy} \ Q_x \ Q_y]^T$$

$$\text{Strain } \mathbf{E}^{(a)} = [\kappa_x \ \kappa_y \ 2\kappa_{xy} \ \gamma_x \ \gamma_y]^T, \quad \mathbf{E}^{(b)} = [\kappa_x \ \kappa_y \ 2\kappa_{xy} \ \gamma_x \ \gamma_y]^T$$

The positive rotations ψ_x and ψ_y of the normal line rotate from x to z and from y to z , respectively; the bending moment M_x and M_y are positive when the bottom of the plate is under tension; the twisting moment M_{xy} is positive when it produces positive shear stress τ_{xy} at the bottom of the plate; the positive shear forces Q_x and Q_y on the positive surfaces are all downward. The positive curvatures κ_x , κ_y and κ_{xy} , shear strains γ_x (γ_{xz}) and γ_y (γ_{yz}) are all corresponding to the deformations caused by the positive M_x , M_y , M_{xy} , Q_x and Q_y , respectively. The above three-field variables are not required to satisfy any conditions in advance within the domain and on the boundaries and interfaces.

2. Definition of the functional

Let the region a be the potential energy region, and the region b be the complementary energy region. Then, the definition of the functional is

$$\Pi_3 = \Pi_{3p}^{(a)} - \Pi_{3c}^{(b)} + H_{pc} \quad (2-86)$$

where $\Pi_{3p}^{(a)}$ is the three-field generalized potential energy of the region a (excluding the interface C_{ab}):

$$\begin{aligned} \Pi_{3p}^{(a)} = & \iint_{\Omega_a} [\tilde{U}_b(\boldsymbol{\kappa}) + \tilde{U}_s(\boldsymbol{\gamma}) - M_x \left(\kappa_x + \frac{\partial \psi_x}{\partial x} \right) - M_y \left(\kappa_y + \frac{\partial \psi_y}{\partial y} \right) \\ & - M_{xy} \left(2\kappa_{xy} + \frac{\partial \psi_x}{\partial y} + \frac{\partial \psi_y}{\partial x} \right) - Q_x \left(\gamma_x - \frac{\partial w}{\partial x} + \psi_x \right) - Q_y \left(\gamma_y - \frac{\partial w}{\partial y} + \psi_y \right) \\ & - \bar{m}_x \psi_x - \bar{m}_y \psi_y - \bar{q} w] dx dy + \int_{C_{1a} + C_{2a}} [M_{ns} (\psi_s - \bar{\psi}_s) - Q_n (w - \bar{w})] ds \\ & + \int_{C_{3a}} (\bar{M}_{ns} \psi_s - \bar{Q}_n w) ds + \int_{C_{1a}} (\psi_n - \bar{\psi}_n) M_n ds + \int_{C_{2a} + C_{3a}} \bar{M}_n \psi_n ds \end{aligned} \quad (2-87)$$

Here, \bar{q} is the load density, and its positive direction is downward. \bar{m}_x and \bar{m}_y are the couple load densities, and their positive directions are the same as those

of ψ_x and ψ_y , respectively. $\tilde{U}_b(\boldsymbol{\kappa})$ and $\tilde{U}_s(\boldsymbol{\gamma})$ are the densities of bending and shear strain energies, respectively:

$$\tilde{U}_b(\boldsymbol{\kappa}) = \frac{D}{2} [\kappa_x^2 + \kappa_y^2 + 2\mu\kappa_x\kappa_y + 2(1-\mu)\kappa_{xy}^2] \quad (2-88)$$

$$\tilde{U}_s(\boldsymbol{\gamma}) = \frac{C}{2} (\gamma_x^2 + \gamma_y^2) \quad (2-89)$$

where $D = \frac{Eh^3}{12(1-\mu^2)}$ and $C = \frac{Eh}{2(1+\mu)k}$ are the bending and shear stiffness,

respectively; μ is the Poisson's ratio; and coefficient $k = 1.2$.

$\Pi_{3c}^{(b)}$ is the three-field generalized complementary energy of the region b (excluding the interface C_{ab}):

$$\begin{aligned} \Pi_{3c}^{(b)} = & \iint_{\Omega_b} [-\tilde{U}_b(\boldsymbol{\kappa}) - \tilde{U}_s(\boldsymbol{\gamma}) + M_x\kappa_x + M_y\kappa_y + 2M_{xy}\kappa_{xy} + Q_x\gamma_x + Q_y\gamma_y \\ & - \left(\frac{\partial M_x}{\partial x} + \frac{\partial M_{xy}}{\partial y} - Q_x - \bar{m}_x \right) \psi_x - \left(\frac{\partial M_{xy}}{\partial x} + \frac{\partial M_y}{\partial y} - Q_y - \bar{m}_y \right) \psi_y \\ & + \left(\frac{\partial Q_x}{\partial x} + \frac{\partial Q_y}{\partial y} + \bar{q} \right) w] dx dy + \int_{C_{1b}+C_{2b}} (\bar{\psi}_s M_{ns} - \bar{w} Q_n) ds \\ & + \int_{C_{3b}} [(M_{ns} - \bar{M}_{ns}) \psi_s - (Q_n - \bar{Q}_n) w] ds + \int_{C_{1b}} \bar{\psi}_n M_n ds \\ & + \int_{C_{2b}+C_{3b}} (M_n - \bar{M}_n) \psi_n ds \end{aligned} \quad (2-90)$$

H_{pc} is the additional energy term on the interface C_{ab} :

$$H_{pc} = \int_{C_{ab}} (M_n^{(b)} \psi_n^{(a)} + M_{ns}^{(b)} \psi_s^{(a)} + Q_n^{(b)} w^{(a)}) ds \quad (2-91)$$

3. Stationary condition

The stationary condition of the functional is

$$\delta \Pi_3 = \delta \Pi_{3p}^{(a)} - \delta \Pi_{3c}^{(b)} + \delta H_{pc} = 0 \quad (2-92)$$

which is equivalent to all field equations, boundary conditions and interface conditions of the thick plate sub-region system, including:

The constitutive, geometrical and equilibrium equations within Ω_a and Ω_b :

$$M_x = D(\kappa_x + \mu\kappa_y), \quad M_y = D(\kappa_y + \mu\kappa_x), \quad M_{xy} = D(1-\mu)\kappa_{xy} \quad (2-93)$$

$$\kappa_x = -\frac{\partial \psi_x}{\partial x}, \quad \kappa_y = -\frac{\partial \psi_y}{\partial y}, \quad 2\kappa_{xy} = -\left(\frac{\partial \psi_x}{\partial y} + \frac{\partial \psi_y}{\partial x} \right) \quad (2-94)$$

$$\left. \begin{aligned} \frac{\partial M_x}{\partial x} + \frac{\partial M_{xy}}{\partial y} - Q_x - \bar{m}_x &= 0 \\ \frac{\partial M_{xy}}{\partial x} + \frac{\partial M_y}{\partial y} - Q_y - \bar{m}_y &= 0 \\ \frac{\partial Q_x}{\partial x} + \frac{\partial Q_y}{\partial y} + \bar{q} &= 0 \end{aligned} \right\} \quad (2-95)$$

The geometrical and force boundary conditions:

$$\left. \begin{aligned} \psi_s &= \bar{\psi}_s, \quad w = \bar{w} && (\text{on } C_{1a} + C_{2a} + C_{1b} + C_{2b}) \\ \psi_n &= \bar{\psi}_n && (\text{on } C_{1a} + C_{1b}) \end{aligned} \right\} \quad (2-96)$$

$$\left. \begin{aligned} M_{ns} &= \bar{M}_{ns}, \quad Q_n = \bar{Q}_n && (\text{on } C_{3a} + C_{3b}) \\ M_n &= \bar{M}_n && (\text{on } C_{2a} + C_{3a} + C_{2b} + C_{3b}) \end{aligned} \right\} \quad (2-97)$$

The interface conditions on C_{ab} :

$$Q_n^{(a)} = -Q_n^{(b)}, \quad M_n^{(a)} = M_n^{(b)}, \quad M_{ns}^{(a)} = M_{ns}^{(b)} \quad (2-98)$$

$$w^{(a)} = w^{(b)}, \quad \psi_n^{(a)} = -\psi_n^{(b)}, \quad \psi_s^{(a)} = -\psi_s^{(b)} \quad (2-99)$$

2.4.2 The Sub-Region Three-Field Generalized Potential and Complementary Energy Principles for Thick Plate

1. The transformation relation between $\Pi_{3p}^{(a)}$ and $\Pi_{3c}^{(a)}$

The three-field generalized potential energy $\Pi_{3p}^{(a)}$ and generalized complementary energy $\Pi_{3c}^{(a)}$ of the region a (excluding the interface C_{ab}) have the following transformation relation:

$$\Pi_{3p}^{(a)} + \Pi_{3c}^{(a)} = \int_{C_{ab}} [Q_n^{(a)} w^{(a)} - M_n^{(a)} \psi_n^{(a)} - M_{ns}^{(a)} \psi_s^{(a)}] ds \quad (2-100)$$

Proof From Eqs. (2-87) and (2-90) (replace b by a in Eq. (2-90)), we have

$$\begin{aligned} \Pi_{3p}^{(a)} + \Pi_{3c}^{(a)} &= \iint_{\Omega_a} \left[-M_x \frac{\partial \psi_x}{\partial x} - M_y \frac{\partial \psi_y}{\partial y} - M_{xy} \left(\frac{\partial \psi_x}{\partial y} + \frac{\partial \psi_y}{\partial x} \right) + Q_x \left(\frac{\partial w}{\partial x} - \psi_x \right) \right. \\ &+ Q_y \left(\frac{\partial w}{\partial y} - \psi_y \right) - \left(\frac{\partial M_x}{\partial x} + \frac{\partial M_{xy}}{\partial y} - Q_x \right) \psi_x - \left(\frac{\partial M_{xy}}{\partial x} + \frac{\partial M_y}{\partial y} - Q_y \right) \psi_y \\ &\left. + \left(\frac{\partial Q_x}{\partial x} + \frac{\partial Q_y}{\partial y} \right) w \right] dx dy - \int_{C_{1a} + C_{2a} + C_{3a}} (Q_n w - M_n \psi_n - M_{ns} \psi_s) ds \end{aligned} \quad (2-101)$$

By using integration by parts, the following identical relation can be obtained:

$$\begin{aligned}
 & \iint_{\Omega_a} \left[-M_x \frac{\partial \psi_x}{\partial x} - M_y \frac{\partial \psi_y}{\partial y} - M_{xy} \left(\frac{\partial \psi_x}{\partial y} + \frac{\partial \psi_y}{\partial x} \right) + Q_x \left(\frac{\partial w}{\partial x} - \psi_x \right) + Q_y \left(\frac{\partial w}{\partial y} - \psi_y \right) \right] dx dy \\
 &= \iint_{\Omega_a} \left[\left(\frac{\partial M_x}{\partial x} + \frac{\partial M_{xy}}{\partial y} - Q_x \right) \psi_x + \left(\frac{\partial M_{xy}}{\partial x} + \frac{\partial M_y}{\partial y} - Q_y \right) \psi_y - \left(\frac{\partial Q_x}{\partial x} + \frac{\partial Q_y}{\partial y} \right) w \right] dx dy \\
 &+ \int_{C_{1a}+C_{2a}+C_{3a}+C_{ab}} (Q_n w - M_n \psi_n - M_{ns} \psi_s) ds
 \end{aligned} \tag{2-102}$$

Substitution of Eq. (2-102) into Eq. (2-101) yields Eq. (2-100). \square

If the whole domain is not divided into sub-regions, C_{ab} will no longer exist, so we have

$$\Pi_{3p}^{(a)} + \Pi_{3c}^{(a)} = 0 \tag{2-103}$$

2. The sub-region three-field generalized potential energy principle

In the functional expression (2-86) of the sub-region three-field generalized mixed variational principle, the region a represents the generalized potential energy region, and the region b represents the generalized complementary region. Now, if the region b is changed to represent the generalized potential region, then from Eq. (2-100), we have

$$\Pi_{3c}^{(b)} = -\Pi_{3p}^{(b)} + \int_{C_{ab}} [Q_n^{(b)} w^{(b)} - M_n^{(b)} \psi_n^{(b)} - M_{ns}^{(b)} \psi_s^{(b)}] ds$$

Substitution of this equation into (2-86) yields

$$\Pi_3 = \Pi_{3p}^{(a)} + \Pi_{3p}^{(b)} + H_{pp} \tag{2-104}$$

where H_{pp} is the additional potential energy term on the interface C_{ab} :

$$H_{pp} = \int_{C_{ab}} [Q_n^{(b)} (w^{(a)} - w^{(b)}) + M_n^{(b)} (\psi_n^{(a)} + \psi_n^{(b)}) + M_{ns}^{(b)} (\psi_s^{(a)} + \psi_s^{(b)})] ds \tag{2-105a}$$

Equations (2-104) and (2-105a) are the functional expressions of the sub-region three-field generalized potential energy principle. It can be shown that the stationary conditions of this functional is equivalent to all field equations, boundary conditions and interface conditions of the thick plate with sub-regions.

Another expression of H_{pp} can also be obtained by interchanging a and b in Eq. (2-105a):

$$H_{pp} = \int_{C_{ab}} [Q_n^{(a)} (w^{(b)} - w^{(a)}) + M_n^{(a)} (\psi_n^{(a)} + \psi_n^{(b)}) + M_{ns}^{(a)} (\psi_s^{(a)} + \psi_s^{(b)})] ds \tag{2-105b}$$

If the displacement continuous conditions (2-99) on the interface C_{ab} are satisfied in advance, then from Eqs. (2-105a) and (2-105b), we can obtain

$$H_{pp} = 0 \quad (2-106)$$

3. The sub-region three-field generalized complementary energy principle

In Eq. (2-86), if the sub-region a is changed to represent the generalized complementary energy region, substitution of (2-100) into (2-86) will yield

$$\Pi_3 = -\Pi_{3c}^{(a)} - \Pi_{3c}^{(b)} + H_{cc} \quad (2-107)$$

where H_{cc} is the additional complementary energy term on the interface C_{ab} :

$$H_{cc} = \int_{C_{ab}} [(Q_n^{(a)} + Q_n^{(b)})w^{(a)} + (M_n^{(b)} - M_n^{(a)})\psi_n^{(a)} + (M_{ns}^{(b)} - M_{ns}^{(a)})\psi_s^{(a)}] ds \quad (2-108a)$$

Equations (2-107) and (2-108a) are the functional expressions of the sub-region three-field generalized complementary energy principle. Another expression of H_{cc} can also be obtained by interchanging a and b in equation (2-108a):

$$H_{cc} = \int_{C_{ab}} [(Q_n^{(a)} + Q_n^{(b)})w^{(b)} + (M_n^{(a)} - M_n^{(b)})\psi_n^{(b)} + (M_{ns}^{(a)} - M_{ns}^{(b)})\psi_s^{(b)}] ds \quad (2-108b)$$

If the traction conditions (2-98) on the interface C_{ab} are satisfied in advance, then from Eqs. (2-108), we can obtain:

$$H_{cc} = 0 \quad (2-109)$$

2.4.3 The Sub-Region Two-Field and Single-Field Variational Principle for Thick Plate

1. The sub-region two-field generalized variational principle

By using the following relations between the strain energy density, $\tilde{U}_b(\boldsymbol{\kappa})$ and $\tilde{U}_s(\boldsymbol{\gamma})$, and the strain complementary energy density, $\tilde{V}_b(\mathbf{M})$ and $\tilde{V}_s(\mathbf{Q})$:

$$\left. \begin{aligned} \tilde{V}_b(\mathbf{M}) &= M_x \kappa_x + M_y \kappa_y + 2M_{xy} \kappa_{xy} - \tilde{U}_b(\boldsymbol{\kappa}) \\ \tilde{V}_s(\mathbf{Q}) &= Q_x \gamma_x + Q_y \gamma_y - \tilde{U}_s(\boldsymbol{\gamma}) \end{aligned} \right\} \quad (2-110)$$

the strain \mathbf{E} in the three-field generalized potential energy $\Pi_{3p}^{(a)}$ and the three-field

generalized complementary energy $\Pi_{3c}^{(a)}$ of the region a (excluding the interface C_{ab}) can be eliminated. Thereby, the two-field (displacement \mathbf{d} and internal force \mathbf{S}) generalized potential energy $\Pi_{2p}^{(a)}$ and the two-field generalized complementary energy $\Pi_{2c}^{(a)}$ can be written as follows:

$$\begin{aligned}
 \Pi_{2p}^{(a)} = & \iint_{\Omega_a} \left[-M_x \frac{\partial \psi_x}{\partial x} - M_y \frac{\partial \psi_y}{\partial y} - M_{xy} \left(\frac{\partial \psi_x}{\partial y} + \frac{\partial \psi_y}{\partial x} \right) + Q_x \left(\frac{\partial w}{\partial x} - \psi_x \right) \right. \\
 & \left. + Q_y \left(\frac{\partial w}{\partial y} - \psi_y \right) - \tilde{V}_b(\mathbf{M}) - \tilde{V}_s(\mathbf{Q}) - \bar{m}_x \psi_x - \bar{m}_y \psi_y - \bar{q} w \right] dx dy \\
 & + \int_{C_{3a}} (\bar{M}_{ns} \psi_s - \bar{Q}_n w) ds + \int_{C_{1a}+C_{2a}} [(\psi_s - \bar{\psi}_s) M_{ns} - (w - \bar{w}) Q_n] ds \\
 & + \int_{C_{1a}} (\psi_n - \bar{\psi}_n) M_n ds + \int_{C_{2a}+C_{3a}} \bar{M}_n \psi_n ds \quad (2-111)
 \end{aligned}$$

$$\begin{aligned}
 \Pi_{2c}^{(a)} = & \iint_{\Omega_a} \left[\tilde{V}_b(\mathbf{M}) + \tilde{V}_s(\mathbf{Q}) - \left(\frac{\partial M_x}{\partial x} + \frac{\partial M_{xy}}{\partial y} - Q_x - \bar{m}_x \right) \psi_x \right. \\
 & \left. - \left(\frac{\partial M_{xy}}{\partial x} + \frac{\partial M_y}{\partial y} - Q_y - \bar{m}_y \right) \psi_y + \left(\frac{\partial Q_x}{\partial x} + \frac{\partial Q_y}{\partial y} + \bar{q} \right) w \right] dx dy \\
 & + \int_{C_{1a}+C_{2a}} (\bar{\psi}_s M_{ns} - \bar{w} Q_n) ds + \int_{C_{3a}} [(M_{ns} - \bar{M}_{ns}) \psi_s - (Q_n - \bar{Q}_n) w] ds \\
 & + \int_{C_{1a}} \bar{\psi}_n M_n ds + \int_{C_{2a}+C_{3a}} (M_n - \bar{M}_n) \psi_n ds \quad (2-112)
 \end{aligned}$$

From equations (2-86), (2-104) and (2-107), the functional expressions of the sub-region two-field generalized mixed energy, potential energy and complementary energy principles can be obtained:

$$\Pi_2 = \Pi_{2p}^{(a)} - \Pi_{2c}^{(b)} + H_{pc} \quad (2-113)$$

$$\Pi_2 = \Pi_{2p}^{(a)} + \Pi_{2p}^{(b)} + H_{pp} \quad (2-114)$$

$$\Pi_2 = -\Pi_{2c}^{(a)} - \Pi_{2c}^{(b)} + H_{cc} \quad (2-115)$$

where H_{pc} , H_{pp} and H_{cc} are still given by Eqs. (2-91), (2-105) and (2-108), respectively.

2. The sub-region single-field variational principle

Now we consider the case where each sub-region is a single-field region.

If the region a is a potential energy region, only the displacement \mathbf{d} will be taken as the field variable. Thus, the $\Pi_{3p}^{(a)}$ in Eq. (2-87) or the $\Pi_{2p}^{(a)}$ in Eq. (2-111) will transform to the single-field potential energy $\Pi_{1p}^{(a)}$ of the region a :

$$\begin{aligned}
 \Pi_{1p}^{(a)} = & \iint_{\Omega_a} [\tilde{U}_b(\mathbf{d}) + \tilde{U}_s(\mathbf{d}) - \bar{m}_x \psi_x - \bar{m}_y \psi_y - \bar{q}w] dx dy \\
 & + \int_{C_{1a}+C_{2a}} [(\psi_s - \bar{\psi}_s) \hat{M}_{ns} - (w - \bar{w}) \hat{Q}_n] ds + \int_{C_{3a}} (\bar{M}_{ns} \psi_s - \bar{Q}_n w) ds \\
 & + \int_{C_{1a}} (\psi_n - \bar{\psi}_n) \hat{M}_n ds + \int_{C_{2a}+C_{3a}} \bar{M}_n \psi_n ds
 \end{aligned} \tag{2-116a}$$

where \hat{Q}_n , \hat{M}_n and \hat{M}_{ns} are the boundary force variables, and can also be expressed by the functions of the displacement \mathbf{d} ; $\tilde{U}_b(\mathbf{d})$ and $\tilde{U}_s(\mathbf{d})$ are the strain energy densities expressed by the displacement \mathbf{d} :

$$\tilde{U}_b(\mathbf{d}) = \frac{D}{2} \left[\left(\frac{\partial \psi_x}{\partial x} \right)^2 + \left(\frac{\partial \psi_y}{\partial y} \right)^2 + 2\mu \frac{\partial \psi_x}{\partial x} \frac{\partial \psi_y}{\partial y} + \frac{1-\mu}{2} \left(\frac{\partial \psi_x}{\partial y} + \frac{\partial \psi_y}{\partial x} \right)^2 \right] \tag{2-117}$$

$$\tilde{U}_s(\mathbf{d}) = \frac{C}{2} \left[\left(\frac{\partial w}{\partial x} - \psi_x \right)^2 + \left(\frac{\partial w}{\partial y} - \psi_y \right)^2 \right] \tag{2-118}$$

If the displacement \mathbf{d} satisfies the geometrical boundary conditions in advance, then

$$\begin{aligned}
 \Pi_{1p}^{(a)} = & \iint_{\Omega_a} [\tilde{U}_b(\mathbf{d}) + \tilde{U}_s(\mathbf{d}) - \bar{m}_x \psi_x - \bar{m}_y \psi_y - \bar{q}w] dx dy \\
 & + \int_{C_{3a}} (\bar{M}_{ns} \psi_s - \bar{Q}_n w) ds + \int_{C_{2a}+C_{3a}} \bar{M}_n \psi_n ds
 \end{aligned} \tag{2-116b}$$

If the sub-region a is a complementary energy region, only the internal force \mathbf{S} will be taken as the field variable, and \mathbf{S} should satisfy the equilibrium differential Eq. (2-95) in advance. Thus, the $\Pi_{3c}^{(a)}$ in Eq. (2-90) or the $\Pi_{2c}^{(a)}$ in Eq. (2-112) will transform to the single-field complementary energy $\Pi_{1c}^{(a)}$:

$$\begin{aligned}
 \Pi_{1c}^{(a)} = & \iint_{\Omega_a} [\tilde{V}_b(\mathbf{M}) + \tilde{V}_s(\mathbf{Q})] dx dy + \int_{C_{1a}+C_{2a}} [(\bar{\psi}_s M_{ns} - \bar{w} Q_n)] ds \\
 & + \int_{C_{3a}} [(M_{ns} - \bar{M}_{ns}) \hat{\psi}_s - (Q_n - \bar{Q}_n) \hat{w}] ds + \int_{C_{1a}} \bar{\psi}_n M_n ds \\
 & + \int_{C_{2a}+C_{3a}} (M_n - \bar{M}_n) \hat{\psi}_n ds
 \end{aligned} \tag{2-119a}$$

where \hat{w} , $\hat{\psi}_n$ and $\hat{\psi}_s$ are the boundary displacement variables.

If \mathbf{S} satisfies the force boundary conditions in advance, then

$$\Pi_{1c}^{(a)} = \iint_{\Omega_a} [\tilde{V}_b(\mathbf{M}) + \tilde{V}_s(\mathbf{Q})] dx dy + \int_{C_{1a}+C_{2a}} [(\bar{\psi}_s M_{ns} - \bar{w} Q_n)] ds + \int_{C_{1a}} \bar{\psi}_n M_n ds \tag{2-119b}$$

From Eqs. (2-86), (2-104), (2-107), or (2-113), (2-114), (2-115), the functional expressions of the sub-region single-field mixed energy principle, potential energy principle and complementary energy principle can be obtained:

$$\Pi_1 = \Pi_{1p}^{(a)} - \Pi_{1c}^{(b)} + H_{pc} \quad (2-120)$$

$$\Pi_1 = \Pi_{1p}^{(a)} + \Pi_{1p}^{(b)} + H_{pp} \quad (2-121)$$

$$\Pi_1 = -\Pi_{1c}^{(a)} - \Pi_{1c}^{(b)} + H_{cc} \quad (2-122)$$

where H_{pc} , H_{pp} and H_{cc} are the same as those in Eq. (2-113) to Eq. (2-115).

2.4.4 The General Form of the Sub-Region Generalized Variational Principle for Thick Plate

From the above discussions, a general form of the sub-region generalized variational principle for elastic thick plate can be obtained. Let an elastic thick plate be divided into several sub-regions. Each sub-region can be arbitrarily appointed as single-field, two-field and three-field potential energy regions (such as the regions Ω_{p1} , Ω_{p2} , Ω_{p3} in Fig. 2.6) or complementary energy regions (such as the regions Ω_{c1} , Ω_{c2} , Ω_{c3} in Fig. 2.6). The interfaces between two adjacent sub-regions are of three types, C_{pc} , C_{pp} and C_{cc} : ① one side of C_{pc} is the potential energy region, while the other side is the complementary one; ② both sides of C_{pp} are potential energy regions; and ③ both sides of C_{cc} are complementary energy regions.

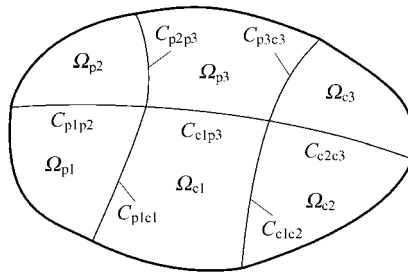


Figure 2.6 A thick plate divided into multi-regions

The general form for the functional of the sub-region variational principle can be written as

$$\Pi = \sum_{\Omega_p} \Pi_p - \sum_{\Omega_c} \Pi_c + \sum_{C_{pc}} H_{pc} + \sum_{C_{pp}} H_{pp} + \sum_{C_{cc}} H_{cc} \quad (2-123)$$

The meanings of the terms on the right-side of this equation are as follows:

The first term denotes the sum of the potential (or generalized potential) energy Π_p of each potential energy region Ω_p , where Π_p can be Π_{1p} or Π_{2p} or Π_{3p} , which is given by Eqs. (2-116), (2-111) and (2-87), respectively;

The second term denotes the sum of the complementary (or generalized complementary) energy Π_c of each complementary energy region Ω_c , where Π_c can be Π_{1c} or Π_{2c} or Π_{3c} , which is given by Eqs. (2-119), (2-112) and (2-90), respectively;

The third term denotes the sum of the additional mixed energy term H_{pc} on the interface C_{pc} , in which H_{pc} is given by Eq. (2-91);

The fourth term denotes the sum of the additional potential energy term H_{pp} on the interface C_{pp} , in which H_{pp} is given by Eq. (2-105);

The fifth term denotes the sum of the additional complementary energy term H_{cc} on the interface C_{cc} , in which H_{cc} is given by Eq. (2-108).

It can be shown that the stationary condition

$$\delta \Pi = 0 \quad (2-124)$$

of the functional Π in Eq. (2-123) is equivalent to all field equations, boundary conditions and interface conditions of the thick plate system with multi-regions.

If all the sub-regions are potential energy regions, the functional of the sub-region potential (or generalized potential) energy principle can be obtained from Eq. (2-123):

$$\Pi = \sum_{\Omega_p} \Pi_p + \sum_{C_{pp}} H_{pp} \quad (2-125)$$

Equations (2-104), (2-114) and (2-121) are all the special cases of (2-125).

If all the sub-regions are complementary energy regions, the functional of the sub-region complementary (or generalized complementary) energy principle can be obtained from Eq. (2-123):

$$\Pi = -\sum_{\Omega_c} \Pi_c + \sum_{C_{cc}} H_{cc} \quad (2-126)$$

Equations (2-107), (2-115) and (2-122) are all the special cases of (2-126).

The functional expression (2-123) of the sub-region generalized variational principle for elastic thick plate is the most general functional form of the variational principle for thick plate, and builds a bridge linking various special functional forms of the variational principle.

By using the relation (2-100), the direct transformation between the different functional forms of the variational principle for thick plate can be performed conveniently.

The sub-region mixed variational principle for thick plate and its functional expression (2-86) provide the fundamentals for the applications of the sub-region mixed finite element method in thick plate problems.

2.5 The Sub-Region Variational Principle for Elastic Shallow Shell

This section will discuss the sub-region variational principle for elastic shallow shell^[14]. The fundamental equations and the variational principles for shallow shell were systematically introduced in [3].

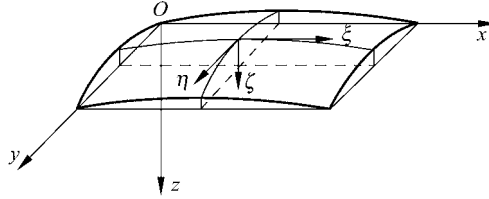


Figure 2.7 The shallow shell

Let the bottom plane of the shallow shell be the xOy plane, and the z -axis be normal to the bottom plane (Fig. 2.7). Then, the mid-surface equation of the shallow shell is

$$z = z(x, y)$$

The initial curvatures of the mid-surface are

$$\kappa_x = -\frac{\partial^2 z}{\partial x^2}, \quad \kappa_y = -\frac{\partial^2 z}{\partial y^2}, \quad \kappa_{xy} = -\frac{\partial^2 z}{\partial x \partial y}$$

And, another movable co-ordinate system (ξ, η, ζ) is also adopted where ζ -axis is the normal of the mid-surface, and ξ -axis and η -axis are the tangents of the mid-surface within xz -plane and yz -plane, respectively.

The load components along ξ , η and ζ directions of an arbitrary point within the mid-surface are p_x, p_y and p_z ; and the displacement components are u, v and w . There are three membrane internal force components N_x, N_y and N_{xy} in shallow shell structures, and their corresponding strains are $\varepsilon_x, \varepsilon_y$ and γ_{xy} . There are also three independent internal moment components M_x, M_y and M_{xy} , and their corresponding generalized strains are the curvature variety values κ_x, κ_y and κ_{xy} . Furthermore, the transverse shear forces Q_x and Q_y , are dependent internal force components, and can be determined by M_x, M_y and M_{xy} . In thin shells, the transverse shear strain γ_{xz} and γ_{yz} are both zero.

On the boundary line C of the shallow shell, let n and s be the outer normal and the tangent directions. The displacement components along n, s and ζ directions of an arbitrary point on the boundary line are u_n, v_s and w , and the corresponding boundary forces are normal tension N_n , tangent shear force N_{ns} , and equivalent transverse shear force $V_n = Q_n + \frac{\partial M_{ns}}{\partial s}$ which is synthesized by

the transverse shear force Q_n and the twisting moment M_{ns} . The rotation on the boundary within $n\zeta$ plane is $\psi_n = \frac{\partial w}{\partial n}$, and the corresponding boundary moment is the normal bending moment M_n .

The boundary line C of the shallow shell contains different line segments:

$$C = C_{u_n} + C_{N_n} = C_{v_s} + C_{N_{ns}} = C_w + C_{V_n} = C_{\psi_n} + C_{M_n}$$

where $C_{u_n}, C_{N_n}, C_{v_s}, C_{N_{ns}}, C_w, C_{V_n}, C_{\psi_n}$ and C_{M_n} denote the boundary segments on which $u_n, N_n, v_s, N_{ns}, w, V_n, \psi_n$ and M_n are specified, respectively.

A denotes the corner point on the boundary line, and is generally composed of two types:

$$A = A_w + A_R$$

where A_w and A_R are the corner points where the deflection \bar{w} and transverse concentrated force \bar{R} are specified, respectively. The twisting moment increment of the two sides of corner point A is $(\Delta M_{ns})_A$.

In the sub-region generalized variational principle for shallow shell, the mid and the bottom surfaces of the shallow shell are divided into several sub-regions. Each sub-region can be arbitrarily appointed as single-field, two-field and three-field potential energy regions (such as Ω_{p1}, Ω_{p2} and Ω_{p3} in Fig. 2.8), or the complementary energy regions (such as Ω_{c1}, Ω_{c2} and Ω_{c3} in Fig. 2.8). The interfaces between two adjacent sub-regions are of three types, C_{pc}, C_{pp} and C_{cc} (Fig. 2.8): ① one side of C_{pc} is the potential energy region, while the other side is the complementary one; ② both sides of C_{pp} are potential energy regions; and ③ both sides of C_{cc} are complementary energy regions. The node J of the adjacent sub-regions generally is also classified into two types, J_w and J_R : J_w and J_R are the nodes where the displacement \bar{w} and the transverse concentrated force \bar{R} are specified, respectively. r_p and r_c denote the numbers of the elements e_p in the potential energy regions and the elements e_c in the complementary energy regions around the node J , respectively.

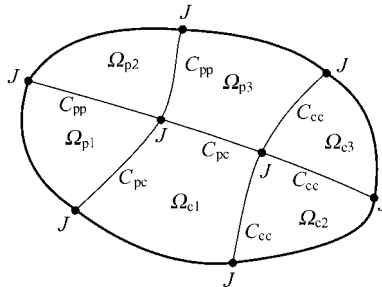


Figure 2.8 A shallow shell divided into multi-regions

The functional of the sub-region generalized variational principle for elastic shallow shell can be written as:

$$\Pi = \sum_{\Omega_p} \Pi_p - \sum_{\Omega_c} \Pi_c + \sum_{C_{pc}} H_{pc} + \sum_{C_{pp}} H_{pp} + \sum_{C_{cc}} H_{cc} + \sum_{J_w} G_w + \sum_{J_R} G_R \quad (2-127)$$

There are seven terms on the right side of the above equation, where the first two terms are the energy of all the sub-regions; the middle three terms are the energy on the interfaces; and the last two terms are the energy at the nodes. Now, the expressions and their meanings of all the terms are given as follows.

The first term on the right side of Eq. (2-127) denotes the sum of the potential (or generalized potential) energy Π_p of each potential energy region Ω_p ; the second term denotes the sum of the complementary (or generalized complementary) energy Π_c of each complementary energy region Ω_c . If the sub-region e is a three-field region, then, Π_p and Π_c are the following $\Pi_{3p}^{(e)}$ and $\Pi_{3c}^{(e)}$, respectively.

$$\Pi_{3p}^{(e)} = \Pi_{3p}^{(e)} + \Pi_{3p}^{n(e)} + I^{(e)} \quad (2-128)$$

$$\Pi_{3c}^{(e)} = \Pi_{3c}^{(e)} + \Pi_{3c}^{n(e)} - I^{(e)} \quad (2-129)$$

where

$$\begin{aligned} \Pi_{3p}^{(e)} = & \iint_{\Omega_e} \left[\tilde{U}'(\boldsymbol{\varepsilon}) - p_x u - p_y v - \left(\varepsilon_x - \frac{\partial u}{\partial x} \right) N_x - \left(\varepsilon_y - \frac{\partial v}{\partial y} \right) N_y \right. \\ & \left. - \left(\gamma_{xy} - \frac{\partial u}{\partial y} - \frac{\partial v}{\partial x} \right) N_{xy} \right] dx dy \\ & - \int_{C_{N_n^e}} \bar{N}_n u_n ds - \int_{C_{N_s^e}} \bar{N}_s v_s ds - \int_{C_{u_n^e}} (u_n - \bar{u}_n) N_n ds \\ & - \int_{C_{v_s^e}} (v_s - \bar{v}_s) N_{ns} ds \end{aligned} \quad (2-130)$$

$$\begin{aligned} \Pi_{3p}^{n(e)} = & \iint_{\Omega_e} \left[\tilde{U}''(\boldsymbol{\kappa}) - p_z w - \left(\kappa_x + \frac{\partial^2 w}{\partial x^2} \right) M_x - \left(\kappa_y + \frac{\partial^2 w}{\partial y^2} \right) M_y \right. \\ & \left. - 2 \left(\kappa_{xy} + \frac{\partial^2 w}{\partial x \partial y} \right) M_{xy} \right] dx dy \\ & - \int_{C_{V_n^e}} \bar{V}_n w ds + \int_{C_{M_n^e}} \bar{M}_n \frac{\partial w}{\partial n} ds - \sum_{A_{R^e}} \bar{R} w - \int_{C_{w^e}} (w - \bar{w}) V_n ds \\ & + \int_{C_{w_n^e}} \left(\frac{\partial w}{\partial n} - \bar{\psi}_n \right) M_n ds - \sum_{A_{w^e}} (w - \bar{w}) \Delta M_{ns} \end{aligned} \quad (2-131)$$

$$I^e = \iint_{\Omega_e} (\kappa_x N_x + \kappa_y N_y + 2\kappa_{xy} N_{xy}) w dx dy \quad (2-132)$$

$$\begin{aligned}
 \Pi_{3c}^{(e)} = & \iint_{\Omega_e} \left[-\tilde{U}'(\boldsymbol{\varepsilon}) + \varepsilon_x N_x + \varepsilon_y N_y + \gamma_{xy} N_{xy} + \left(\frac{\partial N_x}{\partial x} + \frac{\partial N_{xy}}{\partial y} + p_x \right) u \right. \\
 & \left. + \left(\frac{\partial N_{xy}}{\partial x} + \frac{\partial N_y}{\partial y} + p_y \right) v \right] dx dy - \int_{C_{N_n^e}} (N_n - \bar{N}_n) u_n ds \\
 & - \int_{C_{N_{ns}^e}} (N_{ns} - \bar{N}_{ns}) v_s ds - \int_{C_{u_n^e}} \bar{u}_n N_n ds - \int_{C_{v_s^e}} \bar{v}_s N_{ns} ds
 \end{aligned} \quad (2-133)$$

$$\begin{aligned}
 \Pi_{3c}^{(e)} = & \iint_{\Omega_e} \left[-\tilde{U}''(\boldsymbol{\kappa}) + \kappa_x M_x + \kappa_y M_y + 2\kappa_{xy} M_{xy} \right. \\
 & \left. + \left(\frac{\partial^2 M_x}{\partial x^2} + \frac{\partial^2 M_y}{\partial y^2} + 2 \frac{\partial^2 M_{xy}}{\partial x \partial y} + p_z \right) w \right] dx dy \\
 & - \int_{C_{V_n^e}} (V_n - \bar{V}_n) w ds + \int_{C_{M_n^e}} (M_n - \bar{M}_n) \frac{\partial w}{\partial n} ds - \sum_{A_{R^e}} (\Delta M_{ns} - \bar{R}) w \\
 & - \int_{C_{w^e}} \bar{w} V_n ds + \int_{C_{\varphi_n^e}} \bar{\varphi}_n M_n ds - \sum_{A_{w^e}} \bar{w} \Delta M_{ns}
 \end{aligned} \quad (2-134)$$

where $\tilde{U}'(\boldsymbol{\varepsilon})$ and $\tilde{U}''(\boldsymbol{\kappa})$ are the strain energy density of the in-plane action and the thin plate bending, respectively:

$$\tilde{U}'(\boldsymbol{\varepsilon}) = \frac{Eh}{2(1-\mu^2)} \left(\varepsilon_x^2 + \varepsilon_y^2 + 2\mu\varepsilon_x\varepsilon_y + \frac{1-\mu}{2}\gamma_{xy}^2 \right) \quad (2-135)$$

$$\tilde{U}''(\boldsymbol{\kappa}) = \frac{Eh^3}{24(1-\mu^2)} (\kappa_x^2 + \kappa_y^2 + 2\mu\kappa_x\kappa_y + 2(1-\mu)\kappa_{xy}^2) \quad (2-136)$$

E and μ are the Young's modulus and Poisson's ratio, respectively; h is the thickness of the thin shell.

If the sub-region e is a two-field region, then, Π_p and Π_c are the following Π_{2p} and Π_{2c} , respectively:

$$\Pi_{2p}^{(e)} = \Pi_{2p}^{(e)} + \Pi_{2p}^{(e)} + I^{(e)} \quad (2-137)$$

$$\Pi_{2c}^{(e)} = \Pi_{2c}^{(e)} + \Pi_{2c}^{(e)} - I^{(e)} \quad (2-138)$$

where

$$\begin{aligned}
 \Pi_{2p}^{(e)} = & \iint_{\Omega_e} \left[-\tilde{V}'(N) - p_x u - p_y v + N_x \frac{\partial u}{\partial x} + N_y \frac{\partial v}{\partial y} + N_{xy} \left(\frac{\partial u}{\partial y} + \frac{\partial v}{\partial x} \right) \right] dx dy \\
 & - \int_{C_{N_n^e}} \bar{N}_n u_n ds - \int_{C_{N_{ns}^e}} \bar{N}_{ns} v_s ds - \int_{C_{u_n^e}} (u_n - \bar{u}_n) N_n ds - \int_{C_{v_s^e}} (v_s - \bar{v}_s) N_{ns} ds
 \end{aligned} \quad (2-139)$$

$$\begin{aligned}
 \Pi_{2p}^{n(e)} = & \iint_{\Omega_e} \left[-\tilde{V}''(\mathbf{M}) - p_z w - M_x \frac{\partial^2 w}{\partial x^2} - M_y \frac{\partial^2 w}{\partial y^2} - 2M_{xy} \frac{\partial^2 w}{\partial x \partial y} \right] dx dy \\
 & - \int_{C_{\psi_n^e}} \bar{V}_n w ds + \int_{C_{M_n^e}} \bar{M}_n \frac{\partial w}{\partial n} ds - \sum_{A_{R^e}} \bar{R} w - \int_{C_{v_s^e}} (w - \bar{w}) V_n ds \\
 & + \int_{C_{\psi_n^e}} \left(\frac{\partial w}{\partial n} - \bar{\psi}_n \right) M_n ds - \sum_{A_{w^e}} (w - \bar{w}) \Delta M_{ns} \quad (2-140)
 \end{aligned}$$

$$\begin{aligned}
 \Pi_{2c}^{(e)} = & \iint_{\Omega_e} \left[\tilde{V}'(\mathbf{N}) + \left(\frac{\partial N_x}{\partial x} + \frac{\partial N_{xy}}{\partial y} + p_x \right) u + \left(\frac{\partial N_{xy}}{\partial x} + \frac{\partial N_y}{\partial y} + p_y \right) v \right] dx dy \\
 & - \int_{C_{N_n^e}} (N_n - \bar{N}_n) u_n ds - \int_{C_{N_{ns}^e}} (N_{ns} - \bar{N}_{ns}) v_s ds - \int_{C_{\bar{u}_n^e}} \bar{u}_n N_n ds - \int_{C_{\bar{v}_s^e}} \bar{v}_s N_{ns} ds \quad (2-141)
 \end{aligned}$$

$$\begin{aligned}
 \Pi_{2c}^{n(e)} = & \iint_{\Omega_e} \left[\tilde{V}''(\mathbf{M}) + \left(\frac{\partial^2 M_x}{\partial x^2} + \frac{\partial^2 M_y}{\partial y^2} + 2 \frac{\partial^2 M_{xy}}{\partial x \partial y} + p_z \right) w \right] dx dy \\
 & - \int_{C_{V_n^e}} (V_n - \bar{V}_n) w ds + \int_{C_{M_n^e}} (M_n - \bar{M}_n) \frac{\partial w}{\partial n} ds - \sum_{A_{R^e}} (\Delta M_{ns} - \bar{R}) w \\
 & - \int_{C_{w^e}} \bar{w} V_n ds + \int_{C_{\psi_n^e}} \bar{\psi}_n M_n ds - \sum_{A_{w^e}} \bar{w} \Delta M_{ns} \quad (2-142)
 \end{aligned}$$

$I^{(e)}$ is still given by Eq. (2-132); $\tilde{V}'(\mathbf{N})$ and $\tilde{V}''(\mathbf{M})$ are the strain complementary energy density of the in-plane action and the thin plate bending, respectively:

$$\tilde{V}'(\mathbf{N}) = \frac{1}{2} \cdot \frac{1}{Eh} [N_x^2 + N_y^2 - 2\mu N_x N_y + 2(1 + \mu) N_{xy}^2] \quad (2-143)$$

$$\tilde{V}''(\mathbf{M}) = \frac{1}{2} \cdot \frac{12}{Eh^3} [M_x^2 + M_y^2 - 2\mu M_x M_y + 2(1 + \mu) M_{xy}^2] \quad (2-144)$$

If the sub-region e is a single-field region, then, Π_p and Π_c are the following Π_{1p} and Π_{1c} , respectively:

$$\Pi_{1p}^{(e)} = \Pi_{1p}^{(e)} + \Pi_{1p}^{n(e)} \quad (2-145)$$

where

$$\begin{aligned}
 \Pi_{1p}^{(e)} = & \iint_{\Omega_e} [\tilde{U}'(u, v, w) - p_x u - p_y v] dx dy - \int_{C_{N_n^e}} \bar{N}_n u_n ds - \int_{C_{N_{ns}^e}} \bar{N}_{ns} v_s ds \\
 & - \int_{C_{u_n^e}} (u_n - \bar{u}_n) N_n ds - \int_{C_{v_s^e}} (v_s - \bar{v}_s) N_{ns} ds \quad (2-146)
 \end{aligned}$$

$$\begin{aligned} \Pi_{1p}^{n(e)} = & \iint_{\Omega_e} [\tilde{U}''(w) - p_z w] dx dy - \int_{C_{v_n^e}} \bar{V}_n w ds + \int_{C_{M_n^e}} \bar{M}_n \frac{\partial w}{\partial n} ds - \sum_{A_{R^e}} \bar{R} w \\ & - \int_{C_{w^e}} (w - \bar{w}) V_n ds + \int_{C_{\psi_n^e}} \left(\frac{\partial w}{\partial n} - \bar{\psi}_n \right) M_n ds - \sum_{A_{w^e}} (w - \bar{w}) \Delta M_{ns} \end{aligned} \quad (2-147)$$

in which only a single field, i.e. displacement field (u, v, w), exists within the sub-region e ; and N_n, N_{ns}, V_n, M_n and ΔM_{ns} are only the boundary variables or corner point variables defined on the element boundaries and corner points. $\tilde{U}'(u, v, w)$ and $\tilde{U}''(w)$ are the strain energy densities, expressed by the displacement, of the in-plane strain and thin plate bending, respectively.

$$\Pi_{1c}^e = \Pi_{1c}^{Ie} + \Pi_{1c}^{ne} \quad (2-148)$$

where

$$\begin{aligned} \Pi_{1c}^{Ie} = & \int_{\Omega_e} \tilde{V}'(N) dx dy - \int_{C_{N_n^e}} (N_n - \bar{N}_n) u_n ds - \int_{C_{N_{ns}^e}} (N_{ns} - \bar{N}_{ns}) v_s ds \\ & - \int_{C_{\bar{u}_n^e}} \bar{u}_n N_n ds - \int_{C_{\bar{v}_s^e}} \bar{v}_s N_{ns} ds \end{aligned} \quad (2-149)$$

$$\begin{aligned} \Pi_{1c}^{ne} = & \iint_{\Omega_e} \tilde{V}''(M) dx dy - \int_{C_{V_n^e}} (V_n - \bar{V}_n) w ds + \int_{C_{M_n^e}} (M_n - \bar{M}_n) \frac{\partial w}{\partial n} ds \\ & - \sum_{A_{R^e}} (\Delta M_{ns} - \bar{R}) w - \int_{C_{w^e}} \bar{w} V_n ds + \int_{C_{\psi_n^e}} \bar{\psi}_n M_n ds - \sum_{A_{w^e}} \bar{w} \Delta M_{ns} \end{aligned} \quad (2-150)$$

Here, only a single-field, i.e. internal force field ($N_x, N_y, N_{xy}, M_x, M_y, M_{xy}$), exists within the sub-region e , and these internal forces in advance satisfy the equilibrium differential equation of the shallow shell:

$$\left. \begin{aligned} \frac{\partial N_x}{\partial x} + \frac{\partial N_{xy}}{\partial y} + p_x &= 0 \\ \frac{\partial N_{xy}}{\partial x} + \frac{\partial N_y}{\partial y} + p_y &= 0 \\ \frac{\partial^2 M_x}{\partial x^2} + \frac{\partial^2 M_y}{\partial y^2} + 2 \frac{\partial^2 M_{xy}}{\partial x \partial y} - k_x N_x - k_y N_y - 2k_{xy} N_{xy} + p_z &= 0 \end{aligned} \right\} \quad (2-151)$$

u_n, v_s, w and $\frac{\partial w}{\partial n}$ are only the boundary or corner point variables defined on the element boundaries or corner points.

The third, fourth and fifth terms on the right side of Eq. (2-127) are the sum of the additional energy H_{pc}, H_{pp} and H_{cc} on the interfaces C_{pc}, C_{pp} and C_{cc} between the adjacent sub-regions e and e' , respectively, where

$$H_{pc} = \int_{C_{e'}} \left[-N_n^{e'} u_n^e - N_{ns}^{e'} v_s^e + M_n^{e'} \left(\frac{\partial w}{\partial n} \right)^e + V_n^{e'} w^e \right] ds \quad (2-152)$$

(e is the potential energy region; e' is the complementary energy region)

$$\begin{aligned} H_{pp} &= \int_{C_{e'}} \left[-N_n^{e'} (u_n^e + u_n^{e'}) - N_{ns}^{e'} (v_s^e + v_s^{e'}) + M_n^{e'} \left(\left(\frac{\partial w}{\partial n} \right)^e + \left(\frac{\partial w}{\partial n} \right)^{e'} \right) + V_n^{e'} (w^e - w^{e'}) \right] ds \\ &= \int_{C_{e'}} \left[-N_n^e (u_n^e + u_n^{e'}) - N_{ns}^e (v_s^e + v_s^{e'}) + M_n^e \left(\left(\frac{\partial w}{\partial n} \right)^e + \left(\frac{\partial w}{\partial n} \right)^{e'} \right) + V_n^e (w^{e'} - w^e) \right] ds \end{aligned} \quad (2-153)$$

$$\begin{aligned} H_{cc} &= \int_{C_{e'}} \left[(N_n^e - N_n^{e'}) u_n^e + (N_{ns}^e - N_{ns}^{e'}) v_s^e - (M_n^e - M_n^{e'}) \left(\frac{\partial w}{\partial n} \right)^e + (V_n^e + V_n^{e'}) w^e \right] ds \\ &= \int_{C_{e'}} \left[(N_n^{e'} - N_n^e) u_n^{e'} + (N_{ns}^{e'} - N_{ns}^e) v_s^{e'} - (M_n^{e'} - M_n^e) \left(\frac{\partial w}{\partial n} \right)^{e'} + (V_n^{e'} + V_n^e) w^{e'} \right] ds \end{aligned} \quad (2-154)$$

The last two terms on the right side of Eq. (2-127) are the sum of additional energy G_w and G_R at the nodes J_w and J_R , respectively, where

$$G_w = - \sum_{e_p} (\Delta M_{ns})^{(e_p)} (w^{(e_p)} - \bar{w}) + \sum_{e_c} (\Delta M_{ns})^{(e_c)} \bar{w} \quad (2-155)$$

$$G_R = \left[\sum_e (\Delta M_{ns})^{(e)} - \bar{R} \right] w^{(a)} - \sum_{e_p} (\Delta M_{ns})^{(e_p)} w^{(e_p)} \quad (2-156)$$

where \sum_{e_p} , \sum_{e_c} and \sum_e denote the sum of all the potential energy elements e_p , all the complementary energy elements e_c and all the elements e around the nodes, respectively; $w^{(a)}$ is the displacement of any element a around the nodes.

It can be shown that the stationary condition

$$\delta II = 0 \quad (2-157)$$

of the functional II in Eq. (2-127) is equivalent to all field equations, boundary conditions, interface conditions, corner point and node conditions of the shallow shell system with multi-regions.

As a special case, if each sub-region is appointed as a potential energy region (or complementary energy region), then, the functional of the sub-region generalized potential (or complementary) energy principle can be obtained from Eq. (2-127).

2.6 The Sub-Region Mixed Energy Partial Derivative Theorem

This section will discuss the sub-region mixed energy partial derivative theorem and its extensions^[15].

Castigliano first and second theorems are two famous energy partial derivative theorems in history, and both of them are the special cases of the sub-region mixed energy partial derivative theorem.

2.6.1 The Sub-Region Mixed Energy Partial Derivative Theorem and Its Proof

1. The definition of the sub-region mixed energy

Let a structure be divided into two regions: complementary energy region (region a) and potential energy region (region b). The complementary energy region has n_1 independent force variables X_1, X_2, \dots, X_{n_1} , and its complementary energy $(\Pi_c)_a$ is expressed as a function of these force variables. The potential energy region has n_2 displacements at the supports (or constrained displacements) $\Delta_{n_1+1}, \Delta_{n_1+2}, \dots, \Delta_{n_1+n_2}$ as independent displacement variables, and its potential energy $(\Pi_p)_b$ is expressed as a function of these displacement variables. Furthermore, the additional energy Π_J at the interface J between the regions a and b equals to the work done by the constrained force $(\hat{F}_J)_a$ of the region a along the displacement $(\hat{D}_J)_b$ of the region b :

$$\Pi_J = \sum_J (\hat{F}_J)_a (\hat{D}_J)_b$$

The sub-region mixed energy Π_m is defined as:

$$\Pi_m = (\Pi_p)_b - (\Pi_c)_a + \Pi_J = (\Pi_p)_b - (\Pi_c)_a + \sum_J (\hat{F}_J)_a (\hat{D}_J)_b \quad (2-158)$$

As an example, consider a frame shown in Fig. 2.9(a). The left side of the interface J is the complementary energy region (region a), and the right side is the potential energy region (region b). There is force variable X_1 operating in the region a . Let $(M)_a$ be the bending moment of the region a , then the complementary energy $(\Pi_c)_a$ of the region a is

$$(\Pi_c)_a = \sum_a \int \frac{1}{2EI} (M)_a^2 ds \quad (2-159)$$

There is a displacement variable Δ_2 (the nodal rotation) in the region b .

Furthermore, the structure is also under a constant load P . Let $(M)_b$ be the bending moment of the region b , D be the corresponding displacement of load P , then the potential energy $(\Pi_p)_b$ of the region b is

$$(\Pi_p)_b = \sum_b \int \frac{1}{2EI} (M)_b^2 ds - \sum_b (PD)_b \quad (2-160)$$

At the interface J , the displacement $(\hat{D}_J)_b$ of the region b is the nodal rotation Δ_2 , the constrained force $(\hat{F}_J)_a$ of the region a is the bending moment $(M_J)_a$ of cross section J . The additional energy Π_J on the interface is

$$\Pi_J = (\hat{F}_J)_a (\hat{D}_J)_b = (M_J)_a \Delta_2 \quad (2-161)$$

Substitution of Eqs. (2-159), (2-160) and (2-161) into (2-158) yields

$$\Pi_m = \sum_b \int \frac{1}{2EI} (M)_b^2 ds - \sum_b (PD)_b - \sum_a \int \frac{1}{2EI} (M)_a^2 ds + (M_J)_a \Delta_2 \quad (2-162)$$

2. The description of the sub-region mixed energy partial derivative theorem

If the sub-region mixed energy Π_m of the structure is defined by Eq. (2-158), the partial derivative of Π_m with respect to force variable X_i of the complementary energy region will be equal to a minus value of the displacement D_i which corresponds to X_i , and the partial derivative of Π_m with respect to displacement variable Δ_j of the potential energy region will be equal to the constrained force F_j which corresponds to Δ_j , i.e.,

$$\left. \begin{aligned} D_i &= -\frac{\partial \Pi_m}{\partial X_i} & (i = 1, 2, \dots, n_1) \\ F_j &= \frac{\partial \Pi_m}{\partial \Delta_j} & (j = n_1 + 1, n_1 + 2, \dots, n_1 + n_2) \end{aligned} \right\} \quad (2-163)$$

3. The proof for the sub-region mixed energy partial derivative theorem

Consider the frame shown in Fig. 2.9(a), the partial derivative formulae (2-163) can be rewritten as

$$D_1 = -\frac{\partial \Pi_m}{\partial X_1}, \quad F_2 = \frac{\partial \Pi_m}{\partial \Delta_2} \quad (2-164)$$

These two expressions can be derived by the virtual force equation and the virtual displacement equation, respectively.

Firstly, we will deduce the first expression of Eq. (2-164). As shown in Fig. 2.9(b), in order to solve the displacement D_1 , a virtual force system is established: a virtual force increment δX_1 is assumed at point A, then the bending

moment increment of the region a is $(\delta M)_a = \frac{\partial(M)_a}{\partial X_1} \delta X_1$, and the constrained moment increment at interface J is $(\delta M_J)_a = \frac{\partial(M_J)_a}{\partial X_1} \delta X_1$. Let the virtual force system of the region a in Fig. 2.9(b) do virtual work on the deformation state in Fig. 2.9(a), the virtual force equation is

$$(\delta X_1)D_1 + (\delta M_J)_a \Delta_2 = \sum_a \int (\delta M)_a \frac{(M)_a}{EI} ds \quad (2-165)$$

Then we have

$$D_1 = \sum_a \int \frac{1}{EI} (M)_a \frac{\partial(M)_a}{\partial X_1} ds - \frac{\partial(M_J)_a}{\partial X_1} \Delta_2 \quad (2-166)$$

By using Eq. (2-162), the above equation can be rewritten as

$$D_1 = -\frac{\partial \Pi_m}{\partial X_1}$$

Thereby, the first expression of Eq. (2-164) has been derived.

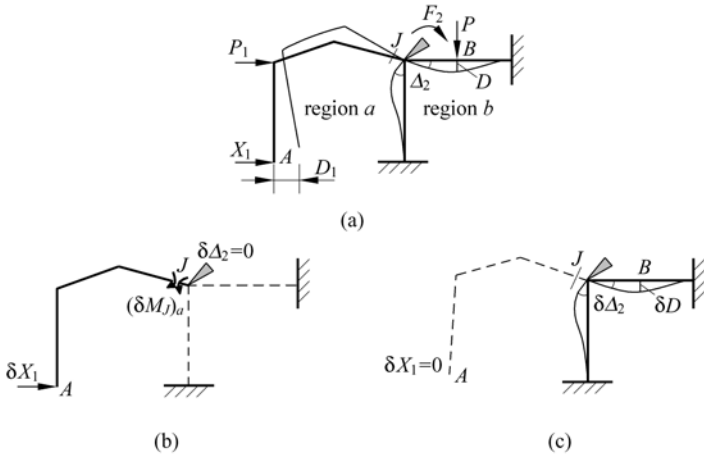


Figure 2.9 A frame divided into two regions

Secondly, we will deduce the second expression of Eq. (2-164). As shown in Fig. 2.9(c), in order to solve the constrained moment F_2 , a virtual displacement system is established: a virtual displacement increment $\delta \Delta_2$ is assumed at point J , then the displacement increment at the point B where the load P acts is $\delta D = \frac{\partial D}{\partial \Delta_2} \delta \Delta_2$, the moment increment of the region b is $(\delta M)_b = \frac{\partial(M)_b}{\partial \Delta_2} \delta \Delta_2$. Let

the force system of the region b (including the interface J) in Fig. 2.9(a) do the virtual work on the virtual displacements of the region b in Fig. 2.9(c), the virtual displacement equation is

$$[F_2 - (M_J)_a] \delta \Delta_2 + \sum_b (P \delta D)_b = \sum_b \int (M)_b \frac{(\delta M)_b}{EI} ds \quad (2-167)$$

Then we have

$$F_2 = \sum_b \int \frac{1}{EI} (M)_b \frac{\partial (M)_b}{\partial \Delta_2} ds - \sum_b P \frac{\partial (D)_b}{\partial \Delta_2} + (M_J)_a \quad (2-168)$$

By using Eq. (2-162), the above equation can be rewritten as

$$F_2 = \frac{\partial \Pi_m}{\partial \Delta_2}$$

Thereby, the second expression of Eq. (2-164) has also been derived.

2.6.2 Three Deductions of the Sub-Region Mixed Energy Partial Derivative Theorem

1. The sub-region mixed energy stationary principle

Let us analyze the frame plotted in Fig. 2.10 by using the sub-region mixed energy method. Node J is the interface, and the region on the left side of the node J is the complementary energy region. Then, according to the force method, the reaction force X_1 along the horizontal bar at point A is taken as the fundamental unknown variable. The region on the right side of the node J is the potential energy region. Then, according to the displacement method, the angular displacement Δ_2 at the node J is taken as the fundamental unknown variable.

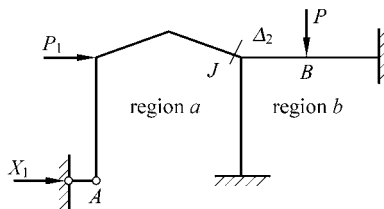


Figure 2.10 A frame

The fundamental system is shown in Fig. 2.9(a): in region a , the horizontal bar at point A is eliminated and replaced by the force variable X_1 ; and in region b , an additional constraint is added at the node J , and the node rotation is made as the

displacement variable Δ_2 . The sub-region mixed energy Π_m of the fundamental system is given by Eq. (2-162), and the displacement D_1 corresponding to X_1 and the constrained moment F_2 corresponding to Δ_2 are given by Eq. (2-164).

The original structure in Fig. 2.10 should satisfy the following fundamental equation

$$D_1 = 0, \quad F_2 = 0 \tag{2-169}$$

Substitution of the above equation into Eq. (2-164) yields

$$\frac{\partial \Pi_m}{\partial X_1} = 0, \quad \frac{\partial \Pi_m}{\partial \Delta_2} = 0 \tag{2-170}$$

The above equation is the stationary conditions of the sub-region mixed energy Π_m . Thereby, the sub-region mixed energy stationary principle can be derived from the sub-region mixed energy partial derivative theorem. Furthermore, the sub-region potential energy principle and the sub-region complementary energy principle are the special cases of the sub-region mixed energy principle.

2. The potential energy partial derivative theorem and related approach, principle and theorem

If the whole structure is looked upon as the potential energy region and no complementary energy region existing, the sub-region mixed energy Π_m will degenerate to the potential energy Π_p of the whole region, and the sub-region mixed energy partial derivative formulae (2-163) will degenerate to the potential energy partial derivative formulae:

$$F_i = \frac{\partial \Pi_p}{\partial \Delta_i} \quad (i = 1, 2, \dots, n) \tag{2-171}$$

This is the mathematical expression of the potential energy partial derivative theorem. And, the theorem can be stated as follows: A structure has n support displacements $\Delta_i (i = 1, 2, \dots, n)$ treated as the independent displacement variables, other support displacements and loads are all specified by the given values, and the potential energy Π_p of the structure is expressed as a function of $\Delta_1, \Delta_2, \dots, \Delta_n$, then the partial derivative of the potential energy Π_p with respect to the displacement variable Δ_i will be equal to the constrained force F_i corresponding to Δ_i .

There are some other deductions which can also be obtained from the potential energy partial derivative theorem.

(1) Both the potential energy partial derivative theorem and the unit support displacement method are the approaches for solving the support reaction force F_i , and they have a close relation. Their differences are as follows: the unit support displacement method possesses a broader application range, and does not involve

physical conditions; the application range of the potential energy partial derivative theorem is relatively narrow, only suitable for elastic structures, but its formulae are quite simple and convenient.

(2) If the constrained force F_i corresponding to the displacement variable Δ_i does not exist, equation (2-171) will degenerate to:

$$\frac{\partial \Pi_p}{\partial \Delta_i} = 0 \quad (i = 1, 2, \dots, n) \quad (2-172)$$

This is the potential energy stationary condition. So, the potential energy stationary principle can also be derived from the potential energy partial derivative theorem.

(3) If there is no other load in the structure except for the displacement variable Δ_i and its constrained force $F_i (i = 1, 2, \dots, n)$, the potential energy Π_p will be equal to the strain energy U , and Eq. (2-171) will be simplified as:

$$F_i = \frac{\partial U}{\partial \Delta_i} \quad (2-173)$$

This is the Castigliano first theorem.

3. The complementary energy partial derivative theorem and related approach, principle and theorem

If the whole structure is looked upon as the complementary energy region and no potential energy region existing, the sub-region mixed energy Π_m will degenerate to the minus value of the complementary energy of the whole region, i.e. $(-\Pi_c)$. Eq. (2-163) will degenerate to:

$$D_i = \frac{\partial \Pi_c}{\partial X_i} \quad (i = 1, 2, \dots, n) \quad (2-174)$$

This is the mathematical expression of the complementary energy partial derivative theorem. And, the theorem can be stated as follows: A structure has n independent variable loads or independent force variables $X_i (i = 1, 2, \dots, n)$, other loads and support displacements are all specified by the given values, and the complementary energy Π_c of the structure is expressed as a function of X_1, X_2, \dots, X_n , then the partial derivative of the complementary energy Π_c with respect to the displacement variable X_i will be equal to the displacement D_i corresponding to X_i .

There are some other deductions which can also be obtained from the complementary energy partial derivative theorem.

(1) Both the complementary energy partial derivative theorem and the unit load method are the approaches for solving the displacement D_i , and they have a close relation. Their differences are as follows: the unit load method possesses a broader application range, and does not involve physical conditions; the application range

of the complementary energy partial derivative theorem is relatively narrow, only suitable for elastic structures, but its formulae are quite simple and convenient.

(2) If the force variables X_1, X_2, \dots, X_n are all redundant constrained forces of the statically indeterminate structure, and their corresponding displacements D_1, D_2, \dots, D_n are all zero, then Eq. (2-174) will degenerate to:

$$\frac{\partial \Pi_c}{\partial X_i} = 0 \quad (i = 1, 2, \dots, n) \quad (2-175)$$

This is the complementary energy stationary conditions. So, the complementary energy stationary principle can also be derived from the complementary energy partial derivative theorem.

(3) If the support displacements of the structure are zero, then, the complementary energy Π_c will be equal to the strain complementary energy V , and Eq. (2-174) will be simplified as

$$D_i = \frac{\partial V}{\partial X_i} \quad (i = 1, 2, \dots, n) \quad (2-176)$$

This is the Crotti-Engesser theorem.

(4) If the structure is linear elastic, and has no initial strain, then the strain complementary energy V and the strain energy U are equal to each other, and Eq. (2-176) can be written as

$$D_i = \frac{\partial U}{\partial X_i} \quad (i = 1, 2, \dots, n) \quad (2-177)$$

This is the Castigliano second theorem.

References

- [1] Washizu K (1968, 1975, 1982) Variational methods in elasticity and plasticity. 1st edn, 2nd edn, 3rd edn, Pergamon Press, Oxford
- [2] Chien WZ (1980) Calculus of variations and finite elements (Vol. I). Science Press, Beijing (in Chinese)
- [3] Hu HC (1984) Variational principles of theory of elasticity with applications. Science Press, Beijing
- [4] Finlayson BA (1972) The method of weighted residuals and variational principles. Academic Press, New York
- [5] Pian THH (1964) Derivation of element stiffness matrices by assumed stress distributions. AIAA Journal, 2: 1333 – 1335
- [6] Atluri SN, Gallagher RH, Zienkiewicz OC (1983) (eds). Hybrid and mixed finite element method. Wiley, Chichester

Chapter 2 The Sub-Region Variational Principles

- [7] Zienkiewicz OC (1983) The generalized finite element method—state of the art and future directions. *Journal of Applied Mechanics* (50th anniversary issue), 50: 1210 – 1217
- [8] Long YQ (1985) Advances in variational principles in China. In: Zhao C et al (eds). *Proceedings of the Second International Conference on Computing in Civil Engineering*. Elsevier Science Publishers, Hangzhou, pp1207 – 1215
- [9] Long YQ (1981) Piecewise generalized variational principles in elasticity. *Shanghai Mechanics*, 2(2): 1 – 9 (in Chinese)
- [10] Long YQ, Zhi BC, Yuan S (1982) Sub-region, sub-item and sub-layer generalized variational principles in elasticity. In: He GQ et al (eds). *Proceedings of international conference on FEM*. Science Press, Shanghai, pp607 – 609
- [11] Long YQ (1987) Sub-region generalized variational principles and sub-region mixed finite element method. In: Chien WZ (eds). *The advances of applied mathematics and mechanics in China*. China Academic Publishers, Beijing, 157 – 179
- [12] Long YQ (1987) Sub-region generalized variational principles in elastic thin plates. In: Yeh KY eds. *Progress in Applied Mechanics*. Martinus Nijhoff Publishers, Dordrecht, Netherlands, pp121 – 134
- [13] Long YQ (1983) Sub-region generalized variational principles for elastic thick plates. *Applied Mathematics and Mechanics (English Edition)* 4(2): 175 – 184
- [14] Long YQ, Long ZF, Xu Y (1996) Sub-region generalized variational principles in shallow shells and applications. In: Zhong WX, Cheng GD and Li XK (eds). *The Advances in computational mechanics*. International Academic Publishers, Beijing, pp69 – 77
- [15] Long YQ (1995) Sub-region mixed energy partial derivative theorem. In: Long YQ (ed). *Proceedings of the Fourth National Conference on Structural Engineering*. Quanzhou, pp188 – 194 (in Chinese)
- [16] Prager W (1968) Variational principles of elastic plates with relaxed continuity requirements. *International Journal of Solids and Structures* 4(9): 837 – 844

Chapter 3 Variational Principles with Several Adjustable Parameters

Yu-Qiu Long

Department of Civil Engineering, School of Civil Engineering,
Tsinghua University, Beijing, 100084, China

Song Cen

Department of Engineering Mechanics, School of Aerospace,
Tsinghua University, Beijing, 100084, China

Zhi-Fei Long

School of Mechanics & Civil Engineering, China University of
Mining & Technology, Beijing, 100083, China

Abstract This chapter also focuses on the development of the variational principles. Firstly, it introduces three patterns of functional transformation, i.e., pattern I, pattern II and pattern III. Then, on the basis of pattern III, some variational principles with several adjustable parameters are formulated. Finally, a variable-substitution-multiplier method is also proposed based on pattern I and pattern II^[1,2].

Keywords variational principle, functional transformation, adjustable parameters, variable-substitution-multiplier method.

3.1 Introduction

There are various forms of the variational principles in elasticity, such as the potential energy principle, the complementary energy principle, the Hellinger-Reissner principle, the Hu-Washizu principle, the sub-region variational principle or the modified variational principle, etc. In order to clarify the transformation relations among these variational principles and their energy functionals, the functional transformations of the variational principles are classified as three patterns in reference [1]:

Pattern I (relaxation pattern) is a generalized equivalent pattern in which the constraint conditions are transformed into natural conditions.

Pattern II (augmented pattern) is a generalized equivalent pattern in which the augmented conditions are transformed into natural conditions.

Pattern III (equivalent pattern) is a pattern in which a non-conditional functional is transformed into an equivalent functional with several adjustable parameters.

In the above patterns, pattern I is the well-known pattern of the Lagrange multiplier method; pattern II and pattern III are new patterns proposed in [1].

Hu-Washizu principle contains three types of functional variables (displacement, strain and stress); Hellinger-Reissner principle contains two types of functional variables (displacement and stress); potential energy principle and complementary energy principle contain a single type of functional variables (displacement or stress), but all of them do not contain adjustable parameters. On the basis of pattern III, references [1, 2] proposed the generalized variational principles with several adjustable parameters and the general and simple forms of their functionals. Many existing variational principles are their special cases.

The Lagrange multiplier method is often used in variational principles. Based on the analysis of the phenomenon of losing effectiveness for the Lagrange multiplier method, reference [3] proposed a high-order Lagrange multiplier method. Reference [2] pointed out the prerequisite for the application of the Lagrange multiplier method, discussed the root leading to the failure phenomenon, and proposed a new transformation pattern: the variable-substitution-multiplier method.

After being proposed in reference [1] in 1986, the variational principles with several adjustable parameters were also introduced in details by special Chapters in monograph [4], encyclopedia [5] and textbook [6]. These variational principles can also be applied to formulate the penalty function method^[7, 8] and other new functionals^[9, 10].

3.2 Several Patterns of Functional Transformation

3.2.1 Preparatory Knowledge

1. Classification of variables and conditions

Here, all the variables in elasticity are classified as functional variables and augmented variables; and all the conditions are classified as forced conditions which should be satisfied in advance by the functional variables, natural conditions (Euler equations and natural boundary conditions) and augmented conditions (the conditions or relations between the augmented and the functional variables, as well as that between various augmented variables). For instance, in the minimum potential energy principle, the functional is the potential energy, the

displacement \mathbf{u} is the functional variable and both strain $\boldsymbol{\varepsilon}$ and stress $\boldsymbol{\sigma}$ are regarded as the augmented variables. The displacement boundary conditions at the fixed boundary are the forced conditions which must be satisfied in advance by the functional variable \mathbf{u} . The differential equilibrium equations and the stress boundary conditions at free boundary, both expressed in terms of displacement, are the natural conditions derived from the stationary condition of potential energy, while the geometrical relations between the functional variable \mathbf{u} and the augmented variable $\boldsymbol{\varepsilon}$, as well as the stress-strain relations between the augmented variables $\boldsymbol{\varepsilon}$ and $\boldsymbol{\sigma}$, are considered as augmented conditions.

When a statement of a variational principle is to be made, three aspects have to be mentioned: ① which variables are chosen to be the functional variables; ② which of the conditions are used as the forced conditions and which of them are the augmented conditions; ③ how to define the energy functional—the natural conditions can be derived from the stationary conditions of the functional.

2. The equivalent relation between two variational principles

The equivalent relation between two variational principles has been discussed frequently in literatures, but sometimes the meaning of the word *equivalent* is not exactly the same in different contexts. In order to have a clear and definite concept, in this Chapter three different cases of the equivalent relations are defined as follows:

(1) Two variational principles are said to be generalized equivalent if both the principles have the same set of variables and the same set of conditions, but their subsets of functional or augmented variables are not the same; their subsets of forced, augmented or natural conditions are not the same.

(2) Two generalized equivalent variational principles are said to be equivalent if their subsets of functional and augmented variables are the same separately; their subsets of forced, augmented and natural conditions are the same separately.

(3) Two equivalent variational principles are said to be identical if their functionals are identical or will be identical if a proportional factor is considered.

3. The fundamental equations and boundary conditions in elasticity

For later convenience of quoting, all the conditions of small displacement theory in elasticity (including basic differential equations and boundary conditions) are listed as follows, where three types of variables, displacement \mathbf{u} , strain $\boldsymbol{\varepsilon}$ and stress $\boldsymbol{\sigma}$, are involved.

(1) Differential equilibrium equations

$$\boldsymbol{\partial}\boldsymbol{\sigma} + \bar{\mathbf{F}} = \mathbf{0} \quad (\text{in volume } V) \quad (3-1)$$

(2) Strain and displacement relations

$$\boldsymbol{\varepsilon} - \boldsymbol{\partial}^T \mathbf{u} = \mathbf{0} \quad (\text{in } V) \quad (3-2)$$

(3) Stress and strain relations

$$\boldsymbol{\sigma} - E\boldsymbol{\varepsilon} = \mathbf{0} \quad \text{or} \quad \boldsymbol{\varepsilon} - G\boldsymbol{\sigma} = \mathbf{0} \quad (\text{in } V) \quad (3-3)$$

in which

$$E = G^{-1}$$

(4) Boundary conditions of the given displacements

$$\mathbf{u} - \bar{\mathbf{u}} = \mathbf{0} \quad (\text{on the fixed boundary } S_u) \quad (3-4)$$

(5) Boundary conditions of the given external forces

$$L\boldsymbol{\sigma} - \bar{\mathbf{T}} = \mathbf{0} \quad (\text{on the free boundary } S_\sigma) \quad (3-5)$$

in which

$$\mathbf{u} = [u \quad v \quad w]^T$$

$$\boldsymbol{\varepsilon} = [\varepsilon_x \quad \varepsilon_y \quad \varepsilon_z \quad \gamma_{yz} \quad \gamma_{zx} \quad \gamma_{xy}]^T$$

$$\boldsymbol{\sigma} = [\sigma_x \quad \sigma_y \quad \sigma_z \quad \tau_{yz} \quad \tau_{zx} \quad \tau_{xy}]^T$$

$$\boldsymbol{\vartheta} = \begin{bmatrix} \frac{\partial}{\partial x} & 0 & 0 & \vdots & 0 & \frac{\partial}{\partial z} & \frac{\partial}{\partial y} \\ 0 & \frac{\partial}{\partial y} & 0 & \vdots & \frac{\partial}{\partial z} & 0 & \frac{\partial}{\partial x} \\ 0 & 0 & \frac{\partial}{\partial z} & \vdots & \frac{\partial}{\partial y} & \frac{\partial}{\partial x} & 0 \end{bmatrix} \quad (3-6)$$

$$G = \frac{1}{E} \begin{bmatrix} 1 & -\mu & -\mu & \vdots & 0 & 0 & 0 \\ -\mu & 1 & -\mu & \vdots & 0 & 0 & 0 \\ -\mu & -\mu & 1 & \vdots & 0 & 0 & 0 \\ \hline 0 & 0 & 0 & \vdots & 2(1+\mu) & 0 & 0 \\ 0 & 0 & 0 & \vdots & 0 & 2(1+\mu) & 0 \\ 0 & 0 & 0 & \vdots & 0 & 0 & 2(1+\mu) \end{bmatrix} \quad (3-7)$$

$$L = \begin{bmatrix} l & 0 & 0 & \vdots & 0 & n & m \\ 0 & m & 0 & \vdots & n & 0 & l \\ 0 & 0 & n & \vdots & m & l & 0 \end{bmatrix} \quad (3-8)$$

where l, m and n are the directional cosines of the outward normal of the boundary.

4. Several energy functionals in elasticity

In elasticity, various variational principles and their functionals have been proposed. Among these functionals, the most important ones may be listed as follows:

(1) Potential energy functional $\Pi_p(\mathbf{u})$ and non-conditional potential energy functional $\Pi_{1p}(\mathbf{u})$

$$\Pi_p(\mathbf{u}) = \iiint_V \left[\frac{1}{2} (\partial^T \mathbf{u})^T \mathbf{E} (\partial^T \mathbf{u}) - \bar{\mathbf{F}}^T \mathbf{u} \right] dV - \iint_{S_\sigma} \bar{\mathbf{T}}^T \mathbf{u} dS \quad (3-9a)$$

$$\begin{aligned} \Pi_{1p}(\mathbf{u}) = & \iiint_V \left[\frac{1}{2} (\partial^T \mathbf{u})^T \mathbf{E} (\partial^T \mathbf{u}) - \bar{\mathbf{F}}^T \mathbf{u} \right] dV - \iint_{S_\sigma} \bar{\mathbf{T}}^T \mathbf{u} dS \\ & - \iint_{S_u} (\mathbf{u} - \bar{\mathbf{u}})^T \mathbf{L} \mathbf{E} (\partial^T \mathbf{u}) dS \end{aligned} \quad (3-9b)$$

(2) Complementary energy functional $\Pi_c(\boldsymbol{\sigma})$

$$\Pi_c(\boldsymbol{\sigma}) = \iiint_V \frac{1}{2} \boldsymbol{\sigma}^T \mathbf{G} \boldsymbol{\sigma} dV - \iint_{S_u} \bar{\mathbf{u}}^T \mathbf{L} \boldsymbol{\sigma} dS \quad (3-10)$$

(3) Hellinger-Reissner functionals $\Pi_{HR}(\mathbf{u}, \boldsymbol{\sigma})$ and $\Pi'_{HR}(\mathbf{u}, \boldsymbol{\sigma})$

$$\Pi_{HR}(\mathbf{u}, \boldsymbol{\sigma}) = \iiint_V \left[\boldsymbol{\sigma}^T (\partial^T \mathbf{u}) - \frac{1}{2} \boldsymbol{\sigma}^T \mathbf{G} \boldsymbol{\sigma} - \bar{\mathbf{F}}^T \mathbf{u} \right] dV - \iint_{S_\sigma} \bar{\mathbf{T}}^T \mathbf{u} dS - \iint_{S_u} (\mathbf{u} - \bar{\mathbf{u}})^T \mathbf{L} \boldsymbol{\sigma} dS \quad (3-11a)$$

$$\Pi'_{HR}(\mathbf{u}, \boldsymbol{\sigma}) = \iiint_V \left[-\frac{1}{2} \boldsymbol{\sigma}^T \mathbf{G} \boldsymbol{\sigma} - \mathbf{u}^T (\partial \boldsymbol{\sigma} + \bar{\mathbf{F}}) \right] dV + \iint_{S_\sigma} \mathbf{u}^T (\mathbf{L} \boldsymbol{\sigma} - \bar{\mathbf{T}}) dS + \iint_{S_u} \bar{\mathbf{u}}^T \mathbf{L} \boldsymbol{\sigma} dS \quad (3-11b)$$

(4) Hu-Washizu functionals $\Pi_{HW}(\mathbf{u}, \boldsymbol{\varepsilon}, \boldsymbol{\sigma})$ and $\Pi'_{HW}(\mathbf{u}, \boldsymbol{\varepsilon}, \boldsymbol{\sigma})$

$$\Pi_{HW}(\mathbf{u}, \boldsymbol{\varepsilon}, \boldsymbol{\sigma}) = \iiint_V \left[\frac{1}{2} \boldsymbol{\varepsilon}^T \mathbf{E} \boldsymbol{\varepsilon} - \boldsymbol{\sigma}^T (\boldsymbol{\varepsilon} - \partial^T \mathbf{u}) - \bar{\mathbf{F}}^T \mathbf{u} \right] dV - \iint_{S_\sigma} \bar{\mathbf{T}}^T \mathbf{u} dS - \iint_{S_u} (\mathbf{u} - \bar{\mathbf{u}})^T \mathbf{L} \boldsymbol{\sigma} dS \quad (3-12a)$$

$$\Pi'_{HW}(\mathbf{u}, \boldsymbol{\varepsilon}, \boldsymbol{\sigma}) = \iiint_V \left[\frac{1}{2} \boldsymbol{\varepsilon}^T \mathbf{E} \boldsymbol{\varepsilon} - \boldsymbol{\sigma}^T \boldsymbol{\varepsilon} - \mathbf{u}^T (\partial \boldsymbol{\sigma} + \bar{\mathbf{F}}) \right] dV + \iint_{S_\sigma} \mathbf{u}^T (\mathbf{L} \boldsymbol{\sigma} - \bar{\mathbf{T}}) dS + \iint_{S_u} \bar{\mathbf{u}}^T \mathbf{L} \boldsymbol{\sigma} dS \quad (3-12b)$$

where $\Pi_p(\mathbf{u})$, $\Pi_{1p}(\mathbf{u})$ and $\Pi_c(\boldsymbol{\sigma})$ are functionals with a single variable; $\Pi_{HR}(\mathbf{u}, \boldsymbol{\sigma})$ and $\Pi'_{HR}(\mathbf{u}, \boldsymbol{\sigma})$ are functionals with two variables; $\Pi_{HW}(\mathbf{u}, \boldsymbol{\varepsilon}, \boldsymbol{\sigma})$ and

$\Pi'_{\text{HW}}(\mathbf{u}, \boldsymbol{\varepsilon}, \boldsymbol{\sigma})$ are functionals with three variables. It should be noted that in all these functionals there is no adjustable parameter involved.

In later discussions, the following formula of integration by parts will be used:

$$\iiint_V (\partial \boldsymbol{\sigma})^T \mathbf{u} dV = - \iiint_V \boldsymbol{\sigma}^T (\partial^T \mathbf{u}) dV + \iint_S (\mathbf{L}\boldsymbol{\sigma})^T \mathbf{u} dS \quad (3-13)$$

From the above equation, we have

$$\Pi_{\text{HR}} = \Pi'_{\text{HR}}, \quad \Pi_{\text{HW}} = \Pi'_{\text{HW}}$$

3.2.2 Transformation Pattern I of the Functional (Relaxation Pattern)

The original functional $\Pi^{(c)}$ is a conditional one; the forced conditions are

$$\phi_i = 0 \quad (\text{in } \tau_i) \quad (3-14)$$

and the new functional $\Pi^{(u)}$ obtained after transformation is a non-conditional one:

$$\Pi^{(u)} = \Pi^{(c)} + \sum_i \int_{\tau_i} \lambda_i^T \phi_i d\tau_i \quad (\text{I})$$

where λ_i is the multiplier, which can be identified by the use of natural conditions of $\Pi^{(u)}$. The functional variables of $\Pi^{(u)}$ consist of the functional variables of $\Pi^{(c)}$ and the identified multiplier variables.

The feature of pattern I is to transform the conditional functional $\Pi^{(c)}$ into a non-conditional functional $\Pi^{(u)}$. $\Pi^{(c)}$ is generalized equivalent but not equivalent to $\Pi^{(u)}$. The forced conditions (3-14) of $\Pi^{(c)}$ is transferred into the natural conditions of $\Pi^{(u)}$.

3.2.3 Transformation Pattern II of the Functional (Augmented Pattern)

The feature of pattern II is that the non-conditional functional $\Pi^{(-)}$ which has fewer variables is transformed into a non-conditional functional $\Pi^{(+)}$ which has more variables. $\Pi^{(+)}$ is generalized equivalent (but not equivalent) to $\Pi^{(-)}$. The augmented conditions of $\Pi^{(-)}$ are transferred into the natural conditions of $\Pi^{(+)}$.

Here we will explain in detail. Assume that the functional $\Pi^{(-)}(\mathbf{y})$ is the non-conditional functional before the transformation which has fewer variables; \mathbf{y} is the functional variable. And, assume that \mathbf{z} is the augmented variable. Thus,

the corresponding augmented conditions are

$$\mathbf{z} - f(\mathbf{y}) = \mathbf{0} \quad (\text{in } V) \quad (3-15)$$

Then, after the transformation, the new functional $\Pi^{(+)}(\mathbf{y}, \mathbf{z})$ is a non-conditional functional with more variables; \mathbf{y} and \mathbf{z} are the functional variables. It will be determined by the following expression:

$$\Pi^{(+)}(\mathbf{y}, \mathbf{z}) = \Pi^{(-)}(\mathbf{y}) + \eta Q(\mathbf{y}, \mathbf{z}) \quad (\text{II})$$

in which Q is a positive definite quadratic integral for the augmented condition expression on the left side of Eq. (3-15):

$$Q = \iiint_V \frac{1}{2} [\mathbf{z} - f(\mathbf{y})]^T \tilde{\mathbf{S}} [\mathbf{z} - f(\mathbf{y})] dV \quad (3-16)$$

where $\tilde{\mathbf{S}}$ is a positive definite symmetric matrix, and η is an arbitrary non-zero parameter. It can be proved that the original and the new functionals $\Pi^{(-)}(\mathbf{y})$ and $\Pi^{(+)}(\mathbf{y}, \mathbf{z})$ are generalized equivalent to each other. For this reason, we present the relevant theorem of pattern II and its proof as follows.

Theorem The new functional $\Pi^{(+)}(\mathbf{y}, \mathbf{z})$ defined by Eq. (II) and the original functional $\Pi^{(-)}(\mathbf{y})$ are generalized equivalent to each other. In other words, the stationary conditions of $\Pi^{(+)}(\mathbf{y}, \mathbf{z})$:

$$\delta \Pi^{(+)}(\mathbf{y}, \mathbf{z}) = 0 \quad (3-17)$$

may be derived from the stationary conditions and augmented conditions of $\Pi^{(-)}(\mathbf{y})$:

$$\delta \Pi^{(-)}(\mathbf{y}) = 0 \quad (3-18a)$$

$$\mathbf{z} - f(\mathbf{y}) = \mathbf{0} \quad (3-18b)$$

Conversely, Eqs. (3-18a) and (3-18b) can also be derived from Eq. (3-17).

Proof Firstly, we will prove that Eq. (3-17) can be derived from Eqs. (3-18a) and (3-18b).

The variation of Eq. (II) is

$$\delta \Pi^{(+)}(\mathbf{y}, \mathbf{z}) = \delta \Pi^{(-)}(\mathbf{y}) + \eta \iiint_V [\mathbf{z} - f(\mathbf{y})]^T \tilde{\mathbf{S}} \delta [\mathbf{z} - f(\mathbf{y})] dV \quad (3-19)$$

We have assumed that Eqs. (3-18a) and (3-18b) are satisfied. Then, substituting Eqs. (3-18a) and (3-18b) into (3-19), Eq. (3-17) can be obtained.

Secondly, it will be proved that (3-18a) and (3-18b) can be derived from Eq. (3-17).

Because both $\delta \mathbf{y}$ and $\delta \mathbf{z}$ are independent variations, both $\delta \mathbf{y}$ and $\delta [\mathbf{z} - f(\mathbf{y})]$

are also independent variations. Since Eq. (3-17) is assured, from Eq. (3-19) we obtain

$$\delta \Pi^{(-)}(\mathbf{y}) = 0 \quad (3-20)$$

$$\tilde{\mathbf{S}}[\mathbf{z} - f(\mathbf{y})] = \mathbf{0} \quad (3-21)$$

Because $\tilde{\mathbf{S}}$ is a positive definite matrix, then from Eq. (3-21) we obtain

$$\mathbf{z} - f(\mathbf{y}) = \mathbf{0} \quad (3-22)$$

According to Eqs. (3-20) and (3-22), Eqs. (3-18a) and (3-18b) can be proved. \square

Example 3.1 Derive the augmented functional of Hellinger-Reissner functional $\Pi'_{\text{HR}}(\mathbf{u}, \boldsymbol{\sigma})$ according to pattern Π .

Solution The original non-conditional functional with fewer variables is

$$\Pi'_{\text{HR}}(\mathbf{u}, \boldsymbol{\sigma}) = \iiint_V \left[-\frac{1}{2} \boldsymbol{\sigma}^T \mathbf{G} \boldsymbol{\sigma} - \mathbf{u}^T (\partial \boldsymbol{\sigma} + \bar{\mathbf{F}}) \right] dV + \iint_{S_\sigma} \mathbf{u}^T (\mathbf{T} - \bar{\mathbf{T}}) dS + \iint_{S_u} \bar{\mathbf{u}}^T \mathbf{T} dS \quad (3-23)$$

And, the augmented condition of which is

$$\boldsymbol{\varepsilon} - \mathbf{G} \boldsymbol{\sigma} = \mathbf{0} \quad (\text{in } V) \quad (3-24)$$

According to the transformation pattern Π , the positive definite quadratic integral for the augmented condition expression on the left side of Eq. (3-24) should be written in the same manner as Eq. (3-16):

$$Q = \iiint_V \frac{1}{2} (\boldsymbol{\varepsilon} - \mathbf{G} \boldsymbol{\sigma})^T \mathbf{E} (\boldsymbol{\varepsilon} - \mathbf{G} \boldsymbol{\sigma}) dV \quad (3-25)$$

Substituting this equation into Eq. (Π), the general form of the new non-conditional functional with more variables can be obtained as follows:

$$\Pi^{(+)}(\mathbf{u}, \boldsymbol{\sigma}, \boldsymbol{\varepsilon}) = \Pi'_{\text{HR}}(\mathbf{u}, \boldsymbol{\sigma}) + \eta \iiint_V \frac{1}{2} (\boldsymbol{\varepsilon} - \mathbf{G} \boldsymbol{\sigma})^T \mathbf{E} (\boldsymbol{\varepsilon} - \mathbf{G} \boldsymbol{\sigma}) dV \quad (3-26)$$

In fact, this functional $\Pi^{(+)}(\mathbf{u}, \boldsymbol{\sigma}, \boldsymbol{\varepsilon})$ is the functional $\Pi_{G\lambda}$ which was firstly proposed in [3].

If the parameter η in Eq. (3-26) equals to 1, special form of the augmented functional can be obtained:

$$\Pi^{(+)}(\mathbf{u}, \boldsymbol{\sigma}, \boldsymbol{\varepsilon}) \Big|_{\eta=1} = \Pi'_{\text{HR}}(\mathbf{u}, \boldsymbol{\sigma}) + \iiint_V \frac{1}{2} (\boldsymbol{\varepsilon} - \mathbf{G} \boldsymbol{\sigma})^T \mathbf{E} (\boldsymbol{\varepsilon} - \mathbf{G} \boldsymbol{\sigma}) dV \quad (3-27)$$

In fact, this functional is the same as the functional $\Pi'_{\text{HW}}(\mathbf{u}, \boldsymbol{\varepsilon}, \boldsymbol{\sigma})$ in Hu-Washizu principle.

3.2.4 Transformation Pattern III of the Functional (Equivalent Pattern)

The feature of pattern III is to transform the non-conditional functional Π into a non-conditional functional Π_L involving several adjustable parameters:

$$\Pi_L = \Pi + \sum_I \eta_i Q_i \quad (\text{III})$$

in which η_i are adjustable parameters; and Q_i are the quadratic integrals constituted by the natural condition expressions of Π in the corresponding domains. In general, the new functional Π_L is the general form of the equivalent functional of the original Π . In the case of degeneration (when η_i equals to a critical value η_{ci}), $\Pi_L|_{\eta_i=\eta_{ci}}$ degenerates into the non-conditional functional with fewer variables.

Some of the functional variables in the original functional are transferred into the augmented variables in the new functional; some of the natural conditions of the original functional are transferred into the augmented conditions of the new functional. Thus, the new functional and the original one are generalized equivalent but not equivalent to each other.

Example 3.2 Derive the equivalent functional $\Pi_L(\mathbf{u}, \boldsymbol{\varepsilon}, \boldsymbol{\sigma})$ of Hu-Washizu functional $\Pi_{\text{HW}}(\mathbf{u}, \boldsymbol{\varepsilon}, \boldsymbol{\sigma})$, according to pattern III.

Solution The Hu-Washizu functional is given by Eq. (3-12), it is a functional with three variables $(\mathbf{u}, \boldsymbol{\varepsilon}, \boldsymbol{\sigma})$. Its natural conditions are the equations which define the problems in small displacement theory of elasticity, i.e. Equations (3-1) to (3-5). Now, we take the natural condition (3-3) as an example, and perform the transformation according to pattern III. We obtain

$$Q_1 = \iiint_V \frac{1}{2} (\mathbf{E}\boldsymbol{\varepsilon} - \boldsymbol{\sigma})^T \mathbf{G} (\mathbf{E}\boldsymbol{\varepsilon} - \boldsymbol{\sigma}) dV \quad (3-28)$$

$$\Pi_{L\eta_1} = \Pi_{\text{HW}}(\mathbf{u}, \boldsymbol{\varepsilon}, \boldsymbol{\sigma}) + \eta_1 \iiint_V \frac{1}{2} (\mathbf{E}\boldsymbol{\varepsilon} - \boldsymbol{\sigma})^T \mathbf{G} (\mathbf{E}\boldsymbol{\varepsilon} - \boldsymbol{\sigma}) dV \quad (3-29)$$

This functional $\Pi_{L\eta_1}$ is the functional Π_{GN} in [3]. When η_1 is an arbitrary constant except -1 , $\Pi_{L\eta_1}(\mathbf{u}, \boldsymbol{\varepsilon}, \boldsymbol{\sigma})$ is the non-conditional functional with three variables $(\mathbf{u}, \boldsymbol{\varepsilon}, \boldsymbol{\sigma})$, and one parameter η_1 is involved in the functional. When $\eta_1 = -1$,

$$\Pi_{L\eta_1} \Big|_{\eta_1=-1} = \Pi_{\text{HR}}(\mathbf{u}, \boldsymbol{\sigma}) \quad (3-30)$$

thus the new functional degenerates into the non-conditional functional with two variables $(\mathbf{u}, \boldsymbol{\sigma})$, ε degenerates into the augmented variable, and condition (3-3) degenerates into the augmented condition.

3.3 Generalized Variational Principle Involving Several Adjustable Parameters

According to pattern III of the functional transformation, generalized variational principles involving several adjustable parameters with one, two and three functional variables will be discussed separately in this section.

3.3.1 Generalized Variational Principle Involving Several Adjustable Parameters with Single Functional Variable \mathbf{u}

If displacement \mathbf{u} is taken as the functional variable, the fundamental equations in elasticity are as follows:

$$\left. \begin{aligned} \partial \mathbf{E}(\partial^T \mathbf{u}) + \bar{\mathbf{F}} &= \mathbf{0} && \text{(in volume } V) \\ \mathbf{u} - \bar{\mathbf{u}} &= \mathbf{0} && \text{(on fixed boundary } S_u) \\ \mathbf{L}\mathbf{E}(\partial^T \mathbf{u}) - \bar{\mathbf{T}} &= \mathbf{0} && \text{(on free boundary } S_\sigma) \end{aligned} \right\} \quad (3-31)$$

where $\bar{\mathbf{F}}$ is the given body force vector; $\bar{\mathbf{u}}$ and $\bar{\mathbf{T}}$ are the given displacement and surface force vectors on the boundaries S_u and S_σ , respectively.

The corresponding non-conditional functional with single functional variable \mathbf{u} of Eq. (3-31) may be expressed in the following form:

$$\Pi_{1p}(\mathbf{u}) = \iiint_V \left[\frac{1}{2} (\partial^T \mathbf{u})^T \mathbf{E}(\partial^T \mathbf{u}) - \bar{\mathbf{F}}^T \mathbf{u} \right] dV - \iint_{S_u} (\mathbf{u} - \bar{\mathbf{u}})^T \mathbf{L}\mathbf{E}(\partial^T \mathbf{u}) dS - \iint_{S_\sigma} \bar{\mathbf{T}}^T \mathbf{u} dS \quad (3-32)$$

in which $\Pi_{1p}(\mathbf{u})$ is the energy functional of the potential energy principle with geometrical boundary condition relaxed. The natural condition of this functional is Eq. (3-31).

Let $\Pi_{1p}(\mathbf{u})$ be the original functional, according to pattern III and by making use of its three natural conditions (3-31), the more general form of its equivalent functional may be obtained as follows:

$$\Pi_{1L}(\mathbf{u}) = \Pi_{1p}(\mathbf{u}) + \sum_{i=1}^5 \alpha_i R_i \quad (3-33)$$

in which R_i are the quadratic integrals constituted by three natural condition

expressions on the left side of Eq. (3-31):

$$\left. \begin{aligned}
 R_1 &= \iiint_V \frac{1}{2} [\partial E(\partial^T \mathbf{u}) + \bar{\mathbf{F}}]^T [\partial E(\partial^T \mathbf{u}) + \bar{\mathbf{F}}] dV \\
 R_2 &= \iint_{S_u} \frac{1}{2} (\mathbf{u} - \bar{\mathbf{u}})^T (\mathbf{u} - \bar{\mathbf{u}}) dS \\
 R_3 &= \iint_{S_u} (\mathbf{u} - \bar{\mathbf{u}})^T (\partial E \partial^T \mathbf{u} + \bar{\mathbf{F}}) dS \\
 R_4 &= \iint_{S_\sigma} \frac{1}{2} (\mathbf{L} E \partial^T \mathbf{u} - \bar{\mathbf{T}})^T (\mathbf{L} E \partial^T \mathbf{u} - \bar{\mathbf{T}}) dS \\
 R_5 &= \iint_{S_\sigma} (\mathbf{L} E \partial^T \mathbf{u} - \bar{\mathbf{T}})^T (\partial E \partial^T \mathbf{u} + \bar{\mathbf{F}}) dS
 \end{aligned} \right\} \quad (3-34)$$

If the highest order of derivatives of \mathbf{u} in the integrand is restricted to first order (in V) and zero order (on S), then the simple form of the functional may be obtained as follows:

$$\Pi_{\text{IL}}(\mathbf{u}) = \Pi_{\text{Ip}}(\mathbf{u}) + \alpha_2 R_2 \quad (3-35)$$

3.3.2 Generalized Variational Principle Involving Several Adjustable Parameters with Two Functional Variables \mathbf{u} and $\boldsymbol{\sigma}$

If displacement \mathbf{u} and stress $\boldsymbol{\sigma}$ are taken as functional variables, the fundamental equations in elasticity are as follows:

$$\left. \begin{aligned}
 \partial \boldsymbol{\sigma} + \bar{\mathbf{F}} &= \mathbf{0} & (\text{in } V) \\
 \partial^T \mathbf{u} - \mathbf{G} \boldsymbol{\sigma} &= \mathbf{0} & (\text{in } V) \\
 \mathbf{u} - \bar{\mathbf{u}} &= \mathbf{0} & (\text{on } S_u) \\
 \mathbf{L} \boldsymbol{\sigma} - \bar{\mathbf{T}} &= \mathbf{0} & (\text{on } S_\sigma)
 \end{aligned} \right\} \quad (3-36)$$

The corresponding non-conditional functional with two functional variables \mathbf{u} and $\boldsymbol{\sigma}$ may be expressed in the following form:

$$\left. \begin{aligned}
 \Pi_{\text{HR}}(\mathbf{u}, \boldsymbol{\sigma}) &= \iiint_V \left[\boldsymbol{\sigma}^T (\partial^T \mathbf{u}) - \frac{1}{2} \boldsymbol{\sigma}^T \mathbf{G} \boldsymbol{\sigma} - \bar{\mathbf{F}}^T \mathbf{u} \right] dV - \iint_{S_u} (\mathbf{u} - \bar{\mathbf{u}})^T \mathbf{L} \boldsymbol{\sigma} dS - \iint_{S_\sigma} \bar{\mathbf{T}}^T \mathbf{u} dS \\
 \text{or} \\
 \Pi'_{\text{HR}}(\mathbf{u}, \boldsymbol{\sigma}) &= \iiint_V \left[-\mathbf{u}^T (\partial \boldsymbol{\sigma} + \bar{\mathbf{F}}) - \frac{1}{2} \boldsymbol{\sigma}^T \mathbf{G} \boldsymbol{\sigma} \right] dV + \iint_{S_u} \bar{\mathbf{u}}^T \mathbf{L} \boldsymbol{\sigma} dS + \iint_{S_\sigma} (\mathbf{L} \boldsymbol{\sigma} - \bar{\mathbf{T}})^T \mathbf{u} dS
 \end{aligned} \right\} \quad (3-37)$$

$\Pi_{\text{HR}}(\mathbf{u}, \boldsymbol{\sigma})$ and $\Pi'_{\text{HR}}(\mathbf{u}, \boldsymbol{\sigma})$ are two expressions of Hellinger-Reissner functional, and are identical to each other.

According to pattern III, the more general form of its equivalent functional may be obtained:

$$\Pi_{2\text{L}}(\mathbf{u}, \boldsymbol{\sigma}) = \Pi_{\text{HR}}(\mathbf{u}, \boldsymbol{\sigma}) + \sum_{i=1}^9 \beta_i P_i = \Pi'_{\text{HR}}(\mathbf{u}, \boldsymbol{\sigma}) + \sum_{i=1}^9 \beta_i P_i \quad (3-38)$$

in which

$$\left. \begin{aligned} P_1 &= \iiint_V \frac{1}{2} (\partial^T \mathbf{u} - \mathbf{G}\boldsymbol{\sigma})^T \mathbf{E} (\partial^T \mathbf{u} - \mathbf{G}\boldsymbol{\sigma}) dV \\ P_2 &= \iiint_V \frac{1}{2} (\partial\boldsymbol{\sigma} + \bar{\mathbf{F}})^T (\partial\boldsymbol{\sigma} + \bar{\mathbf{F}}) dV \\ P_3 &= \iiint_V (\partial\boldsymbol{\sigma} + \bar{\mathbf{F}})^T \mathbf{b} (\boldsymbol{\sigma} - \mathbf{E}\partial^T \mathbf{u}) dV \\ P_4 &= \iint_{S_u} \frac{1}{2} (\mathbf{u} - \bar{\mathbf{u}})^T (\mathbf{u} - \bar{\mathbf{u}}) dS \\ P_5 &= \iint_{S_u} (\mathbf{u} - \bar{\mathbf{u}})^T (\partial\boldsymbol{\sigma} + \bar{\mathbf{F}}) dS \\ P_6 &= \iint_{S_u} (\mathbf{u} - \bar{\mathbf{u}})^T \mathbf{L} (\boldsymbol{\sigma} - \mathbf{E}\partial^T \mathbf{u}) dS \\ P_7 &= \iint_{S_\sigma} \frac{1}{2} (\mathbf{L}\boldsymbol{\sigma} - \bar{\mathbf{T}})^T (\mathbf{L}\boldsymbol{\sigma} - \bar{\mathbf{T}}) dS \\ P_8 &= \iint_{S_\sigma} (\mathbf{L}\boldsymbol{\sigma} - \bar{\mathbf{T}})^T \mathbf{L} (\boldsymbol{\sigma} - \mathbf{E}\partial^T \mathbf{u}) dS \\ P_9 &= \iint_{S_\sigma} (\mathbf{L}\boldsymbol{\sigma} - \bar{\mathbf{T}})^T (\partial\boldsymbol{\sigma} + \bar{\mathbf{F}}) dS \end{aligned} \right\} \quad (3-39)$$

in which

$$\mathbf{b} = \begin{bmatrix} b_1 & 0 & 0 & \vdots & 0 & b_3 & b_2 \\ 0 & b_2 & 0 & \vdots & b_3 & 0 & b_1 \\ 0 & 0 & b_3 & \vdots & b_2 & b_1 & 0 \end{bmatrix} \quad (3-40)$$

b_1, b_2, b_3 are arbitrary given constants. Since

$$\Pi_{\text{HR}}(\mathbf{u}, \boldsymbol{\sigma}) = \Pi_{\text{Ip}}(\mathbf{u}) - P_1 - P_6 \quad (3-41)$$

Equation (3-38) may be rewritten as

$$\Pi_{2\text{L}}(\mathbf{u}, \boldsymbol{\sigma}) = \Pi_{\text{Ip}}(\mathbf{u}) - P_1 - P_6 + \sum_{i=1}^9 \beta_i P_i \quad (3-42)$$

If $\beta_1 = \beta_6 = 1$, $\beta_2 = \beta_3 = \beta_5 = \beta_7 = \beta_8 = \beta_9 = 0$, then from Eq. (3-42), $\Pi_{2L}(\mathbf{u}, \boldsymbol{\sigma})$ will degenerate into the following functional with single functional variable \mathbf{u} :

$$\Pi_{1L}(\mathbf{u}) = \Pi_{1p}(\mathbf{u}) + \beta_4 P_4 = \Pi_{1p}(\mathbf{u}) + \beta_4 R_2$$

Actually, this functional is the same as functional (3-35).

If the highest order of derivatives in the integrand is restricted, then two simple forms of the functional with two functional variables \mathbf{u} and $\boldsymbol{\sigma}$ may be obtained as follows:

$$\Pi_{2L}(\mathbf{u}, \boldsymbol{\sigma}) = \Pi_{HR}(\mathbf{u}, \boldsymbol{\sigma}) + \beta_1 P_1 + \beta_4 P_4 + \beta_7 P_7 \quad (3-43)$$

$$\Pi_{2L}(\mathbf{u}, \boldsymbol{\sigma}) = \Pi'_{HR}(\mathbf{u}, \boldsymbol{\sigma}) + \beta_2 P_2 + \beta_4 P_4 + \beta_7 P_7 \quad (3-44)$$

In Eq. (3-43), \mathbf{u} is restricted to first order (in V) and zero order (on S), $\boldsymbol{\sigma}$ is restricted to zero order. In Eq. (3-44), $\boldsymbol{\sigma}$ is restricted to first order (in V) and zero order (on S), \mathbf{u} is restricted to zero order.

3.3.3 Generalized Variational Principle Involving Several Adjustable Parameters with Two Functional Variables \mathbf{u} and $\boldsymbol{\varepsilon}$

If displacement \mathbf{u} and strain $\boldsymbol{\varepsilon}$ are taken as functional variables, the fundamental equations in elasticity are as follows:

$$\left. \begin{aligned} \partial \mathbf{E}\boldsymbol{\varepsilon} + \bar{\mathbf{F}} &= \mathbf{0} & (\text{in } V) \\ \boldsymbol{\varepsilon} - \partial^T \mathbf{u} &= \mathbf{0} & (\text{in } V) \\ \mathbf{u} - \bar{\mathbf{u}} &= \mathbf{0} & (\text{on } S_u) \\ \mathbf{L}\mathbf{E}\boldsymbol{\varepsilon} - \bar{\mathbf{T}} &= \mathbf{0} & (\text{on } S_\sigma) \end{aligned} \right\} \quad (3-45)$$

The corresponding non-conditional functional with two functional variables \mathbf{u} and $\boldsymbol{\varepsilon}$ may be expressed in the following form:

$$\left. \begin{aligned} \Pi_2(\mathbf{u}, \boldsymbol{\varepsilon}) &= \iiint_V \left[(\partial^T \mathbf{u})^T \mathbf{E}\boldsymbol{\varepsilon} - \frac{1}{2} \boldsymbol{\varepsilon}^T \mathbf{E}\boldsymbol{\varepsilon} - \bar{\mathbf{F}}^T \mathbf{u} \right] dV - \iint_{S_u} (\mathbf{u} - \bar{\mathbf{u}})^T \mathbf{L}\mathbf{E}\boldsymbol{\varepsilon} dS - \iint_{S_\sigma} \bar{\mathbf{T}}^T \mathbf{u} dS \\ \text{or} \\ \Pi'_2(\mathbf{u}, \boldsymbol{\varepsilon}) &= \iiint_V \left[-(\partial(\mathbf{E}\boldsymbol{\varepsilon}) + \bar{\mathbf{F}})^T \mathbf{u} - \frac{1}{2} \boldsymbol{\varepsilon}^T \mathbf{E}\boldsymbol{\varepsilon} \right] dV + \iint_{S_u} \bar{\mathbf{u}}^T \mathbf{L}\mathbf{E}\boldsymbol{\varepsilon} dS + \iint_{S_\sigma} (\mathbf{L}\mathbf{E}\boldsymbol{\varepsilon} - \bar{\mathbf{T}})^T \mathbf{u} dS \end{aligned} \right\} \quad (3-46)$$

in which $\Pi_2(\mathbf{u}, \boldsymbol{\varepsilon})$ and $\Pi'_2(\mathbf{u}, \boldsymbol{\varepsilon})$ are identical.

According to pattern III, the more general form of its equivalent functional may be obtained as follows:

$$\Pi_{2L}(\mathbf{u}, \boldsymbol{\varepsilon}) = \Pi_2(\mathbf{u}, \boldsymbol{\varepsilon}) + \sum_{i=1}^9 \gamma_i S_i = \Pi_2'(\mathbf{u}, \boldsymbol{\varepsilon}) + \sum_{i=1}^9 \gamma_i S_i \quad (3-47)$$

in which

$$\left. \begin{aligned} S_1 &= \iiint_V \frac{1}{2} (\partial^T \mathbf{u} - \boldsymbol{\varepsilon})^T \mathbf{E} (\partial^T \mathbf{u} - \boldsymbol{\varepsilon}) dV \\ S_2 &= \iiint_V \frac{1}{2} (\partial \mathbf{E} \boldsymbol{\varepsilon} + \bar{\mathbf{F}})^T (\partial \mathbf{E} \boldsymbol{\varepsilon} + \bar{\mathbf{F}}) dV \\ S_3 &= \iiint_V (\partial \mathbf{E} \boldsymbol{\varepsilon} + \bar{\mathbf{F}})^T \mathbf{b} \mathbf{E} (\boldsymbol{\varepsilon} - \partial^T \mathbf{u}) dV \\ S_4 &= \iint_{S_u} \frac{1}{2} (\mathbf{u} - \bar{\mathbf{u}})^T (\mathbf{u} - \bar{\mathbf{u}}) dS \\ S_5 &= \iint_{S_u} (\mathbf{u} - \bar{\mathbf{u}})^T \mathbf{L} \mathbf{E} (\boldsymbol{\varepsilon} - \partial^T \mathbf{u}) dS \\ S_6 &= \iint_{S_u} (\mathbf{u} - \bar{\mathbf{u}})^T (\partial \mathbf{E} \boldsymbol{\varepsilon} + \bar{\mathbf{F}}) dS \\ S_7 &= \iint_{S_\sigma} \frac{1}{2} (\mathbf{L} \mathbf{E} \boldsymbol{\varepsilon} - \bar{\mathbf{T}})^T (\mathbf{L} \mathbf{E} \boldsymbol{\varepsilon} - \bar{\mathbf{T}}) dS \\ S_8 &= \iint_{S_\sigma} (\mathbf{L} \mathbf{E} \boldsymbol{\varepsilon} - \bar{\mathbf{T}})^T \mathbf{L} \mathbf{E} (\boldsymbol{\varepsilon} - \partial^T \mathbf{u}) dS \\ S_9 &= \iint_{S_\sigma} (\mathbf{L} \mathbf{E} \boldsymbol{\varepsilon} - \bar{\mathbf{T}})^T (\partial \mathbf{E} \boldsymbol{\varepsilon} + \bar{\mathbf{F}}) dS \end{aligned} \right\} \quad (3-48)$$

Since

$$\Pi_2(\mathbf{u}, \boldsymbol{\varepsilon}) = \Pi_{1p}(\mathbf{u}) - S_1 - S_5 \quad (3-49)$$

Equation (3-47) may be rewritten as

$$\Pi_{2L}(\mathbf{u}, \boldsymbol{\varepsilon}) = \Pi_{1p}(\mathbf{u}) - S_1 - S_5 + \sum_{i=1}^9 \gamma_i S_i \quad (3-50)$$

If $\gamma_1 = \gamma_5 = 1$, $\gamma_2 = \gamma_3 = \gamma_6 = \gamma_7 = \gamma_8 = \gamma_9 = 0$, then from Eq. (3-50), $\Pi_{2L}(\mathbf{u}, \boldsymbol{\varepsilon})$ will degenerate into the following functional with single functional variable \mathbf{u} :

$$\Pi_{1L}(\mathbf{u}) = \Pi_{1p}(\mathbf{u}) + \gamma_4 S_4 = \Pi_{1p} + \gamma_4 R_2$$

Actually, this functional is the same as the functional (3-35).

If the highest order derivatives in the integrand are restricted, then two simple forms of the functional with two variables \mathbf{u} and $\boldsymbol{\varepsilon}$ may be obtained as follows:

$$\Pi_{2L}(\mathbf{u}, \boldsymbol{\varepsilon}) = \Pi_2(\mathbf{u}, \boldsymbol{\varepsilon}) + \gamma_1 S_1 + \gamma_4 S_4 + \gamma_7 S_7 \quad (3-51)$$

$$\Pi_{2L}(\mathbf{u}, \boldsymbol{\varepsilon}) = \Pi'_2(\mathbf{u}, \boldsymbol{\varepsilon}) + \gamma_2 S_2 + \gamma_4 S_4 + \gamma_7 S_7 \quad (3-52)$$

In Eq. (3-51), \mathbf{u} is restricted to first order (in V) and zero order (on S), $\boldsymbol{\varepsilon}$ to zero order. In Eq. (3-52), $\boldsymbol{\varepsilon}$ is restricted to first order (in V) and zero order (on S), \mathbf{u} to zero order.

3.3.4 Generalized Variational Principle Involving Several Adjustable Parameters with Three Functional Variables \mathbf{u} , $\boldsymbol{\varepsilon}$ and $\boldsymbol{\sigma}$

If displacement \mathbf{u} , strain $\boldsymbol{\varepsilon}$ and stress $\boldsymbol{\sigma}$ are taken as functional variables, the fundamental equations in elasticity are as follows

$$\left. \begin{aligned} \partial \boldsymbol{\sigma} + \bar{\mathbf{F}} &= \mathbf{0} & (\text{in } V) \\ \boldsymbol{\varepsilon} - \partial^T \mathbf{u} &= \mathbf{0} & (\text{in } V) \\ \boldsymbol{\sigma} - \mathbf{E} \boldsymbol{\varepsilon} &= \mathbf{0} & (\text{in } V) \\ \mathbf{u} - \bar{\mathbf{u}} &= \mathbf{0} & (\text{on } S_u) \\ \mathbf{L} \boldsymbol{\sigma} - \bar{\mathbf{T}} &= \mathbf{0} & (\text{on } S_\sigma) \end{aligned} \right\} \quad (3-53)$$

The corresponding non-conditional functional with three functional variables \mathbf{u} , $\boldsymbol{\varepsilon}$ and $\boldsymbol{\sigma}$ is usually expressed in the form of Hu-Washizu functional:

$$\left. \begin{aligned} \Pi_{\text{HW}}(\mathbf{u}, \boldsymbol{\varepsilon}, \boldsymbol{\sigma}) &= \iiint_V \left[\frac{1}{2} \boldsymbol{\varepsilon}^T \mathbf{E} \boldsymbol{\varepsilon} - \boldsymbol{\sigma}^T (\boldsymbol{\varepsilon} - \partial^T \mathbf{u}) - \bar{\mathbf{F}}^T \mathbf{u} \right] dV - \iint_{S_u} (\mathbf{u} - \bar{\mathbf{u}})^T \mathbf{L} \boldsymbol{\sigma} dS - \iint_{S_\sigma} \bar{\mathbf{T}}^T \mathbf{u} dS \\ \Pi'_{\text{HW}}(\mathbf{u}, \boldsymbol{\varepsilon}, \boldsymbol{\sigma}) &= \iiint_V \left[\frac{1}{2} \boldsymbol{\varepsilon}^T \mathbf{E} \boldsymbol{\varepsilon} - \boldsymbol{\sigma}^T \boldsymbol{\varepsilon} - (\partial \boldsymbol{\sigma} + \bar{\mathbf{F}})^T \mathbf{u} \right] dV + \iint_{S_u} \bar{\mathbf{u}}^T \mathbf{L} \boldsymbol{\sigma} dS + \iint_{S_\sigma} (\mathbf{L} \boldsymbol{\sigma} - \bar{\mathbf{T}})^T \mathbf{u} dS \end{aligned} \right\} \quad (3-54)$$

According to pattern III, the more general form of its equivalent functional may be obtained as follows:

$$\Pi_{3L}(\mathbf{u}, \boldsymbol{\varepsilon}, \boldsymbol{\sigma}) = \Pi_{\text{HW}}(\mathbf{u}, \boldsymbol{\varepsilon}, \boldsymbol{\sigma}) + \sum_{i=1}^{14} \eta_i Q_i = \Pi'_{\text{HW}}(\mathbf{u}, \boldsymbol{\varepsilon}, \boldsymbol{\sigma}) + \sum_{i=1}^{14} \eta_i Q_i \quad (3-55)$$

in which

$$\left. \begin{aligned}
 Q_1 &= \iiint_V \frac{1}{2} (\boldsymbol{\sigma} - E\boldsymbol{\varepsilon})^T \mathbf{G} (\boldsymbol{\sigma} - E\boldsymbol{\varepsilon}) dV \\
 Q_2 &= \iiint_V \frac{1}{2} (\boldsymbol{\varepsilon} - \partial^T \mathbf{u})^T \mathbf{E} (\boldsymbol{\varepsilon} - \partial^T \mathbf{u}) dV \\
 Q_3 &= \iiint_V \frac{1}{2} (\partial\boldsymbol{\sigma} + \bar{\mathbf{F}})^T (\partial\boldsymbol{\sigma} + \bar{\mathbf{F}}) dV \\
 Q_4 &= \iiint_V (\mathbf{E}\boldsymbol{\varepsilon} - \boldsymbol{\sigma})^T (\boldsymbol{\varepsilon} - \partial^T \mathbf{u}) dV \\
 Q_5 &= \iiint_V (\partial\boldsymbol{\sigma} + \bar{\mathbf{F}})^T \mathbf{b} (\boldsymbol{\sigma} - E\boldsymbol{\varepsilon}) dV \\
 Q_6 &= \iiint_V (\partial\boldsymbol{\sigma} + \bar{\mathbf{F}})^T \mathbf{b} E (\boldsymbol{\varepsilon} - \partial^T \mathbf{u}) dV \\
 Q_7 &= \iint_{S_u} \frac{1}{2} (\mathbf{u} - \bar{\mathbf{u}})^T (\mathbf{u} - \bar{\mathbf{u}}) dS \\
 Q_8 &= \iint_{S_u} \frac{1}{2} (\mathbf{u} - \bar{\mathbf{u}})^T \mathbf{L} (\boldsymbol{\sigma} - E\boldsymbol{\varepsilon}) dS \\
 Q_9 &= \iint_{S_u} (\mathbf{u} - \bar{\mathbf{u}})^T \mathbf{L} E (\boldsymbol{\varepsilon} - \partial^T \mathbf{u}) dS \\
 Q_{10} &= \iint_{S_u} (\mathbf{u} - \bar{\mathbf{u}})^T (\partial\boldsymbol{\sigma} + \bar{\mathbf{F}}) dS \\
 Q_{11} &= \iint_{S_\sigma} \frac{1}{2} (\mathbf{L}\boldsymbol{\sigma} - \bar{\mathbf{T}})^T (\mathbf{L}\boldsymbol{\sigma} - \bar{\mathbf{T}}) dS \\
 Q_{12} &= \iint_{S_\sigma} (\mathbf{L}\boldsymbol{\sigma} - \bar{\mathbf{T}})^T \mathbf{L} (\boldsymbol{\sigma} - E\boldsymbol{\varepsilon}) dS \\
 Q_{13} &= \iint_{S_\sigma} (\mathbf{L}\boldsymbol{\sigma} - \bar{\mathbf{T}})^T \mathbf{L} E (\boldsymbol{\varepsilon} - \partial^T \mathbf{u}) dS \\
 Q_{14} &= \iint_{S_\sigma} (\mathbf{L}\boldsymbol{\sigma} - \bar{\mathbf{T}})^T (\partial\boldsymbol{\sigma} + \bar{\mathbf{F}}) dS
 \end{aligned} \right\} \quad (3-56)$$

Functional (3-55) is the general form of functional involving adjustable parameters with three functional variables \mathbf{u} , $\boldsymbol{\varepsilon}$ and $\boldsymbol{\sigma}$ except the three degenerate cases listed below.

(1) The degenerate case in which $\boldsymbol{\varepsilon}$ is excluded.

If we assume

$$\eta_2 = 1 + \eta_1, \quad \eta_4 = -1 - \eta_1, \quad \eta_5 = \eta_6, \quad \eta_8 = \eta_9, \quad \eta_{12} = \eta_{13}$$

then the functional (3-55) degenerates into the following functional with two functional variables \mathbf{u} and $\boldsymbol{\sigma}$:

$$\begin{aligned} \Pi_{2L}(\mathbf{u}, \boldsymbol{\sigma}) &= (\Pi_{\text{HW}} - Q_1) + (1 + \eta_1)(Q_1 + Q_2 - Q_4) + \eta_3 Q_3 + \eta_5(Q_5 + Q_6) \\ &\quad + \eta_7 Q_7 + \eta_{10} Q_{10} + \eta_8(Q_8 + Q_9) + \eta_{11} Q_{11} + \eta_{12}(Q_{12} + Q_{13}) + \eta_{14} Q_{14} \\ &= \Pi_{\text{HR}}(\mathbf{u}, \boldsymbol{\sigma}) + (1 + \eta_1)P_1 + \eta_3 P_2 + \eta_5 P_3 + \eta_7 P_4 + \eta_{10} P_5 \\ &\quad + \eta_8 P_6 + \eta_{11} P_7 + \eta_{12} P_8 + \eta_{14} P_9 \end{aligned} \quad (3-57)$$

This functional is the same as the functional (3-38).

(2) The degenerate case in which $\boldsymbol{\sigma}$ is excluded.

If we assume

$$\eta_4 = -1, \quad \eta_8 = 1, \quad \eta_1 = \eta_3 = \eta_5 = \eta_6 = \eta_{10} = \eta_{11} = \eta_{12} = \eta_{13} = \eta_{14} = 0$$

then the functional (3-55) degenerates into the following functional with two functional variables \mathbf{u} and $\boldsymbol{\varepsilon}$:

$$\begin{aligned} \Pi_{2L}(\mathbf{u}, \boldsymbol{\varepsilon}) &= (\Pi_{\text{HW}} - Q_4 + Q_8) + \eta_2 Q_2 + \eta_7 Q_7 + \eta_9 Q_9 \\ &= \Pi_2(\mathbf{u}, \boldsymbol{\varepsilon}) + \eta_2 S_1 + \eta_7 S_4 + \eta_9 S_5 \end{aligned} \quad (3-58)$$

This functional is a special case of the functional (3-47). If additional term $\gamma_2 S_2 + \gamma_3 S_3 + \gamma_6 S_6 + \gamma_7 S_7 + \gamma_8 S_8 + \gamma_9 S_9$ is added in the functional (3-55), then this functional may degenerate into the functional (3-47).

(3) The degenerate case in which $\boldsymbol{\varepsilon}$ and $\boldsymbol{\sigma}$ are excluded.

If we assume

$$\eta_2 = \eta_8 = \eta_9 = 1, \quad \eta_4 = -1, \quad \eta_1 = \eta_3 = \eta_5 = \eta_6 = \eta_{10} = \eta_{11} = \eta_{12} = \eta_{13} = \eta_{14} = 0$$

then the functional (3-55) degenerates into the following functional with single functional variable \mathbf{u} :

$$\Pi_{1L}(\mathbf{u}) = (\Pi_{\text{HW}} + Q_2 - Q_4 + Q_8 + Q_9) + \eta_7 Q_7 = \Pi_{1p}(\mathbf{u}) + \eta_7 R_2 \quad (3-59)$$

This functional is the same as the functional (3-35).

If the highest order of derivatives in the integrand is restricted, then two simple forms of the functional with three functional variables \mathbf{u} , $\boldsymbol{\varepsilon}$ and $\boldsymbol{\sigma}$ may be obtained as follows:

$$\Pi_{3L}(\mathbf{u}, \boldsymbol{\varepsilon}, \boldsymbol{\sigma}) = \Pi_{\text{HW}} + \eta_1 Q_1 + \eta_2 Q_2 + \eta_4 Q_4 + \eta_7 Q_7 + \eta_8 Q_8 + \eta_{11} Q_{11} + \eta_{12} Q_{12} \quad (3-60)$$

$$\Pi_{3L}(\mathbf{u}, \boldsymbol{\varepsilon}, \boldsymbol{\sigma}) = \Pi'_{\text{HW}} + \eta_1 Q_1 + \eta_3 Q_3 + \eta_5 Q_5 + \eta_7 Q_7 + \eta_8 Q_8 + \eta_{11} Q_{11} + \eta_{12} Q_{12} \quad (3-61)$$

In Eq. (3-60), \mathbf{u} is restricted to first order (in V) and zero order (on S), $\boldsymbol{\varepsilon}$ and $\boldsymbol{\sigma}$ to

zero order. In Eq. (3.61), σ is restricted to first order (in V) and zero order (on S), ε and u to zero order.

3.4 Variable-Substitution-Multiplier Method

3.4.1 Analysis of the Phenomenon of Losing Effectiveness for the Lagrange Multiplier Method

On the basis of the analysis of the phenomenon of losing effectiveness for the Lagrange multiplier method, the method of high-order Lagrange multiplier was proposed in reference [3].

The objective of the Lagrange multiplier method is to transfer the forced conditions of the original functional into the natural conditions of a new functional. The new functional can be established by absorbing the forced condition expressions of the original functional by means of the multiplier into the original functional. Hence, an essential prerequisite for the application of the Lagrange multiplier method is that the original functional must be a conditional functional, and the forced conditions must exist between the functional variables of the original functional. If this prerequisite is not satisfied, the Lagrange multiplier method will cease to be effective. In other words, the Lagrange multiplier method can only be used to transfer the forced conditions of the original functional into the natural conditions of the new functional, and cannot be used to transfer augmented or natural conditions of the original functional into the natural conditions of the new functional. In the three patterns of the functional transformation, the Lagrange multiplier method can be used only in pattern I but cannot be used in pattern II and pattern III.

Consequently, the question about the reason of losing effectiveness for the Lagrange multiplier method can be answered easily.

For example, by means of the Lagrange multiplier, it is impossible to absorb the stress-strain relation into the Hellinger-Reissner functional Π_{HR} to establish a new functional, since the prerequisite for the application of the Lagrange multiplier method is not satisfied in this case. In fact, strain ε is an augmented variable and not a functional variable of the original functional $\Pi_{HR}(u, \sigma)$; the stress-strain relation between ε and σ is an augmented condition and not a forced condition. An attempt to relax the augmented condition of the original functional by means of the Lagrange multiplier method is doomed to fail.

For another example, it is also impossible to absorb the stress-strain relation into the Hu-Washizu functional Π_{HW} by means of the Lagrange multiplier to establish a new functional, since this relation is a natural condition and not a forced condition of the original functional.

3.4.2 Variable-Substitution-Multiplier Method

It was pointed out in [3] that there are two limitations of the Lagrange multiplier method: ① it is impossible to derive the Hellinger-Reissner principle directly from the potential energy principle; ② it is impossible to derive the Hu-Washizu principle directly from the complementary energy principle.

In order to overcome these limitations of the Lagrange multiplier method, the variable-substitution-multiplier method was proposed in [1, 2]. One limitation of the Lagrange multiplier method is that it is impossible to relax the augmented condition of the original functional and to absorb it to establish the new functional. To surmount the difficulty, the variable-substitution-multiplier method, which consists of two steps, may be used. The first step is the substitution of variables—by means of the augmented condition, the functional variable of the original functional is substituted by the augmented variable, and then a transitional functional is obtained. Now, the augmented condition of the original functional is transferred into the forced condition of this transitional functional. The second step is to apply the Lagrange multiplier method—by means of the multiplier the forced condition is transferred into the natural condition of the new functional. After these two steps, the augmented condition of the original functional is absorbed to establish the new functional.

Example 3.3 Derive the Hellinger-Reissner functional $\Pi_{\text{HR}}(\mathbf{u}, \boldsymbol{\sigma})$ from the functional $\Pi_p(\mathbf{u})$ of the potential energy principle by means of the variable-substitution-multiplier method.

Solution The functional of the potential energy principle is

$$\Pi_p(\mathbf{u}) = \iiint_V \left[\frac{1}{2} (\boldsymbol{\partial}^T \mathbf{u})^T \mathbf{E} (\boldsymbol{\partial}^T \mathbf{u}) - \bar{\mathbf{F}}^T \mathbf{u} \right] dV - \iint_{S_\sigma} \bar{\mathbf{T}}^T \mathbf{u} dS \quad (3-62)$$

The forced condition is

$$\mathbf{u} - \bar{\mathbf{u}} = \mathbf{0} \quad (\text{on } S_u) \quad (3-63)$$

The augmented condition is

$$\boldsymbol{\partial}^T \mathbf{u} - \mathbf{G}\boldsymbol{\sigma} = \mathbf{0} \quad (\text{in } V) \quad (3-64)$$

Firstly, substituting the augmented condition (3-64) into the original functional (3-62), we have the following transitional functional:

$$\Pi(\mathbf{u}, \boldsymbol{\sigma}) = \iiint_V \left[\frac{1}{2} (\boldsymbol{\sigma}^T \mathbf{G}\boldsymbol{\sigma} - \bar{\mathbf{F}}^T \mathbf{u}) \right] dV - \iint_{S_\sigma} \bar{\mathbf{T}}^T \mathbf{u} dS \quad (3-65)$$

Here, Eqs. (3-63) and (3-64) are forced conditions.

Secondly, by means of multiplier $\boldsymbol{\sigma}$ and multiplier $-\mathbf{T} = -\mathbf{L}\boldsymbol{\sigma}$, Eqs. (3-64) and (3-63) are absorbed to establish the new functional. This new functional

is $\Pi_{\text{HR}}(\mathbf{u}, \boldsymbol{\sigma})$:

$$\begin{aligned} \Pi_{\text{HR}}(\mathbf{u}, \boldsymbol{\sigma}) = & \iiint_V \left[\frac{1}{2} \boldsymbol{\sigma}^T \mathbf{G} \boldsymbol{\sigma} - \bar{\mathbf{F}}^T \mathbf{u} \right] dV - \iint_{S_\sigma} \bar{\mathbf{T}}^T \mathbf{u} dS \\ & + \iiint_V \boldsymbol{\sigma}^T (\partial^T \mathbf{u} - \mathbf{G} \boldsymbol{\sigma}) dV - \iint_{S_u} \mathbf{T}^T (\mathbf{u} - \bar{\mathbf{u}}) dS \end{aligned} \quad (3-66)$$

Similarly, by means of the variable-substitution-multiplier method, the Hu-Washizu functional can also be derived from the functional of complementary energy principle.

References

- [1] Long YQ (1986) Several patterns of functional transformation and generalized variational principle with several arbitrary parameters. *International Journal of Solids and Structures* 22(10): 1059 – 1069
- [2] Long YQ (1987) Generalized variational principles with several arbitrary parameters and the variable substitution and multiplier method. *Applied mathematics and Mechanics (English Edition)* 8(7): 617 – 629
- [3] Chien WZ (1983) Method of high-order Lagrange multiplier and generalized variational principles of elasticity with more general forms of functionals. *Applied mathematics and Mechanics (English Edition)* 4(2): 143 – 157
- [4] Xiong ZH, Liu ZT (1988) *Variational principles in elasticity*. Hunan University Press, Changsha, pp88 – 99 (in Chinese)
- [5] DU QH et al (1994) (eds) *An encyclopedia of engineering mechanics*. Higher Education Press, Beijing, pp2304 – 2306 (in Chinese)
- [6] Wang HD, Wu DL (1997) *The finite element method and its computational program*. China Architecture & Building Press, Beijing, pp227 – 232 (in Chinese)
- [7] Zienkiewicz OC (1974) Constrained variational principles and penalty function methods in finite element analysis. In: *Lecture Notes in Mathematics*. Springer-Verlag, Berlin, 363: pp207 – 214
- [8] Wu CC, Pian THH (1997) *Incompatible numerical analysis and hybrid finite element method*. Science Press, Beijing, pp118 – 121 (in Chinese)
- [9] Long ZF, Cen S, Long YQ, Luo JH (2004) Hamiltonian variational principle with arbitrary parameters for thin plates. *Gong Cheng Li Xue/Engineering Mechanics* 21(4): 1 – 5 (in Chinese)
- [10] Hu HC (1992) On the connections between the functionals of equivalent variational principles. *Acta Mechanica Solida Sinica (English Edition)* 5(2): 175 – 182

PART II

Advances in Finite Element Method —Generalized Conforming Elements

- Chapter 4** Generalized Conforming Element Theory
- Chapter 5** Generalized Conforming Thin Plate Element I—Introduction
- Chapter 6** Generalized Conforming Thin Plate Element II—Line-Point and SemiLoof Conforming Schemes
- Chapter 7** Generalized Conforming Thin Plate Element III—Perimeter-Point and Least-Square Conforming Schemes
- Chapter 8** Generalized Conforming Thick Plate Element
- Chapter 9** Generalized Conforming Element for the Analysis of the Laminated Composite Plates
- Chapter 10** Generalized Conforming Element for the Analysis of Piezoelectric Laminated Composite Plates
- Chapter 11** Generalized Conforming Membrane and Shell Elements

Chapter 4 Generalized Conforming Element Theory

Yu-Qiu Long

Department of Civil Engineering, School of Civil Engineering,
Tsinghua University, Beijing, 100084, China

Ke-Gui Xin

Department of Civil Engineering, School of Civil Engineering,
Tsinghua University, Beijing, 100084, China

Abstract As the beginning of Part II, this chapter discusses the fundamental theory and existing construction modes of generalized conforming finite element method. First, by discussion on the different characters of conforming and nonconforming elements, the background and need for the development of the generalized conforming element are described. Second, as an example, the earliest pattern of the generalized conforming element and its excellent performance are exhibited. Third, some theoretical features of the generalized conforming element, including duality of its variational principle basis, flexibility, multiformity and convergence, are discussed in detail.

Keywords finite element, generalized conforming element, conforming, nonconforming, convergence.

4.1 Introduction

This chapter discusses the fundamental theory and construction modes of generalized conforming finite element method^[1-3]. The applications of generalized conforming element method for thin plate, thick plate, laminated composite plate, piezoelectric laminated composite plate, membrane and thin shell will be introduced in Chap. 5 to Chap. 11, respectively.

Generalized conforming element method is a new technique which was developed from the basis of comparison and analysis of conforming and nonconforming element methods. The core problem, which is also the main difference between these three types of displacement-based elements, is the requirement for the displacement compatibility between two adjacent elements.

Generalized conforming element is a kind of limit conforming element which

can ensure convergence: for a coarse mesh, it belongs to nonconforming elements; and for a refined mesh divided by infinite elements, it approaches conforming models.

Variational principle corresponding to the generalized conforming element possesses duality: it starts from the sub-region potential energy principle, and ends with the minimum potential energy principle.

The feature of the generalized conforming method is that it is a combination of energy method and weighted residual method: if the essential generalized conforming conditions are satisfied, the point conforming conditions, line conforming conditions, perimeter conforming conditions can be flexibly applied. Therefore, the generalized conforming method has both flexibility and multiformity.

4.2 Conforming and Nonconforming Elements—Some Consideration about “Conforming”

We have known that the earliest finite element model is displacement-based model, and the earliest displacement-based element is conforming (compatible) element. The theoretical basis of these conforming elements is the minimum potential energy principle, in which displacement is taken as the field variable of energy functional. And the displacement fields of two adjacent elements are required to be conforming exactly at the interface. The name *conforming element* reflects this main feature.

Though the conforming element possesses the longest history, and has an important advantage of ensuring convergence, there are still some embarrassing problems left to solve. For examples, the requirement of exactly conforming is not easy to be satisfied; the performance of the element may be over-stiff in some occasions, and so on. When the conforming element method is used to deal with thin plate/shell problem, which is a kind of C_1 -continuity problem (i.e., the displacement and its first derivative are both required to be compatible between two adjacent elements), the above shortcomings will be especially noticeable. Thereupon, the nonconforming element method was proposed^[4] for overcoming these disadvantages. In this method, only the nodal conforming conditions are required while the exact compatibility between the displacement fields of adjacent elements is not required. And the minimum potential energy principle is still taken as its theoretical start point. Elements constructed by this strategy can exhibit some merits: the relaxed conforming conditions are easier to satisfy; and the accuracy of some nonconforming elements is much better than that of conforming ones. However, some nonconforming models can not converge to correct solutions, which is a fatal defect.

Table 4.1 The contradistinction between conforming and nonconforming elements

	Conforming element	Nonconforming element
Compatibility requirement	Exact compatibility	Inexact compatibility
Variational principle	Minimum potential energy principle: total potential energy $\Pi_p =$ stationary	
Advantages	Simple functional Π_p (contains only single variable: displacement)	
	Convergence ensured	Easily assumed displacement field; and better accuracy in some occasions
Disadvantages	Exact compatibility is not easy to satisfy; element performance is often over-stiff	Convergence can not be ensured

Generalized conforming element is developed on the basis of conforming and nonconforming elements. To understand its background, a comparison should be performed first between conforming and nonconforming elements (Table 4.1). Then, the “puzzle of compatibility” is analyzed and taken into account.

Puzzle of “conforming conditions”

Puzzles: two questions “why”?

- { Why the accuracy of conforming elements is not as good as that of some nonconforming elements?
- { Why some nonconforming elements are not convergent?

Solutions: The requirement of conformity should be moderate and appropriate.

- { The requirement of conforming element is too severe—It is difficult to be satisfied and leads to over-stiff performance.
- { Since the threshold level is too high, it excludes many excellent element models as unacceptable ones.
- { The requirement of nonconforming element is over-relaxed—it can not ensure the convergence.
- { Example: The nonconforming thin plate element BCIZ^[4] can not ensure the convergence.
- { Source: The minimum potential energy principle is not a proper principle to formulate the nonconforming element.
- { ⇒A moderate and rational requirement of conformity is needed—This is the background for creation of the generalized conforming element.

4.3 The First Pattern of Generalized Conforming Element —Replacing Nodal Conforming by Line Conforming Conditions

The first pattern of generalized conforming element was proposed in 1987^[1], in which the new concepts of generalized conforming element and generalized

conforming conditions were established by replacing nodal conforming conditions at element nodes by line conforming conditions of average displacement along each element side. As an example, the triangular generalized conforming thin plate bending element TGC in references [1, 2] utilized the following generalized conforming conditions of average displacements (average deflection, tangent and normal average rotations) along each element side:

$$\left. \begin{aligned} \int_{S_k} (w - \tilde{w}) ds &= 0 \\ \int_{S_k} \left(\frac{\partial w}{\partial n} - \tilde{\psi}_n \right) ds &= 0 \\ \int_{S_k} \left(\frac{\partial w}{\partial s} - \tilde{\psi}_s \right) ds &= 0 \end{aligned} \right\} \quad (\text{along each element side } S_k) \quad (4-1)$$

where w is the deflection function of the element; \tilde{w} , $\tilde{\psi}_n$ and $\tilde{\psi}_s$ are the deflection, tangent and normal rotations along each element side, respectively.

In a traditional pattern, the following nodal conforming conditions

$$\left. \begin{aligned} (w - \tilde{w})_j &= 0 \\ \left(\frac{\partial w}{\partial x} - \tilde{\psi}_x \right)_j &= 0 \\ \left(\frac{\partial w}{\partial y} - \tilde{\psi}_y \right)_j &= 0 \end{aligned} \right\} \quad (\text{at node } j) \quad (4-2)$$

at element nodes are usually used.

The main difference between the generalized conforming element method and the traditional pattern of nonconforming element method is that the former uses Eq. (4-1) instead of Eq. (4-2). In other words, the traditional method emphasizes nodal conforming conditions at nodes, so it is hard to simultaneously satisfy line conforming conditions along each side. On the contrary, the generalized conforming element method pays attention to average displacement conforming conditions of each element side, so it can ensure a kind of limit conforming conditions along each side when the mesh is refined gradually. This is the reason why the generalized conforming element method can ensure the convergence, but traditional nonconforming element scheme can not.

In reference [1], the performance of the generalized conforming element TGC was compared with those of other famous element models, i.e., DKT^[5, 6], HSM^[5, 7], BCIZ^[4] and HCT^[8]. The variations of computation errors with mesh number N for central deflection w_C and central bending moment M_{yC} of a clamped square plate subjected to uniform load are plotted in Fig. 4.1 and Fig. 4.2. It can be seen that the precision of element TGC is the best.

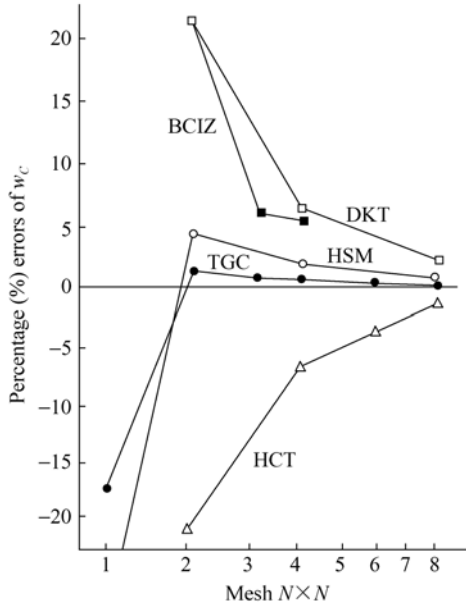


Figure 4.1 Errors for central deflection of a clamped square plate subjected to uniform load

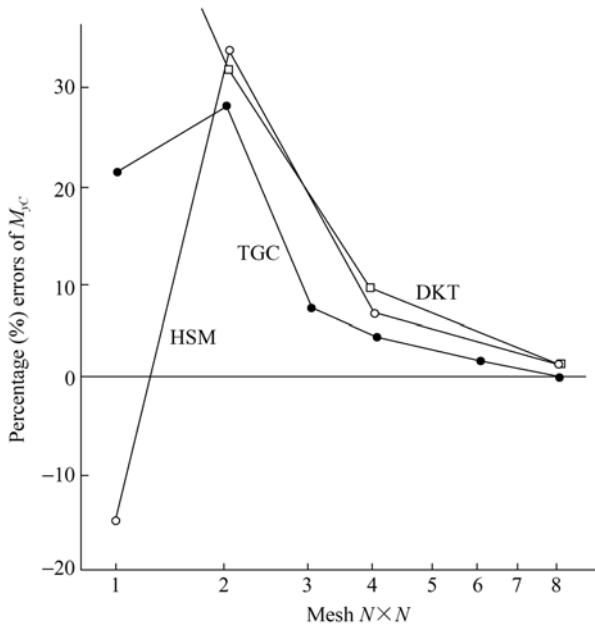


Figure 4.2 Errors for central moment of a clamped square plate subjected to uniform load

4.4 The Variational Basis of Generalized Conforming Element—Duality

Variational principle is the starting point for deriving finite element method. The variational principles corresponding to conforming element, nonconforming element and generalized conforming element as an example for a thin plate bending problem are listed as follows. A clearer understanding for the characters and advantages of generalized conforming element may be obtained by contrasting these three types of elements.

4.4.1 The Variational Principle Corresponding to Conforming Element

Compatibility requirement: In thin plate conforming element, the deflection field $w(x, y)$ must be exactly compatible with deflection \tilde{w} , normal rotation $\tilde{\psi}_n$ and tangent rotation $\tilde{\psi}_s$ along each element side, i.e., at each point of element boundary ∂A^e the following conforming conditions

$$w = \tilde{w}, \quad \frac{\partial w}{\partial n} = \tilde{\psi}_n, \quad \frac{\partial w}{\partial s} = \tilde{\psi}_s \quad (\text{at each point of } \partial A^e) \quad (4-3)$$

must be satisfied precisely.

Variational principle used: The minimum potential energy is the starting point of the conforming element, and its functional Π_p can be written as

$$\Pi_p = \sum_e \Pi_p^e = \sum_e \iint_{A^e} \frac{D}{2} \left\{ \left(\frac{\partial^2 w}{\partial x^2} + \frac{\partial^2 w}{\partial y^2} \right)^2 + 2(1 - \mu) \left[\left(\frac{\partial^2 w}{\partial x \partial y} \right)^2 - \frac{\partial^2 w}{\partial x^2} \frac{\partial^2 w}{\partial y^2} \right] \right\} dA \quad (4-4)$$

where \sum_e denotes the sum of each element e ; D is the bending stiffness of thin plate; μ is the Poisson's ratio. Since in the potential energy Π_p displacement w is the only field variable, Π_p is called a single-field functional. Compared with multi-field functionals, single-field functional is particularly simple.

Disadvantage & advantage: Since the conforming requirement is too severe, it leads to over-stiff performance and the displacement field is difficult to assume. However, the functional is quite simple, and convergence can be guaranteed.

4.4.2 The Variational Principle Corresponding to Nonconforming Element

Compatibility requirement: In nonconforming element, the element deflection field $w(x, y)$ is not required to be exactly compatible, so the conforming conditions (4-3) between elements are relaxed or partially relaxed.

Variational principle used: In order to ensure convergence, the sub-region potential energy principle^[9, 10] (refer to Chap. 2) or modified potential energy principle^[11] must be employed.

Its functional is the sub-region potential energy Π_{mp}

$$\Pi_{mp} = \sum_e (\Pi_p^e + H) \tag{4-5}$$

where H is the additional energy corresponding to incompatible displacement along element boundary

$$H = \oint_{\partial A^e} \left[M_n \left(\frac{\partial w}{\partial n} - \tilde{\psi}_n \right) + M_{ns} \left(\frac{\partial w}{\partial s} - \tilde{\psi}_s \right) - Q_n (w - \tilde{w}) \right] ds \tag{4-6}$$

in which M_n , M_{ns} and Q_n are the Lagrange multipliers, denoting boundary forces. It is worthy of note that, the functional Π_{mp} contains two field variables, displacement and boundary force, which is much more complicated than Π_p with single-field variable. For simplicity, some authors still use potential energy functional Π_p instead of sub-region potential energy functional Π_{mp} when they are constructing nonconforming elements, thereby convergence can not be ensured.

Advantage & disadvantage: The deflection field is easy to assume; however, the functional Π_{mp} is more complicated. If the simplified functional Π_p is improperly employed, convergence will not be guaranteed.

4.4.3 The Variational Principle Corresponding to Generalized Conforming Element

Duality is the feature of generalized conforming element and its variational principle.

Generalized conforming element possesses duality. It is a kind of limit conforming element:

- { For a coarse mesh—It belongs to nonconforming element
- { For a refined mesh divided by infinite elements—It tends to be conforming element

The variational principle corresponding to generalized conforming element also possesses duality. It is a kind of degenerated potential energy principle:

- ⎧ Start point—sub-region potential energy principle: $\Pi_{mp} = \Pi_p + H = \text{stationary}$
 - ⎨ End-result—degenerated potential energy principle: $\Pi_p = \text{stationary}$
- The degenerate condition introduced—generalized conforming condition:

$$H \rightarrow 0 (\Pi_{mp} \rightarrow \Pi_p)$$

The duality of generalized conforming element and its variational principle can also be described in details as follows:

Compatibility requirement: Since the conforming conditions (4-3) are relaxed, the deflection field is easy to assume.

The initial variational principle: In order to ensure convergence, the sub-region potential energy principle is taken as the starting point. However, its functional Π_{mp} is more complicated because it is a two-field -functional.

The degenerate conditions introduced: For simplicity, the two-field-functional Π_{mp} is replaced by its degenerate form—the single-field-functional Π_p . Therefore, following generalized conforming conditions are introduced:

$$H \rightarrow 0 \quad (\text{for any refined mesh divided by infinite elements}) \quad (4-7)$$

or

$$H = 0 \quad (\text{for any constant strain or rigid-body displacement state}) \quad (4-8)$$

When the curvatures of the displacement field tend to be constants, the generalized conforming conditions (4-8) can be written as

$$\oint_{\partial A^e} \left[M_n \left(\frac{\partial w}{\partial n} - \tilde{\psi}_n \right) + M_{ns} \left(\frac{\partial w}{\partial s} - \tilde{\psi}_s \right) - Q_n (w - \tilde{w}) \right] ds = 0 \quad (4-9)$$

(M_n , M_{ns} and Q_n are corresponding to the constant stress state)

The ending variational principle: Since the generalized conforming conditions (4-8) are introduced, the two-field-functional Π_{mp} will degenerate to the single-field-functional Π_p . Then the final variational principle used in practice is the degenerate potential energy principle

$$\Pi_p = \text{stationary} \quad (4-10)$$

Advantages: The deflection field is easy to assume, and the variational principle used in practice is still the single-field-functional Π_p , which is very simple; since the sub-region potential energy principle is taken as the starting point, convergence can be guaranteed. Hereby, both advantages of convenience and convergence are available because of generalized conforming conditions (4-7) or (4-8).

4.4.4 Some Discussions

The key problems for constructing displacement-based elements are how to

rationally deal with compatibility problem between elements and how to rationally select a corresponding variational principle.

Conforming element starts from the minimum potential principle. Thereby, the displacement between elements must be exactly compatible. For conforming models, the functional Π_p is simple (since Π_p is a single-field-functional) while the displacement field is difficult to assume.

Nonconforming element does not require exact compatibility. Thereby, it must start from the sub-region potential energy principle. For nonconforming models, the displacement field is easy to assume, but functional Π_{mp} is complicated (since Π_{mp} is a multi-field-functional). Some workers still take the minimum potential principle as the starting point. This strategy is illegal and leads to non-convergence.

Generalized conforming element does not require exact compatibility either. Thereby, in theory, it also must start from the multi-field-functional Π_{mp} . On the other hand, since the generalized conforming conditions (4-8) are introduced, functional Π_{mp} will return to its degenerate form—single-field-functional Π_p in practice. Thus, for generalized conforming models, the displacement field is easy to assume while the functional Π_p is very simple in operation. It represents the best of both worlds and is never illegal. Thus, it can be concluded that generalized conforming method is the first successful attempt for applying the degenerate functional.

4.5 The Synthesis of Energy Method and Weighted Residual Method—Flexibility

Generalized conforming element method can be looked upon as a combination of energy method and weighted residual method^[12]. In fact, generalized conforming condition (4-9) can be looked upon as a weighted residual equation, in which boundary forces M_n , M_{ns} and Q_n are weighting functions, i.e.,

$$\oint_{\partial A^e} \left[M_n \left(\frac{\partial w}{\partial n} - \tilde{\psi}_n \right) + M_{ns} \left(\frac{\partial w}{\partial s} - \tilde{\psi}_s \right) - Q_n (w - \tilde{w}) \right] ds = 0 \quad (4-11)$$

(M_n , M_{ns} and Q_n are weighting functions)

If weighting functions M_n , M_{ns} and Q_n are assumed to be arbitrary functions, the weighted residual Eq. (4-11) will be equivalent to the boundary conforming conditions (4-3), which corresponds to the exactly compatible case.

If weighting functions M_n , M_{ns} and Q_n are assumed to contain only n arbitrary parameters, the weighted residual Eq. (4-11) will be equivalent to n conforming conditions in integral form. Generally, this corresponds to the approximate conforming case. If different weighting functions are selected, the corresponding weighted residual equation will represent conforming conditions with different

physical meanings. Table 4.2 lists physical meanings of several commonly used weighting functions and their corresponding weighted residual equations.

Table 4.2 The physical meanings of weighting functions and their weighted residual equations in common use

Weighting functions in common use	Physical meanings of the weighted residual equations
Concentrated force } Concentrated couple } at a point	Point conforming { deflection rotation
Uniform load } High order load } along a side	Line conforming { average high order
Constant stress } High order stress } along perimeter	Perimeter conforming { constant stress high order stress

It can be seen from Table 4.2 and Eq. (4-11) that, unlike the traditional method in which only the nodal conforming conditions are used, generalized conforming element method possesses great flexibility. It allows to choose various conditions, including point conforming, line conforming, perimeter conforming conditions and their combination forms. For convergence, the conditions employed in the generalized conforming element method should at least contain the fundamental generalized conforming conditions. i.e., the generalized conforming conditions or their equivalent conditions for constant strain and rigid-body displacement states of an element.

Since generalized conforming conditions can be explained as the weighted residual Eq. (4-11) along element boundary perimeter ∂A^e , then when establishing generalized conforming conditions, one can flexibly employ five conventional classical methods in a weighted residual method:

Collocation method, Sub-domain method, Least square method, Galerkin method, Method of moment

In fact, the usual methods for constructing generalized conforming elements in literature are the applications and generalizations of the above classical weighted residual methods, for example,

Line conforming method—Application of Sub-domain method

Perimeter conforming method—Applied on the boundary perimeter, which is similar to the method of moments

Least square conforming method—Application of Least square method

Point conforming method—In the conventional point conforming method, the element nodes are taken as collocation points; besides, there is still SemiLoof

point conforming method in which the Gauss points at element boundary are taken as collocation points. All these belong to applications of Collocation method.

The combination forms of the above methods can also be used.

4.6 The Convergence of Generalized Conforming Element

From the viewpoint of mechanics, if the fundamental generalized conforming conditions, i.e. the generalized conforming conditions for constant strain and rigid-body displacement states of an element, have been already satisfied when constructing generalized conforming elements, the convergence can be guaranteed. Numerous numerical examples have demonstrated this.

For convergence of the generalized conforming element TGC^[1], Shi Zhongci et al. presented a strict mathematical proof^[13]. Moreover, Shi Zhongci also discussed the accuracy of the generalized conforming element TGC^[14], and pointed out that the accuracy of element TGC is higher than those of elements BCIZ^[4] and Specht^[15].

In reference [16], Shi Zhongci proposed the FEM test and its test conditions for testing the convergence of nonconforming elements. By applying the test conditions, the convergence and uniqueness for the solutions of the line conforming and perimeter conforming modes were demonstrated^[17].

References

- [1] Long YQ, Xin KG (1987) Generalized conforming element. *Tumu Gongcheng Xuebao/China Civil Engineering Journal* 20(1): 1 – 14 (in Chinese)
- [2] Long YQ, Xin KG (1989) Generalized conforming element for bending and buckling analysis of plates. *Finite Elements in Analysis and Design* 5: 15 – 30
- [3] Long YQ, Long ZF, Xu Y (1997) The generalized conforming element (GCE)-theory and applications. *Advances in Structural Engineering* 1(1): 63 – 70
- [4] Bazeley GP, Cheung YK, Irons BM, Zienkiewicz OC (1965) Triangular elements in bending-conforming and nonconforming solution. In: *Proceedings of the Conference on Matrix Methods in Structural Mechanics*. Air Force Institute of Technology, Ohio: Wright-Patterson A. F. Base, pp547 – 576
- [5] Batoz JL, Bathe KJ, Ho LW (1980) A study of three-node triangular plate bending elements. *International Journal for Numerical Methods in Engineering* 15: 1771 – 1812
- [6] Stricklin JA, Haisler WE, Tisdale PR, Gunderson R (1969) A rapidly converging triangular plate element. *AIAA Journal* 7: 180 – 181
- [7] Allman DJ (1971) Triangular finite element plate bending with constant and linearly varying bending moments. In: BF de Veubeke (ed) *High Speed Computing of Elastic Structures*. Liege, Belgium, pp105 – 136

Advanced Finite Element Method in Structural Engineering

- [8] Clough R W, Tocher J L (1965) Finite element stiffness matrices for analysis of plate bending. In: Proceedings of the Conference on Matrix Methods in Structural Mechanics. Air Force Institute of Technology, Ohio: Wright-Patterson A. F. Base, pp515 – 545
- [9] Long YQ, Zhi BC, Yuan S (1982) Sub-region, sub-item and sub-layer generalized variational principles in elasticity. In: He GQ et al. (eds) Proceedings of International Conference on FEM, Shanghai Science Press, pp607 – 609
- [10] Long YQ (1987) Sub-region generalized variational principles in elastic thin plates. In: Yeh KY (eds) Progress in Applied Mechanics. Martinus Nijhoff Publishers, pp121 – 134
- [11] Washizu K (1968, 1975, 1982) Variational methods in elasticity and plasticity. 1st edn, 2nd edn, 3rd edn. Pergamon Press
- [12] Long YQ, Zhao JQ (1992) Combined application of the energy method and the weighted residual method—a new way to construct the finite elements. Chinese Journal of Aeronautics 5(2): 130 – 136
- [13] Shi ZC, Chen SC (1991) Convergence of a nine parameter generalized conforming element. Ji Suan Shu Xue/Mathematica Numerica Sinica 13(2): 193 – 203 (in Chinese)
- [14] Shi ZC (1990) On the accuracy of the quasi-conforming and generalized conforming finite elements. Chinese Annals of Mathematics Series B 11(2): 148 – 155
- [15] Specht B (1988) Modified shape functions for the three-node plate bending element passing the patch test. International Journal for Numerical Methods in Engineering 26: 705 – 715
- [16] Shi ZC (1987) The FEM test for convergence of nonconforming finite element. Mathematics of Computation 49: 391 – 405
- [17] Li JX, Long YQ (1996) The convergence of the generalized conforming element method. Gong Cheng Li Xue/Engineering Mechanics 13(1): 75 – 80 (in Chinese)

Chapter 5 Generalized Conforming Thin Plate Element I—Introduction

Zhi-Fei Long

School of Mechanics & Civil Engineering, China University of Mining & Technology, Beijing, 100083, China

Song Cen

Department of Engineering Mechanics, School of Aerospace, Tsinghua University, Beijing, 100084, China

Abstract This chapter presents a brief summary of the construction methods of the generalized conforming thin plate elements. Following the Introduction in Sect. 5.1, the generalized conforming conditions and their equivalent forms for the thin plate elements are derived in Sect. 5.2. Then, Sect. 5.3 presents the general formulations of the generalized conforming thin plate element. And subsequently, five construction scheme groups of the generalized conforming thin plate elements are proposed in Sect. 5.4. Finally, a collection of the recent generalized conforming thin plate elements is provided in Sect. 5.5.

Keywords thin plate element, generalized conforming, construction scheme.

5.1 Introduction

This chapter firstly gives a review of the construction methods of the generalized conforming thin plate elements. Then, several construction schemes will be discussed in details in Chaps. 6 and 7.

The classical Kirchhoff thin plate theory is generally taken as the theoretical basis for the construction of the thin plate bending elements. It introduces a straight normal assumption, and neglects the effects due to transverse shear deformation. In displacement-based conforming thin plate elements, since they require C_1 continuity between two adjacent elements, their construction procedures are more complicated than those in C_0 problems. In addition, there still are other types of thin plate element models, such as non-conforming elements, quasi-conforming elements, and hybrid mixed elements, and so on.

Universal element models for the analysis of both thick and thin plates can also be developed, in which the thin plate element is only a special case of them. Here, the theoretical basis will be changed to the Reissner-Mindlin plate theory, which considers the effects due to transverse shear deformation, and assumes that the original normal of the plate mid-surface will still keep straight but not be normal to the plate mid-surface anymore after deformation. Some elements based on the Reissner-Mindlin theory actually are not universal element models for both thick and thin plates, because they have good accuracy only for thick plate cases but exhibit an over-stiff performance for thin plate cases. This is the *shear locking* phenomenon which leads to far small deflection results in the thin plate analysis.

There are numerous thin plate bending elements proposed in literatures, detailed reviews on this topic can be found in^[1-3].

A good thin plate bending element should possess the following properties:

- (1) It can converge to exact solution, and pass the patch test.
- (2) It has no spurious zero-energy modes except for rigid-body displacement modes.
- (3) It has high precision and is insensitive to mesh distortion.
- (4) The shear locking phenomenon will not happen when analyzing thin plates by the elements based on the Reissner-Mindlin plate theory.
- (5) The formulations and degrees of freedom (DOFs) are relatively simple; only engineering DOFs (nodal deflection w , and nodal rotations ψ_x and ψ_y) are used.

The generalized conforming element method provides a new effective way for constructing excellent thin plate bending elements.

5.2 The Generalized Conforming Conditions and Their Equivalent Forms for Thin Plate Elements

For the thin plate bending elements, the exact forms of conforming conditions between the elements are given by Eq. (4-3), i.e.,

$$w = \tilde{w}, \quad \frac{\partial w}{\partial n} = \tilde{\psi}_n, \quad \frac{\partial w}{\partial s} = \tilde{\psi}_s \quad (\text{at each point on } \partial A^e) \quad (5-1)$$

in which $w(x, y)$ is the deflection field; \tilde{w} , $\tilde{\psi}_n$ and $\tilde{\psi}_s$ are the deflection, normal and tangent slopes along element boundary ∂A^e , respectively.

In integration form, the generalized conforming conditions given by Eq. (4-11) can be written as:

$$\oint_{\partial A^e} \left[M_n \left(\frac{\partial w}{\partial n} - \tilde{\psi}_n \right) + M_{ns} \left(\frac{\partial w}{\partial s} - \tilde{\psi}_s \right) - Q_n (w - \tilde{w}) \right] ds = 0 \quad (5-2a)$$

where weighting functions M_n , M_{ns} and Q_n denote boundary forces, i.e., the bending moment, twisting moment and transverse shear force along the element boundary.

Two equivalent forms can also be derived from Eq. (5-2a):

$$\oint_{\partial A^e} \left[M_n \left(\frac{\partial w}{\partial n} - \tilde{\psi}_n \right) - \left(Q_n + \frac{\partial M_{ns}}{\partial s} \right) (w - \tilde{w}) \right] ds - \sum_J (\Delta M_{ns}) (w - \tilde{w}) = 0 \quad (5-2b)$$

$$\iint_{A^e} \left(M_x \frac{\partial^2 w}{\partial x^2} + M_y \frac{\partial^2 w}{\partial y^2} + 2M_{xy} \frac{\partial^2 w}{\partial x \partial y} \right) dA - \oint_{\partial A^e} (M_n \tilde{\psi}_n + M_{ns} \tilde{\psi}_s - Q_n \tilde{w}) ds = 0 \quad (5-2c)$$

In Eq. (5-2c), the internal moments M_x , M_y and M_{xy} satisfy the following formula for homogeneous equilibrium equation:

$$\frac{\partial^2 M_x}{\partial x^2} + \frac{\partial^2 M_y}{\partial y^2} + 2 \frac{\partial^2 M_{xy}}{\partial x \partial y} = 0 \quad (5-3)$$

Firstly, in order to derive Eq. (5-2b), the following formula for integration by parts is needed:

$$\oint_{\partial A^e} M_{ns} \frac{\partial}{\partial s} (w - \tilde{w}) ds = - \oint_{\partial A^e} (w - \tilde{w}) \frac{\partial M_{ns}}{\partial s} ds - \sum_J (w - \tilde{w})_J (\Delta M_{ns})_J \quad (5-4)$$

where J denotes the corner node on boundary ∂A^e ; $(\Delta M_{ns})_J$ denotes the increment of the twisting moment M_{ns} crossing the corner node J :

$$(\Delta M_{ns})_J = (M_{ns})_{J_+} - (M_{ns})_{J_-} \quad (5-5)$$

Substitution of Eq. (5-4) into Eq. (5-2a) yields Eq. (5-2b).

Secondly, in order to derive Eq. (5-2c), the following formula for integration by parts is needed:

$$\begin{aligned} & \iint_{A^e} \left[M_x \frac{\partial^2 w}{\partial x^2} + M_y \frac{\partial^2 w}{\partial y^2} + 2M_{xy} \frac{\partial^2 w}{\partial x \partial y} \right] dx dy \\ &= \iint_{A^e} \left(\frac{\partial^2 M_x}{\partial x^2} + \frac{\partial^2 M_y}{\partial y^2} + 2 \frac{\partial^2 M_{xy}}{\partial x \partial y} \right) w dx dy + \oint_{\partial A^e} \left(M_n \frac{\partial w}{\partial n} + M_{ns} \frac{\partial w}{\partial s} - Q_n w \right) ds \end{aligned} \quad (5-6)$$

Substitution of Eq. (5-3) into Eq. (5-6) yields

$$\iint_{A^e} \left[M_x \frac{\partial^2 w}{\partial x^2} + M_y \frac{\partial^2 w}{\partial y^2} + 2M_{xy} \frac{\partial^2 w}{\partial x \partial y} \right] dx dy = \oint_{\partial A^e} \left(M_n \frac{\partial w}{\partial n} + M_{ns} \frac{\partial w}{\partial s} - Q_n w \right) ds \quad (5-7)$$

Then, substitution of Eq. (5-7) into Eq. (5-2a) yields Eq. (5-2c).

The proof of the formula for integration by parts (5-6) is given as follows:

Proof Let l and m be the direction cosines of the outer normal along the boundary. Then, the boundary forces Q_n , M_n and M_{ns} can be expressed in terms of internal moments M_x , M_y and M_{xy} :

$$Q_n = l \left(\frac{\partial M_x}{\partial x} + \frac{\partial M_{xy}}{\partial y} \right) + m \left(\frac{\partial M_{xy}}{\partial x} + \frac{\partial M_y}{\partial y} \right) \quad (5-8a)$$

$$M_n = l^2 M_x + m^2 M_y + 2lm M_{xy} \quad (5-8b)$$

$$M_{ns} = lm(-M_x + M_y) + (l^2 - m^2) M_{xy} \quad (5-8c)$$

And, the derivatives $\frac{\partial w}{\partial n}$ and $\frac{\partial w}{\partial s}$ with respect to normal and tangent directions of the boundary can be expressed in terms of $\frac{\partial w}{\partial x}$ and $\frac{\partial w}{\partial y}$:

$$\begin{aligned} \frac{\partial w}{\partial n} &= l \frac{\partial w}{\partial x} + m \frac{\partial w}{\partial y} \\ \frac{\partial w}{\partial s} &= -m \frac{\partial w}{\partial x} + l \frac{\partial w}{\partial y} \end{aligned} \quad (5-9)$$

From the above two equations, we can obtain

$$M_n \frac{\partial w}{\partial n} + M_{ns} \frac{\partial w}{\partial s} = l M_x \frac{\partial w}{\partial x} + m M_y \frac{\partial w}{\partial y} + M_{xy} \left(m \frac{\partial w}{\partial x} + l \frac{\partial w}{\partial y} \right) \quad (5-10)$$

Now, by using integration by parts two times, the left side of Eq. (5-6) can be expressed as follows:

$$\begin{aligned} \text{Left side of Eq. (5-6)} &= - \iint_{A^e} \left[\left(\frac{\partial M_x}{\partial x} + \frac{\partial M_{xy}}{\partial y} \right) \frac{\partial w}{\partial x} + \left(\frac{\partial M_{xy}}{\partial x} + \frac{\partial M_y}{\partial y} \right) \frac{\partial w}{\partial y} \right] dx dy \\ &\quad + \oint_{\partial A^e} \left[M_x \frac{\partial w}{\partial x} l + M_y \frac{\partial w}{\partial y} m + M_{xy} \left(\frac{\partial w}{\partial x} m + \frac{\partial w}{\partial y} l \right) \right] ds \\ &= \iint_{A^e} \left(\frac{\partial^2 M_x}{\partial x^2} + \frac{\partial^2 M_y}{\partial y^2} + 2 \frac{\partial^2 M_{xy}}{\partial x \partial y} \right) w dx dy \end{aligned}$$

$$\begin{aligned}
 & - \oint_{\partial A^e} w \left[l \left(\frac{\partial M_x}{\partial x} + \frac{\partial M_{xy}}{\partial y} \right) + m \left(\frac{\partial M_{xy}}{\partial x} + \frac{\partial M_y}{\partial y} \right) \right] ds \\
 & + \oint_{\partial A^e} \left[M_x \frac{\partial w}{\partial x} l + M_y \frac{\partial w}{\partial y} m + M_{xy} \left(\frac{\partial w}{\partial x} m + \frac{\partial w}{\partial y} l \right) \right] ds
 \end{aligned}$$

Then by using Eqs. (5-8a) and (5-10), we have

Left side of Eq. (5-6) = Right side of Eq. (5-6) □

5.3 General Formulations of the Generalized Conforming Thin Plate Elements

5.3.1 Element DOFs and Basis Functions of the Deflection Field

Here, an element is assumed to have n DOFs. For the thin plate bending problem, the element DOF vector \mathbf{q}^e usually contains only deflections and rotations w_i , ψ_{xi} , ψ_{yi} ($i=1, 2, \dots, p$) at corner nodes, i.e., $n=3p$, in which p is the number of corner nodes or element sides. Thereby, \mathbf{q}^e is defined as

$$\mathbf{q}^e = [w_1 \quad \psi_{x1} \quad \psi_{y1} \quad \cdots \quad w_p \quad \psi_{xp} \quad \psi_{yp}]^T \quad (5-11)$$

The element deflection field $w(x, y)$ is assumed to be a polynomial with m unknown coefficients:

$$w = \mathbf{F}(x, y)\boldsymbol{\lambda} \quad (5-12)$$

where $\boldsymbol{\lambda}$ is the unknown coefficient vector; \mathbf{F} is the row matrix of basis (or trial) functions:

$$\begin{aligned}
 \boldsymbol{\lambda} &= [\lambda_1 \quad \lambda_2 \quad \cdots \quad \lambda_m]^T \\
 \mathbf{F} &= [F_1 \quad F_2 \quad \cdots \quad F_m]
 \end{aligned}$$

in which $m \geq n$. In usual schemes, let $m=n$, i.e., the number of the unknown coefficients in the deflection field is assumed to be equal to the number of element DOFs. If $m > n$, the element can be called super-basis generalized conforming element.

5.3.2 Generalized Conforming Conditions

In order to obtain the expression of $\boldsymbol{\lambda}$ in terms of \mathbf{q}^e , it needs selecting m generalized conforming conditions, in which the fundamental generalized

conforming conditions or their equivalent conditions must be included. m equations between λ and \mathbf{q}^e are established by these m generalized conforming conditions, and can be written as the following matrix forms:

$$\hat{\mathbf{C}}_{m \times m} \lambda = \hat{\mathbf{G}}_{m \times n} \mathbf{q}^e \quad (5-13)$$

This matrix equation should satisfy the following two conditions:

- (1) $\hat{\mathbf{C}}$ is a nonsingular square matrix;
- (2) The rank of $\hat{\mathbf{G}}$ is n , i.e.,

$$\text{Rank of } \hat{\mathbf{G}} = n \quad (5-14)$$

According to condition (1), λ can be derived from Eq. (5-13):

$$\lambda = \hat{\mathbf{A}}_{m \times n} \mathbf{q}^e \quad (5-15)$$

in which

$$\hat{\mathbf{A}}_{m \times n} = \hat{\mathbf{C}}_{m \times m}^{-1} \hat{\mathbf{G}} \quad (5-16)$$

According to Eqs. (5-14) and (5-16), we have

$$\text{Rank of } \hat{\mathbf{A}} = n \quad (5-17)$$

Meanwhile, the following homogeneous equation set

$$\hat{\mathbf{A}} \mathbf{q}^e = \mathbf{0}$$

has no nonzero solutions. That is to say, when $\lambda = \mathbf{0}$, w will also be zero, the corresponding \mathbf{q}^e must be a zero vector, i.e., there are no spurious zero-energy modes existing.

For the case $m = n$, $\hat{\mathbf{G}}$ and $\hat{\mathbf{A}}$ are both $n \times n$ square matrices. Then, conditions (1) and (2) can be summarized as: $\hat{\mathbf{G}}$ and $\hat{\mathbf{A}}$ are nonsingular square matrices.

5.3.3 Shape Functions

Substitution of Eq. (5-15) into Eq. (5-12) yields

$$\mathbf{w} = \mathbf{N} \mathbf{q}^e \quad (5-18)$$

where \mathbf{N} is the shape function matrix:

$$\mathbf{N} = \mathbf{F} \hat{\mathbf{A}} = \mathbf{F} \hat{\mathbf{C}}^{-1} \hat{\mathbf{G}} \quad (5-19)$$

After the determination of the shape functions, the element stiffness matrix can be obtained by following standard procedure.

5.4 Several Construction Schemes of the Generalized Conforming Thin Plate Elements

The construction methods of the generalized conforming elements have great flexibility. The following two points are worthy of being discussed:

(1) Under the premise that the fundamental generalized conforming conditions are satisfied, various conforming conditions, including point conforming, line conforming, perimeter conforming and their combination forms, can be selected flexibly, which is different from the common practice that only nodal conforming form is used.

(2) The number m of the basis functions (or unknown coefficients) in the interpolation formulae of element deflection field can be equal to or larger than the number of element DOFs n , which is different from the common practice of $m = n$. An element with $m > n$ can be called a super-basis element.

Respectable construction schemes of the generalized conforming thin plate elements have been proposed in many literatures, and they can be classified into five types:

- (1) Line conforming scheme;
- (2) Line-point conforming scheme (equal-basis or super-basis);
- (3) Super-basis point conforming scheme and SemiLoof conforming scheme;
- (4) Perimeter-point conforming scheme (equal-basis or super-basis);
- (5) Least square conforming scheme.

In addition, the thick/thin plate elements introduced in Chap. 8 can also be used for the analysis of the thin plate structures.

The conforming conditions used by the various schemes are briefly described as follows.

5.4.1 Line Conforming Scheme ($m \geq n$)

Now, we start from the first expression of the generalized conforming conditions (5-2a). The whole boundary ∂A^e is looked upon as a sub-domain, and the conforming conditions will be selected according to the sub-domain method. Firstly, the weighting functions M_n , M_{ns} and Q_n are selected independently along each element side; secondly, they are expanded into power series of the tangent coordinate s along the side:

$$M_n = \sum_{k=0}^{\infty} a_k s^k, \quad M_{ns} = \sum_{k=0}^{\infty} b_k s^k, \quad Q_n = \sum_{k=0}^{\infty} c_k s^k \quad (5-20)$$

thirdly, substitute the above equation into Eq. (5-2a). Since parameters a_k , b_k and c_k of each side can be looked upon as independent parameters, the zero-order and

high-order line conforming conditions can be obtained:

$$\left. \begin{aligned} \int_{\Gamma_i} s^k \left(\frac{\partial w}{\partial n} - \tilde{\psi}_n \right) ds &= 0 \\ \int_{\Gamma_i} s^k \left(\frac{\partial w}{\partial s} - \tilde{\psi}_s \right) ds &= 0 \\ \int_{\Gamma_i} s^k (w - \tilde{w}) ds &= 0 \end{aligned} \right\} \begin{aligned} & \left(i = 1, 2, \dots, p \right) \\ & \left(k = 0, 1, \dots, \infty \right) \end{aligned} \quad (5-21)$$

where p denotes the number of element sides expressed by $\Gamma_1, \Gamma_2, \dots, \Gamma_p$. The zero-order line conforming conditions

$$\left. \begin{aligned} \int_{\Gamma_i} \left(\frac{\partial w}{\partial n} - \tilde{\psi}_n \right) ds &= 0 \\ \int_{\Gamma_i} \left(\frac{\partial w}{\partial s} - \tilde{\psi}_s \right) ds &= 0 \\ \int_{\Gamma_i} (w - \tilde{w}) ds &= 0 \end{aligned} \right\} \quad (5-22)$$

are the average displacement conforming conditions of each element side.

In order to determine m unknown coefficients in the element deflection field, m independent generalized conforming conditions are needed. In the line conforming scheme, the average line conforming conditions (5-22) of w, ψ_n and ψ_s along each side should be selected firstly; then, other conforming condition form can also be supplemented, such as one-order line conforming conditions, point and perimeter conforming conditions, and so on. It can be seen that, if the average displacement conforming conditions of each element side have already been satisfied, the six fundamental generalized conforming conditions for rigid body displacement and constant strain states are also satisfied naturally. Thereby, the convergence can be guaranteed. The feature of this construction scheme is: starting from Eq. (5-2a), all or main conforming conditions are line conforming modes, especially, the average line conforming conditions (5-22).

By the way, the selected m generalized conforming conditions should be independent, i.e., they are linearly independent.

5.4.2 Line-Point Conforming Scheme ($m \geq n$)

Now, we start from the second expression of the generalized conforming conditions (5-2b). Here, the line conforming condition related to tangent rotation ψ_s in Eq. (5-2a) has been replaced by the point conforming condition related to deflection w at the corner node in Eq. (5-2b), and the pure line conforming

conditions (5-21) have also correspondingly been replaced by the following combination form:

$$\left. \begin{aligned} w - \tilde{w} &= 0 && \text{(at each corner node)} \\ \int_{r_i} s^k \left(\frac{\partial w}{\partial n} - \tilde{\psi}_n \right) ds &= 0 && \text{(along each side)} \\ \int_{r_i} s^k (w - \tilde{w}) ds &= 0 && \text{(along each side)} \end{aligned} \right\} \quad (5-23)$$

The feature of this construction scheme is: starting from Eq. (5-2b), the point conforming conditions and the line conforming conditions are used jointly. So, this scheme is called the line-point conforming mixed scheme.

5.4.3 Super-Basis Point Conforming and SemiLoof Conforming Schemes ($m > n$)

These are the improved schemes of the conventional non-conforming element method. In the conventional non-conforming element method, $m = n$, all the conforming conditions used are point conforming conditions at the corner nodes. Sometimes this method cannot ensure convergence. Therefore, one of its improved schemes is proposed as follows: let $m > n$ (i.e., increase the number of the unknown coefficients and the basis functions in the element deflection interpolation formulae so that the number m of the basis functions is larger than the number n of element DOFs); besides the n conventional point conforming conditions at the corner nodes, $m - n$ additional point conforming conditions must be supplemented for ensuring element convergence. The feature of this construction scheme is: all the conforming conditions used are point conforming modes, and $m > n$ so that convergence can be guaranteed. So, this scheme is called the super-basis point conforming scheme.

SemiLoof conforming scheme also belongs to the super-basis point conforming scheme, it is a mixed scheme of the generalized conforming element and the SemiLoof element.

5.4.4 Perimeter-Point Conforming Scheme ($m \geq n$)

The line conforming scheme mentioned above is a kind of sub-domain method (takes each element side as a sub-domain), while the scheme in this section is a whole-domain method in which the generalized conforming conditions (5-2a) are used on the whole element boundary line ∂A^e . That is to say, the perimeter conforming conditions are adopted.

Instead, the equivalent condition (5-2c) can also be used. Here, the boundary integration of the element deflection field w in Eq. (5-2a) has been changed to area integration, which is more convenient in applications.

In Eq. (5-2c), the weighting functions M_x , M_y and M_{xy} are the arbitrary internal force fields which satisfy homogeneous equilibrium Eq. (5-3). Corresponding to these internal force fields, Eq. (5-2c) represents a series of generalized conforming conditions, in which the most important generalized conditions are those corresponding to the constant internal force fields. Let the constant internal force fields be:

$$M_x = \beta_1, \quad M_y = \beta_2, \quad M_{xy} = \beta_3 \tag{5-24}$$

where β_1 , β_2 and β_3 are three arbitrary constants. Let l and m be the direction cosines of the outer normal on the element boundary, then the boundary forces can be written as:

$$\left. \begin{aligned} M_n &= l^2 \beta_1 + m^2 \beta_2 + 2lm \beta_3 \\ M_{ns} &= -lm \beta_1 + lm \beta_2 + (l^2 - m^2) \beta_3 \\ Q_n &= 0 \end{aligned} \right\} \tag{5-25}$$

After substituting the above equation into Eq. (5-2c), three independent perimeter conforming conditions can be obtained:

$$\left. \begin{aligned} \iint_{A^e} \frac{\partial^2 w}{\partial x^2} dA - \oint_{\partial A^e} (l^2 \tilde{\psi}_n - lm \tilde{\psi}_s) ds &= 0 \\ \iint_{A^e} \frac{\partial^2 w}{\partial y^2} dA - \oint_{\partial A^e} (m^2 \tilde{\psi}_n + lm \tilde{\psi}_s) ds &= 0 \\ \iint_{A^e} 2 \frac{\partial^2 w}{\partial x \partial y} dA - \oint_{\partial A^e} [2lm \tilde{\psi}_n + (l^2 - m^2) \tilde{\psi}_s] ds &= 0 \end{aligned} \right\} \tag{5-26}$$

The expressions in Eq. (5-26) are perimeter conforming conditions corresponding to the constant internal force fields. The perimeter conforming conditions corresponding to first-order and high-order internal force fields are also derived by similar methods.

In this scheme, the perimeter conforming conditions (5-26) are selected firstly, then the point conforming or the high-order perimeter conforming conditions can be supplemented according to the requirements. The feature of this construction scheme is: starting from Eq. (5-2c), the perimeter conforming conditions and the point conforming conditions are used jointly. So, this scheme is called the perimeter-point conforming mixed scheme.

5.4.5 Least Square Scheme ($m \geq n$)

The feature of this construction scheme is that the generalized conforming conditions are established by least square methods. The interpolation formulae of the element deflection field is assumed as

$$w = F\lambda$$

where λ denotes the unknown coefficient vector; F denotes the row matrix of the basis functions. By applying the least square method, the generalized conforming conditions can be obtained:

$$\frac{\partial}{\partial \lambda} \oint_{\partial A^e} \left[(w - \tilde{w})^2 + \left(\frac{\partial w}{\partial n} - \tilde{\psi}_n \right)^2 \right] ds = \mathbf{0} \tag{5-27}$$

This least square method can also be used jointly with other methods.

5.5 A Collection of the Recent Generalized Conforming Thin Plate Elements

Some recent generalized conforming thin plate elements proposed by authors' group, including 28 new elements, are listed in Table 5.1.

Table 5.1 Some generalized conforming thin plate elements

Symbol of elements	DOFs	No. of basis functions	The interpolation formula for deflection and its basis functions	Conforming conditions used	References
1. TGC-9 Triangular element	9	9	$w = \lambda_1 L_1 + \lambda_2 L_2 + \lambda_3 L_3 + \lambda_4 L_1 L_2 \left(L_1 + \frac{1}{2} L_3 \right) + \lambda_5 L_2 L_3 \left(L_2 + \frac{1}{2} L_1 \right) + \lambda_6 L_3 L_1 \left(L_3 + \frac{1}{2} L_2 \right) + \lambda_7 L_1 L_2 \left(L_2 + \frac{1}{2} L_3 \right) + \lambda_8 L_2 L_3 \left(L_3 + \frac{1}{2} L_1 \right) + \lambda_9 L_3 L_1 \left(L_1 + \frac{1}{2} L_2 \right)$	Average conforming conditions of w , ψ_n , ψ_s along each side (8 independent conditions); in addition, a first moment line conforming condition of w is supplemented: $\int_0^1 (w - \tilde{w})_{23} \left(L_3 - \frac{1}{2} \right) dL_3 + \int_0^1 (w - \tilde{w})_{31} \left(L_1 - \frac{1}{2} \right) dL_1 + \int_0^1 (w - \tilde{w})_{12} \left(L_2 - \frac{1}{2} \right) dL_2 = 0$	[4], [5]

(1) Line conforming scheme

(Continued)

2. TGC-9-1 Triangular element	9	9+1	$w = w(\text{TGC-9}) + F_\alpha \alpha$ where $\alpha =$ internal parameter $F_\alpha = 1 - 6(L_1L_2 + L_2L_3 + L_3L_1)$ $\quad + 18L_1L_2L_3$ $=$ generalized bubble function	$\lambda_1, \lambda_2, \dots, \lambda_9$ are solved by the conforming conditions of element TGC-9; Eliminate α by condensation	[4], [5]
3. RGC-12 Rectangular element	12	12	$w = \lambda_1 + \lambda_2\xi + \lambda_3\eta + \lambda_4\xi^2$ $\quad + \lambda_5\xi\eta + \lambda_6\eta^2 + \lambda_7\xi^3$ $\quad + \lambda_8\xi^2\eta + \lambda_9\xi\eta^2 + \lambda_{10}\eta^3$ $\quad + \lambda_{11}\xi^3\eta + \lambda_{12}\xi\eta^3$	Average line conforming conditions of w, ψ_n and ψ_s along each side (10 independent conditions); Point conforming conditions of ψ_x and ψ_y at a corner node (2 conditions)	[4], [5]
4. CGC-R12 Rectangular element	12	12	$w = \lambda_1 + \lambda_2\xi + \lambda_3\eta + \lambda_4\xi\eta$ $\quad + (\xi^2 - 1)(\lambda_5 + \lambda_7\eta + \lambda_9\xi)$ $\quad + (\eta^2 - 1)(\lambda_6 + \lambda_8\xi + \lambda_{10}\eta)$ $\quad + \lambda_{11}(\xi^4 - 1) + \lambda_{12}(\eta^4 - 1)$	Average line conforming conditions of w and ψ_n along each side (8 conditions); Point conforming conditions of w at each corner node (4 conditions)	[6]
5. LGC-R12 Rectangular element	12	12	$w = \lambda_1 + \lambda_2\xi + \lambda_3\eta + \lambda_4\xi\eta$ $\quad + (\xi^2 - 1)(\lambda_5 + \lambda_7\eta + \lambda_9\xi$ $\quad + \lambda_{11}\xi\eta) + (\eta^2 - 1)(\lambda_6$ $\quad + \lambda_8\xi + \lambda_{10}\eta + \lambda_{12}\xi\eta)$	Point conforming conditions of w at each corner node (4 conditions); Average line conforming conditions of w along each side; average and first moment line conforming conditions of ψ_n along each side (select 8 independent conditions)	[7]
6. LZ1 Triangular element	9	9	$w = \lambda_1L_1 + \lambda_2L_2 + \lambda_3L_3$ $\quad + \lambda_4L_1L_2 + \lambda_5L_2L_3$ $\quad + \lambda_6L_3L_1 + \lambda_7L_1^2L_2$ $\quad + \lambda_8L_2^2L_3 + \lambda_9L_3^2L_1$	Average line conforming conditions of w and ψ_n along each side (6 conditions); Point conforming conditions of w at each corner node (3 conditions)	[8]
7. LZ2 Triangular element	9	9+1	$w = w(\text{LZ1}) + F_\alpha \alpha$ where $\alpha =$ internal parameter $F_\alpha =$ generalized bubble function $= -(L_1L_2 + L_2L_3 + L_3L_1)$ $\quad + 2(L_1^2L_2 + L_2^2L_3 + L_3^2L_1)$ $\quad + 3L_1L_2L_3$	$\lambda_1, \lambda_2, \dots, \lambda_9$ are solved by the conforming conditions of element LZ1; Eliminate α by condensation	[8]

(Continued)

8. GPL-T9 Triangular element	9	9	$w = \lambda_1 L_1 + \lambda_2 L_2 + \lambda_3 L_3$ $+ \lambda_4 L_1 L_2 + \lambda_5 L_2 L_3 + \lambda_6 L_3 L_1$ $+ \lambda_7 L_1 \left(L_1 - \frac{1}{2} \right) (L_1 - 1)$ $+ \lambda_8 L_2 \left(L_2 - \frac{1}{2} \right) (L_2 - 1)$ $+ \lambda_9 L_3 \left(L_3 - \frac{1}{2} \right) (L_3 - 1)$	Average line conforming conditions of w and ψ_n along each side (6 conditions); Point conforming conditions of w at each corner node (3 conditions)	[9]
9. GCIV-T9 Triangular element	9	9	$w = \lambda_1 L_1 + \lambda_2 L_2 + \lambda_3 L_3$ $+ \lambda_4 L_1 L_2 + \lambda_5 L_2 L_3 + \lambda_6 L_3 L_1$ $+ \lambda_7 L_1^2 (L_2 + L_3)$ $+ \lambda_8 L_2^2 (L_3 + L_1)$ $+ \lambda_9 L_3^2 (L_1 + L_2)$	Average line conforming conditions of w and ψ_n along each side (6 conditions); Point conforming conditions of w at each corner node (3 conditions)	[10]
10.LGC-Q12 Quadrilatera l element	12	12	$w = \lambda_1 + \lambda_2 \xi + \lambda_3 \eta + \lambda_4 \xi \eta$ $+ (\xi^2 - 1)(\lambda_5 + \lambda_7 \eta + \lambda_9 \xi$ $+ \lambda_{11} \xi \eta) + (\eta^2 - 1)(\lambda_6$ $+ \lambda_8 \xi + \lambda_{10} \eta + \lambda_{12} \xi \eta)$	Point conforming conditions of w at each corner node (4 conditions); Average line conforming conditions of w along each side; average and first moment line conforming conditions of ψ_n along each side (select 8 independent conditions)	[11]
11. GC-S12 Sector element	12	12	$w = \sum_{i=1}^4 \frac{1}{4} (1 + R_i R) \left(1 + \alpha_i \sin \frac{\alpha \pi}{2} \right) \lambda_i$ $+ (R^2 - 1) \left(\lambda_5 + \lambda_7 \sin \frac{\alpha \pi}{2} \right.$ $\left. + \lambda_9 R + \lambda_{11} R \sin \frac{\alpha \pi}{2} \right)$ $+ \cos \frac{\alpha \pi}{2} (\lambda_6 + \lambda_8 R + \lambda_{10} \sin \frac{\alpha \pi}{2}$ $+ \lambda_{12} R \sin \frac{\alpha \pi}{2})$	Point conforming conditions of w at each corner node (4 conditions); Average line conforming conditions of w along each side; average and first moment line conforming conditions of ψ_n along each side (select 8 independent conditions)	[12]

(2a) Line-point conforming scheme

12. GCIII-R12 Rectangular element	12	14	$w = \lambda_1 + \lambda_2 \xi + \lambda_3 \eta + \lambda_4 \xi^2$ $+ \lambda_5 \xi \eta + \lambda_6 \eta^2 + \lambda_7 \xi^3$ $+ \lambda_8 \xi^2 \eta + \lambda_9 \xi \eta^2 + \lambda_{10} \eta^3$ $+ \lambda_{11} \xi^3 \eta + \lambda_{12} \xi \eta^3$ $+ (\xi^2 - 1)(\eta^2 - 1)(\lambda_{13} \xi + \lambda_{14} \eta)$	Point conforming conditions of w , ψ_x and ψ_y at each corner node (12 conditions); Average line conforming conditions of ψ_n along each side (2 independent conditions)	[13]
---	----	----	--	---	------

(Continued)

<p>13. GPL-R12 Rectangular element</p>	<p>12</p>	<p>16</p>	$w = \lambda_1 + \lambda_2\xi + \lambda_3\eta + \lambda_4\xi\eta + (\xi^2 - 1)(\lambda_5 + \lambda_7\eta + \lambda_9\xi + \lambda_{11}\xi\eta) + (\eta^2 - 1)(\lambda_6 + \lambda_8\xi + \lambda_{10}\eta + \lambda_{12}\xi\eta) + (\xi^2 - 1)\left(\xi^2 - \frac{1}{5}\right)(\lambda_{13} + \lambda_{15}\eta) + (\eta^2 - 1)\left(\eta^2 - \frac{1}{5}\right)(\lambda_{14} + \lambda_{16}\xi)$	<p>Point conforming conditions of w at each corner node (4 conditions); Average line conforming conditions of w along each side; average and first moment line conforming conditions of ψ_n along each side (12 conditions)</p>	<p>[9]</p>
<p>14. GCIII-T9 Triangular element</p>	<p>9</p>	<p>12</p>	$w = \lambda_1L_1 + \lambda_2L_2 + \lambda_3L_3 + \lambda_4L_2L_3 + \lambda_5L_3L_1 + \lambda_6L_1L_2 + \lambda_7L_2L_3(L_3 - L_2) + \lambda_8L_3L_1(L_1 - L_3) + \lambda_9L_1L_2(L_2 - L_1) + \lambda_{10}L_1L_2L_3^2 + \lambda_{11}L_2L_3L_1^2 + \lambda_{12}L_3L_1L_2^2$	<p>Point conforming conditions of w, ψ_x and ψ_y at each corner node (9 conditions); Average line conforming conditions of ψ_n along each side (3 conditions)</p>	<p>[13]</p>
<p>15. LZ3 Triangular element</p>	<p>9</p>	<p>10</p>	$w = \lambda_1L_1 + \lambda_2L_2 + \lambda_3L_3 + \lambda_4L_1L_2 + \lambda_5L_2L_3 + \lambda_6L_3L_1 + \lambda_7L_1^2L_2 + \lambda_8L_2^2L_3 + \lambda_9L_3^2L_1 + \lambda_{10}L_1L_2L_3$	<p>Point conforming conditions of w at each corner node (3 conditions); Average line conforming conditions of w and ψ_n along each side (6 conditions); Line conforming condition of the sum of first moments of w along three sides (1 condition)</p>	<p>[8]</p>

(2b) Super-basis Line-Point conforming scheme

<p>16. MB1-T9 Triangular element</p>	<p>9</p>	<p>12</p>	$w = \lambda_1L_1 + \lambda_2L_2 + \lambda_3L_3 + \lambda_4L_1L_2 + \lambda_5L_2L_3 + \lambda_6L_3L_1 + \lambda_7L_1^2L_2 + \lambda_8L_2^2L_3 + \lambda_9L_3^2L_1 + \lambda_{10}L_2^2L_3^2 + \lambda_{11}L_3^2L_1^2 + \lambda_{12}L_1^2L_2^2$	<p>Point conforming conditions of w, ψ_x and ψ_y at each corner node (9 conditions); Point conforming conditions of ψ_n at midpoint of each side (3 conditions)</p>	<p>[14]</p>
<p>17. MB2-T9 Triangular element</p>	<p>9</p>	<p>12</p>	$w = \lambda_1L_1 + \lambda_2L_2 + \lambda_3L_3 + \lambda_4L_1L_2 + \lambda_5L_2L_3 + \lambda_6L_3L_1 + \lambda_7L_1^2L_2 + \lambda_8L_2^2L_3 + \lambda_9L_3^2L_1 + \lambda_{10}L_1^2L_2L_3 + \lambda_{11}L_2^2L_3L_1 + \lambda_{12}L_3^2L_1L_2$	<p>Same as element MB1-T9</p>	<p>[14]</p>

(Continued)

18. LQ12 Quadrilateral element	12	16	$w = \lambda_1 + \lambda_2\xi + \lambda_3\eta + \lambda_4\xi^2 + \lambda_5\xi\eta + \lambda_6\eta^2 + \lambda_7\xi^3 + \lambda_8\xi^2\eta + \lambda_9\xi\eta^2 + \lambda_{10}\eta^3 + \lambda_{11}\xi^3\eta + \lambda_{12}\xi\eta^3 + (\xi^2 - 1)(\eta^2 - 1)[\lambda_{13} + \lambda_{14}\xi + \lambda_{15}\eta + \lambda_{16}(\xi^2 - \eta^2)]$	Point conforming conditions of w , ψ_x and ψ_y at each corner node (12 conditions); Point conforming conditions of ψ_n at mid-side point of each side (4 conditions)	[15]
19. LSL-T9 Triangular element	9	12	$w = \lambda_1L_1 + \lambda_2L_2 + \lambda_3L_3 + \lambda_4L_2L_3 + \lambda_5L_3L_1 + \lambda_6L_1L_2 + \lambda_7L_2L_3(L_2 - L_3) + \lambda_8L_3L_1(L_3 - L_1) + \lambda_9L_1L_2(L_1 - L_2) + \lambda_{10}L_1^2L_2L_3 + \lambda_{11}L_2^2L_3L_1 + \lambda_{12}L_3^2L_1L_2$	Point conforming conditions of w at each corner node and mid-side point of each side (6 conditions); Point conforming conditions of ψ_n at two Gauss points of each side (6 conditions)	[16]
20. LSL-R12 Rectangular element	12	16	$w = \lambda_1 + \lambda_2\xi + \lambda_3\eta + \lambda_4\xi\eta + (\xi^2 - 1)(\lambda_5 + \lambda_6\xi + \lambda_7\eta + \lambda_8\xi\eta) + (\eta^2 - 1)(\lambda_9 + \lambda_{10}\xi + \lambda_{11}\eta + \lambda_{12}\xi\eta) + (\xi^2 - 1)(\eta^2 - 1)[\lambda_{13} + \lambda_{14}\xi + \lambda_{15}\eta + \lambda_{16}(\xi^2 - \eta^2)]$	Point conforming conditions of w at each corner node and mid-side point of each side (8 conditions); Point conforming conditions of ψ_n at two Gauss points of each side (8 conditions)	[16]
21. LSL-Q12 Quadrilateral element	12	16	$w = \lambda_1 + \lambda_2\xi + \lambda_3\eta + \lambda_4\xi\eta + (\xi^2 - 1)(\lambda_5 + \lambda_6\xi + \lambda_7\eta + \lambda_8\xi\eta) + (\eta^2 - 1)(\lambda_9 + \lambda_{10}\xi + \lambda_{11}\eta + \lambda_{12}\xi\eta) + (\xi^2 - 1)(\eta^2 - 1)(\lambda_{13} + \lambda_{14}\xi + \lambda_{15}\eta) + \lambda_{16}[\xi^2(\xi^2 - 1) - \eta^2(\eta^2 - 1)]$	Point conforming conditions of w at each corner node and mid-side point of each side (8 conditions); Point conforming conditions of ψ_n at two Gauss points of each side (8 conditions)	[17]

(3) Super-basis point conforming and SemiLoof conforming scheme

22. LR12-1 Rectangular element	12	12	$w = \lambda_1 + \lambda_2\xi + \lambda_3\eta + \lambda_4\xi^2 + \lambda_5\xi\eta + \lambda_6\eta^2 + \lambda_7\xi^3 + \lambda_8\xi^2\eta + \lambda_9\xi\eta^2 + \lambda_{10}\eta^3 + \lambda_{11}\xi^3\eta + \lambda_{12}\xi\eta^3$	Point conforming conditions of w at each corner node (select 3 conditions); 9 perimeter conforming conditions, and the corresponding internal moment fields are: $M_x = \beta_1 + \beta_2\xi + \beta_3\eta + \beta_4\xi\eta$ $M_y = \beta_5 + \beta_6\xi + \beta_7\eta + \beta_8\xi\eta$ $M_{xy} = \beta_9$	[18]
--------------------------------------	----	----	--	---	------

(Continued)

23. LR12-2 Rectangular element	12	12	Same as element LR12-1	Similar to element LR12-1, but the internal moment fields are changed to $M_x = \beta_1 + \beta_2\xi + \beta_3\eta$ $M_y = \beta_4 + \beta_5\xi + \beta_6\eta$ $M_{xy} = \beta_7 + \beta_8\xi^2 + \beta_9\eta^2$	[18]
24. Coons method Rectangular element	12	12	$w = w_1(1 - 3\xi^2 + 2\xi^3) \times (1 - 3\eta^2 + 2\eta^3) + w_2(3\xi^2 - 2\xi^3)(1 - 3\eta^2 + 2\eta^3) + w_3(1 - 3\xi^2 + 2\xi^3)(1 - \eta)^2\eta + w_4(3\xi^2 - 2\xi^3)(1 - \eta)^2\eta + w_{,\xi 1}\xi(1 - \xi)^2(1 - \eta) + w_{,\xi 2}\xi^2(\xi - 1)(1 - \eta) + w_{,\xi 3}\xi(1 - \xi)^2\eta + w_{,\xi 4}\xi^2(\xi - 1)\eta + w_{,\eta 1}(1 - \xi)\eta(1 - \eta)^2 + w_{,\eta 2}\xi\eta(1 - \eta)^2 + w_{,\eta 3}(1 - \xi)\eta^2(\eta - 1) + w_{,\eta 4}\xi\eta^2(\eta - 1)$	w of each side is exactly compatible; ψ_n of each side satisfies the perimeter conforming conditions under constant moment fields	[19]

(4a) Perimeter-point conforming scheme

25. GC II - T9 Triangular element	9	12	$w = \lambda_1 L_1 + \lambda_2 L_2 + \lambda_3 L_3 + \lambda_4 L_1 L_2 (L_1 + \frac{L_3}{2}) + \lambda_5 L_2 L_3 (L_2 + \frac{L_1}{2}) + \lambda_6 L_3 L_1 (L_3 + \frac{L_2}{2}) + \lambda_7 L_1 L_3 (L_1 + \frac{L_2}{2}) + \lambda_8 L_2 L_1 (L_2 + \frac{L_3}{2}) + \lambda_9 L_3 L_2 (L_3 + \frac{L_1}{2}) + \lambda_{10} L_1^2 L_2^2 + \lambda_{11} L_2^2 L_3^2 + \lambda_{12} L_3^2 L_1^2$	Point conforming conditions of w , ψ_x and ψ_y at each corner node (9 conditions); Perimeter conforming conditions under constant moment fields (3 conditions)	[20]
-----------------------------------	---	----	--	--	------

(Continued)

26. LT9 Triangular element	9	12	$w = \lambda_1 L_1 + \lambda_2 L_2 + \lambda_3 L_3$ $+ \lambda_4 L_1 L_2 + \lambda_5 L_2 L_3 + \lambda_6 L_3 L_1$ $+ \lambda_7 L_1^2 L_2 + \lambda_8 L_2^2 L_3 + \lambda_9 L_3^2 L_1$ $+ \lambda_{10} L_1^2 L_2 L_3 + \lambda_{11} L_2^2 L_3 L_1$ $+ \lambda_{12} L_3^2 L_1 L_2$	Point conforming conditions of w at each corner node (3 conditions); Perimeter conforming conditions under linear moment fields (9 conditions)	[18]
----------------------------------	---	----	--	---	------

(4b) Super-basis perimeter-point conforming scheme

27. LSGC-R12 Rectangular element	12	14	$w = \lambda_1 + \lambda_2 \xi + \lambda_3 \eta + \lambda_4 \xi^2$ $+ \lambda_5 \xi \eta + \lambda_6 \eta^2 + \lambda_7 \xi^3 + \lambda_8 \xi^2 \eta$ $+ \lambda_9 \xi \eta^2 + \lambda_{10} \eta^3 + \lambda_{11} \xi^3 \eta$ $+ \lambda_{12} \xi \eta^3 + \lambda_{13} \eta (\eta^2 - 1)(\xi^2 - 1)$ $+ \lambda_{14} \xi (\xi^2 - 1)(\eta^2 - 1)$	Point conforming conditions of w , ψ_x and ψ_y at each corner node (12 conditions); The extreme conditions by least square method are (2 conditions): $\frac{\partial}{\partial \lambda_i} \oint \left(\frac{\partial w}{\partial n} - \tilde{\psi}_n \right)^2 ds = 0$ ($i = 13, 14$)	[21]
28. LSGC-T9 Triangular element	9	12	$w = \lambda_1 L_1 + \lambda_2 L_2 + \lambda_3 L_3$ $+ \lambda_4 (L_1^2 L_2 + \frac{1}{2} L_1 L_2 L_3) + \lambda_5 (L_2^2 L_3$ $+ \frac{1}{2} L_1 L_2 L_3) + \lambda_6 (L_3^2 L_1 + \frac{1}{2} L_1 L_2 L_3)$ $+ \lambda_7 (L_1^2 L_3 + \frac{1}{2} L_1 L_2 L_3) + \lambda_8 (L_2^2 L_1$ $+ \frac{1}{2} L_1 L_2 L_3) + \lambda_9 (L_3^2 L_2 + \frac{1}{2} L_1 L_2 L_3)$ $+ \lambda_{10} L_1^2 L_2 L_3 + \lambda_{11} L_2^2 L_3 L_1 + \lambda_{12} L_3^2 L_1 L_2$	Point conforming conditions of w , ψ_x and ψ_y at each corner node (9 conditions); The extreme conditions by least square method are (3 conditions): $\frac{\partial}{\partial \lambda_i} \oint \left(\frac{\partial w}{\partial n} - \tilde{\psi}_n \right)^2 ds = 0$ ($i = 10, 11, 12$)	[21]

(5) Least square scheme

The generalized conforming thin plate elements for geometrically nonlinear analysis, including 8 elements, are listed in Table 5.2. All of them use the corresponding displacement field modes given by Table 5.1, and their Total Lagrangian formulations of the tangent stiffness matrices for the geometrically nonlinear analysis are derived.

In these Tables, brief introductions on the construction features of each element are given, including the assumed element deflection interpolation formula and the conforming conditions used, and the original literatures of these elements are also given for reference.

Advanced Finite Element Method in Structural Engineering

Table 5.2 Some generalized conforming thin plate elements for geometrically nonlinear analysis

Generalized conforming thin plate elements for geometrically nonlinear analysis	The displacement field mode	References
29. NLT-1: nonlinear triangular element	Same as triangular element TGC-9 (No. 1)	[22 – 24]
30. NLT-2: nonlinear triangular element	Same as triangular element GCIII-T9 (No. 14)	
31. NLT-3: nonlinear triangular element	Same as triangular element GC II -T9 (No. 25)	
32. NLR-1 nonlinear rectangular element	Same as rectangular element RGC-12 (No.3)	
33. NLR-2 nonlinear rectangular element	Same as rectangular element LGC-R12 (No.5)	
34. NLR-3 nonlinear rectangular element	Same as rectangular element GC III -R12 (No.12)	
35. NLQ-1 nonlinear quadrilateral element	Same as quadrilateral element LGC-Q12 (No.10)	
36. NLQ-2 nonlinear quadrilateral element	Same as quadrilateral element LSL-Q12 (No.21)	

In Chaps. 6 and 7, several typical elements by different construction schemes will be discussed in detail.

References

- [1] Hrabok MM, Hrudehy TM (1984) A review and catalogue of plate bending finite elements. Computers & Structures 19: 474 – 498
- [2] Yang HTY, Saigal S, Liaw DG (1990) Advances of thin shell finite elements and some applications—version I. Computers & Structures 35: 481 – 504
- [3] Kardestuncer H (1987) Finite element handbook. Mc Graw-Hill
- [4] Long YQ, Xin KG (1987) Generalized conforming element. Tumu Gongcheng Xuebao/China Civil Engineering Journal 20(1): 1 – 14 (in Chinese)
- [5] Long YQ, Xin KG (1989) Generalized conforming element for bending and buckling analysis of plates. Finite Elements in Analysis and Design 5: 15 – 30
- [6] Xu Y, Long ZF (1995) A simple generalized conforming rectangular plate bending element. In: Proceedings of the Fourth National Conference on Structural Engineering 315 – 319 (in Chinese)
- [7] Bu XM, Long YQ (1991) A high-precise rectangular element for thin plate bending analysis. Tumu Gongcheng Xuebao/China Civil Engineering Journal 24(1): 17 – 22 (in Chinese)

- [8] Long ZF (1993) Generalized conforming triangular elements for plate bending. *Communications in Numerical Methods in Engineering* 9: 53 – 65
- [9] Long YQ, Bu XM, Long ZF, Xu Y (1995) Generalized conforming plate bending elements using point and line compatibility conditions. *Computers & Structures* 54(4):717 – 723
- [10] Bu XM, Long YQ (1991) A triangular displacement element based on modified potential energy functional. *Journal of Tsinghua University* 31(2): 9 – 16 (in Chinese)
- [11] Bu XM, Long YQ (1991) A quadrilateral element for thin plate bending. *Acta Mechanica Sinica* 23(1): 53 – 60 (in Chinese)
- [12] Bu XM, Long YQ (1991) A generalized conforming sector element for thin plate bending. *Computational Structural Mechanics and Applications* 8(2): 208 – 213 (in Chinese)
- [13] Long YQ, Bu XM (1990) A family of efficient elements for thin plate bending. *Journal of Tsinghua University* 30(5): 9 – 15 (in Chinese)
- [14] Long ZF (1991) Low-order and high-precision triangular elements for plate bending. In: Cheung, Lee & Leung (eds) *Computational Mechanics*. Rotterdam: Balkema, pp1793 – 1797
- [15] Long ZF (1992) An improved quadrilateral element for thin plate bending. *Journal of Northern Jiaotong University* 16(2): 39 – 45 (in Chinese)
- [16] Long ZF (1993) Two generalized conforming plate elements based on SemiLoof constraints. *Computers & Structures* 47(2): 299 – 304
- [17] Long ZF (1993) Generalized conforming quadrilateral plate element by using SemiLoof constraints. *Communications in Numerical Methods in Engineering* 9: 417 – 426
- [18] Long ZF (1992) Triangular and rectangular plate elements based on generalized compatibility conditions. *Computational Mechanics* 10(3/4): 281 – 288
- [19] Zhang YQ, Zheng ZB, Long YQ (1992) A generalized conforming element for thin plates by Coons surface approach. *Gong Cheng Li Xue/Engineering Mechanics* 9(2): 86 – 90 (in Chinese)
- [20] Long YQ, Zhao JQ (1988) A new generalized conforming triangular element for thin plates. *Communications in Applied Numerical Methods* 4: 781 – 792
- [21] Bu XM, Long YQ (1991) A generalized conforming technique using the least squares method. *Gong Cheng Li Xue/Engineering Mechanics* 8(2): 20 – 24 (in Chinese)
- [22] Sun JH, Long ZF, Long YQ, Zhang CS (2001) Geometrically nonlinear stability analysis of shells using generalized conforming shallow shell element. *International Journal of Structural Stability and Dynamics* 1(3): 313 – 332
- [23] Sun JH, Xia HX, Long YQ (1999) A generalized conforming rectangular shallow shell element. In: Long YQ, ed. *The Proceedings of the First International Conference on Structural Engineering*. KunMing, China, pp803 – 810
- [24] Sun JH, Long ZF, Long YQ (1999) A generalized conforming element with vertex rotational freedoms for thin shell analysis. In: Long YQ, ed. *The Proceedings of the First International Conference on Structural Engineering*. KunMing, China, pp811 – 818

Chapter 6 Generalized Conforming Thin Plate Element II—Line-Point and SemiLoof Conforming Schemes

Zhi-Fei Long

School of Mechanics & Civil Engineering, China University of Mining & Technology, Beijing, 100083, China

Song Cen

Department of Engineering Mechanics, School of Aerospace, Tsinghua University, Beijing, 100084, China

Abstract Five groups of construction schemes for the generalized conforming thin plate elements are proposed in Sect. 5.4. This chapter discusses the first three groups: (1) line conforming scheme (Sect. 6.1); (2) line-point conforming scheme (Sects. 6.2 and 6.3) and super-basis line-point conforming scheme (Sect. 6.4); and (3) super-basis point conforming scheme (Sect. 6.5) and SemiLoof conforming scheme (Sect. 6.6). Formulations of 13 triangular, rectangular and quadrilateral generalized conforming thin plate elements, which are constructed by the above schemes, are introduced in detail. The elements formulated in Sects. 6.1 to 6.3 belong to the equal-basis elements, in which the number m of the unknown coefficients or basis functions in an interpolation formula for the element deflection field equals to the number n of DOFs. And, the elements formulated in Sects. 6.4 to 6.6 belong to the super-basis elements, in which $m > n$. Numerical examples show that these models exhibit excellent performance in the analysis of thin plates. This denotes that the difficulty of C_1 continuity problem can be solved completely.

Keywords thin plate element, generalized conforming, line-point conforming, SemiLoof conforming.

6.1 Line Conforming Scheme—Elements TGC-9 and TGC-9-1

In this section, the generalized conforming thin plate elements TGC-9 and TGC-9-1 will be taken as examples for illustrating the procedure of the line conforming

scheme. The outlines of the procedure are as follows: all conforming conditions are line conforming ones, especially, the average line conforming conditions (5-22) are taken as the main conditions; for the element TGC-9, let $m = n$; and for the element TGC-9-1, it is extended from the element TGC-9 by introducing an internal parameter α , which will be eliminated by condensation.

6.1.1 Element TGC-9

A triangular thin plate element with 9 DOFs is shown in Fig. 6.1. Its nodal displacement vector q^e is

$$q^e = [w_1 \ \psi_{x1} \ \psi_{y1} \ w_2 \ \psi_{x2} \ \psi_{y2} \ w_3 \ \psi_{x3} \ \psi_{y3}]^T \quad (6-1)$$

Along each element side, the deflection \tilde{w} is assumed to be cubic and the normal slope $\tilde{\psi}_n$ linear.

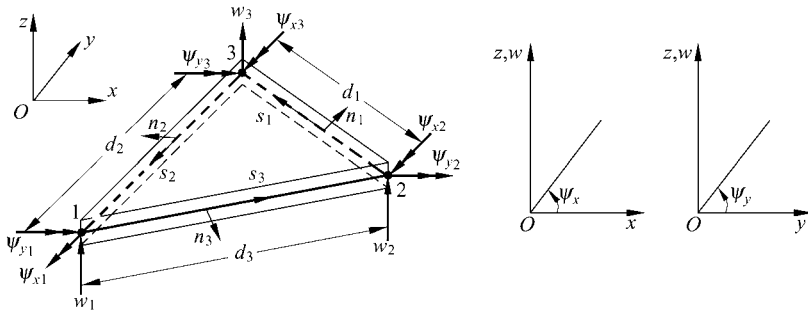


Figure 6.1 A triangular thin plate bending element

According to the element BCIZ in reference [1], the element deflection field $w(x, y)$ is described by an incomplete cubic polynomial and expressed in terms of the area coordinates L_1, L_2, L_3 :

$$w = F_\lambda \lambda \quad (6-2)$$

where λ is a vector containing 9 unknown coefficients:

$$\lambda = [\lambda_1 \ \lambda_2 \ \lambda_3 \ \lambda_4 \ \lambda_5 \ \lambda_6 \ \lambda_7 \ \lambda_8 \ \lambda_9]^T$$

and F_λ is a row matrix containing 9 basis functions:

$$\left. \begin{aligned} F_\lambda &= [L_1 \ L_2 \ L_3 \ F_4 \ F_5 \ F_6 \ F_7 \ F_8 \ F_9] \\ F_4 &= L_1 L_2 (L_1 + \frac{1}{2} L_3), \quad F_5 = L_2 L_3 (L_2 + \frac{1}{2} L_1), \quad F_6 = L_3 L_1 (L_3 + \frac{1}{2} L_2) \\ F_7 &= L_1 L_3 (L_1 + \frac{1}{2} L_2), \quad F_8 = L_2 L_1 (L_2 + \frac{1}{2} L_3), \quad F_9 = L_3 L_2 (L_3 + \frac{1}{2} L_1) \end{aligned} \right\} \quad (6-3)$$

In order to determine the 9 unknown coefficients of λ in terms of q^e , 9 generalized conforming conditions are needed. Here, the line conforming scheme, especially the average line conforming conditions (5-22), are firstly considered. Each element has three sides, along which the average deflection, average normal slope and average tangential slope conforming conditions are used. So, to outward seaming, there are just 9 generalized conforming conditions here. But, if $w - \tilde{w}$ is a continuous function along the boundary perimeter ∂A^e , the following identity relation

$$\oint_{\partial A^e} \frac{\partial}{\partial S} (w - \tilde{w}) ds = 0 \tag{6-4}$$

will come into existence, i.e.,

$$\sum_{i=1}^3 \int_{r_i} \left(\frac{\partial w}{\partial S} - \tilde{\psi}_s \right) ds = 0 \tag{6-5}$$

Therefore, there are only two independent conditions actually active for the tangential slop ψ_s . That is to say, when Eq. (5-22) is used along each element side, there are only 8 independent generalized conforming conditions, which are the first eight equations of the following equation set:

$$\left. \begin{aligned} \int_0^1 w_{23} dL_3 &\equiv d_4 = \int_0^1 \tilde{w}_{23} dL_3 \\ \int_0^1 w_{31} dL_1 &\equiv d_5 = \int_0^1 \tilde{w}_{31} dL_1 \\ \int_0^1 w_{12} dL_2 &\equiv d_6 = \int_0^1 \tilde{w}_{12} dL_2 \\ \int_0^1 \left(\frac{\partial w}{\partial n} \right)_{23} dL_3 &\equiv d_7 = \int_0^1 (\tilde{\psi}_n)_{23} dL_3 \\ \int_0^1 \left(\frac{\partial w}{\partial n} \right)_{31} dL_1 &\equiv d_8 = \int_0^1 (\tilde{\psi}_n)_{31} dL_1 \\ \int_0^1 \left(\frac{\partial w}{\partial n} \right)_{12} dL_2 &\equiv d_9 = \int_0^1 (\tilde{\psi}_n)_{12} dL_2 \\ \int_0^1 \left(\frac{\partial w}{\partial S} \right)_{23} dL_3 &\equiv d_1 = \int_0^1 (\tilde{\psi}_s)_{23} dL_3 \\ \int_0^1 \left(\frac{\partial w}{\partial S} \right)_{31} dL_1 &\equiv d_2 = \int_0^1 (\tilde{\psi}_s)_{31} dL_1 \\ \int_0^1 w_{23} \left(L_3 - \frac{1}{2} \right) dL_3 + \int_0^1 w_{31} \left(L_1 - \frac{1}{2} \right) dL_1 + \int_0^1 w_{12} \left(L_2 - \frac{1}{2} \right) dL_2 &\equiv d_3 \\ = \int_0^1 \tilde{w}_{23} \left(L_3 - \frac{1}{2} \right) dL_3 + \int_0^1 \tilde{w}_{31} \left(L_1 - \frac{1}{2} \right) dL_1 + \int_0^1 \tilde{w}_{12} \left(L_2 - \frac{1}{2} \right) dL_2 & \end{aligned} \right\} \tag{6-6}$$

The ninth equation in Eq. (6-6) is the supplementary generalized conforming condition, which denotes the generalized conforming condition that the sum of the first moments of the deflections along three sides should satisfy.

By using the symbol of Eq. (5-13) and arranging in the sequence of d_1, d_2, \dots, d_9 , Eq. (6-6) can be rewritten in the following matrix form:

$$\hat{C}\lambda = \hat{G}q^e \tag{6-7}$$

where

$$\hat{G} = \begin{bmatrix} 0 & 0 & 0 & -1 & 0 & 0 & 1 & 0 & 0 \\ 1 & 0 & 0 & 0 & 0 & 0 & -1 & 0 & 0 \\ 0 & c_1 & -b_1 & 0 & c_2 & -b_2 & 0 & c_3 & -b_3 \\ 0 & 0 & 0 & 6 & c_1 & -b_1 & 6 & -c_1 & b_1 \\ 6 & -c_2 & b_2 & 0 & 0 & 0 & 6 & c_2 & -b_2 \\ 6 & c_3 & -b_3 & 6 & -c_3 & b_3 & 0 & 0 & 0 \\ 0 & 0 & 0 & 0 & b_1 & c_1 & 0 & b_1 & c_1 \\ 0 & b_2 & c_2 & 0 & 0 & 0 & 0 & b_2 & c_2 \\ 0 & b_3 & c_3 & 0 & b_3 & c_3 & 0 & 0 & 0 \end{bmatrix} \tag{6-8}$$

$$\hat{C} = \begin{bmatrix} 0 & -1 & 1 & 0 & 0 & 0 & 0 & 0 & 0 \\ 1 & 0 & -1 & 0 & 0 & 0 & 0 & 0 & 0 \\ 0 & 0 & 0 & -1 & -1 & -1 & 1 & 1 & 1 \\ 0 & 6 & 6 & 0 & 1 & 0 & 0 & 0 & 1 \\ 6 & 0 & 6 & 0 & 0 & 1 & 1 & 0 & 0 \\ 6 & 6 & 0 & 1 & 0 & 0 & 0 & 1 & 0 \\ \hat{C}_1 & & & \hat{C}_2 & & & \hat{C}_3 & & \end{bmatrix} \tag{6-9}$$

and

$$\hat{C}_1 = \begin{bmatrix} \frac{f_2 + f_3}{A} & -\frac{f_3}{A} & -\frac{f_2}{A} \\ -\frac{f_3}{A} & \frac{f_3 + f_1}{A} & -\frac{f_1}{A} \\ -\frac{f_2}{A} & -\frac{f_1}{A} & \frac{f_1 + f_2}{A} \end{bmatrix} \tag{6-10}$$

$$\hat{\mathbf{C}}_2 = \begin{bmatrix} \frac{f_2 + f_3}{12A} & -3\frac{f_2 + f_3}{12A} & 5\frac{f_2 + f_3}{12A} \\ 5\frac{f_3 + f_1}{12A} & \frac{f_3 + f_1}{12A} & -3\frac{f_3 + f_1}{12A} \\ -3\frac{f_1 + f_2}{12A} & 5\frac{f_1 + f_2}{12A} & \frac{f_1 + f_2}{12A} \end{bmatrix} \quad (6-11)$$

$$\hat{\mathbf{C}}_3 = \begin{bmatrix} \frac{f_2 + f_3}{12A} & 5\frac{f_2 + f_3}{12A} & -3\frac{f_2 + f_3}{12A} \\ -3\frac{f_3 + f_1}{12A} & \frac{f_3 + f_1}{12A} & 5\frac{f_3 + f_1}{12A} \\ 5\frac{f_1 + f_2}{12A} & -3\frac{f_1 + f_2}{12A} & \frac{f_1 + f_2}{12A} \end{bmatrix} \quad (6-12)$$

in which A is the area of the triangle; and

$$\left. \begin{array}{l} b_i = y_j - y_k \\ c_i = x_k - x_j \\ f_i = -(b_j b_k + c_j c_k) \end{array} \right\} (i = \overline{1,2,3}; \quad j = \overline{2,3,1}; \quad k = \overline{3,1,2}) \quad (6-13)$$

It can be verified that $\hat{\mathbf{G}}$ and $\hat{\mathbf{C}}$ are not singular. So, from Eqs. (6-7) and (6-2), we have

$$w = \mathbf{F}_\lambda \hat{\mathbf{C}}^{-1} \hat{\mathbf{G}} \mathbf{q}^e$$

Then, the element stiffness matrix can be obtained following the standard procedure.

6.1.2 Element TGC-9-1

Assume that the element deflection field w is constituted of two parts

$$w = w_q + w_\alpha \quad (6-14)$$

where the first part is the deflection field expressed in Eq. (6-2)

$$w_q = \mathbf{F}_\lambda \boldsymbol{\lambda} = \mathbf{F}_\lambda (\hat{\mathbf{C}}^{-1} \hat{\mathbf{G}}) \mathbf{q}^e \quad (6-15)$$

The second part is a generalized bubble deflection field

$$w_\alpha = F_\alpha \alpha \quad (6-16)$$

where α is an internal displacement parameter and F_α is a generalized bubble function:

$$F_\alpha = 1 - 6(L_1L_2 + L_2L_3 + L_3L_1) + 18L_1L_2L_3 \quad (6-17)$$

It can be verified that all the 9 generalized displacements d_1, \dots, d_9 corresponding to w_α vanish.

The deflection field (6-14) is a complete cubic polynomial with 10 DOFs. α is eliminated by a condensation process, only 9 external DOFs in \mathbf{q}^e are retained.

From the expression (6-14) of the deflection field, the curvature field $\boldsymbol{\kappa}$ can be expressed as

$$\boldsymbol{\kappa} = \begin{bmatrix} -\frac{\partial^2 w}{\partial x^2} & -\frac{\partial^2 w}{\partial y^2} & -2\frac{\partial^2 w}{\partial x \partial y} \end{bmatrix}^T = \mathbf{B}\mathbf{q}^e + \mathbf{B}_\alpha \alpha \quad (6-18)$$

and the element strain energy U is

$$U = \frac{1}{2} \iint_{A^e} \boldsymbol{\kappa}^T \mathbf{D}\boldsymbol{\kappa} dA = \frac{1}{2} \mathbf{q}^{eT} \mathbf{K}_{qq} \mathbf{q}^e + \alpha \mathbf{K}_{\alpha q} \mathbf{q}^e + \frac{1}{2} \alpha^2 k_{\alpha\alpha} \quad (6-19)$$

where

$$\left. \begin{aligned} \mathbf{K}_{qq} &= \iint_{A^e} \mathbf{B}^T \mathbf{D}\mathbf{B} dA \\ \mathbf{K}_{\alpha q} &= \iint_{A^e} \mathbf{B}_\alpha^T \mathbf{D}\mathbf{B} dA \\ k_{\alpha\alpha} &= \iint_{A^e} \mathbf{B}_\alpha^T \mathbf{D}\mathbf{B}_\alpha dA \end{aligned} \right\} \quad (6-20)$$

Applying a condensation process, we can solve α from $\frac{\partial U}{\partial \alpha} = 0$:

$$\alpha = -k_{\alpha\alpha}^{-1} \mathbf{K}_{\alpha q} \mathbf{q}^e$$

Substitution of the above equation into Eq. (6-19) yields

$$U = \frac{1}{2} \mathbf{q}^{eT} \mathbf{K}^e \mathbf{q}^e$$

where \mathbf{K}^e is the element stiffness matrix after condensation:

$$\mathbf{K}^e = \mathbf{K}_{qq} - \mathbf{K}_{\alpha q}^T k_{\alpha\alpha}^{-1} \mathbf{K}_{\alpha q} \quad (6-21)$$

6.1.3 Numerical Examples

Example 6.1 Simply-supported and clamped square plates subjected to uniformly distributed load q or central concentrated load P —comparison of five triangular thin plate elements. L is the length of the plate side; and Poisson's ratio $\mu = 0.3$.

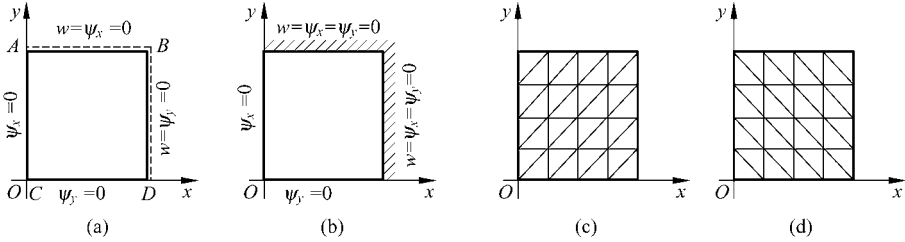


Figure 6.2 Meshes for a quarter square plate

(a) A quarter simply-supported square plate; (b) A quarter clamped square plate; (c) Mesh orientation *A* Mesh density $N = 4$; (d) Mesh orientation *B* Mesh density $N = 4$

Owing to symmetry, only one-quarter of the plate is modelled. As shown in Fig. 6.2, two mesh orientations (*A* and *B*) are considered. For comparison, the results by the five triangular element models with 9 DOFs, the generalized conforming element TGC-9-1, the discrete Kirchhoff theory element DKT^[2, 3], the hybrid-stress element HSM^[2, 4], the non-conforming element BCIZ^[1] and the conforming element HCT^[5], are given together.

The results of the central deflection w_C for the uniformly distributed load case are plotted in Figs. 6.3 and 6.4. And, the results for the concentrated load case are given in Figs. 6.5 and 6.6. Among the five elements used, the generalized conforming element TGC-9-1 gives the most accurate answers, and the elements HSM and DKT give the second best ones.

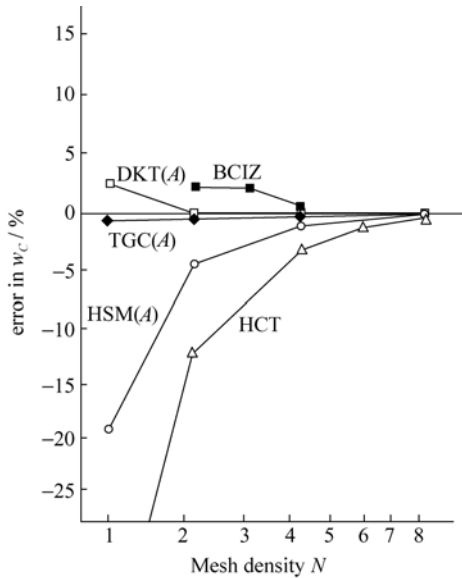


Figure 6.3 The percentage error for central deflection of the simply-supported square plate subjected to uniform load

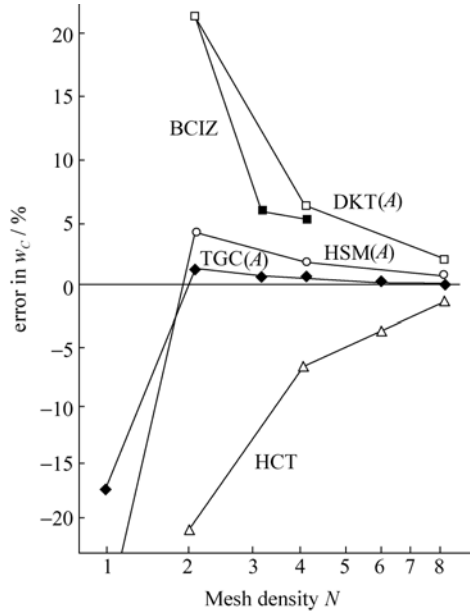


Figure 6.4 The percentage error for central deflection of the clamped square plate subjected to uniform load

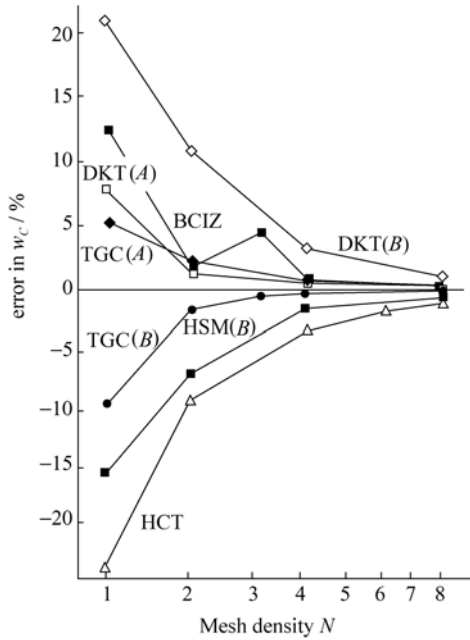


Figure 6.5 The percentage error for central deflection of the simply-supported square plate subjected to concentrated load

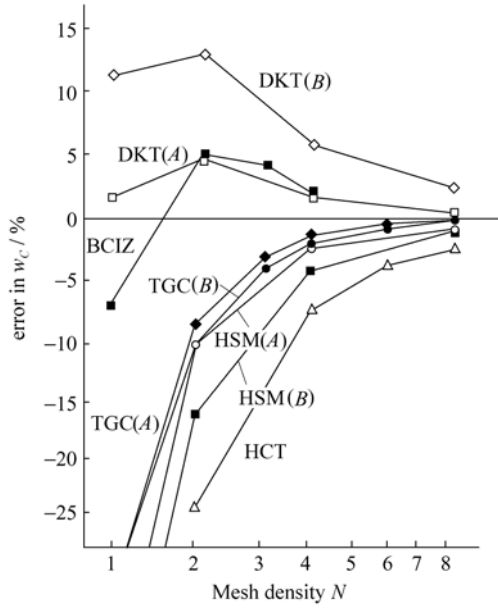


Figure 6.6 The percentage error for central deflection of the clamped square plate subjected to concentrated load

The results of the central moment M_C are given in Figs. 6.7 and 6.8. The accuracy of the generalized conforming element is still the best. And, the results

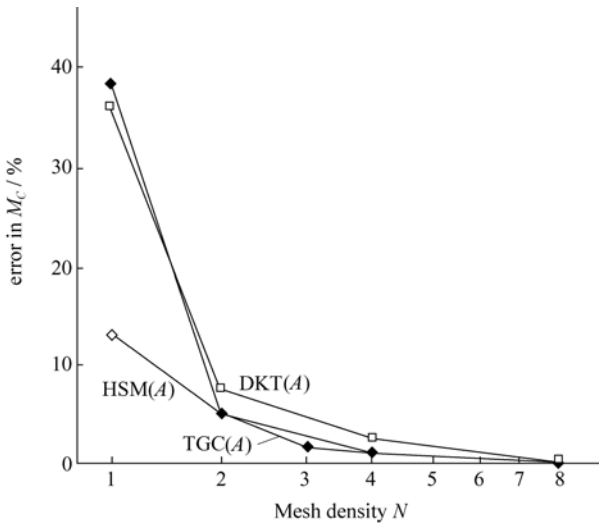


Figure 6.7 The percentage error for central moment of the simply-supported square plate subjected to uniform load

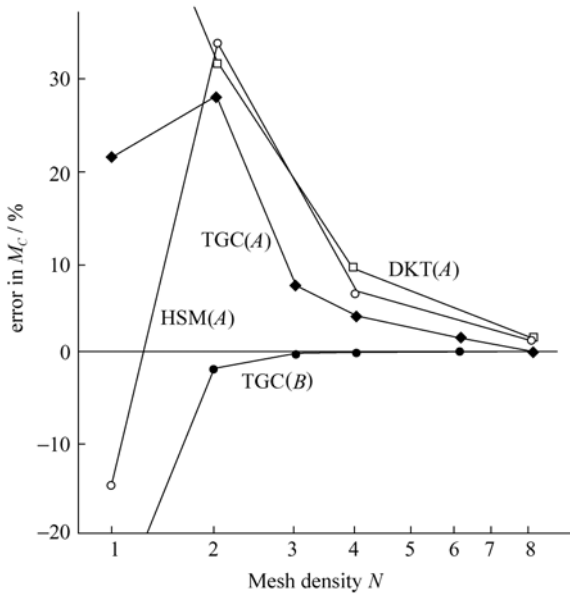


Figure 6.8 The percentage error for central moment of the clamped square plate subjected to uniform load

of the moment M_D at the mid-side point of the plate are given in Figs. 6.9 and 6.10. The elements TGC, HSM and DKT are at the same level of accuracy.

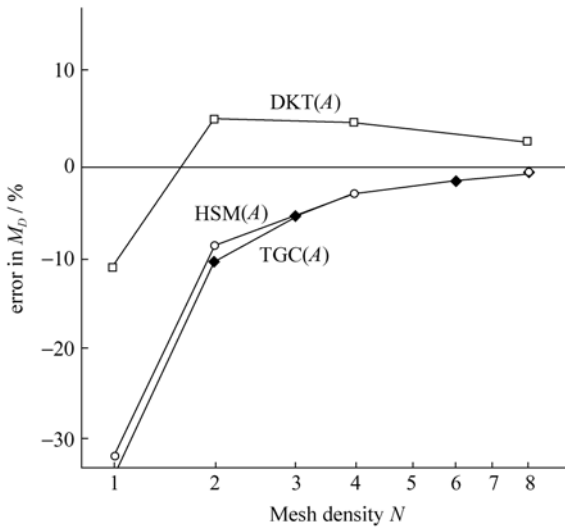


Figure 6.9 The percentage error for moment at mid-side point of the clamped square plate subjected to uniform load

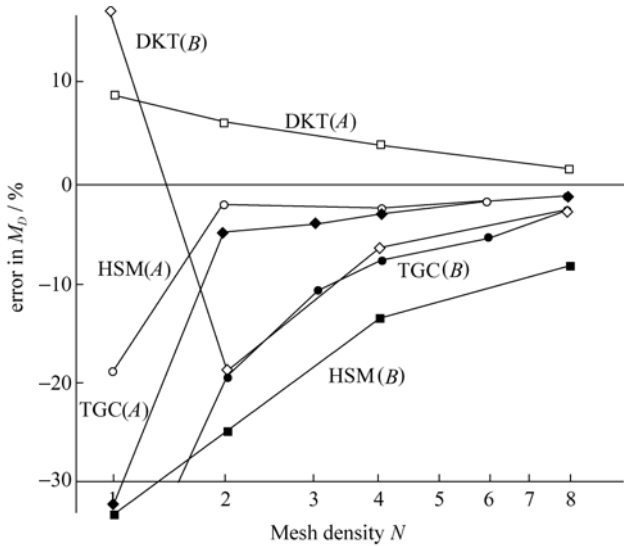


Figure 6.10 The percentage error for moment at mid-side point of the clamped square plate subjected to concentrated load

Different mesh orientations lead to different results for these elements, and the smallest difference is obtained by the generalized conforming element.

6.2 Line-Point Conforming Scheme—Rectangular Elements

The mixed scheme of line and point conforming is one of the most popular schemes for constructing the generalized conforming thin plate elements. We will introduce it in two sections: rectangular elements in this section and triangular elements in the next.

The no. 3, 4, 5 elements RGC-12, CGC-R12 and LGC-R12 in Table 5.1 are all rectangular elements constructed by the line-point conforming scheme, in which $m = n = 12$. Besides, some other contents, including the simplification by using the symmetry of rectangular elements, and the buckling analysis of thin plates, are also introduced.

6.2.1 Rectangular Element RGC-12 (Bending Problem)

A 12-DOF rectangular thin plate element is shown in Fig. 6.11. The element nodal displacement vector q^e is

$$\mathbf{q}^e = [w_1 \quad \psi_{x1} \quad \psi_{y1} \quad w_2 \quad \psi_{x2} \quad \psi_{y2} \quad w_3 \quad \psi_{x3} \quad \psi_{y3} \quad w_4 \quad \psi_{x4} \quad \psi_{y4}]^T$$

where w denotes the deflection; $\psi_x = \frac{\partial w}{\partial x}$ and $\psi_y = \frac{\partial w}{\partial y}$ denote the rotations.

Along each element side, the deflection \tilde{w} is assumed to be cubic and the normal slope $\tilde{\psi}_n$ linearly distributed.

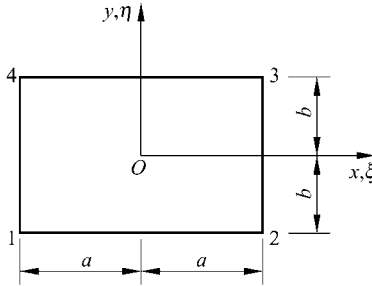


Figure 6.11 Rectangular plate

Let ξ, η be the dimensionless coordinates: $\xi = \frac{x}{a}, \eta = \frac{y}{b}$.

According to the element ACM^[6], the element deflection field w is described by an incomplete quartic polynomial

$$w = \mathbf{F}_\lambda \boldsymbol{\lambda} \tag{6-22}$$

in which

$$\left. \begin{aligned} \boldsymbol{\lambda} &= [\lambda_1 \quad \lambda_2 \quad \lambda_3 \quad \lambda_4 \quad \lambda_5 \quad \lambda_6 \quad \lambda_7 \quad \lambda_8 \quad \lambda_9 \quad \lambda_{10} \quad \lambda_{11} \quad \lambda_{12}]^T \\ \mathbf{F}_\lambda &= [1 \quad \xi \quad \eta \quad \xi^2 \quad \xi\eta \quad \eta^2 \quad \xi^3 \quad \xi^2\eta \quad \xi\eta^2 \quad \eta^3 \quad \xi^3\eta \quad \xi\eta^3] \end{aligned} \right\} \tag{6-23}$$

In order to solve $\boldsymbol{\lambda}$, it is necessary to choose 12 generalized conforming conditions and their corresponding generalized displacements \mathbf{d} .

$$\mathbf{d} = [d_1 \quad d_2 \quad d_3 \quad d_4 \quad d_5 \quad d_6 \quad d_7 \quad d_8 \quad d_9 \quad d_{10} \quad d_{11} \quad d_{12}]^T$$

First of all, we consider the average deflection, the average tangential slope and the average normal slope of each element side, thus 12 average displacements are involved. But, there are two identity relations for these quantities, so only 10 of the average displacements are independent, which may be chosen as the first ten generalized displacements d_1, d_2, \dots, d_{10} . And, the rotations of node 1, ψ_{x1}

and ψ_{y1} , could be chosen as the other two generalized displacements d_{11} and d_{12} . Thus, 12 generalized conforming conditions are established as follows:

$$\left. \begin{aligned}
 \int_{-1}^1 \left(\frac{\partial w}{\partial y} \right)_{12} d\xi &= d_1 = \int_{-1}^1 \bar{\psi}_{y12} d\xi \\
 \int_{-1}^1 \left(\frac{\partial w}{\partial x} \right)_{23} d\eta &= d_2 = \int_{-1}^1 \bar{\psi}_{x23} d\eta \\
 \int_{-1}^1 \left(\frac{\partial w}{\partial y} \right)_{43} d\xi &= d_3 = \int_{-1}^1 \bar{\psi}_{y43} d\xi \\
 \int_{-1}^1 \left(\frac{\partial w}{\partial x} \right)_{14} d\eta &= d_4 = \int_{-1}^1 \bar{\psi}_{x14} d\eta \\
 \int_{-1}^1 \left(\frac{\partial w}{\partial x} \right)_{12} d\xi &= d_5 = \int_{-1}^1 \left(\frac{\partial \tilde{w}}{\partial x} \right)_{12} d\xi \\
 \int_{-1}^1 \left(\frac{\partial w}{\partial y} \right)_{23} d\eta &= d_6 = \int_{-1}^1 \left(\frac{\partial \tilde{w}}{\partial y} \right)_{23} d\eta \\
 \int_{-1}^1 \left(\frac{\partial w}{\partial x} \right)_{43} d\xi &= d_7 = \int_{-1}^1 \left(\frac{\partial \tilde{w}}{\partial x} \right)_{43} d\xi \\
 \int_{-1}^1 w_{12} d\xi &= d_8 = \int_{-1}^1 \tilde{w}_{12} d\xi \\
 \int_{-1}^1 w_{23} d\eta &= d_9 = \int_{-1}^1 \tilde{w}_{23} d\eta \\
 \int_{-1}^1 w_{43} d\xi &= d_{10} = \int_{-1}^1 \tilde{w}_{43} d\xi \\
 \left(\frac{\partial w}{\partial x} \right)_1 &= d_{11} = \psi_{x1} \\
 \left(\frac{\partial w}{\partial y} \right)_1 &= d_{12} = \psi_{y1}
 \end{aligned} \right\} \quad (6-24)$$

Equation (6-24) can be written as

$$\hat{C}\lambda = \hat{G}q^e \quad (6-25)$$

where

$$\hat{\mathbf{G}} = \begin{bmatrix} 0 & 0 & 1 & 0 & 0 & 1 & 0 & 0 & 0 & 0 & 0 & 0 \\ 0 & 0 & 0 & 0 & 1 & 0 & 0 & 1 & 0 & 0 & 0 & 0 \\ 0 & 0 & 0 & 0 & 0 & 0 & 0 & 0 & 1 & 0 & 0 & 1 \\ 0 & 1 & 0 & 0 & 0 & 0 & 0 & 0 & 0 & 0 & 1 & 0 \\ -1 & 0 & 0 & 1 & 0 & 0 & 0 & 0 & 0 & 0 & 0 & 0 \\ 0 & 0 & 0 & -1 & 0 & 0 & 1 & 0 & 0 & 0 & 0 & 0 \\ 0 & 0 & 0 & 0 & 0 & 0 & -1 & 0 & 0 & 1 & 0 & 0 \\ 1 & \frac{a}{3} & 0 & 1 & -\frac{a}{3} & 0 & 0 & 0 & 0 & 0 & 0 & 0 \\ 0 & 0 & 0 & 1 & 0 & \frac{b}{3} & 1 & 0 & -\frac{b}{3} & 0 & 0 & 0 \\ 0 & 0 & 0 & 0 & 0 & 0 & 1 & -\frac{a}{3} & 0 & 1 & \frac{a}{3} & 0 \\ 0 & 1 & 0 & 0 & 0 & 0 & 0 & 0 & 0 & 0 & 0 & 0 \\ 0 & 0 & 1 & 0 & 0 & 0 & 0 & 0 & 0 & 0 & 0 & 0 \end{bmatrix} \quad (6-26a)$$

$$\hat{\mathbf{C}} = \begin{bmatrix} 0 & 0 & \frac{2}{b} & 0 & 0 & -\frac{4}{b} & 0 & \frac{2}{3b} & 0 & \frac{6}{b} & 0 & 0 \\ 0 & \frac{2}{a} & 0 & \frac{4}{a} & 0 & 0 & \frac{6}{a} & 0 & \frac{2}{3a} & 0 & 0 & 0 \\ 0 & 0 & \frac{2}{b} & 0 & 0 & \frac{4}{b} & 0 & \frac{2}{3b} & 0 & \frac{6}{b} & 0 & 0 \\ 0 & \frac{2}{a} & 0 & -\frac{4}{a} & 0 & 0 & \frac{6}{a} & 0 & \frac{2}{3a} & 0 & 0 & 0 \\ 0 & 2 & 0 & 0 & -2 & 0 & 2 & 0 & 2 & 0 & -2 & -2 \\ 0 & 0 & 2 & 0 & 2 & 0 & 0 & 2 & 0 & 2 & 2 & 2 \\ 0 & -2 & 0 & 0 & -2 & 0 & -2 & 0 & -2 & 0 & -2 & -2 \\ 2 & 0 & -2 & \frac{2}{3} & 0 & 2 & 0 & -\frac{2}{3} & 0 & -2 & 0 & 0 \\ 2 & 2 & 0 & 2 & 0 & \frac{2}{3} & 2 & 0 & \frac{2}{3} & 0 & 0 & 0 \\ 2 & 0 & 2 & \frac{2}{3} & 0 & 2 & 0 & \frac{2}{3} & 0 & 2 & 0 & 0 \\ 0 & \frac{1}{a} & 0 & -\frac{2}{a} & -\frac{1}{a} & 0 & \frac{3}{a} & \frac{2}{a} & \frac{1}{a} & 0 & -\frac{3}{a} & -\frac{1}{a} \\ 0 & 0 & \frac{1}{b} & 0 & -\frac{1}{b} & -\frac{2}{b} & 0 & \frac{1}{b} & \frac{2}{b} & \frac{3}{b} & -\frac{1}{b} & -\frac{3}{b} \end{bmatrix} \quad (6-26b)$$

From Eqs. (6-25) and (6-22), we have

$$w = F_2 \hat{C}^{-1} Gq^e \tag{6-27}$$

And then, the element stiffness matrix can be obtained by the conventional procedure.

Example 6.2 Simply-supported and clamped square plates subjected to uniformly distributed load q or central concentrated load P —comparison of different rectangular thin plate elements. L is the length of the plate side; and Poisson’s ratio $\mu = 0.3$.

The deflection coefficients at the plate center are given in Table 6.1. For the sake of comparison, not only the results by the generalized conforming element RGC-12 but also those by the element ACM^[7] are given (the numbers in parentheses are relative errors). It can be seen from Table 6.1 that the precision of the element RGC-12 is better than that of the element ACM. The moment coefficients are given in Table 6.2, and also exhibit high precision.

Table 6.1 The deflection coefficients at central point

Mesh (whole plate)	Simply-supported			
	α (uniform)		β (concentrated)	
	ACM ^[7]	RGC-12	ACM ^[7]	RGC-12
2 × 2	0.3446(−15%)	0.4003(−1.5%)	1.378(+18.8%)	1.116(−3.8%)
4 × 4	0.3939(−3%)	0.4034(−0.7%)	1.233(+6.3%)	1.146(−1.2%)
8 × 8	0.4033(−0.7%)	0.4053(−0.2%)	1.183(+2%)	1.155(−0.4%)
16 × 16	0.4056(−0.15%)	0.4061(−0.02%)	1.167(+0.6%)	1.159(−0.1%)
Analytical solution	0.4062		1.160	
Mesh (whole plate)	Clamped			
	α (uniform)		β (concentrated)	
	ACM ^[7]	RGC-12	ACM ^[7]	RGC-12
2 × 2	0.1480(+17.0%)	0.1479(+16.9%)	0.5919(+5.5%)	0.5918(+5.5%)
4 × 4	0.1403(+10.9%)	0.1228(−2.9%)	0.6134(+9.3%)	0.5433(−3.2%)
8 × 8	0.1304(+3.1%)	0.1253(−0.09%)	0.5803(+3.4%)	0.5550(−1.1%)
16 × 16	0.1275(+0.08%)	0.1262(−0.02%)	0.5672(+1.1%)	0.5596(−0.3%)
Analytical solution	0.1265		0.5612	

Note:
$$\begin{cases} w_{\max} = \alpha \frac{qL^4}{D} \left(\frac{1}{100} \right) & \text{(uniform)} \\ w_{\max} = \beta \frac{PL^2}{D} \left(\frac{1}{100} \right) & \text{(concentrated)} \end{cases}, \quad D = \frac{Eh^3}{12(1-\mu^2)}, \quad E \text{ is the Young's modulus, } \mu \text{ is the}$$

Poisson’s ratio.

Table 6.2 Moment coefficients

Mesh (whole plate)	Central moment		Moment at mid point of boundary	
	Simply-supported	Clamped	Clamped	
	α_1 (load q)	α_1 (load q)	α_1 (load q)	β_1 (load P)
2×2	0.0521(+8.8%)	0.0462(+102%)	-0.0355(+30.8%)	-0.1420(-13.0%)
4×4	0.0484(+1.0%)	0.0239(+4.4%)	-0.0438(+14.6%)	-0.1156(+8.0%)
8×8	0.0479(0%)	0.0230(+0.4%)	-0.0489(+4.7%)	-0.1221(+2.9%)
16×16	0.0479(0%)	0.0230(+0.4%)	-0.0506(+1.4%)	-0.1245(1.0%)
Analytical solution	0.0479	0.0229	-0.0513	-0.1257

Note: $\begin{cases} M = \alpha_1 q L^2 & \text{(uniform)} \\ M = \beta_1 P & \text{(concentrated)} \end{cases}$

6.2.2 Utilization of the Symmetry of Rectangular Elements

We consider the case $m = n = 12$ for the rectangular thin plate elements, and take the element RGC-12 as an example. The main construction procedure is how to establish 12 generalized conforming conditions, i.e. Eq. (6-25), in which \hat{C} is a 12×12 matrix. When solving λ , the inverse matrix \hat{C}^{-1} is needed. It is not an easy work to obtain the inverse matrix of a 12×12 matrix. So, for simplification, the symmetry of the rectangular elements may be used.

In a rectangular element, there are two symmetry axes, that is, x -axis and y -axis in Fig. 6.11. If the symmetry is fully used, the 12 generalized conforming conditions can be classified into four equation groups:

- ◆ Symmetry-Symmetry (SS) group—symmetry with respect to both x -axis and y -axis;
- ◆ Symmetry-Antisymmetry (SA) group—symmetry with respect to the x -axis, antisymmetry with respect to the y -axis;
- ◆ Antisymmetry-Symmetry (AS) group—antisymmetry with respect to the x -axis, symmetry with respect to the y -axis;
- ◆ Antisymmetry-Antisymmetry (AA) group—antisymmetry with respect to both x -axis and y -axis.

Thus, each conforming equation group is usually a set of equations with only three unknown variables, which is much simpler to be solved.

Now, let us take the element RGC-12 as an example to illustrate the whole procedure.

Firstly, the element deflection field is expressed by Eqs. (6-22) and (6-23), in which 12 unknown coefficients and their basis functions have already been classified into four groups:

$$\left. \begin{aligned} \text{SS group} &-\lambda_1, \lambda_4\xi^2, \lambda_6\eta^2 \\ \text{SA group} &-\lambda_2\xi, \lambda_7\xi^3, \lambda_9\xi\eta^2 \\ \text{AS group} &-\lambda_3\eta, \lambda_8\xi^2\eta, \lambda_{10}\eta^3 \\ \text{AA group} &-\lambda_5\xi\eta, \lambda_{11}\xi^3\eta, \lambda_{12}\xi\eta^3 \end{aligned} \right\} \quad (6-28)$$

Secondly, the selected generalized conforming conditions should also possess symmetry or antisymmetry. In fact, all the average line conforming and point conforming conditions about w , ψ_x and ψ_y in Eq. (6-24) do not satisfy this requirement. Therefore, the conforming conditions should be recombined so that the new combination conditions should possess symmetry and antisymmetry, and then, can be vested in one of the above four groups.

For instance, the average line conforming conditions of the rectangular elements can be treated as follows.

In a rectangular element, there are 12 average line conforming conditions about w , ψ_n , ψ_s of each side (the number of independent conditions will be discussed later). According to symmetry or antisymmetry, these conditions can be re-combined to form 12 new combination conditions which are classified as:

(1) Combination conditions belonging to SS group (4 conditions)

$$\int_{-1}^1 (w_{43} + w_{12})d\xi = \int_{-1}^1 (\tilde{w}_{43} + \tilde{w}_{12})d\xi \quad (6-A1)$$

$$\int_{-1}^1 (w_{23} + w_{14})d\eta = \int_{-1}^1 (\tilde{w}_{23} + \tilde{w}_{14})d\eta \quad (6-A2)$$

$$\int_{-1}^1 \left[\left(\frac{\partial w}{\partial x} \right)_{23} - \left(\frac{\partial w}{\partial x} \right)_{14} \right] d\eta = \int_{-1}^1 (\tilde{\psi}_{n23} + \tilde{\psi}_{n14})d\eta \quad (6-A3)$$

$$\int_{-1}^1 \left[\left(\frac{\partial w}{\partial y} \right)_{43} - \left(\frac{\partial w}{\partial y} \right)_{12} \right] d\xi = \int_{-1}^1 (\tilde{\psi}_{s43} + \tilde{\psi}_{s12})d\xi \quad (6-A4)$$

(2) Combination conditions belonging to SA group (3 conditions)

$$\int_{-1}^1 (w_{23} - w_{14})d\eta = \int_{-1}^1 (\tilde{w}_{23} - \tilde{w}_{14})d\eta \quad (6-B1)$$

$$\int_{-1}^1 \left[\left(\frac{\partial w}{\partial x} \right)_{23} + \left(\frac{\partial w}{\partial x} \right)_{14} \right] d\eta = \int_{-1}^1 (\tilde{\psi}_{n23} - \tilde{\psi}_{n14})d\eta \quad (6-B2)$$

$$\int_{-1}^1 \left[\left(\frac{\partial w}{\partial x} \right)_{43} + \left(\frac{\partial w}{\partial x} \right)_{12} \right] d\xi = \int_{-1}^1 (-\tilde{\psi}_{s43} + \tilde{\psi}_{s12})d\xi \quad (6-B3)$$

(3) Combination conditions belonging to AS group (3 conditions)

$$\int_{-1}^1 (w_{43} - w_{12}) d\xi = \int_{-1}^1 (\tilde{w}_{43} - \tilde{w}_{12}) d\xi \quad (6-C1)$$

$$\int_{-1}^1 \left[\left(\frac{\partial w}{\partial y} \right)_{43} + \left(\frac{\partial w}{\partial y} \right)_{12} \right] d\xi = \int_{-1}^1 (\tilde{\psi}_{n43} - \tilde{\psi}_{n12}) d\xi \quad (6-C2)$$

$$\int_{-1}^1 \left[\left(\frac{\partial w}{\partial y} \right)_{23} + \left(\frac{\partial w}{\partial y} \right)_{14} \right] d\eta = \int_{-1}^1 (\tilde{\psi}_{s23} - \tilde{\psi}_{s14}) d\eta \quad (6-C3)$$

(4) Combination conditions belonging to AA group (2 conditions)

$$\int_{-1}^1 \left[\left(\frac{\partial w}{\partial x} \right)_{43} - \left(\frac{\partial w}{\partial x} \right)_{12} \right] d\xi = \int_{-1}^1 -(\tilde{\psi}_{s43} + \tilde{\psi}_{s12}) d\xi \quad (6-D1)$$

$$\int_{-1}^1 \left[\left(\frac{\partial w}{\partial y} \right)_{23} - \left(\frac{\partial w}{\partial y} \right)_{14} \right] d\eta = \int_{-1}^1 (\tilde{\psi}_{s23} + \tilde{\psi}_{s14}) d\eta \quad (6-D2)$$

The combination conforming conditions are derived by selecting the combination boundary forces as weighting functions. The above conforming condition groups are just classified by the symmetry or antisymmetry of the selected combination boundary forces.

Substitution of the element deflection field (6-22) and the interpolation formulae for boundary displacements into the above 12 conditions yields

(1) SS group

$$\lambda_1 + \frac{1}{3}\lambda_4 + \lambda_6 = \frac{1}{4} \sum_{i=1}^4 w_i - \frac{a}{12} \sum_{i=1}^4 \psi_{xi} \xi_i \quad (6-A1)'$$

$$\lambda_1 + \lambda_4 + \frac{1}{3}\lambda_6 = \frac{1}{4} \sum_{i=1}^4 w_i - \frac{b}{12} \sum_{i=1}^4 \psi_{yi} \eta_i \quad (6-A2)'$$

$$\lambda_4 = \frac{a}{8} \sum_{i=1}^4 \psi_{xi} \xi_i \quad (6-A3)'$$

$$\lambda_6 = \frac{b}{8} \sum_{i=1}^4 \psi_{yi} \eta_i \quad (6-A4)'$$

(2) SA group

$$\lambda_2 + \lambda_7 + \frac{1}{3}\lambda_9 = \frac{1}{4}\sum_{i=1}^4 w_i \xi_i - \frac{b}{12}\sum_{i=1}^4 \psi_{yi} \xi_i \eta_i \quad (6-B1)'$$

$$\lambda_2 + 3\lambda_7 + \frac{1}{3}\lambda_9 = \frac{a}{4}\sum_{i=1}^4 \psi_{xi} \quad (6-B2)'$$

$$\lambda_2 + \lambda_7 + \lambda_9 = \frac{1}{4}\sum_{i=1}^4 w_i \xi_i \quad (6-B3)'$$

(3) AS group

$$\lambda_3 + \frac{1}{3}\lambda_8 + \lambda_{10} = \frac{1}{4}\sum_{i=1}^4 w_i \eta_i - \frac{a}{12}\sum_{i=1}^4 \psi_{xi} \xi_i \eta_i \quad (6-C1)'$$

$$\lambda_3 + \frac{1}{3}\lambda_8 + 3\lambda_{10} = \frac{b}{4}\sum_{i=1}^4 \psi_{yi} \quad (6-C2)'$$

$$\lambda_3 + \lambda_8 + \lambda_{10} = \frac{1}{4}\sum_{i=1}^4 w_i \eta_i \quad (6-C3)'$$

(4) AA group

$$\lambda_5 + \lambda_{11} + \lambda_{12} = \frac{1}{4}\sum_{i=1}^4 w_i \xi_i \eta_i \quad (6-D1)'$$

$$\lambda_5 + \lambda_{11} + \lambda_{12} = \frac{1}{4}\sum_{i=1}^4 w_i \xi_i \eta_i \quad (6-D2)'$$

There are total 12 equations above, in which only 10 are independent, that is, 2 equations are not independent.

Firstly, the two Eqs. (6-D1)' and (6-D2)' in the AA group are actually the same, so one of these two conditions is not independent. This is an inevitable result produced by the identical Eq. (6-4), which shows that four average line conforming conditions about ψ_s along four element sides should contain an independent one.

Secondly, there is an independent equation among the four Eqs. (6-A1)', (6-A2)', (6-A3)' and (6-A4)' in the SS group. For example, Eq. (6-A2)' can be derived from the other three equations. This is because only three unknown coefficients ($\lambda_1, \lambda_2, \lambda_3$) are involved in the four equations of the SS group. If it is not a contradictory equation set, it must contain an independent equation.

Anyway, we have only 10 independent conditions here. The first three groups separately have three independent equations, from which three unknown coefficients of each group can be solved.

SS group

$$\left. \begin{aligned} \lambda_1 &= \frac{1}{4} \sum_{i=1}^4 w_i - \frac{a}{8} \sum_{i=1}^4 \psi_{xi} \xi_i - \frac{b}{8} \sum_{i=1}^4 \psi_{yi} \eta_i \\ \lambda_4 &= \frac{a}{8} \sum_{i=1}^4 \psi_{xi} \xi_i \\ \lambda_6 &= \frac{b}{8} \sum_{i=1}^4 \psi_{yi} \eta_i \end{aligned} \right\} \quad (6-29)$$

SA group

$$\left. \begin{aligned} \lambda_2 &= \frac{3}{8} \sum_{i=1}^4 w_i \xi_i - \frac{a}{8} \sum_{i=1}^4 \psi_{xi} - \frac{b}{6} \sum_{i=1}^4 \psi_{yi} \xi_i \eta_i \\ \lambda_7 &= -\frac{1}{8} \sum_{i=1}^4 w_i \xi_i + \frac{a}{8} \sum_{i=1}^4 \psi_{xi} + \frac{b}{24} \sum_{i=1}^4 \psi_{yi} \xi_i \eta_i \\ \lambda_9 &= \frac{b}{8} \sum_{i=1}^4 \psi_{yi} \xi_i \eta_i \end{aligned} \right\} \quad (6-30)$$

AS group

$$\left. \begin{aligned} \lambda_3 &= \frac{3}{8} \sum_{i=1}^4 w_i \eta_i - \frac{a}{6} \sum_{i=1}^4 \psi_{xi} \xi_i \eta_i - \frac{b}{8} \sum_{i=1}^4 \psi_{yi} \\ \lambda_8 &= \frac{a}{8} \sum_{i=1}^4 \psi_{xi} \xi_i \eta_i \\ \lambda_{10} &= -\frac{1}{8} \sum_{i=1}^4 w_i \eta_i + \frac{a}{24} \sum_{i=1}^4 \psi_{xi} \xi_i \eta_i + \frac{b}{8} \sum_{i=1}^4 \psi_{yi} \end{aligned} \right\} \quad (6-31)$$

As for the AA group, there is only one independent condition (6-D1)'. So, two conforming conditions should be supplemented for solving the three unknown coefficients $\lambda_5, \lambda_{11}, \lambda_{12}$.

In the element RGC-12, the two supplementary conditions are the last two point conforming conditions,

$$\left(\frac{\partial w}{\partial x} \right)_1 = \psi_{x1}, \quad \left(\frac{\partial w}{\partial y} \right)_1 = \psi_{y1}$$

that is

$$\begin{aligned} -2\lambda_4 + (\lambda_2 + 3\lambda_7 + \lambda_9) + 2\lambda_8 - (\lambda_5 + 3\lambda_{11} + \lambda_{12}) &= a\psi_{x1} \\ -2\lambda_6 + 2\lambda_9 + (\lambda_3 + \lambda_8 + 3\lambda_{10}) - (\lambda_5 + \lambda_{11} + 3\lambda_{12}) &= b\psi_{y1} \end{aligned}$$

Solving the simultaneous equations of the above two equations and Eq. (6-D1)', the

remaining three unknown coefficients can be obtained:

$$\left. \begin{aligned} \lambda_5 &= \frac{1}{2} \sum_{i=1}^4 w_i \xi_i \eta_i - \frac{a}{8} \sum_{i=1}^4 \psi_{xi} \left(1 + \frac{1}{3} \xi_i \right) \eta_i - \frac{b}{8} \sum_{i=1}^4 \psi_{yi} \xi_i \left(1 + \frac{1}{3} \eta_i \right) \\ \lambda_{11} &= -\frac{1}{8} \sum_{i=1}^4 w_i \xi_i \eta_i + \frac{a}{8} \sum_{i=1}^4 \psi_{xi} \eta_i + \frac{b}{24} \sum_{i=1}^4 \psi_{yi} \xi_i \eta_i \\ \lambda_{12} &= -\frac{1}{8} \sum_{i=1}^4 w_i \xi_i \eta_i + \frac{a}{24} \sum_{i=1}^4 \psi_{xi} \xi_i \eta_i + \frac{b}{8} \sum_{i=1}^4 \psi_{yi} \xi_i \end{aligned} \right\} \quad (6-32)$$

Though the above two supplementary conditions are simple and feasible, they are related to the numbering of the element nodes. So, the following two combination point conforming conditions are more reasonable (belong to the AA group):

$$\left. \begin{aligned} \sum_{i=1}^4 \left(\frac{\partial w}{\partial x} \right)_i \eta_i &= \sum_{i=1}^4 \psi_{xi} \eta_i \\ \sum_{i=1}^4 \left(\frac{\partial w}{\partial y} \right)_i \xi_i &= \sum_{i=1}^4 \psi_{yi} \xi_i \end{aligned} \right\} \quad (6-33)$$

that is

$$\left. \begin{aligned} \lambda_5 + 3\lambda_{11} + \lambda_{12} &= \frac{a}{4} \sum_{i=1}^4 \psi_{xi} \eta_i \\ \lambda_5 + \lambda_{11} + 3\lambda_{12} &= \frac{b}{4} \sum_{i=1}^4 \psi_{yi} \xi_i \end{aligned} \right\} \quad (6-34)$$

Solving Eqs. (6-34) and (6-D1)' simultaneously, we obtain

$$\left. \begin{aligned} \lambda_5 &= \frac{1}{2} \sum_{i=1}^4 w_i \xi_i \eta_i - \frac{a}{8} \sum_{i=1}^4 \psi_{xi} \eta_i - \frac{b}{8} \sum_{i=1}^4 \psi_{yi} \xi_i \\ \lambda_{11} &= -\frac{1}{8} \sum_{i=1}^4 w_i \xi_i \eta_i + \frac{a}{8} \sum_{i=1}^4 \psi_{xi} \eta_i \\ \lambda_{12} &= -\frac{1}{8} \sum_{i=1}^4 w_i \xi_i \eta_i + \frac{b}{8} \sum_{i=1}^4 \psi_{yi} \xi_i \end{aligned} \right\} \quad (6-35)$$

The element obtained by this scheme is the same as no. 23 element LR12-2 in Table 5.1, only the derivation procedures are different.

6.2.3 Rectangular Element RGC-12 (Buckling Problem)

Now, consider the buckling problem for thin plates. The in-plane stress resultants N_x , N_y and N_{xy} of the mid-plane are assumed to be linearly distributed (as shown

in Fig. 6.12):

$$\left. \begin{aligned} N_x &= -(P_x + \xi Q_x + \eta R_x) \\ N_y &= -(P_y + \xi Q_y + \eta R_y) \\ N_{xy} &= -(P_{xy} + \xi Q_{xy} + \eta R_{xy}) \end{aligned} \right\} \quad (6-36)$$

where $P_x, P_y, P_{xy}, Q_x, Q_y, Q_{xy}, R_x, R_y, R_{xy}$ are all constants.

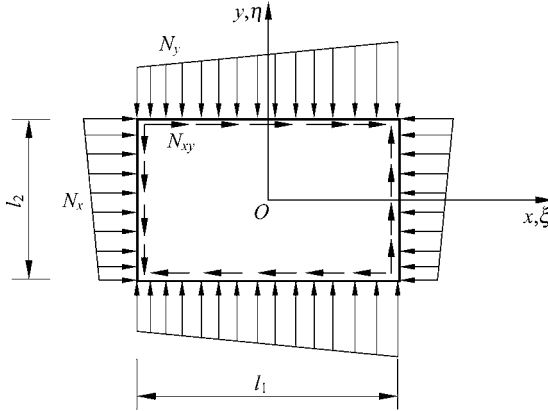


Figure 6.12 Stability problem for thin plates

The geometric stiffness matrix of the generalized conforming element is given by

$$\mathbf{g}^e = (\hat{\mathbf{C}}^{-1} \hat{\mathbf{G}})^T \mathbf{g}_{\lambda\lambda}^e (\hat{\mathbf{C}}^{-1} \hat{\mathbf{G}}) \quad (6-37)$$

where

$$\begin{aligned} \mathbf{g}_{\lambda\lambda}^e = \int_{-1}^1 \int_{-1}^1 & \left\{ \frac{b}{a} (P_x + \xi Q_x + \eta R_x) \mathbf{F}_{\lambda,\xi}^T \mathbf{F}_{\lambda,\xi} + \frac{a}{b} (P_y + \xi Q_y + \eta R_y) \mathbf{F}_{\lambda,\eta}^T \mathbf{F}_{\lambda,\eta} \right. \\ & \left. + (P_{xy} + \xi Q_{xy} + \eta R_{xy}) (\mathbf{F}_{\lambda,\xi}^T \mathbf{F}_{\lambda,\eta} + \mathbf{F}_{\lambda,\eta}^T \mathbf{F}_{\lambda,\xi}) \right\} d\xi d\eta \end{aligned} \quad (6-38)$$

in which $\mathbf{F}_{\lambda,\xi}$ and $\mathbf{F}_{\lambda,\eta}$ denote the derivatives of \mathbf{F}_λ with respect to ξ and η , respectively.

Then the critical load of the thin plate can be calculated by the above stiffness matrix \mathbf{K}^e and geometric stiffness matrix \mathbf{g}^e of the generalized conforming element.

Example 6.3 The buckling critical load P_{cr} for the simply-supported and clamped square plates subjected to uniform compression in one direction. The length of the plate side is L .

The results of the buckling critical load P_{xcr} calculated from the element RGC-12 are given in Table 6.3. Compared with the results given by reference [8], this generalized conforming element gives more accurate results. The numbers in parentheses are relative errors.

Table 6.3 Coefficient k for square plate under compression in one direction

Mesh (whole plate)	Simply-supported		Clamped	
	Kapur [8]	RGC-12	Kapur [8]	RGC-12
4 × 4	3.770(-5.8%)	4.128(+3.2%)	9.28(-7.8%)	9.70(-3.7%)
6 × 6	3.887(-2.8%)	4.028(+0.7%)	9.61(-4.6%)	10.12(+0.5%)
8 × 8	3.933(-1.7%)	4.009(+0.2%)	9.78(-2.9%)	10.12(+0.5%)
10 × 10	3.960(-1.0%)	4.002(+0.05%)	9.89(-1.8%)	10.12(+0.5%)
Analytical solution	4.000		10.07	

Note: $P_{xcr} = k \frac{\pi^2 D}{l^2}$

Example 6.4 The buckling critical load P_{xycr} for a simply-supported rectangular plate $\left(\frac{L_1}{L_2} = 1.25\right)$ under shear load.

The results are given in Table 6.4. Compared with those given in reference [8], the generalized conforming element gives more accurate results.

Table 6.4 Coefficient k for a simply-supported rectangular plate $\left(\frac{L_1}{L_2} = \frac{5}{4}\right)$ under shear load

Mesh (whole plate)	Kapur ^[8]	RGC-12
4 × 4	6.95(-9.9%)	7.84(+1.7%)
6 × 6	7.25(-6.0%)	7.74(+0.4%)
8 × 8	7.45(-3.4%)	7.74(+0.4%)
10 × 10	—	7.72(+0.1%)
Analytical solution	7.71	

Note: $P_{xycr} = k \frac{\pi^2 D}{l_2^2}$

6.2.4 Rectangular Element CGC-R12^[9]

The element CGC-R12 is also a rectangular thin plate element with 12 DOFs, which are still the deflection w_i , rotations ψ_{xi} and ψ_{yi} ($i = 1, 2, 3, 4$) at each corner node.

The element deflection field is assumed to be an incomplete quartic polynomial containing 12 unknown coefficients, and expressed in terms of the dimensionless rectangular coordinates ξ and η as follows:

$$w = \lambda_1 + \lambda_2\xi + \lambda_3\eta + \lambda_4\xi\eta + (\xi^2 - 1)(\lambda_5 + \lambda_7\eta + \lambda_9\xi) + (\eta^2 - 1)(\lambda_6 + \lambda_8\xi + \lambda_{10}\eta) + \lambda_{11}(\xi^4 - 1) + \lambda_{12}(\eta^4 - 1) \quad (6-39)$$

According to the line-point conforming scheme, 12 conforming conditions are selected as follows:

(1) point conforming conditions of w at the corner nodes (4 conditions)

$$w_i - \tilde{w}_i = 0 \quad (i = 1,2,3,4) \quad (6-40)$$

(2) average line conforming conditions of w and ψ_n along the element sides (8 conditions)

$$\int_{d_{ij}} (w - \tilde{w}) ds = 0 \quad (ij = 12,23,34,41) \quad (6-41)$$

$$\int_{d_{ij}} \left(\frac{\partial w}{\partial n} - \tilde{\psi}_n \right) ds = 0 \quad (ij = 12,23,34,41) \quad (6-42)$$

From the four point conforming conditions in Eq. (6-40), the first four unknown coefficients can be obtained:

$$\lambda_1 = \frac{1}{4} \sum_{i=1}^4 w_i, \quad \lambda_2 = \frac{1}{4} \sum_{i=1}^4 w_i \xi_i, \quad \lambda_3 = \frac{1}{4} \sum_{i=1}^4 w_i \eta_i, \quad \lambda_4 = \frac{1}{4} \sum_{i=1}^4 w_i \xi_i \eta_i \quad (6-43)$$

Substitution of the above equation into Eq. (6-39) yields

$$w = \frac{1}{4} \sum_{i=1}^4 w_i (1 + \xi_i \xi) (1 + \eta_i \eta) + (\xi^2 - 1)(\lambda_5 + \lambda_7\eta + \lambda_9\xi) + (\eta^2 - 1)(\lambda_6 + \lambda_8\xi + \lambda_{10}\eta) + \lambda_{11}(\xi^4 - 1) + \lambda_{12}(\eta^4 - 1) \quad (6-44)$$

And, the residual eight unknown coefficients can be determined by the line conforming conditions (6-41) and (6-42). For simplification, the combination conforming conditions with symmetry or antisymmetry can be used again.

Firstly, in Eq. (6-44), four unknown coefficients λ_5 , λ_6 , λ_{11} and λ_{12} belong to the SS group; two unknown coefficients λ_8 and λ_9 belong to the SA group; and two unknown coefficients λ_7 and λ_{10} belong to the AS group.

Secondly, eight combination conditions can be formed from Eqs. (6-41) and (6-42), in which four conditions (6-A1), (6-A2), (6-A3) and (6-A4) of the SS group can just be used to solve λ_5 , λ_6 , λ_{11} and λ_{12} ; two conditions (6-B1) and

(6-B2) of the SA group can just be used to solve λ_8 and λ_9 ; and two conditions (6-C1) and (6-C2) of the AS group can just be used to solve λ_7 and λ_{10} . After substituting the deflection field (6-44) and the interpolation formulae for boundary, equations of these three groups can be written as:

SS group

$$\left. \begin{aligned} \sum_{i=1}^4 w_i - \frac{8}{3} \lambda_5 - \frac{16}{5} \lambda_{11} &= \sum_{i=1}^4 w_i - \frac{a}{3} \sum_{i=1}^4 \psi_{xi} \xi_i \\ \sum_{i=1}^4 w_i - \frac{8}{3} \lambda_6 - \frac{16}{5} \lambda_{12} &= \sum_{i=1}^4 w_i - \frac{b}{3} \sum_{i=1}^4 \psi_{yi} \eta_i \\ \frac{8}{a} (\lambda_5 + 2\lambda_{11}) &= \sum_{i=1}^4 \psi_{xi} \xi_i \\ \frac{8}{b} (\lambda_6 + 2\lambda_{12}) &= \sum_{i=1}^4 \psi_{yi} \eta_i \end{aligned} \right\} \quad (6-45)$$

SA group

$$\left. \begin{aligned} \sum_{i=1}^4 w_i \xi_i - \frac{8}{3} \lambda_8 &= \sum_{i=1}^4 w_i \xi_i - \frac{b}{3} \sum_{i=1}^4 \psi_{yi} \xi_i \eta_i \\ \frac{1}{a} \sum_{i=1}^4 w_i \xi_i + \frac{8}{a} \lambda_9 - \frac{8}{3a} \lambda_8 &= \sum_{i=1}^4 \psi_{xi} \end{aligned} \right\} \quad (6-46)$$

AS group

$$\left. \begin{aligned} \sum_{i=1}^4 w_i \eta_i - \frac{8}{3} \lambda_7 &= \sum_{i=1}^4 w_i \eta_i - \frac{a}{3} \sum_{i=1}^4 \psi_{xi} \xi_i \eta_i \\ \frac{1}{b} \sum_{i=1}^4 w_i \eta_i - \frac{8}{3b} \lambda_7 + \frac{8}{b} \lambda_{10} &= \sum_{i=1}^4 \psi_{yi} \end{aligned} \right\} \quad (6-47)$$

Thus, we can obtain

$$\left. \begin{aligned} \lambda_5 &= \frac{a}{8} \sum_{i=1}^4 \psi_{xi} \xi_i, \quad \lambda_6 = \frac{b}{8} \sum_{i=1}^4 \psi_{yi} \eta_i, \quad \lambda_{11} = 0, \quad \lambda_{12} = 0 \\ \lambda_8 &= \frac{b}{8} \sum_{i=1}^4 \psi_{yi} \xi_i \eta_i, \quad \lambda_9 = -\frac{1}{8} \sum_{i=1}^4 w_i \xi_i + \frac{a}{8} \sum_{i=1}^4 \psi_{xi} + \frac{b}{24} \sum_{i=1}^4 \psi_{yi} \xi_i \eta_i \\ \lambda_7 &= \frac{a}{8} \sum_{i=1}^4 \psi_{xi} \xi_i \eta_i, \quad \lambda_{10} = -\frac{1}{8} \sum_{i=1}^4 w_i \eta_i + \frac{a}{24} \sum_{i=1}^4 \psi_{xi} \xi_i \eta_i + \frac{b}{8} \sum_{i=1}^4 \psi_{yi} \end{aligned} \right\} \quad (6-48)$$

Substitution of Eqs. (6-48) into (6-44) yields

$$w = \sum_{i=1}^4 (N_i w_i + N_{xi} \psi_{xi} + N_{yi} \psi_{yi}) \quad (6-49)$$

where N_i , N_{xi} and N_{yi} are shape functions

$$\left. \begin{aligned} N_i &= \frac{1}{8} [2(1 + \xi_i \xi)(1 + \eta_i \eta) - \xi_i \xi (\xi^2 - 1) - \eta_i \eta (\eta^2 - 1)] \\ N_{xi} &= \frac{a \xi_i}{24} [3(1 + \xi_i \xi + \eta_i \eta)(\xi^2 - 1) + \eta_i \eta (\eta^2 - 1)] \\ N_{yi} &= \frac{b \eta_i}{24} [3(1 + \xi_i \xi + \eta_i \eta)(\eta^2 - 1) + \xi_i \xi (\xi^2 - 1)] \end{aligned} \right\} \quad (6-50)$$

Then, the element stiffness matrix can be obtained by the conventional procedure.

Example 6.5 The central deflection and moment of the simply-supported and clamped square plates subjected to vertical uniformly distributed load q and concentrated load P .

Table 6.5 The central deflection and moment of plates subjected to uniform load

Elements	Central deflection w				Central moment M			
	Simply-supported		Clamped		Simply-supported		Clamped	
	ACM	CGC-R12	ACM	CGC-R12	ACM	CGC-R12	ACM	CGC-R12
2 × 2	0.432 82	0.405 23	0.140 33	0.124 47	0.521 69	0.510 60	0.277 83	0.271 16
4 × 4	0.412 94	0.406 16	0.133 23	0.126 26	0.489 20	0.487 72	0.240 50	0.240 69
6 × 6	0.409 21	0.406 22	0.128 28	0.126 47	0.483 42	0.482 72	0.234 09	0.234 43
8 × 8	0.408 09	0.406 23	0.127 54	0.126 51	0.481 66	0.481 01	0.231 91	0.232 13
Analytical	0.406 24qL ⁴ /(100D)		0.126 53qL ⁴ /(100D)		0.478 86qL ² /10		0.229 05qL ² /10	

Table 6.6 The central deflection of plates subjected to concentrated load

Elements	Simply-supported		Clamped	
	ACM	CGC-R12	ACM	CGC-R12
2 × 2	0.123 27	0.118 71	0.613 45	0.580 62
4 × 4	0.118 29	0.116 89	0.580 26	0.568 89
6 × 6	0.117 14	0.116 42	0.570 99	0.565 03
8 × 8	0.116 74	0.116 24	0.567 30	0.563 44
Analytical	0.1160PL ² /(10D)		0.5612PL ² /(100D)	

The length of the plate side is L , and Poisson’s ratio is 0.3.

Due to symmetry, only one quarter of the plate is meshed. Results by the elements CGC-R12 and ACM are listed in Tables 6.5 and 6.6.

6.3 Line-Point Conforming Scheme—Triangular Elements

This section will introduce the triangular thin plate elements ($m = n = 9$) constructed by the combination scheme of line conforming and point conforming. The no. 6, 7, 8 and 9 elements LZ1, LZ2, GPL-T9 and GCIV-T9 in Table 5.1 all belong to this element group.

6.3.1 Triangular Element LZ1^[10]

A triangular thin plate bending element with 9 DOFs is shown in Fig. 6.1. The nodal displacement vector \mathbf{q}^e is

$$\mathbf{q}^e = [w_1 \quad \psi_{x1} \quad \psi_{y1} \quad w_2 \quad \psi_{x2} \quad \psi_{y2} \quad w_3 \quad \psi_{x3} \quad \psi_{y3}]^T$$

The displacements along each element side are interpolated by \mathbf{q}^e , i.e., along each element side, the deflection \tilde{w} is assumed to be cubic and the normal slope $\tilde{\psi}_n$ linearly distributed.

The element deflection field is assumed to be an incomplete cubic polynomial with 9 unknown coefficients, and expressible in terms of the area coordinates L_1, L_2, L_3 as

$$w = \mathbf{F}_\lambda \boldsymbol{\lambda} \tag{6-51}$$

where $\boldsymbol{\lambda}$ contains 9 unknown coefficients

$$\boldsymbol{\lambda} = [\lambda_1 \quad \lambda_2 \quad \dots \quad \lambda_9]^T$$

\mathbf{F}_λ contains 9 basis functions

$$\mathbf{F}_\lambda = [L_1 \quad L_2 \quad L_3 \quad L_1 L_2 \quad L_2 L_3 \quad L_3 L_1 \quad L_1^2 L_2 \quad L_2^2 L_3 \quad L_3^2 L_1] \tag{6-52}$$

In order to solve the 9 unknown coefficients in terms of \mathbf{q}^e , according to the line-point conforming combination scheme, 9 conforming conditions can be selected as follows:

$$(w - \tilde{w})_j = 0 \quad (j=1, 2, 3) \tag{6-53}$$

$$\int_{S_k} (w - \tilde{w}) ds = 0, \quad \int_{S_k} \left(\frac{\partial w}{\partial n} - \tilde{\psi}_n \right) ds = 0 \quad (k = 1, 2, 3) \tag{6-54}$$

Equation (6-53) denotes the point conforming conditions at three corner nodes; Eq. (6-54) denotes the average line conforming conditions of deflections and rotations along three sides.

From Eq. (6-53), the first three unknown coefficients can be obtained

$$\lambda_1 = w_1, \quad \lambda_2 = w_2, \quad \lambda_3 = w_3 \quad (6-55)$$

From Eq. (6-54), the following six equations can be obtained

$$\left. \begin{aligned} 2\lambda_4 + \lambda_7 &= c_3(\psi_{x1} - \psi_{x2}) - b_3(\psi_{y1} - \psi_{y2}) \\ 2\lambda_5 + \lambda_8 &= c_1(\psi_{x2} - \psi_{x3}) - b_1(\psi_{y2} - \psi_{y3}) \\ 2\lambda_6 + \lambda_9 &= c_2(\psi_{x3} - \psi_{x1}) - b_2(\psi_{y3} - \psi_{y1}) \end{aligned} \right\} \quad (6-56)$$

$$\left. \begin{aligned} \lambda_4 - \lambda_5 - \lambda_6 + \frac{2}{3}\lambda_7 - \frac{2}{3}\lambda_8 &= -(1+r_3)w_1 - (1-r_3)w_2 + 2w_3 \\ &\quad - \frac{2A}{d_3^2} [b_3(\psi_{x1} + \psi_{x2}) + c_3(\psi_{y1} + \psi_{y2})] \\ -\lambda_4 + \lambda_5 - \lambda_6 + \frac{2}{3}\lambda_8 - \frac{2}{3}\lambda_9 &= 2w_1 - (1+r_1)w_2 - (1-r_1)w_3 \\ &\quad - \frac{2A}{d_1^2} [b_1(\psi_{x2} + \psi_{x3}) + c_1(\psi_{y2} + \psi_{y3})] \\ -\lambda_4 - \lambda_5 + \lambda_6 - \frac{2}{3}\lambda_7 + \frac{2}{3}\lambda_9 &= -(1-r_2)w_1 + 2w_2 - (1+r_2)w_3 \\ &\quad - \frac{2A}{d_2^2} [b_2(\psi_{x3} + \psi_{x1}) + c_2(\psi_{y3} + \psi_{y1})] \end{aligned} \right\} \quad (6-57)$$

where

$$b_i = y_j - y_k, \quad c_i = x_k - x_j, \quad r_i = \frac{d_j^2 - d_k^2}{d_i^2} \quad (i = \overline{1,2,3}; \quad j = \overline{2,3,1}; \quad k = \overline{3,1,2}) \quad (6-58)$$

$d_1, d_2,$ and d_3 denote the side lengths of the element; A is the area of the triangle.

The last six unknown coefficients can be determined from Eqs. (6-56) and (6-57).

Combining the above results, we have

$$\lambda = \hat{A}q^e \quad (6-59)$$

where

$$\hat{A} = [\hat{A}_1 \quad \hat{A}_2 \quad \hat{A}_3] \quad (6-60)$$

with

$$\hat{A}_1 = \begin{bmatrix} 1 & 0 & 0 \\ 0 & 0 & 0 \\ 0 & 0 & 0 \\ -\frac{1}{6}(9-r_2-2r_3) & -\frac{1}{12}(r_2c_2-2r_3c_3-3c_2) & \frac{1}{12}(r_2b_2-2r_3b_3-3b_2) \\ -\frac{1}{6}(5r_2+r_3) & -\frac{1}{12}(-5r_2c_2+r_3c_3+3c_1) & \frac{1}{12}(-5r_2b_2+r_3b_3+3b_1) \\ -\frac{1}{6}(-9+2r_2-5r_3) & -\frac{1}{12}(-2r_2c_2-5r_3c_3+12c_2-3c_3) & \frac{1}{12}(-2r_2b_2-5r_3b_3+12b_2-3b_3) \\ \frac{1}{3}(9-r_2-2r_3) & \frac{1}{6}(r_2c_2-2r_3c_3-3c_2+6c_3) & -\frac{1}{6}(r_2b_2-2r_3b_3-3b_2+6b_3) \\ \frac{1}{3}(5r_2+r_3) & \frac{1}{6}(-5r_2c_2+r_3c_3+3c_1) & -\frac{1}{6}(-5r_2b_2+r_3b_3+3b_1) \\ \frac{1}{3}(-9+2r_2-5r_3) & \frac{1}{6}(-2r_2c_2-5r_3c_3+6c_2-3c_3) & -\frac{1}{6}(-2r_2b_2-5r_3b_3+6b_2-3b_3) \end{bmatrix} \quad (6-61)$$

$$\hat{A}_2 = \begin{bmatrix} 0 & 0 & 0 \\ 1 & 0 & 0 \\ 0 & 0 & 0 \\ -\frac{1}{6}(-9+2r_3-5r_1) & -\frac{1}{12}(-2r_3c_3-5r_1c_1+12c_3-3c_1) & \frac{1}{12}(-2r_3b_3-5r_1b_1+12b_3-3b_1) \\ -\frac{1}{6}(9-r_3-2r_1) & -\frac{1}{12}(r_3c_3-2r_1c_1-3c_3) & \frac{1}{12}(r_3b_3-2r_1b_1-3b_3) \\ -\frac{1}{6}(5r_3+r_1) & -\frac{1}{12}(-5r_3c_3+r_1c_1+3c_2) & \frac{1}{12}(-5r_3b_3+r_1b_1+3b_2) \\ \frac{1}{3}(-9+2r_3-5r_1) & \frac{1}{6}(-2r_3c_3-5r_1c_1+6c_3-3c_1) & -\frac{1}{6}(-2r_3b_3-5r_1b_1+6b_3-3b_1) \\ \frac{1}{3}(9-r_3-2r_1) & \frac{1}{6}(r_3c_3-2r_1c_1-3c_3+6c_1) & -\frac{1}{6}(r_3b_3-2r_1b_1-3b_3+6b_1) \\ \frac{1}{3}(5r_3+r_1) & \frac{1}{6}(-5r_3c_3+r_1c_1+3c_2) & -\frac{1}{6}(-5r_3b_3+r_1b_1+3b_2) \end{bmatrix} \quad (6-62)$$

$$\hat{A}_3 = \begin{bmatrix} 0 & 0 & 0 \\ 0 & 0 & 0 \\ 1 & 0 & 0 \\ -\frac{1}{6}(5r_1 + r_2) & -\frac{1}{12}(-5r_1c_1 + r_2c_2 + 3c_3) & \frac{1}{12}(-5r_1b_1 + r_2b_2 + 3b_3) \\ -\frac{1}{6}(-9 + 2r_1 - 5r_2) & -\frac{1}{12}(-2r_1c_1 - 5r_2c_2 + 12c_1 - 3c_2) & \frac{1}{12}(-2r_1b_1 - 5r_2b_2 + 12b_1 - 3b_2) \\ -\frac{1}{6}(9 - r_1 - 2r_2) & -\frac{1}{12}(r_1c_1 - 2r_2c_2 - 3c_1) & \frac{1}{12}(r_1b_1 - 2r_2b_2 - 3b_1) \\ \frac{1}{3}(5r_1 + r_2) & \frac{1}{6}(-5r_1c_1 + r_2c_2 + 3c_3) & -\frac{1}{6}(-5r_1b_1 + r_2b_2 + 3b_3) \\ \frac{1}{3}(-9 + 2r_1 - 5r_2) & \frac{1}{6}(-2r_1c_1 - 5r_2c_2 + 6c_1 - 3c_2) & -\frac{1}{6}(-2r_1b_1 - 5r_2b_2 + 6b_1 - 3b_2) \\ \frac{1}{3}(9 - r_1 - 2r_2) & \frac{1}{6}(r_1c_1 - 2r_2c_2 - 3c_1 + 6c_2) & -\frac{1}{6}(r_1b_1 - 2r_2b_2 - 3b_1 + 6b_2) \end{bmatrix} \quad (6-63)$$

Substituting Eq. (6-59) into Eq. (6-51), we obtain

$$w = F_\lambda \hat{A} q^e \quad (6-64)$$

The element shape function matrix is

$$N = F_\lambda \hat{A} \quad (6-65)$$

Then, the element stiffness matrix K^e can be derived by the conventional procedure.

6.3.2 Triangular Element LZ2^[10]

Assume that the element deflection field w consists of two parts,

$$w = w_q + w_\alpha \quad (6-66)$$

where the first part is the deflection field expressed in Eq. (6-64)

$$w_q = F_\lambda \hat{A} q^e$$

and the second part is a generalized bubble deflection field

$$w_\alpha = F_\alpha \alpha \quad (6-67)$$

in which α is an internal displacement parameter and F_α is a generalized bubble function

$$F_\alpha = -(L_1L_2 + L_2L_3 + L_3L_1) + 2(L_1^2L_2 + L_2^2L_3 + L_3^2L_1) + 3L_1L_2L_3 \quad (6-68)$$

It can be verified that all the nine generalized displacements (3 nodal deflections, average deflections and average normal slopes along three sides) corresponding to w_α vanish.

The deflection field (6-66) is a complete cubic polynomial with 10 DOFs. When the internal DOF α is eliminated by a condensation process, only 9 external DOFs in q^e are retained.

From the deflection expression (6-66), the element curvature field κ can be expressed as

$$\kappa = B_q q^e + B_\alpha \alpha \tag{6-69}$$

The element stiffness matrix after condensation is

$$K^e = K_{qq} - K_{\alpha q}^T k_{\alpha\alpha}^{-1} K_{\alpha q} \tag{6-70}$$

with

$$K_{qq} = \iint_{A^e} B_q^T D B_q dA$$

$$K_{\alpha q} = \iint_{A^e} B_\alpha^T D B_q dA$$

$$k_{\alpha\alpha} = \iint_{A^e} B_\alpha^T D B_\alpha dA$$

D is the elastic matrix.

Example 6.6 The central deflection w_C (in Table 6.7) and central moment M_C (in Table 6.8) of a simply-supported square plate subjected to uniform load q . The length of the square plate side is L ; the Poisson's ratio is 0.3. Two mesh orientations A and B (see Fig. 6.2) are considered. And, the numbers in parentheses are relative errors.

Table 6.7 The central deflection of a simply-supported square plate

Mesh	LZ1		LZ2		CT		E-1	
	Mesh A	Mesh B	Mesh A	Mesh B	Mesh A	Mesh B	Mesh A	Mesh B
1/4 plate								
2 × 2	0.3817 (-6.0%)	0.3947 (-2.8%)	0.4005 (-1.4%)	0.4023 (-1.0%)	0.399 30 (-1.7%)	0.351 18 (-13.6%)	0.399 19 (-1.7%)	0.356 20 (-12.3%)
4 × 4	0.4009 (-1.3%)	0.4038 (-0.6%)	0.4047 (-0.4%)	0.4058 (-0.1%)	0.404 39 (-0.5%)	0.392 80 (-3.3%)	0.404 71 (-0.4%)	0.394 17 (-3.0%)
6 × 6	0.4040 (-0.6%)	0.4053 (-0.2%)	0.4056 (-0.2%)	0.4061 (0.0%)	0.405 40 (-0.2%)	0.400 28 (-1.5%)	0.405 61 (-0.2%)	0.400 92 (-1.3%)
8 × 8	0.4050 (-0.3%)	0.4057 (-0.1%)	0.4059 (-0.1%)	0.4062 (0.0%)				
Analytical	0.406 235qL ⁴ /(100D)							

Table 6.8 The central moment of a simply-supported square plate

Mesh 1/4 plate	LZ1		LZ2		CT		E-1	
	Mesh A	Mesh B	Mesh A	Mesh B	Mesh A	Mesh B	Mesh A	Mesh B
2 × 2	0.4931 (3.0%)	0.5004 (4.5%)	0.5046 (5.4%)	0.5151 (7.6%)	0.499 88 (4.4%)	0.439 58 (-8.2%)	0.513 01 (7.1%)	0.468 71 (-2.1%)
4 × 4	0.4873 (1.8%)	0.4874 (1.8%)	0.4792 (0.1%)	0.4919 (2.7%)	0.483 47 (1.0%)	0.470 05 (-1.8%)	0.487 31 (1.8%)	0.477 97 (-0.2%)
6 × 6	0.4762 (-0.6%)	0.4839 (1.0%)	0.4778 (-0.2%)	0.4857 (1.4%)	0.480 90 (0.4%)	0.474 93 (-0.8%)	0.482 44 (0.7%)	0.478 71 (0.0%)
8 × 8	0.4768 (-0.4%)	0.4822 (0.7%)	0.4777 (-0.2%)	0.4832 (0.9%)				
Analytical	0.478 86qL ² /10							

Since the elements CT^[11], E-1 and E-2^[12] have ever been identified as the most accurate nine-DOF triangular thin plate elements, the accuracy of the present two elements LZ1 and LZ2 is compared with those models.

From Tables 6.7 and 6.8, it can be seen that both elements LZ1 and LZ2 have high precision, their accuracy is at the same level as that of the elements CT and E-1.

6.3.3 Triangular Element GPL-T9^[13]

The element nodal displacement vector q^e is the same as that of the elements LZ1 and LZ2. The element deflection field w is still assumed to be an incomplete cubic polynomial with nine unknown coefficients, i.e., Eq. (6-51). But, the nine basis functions are different and selected as follows

$$F_\lambda = [L_1 \quad L_2 \quad L_3 \quad L_1L_2 \quad L_2L_3 \quad L_3L_1 \quad F_7 \quad F_8 \quad F_9] \quad (6-71)$$

where

$$\left. \begin{aligned} F_7 &= L_1 \left(L_1 - \frac{1}{2} \right) (L_1 - 1) \\ F_8 &= L_2 \left(L_2 - \frac{1}{2} \right) (L_2 - 1) \\ F_9 &= L_3 \left(L_3 - \frac{1}{2} \right) (L_3 - 1) \end{aligned} \right\} \quad (6-72)$$

In order to solve the nine unknown coefficients in λ , we still select 9 conforming conditions according to the line-point conforming combination scheme, as shown in Eqs. (6-53) and (6-54).

Firstly, from the point condition (6-53), we obtain

$$\lambda_1 = w_1, \quad \lambda_2 = w_2, \quad \lambda_3 = w_3 \quad (6-73)$$

Secondly, from the first three average line conforming conditions about w in Eq. (6-54), λ_4 , λ_5 and λ_6 can be obtained as

$$\left. \begin{aligned} \lambda_4 &= \frac{c_3}{2}(\psi_{x1} - \psi_{x2}) - \frac{b_3}{2}(\psi_{y1} - \psi_{y2}) \\ \lambda_5 &= \frac{c_1}{2}(\psi_{x2} - \psi_{x3}) - \frac{b_1}{2}(\psi_{y2} - \psi_{y3}) \\ \lambda_6 &= \frac{c_2}{2}(\psi_{x3} - \psi_{x1}) - \frac{b_2}{2}(\psi_{y3} - \psi_{y1}) \end{aligned} \right\} \quad (6-74)$$

Finally, from the last three average line conforming conditions about ψ_n in Eq. (6-54), λ_7 , λ_8 and λ_9 can be obtained as

$$\left. \begin{aligned} \lambda_7 &= -2w_1 + (1+r_1)w_2 + (1-r_1)w_3 + \frac{1}{2}(c_2 - c_3)\psi_{x1} + \frac{1}{2}(r_1c_1 - c_3)\psi_{x2} \\ &\quad + \frac{1}{2}(r_1c_1 + c_2)\psi_{x3} - \frac{1}{2}(b_2 - b_3)\psi_{y1} - \frac{1}{2}(r_1b_1 - b_3)\psi_{y2} - \frac{1}{2}(r_1b_1 + b_2)\psi_{y3} \\ \lambda_8 &= (1-r_2)w_1 - 2w_2 + (1+r_2)w_3 + \frac{1}{2}(r_2c_2 + c_3)\psi_{x1} + \frac{1}{2}(c_3 - c_1)\psi_{x2} \\ &\quad + \frac{1}{2}(r_2c_2 - c_1)\psi_{x3} - \frac{1}{2}(r_2b_2 + b_3)\psi_{y1} - \frac{1}{2}(b_3 - b_1)\psi_{y2} - \frac{1}{2}(r_2b_2 - b_1)\psi_{y3} \\ \lambda_9 &= (1+r_3)w_1 + (1-r_3)w_2 - 2w_3 + \frac{1}{2}(r_3c_3 - c_2)\psi_{x1} + \frac{1}{2}(r_3c_3 + c_1)\psi_{x2} \\ &\quad + \frac{1}{2}(c_1 - c_2)\psi_{x3} - \frac{1}{2}(r_3b_3 - b_2)\psi_{y1} - \frac{1}{2}(r_3b_3 + b_1)\psi_{y2} - \frac{1}{2}(b_1 - b_2)\psi_{y3} \end{aligned} \right\} \quad (6-75)$$

After λ is solved, the deflection field w can be expressed in terms of the shape functions

$$w = \sum_{i=1}^3 (N_i w_i + N_{xi} \psi_{xi} + N_{yi} \psi_{yi}) \quad (6-76)$$

where

$$\left. \begin{aligned} N_1 &= L_1 - 2F_7 + (1-r_2)F_8 + (1+r_3)F_9 \\ N_{x1} &= \frac{c_3}{2}L_1L_2 - \frac{c_2}{2}L_3L_1 + \frac{1}{2}(c_2 - c_3)F_7 + \frac{1}{2}(r_2c_2 + c_3)F_8 + \frac{1}{2}(r_3c_3 - c_2)F_9 \\ N_{y1} &= -\frac{b_3}{2}L_1L_2 + \frac{b_2}{2}L_3L_1 - \frac{1}{2}(b_2 - b_3)F_7 - \frac{1}{2}(r_2b_2 + b_3)F_8 - \frac{1}{2}(r_3b_3 - b_2)F_9 \end{aligned} \right\} \quad (6-77)$$

The expressions for the other six shape functions can be obtained by permutation.

And, b_i , c_i and r_i are given by Eq. (6-58). Based on these shape functions, the element stiffness matrix can be derived by the conventional procedure.

Example 6.7 The central deflection and central moment for the simply-supported and clamped square plates subjected to uniform load q and central concentrated load P . The meshes A and B in Fig. 6.2, and mesh C in Fig. 6.13 are used. Results by the element GPL-T9 are listed in Tables 6.9 to 6.11.

Example 6.8 The central deflection of a simply-supported circular plate subjected to uniform load.

Due to symmetry, only one quarter of the plate is modelled. Two meshes shown in Fig. 6.14 are used. The computational errors of the central deflection obtained by the element GPL-T9 are given in Table 6.12. And, the results of reference [14] are also listed for comparison.

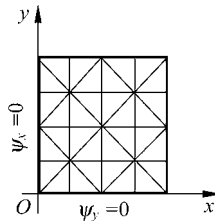


Figure 6.13 Mesh C 4×4 for a quarter square plate

Table 6.9 The central deflection of simply-supported and clamped square plates subjected to uniform load q

Mesh (1/4 plate)	Clamped			Simply-supported		
	Mesh A	Mesh B	Mesh C	Mesh A	Mesh B	Mesh C
2×2	0.1170	0.0995	0.0985	0.3804	0.3948	0.3829
4×4	0.1241	0.1192	0.1210	0.4007	0.4038	0.4008
6×6	0.1256	0.1233	0.1240	0.4040	0.4054	0.4039
8×8	0.1261	0.1246	0.1251	0.4046	0.4049	0.4044
Analytical	$0.12653qL^4/(100D)$			$0.40624qL^4/(100D)$		

Table 6.10 The central moment of simply-supported and clamped square plates subjected to uniform load q

Mesh (1/4 plate)	Clamped			Simply-supported		
	Mesh A	Mesh B	Mesh C	Mesh A	Mesh B	Mesh C
2×2	0.3054	0.2185	0.2216	0.4958	0.4986	0.5296
4×4	0.2395	0.2274	0.2405	0.4775	0.4869	0.4967
6×6	0.2329	0.2286	0.2342	0.4770	0.4838	0.4871
8×8	0.2309	0.2288	0.2319	0.4777	0.4811	0.4829
Analytical	$0.2291qL^2/10$			$0.4789qL^2/10$		

Table 6.11 The central deflection of simply-supported and clamped square plates subjected to central concentrated load P

Mesh (1/4 plate)	Clamped			Simply-supported		
	Mesh A	Mesh B	Mesh C	Mesh A	Mesh B	Mesh C
2 × 2	0.4655	0.4466	0.4235	1.0183	1.0912	1.0501
4 × 4	0.5311	0.5269	0.5257	1.1211	1.1382	1.1253
6 × 6	0.5470	0.5448	0.5434	1.1422	1.1498	1.1430
8 × 8	0.5527	0.5513	0.5503	1.1484	1.1518	1.1485
Analytical	0.5612PL ² /(100D)			1.160PL ² /(100D)		

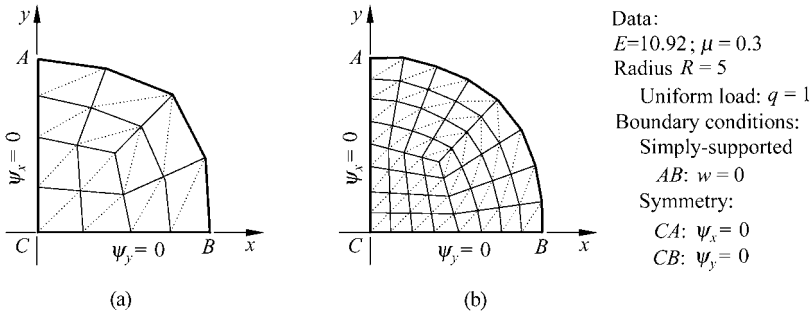


Figure 6.14 The typical mesh for 1/4 circular plate
 (a) 24 triangular elements or 12 quadrilateral elements; (b) 96 triangular elements or 48 quadrilateral elements

Table 6.12 The computational errors of the central deflection of a simply-supported circular plate subjected to uniform load

Mesh (1/4 plate)	GPL-T9	Reference [14]
Mesh A	0.63%	2.87%
Mesh B	0.10%	0.70%

Example 6.9 The central deflection w and central moment M_y of a rhombus plate (Fig. 6.15) subjected to uniform load (Razzaque’s skew plate problem).

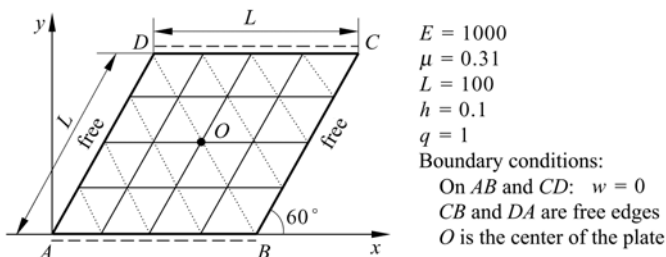


Figure 6.15 Razzaque’s skew plate: typical mesh 4 × 4

The mesh used is shown in Fig. 6.15 and the results by the element GPL-T9 and other models are listed in Table 6.13. It can be seen that the performance of the element GPL-T9 is better than those of the other elements in references [15] and [16].

Table 6.13 The central deflection and central moment of a rhombus plate subjected to uniform load

DOFs	Mesh	Central deflection w			Central moment M_y		
		GPL-T9	Reference [15]	Reference [16]	GPL-T9	Reference [15]	Reference [16]
27	2 × 2	0.7318	0.7230		1.0140	0.7602	
75	4 × 4	0.7783	0.7718	0.8414	0.9925	0.9172	0.9761
105	4 × 6	0.7941	0.7850		0.9904	0.9473	
243	8 × 8	0.7890		0.8111	0.9565		0.9739
507	12 × 12	0.7913		0.8057	0.9596		0.9688
Difference method ^[15]		0.7945 $qL^4/(100D)$			0.9589 $qL^2/10$		

6.4 Super-Basis Line-Point Conforming Scheme—Elements GCIII-R12 and GCIII-T9

This section will introduce the construction procedure for the super-basis thin plate elements formulated by the combination scheme of the line conforming and point conforming conditions. The no. 12, 13, 14 and 15 elements GCIII-R12, GPL-R1, GCIII-T9 and LZ3 in Table 5.1 all belong to this element group. Two elements GCIII-R12 and GCIII-T9 will be discussed in detail.

6.4.1 Rectangular Element GCIII-R12—Improvement on the Element ACM

The rectangular thin plate element GCIII-R12 is a model developed by improving the element ACM^[6]. Element ACM employed a conventional scheme: let $m = n = 12$, the 12 conforming conditions are all point conforming conditions. Though the deflection along the element boundary is compatible, the normal slope along the element boundary is incompatible, and does not satisfy the average line conforming conditions. Therefore, an improvement scheme is proposed: let $m > n = 12$, then, besides the 12 point conforming conditions, the average line conforming conditions of the normal slope along the element sides are supplemented. Thereupon, the element compatibility is improved, and the new element GCIII-R12 is obtained.

The detailed construction procedure for the element GCIII-R12 is as follows. Assume that the element deflection field w consists of two parts

$$w = \bar{w}(\text{ACM}) + \hat{w} \tag{6-78}$$

where \bar{w} (ACM) is the interpolation formula with 12 unknown coefficients used by the element ACM

$$\begin{aligned} \bar{w} = & \lambda_1 + \lambda_2\xi + \lambda_3\eta + \lambda_4\xi^2 + \lambda_5\xi\eta + \lambda_6\eta^2 + \lambda_7\xi^3 \\ & + \lambda_8\xi^2\eta + \lambda_9\xi\eta^2 + \lambda_{10}\eta^3 + \lambda_{11}\xi^3\eta + \lambda_{12}\xi\eta^3 \end{aligned} \tag{6-79}$$

\hat{w} is the additional deflection field with two new unknown coefficients

$$\hat{w} = \lambda_{13}\xi(\xi^2 - 1)(\eta^2 - 1) + \lambda_{14}\eta(\xi^2 - 1)(\eta^2 - 1) \tag{6-80}$$

\hat{w} possesses the following characteristics:

- (1) At the four corner nodes, \hat{w} , $\frac{\partial\hat{w}}{\partial x}$ and $\frac{\partial\hat{w}}{\partial y}$ are all zero;
- (2) Along four element boundary lines, \hat{w} identically equals to zero (thus $\frac{\partial\hat{w}}{\partial s}$ also identically equals to zero), but $\frac{\partial\hat{w}}{\partial n}$ does not identically equal to zero.

The deflection field expressed by Eq. (6-78) is an incomplete bi-cubic polynomial with 14 unknown coefficients. Owing to $m > n$, this is a super-basis element.

In order to solve 14 unknown coefficients, 14 conforming conditions are needed.

Firstly, the 12 point conforming conditions about w , ψ_x and ψ_y at the 4 corner nodes are applied. Due to the characteristic (1) of the additional deflection \hat{w} , we know that λ_{13} and λ_{14} will not appear in these 12 point conforming conditions. So, the 12 unknown coefficients $\lambda_1, \lambda_2, \dots, \lambda_{12}$ can just be solved by the 12 conditions. That is to say, the solutions of these unknown coefficients are identical with those of the element ACM.

Secondly, we apply the average line conforming conditions about normal slopes:

$$\left. \begin{aligned} \int_{-1}^1 \left(\frac{\partial w}{\partial x} \right)_{23} d\eta &= \int_{-1}^1 \tilde{\psi}_{x23} d\eta \\ \int_{-1}^1 \left(\frac{\partial w}{\partial x} \right)_{14} d\eta &= \int_{-1}^1 \tilde{\psi}_{x14} d\eta \\ \int_{-1}^1 \left(\frac{\partial w}{\partial y} \right)_{43} d\xi &= \int_{-1}^1 \tilde{\psi}_{y43} d\xi \\ \int_{-1}^1 \left(\frac{\partial w}{\partial y} \right)_{12} d\xi &= \int_{-1}^1 \tilde{\psi}_{y12} d\xi \end{aligned} \right\} \tag{6-81}$$

In Eq. (6-81), there seemingly are four conditions, in which only two conditions

are independent. Then λ_{13} and λ_{14} can be derived as follows:

$$\left. \begin{aligned} \lambda_{13} &= -\frac{b}{16} \sum_{i=1}^4 \psi_{yi} \xi_i \eta_i \\ \lambda_{14} &= -\frac{a}{16} \sum_{i=1}^4 \psi_{xi} \xi_i \eta_i \end{aligned} \right\} \quad (6-82)$$

After the determination of the 14 unknown coefficients, the element deflection field and its shape functions can be obtained:

$$w = \sum_{i=1}^4 (N_i w_i + N_{xi} \psi_{xi} + N_{yi} \psi_{yi}) \quad (6-83)$$

where the shape functions are all constituted of two parts:

$$\left. \begin{aligned} N_i &= \bar{N}_i + \hat{N}_i \\ N_{xi} &= \bar{N}_{xi} + \hat{N}_{xi} \\ N_{yi} &= \bar{N}_{yi} + \hat{N}_{yi} \end{aligned} \right\} \quad (i = 1, 2, 3, 4) \quad (6-84)$$

\bar{N}_i , \bar{N}_{xi} and \bar{N}_{yi} belong to the part related to \bar{w} (refer to Eq. (7-19)); \hat{N}_i , \hat{N}_{xi} and \hat{N}_{yi} belong to the part related to \hat{w} :

$$\left. \begin{aligned} \hat{N}_i &= 0 \\ \hat{N}_{xi} &= -\frac{a}{16} \xi_i \eta_i \eta (1 - \eta^2) (1 - \xi^2) \\ \hat{N}_{yi} &= -\frac{b}{16} \xi_i \eta_i \xi (1 - \xi^2) (1 - \eta^2) \end{aligned} \right\} \quad (i = 1, 2, 3, 4) \quad (6-85)$$

Since the shape functions have been obtained, the element stiffness matrix can then be established.

Note that, actually, only one of the first two conditions in Eq. (6-81) is independent, this is because of the following relation

$$\int_{-1}^1 \left[\left(\frac{\partial w}{\partial x} \right)_{23} - \left(\frac{\partial w}{\partial x} \right)_{14} \right] d\eta = \int_{-1}^1 (\tilde{\psi}_{x23} - \tilde{\psi}_{x14}) d\eta \quad (6-86)$$

Here, the proof of Eq. (6-86) is given as follows.

Firstly, from Eq. (6-80), we obtain

$$\int_{-1}^1 \left[\left(\frac{\partial \hat{w}}{\partial x} \right)_{23} - \left(\frac{\partial \hat{w}}{\partial x} \right)_{14} \right] d\eta = 0 \quad (6-87)$$

Secondly, it can be verified that the deflection field \bar{w} of the element ACM

satisfies the perimeter conforming condition under constant internal force state (refer to Sect. 7.2). Now, consider the following constant internal force state:

$$M_x = \beta_1, \quad M_y = 0, \quad M_{xy} = 0$$

Then, the boundary forces of the rectangular element can be obtained from Eq. (5-8):

$$\begin{aligned} Q_n &= 0, & M_{ns} &= 0 \\ (M_n)_{12} &= (M_n)_{34} = 0 \\ (M_n)_{23} &= (M_n)_{14} = \beta_1 \end{aligned}$$

Substitution of the above equation into the perimeter conforming condition (5-2a) yields

$$\int_{-1}^1 \left[\left(\frac{\partial \bar{w}}{\partial n} - \tilde{\psi}_n \right)_{23} + \left(\frac{\partial \bar{w}}{\partial n} - \tilde{\psi}_n \right)_{14} \right] d\eta = 0$$

i.e.,

$$\int_{-1}^1 \left[\left(\frac{\partial \bar{w}}{\partial x} - \tilde{\psi}_x \right)_{23} - \left(\frac{\partial \bar{w}}{\partial x} - \tilde{\psi}_x \right)_{14} \right] d\eta = 0 \tag{6-88}$$

Since $w = \bar{w} + \hat{w}$, by the superposition of Eqs. (6-88) and (6-87), Eq. (6-86) can be obtained.

The above procedure proves that there is only one independent condition existing in the first two conditions of Eq. (6-81). Similarly, it can be verified that there is also only one independent condition existing in the last two conditions of Eq. (6-81).

Example 6.10 The central deflection w_c and central moment M_c of the simply-supported and clamped square plates subjected to uniform load q and central concentrated load P .

For comparison, results by the elements GCIII-R12 and ACM are given in Tables 6.14 and 6.15. The length of the square plate side is L , the Poisson’s ratio is 0.3.

Table 6.14 The central deflection and moment of square plates subjected to uniform load q

Mesh (1/4 plate)	Central deflection w_c				Central moment M_c			
	Simply-supported		Clamped		Simply-supported		Clamped	
	ACM	GCIII-R12	ACM	GCIII-R12	ACM	GCIII-R12	ACM	GCIII-R12
2 × 2	0.433	0.395	0.140	0.120	0.522	0.434	0.278	0.203
4 × 4	0.413	0.403	0.133	0.123	0.489	0.466	0.241	0.221
6 × 6	0.409	0.405	0.128	0.126	0.483	0.473	0.234	0.225
8 × 8	0.408	0.406	0.128	0.126	0.482	0.476	0.232	0.227
Analytical	0.406 $24qL^4/(100D)$		0.126 $53qL^4/(100D)$		0.478 $86qL^2/10$		0.229 $1qL^2/10$	

Table 6.15 The central deflection of square plates subjected to central concentrated load P

Mesh (1/4 plate)	Simply-supported		Clamped	
	ACM	GCIII-R12	ACM	GCIII-R12
2 × 2	0.123	0.111	0.613	0.523
4 × 4	0.118	0.115	0.580	0.549
6 × 6	0.117	0.115	0.571	0.555
8 × 8	0.117	0.116	0.567	0.558
Analytical	0.1160 $PL^2/(10D)$		0.5612 $PL^2/(100D)$	

From Tables 6.14 and 6.15, it can be seen that the accuracy of the element GC III-R12 is better than that of the element ACM.

6.4.2 Triangular Element GCIII-T9

The construction procedure for the element GCIII-T9 is: the assumed element deflection field contains 12 unknown coefficients ($m = 12, n = 9$, it is a super-basis element); the 12 conforming conditions used include 9 point conforming conditions and 3 average line conforming conditions. Following is the detailed derivation procedure of the element.

The element deflection field is assumed as

$$\begin{aligned}
 w = & \lambda_1 L_1 + \lambda_2 L_2 + \lambda_3 L_3 + \lambda_4 L_2 L_3 + \lambda_5 L_3 L_1 + \lambda_6 L_1 L_2 \\
 & + \lambda_7 (L_3 - L_2) L_2 L_3 + \lambda_8 (L_1 - L_3) L_3 L_1 + \lambda_9 (L_2 - L_1) L_1 L_2 \\
 & + \lambda_{10} L_1 L_2 L_3^2 + \lambda_{11} L_2 L_3 L_1^2 + \lambda_{12} L_3 L_1 L_2^2
 \end{aligned} \tag{6-89}$$

The element rotation fields are as follows:

$$\begin{aligned}
 \psi_x = \frac{\partial w}{\partial x} = \frac{1}{2A} \left(b_1 \frac{\partial w}{\partial L_1} + b_2 \frac{\partial w}{\partial L_2} + b_3 \frac{\partial w}{\partial L_3} \right) \\
 \psi_y = \frac{\partial w}{\partial y} = \frac{1}{2A} \left(c_1 \frac{\partial w}{\partial L_1} + c_2 \frac{\partial w}{\partial L_2} + c_3 \frac{\partial w}{\partial L_3} \right)
 \end{aligned} \tag{6-90}$$

In order to solve 12 unknown coefficients, 12 conforming conditions are needed. Firstly, 9 point conforming conditions at the corner nodes are selected as

$$\left. \begin{aligned}
 w_1 &= \lambda_1 \\
 \psi_{x1} &= \frac{1}{2A} [b_1 \lambda_1 + b_2 (\lambda_2 + \lambda_6 - \lambda_9) + b_3 (\lambda_3 + \lambda_5 + \lambda_8)] \\
 \psi_{y1} &= \frac{1}{2A} [c_1 \lambda_1 + c_2 (\lambda_2 + \lambda_6 - \lambda_9) + c_3 (\lambda_3 + \lambda_5 + \lambda_8)] \\
 w_2 &= \lambda_2 \\
 \psi_{x2} &= \frac{1}{2A} [b_1 (\lambda_1 + \lambda_6 + \lambda_9) + b_2 \lambda_2 + b_3 (\lambda_3 + \lambda_4 - \lambda_7)] \\
 \psi_{y2} &= \frac{1}{2A} [c_1 (\lambda_1 + \lambda_6 + \lambda_9) + c_2 \lambda_2 + c_3 (\lambda_3 + \lambda_4 - \lambda_7)] \\
 w_3 &= \lambda_3 \\
 \psi_{x3} &= \frac{1}{2A} [b_1 (\lambda_1 + \lambda_5 - \lambda_8) + b_2 (\lambda_2 + \lambda_4 + \lambda_7) + b_3 \lambda_3] \\
 \psi_{y3} &= \frac{1}{2A} [c_1 (\lambda_1 + \lambda_5 - \lambda_8) + c_2 (\lambda_2 + \lambda_4 + \lambda_7) + c_3 \lambda_3]
 \end{aligned} \right\} \quad (6-91)$$

These 9 conditions do not contain λ_{10} , λ_{11} and λ_{12} , so the first 9 unknown coefficients can be solved as follows:

$$\left. \begin{aligned}
 \lambda_1 &= w_1 \\
 \lambda_2 &= w_2 \\
 \lambda_3 &= w_3 \\
 \lambda_4 &= \frac{c_1}{2} (\psi_{x2} - \psi_{x3}) - \frac{b_1}{2} (\psi_{y2} - \psi_{y3}) \\
 \lambda_5 &= \frac{c_2}{2} (\psi_{x3} - \psi_{x1}) - \frac{b_2}{2} (\psi_{y3} - \psi_{y1}) \\
 \lambda_6 &= \frac{c_3}{2} (\psi_{x1} - \psi_{x2}) - \frac{b_3}{2} (\psi_{y1} - \psi_{y2}) \\
 \lambda_7 &= -w_2 + w_3 - \frac{c_1}{2} (\psi_{x2} + \psi_{x3}) - \frac{b_1}{2} (\psi_{y2} + \psi_{y3}) \\
 \lambda_8 &= -w_3 + w_1 - \frac{c_2}{2} (\psi_{x3} + \psi_{x1}) - \frac{b_2}{2} (\psi_{y3} + \psi_{y1}) \\
 \lambda_9 &= -w_1 + w_2 - \frac{c_3}{2} (\psi_{x1} + \psi_{x2}) - \frac{b_3}{2} (\psi_{y1} + \psi_{y2})
 \end{aligned} \right\} \quad (6-92)$$

From Eq. (6-89), it can be seen that the deflection along each element side is a cubic polynomial (note: three terms corresponding to λ_{10} , λ_{11} , λ_{12} are all zero along the boundary line), and can be determined uniquely according to the values of deflections and tangential rotations at the two ends of the side. Thereby, when

the 9 point conforming conditions at the corner nodes are satisfied, the deflection along each element side is compatible exactly. But, the normal slope $\psi_n = \frac{\partial w}{\partial n}$ along each element side is still incompatible.

Secondly, in order to require the normal slope along each side to satisfy the necessary conforming conditions, 3 average line conforming conditions are imposed on the normal slopes along the element sides:

$$\int_0^{d_3} \left(\frac{\partial w}{\partial n} - \tilde{\psi}_n \right) \Big|_{L_3=0} ds = 0 \quad (6-93a)$$

$$\int_0^{d_1} \left(\frac{\partial w}{\partial n} - \tilde{\psi}_n \right) \Big|_{L_1=0} ds = 0 \quad (6-93b)$$

$$\int_0^{d_2} \left(\frac{\partial w}{\partial n} - \tilde{\psi}_n \right) \Big|_{L_2=0} ds = 0 \quad (6-93c)$$

where d_1 , d_2 and d_3 denote the length of each element side, respectively (Fig. 6.1). Substitution of Eq. (6-90) into the above equation will yield three equations containing λ_{10} , λ_{11} , λ_{12} . Now, we take Eq. (6-93a) as an example, the derivation procedure is listed as follows:

The normal derivative of the deflection field (6-89) along side $\bar{12}$ ($L_3 = 0$) is:

$$\begin{aligned} \frac{\partial w}{\partial n} \Big|_{L_3=0} &= \frac{d_3}{4A} \left[(1+r_3) \frac{\partial w}{\partial L_1} + (1-r_3) \frac{\partial w}{\partial L_2} - 2 \frac{\partial w}{\partial L_3} \right] \Big|_{L_3=0} \\ &= \frac{d_3}{4A} \{ (1+r_3)[\lambda_1 + \lambda_6 L_2 + \lambda_9 L_2 (L_2 - 2L_1)] + (1-r_3)[\lambda_2 + \lambda_6 L_1 + \lambda_9 L_1 (2L_2 - L_1)] \\ &\quad - 2[\lambda_3 + \lambda_4 L_2 + \lambda_5 L_1 - \lambda_7 L_2^2 + \lambda_8 L_1^2 + \lambda_{11} L_2 L_1^2 + \lambda_{12} L_1 L_2^2] \} \end{aligned} \quad (6-94)$$

where

$$r_3 = \frac{d_1^2 - d_2^2}{d_3^2}, \quad r_1 = \frac{d_2^2 - d_3^2}{d_1^2}, \quad r_2 = \frac{d_3^2 - d_1^2}{d_2^2} \quad (6-95)$$

The integration of Eq. (6-94) along side $\bar{12}$ is

$$\int_0^{d_3} \frac{\partial w}{\partial n} \Big|_{L_3=0} ds = \frac{d_3^2}{4A} \left[(1+r_3)\lambda_1 + (1-r_3)\lambda_2 - 2\lambda_3 - \lambda_4 - \lambda_5 + \lambda_6 + \frac{2}{3}\lambda_7 - \frac{2}{3}\lambda_8 - \frac{\lambda_{11}}{6} - \frac{\lambda_{12}}{6} \right] \quad (6-96)$$

And, the integration of the normal slope $\tilde{\psi}_n$ along side $\bar{12}$ is

$$\int_0^{d_3} \tilde{\psi}_n \Big|_{L_3=0} ds = -\frac{b_3}{2} (\psi_{x_1} + \psi_{x_2}) - \frac{c_3}{2} (\psi_{y_1} + \psi_{y_2}) \quad (6-97)$$

Substitution of Eq. (6-91) into the above equation yields

$$\int_0^{d_3} \tilde{\psi}_n \Big|_{L_3=0} ds = \frac{d_3^2}{4A} [(1+r_3)\lambda_1 + (1-r_3)\lambda_2 - 2\lambda_3 - \lambda_4 - \lambda_5 + \lambda_6 + \lambda_7 - \lambda_8 + r_3\lambda_9] \quad (6-98)$$

Substitution of Eqs. (6-96) and (6-98) into Eq. (6-93a) yields the first equation of (6-99)

$$\left. \begin{aligned} \lambda_{11} + \lambda_{12} &= -2\lambda_7 + 2\lambda_8 - 6r_3\lambda_9 \\ \lambda_{12} + \lambda_{10} &= -2\lambda_8 + 2\lambda_9 - 6r_1\lambda_7 \\ \lambda_{10} + \lambda_{11} &= -2\lambda_9 + 2\lambda_7 - 6r_2\lambda_8 \end{aligned} \right\} \quad (6-99)$$

Similarly, the second and third equations in the above equations can also be derived. Then, λ_{10} , λ_{11} and λ_{12} can be solved from Eq. (6-99):

$$\left. \begin{aligned} \lambda_{10} &= (2-3r_1)\lambda_7 - (2+3r_2)\lambda_8 + 3r_3\lambda_9 \\ \lambda_{11} &= 3r_1\lambda_7 + (2-3r_2)\lambda_8 - (2+3r_3)\lambda_9 \\ \lambda_{12} &= -(2+3r_1)\lambda_7 + 3r_2\lambda_8 + (2-3r_3)\lambda_9 \end{aligned} \right\} \quad (6-100)$$

Now, all the 12 unknown coefficients have been obtained, as shown in Eqs. (6-92) and (6-100). Substituting them into Eq. (6-89), the element deflection field and its shape functions can be derived as follows:

$$w = \sum_{i=1}^3 (N_i w_i + N_{xi} \psi_{xi} + N_{yi} \psi_{yi}) \quad (6-101)$$

The three shape functions of the node 1 are

$$\left. \begin{aligned} N_1 &= L_1 + L_1 L_3 (L_1 - L_3) - L_1 L_2 (L_2 - L_1) - (2 + 3r_2 + 3r_3) L_1 L_2 L_3^2 \\ &\quad + (4 - 3r_2 + 3r_3) L_2 L_3 L_1^2 - (2 - 3r_2 - 3r_3) L_3 L_1 L_2^2 \\ N_{x1} &= -\frac{c_2}{2} L_3 L_1 + \frac{c_3}{2} L_1 L_2 - \frac{c_2}{2} (L_1 - L_3) L_3 L_1 - \frac{c_3}{2} (L_2 - L_1) L_1 L_2 + \frac{1}{2} (2c_2 + 3c_2 r_2 \\ &\quad - 3c_3 r_3) L_1 L_2 L_3^2 - \frac{1}{2} (2c_2 - 2c_3 - 3c_2 r_2 - 3c_3 r_3) L_2 L_3 L_1^2 \\ &\quad - \frac{1}{2} (2c_3 + 3c_2 r_2 - 3c_3 r_3) L_3 L_1 L_2^2 \\ N_{y1} &= \frac{b_2}{2} L_3 L_1 - \frac{b_3}{2} L_1 L_2 + \frac{b_2}{2} (L_1 - L_3) L_3 L_1 + \frac{b_3}{2} (L_2 - L_1) L_1 L_2 \\ &\quad - \frac{1}{2} (2b_2 + 3b_2 r_2 - 3b_3 r_3) L_1 L_2 L_3^2 + \frac{1}{2} (2b_2 - 2b_3 - 3b_2 r_2 - 3b_3 r_3) L_2 L_3 L_1^2 \\ &\quad + \frac{1}{2} (2b_3 + 3b_2 r_2 - 3b_3 r_3) L_3 L_1 L_2^2 \end{aligned} \right\} \quad (6-102)$$

The shape functions of the nodes 2 and 3 can be obtained by permutation. By these shape functions, it is easy to derive the element stiffness matrix, which has been given in reference [17].

Note that Eq. (6-99) can also be derived from the point conforming conditions about ψ_n at the mid-points of the element sides. This can be explained as follows: according to the deflection field assumed in Eq. (6-89), the normal slope

$$\psi_n = \frac{\partial w}{\partial n}$$

along each side is cubically distributed. On conditions that ψ_n is cubically

distributed along the element side and has already satisfied the point conforming conditions at the two ends, the average line conforming condition of ψ_n is equivalent to the point conforming condition of ψ_n at mid-side point.

Example 6.11 The central deflection w_C and central moment M_C of the simply-supported and clamped square plates subjected to uniform load q and central concentrated load P .

The length of the square plate side is L , the Poisson's ratio is 0.3. Two mesh types are used: mesh B in Fig. 6.2 and Mesh C in Fig. 6.13. The results by the element GCIII-T9 are given in Tables 6.16 and 6.17.

Table 6.16 The central deflection and moment of square plates subjected to uniform load (GCIII-T9)

Mesh (1/4 plate)	Central deflection w_C				Central moment M_C			
	Simply-supported		Clamped		Simply-supported		Clamped	
	Mesh B	Mesh C	Mesh B	Mesh C	Mesh B	Mesh C	Mesh B	Mesh C
2 × 2	0.394	0.386	0.101	0.100	0.472	0.547	0.198	0.230
4 × 4	0.403	0.402	0.120	0.120	0.479	0.502	0.222	0.244
6 × 6	0.405	0.404	0.123	0.124	0.480	0.489	0.226	0.236
8 × 8	0.404	0.405	0.125	0.125	0.478	0.485	0.227	0.233
Analytical	0.406 24 $qL^4/(100D)$		0.126 53 $qL^4/(100D)$		0.478 86 $qL^2/10$		0.2291 $qL^2/10$	

Table 6.17 The central deflection of square plates subjected to central concentrated load (GCIII-T9)

Mesh (1/4 plate)	Simply-supported		Clamped	
	Mesh B	Mesh C	Mesh B	Mesh C
2 × 2	0.107	0.106	0.438	0.433
4 × 4	0.113	0.113	0.523	0.527
6 × 6	0.115	0.114	0.542	0.544
8 × 8	0.115	0.115	0.550	0.551
Analytical	0.1160 $PL^2/(10D)$		0.5612 $PL^2/(100D)$	

6.5 Super-Basis Point Conforming Scheme—Elements MB1-T9 and MB2-T9

This and the next sections will introduce two construction schemes for the super-basis thin plate elements formulated only by the point conforming conditions, which are also the improvement schemes for the conventional non-conforming elements. Firstly, according to the conventional method of non-conforming elements, the point conforming conditions about w , ψ_x , ψ_y at the corner nodes are selected. Here, the normal slope ψ_n along each side is generally still incompatible. Secondly, for overcoming this shortcoming, the point conforming conditions of ψ_n at the mid-side points are supplemented for improving the compatibility of ψ_n along each side. The no. 16, 17 and 18 elements in Table 5.1 belong to this element group, in which two triangular elements MB1-T9 and MB2-T9 will be introduced in detail^[18].

6.5.1 Triangular Element MB1-T9

Triangular element MB1-T9 has 9 DOFs. Its assumed deflection field contains 12 unknown coefficients, and can be written as the sum of two parts:

$$w = \bar{w} + \hat{w} \tag{6-103}$$

where \bar{w} and \hat{w} contain 9 and 3 unknown coefficients, respectively.

$$\bar{w} = \lambda_1 L_1 + \lambda_2 L_2 + \lambda_3 L_3 + \lambda_4 L_1 L_2 + \lambda_5 L_2 L_3 + \lambda_6 L_3 L_1 + \lambda_7 L_1^2 L_2 + \lambda_8 L_2^2 L_3 + \lambda_9 L_3^2 L_1 \tag{6-104}$$

$$\hat{w} = \lambda_{10} L_2^2 L_3^2 + \lambda_{11} L_3^2 L_1^2 + \lambda_{12} L_1^2 L_2^2 \tag{6-105}$$

The selected 12 conforming conditions are also classified into two groups. The first group involves 9 point conforming conditions about w , ψ_x and ψ_y at three corner nodes. Since \hat{w} , $\frac{\partial \hat{w}}{\partial x}$ and $\frac{\partial \hat{w}}{\partial y}$ at the corner nodes are identically equal zero,

only the first 9 unknown coefficients $\lambda_1, \lambda_2, \dots, \lambda_9$ appear in these 9 equations. Their solutions are

$$\left. \begin{aligned} \lambda_1 &= w_1 \\ \lambda_2 &= w_2 \\ \lambda_3 &= w_3 \\ \lambda_4 &= -w_1 + w_2 - c_3 \psi_{x2} + b_3 \psi_{y2} \\ \lambda_5 &= -w_2 + w_3 - c_1 \psi_{x3} + b_1 \psi_{y3} \\ \lambda_6 &= -w_3 + w_1 - c_2 \psi_{x1} + b_2 \psi_{y1} \\ \lambda_7 &= 2w_1 - 2w_2 + c_3(\psi_{x1} + \psi_{x2}) - b_3(\psi_{y1} + \psi_{y2}) \\ \lambda_8 &= 2w_2 - 2w_3 + c_1(\psi_{x2} + \psi_{x3}) - b_1(\psi_{y2} + \psi_{y3}) \\ \lambda_9 &= 2w_3 - 2w_1 + c_2(\psi_{x3} + \psi_{x1}) - b_2(\psi_{y3} + \psi_{y1}) \end{aligned} \right\} \tag{6-106}$$

In the assumed deflection field \bar{w} of Eq. (6-104), deflection \bar{w} along each side is a cubic polynomial, and normal slope $\frac{\partial \bar{w}}{\partial n}$ is a quadric polynomial. Thereby, along each boundary line, \bar{w} and \tilde{w} conform to each other, but $\frac{\partial \bar{w}}{\partial n}$ and $\tilde{\psi}_n$ are not compatible. In fact, the non-conforming values of the normal slopes at the mid-side points 4, 5 and 6 can be solved as follows:

$$\left\{ \begin{array}{l} \frac{1}{d_1} \left(\frac{\partial \bar{w}}{\partial n} - \tilde{\psi}_n \right)_4 \\ \frac{1}{d_2} \left(\frac{\partial \bar{w}}{\partial n} - \tilde{\psi}_n \right)_5 \\ \frac{1}{d_3} \left(\frac{\partial \bar{w}}{\partial n} - \tilde{\psi}_n \right)_6 \end{array} \right\} = \frac{1}{16A} \begin{bmatrix} 0 & 1+3r_1 & 2 \\ 2 & 0 & 1+3r_2 \\ 1+3r_3 & 2 & 0 \end{bmatrix} \begin{Bmatrix} \lambda_7 \\ \lambda_8 \\ \lambda_9 \end{Bmatrix} \quad (6-107)$$

where d_1 and point 4 are the length and mid-side point of the opposite side of the node 1, respectively; r_1 is given by Eq. (6-58). The rest can be analogized.

The second group involves the point conforming conditions about ψ_n at the mid-side points. Since

$$\left\{ \begin{array}{l} \frac{1}{d_1} \left(\frac{\partial \hat{w}}{\partial n} \right)_4 \\ \frac{1}{d_2} \left(\frac{\partial \hat{w}}{\partial n} \right)_5 \\ \frac{1}{d_3} \left(\frac{\partial \hat{w}}{\partial n} \right)_6 \end{array} \right\} = \frac{1}{8A} \begin{Bmatrix} \lambda_{10} \\ \lambda_{11} \\ \lambda_{12} \end{Bmatrix} \quad (6-108)$$

from Eqs. (6-107) and (6-108), and according to the conforming conditions of ψ_n , we obtain

$$\begin{Bmatrix} \lambda_{10} \\ \lambda_{11} \\ \lambda_{12} \end{Bmatrix} = -\frac{1}{2} \begin{bmatrix} 0 & 1+3r_1 & 2 \\ 2 & 0 & 1+3r_2 \\ 1+3r_3 & 2 & 0 \end{bmatrix} \begin{Bmatrix} \lambda_7 \\ \lambda_8 \\ \lambda_9 \end{Bmatrix} \quad (6-109)$$

Thus, all the unknown coefficients have been solved out, and the shape functions and element stiffness matrix can be obtained by the conventional procedure.

Here, we also give the following two points.

(1) If we substitute Eq. (6-109) into Eq. (6-105), then w in Eq. (6-103) can be written in terms of the first 9 unknown coefficients:

$$w = \lambda_1 L_1 + \lambda_2 L_2 + \lambda_3 L_3 + \lambda_4 L_1 L_2 + \lambda_5 L_2 L_3 + \lambda_6 L_3 L_1 + \lambda_7 L_1^2 \left(L_2 - \frac{1+3r_3}{2} L_2^2 - L_3^2 \right)$$

$$+ \lambda_8 L_2^2 \left(L_3 - \frac{1+3r_1}{2} L_3 - L_1^2 \right) + \lambda_9 L_3^2 \left(L_1 - \frac{1+3r_2}{2} L_1^2 - L_2^2 \right) \tag{6-110}$$

where the 9 basis functions can be called as the modified basis functions.

(2) The normal derivative $\frac{\partial w}{\partial n}$ along each side is a cubic polynomial. If the point conforming conditions are satisfied at the mid-side points and two ends of the side, $\frac{\partial w}{\partial n}$ must satisfy the average line conforming conditions, so this element is a convergent model.

Example 6.12 The deflection and moment of the simply-supported and clamped square plates subjected to uniform load q and central concentrated load P .

Two mesh types are used: mesh A and B in Fig. 6.2. The results by the element MB1-T9 are given in Tables 6.18 and 6.19. It can be seen that this element exhibits good performance.

Table 6.18 The results of the central deflection (MB1-T9)

Mesh (1/4 plate)	Uniform load q				Central concentrated load P			
	Simply-supported		Clamped		Simply-supported		Clamped	
	Mesh A	Mesh B	Mesh A	Mesh B	Mesh A	Mesh B	Mesh A	Mesh B
2×2	0.3969 (-2.3%)	0.4066 (0.1%)	0.1324 (4.7%)	0.1128 (-10.9%)	1.093 (-5.8%)	1.166 (0.5%)	0.5300 (-5.6%)	0.5279 (-5.9%)
4×4	0.4041 (-0.5%)	0.4068 (0.1%)	0.1277 (0.9%)	0.1234 (-2.5%)	1.143 (-1.8%)	1.160 (0.0%)	0.5514 (-1.8%)	0.5526 (-1.5%)
6×6	0.4053 (-0.2%)	0.4066 (0.1%)	0.1270 (0.4%)	0.1251 (-1.1%)	1.152 (-0.8%)	1.160 (0.0%)	0.5564 (-0.9%)	0.5571 (-0.7%)
8×8	0.4057 (-0.1%)	0.4064 (0.0%)	0.1268 (0.2%)	0.1258 (-0.6%)	1.155 (-0.4%)	1.160 (0.0%)	0.5584 (-0.5%)	0.5588 (-0.4%)
Analytical	0.4062($qL^4/100D$)		0.1265($qL^4/100D$)		1.160($PL^2/100D$)		0.5612($PL^2/100D$)	

6.5.2 Triangular Element MB2-T9

Another triangular element MB2-T9 can be derived by a similar scheme. The difference with the element MB1-T9 is that \hat{w} is re-assumed as follows:

$$\hat{w} = \lambda_{10} L_1^2 L_2 L_3 + \lambda_{11} L_2^2 L_3 L_1 + \lambda_{12} L_3^2 L_1 L_2 \tag{6-111}$$

From the point conforming conditions of the normal slope ψ_n at the mid-side points, we obtain

$$\begin{Bmatrix} \lambda_{10} \\ \lambda_{11} \\ \lambda_{12} \end{Bmatrix} = \frac{1}{2} \begin{bmatrix} 3(1+r_3) & 1-3r_1 & -(1-3r_2) \\ -(1-3r_3) & 3(1+r_1) & 1-3r_2 \\ 1-3r_3 & -(1-3r_1) & 3(1+r_2) \end{bmatrix} \begin{Bmatrix} \lambda_7 \\ \lambda_8 \\ \lambda_9 \end{Bmatrix} \quad (6-112)$$

The total deflection w can be expressed in terms of $\lambda_1, \lambda_2, \dots, \lambda_9$ and their modified basis functions, and its expression is the same as that of the element proposed by Specht^[19], but the derivation procedure here is much simpler.

Table 6.19 The results of the central and mid-side moments (MB1-T9)

Mesh (1/4 plate)	Central moment (q)				Mid-side moment (clamped plate)			
	Simply-supported		Clamped		(P)		(q)	
	Mesh A	Mesh B	Mesh A	Mesh B	Mesh A	Mesh B	Mesh A	Mesh B
2×2	0.5468 (14.2%)	0.5477 (14.4%)	0.3077 (34.3%)	0.2720 (18.7%)	-0.1706 (35.7%)	-0.1001 (-20.3%)	-0.0707 (37.8%)	-0.0333 (-35.2%)
4×4	0.5001 (4.4%)	0.4971 (3.8%)	0.2524 (10.2%)	0.2408 (5.1%)	-0.1509 (20.0%)	-0.1162 (-7.6%)	-0.0648 (26.4%)	-0.0429 (-16.4%)
6×6	0.4882 (2.0%)	0.4873 (1.8%)	0.2395 (4.5%)	0.2343 (2.3%)	-0.1439 (14.5%)	-0.1181 (-6.1%)	-0.0613 (19.4%)	-0.0454 (-11.6%)
8×8	0.4828 (0.8%)	0.4837 (1.0%)	0.2350 (2.6%)	0.2319 (1.2%)	-0.1399 (11.3%)	-0.1193 (-5.1%)	-0.0592 (15.4%)	-0.0467 (-9.0%)
Analytical	0.4789($qL^2/10$)		0.2291($qL^2/10$)		-0.1257(P)		-0.0513(qL^2)	

6.6 SemiLoof Conforming Scheme

This section will introduce the second construction scheme for the super-basis thin plate elements formulated only by the point conforming conditions, i.e. SemiLoof conforming scheme. This scheme is a novel scheme by the combination of the generalized conforming element and the SemiLoof element^[20], and possesses the following characteristics:

(1) Unlike the SemiLoof element with DOFs at the corner and mid-side nodes, the elements here only contain DOFs at the corner nodes, which is much simpler and more suitable for applications.

(2) It is not necessary that a one-to-one correspondence exists between the element DOFs and the selected conforming conditions (and a super-basis scheme $m > n$ is used). But, the limit compatibility should be ensured when the mesh is refined by infinite elements, so that the advantages (reliability and convergence) of the generalized conforming elements can be guaranteed.

(3) The integral form conforming conditions (such as line conforming and perimeter conforming conditions), which are usually employed by the generalized conforming elements, are not adopted here. All the conforming conditions used

are discrete point conforming conditions: the point conforming conditions about deflection w at the corner nodes and mid-side points, and the point conforming conditions about the normal slope ψ_n at two Gauss points of each side (the SemiLoof constraint conditions). So the derivation procedure becomes more convenient.

The no. 19, 20 and 21 elements LSL-T9, LSL-R12 and LSL-Q12 in Table 5.1 belong to this element group, in which two elements LSL-T9^[21] and LSL-Q12^[22] will be introduced in detail.

6.6.1 Triangular Element LSL-T9

A triangular thin plate element is shown in Fig. 6.16. The nodal displacement vector (element DOFs) q^e is the same as Eq. (6-1).

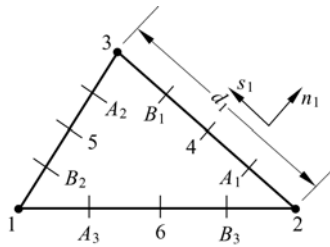


Figure 6.16 A triangular thin plate element with SemiLoof constraint conditions 4,5,6 are mid-side points; and A_i and B_i are two Gauss points along each side

The element deflection field w is assumed to be a polynomial with 12 unknown coefficients, expressible in terms of the area coordinates L_1, L_2 and L_3 as follows

$$\begin{aligned}
 w = & [\lambda_1 L_1 + \lambda_2 L_2 + \lambda_3 L_3] + [\lambda_4 L_2 L_3 + \lambda_5 L_3 L_1 + \lambda_6 L_1 L_2] \\
 & + [\lambda_7 L_2 L_3 (L_2 - L_3) + \lambda_8 L_3 L_1 (L_3 - L_1) + \lambda_9 L_1 L_2 (L_1 - L_2)] \\
 & + [\lambda_{10} L_1^2 L_2 L_3 + \lambda_{11} L_2^2 L_3 L_1 + \lambda_{12} L_3^2 L_1 L_2] \quad (6-113)
 \end{aligned}$$

The following 12 point conforming conditions are selected:

$$(w - \tilde{w})_i = 0 \quad (i = 1, 2, 3) \quad (6-114)$$

$$(w - \tilde{w})_j = 0 \quad (j = 4, 5, 6) \quad (6-115)$$

$$\left(\frac{\partial w}{\partial n} - \tilde{\psi}_n \right)_k = 0 \quad (k = A_1, B_1, A_2, B_2, A_3, B_3) \quad (6-116)$$

Equations (6-114) and (6-115) are the point conforming conditions about deflection at the corner nodes (nodes 1, 2, 3) and mid-side points (points 4, 5, 6); Eq. (6-116) is the point conforming conditions about the normal slope at Gauss points (points $A_1, B_1, A_2, B_2, A_3, B_3$) along the element sides.

Firstly, from Eq. (6-114), we obtain

$$\lambda_1 = w_1, \quad \lambda_2 = w_2, \quad \lambda_3 = w_3 \quad (6-117)$$

Secondly, λ_4 , λ_5 and λ_6 can be obtained from Eq. (6-115), for example, for the mid-side point 4 of side 23, we have

$$w_4 = \frac{1}{2}\lambda_2 + \frac{1}{2}\lambda_3 + \frac{1}{4}\lambda_4$$

$$\tilde{w}_4 = \frac{1}{2}(w_2 + w_3) + \frac{c_1}{8}(\psi_{x2} - \psi_{x3}) - \frac{b_1}{8}(\psi_{y2} - \psi_{y3})$$

Then, as shown in the first equation below, λ_4 can be solved:

$$\left. \begin{aligned} \lambda_4 &= \frac{c_1}{2}(\psi_{x2} - \psi_{x3}) - \frac{b_1}{2}(\psi_{y2} - \psi_{y3}) \\ \lambda_5 &= \frac{c_2}{2}(\psi_{x3} - \psi_{x1}) - \frac{b_2}{2}(\psi_{y3} - \psi_{y1}) \\ \lambda_6 &= \frac{c_3}{2}(\psi_{x1} - \psi_{x2}) - \frac{b_3}{2}(\psi_{y1} - \psi_{y2}) \end{aligned} \right\} \quad (6-118)$$

Finally, the rest of the unknown coefficients can be obtained from Eq. (6-116):

$$\left. \begin{aligned} \lambda_7 &= \frac{1}{2}[(r_2 + r_3)w_1 + (3 - r_3)w_2 - (r_2 + 3)w_3] + \frac{1}{12}[(c_1 - 3r_2c_2 + 3r_3c_3)\psi_{x1} \\ &\quad + (3r_3c_3 - c_3 + 8c_1)\psi_{x2} - (3r_2c_2 + c_2 - 8c_1)\psi_{x3}] - \frac{1}{12}[(b_1 - 3r_2b_2 \\ &\quad + 3r_3b_3)\psi_{y1} + (3r_3b_3 - b_3 + 8b_1)\psi_{y2} - (3r_2b_2 + b_2 - 8b_1)\psi_{y3}] \\ \lambda_8 &= \frac{1}{2}[-(r_3 + 3)w_1 + (r_3 + r_1)w_2 + (3 - r_1)w_3] + \frac{1}{12}[-(3r_3c_3 + c_3 - 8c_2)\psi_{x1} \\ &\quad + (c_2 - 3r_3c_3 + 3r_1c_1)\psi_{x2} + (3r_1c_1 - c_1 + 8c_2)\psi_{x3}] - \frac{1}{12}[-(3r_3b_3 + b_3 \\ &\quad - 8b_2)\psi_{y1} + (b_2 - 3r_3b_3 + 3r_1b_1)\psi_{y2} + (3r_1b_1 - b_1 + 8b_2)\psi_{y3}] \\ \lambda_9 &= \frac{1}{2}[(3 - r_2)w_1 - (r_1 + 3)w_2 + (r_1 + r_2)w_3] + \frac{1}{12}[(3r_2c_2 - c_2 + 8c_3)\psi_{x1} \\ &\quad - (3r_1c_1 + c_1 - 8c_3)\psi_{x2} + (c_3 - 3r_1c_1 + 3r_2c_2)\psi_{x3}] - \frac{1}{12}[(3r_2b_2 - b_2 \\ &\quad + 8b_3)\psi_{y1} - (3r_1b_1 + b_1 - 8b_3)\psi_{y2} + (b_3 - 3r_1b_1 + 3r_2b_2)\psi_{y3}] \\ \lambda_{10} = \lambda_{11} = \lambda_{12} &= (r_3 - r_2)w_1 + (r_1 - r_3)w_2 + (r_2 - r_1)w_3 \\ &\quad + \frac{1}{2}[(r_2c_2 + r_3c_3)\psi_{x1} + (r_3c_3 + r_1c_1)\psi_{x2} + (r_1c_1 + r_2c_2)\psi_{x3}] \\ &\quad - \frac{1}{2}[(r_2b_2 + r_3b_3)\psi_{y1} + (r_3b_3 + r_1b_1)\psi_{y2} + (r_1b_1 + r_2b_2)\psi_{y3}] \end{aligned} \right\} \quad (6-119)$$

where b_i , c_i and r_i are given in Eq. (6-58).

Once λ is solved and expressed in terms of q^e , the element stiffness matrix can be derived following the conventional procedure. Note that the element LT in reference [23] derived with the integral conforming conditions is equivalent to the present element. However, the construction procedure in this section based on the point conforming conditions appears to be simpler, and is easy to be extended to formulate quadrilateral element.

Example 6.13 The central deflection and central moment of the simply-supported and the clamped square plates subjected to uniform load.

Results by the elements LSL-T9 and CT proposed by Fricker^[11] are given in Table 6.20 for comparison. It can be seen that the accuracy of the present element is better than that of the element CT (Meshes *A* and *B* in Fig. 6.2 are used).

Table 6.20 The central deflection and moment of square plates subjected to uniform load (LSL-T9)

	Mesh (1/4 plate)	Simply-supported				Clamped			
		LST-T9		CT		LST-T9		CT	
		Mesh <i>A</i>	Mesh <i>B</i>	Mesh <i>A</i>	Mesh <i>B</i>	Mesh <i>A</i>	Mesh <i>B</i>	Mesh <i>A</i>	Mesh <i>B</i>
Central deflection	2 × 2	0.4014 (-1.2%)	0.4024 (-0.9%)	0.399 30 (-1.7%)	0.351 18 (-13.6%)	0.122 88 (-2.9%)	0.107 68 (-14.9%)	0.147 50 (16.6%)	0.107 32 (-15.2%)
	4 × 4	0.4051 (-0.3%)	0.4058 (-0.1%)	0.404 39 (-0.5%)	0.392 80 (-3.3%)	0.125 44 (-0.8%)	0.122 03 (-3.6%)	0.132 21 (4.5%)	0.122 32 (-3.3%)
	6 × 6	0.405 74 (-0.1%)	0.406 09 (-0.03%)	0.405 40 (-0.2%)	0.400 28 (-1.5%)	0.126 11 (-0.3%)	0.124 52 (-1.6%)	0.129 12 (2.0%)	0.124 68 (-1.5%)
	Analytical	0.406 235 $qL^4/(100D)$				0.126 53 $qL^4/(100D)$			
Central moment	2 × 2	0.5022 (4.9%)	0.5161 (7.8%)	0.499 88 (4.4%)	0.439 58 (-8.2%)	0.2909 (27%)	0.2380 (3.9%)	0.295 10 (28.8%)	0.205 27 (-10.4%)
	4 × 4	0.4798 (0.2%)	0.4917 (2.7%)	0.483 47 (1.0%)	0.470 05 (-1.8%)	0.2386 (4.2%)	0.2343 (2.3%)	0.246 71 (7.7%)	0.223 89 (-2.3%)
	6 × 6	0.478 21 (-0.1%)	0.485 51 (1.4%)	0.480 90 (0.4%)	0.474 93 (-0.8%)	0.232 77 (1.6%)	0.231 55 (1.1%)	0.237 51 (3.7%)	0.226 05 (-1.3%)
	Analytical	0.478 86($qL^2/10$)				0.229 05($qL^2/10$)			

6.6.2 Quadrilateral Element LSL-Q12

A quadrilateral thin plate element with 12 conventional DOFs is shown in Fig. 6.17. Its nodal displacement vector q^e is

$$q^e = [w_1 \quad \psi_{x1} \quad \psi_{y1} \quad w_2 \quad \psi_{x2} \quad \psi_{y2} \quad w_3 \quad \psi_{x3} \quad \psi_{y3} \quad w_4 \quad \psi_{x4} \quad \psi_{y4}]^T \tag{6-120}$$

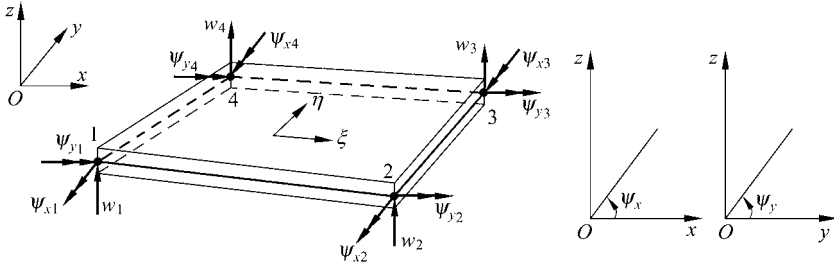


Figure 6.17 A quadrilateral thin plate element

The element deflection w is assumed to be a polynomial with 16 unknown coefficients, and expressed in terms of ξ and η as

$$\begin{aligned}
 w = & \lambda_1 + \lambda_2\xi + \lambda_3\eta + \lambda_4\xi\eta + (\xi^2 - 1)(\lambda_5 + \lambda_6\eta) + (\eta^2 - 1)(\lambda_7 + \lambda_8\xi) \\
 & + \xi(\xi^2 - 1)(\alpha_1 + \alpha_3\eta) + \eta(\eta^2 - 1)(\alpha_2 + \alpha_4\xi) + (\xi^2 - 1)(\eta^2 - 1)(\alpha_5 + \alpha_6\xi + \alpha_7\eta) \\
 & + \alpha_8[\xi^2(\xi^2 - 1) - \eta^2(\eta^2 - 1)]
 \end{aligned} \tag{6-121}$$

Apply the following 16 conforming conditions

$$(w - \tilde{w})_i = 0 \quad (i = 1, 2, \dots, 8) \tag{6-122}$$

$$\left(\frac{\partial w}{\partial n} - \tilde{\psi}_n \right)_j = 0 \quad (j = A_1, B_1, A_2, B_2, A_3, B_3, A_4, B_4) \tag{6-123}$$

where Eq. (6-122) denotes the point conforming conditions about deflections at the corner nodes (nodes 1, 2, 3 and 4) and the mid-side points (points 5, 6, 7 and 8); Eq. (6-123) denotes the point conforming conditions about the normal slopes

at eight Gauss points $A_j \left(\xi_j, \frac{1}{\sqrt{3}}\eta_j \right)$ and $B_j \left(\frac{1}{\sqrt{3}}\xi_j, \eta_j \right)$ ($j = 1, 2, 3, 4$) along the four element sides.

These 16 point conforming conditions are the SemiLoof constraint conditions^[20], as shown in Fig. 6.18.

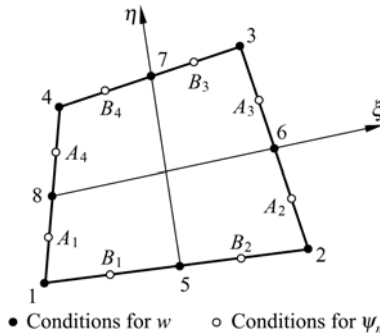


Figure 6.18 SemiLoof constraint conditions

Firstly, by applying the condition (6-122), $\lambda_1, \lambda_2, \dots, \lambda_8$ can be solved as follows:

$$\left. \begin{aligned} \lambda_1 &= \frac{1}{4} \sum_{i=1}^4 w_i, & \lambda_2 &= \frac{1}{4} \sum_{i=1}^4 w_i \xi_i \\ \lambda_3 &= \frac{1}{4} \sum_{i=1}^4 w_i \eta_i, & \lambda_4 &= \frac{1}{4} \sum_{i=1}^4 w_i \xi_i \eta_i \\ \lambda_5 &= \frac{1}{8} \sum_{i=1}^4 [\psi_{xi} \xi_i (\bar{a}_1 + \bar{a}_3 \eta_i) + \psi_{yi} \xi_i (\bar{b}_1 + \bar{b}_3 \eta_i)] \\ \lambda_6 &= \frac{1}{8} \sum_{i=1}^4 [\psi_{xi} \xi_i (\bar{a}_1 \eta_i + \bar{a}_3) + \psi_{yi} \xi_i (\bar{b}_1 \eta_i + \bar{b}_3)] \\ \lambda_7 &= \frac{1}{8} \sum_{i=1}^4 [\psi_{xi} \eta_i (\bar{a}_2 + \bar{a}_3 \xi_i) + \psi_{yi} \eta_i (\bar{b}_2 + \bar{b}_3 \xi_i)] \\ \lambda_8 &= \frac{1}{8} \sum_{i=1}^4 [\psi_{xi} \eta_i (\bar{a}_2 \xi_i + \bar{a}_3) + \psi_{yi} \eta_i (\bar{b}_2 \xi_i + \bar{b}_3)] \end{aligned} \right\} \quad (6-124)$$

where

$$\left. \begin{aligned} \bar{a}_1 &= \frac{1}{4} \sum_{i=1}^4 x_i \xi_i, & \bar{a}_2 &= \frac{1}{4} \sum_{i=1}^4 x_i \eta_i, & \bar{a}_3 &= \frac{1}{4} \sum_{i=1}^4 x_i \xi_i \eta_i \\ \bar{b}_1 &= \frac{1}{4} \sum_{i=1}^4 y_i \xi_i, & \bar{b}_2 &= \frac{1}{4} \sum_{i=1}^4 y_i \eta_i, & \bar{b}_3 &= \frac{1}{4} \sum_{i=1}^4 y_i \xi_i \eta_i \end{aligned} \right\} \quad (6-125)$$

Secondly, $\alpha_1, \alpha_2, \dots, \alpha_8$ can be solved from the condition (6-123). And, their expressions are given in reference [22].

Now, all the unknown coefficients are solved, the element stiffness matrix can be derived following the conventional procedure.

Example 6.14 The central deflection of a simply-supported circular plate subjected to uniform load. For comparison, results by the triangular element proposed by Felippa and Bergan^[14] are also given together with those of the present element LSL-Q12. The Poisson’s ratio $\mu = 0.3$.

Owing to symmetry, only one quarter plate is calculated. The two meshes in Fig. 6.14 are used again, in which mesh *A* contains 12 quadrilateral or 24 triangular elements, and mesh *B* contains 48 quadrilateral or 96 triangular elements.

The computational errors are given in Table 6.21. It can be seen that the precision of the element LSL-Q12 is better than that of the triangular element in reference [14].

Table 6.21 The computational errors for central deflection of a simply-supported circular plate (uniform load)

Mesh for 1/4 circular plate	LSL-Q12	Triangular element ^[14]
Mesh <i>A</i>	0.66%	2.87%
Mesh <i>B</i>	0.17%	0.70%

Example 6.15 The central deflection and moment of the simply-supported and the clamped square plates (the length of side is L) subjected to uniform load. The Poisson's ratio is 0.3.

Three Meshes A , B and C in Fig. 6.19 are used for one quarter plate. And, the results are given in Table 6.22. It can be seen that the element LSL-Q12 possesses high precision for both regular and irregular meshes.

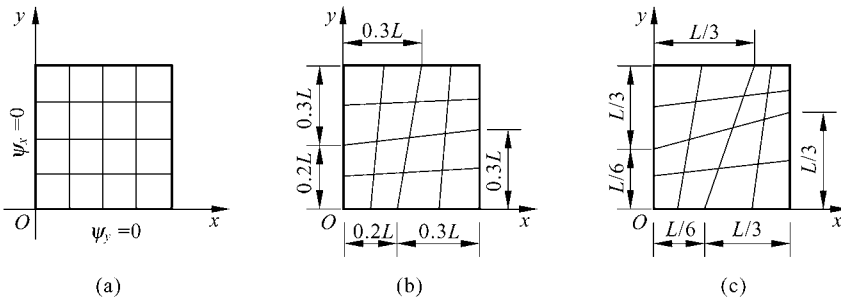


Figure 6.19 Meshes for 1/4 plate
(a) Mesh A 4×4 ; (b) Mesh B 4×4 ; (c) Mesh C 4×4

Table 6.22 Results by element LSL-Q12 for square plates subjected to uniform load

	Mesh (1/4 plate)	Simply-supported			Clamped		
		Mesh A	Mesh B	Mesh C	Mesh A	Mesh B	Mesh C
Central deflection	2×2	0.405 13 (-0.27%)	0.404 42 (-0.45%)	0.403 10 (-0.77%)	0.122 65 (-3.07%)	0.122 34 (-3.31%)	0.121 18 (-4.23%)
	4×4	0.406 16 (-0.02%)	0.406 11 (-0.03%)	0.405 96 (-0.07%)	0.125 86 (-0.53%)	0.125 75 (-0.62%)	0.125 72 (-0.64%)
	8×8	0.406 23 (0.00%)	0.406 14 (-0.02%)	0.405 74 (-0.12%)	0.126 44 (-0.07%)	0.126 41 (-0.09%)	0.126 39 (-0.11%)
	Analytical	0.406 235 $qL^4/(100D)$			0.126 53 $qL^4/(100D)$		
Central moment	2×2	0.512 43 (7.01%)	0.518 02 (8.18%)	0.526 91 (10.03%)	0.257 28 (12.32%)	0.254 25 (11.00%)	0.258 85 (13.01%)
	4×4	0.487 30 (1.76%)	0.486 69 (1.64%)	0.486 56 (1.61%)	0.236 80 (3.38%)	0.235 27 (2.72%)	0.234 63 (2.44%)
	8×8	0.480 98 (0.44%)	0.480 38 (0.32%)	0.479 60 (0.15%)	0.231 07 (0.88%)	0.230 47 (0.62%)	0.230 14 (0.48%)
	Analytical	0.478 86 $qL^2/10$			0.229 05 $qL^2/10$		

Example 6.16 The central deflection w and central moment M_y of a rhombus plate (Fig. 6.15) subjected to uniform load.

The results of central deflection and moment by the element LSL-Q12 and other models are listed in Table 6.23. Compared with the elements in references [15, 16], LSL-Q12 has better precision.

Table 6.23 The central deflection and central moment of a rhombus plate subjected to uniform load

DOF	Mesh	Central deflection w			Central moment M_y		
		LSL-Q12	[15]	[16]	LSL-Q12	[15]	[16]
27	2×2	0.7637	0.7230		1.0006	0.7602	
75	4×4	0.7872	0.7718	0.8414	1.0372	0.9172	0.9761
105	4×6	0.7904	0.7850		0.9478	0.9473	
243	8×8	0.7918		0.8111	0.9777		0.9739
507	12×12	0.7927		0.8057	0.9680		0.9688
Difference method ^[15]		$0.7945qL^4/(100D)$			$0.9589qL^2/10$		

References

[1] Bazeley GP, Cheung YK, Irons BM, Zienkiewicz OC (1965) Triangular elements in bending-conforming and nonconforming solution. In: Proceedings of the Conference on Matrix Methods in Structural Mechanics. Air Force Institute of Technology, Ohio: Wright-Patterson A. F. Base pp 547 – 576

[2] Batoz JL, Bathe KJ, Ho LW (1980) A study of three-node triangular plate bending elements. International Journal for Numerical Methods in Engineering 15: 1771 – 1812

[3] Stricklin JA, Haisler WE, Tisdale PR, Gunderson R (1969) A rapidly converging triangular plate element. AIAA Journal 7: 180 – 181

[4] Allman DJ (1971) Triangular finite element plate bending with constant and linearly varying bending moments. In: BF de Veubeke (ed) High Speed Computing of Elastic Structures. Liege Belgium, pp105 – 136

[5] Clough RW, Tocher JL (1965) Finite element stiffness matrices for analysis of plate bending. In: Proceedings of the Conference on Matrix Methods in Structural Mechanics. Air Force Institute of Technology, Ohio: Wright-Patterson A. F. Base, pp515 – 545

[6] Melosh RJ (1963) Basis for derivation of matrices for the direct stiffness method. AIAA Journal 1(7): 1631 – 1637

[7] Tocher JL, Kapur KK (1965) Comment on “basis of derivation of matrices for direct stiffness method”. AIAA Journal 3(6): 1215 – 1216

[8] Kapur KK, Hartz BJ (1966) Stability of thin plates using the finite element method. In: Proceedings of American Society of Civil Engineering, pp177 – 195

[9] Xu Y, Long ZF (1995) A simple generalized conforming rectangular plate bending element. In: Proceedings of the Fourth National Conference on Structural Engineering, pp315 – 319 (in Chinese)

[10] Long ZF (1993) Generalized conforming triangular elements for plate bending. Communications in Numerical Methods in Engineering 9: 53 – 65

[11] Fricker AJ (1985) An improved three-node triangular element for plate bending. International Journal for Numerical Methods in Engineering 21: 105 – 114

Chapter 6 Generalized Conforming Thin Plate Element II—Line-Point and ...

- [12] Jeyachandrabose C, Kirkhope J (1986) Construction of new efficient three-node triangular thin plate bending elements. *Computers & Structures* 23(5): 587 – 603
- [13] Long YQ, Bu XM, Long ZF, Xu Y (1995) Generalized conforming plate bending elements using point and line compatibility conditions. *Computers & Structures* 54(4): 717 – 723
- [14] Felippa CA, Bergan PG (1987) Triangular bending FE based on energy-orthogonal free formulation. *Computer Methods in Applied Mechanics and Engineering* 61: 129 – 160
- [15] Razzaque A (1973) Program for triangular bending element with derivative smoothing. *International Journal for Numerical Methods in Engineering* 6: 333 – 343
- [16] Zienkiewicz OC, Lefebvre D (1988) A robust triangular plate bending element of the Reissner-Mindlin type. *International Journal for Numerical Methods in Engineering* 26: 1169 – 1184
- [17] Long YQ, Bu XM (1990) A family of efficient elements for thin plate bending. *Journal of Tsinghua University* 30(5): 9 – 15 (in Chinese)
- [18] Long ZF (1991) Low-order and high-precision triangular elements for plate bending. In: Cheung, Lee & Leung (eds) *Computational Mechanics*. Rotterdam: Balkema, pp1793 – 1797
- [19] Specht B (1988) Modified shape functions for the three-node plate bending element passing the patch test. *International Journal for Numerical Methods in Engineering* 26: 705 – 715
- [20] Irons BM (1976) The SemiLoof shell element. In: Gallagher RH, Ashwell DG (eds) *Finite Element for Thin and Curved Member*. Wiley, pp197 – 222
- [21] Long ZF (1992) Two generalized conforming plate elements based on SemiLoof constraints. *Computers & Structures* 9(1): 53 – 65
- [22] Long ZF (1993) Generalized conforming quadrilateral plate element by using SemiLoof constraints. *Communications in Numerical Methods in Engineering* 9: 417 – 426
- [23] Long ZF (1992) Triangular and rectangular plate elements based on generalized compatibility conditions. *Computational Mechanics* 10(3/4): 281 – 288

Chapter 7 Generalized Conforming Thin Plate Element III— Perimeter-Point and Least-Square Conforming Schemes

Song Cen

Department of Engineering Mechanics, School of Aerospace,
Tsinghua University, Beijing, 100084, China

Zhi-Fei Long

School of Mechanics & Civil Engineering, China University of
Mining & Technology, Beijing, 100083, China

Abstract This chapter discusses the last two groups of the construction schemes for the generalized conforming thin plate element: perimeter-point conforming scheme and least-square conforming scheme. Five triangular and rectangular element models formulated by these schemes are presented in detail. Numerical examples show that these generalized conforming models also exhibit excellent performance in the analysis of thin plates. Furthermore, the generalized conforming element theory is applied to verify or improve the convergence of two famous non-conforming element models, ACM and BCIZ, and some valuable conclusions are obtained.

Keywords thin plate element, generalized conforming, perimeter-point conforming, least-square conforming.

7.1 Perimeter-Point Conforming Scheme—Elements LR12-1 and LR12-2

This chapter will take the rectangular generalized conforming elements LR12-1 and LR12-2^[1] as the examples to illustrate the procedure for the combination scheme of perimeter and point conforming conditions. These two elements are both elements with $m = n = 12$: the number of the element DOFs $n = 12$, and the number of the unknown coefficients in the deflection field $m = 12$. The selected 12 conforming conditions include 3 point conforming conditions and 9 perimeter conforming conditions.

7.1.1 Element LR12-1

This rectangular thin plate element is also shown in Fig. 6.11. The element nodal displacement vector \mathbf{q}^e is still composed of $w_i, \psi_{xi}, \psi_{yi}$ ($i = 1,2,3,4$) at four corner nodes. And, the element deflection field w is assumed to be an incomplete quartic polynomial with 12 unknown coefficients, as shown in Eqs. (6-22) and (6-23), i.e.,

$$w = \mathbf{F}_\lambda \boldsymbol{\lambda} \quad (7-1)$$

where

$$\left. \begin{aligned} \boldsymbol{\lambda} &= [\lambda_1 \quad \lambda_2 \quad \lambda_3 \quad \lambda_4 \quad \lambda_5 \quad \lambda_6 \quad \lambda_7 \quad \lambda_8 \quad \lambda_9 \quad \lambda_{10} \quad \lambda_{11} \quad \lambda_{12}]^T \\ \mathbf{F}_\lambda &= [1 \quad \xi \quad \eta \quad \xi^2 \quad \xi\eta \quad \eta^2 \quad \xi^3 \quad \xi^2\eta \quad \xi\eta^2 \quad \eta^3 \quad \xi^3\eta \quad \xi\eta^3] \end{aligned} \right\} \quad (7-2)$$

In order to solve $\boldsymbol{\lambda}$, 12 conforming conditions are needed.

Firstly, 3 conforming conditions for the corner nodal deflections can be established:

$$\left. \begin{aligned} \sum_{i=1}^4 w_i &= 4(\lambda_1 + \lambda_4 + \lambda_6) \\ \sum_{i=1}^4 w_i \xi_i &= 4(\lambda_2 + \lambda_7 + \lambda_9) \\ \sum_{i=1}^4 w_i \eta_i &= 4(\lambda_3 + \lambda_8 + \lambda_{10}) \end{aligned} \right\} \quad (7-3)$$

Secondly, the perimeter conforming condition (5-2c) is used, i.e.,

$$\iint_{A^e} \left(M_x \frac{\partial^2 w}{\partial x^2} + M_y \frac{\partial^2 w}{\partial y^2} + 2M_{xy} \frac{\partial^2 w}{\partial x \partial y} \right) dA = \oint_{\partial A^e} (M_n \tilde{\psi}_n + M_{ns} \tilde{\psi}_s - Q_n \tilde{w}) ds \quad (7-4)$$

where the weighting functions M_n, M_{ns} and Q_n are the boundary forces (bending moment, twisting moment and transverse shear force); M_x, M_y and M_{xy} are the internal moments within the element domain, which are assumed to satisfy the homogeneous equilibrium Eq. (5-3), i.e.,

$$\left. \begin{aligned} \frac{\partial^2 M_x}{\partial x^2} + \frac{\partial^2 M_y}{\partial y^2} + 2 \frac{\partial^2 M_{xy}}{\partial x \partial y} &= 0 \\ Q_x &= \frac{\partial M_x}{\partial x} + \frac{\partial M_{xy}}{\partial y} \\ Q_y &= \frac{\partial M_{xy}}{\partial x} + \frac{\partial M_y}{\partial y} \end{aligned} \right\} \quad (7-5)$$

For the rectangular elements, Eq. (7-4) can be written as

$$\iint_{A^e} \left(M_x \frac{\partial^2 w}{\partial x^2} + M_y \frac{\partial^2 w}{\partial y^2} + 2M_{xy} \frac{\partial^2 w}{\partial x \partial y} \right) dA$$

$$\begin{aligned}
 &= a \int_{-1}^1 [(M_y \tilde{\psi}_y + M_{xy} \tilde{\psi}_x - Q_y \tilde{w})_{43} - (M_y \tilde{\psi}_y + M_{xy} \tilde{\psi}_x - Q_y \tilde{w})_{12}] d\xi \\
 &\quad + b \int_{-1}^1 [(M_x \tilde{\psi}_x + M_{xy} \tilde{\psi}_y - Q_x \tilde{w})_{23} - (M_x \tilde{\psi}_x + M_{xy} \tilde{\psi}_y - Q_x \tilde{w})_{14}] d\eta \quad (7-6)
 \end{aligned}$$

The following equilibrium internal force fields

$$\begin{Bmatrix} M_x \\ M_y \\ M_{xy} \\ Q_x \\ Q_y \end{Bmatrix} = \begin{bmatrix} 1 & \xi & \eta & \xi\eta & 0 & 0 & 0 & 0 & 0 \\ 0 & 0 & 0 & 0 & 1 & \xi & \eta & \xi\eta & 0 \\ 0 & 0 & 0 & 0 & 0 & 0 & 0 & 0 & 1 \\ 0 & \frac{1}{a} & 0 & \frac{1}{a}\eta & 0 & 0 & 0 & 0 & 0 \\ 0 & 0 & 0 & 0 & 0 & 0 & \frac{1}{b} & \frac{1}{b}\xi & 0 \end{bmatrix} \begin{Bmatrix} \beta_1 \\ \beta_2 \\ \vdots \\ \beta_9 \end{Bmatrix} \quad (7-7)$$

are adopted, where $\beta_1, \beta_2, \dots, \beta_9$ are 9 arbitrary parameters.

Since β_i is an arbitrary parameter, substituting Eq. (7-7) into Eq. (7-6), the 9 conforming conditions can be obtained as follows

$$\left. \begin{aligned}
 \iint_{A^e} \frac{\partial^2 w}{\partial x^2} dA &= b \int_{-1}^1 (\tilde{\psi}_{x23} - \tilde{\psi}_{x14}) d\eta \\
 \iint_{A^e} \xi \frac{\partial^2 w}{\partial x^2} dA &= b \int_{-1}^1 (\tilde{\psi}_{x23} + \tilde{\psi}_{x14}) d\eta - \frac{b}{a} \int_{-1}^1 (\tilde{w}_{23} - \tilde{w}_{14}) d\eta \\
 \iint_{A^e} \eta \frac{\partial^2 w}{\partial x^2} dA &= b \int_{-1}^1 (\tilde{\psi}_{x23} - \tilde{\psi}_{x14}) \eta d\eta \\
 \iint_{A^e} \xi \eta \frac{\partial^2 w}{\partial x^2} dA &= b \int_{-1}^1 (\tilde{\psi}_{x23} + \tilde{\psi}_{x14}) \eta d\eta - \frac{b}{a} \int_{-1}^1 (\tilde{w}_{23} - \tilde{w}_{14}) \eta d\eta \\
 \iint_{A^e} \frac{\partial^2 w}{\partial y^2} dA &= a \int_{-1}^1 (\tilde{\psi}_{y43} - \tilde{\psi}_{y12}) d\xi \\
 \iint_{A^e} \xi \frac{\partial^2 w}{\partial y^2} dA &= a \int_{-1}^1 (\tilde{\psi}_{y43} - \tilde{\psi}_{y12}) \xi d\xi \\
 \iint_{A^e} \eta \frac{\partial^2 w}{\partial y^2} dA &= a \int_{-1}^1 (\tilde{\psi}_{y43} + \tilde{\psi}_{y12}) d\xi - \frac{a}{b} \int_{-1}^1 (\tilde{w}_{43} - \tilde{w}_{12}) d\xi \\
 \iint_{A^e} \xi \eta \frac{\partial^2 w}{\partial y^2} dA &= a \int_{-1}^1 (\tilde{\psi}_{y43} + \tilde{\psi}_{y12}) \xi d\xi - \frac{a}{b} \int_{-1}^1 (\tilde{w}_{43} - \tilde{w}_{12}) \xi d\xi \\
 2 \iint_{A^e} \frac{\partial^2 w}{\partial x \partial y} dA &= a \int_{-1}^1 (\tilde{\psi}_{x43} - \tilde{\psi}_{x12}) d\xi + b \int_{-1}^1 (\tilde{\psi}_{y23} - \tilde{\psi}_{y14}) d\eta
 \end{aligned} \right\} \quad (7-8)$$

Then, $\lambda_4, \lambda_5, \dots, \lambda_{12}$ can be solved in turn from Eq. (7-8) as follows

$$\left. \begin{aligned}
 \lambda_4 &= \frac{a}{8} \sum_{i=1}^4 \psi_{xi} \xi_i \\
 \lambda_7 &= -\frac{1}{8} \sum_{i=1}^4 w_i \xi_i + \frac{a}{8} \sum_{i=1}^4 \psi_{xi} + \frac{b}{24} \sum_{i=1}^4 \psi_{yi} \xi_i \eta_i \\
 \lambda_8 &= \frac{a}{8} \sum_{i=1}^4 \psi_{xi} \xi_i \eta_i \\
 \lambda_{11} &= -\frac{3}{20} \sum_{i=1}^4 w_i \xi_i \eta_i + \frac{a}{8} \sum_{i=1}^4 \psi_{xi} \eta_i + \frac{b}{40} \sum_{i=1}^4 \psi_{yi} \xi_i \\
 \lambda_6 &= \frac{b}{8} \sum_{i=1}^4 \psi_{yi} \eta_i \\
 \lambda_9 &= \frac{b}{8} \sum_{i=1}^4 \psi_{yi} \xi_i \eta_i \\
 \lambda_{10} &= -\frac{1}{8} \sum_{i=1}^4 w_i \eta_i + \frac{a}{24} \sum_{i=1}^4 \psi_{xi} \xi_i \eta_i + \frac{b}{8} \sum_{i=1}^4 \psi_{yi} \\
 \lambda_{12} &= -\frac{3}{20} \sum_{i=1}^4 w_i \xi_i \eta_i + \frac{a}{40} \sum_{i=1}^4 \psi_{xi} \eta_i + \frac{b}{8} \sum_{i=1}^4 \psi_{yi} \xi_i \\
 \lambda_5 &= \frac{11}{20} \sum_{i=1}^4 w_i \xi_i \eta_i - \frac{3a}{20} \sum_{i=1}^4 \psi_{xi} \eta_i - \frac{3b}{20} \sum_{i=1}^4 \psi_{yi} \xi_i
 \end{aligned} \right\} \quad (7-9)$$

Substituting the above equation into Eq. (7-3), λ_1, λ_2 and λ_3 can be obtained

$$\left. \begin{aligned}
 \lambda_1 &= \frac{1}{4} \sum_{i=1}^4 w_i - \frac{a}{8} \sum_{i=1}^4 \psi_{xi} \xi_i - \frac{b}{8} \sum_{i=1}^4 \psi_{yi} \eta_i \\
 \lambda_2 &= \frac{3}{8} \sum_{i=1}^4 w_i \xi_i - \frac{a}{8} \sum_{i=1}^4 \psi_{xi} - \frac{b}{6} \sum_{i=1}^4 \psi_{yi} \xi_i \eta_i \\
 \lambda_3 &= \frac{3}{8} \sum_{i=1}^4 w_i \eta_i - \frac{a}{6} \sum_{i=1}^4 \psi_{xi} \xi_i \eta_i - \frac{b}{8} \sum_{i=1}^4 \psi_{yi}
 \end{aligned} \right\} \quad (7-10)$$

Thus, all the coefficients in λ have been obtained. Then, the shape functions and the element stiffness matrix can be derived from them.

7.1.2 Element LR12-2

The construction procedure of this element is basically similar to that of the

element LR12-1. Only the selected equilibrium internal force fields are different from Eq. (7-7), and replaced by

$$\begin{Bmatrix} M_x \\ M_y \\ M_{xy} \\ Q_x \\ Q_y \end{Bmatrix} = \begin{bmatrix} 1 & \xi & \eta & 0 & 0 & 0 & 0 & 0 & 0 \\ 0 & 0 & 0 & 1 & \xi & \eta & 0 & 0 & 0 \\ 0 & 0 & 0 & 0 & 0 & 0 & 1 & \xi^2 & \eta^2 \\ 0 & \frac{1}{a} & 0 & 0 & 0 & 0 & 0 & 0 & \frac{2}{b}\eta \\ 0 & 0 & 0 & 0 & 0 & \frac{1}{b} & 0 & \frac{2}{a}\xi & 0 \end{bmatrix} \begin{Bmatrix} \beta_1 \\ \beta_2 \\ \vdots \\ \beta_9 \end{Bmatrix} \quad (7-11)$$

Following a similar procedure, all the coefficients in λ can be obtained, in which $\lambda_1, \lambda_2, \lambda_3, \lambda_4, \lambda_6, \lambda_7, \lambda_8, \lambda_9, \lambda_{10}$ are the same, and still given by Eqs. (7-9) and (7-10); the other three unknown coefficients are as follows

$$\left. \begin{aligned} \lambda_5 &= \frac{1}{2} \sum_{i=1}^4 w_i \xi_i \eta_i - \frac{a}{8} \sum_{i=1}^4 \psi_{xi} \eta_i - \frac{b}{8} \sum_{i=1}^4 \psi_{yi} \xi_i \\ \lambda_{11} &= -\frac{1}{8} \sum_{i=1}^4 w_i \xi_i \eta_i + \frac{a}{8} \sum_{i=1}^4 \psi_{xi} \eta_i \\ \lambda_{12} &= -\frac{1}{8} \sum_{i=1}^4 w_i \xi_i \eta_i + \frac{b}{8} \sum_{i=1}^4 \psi_{yi} \xi_i \end{aligned} \right\} \quad (7-12)$$

Example 7.1 Central deflection and central moment of the simply-supported and the clamped square plates (the side length is L) subjected to uniform load.

The results by the elements LR12-1 and LR12-2 are listed in Tables 7.1 and 7.2. For comparison, the results by the element ACM^[2] are also given. The Poisson's ratio is 0.3.

Table 7.1 The central deflection of square plates subjected to uniform load

Mesh (1/4 plate)	Simply-supported			Clamped		
	LR12-1	LR12-2	ACM	LR12-1	LR12-2	ACM
2 × 2	0.4051 (-0.3%)	0.4052 (-0.3%)	0.3939 (-3.0%)	0.1238 (-2.0%)	0.1243 (-1.7%)	0.1403 (11.0%)
4 × 4	0.406 16 (-0.02%)	0.406 17 (-0.02%)	0.4033 (-0.7%)	0.1260 (-0.4%)	0.1261 (-0.4%)	0.1304 (4.0%)
8 × 8	0.406 23 (-0.001%)	0.406 23 (-0.001%)	0.4056 (-0.2%)	0.126 45 (-0.06%)	0.126 46 (-0.05%)	0.1275 (0.8%)
Analytical	0.406 235($qL^4/100D$)			0.126 53($qL^4/100D$)		

Table 7.2 The central moment of square plates subjected to uniform load

Mesh (1/4 plate)	Simply-supported			Clamped		
	LR12-1	LR12-2	ACM	LR12-1	LR12-2	ACM
2 × 2	0.512 45 (7.0%)	0.512 23 (7.0%)	0.521 69 (8.9%)	0.255 23 (11.4%)	0.253 23 (10.5%)	0.277 83 (11.3%)
4 × 4	0.487 30 (1.8%)	0.487 32 (1.8%)	0.489 20 (2.2%)	0.236 89 (3.4%)	0.236 96 (3.4%)	0.240 50 (5.0%)
8 × 8	0.480 98 (0.4%)	0.480 98 (0.4%)	0.481 66 (0.6%)	0.231 09 (0.8%)	0.231 10 (0.8%)	0.231 91 (1.2%)
Analytical	0.478 86($qL^2/10$)			0.229 05($qL^2/10$)		

7.2 The Application of Perimeter Conforming Conditions —Verification for the Convergence of the Element ACM

This section will use the perimeter conforming conditions under the constant stress state to verify the convergence of the non-conforming elements. And, as a typical example, the convergence of the well-known element ACM^[2] will be verified.

The element ACM is a non-conforming rectangular thin plate element, which is constructed by the conventional point conforming scheme, i.e., 12 unknown coefficients are determined by 12 point conforming conditions about w , ψ_x , ψ_y at the corner nodes. It can be seen from the deflection field finally determined that the deflection w along the element boundary is exactly compatible, while the normal slope $\frac{\partial w}{\partial n}$ is not. Though the element ACM belongs to the non-conforming elements, it still exhibits good convergence in applications and has been proved in theory that it can pass the patch test.

By starting from the generalized conforming theory, this section will verify the convergence of the element ACM from another point of view. At the same time, this example can also be used to illustrate one of the applications of the generalized conforming theory, that is, the generalized conforming theory can be used to verify or improve the convergence of other non-conforming elements.

7.2.1 Derivation of Element ACM from Symmetry

The rectangular thin plate element ACM, proposed by Adini, Clough and Melosh^[2], is a non-conforming element with 12 DOFs. Its element deflection field is assumed to be an incomplete quartic polynomial, as shown in Eqs. (7-1) and (7-2) (i.e. Eqs. (6-22) and (6-23)), which involves 12 unknown coefficients that will be determined by 12 point conforming conditions about w , ψ_x and ψ_y at the corner

nodes. Since the solution procedure for the 12 unknown coefficients is quite complicated, here we will simplify it by using the symmetry (refer to Sect. 6.2).

Firstly, the 12 unknown coefficients and their basis functions in Eq. (7-1) have already been classified as 4 groups. And, each group contains 3 unknown coefficients, in turn; they are $(\lambda_1, \lambda_4, \lambda_6)$; $(\lambda_2, \lambda_7, \lambda_9)$; $(\lambda_3, \lambda_8, \lambda_{10})$; $(\lambda_5, \lambda_{11}, \lambda_{12})$, as shown in Eq. (6-28).

Secondly, the 12 point conforming conditions at the corner nodes can be recombined. They are classified as 4 independent groups, and each group contains 3 equations and 3 unknown coefficients. Thereupon, the original simultaneous equations with 12 unknowns decompose to be four independent equation groups each with 3 unknowns, which greatly simplifies the problem. The 4 equation groups are listed as follows.

(1) Combination conditions belonging to the SS group (3 conditions)

$$\sum_{i=1}^4 (w - \tilde{w})_i = 0 \tag{7-A1}$$

$$\sum_{i=1}^4 \left(\frac{\partial w}{\partial x} - \tilde{\psi}_x \right)_i \xi_i = 0 \tag{7-A2}$$

$$\sum_{i=1}^4 \left(\frac{\partial w}{\partial y} - \tilde{\psi}_y \right)_i \eta_i = 0 \tag{7-A3}$$

Substitution of Eq. (7-1) into the above equations yields

$$\lambda_1 + \lambda_4 + \lambda_6 = \frac{1}{4} \sum_{i=1}^4 w_i \tag{7-13a}$$

$$\lambda_4 = \frac{a}{8} \sum_{i=1}^4 \psi_{xi} \xi_i \tag{7-13b}$$

$$\lambda_6 = \frac{b}{8} \sum_{i=1}^4 \psi_{yi} \eta_i \tag{7-13c}$$

(2) Combination conditions belonging to the SA group (3 conditions)

$$\sum_{i=1}^4 (w - \tilde{w})_i \xi_i = 0 \tag{7-B1}$$

$$\sum_{i=1}^4 \left(\frac{\partial w}{\partial x} - \tilde{\psi}_x \right)_i = 0 \tag{7-B2}$$

$$\sum_{i=1}^4 \left(\frac{\partial w}{\partial y} - \tilde{\psi}_y \right)_i \xi_i \eta_i = 0 \quad (7-B3)$$

We can obtain

$$\lambda_2 + \lambda_7 + \lambda_9 = \frac{1}{4} \sum_{i=1}^4 w_i \xi_i \quad (7-14a)$$

$$\lambda_2 + 3\lambda_7 + \lambda_9 = \frac{a}{4} \sum_{i=1}^4 \psi_{xi} \quad (7-14b)$$

$$\lambda_9 = \frac{b}{8} \sum_{i=1}^4 \psi_{yi} \xi_i \eta_i \quad (7-14c)$$

(3) Combination conditions belonging to the AS group (3 conditions)

$$\sum_{i=1}^4 (w - \tilde{w})_i \eta_i = 0 \quad (7-C1)$$

$$\sum_{i=1}^4 \left(\frac{\partial w}{\partial x} - \tilde{\psi}_x \right)_i \xi_i \eta_i = 0 \quad (7-C2)$$

$$\sum_{i=1}^4 \left(\frac{\partial w}{\partial y} - \tilde{\psi}_y \right)_i = 0 \quad (7-C3)$$

We can obtain

$$\lambda_3 + \lambda_8 + \lambda_{10} = \frac{1}{4} \sum_{i=1}^4 w_i \eta_i \quad (7-15a)$$

$$\lambda_8 = \frac{a}{8} \sum_{i=1}^4 \psi_{xi} \xi_i \eta_i \quad (7-15b)$$

$$\lambda_3 + \lambda_8 + 3\lambda_{10} = \frac{b}{4} \sum_{i=1}^4 \psi_{yi} \quad (7-15c)$$

(4) Combination conditions belonging to the AA group (3 conditions)

$$\sum_{i=1}^4 (w - \tilde{w})_i \xi_i \eta_i = 0 \quad (7-D1)$$

$$\sum_{i=1}^4 \left(\frac{\partial w}{\partial x} - \tilde{\psi}_x \right)_i \eta_i = 0 \quad (7-D2)$$

$$\sum_{i=1}^4 \left(\frac{\partial w}{\partial y} - \tilde{\psi}_y \right)_i \xi_i = 0 \quad (7-D3)$$

We can obtain

$$\lambda_5 + \lambda_{11} + \lambda_{12} = \frac{1}{4} \sum_{i=1}^4 w_i \xi_i \eta_i \quad (7-16a)$$

$$\lambda_5 + 3\lambda_{11} + \lambda_{12} = \frac{a}{4} \sum_{i=1}^4 \psi_{xi} \eta_i \quad (7-16b)$$

$$\lambda_5 + \lambda_{11} + 3\lambda_{12} = \frac{b}{4} \sum_{i=1}^4 \psi_{yi} \xi_i \quad (7-16c)$$

From the above four groups of simultaneous equations with 3 unknowns, the solutions can be easily obtained:

$$\left. \begin{aligned} \lambda_1 &= \frac{1}{4} \sum_{i=1}^4 w_i - \frac{a}{8} \sum_{i=1}^4 \psi_{xi} \xi_i - \frac{b}{8} \sum_{i=1}^4 \psi_{yi} \eta_i \\ \lambda_4 &= \frac{a}{8} \sum_{i=1}^4 \psi_{xi} \xi_i \\ \lambda_6 &= \frac{b}{8} \sum_{i=1}^4 \psi_{yi} \eta_i \\ \lambda_2 &= \frac{3}{8} \sum_{i=1}^4 w_i \xi_i - \frac{a}{8} \sum_{i=1}^4 \psi_{xi} - \frac{b}{8} \sum_{i=1}^4 \psi_{yi} \xi_i \eta_i \\ \lambda_7 &= -\frac{1}{8} \sum_{i=1}^4 w_i \xi_i + \frac{a}{8} \sum_{i=1}^4 \psi_{xi} \\ \lambda_9 &= \frac{b}{8} \sum_{i=1}^4 \psi_{yi} \xi_i \eta_i \\ \lambda_3 &= \frac{3}{8} \sum_{i=1}^4 w_i \eta_i - \frac{a}{8} \sum_{i=1}^4 \psi_{xi} \xi_i \eta_i - \frac{b}{8} \sum_{i=1}^4 \psi_{yi} \\ \lambda_8 &= \frac{a}{8} \sum_{i=1}^4 \psi_{xi} \xi_i \eta_i \\ \lambda_{10} &= -\frac{1}{8} \sum_{i=1}^4 w_i \eta_i + \frac{b}{8} \sum_{i=1}^4 \psi_{yi} \\ \lambda_5 &= \frac{1}{2} \sum_{i=1}^4 w_i \xi_i \eta_i - \frac{a}{8} \sum_{i=1}^4 \psi_{xi} \eta_i - \frac{b}{8} \sum_{i=1}^4 \psi_{yi} \xi_i \\ \lambda_{11} &= -\frac{1}{8} \sum_{i=1}^4 w_i \xi_i \eta_i + \frac{a}{8} \sum_{i=1}^4 \psi_{xi} \eta_i \\ \lambda_{12} &= -\frac{1}{8} \sum_{i=1}^4 w_i \xi_i \eta_i + \frac{b}{8} \sum_{i=1}^4 \psi_{yi} \xi_i \end{aligned} \right\} \quad (7-17)$$

Finally, substitution of the above solutions into Eq. (7-1) yields the element

deflection field and its shape functions:

$$w = \sum_{i=1}^4 (N_i w_i + N_{xi} \psi_{xi} + N_{yi} \psi_{yi}) \quad (7-18)$$

where the shape functions are

$$\left. \begin{aligned} N_i &= \frac{1}{8}(1 + \xi_i \xi)(1 + \eta_i \eta)(2 + \xi_i \xi + \eta_i \eta - \xi^2 - \eta^2) \\ N_{xi} &= -\frac{a}{8} \xi_i (1 + \xi_i \xi)(1 + \eta_i \eta)(1 - \xi^2) \\ N_{yi} &= -\frac{b}{8} \eta_i (1 + \xi_i \xi)(1 + \eta_i \eta)(1 - \eta^2) \end{aligned} \right\} (i = 1, 2, 3, 4) \quad (7-19)$$

Once the shape functions are obtained, the element stiffness matrix can be derived following the conventional procedure.

7.2.2 The Fundamental Conforming Conditions for Verifying Convergence

According to the generalized conforming theory, the fundamental conditions that ensure convergence are Eq. (4-7) or Eq. (4-8), i.e.,

$$H = 0 \quad (\text{corresponding to constant strain and rigid body displacement states}) \quad (7-20)$$

The above equation is called the fundamental generalized conforming conditions.

Under the limit state that a mesh is refined by the infinite elements, the element strain will tend to be constant. For the thin plate bending problem, the element displacement field in the limit state involves only 6 DOFs, i.e., 3 corresponding to rigid body displacement modes and 3 corresponding to constant strain states. Thereby, the fundamental generalized conforming condition (7-20) should be composed of 6 conforming conditions.

The 3 conditions which the element should satisfy in the rigid body displacement mode can be selected as

$$\sum_{i=1}^p (w - \tilde{w})_i = 0, \quad \sum_{i=1}^p (w - \tilde{w})_i x_i = 0, \quad \sum_{i=1}^p (w - \tilde{w})_i y_i = 0 \quad (7-21)$$

They denote the 3 combination conditions of the point conforming conditions about deflections at the corner nodes, where p is the number of the corner nodes. Besides, they can also be selected as

$$\sum_{i=1}^p (w - \tilde{w})_i = 0, \quad \sum_{i=1}^p \left(\frac{\partial w}{\partial x} - \psi_x \right)_i = 0, \quad \sum_{i=1}^p \left(\frac{\partial w}{\partial y} - \psi_y \right)_i = 0 \quad (7-22)$$

They denote the combination point conforming conditions about w , ψ_x and ψ_y at the corner nodes. For the rigid body displacement modes, the above two sets of equations are equivalent to each other; but for non-rigid body displacement modes, they are not equivalent anymore.

When an element is under constant strain states, the perimeter conforming condition (5-2c) should also be satisfied, in which the weighting functions can be selected according to the constant internal force states. If internal moments are constants and transverse shear forces are zero, Eq. (5-2c) will be simplified as:

$$M_x \iint_{A^e} \frac{\partial^2 w}{\partial x^2} dA + M_y \iint_{A^e} \frac{\partial^2 w}{\partial y^2} dA + 2M_{xy} \iint_{A^e} \frac{\partial^2 w}{\partial x \partial y} dA - \sum_{i=1}^p (M_{ni} \int_0^{d_i} \tilde{\psi}_{ni} ds + M_{nsi} \int_0^{d_i} \tilde{\psi}_{si} ds) = 0 \quad (7-23)$$

If the constant internal force fields are assumed to be those in Eq. (5-24), the perimeter conforming conditions given in Eq. (5-26) are obtained, i.e.,

$$\left. \begin{aligned} \iint_{A^e} \frac{\partial^2 w}{\partial x^2} dA &= \oint_{\partial A^e} (l^2 \tilde{\psi}_n - lm \tilde{\psi}_s) ds \\ \iint_{A^e} \frac{\partial^2 w}{\partial y^2} dA &= \oint_{\partial A^e} (m^2 \tilde{\psi}_n + lm \tilde{\psi}_s) ds \\ \iint_{A^e} 2 \frac{\partial^2 w}{\partial x \partial y} dA &= \oint_{\partial A^e} [2lm \tilde{\psi}_n + (l^2 - m^2) \tilde{\psi}_s] ds \end{aligned} \right\} \quad (7-24)$$

The 6 conditions given in Eq. (7-23) or Eq. (7-24) and Eq. (7-21) or Eq. (7-22) are the fundamental conforming conditions for verifying the convergence of the non-conforming thin plate elements.

7.2.3 Verification for the Convergence of Element ACM

Now, we use the 6 fundamental conforming conditions to verify the convergence of the element ACM.

Firstly, the element ACM has already satisfied the 12 point conforming conditions about w , ψ_x and ψ_y at the corner nodes, thereby, Eq. (7-21) or Eq. (7-22) are satisfied naturally. In fact, the 3 conditions (7-A1), (7-B1) and (7-C1) selected previously are the same as those expressions in Eq. (7-21); and another 3 conditions (7-A1), (7-B2) and (7-C3) are the same as those expressions in Eq. (7-22).

Secondly, verification for the perimeter conforming conditions (7-24) is performed. For the rectangular elements, Eq. (7-24) can be written as

$$\left. \begin{aligned} \iint_{A^e} \frac{\partial^2 w}{\partial x^2} dA &= b \int_{-1}^1 (\tilde{\psi}_{x23} - \tilde{\psi}_{x14}) d\eta \\ \iint_{A^e} \frac{\partial^2 w}{\partial y^2} dA &= a \int_{-1}^1 (\tilde{\psi}_{y43} - \tilde{\psi}_{y12}) d\xi \\ \iint_{A^e} 2 \frac{\partial^2 w}{\partial x \partial y} dA &= a \int_{-1}^1 (\tilde{\psi}_{x43} - \tilde{\psi}_{x12}) d\xi + b \int_{-1}^1 (\tilde{\psi}_{y23} - \tilde{\psi}_{y14}) d\eta \end{aligned} \right\} \quad (7-25)$$

Substituting Eqs. (7-1) and (7-2) into w at the left side of the above equations, and substituting the corresponding interpolation formulae into the boundary rotations at the right sides, we obtain

$$\left. \begin{aligned} \lambda_4 &= \frac{a}{8} \sum_{i=1}^4 \psi_{xi} \xi_i \\ \lambda_6 &= \frac{b}{8} \sum_{i=1}^4 \psi_{yi} \eta_i \\ \lambda_5 + \lambda_{11} + \lambda_{12} &= \frac{1}{4} \sum_{i=1}^4 w_i \xi_i \eta_i \end{aligned} \right\} \quad (7-26)$$

The above 3 equations are the previous Eqs. (7-13b,c) and (7-16a), respectively, and thereby, have been satisfied.

Since the element ACM has already satisfied the 6 fundamental conforming conditions, so, the element ACM is convergent. Actually, it is also a generalized conforming element.

7.3 Super-Basis Perimeter-Point Conforming Scheme — Verification and Improvement of the Element BCIZ

This section will introduce the construction procedure of the super-basis thin plate element formulated by the combination scheme of the perimeter and point conforming conditions. The no. 25 and 26 elements GC II -T9 and LT9 in Table 5.1 belong to this element group. They are both triangular thin plate elements, in which $n=9$ and $m=12$, but the 12 conforming conditions used by them are different: the element GC II -T9 adopts 9 point conforming conditions and 3 perimeter conforming conditions, while the element LT9 adopts 3 point conforming conditions and 9 perimeter conforming conditions.

The conventional scheme that the non-conforming elements usually adopt is: let $m = n$, and only the point conforming conditions at the corner nodes are used. Such non-conforming elements sometimes are convergent (such as the rectangular thin plate element ACM), sometimes are not convergent (such as the triangular thin plate element BCIZ). The super-basis generalized conforming element scheme is an improved strategy for the non-conforming elements. For example, the super-basis element GCIII-R12 in Sect. 6.4 is an improvement on the element ACM (though the element ACM possesses convergence, its accuracy can be improved further), and the super-basis element GCII-T9 in this section is an improvement on the element BCIZ (the number of the basis functions in the element GCII-T9 is more than the number of the element DOFs, thereby, the shortcoming that the element BCIZ cannot ensure convergence will be eliminated). In this section, we firstly apply the fundamental conforming conditions of the generalized conforming element, especially, the 3 perimeter conforming conditions in Eq. (5-26) under constant stress state, to verify the convergence of the element BCIZ; then, by employing the concept of the super-basis elements, we make the perimeter conforming condition (5-26) satisfied, consequently, a new element GCII-T9 is constructed.

7.3.1 Formulations of Element BCIZ

The triangular thin plate element BCIZ is a famous non-conforming model proposed in the past^[3]. And, reference [3] is one of the earliest literatures which pointed out the limitation of the conforming elements and the rationality of the non-conforming elements.

Before verifying the convergence of the element BCIZ, its formulations are introduced briefly as follows.

The element BCIZ has 9 DOFs (Fig. 6.1), and the element nodal displacement vector \mathbf{q}^e is given by Eq. (6-1). The assumed element deflection field w is given by Eqs. (6-2) and (6-3), i.e.,

$$\begin{aligned}
 w = & \lambda_4 L_1 + \lambda_2 L_2 + \lambda_3 L_3 + \lambda_4 L_1 L_2 \left(L_1 + \frac{1}{2} L_3 \right) + \lambda_5 L_2 L_3 \left(L_2 + \frac{1}{2} L_1 \right) \\
 & + \lambda_6 L_3 L_1 \left(L_3 + \frac{1}{2} L_2 \right) + \lambda_7 L_1 L_3 \left(L_1 + \frac{1}{2} L_2 \right) \\
 & + \lambda_8 L_2 L_1 \left(L_2 + \frac{1}{2} L_3 \right) + \lambda_9 L_3 L_2 \left(L_3 + \frac{1}{2} L_1 \right)
 \end{aligned} \tag{7-27}$$

By applying the 9 point conforming conditions about w , ψ_x and ψ_y at the corner nodes, we obtain

$$\left. \begin{aligned}
 w_1 &= \lambda_1 \\
 w_2 &= \lambda_2 \\
 w_3 &= \lambda_3 \\
 \psi_{x1} &= \frac{1}{2A}(b_1\lambda_1 + b_2\lambda_2 + b_3\lambda_3 + b_2\lambda_4 + b_3\lambda_7) \\
 \psi_{x2} &= \frac{1}{2A}(b_1\lambda_1 + b_2\lambda_2 + b_3\lambda_3 + b_3\lambda_5 + b_1\lambda_8) \\
 \psi_{x3} &= \frac{1}{2A}(b_1\lambda_1 + b_2\lambda_2 + b_3\lambda_3 + b_1\lambda_6 + b_2\lambda_9) \\
 \psi_{y1} &= \frac{1}{2A}(c_1\lambda_1 + c_2\lambda_2 + c_3\lambda_3 + c_2\lambda_4 + c_3\lambda_7) \\
 \psi_{y2} &= \frac{1}{2A}(c_1\lambda_1 + c_2\lambda_2 + c_3\lambda_3 + c_3\lambda_5 + c_1\lambda_8) \\
 \psi_{y3} &= \frac{1}{2A}(c_1\lambda_1 + c_2\lambda_2 + c_3\lambda_3 + c_1\lambda_6 + c_2\lambda_9)
 \end{aligned} \right\} \quad (7-28)$$

Then λ can be solved

$$\left. \begin{aligned}
 \lambda_1 &= w_1 \\
 \lambda_2 &= w_2 \\
 \lambda_3 &= w_3 \\
 \lambda_4 &= w_1 - w_2 + c_3\psi_{x1} - b_3\psi_{y1} \\
 \lambda_5 &= w_2 - w_3 + c_1\psi_{x2} - b_1\psi_{y2} \\
 \lambda_6 &= w_3 - w_1 + c_2\psi_{x3} - b_2\psi_{y3} \\
 \lambda_7 &= w_1 - w_3 - c_2\psi_{x1} + b_2\psi_{y1} \\
 \lambda_8 &= w_2 - w_1 - c_3\psi_{x2} + b_3\psi_{y2} \\
 \lambda_9 &= w_3 - w_2 - c_1\psi_{x3} + b_1\psi_{y3}
 \end{aligned} \right\} \quad (7-29)$$

The above equation can be rewritten as

$$\lambda = \hat{A}q^e$$

Substitution of Eq. (7-29) into (7-27) yields

$$w = Nq^e = \sum_{i=1}^3 (N_i w_i + N_{xi} \psi_{xi} + N_{yi} \psi_{yi}) \quad (7-30)$$

in which the 3 shape functions related to the node 1 are

$$\left. \begin{aligned} N_1 &= L_1 + L_1^2 L_2 + L_1^2 L_3 - L_2^2 L_1 - L_3^2 L_1 \\ N_{x1} &= c_3 \left(L_1^2 L_2 + \frac{1}{2} L_1 L_2 L_3 \right) - c_2 \left(L_1^2 L_3 + \frac{1}{2} L_1 L_2 L_3 \right) \\ N_{y1} &= -b_3 \left(L_1^2 L_2 + \frac{1}{2} L_1 L_2 L_3 \right) + b_2 \left(L_1^2 L_3 + \frac{1}{2} L_1 L_2 L_3 \right) \end{aligned} \right\} \quad (7-31)$$

By the permutation of 1, 2 and 3, the other 6 shape functions can be obtained. The element curvature field is

$$\boldsymbol{\kappa} = \begin{Bmatrix} \kappa_x \\ \kappa_y \\ 2\kappa_{xy} \end{Bmatrix} = - \begin{Bmatrix} \frac{\partial^2}{\partial x^2} \\ \frac{\partial^2}{\partial y^2} \\ 2 \frac{\partial^2}{\partial x \partial y} \end{Bmatrix} w \quad (7-32)$$

By using the transformation of second-order derivatives between the Cartesian coordinate system and the area coordinate system:

$$\begin{Bmatrix} \frac{\partial^2}{\partial x^2} \\ \frac{\partial^2}{\partial y^2} \\ 2 \frac{\partial^2}{\partial x \partial y} \end{Bmatrix} = \frac{1}{A} \mathbf{t} \mathbf{s} \boldsymbol{\partial}_2 \quad (7-33)$$

where

$$\mathbf{t} = \frac{1}{4A} \begin{bmatrix} b_1^2 & b_2^2 & b_3^2 \\ c_1^2 & c_2^2 & c_3^2 \\ 2b_1c_1 & 2b_2c_2 & 2b_3c_3 \end{bmatrix} \quad (7-34)$$

$$\mathbf{s} = \begin{bmatrix} 1 & 0 & 0 & | & -1 & 1 & -1 \\ 0 & 1 & 0 & | & -1 & -1 & 1 \\ 0 & 0 & 1 & | & 1 & -1 & -1 \end{bmatrix} \quad (7-35)$$

$$\boldsymbol{\partial}_2 = \left[\frac{\partial^2}{\partial L_1^2} \quad \frac{\partial^2}{\partial L_2^2} \quad \frac{\partial^2}{\partial L_3^2} \quad | \quad \frac{\partial^2}{\partial L_1 \partial L_2} \quad \frac{\partial^2}{\partial L_2 \partial L_3} \quad \frac{\partial^2}{\partial L_3 \partial L_1} \right]^T \quad (7-36)$$

Thus, the expressions of the curvatures can be obtained as follows

$$\boldsymbol{\kappa} = -\frac{1}{A}tsH\boldsymbol{\lambda} \quad (7-37)$$

where

$$H = \left[\begin{array}{ccc|ccc|ccc} 0 & 0 & 0 & 2L_2 & 0 & 0 & 2L_3 & 0 & 0 \\ 0 & 0 & 0 & 0 & 2L_3 & 0 & 0 & 2L_1 & 0 \\ 0 & 0 & 0 & 0 & 0 & 2L_1 & 0 & 0 & 2L_2 \\ \hline 0 & 0 & 0 & 2L_1 + \frac{1}{2}L_3 & \frac{1}{2}L_3 & \frac{1}{2}L_3 & \frac{1}{2}L_3 & 2L_2 + \frac{1}{2}L_3 & \frac{1}{2}L_3 \\ 0 & 0 & 0 & \frac{1}{2}L_1 & 2L_2 + \frac{1}{2}L_1 & \frac{1}{2}L_1 & \frac{1}{2}L_1 & \frac{1}{2}L_1 & 2L_3 + \frac{1}{2}L_1 \\ 0 & 0 & 0 & \frac{1}{2}L_2 & \frac{1}{2}L_2 & 2L_3 + \frac{1}{2}L_2 & 2L_1 + \frac{1}{2}L_2 & \frac{1}{2}L_2 & \frac{1}{2}L_2 \end{array} \right] \quad (7-38)$$

And, the curvature field can also be rewritten as

$$\boldsymbol{\kappa} = B\mathbf{q}^e \quad (7-39)$$

where

$$B = -\frac{1}{A}tsH\hat{A} \quad (7-40)$$

Finally, the element stiffness matrix can be obtained

$$K^e = \iint_{A^e} B^T D B dA \quad (7-41)$$

in which D is the elastic matrix of thin plate.

7.3.2 Verification for the Convergence of the Element BCIZ

According to the generalized conforming element theory, the fundamental conditions which ensure the convergence of the non-conforming elements are given by Eq. (7-20). They involve 6 conforming conditions, such as Eqs. (7-22) and (7-23), which should be satisfied when the element is under the rigid body displacement and constant strain states. Now, we apply these 6 fundamental conforming conditions to verify the convergence of the element BCIZ.

Firstly, the element BCIZ has already satisfied the 9 point conforming conditions about w , ψ_x and ψ_y at the corner nodes, thereby, the point conforming conditions

in Eq. (7-22), which should be satisfied when the element is under rigid body displacement states, are satisfied naturally.

Secondly, we check the perimeter conforming conditions given in Eq. (7-23) which should be satisfied when the element is under constant strain states, i.e.,

$$\mathbf{M}^T \iint_{A^e} \boldsymbol{\kappa} dA = -\sum_{i=1}^3 \left(M_{ni} \int_0^{d_i} \tilde{\psi}_{ni} ds + M_{nsi} \int_0^{d_i} \tilde{\psi}_{si} ds \right) \quad (7-42)$$

where the 3 constant internal force states are usually assumed to be those in Eq. (5-24). But, for the triangular element, they would better be assumed as follows

$$\left. \begin{aligned} M_{n1} &= \frac{4A}{d_1^2} \alpha_1 \\ M_{n2} &= \frac{4A}{d_2^2} \alpha_2 \\ M_{n3} &= \frac{4A}{d_3^2} \alpha_3 \end{aligned} \right\} \quad (7-43)$$

where the arbitrary parameters α_i ($i=1,2,3$) are corresponding to the constant internal force states in which the normal moment of i th side is not zero while the normal moments of the other two sides are zero. The twisting moment M_{nsi} along each element side and the internal moments M_x , M_y , M_{xy} corresponding to this constant internal force state are as follows

$$\left. \begin{aligned} M_{ns1} &= r_1 \alpha_1 - \alpha_2 + \alpha_3 \\ M_{ns2} &= \alpha_1 + r_2 \alpha_2 - \alpha_3 \\ M_{ns3} &= -\alpha_1 + \alpha_2 + r_3 \alpha_3 \end{aligned} \right\} \quad (7-44)$$

$$\left\{ \begin{array}{l} M_x \\ M_y \\ M_{xy} \end{array} \right\} = \frac{1}{A} \begin{bmatrix} -c_2 c_3 & -c_3 c_1 & -c_1 c_2 \\ -b_2 b_3 & -b_3 b_1 & -b_1 b_2 \\ \frac{1}{2}(b_2 c_3 + b_3 c_2) & \frac{1}{2}(b_3 c_1 + b_1 c_3) & \frac{1}{2}(b_1 c_2 + b_2 c_1) \end{bmatrix} \left\{ \begin{array}{l} \alpha_1 \\ \alpha_2 \\ \alpha_3 \end{array} \right\} \quad (7-45)$$

in which r_1 , r_2 and r_3 are given by Eq. (6-58). Equation (7-45) can be written as

$$\mathbf{M} = (\mathbf{t}^{-1})^T \boldsymbol{\alpha} \quad (7-46)$$

Now, we substitute the above constant internal force state into Eq. (7-42).

Firstly, the substitution of Eqs. (7-46) and (7-37) into the left side of Eq. (7-42) yields

$$\begin{aligned}
 \mathbf{M}^T \iint_{A^e} \boldsymbol{\kappa} dA &= -\frac{1}{A} \boldsymbol{\alpha}^T \mathbf{s} \left(\iint_{A^e} \mathbf{H} dA \right) \boldsymbol{\lambda} \\
 &= -\boldsymbol{\alpha}^T \frac{1}{6} \begin{bmatrix} 0 & 0 & 0 & -1 & 3 & -5 & -1 & -5 & 3 \\ 0 & 0 & 0 & -5 & -1 & 3 & 3 & -1 & -5 \\ 0 & 0 & 0 & 3 & -5 & -1 & -5 & 3 & -1 \end{bmatrix} \boldsymbol{\lambda} \\
 &= -\boldsymbol{\alpha}^T \left(\frac{1}{6} \begin{bmatrix} -1 & 3 & -5 \\ -5 & -1 & 3 \\ 3 & -5 & -1 \end{bmatrix} \begin{Bmatrix} \lambda_4 \\ \lambda_5 \\ \lambda_6 \end{Bmatrix} + \frac{1}{6} \begin{bmatrix} -1 & -5 & 3 \\ 3 & -1 & -5 \\ -5 & 3 & -1 \end{bmatrix} \begin{Bmatrix} \lambda_7 \\ \lambda_8 \\ \lambda_9 \end{Bmatrix} \right) \quad (7-47)
 \end{aligned}$$

Secondly, consider the right side of Eq. (7-42). The integrations of rotations along the boundary line are as follows

$$\left. \begin{aligned}
 \int_0^{d_1} \tilde{\psi}_{n1} ds &= -\frac{b_1}{2}(\psi_{x2} + \psi_{x3}) - \frac{c_1}{2}(\psi_{y2} + \psi_{y3}) \\
 \int_0^{d_2} \tilde{\psi}_{n2} ds &= -\frac{b_2}{2}(\psi_{x3} + \psi_{x1}) - \frac{c_2}{2}(\psi_{y3} + \psi_{y1}) \\
 \int_0^{d_3} \tilde{\psi}_{n3} ds &= -\frac{b_3}{2}(\psi_{x1} + \psi_{x2}) - \frac{c_3}{2}(\psi_{y1} + \psi_{y2})
 \end{aligned} \right\} \quad (7-48)$$

$$\left. \begin{aligned}
 \int_0^{d_1} \tilde{\psi}_{s1} ds &= -w_2 + w_3 \\
 \int_0^{d_2} \tilde{\psi}_{s2} ds &= -w_3 + w_1 \\
 \int_0^{d_3} \tilde{\psi}_{s3} ds &= -w_1 + w_2
 \end{aligned} \right\} \quad (7-49)$$

Substitution of Eqs. (7-43), (7-44), (7-48) and (7-49) into the right side of Eq. (7-42) yields

$$\begin{aligned}
 & -\sum_{i=1}^3 (M_{ni} \int_0^{d_i} \tilde{\psi}_{ni} ds + M_{nsi} \int_0^{d_i} \tilde{\psi}_{si} ds) \\
 &= \alpha_1 [-2w_1 + (1+r_1)w_2 + (1-r_1)w_3 + \frac{2Ab_1}{d_1^2}(\psi_{x2} + \psi_{x3}) + \frac{2Ac_1}{d_1^2}(\psi_{y2} + \psi_{y3})] \\
 &+ \alpha_2 [(1-r_2)w_1 - 2w_2 + (1+r_2)w_3 + \frac{2Ab_2}{d_2^2}(\psi_{x3} + \psi_{x1}) + \frac{2Ac_2}{d_2^2}(\psi_{y3} + \psi_{y1})] \\
 &+ \alpha_3 [(1+r_3)w_1 + (1-r_3)w_2 - 2w_3 + \frac{2Ab_3}{d_3^2}(\psi_{x1} + \psi_{x2}) + \frac{2Ac_3}{d_3^2}(\psi_{y1} + \psi_{y2})] \quad (7-50)
 \end{aligned}$$

By employing Eq. (7-28), \mathbf{q}^e on the right side of the above equation can be expressed in terms of $\boldsymbol{\lambda}$

$$\begin{aligned}
 & - \sum_{i=1}^3 (M_{ni} \int_0^{d_i} \tilde{\psi}_{ni} ds + M_{nsi} \int_0^{d_i} \tilde{\psi}_{si} ds) \\
 & = \boldsymbol{\alpha}^T \left(\begin{bmatrix} 0 & -\frac{1}{2}(1-r_1) & 1 \\ 1 & 0 & -\frac{1}{2}(1-r_2) \\ -\frac{1}{2}(1-r_3) & 1 & 0 \end{bmatrix} \begin{Bmatrix} \lambda_4 \\ \lambda_5 \\ \lambda_6 \end{Bmatrix} \right. \\
 & \quad \left. + \begin{bmatrix} 0 & 1 & -\frac{1}{2}(1+r_1) \\ -\frac{1}{2}(1+r_2) & 0 & 1 \\ 1 & -\frac{1}{2}(1+r_3) & 0 \end{bmatrix} \begin{Bmatrix} \lambda_7 \\ \lambda_8 \\ \lambda_9 \end{Bmatrix} \right) \quad (7-51)
 \end{aligned}$$

Substituting Eqs. (7-47) and (7-51) into the two sides of Eq. (7-42), and eliminating the arbitrary parameters $\boldsymbol{\alpha}^T$, we obtain

$$\begin{aligned}
 & \begin{bmatrix} 1 & -3 & 5 \\ 5 & 1 & -3 \\ -3 & 5 & 1 \end{bmatrix} \begin{Bmatrix} \lambda_4 \\ \lambda_5 \\ \lambda_6 \end{Bmatrix} + \begin{bmatrix} 1 & 5 & -3 \\ -3 & 1 & 5 \\ 5 & -3 & 1 \end{bmatrix} \begin{Bmatrix} \lambda_7 \\ \lambda_8 \\ \lambda_9 \end{Bmatrix} \\
 & = \begin{bmatrix} 0 & -3(1-r_1) & 6 \\ 6 & 0 & -3(1-r_2) \\ -3(1-r_3) & 6 & 0 \end{bmatrix} \begin{Bmatrix} \lambda_4 \\ \lambda_5 \\ \lambda_6 \end{Bmatrix} + \begin{bmatrix} 0 & 6 & -3(1+r_1) \\ -3(1+r_2) & 0 & 6 \\ 6 & -3(1+r_3) & 0 \end{bmatrix} \begin{Bmatrix} \lambda_7 \\ \lambda_8 \\ \lambda_9 \end{Bmatrix}
 \end{aligned}$$

i.e.,

$$\begin{bmatrix} 1 & -3r_1 & -1 \\ -1 & 1 & -3r_2 \\ -3r_3 & -1 & 1 \end{bmatrix} \begin{Bmatrix} \lambda_4 - \lambda_8 \\ \lambda_5 - \lambda_9 \\ \lambda_6 - \lambda_7 \end{Bmatrix} = \begin{Bmatrix} 0 \\ 0 \\ 0 \end{Bmatrix} \quad (7-52)$$

If $\boldsymbol{\lambda}$ is expressed in terms of \boldsymbol{q}^e , we obtain

$$\begin{bmatrix} 1 & -3r_1 & -1 \\ -1 & 1 & -3r_2 \\ -3r_3 & -1 & 1 \end{bmatrix} \begin{Bmatrix} 2w_1 - 2w_2 + c_3(\psi_{x1} + \psi_{x2}) - b_3(\psi_{y1} + \psi_{y2}) \\ 2w_2 - 2w_3 + c_1(\psi_{x2} + \psi_{x3}) - b_1(\psi_{y2} + \psi_{y3}) \\ 2w_3 - 2w_1 + c_2(\psi_{x3} + \psi_{x1}) - b_2(\psi_{y3} + \psi_{y1}) \end{Bmatrix} = \begin{Bmatrix} 0 \\ 0 \\ 0 \end{Bmatrix} \quad (7-53)$$

Equations (7-52) and (7-53) are the 3 perimeter conforming conditions for verifying

the convergence of the element BCIZ. When the components in the element DOFs q^e are 9 arbitrary parameters, Eq. (7-53) is not satisfied. Thereby, the convergence of the element BCIZ cannot be guaranteed.

7.3.3 Element GCII-T9—an Improvement on the Element BCIZ

The triangular thin plate element GCII-T9^[4] is an improved model of the element BCIZ.

As described above, the reason why the element BCIZ cannot ensure convergence is that the perimeter conforming condition (7-42) is not satisfied. Therefore, an improvement scheme is proposed as follows: on the basis of the assumed element deflection field given by Eq. (7-27), 3 new unknown coefficients and basis functions are supplemented; and on the basis of the 9 point conforming conditions used, 3 perimeter conforming conditions given in Eq. (7-42) are also supplemented. Since the condition (7-42) has already been satisfied, the convergence can be ensured. This element obtained is called GCII-T9.

The construction procedure of the element GCII-T9 is as follows.

The element deflection field is assumed to be composed of two parts:

$$w = \bar{w}(\text{BCIZ}) + \hat{w} \quad (7-54)$$

where $\bar{w}(\text{BCIZ})$ is the assumed deflection field (7-27) of the element BCIZ with 9 unknown coefficients; \hat{w} is the additional deflection field with 3 new unknown coefficients:

$$\hat{w} = \lambda_{10}L_1^2L_2^2 + \lambda_{11}L_2^2L_3^2 + \lambda_{12}L_3^2L_1^2 \quad (7-55)$$

\hat{w} has the following characteristic: at three corner nodes, \hat{w} , $\frac{\partial \hat{w}}{\partial x}$ and $\frac{\partial \hat{w}}{\partial y}$ are all zero.

The assumed deflection field in Eq. (7-54) contains 12 unknown coefficients, while the number of the element DOFs is still 9, so the new element is a super-basis element.

In order to solve the 12 unknown coefficients, 12 conforming conditions are needed.

Firstly, 9 point conforming conditions about w , ψ_x and ψ_y at three corner nodes are used. Because of the characteristic of the additional deflection \hat{w} mentioned above, we know that λ_{10} , λ_{11} and λ_{12} will not appear in these conditions. So, the first 9 unknown coefficients $\lambda_1, \lambda_2, \dots, \lambda_9$ can be solved just by these 9 conditions, as shown in Eq. (7-29), and are the same as those in the element BCIZ.

Secondly, the 3 new unknown coefficients λ_{10} , λ_{11} and λ_{12} will be solved by applying 3 perimeter conforming conditions given in Eq. (7-42). And, the weighting

functions given in Eq. (7-42) are still the 3 constant internal force states shown in Eqs. (7-43) – (7-46).

For the items at the right side of Eq. (7-42), the derivation results are still given by Eqs. (7-50) and (7-51).

For the items at the left side of Eq. (7-42), the items related to the new unknown coefficients λ_{10} , λ_{11} , λ_{12} should be supplemented on the basis of Eq. (7-47), i.e.,

$$\begin{aligned} \mathbf{M}^T \iint \boldsymbol{\kappa} dA = & -\boldsymbol{\alpha}^T \left(\frac{1}{6} \begin{bmatrix} -1 & 3 & -5 \\ -5 & -1 & 3 \\ 3 & -5 & -1 \end{bmatrix} \begin{Bmatrix} \lambda_4 \\ \lambda_5 \\ \lambda_6 \end{Bmatrix} + \frac{1}{6} \begin{bmatrix} -1 & -5 & 3 \\ 3 & -1 & -5 \\ -5 & 3 & -1 \end{bmatrix} \begin{Bmatrix} \lambda_7 \\ \lambda_8 \\ \lambda_9 \end{Bmatrix} \right) \\ & + \frac{1}{6} \begin{bmatrix} 0 & 2 & 0 \\ 0 & 0 & 2 \\ 2 & 0 & 0 \end{bmatrix} \begin{Bmatrix} \lambda_{10} \\ \lambda_{11} \\ \lambda_{12} \end{Bmatrix} \end{aligned} \quad (7-56)$$

Substitution of Eqs. (7-56) and (7-51) into the two sides of Eq. (7-42) yields

$$\begin{bmatrix} 0 & 2 & 0 \\ 0 & 0 & 2 \\ 2 & 0 & 0 \end{bmatrix} \begin{Bmatrix} \lambda_{10} \\ \lambda_{11} \\ \lambda_{12} \end{Bmatrix} = \begin{bmatrix} 1 & -3r_1 & -1 \\ -1 & 1 & -3r_2 \\ -3r_3 & -1 & 1 \end{bmatrix} \begin{Bmatrix} \lambda_4 - \lambda_8 \\ \lambda_5 - \lambda_9 \\ \lambda_6 - \lambda_7 \end{Bmatrix}$$

From this relation, we obtain

$$\begin{Bmatrix} \lambda_{10} \\ \lambda_{11} \\ \lambda_{12} \end{Bmatrix} = \frac{1}{2} \begin{bmatrix} -3r_3 & -1 & 1 \\ 1 & -3r_1 & -1 \\ -1 & 1 & -3r_2 \end{bmatrix} \begin{Bmatrix} \lambda_4 - \lambda_8 \\ \lambda_5 - \lambda_9 \\ \lambda_6 - \lambda_7 \end{Bmatrix} \quad (7-57)$$

Equation (7-57) can also be expressed in terms of \mathbf{q}^e ,

$$\begin{aligned} \begin{Bmatrix} \lambda_{10} \\ \lambda_{11} \\ \lambda_{12} \end{Bmatrix} = & \begin{bmatrix} -(1+3r_3) & \frac{1}{2}(c_2-3r_3c_3) & -\frac{1}{2}(b_2-3r_3b_3) \\ 2 & \frac{1}{2}(c_3-c_2) & -\frac{1}{2}(b_3-b_2) \\ -(1-3r_2) & -\frac{1}{2}(c_3+3r_2c_2) & \frac{1}{2}(b_3+3r_2b_2) \end{bmatrix} \begin{Bmatrix} w_1 \\ \psi_{x1} \\ \psi_{y1} \end{Bmatrix} \\ & + \begin{bmatrix} -(1-3r_3) & -\frac{1}{2}(c_1+3r_3c_3) & \frac{1}{2}(b_1+3r_3b_3) \\ -(1+3r_1) & \frac{1}{2}(c_3-3r_1c_1) & -\frac{1}{2}(b_3-3r_1b_1) \\ 2 & \frac{1}{2}(c_1-c_3) & -\frac{1}{2}(b_1-b_3) \end{bmatrix} \begin{Bmatrix} w_2 \\ \psi_{x2} \\ \psi_{y2} \end{Bmatrix} \end{aligned}$$

$$+ \begin{bmatrix} 2 & \frac{1}{2}(c_2 - c_1) & -\frac{1}{2}(b_2 - b_1) \\ -(1 - 3r_1) & -\frac{1}{2}(c_2 + 3r_1c_1) & \frac{1}{2}(b_2 + 3r_1b_1) \\ -(1 + 3r_2) & \frac{1}{2}(c_1 - 3r_2c_2) & -\frac{1}{2}(b_1 - 3r_2b_2) \end{bmatrix} \begin{Bmatrix} w_3 \\ \psi_{x3} \\ \psi_{y3} \end{Bmatrix} \quad (7-58)$$

After the 12 unknown coefficients are determined, the element deflection field and its shape functions can then be obtained. All the shape functions are composed of two parts, for examples, for the node 1, we have

$$N_1 = \bar{N}_1 + \hat{N}_1, \quad N_{x1} = \bar{N}_{x1} + \hat{N}_{x1}, \quad N_{y1} = \bar{N}_{y1} + \hat{N}_{y1} \quad (7-59)$$

where $\bar{N}_1, \bar{N}_{x1}, \bar{N}_{y1}$ are the parts related to $\bar{w}(\text{BCIZ})$, and are the same as those given in Eq. (7-31). \hat{N}_1, \hat{N}_{x1} and \hat{N}_{y1} are the parts related to \hat{w} :

$$\left. \begin{aligned} \hat{N}_1 &= -(1 + 3r_3)L_1^2L_2^2 + 2L_2^2L_3^2 - (1 - 3r_2)L_3^2L_1^2 \\ \hat{N}_{x1} &= \frac{1}{2}(c_2 - 3r_3c_3)L_1^2L_2^2 + \frac{1}{2}(c_3 - c_2)L_2^2L_3^2 - \frac{1}{2}(c_3 + 3r_2c_2)L_3^2L_1^2 \\ \hat{N}_{y1} &= -\frac{1}{2}(b_2 - 3r_3b_3)L_1^2L_2^2 - \frac{1}{2}(b_3 - b_2)L_2^2L_3^2 + \frac{1}{2}(b_3 + 3r_2b_2)L_3^2L_1^2 \end{aligned} \right\} \quad (7-60)$$

The other 6 shape functions can be obtained by permutation.

After the shape functions are determined, the element stiffness matrix can then be obtained.

Example 7.2 The central deflection w_C and central moment M_C of a square plate (the side length is L) subjected to uniform load q and central concentrated load P . The Poisson's ratio is 0.3. Meshes A and B in Fig. 6.2 and mesh C in Fig. 6.13 are used. The results by the element GCII-T9 are given in Tables 7.3 and 7.4.

In the tables, $\alpha = w_C/(qL^4/100D)$, $\beta = w_C/(PL^2/10D)$ and $\alpha_1 = M_{xC}/(qL^2)$. And, the numbers in parentheses are the relative errors. From Tables 7.3 and 7.4, two points can be concluded:

(1) The precision of the element GCII-T9 is very high, is better than the Discrete Kirchhoff Theory element DKT and the stress hybrid element HSM.

(2) For mesh C , the element BCIZ cannot pass the patch test, and cannot converge to correct solutions, either; but the computational results of the element GCII-T9 are convergent under this mesh, even better than those obtained by the meshes A and B .

Table 7.3 The central deflection and central moment coefficients of a simply-supported plate (GCII-T9, Mesh *A*)

Mesh (1/4 plate)	Deflection coefficient (uniform load) α	Deflection coefficient (concentrated load) β	Moment coefficient (uniform load) α_1
2 × 2	0.4119(1.41%)	0.1174(1.18%)	0.0499(4.35%)
4 × 4	0.4085(0.57%)	0.1167(0.58%)	0.0488(1.88%)
8 × 8	0.4068(0.15%)	0.1162(0.14%)	0.0480(0.21%)
Analytical	0.4062	0.1160	0.0479

Table 7.4 The central deflection coefficients of simply-supported and clamped plates by using meshes *A*, *B* and *C* (GCII-T9, Mesh 8 × 8)

support \ mesh	α (uniform load)			β (concentrated load)		
	Mesh <i>A</i>	Mesh <i>B</i>	Mesh <i>C</i>	Mesh <i>A</i>	Mesh <i>B</i>	Mesh <i>C</i>
Simply-supported	0.4068 (0.15%)	0.4068 (0.15%)	0.4056 (−0.15%)	0.1162 (0.14%)	0.1182 (1.9%)	0.1163 (0.28%)
Clamped	0.1291 (2.5%)	0.1274 (1.1%)	0.1277 (1.4%)	0.5666 (1.2%)	0.5812 (3.8%)	0.5666 (1.2%)

7.4 Least-Square Scheme—Elements LSGC-R12 and LSGC-T9

This section will introduce the construction procedure of the thin plate element formulated by the least-square scheme. The no. 27 and 28 elements LSGC-R12 and LSGC-T9 in Table 5.1 belong to this element group.

7.4.1 Rectangular Element LSGC-R12^[5] — an Improvement on the Element ACM

Rectangular thin plate element LSGC-R12 is a super-basis element by improving the element ACM^[2] using the least-square scheme. The element DOFs are still the 12 conventional DOFs at the corner nodes. And, the element deflection field is assumed to be composed of two parts:

$$w = \bar{w}(\text{ACM}) + \hat{w} \tag{7-61}$$

where $\bar{w}(\text{ACM})$ is the deflection field (7-1) of the element ACM, and contains 12 unknown coefficients $\lambda_1, \lambda_2, \dots, \lambda_{12}$; \hat{w} is the additional deflection field with 2 new unknown coefficients

$$\hat{w} = \lambda_{13}\eta(\eta^2 - 1)(\xi^2 - 1)^2 + \lambda_{14}\xi(\xi^2 - 1)(\eta^2 - 1)^2 \quad (7-62)$$

\hat{w} possesses the following characteristics:

(1) At 4 corner nodes, \hat{w} , $\frac{\partial \hat{w}}{\partial x}$ and $\frac{\partial \hat{w}}{\partial y}$ are all zero;

(2) Along 4 element sides, \hat{w} identically equals to zero, but $\frac{\partial \hat{w}}{\partial n}$ does not equal to zero.

In order to solve the 14 unknown coefficients, 14 conforming conditions are needed.

Firstly, the 12 point conforming conditions about w , ψ_x and ψ_y at the corner nodes are applied. According to the characteristic (1) of \hat{w} , these 12 conditions do not contain λ_{13} and λ_{14} , thus the 12 unknown coefficients $\lambda_1, \lambda_2, \dots, \lambda_{12}$ can just be solved, and are the same as those of the element ACM.

Since the displacement field \bar{w} of the element ACM is exactly compatible with the deflection \tilde{w} along the element boundary (but incompatible with the normal slope $\tilde{\psi}_n$ along the element boundary), and the value of \hat{w} along the boundary identically equals to zero, so the total displacement $w = \bar{w} + \hat{w}$ is also compatible with the boundary deflection \tilde{w} .

Secondly, the conforming conditions about the normal slope along the element boundary also need to be considered, and then, they are used to determine the other residual 2 unknown coefficients λ_{13} and λ_{14} .

According to the least-square method, the following 2 conditions can be obtained:

$$\left. \begin{aligned} \frac{\partial}{\partial \lambda_{13}} \oint_{\partial A^e} \left(\frac{\partial \bar{w}}{\partial n} + \frac{\partial \hat{w}}{\partial n} - \tilde{\psi}_n \right)^2 ds = 0 \\ \frac{\partial}{\partial \lambda_{14}} \oint_{\partial A^e} \left(\frac{\partial \bar{w}}{\partial n} + \frac{\partial \hat{w}}{\partial n} - \tilde{\psi}_n \right)^2 ds = 0 \end{aligned} \right\} \quad (7-63)$$

From this equation, we obtain

$$\left. \begin{aligned} \lambda_{13} &= \frac{9}{128} a \sum_{i=1}^4 \xi_i \eta_i \psi_{xi} \\ \lambda_{14} &= \frac{9}{128} b \sum_{i=1}^4 \xi_i \eta_i \psi_{yi} \end{aligned} \right\} \quad (7-64)$$

After the 14 unknown coefficients are determined, the element deflection field and its shape functions can be obtained

$$w = \sum_{i=1}^4 (N_i w_i + N_{xi} \psi_{xi} + N_{yi} \psi_{yi}) \quad (7-65)$$

where the shape functions are composed of two parts

$$\left. \begin{aligned} N_i &= \bar{N}_i + \hat{N}_i \\ N_{xi} &= \bar{N}_{xi} + \hat{N}_{xi} \\ N_{yi} &= \bar{N}_{yi} + \hat{N}_{yi} \end{aligned} \right\} \quad (i = 1,2,3,4) \quad (7-66)$$

in which \bar{N}_i , \bar{N}_{xi} and \bar{N}_{yi} are the parts related to \bar{w} , and the same as those given in Eq. (7-19). \hat{N}_i , \hat{N}_{xi} and \hat{N}_{yi} are the parts related to \hat{w} :

$$\left. \begin{aligned} \hat{N}_i &= 0 \\ \hat{N}_{xi} &= \frac{9}{128} a \xi_i \eta_i \eta (\eta^2 - 1) (\xi^2 - 1)^2 \\ \hat{N}_{yi} &= \frac{9}{128} b \xi_i \eta_i \xi (\xi^2 - 1) (\eta^2 - 1)^2 \end{aligned} \right\} \quad (i = 1,2,3,4) \quad (7-67)$$

Once the shape functions are obtained, the element stiffness matrix can be derived.

7.4.2 Triangular Element LSGC-T9^[5] — an Improvement on the Element BCIZ

Triangular thin plate element LSGC-T9 is a super-basis element by improving the element BCIZ^[3] using the least-square scheme. The element DOFs are still the 9 conventional DOFs at the corner nodes. And, the element deflection field is assumed to be composed of two parts:

$$w = \bar{w}(\text{BCIZ}) + \hat{w} \quad (7-68)$$

where \bar{w} (BCIZ) is the deflection field (7-27) of the element BCIZ, and contains 9 unknown coefficients $\lambda_1, \lambda_2, \dots, \lambda_9$; \hat{w} is the additional deflection field with 3 new unknown coefficients:

$$\hat{w} = \lambda_{10} L_1^2 L_2^2 L_3 + \lambda_{11} L_2^2 L_3^2 L_1 + \lambda_{12} L_3^2 L_1^2 L_2 \quad (7-69)$$

The first 9 unknown coefficients can be solved by the point conforming conditions about w , ψ_x , ψ_y , at the corner nodes, as shown in Eq. (7-29). And, the residual 3 unknown coefficients λ_{10} , λ_{11} and λ_{12} can be solved by the following least-square conditions:

$$\frac{\partial}{\partial \lambda_i} \oint_{\partial A^e} \left(\frac{\partial \bar{w}}{\partial n} + \frac{\partial \hat{w}}{\partial n} - \tilde{\psi}_n \right)^2 ds = 0 \quad (i = 10,11,12) \quad (7-70)$$

After the determination of all the unknown coefficients, the shape functions and element stiffness matrix can then be derived.

Example 7.3 The central deflection and central moment of square plates (the side length is L) subjected to uniform load q and central concentrated load P . The Poisson's ratio $\mu = 0.3$.

The results by the elements LSGC-R12 and LSGC-T9 are given in Tables 7.5 and 7.6. And, mesh B in Fig. 6.2 and mesh C in Fig. 6.13 are used for triangular element.

Table 7.5 The central deflection and moment of square plate subjected to uniform load

Mesh (1/4plate)	Clamped				Simply-supported				
	Rectangular elements		Triangular element LSGC-T9		Rectangular elements		Triangular element LSGC-T9		
	ACM	LSGC-R12	Mesh B	Mesh C	ACM	LSGC-R12	Mesh B	Mesh C	
w	2×2	0.1403	0.1222	0.1025	0.1028	0.4328	0.3976	0.3949	0.3918
	4×4	0.1332	0.1241	0.1203	0.1212	0.4129	0.4042	0.4036	0.4032
	8×8	0.1275	0.1262	0.1250	0.1252	0.4081	0.4056	0.4063	0.4055
	Analytical	0.1265($qL^4/100D$)				0.4062($qL^4/100D$)			
M	2×2	0.2778	0.2132	0.2030	0.1624	0.5217	0.4442	0.4734	0.4456
	4×4	0.2405	0.2233	0.2240	0.2241	0.4892	0.4689	0.4810	0.4733
	8×8	0.2319	0.2275	0.2287	0.2267	0.4817	0.4762	0.4829	0.4754
	Analytical	0.2291($qL^2/10$)				0.4789($qL^2/10$)			

Table 7.6 The central deflection of square plate subjected to central concentrated load

Mesh (1/4 plate)	Clamped				Simply-supported			
	Rectangular elements		Triangular element LSGC-T9		Rectangular elements		Triangular element LSGC-T9	
	ACM	LSGC-R12	Mesh B	Mesh C	ACM	LSGC-R12	Mesh B	Mesh C
2×2	0.6135	0.5324	0.4327	0.4482	1.2327	1.1243	1.0622	1.0803
4×4	0.5803	0.5516	0.5207	0.5296	1.1829	1.1501	1.1278	1.1326
8×8	0.5673	0.5585	0.5494	0.5514	1.1674	1.1570	1.1520	1.1515
Analytical	0.5612($PL^2/100D$)				1.160($PL^2/100D$)			

References

- [1] Long ZF (1992) Triangular and rectangular plate elements based on generalized compatibility conditions. *Computational Mechanics* 10(3/4): 281 – 288
- [2] Melosh RJ (1963) Basis for derivation of matrices for the direct stiffness method. *AIAA Journal* 1(7): 1631 – 1637
- [3] Bazeley GP, Cheung YK, Irons BM, Zienkiewicz OC (1965) Triangular elements in bending—conforming and nonconforming solution. In: *Proceedings of the Conference on Matrix Methods in Structural Mechanics*. Air Force Institute of Technology, Ohio: Wright-Patterson A. F. Base, pp 547 – 576
- [4] Long YQ, Zhao JQ (1988) A new generalized conforming triangular element for thin plates. *Communications in Applied Numerical Methods* 4: 781 – 792
- [5] Bu XM, Long YQ (1991) A generalized conforming technique using the least squares method. *Gong Cheng Li Xue/Engineering Mechanics* 8(2): 20 – 24 (in Chinese)

Chapter 8 Generalized Conforming Thick Plate Element

Song Cen

Department of Engineering Mechanics, School of Aerospace,
Tsinghua University, Beijing, 100084, China

Zhi-Fei Long

School of Mechanics & Civil Engineering, China University of
Mining & Technology, Beijing, 100083, China

Abstract This chapter introduces how to use the generalized conforming theory to develop the plate element models for the analysis of both thick and thin plates. In Sects. 8.1 and 8.2, a review of the Reissner-Mindlin (thick) plate theory is firstly given, and then, a comparison between this theory and the Kirchhoff (thin) plate theory is presented. In the subsequent sections, the construction methods for the thick/thin plate elements are firstly summarized; especially, the shear locking difficulty caused by the traditional scheme (assuming deflection and rotation fields) is analyzed. Then, three new schemes which are proposed by the authors and can eliminate shear locking from the outset are introduced in detail, including the schemes of assuming rotation and shear strain fields, assuming deflection and shear strain fields, and introducing the shear strain field into the thin plate elements. The formulations of four triangular and rectangular element models are also presented. Numerical examples show that the proposed models exhibit excellent performance for both thick and thin plates, and no shear locking happens.

Keywords thick plate element, generalized conforming, Reissner-Mindlin (thick) plate theory, thick/thin beam element, shear locking.

8.1 Summary of the Thick Plate Theory

The thick plates discussed here is restricted to moderately-thick plates. Limitation will appear if classical thin plate theory is used to analyze such thick plates.

The fundamental equations of the thick plate theory were firstly proposed by Reissner in the forties of the twentieth century^[1].

Compared with the thin plate theory, the main characteristic of the thick plate theory is that it considers the influences of the transverse shear strain γ_{xz} and γ_{yz} (hereafter referred to as γ_x and γ_y). So, the thick plate theory is also called the shear deformation plate bending theory. Furthermore, in dynamics problems, the influences of rotatory inertia should also be considered^[2].

In the thick plate theory, the shear strain can be expressed in terms of the deflection w and the normal slopes ψ_x and ψ_y as

$$\gamma_x = \frac{\partial w}{\partial x} - \psi_x, \quad \gamma_y = \frac{\partial w}{\partial y} - \psi_y \quad (8-1)$$

in which w , ψ_x , ψ_y are three independent generalized displacements. On the contrary, in the thin plate theory, since γ_x and γ_y are assumed to be zero, Eq. (8-1) will degenerate to be

$$\psi_x = \frac{\partial w}{\partial x}, \quad \psi_y = \frac{\partial w}{\partial y} \quad (8-2)$$

Only one independent displacement w exists, and both ψ_x and ψ_y depend on w . Therefore, the thick plate theory is also called the plate bending theory with three generalized displacements^[3].

Owing to constructional reason, the shear deformation of sandwich plates cannot be ignored. So, the thick plate theory can be used to calculate the sandwich plate problems. Furthermore, it is more reasonable to employ the thick plate theory to analyze the following problems: high-order vibration problem of plates, stress concentration problem, stress distribution problem near free edges, contact problem^[3].

This section compendiously gives the fundamental equations of the thick plate theory, including equilibrium equations, geometrical equations, physical equations, coordinate transformations, boundary conditions, expressions of strain energy and strain complementary energy. For these fundamental equations of the thick plate theory, it is necessary to emphatically understand the difference from those in the thin plate theory and the influence of shear deformation.

8.1.1 Equilibrium Equations

A thick plate in Cartesian coordinates (x, y, z) is shown in Fig. 8.1. The x and y co-ordinates are in the reference middle surface; z is the co-ordinate through the thickness h , and its positive direction is upward.

The load density on the middle surface has three components q , m_x and m_y , in which q is the load density along the z -axis, and its positive direction is also upward; m_x is the couple load density in the xz -plane, and its positive direction is the same

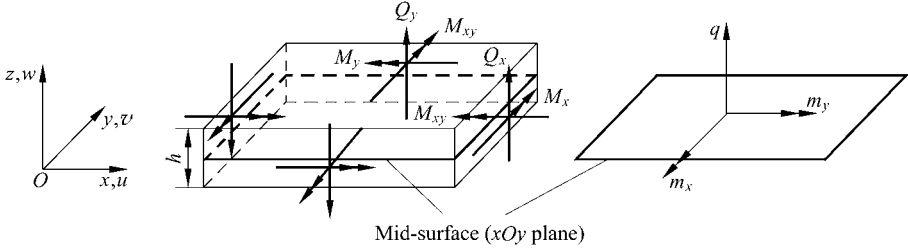


Figure 8.1 The coordinates, internal forces and load density components used in thick plate bending problem

as the rotation from x -axis to z -axis; m_y is the couple load density in the yz -plane, and its positive direction is the same as the rotation from y -axis to z -axis.

In the Cartesian coordinate system, the moderately thick plate has 5 internal force components: bending moments M_x and M_y , twisting moment $M_{xy} = M_{yx}$, transverse shear forces Q_x and Q_y . And, their positive directions are shown in Fig. 8.1. These 5 components can form an internal force vector:

$$\mathbf{S} = [M_x \quad M_y \quad M_{xy} \quad Q_x \quad Q_y]^T$$

which is composed of two sub vectors:

$$\mathbf{M} = [M_x \quad M_y \quad M_{xy}]^T, \quad \mathbf{Q} = [Q_x \quad Q_y]^T$$

Then, the differential equilibrium equations of the thick plate can be written as

$$\left. \begin{aligned} \frac{\partial M_x}{\partial x} + \frac{\partial M_{xy}}{\partial y} - Q_x - m_x &= 0 \\ \frac{\partial M_{xy}}{\partial x} + \frac{\partial M_y}{\partial y} - Q_y - m_y &= 0 \\ \frac{\partial Q_x}{\partial x} + \frac{\partial Q_y}{\partial y} + q &= 0 \end{aligned} \right\} \quad (8-3)$$

One characteristic of the thick plate theory which is different from the thin plate theory is that the number of load densities increases from 1 to 3. Therefore, the shear forces Q_x and Q_y are not only related to the internal moments M_x , M_y and M_{xy} , but also related to the loads m_x and m_y .

8.1.2 Geometrical Equations

The displacements of the thick plate have 3 independent parameters:

$$\mathbf{d} = [w \quad \psi_x \quad \psi_y]^T \quad (8-4)$$

in which w is the deflection, and its positive direction is upward; ψ_x is the normal rotation in the xz -plane, and its positive direction is from x -axis to z -axis; ψ_y is the normal rotation in the yz -plane, and its positive direction is from y -axis to z -axis.

The strains of the thick plate have 5 parameters:

$$\mathbf{E} = [\kappa_x \quad \kappa_y \quad 2\kappa_{xy} \quad \gamma_x \quad \gamma_y]^T \quad (8-5)$$

where κ_x , κ_y and $2\kappa_{xy}$ are the curvatures, and their positive values are corresponding to the deformations caused by positive M_x , M_y and M_{xy} , respectively. They form a bending strain vector:

$$\boldsymbol{\kappa} = [\kappa_x \quad \kappa_y \quad 2\kappa_{xy}]^T \quad (8-6)$$

γ_x (or γ_{xz}) and γ_y (or γ_{yz}) are shear strains, and their positive values are corresponding to the deformations caused by positive Q_x and Q_y , respectively. They form a shear strain vector:

$$\boldsymbol{\gamma} = [\gamma_x \quad \gamma_y]^T \quad (8-7)$$

The geometrical equations between strains and displacements are as follows:

$$\left. \begin{aligned} \kappa_x &= -\frac{\partial \psi_x}{\partial x}, \quad \kappa_y = -\frac{\partial \psi_y}{\partial y}, \quad 2\kappa_{xy} = -\left(\frac{\partial \psi_x}{\partial y} + \frac{\partial \psi_y}{\partial x} \right) \\ \gamma_x &= \frac{\partial w}{\partial x} - \psi_x, \quad \gamma_y = \frac{\partial w}{\partial y} - \psi_y \end{aligned} \right\} \quad (8-8)$$

After the elimination of w , ψ_x and ψ_y in Eq. (8-8), we obtain

$$\left. \begin{aligned} \frac{\partial \kappa_x}{\partial y} - \frac{\partial \kappa_{xy}}{\partial x} &= \frac{1}{2} \frac{\partial}{\partial x} \left(\frac{\partial \gamma_x}{\partial y} - \frac{\partial \gamma_y}{\partial x} \right) \\ \frac{\partial \kappa_y}{\partial x} - \frac{\partial \kappa_{xy}}{\partial y} &= -\frac{1}{2} \frac{\partial}{\partial y} \left(\frac{\partial \gamma_x}{\partial y} - \frac{\partial \gamma_y}{\partial x} \right) \end{aligned} \right\} \quad (8-9)$$

Then, by the elimination of γ_x and γ_y in Eq. (8-9), we have

$$\frac{\partial^2 \kappa_x}{\partial y^2} + \frac{\partial^2 \kappa_y}{\partial x^2} - 2 \frac{\partial^2 \kappa_{xy}}{\partial x \partial y} = 0 \quad (8-10)$$

Equations (8-9) and (8-10) are called the compatibility equations of strains.

Another characteristic of the thick plate theory which is different from the thin plate theory is that the number of displacements increases from 1 to 3. In thin plate, since $\gamma_x = 0$ and $\gamma_y = 0$, from Eq. (8-8), we have

$$\psi_x = \frac{\partial w}{\partial x}, \quad \psi_y = \frac{\partial w}{\partial y}$$

Here, ψ_x and ψ_y can be derived from w , so they are not independent displacement parameters.

8.1.3 Physical Equations

The physical equations between internal forces and strains in a thick plate are as follows:

$$\left. \begin{aligned} M_x &= D(\kappa_x + \mu\kappa_y) \\ M_y &= D(\kappa_y + \mu\kappa_x) \\ M_{xy} &= D(1 - \mu)\kappa_{xy} \\ Q_x &= C\gamma_x \\ Q_y &= C\gamma_y \end{aligned} \right\} \quad (8-11)$$

where D and C are the plate bending stiffness and shear stiffness, respectively; μ is the Poisson's ratio. For an isotropic homogenous thick plate, we have

$$D = \frac{Eh^3}{12(1 - \mu^2)}, \quad C = \frac{Gh}{k} = \frac{Eh}{2(1 + \mu)k} \quad (8-12)$$

where h is the thickness of the plate; E is the Young's modulus; coefficient $k = 1.2$.

For a sandwich plate shown in Fig. 8.2, we have

$$D = \frac{E_f(h + t')^2 t'}{2(1 - \mu_f^2)}, \quad C = G_c(h + t') \quad (8-13)$$

where h is the thickness of the core layer; t' is the thickness of the surface layer; E_f and μ_f are the Young's modulus and Poisson's ratio of the surface layer, respectively; G_c is the shear modulus of the core layer.

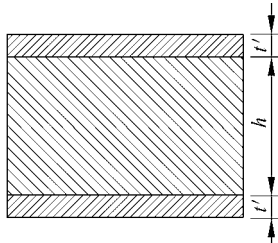


Figure 8.2 A sandwich plate

The physical Eq. (8-11) can be expressed in matrix forms as follows

$$\mathbf{M} = \mathbf{D}\boldsymbol{\kappa} \quad (8-14)$$

$$\mathbf{Q} = \mathbf{C}\boldsymbol{\gamma} \quad (8-15)$$

where

$$\mathbf{D} = D \begin{bmatrix} 1 & \mu & 0 \\ \mu & 1 & 0 \\ 0 & 0 & \frac{1-\mu}{2} \end{bmatrix} \quad (8-16)$$

$$\mathbf{C} = C \begin{bmatrix} 1 & 0 \\ 0 & 1 \end{bmatrix} \quad (8-17)$$

Another form of the physical equations is

$$\left. \begin{aligned} \kappa_x &= \frac{M_x - \mu M_y}{D(1-\mu^2)}, & \gamma_x &= \frac{Q_x}{C} \\ \kappa_y &= \frac{M_y - \mu M_x}{D(1-\mu^2)}, & \gamma_y &= \frac{Q_y}{C} \\ 2\kappa_{xy} &= \frac{2(1+\mu)M_{xy}}{D(1-\mu^2)} \end{aligned} \right\} \quad (8-18)$$

i.e.,

$$\left. \begin{aligned} \boldsymbol{\kappa} &= \mathbf{D}^{-1}\mathbf{M} \\ \boldsymbol{\gamma} &= \mathbf{C}^{-1}\mathbf{Q} \end{aligned} \right\} \quad (8-19)$$

where

$$\mathbf{D}^{-1} = \frac{1}{D(1-\mu^2)} \begin{bmatrix} 1 & -\mu & 0 \\ -\mu & 1 & 0 \\ 0 & 0 & 2(1+\mu) \end{bmatrix} \quad (8-20)$$

$$\mathbf{C}^{-1} = \frac{1}{C} \begin{bmatrix} 1 & 0 \\ 0 & 1 \end{bmatrix} \quad (8-21)$$

In a thick plate, the shear stiffness C is a finite value, while $C = \infty$ is assumed for the thin plate case.

8.1.4 Coordinate Transformation

Assume that Oxy represents the original coordinate system, $Ox'y'$ represents the new coordinate system, and θ is the rotation from x -axis to x' -axis (see Fig. 8.3).

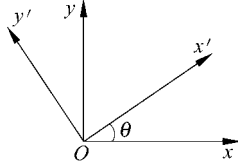


Figure 8.3 Coordinate transformation

Let $l = \cos \theta$, $m = \sin \theta$. Then, the transformation between these two coordinate systems is

$$\begin{Bmatrix} x' \\ y' \end{Bmatrix} = \begin{bmatrix} l & m \\ -m & l \end{bmatrix} \begin{Bmatrix} x \\ y \end{Bmatrix}$$

or written as

$$\mathbf{x}' = \mathbf{L}\mathbf{x} \tag{8-22}$$

where

$$\mathbf{L} = \begin{bmatrix} l & m \\ -m & l \end{bmatrix} \tag{8-23}$$

Since

$$\mathbf{L}^{-1} = \mathbf{L}^T$$

the inverse transformation of Eq. (8-22) is

$$\mathbf{x} = \mathbf{L}^T \mathbf{x}'$$

The transformations of some quantities are the same as Eq. (8-22), for example,

$$(1) \frac{\partial}{\partial \mathbf{x}'} = \mathbf{L} \frac{\partial}{\partial \mathbf{x}}, \text{ i.e., } \begin{Bmatrix} \frac{\partial}{\partial x'} \\ \frac{\partial}{\partial y'} \end{Bmatrix} = \begin{bmatrix} l & m \\ -m & l \end{bmatrix} \begin{Bmatrix} \frac{\partial}{\partial x} \\ \frac{\partial}{\partial y} \end{Bmatrix}$$

$$(2) \boldsymbol{\psi}' = \mathbf{L}\boldsymbol{\psi}, \text{ i.e., } \begin{Bmatrix} \psi'_x \\ \psi'_y \end{Bmatrix} = \begin{bmatrix} l & m \\ -m & l \end{bmatrix} \begin{Bmatrix} \psi_x \\ \psi_y \end{Bmatrix}$$

$$(3) \boldsymbol{\gamma}' = \mathbf{L}\boldsymbol{\gamma}, \text{ i.e., } \begin{Bmatrix} \gamma'_x \\ \gamma'_y \end{Bmatrix} = \begin{bmatrix} l & m \\ -m & l \end{bmatrix} \begin{Bmatrix} \gamma_x \\ \gamma_y \end{Bmatrix}$$

$$(4) \mathbf{Q}' = \mathbf{LQ}, \text{ i.e., } \begin{Bmatrix} Q'_x \\ Q'_y \end{Bmatrix} = \begin{bmatrix} l & m \\ -m & l \end{bmatrix} \begin{Bmatrix} Q_x \\ Q_y \end{Bmatrix} \quad (8-24)$$

The transformation of moments is similar to the transformation of curvatures:

$$(1) \mathbf{M}' = \mathbf{LML}^T, \text{ i.e., } \begin{bmatrix} M_{x'} & M_{x'y'} \\ M_{y'x'} & M_{y'} \end{bmatrix} = \begin{bmatrix} l & m \\ -m & l \end{bmatrix} \begin{bmatrix} M_x & M_{xy} \\ M_{yx} & M_y \end{bmatrix} \begin{bmatrix} l & -m \\ m & l \end{bmatrix}$$

$$(2) \boldsymbol{\kappa}' = \mathbf{L}\boldsymbol{\kappa}\mathbf{L}^T, \text{ i.e., } \begin{bmatrix} \kappa_{x'} & \kappa_{x'y'} \\ \kappa_{y'x'} & \kappa_{y'} \end{bmatrix} = \begin{bmatrix} l & m \\ -m & l \end{bmatrix} \begin{bmatrix} \kappa_x & \kappa_{xy} \\ \kappa_{yx} & \kappa_y \end{bmatrix} \begin{bmatrix} l & -m \\ m & l \end{bmatrix} \quad (8-25)$$

8.1.5 Boundary Conditions

Assume that n and s stand for the outer normal and tangent directions at an arbitrary point on the boundary, respectively. The angle between n and x -axis is θ (see Fig. 8.4). Let

$$l = \cos\theta, \quad m = \sin\theta$$

from Eqs. (8-24) and (8-25), we obtain

$$\begin{Bmatrix} \frac{\partial}{\partial n} \\ \frac{\partial}{\partial s} \end{Bmatrix} = \begin{bmatrix} l & m \\ -m & l \end{bmatrix} \begin{Bmatrix} \frac{\partial}{\partial x} \\ \frac{\partial}{\partial y} \end{Bmatrix} \quad (8-26)$$

$$\begin{Bmatrix} \psi_n \\ \psi_s \end{Bmatrix} = \begin{bmatrix} l & m \\ -m & l \end{bmatrix} \begin{Bmatrix} \psi_x \\ \psi_y \end{Bmatrix} \quad (8-27)$$

$$\left. \begin{aligned} Q_n &= lQ_x + mQ_y \\ M_n &= l^2M_x + m^2M_y + 2lmM_{xy} \\ M_{ns} &= (-M_x + M_y)lm + (l^2 - m^2)M_{xy} \end{aligned} \right\} \quad (8-28)$$

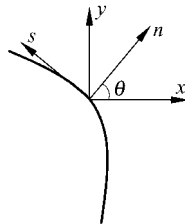


Figure 8.4 The normal and tangent on the boundary

Several typical boundary conditions are given as follows:

$$\left. \begin{aligned} w = \bar{w}, \quad \psi_n = \bar{\psi}_n, \quad \psi_s = \bar{\psi}_s & \quad (\text{on fixed edge } C_1) \\ w = \bar{w}, \quad \psi_s = \bar{\psi}_s, \quad M_n = \bar{M}_n & \quad (\text{on simply-supported (hard) edge } C_2) \\ w = \bar{w}, \quad M_{ns} = \bar{M}_{ns}, \quad M_n = \bar{M}_n & \quad (\text{on simply-supported (soft) edge } C_2') \\ M_n = \bar{M}_n, \quad M_{ns} = \bar{M}_{ns}, \quad Q_n = \bar{Q}_n & \quad (\text{on free edge } C_3) \end{aligned} \right\} \quad (8-29)$$

8.1.6 Strain Energy

Firstly, the definitions of the strain energy density \tilde{U} and the strain energy U of the thick plate are given.

For a given strain vector \mathbf{E} (including bending strain $\boldsymbol{\kappa}$ and shear strain $\boldsymbol{\gamma}$):

$$\begin{aligned} \mathbf{E} &= [\kappa_x \quad \kappa_y \quad 2\kappa_{xy} \quad \gamma_x \quad \gamma_y]^T \\ \boldsymbol{\kappa} &= [\kappa_x \quad \kappa_y \quad 2\kappa_{xy}]^T \\ \boldsymbol{\gamma} &= [\gamma_x \quad \gamma_y]^T \end{aligned}$$

the function $\tilde{U}(\mathbf{E})$ can be defined as

$$\tilde{U}(\mathbf{E}) = \tilde{U}_b(\boldsymbol{\kappa}) + \tilde{U}_s(\boldsymbol{\gamma}) \quad (8-30)$$

where

$$\tilde{U}_b(\boldsymbol{\kappa}) = \frac{1}{2} \boldsymbol{\kappa}^T \mathbf{D} \boldsymbol{\kappa} = \frac{D}{2} [\kappa_x^2 + \kappa_y^2 + 2\mu\kappa_x\kappa_y + 2(1-\mu)\kappa_{xy}^2] \quad (8-31)$$

$$\tilde{U}_s(\boldsymbol{\gamma}) = \frac{1}{2} \boldsymbol{\gamma}^T \mathbf{C} \boldsymbol{\gamma} = \frac{C}{2} (\gamma_x^2 + \gamma_y^2) \quad (8-32)$$

$\tilde{U}(\mathbf{E})$ is the strain energy density of the thick plate; $\tilde{U}_b(\boldsymbol{\kappa})$ is the bending strain energy density; $\tilde{U}_s(\boldsymbol{\gamma})$ is the shear strain energy density.

The strain energy U of the thick plate is defined as the functional of the strain fields \mathbf{E} :

$$\begin{aligned} U(\mathbf{E}) &= \iint_{\Omega} \tilde{U}(\mathbf{E}) \, dx \, dy = \iint_{\Omega} \left(\frac{1}{2} \boldsymbol{\kappa}^T \mathbf{D} \boldsymbol{\kappa} + \frac{1}{2} \boldsymbol{\gamma}^T \mathbf{C} \boldsymbol{\gamma} \right) \, dx \, dy \\ &= \iint_{\Omega} \left\{ \frac{D}{2} [\kappa_x^2 + \kappa_y^2 + 2\mu\kappa_x\kappa_y + 2(1-\mu)\kappa_{xy}^2] + \frac{C}{2} (\gamma_x^2 + \gamma_y^2) \right\} \, dx \, dy \quad (8-33) \end{aligned}$$

Two points should be noted:

(1) For arbitrary strain fields \mathbf{E} , no matter whether these strain fields satisfy the strain compatibility Eq. (8-9), the strain energy corresponding to \mathbf{E} can be defined.

If the strain fields E satisfy the strain compatibility Eq. (8-9), and are derived on the basis of the geometrical Eq. (8-8) from certain displacement fields:

$$\mathbf{d} = [w \quad \psi_x \quad \psi_y]^T$$

then, the strain energy can be expressed as the functional of the displacement fields,

$$U(\mathbf{d}) = \iint_{\Omega} \left\{ \frac{D}{2} \left[\left(\frac{\partial \psi_x}{\partial x} \right)^2 + \left(\frac{\partial \psi_y}{\partial y} \right)^2 + 2\mu \frac{\partial \psi_x}{\partial x} \frac{\partial \psi_y}{\partial y} + \frac{1-\mu}{2} \left(\frac{\partial \psi_x}{\partial y} + \frac{\partial \psi_y}{\partial x} \right)^2 \right] + \frac{C}{2} \left[\left(\frac{\partial w}{\partial x} - \psi_x \right)^2 + \left(\frac{\partial w}{\partial y} - \psi_y \right)^2 \right] \right\} dx dy \quad (8-34)$$

(2) From Eqs. (8-31) and (8-32), it can be seen that $\tilde{U}_b(\boldsymbol{\kappa})$ and $\tilde{U}_s(\boldsymbol{\gamma})$ are the positive definite quadric homogeneous functions of $(\kappa_x, \kappa_y, \kappa_{xy})$ and (γ_x, γ_y) , respectively. According to the properties of the positive definite quadric homogeneous function, the following equalities can be obtained:

$$\left. \begin{aligned} \frac{\partial \tilde{U}_b}{\partial \kappa_x} \kappa_x + \frac{\partial \tilde{U}_b}{\partial \kappa_y} \kappa_y + \frac{\partial \tilde{U}_b}{\partial \kappa_{xy}} \kappa_{xy} &= 2\tilde{U}_b \\ \frac{\partial \tilde{U}_s}{\partial \gamma_x} \gamma_x + \frac{\partial \tilde{U}_s}{\partial \gamma_y} \gamma_y &= 2\tilde{U}_s \\ \frac{\partial \tilde{U}}{\partial \kappa_x} \kappa_x + \frac{\partial \tilde{U}}{\partial \kappa_y} \kappa_y + \frac{\partial \tilde{U}}{\partial \kappa_{xy}} \kappa_{xy} + \frac{\partial \tilde{U}}{\partial \gamma_x} \gamma_x + \frac{\partial \tilde{U}}{\partial \gamma_y} \gamma_y &= 2\tilde{U} \end{aligned} \right\} \quad (8-35)$$

Secondly, the physical equations between internal forces and strains can be expressed in terms of the strain energy density \tilde{U} . For this reason, the derivatives of \tilde{U} are first obtained as follows:

$$\left. \begin{aligned} \frac{\partial \tilde{U}}{\partial \kappa_x} &= D(\kappa_x + \mu\kappa_y), & \frac{\partial \tilde{U}}{\partial \kappa_y} &= D(\kappa_y + \mu\kappa_x), & \frac{\partial \tilde{U}}{2\partial \kappa_{xy}} &= D(1-\mu)\kappa_{xy} \\ \frac{\partial \tilde{U}}{\partial \gamma_x} &= C\gamma_x, & \frac{\partial \tilde{U}}{\partial \gamma_y} &= C\gamma_y \end{aligned} \right\} \quad (8-36)$$

From the above equations, it can be seen that the physical Eq. (8-11) can be expressed in terms of the strain energy density \tilde{U} as follows:

$$\left. \begin{aligned} M_x &= \frac{\partial \tilde{U}}{\partial \kappa_x}, & M_y &= \frac{\partial \tilde{U}}{\partial \kappa_y}, & M_{xy} &= \frac{\partial \tilde{U}}{2\partial \kappa_{xy}} \\ Q_x &= \frac{\partial \tilde{U}}{\partial \gamma_x}, & Q_y &= \frac{\partial \tilde{U}}{\partial \gamma_y} \end{aligned} \right\} \quad (8-37)$$

Finally, the variation of the strain energy is given as:

$$\delta U = \iint_{\Omega} \delta \tilde{U} dx dy \quad (8-38)$$

i.e.,

$$\begin{aligned} \delta U &= \iint_{\Omega} \left[\frac{\partial \tilde{U}}{\partial \kappa_x} \delta \kappa_x + \frac{\partial \tilde{U}}{\partial \kappa_y} \delta \kappa_y + \frac{\partial \tilde{U}}{\partial \kappa_{xy}} \delta \kappa_{xy} + \frac{\partial \tilde{U}}{\partial \gamma_x} \delta \gamma_x + \frac{\partial \tilde{U}}{\partial \gamma_y} \delta \gamma_y \right] dx dy \\ &= \iint_{\Omega} [M_x \delta \kappa_x + M_y \delta \kappa_y + 2M_{xy} \delta \kappa_{xy} + Q_x \delta \gamma_x + Q_y \delta \gamma_y] dx dy \end{aligned} \quad (8-39)$$

The above equation indicates that the variation of the strain energy equals to the work done by the corresponding internal forces on the variation of strains.

8.1.7 Strain Complementary Energy

Firstly, the definitions of the strain complementary energy density \tilde{V} and strain complementary energy V of the thick plate are given.

For a given internal force vector \mathbf{S} (including internal moments \mathbf{M} and shear forces \mathbf{Q}):

$$\left. \begin{aligned} \mathbf{S} &= [M_x \quad M_y \quad M_{xy} \quad Q_x \quad Q_y]^T \\ \mathbf{M} &= [M_x \quad M_y \quad M_{xy}]^T \\ \mathbf{Q} &= [Q_x \quad Q_y]^T \end{aligned} \right\} \quad (8-40)$$

the function $\tilde{V}(\mathbf{S})$ can be defined as:

$$\tilde{V}(\mathbf{S}) = \tilde{V}_b(\mathbf{M}) + \tilde{V}_s(\mathbf{Q}) \quad (8-41)$$

$$\tilde{V}_b(\mathbf{M}) = \frac{1}{2} \mathbf{M}^T \mathbf{D}^{-1} \mathbf{M} = \frac{1}{2(1-\mu^2)D} [M_x^2 + M_y^2 - 2\mu M_x M_y + 2(1+\mu)M_{xy}^2] \quad (8-42)$$

$$\tilde{V}_s(\mathbf{Q}) = \frac{1}{2} \mathbf{Q}^T \mathbf{C}^{-1} \mathbf{Q} = \frac{1}{2C} (Q_x^2 + Q_y^2) \quad (8-43)$$

$\tilde{V}(\mathbf{S})$ is the strain complementary energy density of the thick plate; $\tilde{V}_b(\mathbf{M})$ is the bending strain complementary energy density; $\tilde{V}_s(\mathbf{Q})$ is the shear strain complementary energy density.

The strain complementary energy V of the thick plate is defined as the functional of the internal force fields \mathbf{S} :

$$\begin{aligned}
 V(\mathbf{S}) &= \iint_{\Omega} \tilde{V}(\mathbf{S}) dx dy = \iint_{\Omega} \left(\frac{1}{2} \mathbf{M}^T \mathbf{D}^{-1} \mathbf{M} + \frac{1}{2} \mathbf{Q}^T \mathbf{C}^{-1} \mathbf{Q} \right) dx dy \\
 &= \iint_{\Omega} \left\{ \frac{1}{2(1-\mu^2)D} [M_x^2 + M_y^2 - 2\mu M_x M_y + 2(1+\mu)M_{xy}^2] + \frac{1}{2C} (Q_x^2 + Q_y^2) \right\} dx dy
 \end{aligned} \tag{8-44}$$

Two points should be noted:

(1) For arbitrary internal force fields \mathbf{S} , no matter whether these internal force fields satisfy the equilibrium differential Eq. (8-3) and boundary conditions under given loads, the strain complementary energy corresponding to \mathbf{S} can be defined.

(2) From Eqs. (8-42) and (8-43), it can be seen that $\tilde{V}_b(\mathbf{M})$ and $\tilde{V}_s(\mathbf{Q})$ are the positive definite quadric homogeneous functions of (M_x, M_y, M_{xy}) and (Q_x, Q_y) , respectively. According to the properties of the positive definite quadric homogeneous function, the following equalities can be obtained:

$$\left. \begin{aligned}
 \frac{\partial \tilde{V}_b}{\partial M_x} M_x + \frac{\partial \tilde{V}_b}{\partial M_y} M_y + \frac{\partial \tilde{V}_b}{\partial M_{xy}} M_{xy} &= 2\tilde{V}_b \\
 \frac{\partial \tilde{V}_s}{\partial Q_x} Q_x + \frac{\partial \tilde{V}_s}{\partial Q_y} Q_y &= 2\tilde{V}_s \\
 \frac{\partial \tilde{V}}{\partial M_x} M_x + \frac{\partial \tilde{V}}{\partial M_y} M_y + \frac{\partial \tilde{V}}{\partial M_{xy}} M_{xy} + \frac{\partial \tilde{V}}{\partial Q_x} Q_x + \frac{\partial \tilde{V}}{\partial Q_y} Q_y &= 2\tilde{V}
 \end{aligned} \right\} \tag{8-45}$$

The derivatives of the strain complementary energy density are given as follows:

$$\left. \begin{aligned}
 \frac{\partial \tilde{V}}{\partial M_x} &= \frac{M_x - \mu M_y}{D(1-\mu^2)}, & \frac{\partial \tilde{V}}{\partial Q_x} &= \frac{Q_x}{C} \\
 \frac{\partial \tilde{V}}{\partial M_y} &= \frac{M_y - \mu M_x}{D(1-\mu^2)}, & \frac{\partial \tilde{V}}{\partial Q_y} &= \frac{Q_y}{C} \\
 \frac{\partial \tilde{V}}{\partial M_{xy}} &= \frac{2(1+\mu)}{D(1-\mu^2)} M_{xy}
 \end{aligned} \right\} \tag{8-46}$$

By using the above derivative formulae, the physical Eq. (8-18) between internal forces and strains can be expressed in terms of the strain complementary energy density \tilde{V} as follows:

$$\left. \begin{aligned}
 \kappa_x &= \frac{\partial \tilde{V}}{\partial M_x}, & \gamma_x &= \frac{\partial \tilde{V}}{\partial Q_x} \\
 \kappa_y &= \frac{\partial \tilde{V}}{\partial M_y}, & \gamma_y &= \frac{\partial \tilde{V}}{\partial Q_y} \\
 2\kappa_{xy} &= \frac{\partial \tilde{V}}{\partial M_{xy}}
 \end{aligned} \right\} \tag{8-47}$$

Finally, the variation of the strain complementary energy is given as:

$$\begin{aligned} \delta V &= \iint_{\Omega} \delta \tilde{V} dx dy \\ &= \iint_{\Omega} \left[\frac{\partial \tilde{V}}{\partial M_x} \delta M_x + \frac{\partial \tilde{V}}{\partial M_y} \delta M_y + \frac{\partial \tilde{V}}{\partial M_{xy}} \delta M_{xy} + \frac{\partial \tilde{V}}{\partial Q_x} \delta Q_x + \frac{\partial \tilde{V}}{\partial Q_y} \delta Q_y \right] dx dy \end{aligned} \quad (8-48)$$

Substitution of Eq. (8-47) into the above equation yields

$$\delta V = \iint_{\Omega} [\kappa_x \delta M_x + \kappa_y \delta M_y + 2\kappa_{xy} \delta M_{xy} + \gamma_x \delta Q_x + \gamma_y \delta Q_y] dx dy$$

The above equation indicates that the variation of the strain complementary energy equals to the work done by the variation of internal forces on the corresponding strains.

8.2 Comparison of the Theories for Thick Plates and Thin Plates

According to the contents in the previous section, this section will introduce the differences between the theories for thick plates and thin plates. Comparisons are made in fundamental equations and typical numerical examples.

8.2.1 Comparison of Fundamental Equations

1. Notes on the basic assumptions of deformation

In the thin plate theory, the Kirchhoff normal assumption is adopted—The normal of the mid-surface before deformation will still be the normal of the mid-surface after deformation.

In the thick plate theory, the Reissner-Mindlin straight-line assumption is adopted—The normal of the mid-surface before deformation will still be a straight line after deformation, but generally not the normal of the mid-surface anymore.

One uses the normal assumption while the other uses the straight-line assumption, this exhibits the essential difference of the two theories.

2. Notes on the shear deformation problem

Since the Kirchhoff normal assumption is adopted in the thin plate theory, the transverse shear strains γ_x and γ_y will keep zero during the deformations of the

thin plates, and then, the normal rotations ψ_x and ψ_y will keep being equal to the mid-surface slopes $\frac{\partial w}{\partial x}$ and $\frac{\partial w}{\partial y}$, as shown in Eq. (8-2).

The Reissner-Mindlin straight-line assumption is adopted in the thick plate theory, hence, in general, the normal rotations ψ_x and ψ_y of the thick plates will not keep being equal to the mid-surface slopes $\frac{\partial w}{\partial x}$ and $\frac{\partial w}{\partial y}$. Their differences are the transverse shear strains γ_x and γ_y , as shown in Eq. (8-1).

The essential differences between these two plate theories are:

- (1) Whether the influences of the transverse shear strains are considered or not.
- (2) Whether the normal rotations are equal to the mid-surface slopes or not.

From above, we can also conclude that:

(1) For shear stiffness: $C = \infty$ is assumed in the thin plate theory while C is a finite value in the thick plate theory.

(2) For strain energy: in the thick plate theory, strain energy U is the sum of the bending strain energy U_b and the shear strain energy U_s ; while in the thin plate theory, $U = U_b$ because of $U_s = 0$.

That the shear stiffness C is looked upon as infinite, and the shear strain energy U_s is neglected, are the inevitable results of ignoring the influences of shear deformations in the thin plate theory.

3. Notes on the independent displacements in w , ψ_x and ψ_y

In the thin plate theory, ψ_x and ψ_y are equal to the derivatives of w , so they are not independent displacements. Thus, in the 3 displacements w , ψ_x and ψ_y , only w is independent.

In the thick plate theory, since two new fields γ_x and γ_y appear, w , ψ_x and ψ_y are 3 independent displacement fields.

Independence or dependence between the displacement fields w and (ψ_x, ψ_y) is another essential difference between these two plate theories.

When constructing a universal displacement-based element for both thick and thin plates, one main difficulty encountered is how to deal with the dual requirements of independence and dependence.

Only one independent displacement w is considered for constructing the thin plate element, while 3 independent displacements w , ψ_x and ψ_y must be taken into account for constructing the thick plate element. From this viewpoint, it seems that the development of a thick plate element is more complicated than that of a thin plate element. But, if we observe the expressions of strain energy, it can be seen that the integrands in the strain energy expression (8-34) of the thick plate element contain only first-order derivatives of w , ψ_x and ψ_y , so it belongs to C^0 -continuity problem. On the other hand, the integrands in the strain energy expression of the thin plate element contain second-order derivatives of w , thus, it belongs to C^1 -continuity problem. Therefore, the construction of the thick

plate elements is indeed easier than that of the thin plate element. Anyway, it is easier to construct elements special for the thick plates, but more difficult to construct elements special for the thin plates, and much more difficult to develop universal elements for both thick and thin plates.

4. Notes on the boundary conditions

In the thick plate theory, several typical boundary conditions have been given by Eq. (8-29), in which each boundary has 3 boundary conditions, i.e.,

On fixed edge C_1

$$w = \bar{w}, \quad \psi_s = \bar{\psi}_s, \quad \psi_n = \bar{\psi}_n \quad (8-49a,b,c)$$

On simply-supported (hard) edge C_2

$$w = \bar{w}, \quad \psi_s = \bar{\psi}_s, \quad M_n = \bar{M}_n \quad (8-50a,b,c)$$

On simply-supported (soft) edge C'_2

$$w = \bar{w}, \quad M_{ns} = \bar{M}_{ns}, \quad M_n = \bar{M}_n \quad (8-51a,b,c)$$

On free edge C_3

$$M_n = \bar{M}_n, \quad M_{ns} = \bar{M}_{ns}, \quad Q_n = \bar{Q}_n \quad (8-52a,b,c)$$

Here, the conditions on the fixed edge are all displacement conditions; conditions on the free edge are all force conditions; and conditions on the simply-supported edge are mixed conditions of displacement and force.

In the thin plate theory, since the transverse shear strains are assumed to be zero, the following assumption

$$\psi_s = \frac{\partial w}{\partial s} \quad (8-53)$$

is imposed on the boundary. Thus, the boundary tangent rotation ψ_s is a non-independent displacement relied on boundary deflection w , thereupon, the number of DOFs at each point of the boundary will decrease from 3 (w, ψ_s, ψ_n) to 2 (w, ψ_n), and the number of the boundary conditions will also decrease from 3 to 2.

Firstly, let us consider the fixed edge case. According to the assumption given in Eq. (8-53), the second boundary condition in Eq. (8-49) can be derived from the first boundary condition. So, after the elimination of this non-independent condition, only 2 independent boundary conditions (8-49a,c) remain.

Secondly, let us consider the simply-supported edge case. In the thin plate theory, there are 2 boundary conditions on the simply-supported edge:

$$w = \bar{w}, \quad M_n = \bar{M}_n$$

These are Eqs. (8-50a,c), and also Eqs. (8-51a,c). In the thick plate theory, there are 3 boundary conditions on the simply-supported edge, that is to say, one condition of tangent rotation along the boundary should be supplemented. If the displacement condition (8-50b) $\psi_s = \bar{\psi}_s$ is supplemented, then the boundary is called as hard simply-supported edge; if the force condition (8-51b) $M_{ns} = \bar{M}_{ns}$ is supplemented, then the boundary is called as soft simply-supported edge. Therefore, in the thick plate theory, there are two types of simply-supported edge: hard and soft; but in the thin plate theory, only one type exists.

Finally, let us consider the free edge case. In the thin plate theory, the boundary conditions (8-52) will be replaced by the following two conditions:

On free edge C_3

$$M_n = \bar{M}_n, \quad \frac{\partial M_{ns}}{\partial s} + Q_n = \bar{V}_n \quad (8-54a,b)$$

i.e., two conditions (b) and (c) in Eq. (8-52) are replaced by one condition (b) in Eq. (8-54). Indeed, this is also the inevitable result by introducing the assumption (8-53). Here, \bar{V}_n is the density of the distributed transverse load along the free edge of the thin plate.

Now, from the viewpoint of virtual work, the boundary conditions on the free edge in thick and thin plate theories are explained as follows.

In the thick plate theory, there are 3 independent displacements w , ψ_n and ψ_s on the free boundary edge. Assume that the virtual displacements on the free edge are δw , $\delta \psi_n$ and $\delta \psi_s$, the virtual work done by the boundary forces is

$$\delta W = \int_{C_3} [-M_n \delta \psi_n - M_{ns} \delta \psi_s + Q_n \delta w] ds \quad (8-55)$$

On the other hand, the virtual work done by the given loads on the free edge is

$$\delta \bar{W} = \int_{C_3} [-\bar{M}_n \delta \psi_n - \bar{M}_{ns} \delta \psi_s + \bar{Q}_n \delta w] ds \quad (8-56)$$

Let $\delta W = \delta \bar{W}$, and since the virtual displacements δw , $\delta \psi_n$ and $\delta \psi_s$ are 3 independent arbitrary functions, the 3 boundary conditions in Eqs. (8-52a,b,c) can be obtained.

In the thin plate theory, since the assumption in Eq. (8-53) is introduced, there are only 2 independent virtual displacements δw and $\delta \psi_n$, and $\delta \psi_s = \frac{\partial \delta w}{\partial s}$. The work done by the boundary force is

$$\delta W = \int_{C_3} \left[-M_n \delta \psi_n - M_{ns} \frac{\partial \delta w}{\partial s} + Q_n \delta w \right] ds \quad (8-57)$$

By using the formula of integration by parts, we obtain

$$\delta W = \int_{C_3} \left[-M_n \delta \psi_n + \left(\frac{\partial M_{ns}}{\partial s} + Q_n \right) \delta w \right] ds - M_{ns} \delta w \Big|_{C_3^-}^{C_3^+} \quad (8-58)$$

in which C_3^- and C_3^+ are two ends of the free edge. Since the two ends of the free edge link with the fixed edge or the simply-supported edge, at C_3^- and C_3^+ , $\delta w = 0$, and then the above equation can be written as

$$\delta W = \int_{C_3} \left[-M_n \delta \psi_n + \left(\frac{\partial M_{ns}}{\partial s} + Q_n \right) \delta w \right] ds \quad (8-59)$$

On the other hand, the work done by the given loads on the free edge is

$$\delta \bar{W} = \int_{C_3} [-\bar{M}_n \delta \psi_n + \bar{V}_n \delta w] ds \quad (8-60)$$

Let $\delta W = \delta \bar{W}$, and since $\delta \psi_n$ and δw are 2 arbitrary functions, the 2 boundary conditions on the free edge of the thin plate can be obtained, as shown in Eq. (8-54a,b).

The above discussions about the boundary conditions are expounded from the viewpoint of virtual work. This expatiation method is very natural and evident.

In the thick plate theory, the expression of the boundary virtual work is Eq. (8-55), where ψ_n , ψ_s and w are 3 independent generalized displacements; and $(-M_n)$, $(-M_{ns})$ and Q_n are 3 conjugate (or corresponding) independent generalized forces, respectively. Thereby, in the thick plate theory, there are 3 independent boundary conditions, which are generally expressed by

$$\psi_n = \bar{\psi}_n \quad \text{or} \quad M_n = \bar{M}_n \quad (8-61a)$$

$$\psi_s = \bar{\psi}_s \quad \text{or} \quad M_{ns} = \bar{M}_{ns} \quad (8-61b)$$

$$w = \bar{w} \quad \text{or} \quad Q_n = \bar{Q}_n \quad (8-61c)$$

In the thin plate theory, the expression of boundary virtual work is Eq. (8-59), where ψ_n and w are 2 independent generalized displacements; and $(-M_n)$ and $\left(\frac{\partial M_{ns}}{\partial s} + Q_n \right)$ are 2 conjugate (or corresponding) independent generalized forces, respectively. Thereby, in the thin plate theory, there are 2 independent boundary conditions, which are generally expressed by

$$\psi_n = \bar{\psi}_n \quad \text{or} \quad M_n = \bar{M}_n \quad (8-62a)$$

$$w = \bar{w} \quad \text{or} \quad \frac{\partial M_{ns}}{\partial s} + Q_n = \bar{V}_n \tag{8-62b}$$

where $\frac{\partial M_{ns}}{\partial s}$ is called as the equivalent transverse shear force of the twisting moment M_{ns} ; and $\frac{\partial M_{ns}}{\partial s} + Q_n = V_n$ is called as the resultant transverse shear force.

In the above discussions, the concept that the generalized force P and the generalized displacement Δ are conjugate with each other is mentioned. Its definition can be given as follows.

If the virtual work W done by the generalized force P along the generalized displacement Δ is equal to the product $P\Delta$, i.e.,

$$W = P\Delta \tag{8-63}$$

then, we say that the generalized displacement Δ and the generalized force P are conjugate with each other (or corresponding to each other).

5. Notes on the independent load components and internal force components

Firstly, let us discuss the load components.

In the thick plate theory, since there are 3 independent displacement components w , ψ_x and ψ_y , there should be 3 independent load components q , m_x and m_y corresponding to them. So, the expression of virtual work is

$$\delta W = \iint_A [q\delta w + m_x\delta\psi_x + m_y\delta\psi_y] dA \tag{8-64}$$

From this virtual work expression, it can be seen that 3 load components and 3 displacement components are corresponding to or conjugate with each other.

In the thin plate theory, since there is only one independent transverse displacement component w , and the rotation components ψ_x and ψ_y are both relied on w , there should be only one independent transverse load component q corresponding to it, and the couple load components m_x and m_y should be converted to equivalent transverse load components on dA with line distributed transverse load on the boundary ds . So, the expression of virtual work is

$$\begin{aligned} \delta W &= \iint_A \left[q\delta w + m_x \frac{\partial \delta w}{\partial x} + m_y \frac{\partial \delta w}{\partial y} \right] dA \\ &= \iint_A \left(q - \frac{\partial m_x}{\partial x} - \frac{\partial m_y}{\partial y} \right) \delta w dA + \oint_{\partial A} (m_x l + m_y m) \delta w ds \end{aligned} \tag{8-65}$$

Therefore, after conversion, the surface load q^* and boundary load V_n^* are

$$q^* = q - \frac{\partial m_x}{\partial x} - \frac{\partial m_y}{\partial y} \quad (8-66a)$$

$$V_n^* = m_x l + m_y m \quad (8-66b)$$

Secondly, let us discuss the internal force components.

In the thick plate theory, there are 5 independent internal force components. That is to say, besides the bending moments M_x , M_y and twisting moment M_{xy} , the transverse shear forces Q_x and Q_y are also independent internal force components. It can be seen from the equilibrium differential Eq. (8-3) that, since there are independent couple load components m_x and m_y existing, Q_x and Q_y in the thick plate theory do not completely rely on M_x , M_y and M_{xy} , they are independent internal force components. On the contrary, in the thin plate theory, since $m_x = m_y = 0$ is assumed, Q_x and Q_y completely rely on M_x , M_y and M_{xy} , Q_x and Q_y will not be looked upon as independent internal force components. That is to say, there are only 3 independent internal force components in the thin plate theory.

8.2.2 Comparison of Typical Examples

1. The special case in which the same internal force solution is obtained by both thin beam theory and thick beam theory in beam and frame analysis

The beam theories can be classified as thin beam theory and thick beam theory. Their difference is whether the influence of the shear strain is ignored or not.

When these two theories are employed in beam and frame analysis, except the special case of pure bending state in which the shear strain is zero, the displacement solutions of the two theories are generally different, but the internal force solutions may be either same or different. Now, we discuss the case in which the internal force solutions are the same as each other.

Firstly, if beam and frame are statically determinate structures, the internal force solutions by the two theories will be the same as each other, but for displacement solutions, there will be a discrepancy of an additional displacement purely caused by shear strain, i.e.,

$$M = M^0, \quad Q = Q^0 \quad (8-67)$$

$$\Delta = \Delta^0 + \tilde{\Delta}(\gamma) \quad (8-68)$$

where M , Q and Δ are the bending moment, shear force and displacement of the thick beam theory, respectively; M^0 , Q^0 and Δ^0 are the bending moment, shear

Advanced Finite Element Method in Structural Engineering

force and displacement of the thin beam theory, respectively; $\tilde{\Delta}(\gamma)$ is the additional displacement caused by shear strain.

Secondly, consider the case of the statically indeterminate structures. If the following examples are considered:

- (1) the shear force is statically determinate (Fig. 8.5(a));
- (2) the shear force is statically determinate under symmetrical load (Fig. 8.6(a));
- (3) the shear force of the non-rigid bar is statically determinate (Fig. 8.7(a)), there is still a rigid bar in the frame, but its shear strain is identically equal to zero, so it is not necessary to consider whether its shear forces are statically determinate).

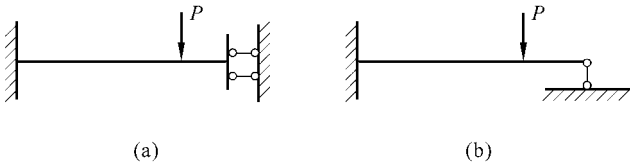


Figure 8.5 Statically indeterminate beams
 (a) A slipping support at the right end; (b) A vertical support at the right end

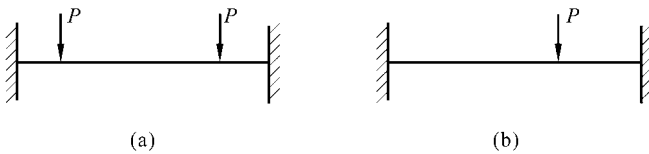


Figure 8.6 Statically indeterminate symmetrical beams
 (a) Symmetrical load; (b) Unsymmetrical load

It follows that the internal force solutions by the two theories will be the same as each other.

For comparison, examples which do not belong to the above cases are given in Figs. 8.5(b), 8.6(b) and 8.7(b).

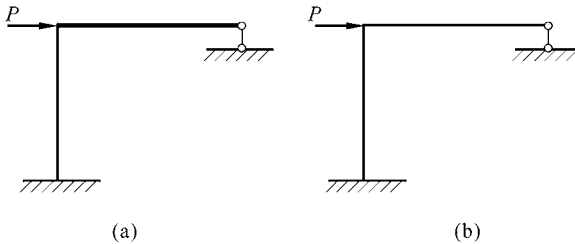


Figure 8.7 Statically indeterminate frames
 (a) Horizontal beam is a rigid bar; (b) Horizontal beam is not a rigid bar

The above conclusion can be proved as follows.

Assume that the degree of statical indeterminacy for the structure is n . The structure is analyzed using the force method, and the corresponding statically

determinate structure is taken as the basic structure. In the n redundant unknown forces, assume that m forces are nonzero ($m \leq n$), then the bending moment M and shear force Q can be expressed as

$$M = M_P + \sum_{i=1}^m \bar{M}_i X_i \quad (8-69a)$$

$$Q = Q_P + \sum_{i=1}^m \bar{Q}_i X_i \quad (8-69b)$$

where M_P and Q_P are the internal forces caused by loads in the basic structure; \bar{M}_i and \bar{Q}_i are the internal forces caused by unit redundant force $X_i = 1$ in the basic structure; X_1, X_2, \dots, X_m are m nonzero redundant unknown forces. $M_P, \bar{M}_i, Q_P, \bar{Q}_i$ are all determined by the equilibrium conditions.

Since the shear forces of each non-rigid bar are assumed to be statically determinate, for each non-rigid bar, we can set

$$\bar{Q}_i = 0 \quad (i = 1, 2, \dots, m) \quad (8-70)$$

The redundant unknown forces X_1, X_2, \dots, X_m can be solved by the fundamental equations of force method.

For the thick beam theory, we have

$$\sum_{j=1}^m \delta_{ij} X_j + \Delta_{iP} = 0 \quad (i = 1, 2, \dots, m)$$

where

$$\delta_{ij} = \sum \int \frac{\bar{M}_i \bar{M}_j}{D} ds + \sum \int \frac{\bar{Q}_i \bar{Q}_j}{C} ds$$

$$\Delta_{iP} = \sum \int \frac{\bar{M}_i M_P}{D} ds + \sum \int \frac{\bar{Q}_i Q_P}{C} ds$$

in which D and C are the section bending and shearing stiffness, respectively.

For the thin beam theory, we have

$$\sum_{j=1}^m \delta_{ij}^0 X_j + \Delta_{iP}^0 = 0 \quad (i = 1, 2, \dots, m)$$

where

$$\delta_{ij}^0 = \sum \int \frac{\bar{M}_i \bar{M}_j}{D} ds$$

$$\Delta_{iP}^0 = \sum \int \frac{\bar{M}_i M_P}{D} ds$$

By using Eq. (8-70), we have

$$\delta_{ij} = \delta_{ij}^0, \quad \Delta_{iP} = \Delta_{iP}^0 \quad (8-71)$$

Therefore, the redundant unknown forces X_1, X_2, \dots, X_m solved by the two theories are the same as each other. Substituting these solutions into Eq. (8-69), it can be seen that the internal force solutions obtained by the two theories are the same as each other. \square

2. The special case in which the same internal force solution is obtained by both thin plate theory and thick plate theory

The following problems belong to this special case:

- (1) Simply-supported polygonal plate;
- (2) Circular plate with axisymmetric deformation;
- (3) The plate problems in which the shear forces Q_x and Q_y are statically determinate.

The proofs about the above conclusions can be referred to reference [3].

3. The concentrated load problem

Consider a clamped circular plate (the radius is a) subjected to a concentrated load P at the center point C .

The displacement solution and the deflection at point C of the thin plate theory are

$$w^0 = \frac{Pr^2}{8\pi D} \ln \frac{r}{a} + \frac{P}{16\pi D} (a^2 - r^2) \quad (8-72a)$$

$$w_C^0 = \frac{Pa^2}{16\pi D} \quad (8-72b)$$

The displacement solutions and the deflection at point C of the thick plate theory are

$$w = w^0 - \frac{P}{2\pi C} \ln \frac{r}{a} \quad (8-73a)$$

$$\psi_r = \frac{dw^0}{dr} \quad (8-73b)$$

$$w_C = \infty \quad (8-73c)$$

From the above results, it can be seen that, the deflection at the load point C of the concentrated load is a finite value by the thin plate theory, but an infinite value

by the thick plate theory. This distinction is completely caused by the influence of the shear strain. In fact, the second term at the right side of Eq. (8-73a) is the additional deflection $\tilde{w}(r)$ purely caused by shear strain.

$$\tilde{w}(r) = -\frac{P}{2\pi C} \ln \frac{r}{a} \quad (8-74)$$

The above equation can be derived as follows.

Firstly, the shear force Q_r is statically determinate, i.e.,

$$Q_r = -\frac{P}{2\pi r} \quad (8-75)$$

The shear strain γ_r is

$$\gamma_r = \frac{Q_r}{C} = -\frac{P}{2\pi r C} \quad (8-76)$$

Secondly, $\tilde{\psi}_r = 0$ should be assumed when the additional deflection \tilde{w} caused by the shear strain is being solved, so we obtain

$$\frac{d\tilde{w}}{dr} = \gamma_r = -\frac{P}{2\pi r C}$$

After integration, we have

$$\tilde{w} = -\frac{P}{2\pi C} \ln r + C_1$$

where constant C_1 can be solved by the boundary condition $w|_{r=a} = 0$ at $r = a$.

Finally, Eq. (8-74) can be obtained. \square

From Eqs. (8-75) and (8-76), it can be seen that the values of Q_r and γ_r at point C are both infinite, which are corresponding to the result $\tilde{w}_C = \infty$.

4. High-order vibration problem

In the vibration analysis of plate, there are two different points between the thick and thin plate theories: one is whether the influence of shear deformation is considered; the other is whether the influence of rotary inertia is considered.

In order to explain the distinction of the second point, the kinetic equations for the natural vibration problem of the thick plate are given as follows:

$$\frac{\partial M_x}{\partial x} + \frac{\partial M_{xy}}{\partial y} - Q_x - \omega^2 \rho J \psi_x = 0 \quad (8-77a)$$

$$\frac{\partial M_{xy}}{\partial x} + \frac{\partial M_y}{\partial y} - Q_y - \omega^2 \rho J \psi_y = 0 \quad (8-77b)$$

$$\frac{\partial Q_x}{\partial x} + \frac{\partial Q_y}{\partial y} + \omega^2 \rho h w = 0 \quad (8-77c)$$

where ω is the natural frequency; ρ is the density of material; ρh is the mass of the unit area on the mid-surface of the plate; ρJ is the rotary inertia. In the thin plate theory, the influence of rotary inertia is ignored.

In high-order vibrations, the effective length and width of the high-order modes become smaller, so the influence of rotary inertia and shear deformation will increase. Thereby, although a plate may belong to the thin plate type, for the analysis of the high-order vibration of this thin plate, it is more reasonable to employ the thick plate theory.

5. Stress concentration problem near a circular hole

Consider an infinite plate with a circular hole (the radius is a). At its infinite edge, the plate is under pure bending state along x -axis, i.e., $M_x = M_0$, and other internal force components are all zero. Now, let us solve the stress concentration coefficient k_B near the circular hole, which is defined as

$$k_B = \frac{M_{\theta \max}}{M_0} \quad (8-78)$$

where $M_{\theta \max}$ denotes the maximum value of the bending moment M_{θ} at the circular hole boundary.

According to the thin plate theory, we have

$$k_B^0 = \frac{5 + 3\mu}{3 + \mu} \quad (8-79)$$

When the Poisson's ratio $\mu = \frac{1}{3}$, $k_B^0 = 1.8$.

According to the Reissner thick plate theory, we have

$$k_B = \frac{3}{2} + \frac{1}{2} \cdot \frac{\frac{3}{2}(1 + \mu)K_2\left(\sqrt{10}\frac{a}{h}\right) - K_0\left(\sqrt{10}\frac{a}{h}\right)}{\frac{1}{2}(1 + \mu)K_2\left(\sqrt{10}\frac{a}{h}\right) + K_0\left(\sqrt{10}\frac{a}{h}\right)} \quad (8-80)$$

where K_0 and K_2 are the modified Bessel functions. When $\mu = \frac{1}{3}$, the variations

of k_B and k_B^0 are plotted in Fig. 8.8 and listed in Table 8.1.

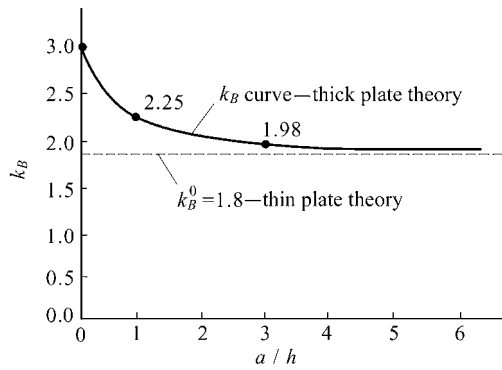


Figure 8.8 The stress concentration coefficient ($\mu = 1/3$)

Table 8.1 The comparison between stress concentration coefficients k_B and k_B^0

a/h	0	1	3
Solution of thick plate theory k_B	3.00	2.25	1.98
Solution of thin plate theory k_B^0	1.80	1.80	1.80
Error $\frac{k_B - k_B^0}{k_B}$	40%	20%	9%

It can be seen that, in the stress concentration problems of plate bending, the influence of the transverse shear strain should not be ignored. The solution of the thin plate theory k_B^0 is always less than the solution of the thick plate theory k_B . Therefore, the solution of the thin plate theory is more unsafe. Errors will increase with the decrease of a/h , and the maximum error is up to 40%.

6. Stress distribution near free edge

As pointed out in the previous sections, for the boundary conditions of the free edge, the expressions from the two theories are different: the thick plate theory requires 3 boundary conditions (8-52a,b,c) to be satisfied, but thin plate theory cannot satisfy them and requires only 2 boundary conditions (8-54a,b) to be satisfied. Therefore, the solutions on or near the free edge of the two theories are always discrepant.

In order to understand the discrepancy in the solutions near the free edge of the two theories, the stress concentration problem near a circular hole mentioned above is still used to illustrate the problem of this section.

Firstly, according to thin plate theory, solutions of Q_r^0 , $M_{r\theta}^0$ and V_r are

$$\left. \begin{aligned} Q_r^0 &= \frac{4}{3+\mu} M_0 \frac{a^2}{r^3} \cos 2\theta \\ M_{r\theta}^0 &= \frac{1}{3+\mu} M_0 \left[-2 + (1-\mu) \left(\frac{a^2}{r^2} - 1 \right) - \frac{3}{2} (1-\mu) \left(\frac{a^4}{r^4} - 1 \right) \right] \sin 2\theta \\ V_r &= \frac{1}{3+\mu} M_0 \frac{1}{r} \left[2(3-\mu) \left(\frac{a^2}{r^2} - 1 \right) - 3(1-\mu) \left(\frac{a^4}{r^4} - 1 \right) \right] \cos 2\theta \end{aligned} \right\} \quad (8-81)$$

It can be seen that at the boundary $r = a$ of the circular hole, only the boundary condition $V_r = 0$ is satisfied, while Q_r^0 and $M_{r\theta}^0$ are both nonzero at the boundary.

Secondly, according to the thick plate theory, the solutions of Q_r and $M_{r\theta}$ are

$$\left. \begin{aligned} Q_r &= Q_r^0 + \tilde{Q}_r \\ M_{r\theta} &= M_{r\theta}^0 + \tilde{M}_{r\theta} \end{aligned} \right\} \quad (8-82)$$

where, when $\frac{a}{h} \gg 1$, we have

$$\left. \begin{aligned} \tilde{Q}_r &= -\frac{4}{3+\mu} M_0 \frac{1}{r} \sqrt{\frac{a}{r}} e^{-\sqrt{10} \left(\frac{r-a}{h} \right)} \cos 2\theta \\ \tilde{M}_{r\theta} &= \frac{2}{3+\mu} M_0 \sqrt{\frac{a}{r}} e^{-\sqrt{10} \left(\frac{r-a}{h} \right)} \sin 2\theta \end{aligned} \right\} \quad (8-83)$$

It can be seen that at the boundary $r = a$ of the circular hole, both the boundary conditions $Q_r = 0$ and $M_{r\theta} = 0$ are satisfied indeed.

Let \tilde{Q}_r and $\tilde{M}_{r\theta}$ be the differences $Q_r - Q_r^0$ and $M_{r\theta} - M_{r\theta}^0$ of the solutions from the two theories, respectively. Both \tilde{Q}_r and $\tilde{M}_{r\theta}$ contain the exponential term $e^{-\sqrt{10} \left(\frac{r-a}{h} \right)}$, which is a rapid attenuation function (refer to Table 8.2). For example, when $\frac{r-a}{h}$ increases from 0 to 1, the function value will decrease

from 1 to 4%. Therefore, the solutions of the two theories are discrepant only within a very small neighborhood near the free edge. The scale of this neighborhood belongs to the same magnitude of the thickness h of the plate. Outside the neighborhood, the internal force solutions of the thin plate theory are still suitable.

The solutions of the thick plate theory contain exponential function which will rapidly decay when they are away from the boundary, and this phenomenon is called as edge effect. The solutions (8-81) of the thin plate theory do not contain this type of exponential function, so there is no edge effect phenomenon.

Table 8.2 Exponential function $e^{-\sqrt{10}\left(\frac{r-a}{h}\right)}$

$\frac{r-a}{h}$	0	1/4	1/2	3/4	1	2
$e^{-\sqrt{10}\left(\frac{r-a}{h}\right)}$	1.0000	0.4538	0.2058	0.0933	0.0424	0.0018

7. Contact problem

Consider the beam contact problem shown in Fig. 8.9^[3]. The left end of the beam is fixed, and the right free end is subjected to a concentrated load P . Below the beam, there is a circular rigid foundation (the radius is r_1). Under the action of load P , the left segment of the beam ($0 \leq x \leq x_1$) will contact with the rigid foundation, and the contact length x_1 will increase with P . This is a contact problem.

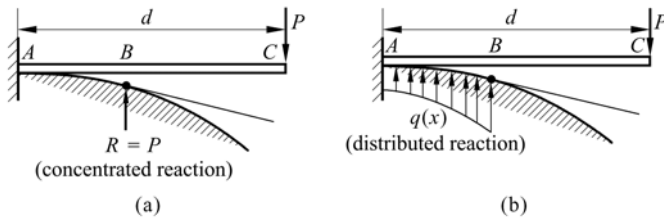


Figure 8.9 Contact problem of beam
 (a) Solutions of thin beam theory; (b) Solutions of thick beam theory

Firstly, we solve this problem according to the thin beam theory. In the contact segment $0 \leq x \leq x_1$, the deflection is

$$w = \frac{x^2}{2r_1} \tag{8-84}$$

From this equation, we obtain

$$\left. \begin{aligned} \text{Rotation} & \quad \psi = \frac{dw}{dx} = \frac{x}{r_1} \\ \text{Bending moment} & \quad M = -\frac{D}{r_1} \\ \text{Shear force} & \quad Q = \frac{dM}{dx} = 0 \\ \text{Distributed reaction} & \quad q = -\frac{dQ}{dx} = 0 \end{aligned} \right\} \tag{8-85}$$

Therefore, it can be concluded that the distributed reaction of the contact segment is zero.

Advanced Finite Element Method in Structural Engineering

In the non-contact segment $x_1 \leq x \leq d$, the bending moment and shear force can be solved by the equilibrium condition:

$$M = -P(d - x), \quad Q = P \tag{8-86}$$

The length x_1 of the contact segment and the concentrated reaction R can be solved by the static continuity conditions at the interface point B :

$$-P(d - x_1) = -\frac{D}{r_1}, \quad x_1 = d - \frac{D}{Pr_1} \tag{8-87}$$

$$R = P \tag{8-88}$$

Here, another conclusion that there is a concentrated reaction $R = P$ at the interface point B is obtained.

There is no distributed reaction along the whole contact segment, and only a concentrated reaction exists at its end, this strange conclusion is formed completely by ignoring the shear deformation. If this problem is solved according to the thick beam theory, more reasonable results will be obtained.

Secondly, we solve this problem according to the thick beam theory.

The deflection of the contact segment is still expressed by Eq. (8-84). Since the influence of the shear strain γ is considered in the thick beam theory, the ψ, M, Q, q in the contact segment are different from those results by the thin beam theory:

$$\left. \begin{aligned} \psi &= \frac{dw}{dx} - \gamma = \frac{x}{r_1} - \gamma \\ M &= -D \frac{d\psi}{dx} = -\frac{D}{r_1} + D \frac{d\gamma}{dx} \\ Q &= C\gamma \\ q &= -\frac{dQ}{dx} = -C \frac{d\gamma}{dx} \end{aligned} \right\} \tag{8-89}$$

So, it can be concluded that, there is distributed reaction existing in the contact segment, and it can be derived from the shear strain.

In order to determine the shear strain γ , the equilibrium differential equation

$\frac{dM}{dx} = Q$ is applied firstly. Substitution of Eq. (8-89) into this equation yields

$$\frac{d^2\gamma}{dx^2} - \lambda^2\gamma = 0 \tag{8-90}$$

where

$$\lambda = \sqrt{\frac{C}{D}} \tag{8-91}$$

The solution of Eq. (8-90) is

$$\gamma = \alpha \operatorname{ch} \lambda x + \beta \operatorname{sh} \lambda x \quad (8-92)$$

From the boundary condition $\psi|_{x=0} = 0$ at the left end, we obtain $\gamma|_{x=0} = 0$, $\alpha = 0$, therefore, we have

$$\gamma = \beta \operatorname{sh} \lambda x \quad (8-93)$$

Then, the bending moment and shear force of the contact segment can be obtained as

$$\left. \begin{aligned} M &= -\frac{D}{r_1} + D\beta\lambda \operatorname{ch} \lambda x \\ Q &= C\beta \operatorname{sh} \lambda x \end{aligned} \right\} \quad (8-94)$$

And, the bending moment and shear force of the non-contact segment are still expressed by Eq. (8-86).

By applying the static continuity conditions at point B :

$$\left. \begin{aligned} -\frac{D}{r_1} + D\beta\lambda \operatorname{ch} \lambda x_1 &= -P(d - x_1) \\ C\beta \operatorname{sh} \lambda x_1 &= P \end{aligned} \right\} \quad (8-95)$$

x_1 and β can be solved as follows:

$$\beta = \frac{P}{C \operatorname{sh} \lambda x_1} \quad (8-96)$$

$$\operatorname{cth} \lambda x_1 = \frac{C}{Pr_1\lambda} - \frac{C(d - x_1)}{D\lambda} \quad (8-97)$$

When x_1 is being solved from Eq. (8-97), the trial method can be used.

Finally, the distributed reaction of the contact segment can be obtained as

$$q = -C\beta\lambda \operatorname{ch} \lambda x = -\frac{P\lambda}{\operatorname{sh} \lambda x_1} \operatorname{ch} \lambda x \quad (8-98)$$

in which the positive direction of q is downward.

So, according to the thick beam theory, there is distributed reaction existing in the contact segment, but no concentrated reaction. This conclusion is more reasonable. In contact problem, the influence of the shear strain should not be ignored.

8.3 Thick/Thin Beam Element

8.3.1 The Fundamental Formulae of Thick/Thin Beam Element

A Timoshenko thick beam element is shown in Fig. 8.10. The formulae of deflection w , rotation ψ and shear strain γ are as follows^[4]:

$$w = w_i(1-t) + w_j t + \frac{d}{2}(\psi_i - \psi_j)F_2 - \frac{d}{2}\Gamma(1-2\delta)F_3 \tag{8-99a}$$

$$\psi = \psi_i(1-t) + \psi_j t + 3(1-2\delta)\Gamma F_2 \tag{8-99b}$$

$$\gamma = \delta\Gamma \tag{8-99c}$$

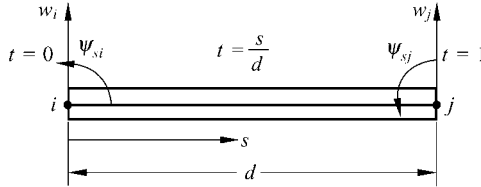


Figure 8.10 Timoshenko thick beam element

where

$$\left. \begin{aligned} \Gamma &= \frac{2}{d}(-w_i + w_j) - \psi_i - \psi_j \\ \delta &= \frac{6\lambda}{1+12\lambda} = \frac{\left(\frac{h}{d}\right)^2}{\frac{5}{6}(1-\mu) + 2\left(\frac{h}{d}\right)^2} \\ \lambda &= \frac{D}{Cd^2} = \frac{h^2}{5(1-\mu)d^2}, \quad D = \frac{Eh^3}{12(1-\mu^2)}, \quad C = \frac{5}{6}Gh = \frac{5Eh}{12(1+\mu)} \\ F_2 &= t(1-t) \\ F_3 &= t(1-t)(1-2t) \end{aligned} \right\} \tag{8-100}$$

8.3.2 Derivation of the Fundamental Formulae

Assume that the shear strain γ , rotation ψ and deflection w are constant, quadratic function and cubic function in the beam element, respectively. According to the

end conditions, let

$$\left. \begin{aligned} \gamma &= \gamma_0 \\ \psi &= \psi_i(1-t) + \psi_j t + \alpha_0 t(1-t) \\ w &= w_i(1-t) + w_j t + \beta_0 dt(1-t) + \beta_1 dt(1-t)(1-2t) \end{aligned} \right\} \quad (8-101)$$

γ , ψ , w should satisfy the following equation:

$$\frac{dw}{dt} - \psi = \gamma \quad (8-102)$$

Substitution of Eq. (8-101) into Eq. (8-102) yields

$$\beta_0 = \frac{1}{2}(\psi_i - \psi_j), \quad \beta_1 = \gamma_0 - \frac{1}{2}\Gamma, \quad \alpha_0 = -6\left(\gamma_0 - \frac{1}{2}\Gamma\right) \quad (8-103)$$

Substitution of Eq. (8-103) into Eq. (8-101) yields

$$\left. \begin{aligned} \gamma &= \gamma_0 \\ \psi &= \psi_i(1-t) + \psi_j t - 6\left(\gamma_0 - \frac{1}{2}\Gamma\right)t(1-t) \\ w &= w_i(1-t) + w_j t + \frac{d}{2}(\psi_i - \psi_j)t(1-t) + d\left(\gamma_0 - \frac{1}{2}\Gamma\right)t(1-t)(1-2t) \end{aligned} \right\} \quad (8-104)$$

in which γ_0 is an internal parameter which can be determined from the condition of minimum strain energy.

Curvature:

$$\begin{aligned} \kappa &= -\frac{d\psi}{dt} = \frac{1}{d}[\psi_i - \psi_j + 6\left(\gamma_0 - \frac{1}{2}\Gamma\right)(1-2t)] = \kappa^0 + \frac{6\gamma_0}{d}(1-2t) \\ \kappa^0 &= \frac{1}{d}[\psi_i - \psi_j - 3\Gamma(1-2t)] \end{aligned}$$

Bending strain energy:

$$\begin{aligned} U_b &= \frac{Dd}{2} \int_0^1 \kappa^2 dt = \frac{Dd}{2} \int_0^1 [(\kappa^0)^2 + \frac{12\gamma_0}{d}\kappa^0(1-2t) + \frac{36\gamma_0^2}{d^2}(1-2t)^2] dt \\ &= U_b^0 - \frac{6D}{d}(\gamma_0\Gamma - \gamma_0^2) \end{aligned}$$

in which

$$U_b^0 = \frac{Dd}{2} \int_0^1 (\kappa^0)^2 dt$$

Shear strain energy:

$$U_s = \frac{Cd}{2} \gamma_0^2$$

The strain energy:

$$U = U_b + U_s = U_b^0 - \frac{6D\gamma_0}{d} \Gamma + \frac{D}{2d} \left(12 + \frac{1}{\lambda} \right) \gamma_0^2 \quad (8-105)$$

From $\frac{\partial U}{\partial \gamma_0} = 0$, we have:

$$\gamma_0 = \frac{6\lambda}{1+12\lambda} \Gamma = \delta \Gamma \quad (8-106)$$

Substitution of Eq. (8-106) into Eq. (8-104) yields Eq. (8-99).

8.3.3 The Stiffness Matrix of Thick/Thin Beam Element

The stiffness matrix \mathbf{K}^e of the thick/thin beam element can be derived from the element strain energy U :

$$U = \frac{1}{2} \mathbf{q}^{eT} \mathbf{K}^e \mathbf{q}^e \quad (8-107)$$

Substitution of Eq. (8-106) into Eq. (8-105) yields the expression of the strain energy as follows:

$$U = U_b^0 + \Delta U \quad (8-108)$$

where U_b^0 is the strain energy of the thin beam element, and the strain energy increment ΔU is

$$\Delta U = -\frac{3D}{d} \delta \Gamma^2 \quad (8-109)$$

The stiffness matrix \mathbf{K}^e of the thick/thin beam element can be written as the sum of two terms:

$$\mathbf{K}^e = \mathbf{K}^{0e} + \Delta \mathbf{K} \quad (8-110)$$

where \mathbf{K}^{0e} is the stiffness of the thin beam element, and by

$$U_b^0 = \frac{1}{2} \mathbf{q}^{eT} \mathbf{K}^{0e} \mathbf{q}^e$$

we have

$$\mathbf{K}^{0e} = \frac{2D}{d^3} \begin{bmatrix} 6 & 3d & -6 & 3d \\ 3d & 2d^2 & -3d & d^2 \\ -6 & -3d & 6 & -3d \\ 3d & d^2 & -3d & 2d^2 \end{bmatrix} \quad (8-111)$$

And, the incremental matrix $\Delta\mathbf{K}$ can be determined by

$$\Delta U = \frac{1}{2} \mathbf{q}^{eT} \Delta\mathbf{K} \mathbf{q}^e$$

i.e.,

$$\Delta\mathbf{K} = -\frac{6D}{d^3} \delta \begin{bmatrix} 4 & 2d & -4 & 2d \\ 2d & d^2 & -2d & d^2 \\ -4 & -2d & 4 & -2d \\ 2d & d^2 & -2d & d^2 \end{bmatrix} \quad (8-112)$$

When the thickness-span ratio $\frac{h}{d}$ decreases gradually, the following limitation relation can be obtained:

$$\delta \rightarrow 0, \quad \Delta\mathbf{K} \rightarrow \mathbf{0}, \quad \mathbf{K}^e \rightarrow \mathbf{K}^{0e}$$

Here, the stiffness matrix \mathbf{K}^e of the thick/thin beam element automatically degenerates to be the stiffness matrix \mathbf{K}^{0e} of the thin beam element. Therefore, no shear locking will happen.

8.4 Review of Displacement-based Thick/Thin Plate Elements

This section will present a brief review of the construction methods of the displacement-based thick/thin plate elements.

The construction methods of the displacement-based thick/thin plate elements are mainly classified into two types: One starts with the thick plate theory, and uses the procedure of transition from the thick plate element to the thick/thin plate element, which is simply denoted as *thick-to-thin scheme* here; the other starts with the thin plate theory, and uses the procedure of transition from the thin plate element to the thin/thick plate element, which is simply denoted as *thin-to-thick scheme* here.

Further explanations are given as follows.

8.4.1 Thick-to-Thin Scheme

The element suitable for the thick plates is firstly constructed based on the thick plate theory; and then, some special treatments are adopted so that the element will satisfy the requirements of the thin plate theory in the thin plate cases.

When constructing the thick plate element, it can be started with assuming the displacement and shear strain fields. In the three variable fields, i.e., the deflection field w , rotation field ψ and shear strain field γ , two of them can be selected to be interpolated rationally, and then the third one can be derived from Eq. (8-1). Since there are three combination forms (w, ψ) , (ψ, γ) and (w, γ) available, accordingly, the corresponding three different schemes are presented. Among these three schemes, the first one which starts with assuming (w, ψ) is the traditional scheme of assuming displacements and is often used in literatures, and the other two are the approaches proposed recently—mixed interpolation schemes partly of displacement and partly of strain.

(1) Scheme starting with assuming (w, ψ)

For the thick plate case, w and ψ should be independent variables; when the plate degenerates to be a thin plate, ψ should be the derivatives of w and not be independent variables anymore. Therefore, the rational assumptions of w and ψ should fulfill the twofold requirements: independence in the thick plate case and non-independence in the thin plate case. This is the main difficulty encountered by this scheme.

In fact, some elements constructed by this scheme possess good precision for the analysis of the thick plates, but an over-stiff performance is obviously exhibited when analyzing the thin plates, i.e., the computational results of deflections are much smaller than correct solutions. This is the shear locking phenomenon. The reason leading to shear locking is that the dual requirements mentioned above are not satisfied when assuming w and ψ , consequently, false shear strain will appear in the thin plate limit state. How to avoid shear locking phenomenon was one of the problems that attracted continuous attention from academia, and many modifications and numerical techniques have been proposed by numerous researchers, such as the reduced integration method^[5], the selective reduced integration method^[6], the substitute shear strain method^[7], and so on.

(2) Scheme starting with assuming (ψ, γ)

In order to avoid the difficulty mentioned above caused by assuming (w, ψ) , the scheme of assuming (ψ, γ) can be used to replace it. For a rational assumption of the shear strain γ , the dual requirements, that γ should be generally nonzero in the thick plate case and tend to be zero in the thin plate case, should be still paid attention to. But then, these dual requirements are much easier to be satisfied, which provides a new way for eliminating shear locking. Some related research achievements^[4,8,9] will be introduced in Sect. 8.5.

By the way, the discrete Kirchhoff theory (DKT) elements for the thin plates indeed belong to a special application of the above scheme.

(3) Scheme starting with assuming (w, γ)

This is another new scheme^[10,11] which can eliminate shear locking, and will be introduced in Sect. 8.6.

8.4.2 Thin-to-Thick Scheme

The element suitable for the thin plates is firstly constructed based on the thin plate theory; and then, some special treatments are adopted so that the influences of shear strain are introduced, thus, the thin plate element is generalized to an element suitable for both thin and thick plates. The shear strain introduced here should automatically degenerate to be zero in the thin plate limit state. Hence, naturally, the elements according to this scheme will not suffer from shear locking phenomenon.

Some high-quality thin plate elements have already been proposed in literatures. Starting with these elements, the corresponding thin/thick plate elements can be constructed by this scheme.

Some related research achievements will be introduced in Sect. 8.7.

By the way, there is another effective method, namely, the Analytical Trial Function (ATF) method, for constructing the universal elements for both thick and thin plates^[12]. This will be introduced in Chap. 14.

8.5 Generalized Conforming Thick/Thin Plate Elements (1) —Starting with Assuming (ψ, γ)

This section will introduce the construction procedure of the thick/thin plate elements starting with assuming (ψ, γ) ^[4,8,9]. The derivation of the triangular element in reference [4] is quite simple and straightforward, and possesses clear physical meaning. So, the procedure in [4] will be introduced here. And, the method of deriving quadrilateral element can be referred to [9].

Main procedure: The functions of rotation and shear strain along each side of the element are firstly determined using the Timoshenko beam theory; Secondly, the rotation and shear strain fields in the domain of the element are then determined using the technique of improved interpolation, and the curvature fields are then determined from the rotation fields; Finally, the element stiffness matrix is determined by the curvature and shear strain fields. This new element is denoted by TMT (Timoshenko-Mindlin Triangular element).

When the thickness becomes small, the thick beam theory will automatically degenerate to be the thin beam theory, and then the shear strain along each element side and the interpolation formulas for shear strain in the domain of the element will all automatically degenerate to be zero. So, the element TMT will

automatically degenerate to be the thin plate element, no shear locking will happen.

8.5.1 Interpolation Formulas for the Rotation Fields of the Thick Plate Element

Consider the triangular thick plate element shown in Fig. 8.11. The element has 3 nodes and 3 engineering DOFs per node. The element nodal displacement vector is:

$$q^e = [w_1 \ \psi_{x1} \ \psi_{y1} \ w_2 \ \psi_{x2} \ \psi_{y2} \ w_3 \ \psi_{x3} \ \psi_{y3}]^T$$

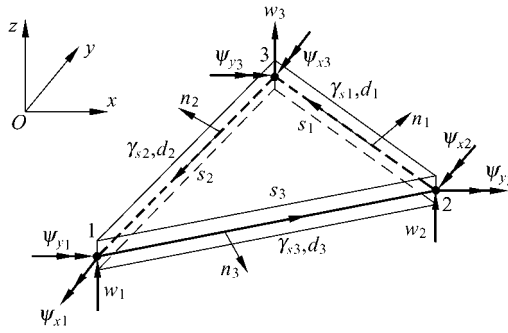


Figure 8.11 A triangular thick plate element

The interpolation formulas for the element rotation fields can be obtained by the rotation formulas along each element side.

1. Formulas of normal rotation ψ_n and tangential rotation ψ_s along each side

The variation of the normal rotation ψ_n along each side is assumed to be linear. For the three sides ($\overline{23}$, $\overline{31}$, $\overline{12}$), we have

$$\left. \begin{aligned} \psi_{n23} &= (\psi_{n23})_2 L_2 + (\psi_{n23})_3 L_3 \\ \psi_{n31} &= (\psi_{n31})_3 L_3 + (\psi_{n31})_1 L_1 \\ \psi_{n12} &= (\psi_{n12})_1 L_1 + (\psi_{n12})_2 L_2 \end{aligned} \right\} \quad (8-113a)$$

The variation of the tangential rotation ψ_s along each side can be determined by Eq. (8-99b). Thus,

$$\left. \begin{aligned} \psi_{s23} &= (\psi_{s23})_2 L_2 + (\psi_{s23})_3 L_3 + 3(1 - 2\delta_1)\Gamma_1 L_2 L_3 \\ \psi_{s31} &= (\psi_{s31})_3 L_3 + (\psi_{s31})_1 L_1 + 3(1 - 2\delta_2)\Gamma_2 L_3 L_1 \\ \psi_{s12} &= (\psi_{s12})_1 L_1 + (\psi_{s12})_2 L_2 + 3(1 - 2\delta_3)\Gamma_3 L_1 L_2 \end{aligned} \right\} \quad (8-113b)$$

where

$$\left. \begin{aligned}
 \delta_i &= \frac{\left(\frac{h}{d_i}\right)^2}{2\left(\frac{h}{d_i}\right)^2 + \frac{5}{6}(1-\mu)} \quad (i=1,2,3) \\
 \Gamma_i &= \frac{1}{d_i} [2(-w_j + w_k) - c_i(\psi_{xj} + \psi_{xk}) + b_i(\psi_{yj} + \psi_{yk})] \\
 b_i &= y_j - y_k \quad (\overline{i, j, k} = \overline{1, 2, 3}) \\
 c_i &= x_k - x_j
 \end{aligned} \right\} \quad (8-114)$$

2. Expressions of rotations ψ_x and ψ_y along each side

By using the relation between (ψ_n, ψ_s) and (ψ_x, ψ_y) , the expression of rotations ψ_x and ψ_y can be obtained as follows:

$$\left. \begin{aligned}
 \psi_{x23} &= -\frac{1}{d_1}(b_1\psi_{n23} - c_1\psi_{s23}) = \psi_{x2}L_2 + \psi_{x3}L_3 + \frac{3c_1}{d_1}(1-2\delta_1)\Gamma_1L_2L_3 \\
 \psi_{x31} &= \psi_{x3}L_3 + \psi_{x1}L_1 + \frac{3c_2}{d_2}(1-2\delta_2)\Gamma_2L_3L_1 \\
 \psi_{x12} &= \psi_{x1}L_1 + \psi_{x2}L_2 + \frac{3c_3}{d_3}(1-2\delta_3)\Gamma_3L_1L_2
 \end{aligned} \right\} \quad (8-115a)$$

$$\left. \begin{aligned}
 \psi_{y23} &= -\frac{1}{d_1}(c_1\psi_{n23} + b_1\psi_{s23}) = \psi_{y2}L_2 + \psi_{y3}L_3 - \frac{3b_1}{d_1}(1-2\delta_1)\Gamma_1L_2L_3 \\
 \psi_{y31} &= \psi_{y3}L_3 + \psi_{y1}L_1 - \frac{3b_2}{d_2}(1-2\delta_2)\Gamma_2L_3L_1 \\
 \psi_{y12} &= \psi_{y1}L_1 + \psi_{y2}L_2 - \frac{3b_3}{d_3}(1-2\delta_3)\Gamma_3L_1L_2
 \end{aligned} \right\} \quad (8-115b)$$

3. Interpolation formulas for element rotation fields ψ_x and ψ_y

The rotation fields ψ_x and ψ_y within the element can then be obtained by the interpolation of the expressions (8-115a,b) of ψ_x and ψ_y on each side, i.e.

$$\left. \begin{aligned}
 \psi_x &= \psi_{x1}L_1 + \psi_{x2}L_2 + \psi_{x3}L_3 + \frac{3c_1}{d_1}(1-2\delta_1)\Gamma_1L_2L_3 \\
 &\quad + \frac{3c_2}{d_2}(1-2\delta_2)\Gamma_2L_3L_1 + \frac{3c_3}{d_3}(1-2\delta_3)\Gamma_3L_1L_2 \\
 \psi_y &= \psi_{y1}L_1 + \psi_{y2}L_2 + \psi_{y3}L_3 - \frac{3b_1}{d_1}(1-2\delta_1)\Gamma_1L_2L_3 \\
 &\quad - \frac{3b_2}{d_2}(1-2\delta_2)\Gamma_2L_3L_1 - \frac{3b_3}{d_3}(1-2\delta_3)\Gamma_3L_1L_2
 \end{aligned} \right\} \quad (8-116)$$

It can be seen that, if $L_i=0$, the expressions of element rotations ψ_x and ψ_y obtained from the above equation are the same as those expressions of rotations along each side given in (8-115a,b). That is to say, The interpolation formulas (8-116) for element rotations are exactly compatible with the formulas (8-115a,b) for rotations along each side.

8.5.2 The Curvature Fields of the Thick Plate Element

The element curvature fields are

$$\boldsymbol{\kappa} = [\kappa_x \quad \kappa_y \quad 2\kappa_{xy}]^T = \left[-\frac{\partial\psi_x}{\partial x} \quad -\frac{\partial\psi_y}{\partial y} \quad -\left(\frac{\partial\psi_x}{\partial y} + \frac{\partial\psi_y}{\partial x} \right) \right]^T \quad (8-117)$$

By using the differential formulae:

$$\left. \begin{aligned} \frac{\partial}{\partial x} &= \frac{1}{2A} \left(b_1 \frac{\partial}{\partial L_1} + b_2 \frac{\partial}{\partial L_2} + b_3 \frac{\partial}{\partial L_3} \right) \\ \frac{\partial}{\partial y} &= \frac{1}{2A} \left(c_1 \frac{\partial}{\partial L_1} + c_2 \frac{\partial}{\partial L_2} + c_3 \frac{\partial}{\partial L_3} \right) \end{aligned} \right\} \quad (8-118)$$

and substituting Eq. (8-116) into Eq. (8-117), we obtain

$$\left. \begin{aligned} \kappa_x &= -\frac{1}{2A} [b_1\psi_{x1} + b_2\psi_{x2} + b_3\psi_{x3} + \frac{3(1-2\delta_1)\Gamma_1}{d_1} c_1(b_2L_3 + b_3L_2) \\ &\quad + \frac{3(1-2\delta_2)\Gamma_2}{d_2} c_2(b_3L_1 + b_1L_3) + \frac{3(1-2\delta_3)\Gamma_3}{d_3} c_3(b_1L_2 + b_2L_1)] \\ \kappa_y &= -\frac{1}{2A} [c_1\psi_{y1} + c_2\psi_{y2} + c_3\psi_{y3} - \frac{3(1-2\delta_1)\Gamma_1}{d_1} b_1(c_2L_3 + c_3L_2) \\ &\quad - \frac{3(1-2\delta_2)\Gamma_2}{d_2} b_2(c_3L_1 + c_1L_3) - \frac{3(1-2\delta_3)\Gamma_3}{d_3} b_3(c_1L_2 + c_2L_1)] \\ 2\kappa_{xy} &= -\frac{1}{2A} (c_1\psi_{x1} + c_2\psi_{x2} + c_3\psi_{x3} + b_1\psi_{y1} + b_2\psi_{y2} + b_3\psi_{y3} + E_1 + E_2 + E_3) \end{aligned} \right\} \quad (8-119)$$

where

$$\left. \begin{aligned} E_1 &= \frac{3(1-2\delta_1)\Gamma_1}{d_1} [(c_1c_2 - b_1b_2)L_3 + (c_3c_1 - b_3b_1)L_2] \\ E_2 &= \frac{3(1-2\delta_2)\Gamma_2}{d_2} [(c_2c_3 - b_2b_3)L_1 + (c_1c_2 - b_1b_2)L_3] \\ E_3 &= \frac{3(1-2\delta_3)\Gamma_3}{d_3} [(c_3c_1 - b_3b_1)L_2 + (c_2c_3 - b_2b_3)L_1] \end{aligned} \right\} \quad (8-120)$$

Equation (8-119) can be written as

$$\boldsymbol{\kappa} = \mathbf{B}_b \mathbf{q}^e \quad (8-121)$$

where

$$\mathbf{B}_b = \mathbf{B}_b^0 + \mathbf{F} \Delta \tilde{\mathbf{G}} \quad (8-122)$$

$$\mathbf{B}_b^0 = -\frac{1}{2A} \begin{bmatrix} 0 & b_1 & 0 & 0 & b_2 & 0 & 0 & b_3 & 0 \\ 0 & 0 & c_1 & 0 & 0 & c_2 & 0 & 0 & c_3 \\ 0 & c_1 & b_1 & 0 & c_2 & b_2 & 0 & c_3 & b_3 \end{bmatrix} \quad (8-123)$$

$$\mathbf{F} = -\frac{3}{2A} \begin{bmatrix} \frac{c_1}{d_1^2}(b_2L_3 + b_3L_2) & \frac{c_2}{d_2^2}(b_3L_1 + b_1L_3) & \frac{c_3}{d_3^2}(b_1L_2 + b_2L_1) \\ -\frac{b_1}{d_1^2}(c_2L_3 + c_3L_2) & -\frac{b_2}{d_2^2}(c_3L_1 + c_1L_3) & -\frac{b_3}{d_3^2}(c_1L_2 + c_2L_1) \\ M_1 & M_2 & M_3 \end{bmatrix} \quad (8-124)$$

$$\left. \begin{aligned} M_1 &= \frac{1}{d_1^2} [(c_1c_2 - b_1b_2)L_3 + (c_3c_1 - b_3b_1)L_2] \\ M_2 &= \frac{1}{d_2^2} [(c_2c_3 - b_2b_3)L_1 + (c_1c_2 - b_1b_2)L_3] \\ M_3 &= \frac{1}{d_3^2} [(c_3c_1 - b_3b_1)L_2 + (c_2c_3 - b_2b_3)L_1] \end{aligned} \right\} \quad (8-125)$$

$$\Delta = \begin{bmatrix} 1 - 2\delta_1 & 0 & 0 \\ 0 & 1 - 2\delta_2 & 0 \\ 0 & 0 & 1 - 2\delta_3 \end{bmatrix} \quad (8-126)$$

$$\tilde{\mathbf{G}} = \begin{bmatrix} 0 & 0 & 0 & -2 & -c_1 & b_1 & 2 & -c_1 & b_1 \\ 2 & -c_2 & b_2 & 0 & 0 & 0 & -2 & -c_2 & b_2 \\ -2 & -c_3 & b_3 & 2 & -c_3 & b_3 & 0 & 0 & 0 \end{bmatrix} \quad (8-127)$$

8.5.3 Interpolation Formulas for Shear Strain Fields of the Thick Plate Element

1. Shear strain along each element side

The transverse shear strain γ_s along the tangential direction (s-direction) of each side is constant. From Eq. (8-99c), we obtain

$$\gamma_{s23} = \delta_1 \Gamma_1, \quad \gamma_{s31} = \delta_2 \Gamma_2, \quad \gamma_{s12} = \delta_3 \Gamma_3 \quad (8-128)$$

in which δ_i and Γ_i are given by Eq. (8-114).

On the boundary line $L_i = 0$, the transformation relations between shear strain components (γ_n, γ_s) and (γ_x, γ_y) are

$$\begin{Bmatrix} \gamma_n \\ \gamma_s \end{Bmatrix}_{L_i=0} = \frac{1}{d_i} \begin{bmatrix} -b_i & -c_i \\ c_i & -b_i \end{bmatrix} \begin{Bmatrix} \gamma_x \\ \gamma_y \end{Bmatrix}_{L_i=0} \quad (8-129)$$

Then, γ_s along each side can be expressed in terms of γ_x and γ_y as follows

$$\begin{Bmatrix} d_1 \gamma_{s23} = c_1 \gamma_{x23} - b_1 \gamma_{y23} \\ d_2 \gamma_{s31} = c_2 \gamma_{x31} - b_2 \gamma_{y31} \\ d_3 \gamma_{s12} = c_3 \gamma_{x12} - b_3 \gamma_{y12} \end{Bmatrix} \quad (8-130)$$

2. Determination of nodal shear strains γ_{xi} and γ_{yi}

Firstly, consider node 1.

There are two sides, $\overline{31}$ and $\overline{12}$, meeting at node 1. According to Eq. (8-130), the tangential shear strains γ_{s31} and γ_{s12} along these two sides can be expressed by the shear strains γ_{x1} and γ_{y1} at node 1, i.e.,

$$\begin{Bmatrix} d_2 \gamma_{s31} \\ d_3 \gamma_{s12} \end{Bmatrix} = \begin{bmatrix} c_2 & -b_2 \\ c_3 & -b_3 \end{bmatrix} \begin{Bmatrix} \gamma_{x1} \\ \gamma_{y1} \end{Bmatrix}$$

Then, we obtain

$$\begin{Bmatrix} \gamma_{x1} \\ \gamma_{y1} \end{Bmatrix} = \frac{1}{2A} \begin{bmatrix} -b_3 & b_2 \\ -c_3 & c_2 \end{bmatrix} \begin{Bmatrix} d_2 \gamma_{s31} \\ d_3 \gamma_{s12} \end{Bmatrix} = \frac{1}{2A} \begin{bmatrix} -b_3 & b_2 \\ -c_3 & c_2 \end{bmatrix} \begin{Bmatrix} d_2 \delta_2 \Gamma_2 \\ d_3 \delta_3 \Gamma_3 \end{Bmatrix} \quad (8-131)$$

Similarly, for nodes 2 and 3, we have

$$\begin{Bmatrix} \gamma_{x2} \\ \gamma_{y2} \end{Bmatrix} = \frac{1}{2A} \begin{bmatrix} -b_1 & b_3 \\ -c_1 & c_3 \end{bmatrix} \begin{Bmatrix} d_3 \delta_3 \Gamma_3 \\ d_1 \delta_1 \Gamma_1 \end{Bmatrix} \quad (8-132)$$

$$\begin{Bmatrix} \gamma_{x3} \\ \gamma_{y3} \end{Bmatrix} = \frac{1}{2A} \begin{bmatrix} -b_2 & b_1 \\ -c_2 & c_1 \end{bmatrix} \begin{Bmatrix} d_1 \delta_1 \Gamma_1 \\ d_2 \delta_2 \Gamma_2 \end{Bmatrix}$$

Thus, from Eqs. (8-131) and (8-132), we obtain

$$\begin{Bmatrix} \gamma_{x1} \\ \gamma_{x2} \\ \gamma_{x3} \end{Bmatrix} = \frac{1}{2A} \begin{bmatrix} 0 & -b_3 & b_2 \\ b_3 & 0 & -b_1 \\ -b_2 & b_1 & 0 \end{bmatrix} \begin{Bmatrix} d_1 \delta_1 \Gamma_1 \\ d_2 \delta_2 \Gamma_2 \\ d_3 \delta_3 \Gamma_3 \end{Bmatrix} \quad (8-133)$$

$$\begin{Bmatrix} \gamma_{y1} \\ \gamma_{y2} \\ \gamma_{y3} \end{Bmatrix} = \frac{1}{2A} \begin{bmatrix} 0 & -c_3 & c_2 \\ c_3 & 0 & -c_1 \\ -c_2 & c_1 & 0 \end{bmatrix} \begin{Bmatrix} d_1 \delta_1 \Gamma_1 \\ d_2 \delta_2 \Gamma_2 \\ d_3 \delta_3 \Gamma_3 \end{Bmatrix} \quad (8-134)$$

3. Interpolation formulas for element shear strain fields

The shear strain fields within the element can be obtained in terms of the nodal shear strains in the following manner

$$\begin{Bmatrix} \gamma_x \\ \gamma_y \end{Bmatrix} = \begin{Bmatrix} \gamma_{x1} L_1 + \gamma_{x2} L_2 + \gamma_{x3} L_3 \\ \gamma_{y1} L_1 + \gamma_{y2} L_2 + \gamma_{y3} L_3 \end{Bmatrix} \quad (8-135)$$

in which the nodal shear strains are given by Eqs.(8-133) and (8-134). After substituting these into the above equation, we obtain

$$\boldsymbol{\gamma} = \begin{Bmatrix} \gamma_x \\ \gamma_y \end{Bmatrix} = \mathbf{H} \begin{Bmatrix} \delta_1 d_1 \Gamma_1 \\ \delta_2 d_2 \Gamma_2 \\ \delta_3 d_3 \Gamma_3 \end{Bmatrix} \quad (8-136)$$

where

$$\mathbf{H} = \frac{1}{2A} \begin{bmatrix} b_3 L_2 - b_2 L_3 & b_1 L_3 - b_3 L_1 & b_2 L_1 - b_1 L_2 \\ c_3 L_2 - c_2 L_3 & c_1 L_3 - c_3 L_1 & c_2 L_1 - c_1 L_2 \end{bmatrix} \quad (8-137)$$

Equation (8-136) can also be written as

$$\boldsymbol{\gamma} = \mathbf{B}_s \mathbf{q}^e \quad (8-138)$$

where

$$\mathbf{B}_s = \mathbf{H} \mathbf{\Delta}' \tilde{\mathbf{G}} \quad (8-139)$$

$$\mathbf{\Delta}' = \begin{bmatrix} \delta_1 & 0 & 0 \\ 0 & \delta_2 & 0 \\ 0 & 0 & \delta_3 \end{bmatrix}$$

$\tilde{\mathbf{G}}$ is given by Eq. (8-127).

4. Expression in Cartesian coordinates for shear strains of the triangular element

For the triangular element, the shear strains γ_x and γ_y are determined by 3 constant shear strains $(\gamma_s)_{12}, (\gamma_s)_{23}, (\gamma_s)_{31}$ along 3 sides, therefore, the general expressions

of γ_x and γ_y can be written as

$$\left. \begin{aligned} \gamma_x &= \gamma_1 + \gamma_3 y \\ \gamma_y &= \gamma_2 - \gamma_3 x \end{aligned} \right\} \quad (8-140)$$

in which 3 parameters γ_1 , γ_2 and γ_3 are involved. This equation can be proved as follows.

For side $\overline{12}$, the shear strain $(\gamma_s)_{12}$ along the side can be expressed by the shear strains at the end point $(\gamma_{x1}, \gamma_{y1})$ or $(\gamma_{x2}, \gamma_{y2})$, as shown in the following Eq. (a)

$$d_3 \gamma_{s12} = c_3 \gamma_{x1} - b_3 \gamma_{y1} = c_3 \gamma_{x2} - b_3 \gamma_{y2} \quad (a)$$

$$d_1 \gamma_{s23} = c_1 \gamma_{x2} - b_1 \gamma_{y2} = c_1 \gamma_{x3} - b_1 \gamma_{y3} \quad (b)$$

$$d_2 \gamma_{s31} = c_2 \gamma_{x3} - b_2 \gamma_{y3} = c_2 \gamma_{x1} - b_2 \gamma_{y1} \quad (c)$$

Equations (b) and (c) can be obtained similarly.

Temporarily assume that γ_x and γ_y are the complete linear polynomials:

$$\left. \begin{aligned} \gamma_x &= \alpha_0 + \alpha_1 x + \alpha_2 y \\ \gamma_y &= \beta_0 + \beta_1 x + \beta_2 y \end{aligned} \right\} \quad (d)$$

in which 6 unknown coefficients are contained. Substitution of Eq. (d) into Eqs. (a), (b), (c) yields

$$\begin{bmatrix} c_3^2 & b_3^2 & -b_3 c_3 \\ c_1^2 & b_1^2 & -b_1 c_1 \\ c_2^2 & b_2^2 & -b_2 c_2 \end{bmatrix} \begin{Bmatrix} \alpha_1 \\ \beta_2 \\ \alpha_2 + \beta_1 \end{Bmatrix} = \begin{Bmatrix} 0 \\ 0 \\ 0 \end{Bmatrix} \quad (e)$$

Since the determinant of the coefficient matrix at the left side is $(2A)^3$, not zero, so, we obtain

$$\alpha_1 = 0, \quad \beta_2 = 0, \quad \alpha_2 = -\beta_1 \quad (f)$$

From Eq. (d), we have

$$\left. \begin{aligned} \gamma_x &= \alpha_0 + \alpha_2 y \\ \gamma_y &= \beta_0 - \alpha_2 x \end{aligned} \right\} \quad (g)$$

Equation (g) is just the form of Eq. (8-140). QED.

By the way, if \mathbf{H} in Eq. (8-137) is expressed in the Cartesian coordinates, the shear strain formulas (8-136) can be expressed by the form of Eq. (8-140).

8.5.4 Stiffness Matrix of the Thick Plate

The element stiffness matrix K^e is composed of two parts

$$K^e = K_b^e + K_s^e \quad (8-141)$$

where K_b^e is the bending stiffness matrix:

$$K_b^e = \iint_{A^e} B_b^T D_b B_b dA \quad (8-142)$$

B_b is given by Eq. (8-122), D_b is the bending elastic matrix:

$$D_b = D \begin{bmatrix} 1 & \mu & 0 \\ \mu & 1 & 0 \\ 0 & 0 & \frac{1-\mu}{2} \end{bmatrix}, \quad D = \frac{Eh^3}{12(1-\mu^2)} \quad (8-143)$$

K_s^e is the shear stiffness matrix:

$$K_s^e = \iint_{A^e} B_s^T D_s B_s dA \quad (8-144)$$

B_s is given by Eq. (8-139), D_s is the shear elastic matrix:

$$D_s = C \begin{bmatrix} 1 & 0 \\ 0 & 1 \end{bmatrix}, \quad C = \frac{5}{6} Gh \quad (8-145)$$

8.5.5 Numerical Examples

Example 8.1 The central deflection and moment of simply-supported (hard) square plates with different thickness-span ratios (h/L) subjected to uniform load.

Assume that the side length of the plate is L , $\mu = 0.3$. Meshes A and B in Fig. 8.12 are used. The results by the element TMT are given in Tables 8.3 to 8.5.

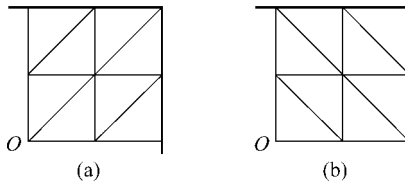


Figure 8.12 Meshes for 1/4 square plate (O is the center of the plate)
 (a) Mesh A 2×2 ; (b) Mesh B 2×2

Advanced Finite Element Method in Structural Engineering

Table 8.3 The central deflection of simply-supported square plates subjected to uniform load $q / \left(\frac{qL^4}{100D} \right)$

Mesh number		2 × 2	4 × 4	8 × 8	16 × 16	Analytical
<i>h/L</i>	Mesh type					
10 ⁻³⁰	<i>A</i>	0.4056	0.4065	0.4064	0.4063	0.4062
	<i>B</i>	0.3676	0.3973	0.4041	0.4057	
0.001	<i>A</i>	0.4056	0.4065	0.4064	0.4063	0.4062
	<i>B</i>	0.3676	0.3973	0.4041	0.4057	
0.01	<i>A</i>	0.4058	0.4066	0.4065	0.4064	0.4064
	<i>B</i>	0.3677	0.3974	0.4042	0.4059	
0.1	<i>A</i>	0.4255	0.4264	0.4270	0.4272	0.4273
	<i>B</i>	0.3845	0.4164	0.4244	0.4266	
0.15	<i>A</i>	0.4520	0.4529	0.4534	0.4536	0.4536
	<i>B</i>	0.4063	0.4414	0.4504	0.4528	
0.20	<i>A</i>	0.4902	0.4905	0.4906	0.4905	0.4906
	<i>B</i>	0.4370	0.4764	0.4867	0.4895	
0.25	<i>A</i>	0.5398	0.5388	0.5383	0.5380	0.5379
	<i>B</i>	0.4769	0.5215	0.5334	0.5366	
0.30	<i>A</i>	0.6009	0.5979	0.5966	0.5960	0.5956
	<i>B</i>	0.5257	0.5767	0.5905	0.5943	
0.35	<i>A</i>	0.6732	0.6679	0.6655	0.6646	0.6641
	<i>B</i>	0.5835	0.6418	0.6580	0.6624	

Table 8.4 The central deflection of clamped square plates subjected to uniform load $q / \left(\frac{qL^4}{100D} \right)$

Mesh number		2 × 2	4 × 4	8 × 8	16 × 16	Analytical
<i>h/L</i>	Mesh type					
10 ⁻³⁰	<i>A</i>	0.1547	0.1347	0.1287	0.1271	0.1265
	<i>B</i>	0.1214	0.1258	0.1264	0.1265	
0.001	<i>A</i>	0.1547	0.1347	0.1287	0.1271	0.1265
	<i>B</i>	0.1214	0.1258	0.1264	0.1265	
0.01	<i>A</i>	0.1550	0.1350	0.1289	0.1273	0.1265
	<i>B</i>	0.1216	0.1260	0.1266	0.1267	
0.1	<i>A</i>	0.1766	0.1575	0.1521	0.1509	0.1499
	<i>B</i>	0.1392	0.1473	0.1495	0.1502	
0.15	<i>A</i>	0.2039	0.1856	0.1805	0.1792	0.1798
	<i>B</i>	0.1617	0.1738	0.1773	0.1784	

(Continued)

Mesh number h/L \ Mesh type		Mesh number				Analytical
		2×2	4×4	8×8	16×16	
0.20	<i>A</i>	0.2423	0.2243	0.2191	0.2177	0.2167
	<i>B</i>	0.1931	0.2101	0.2152	0.2167	
0.25	<i>A</i>	0.2918	0.2735	0.2680	0.2664	0.2675
	<i>B</i>	0.2335	0.2561	0.2630	0.2650	
0.30	<i>A</i>	0.3526	0.3333	0.3271	0.3253	0.3227
	<i>B</i>	0.2827	0.3119	0.3210	0.3236	
0.35	<i>A</i>	0.4246	0.4037	0.3967	0.3945	0.3951
	<i>B</i>	0.3409	0.3776	0.3890	0.3924	

Table 8.5 The central moment of simply-supported square plates subjected to uniform load $q / \left(\frac{qL^2}{10} \right)$

Mesh number h/L \ Mesh type		Mesh number				Analytical
		2×2	4×4	8×8	16×16	
10^{-30}	<i>A</i>	0.5156	0.4885	0.4811	0.4794	0.4789
	<i>B</i>	0.4837	0.4819	0.4799	0.4792	
0.001	<i>A</i>	0.5156	0.4885	0.4811	0.4794	
	<i>B</i>	0.4837	0.4819	0.4799	0.4792	
0.01	<i>A</i>	0.5158	0.4887	0.4813	0.4796	
	<i>B</i>	0.4836	0.4817	0.4797	0.4790	
0.1	<i>A</i>	0.5296	0.4977	0.4849	0.4806	
	<i>B</i>	0.4765	0.4775	0.4781	0.4786	
0.15	<i>A</i>	0.5402	0.5007	0.4854	0.4806	
	<i>B</i>	0.4722	0.4766	0.4781	0.4786	
0.20	<i>A</i>	0.5487	0.5023	0.4855	0.4807	
	<i>B</i>	0.4689	0.4760	0.4780	0.4786	
0.25	<i>A</i>	0.5548	0.5032	0.4856	0.4807	
	<i>B</i>	0.4664	0.4757	0.4780	0.4786	
0.30	<i>A</i>	0.5590	0.5038	0.4857	0.4807	
	<i>B</i>	0.4646	0.4754	0.4780	0.4786	
0.35	<i>A</i>	0.5620	0.5041	0.4857	0.4807	
	<i>B</i>	0.4632	0.4753	0.4780	0.4786	

Example 8.2 The central deflection and moment of simply-supported (soft) and clamped circular plates with different thickness-radius ratios (h/R) subjected to uniform load.

Advanced Finite Element Method in Structural Engineering

Assume that the radius of the circular plate is R , the Young’s modulus $E = 10.92$, the Poisson’s ratio $\mu = 0.3$. Meshes A and B in Fig. 6.14 are used. The results by the element TMT are listed in Tables 8.6 to 8.8.

Table 8.6 The central deflection of simply-supported circular plates subjected to uniform load $q / \left(\frac{qR^4}{D} \right)$

Mesh h/R	A 24 elements	B 96 elements	Analytical solution
10^{-30}	0.063 033 (-1.05%)	0.063 543 (-0.25%)	0.063 702
0.001	0.063 033 (-1.05%)	0.063 543 (-0.25%)	0.063 702
0.01	0.063 039 (-1.05%)	0.063 549 (-0.25%)	0.063 709
0.1	0.063 689 (-1.13%)	0.064 226 (-0.29%)	0.064 416
0.15	0.064 540 (-1.18%)	0.065 109 (-0.31%)	0.065 309
0.20	0.065 754 (-1.21%)	0.066 353 (-0.31%)	0.066 559
0.25	0.067 330 (-1.23%)	0.067 956 (-0.31%)	0.068 166
0.30	0.069 265 (-1.23%)	0.069 917 (-0.30%)	0.070 130
0.35	0.071 557 (-1.24%)	0.072 235 (-0.30%)	0.072 452

Table 8.7 The central deflection of clamped circular plates subjected to uniform load $q / \left(\frac{qR^4}{D} \right)$

Mesh h/R	A 24 elements	B 96 elements	Analytical solution
10^{-30}	0.015 954 (2.11%)	0.015 722 (0.62%)	0.015 625
0.001	0.015 954 (2.11%)	0.015 723 (0.63%)	0.015 625
0.01	0.015 960 (2.10%)	0.157 29 (0.62%)	0.015 632
0.1	0.016 618 (1.71%)	0.016 408 (0.42%)	0.016 339
0.15	0.017 476 (1.42%)	0.017 292 (0.35%)	0.017 232
0.20	0.018 697 (1.16%)	0.018 537 (0.30%)	0.018 482
0.25	0.020 278 (0.94%)	0.020 141 (0.26%)	0.020 089
0.30	0.022 217 (0.74%)	0.022 102 (0.22%)	0.022 054
0.35	0.024 513 (0.57%)	0.024 420 (0.18%)	0.024 375

Table 8.8 The central moment of simply-supported circular plates subjected to uniform load $q/(qR^2)$

h/R \ Mesh	A 24 elements	B 96 elements	Analytical solution
10^{-30}	0.209 51 (1.58%)	0.207 54 (0.63%)	0.206 25
0.001	0.209 51 (1.58%)	0.207 54 (0.63%)	
0.01	0.209 52 (1.59%)	0.207 55 (0.63%)	
0.1	0.210 11 (1.87%)	0.207 84 (0.77%)	
0.15	0.210 52 (2.07%)	0.207 93 (0.81%)	
0.20	0.210 82 (2.22%)	0.207 97 (0.83%)	
0.25	0.211 04 (2.32%)	0.207 99 (0.84%)	
0.30	0.211 19 (2.40%)	0.208 01 (0.85%)	
0.35	0.211 30 (2.45%)	0.208 02 (0.86%)	

The above numerical examples show that the element TMT possesses good performance. It has high precision for both deflection and moment, and for both thick and thin plates. And, no shear locking happens.

The scheme starting with assuming (ψ, γ) proposed in this section is a universal method, it can be generalized to construct similar quadrilateral elements^[9]. Furthermore, Element DKT, which is formulated by the discrete Kirchhoff theory, is a special case of the present element TMT.

8.6 Generalized Conforming Thick/Thin Plate Elements (2) —Starting with Assuming (w, γ)

Schemes starting with assuming (w, γ) for the construction of triangular and quadrilateral thick/thin plate elements have been proposed in references [10] and [11], respectively. This section will introduce the construction procedure of the triangular element TCGC-T9 in [10]. (By the way, another triangular thick/thin element TSL-T9^[13] based on the SemiLoof scheme will also be introduced in Sect. 11.5.3).

Main procedure: The variation functions of deflection \tilde{w} and shear strain γ_s long each side of the element are firstly determined using the Timoshenko beam theory. Secondly, the nodal shear strains γ_{xi} and γ_{yi} and the interpolation formulas of the shear strain fields γ_x and γ_y in the domain of the element are then determined according to the shear strain γ_s along each side. Thirdly, assume that the element deflection w is a polynomial containing 9 unknown coefficients λ . In order to

determine λ , 9 generalized conforming conditions (3 point conforming conditions for deflections at the corner nodes, average line conforming conditions for deflections and normal slopes along 3 element sides) are applied. Finally, the rotation and curvature fields are determined from the deflection and shear strain fields; and the element stiffness matrix is then determined by the curvature and shear strain fields. This new element is denoted by TCGC-T9.

When the thickness becomes small, the element TCGC-T9 will automatically degenerate to be the thin plate element GPL-T9 in reference [14]. So, no shear locking will happen.

Consider the triangular thick plate element shown in Fig. 8.11. The element nodal displacement vector is formed by 9 engineering DOFs:

$$\mathbf{q}^e = [w_1 \quad \psi_{x1} \quad \psi_{y1} \quad w_2 \quad \psi_{x2} \quad \psi_{y2} \quad w_3 \quad \psi_{x3} \quad \psi_{y3}]^T$$

8.6.1 Boundary Displacements of the Element

On the element boundary, the deflection \tilde{w} is assumed according to the thick beam theory, and the normal slope $\tilde{\psi}_n$ is assumed to be a linear function. For example, along the element side 12, we have

$$\left. \begin{aligned} \tilde{w}_{12} &= [L_1 + \mu_{e3}L_1L_2(L_1 - L_2)]w_1 + \frac{1}{2}L_1L_2[1 + \mu_{e3}(L_1 - L_2)](c_3\psi_{x1} - b_3\psi_{y1}) \\ &\quad + [L_2 - \mu_{e3}L_1L_2(L_1 - L_2)]w_2 + \frac{1}{2}L_1L_2[-1 + \mu_{e3}(L_1 - L_2)](c_3\psi_{x2} - b_3\psi_{y2}) \\ \tilde{\psi}_n &= -\frac{L_1}{d_3}(b_3\psi_{x1} + c_3\psi_{y1}) - \frac{L_2}{d_3}(b_3\psi_{x2} + c_3\psi_{y2}) \end{aligned} \right\} \quad (8-146)$$

where

$$\mu_{ei} = 1 - 2\delta_i \quad (i = 1, 2, 3)$$

δ_i is given by Eq. (8-114).

8.6.2 Shear Strain Fields of the Element

Firstly, the shear strain γ_s along each side is determined from the thick beam theory; Then, the shear strains γ_{xi} and γ_{yi} at the corner node i are determined; finally, the interpolation formulas for shear strains γ_x and γ_y in the domain of the element can be obtained. The above derivation procedure has been given in Sect. 8.5.

Formulas in Eq. (8-138) are the interpolation formulas of element shear strains.

8.6.3 Deflection Field of the Element

1. Displacements in the domain of the element

The element deflection field is assumed as

$$w = \mathbf{F}_\lambda \boldsymbol{\lambda} \quad (8-147)$$

where

$$\begin{aligned} \boldsymbol{\lambda} &= [\lambda_1 \quad \lambda_2 \quad \lambda_3 \quad \lambda_4 \quad \lambda_5 \quad \lambda_6 \quad \lambda_7 \quad \lambda_8 \quad \lambda_9]^T \\ \mathbf{F}_\lambda &= [L_1 \quad L_2 \quad L_3 \quad L_1 L_2 \quad L_2 L_3 \quad L_3 L_1 \\ &\quad L_1 \left(L_1 - \frac{1}{2} \right) (L_1 - 1) \quad L_2 \left(L_2 - \frac{1}{2} \right) (L_2 - 1) \quad L_3 \left(L_3 - \frac{1}{2} \right) (L_3 - 1)] \end{aligned} \quad (8-148)$$

Then, the element rotation fields can be obtained as

$$\begin{Bmatrix} \psi_x \\ \psi_y \end{Bmatrix} = \begin{Bmatrix} \frac{\partial w}{\partial x} - \gamma_x \\ \frac{\partial w}{\partial y} - \gamma_y \end{Bmatrix} \quad (8-149)$$

2. Introducing generalized conforming conditions

The same line-point conforming scheme as that of the thin plate element GPL-T9 is used:

$$\left. \begin{aligned} w_i - \tilde{w}_i &= 0 \\ \int_{d_i} (w - \tilde{w}) ds &= 0 \\ \int_{d_i} (\psi_n - \tilde{\psi}_n) ds &= 0 \end{aligned} \right\} \quad (i = 1, 2, 3) \quad (8-150)$$

Substitution of Eqs. (8-146) and (8-147) into the above equation yields

$$\boldsymbol{\lambda} = \hat{\mathbf{A}} \mathbf{q}^e \quad (8-151)$$

where

$$\hat{A} = \begin{bmatrix} 1 & 0 & 0 & 0 & 0 & 0 & 0 & 0 & 0 \\ 0 & 0 & 0 & 1 & 0 & 0 & 0 & 0 & 0 \\ 0 & 0 & 0 & 0 & 0 & 0 & 1 & 0 & 0 \\ 0 & \frac{1}{2}c_3 & -\frac{1}{2}b_3 & 0 & -\frac{1}{2}c_3 & \frac{1}{2}b_3 & 0 & 0 & 0 \\ 0 & 0 & 0 & 0 & \frac{1}{2}c_1 & -\frac{1}{2}b_1 & 0 & -\frac{1}{2}c_1 & \frac{1}{2}b_1 \\ 0 & -\frac{1}{2}c_2 & \frac{1}{2}b_2 & 0 & 0 & 0 & 0 & \frac{1}{2}c_2 & -\frac{1}{2}b_2 \\ \hat{A}_1 & & & \hat{A}_2 & & & & \hat{A}_3 & \end{bmatrix} \quad (8-152)$$

$$\hat{A}_1 = \begin{bmatrix} -(\mu_{e2} + \mu_{e3}) & \frac{1}{2}(c_2\mu_{e2} - c_3\mu_{e3}) & -\frac{1}{2}(b_2\mu_{e2} - b_3\mu_{e3}) \\ \mu_{e3} - r_2\mu_{e2} & \frac{1}{2}(r_2c_2\mu_{e2} + c_3\mu_{e3}) & -\frac{1}{2}(r_2b_2\mu_{e2} + b_3\mu_{e3}) \\ \mu_{e2} + r_3\mu_{e3} & \frac{1}{2}(r_3c_3\mu_{e3} - c_2\mu_{e2}) & -\frac{1}{2}(r_3b_3\mu_{e3} - b_2\mu_{e2}) \end{bmatrix} \quad (8-153a)$$

$$\hat{A}_2 = \begin{bmatrix} \mu_{e3} + r_1\mu_{e1} & \frac{1}{2}(r_1c_1\mu_{e1} - c_3\mu_{e3}) & -\frac{1}{2}(r_1b_1\mu_{e1} - b_3\mu_{e3}) \\ -(\mu_{e3} + \mu_{e1}) & \frac{1}{2}(c_3\mu_{e3} - c_1\mu_{e1}) & -\frac{1}{2}(b_3\mu_{e3} - b_1\mu_{e1}) \\ \mu_{e1} - r_3\mu_{e3} & \frac{1}{2}(r_3c_3\mu_{e3} + c_1\mu_{e1}) & -\frac{1}{2}(r_3b_3\mu_{e3} + b_1\mu_{e1}) \end{bmatrix} \quad (8-153b)$$

$$\hat{A}_3 = \begin{bmatrix} \mu_{e2} - r_1\mu_{e1} & \frac{1}{2}(r_1c_1\mu_{e1} + c_2\mu_{e2}) & -\frac{1}{2}(r_1b_1\mu_{e1} + b_2\mu_{e2}) \\ \mu_{e1} + r_2\mu_{e2} & \frac{1}{2}(r_2c_2\mu_{e2} - c_1\mu_{e1}) & -\frac{1}{2}(r_2b_2\mu_{e2} - b_1\mu_{e1}) \\ -(\mu_{e1} + \mu_{e2}) & \frac{1}{2}(c_1\mu_{e1} - c_2\mu_{e2}) & -\frac{1}{2}(b_1\mu_{e1} - b_2\mu_{e2}) \end{bmatrix} \quad (8-153c)$$

$$r_1 = \frac{d_2^2 - d_3^2}{d_1^2}, \quad r_2 = \frac{d_3^2 - d_1^2}{d_2^2}, \quad r_3 = \frac{d_1^2 - d_2^2}{d_3^2} \quad (8-154)$$

Substitution of Eq. (8-151) into Eq. (8-147) yields

$$w = Nq^e$$

where

$$\begin{aligned}
 \mathbf{N} &= [N_{w1} \quad N_{\psi x1} \quad N_{\psi y1} \quad N_{w2} \quad N_{\psi x2} \quad N_{\psi y2} \quad N_{w3} \quad N_{\psi x3} \quad N_{\psi y3}] \quad (8-155) \\
 N_{wi} &= L_i - (\mu_{ej} + \mu_{em})L_i \left(L_i - \frac{1}{2} \right) (L_i - 1) + (\mu_{em} - r_j \mu_{ej})L_j \left(L_j - \frac{1}{2} \right) (L_j - 1) \\
 &\quad + (\mu_{ej} + r_m \mu_{em})L_m \left(L_m - \frac{1}{2} \right) (L_m - 1) \\
 N_{\psi xi} &= \frac{1}{2} \left[L_i (c_m L_j - c_j L_m) + (c_j \mu_{ej} - c_m \mu_{em})L_i \left(L_i - \frac{1}{2} \right) (L_i - 1) \right. \\
 &\quad \left. + (r_j c_j \mu_{ej} + c_m \mu_{em})L_j \left(L_j - \frac{1}{2} \right) (L_j - 1) \right. \\
 &\quad \left. + (r_m c_m \mu_{em} - c_j \mu_{ej})L_m \left(L_m - \frac{1}{2} \right) (L_m - 1) \right] \\
 N_{\psi yi} &= \frac{1}{2} \left[L_i (-b_m L_j + b_j L_m) - (b_j \mu_{ej} - b_m \mu_{em})L_i \left(L_i - \frac{1}{2} \right) (L_i - 1) \right. \\
 &\quad \left. - (r_j b_j \mu_{ej} + b_m \mu_{em})L_j \left(L_j - \frac{1}{2} \right) (L_j - 1) \right. \\
 &\quad \left. - (r_m b_m \mu_{em} - b_j \mu_{ej})L_m \left(L_m - \frac{1}{2} \right) (L_m - 1) \right] \quad (\overline{i, j, m} = \overline{1, 2, 3})
 \end{aligned} \quad (8-156)$$

8.6.4 Stiffness Matrix of the Element

1. The element bending strain matrix

The element curvature fields are

$$\boldsymbol{\kappa} = [\kappa_x \quad \kappa_y \quad 2\kappa_{xy}]^T = \left[-\frac{\partial \psi_x}{\partial x} \quad -\frac{\partial \psi_y}{\partial y} \quad -\left(\frac{\partial \psi_x}{\partial y} + \frac{\partial \psi_y}{\partial x} \right) \right]^T \quad (8-157)$$

Substitution of Eq. (8-149) into the above equation yields

$$\boldsymbol{\kappa} = \left[-\frac{\partial^2 w}{\partial x^2} + \frac{\partial \gamma_x}{\partial x} \quad -\frac{\partial^2 w}{\partial y^2} + \frac{\partial \gamma_y}{\partial y} \quad -2\frac{\partial^2 w}{\partial x \partial y} + \frac{\partial \gamma_x}{\partial y} + \frac{\partial \gamma_y}{\partial x} \right]^T$$

From Eq. (8-140), we have

$$\frac{\partial \gamma_x}{\partial x} = 0, \quad \frac{\partial \gamma_y}{\partial y} = 0, \quad \frac{\partial \gamma_x}{\partial y} + \frac{\partial \gamma_y}{\partial x} = 0$$

So, we obtain

$$\boldsymbol{\kappa} = \begin{bmatrix} -\frac{\partial^2 w}{\partial x^2} & -\frac{\partial^2 w}{\partial y^2} & -2\frac{\partial^2 w}{\partial x \partial y} \end{bmatrix}^T = \mathbf{B}_b \mathbf{q}^e \quad (8-158)$$

where \mathbf{B}_b is the element bending strain matrix

$$\mathbf{B}_b = [\mathbf{B}_{b1} \quad \mathbf{B}_{b2} \quad \mathbf{B}_{b3}] \quad (8-159)$$

$$\mathbf{B}_{bi} = \begin{bmatrix} B_{bi11} & B_{bi12} & B_{bi13} \\ B_{bi21} & B_{bi22} & B_{bi23} \\ B_{bi31} & B_{bi32} & B_{bi33} \end{bmatrix} \quad (i = 1, 2, 3) \quad (8-160)$$

$$B_{bi11} = -\frac{3}{4A^2}[-b_i^2(\mu_{ej} + \mu_{em})(2L_i - 1) + b_j^2(\mu_{em} - r_j\mu_{ej})(2L_j - 1) + b_m^2(\mu_{ej} + r_m\mu_{em})(2L_m - 1)]$$

$$B_{bi21} = -\frac{3}{4A^2}[-c_i^2(\mu_{ej} + \mu_{em})(2L_i - 1) + c_j^2(\mu_{em} - r_j\mu_{ej})(2L_j - 1) + c_m^2(\mu_{ej} + r_m\mu_{em})(2L_m - 1)]$$

$$B_{bi31} = -\frac{3}{2A^2}[-b_i c_i(\mu_{ej} + \mu_{em})(2L_i - 1) + b_j c_j(\mu_{em} - r_j\mu_{ej})(2L_j - 1) + b_m c_m(\mu_{ej} + r_m\mu_{em})(2L_m - 1)]$$

$$B_{bi12} = -\frac{3}{8A^2}[b_i^2(c_j\mu_{ej} - c_m\mu_{em})(2L_i - 1) + b_j^2(r_j c_j\mu_{ej} + c_m\mu_{em})(2L_j - 1) + b_m^2(r_m c_m\mu_{em} - c_j\mu_{ej})(2L_m - 1) + \frac{2}{3}b_i(b_j c_m - b_m c_j)]$$

$$B_{bi22} = -\frac{3}{8A^2}[c_i^2(c_j\mu_{ej} - c_m\mu_{em})(2L_i - 1) + c_j^2(r_j c_j\mu_{ej} + c_m\mu_{em})(2L_j - 1) + c_m^2(r_m c_m\mu_{em} - c_j\mu_{ej})(2L_m - 1)]$$

$$B_{bi32} = -\frac{3}{4A^2}[b_i c_i(c_j\mu_{ej} - c_m\mu_{em})(2L_i - 1) + b_j c_j(r_j c_j\mu_{ej} + c_m\mu_{em})(2L_j - 1) + b_m c_m(r_m c_m\mu_{em} - c_j\mu_{ej})(2L_m - 1) + \frac{1}{3}c_i(b_j c_m - b_m c_j)]$$

$$B_{bi13} = -\frac{3}{8A^2}[b_i^2(b_m\mu_{em} - b_j\mu_{ej})(2L_i - 1) - b_j^2(r_j b_j\mu_{ej} + b_m\mu_{em})(2L_j - 1) - b_m^2(r_m b_m\mu_{em} - b_j\mu_{ej})(2L_m - 1)]$$

$$B_{bi23} = -\frac{3}{8A^2}[c_i^2(b_m\mu_{em} - b_j\mu_{ej})(2L_i - 1) - c_j^2(r_j b_j\mu_{ej} + b_m\mu_{em})(2L_j - 1) - c_m^2(r_m b_m\mu_{em} - b_j\mu_{ej})(2L_m - 1) + \frac{2}{3}c_i(b_j c_m - b_m c_j)]$$

$$B_{bi33} = -\frac{3}{4A^2} [b_i c_i (b_m \mu_{em} - b_j \mu_{ej})(2L_i - 1) - b_j c_j (r_j b_j \mu_{ej} + b_m \mu_{em})(2L_j - 1) - b_m c_m (r_m b_m \mu_{em} - b_j \mu_{ej})(2L_m - 1) + \frac{1}{3} b_i (b_j c_m - b_m c_j)] \quad (\overline{i, j, m} = \overline{1, 2, 3})$$

2. The element shear strain matrix

The element shear strain matrix is given by Eq. (8-139)

$$\mathbf{B}_s = [\mathbf{B}_{s1} \quad \mathbf{B}_{s2} \quad \mathbf{B}_{s3}] \quad (8-161)$$

where

$$\mathbf{B}_{si} = \frac{1}{2A} \begin{bmatrix} 2\delta_j (b_i L_m - b_m L_i) - 2\delta_m (b_j L_i - b_i L_j) & -c_j \delta_j (b_i L_m - b_m L_i) - c_m \delta_m (b_j L_i - b_i L_j) \\ 2\delta_j (c_i L_m - c_m L_i) - 2\delta_m (c_j L_i - c_i L_j) & -c_j \delta_j (c_i L_m - c_m L_i) - c_m \delta_m (c_j L_i - c_i L_j) \\ b_j \delta_j (b_i L_m - b_m L_i) + b_m \delta_m (b_j L_i - b_i L_j) \\ b_j \delta_j (c_i L_m - c_m L_i) + b_m \delta_m (c_j L_i - c_i L_j) \end{bmatrix} \quad (i, j, m = \overline{1, 2, 3}) \quad (8-162)$$

3. The element stiffness matrix

The element stiffness matrix is

$$\mathbf{K}^e = \begin{bmatrix} \mathbf{K}_{11} & \mathbf{K}_{12} & \mathbf{K}_{13} \\ \mathbf{K}_{21} & \mathbf{K}_{22} & \mathbf{K}_{23} \\ \mathbf{K}_{31} & \mathbf{K}_{32} & \mathbf{K}_{33} \end{bmatrix} \quad (8-163)$$

$$\text{where} \quad \mathbf{K}_{ij} = \iint_{A^e} \mathbf{B}_{bi}^T \mathbf{D}_b \mathbf{B}_{bj} dA + \iint_{A^e} \mathbf{B}_{si}^T \mathbf{D}_s \mathbf{B}_{sj} dA \quad (i, j = 1, 2, 3) \quad (8-164)$$

$$\mathbf{D}_b = D \begin{bmatrix} 1 & \mu & 0 \\ \mu & 1 & 0 \\ 0 & 0 & \frac{1-\mu}{2} \end{bmatrix}, \quad \mathbf{D}_s = C \begin{bmatrix} 1 & 0 \\ 0 & 1 \end{bmatrix}$$

$$D = \frac{Eh^3}{12(1-\mu^2)}, \quad C = \frac{5}{6} Gh = \frac{5D(1-\mu)}{h^2}$$

E is the Young's modulus; G is the shear modulus.

8.6.5 Numerical Examples

Example 8.3 The central deflection and moment of simply-supported (hard) square plates (the side length is L) subjected to uniform load.

Meshes A and B in Fig. 8.12 are still adopted, $\mu = 0.3$. The results by the element TCGC-T9 are given in Tables 8.9 to 8.11.

Table 8.9 The central deflection of simply-supported square plates subjected to uniform load $q / \left(\frac{qL^4}{100D} \right)$

Mesh number		2 × 2	4 × 4	8 × 8	16 × 16	Analytical
h/L	Mesh type					
10 ⁻³⁰	A	0.3803	0.4007	0.4050	0.4059	0.4062
	B	0.3948	0.4038	0.4057	0.4061	
0.001	A	0.3803	0.4007	0.4050	0.4059	0.4062
	B	0.3948	0.4038	0.4057	0.4061	
0.01	A	0.3804	0.4008	0.4051	0.4061	0.4064
	B	0.3950	0.4039	0.4058	0.4062	
0.1	A	0.3978	0.4183	0.4244	0.4265	0.4273
	B	0.4079	0.4194	0.4243	0.4264	
0.15	A	0.4214	0.4434	0.4506	0.4528	0.4536
	B	0.4254	0.4424	0.4500	0.4526	
0.20	A	0.4562	0.4799	0.4876	0.4897	0.4906
	B	0.4519	0.4763	0.4862	0.4893	
0.25	A	0.5025	0.5276	0.5352	0.5372	0.5379
	B	0.4880	0.5207	0.5328	0.5364	
0.30	A	0.5606	0.5863	0.5935	0.5952	0.5956
	B	0.5338	0.5754	0.5899	0.5941	
0.35	A	0.6304	0.6559	0.6624	0.6638	0.6641
	B	0.5892	0.6402	0.6573	0.6622	

Table 8.10 The central deflection of clamped square plates subjected to uniform load $q / \left(\frac{qL^4}{100D} \right)$

Mesh number		2 × 2	4 × 4	8 × 8	16 × 16	Analytical
h/L	Mesh type					
10 ⁻³⁰	A	0.1167	0.1241	0.1261	0.1265	0.1265
	B	0.0997	0.1192	0.1247	0.1260	

(Continued)

Mesh number h/L \ Mesh type		2×2	4×4	8×8	16×16	Analytical
0.001	<i>A</i>	0.1167	0.1241	0.1261	0.1265	0.1265
	<i>B</i>	0.0997	0.1192	0.1247	0.1260	
0.01	<i>A</i>	0.1169	0.1242	0.1263	0.1266	0.1265
	<i>B</i>	0.0998	0.1194	0.1249	0.1262	
0.1	<i>A</i>	0.1363	0.1440	0.1477	0.1496	0.1499
	<i>B</i>	0.1131	0.1376	0.1462	0.1492	
0.15	<i>A</i>	0.1604	0.1704	0.1758	0.1779	0.1798
	<i>B</i>	0.1310	0.1623	0.1737	0.1774	
0.20	<i>A</i>	0.1948	0.2080	0.2144	0.2165	0.2167
	<i>B</i>	0.1579	0.1975	0.2115	0.2157	
0.25	<i>A</i>	0.2403	0.2565	0.2632	0.2652	0.2675
	<i>B</i>	0.1942	0.2427	0.2593	0.2641	
0.30	<i>A</i>	0.2974	0.3158	0.3224	0.3241	0.3227
	<i>B</i>	0.2401	0.2980	0.3172	0.3226	
0.35	<i>A</i>	0.3662	0.3858	0.3919	0.3933	0.3951
	<i>B</i>	0.2956	0.3634	0.3852	0.3914	

Table 8.11 The central moment of simply-supported square plates subjected to uniform load $q / \left(\frac{qL^2}{10} \right)$

Mesh number h/L \ Mesh type		2×2	4×4	8×8	16×16	Analytical
10^{-30}	<i>A</i>	0.4928	0.4768	0.4771	0.4781	0.4789
	<i>B</i>	0.5024	0.4878	0.4823	0.4800	
0.001	<i>A</i>	0.4928	0.4768	0.4771	0.4781	
	<i>B</i>	0.5024	0.4878	0.4823	0.4800	
0.01	<i>A</i>	0.4932	0.4776	0.4780	0.4789	
	<i>B</i>	0.5026	0.4880	0.4824	0.4800	
0.1	<i>A</i>	0.5238	0.4986	0.4858	0.4809	
	<i>B</i>	0.5193	0.4987	0.4867	0.4814	
0.15	<i>A</i>	0.5435	0.5048	0.4870	0.4810	
	<i>B</i>	0.5329	0.5039	0.4877	0.4815	
0.20	<i>A</i>	0.5600	0.5090	0.4876	0.4811	
	<i>B</i>	0.5453	0.5073	0.4882	0.4815	

(Continued)

Mesh number h/L \ Mesh type		2 × 2	4 × 4	8 × 8	16 × 16	Analytical
0.25	A	0.5736	0.5118	0.4880	0.4811	0.4789
	B	0.5557	0.5094	0.4884	0.4815	
0.30	A	0.5849	0.5138	0.4881	0.4811	
	B	0.5639	0.5107	0.4885	0.4816	
0.35	A	0.5941	0.5152	0.4883	0.4811	
	B	0.5704	0.5116	0.4886	0.4816	

Example 8.4 The central deflection and moment of simply-supported (soft) and clamped circular plates subjected to uniform load.

The two meshes (A and B) shown in Fig. 6.14 are still adopted. Assume that $E = 10.92$, $\mu = 0.3$. The results by the element TCGC-T9 are given in Tables 8.12 to 8.14.

The above numerical examples show that the element TCGC-T9 also possesses good performance. It has high precision for both deflection and moment, and for both thick and thin plates. And, no shear locking happens.

By the comparison of the elements TCGC-T9 and TMT, we can conclude that,
 (1) The precisions of these two elements belong to the same magnitude.

(2) For relatively thin plates, the element TCGC-T9 is a little better than the element TMT. This is because for the very thin plate cases, the elements TCGC-T9 and TMT will degenerate to be the thin plate elements GPL-T9 and DKT, respectively. Note that the element GPL-T9 is a little better than the element DKT.

Table 8.12 The central deflection of simply-supported circular plates subjected to uniform load $q / \left(\frac{qR^4}{D} \right)$

h/R \ Mesh	A 24 elements	B 96 elements	Analytical
10^{-30}	0.063 818 (0.18%)	0.063 728 (0.04%)	0.063 702
0.001	0.063 818 (0.18%)	0.063 728 (0.04%)	0.063 702
0.01	0.063 821 (0.18%)	0.063 731 (0.03%)	0.063 709
0.1	0.064 242 (-0.27%)	0.064 247 (-0.26%)	0.064 416
0.15	0.064 901 (-0.62%)	0.065 043 (-0.41%)	0.065 309
0.20	0.065 921 (-0.96%)	0.066 222 (-0.51%)	0.066 559
0.25	0.067 315 (-1.25%)	0.067 777 (-0.57%)	0.068 166
0.30	0.069 088 (-1.49%)	0.069 704 (-0.61%)	0.070 130
0.35	0.071 241 (-1.67%)	0.071 998 (-0.63%)	0.072 452

Table 8.13 The central deflection of clamped circular plates subjected to uniform load $q/\left(\frac{qR^4}{D}\right)$

h/R \ Mesh	A 24 elements	B 96 elements	Analytical
10^{-30}	0.014 515 (-7.10%)	0.015 342 (-1.81%)	0.015 625
0.001	0.014 515 (-7.10%)	0.015 342 (-1.81%)	0.015 625
0.01	0.014 518 (-7.13%)	0.015 345 (-1.84%)	0.015 632
0.1	0.014 938 (-8.57%)	0.015 861 (-2.93%)	0.016 339
0.15	0.015 595 (-9.50%)	0.016 657 (-3.34%)	0.017 232
0.20	0.016 613 (-10.11%)	0.017 836 (-3.50%)	0.018 482
0.25	0.018 007 (-10.36%)	0.019 392 (-3.47%)	0.020 089
0.30	0.019 782 (-10.30%)	0.021 319 (-3.33%)	0.022 054
0.35	0.021 936 (-10.01%)	0.023 613 (-3.13%)	0.024 375

Table 8.14 The central moment of simply-supported circular plates subjected to uniform load $q/(qR^2)$

h/R \ Mesh	A 24 elements	B 96 elements	Analytical
10^{-11}	0.210 28 (1.95%)	0.207 36 (0.54%)	0.206 25
0.001	0.210 28 (1.95%)	0.207 36 (0.54%)	
0.01	0.210 29 (1.96%)	0.207 37 (0.54%)	
0.1	0.211 40 (2.50%)	0.208 15 (0.92%)	
0.15	0.212 42 (2.99%)	0.208 49 (1.09%)	
0.20	0.213 35 (3.44%)	0.208 69 (1.18%)	
0.25	0.214 11 (3.81%)	0.208 82 (1.25%)	
0.30	0.214 70 (4.10%)	0.208 91 (1.29%)	
0.35	0.215 16 (4.32%)	0.208 96 (1.31%)	

(3) For relatively thick plates, the element TMT is a little better than the element TCGC-T9. This is because the shear strain fields of these two elements are the same, only curvature fields are different; the rotation fields of the element TMT are assumed directly, only first-order differential operation is needed when we determine the curvature fields by such rotation fields, so the accuracy loss is relatively less; but in the element TCGC-T9, the deflection field is assumed directly, second-order differential operation must be performed when we determine the curvature fields by such deflection field, so the accuracy loss is relatively more.

(4) When we determine the element equivalent nodal load vector due to transverse distributed load, the element TCGC-T9 is more convenient. This is because the shape functions for the deflection of the element TCGC-T9 have

already been given, so the equivalent nodal load vector can be determined from these shape functions directly; but the deflection field of the element TMT is undetermined, so, before deriving the element equivalent nodal load vector, supplementary work, assumption of rational interpolation formula for deflection field, is needed.

8.7 Generalized Conforming Thin/Thick Plate Elements —From Thin to Thick Plate Elements

By starting with a thin plate element and introducing shear deformation, the thin plate element can be generalized to a new thin/thick plate element. Such transition schemes have been studied in references [15–19].

In 1986, Fricker^[15] proposed a simple method for including shear deformation in the thin plate elements, but the thick plate element he suggested cannot strictly pass the thick plate patch test.

Based on the displacement field of the rectangular thin plate element ACM, reference [16] developed a rectangular thick plate element with 12 DOFs by introducing additional displacement field and linear shear strain fields. The key point is that two generalized conforming conditions are adopted: (1) the conforming conditions for displacements between two adjacent elements; (2) the generalized conforming conditions between shear strains and displacements. The element obtained can pass pure bending, pure twisting and constant shear force patch tests, which provides the first successful experience for the schemes of transition from thin plate elements to thin / thick plate elements.

In reference [17], the displacement fields of the thick plate element were decomposed into two parts: displacement fields for the thin plate element and supplementary displacement fields for the thick plate element. Then, based on the two thin plate elements LR12-2^[20] and ACM^[21], two new thin/thick plate elements LFR1 and LFR2 were constructed. Now, their construction procedure will be introduced as follows.

8.7.1 Decomposition of the Displacement Fields of the Rectangular Thick Plate Element

Consider a rectangular thick plate element shown in Fig. 8.13. Its nodal displacement vector is composed of 12 DOFs

$$\mathbf{q}^e = [w_1 \quad \psi_{x1} \quad \psi_{y1} \quad w_2 \quad \psi_{x2} \quad \psi_{y2} \quad w_3 \quad \psi_{x3} \quad \psi_{y3} \quad w_4 \quad \psi_{x4} \quad \psi_{y4}]^T$$

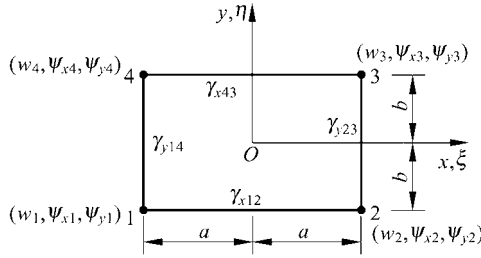


Figure 8.13 Rectangular thick plate element

The displacement fields in the domain of the element are assumed as

$$\left. \begin{aligned} w &= w^0 + w^* \\ \psi_x &= \psi_x^0 + \psi_x^* = \frac{\partial w^0}{\partial x} + \psi_x^* \\ \psi_y &= \psi_y^0 + \psi_y^* = \frac{\partial w^0}{\partial y} + \psi_y^* \end{aligned} \right\} \quad (8-165)$$

where w, ψ_x, ψ_y denote the displacements of the thick plate element; w^0, ψ_x^0, ψ_y^0 denote the displacements of a thin plate element that can be used; and w^*, ψ_x^*, ψ_y^* denote the supplementary displacements of the thick plate element.

The boundary displacements of the thick plate element are assumed as

$$\left. \begin{aligned} \tilde{w} &= \tilde{w}^0 + \tilde{w}^* \\ \tilde{\psi}_s &= \tilde{\psi}_s^0 + \tilde{\psi}_s^* \\ \tilde{\psi}_n &= \tilde{\psi}_n^0 + \tilde{\psi}_n^* \end{aligned} \right\} \quad (8-166)$$

in which n and s denote the normal and tangential directions of the boundary, respectively.

8.7.2 Determination of the Supplementary Displacements of the Thick Plate Element

In order to determine the supplementary displacement fields of the thick plate element, the transverse shear strain γ_s and the supplementary displacements $\tilde{w}^*, \tilde{\psi}_s^*$ and $\tilde{\psi}_n^*$ along each element side are firstly determined from the formulas of thick/thin beam; then the supplementary displacements w^*, ψ_x^* and ψ_y^* in the domain of the element are determined.

Firstly, from Eq. (8-99c), the transverse shear strains along each element side are as follows:

$$\left. \begin{aligned} \gamma_{x12} &= -\frac{\delta_1}{a}[w_1 - w_2 + a(\psi_{x1} + \psi_{x2})] \\ \gamma_{x43} &= -\frac{\delta_1}{a}[w_4 - w_3 + a(\psi_{x4} + \psi_{x3})] \\ \gamma_{y23} &= -\frac{\delta_2}{b}[w_2 - w_3 + b(\psi_{y2} + \psi_{y3})] \\ \gamma_{y14} &= -\frac{\delta_2}{b}[w_1 - w_4 + b(\psi_{y1} + \psi_{y4})] \end{aligned} \right\} \quad (8-167)$$

From Eq. (8-100), we obtain

$$\delta_1 = \frac{\left(\frac{h}{a}\right)^2}{\frac{10}{3}(1-\mu) + 2\left(\frac{h}{a}\right)^2}, \quad \delta_2 = \frac{\left(\frac{h}{b}\right)^2}{\frac{10}{3}(1-\mu) + 2\left(\frac{h}{b}\right)^2} \quad (8-168)$$

h is the thickness of the plate; μ is the Poisson's ratio.

Secondly, the supplementary displacements \tilde{w}^* , $\tilde{\psi}_s^*$ and $\tilde{\psi}_n^*$ along each element side are determined. From the fundamental formulas of the thick beam element (8-99a,b), \tilde{w}^* and $\tilde{\psi}_s^*$ can be written as

$$\left. \begin{aligned} \tilde{w}^* &= \gamma dt(1-t)(1-2t) \\ \tilde{\psi}_s^* &= -6\gamma t(1-t) \end{aligned} \right\} \quad (8-169)$$

Furthermore, $\tilde{\psi}_n^*$ can be assumed to be zero. Therefore, the supplementary displacements along 4 boundary lines can be obtained as

$$\left. \begin{aligned} \text{side 12} \quad \tilde{w}^* &= -\frac{1}{2}\gamma_{x12}a\xi(1-\xi^2), \quad \tilde{\psi}_x^* = -\frac{3}{2}\gamma_{x12}(1-\xi^2), \quad \tilde{\psi}_y^* = 0 \\ \text{side 23} \quad \tilde{w}^* &= -\frac{1}{2}\gamma_{y23}b\eta(1-\eta^2), \quad \tilde{\psi}_y^* = -\frac{3}{2}\gamma_{y23}(1-\eta^2), \quad \tilde{\psi}_x^* = 0 \\ \text{side 43} \quad \tilde{w}^* &= -\frac{1}{2}\gamma_{x43}a\xi(1-\xi^2), \quad \tilde{\psi}_x^* = -\frac{3}{2}\gamma_{x43}(1-\xi^2), \quad \tilde{\psi}_y^* = 0 \\ \text{side 14} \quad \tilde{w}^* &= -\frac{1}{2}\gamma_{y14}b\eta(1-\eta^2), \quad \tilde{\psi}_y^* = -\frac{3}{2}\gamma_{y14}(1-\eta^2), \quad \tilde{\psi}_x^* = 0 \end{aligned} \right\} \quad (8-170)$$

where $\xi = \frac{x}{a}$, $\eta = \frac{y}{b}$.

Finally, the supplementary displacements in the domain of the element are determined. According to Eq. (8-170), the interpolation formulas for the supplementary displacement field in the domain of the element can be written as

$$\left. \begin{aligned} w^* &= -\frac{a}{2} \left[\gamma_{x12} \left(\frac{1-\eta}{2} \right) + \gamma_{x43} \left(\frac{1+\eta}{2} \right) \right] \xi(1-\xi^2) \\ &\quad - \frac{b}{2} \left[\gamma_{y14} \left(\frac{1-\xi}{2} \right) + \gamma_{y23} \left(\frac{1+\xi}{2} \right) \right] \eta(1-\eta^2) \\ \psi_x^* &= -\frac{3}{2} \left[\gamma_{x12} \left(\frac{1-\eta}{2} \right) + \gamma_{x43} \left(\frac{1+\eta}{2} \right) \right] (1-\xi^2) \\ \psi_y^* &= -\frac{3}{2} \left[\gamma_{y14} \left(\frac{1-\xi}{2} \right) + \gamma_{y23} \left(\frac{1+\xi}{2} \right) \right] (1-\eta^2) \end{aligned} \right\} \quad (8-171)$$

It can be seen that, the supplementary displacements in the domain of the element given in Eq. (8-171) are exactly compatible with the boundary supplementary displacements given in Eq. (8-170).

Substituting Eq. (8-167) into Eq. (8-171), the supplementary displacements in the domain of the element can be obtained as:

$$\left. \begin{aligned} w^* &= -\frac{\delta_1}{4} \left[\sum_{i=1}^4 w_i \xi_i (1 + \eta_i \eta) - a \sum_{i=1}^4 \psi_{xi} (1 + \eta_i \eta) \right] \xi(1 - \xi^2) \\ &\quad - \frac{\delta_2}{4} \left[\sum_{i=1}^4 w_i \eta_i (1 + \xi_i \xi) - b \sum_{i=1}^4 \psi_{yi} (1 + \xi_i \xi) \right] \eta(1 - \eta^2) \\ \psi_x^* &= -\frac{3\delta_1}{4a} \left[\sum_{i=1}^4 w_i \xi_i (1 + \eta_i \eta) - a \sum_{i=1}^4 \psi_{xi} (1 + \eta_i \eta) \right] (1 - \xi^2) \\ \psi_y^* &= -\frac{3\delta_2}{4b} \left[\sum_{i=1}^4 w_i \eta_i (1 + \xi_i \xi) - b \sum_{i=1}^4 \psi_{yi} (1 + \xi_i \xi) \right] (1 - \eta^2) \end{aligned} \right\} \quad (8-172)$$

8.7.3 Two Thin/Thick Plate Elements

Two new universal elements LFR1 and LFR2 for both thick and thin plates are constructed based on two high quality thin plate elements (elements LR12-2 and ACM), respectively. The displacement field w^0 of the thin plate element can be expressed by

$$w^0 = \sum_{i=1}^4 N_i^0 \mathbf{q}_i \quad (8-173)$$

where

$$\left. \begin{aligned} N_i^0 &= [N_i^0 \quad N_{xi}^0 \quad N_{yi}^0] \\ \mathbf{q}_i &= [w_i \quad \psi_{xi} \quad \psi_{yi}]^T \end{aligned} \right\} \quad (8-174)$$

For element LFR1

$$\left. \begin{aligned} N_i^0 &= \frac{1}{8}(1 + \xi_i \xi)(1 + \eta_i \eta)(2 + \xi_i \xi + \eta_i \eta - \xi^2 - \eta^2) \\ N_{xi}^0 &= -\frac{a}{8} \xi_i (1 + \xi_i \xi)(1 + \eta_i \eta)(1 - \xi^2) - \frac{a}{24} \xi_i \eta_i \eta (1 - \eta^2) \\ N_{yi}^0 &= -\frac{b}{8} \eta_i (1 + \xi_i \xi)(1 + \eta_i \eta)(1 - \eta^2) - \frac{b}{24} \xi_i \eta_i \xi (1 - \xi^2) \end{aligned} \right\} \quad (8-175)$$

For element LFR2

$$\left. \begin{aligned} N_i^0 &= \frac{1}{8}(1 + \xi_i \xi)(1 + \eta_i \eta)(2 + \xi_i \xi + \eta_i \eta - \xi^2 - \eta^2) \\ N_{xi}^0 &= -\frac{a}{8} \xi_i (1 + \xi_i \xi)(1 + \eta_i \eta)(1 - \xi^2) \\ N_{yi}^0 &= -\frac{b}{8} \eta_i (1 + \xi_i \xi)(1 + \eta_i \eta)(1 - \eta^2) \end{aligned} \right\} \quad (8-176)$$

By the superposition of the displacement fields of the thin plate element given in Eq. (8-173) and the supplementary displacement fields of the thick plate element given in Eq. (8-172), the displacement fields of the thick plate element can be obtained. Then, the element stiffness matrices for two thin/thick plate elements can be derived according to the conventional procedure.

The above schemes have been further applied in references [18,19]. Since the generalized bubble displacement fields are introduced, the accuracy of the elements is improved, and the elements are insensitive to mesh distortion.

8.7.4 Numerical Examples

Example 8.5 The central deflection of simply-supported and clamped square plates (the side length is L) subjected to uniform load q . The Poisson's $\mu = 0.3$. The results by the elements LFR1 and LFR2 are given in Table 8.15.

It can be seen from Table 8.15 that, from thin plates to thick plates, elements LFR1 and LFR2 both provide results with high precision, but their derivation procedures are much simpler than that of the element in [16].

Example 8.6 Examine the convergence of elements LFR1 and LFR2 by refining the mesh. Tables 8.16 and 8.17 give the results for a thin square plate ($h/L = 10^{-3}$) and a thick square plate ($h/L = 0.3$) by using different meshes.

From Tables 8.16 and 8.17, it can be seen that, the elements LFR1 and LFR2 both have good convergence; when $h/L = 0.001$, the elements LFR1 and LFR2 will degenerate to be the thin plate elements LR12-2 and ACM, respectively.

Table 8.15 The central deflection coefficient of square plates subjected to uniform load $\left/ \left(\frac{qL^4}{100D} \right) \right.$

h/L	Simply-supported				Clamped			
	Analytical	LFR1	LFR2	[16]	Analytical	LFR1	LFR2	[16]
10^{-11}	0.4062	0.4062	0.4105	0.4044	0.1265	0.1263	0.1290	0.1290
10^{-3}	0.4062	0.4062	0.4105	0.4044	0.1265	0.1263	0.1290	0.1293
10^{-2}	0.4062	0.4062	0.4106	0.4045	0.1265	0.1264	0.1293	0.1293
0.1	0.4273	0.4224	0.4304	0.4242	0.1499	0.1482	0.1522	0.1521
0.15	0.4536	0.4480	0.4566	0.4502	0.1798	0.1762	0.1802	0.1801
0.20	0.4906	0.4845	0.4933	0.4869	0.2167	0.2144	0.2183	0.2181
0.25	0.5379	0.5312	0.5401	0.5336	0.2675	0.2623	0.2661	0.2658
0.30	0.5956	0.5879	0.5968	0.5902	0.3227	0.3198	0.3235	0.3229
0.35	0.6641	0.6542	0.6631	0.6564	0.3951	0.3866	0.3902	0.3896

Note: a 10×10 mesh is used for the whole plate.

Table 8.16 Results for a thin plate ($h/L = 10^{-3}$) by different meshes (uniform load)

Mesh for whole plate	Central deflection $\left/ \left(\frac{qL^4}{100D} \right) \right.$				Moment $\left/ \left(\frac{qL^2}{10} \right) \right.$			
	Simply-supported		Clamped		Simply-supported (central)		Clamped (mid-side)	
	LFR1	LFR2	LFR1	LFR2	LFR1	LFR2	LFR1	LFR2
2×2	0.3906	0.5063	0.1480	0.1480	0.6094	0.6602	-0.3551	-0.3551
4×4	0.4052	0.4328	0.1243	0.1403	0.5123	0.5217	-0.4706	-0.4761
8×8	0.4062	0.4129	0.1261	0.1304	0.4873	0.4892	-0.5000	-0.5028
16×16	0.4062	0.4079	0.1265	0.1275	0.4810	0.4814	-0.5096	-0.5104
Analytical	0.4062		0.1265		0.4789		-0.5133	

Table 8.17 Results for a thick plate ($h/L = 0.3$) by different meshes (uniform load)

Mesh for whole plate	Central deflection $\left/ \left(\frac{qL^4}{100D} \right) \right.$				Moment $\left/ \left(\frac{qL^2}{10} \right) \right.$			
	Simply-supported		Clamped		Simply-supported (central)		Clamped (mid-side)	
	LFR1	LFR2	LFR1	LFR2	LFR1	LFR2	LFR1	LFR2
2×2	0.5648	0.7081	0.3806	0.3806	0.8422	0.8395	-0.4089	-0.4089
4×4	0.5706	0.6201	0.3207	0.3377	0.5907	0.5739	-0.4927	-0.4604
8×8	0.5855	0.5992	0.3194	0.3250	0.5092	0.5031	-0.4912	-0.4604
16×16	0.5906	0.5942	0.3204	0.3219	0.4867	0.4850	-0.4748	-0.4546
Analytical	0.5956		0.3227		0.4789		-0.4260	

References

- [1] Reissner E (1995) The effect of transverse deformation on the bending of elastic plates. *Journal of Applied Mechanics* 12: A69 – 77
- [2] Mindlin R D (1951) Influence of rotatory inertia and shear on flexural motion of isotropic elastic plates. *Journal of Applied Mechanics* 18: 31 – 38
- [3] Hu HC (1984) *Variational principles of theory of elasticity with applications*. Science Press, Beijing
- [4] Cen S, Long ZF (1998) A Mindlin triangular plate element with improved interpolation for the rotation and shear strain fields. *Gong Cheng Li Xue/Engineering Mechanics* 15(3): 1 – 14 (in Chinese)
- [5] Zienkiewicz OC, Taylor RL, Too JM (1971) Reduced integration techniques in general analysis of plates and shells. *International Journal for Numerical Methods in Engineering* 3(2):275 – 290
- [6] Hughes TJR, Cohen M, Haron M (1978) Reduced and selective integration technique in finite element analysis of plates. *Nuclear Eng. and Design* 46: 203 – 222
- [7] Hinton E, Huang HC (1986) A family of quadrilateral Mindlin plate elements with substitute shear strain fields. *Computers & Structures* 23(3): 409 – 431
- [8] Katili I (1993) A new discrete Kirchhoff-Mindlin element based on Mindlin-Reissner plate theory and assumed shear strain fields-part I : An extended DKT element for thick-plate bending analysis. *International Journal for Numerical Methods in Engineering* 36: 1859 – 1883
- [9] Cen S, Long ZF, Long YQ (1999) A Mindlin quadrilateral plate element with improved interpolation for the rotation and shear strain fields. *Gong Cheng Li Xue/Engineering Mechanics* 16(4): 1 – 15 (in Chinese)
- [10] Cen S, Long ZF (1998) A new triangular generalized conforming element for thin-thick plates. *Gong Cheng Li Xue/Engineering Mechanics* 15(1): 10 – 22 (in Chinese)
- [11] Cen S, Long YQ, Yao ZH, Chiew SP (2006) Application of the quadrilateral area coordinate method: a new element for Mindlin-Reissner plate. *International Journal for Numerical Methods in Engineering* 66(1): 1 – 45
- [12] Long YQ, Fu XR (2002) Two generalized conforming quadrilateral thick plate elements based on analytical trial functions. *Gong Cheng Li Xue/Engineering Mechanics* 19(3): 10 – 15 (in Chinese)
- [13] Chen YL, Cen S, Yao ZH, Long YQ, Long ZF (2003) Development of triangular flat-shell element using a new thin-thick plate bending element based on SemiLoof constrains. *Structural Engineering and Mechanics* 15(1): 83 – 114
- [14] Long YQ, Bu XM, Long ZF, Xu Y (1995) Generalized conforming plate bending elements using point and line compatibility conditions. *Computers & Structures* 54(4): 717 – 723
- [15] Fricker AJ (1986) A simple method for including shear deformation in thin plate elements. *International Journal for Numerical Methods in Engineering* 23: 1355 – 1366
- [16] Long YQ, Xi F (1992) A universal method for including shear deformation in the thin plate elements. *International Journal for Numerical Methods in Engineering* 34: 171 – 177

Chapter 8 Generalized Conforming Thick Plate Element

- [17] Long ZF (1992) Locking-free thick plate rectangular element. *Gong Cheng Li Xue/Engineering Mechanics* 9(1): 88 – 93 (in Chinese)
- [18] Cen S, Long ZF, Kuang WQ (1997) Improved thick plate elements by introducing generalized bubble displacement fields. In: Han DJ, Mo HH (eds) *Computational Methods in Engineering and Science— Theory and Application (Proceedings of the Sixth EPMESC Conference)*. South China University of Technology Press, China, Guangzhou, pp517 – 522
- [19] Cen S, Long ZF, Long YQ, Kuang WQ (1997) Two robust generalized conforming rectangular element for thin-thick plates. In: Han DJ, Mo HH (eds) *Computational Methods in Engineering and Science— Theory and Application (Proceedings of the Sixth EPMESC Conference)*. South China University of Technology Press, China, Guangzhou, pp523 – 527
- [20] Long ZF (1992) Triangular and rectangular plate elements based on generalized compatibility conditions. *Computational Mechanics* 10(3/4): 281 – 288
- [21] Melosh RJ (1963) Basis for derivation of matrices for the direct stiffness method. *AIAA Journal* 1(7): 1631 – 1637

Chapter 9 Generalized Conforming Element for the Analysis of the Laminated Composite Plates

Song Cen

Department of Engineering Mechanics, School of Aerospace,
Tsinghua University, Beijing, 100084, China

Yu-Qiu Long

Department of Civil Engineering, School of Civil Engineering,
Tsinghua University, Beijing, 100084, China

Abstract A simple displacement-based, quadrilateral 20 DOF (5 DOF per node) bending element based on the first-order shear deformation theory (FSDT) for the analysis of the arbitrary laminated composite plates is presented in this chapter. This element is constructed by the following procedure: (1) the variation functions of the rotation and the shear strain along each side of the element are determined using the Timoshenko's beam theory; and (2) the shear strain, rotation and in-plane displacement fields in the domain of the element are then determined using the technique of improved interpolation. In fact, this is the scheme of assuming rotation and shear strain fields which has been introduced in the previous chapter. Furthermore, a simple hybrid procedure is also proposed to improve the stress solutions. The proposed element, denoted as CTMQ20, possesses the advantages of both the displacement-based and hybrid elements. Thus, excellent results for both displacements and stresses, especially for the transverse shear stresses, can be obtained.

Keywords finite element, laminated composite plate, generalized conforming, first-order shear deformation theory (FSDT), hybrid-enhanced post-processing procedure.

9.1 Introduction

During the past 40 years, high performance composite materials have been playing very important roles in the design of modern industrial products and structures for their high strength-to-weight and stiffness-to-weight ratios, and have been broadly used in many high-tech areas, such as aerospace, building, transport,

medicine, and so on. Laminated composite plate is one of the most popular structural components. Due to its particularities and complexity in construction, studies on appropriate computational theories and methods for these structures attract many researchers all the while. The finite element method provides an effective way of solution for such laminated composite plates. Various methods have been proposed based on the following theories^[1]:

- The classical lamination theory based on Kirchhoff hypothesis (CLT);
- First-order shear deformation theory (FSDT);
- Higher-order shear deformation theory (HSDT);
- Layer-wise lamination theory (LLT);
- Three-dimensional (3D) elasticity.

The classical lamination theory (CLT)^[2,3], which is an extension of the classical thin plate theory to laminated plates, neglects the effects due to transverse shear strains and requires C^1 continuity in displacement fields. The errors in such a theory naturally increase as the thickness-span ratio of the plate increases. The first-order shear deformation theory (FSDT) is based on the Reissner-Mindlin plate theory^[4,5]. With the consideration of the transverse shear deformation effect on the plates, FSDT only requires C^0 continuity and can be used from thin to moderately thick plates. But, in FSDT, the transverse shearing strains/stresses are assumed constant through the plate thickness, which is contradictory to the zero shear stress conditions on the bounding planes of the plate. Furthermore, several fictitious shear correction coefficients must be introduced. For overcoming the limitations of FSDT, higher-order shear deformation theories (HSDT) have been proposed by some researchers. Two different approaches have been commonly employed: single-layer and multi-layer formulations. The former increases the order considered for the displacement representation in the thickness coordinates^[6-10]. The latter assumes a representation formula for the displacement field in each layer, similar to that of layer-wise lamination theory^[11,12]. The solutions of these higher order theories are closer to the 3D elasticity theory than those of the two former plate theories. This is especially so for very thick cases. However, the computational cost will be increased significantly.

FSDT is usually considered the best compromise between the capability for prediction and computational cost for a wide class of applications. Some methods have been proposed to solve the above-mentioned problems of the FSDT. For example, the distribution of transverse shear stresses can be evaluated by the 3D elasticity equilibrium equation^[13]; Vlachoutsis^[14] presented a simple procedure to calculate the shear correction factors for laminated plates and shells under cylindrical bending; Auricchio et al.^[15] proposed a numerical method for solving the shear correction coefficients of arbitrary laminated composite plates; Rolfes et al.^[16] presented a simple post-processing approach to obtain improved transverse shear stresses in finite element analysis based on FSDT; and Rolfes et al.^[17] even presented a simple and accurate post-processing method for the FSDT to calculate

the transverse normal stress, which was initially assumed to be zero. These efforts make it more convenient and reasonable to use the FSDT in practical applications.

New finite elements based on the FSDT are still proposed by many researchers^[15, 18, 20]. Since many simple displacement-based elements adopt simple interpolation functions, they are unable to provide a satisfactory recovery of the transverse shear stresses. Therefore, the hybrid or mixed-hybrid elements have been playing a leading role in the analysis of the composite plates^[21]. However, the formulations of the hybrid elements are more complicated than that of the displacement-based elements. Besides, shear locking may also be a problem in the construction of the laminated composite plate elements. How to develop a simple but effective model has been a problem for a long time.

In the first section of this chapter, the first-order shear deformation theory (FSDT) is introduced briefly, and a set of formulae of the Timoshenko's laminated composite beam element are also given for developing the plate element; the subsequent sections will introduce new generalized conforming laminate composite plate elements and a new hybrid-enhanced post-processing procedure for transverse stress solutions which are proposed in [22,23].

9.2 Fundamental Theory

9.2.1 First-Order Shear Deformation Theory for Laminated Composite Plates (FSDT)

With reference to Fig. 9.1, for a linear elastic arbitrary composite plate with n layers, the kinematics is governed by the mid-plane displacements u^0 , v^0 , the transverse displacement (deflection) w and rotations ψ_x and ψ_y :

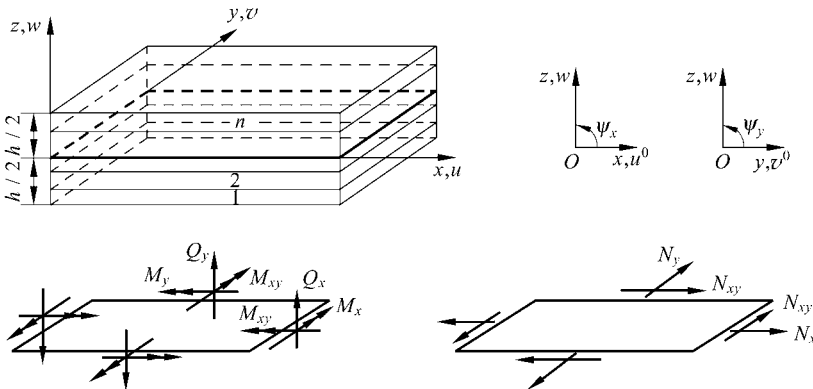


Figure 9.1 Forces and displacements at the mid-plane of a laminated composite plate

$$\begin{cases} u(x, y, z) = u^0(x, y) - z\psi_x(x, y) \\ v(x, y, z) = v^0(x, y) - z\psi_y(x, y) \\ w(x, y, z) = w(x, y) \end{cases} \quad (9-1)$$

Therefore, the total in-plane strain $\boldsymbol{\varepsilon}$ is:

$$\boldsymbol{\varepsilon} = \boldsymbol{\varepsilon}^0 + z\boldsymbol{\kappa} \quad (9-2)$$

where $\boldsymbol{\varepsilon}^0$ and $\boldsymbol{\kappa}$ are the in-plane strain of the mid-plane and the curvature vector of the plate, respectively, which are given below:

$$\boldsymbol{\varepsilon} = [\varepsilon_x \quad \varepsilon_y \quad \gamma_{xy}]^T \quad (9-3)$$

$$\boldsymbol{\varepsilon}^0 = [\varepsilon_x^0 \quad \varepsilon_y^0 \quad \gamma_{xy}^0]^T = \left[\frac{\partial u^0}{\partial x} \quad \frac{\partial v^0}{\partial y} \quad \frac{\partial u^0}{\partial y} + \frac{\partial v^0}{\partial x} \right]^T \quad (9-4)$$

$$\boldsymbol{\kappa} = [\kappa_x \quad \kappa_y \quad 2\kappa_{xy}]^T = \left[-\frac{\partial \psi_x}{\partial x} \quad -\frac{\partial \psi_y}{\partial y} \quad -\frac{\partial \psi_x}{\partial y} - \frac{\partial \psi_y}{\partial x} \right]^T \quad (9-5)$$

The transverse shear strain vector is:

$$\boldsymbol{\gamma} = [\gamma_x \quad \gamma_y]^T = \left[\frac{\partial w}{\partial x} - \psi_x \quad \frac{\partial w}{\partial y} - \psi_y \right]^T \quad (9-6)$$

The stress-strain relationship with respect to the principal material axes, 1-axis and 2-axis, for the k th ($k = 1, 2, \dots, n$) layer is:

$$\begin{Bmatrix} \sigma_1 \\ \sigma_2 \\ \tau_{12} \end{Bmatrix}_k = \begin{bmatrix} Q_{11} & Q_{12} & 0 \\ Q_{12} & Q_{22} & 0 \\ 0 & 0 & Q_{66} \end{bmatrix}_k \begin{Bmatrix} \varepsilon_1 \\ \varepsilon_2 \\ \gamma_{12} \end{Bmatrix}_k \quad (9-7)$$

$$\begin{Bmatrix} \tau_{23} \\ \tau_{13} \end{Bmatrix}_k = \begin{bmatrix} Q_{44} & 0 \\ 0 & Q_{55} \end{bmatrix}_k \begin{Bmatrix} \gamma_{23} \\ \gamma_{13} \end{Bmatrix}_k \quad (9-8)$$

in which

$$\left. \begin{aligned} Q_{11k} &= \frac{E_{1k}}{1 - \mu_{12k}\mu_{21k}}, & Q_{12k} &= \frac{\mu_{21k}E_{1k}}{1 - \mu_{12k}\mu_{21k}} = Q_{21k} \\ Q_{21k} &= \frac{\mu_{12k}E_{2k}}{1 - \mu_{12k}\mu_{21k}}, & Q_{22k} &= \frac{E_{2k}}{1 - \mu_{12k}\mu_{21k}} \\ Q_{66k} &= G_{12k}, & Q_{44k} &= G_{23k}, & Q_{55k} &= G_{13k} \end{aligned} \right\} \quad (9-9)$$

where σ_{1k} , σ_{2k} , τ_{12k} , τ_{23k} and τ_{13k} are the two principal direct stresses, the in-plane shear stresses and the transverse shear stresses of the k th layer, respectively; ε_{1k} , ε_{2k} , γ_{12k} , γ_{23k} and γ_{13k} are the corresponding strains; E_{1k} and E_{2k} are the Young's modulus in the direction of the fibres (1-axis) and transverse to the fibres (2-axis), respectively; G_{12k} is the in-plane shear modulus, G_{23k} and G_{13k} are the transverse shear modulus, μ_{12k} is the major Poisson's ratio, and $\mu_{21k} = \mu_{12k} \frac{E_{2k}}{E_{1k}}$.

Thus, the stress-strain relationship with respect to x -axis and y -axis for the k th ($k = 1, 2, \dots, n$) layer is

$$\boldsymbol{\sigma}_k = \begin{Bmatrix} \sigma_x \\ \sigma_y \\ \tau_{xy} \end{Bmatrix}_k = \begin{bmatrix} \bar{Q}_{11} & \bar{Q}_{12} & \bar{Q}_{16} \\ \bar{Q}_{12} & \bar{Q}_{22} & \bar{Q}_{26} \\ \bar{Q}_{16} & \bar{Q}_{26} & \bar{Q}_{66} \end{bmatrix}_k \begin{Bmatrix} \varepsilon_x \\ \varepsilon_y \\ \gamma_{xy} \end{Bmatrix} = \bar{\mathbf{Q}}_k \boldsymbol{\varepsilon} \quad (9-10)$$

$$\boldsymbol{\tau}_{zk} = \begin{Bmatrix} \tau_{xz} \\ \tau_{yz} \end{Bmatrix}_k = \begin{bmatrix} k_1^2 \bar{Q}_{55} & k_1 k_2 \bar{Q}_{45} \\ k_1 k_2 \bar{Q}_{45} & k_2^2 \bar{Q}_{44} \end{bmatrix}_k \begin{Bmatrix} \gamma_{xz} \\ \gamma_{yz} \end{Bmatrix} = \bar{\mathbf{C}}_{sk} \boldsymbol{\gamma} \quad (9-11)$$

in which k_1^2 , $k_1 k_2$ and k_2^2 are the shear correction coefficients;

$$\begin{cases} \bar{Q}_{11k} = Q_{11k} l_k^4 + 2(Q_{12k} + 2Q_{66k}) l_k^2 m_k^2 + Q_{22k} m_k^4 \\ \bar{Q}_{12k} = (Q_{11k} + Q_{22k} - 4Q_{66k}) l_k^2 m_k^2 + Q_{12k} (l_k^4 + m_k^4) \\ \bar{Q}_{22k} = Q_{11k} m_k^4 + 2(Q_{12k} + 2Q_{66k}) l_k^2 m_k^2 + Q_{22k} l_k^4 \\ \bar{Q}_{16k} = (Q_{11k} - Q_{12k} - 2Q_{66k}) l_k^3 m_k + (Q_{12k} - Q_{22k} + 2Q_{66k}) l_k m_k^3 \\ \bar{Q}_{26k} = (Q_{11k} - Q_{12k} - 2Q_{66k}) l_k m_k^3 + (Q_{12k} - Q_{22k} + 2Q_{66k}) l_k^3 m_k \\ \bar{Q}_{66k} = (Q_{11k} + Q_{22k} - 2Q_{12k} - 2Q_{66k}) l_k^2 m_k^2 + Q_{66k} (l_k^4 + m_k^4) \\ \bar{Q}_{44k} = Q_{44k} l_k^2 + Q_{55k} m_k^2 \\ \bar{Q}_{45k} = (Q_{55k} - Q_{44k}) l_k m_k \\ \bar{Q}_{55k} = Q_{44k} m_k^2 + Q_{55k} l_k^2 \end{cases} \quad (9-12)$$

$$l_k = \cos \theta_k, \quad m_k = \sin \theta_k \quad (9-13)$$

θ_k is the angle between the x -axis and the fiber direction 1-axis of the k th layer.

The constitutive relationship of the laminated composite plate can be expressed as:

$$\boldsymbol{\sigma}_p = \begin{Bmatrix} \mathbf{N} \\ \mathbf{M} \end{Bmatrix} = \begin{bmatrix} \mathbf{A} & \mathbf{B} \\ \mathbf{B} & \mathbf{D} \end{bmatrix} \begin{Bmatrix} \boldsymbol{\varepsilon}^0 \\ \boldsymbol{\kappa} \end{Bmatrix} = \mathbf{C}_p \boldsymbol{\varepsilon}_p \quad (9-14)$$

$$\mathbf{Q} = \mathbf{C}_s \boldsymbol{\gamma} \quad (9-15)$$

where \mathbf{N} is the membrane force vector of the mid-plane; \mathbf{M} is the bending

moment vector; \underline{Q} is the transverse shear force vector; \underline{A} is the extensional stiffness; \underline{B} is the bending-extension stiffness; \underline{D} is the bending stiffness; \underline{C}_s is the shear stiffness. These matrices can be expressed in the following forms:

$$\underline{N} = [N_x \quad N_y \quad N_{xy}]^T, \quad \underline{M} = [M_x \quad M_y \quad M_{xy}]^T \quad (9-16)$$

$$\underline{Q} = [Q_x \quad Q_y]^T \quad (9-17)$$

$$\underline{A} = \begin{bmatrix} A_{11} & A_{12} & A_{16} \\ A_{12} & A_{22} & A_{26} \\ A_{16} & A_{26} & A_{66} \end{bmatrix}, \quad \underline{B} = \begin{bmatrix} B_{11} & B_{12} & B_{16} \\ B_{12} & B_{22} & B_{26} \\ B_{16} & B_{26} & B_{66} \end{bmatrix}, \quad \underline{D} = \begin{bmatrix} D_{11} & D_{12} & D_{16} \\ D_{12} & D_{22} & D_{26} \\ D_{16} & D_{26} & D_{66} \end{bmatrix} \quad (9-18)$$

$$\underline{C}_s = \begin{bmatrix} C_{55} & C_{45} \\ C_{45} & C_{44} \end{bmatrix} = \begin{bmatrix} k_1^2 C_{55}^0 & k_1 k_2 C_{45}^0 \\ k_1 k_2 C_{45}^0 & k_2^2 C_{44}^0 \end{bmatrix} \quad (9-19)$$

$$\left. \begin{aligned} A_{ij} &= \int_{-h/2}^{h/2} \bar{Q}_{ij} dz = \sum_{k=1}^n \bar{Q}_{ijk} (h_k - h_{k-1}) \\ B_{ij} &= \int_{-h/2}^{h/2} \bar{Q}_{ij} z dz = \frac{1}{2} \sum_{k=1}^n \bar{Q}_{ijk} (h_k^2 - h_{k-1}^2) \\ D_{ij} &= \int_{-h/2}^{h/2} \bar{Q}_{ij} z^2 dz = \frac{1}{3} \sum_{k=1}^n \bar{Q}_{ijk} (h_k^3 - h_{k-1}^3) \end{aligned} \right\} (i, j = 1, 2, 6) \quad (9-20)$$

$$C_{ij}^0 = \int_{-h/2}^{h/2} \bar{Q}_{ij} dz = \sum_{k=1}^n \bar{Q}_{ijk} (h_k - h_{k-1}) \quad (i, j = 4, 5) \quad (9-21)$$

where h_k is the z-coordinate of the upper surface for the k th layer, $h_0 = -h/2$ and $h_n = h/2$, h is the thickness of the plate.

The inverse relations of Eqs. (9-14) and (9-15) are as follows:

$$\underline{\epsilon}_p = \underline{S}_p \underline{\sigma}_p \quad (9-22)$$

$$\underline{\gamma} = \underline{S}_s \underline{Q} \quad (9-23)$$

where

$$\underline{S}_p = \underline{C}_p^{-1} = \begin{bmatrix} \underline{A} & \underline{B} \\ \underline{B} & \underline{D} \end{bmatrix}^{-1} = \begin{bmatrix} \underline{S}_{e3 \times 6} \\ \underline{S}_{b3 \times 6} \end{bmatrix} \quad (9-24)$$

$$\underline{S}_s = \underline{C}_s^{-1} \quad (9-25)$$

Substitution of Eq. (9-2) into Eq. (9-10) yields:

$$\sigma_k = \bar{Q}_k (\epsilon^0 + z\kappa) \tag{9-26}$$

Then, substitution of Eqs. (9-14) and (9-24) into the above equation yields:

$$\sigma_k = \bar{Q}_k (S_e + zS_b)\sigma_p \tag{9-27}$$

9.2.2 Locking-free Timoshenko Laminated Composite Beam Element

As shown in Fig. 9.2, for a Timoshenko laminated composite beam element, the formulas of deflection w , rotation ψ and shear strain γ for the element are still given by Eqs. (8-99) and (8-100), in which D and C should be replaced by the following D_d and C_d :

$$D_d = \frac{1}{3} \sum_{k=1}^n (\bar{Q}_{11k})_{\bar{ij}} (h_k^3 - h_{k-1}^3) \tag{9-28}$$

with

$$(\bar{Q}_{11k})_{\bar{ij}} = Q_{11k} l_{k\bar{ij}}^4 + 2(Q_{12k} + 2Q_{66k}) l_{k\bar{ij}}^2 m_{k\bar{ij}}^2 + Q_{22k} m_{k\bar{ij}}^4 \tag{9-29}$$

$$l_{k\bar{ij}} = \cos(\theta_k - \theta_{\bar{ij}}), \quad m_{k\bar{ij}} = \sin(\theta_k - \theta_{\bar{ij}}) \tag{9-30}$$

where $\theta_{\bar{ij}}$ is the angle between the x -axis and the beam (see Fig. 9.2). $\theta_k - \theta_{\bar{ij}}$ is the angle between the beam \bar{ij} and the 1-axis of the k th layer.

$$C_d = (k_1^2 l_{\bar{ij}}^2 + k_2^2 m_{\bar{ij}}^2) \sum_{k=1}^n (\bar{Q}_{55k})_{\bar{ij}} (h_k - h_{k-1}) \tag{9-31}$$

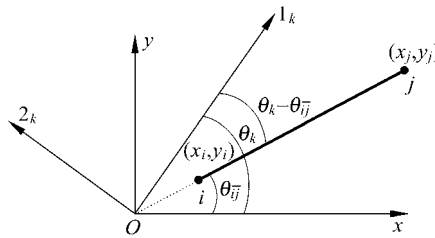


Figure 9.2 The orientation of a Timoshenko beam element \bar{ij} in the coordinate system xOy and the material principal coordinate system $O12$ of the k th layer

with

$$(\bar{Q}_{55k})_{ij} = Q_{55k} l_{ij}^2 + Q_{44k} m_{ij}^2 \tag{9-32}$$

$$l_{ij} = \cos \theta_{ij}, \quad m_{ij} = \sin \theta_{ij} \tag{9-33}$$

9.3 New Element CTMQ20 for the Analysis of Laminated Composite Plates

To construct the new laminated composite plate elements by using the generalized conforming thick-thin plate elements is a new scheme proposed recently. In references [22] and [23], two new models based on FSDT, TMQ20 and CTMQ20, have been successfully developed. They are constructed by adding the bilinear in-plane displacement field to the formulations of the quadrilateral thick-thin elements TMQ^[24] and ARS-Q12^[25], respectively. This section will introduce the construction procedure of the element CTMQ20 proposed in [23].

Consider the quadrilateral arbitrary laminated composite plate element shown in Fig. 9.3. The element nodal displacement vector is:

$$\left. \begin{aligned} \mathbf{q}^e &= [\mathbf{q}_1 \quad \mathbf{q}_2 \quad \mathbf{q}_3 \quad \mathbf{q}_4]^T \\ \mathbf{q}_i &= [u_i \quad v_i \quad w_i \quad \psi_{xi} \quad \psi_{yi}]^T \quad (i=1,2,3,4) \end{aligned} \right\} \tag{9-34}$$

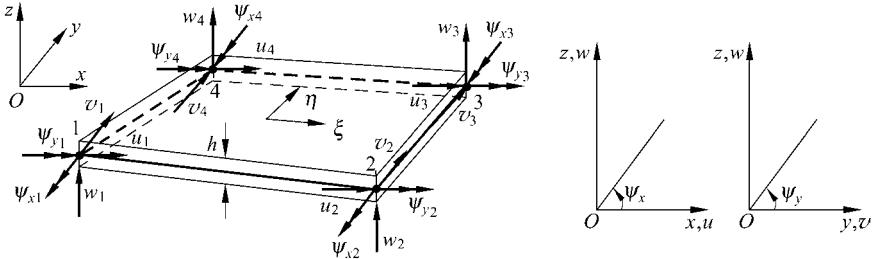


Figure 9.3 A 4-node quadrilateral laminated composite plate element

9.3.1 Interpolation Formulas for the Shear Strain Fields

1. Shear strain along the element sides

According to Eq. (8-99c), the transverse shear strain along the tangential direction (s-direction) of each side can be written as:

$$\left. \begin{aligned} \gamma_{s1} &= -\frac{\delta_1}{d_1} [2(w_2 - w_3) + (c_1\psi_{x_2} - b_1\psi_{y_2}) + (c_1\psi_{x_3} - b_1\psi_{y_3})] \\ \gamma_{s2} &= -\frac{\delta_2}{d_2} [2(w_3 - w_4) + (c_2\psi_{x_3} - b_2\psi_{y_3}) + (c_2\psi_{x_4} - b_2\psi_{y_4})] \\ \gamma_{s3} &= -\frac{\delta_3}{d_3} [2(w_4 - w_1) + (c_3\psi_{x_4} - b_3\psi_{y_4}) + (c_3\psi_{x_1} - b_3\psi_{y_1})] \\ \gamma_{s4} &= -\frac{\delta_4}{d_4} [2(w_1 - w_2) + (c_4\psi_{x_1} - b_4\psi_{y_1}) + (c_4\psi_{x_2} - b_4\psi_{y_2})] \end{aligned} \right\} \quad (9-35)$$

where $\gamma_{s1}, \gamma_{s2}, \gamma_{s3}$ and γ_{s4} are the shear strains along sides $\overline{23}, \overline{34}, \overline{41}$ and $\overline{12}$, respectively; d_1, d_2, d_3 and d_4 are the lengths of sides $23, 34, 41$ and 12 , respectively (refer to Fig. 9.4).

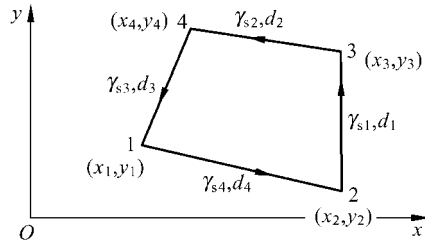


Figure 9.4 The shear strain γ_{si} along each element side and the side length $d_i (i=1,2,3,4)$

$$\begin{aligned} b_1 &= y_2 - y_3 & b_2 &= y_3 - y_4 & b_3 &= y_4 - y_1 & b_4 &= y_1 - y_2 \\ c_1 &= x_3 - x_2 & c_2 &= x_4 - x_3 & c_3 &= x_1 - x_4 & c_4 &= x_2 - x_1 \end{aligned} \quad (9-36)$$

$$\delta_i = \frac{6\lambda_i}{1 + 12\lambda_i}, \quad \lambda_i = \frac{D_{di}}{C_{di}d_i^2} \quad (i=1,2,3,4) \quad (9-37)$$

where D_{di} and C_{di} are given by Eqs. (9-28) and (9-31), respectively. Note that when h approaches zero, δ_i will approach zero. Hence, the transverse shear strains given by Eq. (9-35) will also approach zero.

Let

$$\gamma_{si}^* = d_i \gamma_{si} \quad (i=1,2,3,4) \quad (9-38)$$

$$\gamma_s^* = [\gamma_{s1}^* \quad \gamma_{s2}^* \quad \gamma_{s3}^* \quad \gamma_{s4}^*]^T \quad (9-39)$$

Then we have

$$\gamma_s^* = \Gamma^* \mathbf{q}^e \quad (9-40)$$

where

$$\Gamma^* = [\Gamma_1^* \quad \Gamma_2^* \quad \Gamma_3^* \quad \Gamma_4^*]^T$$

$$\Gamma_1^* = \begin{bmatrix} 0 & 0 & 0 & 0 & 0 \\ 0 & 0 & 0 & 0 & 0 \\ 0 & 0 & 2\delta_3 & -c_3\delta_3 & b_3\delta_3 \\ 0 & 0 & -2\delta_4 & -c_4\delta_4 & b_4\delta_4 \end{bmatrix} \quad \Gamma_2^* = \begin{bmatrix} 0 & 0 & -2\delta_1 & -c_1\delta_1 & b_1\delta_1 \\ 0 & 0 & 0 & 0 & 0 \\ 0 & 0 & 0 & 0 & 0 \\ 0 & 0 & 2\delta_4 & -c_4\delta_4 & b_4\delta_4 \end{bmatrix}$$

$$\Gamma_3^* = \begin{bmatrix} 0 & 0 & 2\delta_1 & -c_1\delta_1 & b_1\delta_1 \\ 0 & 0 & -2\delta_2 & -c_2\delta_2 & b_2\delta_2 \\ 0 & 0 & 0 & 0 & 0 \\ 0 & 0 & 0 & 0 & 0 \end{bmatrix} \quad \Gamma_4^* = \begin{bmatrix} 0 & 0 & 0 & 0 & 0 \\ 0 & 0 & 2\delta_2 & -c_2\delta_2 & b_2\delta_2 \\ 0 & 0 & -2\delta_3 & -c_3\delta_3 & b_3\delta_3 \\ 0 & 0 & 0 & 0 & 0 \end{bmatrix}$$

(9-41)

2. Nodal shear strains γ_{xi} and γ_{yi}

The direction cosines of each element side are defined as follows (refer to Fig. 9.5):

$$\left. \begin{aligned} \cos(s_{12}, x) = \cos \theta_1 = \frac{c_4}{d_4}, \cos(s_{12}, y) = \sin \theta_1 = -\frac{b_4}{d_4} \\ \cos(s_{23}, x) = \frac{c_1}{d_1}, \cos(s_{23}, y) = -\frac{b_1}{d_1} \\ \cos(s_{34}, x) = \frac{c_2}{d_2}, \cos(s_{34}, y) = -\frac{b_2}{d_2} \\ \cos(s_{41}, x) = \cos \theta_2 = \frac{c_3}{d_3}, \cos(s_{41}, y) = \sin \theta_2 = -\frac{b_3}{d_3} \end{aligned} \right\} \quad (9-42)$$

With reference to Fig. 9.5, there are two sides, $\overline{41}$ and $\overline{12}$, meeting at the node 1. The shear strain along $\overline{41}$ and $\overline{12}$, γ_{s_3} and γ_{s_4} , respectively, which are constants, can be expressed in terms of the nodal shear strain (γ_{x1}, γ_{y1}) according to the geometric relation as follows:

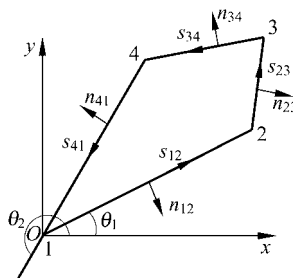


Figure 9.5 The normal and tangential direction along element sides

$$\begin{Bmatrix} \gamma_{s4} \\ \gamma_{s3} \end{Bmatrix} = \begin{bmatrix} \cos(s_{12}, x) & \cos(s_{12}, y) \\ \cos(s_{41}, x) & \cos(s_{41}, y) \end{bmatrix} \begin{Bmatrix} \gamma_{x1} \\ \gamma_{y1} \end{Bmatrix} = \begin{bmatrix} \cos \theta_1 & \sin \theta_1 \\ \cos \theta_2 & \sin \theta_2 \end{bmatrix} \begin{Bmatrix} \gamma_{x1} \\ \gamma_{y1} \end{Bmatrix} \quad (9-43)$$

Note

$$\sin(\theta_2 - \theta_1) = \sin \theta_2 \cos \theta_1 - \cos \theta_2 \sin \theta_1 = \frac{-b_3 c_4 + b_4 c_3}{d_3 d_4} \quad (9-44)$$

therefore, Eqs. (9-43), (9-42) and (9-38) yield

$$\begin{Bmatrix} \gamma_{x1} \\ \gamma_{y1} \end{Bmatrix} = \frac{1}{b_3 c_4 - b_4 c_3} \begin{bmatrix} b_3 & -b_4 \\ c_3 & -c_4 \end{bmatrix} \begin{Bmatrix} \gamma_{s4}^* \\ \gamma_{s3}^* \end{Bmatrix} \quad (9-45a)$$

Similarly, for node 2 , node 3 and node 4, we obtain

$$\begin{Bmatrix} \gamma_{x2} \\ \gamma_{y2} \end{Bmatrix} = \frac{1}{b_4 c_1 - b_1 c_4} \begin{bmatrix} b_4 & -b_1 \\ c_4 & -c_1 \end{bmatrix} \begin{Bmatrix} \gamma_{s1}^* \\ \gamma_{s4}^* \end{Bmatrix} \quad (9-45b)$$

$$\begin{Bmatrix} \gamma_{x3} \\ \gamma_{y3} \end{Bmatrix} = \frac{1}{b_1 c_2 - b_2 c_1} \begin{bmatrix} b_1 & -b_2 \\ c_1 & -c_2 \end{bmatrix} \begin{Bmatrix} \gamma_{s2}^* \\ \gamma_{s1}^* \end{Bmatrix} \quad (9-45c)$$

$$\begin{Bmatrix} \gamma_{x4} \\ \gamma_{y4} \end{Bmatrix} = \frac{1}{b_2 c_3 - b_3 c_2} \begin{bmatrix} b_2 & -b_3 \\ c_2 & -c_3 \end{bmatrix} \begin{Bmatrix} \gamma_{s3}^* \\ \gamma_{s2}^* \end{Bmatrix} \quad (9-45d)$$

Then we have

$$\begin{Bmatrix} \gamma_{xi} = \mathbf{X}_s \gamma_s^* \\ \gamma_{yi} = \mathbf{Y}_s \gamma_s^* \end{Bmatrix} \quad (9-46)$$

where

$$\gamma_{xi} = [\gamma_{x1} \quad \gamma_{x2} \quad \gamma_{x3} \quad \gamma_{x4}]^T, \quad \gamma_{yi} = [\gamma_{y1} \quad \gamma_{y2} \quad \gamma_{y3} \quad \gamma_{y4}]^T \quad (9-47)$$

$$\mathbf{X}_s = \begin{bmatrix} 0 & 0 & -\frac{b_4}{b_3 c_4 - b_4 c_3} & \frac{b_3}{b_3 c_4 - b_4 c_3} \\ \frac{b_4}{b_4 c_1 - b_1 c_4} & 0 & 0 & -\frac{b_1}{b_4 c_1 - b_1 c_4} \\ -\frac{b_2}{b_1 c_2 - b_2 c_1} & \frac{b_1}{b_1 c_2 - b_2 c_1} & 0 & 0 \\ 0 & -\frac{b_3}{b_2 c_3 - b_3 c_2} & \frac{b_2}{b_2 c_3 - b_3 c_2} & 0 \end{bmatrix} \quad (9-48a)$$

$$\mathbf{Y}_s = \begin{bmatrix} 0 & 0 & -\frac{c_4}{b_3c_4 - b_4c_3} & \frac{c_3}{b_3c_4 - b_4c_3} \\ \frac{c_4}{b_4c_1 - b_1c_4} & 0 & 0 & -\frac{c_1}{b_4c_1 - b_1c_4} \\ -\frac{c_2}{b_1c_2 - b_2c_1} & \frac{c_1}{b_1c_2 - b_2c_1} & 0 & 0 \\ 0 & -\frac{c_3}{b_2c_3 - b_3c_2} & \frac{c_2}{b_2c_3 - b_3c_2} & 0 \end{bmatrix} \quad (9-48b)$$

3. Interpolation formula for the shear strain fields within the element

The element shear strain fields are assumed as:

$$\left. \begin{aligned} \gamma_x &= \gamma_{x1}N_1^0 + \gamma_{x2}N_2^0 + \gamma_{x3}N_3^0 + \gamma_{x4}N_4^0 \\ \gamma_y &= \gamma_{y1}N_1^0 + \gamma_{y2}N_2^0 + \gamma_{y3}N_3^0 + \gamma_{y4}N_4^0 \end{aligned} \right\} \quad (9-49)$$

where N_i^0 is the bilinear shape function, i.e.,

$$\left. \begin{aligned} N_1^0 &= \frac{1}{4}(1-\xi)(1-\eta) \\ N_2^0 &= \frac{1}{4}(1+\xi)(1-\eta) \\ N_3^0 &= \frac{1}{4}(1+\xi)(1+\eta) \\ N_4^0 &= \frac{1}{4}(1-\xi)(1+\eta) \end{aligned} \right\} \quad (9-50)$$

Substitution of Eqs. (9-40) and (9-46) into Eq. (9-49) yields

$$\boldsymbol{\gamma} = \begin{Bmatrix} \gamma_x \\ \gamma_y \end{Bmatrix} = \begin{bmatrix} N_s^0 \mathbf{X}_s \boldsymbol{\Gamma}^* \\ N_s^0 \mathbf{Y}_s \boldsymbol{\Gamma}^* \end{bmatrix} \mathbf{q}^e = \mathbf{B}_s \mathbf{q}^e \quad (9-51)$$

where \mathbf{B}_s is the shear strain matrix of the element,

$$\mathbf{B}_s = \begin{bmatrix} N_s^0 \mathbf{X}_s \boldsymbol{\Gamma}^* \\ N_s^0 \mathbf{Y}_s \boldsymbol{\Gamma}^* \end{bmatrix} \quad (9-52)$$

$$\mathbf{N}_s^0 = [N_1^0 \quad N_2^0 \quad N_3^0 \quad N_4^0] \quad (9-53)$$

9.3.2 Interpolation Formulas for the Rotation Fields

1. The mid-side normal and tangential rotations of each element side

Let node 5, 6, 7 and 8 be the mid-side nodes of the sides $\overline{23}$, $\overline{34}$, $\overline{41}$ and $\overline{12}$, respectively (refer to Fig. 9.6).

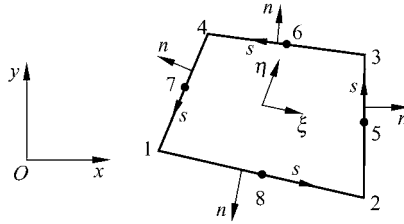


Figure 9.6 The mid-side node of each element side

The normal rotation ψ_n and the tangential rotation ψ_s along side $\overline{23}$ can be expressed as

$$\begin{Bmatrix} \psi_n \\ \psi_s \end{Bmatrix}_{\overline{23}} = \frac{1}{d_1} \begin{bmatrix} -b_1 & -c_1 \\ c_1 & -b_1 \end{bmatrix} \begin{Bmatrix} \psi_{x_2} \\ \psi_{y_2} \end{Bmatrix} \quad (9-54)$$

Then, for the node 2 and 3 of the side $\overline{23}$, we obtain

$$\begin{Bmatrix} \psi_{n2} \\ \psi_{s2} \end{Bmatrix}_{\overline{23}} = \frac{1}{d_1} \begin{bmatrix} -b_1 & -c_1 \\ c_1 & -b_1 \end{bmatrix} \begin{Bmatrix} \psi_{x_2} \\ \psi_{y_2} \end{Bmatrix}, \quad \begin{Bmatrix} \psi_{n3} \\ \psi_{s3} \end{Bmatrix}_{\overline{23}} = \frac{1}{d_1} \begin{bmatrix} -b_1 & -c_1 \\ c_1 & -b_1 \end{bmatrix} \begin{Bmatrix} \psi_{x_3} \\ \psi_{y_3} \end{Bmatrix} \quad (9-55)$$

The variation of the normal rotation ψ_n along each side is assumed to be linear. Therefore, for node 5, we obtain

$$\psi_{n5} = \frac{1}{2} [(\psi_{n2})_{\overline{23}} + (\psi_{n3})_{\overline{23}}] = -\frac{1}{2d_1} [b_1(\psi_{x_2} + \psi_{x_3}) + c_1(\psi_{y_2} + \psi_{y_3})] \quad (9-56a)$$

Similarly, for node 6, 7 and 8, we obtain

$$\psi_{n6} = -\frac{1}{2d_2} [b_2(\psi_{x_3} + \psi_{x_4}) + c_2(\psi_{y_3} + \psi_{y_4})] \quad (9-56b)$$

$$\psi_{n7} = -\frac{1}{2d_3} [b_3(\psi_{x_4} + \psi_{x_1}) + c_3(\psi_{y_4} + \psi_{y_1})] \quad (9-56c)$$

$$\psi_{n8} = -\frac{1}{2d_4} [b_4(\psi_{x_1} + \psi_{x_2}) + c_4(\psi_{y_1} + \psi_{y_2})] \quad (9-56d)$$

The tangential rotation ψ_s on the nodes 5,6,7 and 8 can be determined by Eq. (8-99b):

$$\left. \begin{aligned} \psi_{s5} &= \frac{3}{2d_1}(1-2\delta_1)(w_3 - w_2) - \frac{1}{4d_1}(1-6\delta_1)[c_1(\psi_{x2} + \psi_{x3}) - b_1(\psi_{y2} + \psi_{y3})] \\ \psi_{s6} &= \frac{3}{2d_2}(1-2\delta_2)(w_4 - w_3) - \frac{1}{4d_2}(1-6\delta_2)[c_2(\psi_{x3} + \psi_{x4}) - b_2(\psi_{y3} + \psi_{y4})] \\ \psi_{s7} &= \frac{3}{2d_3}(1-2\delta_3)(w_1 - w_4) - \frac{1}{4d_3}(1-6\delta_3)[c_3(\psi_{x4} + \psi_{x1}) - b_3(\psi_{y4} + \psi_{y1})] \\ \psi_{s8} &= \frac{3}{2d_4}(1-2\delta_4)(w_2 - w_1) - \frac{1}{4d_4}(1-6\delta_4)[c_4(\psi_{x1} + \psi_{x2}) - b_4(\psi_{y1} + \psi_{y2})] \end{aligned} \right\} \quad (9-57)$$

2. The rotations ψ_x and ψ_y of the mid-side nodes

For node 5, which is the mid-side node of side $\bar{23}$, (ψ_{5x}, ψ_{5y}) can be obtained from Eq. (9-54) as follows:

$$\begin{Bmatrix} \psi_{x5} \\ \psi_{y5} \end{Bmatrix} = \frac{1}{d_1} \begin{bmatrix} -b_1 & c_1 \\ -c_1 & -b_1 \end{bmatrix} \begin{Bmatrix} \psi_{n5} \\ \psi_{s5} \end{Bmatrix} \quad (9-58)$$

Similarly, (ψ_{6x}, ψ_{6y}) , (ψ_{7x}, ψ_{7y}) and (ψ_{8x}, ψ_{8y}) can be obtained. By coupling these expressions with Eqs. (9-56) and (9-57), we obtain

$$\begin{Bmatrix} \tilde{\psi}_x = \mathbf{F}_x \mathbf{q}^e \\ \tilde{\psi}_y = \mathbf{F}_y \mathbf{q}^e \end{Bmatrix} \quad (9-59)$$

where

$$\begin{Bmatrix} \tilde{\psi}_x = [\psi_{x5} & \psi_{x6} & \psi_{x7} & \psi_{x8}]^T \\ \tilde{\psi}_y = [\psi_{y5} & \psi_{y6} & \psi_{y7} & \psi_{y8}]^T \end{Bmatrix} \quad (9-60)$$

$$\mathbf{F}_x = [\mathbf{F}_{x1} \quad \mathbf{F}_{x2} \quad \mathbf{F}_{x3} \quad \mathbf{F}_{x4}] \quad (9-61)$$

$$\mathbf{F}_y = [\mathbf{F}_{y1} \quad \mathbf{F}_{y2} \quad \mathbf{F}_{y3} \quad \mathbf{F}_{y4}] \quad (9-62)$$

$$\mathbf{F}_{x1} = \begin{bmatrix} 0 & 0 & 0 & 0 & 0 \\ 0 & 0 & 0 & 0 & 0 \\ 0 & 0 & \frac{3c_3}{2d_3^2}(1-2\delta_3) & \frac{1}{2d_3^2} \left[b_3^2 - \frac{c_3^2}{2}(1-6\delta_3) \right] & \frac{3b_3c_3}{4d_3^2}(1-2\delta_3) \\ 0 & 0 & -\frac{3c_4}{2d_4^2}(1-2\delta_4) & \frac{1}{2d_4^2} \left[b_4^2 - \frac{c_4^2}{2}(1-6\delta_4) \right] & \frac{3b_4c_4}{4d_4^2}(1-2\delta_4) \end{bmatrix} \quad (9-63a)$$

$$\mathbf{F}_{x_2} = \begin{bmatrix} 0 & 0 & -\frac{3c_1}{2d_1^2}(1-2\delta_1) & \frac{1}{2d_1^2} \left[b_1^2 - \frac{c_1^2}{2}(1-6\delta_1) \right] & \frac{3b_1c_1}{4d_1^2}(1-2\delta_1) \\ 0 & 0 & 0 & 0 & 0 \\ 0 & 0 & 0 & 0 & 0 \\ 0 & 0 & \frac{3c_4}{2d_4^2}(1-2\delta_4) & \frac{1}{2d_4^2} \left[b_4^2 - \frac{c_4^2}{2}(1-6\delta_4) \right] & \frac{3b_4c_4}{4d_4^2}(1-2\delta_4) \end{bmatrix} \quad (9-63b)$$

$$\mathbf{F}_{x_3} = \begin{bmatrix} 0 & 0 & \frac{3c_1}{2d_1^2}(1-2\delta_1) & \frac{1}{2d_1^2} \left[b_1^2 - \frac{c_1^2}{2}(1-6\delta_1) \right] & \frac{3b_1c_1}{4d_1^2}(1-2\delta_1) \\ 0 & 0 & -\frac{3c_2}{2d_2^2}(1-2\delta_2) & \frac{1}{2d_2^2} \left[b_2^2 - \frac{c_2^2}{2}(1-6\delta_2) \right] & \frac{3b_2c_2}{4d_2^2}(1-2\delta_2) \\ 0 & 0 & 0 & 0 & 0 \\ 0 & 0 & 0 & 0 & 0 \end{bmatrix} \quad (9-63c)$$

$$\mathbf{F}_{x_4} = \begin{bmatrix} 0 & 0 & 0 & 0 & 0 \\ 0 & 0 & \frac{3c_2}{2d_2^2}(1-2\delta_2) & \frac{1}{2d_2^2} \left[b_2^2 - \frac{c_2^2}{2}(1-6\delta_2) \right] & \frac{3b_2c_2}{4d_2^2}(1-2\delta_2) \\ 0 & 0 & -\frac{3c_3}{2d_3^2}(1-2\delta_3) & \frac{1}{2d_3^2} \left[b_3^2 - \frac{c_3^2}{2}(1-6\delta_3) \right] & \frac{3b_3c_3}{4d_3^2}(1-2\delta_3) \\ 0 & 0 & 0 & 0 & 0 \end{bmatrix} \quad (9-63d)$$

$$\mathbf{F}_{y_1} = \begin{bmatrix} 0 & 0 & 0 & 0 & 0 \\ 0 & 0 & 0 & 0 & 0 \\ 0 & 0 & -\frac{3b_3}{2d_3^2}(1-2\delta_3) & \frac{3b_3c_3}{4d_3^2}(1-2\delta_3) & \frac{1}{2d_3^2} \left[c_3^2 - \frac{b_3^2}{2}(1-6\delta_3) \right] \\ 0 & 0 & \frac{3b_4}{2d_4^2}(1-2\delta_4) & \frac{3b_4c_4}{4d_4^2}(1-2\delta_4) & \frac{1}{2d_4^2} \left[c_4^2 - \frac{b_4^2}{2}(1-6\delta_4) \right] \end{bmatrix} \quad (9-64a)$$

$$\mathbf{F}_{y_2} = \begin{bmatrix} 0 & 0 & \frac{3b_1}{2d_1^2}(1-2\delta_1) & \frac{3b_1c_1}{4d_1^2}(1-2\delta_1) & \frac{1}{2d_1^2} \left[c_1^2 - \frac{b_1^2}{2}(1-6\delta_1) \right] \\ 0 & 0 & 0 & 0 & 0 \\ 0 & 0 & 0 & 0 & 0 \\ 0 & 0 & -\frac{3b_4}{2d_4^2}(1-2\delta_4) & \frac{3b_4c_4}{4d_4^2}(1-2\delta_4) & \frac{1}{2d_4^2} \left[c_4^2 - \frac{b_4^2}{2}(1-6\delta_4) \right] \end{bmatrix} \quad (9-64b)$$

$$\mathbf{F}_{y^3} = \begin{bmatrix} 0 & 0 & -\frac{3b_1}{2d_1^2}(1-2\delta_1) & \frac{3b_1c_1}{4d_1^2}(1-2\delta_1) & \frac{1}{2d_1^2} \left[c_1^2 - \frac{b_1^2}{2}(1-6\delta_1) \right] \\ 0 & 0 & \frac{3b_2}{2d_2^2}(1-2\delta_2) & \frac{3b_2c_2}{4d_2^2}(1-2\delta_2) & \frac{1}{2d_2^2} \left[c_2^2 - \frac{b_2^2}{2}(1-6\delta_2) \right] \\ 0 & 0 & 0 & 0 & 0 \\ 0 & 0 & 0 & 0 & 0 \end{bmatrix} \quad (9-64c)$$

$$\mathbf{F}_{y^4} = \begin{bmatrix} 0 & 0 & 0 & 0 & 0 \\ 0 & 0 & -\frac{3b_2}{2d_2^2}(1-2\delta_2) & \frac{3b_2c_2}{4d_2^2}(1-2\delta_2) & \frac{1}{2d_2^2} \left[c_2^2 - \frac{b_2^2}{2}(1-6\delta_2) \right] \\ 0 & 0 & \frac{3b_3}{2d_3^2}(1-2\delta_3) & \frac{3b_3c_3}{4d_3^2}(1-2\delta_3) & \frac{1}{2d_3^2} \left[c_3^2 - \frac{b_3^2}{2}(1-6\delta_3) \right] \\ 0 & 0 & 0 & 0 & 0 \end{bmatrix} \quad (9-64d)$$

3. Interpolation formulas for the rotation fields ψ_x and ψ_y within the element

The rotation fields ψ_x and ψ_y within the element can be expressed in terms of the node rotations ψ_{xi} and ψ_{yi} ($i = 1, 2, \dots, 8$):

$$\left. \begin{aligned} \psi_x &= \sum_{i=1}^8 N_i \psi_{xi} \\ \psi_y &= \sum_{i=1}^8 N_i \psi_{yi} \end{aligned} \right\} \quad (9-65)$$

where

$$\left. \begin{aligned} N_1 &= -\frac{1}{4}(1-\xi)(1-\eta)(1+\xi+\eta) & N_5 &= \frac{1}{2}(1-\eta^2)(1+\xi) \\ N_2 &= -\frac{1}{4}(1+\xi)(1-\eta)(1-\xi+\eta) & N_6 &= \frac{1}{2}(1-\xi^2)(1+\eta) \\ N_3 &= -\frac{1}{4}(1+\xi)(1+\eta)(1-\xi-\eta) & N_7 &= \frac{1}{2}(1-\eta^2)(1-\xi) \\ N_4 &= -\frac{1}{4}(1-\xi)(1+\eta)(1+\xi-\eta) & N_8 &= \frac{1}{2}(1-\xi^2)(1-\eta) \end{aligned} \right\} \quad (9-66)$$

Substituting Eq. (9-59) into Eq. (9-65), the element rotation fields ψ_x and ψ_y can be expressed by the element nodal displacement vector \mathbf{q}^e .

9.3.3 Interpolation Formulas for the In-Plane Displacement Fields of the Mid-Plane

The in-plane displacement fields u^0 and v^0 of the mid-plane can be expressed as:

$$\left. \begin{aligned} u^0 &= \sum_{i=1}^4 N_i^0 u_i \\ v^0 &= \sum_{i=1}^4 N_i^0 v_i \end{aligned} \right\} \quad (9-67)$$

where N_i^0 is given by Eq. (9-50).

9.3.4 The In-Plane Strain and Curvature Fields

The in-plane strain (9-4) of the mid-plane can be rewritten as:

$$\boldsymbol{\varepsilon}^0 = \mathbf{B}^0 \mathbf{q}^e \quad (9-68)$$

where

$$\mathbf{B}^0 = [\mathbf{B}_1^0 \quad \mathbf{B}_2^0 \quad \mathbf{B}_3^0 \quad \mathbf{B}_4^0] \quad (9-69)$$

$$\mathbf{B}_i^0 = \begin{bmatrix} \frac{\partial N_i^0}{\partial x} & 0 & 0 & 0 & 0 \\ 0 & \frac{\partial N_i^0}{\partial y} & 0 & 0 & 0 \\ \frac{\partial N_i^0}{\partial y} & \frac{\partial N_i^0}{\partial x} & 0 & 0 & 0 \end{bmatrix} \quad (i = 1,2,3,4) \quad (9-70)$$

$$\begin{Bmatrix} \frac{\partial}{\partial x} \\ \frac{\partial}{\partial y} \end{Bmatrix} = \mathbf{J}^{-1} \begin{Bmatrix} \frac{\partial}{\partial \xi} \\ \frac{\partial}{\partial \eta} \end{Bmatrix} \quad (9-71)$$

\mathbf{J}^{-1} is the Jacobian inverse, and it is the same as that of the bilinear isoparametric quadrilateral element Q4.

From Eqs. (9-5), (9-65) and (9-59), the curvature fields can be rewritten as:

$$\boldsymbol{\kappa} = -(\mathbf{H}_0 + \mathbf{H}_1 \mathbf{F}_x + \mathbf{H}_2 \mathbf{F}_y) \mathbf{q}^e = \mathbf{B}_b \mathbf{q}^e \quad (9-72)$$

where \mathbf{B}_b is the bending strain matrix:

$$\mathbf{B}_b = [\mathbf{B}_{b1} \quad \mathbf{B}_{b2} \quad \mathbf{B}_{b3} \quad \mathbf{B}_{b4}] \quad (9-73)$$

$$\mathbf{H}_0 = [\mathbf{H}_{01} \quad \mathbf{H}_{02} \quad \mathbf{H}_{03} \quad \mathbf{H}_{04}] \quad (9-74)$$

$$\mathbf{H}_{0i} = \begin{bmatrix} 0 & 0 & 0 & \frac{\partial N_i}{\partial x} & 0 \\ 0 & 0 & 0 & 0 & \frac{\partial N_i}{\partial y} \\ 0 & 0 & 0 & \frac{\partial N_i}{\partial y} & \frac{\partial N_i}{\partial x} \end{bmatrix} \quad (i = 1,2,3,4) \quad (9-75)$$

$$\mathbf{H}_1 = \begin{bmatrix} \frac{\partial N_5}{\partial x} & \frac{\partial N_6}{\partial x} & \frac{\partial N_7}{\partial x} & \frac{\partial N_8}{\partial x} \\ 0 & 0 & 0 & 0 \\ \frac{\partial N_5}{\partial y} & \frac{\partial N_6}{\partial y} & \frac{\partial N_7}{\partial y} & \frac{\partial N_8}{\partial y} \end{bmatrix}, \quad \mathbf{H}_2 = \begin{bmatrix} 0 & 0 & 0 & 0 \\ \frac{\partial N_5}{\partial y} & \frac{\partial N_6}{\partial y} & \frac{\partial N_7}{\partial y} & \frac{\partial N_8}{\partial y} \\ \frac{\partial N_5}{\partial x} & \frac{\partial N_6}{\partial x} & \frac{\partial N_7}{\partial x} & \frac{\partial N_8}{\partial x} \end{bmatrix} \quad (9-76a,b)$$

where $N_i (i = 1,2, \dots, 8)$ is given by Eq. (9-66).

Then, the $\boldsymbol{\varepsilon}_p$ in Eq. (9-14) can be expressed as:

$$\boldsymbol{\varepsilon}_p = \begin{Bmatrix} \boldsymbol{\varepsilon}^0 \\ \boldsymbol{\kappa} \end{Bmatrix} = \begin{bmatrix} \mathbf{B}^0 \\ \mathbf{B}_b \end{bmatrix} \mathbf{q}^e = \mathbf{B}_p \mathbf{q}^e \quad (9-77)$$

9.3.5 The Stiffness Matrix of the Element

The element strain energy is:

$$U^e = \frac{1}{2} \mathbf{q}^{eT} \iint_{A^e} \mathbf{B}_p^T \mathbf{C}_p \mathbf{B}_p dA \mathbf{q}^e + \frac{1}{2} \mathbf{q}^{eT} \iint_{A^e} \mathbf{B}_s^T \mathbf{C}_s \mathbf{B}_s dA \mathbf{q}^e \quad (9-78)$$

where A^e is the area of the element; \mathbf{C}_p and \mathbf{C}_s are given by Eqs. (9-14) and (9-19), respectively. The element stiffness matrix is

$$\begin{aligned} \mathbf{K}^e &= \iint_{A^e} \mathbf{B}_p^T \mathbf{C}_p \mathbf{B}_p dA + \iint_{A^e} \mathbf{B}_s^T \mathbf{C}_s \mathbf{B}_s dA \\ &= \int_{-1}^1 \int_{-1}^1 \mathbf{B}_p^T \mathbf{C}_p \mathbf{B}_p |J| d\xi d\eta + \int_{-1}^1 \int_{-1}^1 \mathbf{B}_s^T \mathbf{C}_s \mathbf{B}_s |J| d\xi d\eta \end{aligned} \quad (9-79)$$

where $|J|$ is the Jacobian determinant.

A standard 2×2 Gauss integration scheme is found to be sufficient for the calculation of Eq. (9-79), even though 3×3 integration is theoretically necessary. No spurious mode is presented in the element. Note that this 2×2 scheme should not be confused with the standard reduced integration scheme because both 2×2 and 3×3 integration schemes can avoid the shear locking problem and give proper solutions.

This element is denoted as CTMQ20.

9.3.6 Element Load Vector

The deflection field w is not used during the course of calculating the element stiffness matrix. But, for calculating the effective load vector, w can be assumed as follows:

$$w = N_w \mathbf{q}^e \tag{9-80}$$

with

$$N_w = [0 \quad 0 \quad N_1^0 \quad 0 \quad 0 \quad 0 \quad N_2^0 \quad 0 \quad 0 \quad 0 \quad N_3^0 \quad 0 \quad 0 \quad 0 \quad N_4^0 \quad 0 \quad 0] \tag{9-81}$$

where N_i^0 is given in Eq. (9-50). Then, the element equivalent nodal forces due to a pressure $\bar{q}(x, y)$ can be given by

$$\mathbf{f}^e = [0 \quad 0 \quad f_{z1} \quad 0 \quad 0 \quad 0 \quad f_{z2} \quad 0 \quad 0 \quad 0 \quad f_{z3} \quad 0 \quad 0 \quad 0 \quad f_{z4} \quad 0 \quad 0]^T \tag{9-82}$$

with $f_{zi} = \int_{A^e} \bar{q}(x, y) N_i^0 dA = \int_{-1}^1 \int_{-1}^1 \bar{q}^*(\xi, \eta) N_i^0 |J| d\xi d\eta \quad (i = 1, 2, 3, 4)$ (9-83)

9.4 The Hybrid-Enhanced Post-Processing Procedure for Element Stresses

According to the standard procedure of displacement-based elements, the stress solutions of the plate element can be solved from the stress-strain relations (9-10) and (9-11). But, the transverse shear stress solutions obtained from Eq. (9-11) are all constants at each layer of the plate, which neither reflect the actual nonlinear continuous distributions of the transverse shear stresses, nor satisfy the zero shear stress conditions on the bounding planes of the plate. When the 3D elasticity differential equilibrium equations are used to compute the transverse shear stresses, the procedure for the displacement-based elements is quite complicated, and hard

to obtain satisfactory results. Reference [26] proposed a simple hybrid-enhanced post-processing procedure to improve the internal force solutions of the displacement-based plate elements, and references [22,23] employed this procedure to evaluate the internal forces and stresses of the laminated composite plate elements. More accurate results for stresses, especially for the transverse shear stresses, can be obtained. So the element CTMQ20, which uses this treatment, possesses the advantages of both the displacement-based and hybrid elements.

9.4.1 The Bending Moment and Shear Force Fields

The bending moment field \mathbf{M} can be assumed as follows^[26,27]:

$$\mathbf{M} = \mathbf{P}_M \boldsymbol{\lambda}_M \quad (9-84)$$

in which

$$\mathbf{M} = [M_x \quad M_y \quad M_{xy}]^T \quad (9-85)$$

$$\mathbf{P}_M = \begin{bmatrix} 1 & \xi & \eta & \xi\eta & 0 & 0 & 0 & 0 & 0 & 0 & 0 & 0 \\ 0 & 0 & 0 & 0 & 1 & \xi & \eta & \xi\eta & 0 & 0 & 0 & 0 \\ 0 & 0 & 0 & 0 & 0 & 0 & 0 & 0 & 1 & \xi & \eta & \xi\eta \end{bmatrix} \quad (9-86)$$

$$\boldsymbol{\lambda}_M = [\lambda_1 \quad \lambda_2 \quad \lambda_3 \quad \lambda_4 \quad \lambda_5 \quad \lambda_6 \quad \lambda_7 \quad \lambda_8 \quad \lambda_9 \quad \lambda_{10} \quad \lambda_{11} \quad \lambda_{12}]^T \quad (9-87)$$

where (ξ, η) are the isoparametric coordinates of the quadrilateral element; λ_i ($i = 1, 2, \dots, 12$) are 12 unknown parameters.

And, the shear field is assumed to satisfy the homogeneous equilibrium equation,

$$\mathbf{Q} = \begin{Bmatrix} Q_x \\ Q_y \end{Bmatrix} = \begin{Bmatrix} M_{x,x} + M_{xy,y} \\ M_{xy,x} + M_{y,y} \end{Bmatrix} = \mathbf{P}_Q \boldsymbol{\lambda}_M \quad (9-88)$$

in which

$$\mathbf{P}_Q = \begin{bmatrix} 0 & j_{11} & j_{12} & j_{11}\eta + j_{12}\xi & 0 & 0 & 0 & 0 & 0 & j_{21} & j_{22} & j_{21}\eta + j_{22}\xi \\ 0 & 0 & 0 & 0 & 0 & j_{21} & j_{22} & j_{21}\eta + j_{22}\xi & 0 & j_{11} & j_{12} & j_{11}\eta + j_{12}\xi \end{bmatrix} \quad (9-89)$$

j_{11} , j_{12} , j_{21} and j_{22} are the components of the Jacobian inverse.

9.4.2 The Membrane Force Field of the Mid-Plane

The membrane force field \mathbf{N} can be assumed as follows^[28]:

$$N = P_N \lambda_N \quad (9-90)$$

in which

$$P_N = \begin{bmatrix} 1 & 0 & 0 & \bar{a}_1^2 \eta & \bar{a}_3^2 \xi \\ 0 & 1 & 0 & \bar{b}_1^2 \eta & \bar{b}_3^2 \xi \\ 0 & 0 & 1 & \bar{a}_1 \bar{b}_1 \eta & \bar{a}_3 \bar{b}_3 \xi \end{bmatrix} \quad (9-91)$$

$$\left. \begin{aligned} \bar{a}_1 &= \frac{1}{4}(-x_1 + x_2 + x_3 - x_4) & \bar{b}_1 &= \frac{1}{4}(-y_1 + y_2 + y_3 - y_4) \\ \bar{a}_3 &= \frac{1}{4}(-x_1 - x_2 + x_3 + x_4) & \bar{b}_3 &= \frac{1}{4}(-y_1 - y_2 + y_3 + y_4) \end{aligned} \right\} \quad (9-92)$$

$$\lambda_N = [\lambda_{13} \quad \lambda_{14} \quad \lambda_{15} \quad \lambda_{16} \quad \lambda_{17}]^T \quad (9-93)$$

λ_i ($i = 13, 14, \dots, 17$) are 5 unknown parameters.

9.4.3 The Condensation Procedure

Equations (9-14) and (9-15) can be rewritten as:

$$\sigma_p = \begin{Bmatrix} N \\ M \end{Bmatrix} = \begin{bmatrix} P_N & \mathbf{0}_{3 \times 12} \\ \mathbf{0}_{3 \times 5} & P_M \end{bmatrix} \begin{Bmatrix} \lambda_N \\ \lambda_M \end{Bmatrix} = P_{NM} \lambda_{NM} \quad (9-94)$$

$$Q = \begin{bmatrix} \mathbf{0}_{2 \times 5} & P_Q \end{bmatrix} \begin{Bmatrix} \lambda_N \\ \lambda_M \end{Bmatrix} = P_{NQ} \lambda_{NM} \quad (9-95)$$

By employing the Hellinger-Reissner variational principle, the energy functional of the laminated composite plate element can be expressed as:

$$\begin{aligned} \Pi_R^e &= -\frac{1}{2} \iint_{A^e} \sigma_p^T S_p \sigma_p dA - \frac{1}{2} \iint_{A^e} Q^T S_s Q dA + \iint_{A^e} \sigma_p^T \epsilon_p dA + \iint_{A^e} Q^T \gamma dA - W_{\text{exp}} \\ &= -\frac{1}{2} \lambda_{NM}^T \iint_{A^e} (P_{NM}^T S_p P_{NM} + P_{NQ}^T S_s P_{NQ}) dA \cdot \lambda_{NM} \\ &\quad + \lambda_{NM}^T \iint_{A^e} (P_{NM}^T B_p + P_{NQ}^T B_s) dA \cdot q^e - W_{\text{exp}} \end{aligned} \quad (9-96)$$

where W_{exp} is the work done by external forces.

From the stationary condition $\frac{\partial \Pi_R^e}{\partial \lambda_{NM}} = \mathbf{0}$, we obtain:

$$\lambda_{NM} = -\mathbf{K}_{\lambda\lambda}^{-1} \mathbf{K}_{\lambda q} \mathbf{q}^e \quad (9-97)$$

where

$$\begin{aligned} \mathbf{K}_{\lambda\lambda} &= -\iint_{A^e} (\mathbf{P}_{NM}^T \mathbf{S}_p \mathbf{P}_{NM} + \mathbf{P}_{NQ}^T \mathbf{S}_s \mathbf{P}_{NQ}) dA \\ \mathbf{K}_{\lambda q} &= \iint_{A^e} (\mathbf{P}_{NM}^T \mathbf{B}_p + \mathbf{P}_{NQ}^T \mathbf{B}_s) dA \end{aligned} \quad (9-98)$$

Substituting Eq. (9-97) into Eqs. (9-94) and (9-95), N , M and Q can be obtained. And, the element stresses of each layer can be obtained by Eq. (9-27).

9.4.4 Recovery of the Transverse Shear Stresses

Ignoring the effects of the body forces, the stresses of the laminated composite plate should satisfy the following homogeneous equations:

$$\left. \begin{aligned} \frac{\partial \sigma_x}{\partial x} + \frac{\partial \tau_{xy}}{\partial y} + \frac{\partial \tau_{xz}}{\partial z} &= 0 \\ \frac{\partial \tau_{xy}}{\partial x} + \frac{\partial \sigma_y}{\partial y} + \frac{\partial \tau_{yz}}{\partial z} &= 0 \end{aligned} \right\} \quad (9-99)$$

For the k th layer of the plate, we obtain

$$\begin{aligned} \tau_{zk} &= -\int_{-h/2}^z \partial \sigma_k dz = -\int_{-h/2}^z \partial \bar{Q}_k (\mathbf{S}_e + z \mathbf{S}_b) \sigma_p dz \\ &= -\int_{-h/2}^z [\bar{B}l_1 \bar{Q}_k (\mathbf{S}_e + z \mathbf{S}_b) \sigma_{p,x} + \bar{B}l_2 \bar{Q}_k (\mathbf{S}_e + z \mathbf{S}_b) \sigma_{p,y}] dz \end{aligned} \quad (9-100)$$

in which

$$\partial = \begin{bmatrix} \frac{\partial}{\partial x} & 0 & \frac{\partial}{\partial y} \\ 0 & \frac{\partial}{\partial y} & \frac{\partial}{\partial x} \end{bmatrix} \quad (9-101)$$

$$\bar{B}l_1 = \begin{bmatrix} 1 & 0 & 0 \\ 0 & 0 & 1 \end{bmatrix}, \quad \bar{B}l_2 = \begin{bmatrix} 0 & 0 & 1 \\ 0 & 1 & 0 \end{bmatrix} \quad (9-102a,b)$$

$$\begin{aligned} \sigma_{p,x} &= -\mathbf{P}_{NM,x} \mathbf{K}_{\lambda\lambda}^{-1} \mathbf{K}_{\lambda q} \mathbf{q}^e \\ \sigma_{p,y} &= -\mathbf{P}_{NM,y} \mathbf{K}_{\lambda\lambda}^{-1} \mathbf{K}_{\lambda q} \mathbf{q}^e \end{aligned} \quad (9-103)$$

(, x) and (, y) denote the derivatives with respect to x and y of all components in a matrix.

Finally, we obtain

$$\begin{aligned}
 \tau_{zk} = & -\overline{Bl}_1 \overline{Q}_k [(z - h_{k-1})S_e + \frac{1}{2}(z^2 - h_{k-1}^2)S_b] \sigma_{p,x} \\
 & - \overline{Bl}_2 \overline{Q}_k [(z - h_{k-1})S_e + \frac{1}{2}(z^2 - h_{k-1}^2)S_b] \sigma_{p,y} \\
 & - \sum_{i=1}^{k-1} \overline{Bl}_1 \overline{Q}_k [(h_i - h_{i-1})S_e + \frac{1}{2}(h_i^2 - h_{i-1}^2)S_b] \sigma_{p,x} \\
 & - \sum_{i=1}^{k-1} \overline{Bl}_2 \overline{Q}_k [(h_i - h_{i-1})S_e + \frac{1}{2}(h_i^2 - h_{i-1}^2)S_b] \sigma_{p,y} \quad (9-104)
 \end{aligned}$$

9.5 Vibration Analysis of Laminated Composite Plates

The in-plane displacement field of the element CTMQ20 can be obtained from Eq. (9-67):

$$\begin{Bmatrix} u^0 \\ v^0 \end{Bmatrix} = N^0 \mathbf{q}^e \quad (9-105)$$

where

$$N^0 = [N_1^0 \quad N_2^0 \quad N_3^0 \quad N_4^0] \quad (9-106)$$

$$N_i^0 = \begin{bmatrix} N_i^0 & 0 & 0 & 0 & 0 \\ 0 & N_i^0 & 0 & 0 & 0 \end{bmatrix} \quad (i=1,2,3,4) \quad (9-107)$$

The rotation field of the element CTMQ20 can be obtained from Eqs. (9-59) and (9-65):

$$\begin{Bmatrix} \psi_x \\ \psi_y \end{Bmatrix} = N_\beta \mathbf{q}^e \quad (9-108)$$

where

$$N_\beta = N_{\beta 1} + N_{\beta 2} \quad (9-109)$$

$$N_{\beta 1} = \begin{bmatrix} 0 & 0 & 0 & N_1 & 0 & 0 & 0 & 0 & N_2 & 0 & 0 & 0 & 0 & N_3 & 0 & 0 & 0 & 0 & N_4 & 0 \\ 0 & 0 & 0 & 0 & N_1 & 0 & 0 & 0 & 0 & N_2 & 0 & 0 & 0 & 0 & N_3 & 0 & 0 & 0 & 0 & N_4 \end{bmatrix} \quad (9-110)$$

$$N_{\beta 2} = \begin{bmatrix} \tilde{N}_{\beta} F_x \\ \tilde{N}_{\beta} F_y \end{bmatrix} \quad (9-111)$$

$$\tilde{N}_{\beta} = [N_5 \quad N_6 \quad N_7 \quad N_8] \quad (9-112)$$

For the deflection field w , the expression (9-80) is not the real deflection field of the element CTMQ20, which must be derived from the relation (9-6). In order to avoid complicated derivation, the following element concentrated mass matrix corresponding to the deflection field w is suggested here:

$$m_w^e = \frac{\rho Ah}{4} \begin{bmatrix} a & & & \\ & a & & \\ & & a & \\ & & & a \end{bmatrix} \quad (9-113)$$

where ρ is mass density of the plate; A is the area of the element, and

$$a = \begin{bmatrix} 0 & & & \\ & 0 & & \\ & & 1 & \\ & & & 0 \\ & & & & 0 \end{bmatrix}$$

Then the expression of the element mass matrix m^e can be written as:

$$m^e = m_w^e + m_0^e + m_{\beta}^e \quad (9-114)$$

where m_0^e is the in-plane mass matrix:

$$m_0^e = \rho h \int_{-1}^1 \int_{-1}^1 (N^0)^T N^0 |J| d\xi d\eta \quad (9-115)$$

m_{β}^e is the mass matrix caused by the moment of inertia:

$$m_{\beta}^e = \frac{\rho h^3}{12} \int_{-1}^1 \int_{-1}^1 N_{\beta}^T N_{\beta} |J| d\xi d\eta \quad (9-116)$$

When the stacking sequences of a laminated composite plate is symmetrical with respect to the mid-plane, there will be no coupling existing between the bending actions and in-plane actions. So, if only the transverse vibration is considered, m_0^e in Eq. (9-114) can be omitted. Thus, the element mass matrix can be rewritten as:

$$m^e = m_w^e + m_{\beta}^e \quad (9-117)$$

After the element stiffness matrix \mathbf{K}^e and mass matrix \mathbf{m}^e are obtained, the vibration analysis of the plate can be performed by the usual procedure, and the natural frequency ω_i can be solved by the following generalized characteristic equation:

$$(\mathbf{K} - \omega^2 \mathbf{m})\mathbf{q} = \mathbf{0} \tag{9-118}$$

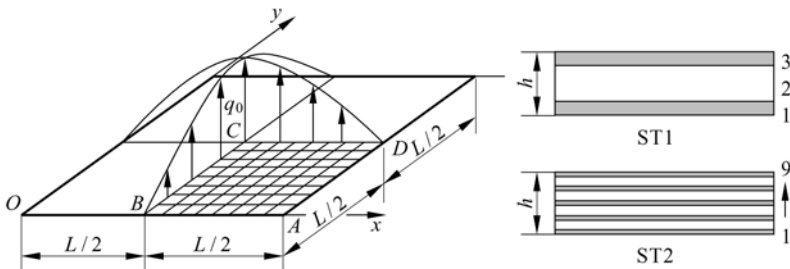
where \mathbf{K} is the global stiffness matrix; \mathbf{m} is the global mass matrix; \mathbf{q} is the global nodal displacement vector.

9.6 Numerical Examples

When dealing with a single layer isotropic plate, the element CTMQ20 will degenerate into the Mindlin plate element ARS-Q12 presented in reference [25]. Good overall results were obtained for displacements, internal forces and stresses. The focus of this section is only on the composite plates.

Example 9.1 Simply supported square symmetric cross-ply laminated plate with 3 (0/90/0) or 9 (0/90/0/90/0/90/0/90/0) layers subjected to a doubly sinusoidal load.

This example, proposed by Pagano and Hatfield^[29], is presented in Fig. 9.7. Each layer is strongly orthotropic and two stacking sequences are studied: ST1 corresponds to 3 layers (0/90/0) whereas ST2 corresponds to 9 layers (0/90/0/90/0/90/0/90/0). In both cases, the total thickness of all the 0° layers is the



GEOMETRY

$L=1000$; $h=250, 100, 20, 10, 1, 0.1$

MATERIAL (orthotropic)

Skins: $E_1=25.0$; $E_2=1.0$; $G_{12}=0.5$; $G_{13}=0.5$; $G_{23}=0.2$; $\mu_{12}=0.25$

ST1: 0/90/0 symmetric

ST2: 0/90/0/90/0/90/0/90/0 symmetric

BOUNDARY CONDITIONS (simply-supported: hard support mode I)

on AB : $u=w=\psi_x=0$; on BC : $u=\psi_x=0$

on CD : $v=\psi_y=0$; on DA : $v=w=\psi_y=0$

LOADING (doubly sinusoidal)

$$q = q_0 \sin \frac{\pi x}{L} \sin \frac{\pi y}{L}$$

Figure 9.7 Square plate with 3 and 9 layers subjected to doubly sinusoidal load

same as that of all the 90° layers; and those layers having the same orientation have the same thickness. Three different meshes, i.e., 4 × 4, 8 × 8 and 16 × 16, are used to model a quadrant of the plate, and five L/t aspect ratios are considered. The correction factors can be obtained from reference [14] or [15]: $k_1^2 = 0.5952$, $k_2^2 = 0.7205$ for ST1 and $k_1^2 = 0.689$, $k_2^2 = 0.611$ for ST2.

For comparing with analytical solutions and solutions in other references, deflection and stresses are given in the form:

$$\text{Deflection: } \tilde{w} = \frac{w\pi^4 \hat{Q}}{12S^4 h q_0} \quad \text{with } S = \frac{L}{h}, \quad \hat{Q} = 4G_{12} + \frac{[E_1 + E_2(1 + 2\mu_{23})]}{(1 - \mu_{12}\mu_{21})}$$

(Note: $\mu_{23} = 0.25$ here. It is necessary for the 3D elastic solution, but it is not needed for FDST)

$$\text{In-plane stresses: } (\tilde{\sigma}_x, \tilde{\sigma}_y, \tilde{\tau}_{xy}) = \frac{1}{q_0 S^2} (\sigma_x, \sigma_y, \tau_{xy})$$

$$\text{Transverse shear stresses: } (\tilde{\tau}_{xz}, \tilde{\tau}_{yz}) = \frac{1}{q_0 S} (\tau_{xz}, \tau_{yz})$$

Some results of the element CTMQ20 obtained together with some other solutions are presented in Tables 9.1 and 9.2, and the distributions of selective normal and transverse shear stresses along the thickness obtained by 8 × 8 mesh are plotted in Figs. 9.8 to 9.15.

Table 9.1 Maximum deflection and stresses in 3-ply (0/90/0) square laminate composite plate (hard simply-supported mode I) subjected to doubly sinusoidal load

$S = L/h$	Mesh & models	\tilde{w} $\left(\frac{L}{2}, \frac{L}{2}, 0\right)$	$\tilde{\sigma}_x$ $\left(\frac{L}{2}, \frac{L}{2}, \pm \frac{h}{2}\right)$	$\tilde{\sigma}_y$ $\left(\frac{L}{2}, \frac{L}{2}, \pm \frac{h}{4}\right)$	$\tilde{\tau}_{xy}$ $\left(0, 0, \pm \frac{h}{2}\right)$	$\tilde{\tau}_{xz}$ $\left(0, \frac{L}{2}, 0\right)$	$\tilde{\tau}_{yz}$ $\left(\frac{L}{2}, 0, 0\right)$
4	4 × 4	4.888	± 0.374	± 0.674	∓ 0.0330	0.245	0.331
	CTMQ20 8 × 8	4.856	± 0.371	± 0.664	∓ 0.0333	0.247	0.334
	16 × 16	4.848	± 0.370	± 0.661	∓ 0.0334	0.248	0.335
	DST 10 × 10 ^[30]	4.490	± 0.518	± 0.296		0.202	0.422
	FSDT	4.845	± 0.370	± 0.661	∓ 0.0334	0.249	0.319
10	4 × 4	1.735	± 0.488	± 0.407	∓ 0.0250	0.304	0.204
	CTMQ20 8 × 8	1.729	± 0.484	± 0.401	∓ 0.0252	0.307	0.207
	16 × 16	1.728	± 0.483	± 0.399	∓ 0.0253	0.308	0.208
	DST 10 × 10 ^[30]	1.727	± 0.549	± 0.253		0.213	0.409
	REC56-Z0 2 × 2 ^[19]	1.445	± 0.529	± 0.363	∓ 0.0250		
	REC72-Z0 2 × 2 ^[19]	1.663	± 0.583	± 0.408	∓ 0.0290		
	3D elasticity ^[29]	1.709	± 0.559	0.401/-0.403	-0.0275/0.0276	0.301	0.196
FSDT	1.727	± 0.483	± 0.399	∓ 0.0253	0.310	0.198	

(Continued)

$S=L/h$	Mesh & models	\tilde{w} $\left(\frac{L}{2}, \frac{L}{2}, 0\right)$	$\tilde{\sigma}_x$ $\left(\frac{L}{2}, \frac{L}{2}, \pm \frac{h}{2}\right)$	$\tilde{\sigma}_y$ $\left(\frac{L}{2}, \frac{L}{2}, \pm \frac{h}{4}\right)$	$\tilde{\tau}_{xy}$ $\left(0, 0, \pm \frac{h}{2}\right)$	$\tilde{\tau}_{xz}$ $\left(0, \frac{L}{2}, 0\right)$	$\tilde{\tau}_{yz}$ $\left(\frac{L}{2}, 0, 0\right)$
50	4 × 4	1.031	± 0.543	± 0.280	∓ 0.0212	0.330	0.135
	CTMQ20 8 × 8	1.031	± 0.538	± 0.277	∓ 0.0214	0.335	0.142
	16 × 16	1.031	± 0.536	± 0.276	∓ 0.0215	0.336	0.146
	DST 10 × 10 ^[30]	1.067	± 0.494	± 0.331		0.160	0.436
	REC56-Z0 2 × 2 ^[19]	0.993	± 0.535	± 0.261	∓ 0.0226		
	REC72-Z0 2 × 2 ^[19]	1.006	± 0.537	± 0.265	∓ 0.0230		
	3D elasticity ^[29]	1.031	± 0.539	± 0.276	∓ 0.0216	0.337	0.141
	FSDT	1.031	± 0.536	± 0.276	∓ 0.0215	0.338	0.141
100	4 × 4	1.007	± 0.545	± 0.274	∓ 0.0210	0.329	0.130
	CTMQ20 8 × 8	1.008	± 0.540	± 0.272	∓ 0.0213	0.335	0.134
	16 × 16	1.008	± 0.538	± 0.271	∓ 0.0213	0.337	0.140
	REC56-Z0 2 × 2 ^[19]	0.956	± 0.506	± 0.248	∓ 0.0223		
	REC72-Z0 2 × 2 ^[19]	0.962	± 0.509	± 0.249	∓ 0.0225		
	3D elasticity ^[29]	1.008	± 0.539	± 0.271	∓ 0.0214	0.339	0.139
	FSDT	1.008	± 0.538	± 0.271	∓ 0.0213	0.339	0.139
100 000	4 × 4	1.000	± 0.545	± 0.273	∓ 0.0210	0.326	0.128
	CTMQ20 8 × 8	1.000	± 0.540	± 0.270	∓ 0.0212	0.330	0.129
	16 × 16	1.000	± 0.539	± 0.270	∓ 0.0213	0.331	0.130
	FSDT	1.000	± 0.539	± 0.269	∓ 0.0213	0.339	0.138
	CLT ^[31]	1.000	± 0.539	± 0.269	∓ 0.0213	0.339	0.138

Table 9.2 Maximum deflection and stresses in 9-ply (0/90/0/90/0/90/0/90/0) square laminate composite plate (hard simply-supported mode I) subjected to doubly sinusoidal load

$S=L/h$	Mesh & models	\tilde{w} $\left(\frac{L}{2}, \frac{L}{2}, 0\right)$	$\tilde{\sigma}_x$ $\left(\frac{L}{2}, \frac{L}{2}, \pm \frac{h}{2}\right)$	$\tilde{\sigma}_y$ $\left(\frac{L}{2}, \frac{L}{2}, \pm \frac{2h}{5}\right)$	$\tilde{\tau}_{xy}$ $\left(0, 0, \frac{h}{2}\right)$	$\tilde{\tau}_{xz}$ $\left(0, \frac{L}{2}, 0\right)$	$\tilde{\tau}_{yz}$ $\left(\frac{L}{2}, 0, 0\right)$
4	4 × 4	4.283	± 0.498	± 0.494	∓ 0.0214	0.234	0.243
	CTMQ20 8 × 8	4.252	± 0.493	± 0.489	∓ 0.0217	0.237	0.245
	16 × 16	4.244	± 0.492	± 0.487	∓ 0.0217	0.237	0.246
	DST 10 × 10 ^[30]	4.242	± 0.547	± 0.419		0.225	0.231
	FSDT	4.242	± 0.491	± 0.487	∓ 0.0217	0.238	0.245
	10	4 × 4	1.529	± 0.526	± 0.461	∓ 0.0212	0.246
CTMQ20 8 × 8	1.524	± 0.521	± 0.456	∓ 0.0214	0.249	0.230	
16 × 16	1.523	± 0.519	± 0.455	∓ 0.0214	0.249	0.231	
DST 10 × 10 ^[30]	1.526	± 0.541	± 0.425		0.219	0.257	
LPL-20β 8 × 8 ^[21]	①	± 0.520	± 0.458	∓ 0.0216	0.248	0.228	
3D elasticity ^[29]	1.512	± 0.551	± 0.477	∓ 0.0233	0.247	0.226	
FSDT	1.522	± 0.519	± 0.454	∓ 0.0215	0.250	0.230	

(Continued)

$S=L/h$	Mesh & models	\bar{w} $\left(\frac{L}{2}, \frac{L}{2}, 0\right)$	$\bar{\sigma}_x$ $\left(\frac{L}{2}, \frac{L}{2}, \pm \frac{h}{2}\right)$	$\bar{\sigma}_y$ $\left(\frac{L}{2}, \frac{L}{2}, \pm \frac{2h}{5}\right)$	$\bar{\tau}_{xy}$ $\left(0, 0, \frac{h}{2}\right)$	$\bar{\tau}_{xz}$ $\left(0, \frac{L}{2}, 0\right)$	$\bar{\tau}_{yz}$ $\left(\frac{L}{2}, 0, 0\right)$
50	4 × 4	1.021	± 0.545	± 0.438	∓ 0.0210	0.251	0.213
	CTMQ20 8 × 8	1.021	± 0.539	± 0.434	∓ 0.0212	0.256	0.218
	16 × 16	1.021	± 0.538	± 0.433	∓ 0.0213	0.257	0.220
	DST 10 × 10 ^[30]	1.020	± 0.522	± 0.447		0.190	0.263
	LPL-20β 8 × 8 ^[21]	①	± 0.540	± 0.434	∓ 0.0214	0.256	0.217
	3D elasticity ^[29]	1.021	± 0.539	± 0.433	∓ 0.0214	0.258	0.219
	FSDT	1.021	± 0.538	± 0.432	∓ 0.0213	0.258	0.219
100	4 × 4	1.005	± 0.545	± 0.437	∓ 0.0209	0.249	0.210
	CTMQ20 8 × 8	1.005	± 0.540	± 0.433	∓ 0.0212	0.254	0.215
	16 × 16	1.005	± 0.539	± 0.432	∓ 0.0213	0.257	0.218
	LPL-20β 8 × 8 ^[21]	①	± 0.541	± 0.433	∓ 0.0214	0.257	0.217
	3D elasticity ^[29]	1.005	± 0.539	± 0.431	∓ 0.0213	0.259	0.219
	FSDT	1.005	± 0.538	± 0.431	∓ 0.0213	0.259	0.219
100 000	4 × 4	1.000	± 0.545	± 0.436	∓ 0.0210	0.247	0.207
	CTMQ20 8 × 8	1.000	± 0.540	± 0.432	∓ 0.0212	0.250	0.210
	16 × 16	1.000	± 0.539	± 0.431	∓ 0.0213	0.250	0.210
	FSDT	1.000	± 0.539	± 0.431	∓ 0.0213	0.259	0.219
	CLT ^[31]	1.000	± 0.539	± 0.431	∓ 0.0213	0.259	0.219

① Reference [21] pointed out that the computational error of the deflection by the element LPL-20β is big, so the results were not given.

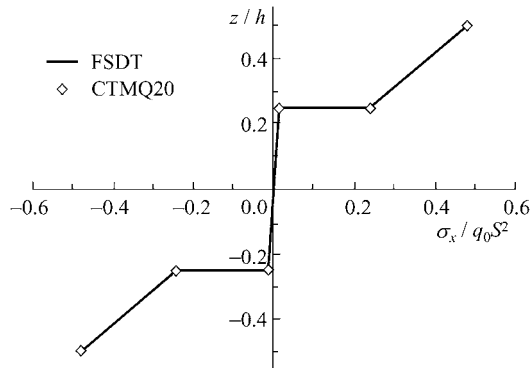


Figure 9.8 The distribution of central stress σ_x along thickness for a square 3-ply plate (doubly sinusoidal load, $L/h = 10$, 8×8 mesh)

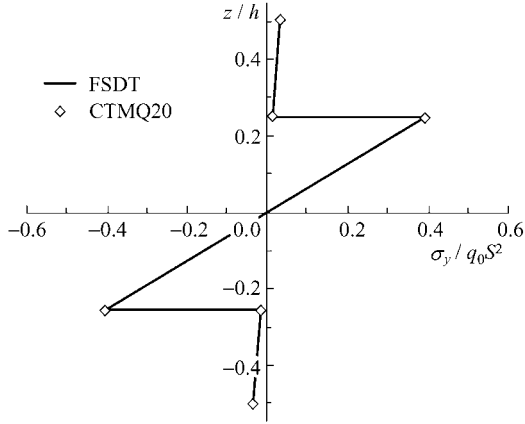


Figure 9.9 The distribution of central stress σ_y along thickness for a square 3-ply plate (doubly sinusoidal load, $L/h = 10$, 8×8 mesh)

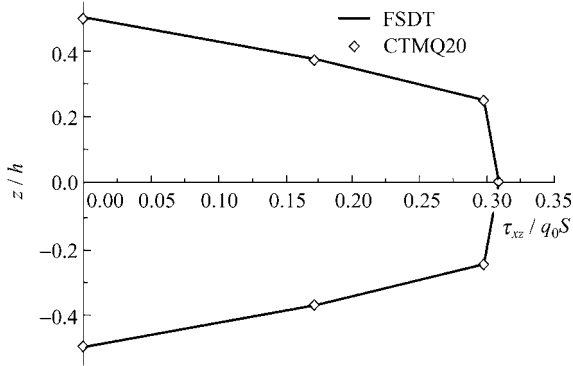


Figure 9.10 The distribution of τ_{xz} at $(0, L/2)$ along thickness of a square 3-ply plate (doubly sinusoidal load, $L/h = 10$, 8×8 mesh)

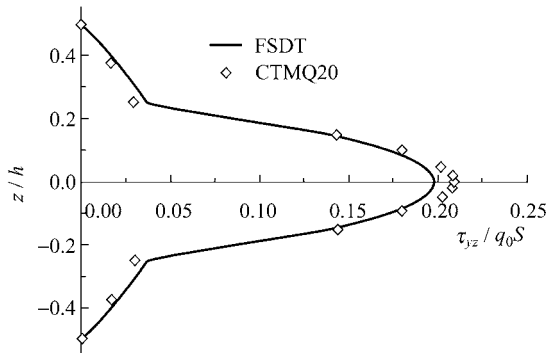


Figure 9.11 The distribution of τ_{yz} at $(L/2, 0)$ along thickness of a square 3-ply plate (doubly sinusoidal load, $L/h = 10$, 8×8 mesh)

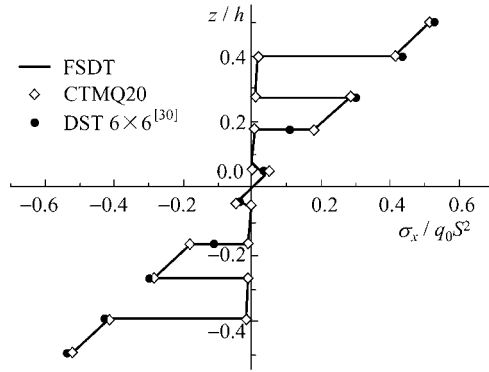


Figure 9.12 The distribution of central stress σ_x along thickness for a square 9-ply plate (doubly sinusoidal load, $L/h = 10$, 8×8 mesh)

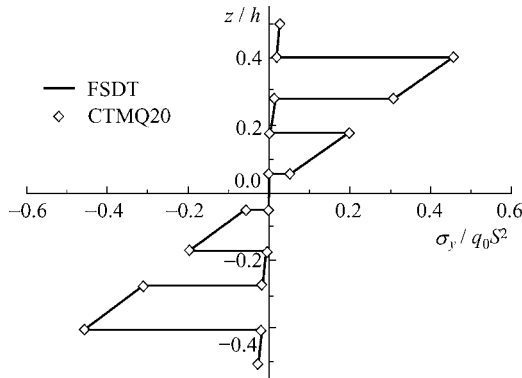


Figure 9.13 The distribution of central stress σ_y along thickness for a square 9-ply plate (doubly sinusoidal load, $L/h = 10$, 8×8 mesh)

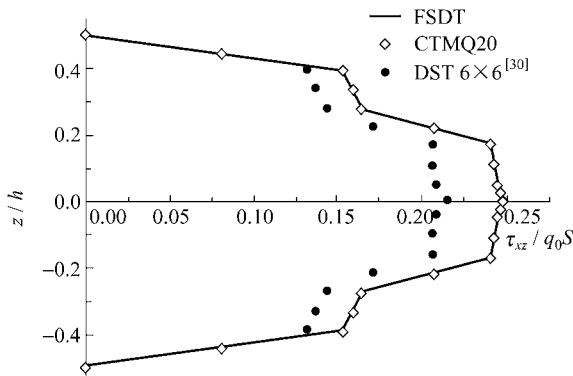


Figure 9.14 The distribution of τ_{xz} at $(0, L/2)$ along thickness of a square 9-ply plate (doubly sinusoidal load, $L/h = 10$, 8×8 mesh)

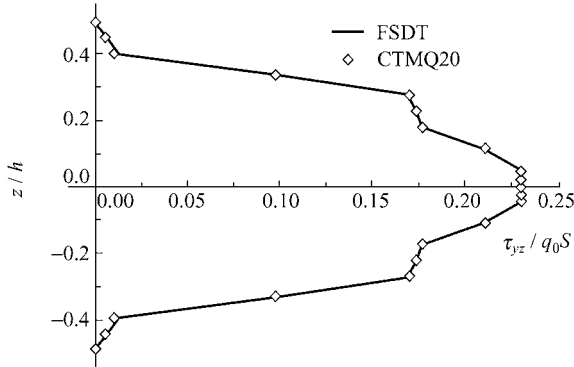


Figure 9.15 The distribution of τ_{yz} at $(L/2, 0)$ along thickness of a square 9-ply plate (doubly sinusoidal load, $L/h = 10$, 8×8 mesh)

With regards to the central deflection w_C and maximum plane stresses σ_x , σ_y and τ_{xy} , the results obtained using the CTMQ20 element are in excellent agreement with those of the exact FSDT for all span-thickness ratio L/t . No shear locking happens in the thin plate limit. The results obtained using three different meshes show rapid convergence for the above-mentioned deflection and stresses. For transverse shear stresses, the element CTMQ20 can still produces good results, which the usual displacement-based element cannot do.

It is obvious that the performance of the element CTMQ20 is much better than those obtained using the quadrilateral hybrid element LPL- 20β by Wu et al.^[21], the element DST (a discrete shear triangular plate-bending element) by Lardeur et al.^[30], REC56-Z0 (56 DOFs per element) and REC72-Z0 (72 DOFs per element) by Sadek^[19].

Example 9.2 Simply supported (hard support mode II) anti-symmetric angle-ply square plate with 2 $(-45/45)$ or 8 $[(-45/45)_4]_s$ layers subjected to doubly sinusoidal load.

The geometry, the material constants and the loading are the same as those given in Example 9.1. All the layers have the same thickness. The boundary conditions (hard simply-supported mode II) are:

$$\text{at } x = 0 \text{ and } x = L: u = w = \psi_y = 0; \text{ at } y = 0 \text{ and } y = L, v = w = \psi_x = 0.$$

Six different meshes, i.e., 4×4 , 8×8 , 16×16 , 32×32 , 64×64 and 80×80 , are used to model the whole plate and three L/h aspect ratios are considered. For comparison with the analytical solution in reference [1], the shear correction factors are taken as: $k_1^2 = k_2^2 = 5/6$. The results are shown in Tables 9.3 and 9.4. It can be seen that excellent solutions for deflection and in-plane stresses can be obtained from the element CTMQ20. For the anti-symmetric or unsymmetric cases, most of the simple displacement-based elements cannot produce good results for the transverse shear stresses using the equilibrium equation^[18]. Since

Table 9.3 Maximum deflection and stresses in 2-ply (−45/45) square laminate composite plate (hard simply-supported mode II) subjected to doubly sinusoidal load

L/h	Model & mesh	$w(L/2, L/2) \times 100E_2h^3/(L^4q_0)$	$\sigma_x(L/2, L/2, h/2) \times h^2/(L^2q_0)$	$\tau_{xy}(0, 0, -h/2) \times h^2/(L^2q_0)$	$\tau_{xz}(0, L/2, h/4) \times h/(Lq_0)$	
10	CTMQ20	4 × 4	0.8042	0.2628	0.2291	0.1683
		8 × 8	0.8218	0.2543	0.2349	0.2005
		16 × 16	0.8267	0.2510	0.2341	0.2107
		32 × 32	0.8280	0.2501	0.2337	0.2134
		64 × 64	0.8283	0.2499	0.2336	0.2141
		80 × 80	0.8283	0.2498	0.2336	0.2142
	FSDT ^[1]		0.8284	0.2498	0.2336	0.2143
20	CTMQ20	4 × 4	0.6733	0.2501	0.2211	0.1324
		8 × 8	0.6906	0.2523	0.2333	0.1773
		16 × 16	0.6961	0.2508	0.2339	0.2027
		32 × 32	0.6976	0.2501	0.2337	0.2112
		64 × 64	0.6980	0.2499	0.2336	0.2136
		80 × 80	0.6980	0.2498	0.2336	0.2138
	FSDT ^[1]		0.6981	0.2498	0.2336	0.2143
100	CTMQ20	4 × 4	0.6399	0.2399	0.2157	0.1049
		8 × 8	0.6519	0.2474	0.2295	0.1194
		16 × 16	0.6550	0.2495	0.2328	0.1362
		32 × 32	0.6560	0.2499	0.2335	0.1691
		64 × 64	0.6563	0.2499	0.2336	0.1980
		80 × 80	0.6564	0.2498	0.2336	0.2033
	FSDT ^[1]		0.6564	0.2498	0.2336	0.2143

Table 9.4 Maximum deflection and stresses in 8-ply [(−45/45)₄]_s square laminate composite plate (hard simply-supported mode II) subjected to doubly sinusoidal load

L/h	Model & mesh	$w(L/2, L/2) \times 100E_2h^3/(L^4q_0)$	$\sigma_x(L/2, L/2, h/2) \times h^2/(L^2q_0)$	$\tau_{xy}(0, 0, -h/2) \times h^2/(L^2q_0)$	$\tau_{xz}(0, L/2, 0) \times h/(Lq_0)$	
10	CTMQ20	4 × 4	0.4063	0.1657	0.1268	0.2131
		8 × 8	0.4157	0.1507	0.1361	0.2384
		16 × 16	0.4188	0.1461	0.1379	0.2460
		32 × 32	0.4196	0.1449	0.1383	0.2480
		64 × 64	0.4198	0.1446	0.1384	0.2485
		80 × 80	0.4198	0.1446	0.1384	0.2486
	FSDT ^[1]		0.4198	0.1445	0.1384	0.2487
20	CTMQ20	4 × 4	0.2764	0.1575	0.1223	0.1850
		8 × 8	0.2846	0.1496	0.1353	0.2225
		16 × 16	0.2881	0.1460	0.1378	0.2408
		32 × 32	0.2892	0.1449	0.1383	0.2466
		64 × 64	0.2895	0.1446	0.1384	0.2481
		80 × 80	0.2895	0.1446	0.1384	0.2483
	FSDT ^[1]		0.2896	0.1445	0.1384	0.2487
100	CTMQ20	4 × 4	0.2440	0.1499	0.1283	0.1674
		8 × 8	0.2463	0.1459	0.1356	0.1791
		16 × 16	0.2471	0.1451	0.1374	0.1904
		32 × 32	0.2476	0.1448	0.1380	0.2172
		64 × 64	0.2478	0.1446	0.1383	0.2380
		80 × 80	0.2478	0.1446	0.1383	0.2416
	FSDT ^[1]		0.2479	0.1445	0.1384	0.2487

the hybrid-enhanced post-processing procedure is used by the present element, it is obvious that good results of transverse shear stresses can be obtained.

Example 9.3 Free vibration analysis of a 3-ply (0/90/0) square plate (hard simply-supported mode I).

All the layers have the same thickness. Other geometry, the material constants, the load and the boundary conditions are the same as those given in Example 9.1. A 16×16 mesh is used for the whole plate and two span-thickness ratios are considered. For comparison with the analytical solution in reference [1], the shear correction factors are taken as: $k_1^2 = k_2^2 = 1$. The first seven dimensionless natural frequencies obtained are listed in Table 9.5. It can be seen that the element CTMQ20 can provide accurate results.

Table 9.5 The free frequency coefficients $\tilde{\omega} = \omega(L^2/h)\sqrt{\rho/E_2}$ for a 3-ply (0/90/0) square laminate composite plate (hard simply-supported mode I)

L/h	Mode m in x -direction	Mode n in y -direction	CLT ^[1]	FSDT ^[1]	CTMQ20 16×16 ^①
10	1	1	15.104	12.527	12.464 (- 0.50%)
	1	2	22.421	19.203	18.974 (- 1.19%)
	1	3	38.738	31.921	31.377 (- 1.70%)
	2	1	55.751	32.931	32.641 (- 0.88%)
	2	2	59.001	36.362	35.641 (- 1.98%)
	1	4	62.526	44.720	43.350 (- 3.06%)
	2	3	67.980	47.854	46.722 (- 2.36%)
100	1	1	15.227	15.191	15.142 (- 0.32%)
	1	2	22.873	22.827	22.659 (- 0.74%)
	1	3	40.283	40.174	39.871 (- 0.75%)
	2	1	56.874	56.319	56.123 (- 0.35%)
	2	2	60.891	60.322	59.556 (- 1.27%)
	1	4	66.708	66.421	65.939 (- 0.73%)
	2	3	71.484	70.764	69.244 (- 2.14%)

① The numbers in parentheses are percentage errors.

Example 9.4 Free vibration analysis of anti-symmetric angle-ply square plates (hard simply-supported mode II) with 2 (- 45/45) and 8 [(- 45/45)₄]_s layers.

All the layers have the same thickness. Boundary conditions are the same as those given in Example 9.2. There are two material cases:

Material 1: $E_1 = 25.0; E_2 = 1.0; G_{12} = 0.5; G_{13} = 0.5; G_{23} = 0.2; \mu_{12} = 0.25$

Material 2: $E_1 = 40.0; E_2 = 1.0; G_{12} = 0.6; G_{13} = 0.6; G_{23} = 0.5; \mu_{12} = 0.25$

A 16×16 mesh is used for the whole plate, and four span-thickness ratios are considered. For comparison with the analytical solution in reference [1], the shear

correction factors are taken as: $k_1^2 = k_2^2 = 5/6$. The results of the first natural frequency are listed in Table 9.6.

Table 9.6 The first natural frequency coefficients $\tilde{\omega} = \omega(L^2/h)\sqrt{\rho/E_2}$ for anti-symmetric angle-ply square laminate composite plate (hard simply-supported mode II)

<i>L/h</i>		Material 1		Material 2	
		2-ply (-45/45)	8-ply [(-45/45) ₄] _s	2-ply (-45/45)	8-ply [(-45/45) ₄] _s
5	CTMQ20	8.457	10.244	10.285	12.842
	16 × 16 FSDT ^[1]	(-0.48%) 8.498	(-0.40%) 10.285	(-4.76%) 10.799	(-0.40%) 12.893
10	CTMQ20	10.860	15.349	13.002	19.242
	16 × 16 FSDT ^[1]	(-0.32%) 10.895	(-0.25%) 15.388	(-4.60%) 13.629	(-0.24%) 19.289
20	CTMQ20	11.908	18.535	14.149	23.237
	16 × 16 FSDT ^[1]	(-0.21%) 11.933	(-0.11%) 18.555	(-4.50%) 14.815	(-0.09%) 23.259
100	CTMQ20	12.315	20.049	14.581	25.134
	16 × 16 FSDT ^[1]	(-0.21%) 12.341	(-0.17%) 20.084	(-4.54%) 15.274	(-0.17%) 25.176

Note: The numbers in parentheses are percentage errors.

References

- [1] Reddy JN (1997) Mechanics of laminated composite plates—theory and analysis. CRC Press, Boca Raton
- [2] Calcote LR (1969) The analysis of laminated composite structures. Van Nostrand Reinhold, New York
- [3] Jones RM (1975) Mechanics of composite material. MacGraw-Hill Kogakusha, Tokyo
- [4] Medwadowski SJ (1958) A refined theory of elastic orthotropic plates. ASME J Appl Mech, 25: 437 – 443
- [5] Yang PC, Norris CH, Stavsky Y (1966) Elastic wave propagation in heterogeneous plates. International Journal of Solids and Structures 2: 665 – 684
- [6] Lo KH, Christensen RM, Wu EM (1977) A higher-order theory of plate deformation, Part II: Laminated plates. Journal of Applied Methanics 44(4): 663 – 668
- [7] Reddy JN (1984) A simple higher-order theory for laminated composite plates. Journal of Applied Methanics 51: 745 – 752
- [8] Phan ND, Reddy JN (1985) Analysis of laminated composite plates using a higher-order shear deformation theory. International Journal for Numerical Methods in Engineering 21: 2201 – 2219

Advanced Finite Element Method in Structural Engineering

- [9] Pandya BN, Kant T (1988) Flexural analysis of laminated composites using refined higher-order C^0 plate bending elements. *Computer Methods in Applied Mechanics and Engineering* 66: 173 – 198
- [10] Kant T, Owen DRJ, Zienkiewicz OC (1982) A refined higher-order C^0 plate bending element. *Computers & Structures* 15: 177 – 183
- [11] Reddy JN (1987) A generalization of two-dimensional theories of laminated composite plates. *Communications in Applied Numerical Methods* 3: 173 – 180
- [12] Robbins DH, Reddy JN (1993) Modelling of thick composites using a layerwise laminate theory. *International Journal for Numerical Methods in Engineering* 36: 655 – 677
- [13] Pryor CW, Barker RM (1971) A finite element analysis including transverse shear effects for application to laminated plates. *AIAA Journal* 9: 912 – 917
- [14] Vlachoutsis S (1992) Shear correction factors for plates and shells. *International Journal for Numerical Methods in Engineering* 33: 1537 – 1552
- [15] Auricchio F, Sacco E (199) A mixed-enhanced finite-element for the analysis of laminated composite plates. *International Journal for Numerical Methods in Engineering* 44: 1481 – 1504
- [16] Rolfes R, Rohwer K (1997) Improved transverse shear stresses in composite finite elements based on first order shear deformation theory. *International Journal for Numerical Methods in Engineering* 40: 51 – 60
- [17] Rolfes R, Rohwer K, Ballerstaedt M (1998) Efficient linear transverse normal stress analysis of layered composite plates. *Computers & Structures* 68: 643 – 652
- [18] Singh G, Raju KK, Rao GV (1998) A new lock-free, material finite element for flexure of moderately thick rectangular composite plates. *Computers & Structures* 69: 609 – 623
- [19] Sadek EA (1998) Some serendipity finite element for the analysis of laminated plates. *Computers & Structures* 69: 37 – 51
- [20] Alfano G, Auricchio F, Rosati L, Sacco E (2001) MITC finite elements for laminated composite plates. *International Journal for Numerical Methods in Engineering* 50: 707 – 738
- [21] Wu CC, Pian THH (1997) *Incompatible Numerical Analysis and Hybrid Finite Element Method*. Beijing: Science Press (in Chinese)
- [22] Cen S, Long YQ, Yao ZH (2002) A new element based on the first-order shear deformation theory for the analysis of laminated composite plates. *Gong Cheng Li Xue/Engineering Mechanics* 19(1): 1 – 8 (in Chinese)
- [23] Cen S, Long YQ, Yao ZH (2002) A new hybrid-enhanced displacement-based element for the analysis of laminated composite plates. *Computers & Structures* 80 (9-10): 819 – 833
- [24] Cen S, Long ZF, Long YQ (1999) A Mindlin quadrilateral plate element with improved interpolation for the rotation and shear strain fields. *Gong Cheng Li Xue/Engineering Mechanics* 16(4): 1 – 15 (in Chinese)
- [25] Soh AK, Cen S, Long YQ, Long ZF (2001) A new twelve DOF quadrilateral element for analysis of thick and thin plates. *European Journal of Mechanics A/Solids* 20: 299 – 326
- [26] Cen S, Long YQ, Yao ZH (2001) An enhanced hybrid post-processing procedure for improving stress solutions of displacement-based plate bending elements. *Gong Cheng Li Xue/Engineering Mechanics* 18(3): 21 – 27 (in Chinese)

- [27] Ayad R, Dhatt G, Batoz JL (1998) A new hybrid-mixed variational approach for Reissner-Mindlin plates: The MiSP model. *International Journal for Numerical Methods in Engineering* 42:1149 – 1179
- [28] Pian THH, Sumihara K (1984) Rational approach for assumed stress finite element. *International Journal for Numerical Methods in Engineering* 20: 1685 – 1695
- [29] Pagano NJ, Hatfield SJ (1972) Elastic behavior of multilayered bidirectional composites. *AIAA Journal* 10: 931 – 933
- [30] Lardeur P, Batoz JL (1989) Composite plate analysis using a new discrete shear triangular finite element. *International Journal for Numerical Methods in Engineering* 27: 343 – 359
- [31] Pagano NJ (1970) Exact solutions for rectangular bidirectional composites and sandwich plates. *J Compos Mater* 4: 20 – 34

Chapter 10 Generalized Conforming Element for the Analysis of Piezoelectric Laminated Composite Plates

Song Cen

Department of Engineering Mechanics, School of Aerospace,
Tsinghua University, Beijing, 100084, China

Yu-Qiu Long

Department of Civil Engineering, School of Civil Engineering,
Tsinghua University, Beijing, 100084, China

Abstract A new 4-node quadrilateral finite element is developed for the analysis of the laminated composite plates containing distributed piezoelectric layers (surface bonded or embedded). The mechanical part of the element formulation is based on the first-order shear deformation theory (FSDT). The formulation is established by generalizing that of the generalized conforming laminated plate element CTMQ20 presented in the previous chapter. The layer-wise linear theory is applied to deal with electric potential. Therefore, the number of the electrical DOF is a variable depending on the number of the plate sub-layers. Thus, there is no need to make any special assumptions with regard to the through-thickness variation of the electric potential, which is the true situation. Furthermore, a new “partial hybrid”-enhanced procedure is presented to improve the stress solutions, especially for the calculation of the transverse shear stresses. The proposed element, denoted as CTMQE, is free of shear locking and it exhibits excellent capability in the analysis of thin to moderately thick piezoelectric laminated composite plates.

Keywords finite element, piezoelectric, laminated composite plate, generalized conforming, first-order shear deformation theory (FSDT), layerwise theory, partial hybrid-enhanced post-processing procedure.

10.1 Introduction

The finite element method is a powerful tool in the analysis of the adaptive/smart structures. Since the early 1970s, many finite element models have been proposed

for analyzing such structures. Benjeddou^[1] made a survey on the advances and trends in the aforementioned area and he found more than one hundred related literatures, which were mostly published in the 1990s. Many researchers are still actively involved in the development of new special elements, as can be seen from the recent publications^[2-4].

The fibre-reinforced laminate composite plates play an important role in the modern industry due to its high strength-to-weight ratio. When the piezoelectric materials, which can be used for both sensors and actuators, are bonded on the top/bottom surface or embedded in the composite structures, their performance could be effectively enhanced. The design and analysis of these complicated coupled systems require the development of new finite elements. Most of the earlier models were devised using the solid 3D elements^[5,6]. Such models lead to high computational costs. Moreover, some numerical problems, such as shear locking, often take place when relatively thin structures are being analyzed. Therefore, many researchers prefer to develop new plate elements based on the 2D theory.

Reddy^[7] has presented theoretical formulations and finite element models based on the classical thin plate theory (CLT) and the third-order shear deformation theory (TSDT). Huang et al.^[8] has also presented FSDT for studying the fully coupled system. To date, FSDT is usually considered the best compromise between the capability for prediction and computational cost for a wide class of applications. By simplifying the effects of the electrical potential, Jonnalagadda et al.^[9] presented a 9-node Lagrangian element without electric DOF based on FSDT. Detwiler et al.^[10] presented a 4-node element model generalized from the Mindlin-plate element, QUAD4, based on the assumption of linear variation through-thickness and constant in-plane electric potential. But, it may suffer from locking or spurious zero energy modes. Another model with one potential DOF per piezoelectric layer, and using uniform reduced numerical integration and hourglass stabilization was also proposed in [11]. Most piezoelectric plate finite element formulations assume the electric potential variation and poling direction along the piezoelectric patch thickness. Reference [4] presented a new 9-node mixed-theory element: The structural deformation was modelled using the FSDT whereas the layer-wise theory was adopted for the modeling of electrical potential. Thus, no specific pattern was imposed on the through-thickness variation of the electric potential.

Reference [12] developed a 4-node quadrilateral generalized conforming element CTMQE for the analysis of the piezoelectric laminated composite plates. The mechanical part of the element formulation is based on the first-order shear deformation theory (FSDT) and comes from those of the element CTMQ20 presented in the previous chapter. And, the layer-wise linear theory is applied to deal with electric potential. Therefore, the number of electrical DOF is a variable depending on the number of the plate sub-layers, and there is no need to make any special assumptions with regard to the through-thickness variation of the electric potential, which is the true situation. Furthermore, a new “partial

hybrid”-enhanced post-processing procedure is presented to improve the stress solutions, especially for the calculation of transverse shear stresses. This chapter will introduce the above formulations.

10.2 The First-Order Shear Deformation Theory of Piezoelectric Laminated Composite Plate

With reference to Fig. 10.1, for the n -layer linear elastic piezoelectric laminated composite plate considered, the kinematics is governed by the mid-plane displacements u^0, v^0 , the transverse displacement w and rotations ψ_x and ψ_y . All the governing equations and the expressions of the strains $\boldsymbol{\varepsilon}, \boldsymbol{\varepsilon}^0, \boldsymbol{\kappa}$ and $\boldsymbol{\gamma}$ are the same as Eqs. (9-1) to (9-6).

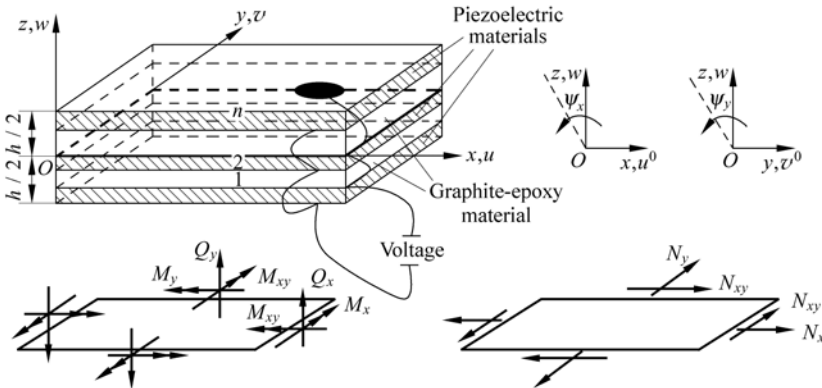


Figure 10.1 Internal forces and displacements at mid-plane of a piezoelectric laminated composite plate

The electric field vector is:

$$\boldsymbol{\varepsilon}_e = [E_x^e \quad E_y^e \quad E_z^e]^T = \begin{bmatrix} -\frac{\partial \phi}{\partial x} & -\frac{\partial \phi}{\partial y} & -\frac{\partial \phi}{\partial z} \end{bmatrix}^T \tag{10-1}$$

where ϕ is the electric field potential; E_x^e, E_y^e and E_z^e are the electric-field intensities in x, y and z directions, respectively.

The stress-strain relationship with respect to principal 1-axis and 2-axis for the k th ($k = 1, 2, \dots, n$) layer is:

$$\begin{Bmatrix} \sigma_1 \\ \sigma_2 \\ \tau_{12} \end{Bmatrix}^k = \begin{bmatrix} Q_{11} & Q_{12} & 0 \\ Q_{12} & Q_{22} & 0 \\ 0 & 0 & Q_{66} \end{bmatrix}^k \begin{Bmatrix} \varepsilon_1 \\ \varepsilon_2 \\ \gamma_{12} \end{Bmatrix}^k - \begin{bmatrix} 0 & 0 & e_{31} \\ 0 & 0 & e_{32} \\ 0 & 0 & 0 \end{bmatrix}^k \begin{Bmatrix} E_1^e \\ E_2^e \\ E_3^e \end{Bmatrix}^k \tag{10-2}$$

$$\begin{Bmatrix} \tau_{23} \\ \tau_{13} \end{Bmatrix}^k = \begin{bmatrix} Q_{44} & 0 \\ 0 & Q_{55} \end{bmatrix}^k \begin{Bmatrix} \gamma_{23} \\ \gamma_{13} \end{Bmatrix}^k - \begin{bmatrix} 0 & e_{24} & 0 \\ e_{15} & 0 & 0 \end{bmatrix}^k \begin{Bmatrix} E_1^e \\ E_2^e \\ E_3^e \end{Bmatrix}^k \quad (10-3)$$

where E_1^e , E_2^e and E_3^e are the electric-field intensities in 1-axis, 2-axis and 3-axis (3-axis is an axis which is normal to the plane constructed by 1-axis and 2-axis, and generally coincides with z -axis), respectively; e_{ij} are the piezoelectric constants defined in the 123 coordinate system; the other symbols are the same as those in Eq. (9-7) to Eq. (9-9).

The electrical displacements of the k th layer is related to the components of strains and electrical field by

$$\begin{Bmatrix} D_1^e \\ D_2^e \\ D_3^e \end{Bmatrix}^k = \begin{bmatrix} 0 & 0 & 0 \\ 0 & 0 & 0 \\ e_{31} & e_{32} & 0 \end{bmatrix}^k \begin{Bmatrix} \varepsilon_1 \\ \varepsilon_2 \\ \gamma_{12} \end{Bmatrix}^k + \begin{bmatrix} \varepsilon_{11} & 0 & 0 \\ 0 & \varepsilon_{22} & 0 \\ 0 & 0 & \varepsilon_{33} \end{bmatrix}^k \begin{Bmatrix} E_1^e \\ E_2^e \\ E_3^e \end{Bmatrix}^k + \begin{bmatrix} e_{15} & 0 \\ 0 & e_{24} \\ 0 & 0 \end{bmatrix}^k \begin{Bmatrix} \gamma_{13} \\ \gamma_{23} \end{Bmatrix}^k \quad (10-4)$$

where D_1^e , D_2^e and D_3^e are the electric displacements in 1-axis, 2-axis and 3-axis, respectively; ε_{11} , ε_{22} and ε_{33} are the dielectric constants.

The stress-strain relationships in the xyz coordinate system for the k th ($k = 1, 2, \dots, n$) layer are:

$$\begin{aligned} \boldsymbol{\sigma}^k &= \begin{Bmatrix} \sigma_x \\ \sigma_y \\ \tau_{xy} \end{Bmatrix}^k = \begin{bmatrix} \bar{Q}_{11} & \bar{Q}_{12} & \bar{Q}_{16} \\ \bar{Q}_{12} & \bar{Q}_{22} & \bar{Q}_{26} \\ \bar{Q}_{16} & \bar{Q}_{26} & \bar{Q}_{66} \end{bmatrix}^k \begin{Bmatrix} \varepsilon_x \\ \varepsilon_y \\ \gamma_{xy} \end{Bmatrix}^k - \begin{bmatrix} 0 & 0 & \bar{e}_{31} \\ 0 & 0 & \bar{e}_{32} \\ 0 & 0 & \bar{e}_{36} \end{bmatrix}^k \begin{Bmatrix} E_x^e \\ E_y^e \\ E_z^e \end{Bmatrix}^k \\ &= \begin{bmatrix} \bar{Q}_{11} & \bar{Q}_{12} & \bar{Q}_{16} \\ \bar{Q}_{12} & \bar{Q}_{22} & \bar{Q}_{26} \\ \bar{Q}_{16} & \bar{Q}_{26} & \bar{Q}_{66} \end{bmatrix}^k \begin{Bmatrix} \varepsilon_x \\ \varepsilon_y \\ \gamma_{xy} \end{Bmatrix}^k - \begin{bmatrix} \bar{e}_{31} \\ \bar{e}_{32} \\ \bar{e}_{36} \end{bmatrix}^k \cdot E_z^e = \bar{\mathbf{Q}}^k \boldsymbol{\varepsilon} - E_z^e \bar{\mathbf{e}}_z^k \end{aligned} \quad (10-5)$$

$$\begin{aligned} \boldsymbol{\tau}_z^k &= \begin{Bmatrix} \tau_{xz} \\ \tau_{yz} \end{Bmatrix}^k = \begin{bmatrix} k_1^2 \bar{Q}_{55} & k_1 k_2 \bar{Q}_{45} \\ k_1 k_2 \bar{Q}_{45} & k_2^2 \bar{Q}_{44} \end{bmatrix}^k \begin{Bmatrix} \gamma_{xz} \\ \gamma_{yz} \end{Bmatrix}^k - \begin{bmatrix} \bar{e}_{15} & \bar{e}_{25} & 0 \\ \bar{e}_{14} & \bar{e}_{24} & 0 \end{bmatrix}^k \begin{Bmatrix} E_x^e \\ E_y^e \\ E_z^e \end{Bmatrix}^k \\ &= \begin{bmatrix} k_1^2 \bar{Q}_{55} & k_1 k_2 \bar{Q}_{45} \\ k_1 k_2 \bar{Q}_{45} & k_2^2 \bar{Q}_{44} \end{bmatrix}^k \begin{Bmatrix} \gamma_{xz} \\ \gamma_{yz} \end{Bmatrix}^k - \begin{bmatrix} \bar{e}_{15} & \bar{e}_{25} \\ \bar{e}_{14} & \bar{e}_{24} \end{bmatrix}^k \begin{Bmatrix} E_x^e \\ E_y^e \end{Bmatrix}^k \\ &= \bar{\mathbf{C}}_s^k \boldsymbol{\gamma} - \bar{\mathbf{e}}_{xy}^k \mathbf{E}_{xy} \end{aligned} \quad (10-6)$$

in which \bar{e}_{ij} are the piezoelectric constants defined in the xyz coordinate system,

$$\left. \begin{aligned} \bar{e}_{31} &= e_{31}l^2 + e_{32}m^2, & \bar{e}_{32} &= e_{31}m^2 + e_{32}l^2, & \bar{e}_{36} &= (e_{31} - e_{32})lm \\ \bar{e}_{14} &= (e_{15} - e_{24})lm, & \bar{e}_{24} &= e_{24}l^2 + e_{15}m^2 \\ \bar{e}_{15} &= e_{24}m^2 + e_{15}l^2, & \bar{e}_{25} &= (e_{15} - e_{24})lm \end{aligned} \right\} \quad (10-7)$$

where the definitions of l and m are the same as Eq. (9-13).

The relation of electric displacements, strains and electric-field intensities in the xyz coordinate system can be written as:

$$\begin{aligned} \begin{Bmatrix} D_x^e \\ D_y^e \\ D_z^e \end{Bmatrix}^k &= \begin{bmatrix} 0 & 0 & 0 \\ 0 & 0 & 0 \\ \bar{e}_{31} & \bar{e}_{32} & \bar{e}_{36} \end{bmatrix}^k \begin{Bmatrix} \mathcal{E}_x \\ \mathcal{E}_y \\ \gamma_{xy} \end{Bmatrix} + \begin{bmatrix} \bar{\epsilon}_{11} & \bar{\epsilon}_{12} & 0 \\ \bar{\epsilon}_{12} & \bar{\epsilon}_{22} & 0 \\ 0 & 0 & \bar{\epsilon}_{33} \end{bmatrix}^k \begin{Bmatrix} E_x^e \\ E_y^e \\ E_z^e \end{Bmatrix} \\ &+ \begin{bmatrix} \bar{e}_{15} & \bar{e}_{14} \\ \bar{e}_{25} & \bar{e}_{24} \\ 0 & 0 \end{bmatrix}^k \begin{Bmatrix} \gamma_{xz} \\ \gamma_{yz} \end{Bmatrix} \end{aligned} \quad (10-8)$$

where $\bar{\epsilon}_{ij}$ are the dielectric constants in the xyz coordinate system,

$$\left. \begin{aligned} \bar{\epsilon}_{11} &= \epsilon_{11}l^2 + \epsilon_{22}m^2, & \bar{\epsilon}_{12} &= (\epsilon_{11} - \epsilon_{22})lm \\ \bar{\epsilon}_{22} &= \epsilon_{11}m^2 + \epsilon_{22}l^2, & \bar{\epsilon}_{33} &= \epsilon_{33} \end{aligned} \right\} \quad (10-9)$$

For convenience, Eq. (10-8) can be rewritten as

$$\begin{aligned} D_{xy}^k &= \begin{Bmatrix} D_x^e \\ D_y^e \end{Bmatrix}^k = \begin{bmatrix} \bar{\epsilon}_{11} & \bar{\epsilon}_{12} \\ \bar{\epsilon}_{12} & \bar{\epsilon}_{22} \end{bmatrix}^k \begin{Bmatrix} E_x^e \\ E_y^e \end{Bmatrix} + \begin{bmatrix} \bar{e}_{15} & \bar{e}_{14} \\ \bar{e}_{25} & \bar{e}_{24} \end{bmatrix}^k \begin{Bmatrix} \gamma_{xz} \\ \gamma_{yz} \end{Bmatrix} \\ &= \bar{\mathbf{e}}_{xy}^k \mathbf{E}_{xy}^e + \bar{\mathbf{e}}_{xy}^{kT} \boldsymbol{\gamma} \end{aligned} \quad (10-10)$$

$$D_z^k = [\bar{e}_{31} \quad \bar{e}_{32} \quad \bar{e}_{36}]^k \begin{Bmatrix} \mathcal{E}_x \\ \mathcal{E}_y \\ \gamma_{xy} \end{Bmatrix} + \bar{\epsilon}_{33}^k E_z = \bar{\mathbf{e}}_z^{kT} \boldsymbol{\epsilon} + \bar{\epsilon}_{33}^k E_z^e \quad (10-11)$$

Then, the mechanical constitutive relationship of the plate can be expressed as:

$$\boldsymbol{\sigma}_p = \begin{Bmatrix} \mathbf{N} \\ \mathbf{M} \end{Bmatrix} = \begin{bmatrix} \mathbf{A} & \mathbf{B} \\ \mathbf{B} & \mathbf{D} \end{bmatrix} \begin{Bmatrix} \boldsymbol{\epsilon}^0 \\ \boldsymbol{\kappa} \end{Bmatrix} - \begin{Bmatrix} \mathbf{N}_e \\ \mathbf{M}_e \end{Bmatrix} = \mathbf{C}_p \boldsymbol{\epsilon}_p - \boldsymbol{\sigma}_e \quad (10-12a)$$

$$\mathbf{Q} = \mathbf{C}_s \boldsymbol{\gamma} - \mathbf{Q}_e \quad (10-12b)$$

in which \mathbf{N}_e , \mathbf{M}_e and \mathbf{Q}_e are the membrane force, bending moment and shear force vectors caused by the electrical field, respectively,

$$\left. \begin{aligned} \mathbf{N}_e &= [N_x^e \quad N_y^e \quad N_z^e]^T = \int_{-h/2}^{h/2} E_z^e \bar{\mathbf{e}}_z^k \, dz \\ \mathbf{M}_e &= [M_x^e \quad M_y^e \quad M_z^e]^T = \int_{-h/2}^{h/2} z E_z^e \bar{\mathbf{e}}_z^k \, dz \\ \mathbf{Q}_e &= [Q_x^e \quad Q_y^e \quad Q_z^e]^T = \int_{-h/2}^{h/2} \bar{\mathbf{e}}_{xy}^k \mathbf{E}_{xy}^e \, dz \end{aligned} \right\} \quad (10-13)$$

Other symbols are the same as those in Eq. (9-16) to Eq. (9-21).

10.3 New Piezoelectric Laminated Composite Plate Element CTMQE

Consider the quadrilateral plate element shown in Fig. 10.2. The generalized nodal displacement vector of the 4-node element is:

$$\left. \begin{aligned} \mathbf{q}^e &= [\mathbf{q}_1^{eT} \quad \mathbf{q}_2^{eT} \quad \mathbf{q}_3^{eT} \quad \mathbf{q}_4^{eT}]^T \\ \mathbf{q}_i^e &= [u_i \quad v_i \quad w_i \quad \psi_{xi} \quad \psi_{yi} \quad \phi_i^0 \quad \phi_i^1 \quad \dots \quad \phi_i^k \quad \dots \quad \phi_i^n]^T \end{aligned} \right\} \quad (i = 1, 2, 3, 4) \quad (10-14)$$

where ϕ_i^k ($k = 0, 1, 2, \dots, n$) are the nodal electrical potential at the interface between k th and $(k + 1)$ th layers.

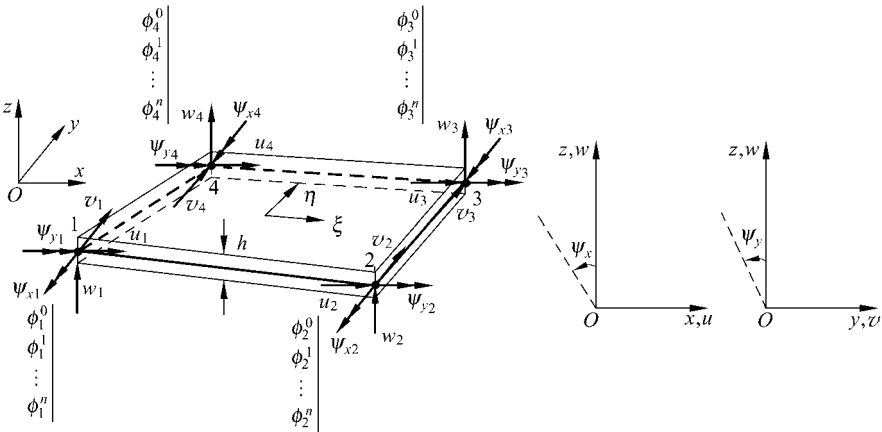


Figure 10.2 The quadrilateral piezoelectric laminated composite plate element CTMQE

10.3.1 Interpolation Formulas for the Shear Strain Fields

The interpolation procedure for the shear strain fields is the same as that in Sect. 9.3.1, and the shear strain fields are as follows:

$$\boldsymbol{\gamma} = \begin{Bmatrix} \gamma_{xz} \\ \gamma_{yz} \end{Bmatrix} = \begin{bmatrix} N_s^0 \mathbf{X}_s \boldsymbol{\Gamma}^* \\ N_s^0 \mathbf{Y}_s \boldsymbol{\Gamma}^* \end{bmatrix} \mathbf{q}^e = \mathbf{B}_s \mathbf{q}^e \quad (10-15)$$

in which

$$\boldsymbol{\Gamma}^* = [\boldsymbol{\Gamma}_1^* \quad \mathbf{0}_{4 \times (n+1)} \quad \boldsymbol{\Gamma}_2^* \quad \mathbf{0}_{4 \times (n+1)} \quad \boldsymbol{\Gamma}_3^* \quad \mathbf{0}_{4 \times (n+1)} \quad \boldsymbol{\Gamma}_4^* \quad \mathbf{0}_{4 \times (n+1)}] \quad (10-16)$$

$$\boldsymbol{\Gamma}_1^* = \begin{bmatrix} 0 & 0 & 0 & 0 & 0 \\ 0 & 0 & 0 & 0 & 0 \\ 0 & 0 & 2\delta_3 & -c_3\delta_3 & b_3\delta_3 \\ 0 & 0 & -2\delta_4 & -c_4\delta_4 & b_4\delta_4 \end{bmatrix}, \quad \boldsymbol{\Gamma}_2^* = \begin{bmatrix} 0 & 0 & -2\delta_1 & -c_1\delta_1 & b_1\delta_1 \\ 0 & 0 & 0 & 0 & 0 \\ 0 & 0 & 0 & 0 & 0 \\ 0 & 0 & 2\delta_4 & -c_4\delta_4 & b_4\delta_4 \end{bmatrix} \quad (10-17a,b)$$

$$\boldsymbol{\Gamma}_3^* = \begin{bmatrix} 0 & 0 & 2\delta_1 & -c_1\delta_1 & b_1\delta_1 \\ 0 & 0 & -2\delta_2 & -c_2\delta_2 & b_2\delta_2 \\ 0 & 0 & 0 & 0 & 0 \\ 0 & 0 & 0 & 0 & 0 \end{bmatrix}, \quad \boldsymbol{\Gamma}_4^* = \begin{bmatrix} 0 & 0 & 0 & 0 & 0 \\ 0 & 0 & 2\delta_2 & -c_2\delta_2 & b_2\delta_2 \\ 0 & 0 & -2\delta_3 & -c_3\delta_3 & b_3\delta_3 \\ 0 & 0 & 0 & 0 & 0 \end{bmatrix} \quad (10-17c,d)$$

where b_i , c_i and δ_i are given in Eqs. (9-36) and (9-37); N_s^0 is given in Eq. (9-53); \mathbf{X}_s and \mathbf{Y}_s are given in Eq. (9-48); $\mathbf{0}_{4 \times (n+1)}$ denotes a zero matrix with 4 lines and $n+1$ columns.

10.3.2 Interpolation Formulas for the Rotation Fields

The interpolation procedure for the rotation fields is similar to that in Sect. 9.3.2, and the interpolation formulas are also the same as Eq. (9-65). Besides, the rotations at the mid-side node can still be expressed in terms of the DOFs at corner nodes. Then, Eq. (9-59) to Eq. (9-64) can be rewritten as:

$$\tilde{\boldsymbol{\psi}}_x = \mathbf{F}_x \mathbf{q}^e, \quad \tilde{\boldsymbol{\psi}}_y = \mathbf{F}_y \mathbf{q}^e \quad (10-18)$$

in which

$$\left. \begin{aligned} \mathbf{F}_x &= [\mathbf{F}_{x1} \quad \mathbf{0}_{4 \times (n+1)} \quad \mathbf{F}_{x2} \quad \mathbf{0}_{4 \times (n+1)} \quad \mathbf{F}_{x3} \quad \mathbf{0}_{4 \times (n+1)} \quad \mathbf{F}_{x4} \quad \mathbf{0}_{4 \times (n+1)}] \\ \mathbf{F}_y &= [\mathbf{F}_{y1} \quad \mathbf{0}_{4 \times (n+1)} \quad \mathbf{F}_{y2} \quad \mathbf{0}_{4 \times (n+1)} \quad \mathbf{F}_{y3} \quad \mathbf{0}_{4 \times (n+1)} \quad \mathbf{F}_{y4} \quad \mathbf{0}_{4 \times (n+1)}] \end{aligned} \right\} \quad (10-19)$$

where \mathbf{F}_{xi} and \mathbf{F}_{yi} ($i=1,2,3,4$) have been given in Eqs. (9-63) and (9-64).

10.3.3 Interpolation Formulas for In-Plane Displacement Fields of the Mid-Plane

The interpolation formulas of the element in-plane displacements are the same as that of Eq. (9-67).

10.3.4 The In-Plane Strain and Curvature Fields

The in-plane strain field of the mid-plane is

$$\boldsymbol{\varepsilon}^0 = \mathbf{B}^0 \mathbf{q}^e \quad (10-20)$$

in which

$$\mathbf{B}^0 = [\mathbf{B}_1^0 \quad \mathbf{0}_{3 \times (n+1)} \quad \mathbf{B}_2^0 \quad \mathbf{0}_{3 \times (n+1)} \quad \mathbf{B}_3^0 \quad \mathbf{0}_{3 \times (n+1)} \quad \mathbf{B}_4^0 \quad \mathbf{0}_{3 \times (n+1)}] \quad (10-21)$$

where \mathbf{B}_i^0 ($i = 1, 2, 3, 4$) are given in equation (9-70); $\mathbf{0}_{3 \times (n+1)}$ denotes a zero matrix with 3 lines and $n + 1$ columns.

The curvature field can be written as

$$\boldsymbol{\kappa} = -(\mathbf{H}_0 + \mathbf{H}_1 \mathbf{F}_x + \mathbf{H}_2 \mathbf{F}_y) \mathbf{q}^e = \mathbf{B}_b \mathbf{q}^e \quad (10-22)$$

in which

$$\mathbf{H}_0 = [\mathbf{H}_{01} \quad \mathbf{0}_{3 \times (n+1)} \quad \mathbf{H}_{02} \quad \mathbf{0}_{3 \times (n+1)} \quad \mathbf{H}_{03} \quad \mathbf{0}_{3 \times (n+1)} \quad \mathbf{H}_{04} \quad \mathbf{0}_{3 \times (n+1)}] \quad (10-23)$$

\mathbf{H}_{0i} , \mathbf{H}_1 and \mathbf{H}_2 are given in Eqs. (9-75) and (9-76).

Then we have

$$\boldsymbol{\varepsilon}_p = \begin{Bmatrix} \boldsymbol{\varepsilon}^0 \\ \boldsymbol{\kappa} \end{Bmatrix} = \begin{bmatrix} \mathbf{B}^0 \\ \mathbf{B}_b \end{bmatrix} \mathbf{q}^e = \mathbf{B}_p \mathbf{q}^e \quad (10-24)$$

10.3.5 Interpolation Formulas for Electric Potential

Following the layer-wise theory, the electric potential within the k th layer can be expressed as^[3,4]:

$$\phi_k(x, y, z) = \frac{z - h_k}{h_{k-1} - h_k} \phi^{k-1}(x, y) + \frac{z - h_{k-1}}{h_k - h_{k-1}} \phi^k(x, y) \quad (h_{k-1} \leq z \leq h_k) \\ (k = 1, 2, \dots, n) \quad (10-25)$$

where $\phi^k(x, y)$ ($k = 1, 2, \dots, n$) are the electric potential function at the interface between the $(k - 1)$ th and the k th layers. And, within the element, they are defined as follows:

$$\phi^k(x, y) = \sum_{i=1}^4 N_i^0 \phi_i^k \quad (k = 1, 2, \dots, n) \quad (10-26)$$

So the $\phi_k(x, y, z)$ in Eq. (10-25) can be rewritten as

$$\phi_k(x, y, z) = \mathbf{L}_k \mathbf{N}_\phi \mathbf{q}^e \quad (10-27)$$

with

$$\mathbf{L}_k = \left[\mathbf{0}_{1 \times (k-1)} \quad \frac{z-h_k}{h_{k-1}-h_k} \quad \frac{z-h_{k-1}}{h_k-h_{k-1}} \quad \mathbf{0}_{1 \times (n-k)} \right] \quad (10-28)$$

$$\mathbf{N}_\phi = [\mathbf{0}_{(n+1) \times 5} \quad N_1^0 \mathbf{I} \quad \mathbf{0}_{(n+1) \times 5} \quad N_2^0 \mathbf{I} \quad \mathbf{0}_{(n+1) \times 5} \quad N_3^0 \mathbf{I} \quad \mathbf{0}_{(n+1) \times 5} \quad N_4^0 \mathbf{I}] \quad (10-29)$$

$$\mathbf{I} = \begin{bmatrix} 1 & & & & \\ & 1 & & & \\ & & \ddots & & \\ & & & 1 & \\ & & & & 1 \end{bmatrix}_{(n+1) \times (n+1)} \quad (10-30)$$

10.3.6 Electric Field

From Eqs. (10-1) and (10-27), the element electric fields within the k th layer can be obtained:

$$\boldsymbol{\varepsilon}_e^k = \begin{Bmatrix} E_x^e \\ E_y^e \\ E_z^e \end{Bmatrix}^k = - \begin{Bmatrix} \frac{\partial \phi}{\partial x} \\ \frac{\partial \phi}{\partial y} \\ \frac{\partial \phi}{\partial z} \end{Bmatrix}^k = - \begin{pmatrix} \mathbf{L}^k \mathbf{N}_{\phi,x} \\ \mathbf{L}^k \mathbf{N}_{\phi,y} \\ \mathbf{L}^k \mathbf{N}_{\phi,z} \end{pmatrix} \cdot \mathbf{q}^e \quad (10-31)$$

where the subscripts $(, x)$, $(, y)$ and $(, z)$ mean the derivatives with respect to x , y and z , respectively.

10.3.7 The Stiffness Matrix of the Element

The element strain energy is

$$U^e = \frac{1}{2} \int_{V^e} (\sigma_{ij} \varepsilon_{ij} - D_i E_i) dV \quad (10-32)$$

in which σ_{ij} , ε_{ij} , D_i and E_i are the stress tensor, strain tensor, electric-displacement tensor and the electric-field intensity tensor. The discrete form of Eq. (10-32) can be written as:

$$U^e = \frac{1}{2} \mathbf{q}^{eT} (\mathbf{K}_{uu}^e - \mathbf{K}_{u\phi}^e - \mathbf{K}_{\phi u}^e - \mathbf{K}_{\phi\phi}^e) \mathbf{q}^e \quad (10-33)$$

where \mathbf{K}_{uu}^e is the mechanical stiffness matrix; $\mathbf{K}_{\phi\phi}^e$ is the electrical stiffness matrix; $\mathbf{K}_{u\phi}^e$ and $\mathbf{K}_{\phi u}^e$ are the mechanical-electrical and electrical-mechanical coupling matrices, respectively. Since all the integrations along the z -direction can be obtained easily, the above matrices may be expressed as follows:

$$\begin{aligned} \mathbf{K}_{uu}^e &= \iint_{A^e} (\mathbf{B}_p^T \mathbf{C}_p \mathbf{B}_p + \mathbf{B}_s^T \mathbf{C}_s \mathbf{B}_s) dA \\ &= \int_{-1}^1 \int_{-1}^1 (\mathbf{B}_p^T \mathbf{C}_p \mathbf{B}_p + \mathbf{B}_s^T \mathbf{C}_s \mathbf{B}_s) |J| d\xi d\eta \end{aligned} \quad (10-34)$$

$$\begin{aligned} \mathbf{K}_{u\phi}^e &= \iint_{A^e} (\mathbf{B}_p^T \mathbf{A}_p + \mathbf{B}_s^T \mathbf{A}_s) dA \\ &= \int_{-1}^1 \int_{-1}^1 (\mathbf{B}_p^T \mathbf{A}_p + \mathbf{B}_s^T \mathbf{A}_s) |J| d\xi d\eta \end{aligned} \quad (10-35)$$

$$\mathbf{K}_{\phi u}^e = \iint_{A^e} (\mathbf{A}_p^T \mathbf{B}_p + \mathbf{A}_s^T \mathbf{B}_s) dA = (\mathbf{K}_{u\phi}^e)^T \quad (10-36)$$

$$\begin{aligned} \mathbf{K}_{\phi\phi}^e &= \iint_{A^e} (N_{\phi,x}^T \boldsymbol{\Theta}_{11} N_{\phi,x} + 2N_{\phi,y}^T \boldsymbol{\Theta}_{12} N_{\phi,x} \\ &\quad + N_{\phi,y}^T \boldsymbol{\Theta}_{22} N_{\phi,y} + N_{\phi}^T \boldsymbol{\Theta}'_{33} N_{\phi}) dA \\ &= \int_{-1}^1 \int_{-1}^1 (N_{\phi,x}^T \boldsymbol{\Theta}_{11} N_{\phi,x} + 2N_{\phi,y}^T \boldsymbol{\Theta}_{12} N_{\phi,x} \\ &\quad + N_{\phi,y}^T \boldsymbol{\Theta}_{22} N_{\phi,y} + N_{\phi}^T \boldsymbol{\Theta}'_{33} N_{\phi}) |J| d\xi d\eta \end{aligned} \quad (10-37)$$

where $|J|$ is the Jacobian determinant; and

$$\mathbf{A}_p = \begin{bmatrix} \mathbf{A}_N \\ \mathbf{A}_M \end{bmatrix} \quad (10-38)$$

$$\mathbf{A}_N = -\sum_{k=1}^n \int_{h_{k-1}}^{h_k} \bar{\mathbf{e}}_z^k L_{,z}^k N_{\phi} dz = \sum_{k=1}^n (\bar{\mathbf{e}}_z^k \mathbf{I}_1^k N_{\phi}) \quad (10-39)$$

$$\mathbf{A}_M = -\sum_{k=1}^n \int_{h_{k-1}}^{h_k} z \bar{\mathbf{e}}_z^k L_{,z}^k N_{\phi} dz = \sum_{k=1}^n \left(\frac{h_{k-1} + h_k}{2} \bar{\mathbf{e}}_z^k \mathbf{I}_1^k N_{\phi} \right) \quad (10-40)$$

$$\mathbf{I}_1^k = [\mathbf{0}_{1 \times (k-1)} \quad 1 \quad -1 \quad \mathbf{0}_{1 \times (n-k)}] \quad (10-41)$$

$$\mathbf{A}_s = -\sum_{k=1}^n \int_{h_{k-1}}^{h_k} \bar{\mathbf{e}}_{xy}^k \begin{bmatrix} \mathbf{L}^k \mathbf{N}_{\phi,x} \\ \mathbf{L}^k \mathbf{N}_{\phi,y} \end{bmatrix} dz = \sum_{k=1}^n \bar{\mathbf{e}}_{xy}^k \begin{bmatrix} \mathbf{I}_2^k \mathbf{N}_{\phi,x} \\ \mathbf{I}_2^k \mathbf{N}_{\phi,y} \end{bmatrix} \quad (10-42)$$

$$\mathbf{I}_2^k = \begin{bmatrix} \mathbf{0}_{1 \times (k-1)} & \frac{h_{k-1} - h_k}{2} & \frac{h_{k-1} - h_k}{2} & \mathbf{0}_{1 \times (n-k)} \end{bmatrix} \quad (10-43)$$

$$\boldsymbol{\Phi}_{ij} = \sum_{k=1}^n \bar{\mathbf{e}}_{ij}^k \int_{h_{k-1}}^{h_k} \mathbf{L}^{kT} \mathbf{L}^k dz = \sum_{k=1}^n \bar{\mathbf{e}}_{ij}^k \begin{bmatrix} 0 & \dots & 0 & 0 & \dots & 0 \\ \vdots & \ddots & & & & \vdots \\ 0 & \frac{h_k - h_{k-1}}{3} & \frac{h_k - h_{k-1}}{6} & & & 0 \\ 0 & \frac{h_k - h_{k-1}}{6} & \frac{h_k - h_{k-1}}{3} & & & 0 \\ \vdots & \ddots & & & \ddots & \vdots \\ 0 & \dots & 0 & 0 & \dots & 0 \end{bmatrix} \quad (i, j = 1, 2) \quad (10-44)$$

$$\boldsymbol{\Phi}'_{33} = \sum_{k=1}^n \bar{\mathbf{e}}_{33}^k \int_{h_{k-1}}^{h_k} \mathbf{L}_{,z}^{kT} \mathbf{L}_{,z}^k dz = \sum_{k=1}^n \bar{\mathbf{e}}_{33}^k \begin{bmatrix} 0 & \dots & 0 & 0 & \dots & 0 \\ \vdots & \ddots & & & & \vdots \\ 0 & \frac{1}{h_k - h_{k-1}} & -\frac{1}{h_k - h_{k-1}} & & & 0 \\ 0 & -\frac{1}{h_k - h_{k-1}} & \frac{1}{h_k - h_{k-1}} & & & 0 \\ \vdots & \ddots & & & \ddots & \vdots \\ 0 & \dots & 0 & 0 & \dots & 0 \end{bmatrix} \quad (10-45)$$

A 2×2 integration scheme can still be used to evaluate the element stiffness matrix. This element is denoted as CTMQE.

10.4 The “Partial Hybrid”-Enhanced Post-Processing Procedure for Element Stresses

This chapter still employs the hybrid-enhanced post-processing procedure to evaluate the element stresses. But, if a full hybrid procedure is used, we must assume not only the stress field, but also the electric displacement field. Since the stress solutions are more important, a “Partial Hybrid”-enhanced post-processing procedure is proposed in this section, in which only the stress field is assumed while the electric displacement field is still evaluated by the piezoelectric

constitutive equation. Thus, more accurate stress solutions can be obtained by a relatively simple procedure.

10.4.1 The Bending Moment, Shear Force and In-Plane Membrane Force Fields

The formulas of the element bending moment, shear force and in-plane membrane force fields are the same as Eq. (9-84) to Eq. (9-95).

10.4.2 The Condensation Procedure of the “Partial Hybrid”-Enhanced Post-Processing Procedure

By employing the Hellinger-Reissner variational principle, the full hybrid energy functional of the piezoelectric laminated composite plate element can be expressed as reference [13]:

$$\begin{aligned}
 \Pi_R^e = & -\frac{1}{2} \iint_{A^e} (\boldsymbol{\sigma}_p^T \mathbf{S}_p \boldsymbol{\sigma}_p + \mathbf{Q}^T \mathbf{S}_s \mathbf{Q}) dA + \iint_{A^e} (\boldsymbol{\sigma}_p^T \boldsymbol{\varepsilon}_p + \mathbf{Q}^T \boldsymbol{\gamma}) dA \\
 & - \iint_{A^e} (\boldsymbol{\sigma}_p^T \mathbf{S}_p \boldsymbol{\sigma}_e + \mathbf{Q}^T \mathbf{S}_s \mathbf{Q}_e) dA \\
 & + \frac{1}{2} \iiint_{V^e} (\mathbf{D}_{xy}^k{}^T \bar{\boldsymbol{\varepsilon}}_{xy}^{k-1} \mathbf{D}_{xy}^k + \frac{1}{\bar{\varepsilon}_{33}^k} D_z^k D_z^k) dV \\
 & - \iiint_{V^e} (\mathbf{D}_{xy}^k{}^T \mathbf{E}_{xy} + D_z^k E_z) dV - W_{\text{exp}}
 \end{aligned} \tag{10-46}$$

where \mathbf{S}_p and \mathbf{S}_s are given in Eqs. (9-24) and (9-25).

For simplicity, only the mechanical stresses ($\boldsymbol{\sigma}_p$ and \mathbf{Q}), mechanical strains ($\boldsymbol{\varepsilon}_p$ and $\boldsymbol{\gamma}$) and electrical fields (\mathbf{E}_{xy} and E_z^e) are taken as independent variables here. The electrical displacements (\mathbf{D}_{xyk} and D_{zk}) are still obtained by the piezoelectric constitutive relationship, i.e. Eqs. (10-10) and (10-11). Thus, the modified “partial hybrid” energy functional can be established:

$$\begin{aligned}
 \Pi_{mR}^e = & -\frac{1}{2} \iint_{A^e} (\boldsymbol{\sigma}_p^T \mathbf{S}_p \boldsymbol{\sigma}_p + \mathbf{Q}^T \mathbf{S}_s \mathbf{Q}) dA + \iint_{A^e} (\boldsymbol{\sigma}_p^T \boldsymbol{\varepsilon}_p + \mathbf{Q}^T \boldsymbol{\gamma}) dA \\
 & - \iint_{A^e} (\boldsymbol{\sigma}_p^T \mathbf{S}_p \boldsymbol{\sigma}_e + \mathbf{Q}^T \mathbf{S}_s \mathbf{Q}_e) dA - \frac{1}{2} \mathbf{q}^{eT} \mathbf{K}_{\phi\phi} \mathbf{q}^e - W_{\text{exp}} \\
 = & -\frac{1}{2} \boldsymbol{\lambda}_{NM}^T \iint_{A^e} (\mathbf{P}_{NM}^T \mathbf{S}_p \mathbf{P}_{NM} + \mathbf{P}_{NQ}^T \mathbf{S}_s \mathbf{P}_{NQ}) dA \cdot \boldsymbol{\lambda}_{NM}
 \end{aligned}$$

$$\begin{aligned}
 & + \lambda_{NM}^T \iint_{A^e} (\mathbf{P}_{NM}^T \mathbf{B}_p + \mathbf{P}_{NQ}^T \mathbf{B}_s - \mathbf{P}_{NM}^T \mathbf{A}_p - \mathbf{P}_{NQ}^T \mathbf{A}_s) dA \cdot \mathbf{q}^e \\
 & - \frac{1}{2} \mathbf{q}^{eT} \mathbf{K}_{\phi\phi} \mathbf{q}^e - W_{\text{exp}}
 \end{aligned} \tag{10-47}$$

From the stationary condition $\frac{\partial \Pi_R^e}{\partial \lambda_{NM}} = \mathbf{0}$, we have

$$\lambda_{NM} = -\mathbf{K}_{\lambda\lambda}^{-1} \mathbf{K}_{\lambda q} \mathbf{q}^e \tag{10-48}$$

where

$$\left. \begin{aligned}
 \mathbf{K}_{\lambda\lambda} &= \iint_{A^e} (\mathbf{P}_{NM}^T \mathbf{S}_p \mathbf{P}_{NM} + \mathbf{P}_{NQ}^T \mathbf{S}_s \mathbf{P}_{NQ}) dA \\
 \mathbf{K}_{\lambda q} &= \iint_{A^e} (\mathbf{P}_{NM}^T \mathbf{B}_p + \mathbf{P}_{NQ}^T \mathbf{B}_s - \mathbf{P}_{NM}^T \mathbf{A}_p - \mathbf{P}_{NQ}^T \mathbf{A}_s) dA
 \end{aligned} \right\} \tag{10-49}$$

Substituting Eq. (10-48) into Eqs. (9-94) and (9-95), N , \mathbf{M} and \mathbf{Q} can be obtained.

10.4.3 The In-Plane Stresses for the k th Layer

Substitution of Eq. (9-2) into Eq. (10-5) yields:

$$\boldsymbol{\sigma}^k = \bar{\mathbf{Q}}^k (\boldsymbol{\varepsilon}^0 + z\boldsymbol{\kappa}) - E_z^e \bar{\mathbf{e}}_z^k \tag{10-50}$$

Moreover, from Eqs. (10-12a), (9-24) and (9-25), we have

$$\boldsymbol{\varepsilon}_p = \begin{Bmatrix} \boldsymbol{\varepsilon}^0 \\ \boldsymbol{\kappa} \end{Bmatrix} = \mathbf{S}_p (\boldsymbol{\sigma}_p - \boldsymbol{\sigma}_e) = \begin{bmatrix} \mathbf{S}_N \\ \mathbf{S}_M \end{bmatrix} (\boldsymbol{\sigma}_p - \boldsymbol{\sigma}_e) \tag{10-51}$$

where \mathbf{S}_N and \mathbf{S}_M are both 3×6 matrices.

Substitution of Eq. (10-51) into Eq. (10-50) yields:

$$\boldsymbol{\sigma}^k = \bar{\mathbf{Q}}^k (\mathbf{S}_N + z\mathbf{S}_M) (\boldsymbol{\sigma}_p - \boldsymbol{\sigma}_e) - E_z^e \bar{\mathbf{e}}_z^k \tag{10-52}$$

10.4.4 Recovery of the Transverse Shear Stresses

The transverse shear stresses are still evaluated by the homogeneous 3D differential equilibrium Eq. (9-99), then for the k th layer of the plate, we obtain

$$\begin{aligned}
 \tau_z^k &= - \int_{-h/2}^z \partial \sigma^k dz \\
 &= - \int_{-h/2}^z \partial [\bar{\mathbf{Q}}^k (\mathbf{S}_N + z \mathbf{S}_M) (\sigma_p - \sigma_e) - E_z^e \bar{\mathbf{e}}_z^k] dz \\
 &= - \int_{-h/2}^z \{ \bar{\mathbf{B}}\mathbf{I}_1 [\bar{\mathbf{Q}}^k (\mathbf{S}_N + z \mathbf{S}_M) (\sigma_{p,x} - \sigma_{e,x}) - E_{z,x}^e \bar{\mathbf{e}}_z^k] \\
 &\quad + \bar{\mathbf{B}}\mathbf{I}_2 [\bar{\mathbf{Q}}^k (\mathbf{S}_N + z \mathbf{S}_M) (\sigma_{p,y} - \sigma_{e,y}) - E_{z,y}^e \bar{\mathbf{e}}_z^k] \} dz \quad (10-53)
 \end{aligned}$$

where

$$\partial = \begin{bmatrix} \frac{\partial}{\partial x} & 0 & \frac{\partial}{\partial y} \\ 0 & \frac{\partial}{\partial y} & \frac{\partial}{\partial x} \end{bmatrix}, \quad \bar{\mathbf{B}}\mathbf{I}_1 = \begin{bmatrix} 1 & 0 & 0 \\ 0 & 0 & 1 \end{bmatrix}, \quad \bar{\mathbf{B}}\mathbf{I}_2 = \begin{bmatrix} 0 & 0 & 1 \\ 0 & 1 & 0 \end{bmatrix} \quad (10-54)$$

$$\sigma_{p,x} = \mathbf{P}_{NM,x} \mathbf{K}_{\lambda\lambda}^{-1} \mathbf{K}_{\lambda q} \mathbf{q}^e, \quad \sigma_{p,y} = \mathbf{P}_{NM,y} \mathbf{K}_{\lambda\lambda}^{-1} \mathbf{K}_{\lambda q} \mathbf{q}^e \quad (10-55)$$

$$\sigma_{e,x} = \mathbf{A}_{p,x} \mathbf{q}^e = \begin{bmatrix} \sum_{k=1}^n \bar{\mathbf{e}}_z^k \mathbf{I}_1^k N_{\phi,x} \\ \sum_{k=1}^n \frac{h_{k-1} + h_k}{2} \bar{\mathbf{e}}_z^k \mathbf{I}_1^k N_{\phi,x} \end{bmatrix} \mathbf{q}^e \quad (10-56a)$$

$$\sigma_{e,y} = \mathbf{A}_{p,y} \mathbf{q}^e = \begin{bmatrix} \sum_{k=1}^n \bar{\mathbf{e}}_z^k \mathbf{I}_1^k N_{\phi,y} \\ \sum_{k=1}^n \frac{h_{k-1} + h_k}{2} \bar{\mathbf{e}}_z^k \mathbf{I}_1^k N_{\phi,y} \end{bmatrix} \mathbf{q}^e \quad (10-56b)$$

$$E_{z,x}^e = -\mathbf{L}_{,z}^k \mathbf{N}_{\phi,x} \mathbf{q}^e, \quad E_{z,y}^e = -\mathbf{L}_{,z}^k \mathbf{N}_{\phi,y} \mathbf{q}^e \quad (10-57)$$

Finally, we obtain

$$\begin{aligned}
 \tau_z^k &= -\bar{\mathbf{B}}\mathbf{I}_1 \left\{ \bar{\mathbf{Q}}_k [(z - h_{k-1}) \mathbf{S}_N + \frac{1}{2} (z^2 - h_{k-1}^2) \mathbf{S}_M] (\sigma_{p,x} - \sigma_{e,x}) - E_{z,x}^e \bar{\mathbf{e}}_z^k \right\} \\
 &\quad - \bar{\mathbf{B}}\mathbf{I}_2 \left\{ \bar{\mathbf{Q}}_k [(z - h_{k-1}) \mathbf{S}_N + \frac{1}{2} (z^2 - h_{k-1}^2) \mathbf{S}_M] (\sigma_{p,y} - \sigma_{e,y}) - E_{z,y}^e \bar{\mathbf{e}}_z^k \right\} \\
 &\quad - \sum_{i=1}^k \bar{\mathbf{B}}\mathbf{I}_1 \left\{ \bar{\mathbf{Q}}_i [(h_i - h_{i-1}) \mathbf{S}_N + \frac{1}{2} (h_i^2 - h_{i-1}^2) \mathbf{S}_M] (\sigma_{p,x} - \sigma_{e,x}) - E_{z,x}^e \bar{\mathbf{e}}_{zi} \right\} \\
 &\quad - \sum_{i=1}^k \bar{\mathbf{B}}\mathbf{I}_2 \left\{ \bar{\mathbf{Q}}_i [(h_i - h_{i-1}) \mathbf{S}_N + \frac{1}{2} (h_i^2 - h_{i-1}^2) \mathbf{S}_M] (\sigma_{p,y} - \sigma_{e,y}) - E_{z,y}^e \bar{\mathbf{e}}_{zi} \right\} \quad (10-58)
 \end{aligned}$$

10.5 Numerical Examples

The new element CTMQE will degenerate into the CTMQ20 element proposed in Chap. 9 for modeling ordinary composite plates.

Example 10.1 Bimorph Pointer.

This example was proposed by Tzou^[5] to examine the validation of the piezoelectric finite element model. As shown in Fig. 10.3, a cantilever piezoelectric bimorph pointer is made of two piezoelectric layers laminated with opposite polarity. It will bend when a unit electric field is applied in the *z*-direction. The material constants are as follows:

- (1) isotropic material, elastic modulus: $E = 2\text{GPa}$, Poisson’s ratio $\mu = 0.29$;
- (2) $e_{31} = 0.046\text{C/m}^2$; $e_{32} = 0.046\text{C/m}^2$; $\epsilon_{11} = \epsilon_{22} = \epsilon_{33} = 0.1062 \times 10^{-9}\text{F/m}$.

Only 5 elements for CTMQE are used (Refer to Fig. 10.3) to solve this problem. To assess the element accuracy by the beam theory solution, the Poisson’s ratio is also set to zero for mimicking the required plane stress condition. The results with some other solutions are reported in Table 10.1 and Fig. 10.4. It can be seen that the presented element CTMQE exhibits the best performance. Exact solutions for the beam theory by CTMQE can be obtained when the Poisson’s ratio equals zero.

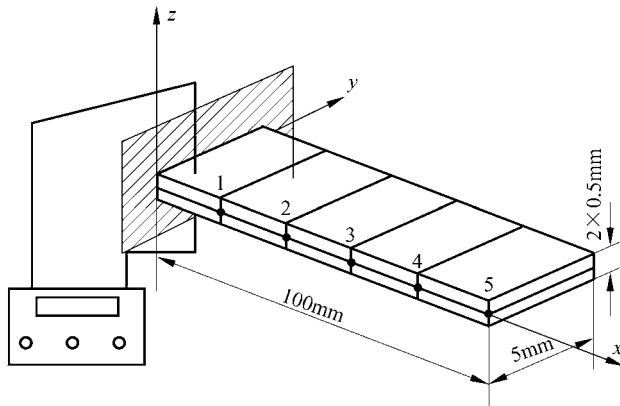


Figure 10.3 The cantilever bimorph pointer problem

Table 10.1 Nodal deflections of the piezoelectric bimorph pointer, μm

Nodes	1	2	3	4	5
Beam theory ^[5]	0.0138	0.0552	0.124	0.221	0.345
Solid FE ^[5]	0.0124	0.0508	0.116	0.210	0.330
Shell FE ^[14]	0.0132	0.0528	0.119	0.211	0.330
QUAD4 ^{[10]①}	0.014	0.055	0.210	0.221	0.345
Experiment ^[5]					0.315
CTMQE ($\mu = 0.29$)	0.0131	0.0538	0.1220	0.2178	0.3412
CTMQE ($\mu = 0.0$)	0.0138	0.0552	0.1242	0.2208	0.3450

① Reference [10] does not give the Poisson’s ratio used.

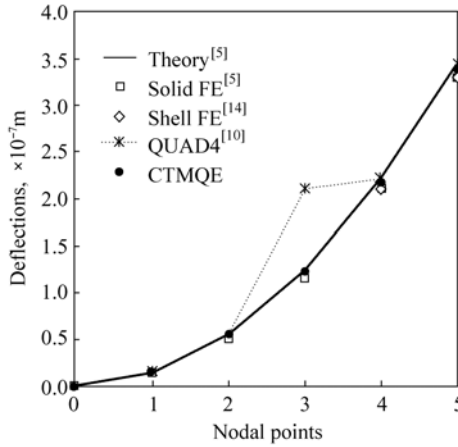


Figure 10.4 Deflections of the bimorph pointer solved by different models

In order to examine the performance of the element CTMQE under distorted meshes, this example is recalculated using the 4 elements shown in Fig. 10.5, where Δ is the distortion parameter and varies from 0 to 25mm. The results with the solutions by the other two brick elements in ABAQUS^[15], C3D8E (8-node linear piezoelectric brick element) and C3D20ER (20-node quadratic piezoelectric brick element with reduced integration), are plotted in Fig. 10.6. It is obvious that the element CTMQE is insensitive to mesh distortion. Exact solution of the tip deflection can also be obtained even when the distortion parameter $\Delta = 25\text{mm}$.

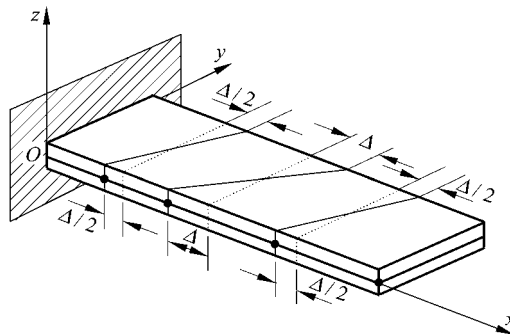


Figure 10.5 Sensitivity test of mesh distortion

Example 10.2 Simply supported square symmetric cross-ply piezoelectric laminated plate with 5 (p/0/90/0/p) layers, p denotes the piezoelectric layer.

Ray et al.^[16] have presented the analytical solutions of the simply supported square composite laminate surface bonded with very thin piezoelectric layers under electrical and/or mechanical loading, which is based on the approach of Pagano^[17].

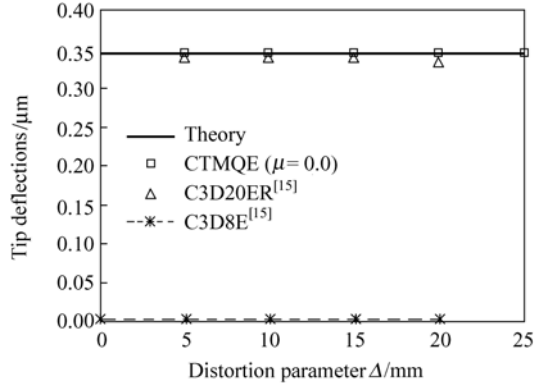


Figure 10.6 Tip deflections due to mesh distortion

A cross-ply laminate (0/90/0) consisting of three identical laminate each of 3mm thickness has been used as the core of the structure. The material properties of the core are as follows:

$$E_1 / E_2 = 25, \quad G_{12} = G_{13} = 0.5E_2, \quad G_{23} = 0.2E_2,$$

$$\mu_{12} = \mu_{13} = \mu_{23} = 0.25, \quad E_2 = 6.9\text{GPa},$$

$$\epsilon_{11} = \epsilon_{22} = \epsilon_{33} = 8.85 \times 10^{-12} \text{F/m}$$

The thickness of each piezoelectric layer bonded on the top and bottom surfaces of the laminate is $40\mu\text{m}$, and they are made of isotropic material with the following material properties:

$$E = 2\text{GPa}, \quad \mu = 0.29, \quad \epsilon_{11} = \epsilon_{22} = \epsilon_{33} = 0.1062 \times 10^{-9} \text{F/m}$$

$$e_{31} = e_{32} = 0.0046 \text{C/m}^2, \quad e_{33} = e_{24} = e_{15} = 0.0$$

According to the method in reference [18], the shear correction factors for this 5-layer plate should be: $k_1^2 = 0.581$, $k_2^2 = 0.802$. Both the mechanical load q and surface potential V acting at the top surface of the plate are doubly sinusoidal (similar to the load in Example 9.1). q_0 and V_0 are the peak values.

The mechanical boundary conditions are the same as those of the Example 9.1 in Chap. 9, and the electrical potential boundary conditions are:

$$\phi = 0 \text{ at } x = 0 \text{ and } L, \quad y = 0 \text{ and } L$$

$$\phi = 0 \text{ at } z = \pm h'/2,$$

$$\phi = V_0 \sin \frac{\pi x}{L} \sin \frac{\pi y}{L} \text{ at } z = h/2$$

where h' and h are the thickness of the elastic core and the whole structure, respectively.

The results are nondimensionalized as:

$$\tilde{w} = \frac{100E_2}{q_0S^4h} w \left(\text{with } S = \frac{L}{h} \right); \quad (\tilde{\sigma}_x, \tilde{\sigma}_y, \tilde{\tau}_{xy}) = \frac{1}{q_0S^2} (\sigma_x, \sigma_y, \tau_{xy});$$

$$(\tilde{\tau}_{xz}, \tilde{\tau}_{yz}) = \frac{1}{q_0S} (\tau_{xz}, \tau_{yz})$$

Table 10.2 Deflection and stresses of ordinary 3-layer (0/90/0) laminated composite plates

L/h	Models	\tilde{w} $\left(\frac{L}{2}, \frac{L}{2}, 0\right)$	$\tilde{\sigma}_x$ $\left(\frac{L}{2}, \frac{L}{2}, \pm \frac{h}{2}\right)$	$\tilde{\sigma}_y$ $\left(\frac{L}{2}, \frac{L}{2}, \pm \frac{h}{6}\right)$	$\tilde{\tau}_{xy}$ $\left(0, 0, \pm \frac{h}{2}\right)$	$\tilde{\tau}_{xz}$ $\left(0, \frac{L}{2}, 0\right)$	$\tilde{\tau}_{yz}$ $\left(\frac{L}{2}, 0, 0\right)$
10	CTMQE 8 × 8	0.764 ^①	0.503 ^①	0.291 ^①	0.0269 ^①	0.372 ^①	0.1376 ^①
		0.670 ^②	0.515 ^②	0.255 ^②	0.0251 ^②	0.379 ^②	0.1227 ^②
	Manjunatha et al. ^[20]	0.669	± 0.521				
	Sheikh et al. ^[4]	0.669 ^②	± 0.517 ^②				
	3D elasticity ^[19]	0.753	± 0.590	0.288/-0.285	∓ 0.0289	0.357	0.1228
100	CTMQE 8×8	0.435 ^①	± 0.540 ^①	± 0.181 ^①	∓ 0.0213 ^①	0.391 ^①	0.0765 ^①
		0.434 ^②	± 0.540 ^②	± 0.181 ^②	∓ 0.0212 ^②	0.390 ^②	0.0763 ^②
	Manjunatha et al. ^[20]	0.434	± 0.544				
	Sheikh et al. ^[4]	0.434 ^②	± 0.542 ^②				
	3D elasticity ^[19]	0.435	± 0.539	± 0.181	∓ 0.0213	0.395	0.0828
	Ray et al. ^[16]	0.470	± 0.539	± 0.181	∓ 0.0214	0.395	0.0828

① Solutions with shear correction factors $k_1^2 = 0.581, k_2^2 = 0.802$.

② Solutions with shear correction factors $k_1^2 = k_2^2 = 5/6$.

Before performing the actual investigation, Ray et al.^[16] studied the performance of their method with the plate without the piezoelectric layer (Example 9.1 or reference^[19]). Table 10.2 lists their results with other solutions by the finite element method. But, as the statement in [4], there is a mistake in the calculation of deflection values, which is shown in Table 10.2. So, their results for the piezoelectric composite plates are not guaranteed.

Table 10.3 shows the results of the whole structure for two load cases: the first one is with $q_0 = 1.0$ and $V_0 = 0.0$ and the second one is with $q_0 = 1.0$ and $V_0 = 100V$. It can be seen that most stress solutions of the CTMQE (8 × 8 mesh for quarter plate) are in agreement with those of Ray et al.^[16]. And, it is worthwhile to mention that the presented 4-node element CTMQE exhibits better performance than the 8-node element proposed by Sheikh et al.^[4], which is based on the same theory and under the same mesh division.

Example 10.3 The distribution of the electrical potential for a simply-supported thick piezoelectric laminated plate with 4 layers (p/0/90/p).

The behaviors of a simply-supported square laminated plate similar to that used in the previous example have been investigated by Heyliger^[21]. But, the major difference is that the electrical potential across the core is not made zero unlike that by Ray et al.^[16]. The plate has an overall thickness h of 1.0m where the core consists of two elastic layers (0/90) each of thickness $0.4h$, and their material constants are as follows:

$$E_1=132.39\text{GPa}, E_2=E_3=10.756\text{GPa}, G_{12}=G_{13}=5.654\text{GPa}, G_{23}=3.606\text{GPa}$$

$$\mu_{12} = \mu_{13} = 0.24, \quad \mu_{23} = 0.49$$

$$\epsilon_{11} / \epsilon_0 = 3.5, \quad \epsilon_{22} / \epsilon_0 = \epsilon_{33} / \epsilon_0 = 3, \quad \epsilon_0 = 8.85 \times 10^{-12} \text{ F/m}$$

Table 10.3 Deflection and stresses of smart laminated composite plates

L/h	Models	\tilde{w} $\left(\frac{L}{2}, \frac{L}{2}, 0\right)$	$\tilde{\sigma}_x$ $\left(\frac{L}{2}, \frac{L}{2}, \pm \frac{h}{2}\right)$	$\tilde{\sigma}_y$ $\left(\frac{L}{2}, \frac{L}{2}, \pm \frac{h}{6}\right)$	$\tilde{\tau}_{xy}$ $\left(0, 0, \pm \frac{h}{2}\right)$	$\tilde{\tau}_{xz}$ $\left(0, \frac{L}{2}, 0\right)$	$\tilde{\tau}_{yz}$ $\left(\frac{L}{2}, 0, 0\right)$
$q_0 = 1.0, V_0 = 0.0$							
10	CTMQE 8×8	0.764 ^①	± 0.502 ^①	± 0.290 ^①	∓ 0.0269 ^①	0.371 ^①	0.137 ^①
	Sheikh et al. ^[4]	0.669 ^②	± 0.514 ^②	± 0.255 ^②	∓ 0.0250 ^②	0.378 ^②	0.122 ^②
	Ray et al. ^[16]	0.668 ^②	± 0.520 ^②				
20	CTMQE 8×8	0.517 ^①	± 0.529 ^①	± 0.211 ^①	∓ 0.0228 ^①	0.386 ^①	0.100 ^①
	Sheikh et al. ^[4]	0.492 ^②	± 0.533 ^②	± 0.201 ^②	∓ 0.0222 ^②	0.388 ^②	0.097 ^②
	Ray et al. ^[16]	0.549	± 0.552	± 0.209	∓ 0.023	0.384	0.094
100	CTMQE 8×8	0.434 ^①	± 0.539 ^①	± 0.181 ^①	∓ 0.0212 ^①	0.390 ^①	0.076 ^①
	Sheikh et al. ^[4]	0.433 ^②	± 0.540 ^②	± 0.181 ^②	∓ 0.0212 ^②	0.390 ^②	0.076 ^②
	Ray et al. ^[16]	0.471	± 0.538	± 0.181	∓ 0.021	0.394	0.083
$q_0 = 1.0, V_0 = 100.0V$							
10	CTMQE 8×8	-2.00 ^①	-2.73/1.35 ^①	-2.45/-0.146 ^①	0.149/-0.072 ^①	-0.710 ^①	0.450 ^①
	Sheikh et al. ^[4]	-1.91 ^②	-2.75/1.37 ^②	-2.40/-0.194 ^②	0.146/-0.069 ^②	-0.720 ^②	0.470 ^②
	Ray et al. ^[16]	-1.91 ^②	-2.78/1.39 ^②				
20	CTMQE 8×8	-0.068 ^①	-0.312/-0.032 ^①	-0.377/-0.273 ^①	0.016/0.003 ^①	0.097 ^①	0.207 ^①
	Sheikh et al. ^[4]	-0.080 ^②	-0.311/-0.034 ^②	-0.381/-0.269 ^②	0.016/0.003 ^②	0.098 ^②	0.204 ^②
	Ray et al. ^[16]	-0.095	-0.321/-0.039	-0.372/-0.277	0.017/0.005	0.096	0.145
100	CTMQE 8×8	0.412 ^①	0.505/-0.519 ^①	0.159/-0.185 ^①	-0.0198/0.0206 ^①	0.378 ^①	0.080 ^①
	Sheikh et al. ^[4]	0.411 ^②	0.505/-0.519 ^②	0.159/-0.185 ^②	-0.0198/0.0205 ^②	0.378 ^②	0.080 ^②
	Ray et al. ^[16]	0.411 ^②	0.510/-0.514 ^②				
		0.447	0.504/-0.518	0.158/-0.184	-0.019/0.021	0.382	0.086

① Solutions with shear correction factors $k_1^2 = 0.581, k_2^2 = 0.802$.

② Solutions with shear correction factors $k_1^2 = k_2^2 = 5/6$.

The piezoelectric layers with thickness $0.1h$ each are bonded to the top and bottom surface of the core, and their material constants are as follows:

$$E_1 = E_2 = 81.3\text{GPa}, \quad E_3 = 64.5\text{GPa}, \quad G_{12} = 30.6\text{GPa}, \quad G_{13} = G_{23} = 25.6\text{GPa}$$

$$\mu_{12} = 0.329, \quad \mu_{13} = \mu_{23} = 0.432$$

$$\epsilon_{11} / \epsilon_0 = \epsilon_{22} / \epsilon_0 = 1475, \quad \epsilon_{33} / \epsilon_0 = 1300, \quad \epsilon_0 = 8.85 \times 10^{-12} \text{F/m}$$

$$e_{31} = e_{32} = -5.20\text{C/m}^2, \quad e_{33} = 15.08\text{C/m}^2, \quad e_{24} = e_{15} = 12.72\text{C/m}^2$$

However, it is too thick as the thickness ratio of the plate is 0.25. So, it is not expected that the proposed model, which is based on FSDT, perform well under mechanical loading. But, on the other hand, a very good agreement between the results from CTMQE and Heyliger^[21] can be obtained for the through-thickness variation of the potential under the electrical loading. This validates the electrical component of the present formulation.

From Table 10.4, it can be seen that both CTMQE and the 8-node element model proposed by Sheikh et al.^[4] can all give the excellent solutions of the electrical potential in the thickness direction. But, the active DOFs of the CTMQE are much less than those of Sheikh et al.^[4].

Table 10.4 The distribution of the electrical potential in thickness direction at the plate center

$z(\text{m})$	CTMQE $4 \times 4 \times 4$	CTMQE $4 \times 4 \times 12$ ^①	Sheikh et al. $4 \times 4 \times 12$ ^{①[4]}	Heyliger ^[21]
0.5	1.0000	1.0000	1.0000	1.0000
0.45	0.9959 ^②	0.9939	0.9951	0.9950
0.4	0.9918	0.9918	0.9935	0.9929
0.2	0.7185 ^②	0.6997	0.7018	0.7014
0.0	0.4452	0.4461	0.4477	0.4476
-0.2	0.2221 ^②	0.2167	0.2178	0.2179
-0.4	-0.0009	-0.0009	-0.0005	-0.0010
-0.45	-0.0005 ^②	-0.0007	-0.0005	-0.0008
-0.5	0.0000	0.0000	0.0000	0.0000

① Each of the elastic layers and the piezoelectric layers are divided into four and two sub-layers, respectively.

② Obtained by linear interpolation.

References

- [1] Benjeddou A (2000) Advances in piezoelectric finite element modeling of adaptive structural elements: a survey. *Computers & Structures* 76: 347 – 363
- [2] Sze KY, Yao LQ, Yi S (2000) A hybrid stress ANS solid-shell element and its generalization for smart structure modeling. Part II-smart structure modeling. *International Journal for Numerical Methods in Engineering* 48: 565 – 582

Advanced Finite Element Method in Structural Engineering

- [3] Chee C, Tong L, Steven G (2000) A mixed model for adaptive composite plates with piezoelectric for anisotropic actuation. *Computers & Structures* 77: 253 – 268
- [4] Sheikh AH, Topdar P, Halder S (2001) An appropriate FE model for through-thickness variation of displacement and potential in thin/moderately thick smart laminates. *Composite Structures* 51: 401 – 409
- [5] Tzou HS (1993) *Piezoelectric Shells: Distributed Sensing and Control of Continua*. Netherlands: Kluwer Academic Publishers
- [6] Ha SK, Keilers C, Chang FK (1992) Finite element analysis of composite structures containing distributed piezoelectric sensors and actuators. *AIAA Journal* 30(3): 772 – 780
- [7] Reddy JN (1999) On laminated composite plates with integrated sensors and actuators. *Engineering Structures* 21: 568 – 593
- [8] Huang JH, Wu TL (1996) Analysis of hybrid multilayered piezoelectric plates. *International Journal of Engineering Science* 34(2): 171 – 181
- [9] Jonnalagadda KD, Blandford GE, Tauchert TR (1992) Piezothermoelastic composite plate analysis using first-order shear deformation theory. *Computers & Structures* 5(1): 79 – 89
- [10] Detwiler DT, Shen MHH, Venkayya VB (1995) Finite element analysis of laminated composite structures containing distributed piezoelectric actuators and sensors. *Finite Elements in Analysis and Design* 20: 87 – 100
- [11] Suleman A, Venkayya VB (1995) A simple finite element formulation for a laminated composite with piezoelectric layers. *Journal of Intelligent Material Systems and Structures* 6: 776 – 782
- [12] Cen S, Soh AK, Long YQ, Yao ZH (2002) A new 4-node quadrilateral FE model with variable electrical degrees of freedom for the analysis of piezoelectric laminated composite plates. *Composite Structures* 58(4): 583 – 599
- [13] Wu CC, Sze KY, Huang YQ (2001) Numerical solutions on fracture of piezoelectric materials by hybrid element. *International Journal of Solids and Structures* 38: 4315 – 4329
- [14] Tzou HS, Ye R (1996) Analysis of piezoelectric structures with laminated piezoelectric triangle shell element. *AIAA Journal* 34(1):110 – 115
- [15] ABAQUS/Standard User's Manual, Version 5.8 (1998) Hibbit, Karlsson & Sorensen, Inc.: Rawtucket, Rhode Island
- [16] Ray MC, Bhattacharya R, Samanta B (1972) Exact solutions for static analysis of intelligent structures. *AIAA Journal* 31(9): 1684 – 1691
- [17] Pagano NJ, Hatfield SJ (1992) Elastic behavior of multilayered bidirectional composites. *AIAA Journal* 10: 931 – 933
- [18] Vlachoutsis S (1992) Shear correction factors for plates and shells. *International Journal for Numerical Methods in Engineering* 33: 1537 – 1552
- [19] Pagano NJ (1970) Exact solutions for rectangular bidirectional composites and sandwich plates. *Journal of Composite Materials* 4: 20 – 34
- [20] Manjunatha BS, Kant T (1994) A comparison of 9 and 16 noded quadrilateral elements based on higher order laminated theories for estimation of transverse stresses. *Journal of Reinforced Plastics and Composites* 11: 986 – 1002
- [21] Heyliger P (1994) Static behavior of laminated elastic/piezoelectric plates. *AIAA Journal* 32(12): 2481 – 2484

Chapter 11 Generalized Conforming Membrane and Shell Elements

Zhi-Fei Long

School of Mechanics & Civil Engineering, China University of
Mining & Technology, Beijing, 100083, China

Song Cen

Department of Engineering Mechanics, School of Aerospace,
Tsinghua University, Beijing, 100084, China

Abstract Besides the various plate problems discussed in the previous chapters, the idea of the generalized conforming element has already been successfully generalized to many other areas. As the final chapter of Part II, this chapter mainly introduces some research achievements on the applications of the generalized conforming element method for isoparametric membrane element (Sect. 11.2), membrane element with drilling freedoms (Sects. 11.3 and 11.4), flat-shell element (Sect. 11.5), curved shell element (Sects. 11.6 and 11.7) and shell element for geometrically nonlinear analysis (Sects. 11.8 and 11.9). Thus, the universal significance of the generalized conforming theory can be clearly illustrated.

Keywords finite element, generalized conforming, membrane element, shell element.

11.1 Introduction

The generalized conforming element method was originally proposed for solving the difficulty of C^1 -continuity required by thin plate elements. It opens a new way between the conforming and non-conforming elements: on the one hand, the shortcomings that sometimes the conforming elements are over-stiff and even difficult to be constructed are overcome; on the other hand, the major weakness that the non-conforming elements may not be convergent is also eliminated. As described in Chap. 5 to Chap. 7, first it obtains success in the construction of thin plate elements, and various high-performance thin plate element models of different types are then successfully constructed.

At the same time, the idea of the generalized conforming element has also been successfully generalized to many other areas: besides the applications of thick plate in Chap. 8, laminated composite plate in Chap. 9 and piezoelectric laminated composite plate in Chap. 10, generalized conforming isoparametric membrane elements are proposed in reference [1], generalized conforming membrane elements with drilling freedoms are proposed in references [2,3], generalized conforming flat-shell elements are proposed in references [4–9], generalized conforming curved shallow shell elements are proposed in references [10,11], and generalized conforming plate and shell elements for geometrically nonlinear analysis are also proposed in [9–12].

This chapter will mainly introduce some research achievements on the applications of the generalized conforming element method for isoparametric membrane element, membrane element with drilling freedoms, flat-shell element, curved shell element and shell element for geometrically nonlinear analysis. Thus, the universal significance of the generalized conforming theory can be exhibited.

11.2 Generalized Conforming Isoparametric Membrane Element

This section will introduce the construction mode of the generalized conforming isoparametric element GC-Q6^[1].

For the plane 4-node isoparametric element Q4 (Fig. 11.1), its nodal DOFs are defined as:

$$\mathbf{q}^e = [u_1 \quad v_1 \quad u_2 \quad v_2 \quad u_3 \quad v_3 \quad u_4 \quad v_4]^T \tag{11-1}$$

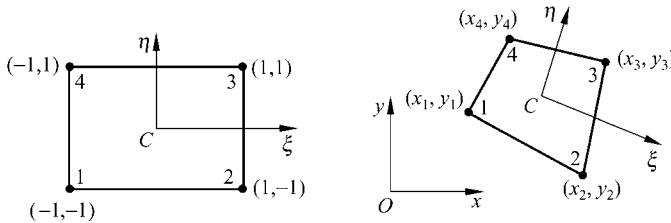


Figure 11.1 4-node quadrilateral plane isoparametric element

The interpolation functions for displacements u and v are given by

$$u = \sum_{i=1}^4 N_i u_i, \quad v = \sum_{i=1}^4 N_i v_i \tag{11-2}$$

where u_i and v_i ($i = 1,2,3,4$) are the nodal displacements; N_i the shape functions

which are bilinear functions of the natural coordinates ξ, η

$$N_i = \frac{1}{4}(1 + \xi_i \xi)(1 + \eta_i \eta) \quad (i = 1, 2, 3, 4) \quad (11-3)$$

Element Q4 is very popular. However, for bending problems it gives results with low accuracy.

In order to improve the bending behavior of the element Q4, Wilson et al.^[13] propose a non-conforming element in which the displacements are split into compatible and incompatible parts:

$$\mathbf{u} = \mathbf{u}_q + \mathbf{u}_\lambda \quad (11-4)$$

where $\mathbf{u}_q = [u \quad v]^T$ are the compatible displacements and given by Eqs. (11-2) and (11-3); and \mathbf{u}_λ are the incompatible displacements given by

$$\mathbf{u}_\lambda = \begin{Bmatrix} u_\lambda \\ v_\lambda \end{Bmatrix} = \begin{bmatrix} 1 - \xi^2 & 1 - \eta^2 & 0 & 0 \\ 0 & 0 & 1 - \xi^2 & 1 - \eta^2 \end{bmatrix} \begin{Bmatrix} \lambda_1 \\ \lambda_2 \\ \lambda_3 \\ \lambda_4 \end{Bmatrix} \quad (11-5)$$

where λ_i ($i = 1, 2, 3, 4$) are 4 internal displacement parameters. This element is denoted as Q6. Some excellent numerical results are obtained by the element Q6, however, it cannot pass the patch test for irregular mesh.

In this section, according to the basic idea of the generalized conforming element, the generalized conforming isoparametric element GC-Q6 is obtained based on the generalized conforming conditions under constant and linear stress fields. Here, the generalized conforming conditions under constant stresses are used to ensure convergence, and the generalized conforming conditions under linear stresses are used to improve computational accuracy.

11.2.1 Generalized Conforming Conditions under Constant and Linear Stress Fields

For the conforming element, the element displacement fields \mathbf{u} must satisfy the conforming conditions along the element boundary ∂A^e

$$\mathbf{u} - \tilde{\mathbf{u}} = \mathbf{0} \quad (\text{on } \partial A^e) \quad (11-6)$$

where $\tilde{\mathbf{u}}$ denote the boundary displacement of the element.

For the generalized conforming element, the conforming condition (11-6) are relaxed and replaced by the following generalized conforming conditions in the limit of mesh refinement (the stresses and strains of each element tends to be constant):

$$\oint_{\partial A^e} \mathbf{T}_c^T (\mathbf{u} - \tilde{\mathbf{u}}) ds = 0 \quad (11-7)$$

where \mathbf{T}_c denotes the boundary tractions of the constant stress field.

In reference [14], during the derivation of the generalized conforming element, the following conforming conditions of the average displacement along each element side S_i are used:

$$\int_{S_i} (\mathbf{u} - \tilde{\mathbf{u}}) ds = \mathbf{0} \quad (11-8)$$

Obviously, the condition (11-8) are the strong forms of the condition (11-7).

In reference [1], a new kind of generalized conforming element is established by using another strong form of the condition (11-7), i.e.,

$$\oint_{\partial A^e} \mathbf{T}^T (\mathbf{u} - \tilde{\mathbf{u}}) ds = 0 \quad (11-9)$$

where \mathbf{T} denotes the boundary tractions under both the constant and linear stress fields. Substituting Eq. (11-4) into Eq. (11-9), and applying the following condition satisfied by the conforming displacement \mathbf{u}_q :

$$\mathbf{u}_q - \tilde{\mathbf{u}} = \mathbf{0} \quad (\text{on } \partial A^e) \quad (11-10)$$

we have

$$\oint_{\partial A^e} \mathbf{T}^T \mathbf{u}_\lambda ds = 0 \quad (11-11)$$

Considering the following linear stress state:

$$\sigma_x = \beta_1 + \beta_4 \eta, \quad \sigma_y = \beta_2 + \beta_5 \xi, \quad \tau_{xy} = \beta_3 \quad (11-12)$$

we obtain

$$T_x = l\beta_1 + m\beta_3 + l\eta\beta_4, \quad T_y = m\beta_2 + l\beta_3 + m\xi\beta_5 \quad (11-13)$$

where l and m are the directional cosines of the outward normal to the boundary.

Substitution of Eq. (11-13) into Eq. (11-11) yields

$$\oint_{\partial A^e} [\beta_1 l u_\lambda + \beta_2 m v_\lambda + \beta_3 (m u_\lambda + l v_\lambda) + \beta_4 l \eta u_\lambda + \beta_5 m \xi v_\lambda] ds = 0 \quad (11-14)$$

Since the 5 parameters β_i are independent to each other, 5 conditions can be obtained as follows:

$$\left. \begin{aligned} \oint_{\partial A^e} l u_\lambda ds = 0, \quad \oint_{\partial A^e} m v_\lambda ds = 0 \\ \oint_{\partial A^e} (m u_\lambda + l v_\lambda) ds = 0 \\ \oint_{\partial A^e} l \eta u_\lambda ds = 0, \quad \oint_{\partial A^e} m \xi v_\lambda ds = 0 \end{aligned} \right\} \quad (11-15)$$

The conditions given by Eq. (11-15) are the generalized conforming conditions under constant and linear stress fields.

11.2.2 Determination of the Generalized Conforming Displacements u_λ

Firstly, the generalized conforming displacements u_λ and v_λ are expressed in a complete quadratic polynomial form:

$$\left. \begin{aligned} u_\lambda &= \lambda_1 + \lambda_2\xi + \lambda_3\eta + \lambda_4\xi^2 + \lambda_5\xi\eta + \lambda_6\eta^2 \\ v_\lambda &= \lambda'_1 + \lambda'_2\xi + \lambda'_3\eta + \lambda'_4\xi^2 + \lambda'_5\xi\eta + \lambda'_6\eta^2 \end{aligned} \right\} \quad (11-16)$$

From this equation, the displacements u_C , v_C and rotation ω_C at the centroid C ($\xi=0, \eta=0$) of the element can be obtained as follows:

$$u_C = \lambda_1, \quad v_C = \lambda'_1, \quad \omega_C = \frac{1}{2|J|_C}(a_3\lambda_2 - a_1\lambda_3 + b_3\lambda'_2 - b_1\lambda'_3) \quad (11-17)$$

where the following notations are used:

$$\left. \begin{aligned} a_1 &= \frac{1}{4}(-x_1 + x_2 + x_3 - x_4), \quad a_2 = \frac{1}{4}(x_1 - x_2 + x_3 - x_4) \\ a_3 &= \frac{1}{4}(-x_1 - x_2 + x_3 + x_4) \\ b_1 &= \frac{1}{4}(-y_1 + y_2 + y_3 - y_4), \quad b_2 = \frac{1}{4}(y_1 - y_2 + y_3 - y_4) \\ b_3 &= \frac{1}{4}(-y_1 - y_2 + y_3 + y_4) \\ |J|_C &= a_1b_3 - a_3b_1 \neq 0 \end{aligned} \right\} \quad (11-18)$$

Secondly, substitution of Eq. (11-16) into the generalized conforming condition (11-15) yields

$$\left. \begin{aligned} 3b_3\lambda_2 - 3b_1\lambda_3 + 2b_2(\lambda_4 - \lambda_6) &= 0 \\ 3a_3\lambda'_2 - 3a_1\lambda'_3 + 2a_2(\lambda'_4 - \lambda'_6) &= 0 \\ [3a_3\lambda_2 - 3a_1\lambda_3 + 2a_2(\lambda_4 - \lambda_6)] + [3b_3\lambda'_2 - 3b_1\lambda'_3 + 2b_2(\lambda'_4 - \lambda'_6)] &= 0 \\ 3b_1\lambda_1 + 2b_2\lambda_3 + b_1\lambda_4 - b_3\lambda_5 + 3b_1\lambda_6 &= 0 \\ 3a_3\lambda'_1 + 2a_2\lambda'_2 + 3a_3\lambda'_4 - a_1\lambda'_5 + a_3\lambda'_6 &= 0 \end{aligned} \right\} \quad (11-19)$$

From Eqs. (11-19) and (11-17), 8 parameters $\lambda_1, \lambda_2, \lambda_3, \lambda_5, \lambda'_1, \lambda'_2, \lambda'_3$ and λ'_5 can be expressed in terms of another 4 independent parameters $\lambda_4, \lambda_6, \lambda'_4, \lambda'_6$

and three centroid displacements u_C, v_C, ω_C .

Finally, if we let

$$u_C = -\lambda_4 - \lambda_6, \quad v_C = -\lambda'_4 - \lambda'_6, \quad \omega_C = 0 \quad (11-20)$$

then from Eq. (11-16) we obtain

$$\begin{Bmatrix} u_\lambda \\ v_\lambda \end{Bmatrix} = \begin{bmatrix} \xi^2 - 1 + F_1 & \eta^2 - 1 + F_2 & F_3 & -F_3 \\ F'_3 & -F'_3 & \xi^2 - 1 + F'_1 & \eta^2 - 1 + F'_2 \end{bmatrix} \begin{Bmatrix} \lambda_4 \\ \lambda_6 \\ \lambda'_4 \\ \lambda'_6 \end{Bmatrix} \quad (11-21)$$

where

$$\left. \begin{aligned} F_1 &= \frac{1}{3|\mathbf{J}|_C} \left\{ -(2a_1b_2 - a_2b_1)\xi - (2a_3b_2 - a_2b_3)\eta \right. \\ &\quad \left. + \left[(3a_1b_1 + 2a_2b_2) - \frac{a_3}{b_3}(3b_1^2 + 4b_2^2) - \frac{b_1}{b_3}|\mathbf{J}|_C \right] \xi\eta \right\} \\ F'_1 &= \frac{1}{3|\mathbf{J}|_C} \left\{ (2a_2b_1 - a_1b_2)\xi + (2a_2b_3 - a_3b_2)\eta \right. \\ &\quad \left. + \left[(9a_3b_3 - 2a_2b_2) + \frac{b_1}{a_1}(4a_2^2 - 9a_3^2) - \frac{a_3}{a_1}|\mathbf{J}|_C \right] \xi\eta \right\} \\ F_2 &= -F_1 - \frac{2b_1}{b_3}\xi\eta, \quad F'_2 = -F'_1 - \frac{2a_3}{a_1}\xi\eta \\ F_3 &= \frac{-1}{3|\mathbf{J}|_C} [b_1b_2\xi + b_2b_3\eta + 2b_2^2\xi\eta] \\ F'_3 &= \frac{1}{3|\mathbf{J}|_C} [a_1a_2\xi + a_2a_3\eta + 2a_2^2\xi\eta] \end{aligned} \right\} \quad (11-22)$$

Equation (11-21), involving 4 internal displacement parameters $\lambda_4, \lambda_6, \lambda'_4$ and λ'_6 , represents the required generalized conforming displacement mode which satisfies the condition (11-15). If the element is a parallelogram, Eq. (11-21) degenerates to Eq. (11-5).

11.2.3 Stiffness Matrix of the Element GC-Q6

As soon as the generalized conforming displacement mode (11-21) is determined, the stiffness matrix may be derived by the conventional procedure.

Substituting Eqs. (11-2) and (11-21) into Eq. (11-4), the element displacement may be written as

$$\mathbf{u} = \mathbf{u}_q + \mathbf{u}_\lambda = N\mathbf{q}^e + N_\lambda \boldsymbol{\lambda} \quad (11-23)$$

Element strain may be expressed as

$$\boldsymbol{\varepsilon} = \mathbf{B}\mathbf{q}^e + \mathbf{B}_\lambda \boldsymbol{\lambda} \quad (11-24)$$

And, the element strain energy is

$$U = \frac{h}{2} \iint_{A^e} \boldsymbol{\varepsilon}^T \mathbf{D} \boldsymbol{\varepsilon} dA = \frac{1}{2} \mathbf{q}^{eT} \mathbf{K}_{qq} \mathbf{q}^e + \frac{1}{2} \boldsymbol{\lambda}^T \mathbf{K}_{\lambda\lambda} \boldsymbol{\lambda} + \boldsymbol{\lambda}^T \mathbf{K}_{\lambda q} \mathbf{q}^e \quad (11-25)$$

in which h is the thickness of the element;

$$\left. \begin{aligned} \mathbf{K}_{qq} &= h \int_{-1}^1 \int_{-1}^1 \mathbf{B}^T \mathbf{D} \mathbf{B} |J| d\xi d\eta \\ \mathbf{K}_{\lambda\lambda} &= h \int_{-1}^1 \int_{-1}^1 \mathbf{B}_\lambda^T \mathbf{D} \mathbf{B}_\lambda |J| d\xi d\eta \\ \mathbf{K}_{\lambda q} &= h \int_{-1}^1 \int_{-1}^1 \mathbf{B}_\lambda^T \mathbf{D} \mathbf{B} |J| d\xi d\eta \end{aligned} \right\} \quad (11-26)$$

where $|J|$ is the determinant of the Jacobian matrix; \mathbf{D} is the matrix of the elasticity coefficients, for the plane stress problem, we have

$$\mathbf{D} = \frac{E}{1-\mu^2} \begin{bmatrix} 1 & \mu & 0 \\ \mu & 1 & 0 \\ 0 & 0 & \frac{1-\mu}{2} \end{bmatrix} \quad (11-27)$$

in which E and μ are the Young's modulus and Poisson's ratio, respectively. For the plane strain problem, the E and μ in the above equation should be replaced by $E/(1-\mu^2)$ and $\mu/(1-\mu)$, respectively.

From $\partial U / \partial \boldsymbol{\lambda} = \mathbf{0}$, we obtain

$$\boldsymbol{\lambda} = -\mathbf{K}_{\lambda\lambda}^{-1} \mathbf{K}_{\lambda q} \mathbf{q}^e \quad (11-28)$$

and finally the element stiffness matrix can be written as

$$\mathbf{K}^e = \mathbf{K}_{qq} - \mathbf{K}_{\lambda q}^T \mathbf{K}_{\lambda\lambda}^{-1} \mathbf{K}_{\lambda q} \quad (11-29)$$

11.2.4 Numerical Examples

Example 11.1 Analysis of a rectangular plate using irregular mesh (Fig. 11.2).

Two load cases are considered: Uniform tension under load 1 (an experiment problem for patch test) and pure bending under load 2. Owing to the symmetry of the plate, only 1/4 of the plate is modelled. Irregular mesh as shown in Fig. 11.2 is used. Computational results are given in Table 11.1. For comparison, the results by the other 6 element models and exact results are also given. From Table 11.1, it can be seen that, except the element Q6, the other models can all pass the patch test.

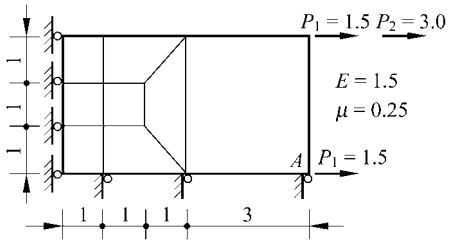


Figure 11.2 A 1/4 rectangular plate subjected to uniform tension and pure bending loads

Table 11.1 Comparison of results for Example 11.1 (7 elements)

Element type	Load 1 (uniform tension)		Load 2 (bending)
	u_A	Patch test	v_A
Q4 (isoparametric)	6.00	pass	- 17.00
Q6 ^[13]	6.70	fail	- 19.66
QM6 ^[15]	6.00	pass	- 17.61
QP6 ^[16]	6.00	pass	- 17.61
NQ6 ^[17]	6.00	pass	- 17.61
QC6 ^[18]	6.00	pass	- 17.61
GC-Q6 (presented)	6.00	pass	- 17.62
Analytical solution	6.00		- 18.00

Example 11.2 Analysis of a cantilever beam using irregular mesh (Fig. 11.3).

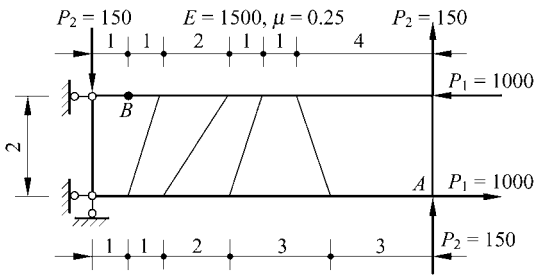


Figure 11.3 A cantilever beam subjected to pure bending and transverse bending loads

Two load cases are considered: pure bending under load 1 and transverse bending under load 2.

From Table 11.2, it can be seen that the accuracy of the isoparametric element Q4 is the worst, but the other 4 elements can provide good accuracy, especially the element QC-Q6 which gives the best answers.

Table 11.2 Comparison of results for Example 11.2 (5 elements)

Element type	Load 1 (pure bending)		Load 2 (transverse bending)	
	v_A	σ_{xB}	v_A	σ_{xB}
Q4 (isoparametric)	45.7	- 1761	50.7	- 2448
Q6 ^[13]	98.4	- 2428	100.4	- 3354
QC6 ^[18]	96.1	- 2439	98.1	- 3339
NQ6 ^[17]	96.1	- 2439	98.0	- 3294
GC-Q6 (presented)	95.0	- 3036 ^①	96.1	- 4182 ^①
Analytical solution	100	- 3000	102.6	- 4050

① Stress at point B is computed by extrapolation from the stresses at the 2×2 Gauss quadrature points.

Example 11.3 Cook’s skew beam problem: analysis of a tapered and swept panel with unit load uniformly distributed along the right edge (Fig. 11.4, mesh by real line).

This example has been discussed in reference [30]. From Table 11.3, it can be seen that the presented element GC-Q6 gives more accurate results than the element HL for coarser meshes.

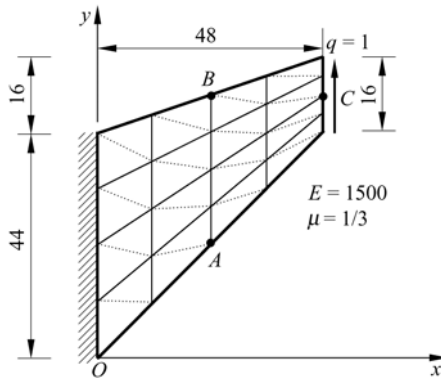


Figure 11.4 Cook’s skew beam problem, mesh 4×4

Table 11.3 Comparison of results for Cook’s skew beam problem (5 elements)

Element	v_C (the vertical displacement at point C)			σ_{Amax} (the maximum stress at point A)			σ_{Bmin} (the minimum stress at point B)		
	2×2	4×4	8×8	2×2	4×4	8×8	2×2	4×4	8×8
Q4	11.80	18.29	22.08	0.1217	0.1873	0.2242	-0.0960	-0.1524	-0.1869
Q6 ^[13]	22.94	23.48		0.2029	0.2258		-0.1734	-0.1915	
QM6 ^[15]	21.05	23.02		0.1928	0.2243		-0.1580	-0.1856	
HL ^[19]	18.17	22.03	23.39	0.1582	0.1980	0.2205	-0.1335	-0.1770	-0.1931
GC-Q6 ^①	27.61	24.31	23.99	0.2538	0.2349	0.2318	-0.1688	-0.1930	-0.1965
Reference ^②	23.96			0.2362			-0.2023		

① Nodal stresses are computed by extrapolation from the stresses at 2×2 Gauss quadrature points and nodal stresses of neighboring element are averaged.

② Results by the element GT9M8^[3] using 64×64 mesh.

11.3 Membrane Elements with Drilling Freedoms— Definition of the Drilling Freedom and the Corresponding Rectangular and Quadrilateral Elements

The introduction of drilling freedom at each node in a plane stress element can improve the order of the element displacement fields, so it can enhance the element performance without increasing the number of the element nodes. And, such drilling freedoms in membrane elements possess special significance for the finite element analysis of shells. The membrane elements with drilling freedoms can be combined with plate bending elements to form flat-shell elements, which contain 3 translational freedoms and 3 rotational freedoms at each node. Thus, when a flat-shell element is used for the analysis of shell structures, the problem that the global stiffness matrix may be singular can be naturally solved. And, the troubles caused by some other treatments^[20,21] for this problem can also be avoided.

11.3.1 Notes on the Definition of Nodal Drilling Freedom θ_z in a Membrane Element

Following are 3 definitions of the drilling freedom θ_z at the node in a membrane element, and comparisons of their advantages and disadvantages are also given.

(1) Definition in the early time—the nodal drilling freedom θ_z in a membrane element is defined as the nodal rigid rotation

In the early definition of the nodal drilling freedom in a membrane element, the rotation of two adjacent sides of the element is assumed to be equal. So, during the whole deformation process of the element under this definition, the angle

between two adjacent sides which meet at the same corner node will indeed keep invariant. The introduction of this improper constraint will make the deformation state of the element quite different from the real situation. And, the triangular membrane element established by this method in [22] cannot be convergent to correct solutions.

(2) The second definition—the nodal drilling freedom θ_z in a membrane element is defined as the nodal rotation ω according to the concept of continuum mechanics

From the displacements u and v of the membrane element, its rotation can be derived by the concept of continuum mechanics as follows:

$$\omega = \frac{1}{2} \left(\frac{\partial v}{\partial x} - \frac{\partial u}{\partial y} \right) \quad (11-30)$$

In many recent literatures, this concept of rotation ω was adopted to define the nodal drilling freedom θ_z of the membrane element as

$$\theta_z = \omega = \frac{1}{2} \left(\frac{\partial v}{\partial x} - \frac{\partial u}{\partial y} \right) \quad (11-31)$$

Now, the properties of the rotation ω are listed as follows.

Property 1 When the axes of the Cartesian coordinate system rotate, ω is an invariant.

Assume that the Cartesian coordinate system xOy will change to another Cartesian coordinate system $x'Oy'$ after it rotates an arbitrary angle. Then, the corresponding rotations of these two coordinate systems are

$$\omega_{xy} = \frac{1}{2} \left(\frac{\partial v}{\partial x} - \frac{\partial u}{\partial y} \right), \quad \omega_{x'y'} = \frac{1}{2} \left(\frac{\partial v'}{\partial x'} - \frac{\partial u'}{\partial y'} \right) \quad (11-32)$$

By using the coordinate transformation (8-22), it can be proved that

$$\omega_{xy} = \omega_{x'y'} \quad (11-33)$$

i.e., ω is an invariant.

That ω is an invariant is just one of the important reasons why it has been selected as the definition of the nodal drilling freedom θ_z .

Property 2 The rotation of the x -axis is $\theta_x = \frac{\partial v}{\partial x}$, and the rotation of the y -axis is $\theta_y = -\frac{\partial u}{\partial y}$. Then, the shear strain γ_{xy} and rotation ω can be expressed in terms of θ_x and θ_y as

$$\gamma_{xy} = \theta_x - \theta_y, \quad \omega = \frac{1}{2}(\theta_x + \theta_y) \quad (11-34)$$

i.e., the shear strain γ_{xy} is the difference value of θ_x and θ_y , and the rotation ω is the average value of θ_x and θ_y .

Property 3 θ_x and θ_y can be expressed in terms of ω and γ_{xy} as follows:

$$\theta_x = \omega + \frac{1}{2}\gamma_{xy}, \quad \theta_y = \omega - \frac{1}{2}\gamma_{xy} \quad (11-35)$$

Similarly, we have

$$\theta_{x'} = \omega + \frac{1}{2}\gamma_{x'y'}, \quad \theta_{y'} = \omega - \frac{1}{2}\gamma_{x'y'} \quad (11-36)$$

Property 4 Under the general strain state in which the strain circle does not degenerate to be a point, when the coordinate axes $x'O'y'$ rotate, $\gamma_{x'y'}$ is a variant, so $\theta_{x'}$ and $\theta_{y'}$ are also variants.

Since $\theta_{x'}$ and $\theta_{y'}$ are variants, it is impossible that they are identically equal to the invariant ω . Only for the special case in which the x' -axis and the y' -axis are the strain principal axes, and then $\gamma_{x'y'} = 0$, ω will be equal to θ_x and θ_y . Thus, we can obtain:

$$(\theta)_{\text{principal axis}} = \omega, \quad (\theta)_{\text{non principal axis}} \neq \omega \quad (11-37)$$

Property 5 Under the special strain state in which the strain circle degenerates to be a point (isotropic spherical stress-strain state), axes along arbitrary directions are all strain principal axes. Therefore, the rotation θ of a line segment in the arbitrary direction will be identically equal to ω , it is an invariant, i.e.,

$$(\theta)_{\text{line segment in arbitrary direction}} = \omega \quad (\text{Under isotropic spherical stress state}) \quad (11-38)$$

From the above properties of rotation ω , it can be seen that the second definition described in this section is inappropriate, either. Its main shortcoming is: in general cases, the nodal rotation ω and the rotation θ of the element side are two different geometric quantities, and there is no definitive relation between them. For instance, from Property 2, it can be seen that ω is the average value of the rotation θ_x of the element side and the rotation θ_y of the side normal, and has no definitive relation with the rotation $\theta_{x'}$ of the element side; and from property 4, it can be seen that, if the element side is not the strain principal axis, the rotation θ of the element side will not be equal to ω .

In order to explain the reason why the second definition is inappropriate, three other examples are given as follows:

Example 1 At common nodes, the values of ω in adjacent elements are generally not equal to each other, thereby, ω is not suitable for being taken as the nodal freedom.

In Fig. 11.5, e and e' represent two adjacent elements, and point 1 is the common

node. Let the common side 12 be the x' -axis, then the rotation at the common node 1 of elements e and e' are

$$\omega^e = \theta_{x'}^e - \frac{1}{2}\gamma_{x'y'}^e, \quad \omega^{e'} = \theta_{x'}^{e'} - \frac{1}{2}\gamma_{x'y'}^{e'} \quad (11-39)$$

where $\theta_{x'}^e$ and $\theta_{x'}^{e'}$ are the rotations along the common side of the two elements at node 1, and should be equal; and $\gamma_{x'y'}^e$ and $\gamma_{x'y'}^{e'}$ are the shear strains of the two elements at node 1, but they are generally not equal. Hence, at common node 1, ω^e and $\omega^{e'}$ are generally not equal, either. So, ω is not suitable for being taken as the nodal freedom.

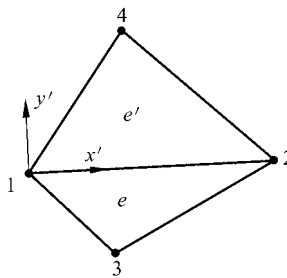


Figure 11.5 Two adjacent elements

Example 2 Assume that the two elements e and e' in Fig. 11.6 are both triangular element CST (Constant Strain Triangle), their strains are constants, and displacements are linear, so the rotations ω^e and $\omega^{e'}$ are also both constants (expressed by constants C_1 and C_2 , respectively), i.e.,

$$\omega_1^e = \omega_2^e = \omega_3^e = C_1, \quad \omega_1^{e'} = \omega_2^{e'} = \omega_4^{e'} = C_2 \quad (11-40)$$

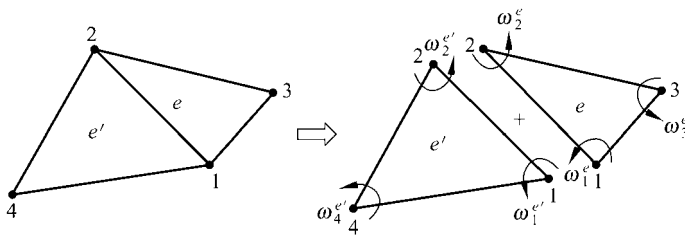


Figure 11.6 Two adjacent CST elements

Since constants C_1 and C_2 are generally not equal, it can also be concluded that ω^e and $\omega^{e'}$ at the common nodes 1 and 2 are generally not equal. So, ω is not suitable for being taken as the nodal freedom.

By the way, for the CST elements, stress σ , strain ε and rotation ω within each element are all constants, but generally different in adjacent elements, and

discontinuity phenomena will happen at two sides of the common side. Thereby, the quantities related to the derivatives of the displacements, such as σ , ε , ω , and so on, are not suitable for being selected as the nodal freedoms.

Example 3 Along a fixed edge where the displacements are specified as zero, the boundary conditions of the translational displacements u and v can be expressed as follows:

$$u = 0, \quad v = 0 \quad (\text{at the nodes on the fixed edge}) \quad (11-41)$$

But, the rotation ω on the fixed edge generally cannot be expressed by

$$\omega = 0 \quad (\text{at the nodes on the fixed edge}) \quad (11-42)$$

Therefore, ω is not suitable for being selected as the nodal freedom.

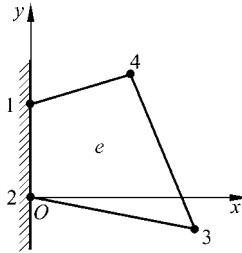


Figure 11.7 The boundary conditions on fixed edge

In Fig. 11.7, side $\bar{12}$ is a fixed edge. The boundary conditions of the element e at nodes 1 and 2 are

$$u_1 = u_2 = 0, \quad v_1 = v_2 = 0 \quad (11-43)$$

And, the following conditions can also be obtained:

$$\left(\frac{\partial u}{\partial y} \right)_1 = \left(\frac{\partial u}{\partial y} \right)_2 = 0 \quad (11-44)$$

Then, the rotation at node 1 can be derived from the above conditions:

$$\omega_1 = \frac{1}{2} \left(\frac{\partial v}{\partial x} - \frac{\partial u}{\partial y} \right)_1 = \frac{1}{2} \left(\frac{\partial v}{\partial x} \right)_1 \quad (11-45)$$

Since the term $\left(\frac{\partial v}{\partial x} \right)_1$ at the right side of the above equation is generally nonzero, so the following boundary condition

$$\omega = 0 \quad (11-46)$$

generally cannot come into existence. Therefore, ω is not suitable for being selected as the nodal freedom.

While the second definition possesses the above disadvantages, references [2, 3] proposed the third definition for the nodal drilling freedom θ_z of the membrane element.

(3) The third definition—the nodal drilling freedom θ_z in the membrane element is defined as the additional rigid rotation at the element node.

In this definition, the displacement fields within the domain of an element are assumed to include two parts:

$$\mathbf{u} = \mathbf{u}^0 + \mathbf{u}_\theta \tag{11-47}$$

where $\mathbf{u}^0 = [u^0 \ v^0]^T$ are the displacement fields determined by the nodal translational displacements; $\mathbf{u}_\theta = [u_\theta \ v_\theta]^T$ are the additional displacement fields only determined by the vertex rigid rotations. According to Eq. (11-47), the deformation process of the element under external load can be expressed by Fig. 11.8. The element deformation caused by the nodal translational displacements is shown in Fig. 11.8(a), and the element deformation caused by the vertex rigid rotations is shown in Fig. 11.8(b). It should be emphatically pointed out that the above two deformation states are independent of each other.

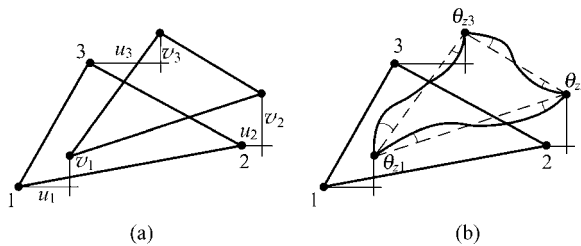


Figure 11.8 The deformation process of a plane membrane element

The characteristics of the nodal drilling freedom defined in Fig. 11.8 are as follows:

(1) The change of the angle between two adjacent sides along with the element deformation is allowed (see Fig. 11.8(a)), which overcomes the shortcomings caused by the improper constraint introduced by the early definition.

(2) The rotation θ of the element side has definite relation with the nodal drilling freedom θ_z . In fact, the rotation θ of element side is composed of two parts θ' and θ'' , in which θ' is given by Fig. 11.8(a), and θ'' is just θ_z .

Just because of these two characteristics, the irrationalities in the former two definitions are avoided.

11.3.2 The Rectangular Membrane Element with Drilling Freedoms GR12

A rectangular membrane element with 12 DOFs is shown in Fig. 11.9, and the freedoms at each node are:

$$\mathbf{q}_i = [u_i \quad v_i \quad \theta_i]^T \quad (i = 1, 2, 3, 4) \quad (11-48)$$

where u_i and v_i are the translational freedoms; and θ_i is just the additional in-plane rigid rotational freedom which is defined previously.

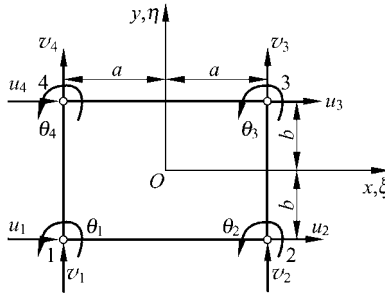


Figure 11.9 Rectangular membrane element

Assume that the element displacement mode is given by Eq. (11-47), which includes two parts \mathbf{u}^0 and \mathbf{u}_θ . \mathbf{u}^0 are the bilinear compatible displacement fields expressed by the translational freedoms as

$$\mathbf{u}^0 = \begin{Bmatrix} u^0 \\ v^0 \end{Bmatrix} = \sum_{i=1}^4 N_i^0 \begin{Bmatrix} u_i \\ v_i \end{Bmatrix} \quad (11-49)$$

where

$$N_i^0 = \frac{1}{4}(1 + \xi_i \xi)(1 + \eta_i \eta) \quad (11-50)$$

And, $\mathbf{u}_\theta = [u_\theta \quad v_\theta]^T$ in Eq. (11-47) are only the additional displacement fields caused by the additional vertex rigid rotations θ_i ($i = 1, 2, 3, 4$), as shown in Fig. 11.10. Here, θ_i is only related to the additional displacement fields \mathbf{u}_θ and independent of \mathbf{u}^0 . The rotational freedom defined as above can describe the deformation behavior of the element boundary more clearly.

The additional displacement fields \mathbf{u}_θ can be assumed as

$$\left. \begin{aligned} u_\theta &= (1 - \xi^2)(\alpha_1 + \alpha_2 \eta) + (1 - \eta^2)(\alpha_3 + \alpha_4 \xi) \\ v_\theta &= (1 - \eta^2)(\beta_1 + \beta_2 \xi) + (1 - \xi^2)(\beta_3 + \beta_4 \eta) \end{aligned} \right\} \quad (11-51)$$

The values of the displacement fields expressed by the above equation at the element corner nodes are all zero.

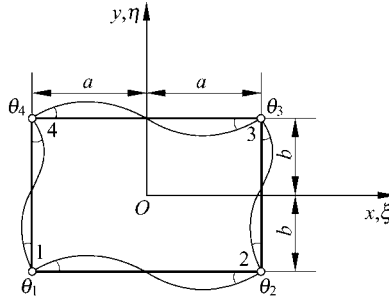


Figure 11.10 Additional displacement field

The element boundary displacements $\bar{\mathbf{u}}_{\theta}$ caused by the additional vertex rigid rotations can be written as:

$$\left. \begin{aligned} \bar{\mathbf{u}}_{\theta 12} &= \begin{Bmatrix} \bar{u}_{\theta 12} \\ \bar{v}_{\theta 12} \end{Bmatrix} = \frac{a}{4}(1-\xi^2)[\theta_1(1-\xi) - \theta_2(1+\xi)] \begin{Bmatrix} 0 \\ 1 \end{Bmatrix} \\ \bar{\mathbf{u}}_{\theta 43} &= \begin{Bmatrix} \bar{u}_{\theta 43} \\ \bar{v}_{\theta 43} \end{Bmatrix} = \frac{a}{4}(1-\xi^2)[\theta_4(1-\xi) - \theta_3(1+\xi)] \begin{Bmatrix} 0 \\ 1 \end{Bmatrix} \\ \bar{\mathbf{u}}_{\theta 23} &= \begin{Bmatrix} \bar{u}_{\theta 23} \\ \bar{v}_{\theta 23} \end{Bmatrix} = -\frac{b}{4}(1-\eta^2)[\theta_2(1-\eta) - \theta_3(1+\eta)] \begin{Bmatrix} 1 \\ 0 \end{Bmatrix} \\ \bar{\mathbf{u}}_{\theta 14} &= \begin{Bmatrix} \bar{u}_{\theta 14} \\ \bar{v}_{\theta 14} \end{Bmatrix} = -\frac{b}{4}(1-\eta^2)[\theta_1(1-\eta) - \theta_4(1+\eta)] \begin{Bmatrix} 1 \\ 0 \end{Bmatrix} \end{aligned} \right\} \quad (11-52)$$

From the generalized conforming condition (11-8), which can be written as

$$\int_{S_k} (\mathbf{u}_{\theta} - \bar{\mathbf{u}}_{\theta}) ds = \mathbf{0} \quad (k = 1, 2, 3, 4) \quad (11-53)$$

the unknown coefficients α_i and β_i ($i = 1, 2, 3, 4$) in Eq. (11-51) can be solved. Then, substituting them back into Eq. (11-51), we have

$$\mathbf{u}_{\theta} = \begin{Bmatrix} u_{\theta} \\ v_{\theta} \end{Bmatrix} = \sum_{i=1}^4 \begin{Bmatrix} N_{u\theta i} \\ N_{v\theta i} \end{Bmatrix} \theta_i \quad (11-54)$$

where

$$\left. \begin{aligned} N_{u\theta i} &= \frac{b}{8}(1-\eta^2)(1+\xi_i\xi)\eta_i \\ N_{v\theta i} &= -\frac{a}{8}(1-\xi^2)(1+\eta_i\eta)\xi_i \end{aligned} \right\} \quad (11-55)$$

Substitution of Eqs. (11-49) and (11-54) into Eq. (11-47) yields the displacement fields expressed in terms of the shape functions:

$$\mathbf{u} = \mathbf{u}^0 + \mathbf{u}_\theta = \mathbf{N}\mathbf{q}^e = \sum_{i=1}^4 N_i \mathbf{q}_i \quad (11-56)$$

where

$$\mathbf{q}^e = [\mathbf{q}_1^T \quad \mathbf{q}_2^T \quad \mathbf{q}_3^T \quad \mathbf{q}_4^T]^T \quad (11-57)$$

$$\mathbf{N} = [N_1 \quad N_2 \quad N_3 \quad N_4] \quad (11-58)$$

$$N_i = \begin{bmatrix} N_i^0 & 0 & N_{u\theta i} \\ 0 & N_i^0 & N_{v\theta i} \end{bmatrix} \quad (11-59)$$

and N_i^0 , $N_{u\theta i}$ and $N_{v\theta i}$ are given by Eqs. (11-50) and (11-55), respectively.

Though the displacement fields expressed by Eq. (11-56) are not exactly compatible on the element boundary, they have already satisfied the generalized conforming conditions in Eq. (11-53). Therefore, the finite element formulations can be established by the potential energy principle. This element is denoted as GR12. According to the conventional procedure, the element stiffness matrix \mathbf{K}^e can be obtained:

$$\mathbf{K}^e = \begin{bmatrix} \mathbf{K}_{11} & \mathbf{K}_{12} & \mathbf{K}_{13} & \mathbf{K}_{14} \\ \mathbf{K}_{21} & \mathbf{K}_{22} & \mathbf{K}_{23} & \mathbf{K}_{24} \\ \mathbf{K}_{31} & \mathbf{K}_{32} & \mathbf{K}_{33} & \mathbf{K}_{34} \\ \mathbf{K}_{41} & \mathbf{K}_{42} & \mathbf{K}_{43} & \mathbf{K}_{44} \end{bmatrix} \quad (11-60)$$

where

$$\mathbf{K}_{ij} = \frac{habE}{24(1-\mu^2)} \begin{bmatrix} \bar{k}_{11} & \bar{k}_{12} & \bar{k}_{13} \\ \bar{k}_{21} & \bar{k}_{22} & \bar{k}_{23} \\ \bar{k}_{31} & \bar{k}_{32} & \bar{k}_{33} \end{bmatrix} \quad (11-61)$$

with

$$\bar{k}_{11} = \frac{2}{a^2} \xi_i \xi_j (3 + \eta_i \eta_j) + \frac{1-\mu}{b^2} \eta_i \eta_j (3 + \xi_i \xi_j)$$

$$\bar{k}_{12} = \frac{6\mu}{ab} \xi_i \eta_j + \frac{3(1-\mu)}{ab} \eta_i \xi_j$$

$$\bar{k}_{13} = \frac{2b}{a^2} \xi_i \xi_j \eta_j - \frac{1}{b} \xi_i \xi_j [2\mu \eta_j - (1-\mu) \eta_i]$$

$$\bar{k}_{21} = \frac{6\mu}{ab} \eta_i \xi_j + \frac{3(1-\mu)}{ab} \xi_i \eta_j$$

$$\begin{aligned}\bar{k}_{22} &= \frac{2}{b^2} \eta_i \eta_j (3 + \xi_i \xi_j) + \frac{1-\mu}{a^2} \xi_i \xi_j (3 + \eta_i \eta_j) \\ \bar{k}_{23} &= -\frac{2a}{b^2} \eta_i \eta_j \xi_j + \frac{1}{a} \eta_i \eta_j [2\mu \xi_j - (1-\mu) \xi_i] \\ \bar{k}_{31} &= \frac{2b}{a^2} \eta_i \xi_i \xi_j - \frac{1}{b} \xi_i \xi_j [2\mu \eta_i - (1-\mu) \eta_j] \\ \bar{k}_{32} &= -\frac{2a}{b^2} \xi_i \eta_i \eta_j + \frac{1}{a} \eta_i \eta_j [2\mu \xi_i - (1-\mu) \xi_j] \\ \bar{k}_{33} &= \frac{4}{5} \left(\frac{a^2}{b^2} + \frac{b^2}{a^2} - \frac{5}{3} \mu \right) \xi_i \xi_j \eta_i \eta_j + (1-\mu) (\xi_i \xi_j + \eta_i \eta_j)\end{aligned}$$

11.3.3 The Rectangular Membrane Element with Drilling Freedoms GR12M—with Internal Freedoms

Consider the following bubble displacement fields:

$$\mathbf{u}_\lambda = \begin{Bmatrix} u_\lambda \\ v_\lambda \end{Bmatrix} = N_\lambda \boldsymbol{\lambda} = \begin{bmatrix} N_\lambda & 0 \\ 0 & N_\lambda \end{bmatrix} \begin{Bmatrix} \lambda_1 \\ \lambda_2 \end{Bmatrix} \quad (11-62)$$

where

$$N_\lambda = (1 - \xi^2)(1 - \eta^2) \quad (11-63)$$

λ_1 and λ_2 are arbitrary parameters.

By the superposition of Eqs. (11-62) and (11-47), the displacement fields with three parts can be obtained

$$\mathbf{u} = \mathbf{u}^0 + \mathbf{u}_\theta + \mathbf{u}_\lambda \quad (11-64)$$

This is the displacement mode of the element GR12M. Substitution of Eqs. (11-56) and (11-62) into the above equation yields

$$\mathbf{u} = N\mathbf{q}^e + N_\lambda \boldsymbol{\lambda} \quad (11-65)$$

The corresponding strain fields can be expressed as

$$\boldsymbol{\varepsilon} = \mathbf{B}\mathbf{q}^e + \mathbf{B}_\lambda \boldsymbol{\lambda} \quad (11-66)$$

in which \mathbf{B} and \mathbf{B}_λ are the strain matrices corresponding to Eqs. (11-56) and (11-62), respectively.

According to Eq. (11-66), the strain energy of element GR12M can be written as

$$U = \frac{h}{2} \iint_{A^e} \boldsymbol{\varepsilon}^T \mathbf{D} \boldsymbol{\varepsilon} dA = \frac{1}{2} \mathbf{q}^{eT} \mathbf{K}_{qq} \mathbf{q}^e + \boldsymbol{\lambda}^T \mathbf{K}_{\lambda q} \mathbf{q}^e + \frac{1}{2} \boldsymbol{\lambda}^T \mathbf{K}_{\lambda\lambda} \boldsymbol{\lambda} \quad (11-67)$$

in which

$$\mathbf{K}_{qq} = abh \int_{-1}^1 \int_{-1}^1 \mathbf{B}^T \mathbf{D} \mathbf{B} d\xi d\eta \quad (11-68a)$$

$$\mathbf{K}_{\lambda q} = abh \int_{-1}^1 \int_{-1}^1 \mathbf{B}_\lambda^T \mathbf{D} \mathbf{B} d\xi d\eta \quad (11-68b)$$

$$\mathbf{K}_{\lambda\lambda} = abh \int_{-1}^1 \int_{-1}^1 \mathbf{B}_\lambda^T \mathbf{D} \mathbf{B}_\lambda d\xi d\eta \quad (11-68c)$$

From the stationary condition

$$\frac{\partial U}{\partial \boldsymbol{\lambda}} = \mathbf{0} \quad (11-69)$$

the arbitrary parameters $\boldsymbol{\lambda}$ can be expressed in terms of the external DOFs as

$$\boldsymbol{\lambda} = -\mathbf{K}_{\lambda\lambda}^{-1} \mathbf{K}_{\lambda q} \mathbf{q}^e \quad (11-70)$$

Substitution of the above equation into Eq. (11-65) yields

$$\mathbf{u} = \mathbf{N}^* \mathbf{q}^e \quad (11-71)$$

where

$$\mathbf{N}^* = \mathbf{N} - \mathbf{N}_\lambda \mathbf{K}_{\lambda\lambda}^{-1} \mathbf{K}_{\lambda q} \quad (11-72)$$

The above equation includes the shape functions of the element GR12M, in which $\mathbf{K}_{\lambda q}$ and $\mathbf{K}_{\lambda\lambda}^{-1}$ are evaluated from Eqs. (11-68b) and (11-68c), respectively,

$$\mathbf{K}_{\lambda q} = [\mathbf{K}'_1 \quad \mathbf{K}'_2 \quad \mathbf{K}'_3 \quad \mathbf{K}'_4] \quad (11-73)$$

where

$$\mathbf{K}'_i = -\frac{2Eh}{9(1-\mu^2)} \begin{bmatrix} 0 & (1+\mu)\xi_i\eta_i & -a(1-\mu)\eta_i \\ (1+\mu)\xi_i\eta_i & 0 & b(1-\mu)\xi_i \end{bmatrix} \quad (i = 1, 2, 3, 4) \quad (11-74)$$

$$\mathbf{K}_{\lambda\lambda}^{-1} = \frac{45(1-\mu^2)ab}{128E} \begin{bmatrix} \frac{1}{b^2 + \frac{1-\mu}{2}a^2} & 0 \\ 0 & \frac{1}{a^2 + \frac{1-\mu}{2}b^2} \end{bmatrix} \quad (11-75)$$

According to the element shape function (11-72), the element stiffness matrix can be written as

$$\mathbf{K}^e = \mathbf{K}_{qq} - \mathbf{K}_{\lambda q}^T \mathbf{K}_{\lambda\lambda}^{-1} \mathbf{K}_{\lambda q} \quad (11-76)$$

here \mathbf{K}_{qq} is the same as the element stiffness matrix of the element GR12.

The stress vector of the element GR12 is $\boldsymbol{\sigma} = \mathbf{S}\mathbf{q}^e$, in which the stress matrix \mathbf{S} is

$$\mathbf{S} = [\mathbf{S}_1 \quad \mathbf{S}_2 \quad \mathbf{S}_3 \quad \mathbf{S}_4] \quad (11-77)$$

in which

$$\mathbf{S}_i = \frac{E}{8ab(1-\mu^2)} \begin{bmatrix} s_{11} & s_{12} & s_{13} \\ s_{21} & s_{22} & s_{23} \\ s_{31} & s_{32} & s_{33} \end{bmatrix} \quad (i = 1,2,3,4) \quad (11-78)$$

with

$$\begin{aligned} s_{11} &= 2b\xi_i(1 + \eta_i\eta), & s_{12} &= 2a\mu\eta_i(1 + \xi_i\xi) \\ s_{13} &= [b^2(1 - \eta^2) - \mu a^2(1 - \xi^2)]\xi_i\eta_i \\ s_{21} &= 2b\mu\xi_i(1 + \eta_i\eta), & s_{22} &= 2a\eta_i(1 + \xi_i\xi) \\ s_{23} &= [\mu b^2(1 - \eta^2) - a^2(1 - \xi^2)]\xi_i\eta_i \\ s_{31} &= a(1 - \mu)\eta_i(1 + \xi_i\xi) \\ s_{32} &= b(1 - \mu)\xi_i(1 + \eta_i\eta) \\ s_{33} &= ab(1 - \mu)(\xi_i\xi - \eta_i\eta) \end{aligned}$$

And the stress vector of the element GR12M can be written as

$$\boldsymbol{\sigma} = \mathbf{D}(\boldsymbol{\varepsilon} - \boldsymbol{\varepsilon}') = (\mathbf{S} - \mathbf{S}')\mathbf{q}^e = \sum_{i=1}^4 (\mathbf{S}_i - \mathbf{S}'_i)\mathbf{q}_i \quad (11-79)$$

in which \mathbf{S}_i is given by Eq. (11-78), and \mathbf{S}'_i is

$$\mathbf{S}'_i = \mathbf{D}\mathbf{B}_\lambda \mathbf{K}_{\lambda\lambda}^{-1} \mathbf{K}'_i = \mathbf{S}_\lambda \mathbf{K}_{\lambda\lambda}^{-1} \mathbf{K}'_i \quad (i = 1,2,3,4) \quad (11-80)$$

where

$$\mathbf{S}_\lambda = -\frac{2E}{ab(1-\mu^2)} \begin{bmatrix} b(1-\eta^2)\xi & a\mu(1-\xi^2)\eta \\ b\mu(1-\eta^2)\xi & a(1-\xi^2)\eta \\ \frac{a(1-\mu)}{2}(1-\xi^2)\eta & \frac{b(1-\mu)}{2}(1-\eta^2)\xi \end{bmatrix} \quad (11-81)$$

\mathbf{K}'_i and $\mathbf{K}_{\lambda\lambda}^{-1}$ are given by Eqs. (11-74) and (11-75), respectively.

11.3.4 Quadrilateral Membrane Elements with Drilling Freedoms GQ12 and GQ12M

The rectangular elements GR12 and GR12M can be generalized to quadrilateral elements, the details can be found in reference [2].

11.4 Membrane Elements with Drilling Freedoms — Triangular Elements

On the basis of the constant strain triangular element, if we use the additional rigid rotational freedom proposed previously, the additional displacement fields caused only by the vertex rigid rotations can be introduced into the constant-strain displacement fields, and then, the triangular membrane element with drilling freedoms, GT9, can be derived. On the basis of the element GT9, by adding the generalized bubble displacement field, the new triangular membrane elements with higher accuracy, GT9M and GT9M8, can be obtained. These three elements can pass the patch test with arbitrary shape, so they are convergent models.

11.4.1 Triangular Membrane Element with Drilling Freedoms GT9

A triangular membrane element is shown in Fig. 11.11. At each node, there are two translational freedoms and one in-plane rotational freedom. The element nodal displacement vector is

$$\mathbf{q}^e = [\mathbf{q}_1^T \quad \mathbf{q}_2^T \quad \mathbf{q}_3^T]^T \tag{11-82}$$

where

$$\mathbf{q}_i = [u_i \quad v_i \quad \theta_i]^T \quad (i = 1, 2, 3) \tag{11-83}$$

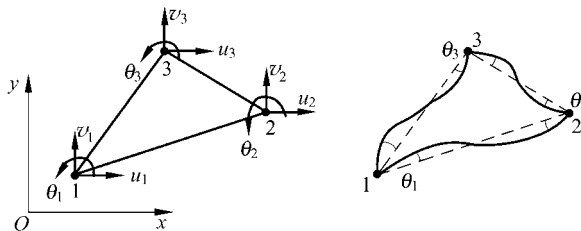


Figure 11.11 A triangular membrane element and its additional displacement field

in which u_i and v_i are the translational displacements at the corner node; θ_i is the additional rigid rotation at the corner node. As described in Sect. 11.3.1, θ_i used here is different from the rotation defined in continuum mechanics.

The basic displacement fields are assumed to be composed of two parts:

$$\mathbf{u}_b = \mathbf{u}^0 + \mathbf{u}_\theta \quad (11-84)$$

where $\mathbf{u}^0 = [u^0 \ v^0]^T$ are the linear displacement fields, which are determined by the translational freedoms at the corner nodes uniquely. These are compatible displacement fields, and can be expressed in terms of the triangular area coordinates as

$$\mathbf{u}^0 = \begin{Bmatrix} u^0 \\ v^0 \end{Bmatrix} = \sum_{i=1}^3 \begin{bmatrix} L_i & 0 \\ 0 & L_i \end{bmatrix} \begin{Bmatrix} u_i \\ v_i \end{Bmatrix} \quad (11-85)$$

And, $\mathbf{u}_\theta = [u_\theta \ v_\theta]^T$ are the additional displacement fields only caused by the in-plane vertex rigid rotational freedoms. It can be assumed to be the pure quadric polynomial in terms of the area coordinates

$$\mathbf{u}_\theta = \begin{Bmatrix} u_\theta \\ v_\theta \end{Bmatrix} = L_2 L_3 \begin{Bmatrix} \alpha_1 \\ \beta_1 \end{Bmatrix} + L_3 L_1 \begin{Bmatrix} \alpha_2 \\ \beta_2 \end{Bmatrix} + L_1 L_2 \begin{Bmatrix} \alpha_3 \\ \beta_3 \end{Bmatrix} \quad (11-86)$$

The value of \mathbf{u}_θ in the above equation at the corner node i is zero.

Along the sides of triangular element, the normal displacements due to the vertex rigid rotations can be written as the cubic interpolation formulas

$$\left. \begin{aligned} \bar{u}_{n\theta 23} &= -d_1 L_2 L_3 (\theta_2 L_2 - \theta_3 L_3) \\ \bar{u}_{n\theta 31} &= -d_2 L_3 L_1 (\theta_3 L_3 - \theta_1 L_1) \\ \bar{u}_{n\theta 12} &= -d_3 L_1 L_2 (\theta_1 L_1 - \theta_2 L_2) \end{aligned} \right\} \quad (11-87)$$

in which $d_i (i = 1, 2, 3)$ are the lengths of the triangular element sides. And, the vertex rotations will not produce the tangent displacements along the element sides, i.e.,

$$\bar{u}_{s\theta 23} = \bar{u}_{s\theta 12} = \bar{u}_{s\theta 31} = 0 \quad (11-88)$$

The direction cosines of the normal on the element side ($L_i=0$) are

$$n_{xi} = -\frac{b_i}{d_i}, \quad n_{yi} = -\frac{c_i}{d_i} \quad (i = 1, 2, 3) \quad (11-89)$$

where b_i and c_i are given by Eq. (6-13). The projections of the normal displacements in Eq. (11-87) on x -axes and y -axes are

Since the displacement fields (11-94) satisfy the generalized conforming conditions (11-8), therefore, the element stiffness matrix \mathbf{K}^e can be derived by the conventional procedure:

$$\mathbf{K}^e = \begin{bmatrix} \mathbf{K}_{11} & \mathbf{K}_{12} & \mathbf{K}_{13} \\ \mathbf{K}_{21} & \mathbf{K}_{22} & \mathbf{K}_{23} \\ \mathbf{K}_{31} & \mathbf{K}_{32} & \mathbf{K}_{33} \end{bmatrix} \quad (11-97)$$

where the sub-matrices are

$$\mathbf{K}_{ij} = h \iint_{A^e} \mathbf{B}_i^T \mathbf{D} \mathbf{B}_j dA \quad (i, j = 1, 2, 3) \quad (11-98)$$

in which

$$\mathbf{B}_i = \frac{1}{4A} \begin{bmatrix} 2b_i & 0 & b_i(b_m L_j - b_j L_m) \\ 0 & 2c_i & c_i(c_m L_j - c_j L_m) \\ 2c_i & 2b_i & (c_i b_m + b_i c_m) L_j - (c_i b_j + b_i c_j) L_m \end{bmatrix} \quad (i, j, m = \overline{1, 2, 3}) \quad (11-99)$$

11.4.2 Triangular Membrane Element with Drilling Freedoms GT9M—with an Internal Freedom

The displacement functions with one arbitrary internal parameter λ can be assumed as

$$\mathbf{u}_\lambda = \begin{Bmatrix} u_\lambda \\ v_\lambda \end{Bmatrix} = \mathbf{N}_\lambda \lambda = \begin{Bmatrix} N_{u\lambda} \\ N_{v\lambda} \end{Bmatrix} \lambda \quad (11-100)$$

where

$$\mathbf{N}_\lambda = [N_{u\lambda} \quad N_{v\lambda}]^T \quad (11-101)$$

$$N_{u\lambda} = \sum_{i=1}^3 b_i F_i, \quad N_{v\lambda} = \sum_{i=1}^3 c_i F_i \quad (11-102)$$

and

$$F_i = L_j L_m (L_j - L_m) \quad (11-103)$$

It can be easily verified that Eq. (11-100) satisfies the following equation:

$$\int_{L_i=0} \mathbf{u}_\lambda ds = \mathbf{0} \quad (i = 1, 2, 3) \quad (11-104)$$

and is equal to zero at 3 corner nodes. Hence, the displacement functions given by Eq. (11-100) are the generalized bubble displacements whose average values along the element sides are zero.

The displacement fields of the element GT9M are composed of 3 parts:

$$\mathbf{u} = \mathbf{u}^0 + \mathbf{u}_\theta + \mathbf{u}_\lambda \quad (11-105)$$

From Eqs. (11-94) and (11-100), the above equation can be expressed as

$$\mathbf{u} = \mathbf{N}\mathbf{q}^e + \mathbf{N}_\lambda\lambda \quad (11-106)$$

in which \mathbf{N} and \mathbf{N}_λ are given by Eqs. (11-95) and (11-101), respectively. The strain fields corresponding to Eq. (11-106) are

$$\boldsymbol{\varepsilon} = \mathbf{B}\mathbf{q}^e + \mathbf{B}_\lambda\lambda \quad (11-107)$$

where \mathbf{B} is the strain matrix corresponding to Eq. (11-94); \mathbf{B}_λ is the strain vector corresponding to Eq. (11-100). From Eq. (11-107), the strain energy of the element GT9M can be written as

$$U = \frac{h}{2} \iint_{A^e} \boldsymbol{\varepsilon}^T \mathbf{D} \boldsymbol{\varepsilon} dA = \frac{1}{2} \mathbf{q}^{eT} \mathbf{K}_{qq} \mathbf{q}^e + \lambda \mathbf{K}_{\lambda q} \mathbf{q}^e + \frac{1}{2} \lambda^2 k_{\lambda\lambda} \quad (11-108)$$

where

$$\mathbf{K}_{qq} = h \iint_{A^e} \mathbf{B}^T \mathbf{D} \mathbf{B} dA \quad (11-109a)$$

$$\mathbf{K}_{\lambda q} = h \iint_{A^e} \mathbf{B}_\lambda^T \mathbf{D} \mathbf{B} dA \quad (11-109b)$$

$$k_{\lambda\lambda} = h \iint_{A^e} \mathbf{B}_\lambda^T \mathbf{D} \mathbf{B}_\lambda dA \quad (11-109c)$$

with

$$\mathbf{B} = [\mathbf{B}_1 \quad \mathbf{B}_2 \quad \mathbf{B}_3] \quad (11-110)$$

in which \mathbf{B}_i ($i = 1, 2, 3$) are given by Eq. (11-99); and

$$\mathbf{B}_\lambda = \frac{1}{A} \sum_{i=1}^3 \left\{ \begin{array}{l} b_m^2 - b_j^2 \\ c_m^2 - c_j^2 \\ 2(b_m c_m - b_j c_j) \end{array} \right\} L_m L_j \quad (i, j, m = \overline{1, 2, 3}) \quad (11-111)$$

From the stationary condition

$$\frac{\partial U}{\partial \lambda} = 0 \quad (11-112)$$

the arbitrary parameter λ in Eq. (11-106) can be expressed in terms of \mathbf{q}^e

$$\lambda = -\frac{1}{k_{\lambda\lambda}} \mathbf{K}_{\lambda q} \mathbf{q}^e \quad (11-113)$$

Substituting the above equation into Eq. (11-106), the displacement fields of the element GT9M expressed only in terms of external freedoms \mathbf{q}^e can be obtained

$$\mathbf{u} = \mathbf{N}^* \mathbf{q}^e \quad (11-114)$$

where

$$\mathbf{N}^* = \mathbf{N} - \frac{1}{k_{\lambda\lambda}} \mathbf{N}_{\lambda} \mathbf{K}_{\lambda q} \quad (11-115)$$

The stiffness matrix of the element GT9M is

$$\mathbf{K}^e = \mathbf{K}_{qq} - \frac{1}{k_{\lambda\lambda}} \mathbf{K}_{\lambda q}^T \mathbf{K}_{\lambda q} \quad (11-116)$$

in which \mathbf{K}_{qq} is the same as \mathbf{K}^e in Eq. (11-97).

11.4.3 Triangular Membrane Element with Drilling Freedoms GT9M8—with 8 Internal Freedoms

The element GT9M derived above contains one internal freedom, and the corresponding generalized bubble displacement is cubic. Now, we will develop a new element GT9M8 with 8 internal freedoms, and the corresponding generalized bubble displacement is still cubic.

Assume that the element displacement fields are composed of two parts:

$$\mathbf{u} = \mathbf{u}_b + \mathbf{u}_{\lambda} \quad (11-117)$$

where \mathbf{u}_b are the basic displacement functions given by Eq. (11-94); \mathbf{u}_{λ} are the additional displacement fields expressed by internal freedoms, here they are assumed to be complete cubic polynomials in the area coordinates

$$\begin{aligned} \mathbf{u}_{\lambda} = \begin{Bmatrix} u_{\lambda} \\ v_{\lambda} \end{Bmatrix} = & L_1 \begin{Bmatrix} \alpha_1 \\ \beta_1 \end{Bmatrix} + L_2 \begin{Bmatrix} \alpha_2 \\ \beta_2 \end{Bmatrix} + L_3 \begin{Bmatrix} \alpha_3 \\ \beta_3 \end{Bmatrix} + L_2 L_3 \begin{Bmatrix} \alpha_4 \\ \beta_4 \end{Bmatrix} + L_3 L_1 \begin{Bmatrix} \alpha_5 \\ \beta_5 \end{Bmatrix} \\ & + L_1 L_2 \begin{Bmatrix} \alpha_6 \\ \beta_6 \end{Bmatrix} + L_2^2 L_3 \begin{Bmatrix} \lambda_1 \\ \lambda_2 \end{Bmatrix} + L_3^2 L_1 \begin{Bmatrix} \lambda_3 \\ \lambda_4 \end{Bmatrix} + L_1^2 L_2 \begin{Bmatrix} \lambda_5 \\ \lambda_6 \end{Bmatrix} + L_1 L_2 L_3 \begin{Bmatrix} \lambda_7 \\ \lambda_8 \end{Bmatrix} \end{aligned} \quad (11-118)$$

where α_i and β_i ($i = 1, 2, \dots, 6$), λ_i ($i = 1, 2, \dots, 8$) are the arbitrary parameters. Substitution of Eq. (11-118) into the generalized conforming conditions corresponding to zero average side displacements and zero vertex displacement conditions:

$$\int_{L_i=0} \mathbf{u}_\lambda ds = \mathbf{0}, \quad \mathbf{u}_\lambda|_{L_i=1} = \mathbf{0} \quad (i = 1, 2, 3) \quad (11-119)$$

yields the additional displacement functions expressed by 8 arbitrary parameters λ_i ($i = 1, 2, \dots, 8$):

$$\mathbf{u}_\lambda = \begin{Bmatrix} u_\lambda \\ v_\lambda \end{Bmatrix} = \sum_{i=1}^3 L_j L_m \left(L_j - \frac{1}{2} \right) \begin{Bmatrix} \lambda_{2i-1} \\ \lambda_{2i} \end{Bmatrix} + L_1 L_2 L_3 \begin{Bmatrix} \lambda_7 \\ \lambda_8 \end{Bmatrix} \quad (11-120)$$

The above formulas are the generalized bubble functions which satisfy the generalized conforming conditions. And $\lambda_1, \lambda_2, \dots, \lambda_8$ are 8 internal freedoms.

By the way, the internal displacement field that is exactly compatible with zero boundary displacement is called bubble displacement, and that is generalized conforming to zero boundary displacement is called generalized bubble displacement. Equation (11-120) contains 8 internal freedoms, in which λ_7 and λ_8 are corresponding to the bubble displacements, while $\lambda_1, \lambda_2, \dots, \lambda_6$ are corresponding to the generalized bubble displacements.

The additional displacements (11-120) expressed by internal freedoms can be written as the following matrix form:

$$\mathbf{u}_\lambda = \mathbf{N}_\lambda \boldsymbol{\lambda} \quad (11-121)$$

in which

$$\mathbf{N}_\lambda = \begin{bmatrix} F_1 & 0 & F_2 & 0 & F_3 & 0 & F_4 & 0 \\ 0 & F_1 & 0 & F_2 & 0 & F_3 & 0 & F_4 \end{bmatrix} \quad (11-122)$$

where

$$F_i = L_j L_m \left(L_j - \frac{1}{2} \right) \quad (i = 1, 2, 3), \quad F_4 = L_1 L_2 L_3 \quad (11-123)$$

And, $\boldsymbol{\lambda}$ in Eq. (11-121) is the internal freedom vector:

$$\boldsymbol{\lambda} = [\lambda_1 \quad \lambda_2 \quad \lambda_3 \quad \lambda_4 \quad \lambda_5 \quad \lambda_6 \quad \lambda_7 \quad \lambda_8]^T \quad (11-124)$$

From Eqs. (11-117), (11-94) and (11-121), the displacement fields of the element GT9M8 can be expressed in terms of the shape functions

$$\mathbf{u} = \mathbf{N}\mathbf{q}^e + \mathbf{N}_\lambda \boldsymbol{\lambda} \quad (11-125)$$

where \mathbf{N} and \mathbf{N}_λ are given by Eqs. (11-95) and (11-122), respectively.

From the element displacement given by Eq. (11-125), and according to the procedure similar to those in Sects. 11.3.2 and 11.3.3, the internal freedoms λ can be expressed in terms of q^e by condensation

$$\lambda = -\mathbf{K}_{\lambda\lambda}^{-1} \mathbf{K}_{\lambda q} q^e \quad (11-126)$$

where

$$\mathbf{K}_{\lambda q} = h \iint_{A^e} \mathbf{B}_\lambda^T \mathbf{D} \mathbf{B} dA \quad (11-127a)$$

$$\mathbf{K}_{\lambda\lambda} = h \iint_{A^e} \mathbf{B}_\lambda^T \mathbf{D} \mathbf{B}_\lambda dA \quad (11-127b)$$

in which \mathbf{B} in Eq. (11-127a) is given by Eq. (11-110); and \mathbf{B}_λ in Eq. (11-127) is

$$\mathbf{B}_\lambda = \begin{bmatrix} F_{1x} & 0 & F_{2x} & 0 & F_{3x} & 0 & F_{4x} & 0 \\ 0 & F_{1y} & 0 & F_{2y} & 0 & F_{3y} & 0 & F_{4y} \\ F_{1y} & F_{1x} & F_{2y} & F_{2x} & F_{3y} & F_{3x} & F_{4y} & F_{4x} \end{bmatrix} \quad (11-128)$$

$$\left. \begin{aligned} F_{ix} &= \frac{1}{2A} \left[b_j L_m \left(2L_j - \frac{1}{2} \right) + b_m L_j \left(L_j - \frac{1}{2} \right) \right] \\ F_{iy} &= \frac{1}{2A} \left[c_j L_m \left(2L_j - \frac{1}{2} \right) + c_m L_j \left(L_j - \frac{1}{2} \right) \right] \\ F_{4x} &= \frac{1}{2A} (b_1 L_2 L_3 + b_2 L_3 L_1 + b_3 L_1 L_2) \\ F_{4y} &= \frac{1}{2A} (c_1 L_2 L_3 + c_2 L_3 L_1 + c_3 L_1 L_2) \end{aligned} \right\} (i, j, m = \overline{1, 2, 3}) \quad (11-129)$$

Thus, Eq. (11-125) can be expressed in terms of external freedoms as

$$\mathbf{u} = \mathbf{N}^* q^e \quad (11-130)$$

where

$$\mathbf{N}^* = \mathbf{N} - \mathbf{N}_\lambda \mathbf{K}_{\lambda\lambda}^{-1} \mathbf{K}_{\lambda q} \quad (11-131)$$

According to the displacement field (11-130) expressed by the shape functions, the element stiffness matrix can be obtained

$$\mathbf{K}^e = \mathbf{K}_{qq} - \mathbf{K}_{\lambda q}^T \mathbf{K}_{\lambda\lambda}^{-1} \mathbf{K}_{\lambda q} \quad (11-132)$$

where \mathbf{K}_{qq} is evaluated by Eq. (11-97).

Example 11.4 Pure in-plane bending of a square plate.

A square plate of side length L is shown in Fig. 11.12. It is subjected to a linear

varying normal stress on the left and right sides:

$$\sigma_x \Big|_{x=\pm(L/2)} = 2\left(\frac{y}{L}\right)\sigma_0$$

In view of the symmetry of the problem, only 1/4 of the plate is considered and meshed. Numerical results of the displacement and stress at corner point *C* are listed in Table 11.4. For comparison, the other results obtained by Allman^[23] and the bilinear rectangular element R4 are also given.

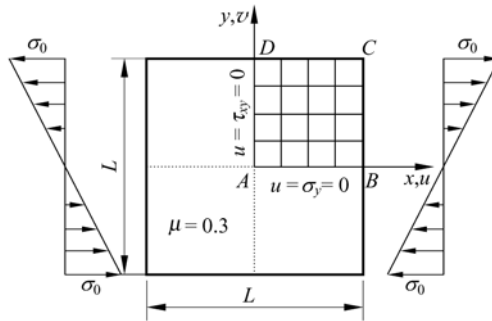


Figure 11.12 Pure in-plane bending of a square plate (Mesh 4 × 4)

From Table 11.4, it can be seen that the presented two rectangular elements GR12 and GR12M can provide more accurate results for displacement and stress.

Table 11.4 The displacement and stress at point *C* of a square plate under pure in-plane bending

Mesh (1/4 plate)	(1 × 1)			(2 × 2)		
Element	$\frac{Eu_C}{\sigma_0 L}$	$\frac{Ev_C}{\sigma_0 L}$	$\frac{\sigma_{xC}}{\sigma_0}$	$\frac{Eu_C}{\sigma_0 L}$	$\frac{Ev_C}{\sigma_0 L}$	$\frac{\sigma_{xC}}{\sigma_0}$
R4	0.4461	- 0.2900	0.9363	0.4797	- 0.3120	0.9770
Allman ^[23]	0.4738	- 0.3070	0.9784	0.4910	- 0.3191	0.9912
GR12	0.4823	- 0.3108	1.0220	0.4941	- 0.3206	1.0129
GR12M	0.4961	- 0.3218	1.0055	0.4987	- 0.3241	1.0029
Mesh (1/4 plate)	(4 × 4)			(8 × 8)		
Element	$\frac{Eu_C}{\sigma_0 L}$	$\frac{Ev_C}{\sigma_0 L}$	$\frac{\sigma_{xC}}{\sigma_0}$	$\frac{Eu_C}{\sigma_0 L}$	$\frac{Ev_C}{\sigma_0 L}$	$\frac{\sigma_{xC}}{\sigma_0}$
R4	0.4931	- 0.3206	0.9894	0.4978	- 0.3236	0.9947
Allman ^[23]	0.4971	- 0.3231	0.9956	0.4991	- 0.3244	0.9978
GR12	0.4982	- 0.3237	1.0066	0.4994	- 0.3246	1.0033
GR12M	0.4996	- 0.3247	1.0015	0.4999	- 0.3249	1.0007

Note: Exact solutions are given by [23] $\frac{Eu_C}{\sigma_0 L} = 0.5000$, $\frac{Ev_C}{\sigma_0 L} = -0.3250$, $\frac{\sigma_{xC}}{\sigma_0} = 1.0000$.

Example 11.5 Cantilever beam under a tip shear load.

As shown in Fig. 11.13, a cantilever beam is subjected to a tip parabolic shear load

$$\tau_{xy}|_{x=L} = \frac{3W}{2Hh} \left[1 - 4 \left(\frac{y}{H} \right)^2 \right]$$

where L , H and h are the length, height and thickness of the beam, respectively. 3 finite element meshes plotted in the figure are used. Numerical results for the deflection at the mid-side point C of the beam tip and stress of point A are listed in Table 11.5, where the coordinates of the point A is (12, 6).

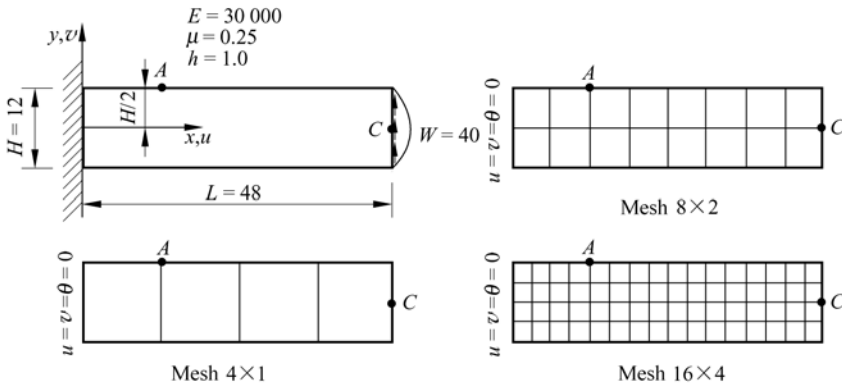


Figure 11.13 A cantilever beam under tip shear load

It can be seen from the results that, the performance of the bilinear element R4 is obviously lower than those of the other elements. And, the precisions of the presented two elements GR12 and GR12M are both better than that of similar element proposed by Allman.

Table 11.5 Deflection and stress at selected points of a cantilever

Element	(4 × 1) mesh		(8 × 2) mesh		(16 × 4) mesh	
	v_C	σ_{xA}	v_C	σ_{xA}	v_C	σ_{xA}
R4	0.2424	-43.64	0.3162	-55.70	0.3447	-59.28
Allman ^[23]	0.3026	-52.70	0.3394	-58.40	0.3512	-59.70
GR12	0.3283	-60.00	0.3475	-61.31	0.3535	-60.76
GR12M	0.3446	-60.00	0.3527	-60.65	0.3550	-60.20
Comparison solutions ^[23]	$v_C = 0.3558$			$\sigma_{xA} = -60.0 (x = 12, y = 6)$		

Example 11.6 Cantilever beam under a tip shear load (3-node triangular element).

This problem is the same as the Example 11.5. Numerical results for deflection at the mid-side point at the beam tip by using different meshes are listed in Table 11.6. Two different meshes are shown in Fig. 11.14(a) and (b), respectively. Mesh I is for the three presented elements GT9, GT9M and GT9M8. And mesh II, in which each rectangle is divided into four half-thickness overlaid triangles, is for the elements in reference [24], so the computing work will be twice as much as that for mesh I.

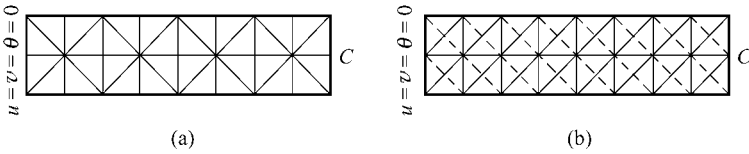


Figure 11.14 Meshes for Example 11.6

(a) Mesh I 8×2 ; (b) Mesh II 8×2

Table 11.6 The tip deflection of cantilever beam under tip shear load

Element	$100v_C/0.356\ 01$				
	8×2	16×4	32×8	64×16	
Mesh I					
T3(CST)	46.73	81.14	94.69	99.01	
GT9	94.41	98.74	99.76	99.98	
GT9M	95.60	99.10	99.86	99.85	
GT9M8	103.15	100.59	100.10	100.02	
Mesh II					
EFFAND ^[24]	101.68	100.30	100.03	100.00	
FF ^[24]	99.15	99.71	99.87	99.96	
	2×2	4×4	8×8	16×16	32×32
Mesh I					
T3(CST)	18.39	45.06	76.02	92.53	98.18
GT9	60.47	85.64	95.72	98.79	98.87
GT9M	61.65	86.24	95.91	98.84	99.88
GT9M8	92.13	97.37	99.08	99.67	99.89
Mesh II					
EFFAND ^[24]	92.24	96.99	98.70	99.48	98.81
FF ^[24]	89.26	96.37	98.66	99.50	99.83

Numerical results in Table 11.6 show that, the computational precision by the three presented elements GT9, GT9M and GT9M8 using mesh I is close to that of the elements in reference [24] using mesh II. And, in the 2 × 2 and 4 × 4 slim triangular meshes, the element GT9M8 exhibits much higher precision.

Example 11.7 Cook’s skew beam problem (3-node triangular element).

This problem is the same as Example 11.3. The mesh division can be referred to Fig. 11.4, and the results are listed in Table 11.7. It can be seen that the generalized conforming elements proposed in this chapter possess better performance than those of the other elements.

Table 11.7 Comparison of results for Cook’s skew beam problem (triangular elements)

Element	v_C (the vertical displacement at point C)			σ_{Amax} (the maximum stress at point A)			σ_{Bmin} (the minimum stress at point B)		
	2 × 2	4 × 4	8 × 8	2 × 2	4 × 4	8 × 8	2 × 2	4 × 4	8 × 8
T3(CST)	11.99	18.28	22.02	0.0760	0.1498	0.1999	-0.0360	-0.1002	-0.1567
EFFAND ^[24]	20.56	22.45	23.43						
FF ^[25]	20.36	22.42	23.41	0.1700	0.2129	0.2309	-0.1804	-0.1706	-0.1902
GT9	20.08	22.71	23.61	0.1610	0.2073	0.2266	-0.1467	-0.1721	-0.1900
GT9M	20.36	22.80	23.63	0.1650	0.2093	0.2274	-0.1519	-0.1734	-0.1905
GT9M8	21.75	23.21	23.74	0.1827	0.2171	0.2304	-0.1981	-0.1777	-0.1924
reference ^①	23.96			0.2362			-0.2023		

① Results by the element GT9M8 using 64 × 64 mesh.

11.5 Flat-Shell Elements—Triangular Thick/Thin Shell Element GMST18

The flat-shell element, which is composed of plate bending element and plane membrane element^[20], is the simplest shell element model, and widely used in the linear and nonlinear problems. Reviews on the general formulations and characteristics of the flat-shell element can be found in reference [26]. The appearance of the new generalized conforming membrane element with drilling freedoms and the new generalized conforming thin plate element makes it possible to construct high performance flat-shell elements.

Sects. 11.3 and 11.4 have introduced the concept of drilling freedom (the additional in-plane rigid vertex rotational freedom), and given the formulations of the new generalized conforming rectangular membrane element GR12 and triangular membrane elements GT9 and GT9M8 with drilling freedoms. Furthermore, in reference [27], the generalized conforming rectangular thin plate element GPL-R12 and triangular thin plate element GPL-T9 (this element has been

introduced in Sect. 6.3 of this book) are constructed. Then, in references [4–8], by starting with the generalized conforming theory and the degenerated potential energy principle, the above plane membrane and plate bending elements are used to formulate several generalized conforming flat-shell elements for the analysis of cylindrical and arbitrary shells:

(1) Generalized conforming rectangular flat-shell element GCR24^[5]: developed by the combination of the generalized conforming rectangular membrane element GR12 and the rectangular thin plate element GPL-R12;

(2) Generalized conforming triangular flat-shell element GST18^[4]: developed by the combination of the generalized conforming triangular membrane element GT9 and the triangular thin plate element GPL-T9, and one-point reduced integration scheme is used for GT9;

(3) Generalized conforming triangular flat-shell element GST18M^[8]: developed by the combination of the generalized conforming triangular membrane element GT9M8 and the triangular thin plate element GPL-T9.

Furthermore, reference [9] developed a generalized conforming triangular thick/thin flat-shell element GMST18. Firstly, the formulation of the generalized conforming triangular membrane element GT9 is employed as the membrane component of the shell element. Both one-point reduced integration scheme and a corresponding stabilization matrix proposed by Fish et al.^[27] are adopted for avoiding membrane locking and hourglass phenomenon. Secondly, the bending component of the element comes from a new generalized conforming thick/thin plate element TSL-T9, which is derived based on the rational shear interpolation proposed in Chap. 8 and the SemiLoof conforming scheme in Sect. 6.6. In this section, as an example, the element GMST18 will be used to describe the construction procedure of the generalized conforming flat-shell element.

11.5.1 Two Component Parts of the Flat-Shell Element

As shown in Fig. 11.15, the flat-shell element in the local coordinate system $Oxyz$ is assembled by plane membrane and plate bending element.

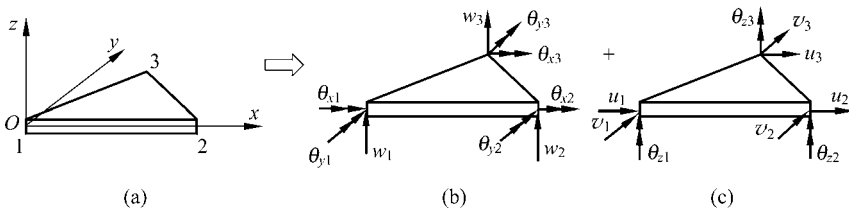


Figure 11.15 Flat-shell element in the local coordinate system $Oxyz$
 (a) Flat-shell element; (b) Plate bending element; (c) Membrane element

The element nodal displacement vector \mathbf{q}^e in local coordinate system $Oxyz$ is composed of the vertex freedoms:

$$\mathbf{q}^e = \begin{Bmatrix} \mathbf{q}_1^e \\ \mathbf{q}_2^e \\ \mathbf{q}_3^e \end{Bmatrix}, \quad \mathbf{q}_i^e = [u_i \quad v_i \quad w_i \quad \theta_{xi} \quad \theta_{yi} \quad \theta_{zi}]^T \quad (i = 1, 2, 3) \quad (11-133)$$

Let \mathbf{q}_m^e be the nodal displacement vector related to the membrane element, \mathbf{q}_p^e be the nodal displacement vector related to the plate element, then we have

$$\mathbf{q}_m^e = \begin{Bmatrix} \mathbf{q}_{m1}^e \\ \mathbf{q}_{m2}^e \\ \mathbf{q}_{m3}^e \end{Bmatrix}, \quad \mathbf{q}_{mi}^e = \begin{Bmatrix} u_i \\ v_i \\ \theta_{zi} \end{Bmatrix}, \quad \mathbf{q}_p^e = \begin{Bmatrix} \mathbf{q}_{p1}^e \\ \mathbf{q}_{p2}^e \\ \mathbf{q}_{p3}^e \end{Bmatrix}, \quad \mathbf{q}_{pi}^e = \begin{Bmatrix} w_i \\ \theta_{xi} \\ \theta_{yi} \end{Bmatrix} \quad (i = 1, 2, 3) \quad (11-134)$$

11.5.2 Membrane Part—Triangular Membrane Element GT9

The plane membrane element GT9 introduced in Sect. 11.4.1 is a triangular generalized conforming membrane element with additional rigid rotational freedoms, its element stiffness matrix \mathbf{K}_m^e is given by Eq. (11-97) to Eq. (11-99). In order to avoid membrane locking in the calculation of shells, one-point reduced integration is often employed for computing \mathbf{K}_m^e . But unfortunately, extra zero energy modes of the element will appear, and for some special cases, such as the twisted cantilever beam problem, the hourglass phenomenon may occur. Reference [28] suggested a method of adding a stabilization matrix to overcome this shortcoming. According to their approach, the stabilization matrix of the element GT9 is given as follows:

$$\mathbf{K}_{m \text{ stab}}^e = \bar{\omega} \begin{bmatrix} 0 & 0 & 0 & 0 & 0 & 0 & 0 & 0 & 0 \\ 0 & 0 & 0 & 0 & 0 & 0 & 0 & 0 & 0 \\ 0 & 0 & 2 & 0 & 0 & -1 & 0 & 0 & -1 \\ \hline 0 & 0 & 0 & 0 & 0 & 0 & 0 & 0 & 0 \\ 0 & 0 & 0 & 0 & 0 & 0 & 0 & 0 & 0 \\ 0 & 0 & -1 & 0 & 0 & 2 & 0 & 0 & -1 \\ \hline 0 & 0 & 0 & 0 & 0 & 0 & 0 & 0 & 0 \\ 0 & 0 & 0 & 0 & 0 & 0 & 0 & 0 & 0 \\ 0 & 0 & -1 & 0 & 0 & -1 & 0 & 0 & 2 \end{bmatrix} \quad (11-135)$$

in which

$$\bar{\omega} = \frac{1}{3} \chi \left[\mathbf{K}_m^1(3, 3)^e + \mathbf{K}_m^1(6, 6)^e + \mathbf{K}_m^1(9, 9)^e \right] \quad (11-136)$$

where \mathbf{K}_m^{1e} denotes the element stiffness matrix of GT9 using one-point integration; χ is a perturbation factor. From numerical experiments, it is found that, when χ is not less than 10^{-6} , the rank and eigenvalues of the new shell element are correct. So, $\chi = 10^{-6}$ is adopted. Thus, the element stiffness matrix of GT9 in the local coordinate system can be modified as

$$\mathbf{K}_m^e = \mathbf{K}_m^{1e} + \mathbf{K}_{m \text{ stab}}^e \quad (11-137)$$

11.5.3 Plate Bending Part—Triangular Thick/Thin Plate Element TSL-T9

The triangular plate bending element TSL-T9 in the local coordinate system $Oxyz$ is shown in Fig. 11.16. The element nodal displacement vector is composed of deflection w and normal slopes ψ_x and ψ_y of the mid-surface

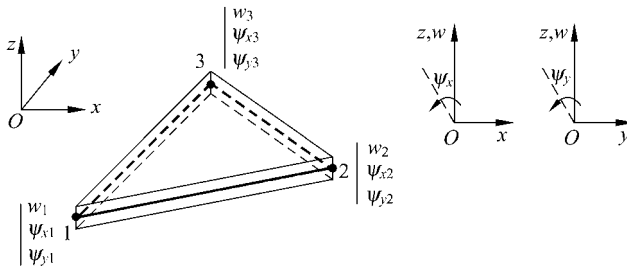


Figure 11.16 Triangular plate bending element TSL-T9

$$\bar{\mathbf{q}}^e = [w_1 \quad \psi_{x1} \quad \psi_{y1} \quad w_2 \quad \psi_{x2} \quad \psi_{y2} \quad w_3 \quad \psi_{x3} \quad \psi_{y3}]^T \quad (11-138)$$

Note that, since the definitions of the rotations (ψ_x , ψ_y and θ_x , θ_y) are different, there exists the following relation between $\bar{\mathbf{q}}^e$ and \mathbf{q}_p^e in Eq. (11-134):

$$\bar{\mathbf{q}}^e = \mathbf{L} \mathbf{q}_p^e, \quad \mathbf{L} = \begin{bmatrix} \mathbf{I} & \mathbf{0} & \mathbf{0} \\ \mathbf{0} & \mathbf{I} & \mathbf{0} \\ \mathbf{0} & \mathbf{0} & \mathbf{I} \end{bmatrix}, \quad \mathbf{I} = \begin{bmatrix} 1 & 0 & 0 \\ 0 & 0 & -1 \\ 0 & 1 & 0 \end{bmatrix}, \quad \mathbf{0} = \begin{bmatrix} 0 & 0 & 0 \\ 0 & 0 & 0 \\ 0 & 0 & 0 \end{bmatrix} \quad (11-139)$$

The construction procedure of the element shear strain fields is the same as that described in Sect. 8.5.3, then the final element shear strain field is

$$\boldsymbol{\gamma} = \mathbf{B}_s \mathbf{q}_p^e = \mathbf{H} \boldsymbol{\Delta}' \tilde{\mathbf{G}} \mathbf{L} \mathbf{q}_p^e \quad (11-140)$$

where \mathbf{B}_s is the element shear strain matrix; \mathbf{H} , $\boldsymbol{\Delta}'$ and $\tilde{\mathbf{G}}$ are given by Eqs. (8-137), (8-139) and (8-127), respectively.

The element deflection field is assumed to be the same as that of the thin plate element LSL-T9 introduced in Sect. 6.6, i.e.,

$$w = \mathbf{F}_\lambda \boldsymbol{\lambda} \quad (11-141)$$

where

$$\boldsymbol{\lambda} = [\lambda_1 \quad \lambda_2 \quad \lambda_3 \quad \lambda_4 \quad \lambda_5 \quad \lambda_6 \quad \lambda_7 \quad \lambda_8 \quad \lambda_9 \quad \lambda_{10} \quad \lambda_{11} \quad \lambda_{12}]^T \quad (11-142)$$

$$\mathbf{F}_\lambda = \begin{bmatrix} L_1 & L_2 & L_3 & L_2 L_3 & L_3 L_1 & L_1 L_2 & L_2 L_3 (L_2 - L_3) & L_3 L_1 (L_3 - L_1) \\ L_1 L_2 (L_1 - L_2) & L_1^2 L_2 L_3 & L_2^2 L_3 L_1 & L_3^2 L_1 L_2 \end{bmatrix} \quad (11-143)$$

According to the Mindlin plate theory, the element rotation fields are

$$\boldsymbol{\psi} = \begin{Bmatrix} \psi_x \\ \psi_y \end{Bmatrix} = \begin{Bmatrix} \frac{\partial w}{\partial x} - \gamma_{xz} \\ \frac{\partial w}{\partial y} - \gamma_{yz} \end{Bmatrix} = \begin{bmatrix} \mathbf{F}_{\lambda,x} \\ \mathbf{F}_{\lambda,y} \end{bmatrix} \boldsymbol{\lambda} - \mathbf{B}_s \mathbf{q}_p^e. \quad (11-144)$$

where $\mathbf{F}_{\lambda,x}$ and $\mathbf{F}_{\lambda,y}$ denote the derivative matrices of \mathbf{F}_λ with respect to x and y , respectively.

Along the element sides, deflection \tilde{w} is interpolated according to the thick beam theory, and the normal slope $\tilde{\psi}_n$ is assumed to be linearly distributed, as shown in Eq. (8-146).

The following 12 SemiLoof point conforming conditions (refer to Fig. 6.16)

$$(w - \tilde{w})_i = 0 \quad (i = 1, 2, 3) \quad (11-145)$$

$$(w - \tilde{w})_j = 0 \quad (j = 4, 5, 6) \quad (11-146)$$

$$(\psi_n - \tilde{\psi}_n)_k = 0 \quad (k = A_1, B_1, A_2, B_2, A_3, B_3) \quad (11-147)$$

are introduced. Equations (11-145) and (11-146) are the point conforming conditions about deflections at the corner nodes (nodes 1, 2, 3) and mid-side points (points 4, 5, 6), respectively; Eq. (11-147) denotes the point conforming conditions about the normal slopes at the Gauss points on the element side (points $A_1, B_1, A_2, B_2, A_3, B_3$).

Then, $\lambda_1, \lambda_2, \dots, \lambda_{12}$ can be obtained, in which the last 3 coefficients are equal to each other, i.e., $\lambda_{10} = \lambda_{11} = \lambda_{12}$. Therefore, Eq. (11-141) can be rewritten as

$$w = \mathbf{F}'_\lambda \boldsymbol{\lambda}' \quad (11-148)$$

where

$$\lambda' = [\lambda_1 \ \lambda_2 \ \lambda_3 \ \lambda_4 \ \lambda_5 \ \lambda_6 \ \lambda_7 \ \lambda_8 \ \lambda_9 \ \lambda_{10}]^T \quad (11-149)$$

$$F'_\lambda = [L_1 \ L_2 \ L_3 \ L_2 L_3 \ L_3 L_1 \ L_1 L_2 \ L_2 L_3 (L_2 - L_3) \ L_3 L_1 (L_3 - L_1) \ L_1 L_2 (L_1 - L_2) \ L_1 L_2 L_3] \quad (11-150)$$

λ' can be expressed in terms of the element nodal displacement vector

$$\lambda' = C \bar{q}^e \quad (11-151)$$

where

$$C = [C_1 \ C_2 \ C_3] \quad (11-152)$$

$$C_1 = \begin{bmatrix} 1 & 0 & 0 \\ 0 & 0 & 0 \\ 0 & 0 & 0 \\ 0 & 0 & 0 \\ 0 & -\frac{1}{2}c_2 & \frac{1}{2}b_2 \\ 0 & \frac{1}{2}c_3 & -\frac{1}{2}b_3 \\ \frac{1}{2}(r_2 + r_3) - \left(\frac{1}{3} + r_2\right)\delta_2 & \frac{1}{12}(c_1 - 3r_2c_2 + 3r_3c_3) & -\frac{1}{12}(b_1 - 3r_2b_2 + 3r_3b_3) \\ + \left(\frac{1}{3} - r_3\right)\delta_3 & + \frac{1}{6}(1 + 3r_2)c_2\delta_2 & -\frac{1}{6}(1 + 3r_2)b_2\delta_2 \\ & + \frac{1}{6}(1 - 3r_3)c_3\delta_3 & -\frac{1}{6}(1 - 3r_3)b_3\delta_3 \\ -\frac{1}{2}(3 + r_3) + \frac{8}{3}\delta_2 & -\frac{1}{12}(3r_3c_3 + c_3 - 8c_2) & \frac{1}{12}(3r_3b_3 + b_3 - 8b_2) + \frac{4}{3}b_2\delta_2 \\ + \left(\frac{1}{3} + r_3\right)\delta_3 & -\frac{4}{3}c_2\delta_2 + \frac{1}{6}(1 + 3r_3)c_3\delta_3 & -\frac{1}{6}(1 + 3r_3)b_3\delta_3 \\ \frac{1}{2}(3 - r_2) - \left(\frac{1}{3} - r_2\right)\delta_2 & \frac{1}{12}(3r_2c_2 - c_2 + 8c_3) & -\frac{1}{12}(3r_2b_2 - b_2 + 8b_3) \\ -\frac{8}{3}\delta_3 & + \frac{1}{6}(1 - 3r_2)c_2\delta_2 - \frac{4}{3}c_3\delta_3 & -\frac{1}{6}(1 - 3r_2)b_2\delta_2 + \frac{4}{3}b_3\delta_3 \\ (r_3 - r_2) + 2(r_2\delta_2 - r_3\delta_3) & \frac{1}{2}(r_2c_2 + r_3c_3) & -\frac{1}{2}(r_2b_2 + r_3b_3) \\ & -r_2c_2\delta_2 - r_3c_3\delta_3 & +r_2b_2\delta_2 + r_3b_3\delta_3 \end{bmatrix} \quad (11-153a)$$

$$\mathbf{C}_2 = \begin{bmatrix}
 0 & 0 & 0 \\
 1 & 0 & 0 \\
 0 & 0 & 0 \\
 0 & \frac{1}{2}c_1 & -\frac{1}{2}b_1 \\
 0 & 0 & 0 \\
 0 & -\frac{1}{2}c_3 & \frac{1}{2}b_3 \\
 \frac{1}{2}(3-r_3) - \left(\frac{1}{3}-r_3\right)\delta_3 & \frac{1}{12}(3r_3c_3 - c_3 + 8c_1) & -\frac{1}{12}(3r_3b_3 - b_3 + 8b_1) \\
 -\frac{8}{3}\delta_1 & +\frac{1}{6}(1-3r_3)c_3\delta_3 - \frac{4}{3}c_1\delta_1 & -\frac{1}{6}(1-3r_3)b_3\delta_3 + \frac{4}{3}b_1\delta_1 \\
 \frac{1}{2}(r_3+r_1) - \left(\frac{1}{3}+r_3\right)\delta_3 & \frac{1}{12}(c_2 - 3r_3c_3 + 3r_1c_1) & -\frac{1}{12}(b_2 - 3r_3b_3 + 3r_1b_1) \\
 +\left(\frac{1}{3}-r_1\right)\delta_1 & +\frac{1}{6}(1+3r_3)c_3\delta_3 & -\frac{1}{6}(1+3r_3)b_3\delta_3 \\
 & +\frac{1}{6}(1-3r_1)c_1\delta_1 & -\frac{1}{6}(1-3r_1)b_1\delta_1 \\
 -\frac{1}{2}(3+r_1) + \frac{8}{3}\delta_3 & -\frac{1}{2}(3r_1c_1 + c_1 - 8c_3) - \frac{4}{3}c_3\delta_3 & \frac{1}{12}(3r_1b_1 + b_1 - 8b_3) + \frac{4}{3}b_3\delta_3 \\
 +\left(\frac{1}{3}+r_1\right)\delta_1 & +\frac{1}{6}(1+3r_1)c_1\delta_1 & -\frac{1}{6}(1+3r_1)b_1\delta_1 \\
 (r_1-r_3) + 2(r_3\delta_3 - r_1\delta_1) & \frac{1}{2}(r_3c_3 + r_1c_1) & -\frac{1}{2}(r_3b_3 + r_1b_1) \\
 & -r_3c_3\delta_3 - r_1c_1\delta_1 & +r_3b_3\delta_3 + r_1b_1\delta_1
 \end{bmatrix}$$

(11-153b)

$$\mathbf{C}_3 = \begin{bmatrix}
 0 & 0 & 0 \\
 0 & 0 & 0 \\
 1 & 0 & 0 \\
 0 & -\frac{1}{2}c_1 & \frac{1}{2}b_1 \\
 0 & \frac{1}{2}c_2 & -\frac{1}{2}b_2 \\
 0 & 0 & 0 \\
 -\frac{1}{2}(3+r_2)+\frac{8}{3}\delta_1 & -\frac{1}{12}(3r_2c_2+c_2-8c_1)-\frac{4}{3}c_1\delta_1 & \frac{1}{12}(3r_2b_2+b_2-8b_1)+\frac{4}{3}b_1\delta_1 \\
 +\left(\frac{1}{3}+r_2\right)\delta_2 & +\frac{1}{6}(1+3r_2)c_2\delta_2 & -\frac{1}{6}(1+3r_2)b_2\delta_2 \\
 \frac{1}{2}(3-r_1)-\left(\frac{1}{3}-r_1\right)\delta_1 & \frac{1}{12}(3r_1c_1-c_1+8c_2) & -\frac{1}{12}(3r_1b_1-b_1+8b_2) \\
 -\frac{8}{3}\delta_2 & +\frac{1}{6}(1-3r_1)c_1\delta_1-\frac{4}{3}c_2\delta_2 & -\frac{1}{6}(1-3r_1)b_1\delta_1+\frac{4}{3}b_2\delta_2 \\
 \frac{1}{2}(r_1+r_2)-\left(\frac{1}{3}+r_1\right)\delta_1 & \frac{1}{12}(c_3-3r_1c_1+3r_2c_2) & -\frac{1}{12}(b_3-3r_1b_1+3r_2b_2) \\
 +\left(\frac{1}{3}-r_2\right)\delta_2 & +\frac{1}{6}(1+3r_1)c_1\delta_1 & -\frac{1}{6}(1+3r_1)b_1\delta_1 \\
 & +\frac{1}{6}(1-3r_2)c_2\delta_2 & -\frac{1}{6}(1-3r_2)b_2\delta_2 \\
 (r_2-r_1)+2(r_1\delta_1-r_2\delta_2) & \frac{1}{2}(r_1c_1+r_2c_2) & -\frac{1}{2}(r_1b_1+r_2b_2) \\
 & -r_1c_1\delta_1-r_2c_2\delta_2 & +r_1b_1\delta_1+r_2b_2\delta_2
 \end{bmatrix}$$

(11-153c)

in which b_i , c_i and r_i ($i=1,2,3$) are given by Eq. (6-58); δ_i ($i=1,2,3$) are given by the first equation in (8-114).

Substitution of Eq. (11-151) into Eq. (11-148) yields

$$w = \mathbf{F}'_{\lambda} \mathbf{C} \bar{\mathbf{q}}^e = \mathbf{F}'_{\lambda} \mathbf{C} \mathbf{L} \mathbf{q}_p^e = \mathbf{N}^e \mathbf{q}_p^e, \quad \mathbf{N}^e = \mathbf{F}'_{\lambda} \mathbf{C} \mathbf{L} \quad (11-154)$$

where N^e is the shape function matrix of the deflection w . It can be verified that, this deflection field and the rotation fields given by Eq. (11-144) determined by this deflection field satisfy the following generalized conforming condition

$$\oint_{\partial A^e} [Q_n(w - \tilde{w}) - M_n(\psi_n - \tilde{\psi}_n) - M_{ns}(\psi_s - \tilde{\psi}_s)] = 0 \quad (11-155)$$

where Q_n , M_n and M_{ns} denote the shear force, normal bending moment and tangent bending moment along the element boundary ∂A^e . Hence, the element derived here is a generalized conforming element, and its convergence can be ensured.

The rotation field ψ in Eq. (11-144) can be rewritten as

$$\psi = \begin{Bmatrix} \psi_x \\ \psi_y \end{Bmatrix} = \begin{Bmatrix} \frac{\partial w}{\partial x} - \gamma_{xz} \\ \frac{\partial w}{\partial y} - \gamma_{yz} \end{Bmatrix} = \left(\begin{bmatrix} F'_{\lambda,x} \\ F'_{\lambda,y} \end{bmatrix} C - B_s \right) L q_p^e \quad (11-156)$$

Then, the curvature field κ of the plate element is

$$\kappa = \begin{Bmatrix} \kappa_x \\ \kappa_y \\ 2\kappa_{xy} \end{Bmatrix} = \begin{Bmatrix} -\frac{\partial \psi_x}{\partial x} \\ -\frac{\partial \psi_y}{\partial y} \\ -\frac{\partial \psi_x}{\partial y} - \frac{\partial \psi_y}{\partial x} \end{Bmatrix} = \left(- \begin{bmatrix} F'_{\lambda,xx} \\ F'_{\lambda,yy} \\ 2F'_{\lambda,xy} \end{bmatrix} CL \right) q_p^e = B_b q_p^e \quad (11-157)$$

in which B_b is the bending strain matrix.

Thus, the element stiffness matrix of the thick/thin bending element TSL-T9 can be obtained

$$K_p^e = \iint_{A^e} B_b^T D_b B_b dA + \iint_{A^e} B_s^T D_s B_s dA \quad (11-158)$$

Numerical results show that the element TSL-T9 possesses excellent performance for both thin and thick plate bending problems. And, its stress solutions are also improved by the hybrid-enhanced post-processing procedure in reference [9]. Here we will not expand this in detail. Readers who are interested in it can refer to reference [9].

11.5.4 Stiffness Matrix of the Flat-Shell Element GMST18

Assembling Eqs.(11-137) and (11-158) according to the DOF's sequence given by Eq. (11-133), we obtain the element stiffness matrix K^e of the flat-shell element GMST18 in the local co-ordinates. And, after transforming K^e to the global

coordinates by standard procedure, the element can be used to calculate shell structures.

11.5.5 Numerical Examples

Here, the numerical results of the flat-shell element are given. For comparison, the results by other elements are also listed. All element models used are listed in Table 11.8.

Table 11.8 Shell elements for comparison (17 elements)

Element symbol	Element types	References
1. GMST18	3-node triangular generalized conforming thick/thin flat-shell element	[9]
2. GST18	3-node triangular generalized conforming thin flat-shell element	[4]
3. GST18M	3-node triangular generalized conforming thin flat-shell element	[8]
4. RTS18	3-node triangular thin flat-shell element	[29]
5. PROVIDAS	3-node triangular thin flat-shell element	[30]
6. DKT-CST-15RB	3-node triangular thin flat-shell element	[31]
7. OLSON	triangular thin flat-shell element	[22]
8. STRI3	3-node triangular thin flat-shell element in ABAQUS	[32]
9. S3R	3-node triangular 3D degenerated shell element in ABAQUS	[32]
10. GCR24	4-node rectangular generalized conforming thin flat-shell element	[5]
11. QUAD4	4-node quadrilateral 3D degenerated shell element	[33]
12. AQR8	8-node quadrilateral hybrid stress shell element	[34]
13. GUAN	9-node quadrilateral quasi-conforming 3D degenerated shell element	[35]
14. DKQ	4-node quadrilateral plate element based on discrete Kirchhoff assumption	[36]
15. MITC4	4-node quadrilateral plate element based on the mixed interpolation technique	[37]
16. T15-R	Reduced or selected reduced integration triangular degenerated shell element	[38]
17. RDTS15	Discrete refined 3-node triangular degenerated shell element	[38]

Example 11.8 Test of applicability for both thick and thin plates—a clamped square plate under uniform load.

A clamped square plate is subjected to a uniform load q . The side length $L = 100$, the thickness-span ratio varies from 10^{-15} to 0.6, and the material

constants are: $E = 10^6$ and $\mu = 0.3$. The whole plate is analyzed using the irregular mesh shown in Fig. 11.17. In Fig. 11.18, the deflection coefficients $w_c / (qL^4 / D)$ obtained by the several shell elements under different thickness-span ratios are given. It can be seen that, the element GMST18 can produce satisfactory results for both thin and thick plates, only the element RDTS15 is close to this element.

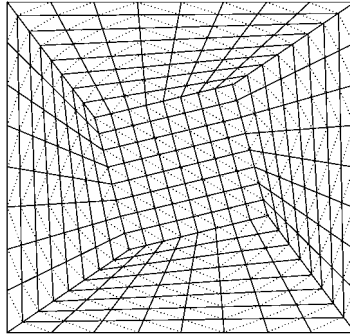


Figure 11.17 Irregular mesh for a square plate

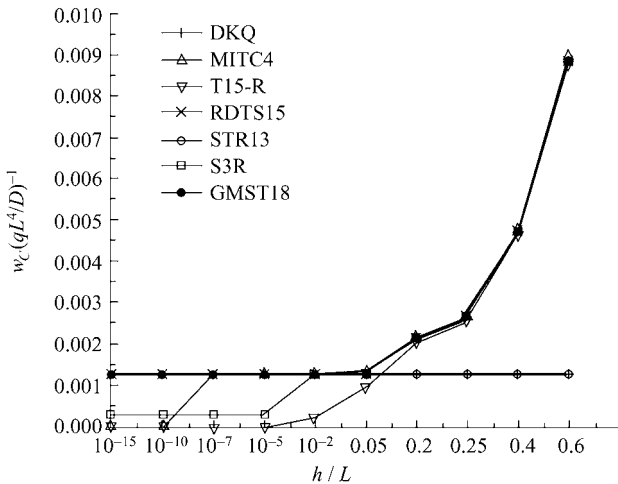


Figure 11.18 The variation of deflection coefficient with thickness-span ratio

Example 11.9 Scordelis-Lo Roof.

The cylindrical shell in Fig. 11.19 is supported by a rigid diaphragm at two ends and loaded vertically by its uniform dead weight. The theoretical solution from the deep shell theory for the vertical displacement at the midpoint of the free edge is $0.3008^{[39]}$. Because the shell is symmetric, only a quarter is taken for calculation.

Nondimensional results by different shell elements are listed in Tables 11.9

and 11.10. It can be seen that all the generalized conforming elements have good accuracy.

Example 11.10 Twisted Cantilever Beam.

A twisted cantilever beam is shown in Fig. 11.20. The free end is twisted 90° from the clamped end. Two types of load are applied to the free end of the beam: $P = 1.0, Q = 0.0$ and $P = 0.0, Q = 1.0$. The displacements in the direction of the load are reported in Table 11.11.

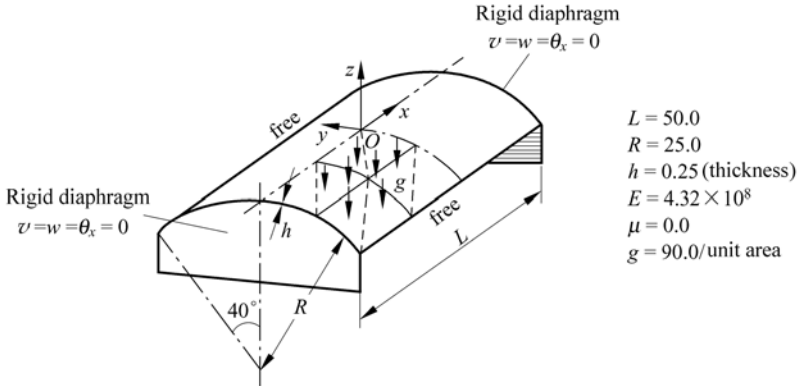


Figure 11.19 Scordelis-Lo roof

Table 11.9 Vertical displacement at the midpoint of free edge for Scordelis-Lo roof (rectangular and quadrilateral elements)

Mesh (1/4 shell)	QUAD4	AQR8	GUAN	GCR24
2 × 2	0.4161	0.3683	0.3078	0.3533
4 × 4	0.3175	0.3088	0.3033	0.3037
6 × 6	0.3078	0.3042		0.3011
8 × 8	0.3048	0.3033		0.3007
10 × 10	0.3036	0.3027		0.3006

Table 11.10 Vertical displacement at the midpoint of free edge for Scordelis-Lo roof (triangular elements)

Mesh (1/4 shell)	DKT-CST-15RB	OLSON	S3R	STRI3	GST18	GST18M	GMST18
2 × 2	0.2976	0.3809	0.2390	0.3310	0.3361	0.3525	0.3349
3 × 3		0.3024	0.2150	0.2221	0.2968	0.3027	0.2943
4 × 4	0.2144	0.2942			0.2921	0.2950	
5 × 5		0.2939			0.2931	0.2947	
6 × 6	0.2428		0.2438	0.2464	0.2947	0.2957	0.2946
8 × 8	0.2622		0.2627	0.2642	0.2969	0.2974	0.2965
10 × 10	0.2737	0.2970	0.2742	0.2751	0.2981	0.2984	0.2978

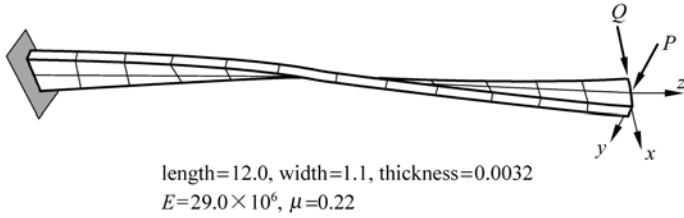


Figure 11.20 Twisted beam divided into 2 × 12 mesh

Table 11.11 Normalized deflection at the free edge of a cantilever twisted beam

Mesh	QUAD4	S3R	STRI3	RTS18	GST18	GST18M	GMST18
$P = 1.0, Q = 0.0$							
2 × 4		0.513	0.046	0.658			0.676
2 × 8		0.920	0.352	0.957			0.991
2 × 12	0.985	0.970	0.709	0.989	0.994	0.994	0.999
2 × 16		0.985	0.885	0.997			1.001
Theory	1294						
$P = 0.0, Q = 1.0$							
2 × 4		0.472	0.035	0.709			0.688
2 × 8		0.931	0.331	0.974			0.994
2 × 12	0.993	0.969	0.700	0.997	0.993	1.000	1.002
2 × 16		0.980	0.883	1.002			1.004
Theory	5256						

Example 11.11 Hemispherical shell.

As shown in Fig. 11.21, a hemispherical shell with a hole at the top is under two pairs of opposite radial concentrated loads at points *A* and *B*. Due to symmetry, only 1/4 of the hemispherical shell is analyzed. Results of the radial deflection at load points *A* and *B* are given in Table 11.12.

Table 11.12 Radial deflection at point *A* of the spherical under concentrated loads at *A* and *B*

Mesh	STRI3	S3R	RTS18	Providas	GST18	GST18M	GMST18
4 × 4	0.094	0.055	0.091	0.095	0.072	0.082	0.082
8 × 8	0.094	0.084	0.096	0.093	0.092	0.092	0.092
16 × 16	0.093	0.092	0.094 (14 × 14)		0.093	0.093	0.093
64 × 64	0.093	0.093					0.094
Comparison solution ^[29]						0.094	

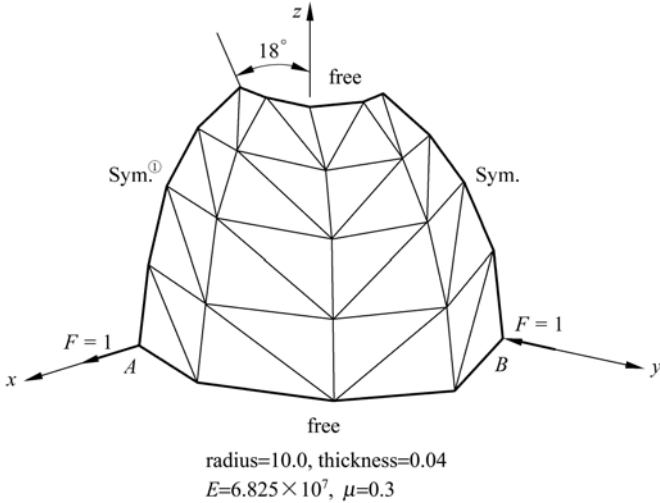


Figure 11.21 Hemispherical shell with hole at the top, mesh 8×8

11.6 Shallow Shell Element—Variational Principle and Membrane Locking Problem

Shell elements mainly have four discrete forms in geometry. Besides the flat-shell elements described above, there still are curved shell elements, degenerated shell elements derived from three-dimensional elements, and axisymmetric shell elements for the analysis of the shells of revolution. This section will introduce the construction procedure of the generalized conforming curved shell elements for shallow shells.

Reference [40] firstly takes the modified Hu-Washizu principle as the starting point, then, by introducing two types of the generalized conforming conditions and using the degenerated potential energy principle, it establishes a thick shallow shell element GC-S20 with 20 DOFs. For the bending part of the shell, the scheme proposed in reference [41] is adopted to eliminate the shear locking phenomenon; and for the membrane strain part of the shell, both displacement fields and membrane strain fields are assumed independently, and then by using the related generalized conforming conditions, membrane locking phenomenon can be eliminated. Reference [42] extends the generalized conforming rectangular thin plate elements RGC-12^[14], LGC-R12^[43] and triangular element TGC-9^[14] to various shallow shell elements for the first time, but only the rectangular elements can pass the membrane locking test. Thereupon reference [42] continues the study on the membrane locking problem, and successfully constructs the generalized conforming rectangular and triangular shallow shell elements with mid-side nodes, which can completely avoid the membrane locking phenomenon.

① Sym. is the abbreviation for symmetrical.

11.6.1 Variational Principle for Shallow Shells and Its Degenerate Form

Let the base plane of the shallow shell be the xOy plane, and the z -axis be normal to the base plane. Then, the mid-surface equation of the shallow shell is

$$z = z(x, y) \quad (11-159)$$

The initial curvatures of the mid-surface are

$$\kappa_x^0 = -\frac{\partial^2 z}{\partial x^2} = \frac{1}{R_x}, \quad \kappa_y^0 = -\frac{\partial^2 z}{\partial y^2} = \frac{1}{R_y}, \quad \kappa_{xy}^0 = -\frac{\partial^2 z}{\partial x \partial y} = \frac{1}{R_{xy}} \quad (11-160)$$

where R_x , R_y and R_{xy} are the reciprocal values of the corresponding curvatures, respectively.

In shallow shell elements, the following quantities need to be assumed:

Displacements of mid-surface u, v, w

Membrane strains $\boldsymbol{\varepsilon} = [\varepsilon_x \quad \varepsilon_y \quad \gamma_{xy}]^T$

The curvatures derived from the displacements are

$$\boldsymbol{\kappa} = [\kappa_x \quad \kappa_y \quad 2\kappa_{xy}]^T = \left[-\frac{\partial^2 w}{\partial x^2} \quad -\frac{\partial^2 w}{\partial y^2} \quad -2\frac{\partial^2 w}{\partial x \partial y} \right]^T \quad (11-161)$$

And, the membrane strains derived from the displacements are

$$\hat{\boldsymbol{\varepsilon}} = [\hat{\varepsilon}_x \quad \hat{\varepsilon}_y \quad \hat{\gamma}_{xy}]^T = \left[\frac{\partial u}{\partial x} + \frac{w}{R_x} \quad \frac{\partial v}{\partial y} + \frac{w}{R_y} \quad \frac{\partial v}{\partial x} + \frac{\partial u}{\partial y} + 2\frac{w}{R_{xy}} \right]^T \quad (11-162)$$

For thin shallow shell, the modified Hu-Washizu functional can be written as

$$\Pi^e = \Pi_1^e + \Pi_2^e \quad (11-163)$$

where Π_1^e is the energy due to the bending deformation of the shallow shell element,

$$\Pi_1^e = \iint_{A^e} \frac{1}{2} \boldsymbol{\kappa}^T \mathbf{D}_b \boldsymbol{\kappa} dA + \oint_{\partial A^e} [M_n \left(\frac{\partial w}{\partial n} - \frac{\partial \tilde{w}}{\partial n} \right) + M_{ns} \left(\frac{\partial w}{\partial s} - \frac{\partial \tilde{w}}{\partial s} \right) - Q_n (w - \tilde{w})] ds \quad (11-164)$$

in which A^e is the projection area of the element; ∂A^e is the element boundary; M_n , M_{ns} and Q_n are the bending moment, twisting moment and transverse shear force on the element boundary; w , $\frac{\partial w}{\partial n}$ and $\frac{\partial w}{\partial s}$ are the displacements on the

element boundary determined by the element deflection field; \tilde{w} , $\frac{\partial \tilde{w}}{\partial n}$ and $\frac{\partial \tilde{w}}{\partial s}$ are the given displacements on the element boundary; \mathbf{D}_b is the elastic matrix for thin plate bending,

$$\mathbf{D}_b = \frac{Eh^3}{12(1-\mu^2)} \begin{bmatrix} 1 & \mu & 0 \\ \mu & 1 & 0 \\ 0 & 0 & \frac{1-\mu}{2} \end{bmatrix}$$

where h is the thickness of the shell; E is the Young's modulus; μ is the Poisson's ratio.

Π_2^e is the energy due to the membrane deformation of the shallow shell element,

$$\Pi_2^e = \iint_{A^e} \left[\frac{1}{2} \boldsymbol{\varepsilon}^T \mathbf{D}_m \boldsymbol{\varepsilon} - \mathbf{N}^T (\boldsymbol{\varepsilon} - \hat{\boldsymbol{\varepsilon}}) \right] dA \quad (11-165)$$

in which $\boldsymbol{\varepsilon}$ is the assumed element membrane strain vector; \mathbf{N} is the element membrane stress vector; \mathbf{D}_m is the elastic matrix for thin membrane deformation (i.e., the elastic matrix for plane stress problem),

$$\mathbf{D}_m = \frac{Eh}{1-\mu^2} \begin{bmatrix} 1 & \mu & 0 \\ \mu & 1 & 0 \\ 0 & 0 & \frac{1-\mu}{2} \end{bmatrix}$$

The displacement mode of the generalized conforming thin plate element is taken as the interpolation function for the normal displacement of the shallow shell element, when the mesh is refined by infinite elements, it satisfies

$$\oint_{\partial A^e} \left[M_n \left(\frac{\partial w}{\partial n} - \frac{\partial \tilde{w}}{\partial n} \right) + M_{ns} \left(\frac{\partial w}{\partial s} - \frac{\partial \tilde{w}}{\partial s} \right) - Q_n (w - \tilde{w}) \right] ds = 0 \quad (11-166)$$

When the mesh is refined by infinite elements, i.e., the element is under the limit state of constant internal forces, the second term in Eq. (11-165) should satisfy the following generalized conforming conditions

$$\iint_{A^e} \mathbf{N}^T (\boldsymbol{\varepsilon} - \hat{\boldsymbol{\varepsilon}}) dA = 0 \quad (11-167)$$

Here, the energy functional degenerates to the following simplified form

$$\Pi^e = \iint_{A^e} \left[\frac{1}{2} \boldsymbol{\kappa}^T \mathbf{D}_b \boldsymbol{\kappa} + \frac{1}{2} \boldsymbol{\varepsilon}^T \mathbf{D}_m \boldsymbol{\varepsilon} \right] dA \quad (11-168)$$

Then, according to Eq. (1-168), the stiffness matrix for the shallow shell element can be derived conveniently.

11.6.2 Notes on the Membrane Locking Problem

From Eq. (11-162), it can be seen that, the membrane strains are not only related to the tangential displacements u and v , but also related to the normal displacement w . The reason leading to membrane locking comes from the mismatching between the tangential displacements u , v and the normal displacement w in the assumed displacement mode for the shallow shell element, so that the displacement state of the rigid-body motion of the element cannot be presented. In order that the rigid-body motion of the element can be presented, the following zero strain state must come into existence

$$\kappa_x = -\frac{\partial^2 w}{\partial x^2} = 0, \quad \kappa_y = -\frac{\partial^2 w}{\partial y^2} = 0, \quad \kappa_{xy} = -2\frac{\partial^2 w}{\partial x \partial y} = 0 \quad (11-169)$$

$$\varepsilon_x = \frac{\partial u}{\partial x} + \frac{w}{R_x} = 0, \quad \varepsilon_y = \frac{\partial v}{\partial y} + \frac{w}{R_y} = 0, \quad \gamma_{xy} = \frac{\partial v}{\partial x} + \frac{\partial u}{\partial y} + \frac{2w}{R_{xy}} = 0 \quad (11-170)$$

From the first expression of Eq. (11-169), we obtain

$$w = xf_1(y) + f_2(y) \quad (11-171)$$

Substitution of the above equation into the last two expressions of Eq. (11-169) yields

$$f_1(y) = C_1, \quad f_2(y) = C_2 y + C_3 \quad (11-172)$$

where C_1 , C_2 and C_3 are constants. Thereby, the normal displacement should be the following linear function

$$w = C_1 x + C_2 y + C_3 \quad (11-173)$$

Substituting Eq. (11-173) into the first two expressions of Eq. (11-170), and assume that R_x , R_y and R_{xy} are constants, we can obtain

$$\left. \begin{aligned} u &= -\frac{1}{R_x} \left[\frac{C_1}{2} x^2 + C_2 xy + C_3 x + g_1(y) \right] \\ v &= -\frac{1}{R_y} \left[C_1 xy + \frac{C_2}{2} y^2 + C_3 y + g_2(x) \right] \end{aligned} \right\} \quad (11-174)$$

Substitution of u and v into the third expression of Eq. (11-170) yields

$$-\frac{1}{R_y} g_2'(x) - \frac{C_2}{R_x} x + \frac{2C_1}{R_{xy}} x + \frac{2C_3}{R_{xy}} = \frac{1}{R_x} g_1'(y) + \frac{C_1}{R_y} y - \frac{2C_2}{R_{xy}} y \quad (11-175)$$

The above equation exists for arbitrary x and y , then we have

$$\left. \begin{aligned} g_2'(x) &= -\frac{R_y}{R_x} C_2 x + \frac{2R_y}{R_{xy}} C_1 x + \frac{2R_y}{R_{xy}} C_3 - C_4 R_y \\ g_1'(y) &= -\frac{R_x}{R_y} C_1 y + \frac{2R_x}{R_{xy}} C_2 y + C_4 R_x \end{aligned} \right\} \quad (11-176)$$

Thereupon, it can be easily obtained that

$$\left. \begin{aligned} g_2(x) &= -\frac{R_y}{2R_x} C_2 x^2 + \frac{R_y}{R_{xy}} C_1 x^2 + \frac{2R_y}{R_{xy}} C_3 x - C_4 R_y x + C_5 \\ g_1(y) &= -\frac{R_x}{2R_y} C_1 y^2 + \frac{R_x}{R_{xy}} C_2 y^2 + C_4 R_x y + C_6 \end{aligned} \right\} \quad (11-177)$$

in which C_4 , C_5 and C_6 are all constants. Substitution of Eq. (11-177) into Eq. (11-174) yields

$$\left. \begin{aligned} u &= -\frac{1}{2R_x} C_1 x^2 - \frac{1}{R_x} C_2 xy + \left(\frac{1}{2R_y} C_1 - \frac{1}{R_{xy}} C_2 \right) y^2 - \frac{1}{R_x} C_3 x - C_4 y - \frac{1}{R_x} C_6 \\ v &= \left(\frac{1}{2R_x} C_2 - \frac{1}{R_{xy}} C_1 \right) x^2 - \frac{1}{R_y} C_1 xy - \frac{1}{2R_y} C_2 y^2 - \left(\frac{2}{R_{xy}} C_3 - C_4 \right) x - \frac{1}{R_y} C_3 y - \frac{1}{R_y} C_5 \end{aligned} \right\} \quad (11-178)$$

Let

$$\theta_0 = C_4 - \frac{C_3}{R_{xy}}, \quad u_0 = -\frac{C_6}{R_x}, \quad v_0 = -\frac{C_5}{R_y} \quad (11-179)$$

Then, Eq. (11-178) can be rewritten as

$$\left. \begin{aligned} u &= -\frac{1}{2R_x} C_1 x^2 - \frac{1}{R_x} C_2 xy + \left(\frac{1}{2R_y} C_1 - \frac{1}{R_{xy}} C_2 \right) y^2 - \frac{1}{R_x} C_3 x - \frac{1}{R_{xy}} C_3 y - \theta_0 y + u_0 \\ v &= \left(\frac{1}{2R_x} C_2 - \frac{1}{R_{xy}} C_1 \right) x^2 - \frac{1}{R_y} C_1 xy - \frac{1}{2R_y} C_2 y^2 - \frac{1}{R_{xy}} C_3 x - \frac{1}{R_y} C_3 y + \theta_0 x + v_0 \end{aligned} \right\} \quad (11-180)$$

Equations (11-173) and (11-180) can be written together in the following form

$$\begin{Bmatrix} w \\ u \\ v \end{Bmatrix} = \begin{bmatrix} x & y & 1 \\ -\frac{x^2}{2R_x} + \frac{y^2}{2R_y} & -\frac{xy}{R_x} - \frac{y^2}{R_{xy}} & -\frac{x}{R_x} - \frac{y}{R_{xy}} \\ -\frac{x^2}{R_{xy}} - \frac{xy}{R_y} & \frac{x^2}{2R_x} - \frac{y^2}{2R_y} & -\frac{x}{R_{xy}} - \frac{y}{R_y} \end{bmatrix} \begin{Bmatrix} C_1 \\ C_2 \\ C_3 \end{Bmatrix} + \begin{Bmatrix} 0 \\ u_0 - \theta_0 y \\ v_0 + \theta_0 x \end{Bmatrix} \quad (11-181)$$

The second term on the right-side of the above equation denotes the displacement of the rigid-body motion when there is no normal displacement, and the first term denotes the displacement of the rigid-body motion when the normal displacement exists.

According to the above demonstration, the following deduction can be obtained.

Deduction If the shallow shell element can embody the displacement state of the rigid-body motion, the interpolation formulas for tangential displacements u, v should at least include the complete quadric polynomial.

From this conclusion, it follows that, the appearance of the membrane locking phenomena of some curved shell elements is just because the assumed tangential displacement trial functions cannot satisfy the above requirement.

11.7 Shallow Shell Element—Triangular Element SST21 with Mid-Side Nodes

Triangular shallow shell elements often suffer from the membrane locking phenomenon. In order to overcome this difficulty, some successful displacement-based triangular shallow shell elements are almost the high-order elements using high-order interpolation functions for tangential displacements. For example, in reference [44], tangential and normal displacements all adopt the cubic interpolation functions, and the triangular shallow shell elements with 36 and 27 DOFs are then constructed, respectively; in reference [45], the interpolation functions for the tangential and normal displacements are assumed to be complete cubic and incomplete quintic polynomials, respectively, and a triangular shallow shell element with 2 internal DOFs and 36 external DOFs is then constructed. In order to increase the order of the tangential displacement functions to quadric, the tangential freedoms at the mid-side nodes are considered. This is the scheme for the generalized conforming shallow shell element SST21. Here, we will introduce the construction procedure of this model.

11.7.1 The Local Coordinate System and the Geometric Description of the Element Surface

A triangular shallow shell element is shown in Fig. 11.22. The base plane of the element is formed by linking three corner nodes; let node 1 be the origin of the local coordinate system $Oxyz$, the linking line of nodes 1 and 2 be the x -axis, and xy plane be within the base plane of the element.

Assume that the element surface is a quadric surface in the local coordinate system, and can be expressed in terms of the area coordinates as

$$z = h_1L_1 + h_2L_2 + h_3L_3 + h_4L_1L_2 + h_5L_2L_3 + h_6L_3L_1 \tag{11-182}$$

Substituting the coordinates of the three corner nodes and three mid-side nodes into the above equation in turn, the coefficients h_i can be obtained:

$$\mathbf{h} = \begin{Bmatrix} h_1 \\ h_2 \\ h_3 \\ h_4 \\ h_5 \\ h_6 \end{Bmatrix} = \begin{bmatrix} 1 & 0 & 0 & 0 & 0 & 0 \\ 0 & 1 & 0 & 0 & 0 & 0 \\ 0 & 0 & 1 & 0 & 0 & 0 \\ -2 & -2 & 0 & 4 & 0 & 0 \\ 0 & -2 & -2 & 0 & 4 & 0 \\ -2 & 0 & -2 & 0 & 0 & 4 \end{bmatrix} \begin{Bmatrix} z_1 \\ z_2 \\ z_3 \\ z_4 \\ z_5 \\ z_6 \end{Bmatrix} \tag{11-183}$$

Substituting Eq. (11-183) into Eq. (11-182) (note that the local z -coordinates of the 3 corner nodes in Fig. 11.22 are all zero), we can obtain

$$z = 4(z_4L_1L_2 + z_5L_2L_3 + z_6L_3L_1) \tag{11-184}$$

From the above equation, the initial curvatures of the element, and the transformations between local and global coordinates can be derived.

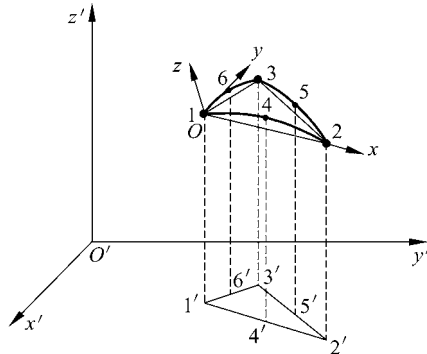


Figure 11.22 Triangular shallow shell element

11.7.2 Selection of DOFs and Determination of Displacement Functions

A triangular shallow shell element with mid-side nodes is shown in Fig. 11.23(a), it is composed of the 3-node bending element in Fig. 11.23(b) and 6-node membrane element in Fig. 11.23(c).

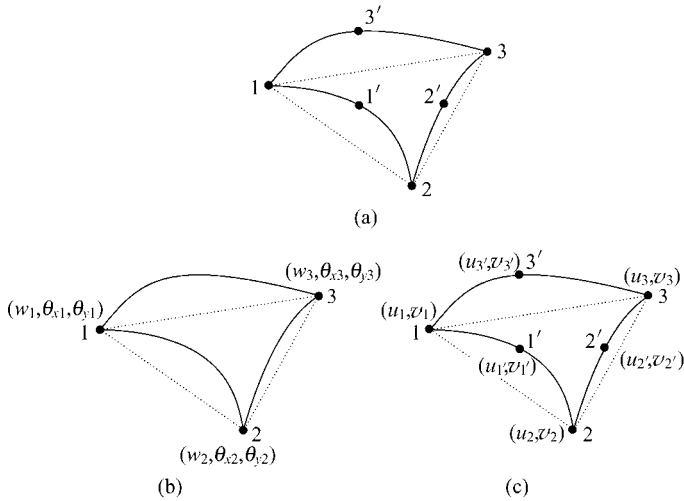


Figure 11.23 Triangular shallow shell element SST21

- (a) Triangular shallow shell element with mid-side nodes;
- (b) 3-node bending element; (c) 6-node membrane element

The element nodal displacement vector in local coordinate system is

$$\bar{\mathbf{q}}^e = [\mathbf{q}_1^T \quad \mathbf{q}_{1'}^T \quad \mathbf{q}_2^T \quad \mathbf{q}_{2'}^T \quad \mathbf{q}_3^T \quad \mathbf{q}_{3'}^T]^T \quad (11-185)$$

where

$$\mathbf{q}_i = [u_i \quad v_i \quad w_i \quad \theta_{xi} \quad \theta_{yi}]^T, \quad \mathbf{q}_{i'} = [u_{i'} \quad v_{i'}]^T, \quad \theta_{xi} = \left(\frac{\partial w}{\partial y} \right)_i, \quad \theta_{yi} = - \left(\frac{\partial w}{\partial x} \right)_i \quad (11-186)$$

For convenience, the bending displacements and membrane displacements are separated as

$$\mathbf{q}^{me} = [u_1 \quad v_1 \quad u_{1'} \quad v_{1'} \quad u_2 \quad v_2 \quad u_{2'} \quad v_{2'} \quad u_3 \quad v_3 \quad u_{3'} \quad v_{3'}]^T \quad (11-187)$$

$$\mathbf{q}^{be} = [w_1 \quad \theta_{x1} \quad \theta_{y1} \quad w_2 \quad \theta_{x2} \quad \theta_{y2} \quad w_3 \quad \theta_{x3} \quad \theta_{y3}]^T \quad (11-188)$$

The tangential displacements of the shell element are assumed to be the displacement fields of the 6-node quadric triangular membrane element, which are the compatible displacement modes:

$$\mathbf{u} = \begin{Bmatrix} u \\ v \end{Bmatrix} = \sum_{i=1}^3 \mathbf{N}_i \mathbf{q}_i^m \quad (11-189)$$

in which

$$\mathbf{N}_i = \begin{bmatrix} (2L_i - 1)L_i & 0 & 4L_j L_m & 0 \\ 0 & (2L_i - 1)L_i & 0 & 4L_j L_m \end{bmatrix} \quad (i, j, m = 1, 2, 3) \quad (11-190)$$

$$\mathbf{q}_i^m = [u_i \quad v_i \quad u_{i'} \quad v_{i'}]^T \quad (11-191)$$

And, the normal displacements of the shell element are assumed to be displacement fields of the generalized conforming 3-node triangular plate element TGC-9 introduced in Sect. 6.1.1.

11.7.3 Element Stiffness Matrix

The element membrane strains are

$$\boldsymbol{\varepsilon} = [\varepsilon_x \quad \varepsilon_y \quad \gamma_{xy}]^T = \left[\frac{\partial u}{\partial x} + \frac{w}{R_x} \quad \frac{\partial v}{\partial y} + \frac{w}{R_y} \quad \frac{\partial v}{\partial x} + \frac{\partial u}{\partial y} + 2 \frac{w}{R_{xy}} \right]^T = \mathbf{B}_m \mathbf{q}^{me} + \mathbf{B}_{mw} \mathbf{q}^{be} \quad (11-192)$$

where

$$\mathbf{B}_m = [\mathbf{B}_{m1} \quad \mathbf{B}_{m2} \quad \mathbf{B}_{m3}] \quad (11-193)$$

$$\mathbf{B}_{mi} = \frac{1}{2A} \begin{bmatrix} b_i(2L_i - 1) & 0 & 4(b_j L_m + b_m L_j) & 0 \\ 0 & c_i(2L_i - 1) & 0 & 4(c_j L_m + c_m L_j) \\ c_i(2L_i - 1) & b_i(2L_i - 1) & 4(c_j L_m + c_m L_j) & 4(b_j L_m + b_m L_j) \end{bmatrix} \quad (11-194)$$

$(i, j, m = 1, 2, 3)$

$$b_i = y_j - y_m, \quad c_i = -(x_j - x_m) \quad (11-195)$$

A is the area of the base plane of the element; and

$$\mathbf{B}_{mw} = \begin{bmatrix} \frac{1}{R_x} F_\lambda \hat{\mathbf{C}}^{-1} \hat{\mathbf{G}} \\ \frac{1}{R_y} F_\lambda \hat{\mathbf{C}}^{-1} \hat{\mathbf{G}} \\ \frac{2}{R_{xy}} F_\lambda \hat{\mathbf{C}}^{-1} \hat{\mathbf{G}} \end{bmatrix} \quad (11-196)$$

where F_λ is given by Eq. (6-3), $\hat{\mathbf{G}}$ and $\hat{\mathbf{C}}$ can be expressed as follows:

$$\hat{\mathbf{G}} = \begin{bmatrix} 0 & 0 & 0 & -1 & 0 & 0 & 1 & 0 & 0 \\ 1 & 0 & 0 & 0 & 0 & 0 & -1 & 0 & 0 \\ 0 & -b_1 & -c_1 & 0 & -b_2 & -c_2 & 0 & -b_3 & -c_3 \\ 0 & 0 & 0 & 6 & -b_1 & -c_1 & 6 & b_1 & c_1 \\ 6 & b_2 & c_2 & 0 & 0 & 0 & 6 & -b_2 & -c_2 \\ 6 & -b_3 & -c_3 & 6 & b_3 & c_3 & 0 & 0 & 0 \\ 0 & 0 & 0 & 0 & c_1 & -b_1 & 0 & c_1 & -b_1 \\ 0 & c_2 & -b_2 & 0 & 0 & 0 & 0 & c_2 & -b_2 \\ 0 & c_3 & -b_3 & 0 & c_3 & -b_3 & 0 & 0 & 0 \end{bmatrix} \quad (11-197)$$

$$\hat{\mathbf{C}} = \begin{bmatrix} 0 & -1 & 1 & 0 & 0 & 0 & 0 & 0 & 0 \\ 1 & 0 & -1 & 0 & 0 & 0 & 0 & 0 & 0 \\ 0 & 0 & 0 & -1 & -1 & -1 & 1 & 1 & 1 \\ 0 & 6 & 6 & 0 & 1 & 0 & 0 & 0 & 1 \\ 6 & 0 & 6 & 0 & 0 & 1 & 1 & 0 & 0 \\ 6 & 6 & 0 & 1 & 0 & 0 & 0 & 1 & 0 \\ \frac{f_2 + f_3}{A} & \frac{-f_3}{A} & \frac{-f_2}{A} & F_2 & -3F_2 & 5F_2 & F_2 & 5F_2 & -3F_2 \\ \frac{-f_3}{A} & \frac{f_3 + f_1}{A} & \frac{-f_1}{A} & 5F_3 & F_3 & -3F_3 & -3F_3 & F_3 & 5F_3 \\ \frac{-f_2}{A} & \frac{-f_1}{A} & \frac{f_1 + f_2}{A} & -3F_1 & 5F_1 & F_1 & 5F_1 & -3F_1 & F_1 \end{bmatrix} \quad (11-198)$$

$$\left. \begin{aligned} f_i &= -(b_j b_m + c_j c_m) \\ F_i &= \frac{f_i + f_j}{12A} \end{aligned} \right\} (i, j, m = 1, 2, 3) \quad (11-199)$$

The element bending strain matrix B_b can be obtained by the conventional procedure. According to the sequence of DOFs given in Eq. (11-185), B_m , B_{mw} and B_b can be expanded to 3×21 matrices, and then, can be assembled to form the total strain matrix B . Thus, the element stiffness matrix in the element local coordinate system can be written as

$$\bar{K}^e = \iint_{A^e} B^T D B dA \tag{11-200}$$

with

$$D = \begin{bmatrix} D_m & 0 \\ 0 & D_b \end{bmatrix} \tag{11-201}$$

Then, it can be transformed to the global coordinate system for the finite element solution.

11.7.4 Numerical Examples

Example 11.12 Scordelis-Lo roof problem.

As shown in Fig. 11.24, this problem is the same as the Example 11.9. The analytical solution of the shallow shell is used for comparison. The results are listed in Tables 11.13 and 11.14, in which Table 11.13 gives the vertical displacements of the center point of the roof and the mid-side point of the free edge obtained by different meshes; Table 11.14 gives the displacement results of the different points using 8×12 mesh. It can be seen that the element SST21 can successfully pass the membrane locking test, and converge to the analytical solution of the shallow shell.

Table 11.13 The vertical displacements of the center point of the cylindrical shell and the mid-side point of the free edge (membrane locking test)

Mesh	SST21 (21 DOFs)		Reference [44] (27 DOFs)		Reference [44] (36 DOFs)	
	w_B	w_C	w_B	w_C	w_B	w_C
2×3	0.171	-0.0068	0.211		0.323	-0.044
4×5	0.287	-0.0416	0.297	-0.0400	0.315	-0.0448
8×12	0.307	-0.0433	0.309	-0.0436		
Analytical solution of shallow shell ^[46]	0.308	-0.046	0.308	-0.046	0.308	-0.046

Table 11.14 The displacements of different points on the cylindrical shell (8×12 mesh)

Point		A	B	2	3	4	C
u	SST21	0.0126	0	0	0	0	0
	Analytical ^[46]	0.0126	0	0	0	0	0
v	SST21	0	-0.164	-0.0836	-0.0294	-0.0046	0
	Analytical ^[46]	0	-0.164	-0.082	-0.028	-0.004	0
w	SST21	0	0.307	0.192	0.0774	-0.0104	-0.0433
	Analytical ^[46]	0	0.308	0.190	0.076	-0.012	-0.046

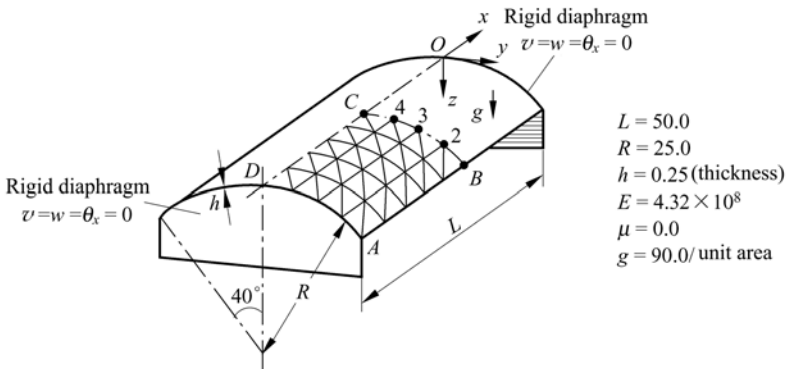


Figure 11.24 Scordelis-Lo roof. Mesh by shallow shell element 4×5

Example 11.13 Doubly curved shallow shell.

A simply-supported doubly curved shallow shell subjected to uniform vertical load q is shown in Fig. 11.25. Equation of its mid-surface is $z = 0.5k(x^2 + y^2)$. Due to symmetry, only 1/4 of the shell is analyzed. The results are listed in Table 11.15.

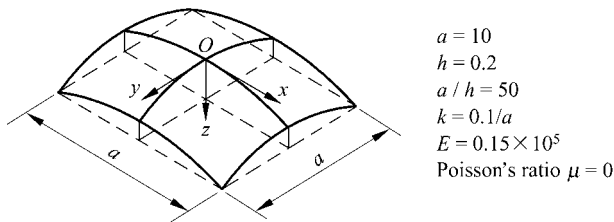


Figure 11.25 A doubly curved shallow shell

Table 11.15 The central vertical displacement of the doubly curved shallow shell $w/(10^{-3}qaD^{-1})$

Mesh for 1/4 shell	1×1	2×2	4×4	6×6
SST21	4.29	4.01	3.99	3.99
Analytical solution	3.99			

Example 11.14 Hyperbolic paraboloid shell.

A clamped hyperbolic paraboloid shell subjected to uniformly distributed normal load q is shown in Fig. 11.26. The results are listed in Table 11.16.

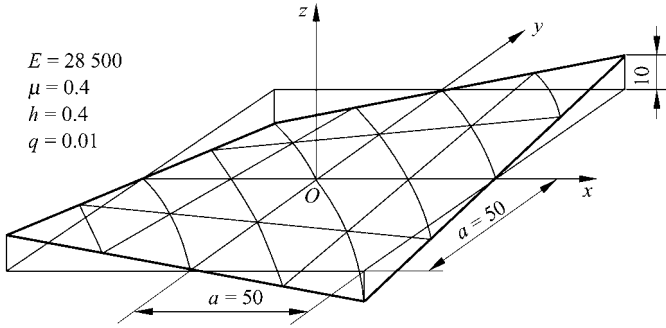


Figure 11.26 Hyperbolic paraboloid shell

Table 11.16 The central vertical displacement of the hyperbolic paraboloid shell

Element \ Mesh	2 × 2	4 × 4	8 × 8	12 × 12
SST21 (21 DOFs)	-0.0326	-0.0315	-0.0250	-0.0248
Reference [44] (27 DOFs)		-0.0345	-0.0283	
Reference [44] (36 DOFs)	-0.044	-0.0275	-0.0263	
Finite difference solution	-0.02459			

11.8 Shell Element for Geometrically Nonlinear Analysis — Triangular Flat-Shell Element GMST18

On the basis of the generalized conforming thick/thin triangular flat-shell element GMST18 (refer to Sect. 11.4), reference [9] derives the UL (Updated Lagrangian) formulations of the element for the analysis of geometrically nonlinear problems, which exhibit good performance for numerical examples.

In the incremental method, all the physical components of a structure from time 0 to time t are assumed to have been obtained. What we are interested in is the increment that occurs from time t to time $t + \Delta t$. The reference configuration is the configuration at time t . The principle of virtual displacement expressed by the UL method can be written as

$$\iiint_V ({}^{t+\Delta t}\sigma_{ij}) \delta ({}^{t+\Delta t}\epsilon_{ij}) dV = {}^{t+\Delta t}W \tag{11-202}$$

where ${}^{t+\Delta t}\sigma_{ij}$ and ${}^{t+\Delta t}\varepsilon_{ij}$ are the modified Kirchhoff stress tensor and the modified Green strain tensor, respectively; ${}^{t+\Delta t}W$ is the virtual work done by external loadings at the time $t + \Delta t$.

$${}^{t+\Delta t}\sigma_{ij} = \sigma_{ij}^E + \Delta\sigma_{ij} \quad (11-203)$$

where σ_{ij}^E is the Cauchy stress tensor at the time t , and $\Delta\sigma_{ij}$ is the Kirchhoff stress tensor increment from time t to time $t + \Delta t$.

$$\left. \begin{aligned} {}^{t+\Delta t}\varepsilon_{ij} &= \Delta\varepsilon_{ij} = \Delta e_{ij} + \Delta\eta_{ij} \\ \Delta e_{ij} &= \frac{1}{2}(\Delta u_{i,j} + \Delta u_{j,i}), \quad \Delta\eta_{ij} = \frac{1}{2}\Delta u_{k,i}\Delta u_{k,j} \end{aligned} \right\} \quad (11-204)$$

where Δe_{ij} and $\Delta\eta_{ij}$ are the linear and non-linear Green strain tensor increment from time t to time $t + \Delta t$, respectively. And, Δu_i is the displacement increment from time t to time $t + \Delta t$.

If Δt is small enough, the following relationship can be established

$$\Delta\sigma_{ij} = D_{ijkl}\Delta\varepsilon_{kl} \quad (11-205)$$

where D_{ijkl} is the elastic tensor.

Substitution of Eqs. (11-203), (11-204) and (11-205) into Eq. (11-202) yields (the higher-order terms have been neglected)

$$I_1 + I_2 = ({}^{t+\Delta t}W) - I_3 \quad (11-206)$$

with

$$I_1 = \int_V D_{ijkl}\Delta e_{kl}\delta\Delta e_{ij}dV, \quad I_2 = \int_V \sigma_{ij}^E\delta\Delta\eta_{ij}dV, \quad I_3 = \int_V \sigma_{ij}^E\delta\Delta e_{ij}dV \quad (11-207)$$

where I_1 is the linear increment of virtual work; I_2 is the incremental virtual work relevant to the initial stresses; I_3 is the incremental virtual work done by the internal forces.

For the flat-shell element in the local co-ordinates, I_1 , I_2 and I_3 in Eq. (11-207) can be rewritten in the following discrete form

$$\left. \begin{aligned} I_1 &= \iint_{A^e} (\delta\Delta\varepsilon_m^T \mathbf{D}_m \Delta\varepsilon_m + \delta\Delta\kappa^T \mathbf{D}_b \Delta\kappa + \delta\Delta\gamma^T \mathbf{D}_s \Delta\gamma) dA \\ I_2 &= \iint_{A^e} \delta\Delta\mathbf{w}'^T \bar{\mathbf{N}}^E \Delta\mathbf{w}' dA \\ I_3 &= \iint_{A^e} (\delta\Delta\varepsilon_m^T \mathbf{N}_m^E + \delta\Delta\kappa^T \mathbf{M}^E + \delta\Delta\gamma^T \mathbf{Q}^E) dA \end{aligned} \right\} \quad (11-208)$$

where Δ means the increment of relevant variables; $\Delta\varepsilon_m$ is the linear increment

of the membrane strain and given by

$$\Delta \boldsymbol{\varepsilon}_m = \left[\frac{\partial \Delta u}{\partial x} \quad \frac{\partial \Delta v}{\partial y} \quad \frac{\partial \Delta u}{\partial y} + \frac{\partial \Delta v}{\partial x} \right]^T = \mathbf{B}_m \Delta \mathbf{q}_m^e \quad (11-209)$$

$\Delta \boldsymbol{\kappa}$ is the linear increment of the curvature vector given in Eq. (11-157); $\Delta \boldsymbol{\gamma}$ is the increment of the transverse shear strain vector given in Eq. (11-140);

$$\Delta \mathbf{w}' = \begin{Bmatrix} \frac{\partial \Delta w}{\partial x} \\ \frac{\partial \Delta w}{\partial y} \end{Bmatrix} = \begin{bmatrix} \mathbf{F}'_{\lambda,x} \\ \mathbf{F}'_{\lambda,y} \end{bmatrix} \mathbf{CL} \Delta \mathbf{q}_p^e = \mathbf{B}_G \Delta \mathbf{q}_p^e, \quad \mathbf{B}_G = \begin{bmatrix} \mathbf{F}'_{\lambda,x} \\ \mathbf{F}'_{\lambda,y} \end{bmatrix} \mathbf{CL} \quad (11-210)$$

$$\bar{\mathbf{N}}^E = \begin{bmatrix} \int_{-h/2}^{h/2} \sigma_x^E dz & \int_{-h/2}^{h/2} \tau_{xy}^E dz \\ \int_{-h/2}^{h/2} \tau_{xy}^E dz & \int_{-h/2}^{h/2} \sigma_y^E dz \end{bmatrix} = \begin{bmatrix} N_x^E & N_{xy}^E \\ N_{xy}^E & N_y^E \end{bmatrix} \quad (11-211)$$

N_m^E , M^E and Q^E are the membrane force, bending moment and shear force vectors at the time t , respectively,

$$\mathbf{N}_m^E = [N_x^E \quad N_y^E \quad N_{xy}^E]^T, \quad \mathbf{M}^E = [M_x^E \quad M_y^E \quad M_{xy}^E]^T, \quad \mathbf{Q}^E = [Q_x^E \quad Q_y^E]^T \quad (11-212)$$

Substitution of the geometric relation Eqs. (11-140), (11-157) and (11-209) into Eq. (11-208) yields

$$\left. \begin{aligned} I_1 &= \delta \Delta \mathbf{q}_m^{eT} \left(\iint_{A^e} \mathbf{B}_m^T \mathbf{D}_m \mathbf{B}_m dA \right) \Delta \mathbf{q}_m^e \\ &+ \delta \Delta \mathbf{q}_p^{eT} \left(\iint_{A^e} (\mathbf{B}_b^T \mathbf{D}_b \mathbf{B}_b + \mathbf{B}_s^T \mathbf{D}_s \mathbf{B}_s) dA \right) \Delta \mathbf{q}_p^e \\ I_2 &= \delta \Delta \mathbf{q}_p^{eT} \left(\iint_{A^e} \mathbf{B}_G^T \bar{\mathbf{N}}^E \mathbf{B}_G dA \right) \Delta \mathbf{q}_p^e \\ I_3 &= \delta \Delta \mathbf{q}_m^{eT} \left(\iint_{A^e} \mathbf{B}_m^T \mathbf{N}_m^E dA \right) \Delta \mathbf{q}_m^e \\ &+ \delta \Delta \mathbf{q}_p^{eT} \left(\iint_{A^e} (\mathbf{B}_b^T \mathbf{M}^E + \mathbf{B}_s^T \mathbf{Q}^E) dA \right) \Delta \mathbf{q}_p^e \end{aligned} \right\} \quad (11-213)$$

And, ${}^{t+\Delta t}W$ can be rewritten as

$${}^{t+\Delta t}W = \delta \Delta \mathbf{q}_m^{eT} {}^{t+\Delta t} \mathbf{R}_m^e + \delta \Delta \mathbf{q}_p^{eT} {}^{t+\Delta t} \mathbf{R}_p^e \quad (11-214)$$

where ${}^{t+\Delta t}\mathbf{R}_m^e$ and ${}^{t+\Delta t}\mathbf{R}_p^e$ are the equivalent nodal force vectors at the time $t + \Delta t$ of the membrane element and plate bending element, respectively.

Since $\delta\Delta\mathbf{q}_m^e$ and $\delta\Delta\mathbf{q}_p^e$ are arbitrary, thus, according to the variational principle and Eqs. (11-206), (11-213) and (11-214), we can obtain the element incremental equations in the local co-ordinates:

$$\begin{bmatrix} \mathbf{K}_m^e & \mathbf{0} \\ \mathbf{0} & \mathbf{K}_p^e + \mathbf{K}_\sigma^e \end{bmatrix} \begin{Bmatrix} \Delta\mathbf{q}_m^e \\ \Delta\mathbf{q}_p^e \end{Bmatrix} = \begin{Bmatrix} {}^{t+\Delta t}\mathbf{R}_m^e \\ {}^{t+\Delta t}\mathbf{R}_p^e \end{Bmatrix} - \begin{Bmatrix} \boldsymbol{\Psi}_m^e \\ \boldsymbol{\Psi}_p^e \end{Bmatrix} \quad (11-215)$$

where \mathbf{K}_m^e is the linear stiffness matrix of the membrane element and given by Eq. (11-97); \mathbf{K}_p^e is the linear stiffness matrix of the plate bending element and given by Eq. (11-158); \mathbf{K}_σ^e is the geometric stiffness matrix,

$$\mathbf{K}_\sigma^e = \iint_{A^e} \mathbf{B}_G^T \bar{\mathbf{N}}^E \mathbf{B}_G dA \quad (11-216)$$

$\boldsymbol{\Psi}_m^e$ is the equivalent nodal internal force vector of the membrane element; $\boldsymbol{\Psi}_p^e$ is the equivalent nodal internal force vector of the plate bending element,

$$\boldsymbol{\Psi}_m^e = \iint_{A^e} \mathbf{B}_m^T \mathbf{N}_m^E dA, \quad \boldsymbol{\Psi}_p^e = \iint_{A^e} (\mathbf{B}_b^T \mathbf{M}^E + \mathbf{B}_s^T \mathbf{Q}^E) dA \quad (11-217)$$

Rewriting (11-215) according to the DOF's sequence yields

$$(\mathbf{K}^e + \mathbf{K}_\sigma^e)\Delta\mathbf{q}^e = {}^{t+\Delta t}\mathbf{R}^e - \boldsymbol{\Psi}^e \quad (11-218)$$

After transforming (11-218) to the global co-ordinates by standard procedure, the element GMST18 can be used to analyze the geometrically nonlinear problem of shells.

Example 11.15 Post-buckling analysis of a square plate.

As shown in Fig. 11.27, a square plate is controlled by four clamps along each edge. Thus, the displacements in the controlled directions are uniform. This plate is subjected to a pair of concentrated loads on two opposite sides. Only a quarter of the plate using 4×4 mesh division is analyzed because of symmetry.

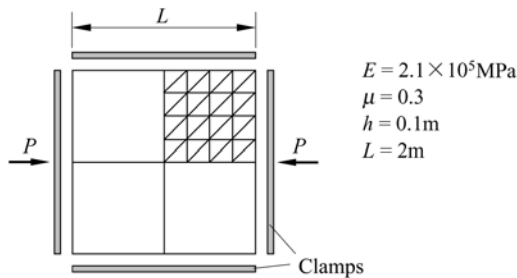


Figure 11.27 Post-buckling problem for a square plate

According to the series method presented by Budiansky^[47], the critical load and post-buckling path are given by

$$P_{cr} = \frac{4\pi^2 D}{L} \quad \text{and} \quad \frac{P}{P_{cr}} = 1 + \frac{3}{8}(1 - \mu^2) \left(\frac{w_{max}}{h} \right)^2$$

where w_{max} is the central deflection of the square plate. The post-buckling paths obtained by presented element GMST18 and element STRI3 in ABAQUS are plotted in Fig. 11.28. It can be seen that the results of GMST18 are more consistent with Budiansky’s solutions than those of STRI3.

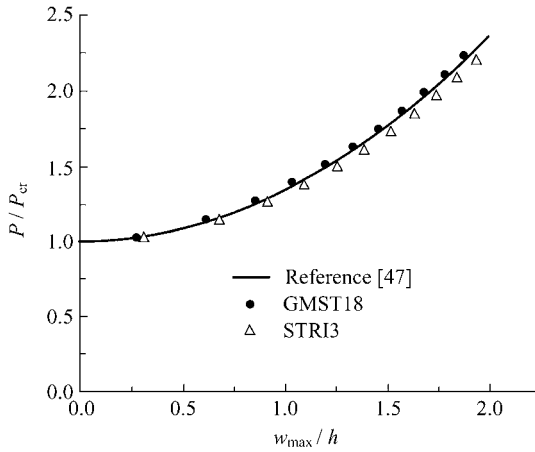


Figure 11.28 Post-buckling path for a square plate, mesh 4×4

11.9 Shell Element for Geometrically Nonlinear Analysis —Rectangular Shallow Shell Element SSR28

11.9.1 Nonlinear Strains and TL (Total Lagrangian) Formulations

The simplified nonlinear strain components of the shallow shell element given by reference [48] have already been successfully applied in the nonlinear analysis of the shell structures. Here, these nonlinear strain components will be adopted to construct the generalized conforming rectangular shallow shell element for geometrically nonlinear analysis. The expressions of these strains are as follows:

$$\epsilon_{11} = \frac{\partial u}{\partial x} + \frac{w}{R_1} + \frac{1}{2} \left(\frac{\partial w}{\partial x} - \frac{u}{R_1} \right)^2 + z \left(-\frac{\partial^2 w}{\partial x^2} + \frac{1}{R_1} \frac{\partial u}{\partial x} \right) \quad (11-219a)$$

$$\varepsilon_{22} = \frac{\partial v}{\partial y} + \frac{w}{R_2} + \frac{1}{2} \left(\frac{\partial w}{\partial y} - \frac{v}{R_2} \right)^2 + z \left(-\frac{\partial^2 w}{\partial y^2} + \frac{1}{R_2} \frac{\partial v}{\partial y} \right) \quad (11-219b)$$

$$\varepsilon_{12} = \frac{\partial u}{\partial y} + \frac{\partial v}{\partial x} + \left(\frac{\partial w}{\partial x} - \frac{u}{R_1} \right) \left(\frac{\partial w}{\partial y} - \frac{v}{R_2} \right) + z \left(-2 \frac{\partial^2 w}{\partial x \partial y} + \frac{1}{R_1} \frac{\partial u}{\partial y} + \frac{1}{R_2} \frac{\partial v}{\partial x} \right) \quad (11-219c)$$

where $\varepsilon_{11} = \varepsilon_x$, $\varepsilon_{22} = \varepsilon_y$, $\varepsilon_{12} = \varepsilon_{xy}$, $R_1 = R_x$, $R_2 = R_y$.

The above strain components can be decomposed as follows:

$$\boldsymbol{\varepsilon}^m = [e_{11} \quad e_{22} \quad e_{12} + e_{21}]^T = \left[\frac{\partial u}{\partial x} + \frac{w}{R_1} \quad \frac{\partial v}{\partial y} + \frac{w}{R_2} \quad \frac{\partial u}{\partial y} + \frac{\partial v}{\partial x} \right]^T \quad (11-220a)$$

$$\boldsymbol{\varepsilon}^b = [\kappa_{11} \quad \kappa_{22} \quad \kappa_{12} + \kappa_{21}]^T = \left[-\frac{\partial^2 w}{\partial x^2} + \frac{1}{R_1} \frac{\partial u}{\partial x} \quad -\frac{\partial^2 w}{\partial y^2} + \frac{1}{R_2} \frac{\partial v}{\partial y} \quad -2 \frac{\partial^2 w}{\partial x \partial y} + \frac{1}{R_1} \frac{\partial u}{\partial y} + \frac{1}{R_2} \frac{\partial v}{\partial x} \right]^T \quad (11-220b)$$

$$\boldsymbol{\varepsilon}^s = [e_{13} \quad e_{23}]^T = \left[\frac{\partial w}{\partial x} - \frac{u}{R_1} \quad \frac{\partial w}{\partial y} - \frac{v}{R_2} \right]^T \quad (11-220c)$$

Compared with von Kármán nonlinear strain components, it can be seen that in the above expressions, $\frac{\partial w}{\partial x}$ and $\frac{\partial w}{\partial y}$ are replaced by $\frac{\partial w}{\partial x} - \frac{u}{R_1}$ and $\frac{\partial w}{\partial y} - \frac{v}{R_2}$, respectively; $-\frac{\partial^2 w}{\partial x^2}$ and $-\frac{\partial^2 w}{\partial y^2}$ are replaced by $-\frac{\partial^2 w}{\partial x^2} + \frac{1}{R_1} \frac{\partial u}{\partial x}$ and $-\frac{\partial^2 w}{\partial y^2} + \frac{1}{R_2} \frac{\partial v}{\partial y}$, respectively; and $-2 \frac{\partial^2 w}{\partial x \partial y}$ is replaced by $-2 \frac{\partial^2 w}{\partial x \partial y} + \frac{1}{R_1} \frac{\partial u}{\partial y} + \frac{1}{R_2} \frac{\partial v}{\partial x}$. In total Lagrangian coordinates, the increments of strain components are

$$\Delta \varepsilon_{11} = \Delta e_{11} + e_{13} \Delta e_{13} + \frac{1}{2} \Delta e_{13}^2 + z \Delta \kappa_{11} \quad (11-221a)$$

$$\Delta \varepsilon_{22} = \Delta e_{22} + e_{23} \Delta e_{23} + \frac{1}{2} \Delta e_{23}^2 + z \Delta \kappa_{22} \quad (11-221b)$$

$$\Delta \varepsilon_{12} = \Delta e_{12} + \Delta e_{21} + e_{13} \Delta e_{23} + e_{23} \Delta e_{13} + \Delta e_{13} \Delta e_{23} + z (\Delta \kappa_{12} + \Delta \kappa_{21}) \quad (11-221c)$$

where Δe_{11} and Δe_{22} are the strains caused by displacement increments; e_{13} and e_{23} are the strains caused by total displacements corresponding to original coordinate system. After the determination of the normal and tangential displacement functions, the linear strains in Eq. (11-221) can be written as

$$\begin{aligned} \Delta \bar{\boldsymbol{\varepsilon}}^m &= \left\{ \begin{array}{l} \Delta \bar{e}_{11} \\ \Delta \bar{e}_{22} \\ \Delta \bar{e}_{12} + \Delta \bar{e}_{21} \end{array} \right\} = \left\{ \begin{array}{l} \Delta e_{11} + e_{13} \Delta e_{13} \\ \Delta e_{22} + e_{23} \Delta e_{23} \\ \Delta e_{12} + \Delta e_{21} + e_{13} \Delta e_{23} + e_{23} \Delta e_{13} \end{array} \right\} \\ &= \Delta \boldsymbol{\varepsilon}^m + \Delta \boldsymbol{\varepsilon}^{m\theta} = (\mathbf{B}^{mp} + \mathbf{B}^{m\theta}) \Delta \bar{\mathbf{q}}^e \end{aligned} \quad (11-222)$$

where

$$\Delta \boldsymbol{\varepsilon}^m = \left\{ \begin{array}{l} \Delta e_{11} \\ \Delta e_{22} \\ \Delta e_{12} + \Delta e_{21} \end{array} \right\} = \mathbf{B}^{mp} \Delta \bar{\mathbf{q}}^e \quad (11-223)$$

$$\Delta \boldsymbol{\varepsilon}^{m\theta} = \left\{ \begin{array}{l} e_{13} \Delta e_{13} \\ e_{23} \Delta e_{23} \\ e_{13} \Delta e_{23} + e_{23} \Delta e_{13} \end{array} \right\} = \left\{ \begin{array}{l} e_{13} \mathbf{B}_{13}^g \\ e_{23} \mathbf{B}_{23}^g \\ e_{13} \mathbf{B}_{23}^g + e_{23} \mathbf{B}_{13}^g \end{array} \right\} \Delta \bar{\mathbf{q}}^e = \mathbf{B}^{m\theta} \Delta \bar{\mathbf{q}}^e \quad (11-224)$$

From Eqs. (11-220b) and (11-220c), the following incremental strains can be obtained:

$$\Delta \boldsymbol{\varepsilon}^g = \left\{ \begin{array}{l} \Delta e_{13} \\ \Delta e_{23} \end{array} \right\} = \left\{ \begin{array}{l} \mathbf{B}_{13}^g \\ \mathbf{B}_{23}^g \end{array} \right\} \Delta \bar{\mathbf{q}}^e = \mathbf{B}^g \Delta \bar{\mathbf{q}}^e \quad (11-225)$$

$$\Delta \boldsymbol{\varepsilon}^b = \left\{ \begin{array}{l} \Delta \kappa_{11} \\ \Delta \kappa_{22} \\ \Delta \kappa_{12} + \Delta \kappa_{21} \end{array} \right\} = \mathbf{B}^{bp} \Delta \bar{\mathbf{q}}^e \quad (11-226)$$

Then, the TL formulations for nonlinear tangential stiffness matrix of the shallow shell element can be written as

$$\bar{\mathbf{K}}_T^e = \bar{\mathbf{K}}^{me} + \bar{\mathbf{K}}^{m\theta e} + \bar{\mathbf{K}}^{be} + \bar{\mathbf{K}}^{ge} + \Delta \bar{\mathbf{K}}^e \quad (11-227)$$

where

$$\begin{aligned} \bar{\mathbf{K}}^{me} &= \iint_{A^e} \mathbf{B}^{mpT} \mathbf{D}_m \mathbf{B}^{mp} dA \\ \bar{\mathbf{K}}^{m\theta e} &= \bar{\mathbf{K}}_1^{m\theta e} + \bar{\mathbf{K}}_2^{m\theta e} + \bar{\mathbf{K}}_2^{m\theta eT} \\ \bar{\mathbf{K}}_1^{m\theta e} &= \frac{Eh}{1-\mu^2} \iint_{A^e} \mathbf{B}^{gT} \begin{bmatrix} e_{13}^2 + \frac{1-\mu}{2} e_{23}^2 & \frac{1+\mu}{2} e_{13} e_{23} \\ \frac{1+\mu}{2} e_{13} e_{23} & e_{23}^2 + \frac{1-\mu}{2} e_{13}^2 \end{bmatrix} \mathbf{B}^g dA \end{aligned}$$

$$\bar{\mathbf{K}}_2^{m\theta e} = \frac{Eh}{1-\mu^2} \iint_{A^e} \mathbf{B}^{gT} \begin{bmatrix} e_{13} & \mu e_{13} & \frac{1-\mu}{2} e_{23} \\ \mu e_{23} & e_{23} & \frac{1-\mu}{2} e_{13} \end{bmatrix} \mathbf{B}^{mp} dA$$

$$\bar{\mathbf{K}}^{be} = \iint_{A^e} \mathbf{B}^{bpT} \mathbf{D}_b \mathbf{B}^{bp} dA$$

$$\bar{\mathbf{K}}^{ge} = h \iint_{A^e} \mathbf{B}^{gT} \begin{bmatrix} \sigma_{11} & \tau_{12} \\ \tau_{12} & \sigma_{22} \end{bmatrix} \mathbf{D}_m \mathbf{B}^g dA$$

$$\Delta \bar{\mathbf{K}}^e = \Delta \bar{\mathbf{K}}_1^e + \Delta \bar{\mathbf{K}}_2^e + \Delta \bar{\mathbf{K}}_2^{eT} + \Delta \bar{\mathbf{K}}_3^e$$

$$\Delta \bar{\mathbf{K}}_1^e = \frac{Eh}{1-\mu^2} \iint_{A^e} \mathbf{B}^{gT} \begin{bmatrix} \frac{1}{2}(3\Delta e_{13}^2 + \Delta e_{23}^2) & \Delta e_{13} \Delta e_{23} \\ \Delta e_{13} \Delta e_{23} & \frac{1}{2}(3\Delta e_{23}^2 + \Delta e_{13}^2) \end{bmatrix} \mathbf{B}^g dA$$

$$\Delta \bar{\mathbf{K}}_2^e = \frac{Eh}{1-\mu^2} \iint_{A^e} \mathbf{B}^{gT} \begin{bmatrix} \Delta e_{13} & \mu \Delta e_{13} & \frac{1}{2}(1-\mu) \Delta e_{23} \\ \mu \Delta e_{23} & \Delta e_{23} & \frac{1}{2}(1-\mu) \Delta e_{13} \end{bmatrix} (\mathbf{B}^{mp} + \mathbf{B}^{m\theta}) dA$$

$$\Delta \bar{\mathbf{K}}_3^e = \frac{Eh}{1-\mu^2} \iint_{A^e} \mathbf{B}^{gT} \begin{bmatrix} \Delta \bar{e}_{11} + \mu \Delta \bar{e}_{22} & \frac{1}{2}(1-\mu)(\Delta \bar{e}_{12} + \Delta \bar{e}_{21}) \\ \frac{1}{2}(1-\mu)(\Delta \bar{e}_{12} + \Delta \bar{e}_{21}) & \Delta \bar{e}_{22} + \mu \Delta \bar{e}_{11} \end{bmatrix} \mathbf{B}^g dA$$

where σ_{11} , σ_{22} and τ_{12} are the second Piola-Kirchhoff stresses.

11.9.2 The Formulations of the Rectangular Shallow Shell Element SSR28

A generalized conforming rectangular shallow shell element with tangential DOFs at the mid-side points is shown in Fig. 11.29. It is composed of two parts: 4-node bending element and 8-node membrane element.

The element nodal displacement vector is

$$\bar{\mathbf{q}}^e = [\mathbf{q}_1^T \quad \mathbf{q}_{1'}^T \quad \mathbf{q}_2^T \quad \mathbf{q}_{2'}^T \quad \mathbf{q}_3^T \quad \mathbf{q}_{3'}^T \quad \mathbf{q}_4^T \quad \mathbf{q}_{4'}^T]^T \quad (11-228)$$

where the definition of \mathbf{q}_i and $\mathbf{q}_{i'}$ are given by Eq. (11-186).

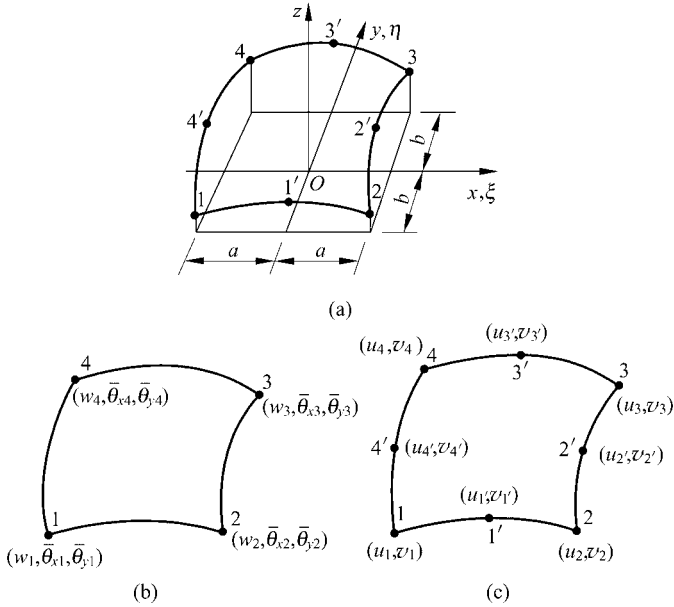


Figure 11.29 (a) = (b) + (c)

(a) nodes of rectangular shallow shell element; (b) nodes of bending element; (c) nodes of membrane element

Similar to Eqs. (11-187) and (11-188), for convenience, the displacement vector (11-228) is decomposed into membrane displacement and bending displacement vectors:

$$\mathbf{q}^{me} = [u_1 \quad v_1 \quad u_{1'} \quad v_{1'} \quad u_2 \quad v_2 \quad u_{2'} \quad v_{2'} \quad u_3 \quad v_3 \quad u_{3'} \quad v_{3'} \quad u_4 \quad v_4 \quad u_{4'} \quad v_{4'}]^T \quad (11-229)$$

$$\mathbf{q}^{be} = [w_1 \quad \theta_{x1} \quad \theta_{y1} \quad w_2 \quad \theta_{x2} \quad \theta_{y2} \quad w_3 \quad \theta_{x3} \quad \theta_{y3} \quad w_4 \quad \theta_{x4} \quad \theta_{y4}]^T \quad (11-230)$$

Assume that the tangential displacement fields are cubic polynomials:

$$\bar{\mathbf{u}}^e = \begin{Bmatrix} u \\ v \end{Bmatrix} = \sum_{i=1}^4 N_i \mathbf{q}_i^m \quad (11-231)$$

where

$$N_i = \begin{bmatrix} N_i & 0 & N_{i'} & 0 \\ 0 & N_i & 0 & N_{i'} \end{bmatrix}, \quad \mathbf{q}_i^m = [u_i \quad v_i \quad u_{i'} \quad v_{i'}]^T \quad (i = 1, 2, 3, 4) \quad (11-232)$$

$$\left. \begin{aligned}
 N_{1'} &= \frac{1}{2}(1-\xi^2)(1-\eta), & N_{2'} &= \frac{1}{2}(1-\eta^2)(1+\xi) \\
 N_{3'} &= \frac{1}{2}(1-\xi^2)(1+\eta), & N_{4'} &= \frac{1}{2}(1-\eta^2)(1-\xi) \\
 N_1 &= N_1^0 - \frac{1}{2}N_{1'} - \frac{1}{2}N_{4'}, & N_2 &= N_2^0 - \frac{1}{2}N_{1'} - \frac{1}{2}N_{2'} \\
 N_3 &= N_3^0 - \frac{1}{2}N_{2'} - \frac{1}{2}N_{3'}, & N_4 &= N_4^0 - \frac{1}{2}N_{3'} - \frac{1}{2}N_{4'} \\
 N_i^0 &= \frac{1}{4}(1+\xi_i\xi)(1+\eta_i\eta) \quad (i=1,2,3,4)
 \end{aligned} \right\} \quad (11-233)$$

The above tangential displacement functions not only are complete quadric polynomials, but also include the cubic terms $\xi^2\eta$ and $\xi\eta^2$. The displacement functions of the generalized conforming rectangular plate element RGC-12^[14] are adopted to form the normal displacement field of the shallow shell element:

$$w = F_\lambda (\hat{C}^{-1} \hat{G}) q^{be} \quad (11-234)$$

where

$$F_\lambda = [1 \quad \xi \quad \eta \quad \mid \quad \xi^2 \quad \xi\eta \quad \eta^2 \quad \mid \quad \xi^3 \quad \xi^2\eta \quad \xi\eta^2 \quad \eta^3 \quad \mid \quad \xi^3\eta \quad \xi\eta^3]^T \quad (11-235)$$

$$\hat{C} = \begin{bmatrix}
 0 & 0 & \frac{2}{b} & 0 & 0 & -\frac{4}{b} & 0 & \frac{2}{3b} & 0 & \frac{6}{b} & 0 & 0 \\
 0 & \frac{2}{a} & 0 & \frac{4}{a} & 0 & 0 & \frac{6}{a} & 0 & \frac{2}{3a} & 0 & 0 & 0 \\
 0 & 0 & \frac{2}{b} & 0 & 0 & \frac{4}{b} & 0 & \frac{2}{3b} & 0 & \frac{6}{b} & 0 & 0 \\
 0 & \frac{2}{a} & 0 & -\frac{4}{a} & 0 & 0 & \frac{6}{a} & 0 & \frac{2}{3a} & 0 & 0 & 0 \\
 \hline
 0 & 2 & 0 & 0 & -2 & 0 & 2 & 0 & 2 & 0 & -2 & -2 \\
 0 & 0 & 2 & 0 & 2 & 0 & 0 & 2 & 0 & 2 & 2 & 2 \\
 0 & -2 & 0 & 0 & -2 & 0 & -2 & 0 & -2 & 0 & -2 & -2 \\
 \hline
 2 & 0 & -2 & \frac{2}{3} & 0 & 2 & 0 & -\frac{2}{3} & 0 & -2 & 0 & 0 \\
 2 & 2 & 0 & 2 & 0 & \frac{2}{3} & 2 & 0 & \frac{2}{3} & 0 & 0 & 0 \\
 2 & 0 & 2 & \frac{2}{3} & 0 & 2 & 0 & \frac{2}{3} & 0 & 2 & 0 & 0 \\
 \hline
 0 & \frac{1}{a} & 0 & -\frac{2}{a} & -\frac{1}{a} & 0 & \frac{3}{a} & \frac{2}{a} & \frac{1}{a} & 0 & -\frac{3}{a} & -\frac{1}{a} \\
 0 & 0 & \frac{1}{b} & 0 & -\frac{1}{b} & -\frac{2}{b} & 0 & \frac{1}{b} & \frac{2}{b} & \frac{3}{b} & -\frac{1}{b} & -\frac{3}{b}
 \end{bmatrix} \quad (11-236)$$

$$\hat{\mathbf{G}} = \begin{bmatrix} 0 & 1 & 0 & 0 & 1 & 0 & 0 & 0 & 0 & 0 & 0 & 0 & 0 \\ 0 & 0 & 0 & 0 & 0 & -1 & 0 & 0 & -1 & 0 & 0 & 0 & 0 \\ 0 & 0 & 0 & 0 & 0 & 0 & 0 & 1 & 0 & 0 & 1 & 0 & 0 \\ 0 & 0 & -1 & 0 & 0 & 0 & 0 & 0 & 0 & 0 & 0 & 0 & -1 \\ \hline -1 & 0 & 0 & 1 & 0 & 0 & 0 & 0 & 0 & 0 & 0 & 0 & 0 \\ 0 & 0 & 0 & -1 & 0 & 0 & 1 & 0 & 0 & 0 & 0 & 0 & 0 \\ 0 & 0 & 0 & 0 & 0 & 0 & -1 & 0 & 0 & 1 & 0 & 0 & 0 \\ \hline 1 & 0 & -\frac{a}{3} & 1 & 0 & \frac{a}{3} & 0 & 0 & 0 & 0 & 0 & 0 & 0 \\ 0 & 0 & 0 & 1 & \frac{b}{3} & 0 & 1 & -\frac{3}{b} & 0 & 0 & 0 & 0 & 0 \\ 0 & 0 & 0 & 0 & 0 & 0 & 1 & 0 & \frac{a}{3} & 1 & 0 & -\frac{a}{3} & 0 \\ \hline 0 & 0 & -1 & 0 & 0 & 0 & 0 & 0 & 0 & 0 & 0 & 0 & 0 \\ 0 & 1 & 0 & 0 & 0 & 0 & 0 & 0 & 0 & 0 & 0 & 0 & 0 \end{bmatrix} \quad (11-237)$$

The incremental displacement vector of the element is

$$\Delta \bar{\mathbf{q}}^e = [\Delta \mathbf{q}_1^T \quad \Delta \mathbf{q}_{1'}^T \quad \Delta \mathbf{q}_2^T \quad \Delta \mathbf{q}_{2'}^T \quad \Delta \mathbf{q}_3^T \quad \Delta \mathbf{q}_{3'}^T \quad \Delta \mathbf{q}_4^T \quad \Delta \mathbf{q}_{4'}^T]^T \quad (11-238)$$

where

$$\Delta \mathbf{q}_i = [\Delta u_i \quad \Delta v_i \quad \Delta w_i \quad \Delta \theta_{xi} \quad \Delta \theta_{yi}]^T, \quad \Delta \mathbf{q}_{i'} = [\Delta u_{i'} \quad \Delta v_{i'}]^T \quad (11-239)$$

The incremental displacements corresponding to Eqs. (11-229) and (11-230) are

$$\Delta \mathbf{q}^{me} = [\Delta u_1 \quad \Delta v_1 \quad \Delta u_{1'} \quad \Delta v_{1'} \quad \Delta u_2 \quad \Delta v_2 \quad \Delta u_{2'} \quad \Delta v_{2'} \quad \Delta u_3 \quad \Delta v_3 \quad \Delta u_{3'} \quad \Delta v_{3'} \quad \Delta u_4 \quad \Delta v_4 \quad \Delta u_{4'} \quad \Delta v_{4'}]^T \quad (11-240)$$

$$\Delta \mathbf{q}^{be} = [\Delta w_1 \quad \Delta \theta_{x1} \quad \Delta \theta_{y1} \quad \Delta w_2 \quad \Delta \theta_{x2} \quad \Delta \theta_{y2} \quad \Delta w_3 \quad \Delta \theta_{x3} \quad \Delta \theta_{y3} \quad \Delta w_4 \quad \Delta \theta_{x4} \quad \Delta \theta_{y4}]^T \quad (11-241)$$

According to Eqs. (11-220a) and (11-222), matrix \mathbf{B}^{mp} can be written as

$$\begin{aligned} \mathbf{B}^{mp} \Delta \bar{\mathbf{q}}^e &= \left[\frac{\partial \Delta u}{\partial x} + \frac{\Delta w}{R_1} \quad \frac{\partial \Delta v}{\partial y} + \frac{\Delta w}{R_2} \quad \frac{\partial \Delta u}{\partial y} + \frac{\partial \Delta v}{\partial x} \right]^T \\ &= \mathbf{B}^m \Delta \mathbf{q}^{me} + \mathbf{B}^{mw} \Delta \mathbf{q}^{be} \end{aligned} \quad (11-242)$$

where

$$\mathbf{B}^m = [\mathbf{B}_1^m \quad \mathbf{B}_{1'}^m \quad \mathbf{B}_2^m \quad \mathbf{B}_{2'}^m \quad \mathbf{B}_3^m \quad \mathbf{B}_{3'}^m \quad \mathbf{B}_4^m \quad \mathbf{B}_{4'}^m]$$

$$\mathbf{B}_{i'}^m = \frac{1}{4ab} \begin{bmatrix} b(1+\eta_0)(2\xi + \xi_i\eta_0) & 0 \\ 0 & a(1-\xi_0)(2\eta + \eta_i\xi_0) \\ a(1-\xi_0)(2\eta + \eta_i\xi_0) & b(1+\eta_0)(2\xi + \xi_i\eta_0) \end{bmatrix}, \quad \xi_0 = \xi_i\xi, \quad \eta_0 = \eta_i\eta$$

$$\mathbf{B}_i^m = \frac{1}{ab} \begin{bmatrix} b_{1i'} & 0 \\ 0 & b_{2i'} \\ b_{2i'} & b_{1i'} \end{bmatrix}$$

$$b_{11'} = -b\xi(1-\eta), \quad b_{12'} = \frac{b}{2}(1-\eta^2), \quad b_{13'} = -b\xi(1+\eta), \quad b_{14'} = -\frac{b}{2}(1-\eta^2)$$

$$b_{21'} = -\frac{a}{2}(1-\xi^2), \quad b_{22'} = -a\eta(1+\xi), \quad b_{23'} = \frac{a}{2}(1-\xi^2), \quad b_{24'} = -a\eta(1-\xi)$$

$$\mathbf{B}^{mw} = \begin{bmatrix} \frac{1}{R_1} \mathbf{F}_\lambda(\hat{\mathbf{C}}^{-1}\hat{\mathbf{G}}) \\ \frac{1}{R_2} \mathbf{F}_\lambda(\hat{\mathbf{C}}^{-1}\hat{\mathbf{G}}) \\ 0 \end{bmatrix}$$

The element bending strain matrix is

$$\begin{aligned} \mathbf{B}^{bp} \Delta \bar{\mathbf{q}}^e &= \begin{bmatrix} -\frac{\partial^2 \Delta w}{\partial x^2} + \frac{1}{R_1} \frac{\partial \Delta u}{\partial x} & -\frac{\partial^2 \Delta w}{\partial y^2} + \frac{1}{R_2} \frac{\partial \Delta v}{\partial y} & -2\frac{\partial^2 \Delta w}{\partial x \partial y} + \frac{1}{R_1} \frac{\partial \Delta u}{\partial y} + \frac{1}{R_2} \frac{\partial \Delta v}{\partial x} \end{bmatrix}^T \\ &= \mathbf{B}^b \Delta \mathbf{q}^{be} + \mathbf{B}^{bm} \Delta \mathbf{q}^{me} \end{aligned} \quad (11-240)$$

where

$$\mathbf{B}^b = \bar{\mathbf{B}}^b (\hat{\mathbf{C}}^{-1}\hat{\mathbf{G}})$$

$$\bar{\mathbf{B}}^b = \frac{-1}{a^2 b^2} \begin{bmatrix} 0 & 0 & 0 & 2b^2 & 0 & 0 & 6b^2\xi & 2b^2\eta & 0 & 0 & 6b^2\xi\eta & 0 \\ 0 & 0 & 0 & 0 & 0 & 2a^2 & 0 & 0 & 2a^2\xi & 6a^2\eta & 0 & 6a^2\xi\eta \\ 0 & 0 & 0 & 0 & 2ab & 0 & 0 & 4ab\xi & 4ab\eta & 0 & 6ab\xi^2 & 6ab\eta^2 \end{bmatrix}$$

$$\mathbf{B}^{bm} = [\mathbf{B}_1^{bm} \quad \mathbf{B}_{1'}^{bm} \quad \mathbf{B}_2^{bm} \quad \mathbf{B}_{2'}^{bm} \quad \mathbf{B}_3^{bm} \quad \mathbf{B}_{3'}^{bm} \quad \mathbf{B}_4^{bm} \quad \mathbf{B}_{4'}^{bm}]$$

$$\mathbf{B}_i^{bm} = \frac{1}{ab} \begin{bmatrix} \frac{1}{R_1} b_{1i'} & 0 \\ 0 & \frac{1}{R_2} b_{2i'} \\ \frac{1}{R_1} b_{2i'} & \frac{1}{R_2} b_{1i'} \end{bmatrix}$$

$$\mathbf{B}_i^{\text{bm}} = \frac{1}{4ab} \begin{bmatrix} \frac{b}{R_1}(1 + \eta_0)(2\xi + \xi_i\eta_0) & 0 \\ 0 & \frac{a}{R_2}(1 - \xi_0)(2\eta + \eta_i\xi_0) \\ \frac{a}{R_1}(1 - \xi_0)(2\eta + \eta_i\xi_0) & \frac{b}{R_2}(1 + \eta_0)(2\xi + \xi_i\eta_0) \end{bmatrix}$$

Matrix \mathbf{B}^g can be expressed by

$$\begin{aligned} \mathbf{B}^g \Delta \bar{\mathbf{q}}^e &= \left[\frac{\partial \Delta w}{\partial x} - \frac{\Delta u}{R_1} \quad \frac{\partial \Delta w}{\partial y} - \frac{\Delta v}{R_2} \right]^T \\ &= \bar{\mathbf{G}} \Delta \mathbf{q}^{\text{be}} - \sum_{i=1}^4 \begin{bmatrix} \frac{1}{R_1} & 0 \\ 0 & \frac{1}{R_2} \end{bmatrix} N_i \Delta \mathbf{q}_i^{\text{me}} \end{aligned} \quad (11-244)$$

where

$$\bar{\mathbf{G}} = \frac{1}{ab} \begin{bmatrix} 0 & b & 0 & 2b\xi & b\eta & 0 & 3b\xi^2 & 2b\xi\eta & b\eta^2 & 0 & 3b\xi^2\eta & b\eta^3 \\ 0 & 0 & a & a & a\xi & 2a\eta & 0 & a\xi^2 & 2a\xi\eta & 3a\eta^2 & a\xi^3 & 3a\xi\eta^2 \end{bmatrix} (\hat{\mathbf{C}}^{-1} \hat{\mathbf{G}})$$

$$\Delta \mathbf{q}_i^{\text{me}} = [\Delta u_i \quad \Delta v_i \quad \Delta u_{,i} \quad \Delta v_{,i}]^T$$

Then, from the above equations, the nonlinear tangential stiffness matrix of the shallow shell element can be obtained according to Eq. (11-227).

11.9.3 Numerical Examples

In the following nonlinear numerical examples, the variable arc length iteration method^[42], in which the current stiffness parameter is taken as the control variable, is used, and the materials are all assumed to be linear elastic.

Example 11.16 The nonlinear analysis of a clamped square plate subjected to uniform load.

A clamped square plate subjected to uniform load q is shown in Fig. 11.30, its Poisson's ratio $\mu = 0.316$. Due to the symmetry, only 1/4 of the plate is analyzed by using two meshes 2×2 and 4×4 . The results are listed in Table 11.17, in which $\bar{W} = w/h$ and $\bar{Q} = qa^4/Eh^4$. It can be seen that the element SSR28 can provide higher precision with less DOFs.

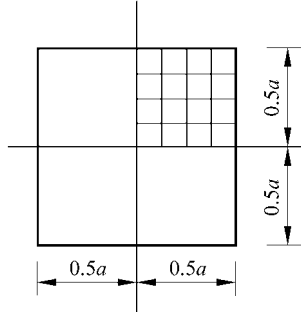


Figure 11.30 A clamped square plate

Table 11.17 The central deflection parameter \bar{W} in nonlinear analysis of a clamped square plate subjected to uniform load

Load parameter \bar{Q}	Analytical ^[49]	QH ^[49]	SSR28 2 × 2	SSR28 4 × 4
17.79	0.237	0.2361	0.2254	0.2333
30.8	0.471	0.4687	0.4509	0.4621
63.4	0.695	0.6902	0.6694	0.6815
95	0.912	0.9015	0.8804	0.8909
134.9	1.121	1.1050	1.0848	1.0936
184	1.323	1.2997	1.2807	1.2942
245	1.521	1.4916	1.4739	1.4900
318	1.714	1.6775	1.6607	1.6834
402	1.902	1.8545	1.8382	1.8643
DOFs		405	69	205

Example 11.17 Post-buckling analysis of a thin cylindrical shell subjected to concentrated load.

A cylindrical shell is shown in Fig. 11.31. Its longitudinal straight edges are hinged while curved edges are free. A concentrated load acts on the center of the

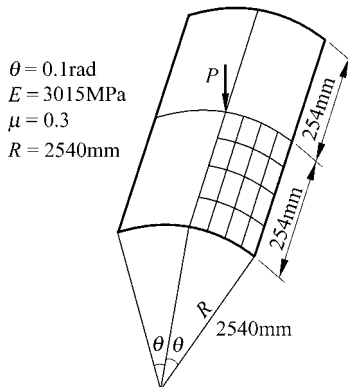


Figure 11.31 Cylindrical shell

shell. Two different thickness cases are considered: $h = 12.7\text{mm}$ and $h = 6.35\text{mm}$. The critical load of this structures obtained by computations are listed in Tables 11.18 and 11.19, and also plotted in Figs. 11.32 and 11.33. It can be seen that the results by the element SSR28 agree with those obtained by the cylindrical shell element^[50], the flat-shell element^[51] and the quasi-conforming rectangular shallow shell element^[52].

Table 11.18 The critical load P_{cr} of a cylindrical shell ($h = 12.7\text{mm}$) subjected to concentrated load

Mesh \ Model	2 × 2		4 × 4		16 × 16	
	Up limit	Low limit	Up limit	Low limit	Up limit	Low limit
SSR28	2.223	0.6066	2.200	0.5169		
Reference [52]					2.222 86	0.546 40
Reference [51]			2.27			
Reference [50]			2.22			

Table 11.19 The critical load P_{cr} of a cylindrical shell ($h = 6.35\text{mm}$) subjected to concentrated load

Mesh \ Model	2 × 2		4 × 4		16 × 16	
	Up limit	Low limit	Up limit	Low limit	Up limit	Low limit
SSR28	0.5956	-0.3324	0.5837	-0.3739		
Reference [52]					0.5907	-0.3794

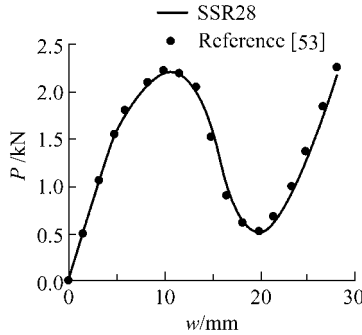


Figure 11.32 Load-central deflection relation curve of a cylindrical shell ($h = 12.7\text{mm}$)

Example 11.18 Post-buckling analysis of a thin cylindrical shell subjected to uniform load.

The dimensions and material properties of a cylindrical shell structure are shown in Fig. 11.31. This cylindrical shell is clamped and subjected to vertical

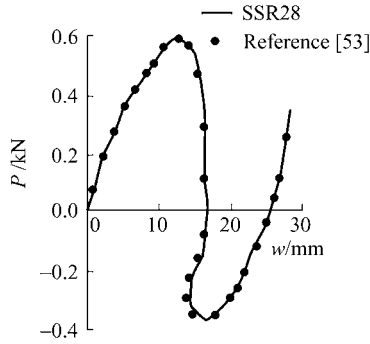


Figure 11.33 Load-central deflection relation curve of a cylindrical shell ($h = 6.35\text{mm}$)

uniformly distributed load q , and its thickness $h = 3.175\text{mm}$. The results of the post-buckling analysis by 4×4 mesh are plotted in Fig. 11.34, in which w is the vertical deflection at central point.

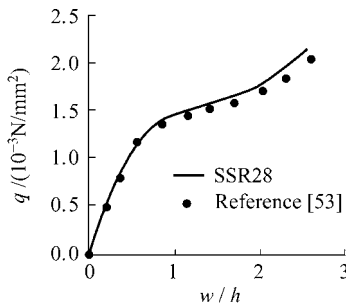
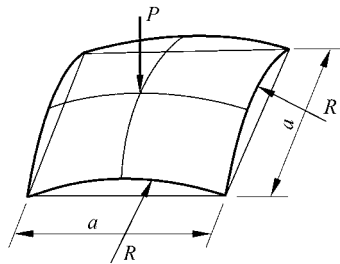


Figure 11.34 Post-buckling analysis of a clamped cylindrical shell ($h = 3.175\text{mm}$)

Example 11.19 Post-buckling analysis of a shallow spheric shell.

A simply-supported shallow spheric shell subjected to a central concentrated load P is shown in Fig. 11.35. Its stability problem has already been analyzed by



$R = 2540\text{mm}$, $a = 1569.8\text{mm}$, $h = 99.45\text{mm}$
 $E = 68.95\text{MPa}$, $\mu = 0.3$

Figure 11.35 A shallow spheric shell

many element models^[51,52,54]. The results of the critical load obtained by the element SSR28 using 2×2 and 4×4 meshes are listed in Table 11.20. A comparison between the results by the element SSR28 using 4×4 mesh and those in reference [51] is given in Fig. 11.36.

Table 11.20 The critical load P_{cr} (kN) of a shallow spheric shell subjected to concentrated load

Model \ Mesh	2×2		4×4		5×5		16×16	
	Up	Low limit	Up limit	Low limit	Up limit	Low limit	Up limit	Low limit
SSR28	48.991	37.360	49.874	36.562				
Reference							48.172	36.951
Reference			52.000					
Reference					51.400			

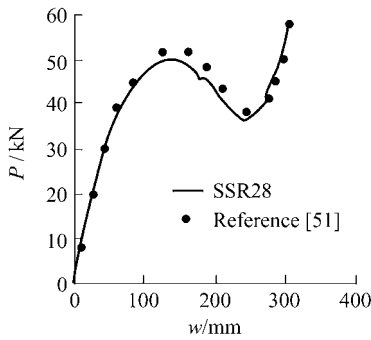


Figure 11.36 Post-buckling analysis of a shallow spheric shell

References

- [1] Long YQ, Huang MF (1988) A generalized conforming isoparametric element. Applied mathematics and Mechanics (English Edition) 9(10): 929 – 936
- [2] Long YQ, Xu Y (1994) Generalized conforming quadrilateral membrane element with vertex rigid rotational freedom. Computers & Structures 52(4): 749 – 755
- [3] Long YQ, Xu Y (1994) Generalized conforming triangular membrane element with vertex rigid rotational freedom. Finite Elements in Analysis and Design 17: 259 – 271
- [4] Long YQ, Xu Y (1993) Generalized conforming triangular flat shell element. Gong Cheng Li Xue/Engineering Mechanics 10(4): 1 – 7 (in Chinese)
- [5] Long YQ, Xu Y (1994) Generalized conforming flat rectangular thin shell element. Computational Structural Mechanics and Applications 11(2): 154 – 160 (in Chinese)
- [6] Xu Y, Long YQ, Long ZF (1994) A triangular shell element with drilling freedoms based on generalized compatibility conditions. In: Proc. WCCMIII. Japan, pp1234 – 1235

Chapter 11 Generalized Conforming Membrane and Shell Elements

- [7] Xu Y, Long ZF (1996) Advances of membrane and thin shell elements with the generalized conforming approach. In: Yuan Si, Ma Zhiliang (eds) *New Developments in Structural Engineering*, pp218 – 223
- [8] Xu Y, Long YQ, Long ZF (1999) A generalized conforming triangular flat shell element with high accuracy. In: Long YQ (ed) *The Proceedings of the First International Conference on Structural Engineering*. China, KunMing, pp700 – 706
- [9] Chen YL, Cen S, Yao ZH, Long YQ, Long ZF (2003) Development of triangular flat-shell element using a new thin-thick plate bending element based on SemiLoof constraints. *Structural Engineering and Mechanics* 15(1): 83 – 114
- [10] Sun JH, Xia HX, Long YQ (1999) A generalized conforming rectangular shallow shell element. In: Long YQ (ed) *The Proceedings of the First International Conference on Structural Engineering*. China, KunMing, pp803 – 810
- [11] Sun JH, Long ZF, Long YQ (1999) A generalized conforming element with vertex rotational freedoms for thin shell analysis. In: Long YQ (ed) *The Proceedings of the First International Conference on Structural Engineering*. China, KunMing, pp811 – 818
- [12] Sun JH, Long ZF, Long YQ, Zhang CS (2001) Geometrically nonlinear stability analysis of shells using generalized conforming shallow shell element. *International Journal of Structural Stability and Dynamics* 1(3): 313 – 332
- [13] Wilson EL, Taylor RL, Doherty WP, Ghabussi T (1973) Incompatible displacement models. In: Fenven ST et al (eds) *Numerical and Computer Methods in Structural Mechanics*. Academic Press, New York, pp43 – 57
- [14] Long YQ, Xin KG (1989) Generalized conforming element for bending and buckling analysis of plates. *Finite Elements in Analysis and Design* 5:15 – 30
- [15] Taylor RL, Beresford PJ, Wilson EL (1976) A non-conforming element for stress analysis. *International Journal for Numerical Methods in Engineering* 10: 1211 – 1219
- [16] Wachspress EL (1978) Incomptiable quadrilateral basis functions. *International Journal for Numerical Methods in Engineering* 12: 589 – 595
- [17] Pian THH, Wu CC (1986) General formulation of incompatible shape function and an incompatible isoparametric element. In: *Proc of the Invitational China-American Workshop on FEM*. Chengde, pp159 – 165
- [18] Chen WJ, Tang LM (1981) Isoparametric quasi-conforming element. *Journal of Dalian Institute of Technology* 20(1): 63 – 74 (in Chinese)
- [19] Cook RD (1974) Improved two-dimensional finite element. *Journal of the Structural Division ASCE*, 100, ST9: 1851 – 1863
- [20] Zienkiewicz OC, Taylor RL (1991) *The finite element method*, 4th edn. Volume 2—Solid and Fluid Mechanics & Dynamics and Non-linearity. McGRAW-HILL Book Company, London
- [21] Clough RW, Johnson CP (1968) A finite element approximation for the analysis of thin shells. *International Journal of Solids and Structures* 4: 43 – 60
- [22] Olsen MD, Bearden TW (1979) A simple flat shell element revisited. *International Journal for Numerical Methods in Engineering* 14: 51 – 68
- [23] Allman DJ (1988) A quadrilateral finite element including vertex rotation for plane elasticity analysis. *International Journal for Numerical Methods in Engineering* 26: 717 – 730
- [24] Felippa CA, Alexander S (1992) Membrane triangles with corner drilling freedom—III. Implementations and performane evolution. *Finite Element in Analysis and Design* 12: 203 – 249

Advanced Finite Element Method in Structural Engineering

- [25] Bergan PG, Felippa CA (1985) A triangular membrane element with rotational degrees of freedom. *Computer Methods in Applied Mechanics and Engineering* 50: 25 – 69
- [26] Long ZF, Cen S (1992) New monograph of finite element method: principle, programming, developments. Hydraulic and Water-power Press, China, Beijing (in Chinese)
- [27] Long YQ, Bu XM, Long ZF, Xu Y (1995) Generalized conforming plate bending elements using point and line compatibility conditions. *Computers & Structures* 54(4): 717 – 723
- [28] Fish J, Belytshko T (1992) Stabilized rapidly convergent 18-degree-of-freedom flat shell triangular element. *International Journal for Numerical Methods in Engineering* 33: 149 – 162
- [29] Chen WJ, Cheung YK (1999) Refined non-conforming triangular elements for analysis of shell structures. *International Journal for Numerical Methods in Engineering* 46: 433 – 455
- [30] Providas E, Kattis MA (2000) An assessment of two fundamental flat triangular shell elements with drilling rotations. *Computers & Structure* 77(2): 129 – 139
- [31] Carpenter N, Stolarski H, Belyschko T (1986) Improvements in 3-node triangular shell elements. *International Journal for Numerical Methods in Engineering* 23: 1643 – 1667
- [32] ABAQUS/Standard User's Manual, Version 5.8 (1998) Hibbit, Karlsson & Sorensen, Inc.: Rawtucket, Rhode Island
- [33] MacNeal RH, Harder RL (1985) A proposed standard set of problems to test finite element accuracy. *Finite Element in Analysis and Design* 1: 3 – 20
- [34] Aminpour MA (1992) An assumed-stress hybrid 4-node shell element with drilling degrees of freedom. *International Journal for Numerical Methods in Engineering* 33: 19 – 38
- [35] Guan Y, Tang L (1992) A quasi-conforming nine-node degenerated shell finite element. *Finite Elements in Analysis and Design* 11: 165 – 176
- [36] Batoz JL, Tahar MB (1982) Evaluation of a new quadrilateral thin plate bending element. *International Journal for Numerical Methods in Engineering* 18: 1655 – 1677
- [37] Bathe KJ, Dvorkin EN (1985) Short communication: a four-node plate bending element based on Mindlin/Ressiner plate theory and mixed interpolation. *International Journal for Numerical Methods in Engineering* 21: 367 – 383
- [38] Chen WJ (2001) Advances in finite element with high performances. In: Yuan MW, Sun SL (eds) *Computational Mechanics in Engineering and Science (Proceedings of the Chinese Conference on Computational Mechanics'2001)*. Peking Univerisuty Press, China, Guangzhou, pp136 – 151 (in Chinese)
- [39] Parish HA (1979) Critical survey of the 9-node degenerated shell element with special emphasis on thin shell application and reduced integration. *Computer Methods in Applied Mechanics and Engineering* 20: 323 – 350
- [40] Long YQ, Zhao JQ (1992) Generalized conforming curved rectangular element for shallow shells. *Gong Cheng Li Xue/Engineering Mechanics*, 9(1): 3 – 10 (in Chinese)
- [41] Long YQ, Xi F (1992) A universal method for including shear deformation in thin plate elements. *International Journal for Numerical Methods in Engineering* 34: 171 – 177
- [42] Sun JH (1998) Research on generalized conforming shallow shell element and nonlinear analysis of plate and shell structures [Doctoral Dissertation]. Tsinghua University, Beijing (in Chinese)
- [43] Bu XM, Long YQ (1991) A high-precise rectangular element for thin plate bending analysis. *Tumu Gongcheng Xuebao/China Civil Engineering Journal* 24(1): 17 – 22 (in Chinese)

Chapter 11 Generalized Conforming Membrane and Shell Elements

- [44] Bonnes G, Dhatt G, Giroux Y, Robichaud (1968) Curved triangular elements for analysis of shell. In: Proceedings of Conference on Matrix Method in Structural Mechanics. A. F. Base, Ohio: Wright Patterson pp617 – 640
- [45] Cowper G, Lindberg GM, Olson MD (1970) A shallow shell finite element of triangular shape. *International Journal of Solids and Structures* 6: 1133 – 1156
- [46] Cook RD (1974) *Concept and Applications of Finite Element Analysis*. John Wiley & Sons, Inc, New York
- [47] Badiansky B (1974) Theory of buckling and post-buckling behavior of elastic structure. In: Yih Chia-Shun (eds) *Advances in Applied Mechanics* (Vol. 14), Academic Press, New York, pp2 – 63
- [48] Jiang HY (1984) Nonlinear finite element method of quasi-conforming technique model. *Computational Structural Mechanics and Applications* 1(2): 49 – 59 (in Chinese)
- [49] Pica A, Wood RD, Hinton E (1980) Finite element analysis of geometrically nonlinear plate behaviour using a Mindlin formulation. *Computers & Structures* 11: 203 – 215
- [50] Sabir AB, Lock AC (1972) The application of finite element to the large deflection geometrically nonlinear behavior of cylindrical shells. In: Brebbia CA (ed) *Variational Methods in Engineering*, Southampton University Press, Southampton pp54 – 65
- [51] Ramesh G, Krishnamoorthy CS (1993) Post-buckling analysis of structures by dynamic relaxation. *International Journal for Numerical Methods in Engineering* 36: 1339 – 1364
- [52] Wei G, Zhao CX (1990) A large deflection quasi-conforming rectangular shallow shell element and applications. *Computational Structural Mechanics and Applications* 7(1): 15 – 43 (in Chinese)
- [53] Crisfield MA (1981) A fast incremental / iterative solution procedure that handles “snap-through”. *Computers & Structures* 13: 55 – 62
- [54] Horrigmoe G, Bergan PG (1978) Nonlinear analysis of free-form shells by flat finite elements. *Computer Methods in Applied Mechanics and Engineering* 16: 11 – 35

PART III

Other Advances in Finite Element Method

- Chapter 12 Sub-Region Mixed Element I — Fundamental Theory at Crack Problem
- Chapter 13 Sub-Region Mixed Element II — V-Notch Problem
- Chapter 14 Analytical Trial Function Method I — Membrane and Plate Bending Elements
- Chapter 15 Analytical Trial Function Method II — Singular Elements with Crack and Notch
- Chapter 16 Quadrilateral Area Coordinate Systems, Part I — Theory and Formulae
- Chapter 17 Quadrilateral Area Coordinate Systems, Part II — A New Tool for Constructing Quadrilateral Elements
- Chapter 18 Spline Element I — Analysis of High-Rise Building Structures
- Chapter 19 Spline Element II — Analysis of Plate/Shell Structures

Chapter 12 Sub-Region Mixed Element I— Fundamental Theory and Crack Problem

Yu-Qiu Long

Department of Civil Engineering, School of Civil Engineering,
Tsinghua University, Beijing, 100084, China

Song Cen

Department of Engineering Mechanics, School of Aerospace,
Tsinghua University, Beijing, 100084, China

Abstract This chapter firstly gives a brief review of the variational fundamentals and computational method of the sub-region mixed element method in the first two sections. Then, in the next three sections, the applications of this method in the 2D crack problem, cracked thick plate problem and surface crack problem in 3D body are introduced, respectively. Numerical examples show that the proposed sub-region mixed element method is an efficient tool for solving the various crack problems.

Keywords finite element, sub-region mixed element, crack problem.

12.1 Review of the Sub-Region Mixed Element Method

The main characteristic of the sub-region mixed element method can be stated as follows: a whole structure is divided into several sub-regions (or sub-domains), and then, the displacement-based elements and the stress-based elements are adopted in different sub-regions, respectively. The finite element mesh used here is a kind of mixed mesh in which both displacement-based element and stress-based element exist and are coupled with each other. This is a new version of the mixed methods—usual mixed-hybrid element method is only a mixed method in the element level, while the sub-region mixed element method is a mixed method in the whole structure level.

The sub-region mixed element method takes the sub-region mixed variational principle (refer to Chap. 2) as its theoretical basis. Thus, the coupling problem and convergence problem at the mixed interface between the displacement-based element and stress-based element can be solved in theory.

The sub-region mixed element method has a broad application range. On the

one hand, it is a universal method which can be used for various mechanics problems. On the other hand, the most suitable application field of this method is the stress concentration problem or singular stress problem (such as crack problem and notch problem). The distinguished characteristic of this kind of problem is that, there are two sub-domain types in the structure: one belongs to the singular stress region, and the other belongs to the even stress region. That is to say, **the stress fields of this kind of problem possess a characteristic of “sub-region mixed”**—the stress fields of the whole structure can be divided into multiple sub-domains with different stress types. They simultaneously exist in the whole structure.

Obviously, this kind of problem in which the stress fields possess the sub-region mixed character is just the problem that the sub-region mixed element method is the most suitable for.

In fact, the sub-region mixed element method was initially established^[1] just for this kind of problem (crack problem). The stress-based element with singular stress terms is used in the singular stress region at the tip of the crack, and the conventional displacement-based elements are used in the even stress region away from the tip of the crack. Due to the ingenious combination of the stress-based element and the displacement-based element (i.e. singular element and conventional element), both advantages of these two elements can be obtained. So, the computational accuracy of this method is very high. In reference [1], results of mode I plane crack problem by Benzley’s method^[2], Qian’s method^[3] and sub-region mixed element method are compared with each other. It can be seen that, the precision of Qian’s method is nearly thrice as good as that of Benzley’s method, but the precision of the sub-region mixed element method using only 17 elements is the same as that of Qian’s method using 448 elements.

Following are the analysis steps of the sub-region mixed element method for the crack problem.

(1) An example of the sub-region mixed problem—stress analysis of a body with crack (Fig. 12.1).

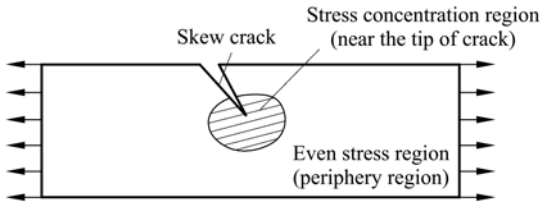


Figure 12.1 Crack problem

Two different region types (stress concentration region and even stress region) exist simultaneously.

(2) The region division of the sub-region mixed element method (Fig. 12.2).

Two different element types (displacement-based element and stress-based element) are used simultaneously.

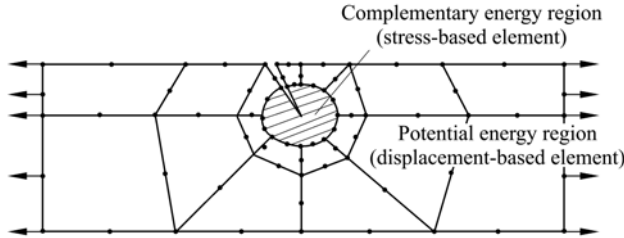


Figure 12.2 The coupling of potential energy region (displacement-based element) and complementary energy region (stress-based element)

Region division	Element type	Basic variables
Stress concentration region (Complementary energy region)	Singular stress element (stresses distribute according to the singular analytical solutions)	Stress parameters β (unknown coefficients in the analytical solutions)
Even stress region (Potential energy region)	Conventional displacement-based element (isoparametric element) (displacements distribute according to polynomial expressions)	Nodal displacements δ

(3) The basic equations of the sub-region mixed element method

From the sub-region mixed variational principle

$$\Pi = \Pi_p(\delta) - \Pi_c(\beta) + H_{pc}(\delta, \beta) = \text{stationary} \quad (12-1)$$

and stationary conditions

$$\frac{\partial \Pi}{\partial \delta} = \mathbf{0}, \quad \frac{\partial \Pi}{\partial \beta} = \mathbf{0},$$

the basic equations of the mixed method can be obtained. Then, δ and β can be solved.

(4) Advances on the applications of the sub-region mixed element method

Applications		References	
Fracture problem	2D fracture problem (mode I)	[1] (1982)	
	2D fracture problem (mixed mode)	[4] (1985)	
	Fracture problem in Reissner plate	[5] (1988)	
	Surface crack problem in 3D elastic body	[6] (1992)	
Notch problem	Plane V-notch problem	[7] (1992)	
	Bi-material notch problem	[8] (1990) [9] (1992)	
	Notch problem in Reissner plate	[10] (1992)	
	Notch problem in 3D elastic body	[11] (1994)	
	Stress concentrated problem in shear wall supported by beam column system		[12] (1984)

(5) The characteristics and merits of the sub-region mixed element method

The knack of the success—smart combinations between the stress-based element and displacement-based element, between singular element and conventional element, and between analytical solution and numerical solution.

12.2 Basic Equations of the Sub-Region Mixed Element Method

This section will briefly narrate the basic concepts and equations of the sub-region mixed element method. The concepts of the sub-region mixed mesh and mixed basic variables, mixed energy functional, and mixed basic equations, are introduced in turn.

12.2.1 Sub-Region Mixed Mesh and Mixed Basic Variables

In the sub-region mixed element method, an elastic body is divided into a mixed body composed of potential energy region (P-region) and complementary energy region (C-region), and then, a mixed mesh containing both displacement-based element and stress-based element is established.

In the potential energy region, the displacement-based element is adopted, and the nodal displacements are taken as the basic variables:

$$\boldsymbol{\delta} = [\delta_1 \quad \delta_2 \quad \cdots \quad \delta_n]^T \quad (12-2)$$

In the complementary energy region, the stress-based element is used, and the stress parameters are taken as the basic variables:

$$\boldsymbol{\beta} = [\beta_1 \quad \beta_2 \quad \cdots \quad \beta_m]^T \quad (12-3)$$

The basic variables of the sub-region mixed element method is formed by the combination of the above two basic variables $\boldsymbol{\delta}$ and $\boldsymbol{\beta}$:

$$\boldsymbol{q} = [\boldsymbol{\beta}^T \quad \boldsymbol{\delta}^T]^T \quad (12-4)$$

Obviously, this set of basic variables is a mixed mode.

12.2.2 Mixed Energy Functional

The sub-region mixed element method takes the sub-region mixed variational principle as its theoretical basis. The energy functional of the sub-region mixed

variational principle is given by Eq. (2-1) in Chap. 2, i.e.,

$$\Pi = \Pi_p - \Pi_c + H_{pc} \quad (12-5)$$

where Π_p is the total potential energy of the potential region (P-region); Π_c is the total complementary energy of the complementary energy region; H_{pc} is the additional energy on the interface S_{pc} .

The expressions of the terms at the right side of Eq. (12-5) are as follows:

The total potential energy Π_p of the potential energy region is expressed in terms of the nodal displacements δ of the potential energy region as

$$\Pi_p = \frac{1}{2} \delta^T \mathbf{K} \delta - \delta^T \mathbf{P} \quad (12-6)$$

where \mathbf{K} is the global stiffness matrix of the potential energy region; \mathbf{P} is the equivalent nodal load vector.

The total complementary energy Π_c of the complementary energy region is expressed in terms of the stress parameters β of the complementary energy region as

$$\Pi_c = \frac{1}{2} \beta^T \mathbf{F} \beta \quad (12-7)$$

where \mathbf{F} is the flexibility matrix of the complementary energy region.

The additional energy H_{pc} at the interface of the two regions is given by Eq. (2-4), i.e.,

$$H_{pc} = \int_{S_{pc}} \mathbf{T}^T \bar{\mathbf{u}} ds \quad (12-8)$$

where \mathbf{T} denotes the boundary forces of the complementary energy region on the interface S_{pc} ; $\bar{\mathbf{u}}$ denotes the boundary displacements of the potential energy region at the interface; and the additional energy H_{pc} at the interface S_{pc} is the work done by the boundary forces \mathbf{T} of the complementary energy region along the boundary displacements $\bar{\mathbf{u}}$ of the potential energy region.

The boundary forces \mathbf{T} can be derived from the stress parameters β , and the boundary displacements $\bar{\mathbf{u}}$ can be derived from the boundary nodal displacements $\bar{\delta}$. Let

$$\mathbf{T} = \mathbf{R} \beta \quad (12-9)$$

$$\bar{\mathbf{u}} = \bar{\mathbf{N}} \bar{\delta} \quad (12-10)$$

Substitution of the above two equations into Eq. (12-8) yields

$$H_{pc} = \beta^T \mathbf{H} \bar{\delta} \quad (12-11)$$

where \mathbf{H} is the mixed matrix at the interface:

$$\mathbf{H} = \int_{S_{pc}} \mathbf{R}^T \bar{\mathbf{N}} ds \quad (12-12)$$

Anyway, substituting Eqs. (12-6), (12-7) and (12-11) into Eq. (12-5), the expression of the energy functional Π of the sub-region mixed element method can be obtained as follows:

$$\Pi = \frac{1}{2} \boldsymbol{\delta}^T \mathbf{K} \boldsymbol{\delta} - \boldsymbol{\delta}^T \mathbf{P} - \frac{1}{2} \boldsymbol{\beta}^T \mathbf{F} \boldsymbol{\beta} + \boldsymbol{\beta}^T \mathbf{H} \bar{\boldsymbol{\delta}} \quad (12-13)$$

Π is a mixed energy functional, and determined by the mixed basic variables $\boldsymbol{\delta}$ and $\boldsymbol{\beta}$.

12.2.3 Mixed Basic Equations

The stationary condition of the sub-region mixed energy functional is

$$\delta \Pi = 0 \quad (12-14)$$

or written in the following form of mixed stationary conditions

$$\frac{\partial \Pi}{\partial \boldsymbol{\beta}} = \mathbf{0} \quad (12-15a)$$

$$\frac{\partial \Pi}{\partial \boldsymbol{\delta}} = \mathbf{0} \quad (12-15b)$$

Firstly, from the condition (12-15a), we have

$$-\mathbf{F} \boldsymbol{\beta} + \mathbf{H} \bar{\boldsymbol{\delta}} = \mathbf{0}$$

Then, the stress parameters $\boldsymbol{\beta}$ can be solved:

$$\boldsymbol{\beta} = \mathbf{F}^{-1} \mathbf{H} \bar{\boldsymbol{\delta}} \quad (12-16)$$

Substituting the above equation into Eq. (12-13), then Π containing only $\boldsymbol{\delta}$ can be obtained

$$\Pi = \frac{1}{2} \boldsymbol{\delta}^T \mathbf{K} \boldsymbol{\delta} + \frac{1}{2} \bar{\boldsymbol{\delta}}^T (\mathbf{H}^T \mathbf{F}^{-1} \mathbf{H}) \bar{\boldsymbol{\delta}} - \boldsymbol{\delta}^T \mathbf{P} \quad (12-17)$$

Secondly, let

$$\boldsymbol{\delta} = \begin{Bmatrix} \bar{\boldsymbol{\delta}} \\ \boldsymbol{\delta}^* \end{Bmatrix} \quad (12-18)$$

here, $\bar{\boldsymbol{\delta}}$ and $\boldsymbol{\delta}^*$ denote the nodal displacements in the potential energy region at the interface and not at the interface, respectively. From the condition (12-15b),

we obtain

$$\left(\mathbf{K} + \begin{bmatrix} \mathbf{H}^T \mathbf{F}^{-1} \mathbf{H} & \mathbf{0} \\ \mathbf{0} & \mathbf{0} \end{bmatrix} \right) \begin{Bmatrix} \bar{\boldsymbol{\delta}} \\ \boldsymbol{\delta}^* \end{Bmatrix} = \mathbf{P} \quad (12-19)$$

Then, from this equation, the nodal displacements $\boldsymbol{\delta}$ can be solved. And, the stress parameters $\boldsymbol{\beta}$ can be evaluated from Eq. (12-16).

The mixed basic Eqs. (12-15a,b) of the sub-region mixed element method are listed above, and Eqs. (12-19) and (12-16), for solving $\boldsymbol{\delta}$ and $\boldsymbol{\beta}$, respectively, are also derived.

12.3 2D Crack Problem

Reference [1] firstly applied the sub-region mixed element method to analyze the 2D fracture problems and discussed the computational problem for the stress intensity factor K_I of mode I. Later, reference [4] discussed the mixed problem of the stress intensity factor K_I of mode I and the stress intensity factor K_{II} of mode II.

In this section, the 2D crack problems are systematically analyzed by the sub-region mixed element method. Firstly, the expansion of stresses near the tip of the crack is introduced. Then, the related computational formulas of the sub-region mixed element method for the mixed crack problem are given.

12.3.1 The Series Expansion of Stresses Near the Tip of a 2D Crack

Let us consider an elastic plane crack shown in Fig. 12.3. The origin of the coordinate is at the tip of the crack. In the series expansion of stresses near the

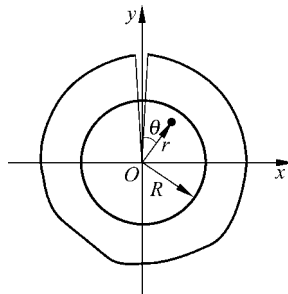


Figure 12.3 Stress analysis near the tip of a crack

crack tip, m_1 terms are taken for both modes I and II stress terms, then we have

$$\boldsymbol{\sigma} = [\sigma_x \quad \sigma_y \quad \tau_{xy}]^T = \mathbf{S}' \boldsymbol{\beta}' + \mathbf{S}'' \boldsymbol{\beta}'' \quad (12-20)$$

in which the two terms at the right side are corresponding to the modes I and II stress terms, respectively:

$$\boldsymbol{\beta}' = [\beta'_1 \quad \beta'_2 \quad \cdots \quad \beta'_{m_1}]^T \quad (12-21)$$

$$\boldsymbol{\beta}'' = [\beta''_1 \quad \beta''_2 \quad \cdots \quad \beta''_{m_1}]^T \quad (12-22)$$

$$\mathbf{S}' = [\mathbf{S}'_1 \quad \mathbf{S}'_2 \quad \cdots \quad \mathbf{S}'_{m_1}] \quad (12-23)$$

$$\mathbf{S}'' = [\mathbf{S}''_1 \quad \mathbf{S}''_2 \quad \cdots \quad \mathbf{S}''_{m_1}] \quad (12-24)$$

In the coordinate system shown in Fig. 12.3, \mathbf{S}'_k and \mathbf{S}''_k can be expressed as

$$\mathbf{S}'_k = \frac{k}{2} \left(\frac{r}{R} \right)^{\frac{k}{2}-1} \cdot \left\{ \begin{array}{l} \left[2 - (-1)^k - \frac{k}{2} \right] \cos\left(\frac{k}{2}-1\right)(\pi-\theta) + \left(\frac{k}{2}-1\right) \cos\left(\frac{k}{2}-3\right)(\pi-\theta) \\ \left[2 + (-1)^k + \frac{k}{2} \right] \cos\left(\frac{k}{2}-1\right)(\pi-\theta) - \left(\frac{k}{2}-1\right) \cos\left(\frac{k}{2}-3\right)(\pi-\theta) \\ \left[(-1)^k + \frac{k}{2} \right] \sin\left(\frac{k}{2}-1\right)(\pi-\theta) - \left(\frac{k}{2}-1\right) \sin\left(\frac{k}{2}-3\right)(\pi-\theta) \end{array} \right\} \quad (12-25)$$

$$\mathbf{S}''_k = \frac{k}{2} \left(\frac{r}{R} \right)^{\frac{k}{2}-1} \cdot \left\{ \begin{array}{l} \left[2 + (-1)^k - \frac{k}{2} \right] \sin\left(\frac{k}{2}-1\right)(\pi-\theta) + \left(\frac{k}{2}-1\right) \sin\left(\frac{k}{2}-3\right)(\pi-\theta) \\ \left[2 - (-1)^k + \frac{k}{2} \right] \sin\left(\frac{k}{2}-1\right)(\pi-\theta) - \left(\frac{k}{2}-1\right) \sin\left(\frac{k}{2}-3\right)(\pi-\theta) \\ \left[(-1)^k - \frac{k}{2} \right] \cos\left(\frac{k}{2}-1\right)(\pi-\theta) + \left(\frac{k}{2}-1\right) \cos\left(\frac{k}{2}-3\right)(\pi-\theta) \end{array} \right\} \quad (k=1,2,\dots,m_1) \quad (12-26)$$

It can be verified that, the above stress terms satisfy the stress equilibrium differential equations and the stress boundary conditions on the crack surface ($\theta = 0, 2\pi$):

$$\sigma_x = \tau_{xy} = 0$$

Then, the stress intensity factors K_I and K_{II} can be expressed in terms of the stress parameters β'_1 and β''_1 as:

$$\left. \begin{aligned} K_{\text{I}} &= \sqrt{2\pi R} \beta' \\ K_{\text{II}} &= \sqrt{2\pi R} \beta'' \end{aligned} \right\} \quad (12-27)$$

The stress expansion (12-20) can also be written as

$$\boldsymbol{\sigma} = \mathbf{S} \boldsymbol{\beta} \quad (12-28)$$

in which

$$\boldsymbol{\beta} = [\boldsymbol{\beta}'^T \quad \boldsymbol{\beta}''^T]^T \quad (12-29a)$$

$$\mathbf{S} = [\mathbf{S}' \quad \mathbf{S}''] \quad (12-29b)$$

12.3.2 Formulation of Sub-Region Mixed Element Method for the 2D Crack Problem

As an example, the plate with a skew crack and under tension load, which is shown in Fig. 12.1, is considered. We will introduce the main ideas of the sub-region mixed element method for this problem. Let the thickness of the plate $h=1$.

(1) Region division and basic variables

Region division is shown in Fig. 12.2. It contains two region types.

The complementary energy region—it is the circular region near the crack tip, in which the crack tip is the center of the circle; R is the radius. This is a singular stress-based element with internal crack, and the $2m_1$ stress parameters in $\boldsymbol{\beta}$ are its basic variables, as shown in Eq. (12-29a).

The potential energy region—it is the region out of the singular element, and takes $2n_1$ nodal displacement components as the basic variables:

$$\boldsymbol{\delta} = [u_1 \quad v_1 \quad \cdots \quad u_{n_1} \quad v_{n_1}]^T \quad (12-30)$$

(2) Mixed energy functional Π

The energy functional of the sub-region mixed variational principle is given initially by Eq. (12-5) and finally by Eq. (12-13), in which the stiffness matrix \mathbf{K} of the potential energy region and the equivalent nodal load vector \mathbf{P} are determined according to the conventional procedure. Furthermore, the flexibility matrix \mathbf{F} of the complementary energy region and the mixed matrix \mathbf{H} at the interface will be derived as follows.

(3) The flexibility matrix \mathbf{F} of the complementary energy region

In the current problem, the total complementary energy of the complementary energy region is equal to the complementary strain energy of the singular element, i.e.,

$$\Pi_c = \frac{1}{2} \iint_A \boldsymbol{\sigma}^T \mathbf{D}^{-1} \boldsymbol{\sigma} dA \quad (12-31)$$

For plane stress problem, we have

$$\mathbf{D}^{-1} = \frac{1}{E} \begin{bmatrix} 1 & -\mu & 0 \\ -\mu & 1 & 0 \\ 0 & 0 & 2(1+\mu) \end{bmatrix} \quad (12-32)$$

E is the Young's modulus; μ is the Poisson's ratio. For the plane strain problem, E and μ in the above equation should be replaced by $\frac{E}{1-\mu^2}$ and $\frac{\mu}{1-\mu}$, respectively.

Substitution of Eq. (12-28) into Eq. (12-31) yields

$$\Pi_c = \frac{1}{2} \boldsymbol{\beta}^T \mathbf{F} \boldsymbol{\beta} \quad (12-33)$$

where

$$\mathbf{F} = \iint_A \mathbf{S}^T \mathbf{D}^{-1} \mathbf{S} dA \quad (12-34)$$

Equation (12-34) gives the expression of the flexibility matrix \mathbf{F} of the complementary energy region.

In consideration of the symmetry of mode I stress terms and antisymmetry of mode II stress terms, the complementary energy Π_c can also be written as

$$\Pi_c = \frac{1}{2} \boldsymbol{\beta}'^T \mathbf{F}' \boldsymbol{\beta}' + \frac{1}{2} \boldsymbol{\beta}''^T \mathbf{F}'' \boldsymbol{\beta}'' \quad (12-35)$$

where

$$\begin{aligned} \mathbf{F}' &= \iint_A \mathbf{S}'^T \mathbf{D}^{-1} \mathbf{S}' dA \\ \mathbf{F}'' &= \iint_A \mathbf{S}''^T \mathbf{D}^{-1} \mathbf{S}'' dA \end{aligned} \quad (12-36)$$

Substituting Eqs. (12-25) and (12-26) into the above equation, and let $m_1 = 4$, we have

$$\mathbf{F}' = \frac{2R^2}{E} \begin{bmatrix} \frac{\pi}{4}(5-3\mu) & \frac{32}{15}(2-3\mu) & \frac{3\pi}{2}(1-\mu) & \frac{64}{105}(6-\mu) \\ & 8\pi & \frac{32}{5}(2-\mu) & 0 \\ \text{Sym.} & & \frac{3\pi}{4}(5-3\mu) & \frac{64}{35}(6+\mu) \\ & & & 8\pi(3+2\mu) \end{bmatrix} \quad (12-37)$$

$$\mathbf{F}'' = \frac{2R^2}{E} \begin{bmatrix} \frac{\pi}{4}(9+\mu) & 0 & -\frac{3\pi}{2}(1-\mu) & -\frac{128}{105}(6-\mu) \\ & 0 & 0 & 0 \\ \text{Sym.} & & \frac{3\pi}{4}(17+9\mu) & \frac{128}{35}(6+\mu) \\ & & & 8\pi \end{bmatrix} \quad (12-38)$$

And,

$$\mathbf{F} = \begin{bmatrix} \mathbf{F}' & \mathbf{0} \\ \mathbf{0} & \mathbf{F}'' \end{bmatrix} \quad (12-39)$$

Substituting Eqs. (12-37) and (12-38) into the above equation, the explicit expressions for the flexibility matrix \mathbf{F} of the complementary energy region can be obtained.

(4) The mixed matrix \mathbf{H} at the interface

From Eqs. (12-8) and (12-11), we have

$$H_{pc} = \int_{S_{pc}} \mathbf{T}^T \bar{\mathbf{u}} ds = \boldsymbol{\beta}^T \mathbf{H} \bar{\boldsymbol{\delta}}$$

In order to determine \mathbf{H} , \mathbf{T} and $\bar{\mathbf{u}}$ should be firstly derived.

Firstly, the boundary forces \mathbf{T} of the complementary energy region at the interface can be derived:

$$\mathbf{T} = \mathbf{L}\boldsymbol{\sigma} = \mathbf{L}\mathbf{S}\boldsymbol{\beta} \quad (12-40)$$

where \mathbf{L} is the direction cosine matrix of the interface

$$\mathbf{L} = \begin{bmatrix} \sin \theta & 0 & \cos \theta \\ 0 & \cos \theta & \sin \theta \end{bmatrix} \quad (12-41)$$

From Eqs. (12-40) and (12-9), we obtain

$$\mathbf{R} = \mathbf{L}\mathbf{S} \quad (12-42)$$

Secondly, the boundary displacements $\bar{\mathbf{u}}$ of the potential energy region at the interface are then derived. From Eq. (12-10), we have

$$\bar{\mathbf{u}} = \begin{Bmatrix} \bar{u} \\ \bar{v} \end{Bmatrix} = \bar{\mathbf{N}} \bar{\boldsymbol{\delta}} \quad (12-43)$$

$\bar{\mathbf{N}}$ is the shape function matrix of the boundary nodes at the interface,

$$\bar{\mathbf{N}} = \begin{bmatrix} \bar{N}_1 & 0 & \bar{N}_2 & 0 & \dots & \bar{N}_{n_2} & 0 \\ 0 & \bar{N}_1 & 0 & \bar{N}_2 & \dots & 0 & \bar{N}_{n_2} \end{bmatrix} \quad (12-44)$$

where n_2 is the number of the nodes on the interface; and the expressions of shape functions \bar{N}_i are given by reference[4].

Substitution of \mathbf{R} in Eq. (12-42) and $\bar{\mathbf{N}}$ in Eq. (12-44) into Eq. (12-12) yields the mixed matrix \mathbf{H} at the interface, i.e.,

$$\mathbf{H} = \int_{S_{pc}} \mathbf{R}^T \bar{\mathbf{N}} \, ds = \int_{S_{pc}} \mathbf{S}^T \mathbf{L}^T \bar{\mathbf{N}} \, ds \quad (12-45)$$

(5) Solution of basic equations

Matrices \mathbf{F} and \mathbf{H} can be obtained from Eqs. (12-39) and (12-45), respectively. Substitution of them into Eq. (12-13) yields the expression of the energy functional Π .

By using the stationary condition of the energy functional, the basic Eqs. (12-19) and (12-16) of the sub-region mixed element method can be derived. From them, the basic variables $\boldsymbol{\delta}$ and $\boldsymbol{\beta}$ can be solved in turn. Finally, the stress intensity factors K_I and K_{II} can be obtained from Eq. (12-27).

The sub-region mixed element method can be denoted by SRM. For the 2D mode I crack problem, it is denoted by SRM-C1; and for the mixed 2D problem, it is denoted by SRM-C2.

Example 12.1 Stress intensity factors of the four 2D crack problems shown in Fig. 12.4.

- (a) single-edge cracked tension plate—SEC (Fig. 12.4(a));
- (b) centre cracked tension plate—CC (Fig. 12.4(b));
- (c) single-edge slant cracked tension plate—SESC (Fig. 12.4(c));
- (d) centre slant cracked tension plate—CSC (Fig. 12.4(d)).

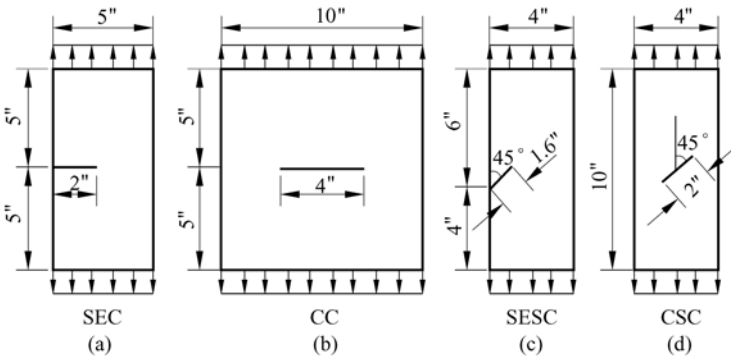


Figure 12.4 Four crack problems

The results by the sub-region mixed element method in reference[4] and the related results for comparison are given in Table 12.1. For comparison with the results in related references, here the original data and the unit given in these references are used for the computations: the loading is 1lb/in²; the Poisson’s ratio is 0.3; the Young’s modulus is 10⁷lb/in²; the length or semi-length of the crack is a .

Table 12.1 Stress intensity factor result comparisons

Problem	References	$K_I / (\sigma\sqrt{\pi a})$		Error Δ_1 (%)	Error Δ_2 (%)	DOF	Standard value
(a) SEC	[13]	2.098		- 0.57		186	2.110 ^[15]
	[14]	2.092		- 0.84		712	
	SRM ^[4]	2.088		- 1.04		90	
(b) CC	[13]	1.229		0.65		186	1.220 ^[16]
	[14]	1.211		- 0.64		88	
	SRM ^[4]	1.225		0.41		90	
(c) SESC	SRM ^[4,17]	1.012	0.508	- 0.78	0.59	210	[17]
		1.020	0.505				
(d) CSC	SRM ^[4,18]	0.614	0.549	0.33	0.73	320	[18]
		0.612	0.545				

The results for the stress intensity factors K_I and K_{II} calculated by the sub-region element method and other methods are listed in Table 12.1.

From the numerical results in Table 12.1 and other examples, it can be concluded that:

(1) The sub-region mixed element method has been successfully applied to 2D crack problem involving single as well as mixed mode of crack deformation. It may provide more accurate results with less work load.

(2) If the radius R of the complementary energy region is too small, then more nodes must be used in the P-region for obtaining better accuracy. When R is about 0.075 a (a is the crack length or semi-length), better results can be obtained by using less nodes in the P-region. In this case, 9 nodes on the interface (semicircular) are enough.

(3) With the increase of the number of the stress parameters in the C-region, the accuracy can in general be improved. However, it is suitable to use the first four terms ($m_1 = 4$) of the known stress function. Fig. 12.5 shows the relation curves of computed errors Δ in the stress intensity factors and $\frac{a}{R}$ when different m_1 is taken for CC specimen.

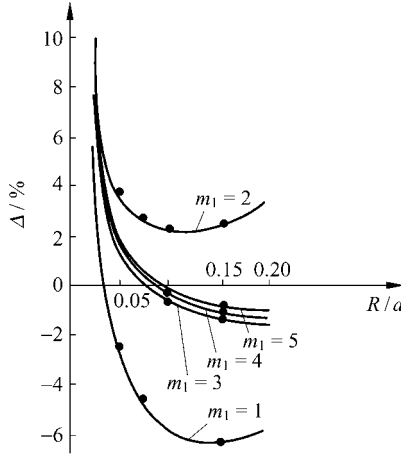


Figure 12.5 The relation curve of Δ and R/a

Δ —the relative error between numerical results and reference values
 m_1 —the number of the terms in stress functions
 R —the radius of the complementary energy region
 a —the semi-length of the crack

12.4 Cracked Thick Plate Problem

The early analysis of the plate fracture problems was based on the Kirchhoff thin plate theory, in which the disadvantage is that the degree of stress singularity of the shear force is different from that of the bending moment. But, if the Reissner thick plate theory is adopted, the correct conclusion that both singularities are equal to each other can then be obtained. The mode I problem has been calculated by Barsoum^[19] who used the degenerated thick plate element as well as distorted isoparametric element, and G. Yagawa^[20] who superimposed the finite element mode on the singular term.

This section discusses the computation of the stress intensity factor in the cracked plate bending problem by using the sub-region mixed element method^[5]. Here, the Reissner thick plate theory is adopted so that the influence of transverse shear deformation is considered. In the computational model, the singular stress element is used near the crack tip, and the isoparametric displacement-based elements are used in the other region. Then, the stress intensity factors of modes I, II and III for some finite and infinite plates are calculated. The relative errors are less than 1%.

In this section, the basic equations of the thick plate theory and the series expansion of the internal forces near the crack tip are introduced firstly; and then the related formulas of the sub-region mixed element method for the cracked thick plate bending problem are given.

12.4.1 Basic Equations of the Thick Plate

In a thick plate, the positive directions of deflection w , normal slopes ψ of mid-surface, shear strains γ , curvatures κ , internal moments \mathbf{M} and transverse shear forces \mathbf{Q} are shown in Fig. 12.6. Here, we have

$$\left. \begin{aligned} \boldsymbol{\psi} &= [\psi_x \quad \psi_y]^T \\ \boldsymbol{\gamma} &= [\gamma_x \quad \gamma_y]^T \\ \boldsymbol{\kappa} &= [\kappa_x \quad \kappa_y \quad 2\kappa_{xy}]^T \\ \mathbf{M} &= [M_x \quad M_y \quad M_{xy}]^T \\ \mathbf{Q} &= [Q_x \quad Q_y]^T \end{aligned} \right\} \quad (12-46)$$

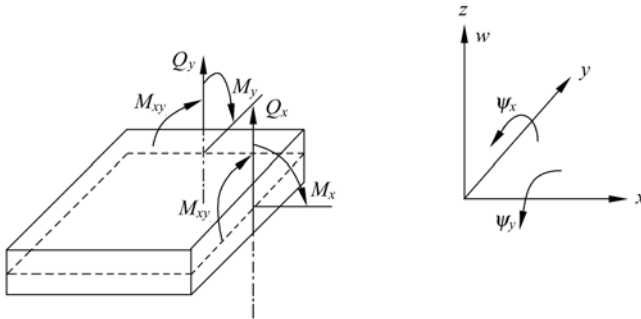


Figure 12.6 The internal forces and displacements of thick plate

The geometrical relations between strains and displacements are

$$\boldsymbol{\gamma} = \left\{ \begin{aligned} \frac{\partial w}{\partial x} - \psi_x \\ \frac{\partial w}{\partial y} - \psi_y \end{aligned} \right\}, \quad \boldsymbol{\kappa} = \left\{ \begin{aligned} -\frac{\partial \psi_x}{\partial x} \\ \frac{\partial \psi_y}{\partial y} \\ -\frac{\partial \psi_x}{\partial y} - \frac{\partial \psi_y}{\partial x} \end{aligned} \right\} \quad (12-47a,b)$$

The elastic relations between internal forces and strains are

$$\mathbf{M} = \mathbf{D}\boldsymbol{\kappa}, \quad \mathbf{Q} = \mathbf{C}\boldsymbol{\gamma} \quad (12-48a,b)$$

in which

$$D = D \begin{bmatrix} 1 & \mu & 0 \\ \mu & 1 & 0 \\ 0 & 0 & \frac{1-\mu}{2} \end{bmatrix}, \quad C = C \begin{bmatrix} 1 & 0 \\ 0 & 1 \end{bmatrix} \quad (12-49a,b)$$

where $D = \frac{Eh^3}{12(1-\mu^2)}$; $C = \frac{Gh}{1.2}$; E is the Young's modulus; G is the shear elastic modulus; μ is the Poisson's ratio; h is the thickness of the plate.

12.4.2 Series Expansion of the Internal Forces Around the Crack Tip

Let the crack tip be the origin of the coordinate system, and the x -axis be along the direction of the crack (Fig. 12.7). r and θ are the polar coordinates. From [21], we know that the internal forces for symmetrical bending can be expressed by

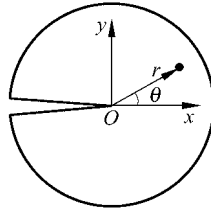


Figure 12.7 Analysis of internal forces around the crack tip in thick plate

$$\begin{aligned} -\frac{M_r}{D} &= 0.5A_{11}r^{-\frac{1}{2}} \left(\cos \frac{3\theta}{2} - 5 \cos \frac{\theta}{2} \right) (1-\mu) + A_{12}(1-\mu)(1 + \cos 2\theta) \\ &+ \frac{C}{2D} D_{12}r(\cos 3\theta - \cos \theta) + 1.5A_{13}r^{\frac{1}{2}}(1-\mu) \\ &\times \left(\cos \frac{5\theta}{2} + 3 \cos \frac{\theta}{2} \right) + 2A_{14}r(1-\mu) \left(\cos 3\theta + \frac{1}{3} \cos \theta \right) + O(r^{\frac{3}{2}}) \quad (12-50a) \end{aligned}$$

$$\begin{aligned} -\frac{M_\theta}{D} &= A_{11}r^{-\frac{1}{2}}(\mu-1) \left(\cos \frac{3\theta}{2} + 3 \cos \frac{\theta}{2} \right) + A_{12}(1-\mu)(1 - \cos 2\theta) \\ &- \frac{C}{2D} D_{12}r(\cos 3\theta - \cos \theta) + 1.5A_{13}r^{\frac{1}{2}}(\mu-1) \\ &\times \left(\cos \frac{5\theta}{2} - 5 \cos \frac{\theta}{2} \right) + 2A_{14}r(\mu-1)(\cos 3\theta - \cos \theta) + O(r^{\frac{3}{2}}) \quad (12-50b) \end{aligned}$$

$$\begin{aligned}
 -\frac{2M_{r\theta}}{D(1-\mu)} = & -A_{11}r^{-\frac{1}{2}}\left(\sin\frac{\theta}{2} + \sin\frac{3\theta}{2}\right) - 2A_{12}\sin 2\theta + 2D_{12}rk^2 \\
 & \times (\sin\theta - \sin 3\theta) + 3A_{13}r^{\frac{1}{2}}\left(\sin\frac{\theta}{2} - \sin\frac{5\theta}{2}\right) \\
 & + 4A_{14}r\left(-\sin 3\theta + \frac{1}{3}\sin\theta\right) + O(r^{\frac{3}{2}}) \quad (12-50c)
 \end{aligned}$$

$$\begin{aligned}
 \frac{Q_r}{C} = & \frac{2}{(1+\mu)}A_{11}r^{\frac{1}{2}}\left(\cos\frac{\theta}{2} + 3\cos\frac{3\theta}{2}\right) + D_{12}[\cos\theta + 0.5k^2r^2 \\
 & \times (\cos\theta - \cos 3\theta)] + \frac{2}{(1+\mu)}A_{13}r^{\frac{3}{2}}\left(\cos\frac{\theta}{2} - 5\cos\frac{5\theta}{2}\right) \\
 & + \frac{2}{(3+3\mu)}A_{14}r^2(\cos\theta - \cos 3\theta) + O(r^{\frac{5}{2}}) \quad (12-50d)
 \end{aligned}$$

$$\begin{aligned}
 \frac{Q_\theta}{C} = & -\frac{6}{(1+\mu)}A_{11}r^{\frac{1}{2}}\left(\sin\frac{\theta}{2} + \sin\frac{3\theta}{2}\right) + D_{12}\left[-\sin\theta - 1.5k^2r^2\right. \\
 & \left.\times\left(\sin\theta - \frac{1}{3}\sin 3\theta\right)\right] + \frac{10}{(1+\mu)}A_{13}r^{\frac{3}{2}}\left(\sin\frac{5\theta}{2} - \sin\frac{\theta}{2}\right) \\
 & + \frac{2}{(1+\mu)}A_{14}r^2\left(-\sin\theta + \frac{1}{3}\sin 3\theta\right) + O(r^{\frac{5}{2}}) \quad (12-50e)
 \end{aligned}$$

and the internal forces for anti-symmetrical bending can be expressed by

$$\begin{aligned}
 -\frac{M_r}{D} = & 0.5A_{21}r^{-\frac{1}{2}}(1-\mu)\left(\sin\frac{3\theta}{2} - \frac{5}{3}\sin\frac{\theta}{2}\right) + \frac{C}{4D}D_{21}r^{\frac{1}{2}} \\
 & \times\left(\sin\frac{5\theta}{2} - \sin\frac{\theta}{2}\right) + 1.5A_{23}r^{\frac{1}{2}}(1-\mu)\left(\sin\frac{5\theta}{2} + 0.6\sin\frac{\theta}{2}\right) \\
 & + 2A_{24}r(1-\mu)(\sin 3\theta + \sin\theta) + O(r^{\frac{3}{2}}) \quad (12-51a)
 \end{aligned}$$

$$\begin{aligned}
 -\frac{M_\theta}{D} = & 0.5A_{21}r^{-\frac{1}{2}}(\mu-1)\left(\sin\frac{3\theta}{2} + \sin\frac{\theta}{2}\right) - \frac{C}{4D}D_{21}r^{\frac{1}{2}} \\
 & \times\left(\sin\frac{5\theta}{2} - \sin\frac{\theta}{2}\right) + 1.5A_{23}r^{\frac{1}{2}}(\mu-1)\left(\sin\frac{5\theta}{2} - \sin\frac{\theta}{2}\right) \\
 & + 2A_{24}r(\mu-1)(\sin 3\theta - 3\sin\theta) + O(r^{\frac{3}{2}}) \quad (12-51b)
 \end{aligned}$$

$$\begin{aligned} -\frac{2M_{r\theta}}{D(1-\mu)} &= A_{21}r^{-\frac{1}{2}}\left(\cos\frac{3\theta}{2} + \frac{1}{3}\cos\frac{\theta}{2}\right) + D_{21}r^{\frac{1}{2}}k^2\left(\cos\frac{5\theta}{2} - \cos\frac{\theta}{2}\right) \\ &\quad + 3A_{23}r^{\frac{1}{2}}\left(\cos\frac{5\theta}{2} - 0.2\cos\frac{\theta}{2}\right) \\ &\quad + 4A_{24}r(\cos 3\theta - \cos\theta) + O(r^{\frac{3}{2}}) \end{aligned} \quad (12-51c)$$

$$\begin{aligned} \frac{Q_r}{C} &= \frac{2}{(3+3\mu)}A_{21}r^{\frac{1}{2}}\left(\sin\frac{\theta}{2} + \sin\frac{3\theta}{2}\right) + D_{21}\left[0.5r^{-\frac{1}{2}}\sin\frac{\theta}{2} \right. \\ &\quad \left. + \frac{1}{3}k^2r^{\frac{3}{2}}\left(\sin\frac{\theta}{2} - \sin\frac{5\theta}{2}\right)\right] + \frac{2}{(5+5\mu)}A_{23}r^{\frac{3}{2}}\left(\sin\frac{\theta}{2} - \sin\frac{5\theta}{2}\right) \\ &\quad + D_{23}\left[1.5r^{\frac{1}{2}}\sin\frac{3\theta}{2} - \frac{3k^2r^{\frac{5}{2}}}{5}\left(\sin\frac{7\theta}{2} - \sin\frac{3\theta}{2}\right)\right] \\ &\quad + \frac{2}{(1+\mu)}A_{24}r^2(\sin\theta - 3\sin 3\theta) + D_{25}r^{\frac{3}{2}}\sin\frac{5\theta}{2} + O(r^{\frac{5}{2}}) \end{aligned} \quad (12-51d)$$

$$\begin{aligned} \frac{Q_\theta}{C} &= \frac{2}{(1+\mu)}A_{21}r^{\frac{1}{2}}\left(\cos\frac{\theta}{2} + \frac{1}{3}\cos\frac{3\theta}{2}\right) + D_{21}\left[0.5r^{-\frac{1}{2}}\cos\frac{\theta}{2} + \frac{5k^2r^{\frac{3}{2}}}{3} \right. \\ &\quad \left. \times\left(\cos\frac{\theta}{2} - 0.2\cos\frac{5\theta}{2}\right)\right] + \frac{2}{(1+\mu)}A_{23}r^{\frac{3}{2}}\left(\cos\frac{\theta}{2} - 0.2\cos\frac{5\theta}{2}\right) \\ &\quad + D_{23}\left[1.5r^{\frac{1}{2}}\cos\frac{3\theta}{2} + \frac{7k^2r^{\frac{5}{2}}}{5}\left(\cos\frac{3\theta}{2} - \frac{3}{7}\cos\frac{7\theta}{2}\right)\right] \\ &\quad + \frac{6}{(1+\mu)}A_{24}r^2(\cos\theta - \cos 3\theta) + 2.5D_{25}r^{\frac{3}{2}}\cos\frac{5\theta}{2} + O(r^{\frac{5}{2}}) \end{aligned} \quad (12-51e)$$

In the above equations, $k^2 = \frac{C}{2D(1-\mu)} = \frac{5}{2h^2}$. Let

$$\boldsymbol{\beta} = [A_{11} \quad A_{12} \quad D_{12} \quad A_{13} \quad A_{14}]^T \quad (\text{symmetry case}) \quad (12-52a)$$

$$\boldsymbol{\beta} = [D_{21} \quad A_{21} \quad A_{23} \quad D_{23} \quad A_{24} \quad D_{25}]^T \quad (\text{anti-symmetry case}) \quad (12-52b)$$

then the above expressions of the internal forces can be written as

$$\mathbf{M} = \mathbf{S}_b \boldsymbol{\beta}, \quad \mathbf{Q} = \mathbf{S}_s \boldsymbol{\beta} \quad (12-53)$$

The stress intensity factors can be obtained from the following relations:

$$\left. \begin{aligned} K_I &= 2\sqrt{2D}(1-\mu)A_{11} \\ K_{II} &= -2\sqrt{2D}(1-\mu)A_{21}/3 \\ K_{III} &= -\sqrt{2}CD_{21}/2 \end{aligned} \right\} \quad (12-54)$$

12.4.3 Formulation of the Sub-Region Mixed Element Method for the Cracked Thick Plate Problem

The final energy functional of the sub-region mixed variational principle is still given by Eq. (12-13), in which the flexibility matrix F of the C-region and the mixed matrix H on the interface will be derived as follows.

(1) The flexibility matrix F of the C-region

The total complementary energy of the C-region in a thick plate is composed of two parts, bending and shear strain complementary energy:

$$\Pi_c = \frac{1}{2} \iint_A (\mathbf{M}^T \mathbf{D}^{-1} \mathbf{M} + \mathbf{Q}^T \mathbf{C}^{-1} \mathbf{Q}) dA \quad (12-55)$$

Substitution of Eqs. (12-50) and (12-51) into the above equation yields

$$\Pi_c = \frac{1}{2} \boldsymbol{\beta}^T \mathbf{F} \boldsymbol{\beta} \quad (12-56)$$

where the flexibility matrix F is

$$\mathbf{F} = \iint_A (\mathbf{S}_b^T \mathbf{D}^{-1} \mathbf{S}_b + \mathbf{S}_s^T \mathbf{C}^{-1} \mathbf{S}_s) dA \quad (12-57)$$

(2) The mixed matrix H on the interface

Let n and s denote the directions of the normal and tangent of the interface S_{pc} . The additional energy H_{pc} on the interface is

$$H_{pc} = \int_{S_{pc}} (Q_n \bar{w} + M_n \bar{\psi}_n + M_{ns} \bar{\psi}_s) ds \quad (12-58)$$

where Q_n , M_n and M_{ns} are the components in the boundary forces T of the C-region on the interface; \bar{w} , $\bar{\psi}_n$ and $\bar{\psi}_s$ are the corresponding components in the boundary displacements \bar{u} of the P-region on the interface.

From the above equation, H_{pc} can be derived, and can be written in the form of Eq. (12-11), i.e.,

$$H_{pc} = \boldsymbol{\beta}^T \mathbf{H} \bar{\boldsymbol{\delta}}$$

Then, the expressions of H are obtained.

(3) Solution of stress intensity factor

Substitution of F and H , which have already been obtained, into Eq. (12-13) yields the expression of the energy functional II . Then, the basic Eqs. (12-19) and (12-16) can be derived from the stationary condition, and the basic unknowns δ and β can be solved in turn. Finally, the stress intensity factors can be solved from Eq. (12-54).

The sub-region mixed element method for the cracked thick plate is denoted as SRM-C3.

Example 12.2 Stress intensity factor of mode I for an infinite cracked plate subjected to uniform bending moment.

A cracked plate subjected to uniform bending moment M along its four edges is shown in Fig. 12.8. The length of the crack is $2a$. In order to approximate the infinite plate, $2L = 2W = 20a$ is taken. The Young's modulus $E = 2 \times 10^6$, and Poisson's ratio $\mu = 0.3$.

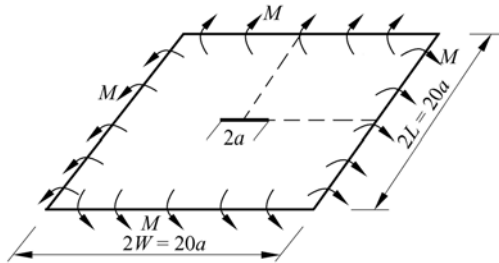


Figure 12.8 An infinite plate with crack

Owing to symmetry, only 1/4 of the plate is calculated. The division of C-region and P-region are shown in Fig. 12.9, in which the C-region is a rectangle, the crack tip O locates at the center of the rectangle; and the dimension of the C-region $r_c = 0.1a$.

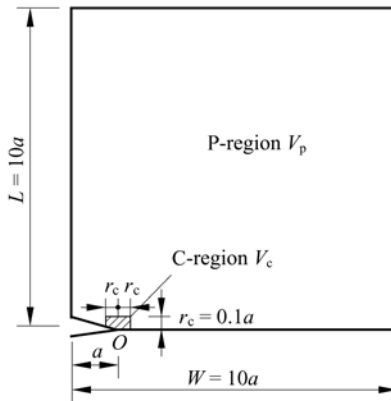


Figure 12.9 The division of C-region and P-region

In the P-region, 8-node isoparametric element is used, and the mesh division is shown in Fig. 12.10.

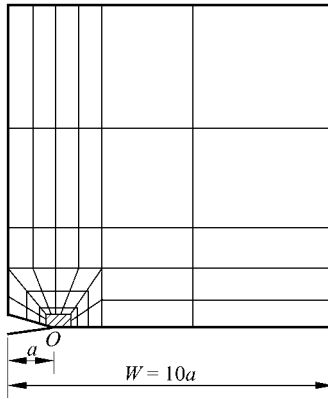


Figure 12.10 Mesh division

The computed results of the stress intensity factor K_I^∞ of mode I by SRM-C3 are listed in Table 12.2, in which a comparison is made with the analytical solutions given by [22] and other finite element results given by [21].

Table 12.2 Comparison of K_I^∞ for infinite plate

h/a	Analytical solution $K_I^\infty / M\sqrt{a}$ [22]	$K_I^\infty / M\sqrt{a}$ (SRM-C3)	$K_I^\infty / M\sqrt{a}$ [21]
0.2	0.647	0.6510 (0.62%)	
0.5	0.693	0.6970 (0.57%)	0.6726 (2.79%)
1.0	0.741	0.745 (0.54%)	0.7352 (1.25%)
1.5	0.781	0.7848 (0.49%)	
2.0	0.816	0.8186 (0.32%)	0.8144 (0.195%)

Note: The numerical values in parentheses are the relative errors with respect to the analytical solutions in [22].

Example 12.3 Stress intensity factor K_I of finite cracked plate with $2L = 2W = 4a$ under uniform moment.

The results of K_I computed by SRM-C3 are listed in Table 12.3. They are in agreement with the results of reference [21]. The values of K_I / K_I^∞ are also given in Table 12.3. When $\frac{h}{a} = 2.0$, K_I is 32.7% higher than K_I^∞ .

Example 12.4 Stress intensity factors of modes II and III of infinite cracked plate subjected to pure twisting moment.

A cracked plate is shown in Fig. 12.8. Assume that it is subjected to uniform twisting moment H along the outer boundary. The meshes shown in Figs. 12.9 and 12.10 are still adopted. Results for the stress intensity factors K_{II} and K_{III} of

modes II and III computed by SRM-C3 are listed in Table 12.4. Compared with the results given by [23], all errors are under 1%.

Table 12.3 Stress intensity factors K_I for finite plate

h/a	K_I [21]	K_I (SRM-C3)	K_I / K_I^∞
0.2		0.7376	1.141
0.5	0.8036	0.8108	1.170
1.0	0.8985	0.8985	1.208
1.5		1.0059	1.288
2.0		1.0830	1.327

Table 12.4 Stress intensity factors of modes II and III for an infinite plate subjected to pure twisting moment

h/a	$K_{II} / H\sqrt{a}$			$K_{III} / \left(\frac{\sqrt{10}}{(1+\mu)h} H\sqrt{a} \right)$		
	SRM-C3	Reference [23]	Relative errors	SRM-C3	Reference [23]	Relative errors
0.2	0.1942	0.193	0.63%	0.1386	0.140	- 1.00%
0.5	0.3974	0.395	0.62%	0.1437	0.145	- 0.92%
1.0	0.5135	0.510	0.59%	0.1219	0.123	- 0.88%
1.5	0.6467	0.643	0.58%	0.0818	0.0825	- 0.89%
2.0	0.7010	0.697	0.59%	0.0605	0.061	- 0.90%

12.5 Surface Crack Problem in a 3D Body

Various solution schemes for the stress intensity factors of the surface crack in a 3D body have been proposed in some references [24–26]. Reference [27] discussed the stress and strain fields around the tip of surface crack in a 3D body.

This section will use the sub-region mixed element method to analyze the surface crack problem in a 3D body^[6]. According to the asymptotic representation of the stress fields in the region of the surface crack, a special singular stress-based element is constructed; and the stress intensity factors of different positions at the tip of crack are computed by the sub-region mixed element method.

12.5.1 The Expression of Stress Fields in the Region of the Surface Crack

The 3D body with the surface elliptic crack shown in Fig. 12.11 is analyzed here.

Let $Oxyz$ be the original coordinate system, in which the xOy plane is a free surface. The semi-elliptical crack is within the xOz plane, and the z -axis points to the inner of the body.

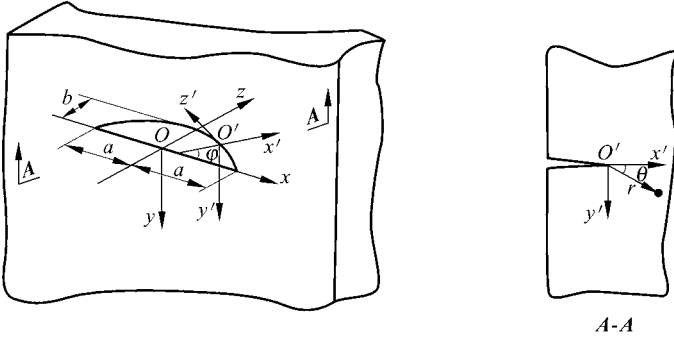


Figure 12.11 A 3D body with surface elliptic crack

For convenience, a special coordinate transformation is introduced here. Let y' -axis be parallel to y -axis, and $x'O'z'$ plane only translate and rotate within xOz plane. The origin O' of the new coordinate system is always at the line of the crack tip; $O'z'$ -axis and $O'x'$ -axis are taken as the tangent and normal of the ellipse, respectively. The angle between $O'x'$ -axis and Ox -axis is ϕ , and polar coordinates r and θ are introduced in $x'O'y'$ plane.

The relation between the new and old coordinate system is as follows:

$$\left. \begin{aligned} x &= \frac{a \cos \varphi}{(1 - e^2 \sin^2 \varphi)^{3/2}} + r \cos \theta \cos \varphi \\ y &= r \sin \theta \\ z &= \frac{b^2 \sin \varphi}{a(1 - e^2 \sin^2 \varphi)^{3/2}} + r \cos \theta \sin \varphi \end{aligned} \right\} \quad (12-59)$$

where $e^2 = (a^2 - b^2) / a^2$.

The equilibrium differential equations in the curved coordinate system are

$$\left. \begin{aligned} \frac{\partial \sigma_r}{\partial r} + \frac{\partial \sigma_{\theta r}}{r \partial \theta} + \frac{\sigma_r - \sigma_\theta}{r} + \frac{1}{\Phi} \left[\frac{\partial \sigma_{r\varphi}}{\partial \varphi} + (\sigma_r - \sigma_\varphi) \cos \theta - \sigma_{\theta r} \sin \theta \right] &= 0 \\ \frac{\partial \sigma_{r\theta}}{\partial r} + \frac{\partial \sigma_\theta}{r \partial \theta} + \frac{2\sigma_{\theta r}}{r} + \frac{1}{\Phi} \left[\frac{\partial \sigma_{\theta\varphi}}{\partial \varphi} + \sigma_{r\theta} \cos \theta + (\sigma_\varphi - \sigma_\theta) \sin \theta \right] &= 0 \\ \frac{\partial \sigma_{r\varphi}}{\partial r} + \frac{\partial \sigma_{\theta\varphi}}{r \partial \theta} + \frac{\sigma_{r\varphi}}{r} + \frac{1}{\Phi} \left[\frac{\partial \sigma_\varphi}{\partial \varphi} + 2\sigma_{r\varphi} \cos \theta - 2\sigma_{\theta\varphi} \sin \theta \right] &= 0 \end{aligned} \right\} \quad (12-60)$$

in which

$$\Phi = \frac{b^2}{a(1 - e^2 \sin^2 \varphi)^{2/3}} + r \cos \theta \tag{12-61}$$

The geometric equations in the curved coordinate system are

$$\left. \begin{aligned} \varepsilon_r &= \frac{\partial u_r}{\partial r} \\ \varepsilon_\theta &= \frac{\partial u_\theta}{r \partial \theta} + \frac{u_r}{r} \\ \varepsilon_\varphi &= \frac{1}{\Phi} \left(\frac{\partial u_\varphi}{\partial \varphi} + u_r \cos \theta - u_\theta \sin \theta \right) \\ \varepsilon_{r\theta} &= \frac{\partial u_r}{r \partial \theta} + \frac{\partial u_\theta}{\partial r} - \frac{u_\theta}{r} \\ \varepsilon_{r\varphi} &= \frac{1}{\Phi} \left(\frac{\partial u_r}{\partial \varphi} - u_\varphi \cos \theta \right) + \frac{\partial u_\varphi}{\partial r} \\ \varepsilon_{\theta\varphi} &= \frac{1}{\Phi} \left(\frac{\partial u_\theta}{\partial \varphi} + u_\varphi \sin \theta \right) + \frac{\partial u_\varphi}{r \partial \theta} \end{aligned} \right\} \tag{12-62}$$

And, the boundary conditions at the crack are

$$\sigma_{\theta\theta} = \sigma_{r\theta} = \sigma_{\theta\varphi} = 0 \quad (\text{at } \theta = \pm\pi) \tag{12-63}$$

By eigenfunction method, the expression of stress at the tip of the crack can be derived^[42]. Some low order solutions are listed as follows.

(a) zero-order solution

$$(\sigma_r)_0 = (\sigma_\theta)_0 = (\sigma_\varphi)_0 = (\sigma_{r\theta})_0 = (\sigma_{r\varphi})_0 = (\sigma_{\theta\varphi})_0 = 0 \tag{12-64a}$$

(b) first-order solution

$$\left. \begin{aligned} (\sigma_r)_1 &= \rho^{-\frac{1}{2}} \frac{E}{2(1+\mu)} \left[K_1 \left(\cos \frac{3}{2}\theta - 5 \cos \frac{\theta}{2} \right) + L_1 \left(\sin \frac{3}{2}\theta - \frac{5}{3} \sin \frac{\theta}{2} \right) \right] \\ (\sigma_\theta)_1 &= -\rho^{-\frac{1}{2}} \frac{E}{2(1+\mu)} \left[K_1 \left(\cos \frac{3}{2}\theta + 3 \cos \frac{\theta}{2} \right) + L_1 \left(\sin \frac{3}{2}\theta + \sin \frac{\theta}{2} \right) \right] \\ (\sigma_\varphi)_1 &= -\rho^{-\frac{1}{2}} \frac{4E\mu}{1+\mu} \left(K_1 \cos \frac{\theta}{2} + \frac{1}{3} L_1 \sin \frac{\theta}{2} \right) \\ (\sigma_{r\theta})_1 &= \rho^{-\frac{1}{2}} \frac{E}{2(1+\mu)} \left[-K_1 \left(\sin \frac{3}{2}\theta + \sin \frac{\theta}{2} \right) + L_1 \left(\cos \frac{3}{2}\theta + \frac{1}{3} \cos \frac{\theta}{2} \right) \right] \\ (\sigma_{r\varphi})_1 &= \rho^{-\frac{1}{2}} \frac{E}{4(1+\mu)} Q_1 \sin \frac{\theta}{2} \\ (\sigma_{\theta\varphi})_1 &= \rho^{-\frac{1}{2}} \frac{E}{4(1+\mu)} Q_1 \cos \frac{\theta}{2} \end{aligned} \right\} \tag{12-64b}$$

where $\rho = \frac{r}{b^2/a}$, K_1, L_1, Q_1 are functions of φ .

(c) second-order solution

$$\left. \begin{aligned}
 (\sigma_r)_2 &= \frac{E}{1+\mu} K_2 (1 + \cos 2\theta) \\
 (\sigma_\theta)_2 &= \frac{E}{1+\mu} K_2 (1 - \cos 2\theta) \\
 (\sigma_\varphi)_2 &= \frac{2E\mu}{1+\mu} K_2 + E\psi(P'_0 + K_0) \\
 (\sigma_{r\theta})_2 &= -\frac{E}{1+\mu} K_2 \sin 2\theta \\
 (\sigma_{r\varphi})_2 &= \frac{E}{2(1+\mu)} [P_2 \cos \theta + \psi(K'_0 - P_0) \cos \theta] \\
 (\sigma_{\theta\varphi})_2 &= -\frac{E}{2(1+\mu)} [P_2 \sin \theta + \psi(K'_0 - P_0) \sin \theta]
 \end{aligned} \right\} \quad (12-64c)$$

where $\psi = (1 - e^2 \sin^2 \varphi)^{\frac{3}{2}}$, K_0, P_0, K_2 and P_2 are the functions of φ ; P'_0 and K'_0 denote the first-order derivatives with respect to φ .

12.5.2 Formulation of the Sub-Region Mixed Element Method for the Surface Crack Problem

A thick plate with the surface elliptic crack is shown in Fig. 12.12. Here, it is analyzed by the sub-region mixed element method.

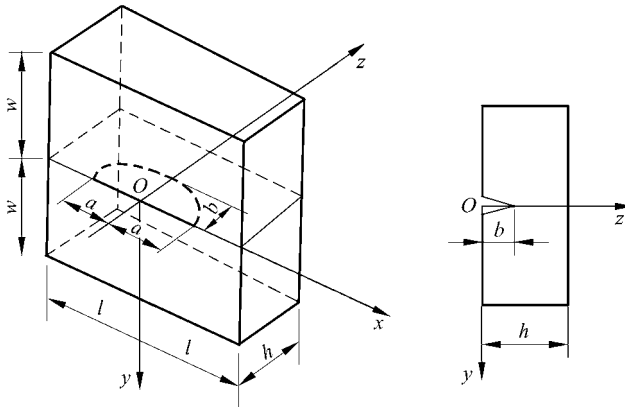


Figure 12.12 A thick plate with surface elliptic crack

In the sub-region mixed element method, the whole structure is divided into two regions (Fig. 12.13):

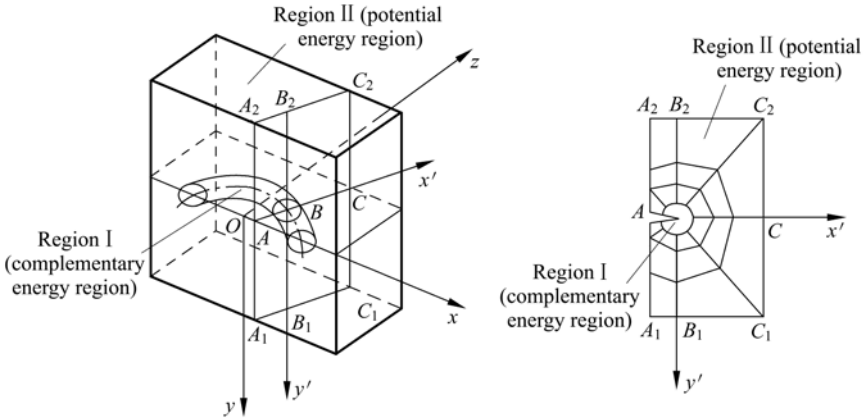


Figure 12.13 The division of the potential and complementary energy regions

(1) Region I is the complementary energy region, an annular region in which the line of the crack tip is taken as the axial line, and the intersection of this annular region with the $x'O'y'$ plane is a circle with radius r_c . Region I is a stress concentration region, in which a singular stress element is constructed and the unknown stress parameters β are taken as the variational variables.

(2) Region II is the potential energy region, an even stress region. In this region, 20-node isoparametric element is used, and the nodal displacements δ are taken as the variational variables.

The final energy functional of the sub-region mixed variational principle is still given by Eq. (12-13), in which matrices F and H will be derived as follows.

(1) The flexibility matrix F in the C-region

Here, the C-region is the annular region with crack. The first and second order solutions of the stress expansion are given by Eq. (12-64). Now, the stress fields can be expressed by

$$\sigma = \bar{S}\alpha \tag{12-65}$$

where σ is a vector formed by 6 stress components

$$\sigma = [\sigma_r \quad \sigma_\theta \quad \sigma_\varphi \quad \sigma_{r\theta} \quad \sigma_{r\varphi} \quad \sigma_{\theta\varphi}]^T \tag{12-66}$$

α is a vector formed by 10 unknown coefficients in Eq. (12-64)

$$\alpha = [K_0 \quad K'_0 \quad K_1 \quad K_2 \quad P_0 \quad P'_0 \quad P_1 \quad P_2 \quad L_1 \quad Q_1]^T \tag{12-67}$$

\bar{S} is formed by related terms in Eq. (12-64).

$$\lambda = \frac{\mu E}{(1 + \mu)(1 - 2\mu)}, \quad G = \frac{E}{2(1 + \mu)} \quad (12-75)$$

$$dV = |J| dr d\theta d\varphi \quad (12-76)$$

$$|J| = -r^2 \cos \theta - \frac{br^2}{a(1 - e^2 \sin^2 \varphi)^{3/2}} \quad (12-77)$$

(2) The mixed matrix H on the interface

The interface S_{pc} is a curved face of the annular shell (Fig. 12.14(a)). The additional energy on the interface is

$$H_{pc} = \iint_{S_{pc}} (\sigma_r \bar{u}_r + \sigma_{r\theta} \bar{u}_\theta + \sigma_{r\varphi} \bar{u}_\varphi) dS \quad (12-78)$$

where $\sigma_r, \sigma_{r\theta}$ and $\sigma_{r\varphi}$ are the boundary force components on the interface, and can be expressed in terms of the stress parameters β as

$$[\sigma_r \quad \sigma_{r\theta} \quad \sigma_{r\varphi}]^T = S' \beta \quad (12-79)$$

$\bar{u}_r, \bar{u}_\theta$ and \bar{u}_φ are the boundary displacement components along r, θ and φ directions on the interface, and can be expressed in terms of the boundary displacement components \bar{u}_x, \bar{u}_y and \bar{u}_z along x, y and z directions as

$$\begin{Bmatrix} \bar{u}_r \\ \bar{u}_\theta \\ \bar{u}_\varphi \end{Bmatrix} = \mathbf{t} \begin{Bmatrix} \bar{u}_x \\ \bar{u}_y \\ \bar{u}_z \end{Bmatrix} \quad (12-80)$$

where \mathbf{t} is the coordinate transformation matrix, from Fig. 12.14, we have

$$\mathbf{t} = \begin{bmatrix} \cos \varphi \cos \theta & \sin \theta & \sin \varphi \cos \theta \\ -\cos \varphi \sin \theta & \cos \theta & -\sin \varphi \sin \theta \\ -\sin \varphi & 0 & \cos \varphi \end{bmatrix} \quad (12-81)$$

And, the boundary displacements \bar{u}_x, \bar{u}_y and \bar{u}_z can be expressed in terms of the boundary nodal displacements $\bar{\delta}$ and shape functions \bar{N} as

$$\begin{Bmatrix} \bar{u}_x \\ \bar{u}_y \\ \bar{u}_z \end{Bmatrix} = \bar{N} \bar{\delta} \quad (12-82)$$

Substitution of the above equation into Eq. (12-80) yields

$$\begin{Bmatrix} \bar{u}_r \\ \bar{u}_\theta \\ \bar{u}_\varphi \end{Bmatrix} = \mathbf{t} \bar{N} \bar{\delta} \quad (12-83)$$

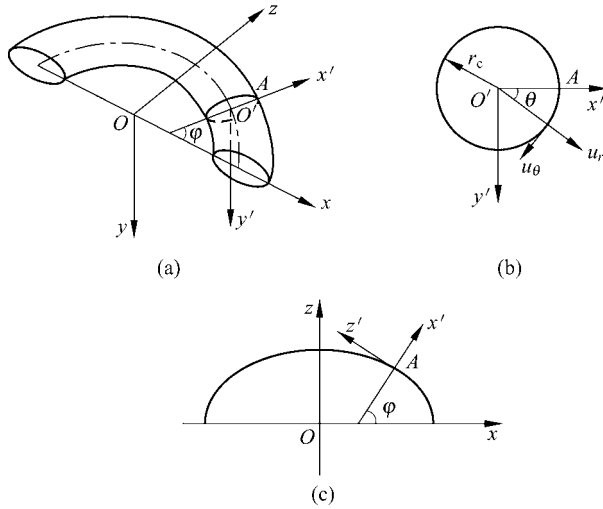


Figure 12.14 The interface S_{pc}

Substitution of Eqs. (12-79) and (12-83) into Eq. (12-78) yields

$$H_{pc} = \beta^T H \bar{\delta} \tag{12-84}$$

where the mixed matrix H on the interface is

$$H = \iint_{S_{pc}} \mathbf{S}^T \mathbf{t} \bar{N} dS \tag{12-85}$$

here the differential area dS on the interface can be derived from Eq. (12-59) as follows:

$$dS = \left(r_c \cos \theta + \frac{b^2}{a(1 - e^2 \sin^2 \varphi)^{3/2}} \right) r_c d\theta d\varphi \tag{12-86}$$

After the determination of matrices H and F , the basic unknowns δ and β can be solved in turn from Eqs. (12-19) and (12-16). Then, the stress intensity factors at different points on the tip line of the crack can be obtained.

The sub-region mixed element method for the surface crack problem in a 3D body is denoted as SRM-C4^[6].

Example 12.5 The dimensionless stress intensity factor of a thick plate with the surface elliptic crack (Fig. 12.12) under tension and bending loads.

In Fig. 12.12, a and b are the half long axis and the half short axis of the ellipse, respectively; h is the thickness of the plate; $2l$ and $2w$ are the length and width of the plate, respectively; and the Poisson's ratio $\mu = 0.3$.

For the different points on the tip line of the crack, their coordinates φ are corresponding to different values. The stress intensity factors K_I at different

points are functions of φ , which can be defined as follows^[28]:

$$K_I = \sigma \sqrt{\frac{\pi b}{Q}} F\left(\frac{b}{h}, \frac{b}{a}, \frac{a}{l}, \varphi\right) \tag{12-87}$$

where F is the dimensionless stress intensity factor; Q is the shape factors, its approximate formula is

$$Q = 1 + 1.46 \left(\frac{b}{a}\right)^{1.65} \quad (a > b) \tag{12-88}$$

and σ is the stress on the plate edge.

Table 12.5 Dimensionless stress intensity factor of a plate with surface crack under tension and bending loads

$$\left(\frac{a}{l} = 0.2, \frac{b}{a} = 0.6, \frac{a}{w} = 0.2, \frac{b}{h} = 0.6, \mu = 0.3\right)$$

$2\varphi/\pi$	Tension		Bending	
	SRM-C4 ^[6]	Reference [28]	SRM-C4 ^[6]	Reference [28]
0	1.111	1.172	0.794	0.862
0.25	1.137	1.142	0.625	0.676
0.5	1.164	1.182	0.464	0.504
0.75	1.182	1.218	0.355	0.370
1.00	1.201	1.230	0.301	0.317

(1) Two load cases, tension and bending, are considered

Results for F given by SRM-C4^[6] are given in Table 12.5, and compared with the results in reference [28].

The present method can provide quite good accuracy, but its workload is only 1/10 of that of [28].

(2) Different ratios $\frac{a}{l}$ are considered

For the cases $\frac{a}{l} = 0.1, 0.2, 0.3, 0.4$, the stress intensity factors of a plate with the surface crack under tension load are given in Table 12.6, and compared with the results of reference [27].

(3) Different ratios $\frac{b}{h}$ are considered

For the cases $\frac{b}{h} = 0.2, 0.4, 0.6$, the stress intensity factors of a plate with the surface crack under bending load are given in Table 12.7, and compared with the results of reference [27].

Table 12.6 Dimensionless stress intensity factors of a plate with surface crack under tension load for different $\frac{a}{l}$

$$\left(\frac{b}{a} = 0.6, \frac{a}{w} = 0.2, \frac{b}{h} = 0.6, \mu = 0.3 \right)$$

a/l	0.1		0.2		0.3		0.4	
$2\varphi/\pi$	SRM-C4	Reference [27]	SRM-C4	Reference [27]	SRM-C4	Reference [27]	SRM-C4	Reference [27]
0	1.015	0.248	1.111	0.253	1.138	0.283	1.164	0.304
0.25	1.117	1.126	1.137	1.150	1.200	1.240	1.258	1.324
0.5	1.153	1.138	1.164	1.160	1.251	1.244	1.301	1.320
0.75	1.149	1.144	1.182	1.178	1.255	1.248	1.312	1.322
1.00	1.199	1.206	1.201	1.225	1.292	1.304	1.354	1.383

Table 12.7 Dimensionless stress intensity factors of a plate with surface crack under bending load for different $\frac{b}{h}$

$$\left(\frac{a}{l} = 0.2, \frac{b}{a} = 0.6, \frac{a}{w} = 0.2, \mu = 0.3 \right)$$

b/h	0.2		0.4		0.6	
$2\varphi/\pi$	SRM-C4	Reference [27]	SRM-C4	Reference [27]	SRM-C4	Reference [27]
0	0.823	0.153	0.801	0.153	0.794	0.101
0.25	0.724	0.732	0.667	0.680	0.625	0.640
0.5	0.735	0.756	0.604	0.632	0.464	0.486
0.75	0.741	0.748	0.558	0.572	0.355	0.364
1.00	0.772	0.792	0.542	0.568	0.301	0.322

References

- [1] Long YQ, Zhi BC, Kuang WQ, Shan J (1982) Sub-region mixed finite element method for the calculation of stress intensity factor. In: He GQ et al (eds) Proceedings of International Conference on FEM. Science Press, Shanghai, pp738 – 740
- [2] Benzley SE (1974) Representation of singularities with isoparametric finite elements. International Journal for Numerical Methods in Engineering 8: 537 – 545
- [3] Chien WZ, Xie ZC, Gu QL, Yang ZF, Zhou CT (1980) The superposition of the finite element method on the singularity terms in determining the stress intensity factors. Journal of Tsinghua University 2: 15 – 24 (in Chinese)
- [4] Long YQ, Zhao YQ (1985) Calculation of stress intensity factors in plane problems by the sub-region mixed finite element method. Engineering Software 7(1): 32 – 35

Advanced Finite Element Method in Structural Engineering

- [5] Huang MF, Long YQ (1988) Calculation of stress intensity factors of cracked Reissner plates by the sub-region mixed finite element method. *Computers & Structures* 30(4): 837 – 840
- [6] Long YQ, Qian J (1992) Calculation of stress intensity factors for surface cracks in a 3D body by the subregion mixed FEM. *Computers & Structures* 44(1/2): 75 – 78
- [7] Fan Z, Long YQ (1992) Sub-region mixed finite element analysis of V-notched plates. *International Journal of Fracture* 56: 333 – 344
- [8] Long YQ, Qian J (1990) Fracture analysis of V-notch in composite material. In: *Proceeding of WCCM-II. Stuttgart*, pp332 – 335
- [9] Long YQ, Qian J (1992) Sub-region mixed finite element analysis of V-notches in a bimaterial. In: *Zhu DC (ed) Advances in Engineering Mechanics. Peking University Press, Beijing*, pp54 – 59
- [10] Qian J, Long YQ (1992) The expression of stress and strain at the tip of notch in Reissner plate. *Applied mathematics and Mechanics (English Edition)* 13(4): 315 – 324
- [11] Qian J, Long YQ (1994) The expression of stress and strain at the tip of 3-D notch. *Applied mathematics and Mechanics (English Edition)* 15(3): 211 – 221
- [12] Bao SH, Yang C, Fan Z (1984) Analysis of shear wall supported by beam column system and shear wall with opening by subregion mixed FEM. In: *Proc. 3rd Int. Conf. on Tall Buildings. Hong Kong*, pp586 – 591
- [13] Atluri SN, Kobayashi AS, Nakagaki M (1975) An assumed displacement hybrid finite element model for linear fracture mechanics. *International Journal of Fracture* 11: 257 – 271
- [14] Kelly JW, Sun CT (1977) A singular finite element for computing stress intensity factors. In: *Sih GC (ed) Proceedings of an International Conference on Fracture Mechanics and Technology (Vol 2), Sijthoff and Noordhoff International Publishers, Hong Kong*, pp1483 – 1498
- [15] Gross B, Strawley JE, Brown WE (1964) Stress intensity factors for a single edge notch tension specimen by boundary collocation of a stress function. *NASA, TN-D-2395*
- [16] Isida M (1971) Effect of width and length on stress intensity factors of internally cracked plates under various boundary conditions. *International Journal of Fracture* 7: 301 – 316
- [17] Rooke DP, Cartwright DJ (1976) *Compendium of Stress Intensity Factors. Her Majesty's Stationery Office, London*
- [18] Wilson WK (1971) Numerical methods for determining stress intensity factors of an interior crack in a finite plate. *ASME Journal of Basic Engineering* 93: 685 – 690
- [19] Barsoum RS (1976) A degenerate solid element for linear fracture analysis of plate bending and general shells. *International Journal for Numerical Methods in Engineering* 10: 551 – 564
- [20] Yagawa G (1979) Finite element analysis of stress intensity factors for plate extension and plate bending problems. *International Journal for Numerical Methods in Engineering* 14(5): 727 – 740
- [21] Li YZ, Liu CT (1983) Analysis of Reissner's plate bending fracture problem. *Acta Mechanica Sinica* 15(4): 366 – 375 (in Chinese)
- [22] Hartranft RJ, Sih GC (1968) Effect of plate thickness on the bending stress distribution around through cracks. *Journal of Mathematics and Physics* 47: 276 – 291

Chapter 12 Sub-Region Mixed Element I— Fundamental Theory and Crack Problem

- [23] Wang NM (1970) Twisting of an elastic plate containing a crack. *International Journal of Fracture* 6: 367 – 378
- [24] Nishioka T, Atluri SN (1983) An alternating method for analysis of surface flawed aircraft structural components. *AIAA Journal* 21(5): 749 – 757
- [25] Niu X, Glinka G (1989) Stress intensity factors for semi-elliptical surface cracks in welded joints. *International Journal of Fracture* 40: 255 – 270
- [26] Heliot J, Labbens R, Pellissier-Tannon A (1979) Semi-elliptical cracks in a cylinder subjected to stress gradients. In: Smith GW (eds) *Fracture Mechanics*. ASTM STP 677, American Society for Testing and Materials, Philadelphia, pp341 – 364
- [27] Li YZ (1988) Crack tip stress and strain fields for surface cracks in 3D body and the calculation of stress intensity factors. *Chinese Science (A)* 8: 828 – 842
- [28] Newman JC, Raju IS (1979) NASA, TP-1578

Chapter 13 Sub-Region Mixed Element II—V-Notch Problem

Yu-Qiu Long

Department of Civil Engineering, School of Civil Engineering,
Tsinghua University, Beijing, 100084, China

Song Cen

Department of Engineering Mechanics, School of Aerospace,
Tsinghua University, Beijing, 100084, China

Abstract This chapter continues discussing the sub-region mixed element method. Here, the applications of the sub-region mixed element method in the analysis of the V-notches in plane problem, bi-material problem, Reissner plate problem, and 3D elastic body problem are focused on and discussed in turn. It is demonstrated again that the proposed sub-region mixed element method is efficient for such singular stress problems.

Keywords finite element, sub-region mixed element, V-notch problem.

13.1 Introduction

This chapter will discuss some topics about the stress analysis of structures with V-notches and the applications of the sub-region mixed element method.

Stress concentration will happen around the notches in structures, i.e., the stress fields at the tip of the notches possess singularity. Angular corners of holes and welding structures are all examples of the V-notch problem. An ideal straight crack can also be regarded as a V-notch with zero opening angle.

In this chapter, the sub-region mixed element analysis of the V-notches in plane problem^[1], bi-material problem^[2], Reissner plate problem^[3] and 3D elastic body problem^[4] will be discussed in turn.

13.2 Plane V-Notch Problem

Plane V-notch problems have always attracted much attention. In 1952, Williams^[5] first established the eigenequations for the V-notch problem. He pointed out that

the stress at the notch-tip possesses singularity, and concluded that such singularity depends on the opening angle of the notch. Gross et al.^[6] extended the concept of the stress intensity factors from ideal cracks into V-notch cases and evaluated the notch-tip stress intensity factors using a boundary collocation method. The boundary integral method has also been applied in reference [7] for the beam bending problem with a V-notch. The reciprocal work contour integral method was extended by Carpenter^[8-10] into the analysis of stress concentration at the notch. Lin and Tong^[11] proposed a hybrid singular element for the analysis of the V-notch problem. Awaji et al.^[12] investigated the V-notches using dense triangular elements.

In this section, the sub-region mixed element method will be used for the analysis of the plane V-notch problem^[1]. Firstly, by starting with the complex potentials of elasticity, the eigenproblem of the V-notch is discussed, and the variation regularity of the eigenvalue with the opening angle is given, in which the embranchment phenomenon of the high-order eigenvalue curve and the concept of the critical angle are also pointed out. Then, the expressions of the stress fields for modes I and II problems are given. Finally, the sub-region mixed element method is used to analyze the V-notch problem, which gives the results of the stress intensity factors K_I and K_{II} of the specimens containing V-notches with various angles.

13.2.1 Eigenproblem of V-Notches

The configuration of the elastic plane with a V-notch is shown in Fig. 13.1, the polar coordinate system is set. The stresses can be expressed in terms of two complex potentials $\phi(z)$ and $\psi(z)$ as follows:

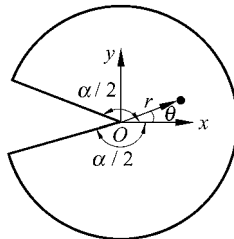


Figure 13.1 Stress analysis around a V-notch tip

$$\sigma_r + \sigma_\theta = 4 \operatorname{Re} \phi'(z) \tag{13-1}$$

$$\sigma_\theta - i \tau_{r,\theta} = \phi'(z) + \overline{\phi'(z)} + \bar{z} \phi''(z) + \bar{z} z^{-1} \overline{\psi'(z)} \tag{13-2}$$

The complex potentials can be expanded in series further

$$\left. \begin{aligned} \phi(x) &= \sum_{n=1}^{\infty} \frac{1}{2} (A_n z^{\lambda_n} + B_n z^{\bar{\lambda}_n}) \\ \psi(x) &= \sum_{n=1}^{\infty} \frac{1}{2} (C_n z^{\lambda_n} + D_n z^{\bar{\lambda}_n}) \end{aligned} \right\} \quad (13-3)$$

The stress boundary conditions for two unloaded surfaces of a V-notch are

$$(\sigma_{\theta} - i \tau_{r\theta}) \Big|_{\theta=\pm \frac{\alpha}{2}} = 0 \quad (13-4)$$

Then, from the above equations, we obtain

$$\left. \begin{aligned} C_n &= -A_n \lambda_n \cos \alpha - \bar{B}_n \cos \lambda_n \alpha \\ \bar{D}_n &= -A_n \cos \lambda_n \alpha - \bar{B}_n \lambda_n \cos \alpha \end{aligned} \right\} \quad (13-5)$$

$$\left. \begin{aligned} A_n \sin \lambda_n \alpha + \bar{B}_n \lambda_n \sin \alpha &= 0 \\ A_n \lambda_n \sin \alpha + \bar{B}_n \sin \lambda_n \alpha &= 0 \end{aligned} \right\} \quad (13-6)$$

Since stresses exist in the neighborhood of the notch-tip, the determinant of the coefficient matrix must be zero. Hence, two eigenequations can be obtained

$$\lambda_n \sin \alpha + \sin \lambda_n \alpha = 0 \quad (\text{mode I - symmetry}) \quad (13-7)$$

$$\lambda_n^* \sin \alpha - \sin \lambda_n^* \alpha = 0 \quad (\text{mode II - antisymmetry}) \quad (13-8)$$

From these eigenequations, two series of eigenvalues can be solved

$$\lambda_n = \xi_n + i \eta_n, \quad \lambda_n^* = \xi_n^* + i \eta_n^* \quad (13-9)$$

The eigenvalues λ_n and λ_n^* for α ranging from π to 2π are listed in Tables 13.1 and 13.2, respectively. And, a series of real part curves $\xi_n - \alpha$ (or $\xi_n^* - \alpha$) and imaginary part curves $\eta_n - \alpha$ (or $\eta_n^* - \alpha$) are also given in Figs. 13.2 and 13.3.

From these tables and figures, the following four points should be mentioned:

(1) The 3 eigenvalues ($\lambda = 0$, $\lambda^* = 0$, $\lambda^* = 1$) are corresponding to the 3 states of rigid-body motion, so they should not be considered in practical analysis.

(2) The first eigenvalue λ_1 (or λ_1^*) is identical to a real number. The imaginary part curves $\eta_1 - \alpha$ and $\eta_1^* - \alpha$ coincide with the abscissa axis. And, the real part curves $\xi_1 - \alpha$ and $\xi_1^* - \alpha$ are smooth curves when $\pi \leq \alpha \leq 2\pi$. For the mode I problem, the relation $0.5 \leq \lambda_1 < 1$ is satisfied when the notch-tip angle α is in the range $[\pi, 2\pi]$, hence, the stress singularity always exists in the notch-tip. For the mode II problem, the relation $0.5 \leq \lambda_1^* < 1$ will not be satisfied unless the notch-tip angle α is in the range $[4.493409, 2\pi]$, thus, the stress singularity at the notch-tip does not always exist. In reference [11], the authors said that the mode II

Table 13.1 Eigenvalues $\lambda_n = \xi_n \pm i\eta_n$ for Mode I (symmetry) problem

α	2π (360°)	6.108 652 (350°)	5.934 119 (340°)	5.855 023 (335.47°)	5.759 587 (330°)	5.499 379 (315.07°)	5.235 988 (300°)	4.712 389 (270°)
λ_1	0.5	0.500 053	0.500 427		0.501 453		0.512 222	0.544 484
λ_2	1.0	1.058 843	1.125 407		1.202 157	1.404 750	1.471 028	1.629 257
λ_3	1.5	1.499 728	1.497 614		1.490 378		$\pm 0.141 853i$	$\pm 0.231 251i$
λ_4	2.0	2.118 822	2.267 187	2.402 415	2.440 492		2.567 762	2.971 844
λ_5	2.5	2.497 980	2.476 770		$\pm 0.114 207i$		$\pm 0.284 901i$	$\pm 0.373 931i$
α	4.188 790 (240°)	3.665 191 (210°)	3.625 739 (207.74°)	3.490 659 (200°)	3.383 923 (193.88°)	3.316 126 (190°)	π (180°)	
λ_1	0.615 731	0.751 973		0.818 703		0.900 042	1.0	
λ_2	1.833 550	2.106 29	2.130 670	2.018 265		2.001 797	2.0	
λ_3	$\pm 0.252 260i$	$\pm 0.096 099i$		2.420 588		2.695 23	3.0	
λ_4	3.343 717	3.828 294		4.025 002	4.156 771	4.022 68	4.0	
λ_5	$\pm 0.414 037i$	$\pm 0.347 177i$		$\pm 0.243 015i$		4.468 954	5.0	

Table 13.2 Eigenvalues $\lambda_n^* = \xi_n^* \pm i\eta_n^*$ for Mode II (antisymmetry) problem

α	2π (360°)	6.108 652 (350°)	5.934 119 (340°)	5.932 123 (339.89°)	5.759 587 (330°)	5.732 235 (328.43°)	5.235 988 (300°)	4.712 389 (270°)
λ_1^*	0.5	0.529 355	0.562 007		0.598 192		0.730 901	0.908 529
λ_2^*	1.5	1.588 609	1.692 250		1.838 934	1.902 246	2.074 826	2.301 328
λ_3^*	2.0	1.999 107	1.991 385		1.948 556		$\pm 0.229 426i$	$\pm 0.315 837i$
λ_4^*	2.5	2.649 696	2.883 887	2.902 967	2.987 005		3.279 767	3.641 420
λ_5^*	3.0	2.996 141	2.920 168		$\pm 0.166 741i$		$\pm 0.326 690i$	$\pm 0.418 787i$
α	4.493 409 (257.45°)	4.188 790 (240°)	3.665 191 (210°)	3.490 659 (200°)	3.463 416 (198.44°)	3.336 226 (191.15°)	3.316 126 (190°)	π (180°)
λ_1^*	1.0	1.148 913	1.485 81	1.630 47			1.798 929	2.0
λ_2^*		2.589 479	2.967 836	3.122 551	3.148 372		3.007 832	3.0
λ_3^*		$\pm 0.348 375i$	$\pm 0.261 186i$	$\pm 0.108 732i$				3.586 718
λ_4^*		4.096 928	4.688 039	4.926 987		5.161 747	5.060 484	5.0
λ_5^*		$\pm 0.464 641i$	$\pm 0.409 575i$	$\pm 0.319 811i$			5.327 916	6.0

problem always possesses stress singularity when $\pi < \alpha \leq 2\pi$. This does not seem to be correct.

(3) The higher-order eigenvalues λ_n and λ_n^* may be complex numbers. The features of the curves of the higher-order eigenvalues can be described in detail as follows:

- ① When $\pi \leq \alpha \leq 2\pi$, these curves, which are not smooth curves any more,

consist of 3-piecewise curves, in which the middle segment and the two end segments are corresponding to complex roots and real roots, respectively. The positions of two conjunction points of 3-piecewise curves are corresponding to critical angles, α_{cr1} and α_{cr2} .

② The higher-order eigenvalues exist in pairs, for instance, λ_2 and λ_3 are a pair; λ_4 and λ_5 are a pair, etc. In addition, the curves of each pair of eigenvalues coincide in some ranges and then separate in other ranges. The real part curves $\xi-\alpha$ and $\xi^*- \alpha$ (see Figs. 13.2(a) and 13.3(a)) are separate curves in the two end ranges, and then coincide in the middle range. For example, the curves for ξ_2 and

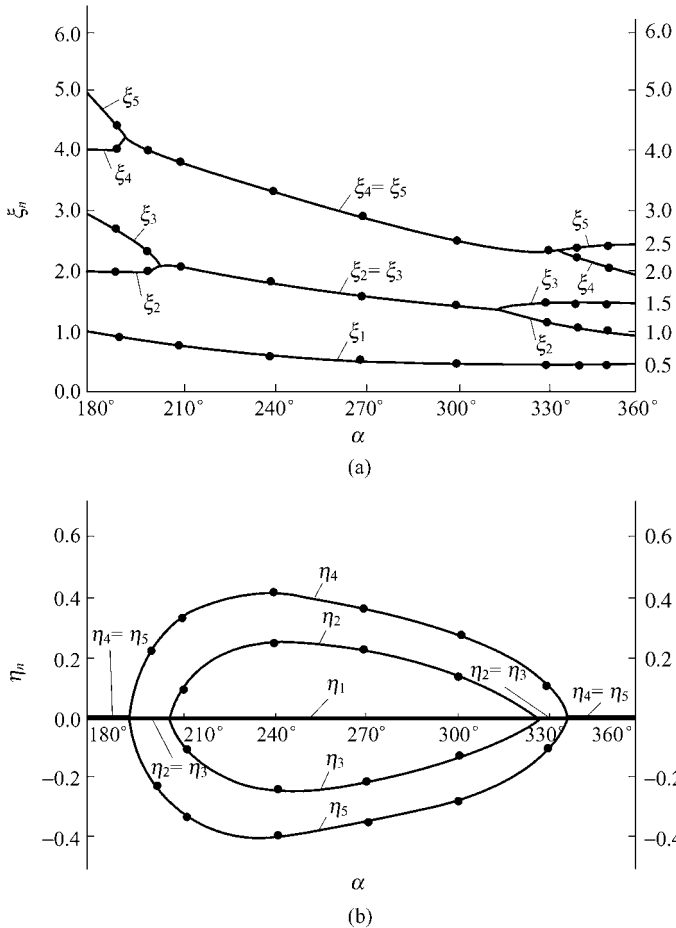


Figure 13.2 Real part and imaginary part curves of eigenvalues for Mode I (symmetry) problem

(a) $\xi_n-\alpha$ curve; (b) $\eta_n-\alpha$ curve

ξ_3 , which are two-branch curves in the two end ranges, will become a one-branch curve in the middle range after meeting at the critical angles α_{cr1} and α_{cr2} . Conversely, the imaginary part curves $\eta-\alpha$ and $\eta^*-\alpha$ (see Figs. 13.2(b) and 13.3(b)) are separated curves in the middle range, but will coincide in the two end ranges. For example, η_2 and η_3 are two symmetric curves (λ_2 and λ_3 are conjugate with each other) on the two sides of the abscissa axis in the middle range (complex root region), and will be merged into the abscissa axis in the two end ranges (real root regions).

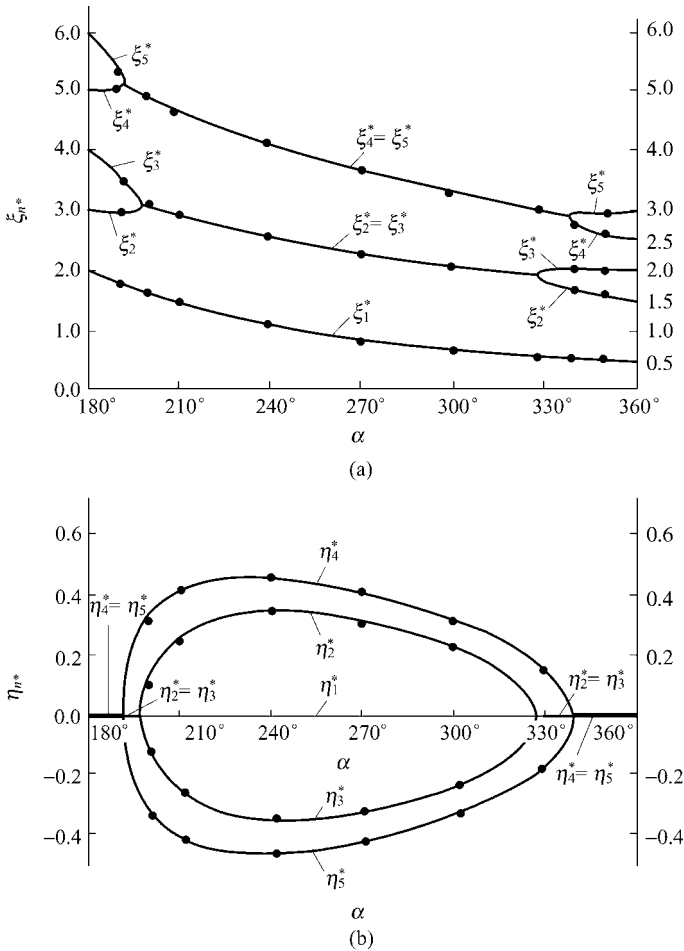


Figure 13.3 Real part and imaginary part curves of eigenvalues for Mode II (antisymmetry) problem

(a) $\xi_n^*-\alpha$ curve; (b) $\eta_n^*-\alpha$ curve

The above features of the curves of the higher-order eigenvalues, such as appearance in pairs and the phenomenon of embranchment, have not been recognized by some authors in the early time. For example, the ξ - α curve in reference [8] does not reflect the characteristic of embranchment.

(4) For a certain notch-angle α , its eigenvalue series λ and λ^* are formed in the following manner: in the first place there are a few real roots in odd number, then followed by a sequence of conjugate complex roots in pairs. The number of real roots varies according to the notch-angle α . For $207.74^\circ < \alpha < 315.07^\circ$, only one real root λ_1 exists among λ . For $198.44^\circ < \alpha < 328.43^\circ$, only one real root λ_1^* exists among λ^* . The number of real roots will increase while α tends to π or 2π . When $\alpha = \pi$ or $\alpha = 2\pi$, only real roots exist.

13.2.2 Stress Fields of the Mode I (Symmetry) Problem

1. For complex eigenvalue λ_n

Substitution of Eq. (13-7) into Eqs. (13-6) and (13-5) yields

$$\bar{B}_n = A_n, \quad C_n = \bar{D}_n = -A_n(\lambda_n \cos \alpha + \cos \lambda_n \alpha) \tag{13-10}$$

The stresses pertaining to the complex eigenvalue λ_n for mode I problem are

$$\sigma_n = \begin{Bmatrix} \sigma_{r,n} \\ \sigma_{\theta,n} \\ \sigma_{r\theta,n} \end{Bmatrix} = \begin{bmatrix} \text{Re } J_n & \text{Im } J_n \\ \text{Re } G_n & \text{Im } G_n \\ \text{Re } H_n & \text{Im } H_n \end{bmatrix} \begin{Bmatrix} \text{Re } A_n \\ -\text{Im } A_n \end{Bmatrix} \tag{13-11}$$

where

$$\left. \begin{aligned} J_n &= r^{\lambda_n-1} \lambda_n [(3 - \lambda_n) \cos(\lambda_n - 1)\theta + (\lambda_n \cos \alpha + \cos \lambda_n \alpha) \cos(\lambda_n + 1)\theta] \\ G_n &= r^{\lambda_n-1} \lambda_n [(\lambda_n + 1) \cos(\lambda_n - 1)\theta - (\lambda_n \cos \alpha + \cos \lambda_n \alpha) \cos(\lambda_n + 1)\theta] \\ H_n &= r^{\lambda_n-1} \lambda_n [(\lambda_n - 1) \sin(\lambda_n - 1)\theta - (\lambda_n \cos \alpha + \cos \lambda_n \alpha) \sin(\lambda_n + 1)\theta] \end{aligned} \right\} \tag{13-12}$$

The eigenroots are pairs of conjugate complex number. Let λ_n and λ_{n+1} be a pair of conjugate complex roots, we have

$$J_{n+1} = \bar{J}_n, \quad G_{n+1} = \bar{G}_n, \quad H_{n+1} = \bar{H}_n \tag{13-13}$$

Therefore, the stresses pertaining to this pair of conjugate complex roots can be written as

$$\sigma_n + \sigma_{n+1} = \begin{bmatrix} \operatorname{Re} J_n & \operatorname{Im} J_n \\ \operatorname{Re} G_n & \operatorname{Im} G_n \\ \operatorname{Re} H_n & \operatorname{Im} H_n \end{bmatrix} \begin{Bmatrix} \beta_n \\ \beta_{n+1} \end{Bmatrix} \quad (13-14)$$

in which two undetermined stress parameters β_n and β_{n+1} are included.

2. For real eigenvalue λ_n

When λ_n is real, J_n , G_n and H_n in Eq. (13-12) are all real numbers. So, Eq. (13-11) will degenerate into

$$\sigma_n = \begin{Bmatrix} J_n \\ G_n \\ H_n \end{Bmatrix} \beta_n \quad (13-15)$$

in which only one undetermined stress parameter β_n is involved.

3. Mode I stress intensity factor K_I

$$K_I = \sqrt{2\pi} \lim_{r \rightarrow 0} r^{1-\lambda_1} \sigma_{\theta,1} \Big|_{\theta=0} = \sqrt{2\pi} \beta_1 \lambda_1 (\lambda_1 + 1 - \lambda_1 \cos \alpha - \cos \lambda_1 \alpha) \quad (13-16)$$

13.2.3 Stress Fields of the Mode II (Antisymmetry) Problem

1. For complex eigenvalue λ_n^*

Substitution of Eq. (13-8) into Eqs. (13-6) and (13-5) yields

$$\bar{B}_n^* = -A_n^*, \quad C_n^* = -\bar{D}_n^* = -A_n^* (\lambda_n^* \cos \alpha - \cos \lambda_n^* \alpha) \quad (13-17)$$

The stresses pertaining to the complex eigenvalue λ_n^* for mode II problem are

$$\sigma_n = \begin{bmatrix} \operatorname{Re} J_n^* & \operatorname{Im} J_n^* \\ \operatorname{Re} G_n^* & \operatorname{Im} G_n^* \\ \operatorname{Re} H_n^* & \operatorname{Im} H_n^* \end{bmatrix} \begin{Bmatrix} \operatorname{Im} A_n^* \\ \operatorname{Re} A_n^* \end{Bmatrix} \quad (13-18)$$

where

$$\left. \begin{aligned} J_n^* &= -r^{\lambda_n^*-1} \lambda_n^* [(3 - \lambda_n^*) \sin(\lambda_n^* - 1)\theta + (\lambda_n^* \cos \alpha - \cos \lambda_n^* \alpha) \sin(\lambda_n^* + 1)\theta] \\ G_n^* &= -r^{\lambda_n^*-1} \lambda_n^* [(\lambda_n^* + 1) \sin(\lambda_n^* - 1)\theta - (\lambda_n^* \cos \alpha - \cos \lambda_n^* \alpha) \sin(\lambda_n^* + 1)\theta] \\ H_n^* &= -r^{\lambda_n^*-1} \lambda_n^* [(1 - \lambda_n^*) \cos(\lambda_n^* - 1)\theta + (\lambda_n^* \cos \alpha - \cos \lambda_n^* \alpha) \cos(\lambda_n^* + 1)\theta] \end{aligned} \right\} \quad (13-19)$$

The stresses pertaining to the conjugate complex roots λ_n^* and λ_{n+1}^* can be written as

$$\sigma_n + \sigma_{n+1} = \begin{bmatrix} \text{Re } J_n^* & \text{Im } J_n^* \\ \text{Re } G_n^* & \text{Im } G_n^* \\ \text{Re } H_n^* & \text{Im } H_n^* \end{bmatrix} \begin{Bmatrix} \beta_n^* \\ \beta_{n+1}^* \end{Bmatrix} \tag{13-20}$$

2. For real eigenvalue λ_n^*

$$\sigma_n = \begin{Bmatrix} J_n^* \\ G_n^* \\ H_n^* \end{Bmatrix} \beta_n^* \tag{13-21}$$

3. Mode II stress intensity factor K_{II}

$$K_{II} = \sqrt{2\pi} \lim_{r \rightarrow 0} r^{1-\lambda_1^*} \tau_{r\theta,1} \Big|_{\theta=0} = \sqrt{2\pi} \beta_1^* (-\lambda_1^*) (1 - \lambda_1^* + \lambda_1^* \cos \alpha - \cos \lambda_1^* \alpha) \tag{13-22}$$

13.2.4 The Sub-Region Mixed Element Method

Now, the plane V-notch problem is considered using the sub-region mixed element method. The sectorial region of radius R , centered on the notch-tip is regarded as the complementary energy region (C-region), and the outside domain as the potential energy region (P-region). And, the P-region is modelled by the 8-node displacement-based isoparametric elements (see Fig. 13.4).

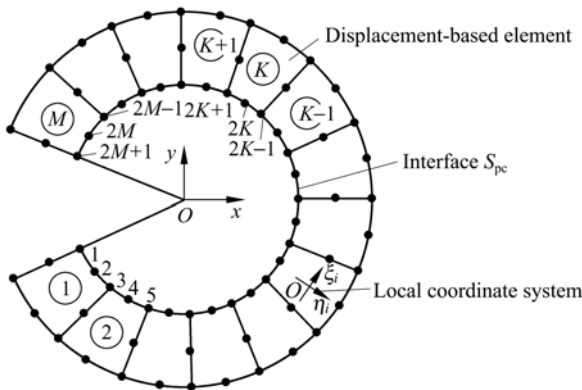


Figure 13.4 Stress-based element and outside 8-node isoparametric elements

The energy functional of the sub-region mixed variational principle is still given by Eq. (12-13), in which the matrices F and H can be derived as follows.

(1) The flexibility matrix F of the C-region

The stress fields of the C-region for modes I and II have already been derived, respectively. Here, the stress fields can be expressed in terms of the stress parameters β as

$$\sigma = [\sigma_r \quad \sigma_\theta \quad \tau_{r\theta}]^T = S\beta \quad (13-23)$$

Then, the complementary energy Π_c of the C-region and its flexibility matrix F can be written as

$$\begin{aligned} \Pi_c &= \frac{1}{2} \beta^T F \beta \\ F &= \int_{A_c} S^T D^{-1} S h dA \end{aligned} \quad (13-24)$$

where D is the elastic coefficient matrix; D^{-1} is given by Eq. (12-32). h is the thickness; and A_c is the area of the sectorial region in the C-region.

(2) The mixed matrix H on the interface

The mixed matrix H on the interface is still given by Eq. (12-45), i.e.,

$$H = \int_{S_{pc}} S^T L^T \bar{N} h ds \quad (13-25)$$

where S is defined by Eq. (13-23); L is the direction cosine matrix, and given by Eq. (12-41); \bar{N} is the shape function matrix of the 8-node isoparametric element. In Fig. 13.4, there are M isoparametric elements along the interface S_{pc} , then the components in matrix \bar{N} are

$$\left. \begin{aligned} \bar{N}_1 &= -\frac{1}{2} \xi_1 (1 - \xi_1) \\ \bar{N}_{2k} &= 1 - \xi_k^2 \\ \bar{N}_{2k+1} &= \begin{cases} \frac{1}{2} \xi_k (1 + \xi_k) & \text{(element } k) \\ -\frac{1}{2} \xi_{k+1} (1 - \xi_{k+1}) & \text{(element } k+1) \end{cases} \\ \bar{N}_{2M+1} &= \frac{1}{2} \xi_M (1 + \xi_M) \end{aligned} \right\} \begin{aligned} &(1 \leq k \leq M) \\ &(1 \leq k \leq M-1) \end{aligned} \quad (13-26)$$

h is the thickness (in Eq. (12-45), $h=1$ is assumed).

(3) The stress intensity factors

Substitution of F and H obtained into Eq. (12-13) yields the expression of the energy functional Π . The basic unknowns δ and β are still solved from the

stationary conditions (12-19) and (12-16). Finally, the stress intensity factors K_I and K_{II} can be obtained from Eqs. (13-16) and (13-22).

The sub-region mixed element method for the plane V-notch problem is denoted as SRM-V1.

Example 13.1 Evaluate the stress intensity factor K_I of a V-notched specimen subjected to uniform tension.

The geometry of the specimen is shown in Fig. 13.5(a), in which $\frac{H}{w} = 1.0$; the Poisson's ratio $\mu = 0.3$. Due to the symmetry, only half of the specimen is considered. Two meshes used here are shown in Figs. 13.5(b) and (c), which contain 11 and 22 elements, respectively.

The numerical results of the dimensionless stress intensity factor $K_I / (\sigma w^{1-\lambda_1})$ for the various angles α are listed in Table 13.3 (assume $\frac{a}{w} = 0.4$). It can be seen that, in comparison with the results given by reference [6], the relative errors are all less than 0.6% for mesh II.

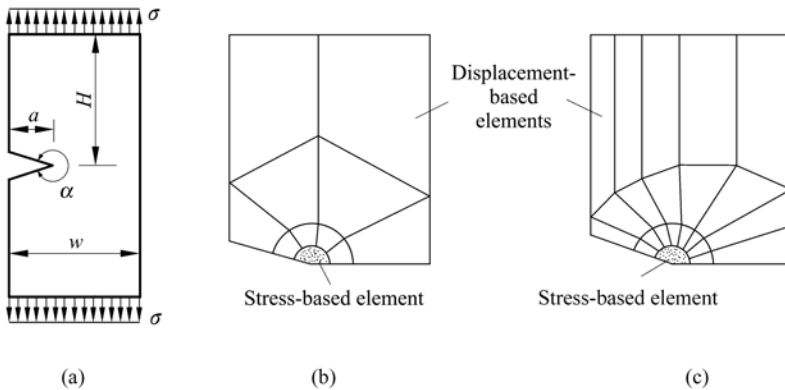


Figure 13.5 A V-notched specimen subjected to uniform tension
(a) Geometry; (b) Mesh I; (c) Mesh II

The results for various a/w are listed in Table 13.4 (assume $\alpha = 300^\circ$). In comparison with the results given by reference [6], the relative errors are no larger than 0.6% for mesh II.

Example 13.2 Evaluate the stress intensity factor K_{II} of a V-notched specimen subjected to antisymmetric load.

A single edge notched specimen is shown in Fig. 13.6(a): $a/w = 0.333$, $H/a = 1.0$, $\mu = 0.3$. And, the mesh used for this example is shown in Fig. 13.6(b).

Table 13.3 $K_I/(\sigma w^{1-\lambda_1})$ for various α ($\frac{a}{w} = 0.4$)

α	λ_1	Reference [6]	Mesh I	Error (%)	Mesh II	Error (%)
360°	0.500 000	2.369	2.314	-2.3	2.357	-0.5
350°	0.500 053	2.369	2.314	-2.3	2.357	-0.5
330°	0.501 453	2.389	2.313	-3.0	2.378	-0.5
300°	0.512 221	2.520	2.437	-3.3	2.514	-0.2
270°	0.544 484	2.888	2.795	-3.2	2.876	-0.4
240°	0.615 731	3.766	3.662	-2.8	3.754	-0.3

Table 13.4 $K_I/(\sigma w^{1-\lambda_1})$ for various a/w ($\alpha = 300^\circ$)

a/w	Reference [6]	Mesh I	Error (%)	Mesh II	Error (%)
0.3	1.724	1.671	-3.1	1.713	-0.6
0.4	2.520	2.436	-3.3	2.511	-0.5
0.5	3.756	3.569	-5.0	3.736	-0.5
0.6	5.859	5.576	-4.8	5.761	-0.6

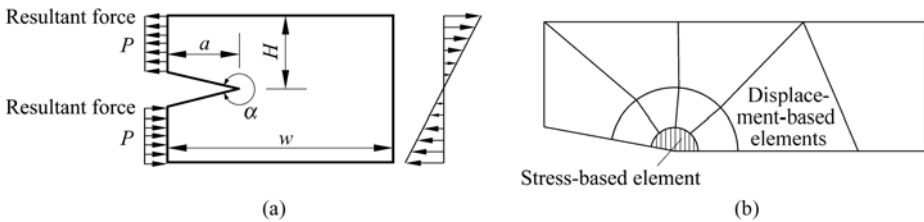


Figure 13.6 Single edge notched specimen subjected to antisymmetric load
(a) Geometry; (b) Mesh

For investigating the effect of the number of the eigenvalues considered on the stress intensity factors, the numerical results with which 1, 2, 3 and 4 eigenvalues are considered are given respectively in Table 13.5. It can be seen that satisfactory results can be obtained when the first 3 eigenvalues are used.

Table 13.5 $K_{II}(H/Pa^{1-\lambda_1^*})$ for various numbers of the first eigenvalues

α	λ_1^*	Number of eigenvalues considered				Reference [6]
		1	2	3	4	
360°	0.500 000	0.521	0.484	0.503	0.502	0.500
350°	0.529 355	0.425	0.388	0.405	0.404	0.401
340°	0.562 007	0.308	0.269	0.283	0.282	0.278

13.3 Plane V-Notch Problem in a Bi-Material

The plane V-notch problem in a bi-material not only keeps the main features of the plane V-notch problem for homogeneous material, but also reflects the characteristic of the interface crack. The singularities of stresses and strains at the notch-tip depend both on the opening angle of the notch and the ratio of the bi-material properties.

The plane V-notch problems in a bi-material have been discussed in references [2] and [13, 14]. In this section, the sub-region mixed element method will be used to analyze the V-notches in a bi-material^[2]. Firstly, by starting with the potential function theory, the eigenequations for the plane V-notch problem in a bi-material are derived. Then, the eigenvalues are solved by Muller iteration method, and the displacement and stress fields around the notch-tip can be obtained. Finally, the stress intensity factors for the various opening angles and ratios of bi-material properties are solved by the sub-region mixed element method.

13.3.1 The Stress Fields Around the Notch-Tip

As shown in Fig. 13.7, the V-notch is composed of two kinds of materials. Their shear elastic moduli are G_1 and G_2 , respectively; and the Poisson's ratios are μ_1 and μ_2 .

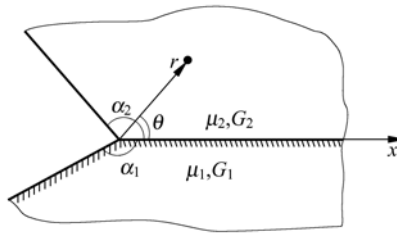


Figure 13.7 A V-notch in a bi-material

Let the notch-tip be the origin of the coordinate system, and the interface line be the x -axis. Then, the two sides of the notch are given by

$$\theta = -\alpha_1, \quad \theta = \alpha_2$$

Let $i = 1, 2$ denote material 1 and material 2, respectively. Then, the stress fields of this bi-material can be derived as follows.

(1) The stress functions φ_1 and φ_2

φ_1 and φ_2 denote the stress functions of material 1 and 2, respectively. In polar coordinates r and θ , they can be expressed in the following form of separated variables:

$$\varphi_i = r^{\lambda+1} f_i(\theta, \lambda) \quad (i = 1, 2) \tag{13-27}$$

where λ is the eigenvalue.

Since both the stress functions φ_1 and φ_2 should satisfy the bi-harmonic equation, f_i in the above equation should be

$$f_i = a_i \sin(\lambda + 1)\theta + b_i \cos(\lambda + 1)\theta + c_i \sin(\lambda - 1)\theta + d_i \cos(\lambda - 1)\theta \quad (i = 1, 2) \quad (13-28)$$

Thus, the stresses and displacements of the bi-material can be expressed in terms of f_i as follows

$$\left. \begin{aligned} \sigma_{rr} &= r^{\lambda-1} [f_i'' + (\lambda + 1)f_i'] \\ \sigma_{\theta\theta} &= r^{\lambda-1} [\lambda(\lambda + 1)f_i] \\ \sigma_{r\theta} &= r^{\lambda-1} [-\lambda f_i'] \\ u_{ir} &= \frac{r^\lambda}{2G_i} \{ -(\lambda + 1)f_i + (\lambda\omega_i)^{-1} [f_i'' + (\lambda + 1)^2 f_i] \} \\ u_{i\theta} &= \frac{r^\lambda}{2G_i} \{ -f_i' - (\lambda(\lambda - 1)\omega_i)^{-1} [f_i'' + (\lambda + 1)^2 f_i] \} \end{aligned} \right\} \quad (i = 1, 2) \quad (13-29)$$

where f_i' is the first-order derivative of f_i with respect to θ , the rest may be inferred by analogy; G_i is the shear modulus; ω_i can be expressed as

$$\omega_i = \begin{cases} 1 + \mu_i & \text{plane stress state} \\ \frac{1}{1 - \mu_i} & \text{plane strain state} \end{cases}$$

in which μ_i is the Poisson's ratio of material i .

(2) The boundary and continuity conditions

From Eq. (13-28), it can be seen that f_1 and f_2 each contain 4 unknown parameters. These 8 unknown parameters can be written as

$$\mathbf{g} = [a_1 \quad b_1 \quad c_1 \quad d_1 \quad a_2 \quad b_2 \quad c_2 \quad d_2]^T \quad (13-30)$$

In order to solve these unknown parameters, the following 8 conditions

$$\left. \begin{aligned} \sigma_{1\theta\theta} = 0 \\ \sigma_{1r\theta} = 0 \end{aligned} \right\} \quad (\theta = -\alpha_1)$$

$$\left. \begin{aligned} \sigma_{2\theta\theta} = 0 \\ \sigma_{2r\theta} = 0 \end{aligned} \right\} \quad (\theta = \alpha_2) \quad (13-31)$$

$$\left. \begin{aligned} \sigma_{1\theta\theta} = \sigma_{2\theta\theta} \\ \sigma_{1r\theta} = \sigma_{2r\theta} \\ u_{1r} = u_{2r} \\ u_{1\theta} = u_{2\theta} \end{aligned} \right\} \quad (\theta = 0)$$

can be introduced.

Substitution of Eq. (13-29) into the above equation yields 8 homogeneous conditions about the unknown parameters \mathbf{g} as follows:

$$-a_1 \sin(\lambda + 1)\alpha_1 + b_1 \cos(\lambda + 1)\alpha_1 - c_1 \sin(\lambda - 1)\alpha_1 + d_1 \cos(\lambda - 1)\alpha_1 = 0 \quad (13-32a)$$

$$a_1(\lambda + 1)\cos(\lambda + 1)\alpha_1 + b_1(\lambda + 1)\sin(\lambda + 1)\alpha_1 + c_1(\lambda - 1)\cos(\lambda - 1)\alpha_1 + d_1(\lambda - 1)\sin(\lambda - 1)\alpha_1 = 0 \quad (13-32b)$$

$$a_2 \sin(\lambda + 1)\alpha_2 + b_2 \cos(\lambda + 1)\alpha_2 + c_2 \sin(\lambda - 1)\alpha_2 + d_2 \cos(\lambda - 1)\alpha_2 = 0 \quad (13-32c)$$

$$a_2(\lambda + 1)\cos(\lambda + 1)\alpha_2 - b_2(\lambda + 1)\sin(\lambda + 1)\alpha_2 + c_2(\lambda - 1)\cos(\lambda - 1)\alpha_2 - d_2(\lambda - 1)\sin(\lambda - 1)\alpha_2 = 0 \quad (13-32d)$$

$$b_1 + d_1 = b_2 + d_2 \quad (13-32e)$$

$$a_1(\lambda + 1) + c_1(\lambda - 1) = a_2(\lambda + 1) + c_2(\lambda - 1) \quad (13-32f)$$

$$\begin{aligned} & -(\lambda + 1)(b_1 + d_1) + (\lambda\omega_1)^{-1}[-b_1(\lambda + 1)^2 - d_1(\lambda - 1)^2 + (\lambda + 1)(b_1 + d_1)] \\ = & -(\lambda + 1)(b_2 + d_2) + (\lambda\omega_2)^{-1}[-b_2(\lambda + 1)^2 - d_2(\lambda - 1)^2 + (\lambda + 1)(b_2 + d_2)] \end{aligned} \quad (13-32g)$$

$$\begin{aligned} & -a_1(\lambda + 1) - c_1(\lambda - 1) - (\lambda(\lambda - 1)\omega_1)^{-1}\{-a_1(\lambda + 1)^3 \\ & - c_1(\lambda - 1)^3 + (\lambda + 1)^2[(\lambda + 1)a_1 + (\lambda - 1)c_1]\} \\ = & -a_2(\lambda + 1) - c_2(\lambda - 1) - (\lambda(\lambda - 1)\omega_2)^{-1}\{-a_2(\lambda + 1)^3 \\ & - c_2(\lambda - 1)^3 + (\lambda + 1)^2[(\lambda + 1)a_2 + (\lambda - 1)c_2]\} \end{aligned} \quad (13-32h)$$

The above 8 homogeneous equations can be rewritten in the following matrix form:

$$\mathbf{G}\mathbf{g} = \mathbf{0} \quad (13-33)$$

where the unknown parameters in \mathbf{g} are defined by Eq. (13-30); and \mathbf{G} is the coefficient matrix of the equation set (13-32).

(3) Eigenequation and the first n eigenvalues

In order to obtain the nonzero solutions of the homogeneous Eq. (13-33), let the determinant of the coefficient matrix \mathbf{G} be zero:

$$|\mathbf{G}| = 0 \quad (13-34)$$

This is the eigenequation of the plane V-notch problem in a bi-material.

By using the Muller iteration method, a series of eigenvalues of the eigenequation (13-34) can be solved. The first n eigenvalues are written by

$$\boldsymbol{\lambda} = [\lambda_1 \quad \lambda_2 \quad \cdots \quad \lambda_n]^T \quad (13-35)$$

(4) Stress expansion around the notch-tip

Substituting any eigenvalue λ_k in $\boldsymbol{\lambda}$ into Eq. (13-33), a set of nonzero solutions $\mathbf{g}^{(k)}$ of \mathbf{g} can be obtained. We can only determine the ratio of each component to the first component a_{1k} in $\mathbf{g}^{(k)}$, but a_{1k} is still an unknown value. That is to say, each component in $\mathbf{g}^{(k)}$ can be expressed as a known multiple of a_{1k} . Substitution of $\mathbf{g}^{(k)}$ into Eq. (13-29) yields the stress terms corresponding to the eigenvalue λ_k :

$$\boldsymbol{\sigma}_{i(k)} = \begin{Bmatrix} \sigma_{irr} \\ \sigma_{i\theta\theta} \\ \sigma_{ir\theta} \end{Bmatrix}_{(k)} = \mathbf{J}_{i(k)} a_{1k} \quad (i=1,2) \quad (13-36)$$

By superposition of the stress terms corresponding to the first n eigenvalues, the stress expansion can be obtained as follows:

$$\boldsymbol{\sigma}_i = \begin{Bmatrix} \sigma_{irr} \\ \sigma_{i\theta\theta} \\ \sigma_{ir\theta} \end{Bmatrix} = \mathbf{S}_i \boldsymbol{\beta} \quad (i=1,2) \quad (13-37)$$

where

$$\left. \begin{aligned} \boldsymbol{\beta} &= [a_{11} \quad a_{12} \quad \cdots \quad a_{1n}]^T \\ \mathbf{S}_i &= [\mathbf{J}_{i(1)} \quad \mathbf{J}_{i(2)} \quad \cdots \quad \mathbf{J}_{i(n)}] \end{aligned} \right\} \quad (13-38)$$

The unknown coefficients in $\boldsymbol{\beta}$ will be determined by the sub-region mixed element method.

13.3.2 The Sub-Region Mixed Element Method

Now, the sub-region mixed element method is used to analyze the plane V-notch problem in a bi-material. The sectorial region centered at the notch-tip is taken as the complementary energy region A_c , which is composed of two kinds of materials and denoted as A_{c1} and A_{c2} , respectively (Fig. 13.8). The outside of the C-region is the potential energy region A_p , which is composed of A_{p1} and A_{p2} and modelled by 8-node displacement-based isoparametric elements. And, the interface S_{pc} is composed of S_{pc1} and S_{pc2} .

The energy functional of the sub-region mixed variational principle is still given by Eq. (12-13), in which the matrices \mathbf{F} and \mathbf{H} can be derived as follows.

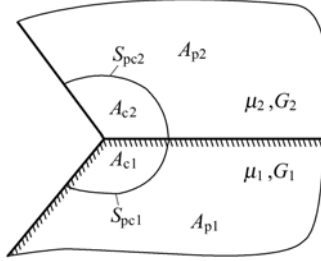


Figure 13.8 Division of the C-region and P-region (V-notch in a bi-material)

(1) The flexibility matrix F of the C-region
 The complementary energy Π_c of the C-region is

$$\Pi_c = \frac{1}{2} \iint_{A_{c1}} \boldsymbol{\sigma}_1^T \mathbf{D}_1^{-1} \boldsymbol{\sigma}_1 h dA + \frac{1}{2} \iint_{A_{c2}} \boldsymbol{\sigma}_2^T \mathbf{D}_2^{-1} \boldsymbol{\sigma}_2 h dA \quad (13-39)$$

in which stresses $\boldsymbol{\sigma}_i$ are expressed by Eq. (13-37), so we have

$$\Pi_c = \frac{1}{2} \boldsymbol{\beta}^T \mathbf{F} \boldsymbol{\beta} \quad (13-40)$$

Then, the flexibility matrix F can be written as

$$\mathbf{F} = \iint_{A_{c1}} \mathbf{S}_1^T \mathbf{D}_1^{-1} \mathbf{S}_1 h dA + \iint_{A_{c2}} \mathbf{S}_2^T \mathbf{D}_2^{-1} \mathbf{S}_2 h dA \quad (13-41)$$

where \mathbf{D}_1 and \mathbf{D}_2 are the elastic matrices of the materials 1 and 2, respectively.

(2) The mixed matrix H on the interface

The additional energy H_{pc} on the interface is composed of two parts. According to Eq. (12-8), H_{pc} can be expressed as

$$H_{pc} = \int_{S_{pe1}} \mathbf{T}_1^T \bar{\mathbf{u}}_1 h ds + \int_{S_{pe2}} \mathbf{T}_2^T \bar{\mathbf{u}}_2 h ds \quad (13-42)$$

\mathbf{T}_i is the boundary force of the C-region on the interface S_{pei} ; $\bar{\mathbf{u}}_i$ is the boundary displacement of the P-region on the interface S_{pei} :

$$\left. \begin{aligned} \mathbf{T}_i &= \mathbf{L}_i \boldsymbol{\sigma}_i = \mathbf{L}_i \mathbf{S}_i \boldsymbol{\beta} \\ \bar{\mathbf{u}}_i &= \bar{\mathbf{N}}_i \bar{\boldsymbol{\delta}} \end{aligned} \right\} \quad (13-43)$$

where \mathbf{L}_1 and \mathbf{L}_2 are the direction cosine matrix of the interface; $\bar{\mathbf{N}}_1$ and $\bar{\mathbf{N}}_2$ are formed by the shape functions of the displacement-based elements; $\bar{\boldsymbol{\delta}}$ is the nodal displacement vector of the nodes on the interface. Substitution of Eq. (13-43) into Eq. (13-42) yields

$$H_{pc} = \beta^T H \bar{\delta} \tag{13-44}$$

And, the mixed matrix H on the interface can be derived:

$$H = \int_{S_{pc1}} S_1^T L_1 \bar{N}_1 h ds + \int_{S_{pc2}} S_2^T L_2 \bar{N}_2 h ds \tag{13-45}$$

(3) The stress intensity factors

Substituting F and H , which have been obtained, into Eq. (12-13), the expression of the energy functional Π can be obtained. The basic unknowns δ and β are still solved by the stationary conditions (12-19) and (12-16).

From β , the stresses $\sigma_{\theta\theta}$ and $\sigma_{r\theta}$ can be determined. And, the stress intensity factor of the notch-tip can be determined from the following definition:

$$\left. \begin{aligned} K_I &= \sqrt{2\pi} \lim_{r \rightarrow 0} r^{1-\lambda_1} \sigma_{\theta\theta} \Big|_{\theta=0} \\ K_{II} &= \sqrt{2\pi} \lim_{r \rightarrow 0} r^{1-\lambda_2} \sigma_{r\theta} \Big|_{\theta=0} \end{aligned} \right\} \tag{13-46}$$

The sub-region mixed element method for the plane V-notch problem in a bi-material is denoted as SRM-V2.

Example 13.3 Evaluate the stress intensity factors K_I and K_{II} of a plate in extension with a V-notch at a bi-material interface by the sub-region mixed element method SRM-V2 (Fig. 13.9). The notch-tip is also at the bi-material interface.

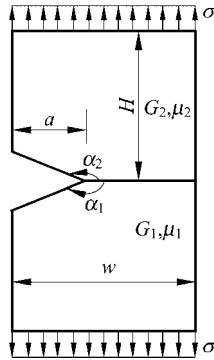


Figure 13.9 A plate in extension with a V-notch at a bi-material interface

Let $\mu_1 = \mu_2 = 0.3$; $H / w = 1.0$; and $\alpha_1 = \alpha_2$.

In order to check the effects on the stress intensity factors with the variations of different factors (ratios of material properties, opening angle of the notch and ratio of the notch length to plate width), the following two cases are considered:

(1) a/w ratio keeps invariant, but opening angles $\alpha_1 = \alpha_2$ of the notch and G_2 / G_1 ratio vary—Numerical results are listed in Table 13.6.

Advanced Finite Element Method in Structural Engineering

(2) Opening angles $\alpha_1 = \alpha_2$ keep invariant, but ratios of a / w and G_2 / G_1 vary—Numerical results are listed in Table 13.7.

From the above results, it can be concluded that

(1) For a symmetric notch subjected to symmetric load, the shear mode stress concentration phenomenon ($K_{II} \neq 0$) will happen due to the difference of materials; when $G_2 / G_1 = 1$, $K_{II} = 0$.

Table 13.6 The stress intensity factors under various ratios of material properties and opening angles of the notch ($a / w = 0.4$)

$\alpha_1 = \alpha_2$	G_2 / G_1	1			3	5	7	10
		SRM-V2	Reference[6]	Error (%)				
240°	$K_I / w^{1-\lambda_1} \sigma$	3.801	3.766	0.93	3.944	4.187	4.336	4.515
	$K_{II} / w^{1-\lambda_2} \sigma$	0.0	0.0		0.234	0.397	0.494	0.631
270°	$K_I / w^{1-\lambda_1} \sigma$	2.913	2.888	0.87	3.340	3.904	4.480	5.397
	$K_{II} / w^{1-\lambda_2} \sigma$	0.0	0.0		1.018	1.564	1.990	2.576

Table 13.7 Variations of the stress intensity factors with various ratios G_2 / G_1 and notch lengths ($\alpha_1 = \alpha_2 = 150^\circ$)

G_2 / G_1	a / w	0.3	0.4	0.5	0.6
		1	$K_I / w^{1-\lambda_1} \sigma$	1.750	2.574
$K_{II} / w^{1-\lambda_2} \sigma$	0.0		0.0	0.0	0.0
3	$K_I / w^{1-\lambda_1} \sigma$	2.400	3.428	4.988	7.554
	$K_{II} / w^{1-\lambda_2} \sigma$	1.278	1.717	2.398	3.541

(2) The singularity at the notch-tip will increase with the increase of the difference of materials.

(3) The singularity at the notch-tip will increase with the decrease of the opening angle of notch.

(4) The singularity at the notch-tip will increase with the increase of the notch length.

The first 4 eigenvalues are taken during the computations. If the radius of the singular element varies within the range $0.1a - 0.08a$, the results are relatively stable.

Example 13.4 Evaluate the stress intensity factors of a central crack at a bi-material interface in an infinite plate.

An infinite plate subjected to a uniform tension load $\sigma_y^\infty = 1\text{kPa}$ along y -direction is shown in Fig. 13.10. There is an interface crack with length $2a = 2\text{m}$ located at

the center of the bi-material interface. And, the Young's modulus $E_1 = 1\text{kPa}$; the Poisson's ratios $\mu_1 = \mu_2 = 0.3$.

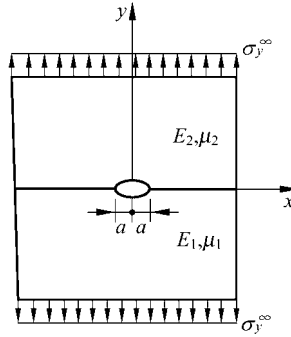


Figure 13.10 An infinite plate in extension with a crack at a bi-material interface

The stress intensity factors of the interface crack are defined as follows:

$$K_I - iK_{II} = 2\sqrt{2}e^{-\pi\text{Im}\lambda_1} \lim_{z \rightarrow 0} z^{\bar{\lambda}_1} \phi_2'(z)$$

where $\phi_2(z)$ denotes the complex potential function of elasticity, and can be expressed in terms of the stress coefficients β .

Numerical results are listed in Table 13.8. In comparison with classical solutions^[15], all relative errors are within 1%.

In practical computations, the infinite plate is replaced by a $20\text{m} \times 20\text{m}$ plate. The radius of the singular element is taken as $0.08a$, and the first 4 terms of λ are used. It can be seen that the results are basically stable. The accuracy of K_{II} is lower than that of K_I . So, for improving the precision of K_{II} , more terms of the eigenvalues are needed.

Table 13.8 Stress intensity factors of a central interface crack in an infinite plate under uniform tension

G_2 / G_1		1	3	10	100	1000
K_I	SRM-V2	1.009	0.999	0.981	0.968	0.957
	Reference [15]	1.000	0.988	0.968	0.953	0.952
K_{II}	SRM-V2	0.0	0.0822	0.1289	0.1401	0.1535
	Reference [15]	0.0	0.0724	0.1171	0.1391	0.1415

13.4 Anti-Plane V-Notch Problem in a Bi-Material

This section will discuss the anti-plane V-notch problem (Mode III) in a bi-material^[16]. Firstly, the stress fields around the notch-tip are derived by the

eigenfunction method; then, the stress intensity factor K_{III} is solved by the sub-region mixed element method. Besides, the anti-plane V-notch problem has already been analyzed by the weight function theory in references [17, 18], and the anti-plane crack problem in a non-homogenous elastic material has also been studied in [19].

13.4.1 The Displacement and Stress Fields around the Notch-Tip

An anti-plane V-notch in a bi-material shown in Fig. 13.11 is considered. Let the interface line of the two materials be the x -axis, then equations of two notch sides are $\theta = \theta_1$ and $\theta = \theta_2$, respectively.

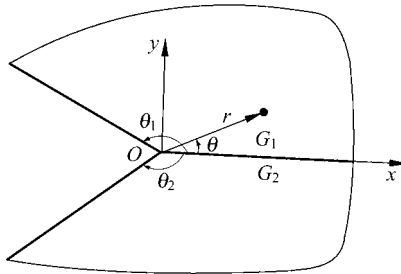


Figure 13.11 An anti-plane V-notch in a bi-material

Under the anti-plane state, only the displacement w in the z -direction exists, so the stresses can be expressed in terms of displacement as follows:

$$\tau_{rzi} = G_i \frac{\partial w_i}{\partial r}, \quad \tau_{\theta zi} = G_i \frac{1}{r} \frac{\partial w_i}{\partial \theta} \tag{13-47}$$

in which G_i denotes the shear modulus of the material i , $i = 1$ and 2 .

Ignoring the influences of body forces, the equilibrium equation can be expressed in terms of stresses as follows:

$$\frac{\partial}{\partial r}(r\tau_{rzi}) + \frac{\partial}{\partial \theta}(\tau_{\theta zi}) = 0 \tag{13-48}$$

Substitution of Eq. (13-47) into Eq. (13-48) yields the equilibrium equation expressed in terms of displacement:

$$\frac{\partial^2 w_i}{\partial r^2} + \frac{1}{r} \frac{\partial w_i}{\partial r} + \frac{1}{r^2} \frac{\partial^2 w_i}{\partial \theta^2} = 0 \tag{13-49}$$

w_i can be rewritten as the following form of separated variables

$$w_i = r^{\lambda+1} F_i(\theta, \lambda)$$

Then, from Eq. (13-49), we obtain

$$w_i(r, \theta) = r^{\lambda+1} [A_i \cos(\lambda + 1)\theta + B_i \sin(\lambda + 1)\theta] \quad (13-50)$$

Assume that there is no external load around the notch-tip, so the boundary conditions of the notch can be expressed as follows:

$$\tau_{z\theta 1} \Big|_{\theta=\theta_1} = 0, \quad \tau_{z\theta 2} \Big|_{\theta=\theta_2} = 0$$

And, the continuity conditions of displacements and stresses between the two materials are

$$w_1 \Big|_{\theta=0} = w_2 \Big|_{\theta=0}, \quad \tau_{z\theta 1} \Big|_{\theta=0} = \tau_{z\theta 2} \Big|_{\theta=0}$$

By Eqs. (13-47) and (13-50), we can obtain

$$\left. \begin{aligned} -A_1 \sin(\lambda + 1)\theta_1 + B_1 \cos(\lambda + 1)\theta_1 &= 0 \\ -A_2 \sin(\lambda + 1)\theta_2 + B_2 \cos(\lambda + 1)\theta_2 &= 0 \\ A_1 = A_2, \quad G_1 B_1 = G_2 B_2 \end{aligned} \right\} \quad (13-51)$$

In order to obtain nonzero solutions from the original problem, the coefficient determinant of Eq. (13-51) must be zero, then we have

$$G_1 \sin(\lambda + 1)\theta_1 \cos(\lambda + 1)\theta_2 - G_2 \sin(\lambda + 1)\theta_2 \cos(\lambda + 1)\theta_1 = 0 \quad (13-52)$$

Equation (13-52) is the eigenequation of the anti-plane V-notch in a bi-material. In general, a series of solutions for λ can be solved by the Muller iteration method. For the following special cases:

$$\text{If } G_1 = G_2, \quad \lambda_n + 1 = n\pi / (\theta_1 - \theta_2) \quad (n = 1, 2, \dots)$$

$$\text{If } \theta_1 = -\theta_2, \quad \lambda_n + 1 = n\pi / (2\theta_1) \quad (n = 1, 2, \dots)$$

The singularities of stresses and strains will increase with the decrease of the corresponding λ . Hence, the influence of the minimum eigenvalue λ_1 is dominant for the singularity of notch-tip. If only λ_1 is considered, the displacement and stress fields around the notch-tip can be derived from Eq. (13-51):

$$\left. \begin{aligned} w_i &= K_{\text{III}} \frac{(2\pi)^{\lambda_1} r^{\lambda_1+1} \cos[(\lambda_1 + 1)(\theta_i - \theta)]}{G_i (\lambda_1 + 1) \sin[(\lambda_1 + 1)\theta_i]} \\ \tau_{zri} &= K_{\text{III}} (2\pi r)^{\lambda_1} \frac{\cos[(\lambda_1 + 1)(\theta_i - \theta)]}{\sin[(\lambda_1 + 1)\theta_i]} \\ \tau_{\theta zi} &= K_{\text{III}} (2\pi r)^{\lambda_1} \frac{\sin[(\lambda_1 + 1)(\theta_i - \theta)]}{\sin[(\lambda_1 + 1)\theta_i]} \end{aligned} \right\} \quad (i = 1, 2) \quad (13-53)$$

in which K_{III} is the stress intensity factor of the anti-plane V-notch in a bi-material, and is defined as:

$$K_{III} = \lim_{r \rightarrow 0} \frac{1}{(2\pi r)^{\lambda_1}} \tau_{\theta zi} \Big|_{\theta=0} \quad (13-54)$$

If let $G_1 = G_2$ and $\theta_1 = -\theta_2 = \pi$ in Eq. (13-53), the displacement and stress fields of the mode III crack in homogenous material can then be obtained, and they are in agreement with those given in reference [20].

Equation (13-53) gives the dominant term of the displacement and stress fields around the notch-tip, in which an undetermined parameter K_{III} is included. And, Eq. (13-53) can be rewritten as:

$$w_i = K_{III} \tilde{w}_i, \quad \tau_{zri} = K_{III} \tilde{\tau}_{zri}, \quad \tau_{\theta zi} = K_{III} \tilde{\tau}_{\theta zi} \quad (13-55)$$

13.4.2 The Sub-Region Mixed Element Method

The energy functional of the sub-region mixed variational principle is still given by Eq. (12-5), i.e.,

$$\Pi = \Pi_p - \Pi_c + H_{pc} \quad (13-56)$$

in which the stress parameter K_{III} of the complementary energy region and the nodal displacements $\boldsymbol{\delta}$ of the potential energy region are the basic unknowns.

(1) The total potential energy Π_p of the potential energy region

$$\Pi_p = \frac{1}{2} \boldsymbol{\delta}^T \mathbf{K} \boldsymbol{\delta} - \boldsymbol{\delta}^T \mathbf{P} = \frac{1}{2} \sum_{k=1}^n \sum_{j=1}^n K_{kj} w_k w_j - \sum_{j=1}^n P_j w_j \quad (13-57)$$

where n is the total number of the nodes of the displacement-based elements in the potential energy region; \mathbf{K} is the stiffness matrix; \mathbf{P} is the equivalent nodal load vector; $\boldsymbol{\delta}$ is the nodal displacement vector:

$$\boldsymbol{\delta} = [w_1 \quad w_2 \quad \cdots \quad w_n]^T$$

(2) The total complementary energy Π_c of the complementary energy region

The complementary energy region A_c is composed of two materials, which are denoted as A_{c1} and A_{c2} , respectively. Thus, the complementary energy Π_c of the complementary energy region is

$$\Pi_c = \frac{1}{2G_1} \iint_{A_{c1}} (\tau_{rz1}^2 + \tau_{\theta z1}^2) dA + \frac{1}{2G_2} \iint_{A_{c2}} (\tau_{rz2}^2 + \tau_{\theta z2}^2) dA$$

Substitution of Eq. (13-53) into the above equation yields

$$\Pi_c = \frac{K_{III}^2}{2G_1 \sin^2(\lambda_1 + 1)\theta_1} \iint_{A_{c1}} (2\pi r)^{2\lambda_1} dA + \frac{K_{III}^2}{2G_2 \sin^2(\lambda_1 + 1)\theta_2} \iint_{A_{c2}} (2\pi r)^{2\lambda_1} dA$$

If the complementary energy region is assumed as a sectorial region with radius r_c , then we have

$$\Pi_c = \frac{1}{2} K_{III}^2 V \quad (13-58)$$

where

$$V = \frac{(2\pi)^{2\lambda_1} r_c^{2\lambda_1+2}}{2(\lambda_1 + 1)} \left[\frac{\theta_1}{G_1 \sin^2(\lambda_1 + 1)\theta_1} - \frac{\theta_2}{G_2 \sin^2(\lambda_1 + 1)\theta_2} \right] \quad (13-59)$$

(3) The additional energy H_{pc} on the interface

The interface line S_{pc} is composed of two segments S_{pc1} and S_{pc2} . The total number of the nodes on the interface is n_1 , and the nodal displacement vector on the interface is

$$\bar{\delta} = [w_1 \quad w_2 \quad \cdots \quad w_{n_1}]^T$$

Then, the additional energy H_{pc} on the interface is

$$H_{pc} = \int_{S_{pc1}} \tau_{rz1} \bar{w} ds + \int_{S_{pc2}} \tau_{rz2} \bar{w} ds \quad (13-60)$$

And, the displacement \bar{w} on the interface can be expressed in terms of the nodal displacement vector $\bar{\delta}$ and shape functions \bar{N} as

$$\bar{w} = \sum_{j=1}^{n_1} \bar{N}_j w_j \quad (13-61)$$

Substituting the above equation into Eq. (13-60), H_{pc} can be expressed in terms of K_{III} and $\bar{\delta}$ as

$$H_{pc} = K_{III} \sum_{j=1}^{n_1} h_j w_j \quad (13-62)$$

where

$$h_j = \int_{S_{pc1}} \tau_{rz1} \bar{N}_j ds + \int_{S_{pc2}} \tau_{rz2} \bar{N}_j ds \quad (13-63)$$

(4) The energy stationary condition

Substituting Eqs. (13-57), (13-58) and (13-62) into Eq. (13-56), the energy Π can be expressed in terms of the basic unknowns K_{III} and δ as

$$\Pi = \frac{1}{2} \sum_{k=1}^n \sum_{j=1}^n k_{kj} w_k w_j - \sum_{j=1}^n P_j w_j - \frac{1}{2} K_{III}^2 V + K_{III} \sum_{j=1}^{n_1} h_j w_j \quad (13-64)$$

From the stationary condition $\frac{\partial \Pi}{\partial w_j} = 0$, we obtain

$$\left. \begin{aligned} \sum_{k=1}^n K_{kj} w_k + K_{III} h_j &= P_j \quad (j = 1, 2, \dots, n_1) \\ \sum_{k=1}^n K_{kj} w_k &= P_j \quad (j = n_1 + 1, \dots, n) \end{aligned} \right\} \quad (13-65)$$

From $\frac{\partial \Pi}{\partial K_{III}} = 0$, we obtain

$$-K_{III} V + \sum_{j=1}^{n_1} h_j w_j = 0 \quad (13-66)$$

By substituting Eq. (13-66) into the first expression in Eq. (13-65), K_{III} can be eliminated, and $\delta = [w_1 \ w_2 \ \dots \ w_n]^T$ can first be solved. Then, K_{III} can be solved from Eq. (13-66).

The sub-region mixed element method for the anti-plane V-notch problem in a bi-material is denoted as SRM-V3.

Example 13.5 Evaluate the stress intensity factor K_{III} of an infinite V-notch in a bi-material. Let the interface of the two materials be the sectrix line for the opening angle of the V-notch, and a pair of concentrated forces P with reverse directions act on the notch boundary (Fig. 13.12).

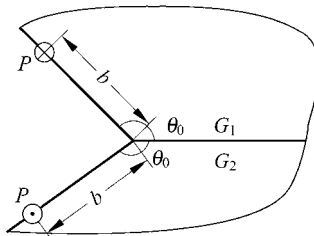


Figure 13.12 An infinite V-notch in a bi-material

The computational formula of K_{III} obtained by weight function method in [17] is

$$K_{III} = (2\pi)^{1-\frac{\pi}{2\theta_0}} \frac{P}{\theta_0 b^{1-\frac{\pi}{2\theta_0}}} \quad (13-67)$$

where b is the distance from load P to the notch-tip.

The results of the stress intensity factor K_{III} calculated by the sub-region

mixed element method are listed in Table 13.9. And for comparison, the results of [17] are also given. Here, $\theta_0 = \frac{3}{4}\pi$ and $b = 10\text{m}$.

Table 13.9 Results of K_{III} with different radius r_c of the complementary energy region

r_c/b	0.2	0.1	0.075	0.05	0.01	Reference [17]
K_{III} / P	0.740	0.761	0.794	0.812	0.832	0.783
Error (%)	- 5.25	- 2.82	1.39	3.68	6.23	

It can be seen from Table 13.9 that, when $\frac{r_c}{b} = 0.075$, the accuracy of the present method (SRM-V3) is the best. And, when $0.01 \leq \frac{r_c}{b} \leq 0.2$, the numerical results are relatively stable. By increasing the number of the displacement-based elements outside the interface S_{pc} , the stress continuity on the interface can be improved, then the computational accuracy of K_{III} can also be improved.

13.5 V-Notch Problem in Reissner Plate

This section will discuss the V-notch problem in a thick plate^[3]. Since limitations may happen for the crack and V-notch problems in plate bending if the Kirchhoff thin plate theory is used, the Reissner plate theory which considers the influence of shear deformation is adopted here. Firstly, the eigenequations and their solutions for the V-notch problem in the Reissner plate are derived; then, the expressions of stress and displacement fields around the notch-tip in the Reissner plate are derived; finally, the stress intensity factor is solved by the sub-region mixed element method.

13.5.1 The Eigenequations and Eigenvalues of V-Notch Problem in Reissner Plate

1. Fundamental equations

As shown in Fig. 13.13, a bending plate with a notch is considered, and the notch-tip is taken as the origin of the coordinate system. By using the Reissner theory and polar coordinates, the fundamental equations of the thick plate can be expressed in terms of 3 generalized displacements ψ_r , ψ_θ and w as

$$\left. \begin{aligned}
 & D \left[\frac{\partial^2 \psi_r}{\partial r^2} + \frac{1}{r} \frac{\partial \psi_r}{\partial r} - \frac{\psi_r}{r^2} + \frac{1-\mu}{2} \frac{\partial^2 \psi_r}{r^2 \partial \theta^2} + \frac{1+\mu}{2} \frac{1}{r} \frac{\partial^2 \psi_\theta}{\partial r \partial \theta} - \frac{3-\mu}{2} \frac{\partial \psi_\theta}{r^2 \partial \theta} \right] \\
 & \quad + C \left(\frac{\partial w}{\partial r} - \psi_r \right) = 0 \\
 & D \left[\frac{1+\mu}{2} \frac{1}{r} \frac{\partial^2 \psi_r}{\partial r \partial \theta} + \frac{3-\mu}{2} \frac{1}{r^2} \frac{\partial \psi_r}{\partial \theta} + \frac{1-\mu}{2} \frac{\partial^2 \psi_\theta}{\partial r^2} + \frac{1-\mu}{2} \frac{1}{r} \frac{\partial \psi_\theta}{\partial r} + \frac{1}{r^2} \frac{\partial^2 \psi_\theta}{\partial \theta^2} - \frac{1-\mu}{2} \frac{\psi_\theta}{r^2} \right] \\
 & \quad + C \left(\frac{1}{r} \frac{\partial w}{\partial \theta} - \psi_\theta \right) = 0 \\
 & C \left[\frac{\partial^2 w}{\partial r^2} + \frac{1}{r} \frac{\partial w}{\partial r} + \frac{1}{r^2} \frac{\partial^2 w}{\partial \theta^2} - \left(\frac{\partial \psi_r}{\partial r} + \frac{\psi_r}{r} + \frac{1}{r} \frac{\partial \psi_\theta}{\partial \theta} \right) \right] + p = 0
 \end{aligned} \right\} \tag{13-68}$$

where ψ_r and ψ_θ are rotating angles of straight lines which are perpendicular to the middle plane before deformation. ψ_r is the rotating angle in the rz -plane, and is positive if rotates from r -axis to z -axis; ψ_θ is the rotating angle in the θz -plane, and is positive if rotates from θ -direction to z -axis; w is the deflection. D and C are bending and shearing stiffness, respectively,

$$D = \frac{Eh^3}{12(1-\mu^2)}, \quad C = \frac{5}{6} Gh$$

in which E is the Young's modulus; G is the shear modulus; μ is the Poisson's ratio; h is the thickness of the plate; p is the density of the external load.

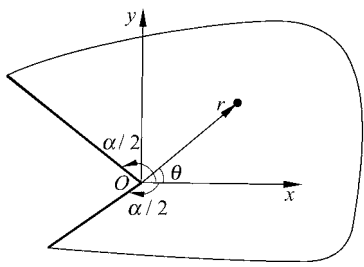


Figure 13.13 V-notch problem in plate bending

The relations between internal forces and displacements are as follows:

$$\left. \begin{aligned} M_r &= -D \left[\frac{\partial \psi_r}{\partial r} + \mu \left(\frac{1}{r} \frac{\partial \psi_\theta}{\partial \theta} + \frac{\psi_r}{r} \right) \right] \\ M_\theta &= -D \left[\frac{1}{r} \frac{\partial \psi_\theta}{\partial \theta} + \frac{\psi_r}{r} + \mu \frac{\partial \psi_r}{\partial r} \right] \\ M_{r\theta} &= -D \frac{1-\mu}{2} \left(\frac{1}{r} \frac{\partial \psi_r}{\partial \theta} + \frac{\partial \psi_\theta}{\partial r} - \frac{\psi_\theta}{r} \right) \\ Q_r &= C \left(\frac{\partial w}{\partial r} - \psi_r \right) \\ Q_\theta &= C \left(\frac{1}{r} \frac{\partial w}{\partial \theta} - \psi_\theta \right) \end{aligned} \right\} \quad (13-69)$$

The boundary conditions of the notch are

$$M_\theta = M_{r\theta} = Q_\theta = 0 \quad (\theta = \pm\alpha/2) \quad (13-70)$$

2. Eigenexpansions and eigenequations

ψ_r, ψ_θ and w can be expanded as follows:

$$\left. \begin{aligned} \psi_r &= \sum_j \sum_n r^{\lambda_j+n} a_{nj}(\theta, \lambda_j) \\ \psi_\theta &= \sum_j \sum_n r^{\lambda_j+n} b_{nj}(\theta, \lambda_j) \\ w &= \sum_j \sum_n r^{\lambda_j+n} c_{nj}(\theta, \lambda_j) \end{aligned} \right\} \quad (13-71)$$

Substitution of Eq. (13-71) into Eq. (13-68) yields

$$\begin{aligned} &\sum_j \sum_n \left\{ D \left[((\lambda_j+n)^2 - 1) a_{nj} + \frac{1-\mu}{2} a_{nj}'' + \left(\frac{1+\mu}{2} (\lambda_j+n) - \frac{3-\mu}{2} \right) b_{nj}' \right] r^{\lambda_j+n-2} \right. \\ &\quad \left. + C(\lambda_j+n) c_{nj} \lambda^{\lambda_j+n-1} - C a_{nj} r^{\lambda_j+n} \right\} = 0 \\ &\sum_j \sum_n \left\{ D \left[\left(\frac{1+\mu}{2} (\lambda_j+n) + \frac{3-\mu}{2} \right) a_{nj}' + \frac{1-\mu}{2} ((\lambda_j+n)^2 - 1) b_{nj} + b_{nj}'' \right] r^{\lambda_j+n-2} \right. \\ &\quad \left. + C c_{nj}' r^{\lambda_j+n-1} - C b_{nj} r^{\lambda_j+n} \right\} = 0 \\ &\sum_j \sum_n \{ [(\lambda_j+n)^2 c_{nj} + c_{nj}''] r^{\lambda_j+n-2} - [(\lambda_j+n+1) a_{nj} + b_{nj}'] r^{\lambda_j+n} \} = 0 \end{aligned}$$

in which $a'_{nj} = \frac{\partial a_{nj}}{\partial \theta}$, and others can be obtained by analogy. In the above equation

set, if we let the sum of the coefficients of r with the same power order be zero, equation sets with various orders can be obtained. For instance, the lowest order equation set (called zero-order equation set) is formed by letting the sum of the coefficients of r^{λ_j-2} terms be zero, i.e.,

$$\left. \begin{aligned} (\lambda_j^2 - 1)a_{0j} + \frac{1-\mu}{2}a_{0j}'' + \left(\frac{1+\mu}{2}\lambda_j - \frac{3-\mu}{2}\right)b_{0j}' &= 0 \\ \left(\frac{1+\mu}{2}\lambda_j + \frac{3-\mu}{2}\right)a_{0j}' + \frac{1-\mu}{2}(\lambda_j^2 - 1)b_{0j} + b_{0j}'' &= 0 \\ c_{0j}'' + \lambda_j^2 c_{0j} &= 0 \end{aligned} \right\} \quad (13-72)$$

This is a homogenous ordinary differential equation set about a_{0j} , b_{0j} and c_{0j} . And, if we let the sum of the coefficients of r^{λ_j-1} terms be zero, the first-order equation set, which is a homogenous ordinary differential equation set about (a_{1j}, b_{1j}, c_{1j}) and (a_{0j}, b_{0j}, c_{0j}) , can be established. Then from this set, a_{1j} , b_{1j} and c_{1j} can be solved. According to this step, equation set of any order can be obtained, and the corresponding coefficients a_{nj} , b_{nj} and c_{nj} can be solved.

The solution strategy for the zero-order equation set (13-72) is discussed in detail as follows. Its solutions can be expressed by

$$\left. \begin{aligned} a_{0j} &= A_{0j} \cos(\lambda_j + 1)\theta + B_{0j} \sin(\lambda_j + 1)\theta + C_{0j} \cos(\lambda_j - 1)\theta + D_{0j} \sin(\lambda_j - 1)\theta \\ b_{0j} &= B_{0j} \cos(\lambda_j + 1)\theta - A_{0j} \sin(\lambda_j + 1)\theta + K_{0j}D_{0j} \cos(\lambda_j - 1)\theta - K_{0j}C_{0j} \sin(\lambda_j - 1)\theta \\ c_{0j} &= E_{0j} \cos \lambda_j \theta + F_{0j} \sin \lambda_j \theta \end{aligned} \right\} \quad (13-73)$$

in which the parameter K_{0j} is

$$K_{0j} = \frac{(1 + \mu)\lambda_j + (3 - \mu)}{(1 + \mu)\lambda_j - (3 - \mu)}$$

$A_{0j}, B_{0j}, C_{0j}, D_{0j}, E_{0j}$ and F_{0j} are 6 undetermined coefficients; λ_j is the eigenvalue, and determined by the eigenequation.

The zero-order boundary conditions which a_{0j} , b_{0j} and c_{0j} should satisfy can be derived from the boundary condition Eq. (13-70). Therefore, substitution of Eq. (13-71) into Eq. (13-69) yields the series expressions of the internal forces. Substituting them into Eq. (13-70), the series expressions of the boundary conditions can also be obtained, in which the zero-order boundary conditions are

$$\left. \begin{aligned} b'_{0j} + (\lambda_j \mu + 1) a_{0j} &= 0 \\ a'_{0j} + (\lambda_j - 1) b_{0j} &= 0 \\ c'_{0j} &= 0 \end{aligned} \right\} \left(\theta = \pm \frac{\alpha}{2} \right) \quad (13-74)$$

Substituting Eq. (13-73) into the above equation, the following 6 conditions can be obtained:

$$2\lambda_j(\mu - 1)A_{0j} \cos(\lambda_j + 1) \frac{\alpha}{2} + 2[-K_{0j}(\lambda_j - 1) + (1 + \lambda_j \mu)]C_{0j} \cos(\lambda_j - 1) \frac{\alpha}{2} = 0 \quad (13-75a)$$

$$2\lambda_j A_{0j} \sin(\lambda_j + 1) \frac{\alpha}{2} + (\lambda_j - 1)(K_{0j} + 1)C_{0j} \sin(\lambda_j - 1) \frac{\alpha}{2} = 0 \quad (13-75b)$$

$$2\lambda_j(\mu - 1)B_{0j} \sin(\lambda_j + 1) \frac{\alpha}{2} + 2[-K_{0j}(\lambda_j - 1) + (1 + \lambda_j \mu)]D_{0j} \sin(\lambda_j - 1) \frac{\alpha}{2} = 0 \quad (13-75c)$$

$$2\lambda_j B_{0j} \cos(\lambda_j + 1) \frac{\alpha}{2} + (\lambda_j - 1)(K_{0j} + 1)D_{0j} \cos(\lambda_j - 1) \frac{\alpha}{2} = 0 \quad (13-75d)$$

$$F_{0j} \cos \lambda_j \frac{\alpha}{2} = 0 \quad (13-75e)$$

$$E_{0j} \sin \lambda_j \frac{\alpha}{2} = 0 \quad (13-75f)$$

This is a homogenous algebraic equation set about 6 undetermined coefficients A_{0j} , B_{0j} , C_{0j} , D_{0j} , E_{0j} and F_{0j} . If the homogenous equation set has nontrivial solutions, its coefficient determinant should be zero, i.e.,

$$(\sin \lambda_j \alpha + \lambda_j \sin \alpha)(\sin \lambda_j \alpha - \lambda_j \sin \alpha) \cos \lambda_j \frac{\alpha}{2} \sin \lambda_j \frac{\alpha}{2} = 0 \quad (13-76)$$

This is the eigenequation for the V-notch problem in the Reissner plate, from which a series of eigenvalues λ_j can be determined.

By the way, the eigenequation (13-76) can be decomposed into the following 4 equations:

$$\sin \lambda_j \alpha + \lambda_j \sin \alpha = 0 \quad (13-77a)$$

$$\sin \lambda_j \alpha - \lambda_j \sin \alpha = 0 \quad (13-77b)$$

$$\cos \lambda_j \frac{\alpha}{2} = 0 \quad (13-77c)$$

$$\sin \lambda_j \frac{\alpha}{2} = 0 \quad (13-77d)$$

They are corresponding to the following 4 conditions, respectively:

- A_{0j} and C_{0j} in Eqs. (13-75a,b) have nontrivial solutions;
- B_{0j} and D_{0j} in Eqs. (13-75c,d) have nontrivial solutions;
- F_{0j} in Eq. (13-75e) has nontrivial solution;
- E_{0j} in Eq. (13-75f) has nontrivial solution.

3. The solution of eigenequation

By comparing the eigenequation (13-76) for the V-notch problem in the Reissner plate with the eigenequations (13-7) and (13-8) for the plane V-notch problem, it can be seen that, besides the first two factors contained in the left side of Eq. (13-76) that are the same as those in Eqs. (13-7) and (13-8), there are still other two factors, $\cos \lambda_j \frac{\alpha}{2}$ and $\sin \lambda_j \frac{\alpha}{2}$, existing here. Hence, the singularities of the V-notches in the Reissner plate and plane problem have some relations, but are different.

By Muller iteration method, all the real and complex roots of Eq. (13-76) can be solved. A series of eigenvalues with various opening angles of notch are listed in Table 13.10.

Along with the decrease of the inner angle of the notch, the minimum eigenvalue λ_1 increases gradually, which means that the singularity at the tip of the notch decreases gradually. When the inner angle of the notch tends to be 180° , the singularity at the tip of the notch will disappear.

For convenience, let us divide the roots of the eigenequation (13-76) into two parts: one is composed of $\{\lambda_1, \lambda_4, \lambda_5, \lambda_8, \dots\}$, which represents the symmetric part; the other is composed of $\{\lambda_2, \lambda_3, \lambda_6, \lambda_7, \dots\}$, which represents the antisymmetric part. The coefficients of displacement corresponding to the symmetric part and antisymmetric part are derived in the following, respectively. Furthermore, the expressions of stresses at the tip of the notch can be obtained.

13.5.2 The Internal Force Fields at Notch-Tip in Reissner Plate —the Symmetric Part

The symmetric part is corresponding to the following eigenvalue series:

$$[\lambda_1, \lambda_4, \lambda_5, \lambda_8, \lambda_9, \lambda_{12}, \dots]$$

which can be divided into two groups, a and b:

group a: $[\lambda_1, \lambda_5, \lambda_9, \dots]$

group b: $[\lambda_4, \lambda_8, \lambda_{12}, \dots]$

Table 13.10 The eigenvalues of V-notch in Reissner plate

α	360°	350°	330°	300°	270°	240°
λ_1	0.500 000	0.500 053	0.0	0.501 453	0.0	0.615 731
λ_2	0.500 000	0.514 286	0.0	0.545 455	0.0	0.750 000
λ_3	0.500 000	0.529 355	0.0	0.598 192	0.0	1.148 913
λ_4	1.000 000	1.028 571	0.0	1.090 909	0.0	1.500 000
λ_5	1.000 000	1.058 843	0.0	1.202 157	0.0	1.833 550
λ_6	1.500 000	1.542 857	0.0	1.636 364	0.0	2.250 000
λ_7	1.500 000	1.588 609	0.0	1.838 934	0.0	2.589 479
λ_8	2.000 000	2.057 143	0.0	2.181 818	0.0	3.000 000
λ_9	1.500 000	1.499 728	0.0	1.490 378	0.0	3.343 717
λ_{10}	2.500 000	2.571 429	0.0	2.727 273	0.0	3.750 000
λ_{11}	2.000 000	1.999 107	0.0	1.948 556	0.0	4.096 928
λ_{12}	3.000 000	3.085 714	0.0	3.272 727	0.0	4.500 000
λ_{13}	2.000 000	2.118 822	0.0	2.440 492	0.114 207	
λ_{14}	3.500 000	3.600 000	0.0	3.818 132	0.0	
λ_{15}	2.500 000	2.649 696	0.0	2.987 005	0.166 741	
λ_{16}	4.000 000	4.114 286	0.0	4.363 636	0.0	
λ_{17}	2.500 000	2.497 980	0.0			
λ_{18}	4.500 000	4.628 571	0.0			
λ_{19}	3.000 000	2.996 141	0.0			
λ_{20}	5.000 000	5.142 857	0.0			

Advanced Finite Element Method in Structural Engineering

The results for the first two orders ($n = 0$ and $n = 1$) are given as follows.

(1a) $n = 0, j = 1, 5, 9, \dots$

In this case, λ_j satisfies Eq. (13-77a). From Eqs. (13-75a) and (13-75b), we have

$$C_{0j} = m_{0j}\beta_j$$

where

$$m_{0j} = -\frac{2\lambda_j \sin(\lambda_j + 1)\frac{\alpha}{2}}{(\lambda_j - 1)(1 + K_{0j})\sin(\lambda_j - 1)\frac{\alpha}{2}}$$

and β_j represents A_{0j} .

And, from Eqs. (13-75c), (13-75d), (13-75e) and (13-75f), we can obtain

$$B_{0j} = D_{0j} = E_{0j} = F_{0j} = 0$$

Therefore, Eq. (13-73) yields

$$\left. \begin{aligned} a_{0j} &= [\cos(\lambda_j + 1)\theta + m_{0j} \cos(\lambda_j - 1)\theta]\beta_j \\ b_{0j} &= -[\sin(\lambda_j + 1)\theta + K_{0j}m_{0j} \sin(\lambda_j - 1)\theta]\beta_j \\ c_{0j} &= 0 \end{aligned} \right\} \quad (13-78)$$

And, the corresponding internal force fields can be written as

$$\left. \begin{aligned} M_r &= -Dr^{\lambda_j-1} \{ (1-\mu)\lambda_j \cos(\lambda_j + 1)\theta + m_{0j} [(\lambda_j + \mu) - K_{0j}\mu(\lambda_j - 1)] \cos(\lambda_j - 1)\theta \} \beta_j \\ M_\theta &= -Dr^{\lambda_j-1} \{ (\mu-1)\lambda_j \cos(\lambda_j + 1)\theta + m_{0j} [1 + \lambda_j\mu - K_{0j}(\lambda_j - 1)] \cos(\lambda_j - 1)\theta \} \beta_j \\ M_{r\theta} &= \frac{D(1-\mu)}{2} r^{\lambda_j-1} [2\lambda_j \sin(\lambda_j + 1)\theta + (\lambda_j - 1)(1 + K_{0j})m_{0j} \sin(\lambda_j - 1)\theta] \beta_j \\ Q_r &= -Cr^{\lambda_j} [\cos(\lambda_j + 1)\theta + m_{0j} \cos(\lambda_j - 1)\theta] \beta_j \\ Q_\theta &= Cr^{\lambda_j} [\sin(\lambda_j + 1)\theta + K_{0j}m_{0j} \sin(\lambda_j - 1)\theta] \beta_j \end{aligned} \right\} \quad (13-79)$$

(1b) $n = 0, j = 4, 8, 12, \dots$

In this case, λ_j only satisfies Eq. (13-77d). Then, from Eq. (13-75), we have

$$E_{0j} \neq 0, \quad \text{and} \quad A_{0j} = B_{0j} = C_{0j} = D_{0j} = F_{0j} = 0$$

From Eq. (13-73), we obtain

$$a_{0j} = 0, \quad b_{0j} = 0, \quad c_{0j} = \beta_j \cos \lambda_j \theta \quad (13-80)$$

in which β_j represents E_{0j} . And, the corresponding internal force fields are

$$\left. \begin{aligned} M_r = 0, \quad M_\theta = 0, \quad M_{r\theta} = 0 \\ Q_r = Cr^{\lambda_j-1}(\lambda_j \cos \lambda_j \theta)\beta_j, \quad Q_\theta = Cr^{\lambda_j-1}(-\lambda_j \sin \lambda_j \theta)\beta_j \end{aligned} \right\} \quad (13-81)$$

(2a) $n = 1, j = 1, 5, 9, \dots$

When $n = 1$, from Eq. (13.71), we have

$$\psi_r = r^{\lambda_j+1} a_{1j}, \quad \psi_\theta = r^{\lambda_j+1} b_{1j}, \quad w = r^{\lambda_j+1} c_{1j} \quad (13-82)$$

Substituting Eq. (13-82) into Eq. (13-68), and making use of Eq. (13-78), the following solutions can be obtained:

$$\left. \begin{aligned} a_{1j} &= A_{1j} \cos(\lambda_j + 2)\theta + B_{1j} \sin(\lambda_j + 2)\theta + C_{1j} \cos \lambda_j \theta + D_{1j} \sin \lambda_j \theta \\ b_{1j} &= B_{1j} \cos(\lambda_j + 2)\theta - A_{1j} \sin(\lambda_j + 2)\theta + K_{1j} D_{1j} \cos \lambda_j \theta - K_{1j} C_{1j} \sin \lambda_j \theta \\ c_{1j} &= E_{1j} \cos(\lambda_j + 1)\theta + F_{1j} \sin(\lambda_j + 1)\theta + \frac{\lambda_j + 1 - K_{0j}(\lambda_j - 1)}{4\lambda_j} \beta_j \cos(\lambda_j - 1)\theta \end{aligned} \right\} \quad (13-83)$$

where

$$K_{1j} = \frac{(1 + \mu)(1 + \lambda_j) + (3 - \mu)}{(1 + \mu)(1 + \lambda_j) - (3 - \mu)}$$

Substituting Eq. (13-82) into Eq. (13-70) and making use of Eq. (13-78), the corresponding boundary conditions can be derived as follows:

$$\left. \begin{aligned} b'_{1j} + a_{1j} + \mu(\lambda_j + 1)a_{1j} &= 0 \\ a'_{1j} + \lambda_j b_{1j} &= 0 \\ c'_{1j} + [\sin(\lambda_j + 1)\theta + K_{0j} m_{0j} \sin(\lambda_j - 1)\theta] \beta_j &= 0 \end{aligned} \right\} \left(\theta = \pm \frac{\alpha}{2} \right) \quad (13-84)$$

Substitution of Eq. (13-83) into Eq. (13-84) yields:

$$A_{1j} = B_{1j} = C_{1j} = D_{1j} = F_{1j} = 0, \quad E_{1j} = f_{1j} \beta_j$$

where

$$\begin{aligned} f_{1j} &= -\frac{\lambda_j + 1 - K_{0j}(\lambda_j - 1)}{4\lambda_j(\lambda_j + 1)} (\lambda_j - 1) \frac{\sin(\lambda_j - 1)\frac{\alpha}{2}}{\sin(\lambda_j + 1)\frac{\alpha}{2}} \\ &+ \frac{1}{\lambda_j + 1} \frac{\sin(\lambda_j + 1)\frac{\alpha}{2} + K_{0j} m_{0j} \sin(\lambda_j - 1)\frac{\alpha}{2}}{\sin(\lambda_j + 1)\frac{\alpha}{2}} \end{aligned}$$

From Eq. (13-83), we can obtain

$$a_{1j} = 0, \quad b_{1j} = 0, \quad c_{1j} = [f_{1j} \cos(\lambda_j + 1)\theta + g_{1j} \cos(\lambda_j - 1)\theta] \beta_j \quad (13-85)$$

where

$$g_{1j} = [\lambda_j + 1 + K_{0j}(\lambda_j - 1)] / 4\lambda_j$$

And, the corresponding internal force fields are

$$\left. \begin{aligned} M_r = 0, \quad M_\theta = 0, \quad M_{r\theta} = 0 \\ Q_r = Cr^{\lambda_j} (\lambda_j + 1) [f_{1j} \cos(\lambda_j + 1)\theta + g_{1j} \cos(\lambda_j - 1)\theta] \beta_j \\ Q_\theta = Cr^{\lambda_j} [-(\lambda_j + 1)f_{1j} \sin(\lambda_j + 1)\theta - (\lambda_j - 1)g_{1j} \sin(\lambda_j - 1)\theta] \beta_j \end{aligned} \right\} \quad (13-86)$$

(2b) $n = 1, j = 4, 8, 12, \dots$

Substituting Eq. (13-82) into Eq. (13-68) and making use of Eq. (13-80), we can obtain:

$$\left. \begin{aligned} a_{1j} &= A_{1j} \cos(\lambda_j + 2)\theta + B_{1j} \sin(\lambda_j + 2)\theta + C_{1j} \cos \lambda_j \theta + D_{1j} \sin \lambda_j \theta \\ &\quad - \frac{C}{D[\lambda_j(1 + \mu)/2 + 2]} \beta_j \cos \lambda_j \theta \\ b_{1j} &= B_{1j} \cos(\lambda_j + 2)\theta - A_{1j} \sin(\lambda_j + 2)\theta + K_{1j} D_{1j} \cos \lambda_j \theta - K_{1j} C_{1j} \sin \lambda_j \theta \\ c_{1j} &= E_{1j} \cos(\lambda_j + 1)\theta + F_{1j} \sin(\lambda_j + 1)\theta \end{aligned} \right\} \quad (13-87)$$

Substituting Eq. (13-82) into Eq. (13-70) and making use of Eq. (13-80), the corresponding boundary conditions can be obtained:

$$\left. \begin{aligned} b'_{1j} + a_{1j} + \mu(\lambda_j + 1)a_{1j} = 0 \\ a'_{1j} + \lambda_j b_{1j} = 0, \quad c'_{1j} = 0 \end{aligned} \right\} \left(\theta = \pm \frac{\alpha}{2} \right) \quad (13-88)$$

Substitution of Eq. (13-87) into Eq. (13-88) yields:

$$\begin{aligned} B_{1j} = D_{1j} = F_{1j} = E_{1j} = 0 \\ A_{1j} = \frac{c_1 a_{22} - c_2 a_{12}}{a_{11} a_{22} - a_{12} a_{21}} \beta_j = l_{1j} \beta_j, \quad C_{1j} = \frac{c_2 a_{11} - c_1 a_{21}}{a_{11} a_{22} - a_{12} a_{21}} \beta_j = v_{1j} \beta_j \end{aligned}$$

where

$$\begin{aligned}
 a_{11} &= 2(\lambda_j + 1)(\mu - 1)\cos(\lambda_j + 1)\frac{\alpha}{2}, & a_{12} &= 2[-K_{1j}\lambda_j + 1 + \mu(\lambda_j + 1)]\cos\lambda_j\frac{\alpha}{2} \\
 a_{21} &= 2(\lambda_j + 1)\sin(\lambda_j + 2)\frac{\alpha}{2}, & a_{22} &= \lambda_j(1 + K_{1j})\sin\lambda_j\frac{\alpha}{2} \\
 c_1 &= \frac{2C[1 + \mu(\lambda_j + 1)]}{D[(1 + \mu)\lambda_j/2 + 2]}\cos\lambda_j\frac{\alpha}{2}, & c_2 &= \frac{C}{D[(1 + \mu)\lambda_j/2 + 2]}\lambda_j\sin\lambda_j\frac{\alpha}{2}
 \end{aligned}$$

Finally, from Eq. (13-87), we obtain

$$\left. \begin{aligned}
 a_{1j} &= [\alpha_{1j}\cos\lambda_j\theta + l_{1j}\cos(\lambda_j + 2)\theta]\beta_j \\
 b_{1j} &= -[K_{1j}v_{1j}\sin\lambda_j\theta + l_{1j}\sin(\lambda_j + 2)\theta]\beta_j \\
 c_{1j} &= 0
 \end{aligned} \right\} \quad (13-89)$$

where

$$\alpha_{1j} = v_{1j} - \frac{C}{D[\lambda_j(1 + \mu)/2 + 2]}$$

And, the corresponding internal force fields are

$$\left. \begin{aligned}
 M_r &= -Dr^{\lambda_j} \{ [\alpha_{1j}(\lambda_j + 1 + \mu) - K_{1j}v_{1j}\mu\lambda_j]\cos\lambda_j\theta \\
 &\quad + [l_{1j}(\lambda_j + 1 + \mu) - \mu l_{1j}(\lambda_j + 2)]\cos(\lambda_j + 2)\theta \} \beta_j \\
 M_\theta &= -Dr^{\lambda_j} \{ [\alpha_{1j}(\lambda_j\mu + \mu + 1) - K_{1j}v_{1j}\lambda_j]\cos\lambda_j\theta \\
 &\quad + [l_{1j}(\lambda_j\mu + \mu + 1) - l_{1j}(\lambda_j + 2)]\cos(\lambda_j + 2)\theta \} \beta_j \\
 M_{r\theta} &= \frac{D(1 - \mu)}{2} r^{\lambda_j} [\lambda_j(\alpha_{1j} + K_{1j}v_{1j})\sin\lambda_j\theta + 2(\lambda_j + 1)l_{1j}\sin(\lambda_j + 2)\theta] \beta_j \\
 Q_r &= -Cr^{\lambda_j+1} [\alpha_{1j}\cos\lambda_j\theta + l_{1j}\cos(\lambda_j + 2)\theta] \beta_j \\
 Q_\theta &= Cr^{\lambda_j+1} [K_{1j}v_{1j}\sin\lambda_j\theta + l_{1j}\sin(\lambda_j + 2)\theta] \beta_j
 \end{aligned} \right\} \quad (13-90)$$

13.5.3 The Internal Force Fields at Notch-Tip in Reissner Plate —the Antisymmetric Part

The antisymmetric part is corresponding to the following eigenvalue series:

$$[\lambda_2, \lambda_3, \lambda_6, \lambda_7, \lambda_{10}, \lambda_{11}, \dots]$$

Advanced Finite Element Method in Structural Engineering

which can also be divided into two groups, a and b:

$$\text{group a: } [\lambda_2, \lambda_6, \lambda_{10}, \dots]$$

$$\text{group b: } [\lambda_3, \lambda_7, \lambda_{11}, \dots]$$

The results for the first two orders ($n = 0$ and $n = 1$) are given as follows.

(1a) $n = 0, j = 2, 6, 10, \dots$

$$a_{0j} = 0, \quad b_{0j} = 0, \quad c_{0j} = \beta_j \sin \lambda_j \theta \quad (13-91)$$

The corresponding internal force fields are

$$\left. \begin{aligned} M_r = 0, \quad M_\theta = 0, \quad M_{r\theta} = 0 \\ Q_r = C\lambda_j r^{\lambda_j-1} \beta_j \sin \lambda_j \theta, \quad Q_\theta = C\lambda_j r^{\lambda_j-1} \beta_j \cos \lambda_j \theta \end{aligned} \right\} \quad (13-92)$$

(1b) $n = 0, j = 3, 7, 11, \dots$

$$\left. \begin{aligned} a_{0j} &= [\sin(\lambda_j + 1)\theta + m'_{0j} \sin(\lambda_j - 1)\theta] \beta_j \\ b_{0j} &= [\cos(\lambda_j + 1)\theta + K_{0j} m'_{0j} \cos(\lambda_j - 1)\theta] \beta_j \\ c_{0j} &= 0 \end{aligned} \right\} \quad (13-93)$$

where

$$m'_{0j} = - \frac{2\lambda_j \cos(\lambda_j + 1) \frac{\alpha}{2}}{(\lambda_j - 1)(1 + K_{0j}) \cos(\lambda_j - 1) \frac{\alpha}{2}}$$

The corresponding internal force fields are

$$\left. \begin{aligned} M_r &= -Dr^{\lambda_j-1} \{ (1 - \mu)\lambda_j \sin(\lambda_j + 1)\theta + m'_{0j} [(\lambda_j + \mu) - K_{0j}\mu(\lambda_j - 1)] \sin(\lambda_j - 1)\theta \} \beta_j \\ M_\theta &= -Dr^{\lambda_j-1} \{ (\mu - 1)\lambda_j \sin(\lambda_j + 1)\theta + m'_{0j} [1 + \lambda_j\mu - K_{0j}(\lambda_j - 1)] \sin(\lambda_j - 1)\theta \} \beta_j \\ M_{r\theta} &= -\frac{D(1 - \mu)}{2} r^{\lambda_j-1} \{ 2\lambda_j \cos(\lambda_j + 1)\theta + m'_{0j} (\lambda_j - 1)(1 + K_{0j}) \cos(\lambda_j - 1)\theta \} \beta_j \\ Q_r &= -Cr^{\lambda_j} [\sin(\lambda_j + 1)\theta + m'_{0j} \sin(\lambda_j - 1)\theta] \beta_j \\ Q_\theta &= -Cr^{\lambda_j} [\cos(\lambda_j + 1)\theta + m'_{0j} K_{0j} \cos(\lambda_j - 1)\theta] \beta_j \end{aligned} \right\} \quad (13-94)$$

(2a) $n = 1, j = 2, 6, 10, \dots$

$$\left. \begin{aligned} a_{1j} &= [a'_{1j} \sin \lambda_j \theta + l'_{1j} \sin(\lambda_j + 2)\theta] \beta_j \\ b_{1j} &= [l'_{1j} \cos(\lambda_j + 2)\theta + K_{1j} v'_{1j} \cos \lambda_j \theta] \beta_j \\ c_{1j} &= 0 \end{aligned} \right\} \quad (13-95)$$

where

$$\begin{aligned} l'_{1j} &= \frac{c'_1 a'_{22} - c'_2 a'_{12}}{a'_{11} a'_{22} - a'_{12} a'_{21}}, \quad v'_{1j} = \frac{c'_2 a'_{11} - c'_1 a'_{21}}{a'_{11} a'_{22} - a'_{12} a'_{21}} \\ a'_{11} &= 2(\lambda_j + 1)(\mu - 1) \sin(\lambda_j + 2) \frac{\alpha}{2} \\ a'_{12} &= 2[-K_{1j} \lambda_j + 1 + \mu(\lambda_j + 1)] \sin \lambda_j \frac{\alpha}{2} \\ a'_{21} &= 2(\lambda_j + 1) \cos(\lambda_j + 2) \frac{\alpha}{2}, \quad a'_{22} = \lambda_j (1 + K_{1j}) \cos \lambda_j \frac{\alpha}{2} \\ c'_1 &= \frac{2[1 + \mu(\lambda_j + 1)]C}{D \left(\frac{1 + \mu}{2} \lambda_j + 2 \right)} \sin \lambda_j \frac{\alpha}{2}, \quad c'_2 = \frac{C}{D \left(\frac{1 + \mu}{2} \lambda_j + 2 \right)} \lambda_j \cos \lambda_j \frac{\alpha}{2} \\ \alpha'_{1j} &= v'_{1j} - \frac{C}{D[\lambda_j(1 + \mu) / 2 + 2]} \end{aligned}$$

The corresponding internal force fields are

$$\left. \begin{aligned} M_r &= -Dr^{\lambda_j} \{ [\alpha'_{1j} (\lambda_j + 1 + \mu) - K_{1j} v'_{1j} \mu \lambda_j] \sin \lambda_j \theta \\ &\quad + [l'_{1j} (\lambda_j + 1 + \mu) - \mu l'_{1j} (\lambda_j + 2)] \sin(\lambda_j + 2)\theta \} \beta_j \\ M_\theta &= -Dr^{\lambda_j} \{ [\alpha'_{1j} (\lambda_j \mu + \mu + 1) - K_{1j} v'_{1j} \lambda_j] \sin \lambda_j \theta \\ &\quad + [l'_{1j} (\lambda_j \mu + \mu + 1) - l'_{1j} (\lambda_j + 2)] \sin(\lambda_j + 2)\theta \} \beta_j \\ M_{r\theta} &= -\frac{D(1 - \mu)}{2} r^{\lambda_j} \{ [\alpha'_{1j} \lambda_j + \lambda_j K_{1j} v'_{1j}] \cos \lambda_j \theta + 2l'_{1j} (\lambda_j + 1) \cos(\lambda_j + 2)\theta \} \beta_j \\ Q_r &= -Cr^{\lambda_j + 1} [\alpha'_{1j} \sin \lambda_j \theta + l'_{1j} \sin(\lambda_j + 2)\theta] \beta_j \\ Q_\theta &= -Cr^{\lambda_j + 1} [l'_{1j} \cos(\lambda_j + 2)\theta + K_{1j} v'_{1j} \cos \lambda_j \theta] \beta_j \end{aligned} \right\} \quad (13-96)$$

$$(2b) \quad n = 1, j = 3, 7, 11, \dots$$

$$a_{1j} = 0, \quad b_{1j} = 0, \quad c_{1j} = [f'_{1j} \sin(\lambda_j + 1)\theta + g'_{1j} \sin(\lambda_j - 1)\theta] \beta_j \quad (13-97)$$

where

$$\begin{aligned}
 f'_{1j} &= -\frac{\lambda_j + 1 - K_{0j}(\lambda_j - 1)}{4\lambda_j(\lambda_j + 1)}(\lambda_j - 1)m'_{0j} \frac{\cos(\lambda_j - 1)\frac{\alpha}{2}}{\cos(\lambda_j + 1)\frac{\alpha}{2}} \\
 &\quad + \frac{\cos(\lambda_j + 1)\alpha + K_{0j}m'_{0j} \cos(\lambda_j - 1)\frac{\alpha}{2}}{(\lambda_j + 1)\cos(\lambda_j + 1)\frac{\alpha}{2}} \\
 g'_{1j} &= m'_{1j}[\lambda_j + 1 - K_{0j}(\lambda_j - 1)]/4\lambda_j
 \end{aligned}$$

The corresponding internal force fields are

$$\left. \begin{aligned}
 M_r &= 0, \quad M_\theta = 0, \quad M_{r\theta} = 0 \\
 Q_r &= C(\lambda_j + 1)r^{\lambda_j} [f'_{1j} \sin(\lambda_j + 1)\theta + g'_{1j} \sin(\lambda_j - 1)\theta] \beta_j \\
 Q_\theta &= Cr^{\lambda_j} [(\lambda_j + 1)f'_{1j} \cos(\lambda_j + 1)\theta + (\lambda_j - 1)g'_{1j} \cos(\lambda_j - 1)\theta] \beta_j
 \end{aligned} \right\} \quad (13-98)$$

The expressions for the zero and first order internal force fields have been given above. According to the above process, some higher order solutions can be derived.

When $\alpha = 2\pi$, the V-notch problem will degenerate into the crack problem. The solution of the internal force fields around the crack-tip in the Reissner plate given in reference [21] can be treated as a special case of the solution in this section.

From the above derived expressions of the internal force fields around the notch-tip, it is found that, around the notch-tip, the order of singularity of the transverse shear stresses τ_{rz} and $\tau_{\theta z}$ is different from that of stresses σ_r , σ_θ and $\tau_{r\theta}$, the former is $r^{\lambda_2 - 1}$ while the latter is $r^{\lambda_1 - 1}$. Only when the opening angle $\alpha = 2\pi$ (crack problem), since $\lambda_1 = \lambda_2 = 0.5$, the order of singularity of τ_{rz} and $\tau_{\theta z}$ will be the same as that of σ_r , σ_θ and $\tau_{r\theta}$, which is identical to that in reference [22].

13.5.4 The Sub-Region Mixed Element Method

Now, the sub-region mixed element method is used to analyze the plane V-notch problem in thick plate. The sectorial region centered at the notch-tip is taken as the complementary energy region (C-region), and the outside of the C-region is the potential energy region (P-region). The P-region is divided by the 8-node isoparametric thick plate elements, and its nodal displacements δ are the undetermined displacement parameters. The above solutions of the internal force fields around the notch-tip can be taken as the internal force fields of the C-region, which can be written as

$$\left. \begin{aligned}
 M &= S_b \beta \\
 Q &= S_s \beta
 \end{aligned} \right\} \quad (13-99)$$

where $\mathbf{M} = [M_x \ M_y \ M_{xy}]^T$ are the bending and twisting moments; $\mathbf{Q} = [Q_x \ Q_y]^T$ are the transverse shear forces; $\boldsymbol{\beta}$ are the undetermined internal force parameters; \mathbf{S}_b and \mathbf{S}_s are formed by the combination of the internal forces around the notch-tip.

The undetermined parameters $\boldsymbol{\delta}$ and $\boldsymbol{\beta}$ can be determined by the stationary condition of the sub-region mixed variational principle.

The energy functional of the sub-region mixed variational principle is still given by Eq. (12-5), i.e.,

$$\Pi = \Pi_p - \Pi_c + H_{pc} \quad (13-100)$$

(1) The total potential energy Π_p of the P-region (see Eq. (12-6))

$$\Pi_p = \frac{1}{2} \boldsymbol{\delta}^T \mathbf{K} \boldsymbol{\delta} - \boldsymbol{\delta}^T \mathbf{P} \quad (13-101)$$

in which \mathbf{K} and \mathbf{P} are the stiffness matrix and the equivalent nodal load vector, respectively.

(2) The total complementary energy Π_c of the C-region

The total complementary energy Π_c of the C-region in the thick plate is composed of two parts, bending strain complementary energy and shearing strain complementary energy (see Eq. (12-55)):

$$\Pi_c = \frac{1}{2} \iint_{A_c} (\mathbf{M}^T \mathbf{D}_b^{-1} \mathbf{M} + \mathbf{Q}^T \mathbf{D}_s^{-1} \mathbf{Q}) dA \quad (13-102)$$

Substitution of Eq. (13-99) into the above equation yields

$$\Pi_c = \frac{1}{2} \boldsymbol{\beta}^T \mathbf{F} \boldsymbol{\beta} \quad (13-103)$$

where \mathbf{F} is the flexibility matrix (see Eq. (12-57)):

$$\mathbf{F} = \iint_{A_c} (\mathbf{S}_b^T \mathbf{D}_b^{-1} \mathbf{S}_b + \mathbf{S}_s^T \mathbf{D}_s^{-1} \mathbf{S}_s) dA \quad (13-104)$$

in which \mathbf{D}_b and \mathbf{D}_s are given by Eq. (12-49).

(3) The additional energy H_{pc} on the interface

The additional energy H_{pc} on the interface line S_{pc} of the two regions is (see Eq. (12-58)):

$$H_{pc} = \int_{S_{pc}} (Q_n \bar{w} + M_n \bar{\psi}_n + M_{ns} \bar{\psi}_s) ds = \int_{S_{pc}} \mathbf{T}^T \bar{\mathbf{u}} ds \quad (13-105)$$

where Q_n , M_n and M_{ns} are the three components of the boundary forces \mathbf{T} of the C-region on the interface; \bar{w} , $\bar{\psi}_n$ and $\bar{\psi}_s$ are the three components of the boundary displacements $\bar{\mathbf{u}}$ of the P-region on the interface.

The boundary forces \mathbf{T} can be expressed in terms of the stress parameters $\boldsymbol{\beta}$, and the boundary displacements $\bar{\mathbf{u}}$ can be expressed in terms of the nodal displacements $\bar{\boldsymbol{\delta}}$ on the interface. Since the C-region is a sectorial region, and the interface S_{pc} is a circular arc, the polar coordinates are used. Let

$$\left. \begin{aligned} \mathbf{T} &= [Q_r \quad M_r \quad M_{r\theta}]^T = \mathbf{R}\boldsymbol{\beta} \\ \bar{\mathbf{u}} &= [\bar{w} \quad \bar{\psi}_r \quad \bar{\psi}_\theta]^T = \mathbf{L}[\bar{w} \quad \bar{\psi}_x \quad \bar{\psi}_y]^T = \mathbf{L}\bar{\mathbf{N}}\bar{\boldsymbol{\delta}} \end{aligned} \right\} \quad (13-106)$$

where \mathbf{R} can be derived from the internal force fields around the notch-tip; \mathbf{L} is a transformation matrix:

$$\mathbf{L} = \begin{bmatrix} 1 & 0 & 0 \\ 0 & \cos\theta & \sin\theta \\ 0 & -\sin\theta & \cos\theta \end{bmatrix} \quad (13-107)$$

$\bar{\mathbf{N}}$ is given by the shape functions of the 8-node isoparametric thick plate element

$$\bar{\mathbf{N}} = \begin{bmatrix} \bar{N}_1 & 0 & 0 & \bar{N}_2 & 0 & 0 & \cdots & \bar{N}_m & 0 & 0 \\ 0 & \bar{N}_1 & 0 & 0 & \bar{N}_2 & 0 & \cdots & 0 & \bar{N}_m & 0 \\ 0 & 0 & \bar{N}_1 & 0 & 0 & \bar{N}_2 & \cdots & 0 & 0 & \bar{N}_m \end{bmatrix} \quad (13-108)$$

m is the number of the nodes on the interface. $\bar{\boldsymbol{\delta}}$ is the nodal displacement vector on the interface.

Substituting Eq. (13-106) into Eq. (13-105), the additional energy on the interface can be written in the form of Eq. (12-11):

$$H_{pc} = \boldsymbol{\beta}^T \mathbf{H} \bar{\boldsymbol{\delta}} \quad (13-109)$$

where

$$\mathbf{H} = \int_{S_{pc}} \mathbf{R}^T \mathbf{L} \bar{\mathbf{N}} ds \quad (13-110)$$

(4) Solutions of the stress intensity factors

The energy functional Π above has already been expressed in terms of $\boldsymbol{\delta}$ and $\boldsymbol{\beta}$. From the stationary conditions, the fundamental Eqs. (12-19) and (12-16) can be derived. Then, $\boldsymbol{\delta}$ and $\boldsymbol{\beta}$ can be solved in turn, and the internal forces can also be obtained. Finally, we obtain

$$\left. \begin{aligned} K_I &= \sqrt{2} \lim_{r \rightarrow 0} r^{1-\lambda_1} M_{\theta} |_{\theta=0} = -\sqrt{2} D \{ (\mu - 1) \lambda_1 + m_{01} [1 + \lambda_1 \mu - K_{01} (\lambda_1 - 1)] \} \beta_1 \\ K_{II} &= \sqrt{2} \lim_{r \rightarrow 0} r^{1-\lambda_3} M_{r\theta} |_{\theta=0} = -\frac{\sqrt{2}}{2} D (1 - \mu) [2\lambda_3 + m'_{03} (\lambda_3 - 1) (1 + K_{03})] \beta_3 \\ K_{III} &= \sqrt{2} \lim_{r \rightarrow 0} r^{1-\lambda_2} Q_{\theta} |_{\theta=0} = \sqrt{2} C \lambda_2 \beta_2 \end{aligned} \right\} \quad (13-111)$$

The sub-region mixed element method for the V-notch problem in thick plate is denoted as SRM-V4.

Several numerical examples are given as follows.

Example 13.6 Stress intensity factor of mode I for the V-notch problem in an infinite plate subjected to uniform bending moment.

An infinite rectangular plate with a rhombic hole is shown in Fig. 13.14. Its periphery is subjected to uniform bending moment M . The inner angle of the rhombic hole is α , and the length of diagonal line is $2a$.

In order to simulate the infinite plate, the side lengths of the rectangular plate are assumed as $2L = 2W = 20a$ during computation. And, $E = 2 \times 10^6$, $\mu = 0.3$. Owing to symmetry, only 1/4 of the plate is used for computation. The division of the C-region and P-region is shown in Fig. 13.15. The C-region is a sector centered at the notch-tip, and its radius is r_c .

The 8-node isoparametric thick plate element is used for the P-region, and the mesh divisions are shown in Fig. 13.16(a),(b).

The results for the stress intensity factor K_I^{∞} (mode I) with various opening angles are listed in Table 13.11. Along with the decrease of the opening angle α ,

Table 13.11 $K_I^{\infty} / M\sqrt{a}$ of an infinite plate with various opening angles of the notch

h/a \ $\alpha/2$	0°	15°	30°	45°	60°
1.0	0.7343	0.7899	0.8010	0.8515	0.9405
1.5	0.7874	0.8423	0.8540	0.8969	0.9890
2.0	0.8236	0.8917	0.8977	0.9305	1.0090

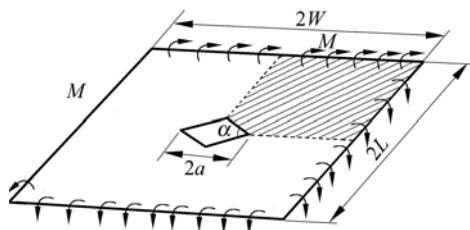


Figure 13.14 An infinite plate with V-notch subjected to uniform bending moment

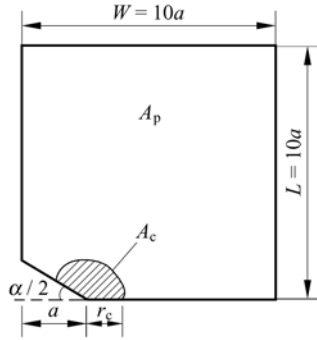


Figure 13.15 The division of the C-region and P-region (V-notch in thick plate)

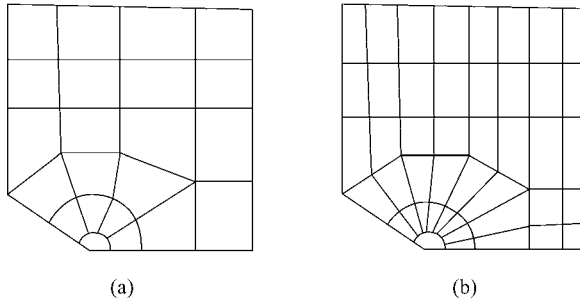


Figure 13.16 The mesh divisions of the P-region

the results will tend to be the analytical solutions of the crack problem^[23], and errors are within 1%.

Example 13.7 The stress intensity factor K_I of the V-notch in a finite plate.

The dimensions of the plate are $2L = 2W = 4a$, and the other data are the same as those in Example 13.6. The results for the stress intensity factor K_I with various opening angles are listed in Table 13.12.

Table 13.12 K_I of a finite plate with various opening angles of the notch

$h/a \backslash \alpha/2$	0°	15°	30°	45°	60°
1.0	0.8962	0.9418	0.9565	1.008	1.146
1.5	0.9901	1.045	1.058	1.115	1.250
2.0	1.055	1.112	1.118	1.162	1.288

In the above two examples, the radius of the C-region $r_c = 0.08a$. And, the highest order terms used here in the asymptotic solutions of the stresses at the notch-tip are r^{λ_2} (for M) and r^{λ_2+1} (for Q), respectively. It can be concluded that the computational results are basically stable.

13.6 3D V-Notch Problem

This section will discuss the 3D V-notch problem^[4]. Firstly, by the expansion of the double power series, the eigenvalue of the 3D V-notch problem is derived. Then, the eigenvalue series for notches with various inner opening angles are solved by the Muller iteration method, in which the minimum positive eigenvalue can be used to reflect the singularity of the notch-tip and the relation between this singularity and the inner angle of the notch. If the inner angle of the notch is equal to π , the problem will degenerate to be a semi-infinite space problem, in which no singularity exists; if the inner angle of the notch increases to be 2π , the problem will transfer to the 3D crack problem, in which the crack-tip possesses singularity with $1/2$ order. For the general notch, the eigenvalue series can be decomposed into two parts, symmetric part and antisymmetric part. The corresponding displacement fields of the notch-tip are first derived; then the stress fields of the notch-tip are solved by the stress-displacement or strain-displacement relations.

13.6.1 The Differential Equations and Boundary Conditions for the 3D V-Notch Problem

As shown in Fig. 13.17, a 3D V-notch is considered. Its inner angle is α , and $\pi < \alpha < 2\pi$. The line of the notch-tip coincides with the z -axis, and can be infinitely extended forward and backward. The equations of the two surfaces of the notch are $\theta = \frac{\alpha}{2}$ and $\theta = -\frac{\alpha}{2}$, respectively.

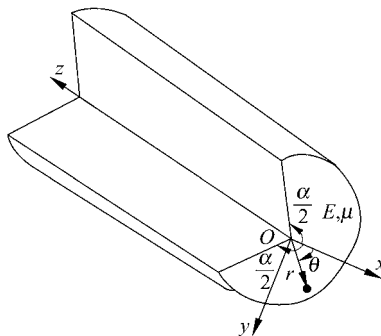


Figure 13.17 3D V-notch problem

By ignoring the influence of body forces and using the cylinder coordinate system, the equilibrium differential equations of this problem can be expressed in

terms of the stress components as follows:

$$\left. \begin{aligned} \frac{\partial \sigma_{rr}}{\partial r} + \frac{1}{r} \frac{\partial \sigma_{r\theta}}{\partial \theta} + \frac{\partial \sigma_{rz}}{\partial z} + \frac{1}{r} (\sigma_{rr} - \sigma_{\theta\theta}) &= 0 \\ \frac{\partial \sigma_{r\theta}}{\partial r} + \frac{1}{r} \frac{\partial \sigma_{\theta\theta}}{\partial \theta} + \frac{\partial \sigma_{\theta z}}{\partial z} + \frac{2}{r} \sigma_{r\theta} &= 0 \\ \frac{\partial \sigma_{rz}}{\partial r} + \frac{1}{r} \frac{\partial \sigma_{\theta z}}{\partial \theta} + \frac{\partial \sigma_{zz}}{\partial z} + \frac{1}{r} \sigma_{rz} &= 0 \end{aligned} \right\} \quad (13-112)$$

The stress-displacement relations are

$$\left. \begin{aligned} \sigma_{rr} &= \frac{E}{1+\mu} \left(\frac{\mu}{1-2\mu} e + \frac{\partial u_r}{\partial r} \right), & \sigma_{\theta\theta} &= \frac{E}{1+\mu} \left(\frac{\mu}{1-2\mu} e + \frac{1}{r} \frac{\partial u_\theta}{\partial \theta} + \frac{u_r}{r} \right) \\ \sigma_{zz} &= \frac{E}{1+\mu} \left(\frac{\mu}{1-2\mu} e + \frac{\partial u_z}{\partial z} \right), & \sigma_{r\theta} &= \frac{E}{2(1+\mu)} \left(\frac{\partial u_\theta}{\partial r} + \frac{1}{r} \frac{\partial u_r}{\partial \theta} - \frac{u_\theta}{r} \right) \\ \sigma_{\theta z} &= \frac{E}{2(1+\mu)} \left(\frac{1}{r} \frac{\partial u_z}{\partial \theta} + \frac{\partial u_\theta}{\partial z} \right), & \sigma_{rz} &= \frac{E}{2(1+\mu)} \left(\frac{\partial u_r}{\partial z} + \frac{\partial u_z}{\partial r} \right) \end{aligned} \right\} \quad (13-113)$$

where E and μ are the Young's modulus and the Poisson's ratio of the material, respectively; and $e = \frac{\partial u_r}{\partial r} + \frac{1}{r} \frac{\partial u_\theta}{\partial \theta} + \frac{u_r}{r} + \frac{\partial u_z}{\partial z}$.

Substitution of Eq. (13-113) into Eq. (13-112) yields the equilibrium differential equations expressed by displacements:

$$\left. \begin{aligned} (X+G) \frac{\partial e}{\partial r} + G \nabla^2 u_r - G \frac{u_r}{r^2} - 2G \frac{1}{r^2} \frac{\partial u_\theta}{\partial \theta} &= 0 \\ (X+G) \frac{1}{r} \frac{\partial e}{\partial \theta} + G \nabla^2 u_\theta + \frac{2G}{r^2} \frac{\partial u_r}{\partial \theta} - \frac{G}{r^2} u_\theta &= 0 \\ (X+G) \frac{\partial e}{\partial z} + G \nabla^2 u_z &= 0 \end{aligned} \right\} \quad (13-114)$$

where

$$X = \frac{E\mu}{(1+\mu)(1-2\mu)}, \quad G = \frac{E}{2(1+\mu)}, \quad \nabla^2 = \frac{\partial^2}{\partial r^2} + \frac{1}{r} \frac{\partial}{\partial r} + \frac{1}{r^2} \frac{\partial^2}{\partial \theta^2} + \frac{\partial^2}{\partial z^2}$$

The boundary conditions of the notch (see Fig. 13.17) can be expressed by

$$\sigma_{\theta\theta} = \sigma_{\theta r} = \sigma_{\theta z} = 0 \quad \left(\theta = \pm \frac{\alpha}{2} \right) \quad (13-115)$$

13.6.2 The Eigenequation and Eigenvalue of the 3D V-Notch Problem

The displacements u_r , u_θ and u_z can be expanded as the following double power series:

$$\left. \begin{aligned} u_r &= \sum_j \sum_n r^{\lambda_j+n} a_{nj}(\lambda_j, \theta, z) \\ u_\theta &= \sum_j \sum_n r^{\lambda_j+n} b_{nj}(\lambda_j, \theta, z) \\ u_z &= \sum_j \sum_n r^{\lambda_j+n} c_{nj}(\lambda_j, \theta, z) \end{aligned} \right\} \quad (13-116)$$

where $n = 0, 1, 2, \dots$; $j = 1, 2, \dots$; and $\lambda_1, \lambda_2, \dots$ are the eigenvalue series.

Substitution of Eq. (13-116) into Eq. (13-114) yields

$$\sum_j \sum_n \{ \{ (X + G)[(\lambda_j + n)^2 - 1] a_{nj} + (\lambda_j + n - 1) b'_{nj} \} + G[(\lambda_j + n)^2 - 1] a_{nj} + a''_{nj} - 2b'_{nj} \} r^{\lambda_j+n-2} + (X + G)(\lambda_j + n) c'_{nj} r^{\lambda_j+n-1} + G a''_{nj} r^{\lambda_j+n} = 0 \quad (13-117a)$$

$$\sum_j \sum_n \{ \{ (X + G)[(\lambda_j + n + 1) a'_{nj} + b''_{nj} \} + G[2a'_{nj} + ((\lambda_j + n)^2 - 1) b_{nj} + b''_{nj} \} \} r^{\lambda_j+n-2} + (X + G) c''_{nj} r^{\lambda_j+n-1} + G b''_{nj} r^{\lambda_j+n} = 0 \quad (13-117b)$$

$$\sum_j \sum_n \{ G[(\lambda_j + n)^2 c_{nj} + c''_{nj}] r^{\lambda_j+n-2} + (X + G)[(\lambda_j + n + 1) a'_{nj} + b'_{nj}] r^{\lambda_j+n-1} + (X + 2G) c''_{nj} r^{\lambda_j+n} \} = 0 \quad (13-117c)$$

where $\frac{\partial a}{\partial \theta}$ and $\frac{\partial a}{\partial z}$ are denoted by a' and a'' , respectively. In the above equation set, by letting the sum of the coefficients of r terms with the same power order to be zero, equation set for each order will be obtained. The lowest order equation set (called the zero-order equation set) can be established by letting the sum of the coefficients of r^{λ_j-2} terms to be zero, i.e.,

$$\left. \begin{aligned} (X + G)[(\lambda_j^2 - 1) a_{0j} + (\lambda_j - 1) b'_{0j}] + G[(\lambda_j^2 - 1) a_{0j} + a''_{0j} - 2b'_{0j}] &= 0 \\ (X + G)[(\lambda_j + 1) a'_{0j} + b''_{0j}] + G[2a'_{0j} + (\lambda_j^2 - 1) b_{0j} + b''_{0j}] &= 0 \\ \lambda_j^2 c_{0j} + c''_{0j} &= 0 \end{aligned} \right\} \quad (13-118)$$

This is a homogenous ordinary differential equation set about a_{0j} , b_{0j} and c_{0j} .

Similarly, the first order equation set is obtained by letting the sum of the coefficients of r^{λ_j-1} terms in Eq. (13-117) be zero. This is a homogenous ordinary differential equation set about (a_{1j}, b_{1j}, c_{1j}) and (a_{0j}, b_{0j}, c_{0j}) , from which a_{1j} , b_{1j} and c_{1j} can be solved.

According to the above procedure, equation set for each order can be derived in turn, and a_{nj} , b_{nj} and c_{nj} ($n = 2, 3, \dots$) of each order can also be solved in turn.

The solution procedure for the zero-order equation set (13-118) (can be compared with that for Eq. (13-72)) will be discussed in detail as follows:

Firstly, the solutions of Eq. (13-118) can be expressed by

$$\left. \begin{aligned} a_{0j} &= A_{0j} \cos(\lambda_j + 1)\theta + B_{0j} \sin(\lambda_j + 1)\theta + D_{0j} \cos(\lambda_j - 1)\theta + F_{0j} \sin(\lambda_j - 1)\theta \\ b_{0j} &= B_{0j} \cos(\lambda_j + 1)\theta - A_{0j} \sin(\lambda_j + 1)\theta + K_{0j}[F_{0j} \cos(\lambda_j - 1)\theta - D_{0j} \sin(\lambda_j - 1)\theta] \\ c_{0j} &= P_{0j} \cos \lambda_j \theta + Q_{0j} \sin \lambda_j \theta \end{aligned} \right\} \quad (13-119)$$

in which A_{0j} , B_{0j} , D_{0j} , F_{0j} , P_{0j} and Q_{0j} are the undetermined coefficients and functions of z ; and $K_{0j} = \frac{\lambda_j + 3 - 4\mu}{\lambda_j - 3 + 4\mu}$.

Secondly, the corresponding boundary conditions are introduced. Substitution of Eq. (13-116) into the boundary conditions (13-115) yields the following zero-order boundary conditions

$$\left. \begin{aligned} b'_{0j} + \left(1 + \frac{\mu\lambda_j}{1-\mu}\right)a_{0j} &= 0 \\ a'_{0j} + (\lambda_j - 1)b_{0j} &= 0 \\ c'_{0j} &= 0 \end{aligned} \right\} \left(\theta = \pm \frac{\alpha}{2} \right) \quad (13-120)$$

Substituting Eq. (13-119) into the above equation, the following 6 conditions can be obtained:

$$\frac{2\mu - 1}{1 - \mu} \lambda_j A_{0j} \cos(\lambda_j + 1) \frac{\alpha}{2} + \left[-K_{0j}(\lambda_j - 1) + 1 + \frac{\lambda_j \mu}{1 - \mu} \right] D_{0j} \cos(\lambda_j - 1) \frac{\alpha}{2} = 0 \quad (13-121a)$$

$$2A_{0j} \lambda_j \sin(\lambda_j + 1) \frac{\alpha}{2} - (\lambda_j - 1)(1 + K_{0j}) D_{0j} \sin(\lambda_j - 1) \frac{\alpha}{2} = 0 \quad (13-121b)$$

$$\frac{2\mu - 1}{1 - \mu} \lambda_j B_{0j} \sin(\lambda_j + 1) \frac{\alpha}{2} + \left[-K_{0j}(\lambda_j - 1) + 1 + \frac{\lambda_j \mu}{1 - \mu} \right] F_{0j} \sin(\lambda_j - 1) \frac{\alpha}{2} = 0 \quad (13-121c)$$

$$2B_{0j}\lambda_j \cos(\lambda_j + 1)\frac{\alpha}{2} + (\lambda_j - 1)(1 + K_{0j})F_{0j} \cos(\lambda_j - 1)\frac{\alpha}{2} = 0 \quad (13-121d)$$

$$Q_{0j}\lambda_j \cos \lambda_j \frac{\alpha}{2} = 0 \quad (13-121e)$$

$$P_{0j}\lambda_j \sin \lambda_j \frac{\alpha}{2} = 0 \quad (13-121f)$$

This is a homogenous equation set about A_{0j} , B_{0j} , D_{0j} , F_{0j} , Q_{0j} and P_{0j} . If this homogenous equation set has nontrivial solutions, its determinant of coefficients should be equal to zero, i.e.,

$$(\sin \lambda_j \alpha + \lambda_j \sin \alpha)(\sin \lambda_j \alpha - \lambda_j \sin \alpha) \sin \frac{\lambda_j \alpha}{2} \cos \frac{\lambda_j \alpha}{2} = 0 \quad (13-122)$$

This is the eigenequation for the 3D V-notch problem, which is completely the same as the eigenequation (13-76) for the V-notch problem in the Reissner plate. Therefore, the eigenvalues of the V-notch problem in the Reissner plate listed in Table 13.10 are still suitable for the 3D V-notch problem.

It can be recalled that, the eigenequation (13-122) can be decomposed into the following four equations (i.e. Eq. (13-77)):

$$\sin \lambda_j \alpha + \lambda_j \sin \alpha = 0 \quad (13-123a)$$

$$\sin \lambda_j \alpha - \lambda_j \sin \alpha = 0 \quad (13-123b)$$

$$\cos \lambda_j \frac{\alpha}{2} = 0 \quad (13-123c)$$

$$\sin \lambda_j \frac{\alpha}{2} = 0 \quad (13-123d)$$

which are corresponding to the following four cases:

A_{0j} and D_{0j} in Eqs. (13-121a,b) have nontrivial solutions—symmetric state;

B_{0j} and F_{0j} in Eqs. (13-121 c,d) have nontrivial solutions—antisymmetric state;

Q_{0j} in Eq. (13-121e) has nontrivial solution—antisymmetric state;

P_{0j} in Eq. (13-121f) has nontrivial solution—symmetric state.

Load states in the 3D V-notch problem can be classified as symmetric state and antisymmetric state. And, the eigenvalue series λ can also be classified as two sub series of symmetry and antisymmetry:

Symmetric sub series $\{\lambda_1, \lambda_4, \lambda_5, \lambda_8, \dots\}$ —the combination of the eigenvalues of Eqs. (13-123a,d).

Antisymmetric sub series $\{\lambda_2, \lambda_3, \lambda_6, \lambda_7, \dots\}$ —the combination of the eigenvalues of Eqs. (13-123b,c).

The following discussions on the displacement and stress fields around notch-tip are also classified as two cases of symmetry and antisymmetry.

13.6.3 Stress Fields Around 3D Notch-Tip—the Symmetric State

The symmetric sub series of eigenvalues can be divided into two groups

$$\text{Group a: } [\lambda_1, \lambda_3, \lambda_9, \dots]$$

$$\text{Group b: } [\lambda_4, \lambda_8, \lambda_{12}, \dots]$$

Here, the results of the first two orders ($n = 0$ and $n = 1$) are given as follows.

(1a) $n = 0, j = 1, 5, 9, \dots$

Eigenvalue λ_j of this group satisfies Eq. (13-123a). Substitution of it into Eq. (13-121b) or Eq. (13-121a) yields

$$A_{0j} = m_{0j} D_{0j}$$

where

$$m_{0j} = \frac{(\lambda_j - 1)(1 + K_{0j}) \sin \frac{1}{2}(\lambda_j - 1)\alpha}{2\lambda_j \sin \frac{1}{2}(\lambda_j + 1)\alpha}$$

Then, from Eq. (13-121c) to Eq. (13-121f), we have

$$B_{0j} = F_{0j} = Q_{0j} = P_{0j} = 0$$

Substituting them into Eqs. (13-119) and (13-116), the corresponding displacement terms can be derived:

$$\left. \begin{aligned} u_r &= r^{\lambda_j} [m_{0j} \cos(\lambda_j + 1)\theta + \cos(\lambda_j - 1)\theta] \beta_j \\ u_\theta &= -r^{\lambda_j} [m_{0j} \sin(\lambda_j + 1)\theta + K_{0j} \sin(\lambda_j - 1)\theta] \beta_j \\ u_z &= 0 \end{aligned} \right\} \quad (13-124)$$

in which β_j is just D_{0j} , it is a function of z ($j = 1, 5, 9, \dots$). By the stress-displacement relation (13-113), the corresponding stress field can be obtained:

$$\left. \begin{aligned} \sigma_{rr} &= r^{\lambda_j - 1} \{ [X(\lambda_j - 1) - XK_{0j}(\lambda_j - 1) + 2G\lambda_j] \cos(\lambda_j - 1)\theta + 2G\lambda_j m_{0j} \cos(\lambda_j + 1)\theta \} \beta_j \\ \sigma_{\theta\theta} &= r^{\lambda_j - 1} \{ [X(\lambda_j + 1) - XK_{0j}(\lambda_j - 1) + 2G \\ &\quad - 2GK_{0j}(\lambda_j - 1)] \cos(\lambda_j - 1)\theta - 2G\lambda_j m_{0j} \cos(\lambda_j + 1)\theta \} \beta_j \\ \sigma_{zz} &= r^{\lambda_j - 1} \{ [X(\lambda_j + 1) - K_{0j}(\lambda_j - 1)] \cos(\lambda_j - 1)\theta \} \beta_j \\ \sigma_{r\theta} &= r^{\lambda_j - 1} G [-2m_{0j} \lambda_j \sin(\lambda_j + 1)\theta - (\lambda_j - 1)(1 + K_{0j}) \sin(\lambda_j - 1)\theta] \beta_j \\ \sigma_{\theta z} &= r^{\lambda_j} G [-m_{0j} \sin(\lambda_j + 1)\theta - K_{0j} \sin(\lambda_j - 1)\theta] \beta_j \\ \sigma_{rz} &= r^{\lambda_j} G [m_{0j} \cos(\lambda_j + 1)\theta + \cos(\lambda_j - 1)\theta] \beta_j \end{aligned} \right\} \quad (13-125)$$

(1b) $n = 0, j = 4, 8, 12, \dots$

The eigenvalue λ_j of this group satisfies Eq. (13-123d). Substitution of it into Eq. (13-121f) yields

$$P_{0j} \neq 0$$

And, from the other expressions in Eq. (13-121), we obtain

$$A_{0j} = D_{0j} = B_{0j} = F_{0j} = Q_{0j} = 0$$

Substituting them into Eqs. (13-119) and (13-116), the corresponding displacement terms can be obtained

$$u_r = 0, \quad u_\theta = 0, \quad u_z = r^{\lambda_j} \beta_j \cos \lambda_j \theta \quad (13-126)$$

in which β_j is just P_{0j} ($j = 4, 8, 12, \dots$).

The corresponding stress terms can be solved from Eq. (13-113) as follows:

$$\left. \begin{aligned} \sigma_{rr} &= r^{\lambda_j} X \beta_j \cos \lambda_j \theta, & \sigma_{\theta\theta} &= r^{\lambda_j} X \beta_j \cos \lambda_j \theta \\ \sigma_{zz} &= r^{\lambda_j} (2G + X) \beta_j \cos \lambda_j \theta, & \sigma_{r\theta} &= 0 \\ \sigma_{\theta z} &= -r^{\lambda_j-1} G \lambda_j \beta_j \sin \lambda_j \theta, & \sigma_{rz} &= r^{\lambda_j-1} G \lambda_j \beta_j \cos \lambda_j \theta \end{aligned} \right\} \quad (13-127)$$

(2a) $n = 1, j = 1, 5, 9, \dots$

The case of $n = 1$ is corresponding to the first-order equation set and the first-order displacement and stress terms. By letting the sum of the coefficients of r^{λ_j-1} terms in Eq. (13-117) be zero, an ordinary differential equation set about (a_{1j}, b_{1j}, c_{1j}) and (a_{0j}, b_{0j}, c_{0j}) can be obtained as follows:

$$\left. \begin{aligned} (X + G)\{[(\lambda_j + 1)^2 - 1]a_{1j} + \lambda_j b'_{1j}\} \\ + G\{[(\lambda_j + 1)^2 - 1]a_{1j} + a''_{1j} - 2b'_{1j}\} + (X + G)\lambda_j c'_{0j} &= 0 \\ (X + G)[(\lambda_j + 2)a'_{1j} + b''_{1j}] + G\{2a'_{1j} + [(\lambda_j + 1)^2 - 1]b'_{1j} + b''_{1j}\} + (X + G)c'_{0j} &= 0 \\ G[(\lambda_j + 1)^2 c_{1j} + c''_{1j}] + (X + G)[(\lambda_j + 1)a'_{0j} + b'_{0j}] &= 0 \end{aligned} \right\} \quad (13-128)$$

When $j = 1, 5, 9, \dots$, (a_{0j}, b_{0j}, c_{0j}) in the above equation can be obtained from Eq. (13-124):

$$\left. \begin{aligned} a_{0j} &= [m_{0j} \cos(\lambda_j + 1)\theta + \cos(\lambda_j - 1)\theta] \beta_j \\ b_{0j} &= -[m_{0j} \sin(\lambda_j + 1)\theta + K_{0j} \sin(\lambda_j - 1)\theta] \beta_j \\ c_{0j} &= 0 \end{aligned} \right\} \quad (13-129)$$

Substituting the above equation into Eq. (13-128), (a_{1j}, b_{1j}, c_{1j}) can be solved as follows:

$$\left. \begin{aligned} a_{1j} &= A_{1j} \cos(\lambda_j + 2)\theta + B_{1j} \sin(\lambda_j + 2)\theta + D_{1j} \cos \lambda_j \theta + F_{1j} \sin \lambda_j \theta \\ b_{1j} &= B_{1j} \cos(\lambda_j + 2)\theta - A_{1j} \sin(\lambda_j + 2)\theta + K_{1j} [F_{1j} \cos \lambda_j \theta - D_{1j} \sin \lambda_j \theta] \\ c_{1j} &= P_{1j} \cos(\lambda_j + 1)\theta + Q_{1j} \sin(\lambda_j + 1)\theta - \frac{X + G}{4\lambda_j G} [\lambda_j + 1 - K_{0j}(\lambda_j - 1)] \beta_j^* \cos(\lambda_j - 1)\theta \end{aligned} \right\} \quad (13-130)$$

where

$$K_{1j} = -\frac{\lambda_j + 1 + 3 - 4\mu}{\lambda_j + 1 - 3 + 4\mu}$$

From the boundary condition (13-115), the first-order boundary conditions can be written by

$$\left. \begin{aligned} b'_{1j} + \frac{\lambda_j \mu + 1}{1 - \mu} a_{1j} &= 0 \\ a'_{1j} + \lambda_j b_{1j} &= 0 \\ c'_{1j} - [m_{0j} \sin(\lambda_j + 1)\theta + K_{0j} \sin(\lambda_j - 1)\theta] \beta_j^* &= 0 \end{aligned} \right\} \left(\theta = \pm \frac{\alpha}{2} \right) \quad (13-131)$$

Substitution of Eq. (13-130) into the above equation, we have

$$\begin{aligned} A_{1j} &= B_{1j} = D_{1j} = F_{1j} = Q_{1j} = 0 \\ P_{1j} &= f_{1j} \beta_j^* \end{aligned}$$

where

$$\begin{aligned} f_{1j} &= \frac{X + G}{4\lambda_j G} [(\lambda_j + 1) - K_{0j}(\lambda_j - 1)] \frac{\lambda_j - 1 \sin \frac{1}{2}(\lambda_j - 1)\alpha}{\lambda_j + 1 \sin \frac{1}{2}(\lambda_j + 1)\alpha} \\ &\quad - \frac{m_{0j} \sin \frac{1}{2}(\lambda_j + 1)\alpha + K_{0j} \sin \frac{1}{2}(\lambda_j - 1)\alpha}{(\lambda_j + 1) \sin \frac{1}{2}(\lambda_j + 1)\alpha} \end{aligned}$$

The corresponding displacement terms can be solved as follows

$$\left. \begin{aligned} u_r &= 0 \\ u_\theta &= 0 \\ u_z &= r^{\lambda_j + 1} [f_{1j} \cos(\lambda_j + 1)\theta + g_{1j} \cos(\lambda_j - 1)\theta] \beta_j^* \end{aligned} \right\} \quad (13-132)$$

where

$$g_{1j} = -\frac{X+G}{4\lambda_j G} [\lambda_j + 1 - K_{0j}(\lambda_j - 1)]$$

And, the corresponding stress terms are

$$\left. \begin{aligned} \sigma_{rr} &= r^{\lambda_j+1} X [f_{1j} \cos(\lambda_j + 1)\theta + g_{1j} \cos(\lambda_j - 1)\theta] \beta_j'' \\ \sigma_{\theta\theta} &= r^{\lambda_j+1} X [f_{1j} \cos(\lambda_j + 1)\theta + g_{1j} \cos(\lambda_j - 1)\theta] \beta_j'' \\ \sigma_{zz} &= r^{\lambda_j+1} (X + 2G) [f_{1j} \cos(\lambda_j + 1)\theta + g_{1j} \cos(\lambda_j - 1)\theta] \beta_j'' \\ \sigma_{r\theta} &= 0 \\ \sigma_{\theta z} &= r^{\lambda_j} G [(\lambda_j + 1)f_{1j} \sin(\lambda_j + 1)\theta + (\lambda_j - 1)g_{1j} \sin(\lambda_j - 1)\theta] \beta_j' \\ \sigma_{rz} &= r^{\lambda_j} G \lambda_j [f_{1j} \cos(\lambda_j + 1)\theta + g_{1j} \cos(\lambda_j - 1)\theta] \beta_j' \end{aligned} \right\} \quad (13-133)$$

(2b) $n = 1, j = 4, 8, 12, \dots$

Now, the cases of $j = 4, 8, 12, \dots$ are considered. Here, a_{0j} , b_{0j} and c_{0j} can be obtained from Eq. (13-126):

$$a_{0j} = 0, \quad b_{0j} = 0, \quad c_{0j} = \beta_j \cos \lambda_j \theta \quad (13-134)$$

Substituting the above equation back into Eq. (13-128), a_{1j} , b_{1j} and c_{1j} can be solved as follows:

$$\left. \begin{aligned} a_{1j} &= A_{1j} \cos(\lambda_j + 2)\theta + B_{1j} \sin(\lambda_j + 2)\theta + D_{1j} \cos \lambda_j \theta + F_{1j} \sin \lambda_j \theta \\ &\quad - \frac{X+G}{(X+G)(\lambda_j + 2) + 2G} \beta_j' \cos \lambda_j \theta \\ b_{1j} &= B_{1j} \cos(\lambda_j + 2)\theta - A_{1j} \sin(\lambda_j + 2)\theta + K_{1j} (F_{1j} \cos \lambda_j \theta - D_{1j} \sin \lambda_j \theta) \\ c_{1j} &= P_{1j} \cos(\lambda_j + 1)\theta + Q_{1j} \sin(\lambda_j + 1)\theta \end{aligned} \right\} \quad (13-135)$$

From the boundary condition (13-115), the corresponding first-order boundary condition can be written as:

$$\left. \begin{aligned} b'_{1j} + \frac{\lambda_j \mu + 1}{1 - \mu} a_{1j} + \frac{\mu}{1 - \mu} \beta_j' \cos \lambda_j \theta &= 0 \\ a'_{1j} + \lambda_j b_{1j} &= 0 \\ c'_{1j} &= 0 \end{aligned} \right\} \quad \left(\theta = \pm \frac{\alpha}{2} \right) \quad (13-136)$$

Substitution of Eq. (13-135) into the above equation yields

$$\left. \begin{aligned} B_{1j} = F_{1j} = Q_{1j} = P_{1j} = 0 \\ A_{1j} = l_{1j}\beta_j^*, \quad D_{1j} = \gamma_{1j}\beta_j^* \end{aligned} \right\} \quad (13-137)$$

where l_{1j} and γ_{1j} are given in Appendix C. The corresponding displacement terms are

$$\left. \begin{aligned} u_r &= r^{\lambda_j+1} [l_{1j} \cos(\lambda_j + 2)\theta + h_{1j} \cos \lambda_j \theta] \beta_j^* \\ u_\theta &= -r^{\lambda_j+1} [l_{1j} \sin(\lambda_j + 2)\theta + K_{1j}\gamma_{1j} \sin \lambda_j \theta] \beta_j^* \\ u_z &= 0 \end{aligned} \right\} \quad (13-138)$$

where

$$h_{1j} = \gamma_{1j} - \frac{X + G}{(X + G)(\lambda_j + 2) + 2G}$$

And, the corresponding stress terms are

$$\left. \begin{aligned} \sigma_{rr} &= r^{\lambda_j} \{ [-XK_{1j}\gamma_{1j}\lambda_j + X(\lambda_j + 2)g_{1j} + 2G\lambda_j g_{1j}] \cos \lambda_j \theta + 2G\lambda_j l_{1j} \cos(\lambda_j + 2)\theta \} \beta_j^* \\ \sigma_{\theta\theta} &= r^{\lambda_j} \{ [-XK_{1j}\gamma_{1j}\lambda_j + X(\lambda_j + 2)g_{1j} \\ &\quad + 2G(g_{1j} - K_{1j}\gamma_{1j}\lambda_j)] \cos \lambda_j \theta - 2Gl_{1j}(\lambda_j + 1) \cos(\lambda_j + 2)\theta \} \beta_j^* \\ \sigma_{zz} &= r^{\lambda_j} \{ X[-K_{1j}\gamma_{1j}\lambda_j + (\lambda_j + 2)g_{1j}] \cos \lambda_j \theta \} \beta_j^* \\ \sigma_{r\theta} &= -r^{\lambda_j} G [2l_{1j}(\lambda_j + 1) \sin(\lambda_j + 2)\theta + (g_{1j} + K_{1j}\gamma_{1j})\lambda_j \sin \lambda_j \theta] \beta_j^* \\ \sigma_{\theta z} &= -r^{\lambda_j+1} G [l_{1j} \sin(\lambda_j + 2)\theta + K_{1j}\gamma_{1j} \sin \lambda_j \theta] \beta_j^* \\ \sigma_{rz} &= r^{\lambda_j+1} G [l_{1j} \cos(\lambda_j + 2)\theta + g_{1j} \cos \lambda_j \theta] \beta_j^* \end{aligned} \right\} \quad (13-139)$$

13.6.4 Stress Fields Around 3D Notch-Tip—the Antisymmetric State

The antisymmetric sub series of eigenvalues can be divided into two groups

$$\text{Group a: } [\lambda_2, \lambda_6, \lambda_{10}, \dots]$$

$$\text{Group b: } [\lambda_3, \lambda_7, \lambda_{11}, \dots]$$

Here, the results of the first two orders ($n = 0$ and $n = 1$) are given as follows.

(1a) $n = 0, j = 2, 6, 10, \dots$

The displacement terms are

$$u_r = 0, \quad u_\theta = 0, \quad u_z = r^{\lambda_j} \beta_j \sin \lambda_j \theta \quad (13-140)$$

And, the stress terms are:

$$\left. \begin{aligned} \sigma_{rr} &= r^{\lambda_j} X \beta_j^* \sin \lambda_j \theta \\ \sigma_{\theta\theta} &= r^{\lambda_j} X \beta_j^* \sin \lambda_j \theta \\ \sigma_{zz} &= r^{\lambda_j} (X + 2G) \beta_j^* \sin \lambda_j \theta \\ \sigma_{r\theta} &= 0 \\ \sigma_{\theta z} &= r^{\lambda_j-1} G \lambda_j \beta_j \cos \lambda_j \theta \\ \sigma_{rz} &= r^{\lambda_j-1} G \lambda_j \beta_j \sin \lambda_j \theta \end{aligned} \right\} \quad (13-141)$$

(1b) $n = 0, j = 3, 7, 11, \dots$

The displacement terms are

$$\left. \begin{aligned} u_r &= r^{\lambda_j} [n_{0j} \sin(\lambda_j + 1)\theta + \sin(\lambda_j - 1)\theta] \beta_j \\ u_\theta &= r^{\lambda_j} [n_{0j} \cos(\lambda_j + 1)\theta + K_{0j} \cos(\lambda_j - 1)\theta] \beta_j \\ u_z &= 0 \end{aligned} \right\} \quad (13-142)$$

And, the stress terms are

$$\left. \begin{aligned} \sigma_{rr} &= r^{\lambda_j-1} \{ [X(\lambda_j + 1) - XK_{0j}(\lambda_j - 1) + 2G\lambda_j] \sin(\lambda_j - 1)\theta \\ &\quad + 2Gn_{0j}\lambda_j \sin(\lambda_j + 1)\theta \} \beta_j \\ \sigma_{\theta\theta} &= r^{\lambda_j-1} \{ [X(\lambda_j + 1) - XK_{0j}(\lambda_j - 1) + 2G \\ &\quad - 2GK_{0j}(\lambda_j - 1)] \sin(\lambda_j - 1)\theta - 2Gn_{0j}\lambda_j \sin(\lambda_j + 1)\theta \} \beta_j \\ \sigma_{zz} &= r^{\lambda_j-1} X \{ [\lambda_j + 1 - K_{0j}(\lambda_j - 1)] \sin(\lambda_j - 1)\theta \} \beta_j \\ \sigma_{r\theta} &= r^{\lambda_j-1} G [2n_{0j}\lambda_j \cos(\lambda_j + 1)\theta + (\lambda_j - 1)(1 + K_{0j}) \cos(\lambda_j - 1)\theta] \beta_j \\ \sigma_{\theta z} &= r^{\lambda_j} G [n_{0j} \cos(\lambda_j + 1)\theta + K_{0j} \cos(\lambda_j - 1)\theta] \beta_j^* \\ \sigma_{rz} &= r^{\lambda_j} G [n_{0j} \sin(\lambda_j + 1)\theta + \sin(\lambda_j - 1)\theta] \beta_j^* \end{aligned} \right\} \quad (13-143)$$

where

$$n_{0j} = - \frac{(\lambda_j - 1)(1 + K_{0j}) \cos \frac{1}{2}(\lambda_j - 1)\alpha}{2\lambda_j \cos \frac{1}{2}(\lambda_j + 1)\alpha}$$

(2a) $n = 1, j = 2, 6, 10, \dots$

The displacement terms are

$$\left. \begin{aligned} u_r &= r^{\lambda_j+1} [s_{1j} \sin(\lambda_j + 2)\theta + p_{1j} \sin \lambda_j \theta] \beta_j^* \\ u_\theta &= r^{\lambda_j+1} [s_{1j} \cos(\lambda_j + 2)\theta + K_{1j} t_{1j} \cos \lambda_j \theta] \beta_j^* \\ u_z &= 0 \end{aligned} \right\} \quad (13-144)$$

where s_{1j} and t_{1j} are given in Appendix D,

$$p_{1j} = t_{1j} - \frac{X + G}{(X + G)(\lambda_j + 2) + 2G}$$

And, the stress terms are

$$\left. \begin{aligned} \sigma_{rr} &= r^{\lambda_j} \{ [X(\lambda_j + 2)v_{1j} - XK_{1j}\gamma_{1j}\lambda_j + 2G\lambda_j v_{1j}] \sin \lambda_j \theta + 2G\lambda_j s_{1j} \sin(\lambda_j + 2)\theta \} \beta_j^* \\ \sigma_{\theta\theta} &= r^{\lambda_j} \{ [X(\lambda_j + 2)v_{1j} - XK_{1j}\gamma_{1j}\lambda_j + 2G(v_{1j} - K_{1j}t_{1j}\lambda_j)] \sin \lambda_j \theta \\ &\quad - 2G(\lambda_j + 1)s_{1j} \sin(\lambda_j + 2)\theta \} \beta_j^* \\ \sigma_{zz} &= r^{\lambda_j} X \{ [(\lambda_j + 2)v_{1j} - K_{1j}t_{1j}\lambda_j] \sin \lambda_j \theta \} \beta_j^* \\ \sigma_{r\theta} &= r^{\lambda_j} G \{ 2(\lambda_j + 1)s_{1j} \cos(\lambda_j + 2)\theta + [v_{1j}\lambda_j + K_{1j}\lambda_j t_{1j}] \cos \lambda_j \theta \} \beta_j^* \\ \sigma_{\theta z} &= r^{\lambda_j+1} G [s_{1j} \sin(\lambda_j + 2)\theta + K_{1j}t_{1j} \cos \lambda_j \theta] \beta_j^{**} \\ \sigma_{rz} &= r^{\lambda_j+1} G [s_{1j} \sin(\lambda_j + 2)\theta + v_{1j} \cos \lambda_j \theta] \beta_j^{**} \end{aligned} \right\} \quad (13-145)$$

(2b) $n = 1, j = 3, 7, 11, \dots$

The displacement terms are

$$u_r = 0, \quad u_\theta = 0, \quad u_z = r^{\lambda_j} [q_{1j} \sin(\lambda_j + 1)\theta + v_{1j} \sin(\lambda_j - 1)\theta] \beta_j^* \quad (13-146)$$

where

$$\begin{aligned} q_{1j} &= \frac{X + G}{4\lambda_j G} [(\lambda_j + 1) - K_{0j}(\lambda_j - 1)] \frac{\lambda_j - 1}{\lambda_j + 1} \frac{\cos \frac{1}{2}(\lambda_j - 1)\alpha}{\cos \frac{1}{2}(\lambda_j + 1)\alpha} \\ &\quad - \frac{n_{0j} \cos \frac{1}{2}(\lambda_j + 1)\alpha + K_{0j} \cos \frac{1}{2}(\lambda_j - 1)\alpha}{(\lambda_j + 1) \cos \frac{1}{2}(\lambda_j + 1)\alpha} \\ v_{1j} &= -\frac{X + G}{4\lambda_j G} [\lambda_j + 1 - K_{0j}(\lambda_j - 1)] \end{aligned}$$

And, the stress terms are

$$\left. \begin{aligned} \sigma_{rr} &= r^{\lambda_j+1} X[q_{1j} \sin(\lambda_j + 1)\theta + v_{1j} \sin(\lambda_j - 1)\theta] \beta_j'' \\ \sigma_{\theta\theta} &= r^{\lambda_j+1} X[q_{1j} \sin(\lambda_j + 1)\theta + v_{1j} \sin(\lambda_j - 1)\theta] \beta_j'' \\ \sigma_{zz} &= r^{\lambda_j+1} (X + 2G)[q_{1j} \sin(\lambda_j + 1)\theta + v_{1j} \sin(\lambda_j - 1)\theta] \beta_j'' \\ \sigma_{r\theta} &= 0 \\ \sigma_{\theta z} &= r^{\lambda_j} G[(\lambda_j + 1)q_{1j} \cos(\lambda_j + 1)\theta + (\lambda_j - 1)v_{1j} \cos(\lambda_j - 1)\theta] \beta_j' \\ \sigma_{rz} &= r^{\lambda_j} G\lambda_j[q_{1j} \sin(\lambda_j + 1)\theta + v_{1j} \sin(\lambda_j - 1)\theta] \beta_j' \end{aligned} \right\} \quad (13-147)$$

When the inner angle tends to be 2π , the above solutions can be transferred to the displacement and stress fields of a crack in 3D space, which are identical with the results given by reference [24].

The sub-region mixed element method for the 3D V-notch problem is denoted by SRM-V5.

References

- [1] Fan Z, Long YQ (1992) Sub-region mixed finite element analysis of V-notched plates. *International Journal of Fracture* 56: 333 – 344
- [2] Long YQ, Qian J (1992) Sub-region mixed finite element analysis of V-notches in a bimaterial. In: Zhu DC (ed) *Advances in Engineering Mechanics*, Peking University Press, Beijing, pp54 – 59
- [3] Qian J, Long YQ (1992) The expression of stress and strain at the tip of notch in Reissner plate. *Applied mathematics and Mechanics (English Edition)* 13(4): 315 – 324
- [4] Qian J, Long YQ (1994) The expression of stress and strain at the tip of 3-D notch. *Applied mathematics and Mechanics (English Edition)* 15(3): 211 – 221
- [5] Williams ML (1952) Stress singularities resulting from various boundary conditions in angular corners of plates in extension. *Journal of Applied Mechanics* 14: 526 – 528
- [6] Gross B, Mendelson A (1972) Plane elastostatic analysis of V-notched plates. *International Journal of Fracture* 8: 267 – 276
- [7] Rzasnicki W, Mendelson A, Albers LU (1973) Application of boundary integral method to elastic analysis of V-notched beams. NASA TN-F-7424
- [8] Carpenter WC (1984) A collocation procedure for determining fracture mechanics parameters at a corner. *International Journal of Fracture* 24: 255 – 266
- [9] Carpenter WC (1985) The eigenvector solution for a general corner or finite opening crack with further studies on the collocation procedure. *International Journal of Fracture* 27: 63 – 74
- [10] Carpenter WC (1987) A path independent integral for computing stress intensities for V-notched cracks in a bi-material. *International Journal of Fracture* 35: 245 – 268

Advanced Finite Element Method in Structural Engineering

- [11] Lin KY, Tong P (1980) Singular finite element for the fracture analysis of V-notch plate. *International Journal for Numerical Methods in Engineering* 15: 1343 – 1354
- [12] Awaji H, Yokobori AT, Yokobori T (1986) The variation of the stress singularity at the notch-tip as notch angle and radius of curvature. *Computers & Structures* 22(1): 25 – 30
- [13] Long YQ (1987) *Variational Principles • Finite Element Method • Shell Analysis*. Liaoning Science and Technology Publishing House, Shenyang (in Chinese)
- [14] Lin KY, Mar JW (1976) Finite element analysis of stress intensity factors for cracks at a bi-material interface. *International Journal of Fracture* 12: 521 – 531
- [15] Rice JR, Sih GC (1965) Plane problems of cracks in dissimilar media. *Journal of Applied Mechanics* 32: 418 – 423
- [16] Qian J, Long YQ (1991) Sub region mixed FEM for calculating stress intensity factor of antiplane notch in bi-material. *Computational Structural Mechanics and Applications* 8(3): 325 – 330 (in Chinese)
- [17] Sham TL, Bueckner HF (1988) The weight function theory for piecewise homogeneous isotropic notches in antiplane strain. *Journal of Applied Mechanics* 55: 956 – 603
- [18] Sham TL (1988) Weight functions for piecewise homogeneous isotropic notches in antiplane strain by finite element method. *Engineering Fracture Mechanics* 31(4): 567 – 576
- [19] Schovanec L (1989) An antiplane shear crack in a nonhomogeneous elastic material. *Engineering Fracture Mechanics* 33: 745 – 751
- [20] Hwang KC, Yu SW (1985) *Fracture mechanics in elasticity and plasticity*. Tsinghua University Press, Beijing (in Chinese)
- [21] Liu CT (1983) Stresses and deformations near the crack tip for bending plate. *Acta Mechanica Solida Sinica* 3: 441 – 448 (in Chinese)
- [22] Knowles JK, Wang NM (1960) On the bending of an elastic plate containing a crack. *Journal of Mathematics and Physics* 39: 223 – 236
- [23] Hartanft RJ, Sih GC (1968) Effect of plate thickness on the bending stress distribution around through cracks. *Journal of Mathematics and Physics* 47: 276 – 291
- [24] Hartranft RJ, Sih GC (1969) The use of eigenfunction expansions in the general solution of three dimensional crack problems. *Journal of Mathematics and Mechanics* 19: 123 – 138

Chapter 14 Analytical Trial Function Method I — Membrane and Plate Bending Elements

Song Cen

Department of Engineering Mechanics, School of Aerospace,
Tsinghua University, Beijing, 100084, China

Zhi-Fei Long

School of Mechanics & Civil Engineering, China University of
Mining & Technology, Beijing, 100083, China

Abstract This chapter introduces a novel finite element method, namely, the analytical trial function method. A detailed discussion on the features of the analytical trial function method is firstly given in Sect. 14.1. Then, in the next five sections, the basic analytical solutions of plane problem, thick plate problem and thin plate problem are derived and taken as the trial functions for the corresponding finite element models. It can be seen that those resulting models exhibit excellent performance. Some challenging problems, such as the trapezoidal locking and shear locking, can be avoided naturally.

Keywords finite element, analytical trial function method, membrane element, plate bending element.

14.1 Recognition of the Analytical Trial Function Method

14.1.1 Trial Function

When constructing a displacement-based element, the first step is usually to assume its displacement mode. For example, the displacement mode of the constant strain triangular element CST is assumed to be

$$\begin{Bmatrix} u \\ v \end{Bmatrix} = \begin{bmatrix} 1 & 0 & x & 0 & y & 0 \\ 0 & 1 & 0 & x & 0 & y \end{bmatrix} \begin{Bmatrix} \lambda_1 \\ \vdots \\ \lambda_6 \end{Bmatrix} = \mathbf{F} \boldsymbol{\lambda} \quad (14-1)$$

and the displacement mode of the rectangular thin plate element ACM is assumed to be

$$w = [1 \quad x \quad y \quad x^2 \quad xy \quad y^2 \quad x^3 \quad x^2y \quad xy^2 \quad y^3 \quad x^3y \quad xy^3] \begin{Bmatrix} \lambda_1 \\ \vdots \\ \lambda_{12} \end{Bmatrix} = \mathbf{F} \boldsymbol{\lambda} \tag{14-2}$$

where $\boldsymbol{\lambda}$ is the undetermined parameter vector; \mathbf{F} is composed of trial functions (or basis functions).

Element performance relies deeply on the selected trial functions. As a result of the irrationally selected trial functions for displacements, trapezoidal locking and shear locking phenomena may exist in some membrane and thick plate elements, respectively.

14.1.2 Analytical Trial Function

In structural matrix analysis, the exact (or analytical) solutions for the displacement of the thin beam theory are used by the thin beam element. That is to say, the selected trial functions are analytical solutions; therefore, they are called as *analytical trial functions*.

Timoshenko thick beam element also uses the exact solutions for the displacements of the thick beam theory. So, it will not suffer from shear locking phenomenon because the analytical trial functions are employed.

2D and 3D elasticity problems, thin and thick plate problems are all problems with infinite DOFs. For their homogeneous problems, the analytical solutions are composed of infinite terms. Finite element method is an approximate method in which such infinite DOF problems are treated as problems with only finite DOFs. And, the corresponding element model also contains finite (n) DOFs, which means that its displacement mode contains only n basic analytical trial functions. These n analytical solutions can be selected in turn from low to high orders.

14.1.3 Analytical Trial Function Method

The construction procedure of the finite element model in which the basic analytical solutions are taken as the trial functions is called *the finite element method based on analytical trial functions*, or *the analytical trial function method*.

The feature of the analytical trial function method is: the finite element method is a discrete approximate method, while the advantages of the analytical method are preserved in it. It exhibits the close relation between the trial function and the

basic analytical solution and the complementarity between discrete and analytical methods.

14.1.4 Recognition of the Analytical Trial Function Method

At the beginning of the finite element method, all people thought of taking the most basic analytical solutions as the trial functions. For instance, in the displacement mode (14-1) of the first membrane element CST, the selected 6 trial functions are just the most basic analytical solutions of the 2D homogenous problem in elasticity (3 rigid body displacements and 3 constant strain states). And, in the displacement mode (14-2) of the first rectangular thin plate element ACM, the selected 12 trial functions are just the most basic analytical solutions of the thin plate homogenous problem, i.e., they are all the analytical solutions of the following homogenous differential equation

$$\nabla^2 \nabla^2 w = 0 \quad (14-3)$$

and are the 12 analytical solutions of the lowest orders which contain 3 rigid body displacement states, 3 constant strain states, 4 linear strain states and 2 quadratic strain states. It can be seen that, for these earliest elements, whether by conscious efforts or not, their construction procedures are in keeping with the requirement of the analytical trial function method. That is to say, the analytical trial function method is the earliest scheme used in the finite element method.

With the flourishing development of the finite element method, various schemes have been proposed one after the other. Especially, after the isoparametric elements were broadly used, the analytical trial function method was almost overlooked.

Owing to the inherent advantages of the analytical trial function method, its new applications are continuously suggested in some references. For example, in 1982, reference [1] used the analytical solutions containing singular stress point as the trial functions for developing the singular element with crack, which provides an effective solution scheme for the crack problem; in 1996, reference [2] proposed a rational finite element method, and constructed a set of high quality elements by using the basic analytical solutions for plane elasticity; reference [3] takes the basic analytical solutions of the thick plate theory as the trial functions to develop the thick plate elements, which rationally resolves the matching problem of the trial functions for deflection and rotations so that shear locking phenomenon can be eliminated from the outset; reference [4] uses the analytical solutions to construct two membrane elements which can keep high precision in distorted mesh, and the trapezoidal locking problem given in reference [5] is thus solved. In 2002, reference [6] gave a systematical review of the analytical trial function method. It points out the advantages and potentialities of the analytical trial function method in dealing with mesh distortion, shear locking and singular

stress point problems, which will induce further studies and developments on the analytical trial function method.

14.2 4-Node Membrane Elements Based on the Analytical Trial Function Method

14.2.1 The Basic Analytical Solutions in Plane Elasticity

In plane elasticity, the analytical solutions of different order which satisfy the basic governing equations, including equilibrium equations, geometrical equations and constitutive law, can be derived. The 12 low-order analytical solutions are listed in Table 14.1 (in which μ is the Poisson’s ratio).

Table 14.1 The basic analytical solutions in plane elasticity

No.of terms	1	2	3	4	5	6	7	8	9	10	11	12
u	1	0	y	y	$-\mu x$	x	$-\mu x^2 - y^2$	$2xy$	$-2\mu xy$	$x^2 - (2 + \mu)y^2$	$-3\mu x^2 y - y^3$	$3yx^2 - (2 + \mu)y^3$
v	0	1	$-x$	x	y	$-\mu y$	$2xy$	$-\mu y^2 - x^2$	$y^2 - (2 + \mu)x^2$	$-2\mu xy$	$3xy^2 - (2 + \mu)x^3$	$-3\mu y^2 x - x^3$
θ	0	0	1	0	0	0	$-2y$	$2x$	$2x$	$-2y$	$3x^2 - 3y^2$	$3x^2 - 3y^2$
ε_x	0	0	0	0	$-\mu$	1	$-2\mu x$	$2y$	$-2\mu y$	$2x$	$-6\mu xy$	$6xy$
ε_y	0	0	0	0	1	$-\mu$	$2x$	$-2\mu y$	$2y$	$-2\mu x$	$6xy$	$-6\mu xy$
γ_{xy}	0	0	0	2	0	0	0	0	$-4(1 + \mu)x$	$-4(1 + \mu)y$	$-6(1 + \mu)x^2$	$-6(1 + \mu)y^2$

14.2.2 3 Membrane Elements Based on the Analytical Trial Functions

A 4-node, 8-DOF membrane element shown in Fig. 14.1 is considered. The element nodal displacement vector is

$$\mathbf{q}^e = [u_1 \quad v_1 \quad u_2 \quad v_2 \quad u_3 \quad v_3 \quad u_4 \quad v_4]^T \tag{14-4}$$

By using the first eight terms of the analytical solutions given in Table 14.1 as the trial functions, the element displacements u and v are assumed to be

$$\begin{Bmatrix} u \\ v \end{Bmatrix} = \begin{bmatrix} 1 & 0 & y & y & -\mu x & x & -\mu x^2 - y^2 & 2xy \\ 0 & 1 & -x & x & y & -\mu y & 2xy & -\mu y^2 - x^2 \end{bmatrix} \begin{Bmatrix} \lambda_1 \\ \lambda_2 \\ \vdots \\ \lambda_8 \end{Bmatrix} \tag{14-5}$$

where $\lambda_1, \lambda_2, \dots, \lambda_8$ are 8 unknown parameters.

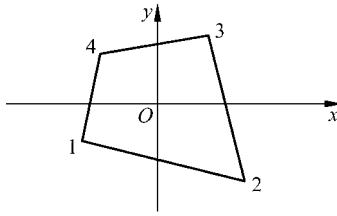


Figure 14.1 A 4-node quadrilateral membrane element

By employing 8 nodal conforming conditions

$$\left. \begin{aligned} (u - \bar{u})_i &= 0 \\ (v - \bar{v})_i &= 0 \end{aligned} \right\} \quad (i = 1, 2, 3, 4) \quad (14-6)$$

the 8 unknown parameters can be solved and expressed in terms of \mathbf{q}^e . This element is denoted as ATF-Q4a.

If the 8 nodal conforming conditions are replaced by the following nodal and perimeter conforming conditions

$$\left. \begin{aligned} \iint_{A^e} \frac{\partial u}{\partial x} dA &= \oint_{\partial A^e} l \bar{u} ds & \iint_{A^e} \frac{\partial v}{\partial x} dA &= \oint l \bar{v} ds \\ \iint_{A^e} \frac{\partial u}{\partial y} dA &= \oint m \bar{u} ds & \iint_{A^e} \frac{\partial v}{\partial y} dA &= \oint m \bar{v} ds \\ \sum_{i=1}^4 (u - \bar{u})_i &= 0 & \sum_{i=1}^4 (v - \bar{v})_i &= 0 \\ \sum_{i=1}^4 (u - \bar{u})_i \xi_i \eta_i &= 0 & \sum_{i=1}^4 (v - \bar{v})_i \xi_i \eta_i &= 0 \end{aligned} \right\} \quad (14-7)$$

in which l and m are the direction cosines of the normal on the element boundary; ξ_i and η_i are the isoparametric coordinates of node i ; \bar{u} and \bar{v} are the displacements of the element boundary. This element is denoted as ATF-Q4b.

For the 4-node membrane element shown in Fig. 14.1, if the rotation θ_i of node i is also taken as the DOF, the element will have 12 DOFs. Thus, the element nodal displacement vector is

$$\mathbf{q}^e = [u_1 \quad v_1 \quad \theta_1 \quad u_2 \quad v_2 \quad \theta_2 \quad u_3 \quad v_3 \quad \theta_3 \quad u_4 \quad v_4 \quad \theta_4]^T \quad (14-8)$$

The 12 analytical solutions given in Table 14.1 are taken as the trial functions, and the following 12 nodal conforming conditions

$$\left. \begin{aligned} (u - \bar{u})_i &= 0 \\ (v - \bar{v})_i &= 0 \\ (\theta - \bar{\theta})_i &= 0 \end{aligned} \right\} (i = 1, 2, 3, 4) \tag{14-9}$$

are also used, in which

$$\theta = \frac{1}{2} \left(\frac{\partial u}{\partial y} - \frac{\partial v}{\partial x} \right) \tag{14-10}$$

This element is denoted as ATF-Q4θ.

14.3 Avoiding Trapezoidal Locking Phenomenon by ATF Elements

As to the trapezoidal locking problem (or sensitivity problem to mesh distortion), the analytical trial function method provides an effective solution countermeasure.

Example 14.1 Sensitivity test I to mesh distortion—A pure bending beam divided by two distorted elements.

A cantilever beam subjected to pure bending load is shown in Fig. 14.2, and it is divided into two elements. δ is a distortion parameter. When δ increases, the distortion will become more serious. The length of the beam is 10; height is 2; thickness is 1. And, $E = 1500$, $\mu = 0.25$. Results of the deflection v_A at tip A are plotted in Fig. 14.3. Besides the present elements ATF-Q4a, ATF-Q4b and ATF-Q4θ, results obtained by the 4-node isoparametric element Q4, the isoparametric element with internal parameters QM6^[7] and the hybrid stress element P-S^[8] are also given for comparison.

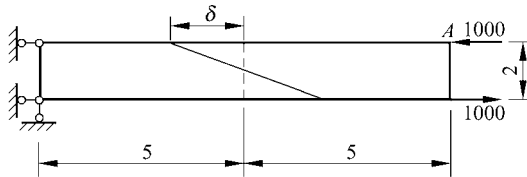


Figure 14.2 A beam divided by two distorted elements

From Fig. 14.3, it can be seen that, the precision of the 4-node isoparametric element Q4 is the lowest: when $\delta = 0$, since the length-height ratio of the rectangular element is high $\left(\frac{L}{h} = \frac{5}{2} \right)$, the precision of v_A has already dropped to 28%. And, with the increase of δ , its precision will continually drop, even below

10%. Though the precisions of the hybrid stress element P-S, the isoparametric element with internal parameters QM6 and element ATF-Q4b are all 100% for the rectangular element case ($\delta=0$), if $\delta>1$, they will be below 60%. The precisions of the other two present elements ATF-Q4a and ATF-Q40 are the best: with the increase of the distortion parameter δ , the precision can always keep 100% which means that both the elements are very insensitive to mesh distortion. From these results, it can be concluded that, if appropriate conforming conditions are selected, ATF elements can exhibit excellent performance for avoiding trapezoidal locking.

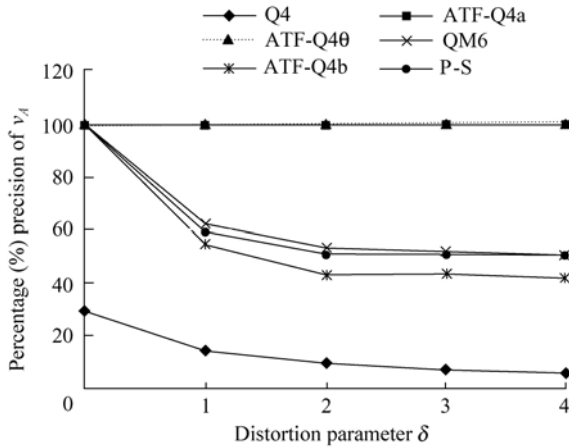


Figure 14.3 Relation between Percentage (%) precision of v_A and distortion parameter δ

Example 14.2 Sensitivity test II to mesh distortion—MacNeal thin beam problem with distorted mesh.

The MacNeal thin beam problem^[5] is shown in Fig. 14.4, in which rectangular, parallelogram and trapezoidal mesh are used. This is a famous benchmark for testing the sensitivity to mesh distortion. The precisions of many 4-node membrane

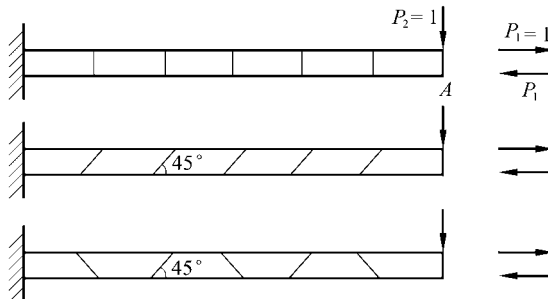


Figure 14.4 MacNeal thin beam with distorted meshes

elements drop dramatically for the trapezoidal mesh case, which is the so-called trapezoidal locking phenomenon. The length of the cantilever beam is 6, the height is 0.2; the elastic constants $E = 10^7$ and $\mu = 0.3$. Two tip load cases are considered: pure bending and transverse shear.

The results of the deflection v_A at tip A are listed in Table 14.2. Besides the present three elements, the results obtained by the 4-node isoparametric element Q4, hybrid stress element P-S^[8], 4-node element QUAD4^[5] with one integration point, assumed strain element PEAS7^[9] and its modification versions, the elements M1PEAS7 and M2PEAS7^[10] are also given for comparison.

Table 14.2 The percentage (%) precision of the tip deflection v_A of MacNeal beam

Load case	Transverse shear			Pure bending		
	Rectangle	Parallelogram	Trapezoid	Rectangle	Parallelogram	Trapezoid
Q4	9.3	3.5	0.3	9.3	3.1	2.2
QUAD4	90.4	8.0	7.1			
P-S	99.3	79.8	22.1	100	85.2	16.7
PEAS7	98.2	79.5	21.7			
M1PEAS7	99.3	94.8	36.7			
M2PEAS7	99.3	94.3	36.8			
ATF-Q4b	99.4	61.3	4.5	100	70.7	4.1
ATF-Q4a	99.4	99.4	99.4	100	100	100
ATF-Q4θ	100	100	100	100	100	100

From Table 14.2, it can be seen that, because the length-height ratio of the element is $1/0.2 = 5$, the precision of the element Q4 drops obviously. The element QUAD 4 using a single integration point is seriously locking in parallelogram and trapezoidal meshes. The precisions of the hybrid stress element P-S, element ATF-Q4b, assumed strain elements PEAS7, M1PEAS7 and M2PEAS7 are similar: for the mesh divided by rectangular elements, the precision is the best; for the mesh divided by parallelogram elements, the precision will drop; and for the mesh divided by trapezoidal elements, locking phenomenon will happen. Only two elements ATF-Q4a and ATF-Q4θ, which are proposed in this section, possess high accuracy for all mesh divisions, i.e., they are insensitive to mesh distortion. And, element ATF-Q4θ can even provide exact solutions for the two load cases and three meshes. The trapezoidal locking problem of MacNeal beam is a serious challenge to the 4-node, 8-DOF membrane elements. The victory of the element ATF-Q4a in this challenge exhibits its advantage again.

Example 14.3 Weak patch test for the element ATF-Q4a.

Patch test is often used for testing the convergence of the non-conforming elements. It has two forms:

Strict form—The boundary conditions are specified according to the constant strain state. Then, by using an arbitrary mesh divided by the elements with finite

dimensions, the finite element solutions will be tested to see whether they are the exact solutions.

Weak form—The boundary conditions are also specified according to the constant strain state. Then, by using meshes refined by more and more elements, the finite element solutions will be tested to see whether they are convergent to the exact ones.

The merit of the strict form is that it can be conveniently performed; and the merit of the weak form is that it possesses the right description and is more coincident with the original idea of the convergence.

The MacNeal beam subjected to a horizontal load (resultant force is 1) is considered. This structure is under a constant strain state. By using the two refined meshes shown in Fig. 14.5, the convergence of the element ATF-Q4a is analyzed. The results of the tip displacement are listed in Table 14.3 (the analytical solution is 0.6).

In Fig. 14.5, the refined mesh *A* firstly contains $n \times n$ rectangular elements; then, each rectangular element is divided into two trapezoidal elements, thus, $2n^2$ elements are totally obtained. And, the refined mesh *B* firstly contains two trapezoidal elements; then, each trapezoidal element is bisected through the midpoints of the element sides so that it is divided into four trapezoidal elements; finally, $2n^2$ elements are totally obtained.

From Table 14.3, it can be seen that the element ATF-Q4a cannot pass the strict patch test because it does not produce the exact solutions of the constant strain state by mesh with finite dimensions. But, with the refinement of the mesh, the finite element solutions can rapidly converge to the exact solutions. So, the element ATF-Q4a can pass the weak patch test.

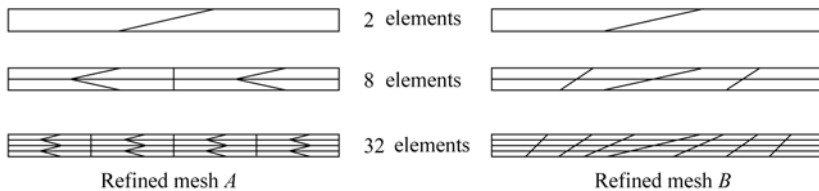


Figure 14.5 Two refined patterns of the meshes for MacNeal beam

Let us make a comparison between the elements ATF-Q4a and ATF-Q4b. From the numerical results of Examples 14.1 and 14.2, it can be seen that the precision of the element ATF-Q4a is obviously higher than that of the element ATF-Q4b. But, the element ATF-Q4b can pass the strict patch test (thereby it can also pass the weak one), and the element ATF-Q4a can only pass the weak patch test. By this token, the ultimate rule for testing the convergence should be the weak patch test, not the strict one. It is not appropriate to deny the element ATF-Q4a, which possesses high accuracy, only according to the results of the strict patch test.

Table 14.3 The tip displacements of the MacNeal beam under tension (ATF-Q4a)

Num. of elements	Refined mesh <i>A</i>		Refined mesh <i>B</i>	
	Result	Relative Precision	Result	Relative Precision
2	0.6923	1.1538	0.6923	1.1538
	0.6923	1.1538	0.6923	1.1538
8	0.5935	0.9892	0.6067	1.0112
	0.6318	1.0530	0.5998	0.9997
	0.5935	0.9892	0.6065	1.0108
32	0.6008	1.0013	0.6014	1.0023
	0.6010	1.0017	0.6003	1.0005
	0.6010	1.0017	0.5997	0.9995
	0.6010	1.0017	0.5988	0.9980
	0.6008	1.0013	0.6029	1.0048

14.4 The Basic Analytical Solutions of the Thick Plate Theory and ATF Elements Free of Shear Locking

14.4.1 Shear Locking Phenomenon in the Thick Plate Element

During the construction procedure of the thick plate element based on the Mindlin-Reissner thick plate theory, the three displacement components w , ψ_x and ψ_y should be independent variables. When the thick plate degenerates to be a thin plate, then, according to the Kirchhoff thin plate theory, the rotations ψ_x and ψ_y will be the derivatives of w , which are not independent anymore. Many displacement-based elements produce false shear strains γ_x and γ_y in thin plate cases, consequently, shear locking phenomenon will happen. Reference [11] claimed that, “The root of this difficulty lies on the contradiction of the double requirements of dependence and independence among the displacements”. In order to overcome such shear locking, many countermeasures have already been proposed in numerous literatures. The most popular countermeasures are reduced integration^[12] and selected reduced integration schemes^[13]. However, though they can provide us temporary solutions, the shear locking is still not eliminated from the outset, and even some new troubles, such as spurious zero energy mode, may be aroused. In some recent references [14–18], the double requirements of dependence and independence among the displacements have been translated into other double requirements of nonzero and zero shear strains, and a rational interpolation scheme for shear strains which satisfies the double requirements is proposed. As a result, a series of thick plate elements which can completely

avoid shear locking are developed successfully. This section will present another way to eliminate shear locking: The basic analytical solutions of the Mindlin-Reissner theory are used in the trial functions of the thick plate displacements w , ψ_x and ψ_y ; when the plate degenerates to be a thin plate, these basic analytical solutions will automatically degenerate to be those of the Kirchhoff theory, and consequently, the shear locking will also be avoided from the outset.

14.4.2 The Basic Analytical Solutions of the Thick Plate Theory

In the equilibrium differential equations of the thick plate, if the internal forces are expressed in terms of the displacements, the basic differential equations of the displacement method for the thick plate can be obtained. For the homogeneous problem when all loads are zero, we have

$$\left. \begin{aligned} D \left(\frac{\partial^2 \psi_x}{\partial x^2} + \frac{1-\mu}{2} \frac{\partial^2 \psi_x}{\partial y^2} + \frac{1+\mu}{2} \frac{\partial^2 \psi_y}{\partial x \partial y} \right) + C \left(\frac{\partial w}{\partial x} - \psi_x \right) &= 0 \\ D \left(\frac{1+\mu}{2} \frac{\partial^2 \psi_x}{\partial x \partial y} + \frac{1-\mu}{2} \frac{\partial^2 \psi_y}{\partial x^2} + \frac{\partial^2 \psi_y}{\partial y^2} \right) + C \left(\frac{\partial w}{\partial y} - \psi_y \right) &= 0 \\ C \left(\frac{\partial^2 w}{\partial x^2} + \frac{\partial^2 w}{\partial y^2} - \frac{\partial \psi_x}{\partial x} - \frac{\partial \psi_y}{\partial y} \right) &= 0 \end{aligned} \right\} \quad (14-11)$$

Let $F(x, y)$ be a bi-harmonic function which satisfies the following bi-harmonic equation

$$\nabla^2 \nabla^2 F = 0 \quad (14-12)$$

where

$$\nabla^2 = \frac{\partial^2}{\partial x^2} + \frac{\partial^2}{\partial y^2}$$

Then, the following expressions

$$w = F - \frac{D}{C} \nabla^2 F, \quad \psi_x = \frac{\partial F}{\partial x}, \quad \psi_y = \frac{\partial F}{\partial y} \quad (14-13)$$

are the solutions of Eq. (14-11). Let d be a characteristic length. By introducing the dimensionless coordinates ξ and η

$$\xi = \frac{x}{d}, \quad \eta = \frac{y}{d} \quad (14-14)$$

and the dimensionless parameter λ

$$\lambda = \frac{D}{Cd^2} = \frac{h^2}{5(1-\mu)d^2} \tag{14-15}$$

the first expression in Eq. (14-13) can be written as

$$w = F - \lambda \left(\frac{\partial^2}{\partial \xi^2} + \frac{\partial^2}{\partial \eta^2} \right) F \tag{14-16}$$

If $\frac{h}{d} \rightarrow 0$, $\lambda \rightarrow 0$, then, the analytical solutions (14-13) of the thick plate theory will degenerate to be the following analytical solutions of the thin plate theory

$$\left. \begin{aligned} w &= F, \quad \psi_x = \frac{\partial F}{\partial x}, \quad \psi_y = \frac{\partial F}{\partial y} \\ \gamma_{xz} &= \frac{\partial w}{\partial x} - \psi_x = 0, \quad \gamma_{yz} = \frac{\partial w}{\partial y} - \psi_y = 0 \end{aligned} \right\} \tag{14-17}$$

From above, it can be concluded that, if the basic analytical solutions (14-13) of the thick plate theory are taken as the trial functions for the thick plate element, once $\frac{h}{d} \rightarrow 0$, these trial functions will automatically degenerate to be the analytical solutions of the thin plate theory, thereby, the shear locking phenomenon can be eliminated from the outset.

14.5 Development of Quadrilateral Thin-Thick Plate Element Based on the Analytical Trial Function Method

14.5.1 Thick Plate Element ATF-MQ Based on the Analytical Trial Function Method

Consider a quadrilateral thick plate element with 12 DOFs, its nodal displacement vector is

$$\mathbf{q}^e = [w_1 \quad \psi_{x1} \quad \psi_{y1} \quad w_2 \quad \psi_{x2} \quad \psi_{y2} \quad w_3 \quad \psi_{x3} \quad \psi_{y3} \quad w_4 \quad \psi_{x4} \quad \psi_{y4}]^T$$

According to the analytical solutions (14-13) of the thick plate theory, the first 12 low-order terms of the analytical solutions are taken as the trial functions. The

element displacements w , ψ_x and ψ_y can be expressed by

$$\begin{Bmatrix} w \\ \psi_x \\ \psi_y \end{Bmatrix} = \begin{bmatrix} 1 & x & y & x^2 - 2\frac{D}{C} & xy & y^2 - 2\frac{D}{C} & x^3 - 6\frac{D}{C}x & x^2y - 2\frac{D}{C}y \\ 0 & 1 & 0 & 2x & y & 0 & 3x^2 & 2xy \\ 0 & 0 & 1 & 0 & x & 2y & 0 & x^2 \\ xy^2 - 2\frac{D}{C}x & y^3 - 6\frac{D}{C}y & x^3y - 6\frac{D}{C}xy & xy^3 - 6\frac{D}{C}xy \\ y^2 & 0 & 3x^2y & y^3 \\ 2xy & 3y^2 & x^3 & 3xy^2 \end{bmatrix} \boldsymbol{\lambda} \quad (14-18)$$

where D is the bending stiffness of the plate; C is the shear stiffness of the plate; $\boldsymbol{\lambda}$ is a vector composed of 12 parameters.

The corresponding curvature fields $\boldsymbol{\kappa} = [\kappa_x \quad \kappa_y \quad 2\kappa_{xy}]^T$ are

$$\begin{Bmatrix} \kappa_x \\ \kappa_y \\ 2\kappa_{xy} \end{Bmatrix} = \begin{bmatrix} 0 & 0 & 0 & -2 & 0 & 0 & -6x & -2y & 0 & 0 & -6xy & 0 \\ 0 & 0 & 0 & 0 & 0 & -2 & 0 & 0 & -2x & -6y & 0 & -6xy \\ 0 & 0 & 0 & 0 & -2 & 0 & 0 & -4x & -4y & 0 & -6x^2 & -6y^2 \end{bmatrix} \boldsymbol{\lambda} \quad (14-19)$$

And, the corresponding shear strain fields $\boldsymbol{\gamma} = [\gamma_{xz} \quad \gamma_{yz}]^T$ are

$$\begin{Bmatrix} \gamma_{xz} \\ \gamma_{yz} \end{Bmatrix} = \begin{bmatrix} 0 & 0 & 0 & 0 & 0 & 0 & -6\frac{D}{C} & 0 & -2\frac{D}{C} & 0 & -6\frac{D}{C}y & -6\frac{D}{C}y \\ 0 & 0 & 0 & 0 & 0 & 0 & 0 & -2\frac{D}{C} & 0 & -6\frac{D}{C} & -6\frac{D}{C}x & -6\frac{D}{C}x \end{bmatrix} \boldsymbol{\lambda} \quad (14-20)$$

The following 12 nodal and line conforming conditions

$$\left. \begin{aligned} (w - \tilde{w})_i &= 0 && \text{(for each node } i = 1,2,3,4) \\ (\psi_s - \tilde{\psi}_s)_i &= 0 && \text{(for the end point } i \text{ of each side } d_{ij}: i = 1,2,3,4) \\ \int_{d_{ij}} (\psi_n - \tilde{\psi}_n) ds &= 0 && \text{(for each side } ij = 12,23,34,41) \end{aligned} \right\} \quad (14-21)$$

are employed, in which n and s are the normal and tangential directions of each element side; \tilde{w} , $\tilde{\psi}_s$ and $\tilde{\psi}_n$ are the displacements along the element boundary. Thus, the 12 parameters in $\boldsymbol{\lambda}$ can be obtained and expressed in terms of \mathbf{q}^e . This element is denoted as ATF-MQ.

14.5.2 Numerical Examples

Example 14.4 The central deflection of the simply-supported and clamped square plates under uniformly distributed load.

Two thickness-span cases, ① thick plate ($h/L = 0.3$) and ② thin plate ($h/L = 0.003$), are considered. The central deflection w_C is computed by the element ATF-MQ using different mesh density. Its relative precision is given in Table 14.4.

Table 14.4 The relative precision for the central deflection w_C of square plate (ATF-MQ)

Mesh	Thick plate ($h/L = 0.3$)		Thin plate ($h/L = 0.003$)	
	Simply-supported	Clamped	Simply-supported	Clamped
2×2	1.009	1.035	1.011	1.009
4×4	1.002	1.006	1.003	1.006
8×8	1.0005	0.9998	1.0007	1.003
16×16	1.0002	0.9984	1.0001	1.002
32×32	1.0001	0.9980	1.0001	1.002

From Table 14.4, it can be seen that the element ATF-MQ exhibits excellent performance for both thick and thin plates, and no shear locking happens. For the simply-supported and clamped square plates, high accuracy can be obtained. When a 8×8 mesh is used, all relative errors are below 0.3%.

Example 14.5 The central deflection and bending moment of the simply-supported and clamped circular plates under uniformly distributed load.

The element ATF-MQ is used for this computation by using two meshes given by Fig. 6.14 in which the numbers of the elements are 12 and 48, respectively. The thickness-radius ratios h/R of the circular plate vary from 10^{-30} to 0.35. And, the relative precisions for the central deflection and bending moment are listed in Table 14.5.

From Table 14.5, it can be seen again that, the element ATF-MQ is universal for both thick and thin plates, and no shear locking happens. It provides high precision for both deflection and bending moment. When 48 elements are used, all errors are around or below 1%.

Example 14.6 Sensitivity test for mesh distortion.

The central deflections of the simply-supported and clamped square plates under uniformly distributed load are computed by using two distorted meshes shown in Fig. 14.6. Three distortion parameter cases: $\frac{\Delta}{0.5L} = 0.05, 0.10$ and 0.12 (or 0.20), are considered. The relative precision is given in Table 14.6.

From Table 14.6, it can be seen that, the element ATF-MQ is insensitive to mesh distortion. For various values of the distortion parameter $\frac{\Delta}{L}$, high accuracy can all be obtained.

Table 14.5 The relative precisions for central deflection w_C and bending moment M_C of circular plate (ATF-MQ)

h/R	Central deflection w_C				Central bending moment M_C			
	Simply-supported		Clamped		Simply-supported		Clamped	
	12 elements	48 elements	12 elements	48 elements	12 elements	48 elements	12 elements	48 elements
10^{-30}	1.0103	1.0024	0.9625	0.9898	1.0208	1.0040	1.0137	1.0002
0.001	1.0103	1.0024	0.9625	0.9898	1.0208	1.0040	1.0137	1.0002
0.01	1.0103	1.0024	0.9625	0.9898	1.0207	1.0041	1.0136	1.0003
0.10	1.0100	1.0025	0.9631	0.9905	1.0199	1.0046	1.0107	1.0014
0.15	1.0099	1.0025	0.9648	0.9913	1.0194	1.0047	1.0086	1.0014
0.20	1.0099	1.0026	0.9673	0.9922	1.0190	1.0047	1.0068	1.0011
0.25	1.0098	1.0026	0.9703	0.9930	1.0188	1.0047	1.0053	1.0007
0.30	1.0097	1.0026	0.9732	0.9938	1.0187	1.0046	1.0041	1.0002
0.35	1.0096	1.0025	0.9762	0.9945	1.0186	1.0045	1.0031	0.9997

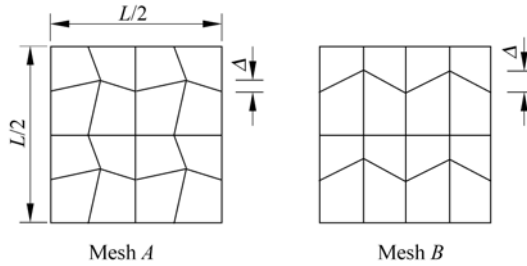


Figure 14.6 Two distorted meshes (for 1/4 square plate)

Table 14.6 The relative precision for central deflection of square plate by using distorted meshes (ATF-MQ)

Mesh	Distortion parameter $\frac{\Delta}{0.5L}$	Clamped		Simply-supported	
		Thickness-span ratio $h/L = 0.1$	Thickness-span ratio $h/L = 0.001$	Thickness-span ratio $h/L = 0.1$	Thickness-span ratio $h/L = 0.001$
Mesh A	0.05	1.0246	1.0152	1.0013	1.0093
	0.10	1.0500	1.0480	1.0074	1.0079
	0.12	1.0559	1.0573	1.0092	1.0071
Mesh B	0.05	1.0186	1.0091	1.0001	1.0096
	0.10	1.0348	1.0284	0.9958	1.0078
	0.20	1.0567	1.0481	1.0075	0.9942

14.6 Analytical Trial Function Method for Developing a Triangular Thick Plate Element Based on a Thin Plate Element

In this section, the analytical trial function (ATF) method is used to extend the existing Kirchhoff triangular thin plate element to the corresponding Mindlin triangular thick plate element. As an example, the triangular thin plate element GPL, proposed in reference [19], is generalized to a thick/thin plate element GPLM (M denotes the Mindlin plate).

14.6.1 Brief Review of the Triangular Thin Plate Element GPL

This element possesses only 9 DOFs. The element nodal displacement vector is

$$\mathbf{q}^e = [w_1 \quad \psi_{x1} \quad \psi_{y1} \quad w_2 \quad \psi_{x2} \quad \psi_{y2} \quad w_3 \quad \psi_{x3} \quad \psi_{y3}]^T \quad (14-22)$$

According to the ATF method, the element deflection and rotation fields are assumed to be

$$\left. \begin{aligned} w &= \mathbf{F}\boldsymbol{\lambda} \\ \psi_x &= \frac{\partial w}{\partial x} = \frac{\partial}{\partial x} \mathbf{F}\boldsymbol{\lambda} \\ \psi_y &= \frac{\partial w}{\partial y} = \frac{\partial}{\partial y} \mathbf{F}\boldsymbol{\lambda} \end{aligned} \right\} \quad (14-23)$$

in which $\boldsymbol{\lambda}$ contains 9 unknown coefficients; and \mathbf{F} is composed of 9 trial functions

$$\mathbf{F} = \left[\begin{array}{ccccccccc} L_1 & L_2 & L_3 & L_1L_2 & L_2L_3 & L_3L_1 & L_1\left(L_1 - \frac{1}{2}\right) & (L_1 - 1) \\ & & & & & & L_2\left(L_2 - \frac{1}{2}\right) & (L_2 - 1) & L_3\left(L_3 - \frac{1}{2}\right) & (L_3 - 1) \end{array} \right] \quad (14-24)$$

Since the highest order of these trial functions F is cubic, thereby, they satisfy the bi-harmonic Eq. (14-12). For the thin plate theory, these trial functions are all the analytical trial functions.

For solving the 9 unknown coefficients, 9 conforming conditions are selected as follows

$$(w - \bar{w})_i = 0 \quad (\text{for each corner node } i = 1, 2, 3) \quad (14-25a)$$

$$\int_{d_j} (w - \bar{w}) ds = 0 \quad (\text{for each side } d_j = d_1, d_2, d_3) \quad (14-25b)$$

$$\int_{d_j} (\psi_n - \bar{\psi}_n) ds = 0 \quad (\text{for each side } d_j = d_1, d_2, d_3) \quad (14-25c)$$

Then, λ can be derived from the above equations, and can be expressed in terms of q^e

$$\lambda = Pq^e \quad (14-26)$$

Substituting the above equation back into Eq. (14-23), the element displacement fields and its shape functions can be determined. And then, the element stiffness matrix K^e can be derived following the conventional procedure.

14.6.2 Generalization of the Element GPL to the Triangular Thick Plate Element GPLM

In the thick plate element, q^e is still given by Eq. (14-22).

Based on the analytical solutions (14-13) of the thick plate theory, the displacement fields (14-23) of the element GPL are generalized to the following forms

$$\left. \begin{aligned} w &= \left(\mathbf{F} - \frac{D}{C} \nabla^2 \mathbf{F} \right) \boldsymbol{\lambda} \\ \psi_x &= \frac{\partial}{\partial x} \mathbf{F} \boldsymbol{\lambda} \\ \psi_y &= \frac{\partial}{\partial y} \mathbf{F} \boldsymbol{\lambda} \end{aligned} \right\} \quad (14-27)$$

The expressions in the above equation are the displacement fields of the thick plate element assumed according to the ATF method. Thus, from the above equation, the shear strains of the thick plate element can be obtained as follows

$$\left. \begin{aligned} \gamma_x &= \frac{\partial w}{\partial x} - \psi_x = -\frac{D}{C} \frac{\partial}{\partial x} \nabla^2 \mathbf{F} \boldsymbol{\lambda} \\ \gamma_y &= \frac{\partial w}{\partial y} - \psi_y = -\frac{D}{C} \frac{\partial}{\partial y} \nabla^2 \mathbf{F} \boldsymbol{\lambda} \end{aligned} \right\} \quad (14-28)$$

It can be seen that, when the plate becomes thinner, Eq. (14-27) will degenerate to be Eq. (14-23) of the thin plate element, and Eq. (14-28) will degenerate to be

$$\gamma_x = 0, \quad \gamma_y = 0 \quad (14-29)$$

In order to solve the unknown coefficients in λ , the conforming conditions (14-25a,b,c) for the thin plate element are still used, in which the original

displacement \bar{w} along the element boundary should be replaced by the boundary displacement \bar{w}^* of the thick plate element

$$\left. \begin{aligned} (\bar{w} - \bar{w}^*)_i &= 0 \quad (\text{for each corner node } i = 1, 2, 3) \\ \int_{d_j} (\bar{w} - \bar{w}^*) ds &= 0 \quad (\text{for each side } d_j = d_1, d_2, d_3) \\ \int_{d_j} (\psi_n - \bar{\psi}_n) ds &= 0 \quad (\text{for each side } d_j = d_1, d_2, d_3) \end{aligned} \right\} \quad (14-30)$$

Then, we can obtain

$$\lambda = P^* q^e \quad (14-31)$$

When the plate becomes thinner, Eqs. (14-30) and (14-31) will degenerate to be Eqs. (14-25) and (14-26) which are used for the thin plate element.

The main procedure for the generalization of the element GPL to the element GPLM has been described above. This generalization can be performed conveniently.

By the comparison of the new and old elements, it can be seen that their derivation procedures are the same, and formulae in each step are also similar. The key step in this procedure is the assumption of displacement fields according to the analytical trial function method, in which Eq. (14-23) of the original element is replaced by Eq. (14-27) of the new element. In these two equations, except that there is a $-\frac{D}{C}\nabla^2 F\lambda$ term in the deflection expression of Eq. (14-27),

the other expressions are exactly the same. Only one term is different, so the new and old elements are quite similar in form.

However, although only one term is different, the effects of this term $\left(-\frac{D}{C}\nabla^2 F\lambda\right)$ is very pivotal—By this term, the shear strains can be introduced into the new thick plate element; and also by this term, the shear locking phenomenon of the new thick plate element can be successfully eliminated.

Though the method proposed in this section is described by taking the element GPL as an example, in fact, it can also be used to generalize other existing triangular and quadrilateral thin plate elements to the corresponding thick/thin elements, as long as the trial functions for the deflections of these existing thin plate elements are the analytical trial functions of thin plate theory, i.e., should be the bi-harmonic functions.

There are several successful schemes that can generalize the thin plate element to thick/thin one. What is introduced here is only one of them, and can be called as the analytical trial function (ATF) method. Another scheme is the rational interpolation technique in which the shear strain fields are directly introduced

into a thin plate (refer to Sects. 8.5 and 8.6). The triangular thick/thin element TCGC given in Sect. 8.6 is just derived by the latter scheme. When the plate becomes thinner, the element TCGC will also degenerate to be the element GPL. (It can be seen that the elements GPLM and TCGC are the two thick/thin plate elements generalized from the element GPL by the above two approaches.)

14.6.3 Numerical Examples

Example 14.7 Simply-supported and clamped square plates subjected to uniform load q .

As shown in Fig. 14.7, due to the symmetry, only a quarter of the plate is considered. The results obtained by four 8×8 meshes are listed in Table 14.7. The side length of the square plate is L , The Poisson's ratio $\mu = 0.3$.

From Table 14.7, it can be seen that

- (1) when the plate becomes thinner, the thin plate element GPL-T9 is the final limit, thus, no shear locking will happen;
- (2) the rational results can all be provided when the thickness-span ratio h/L varies from 10^{-30} to 0.35;
- (3) the present element is insensitive to mesh distortion. For the four meshes I, II, III and IV, errors given in Table 14.7 are all very small.

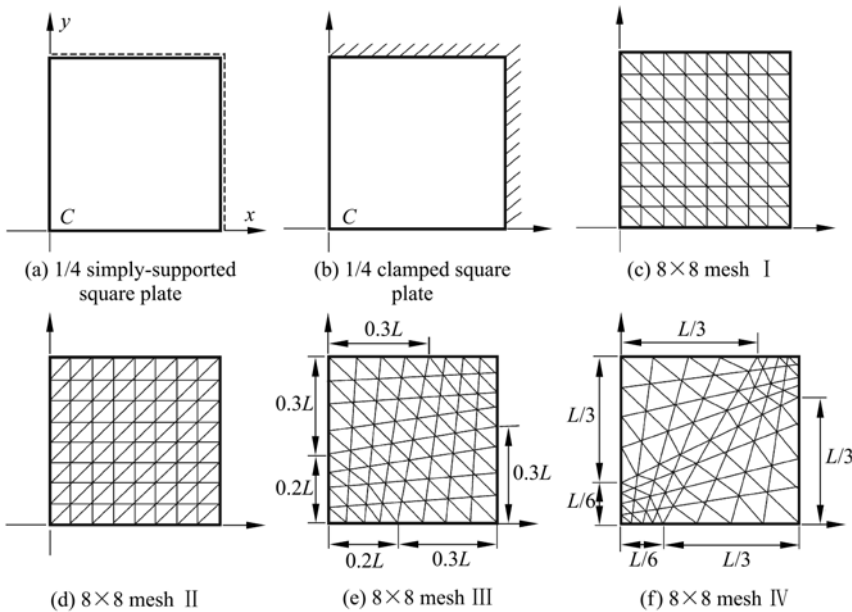


Figure 14.7 Simply-supported and clamped square plates

Table 14.7 The central deflection $w_c / \left(\frac{qL^4}{100D} \right)$ of square plate under uniform load (four 8×8 meshes I, II, III and IV are used)

h/L	Simply-supported square plate					Clamped square plate				
	Mesh I	Mesh II	Mesh III	Mesh IV	Analytical solution	Mesh I	Mesh II	Mesh III	Mesh IV	Analytical solution
10^{-30}	0.4057 (99.88%)	0.4050 (99.70%)	0.4059 (99.93%)	0.4058 (99.90%)	0.4062	0.1247 (98.58%)	0.1261 (99.68%)	0.1252 (98.97%)	0.1254 (99.13%)	0.1265
0.01	0.4058 (99.85%)	0.4051 (99.68%)	0.4060 (99.90%)	0.4060 (99.90%)	0.4064	0.1249 (98.74%)	0.1263 (99.84%)	0.1255 (99.21%)	0.1256 (99.29%)	0.1265
0.10	0.4260 (99.70%)	0.4255 (99.58%)	0.4261 (99.72%)	0.4261 (99.72%)	0.4273	0.1480 (98.73%)	0.1502 (100.20%)	0.1494 (99.67%)	0.1492 (99.53%)	0.1499
0.15	0.4519 (99.63%)	0.4520 (99.65%)	0.4522 (99.69%)	0.4523 (99.71%)	0.4536	0.1759 (97.83%)	0.1788 (99.44%)	0.1780 (99.00%)	0.1773 (98.61%)	0.1798
0.20	0.4882 (99.51%)	0.4891 (99.69%)	0.4887 (99.61%)	0.4889 (99.65%)	0.4906	0.2138 (98.66%)	0.2175 (100.37%)	0.2168 (100.05%)	0.2156 (99.49%)	0.2167
0.25	0.5350 (99.46%)	0.5368 (99.80%)	0.5357 (99.59%)	0.5360 (99.65%)	0.5379	0.2616 (97.79%)	0.2665 (99.63%)	0.2658 (99.36%)	0.2639 (98.65%)	0.2675
0.30	0.5921 (99.41%)	0.5951 (99.92%)	0.5931 (99.58%)	0.5936 (99.66%)	0.5956	0.3195 (99.01%)	0.3257 (100.93%)	0.3251 (100.74%)	0.3224 (99.91%)	0.3227
0.35	0.6595 (99.31%)	0.6640 (99.98%)	0.6610 (99.53%)	0.6616 (99.62%)	0.6641	0.3876 (98.10%)	0.3953 (100.05%)	0.3949 (99.95%)	0.3911 (98.99%)	0.3951

Note: Numbers in () are percentage precisions.

Example 14.8 Circular plate under uniform load.

Two boundary conditions are considered: soft simply-supported and clamped. As shown in Fig. 14.8, due to the symmetry, only a quarter of the circular plate is computed. The radius of the circular plate $R = 5$; and the Poisson’s ratio $\mu = 0.3$.

Numerical results obtained by the present element GPLM are listed in Tables 14.8 and 14.9. For comparison, the results by the other elements T3BL, T3BL(R)^[20], DKMT^[21], DST-BK^[22] and DST-BL^[23] are also given.

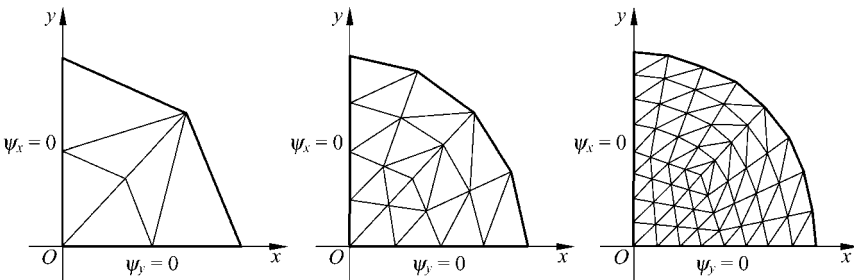


Figure 14.8 Meshes for circular plate

From Table 14.8, it can be seen that, in comparison with the similar elements, the element GPLM can give the best results for the central bending moment of clamped square plate. And, from Table 14.9, it can also be seen that the element GPLM can produce the best answers for the central deflection and bending moment of the simply-supported plate.

Table 14.8 The central deflection $w_c / \left(\frac{qR^4}{D} \right)$ and bending moment M_c / qR^2 of clamped circular plate

	$h/R = 0.002$						$h/R = 0.2$					
	GPLM	T3BL	T3BL (R)	DKMT	DST-BK	DST-BL	GPLM	T3BL	T3BL (R)	DKMT	DST-BK	DST-BL
Central deflection												
6 elements	7.2283	6.0495	9.1192	10.3060	9.8430	10.3060	8.7991	8.0392	10.8377	11.921	11.342	11.951
24 elements	9.0867	8.7750	9.6403	9.9956	9.8551	9.9958	10.7473	10.6006	11.4059	11.703	11.548	11.806
96 elements	9.6038	9.5237	9.7382	9.8748	9.8025	9.8483	11.3344	11.3022	11.5066	11.594	11.554	11.731
Analytical	9.7835						11.5513					
Central bending moment												
6 elements	2.0315	1.2188	1.3304	2.40	2.56	2.40	2.0010	1.2885	1.3296	2.47	2.31	2.43
24 elements	2.0535	1.8187	1.8354	2.17	2.25	2.17	2.0498	1.8258	1.8316	2.22	2.16	2.19
96 elements	2.0383	1.9771	1.9789	2.07	2.09	2.07	2.0317	1.9780	1.9784	2.09	2.07	2.10
Analytical	2.0313											

Table 14.9 The central deflection $w_c / \left(\frac{qR^4}{D} \right)$ and bending moment M_c / qR^2 of simply-supported circular plate

	$h/R = 0.002$						$h/R = 0.2$					
	GPLM	T3BL	T3BL (R)	DKMT	DST-BK	DST-BL	GPLM	T3BL	T3BL (R)	DKMT	DST-BK	DST-BL
Central deflection												
6 elements	40.2358	39.4319	42.2158	37.848	37.391	37.847	41.8163	41.1627	43.9038	39.462	38.888	39.494
24 elements	39.9018	39.6576	40.4609	39.398	39.249	39.397	41.5706	41.4296	42.2235	41.091	40.926	41.185
96 elements	39.8455	39.7848	39.9434	39.729	39.680	39.729	41.5771	41.5555	41.7594	41.473	41.432	41.705
Analytical	39.8315						41.5994					
Central bending moment												
6 elements	5.4548	4.7084	4.7486	5.26	5.43	5.26	5.4238	4.7237	4.7460	5.33	5.27	5.30
24 elements	5.2563	5.0310	5.0380	5.23	5.28	5.23	5.2345	5.0294	5.0342	5.27	5.22	5.25
96 elements	5.1835	5.1242	5.1217	5.18	5.20	5.18	5.1768	5.1239	5.1243	5.20	5.18	5.22
Analytical	5.1563											

References

- [1] Long YQ, Zhi BC, Kuang WQ, Shan J (1982). Sub-region mixed finite element method for the calculation of stress intensity factor. In: He GQ et al. (eds). Proceedings of International Conference on FEM. Science Press, Shanghai, pp738 – 740
- [2] Zhong WX, Ji Z (1996). Rational finite element. Computational Structural Mechanics and Applications 1: 1 – 8 (in Chinese)
- [3] Long YQ, Fu XR (2002) Two generalized conforming quadrilateral thick plate elements based on analytical trial functions. Gong Cheng Li Xue/Engineering Mechanics 19(3): 10 – 15 (in Chinese)
- [4] Fu XR, Long YQ (2002) Generalized conforming quadrilateral plane elements based on analytical trial functions. Gong Cheng Li Xue/Engineering Mechanics 19(4): 12 – 16 (in Chinese)
- [5] MacNeal RH (1989) Toward a defect-free four-noded membrane element. Finite Elements in Analysis and Design 5: 31 – 37
- [6] Long YQ, Fu XR (2002) Generalized conforming elements based on analytical trial functions. In: Proceedings of the Eleventh National Conference on Structural Engineering (Vol. I), plenary lecture. China, Changsha, pp28 – 39 (in Chinese)
- [7] Taylor RL, Beresford PJ, Wilson EL (1976) A non-conforming element for stress analysis. International Journal for Numerical Methods in Engineering 10: 1211 – 1219.
- [8] Pian THH, Sumihara K (1984) Rational approach for assumed stress finite element. International Journal for Numerical Methods in Engineering 20: 1685 – 1695
- [9] Andelfinger U, Ramm E (1993) EAS-elements for two dimensional, three dimensional, plate and shell structures and their equivalence to HR-elements. International Journal for Numerical Methods in Engineering 36: 1311 – 1337
- [10] Cao YP, Hu N, Yao ZH (2002) Improved EAS elements. Gong Cheng Li Xue/Engineering Mechanics 19(1): 47 – 51 (in Chinese)
- [11] Hu HC (1984) Variational principles of theory of elasticity with applications. Science Press, Beijing
- [12] Zienkiewicz OC, Taylor RL, Too JM (1971) Reduced integration techniques in general of plates and shells. International Journal for Numerical Methods in Engineering 3: 275 – 290
- [13] Hughes TJ, Cohen M, Haroun M (1978) Reduced and selective integration techniques in finite element analysis of plates. Nuclear Engineering and Design 46: 203 – 222
- [14] Soh AK, Long ZF, Cen S (1999) A Mindlin plate triangular element with improved interpolation based on Timoshenko's beam theory. Communications in Numerical Methods in Engineering 15(7): 527 – 532
- [15] Soh AK, Long ZF, Cen S (1999) A new nine dof triangular element for analysis of thick and thin plates. Computational Mechanics 24(5): 408 – 417
- [16] Soh AK, Cen S, Long YQ, Long ZF (2001) A new twelve DOF quadrilateral element for analysis of thick and thin plates. European Journal of Mechanics A/Solids 20(2): 299 – 326

Chapter 14 Analytical Trial Function Method I— Membrane and Plate Bending Element

- [17] Cen S, Long YQ, Yao ZH, Chiew SP (2006) Application of the quadrilateral area coordinate method: a new element for Mindlin-Reissner plate. *International Journal for Numerical Methods in Engineering* 66(1): 1 – 45
- [18] Long ZF, Cen S (2001) *New monograph of finite element method: principle, programming, developments*. China Hydraulic and Water-power Press, Beijing (in Chinese)
- [19] Long YQ, Bu XM, Long ZF, Xu Y (1995) Generalized conforming plate bending elements using point and line compatibility conditions. *Computers & Structures* 55(4): 717 – 728
- [20] Taylor RL, Auricchio F (1993) Linked interpolation for Reissner-Mindlin plate element: part II—a simple triangle. *International Journal for Numerical Methods in Engineering* 36: 3057 – 3066
- [21] Katili I (1993) A new discrete Kirchhoff-Mindlin element based on Mindlin-Reissner plate theory and assumed shear strain fields—Part I: An extended DKT element for thick-plate bending analysis. *International Journal for Numerical Methods in Engineering* 36: 1859 – 1883
- [22] Batoz JL, Katili I (1992) On a simple triangular Reissner/Mindlin plate element based on incompatible modes and discrete constraints. *International Journal for Numerical Methods in Engineering* 35: 1603 – 1632
- [23] Batoz JL, Lardeur P (1989) A discrete shear triangular nine d.o.f. element for the analysis of thick to very thin plates. *International Journal for Numerical Methods in Engineering* 28: 533 – 560

Chapter 15 Analytical Trial Function Method II— Singular Elements with Crack and Notch

Song Cen

Department of Engineering Mechanics, School of Aerospace,
Tsinghua University, Beijing, 100084, China

Zhi-Fei Long

School of Mechanics & Civil Engineering, China University of
Mining & Technology, Beijing, 100083, China

Abstract This chapter continues to discuss the analytical trial function method. Here, the analytical trial function method is applied to develop the singular hybrid elements with crack and notch for the analysis of the crack and notch problems. During the analysis, the singular hybrid element is collocated in the region around the tips of the crack and notch, while the conventional displacement-based elements are used in the periphery region. Furthermore, this chapter also gives detailed discussions on the convergence of the singular element, zero energy mode, and improvement for the iteration solution method of eigenvalues. From the contents of this chapter and the previous chapter, it can be seen that, in the analytical trial function method, analytical and discrete methods can complement each other; and as a result, some challenging problems existing in FEM can be successfully solved.

Keywords finite element, analytical trial function method, singular element, crack, notch.

15.1 Introduction

In this chapter, the analytical trial function method is further applied to construct the singular hybrid elements with crack and notch in the analysis of the crack and notch problems. During the analysis, a kind of coupling mesh is employed: the singular hybrid element is collocated in the region around the tips of the crack and notch, while the conventional displacement-based elements are used in the periphery region.

Though the contents of this chapter are consistent with the sub-region mixed element method reported in Chaps. 12 and 13, however, their emphases are

different. Chaps. 12 and 13 emphasize particularly on the joint existence of the complementary and potential energy regions and on the application of the sub-region mixed variational principle, by which the mixed equations containing both stress and displacement variables are finally established. This chapter emphasizes particularly on the joint existence of the singular hybrid element and the conventional displacement-based elements in one mesh division and on the applications of the analytical trial function method and complementary energy principle, by which the stiffness equations containing only nodal displacements are finally obtained. That is to say, both approaches belong to the sub-region mixed element method, one emphasizes particularly on the sub-region mixture of the stress-based and displacement-based elements, and leads to the mixed equations; the other emphasizes particularly on the sub-region mixture of the hybrid and displacement-based elements, and leads to the stiffness equations.

Furthermore, this chapter will give detailed discussions on the convergence of the singular element, zero energy mode, and improvement for the iteration solution method of the eigenvalues.

15.2 The Basic Analytical Solutions of the Plane Crack Problem

According to Williams's theoretical analysis of the stress field at a plane crack tip^[1], the analytical solutions of stresses, which can satisfy the equilibrium equations and boundary conditions, can be derived from the bi-harmonic stress function.

15.2.1 The Basic Analytical Solutions for the Symmetric Problem of Mode I

A structure with a crack shown in Fig. 15.1 is considered. And, the coordinate system used here is also plotted in the figure (note: it is different from that given in Fig. 12.3, so the expressions of the analytical solutions for stresses are also different from those given by Sect. 12.3). In the polar coordinate system, the

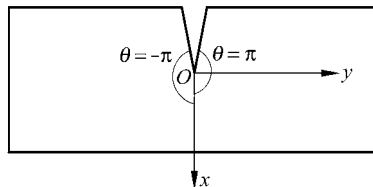


Figure 15.1 A structure with a crack

symmetric part of the bi-harmonic stress functions which satisfy equation $\nabla^4 \phi = 0$ can be written as

$$\phi = r^{\frac{K}{2}+1} \left[A_K \cos\left(\frac{K}{2}-1\right)\theta + B_K \cos\left(\frac{K}{2}+1\right)\theta \right] \quad (K = 1, 2, \dots) \quad (15-1)$$

And, the corresponding stresses are

$$\left. \begin{aligned} \sigma_r &= \frac{1}{r^2} \frac{\partial^2 \phi}{\partial \theta^2} + \frac{1}{r} \frac{\partial \phi}{\partial r} \\ \sigma_\theta &= \frac{\partial^2 \phi}{\partial r^2} \\ \tau_{r\theta} &= \frac{1}{r^2} \frac{\partial \phi}{\partial \theta} - \frac{1}{r} \frac{\partial^2 \phi}{\partial \theta \partial r} = -\frac{\partial}{\partial r} \left(\frac{1}{r} \frac{\partial \phi}{\partial \theta} \right) \end{aligned} \right\} \quad (15-2)$$

i.e.,

$$\left. \begin{aligned} \sigma_r &= r^{\frac{K}{2}-1} \left(-\frac{K}{2} \right) \left[A_K \left(\frac{K}{2}-3 \right) \cos\left(\frac{K}{2}-1\right)\theta + B_K \left(\frac{K}{2}+1 \right) \right. \\ &\quad \left. \times \cos\left(\frac{K}{2}+1\right)\theta \right] \\ \sigma_\theta &= r^{\frac{K}{2}-1} \frac{K}{2} \left(\frac{K}{2}+1 \right) \left[A_K \cos\left(\frac{K}{2}-1\right)\theta + B_K \cos\left(\frac{K}{2}+1\right)\theta \right] \\ \tau_{r\theta} &= r^{\frac{K}{2}-1} \frac{K}{2} \left[A_K \left(\frac{K}{2}-1 \right) \sin\left(\frac{K}{2}-1\right)\theta + B_K \left(\frac{K}{2}+1 \right) \sin\left(\frac{K}{2}+1\right)\theta \right] \end{aligned} \right\} \quad (K = 1, 2, \dots) \quad (15-3)$$

For the surface of the crack with free boundary (Fig. 15.1), we have

$$\sigma_\theta \Big|_{\theta=\pm\pi} = \tau_{r\theta} \Big|_{\theta=\pm\pi} = 0 \quad (15-4)$$

From the last two expressions of Eq. (15-3), we can obtain

$$A_K \cos\left(\frac{K}{2}-1\right)\pi + B_K \cos\left(\frac{K}{2}+1\right)\pi = 0 \quad (15-5)$$

$$A_K \left(\frac{K}{2}-1 \right) \sin\left(\frac{K}{2}-1\right)\pi + B_K \left(\frac{K}{2}+1 \right) \sin\left(\frac{K}{2}+1\right)\pi = 0 \quad (15-6)$$

If A_K and B_K are both nonzero, the determinant of coefficient matrix should be zero, i.e.,

$$\begin{aligned}
 |A| &= \left(\frac{K}{2} + 1\right) \sin\left(\frac{K}{2} + 1\right) \pi \cos\left(\frac{K}{2} - 1\right) \pi - \left(\frac{K}{2} - 1\right) \sin\left(\frac{K}{2} - 1\right) \pi \cos\left(\frac{K}{2} + 1\right) \pi \\
 &= \left(\frac{K}{2} + 1\right) [\sin K\pi + \sin 2\pi] - \left(\frac{K}{2} - 1\right) [\sin K\pi - \sin 2\pi] \\
 &= 2 \left[\sin K\pi + \frac{K}{2} \sin 2\pi \right] = 0
 \end{aligned} \tag{15-7}$$

When K is an arbitrary integer, Eq. (15-7) is an identical equation. From Eqs. (15-5) and (15-6), we can obtain

$$B_K = -\frac{A_K}{K/2 + 1} \left[(-1)^K + \frac{K}{2} \right] \tag{15-8}$$

Let

$$A_K = \beta_{2K-1} \quad (K = 1, 2, \dots) \tag{15-9}$$

then the basic analytical solutions for the stresses of the symmetric part can be written as

$$\left\{ \begin{array}{l} \sigma_r \\ \sigma_\theta \\ \tau_{r\theta} \end{array} \right\} = \beta_{2K-1} \left\{ \begin{array}{l} r^{\frac{K}{2}-1} \frac{K}{2} \left[\left(3 - \frac{K}{2}\right) \cos\left(\frac{K}{2} - 1\right) \theta + \left(\frac{K}{2} + (-1)^K\right) \cos\left(\frac{K}{2} + 1\right) \theta \right] \\ r^{\frac{K}{2}-1} \frac{K}{2} \left[\left(\frac{K}{2} + 1\right) \cos\left(\frac{K}{2} - 1\right) \theta - \left(\frac{K}{2} + (-1)^K\right) \cos\left(\frac{K}{2} + 1\right) \theta \right] \\ r^{\frac{K}{2}-1} \frac{K}{2} \left[\left(\frac{K}{2} - 1\right) \sin\left(\frac{K}{2} - 1\right) \theta - \left(\frac{K}{2} + (-1)^K\right) \sin\left(\frac{K}{2} + 1\right) \theta \right] \end{array} \right\} \tag{15-10}$$

($K = 1, 2, \dots$)

15.2.2 The Basic Analytical Solutions for the Antisymmetric Problem of Mode II

In the polar coordinate system, the antisymmetric part of the bi-harmonic stress functions which satisfy equation $\nabla^4 \phi = 0$ can be written as

$$\phi = r^{\frac{K}{2}+1} \left[C_K \sin\left(\frac{K}{2} - 1\right) \theta + D_K \sin\left(\frac{K}{2} + 1\right) \theta \right] \tag{15-11}$$

Similar to the symmetric problem, from the free boundary conditions of the crack surface, we can obtain

$$D_K = -\frac{C_K}{K/2+1} \left[\frac{K}{2} - (-1)^K \right] \quad (15-12)$$

Let

$$C_K = \beta_{2K} \quad (K=1,2,\dots) \quad (15-13)$$

then the basic analytical solutions for the stresses of the antisymmetric part can be written as

$$\begin{Bmatrix} \sigma_r \\ \sigma_\theta \\ \tau_{r\theta} \end{Bmatrix} = \beta_{2K} \begin{Bmatrix} -r^{\frac{K}{2}-1} \frac{K}{2} \left[\left(3 - \frac{K}{2} \right) \sin\left(\frac{K}{2}-1\right)\theta + \left(\frac{K}{2} - (-1)^K \right) \sin\left(\frac{K}{2}+1\right)\theta \right] \\ -r^{\frac{K}{2}-1} \frac{K}{2} \left[\left(\frac{K}{2} + 1 \right) \sin\left(\frac{K}{2}-1\right)\theta - \left(\frac{K}{2} - (-1)^K \right) \sin\left(\frac{K}{2}+1\right)\theta \right] \\ -r^{\frac{K}{2}-1} \frac{K}{2} \left[\left(1 - \frac{K}{2} \right) \cos\left(\frac{K}{2}-1\right)\theta + \left(\frac{K}{2} - (-1)^K \right) \cos\left(\frac{K}{2}+1\right)\theta \right] \end{Bmatrix} \quad (K=1,2,\dots) \quad (15-14)$$

15.2.3 The Stress Field Subspace and the Stress Intensity Factor

By selecting the first M terms of Eqs. (15-10) and (15-14), a stress field subspace with $2M$ stress parameters is then established. It can be denoted as

$$\begin{Bmatrix} \sigma_r \\ \sigma_\theta \\ \tau_{r\theta} \end{Bmatrix} = \mathbf{S} \begin{Bmatrix} \beta_1 \\ \vdots \\ \beta_{2M} \end{Bmatrix} \quad (15-15)$$

where \mathbf{S} is the matrix of the basic analytical solutions for stresses, which is determined by Eqs. (15-10) and (15-14).

In Eq. (15-14), when $K=2$, the stress vector is a zero vector, this term will disappear in the formulations of the stress fields.

The stress intensity factor K_I of mode I is

$$K_I = \sqrt{2\pi} \lim_{r \rightarrow 0} r^{1/2} \sigma_\theta |_{\theta=0} = \sqrt{2\pi} \beta_1 \quad (15-16)$$

where β_1 is the first stress parameter in Eq. (15-10).

The stress intensity factor K_{II} of mode II is

$$K_{II} = \sqrt{2\pi} \lim_{r \rightarrow 0} r^{1/2} \tau_{r\theta} |_{\theta=0} = -\sqrt{2\pi} \beta_2 \quad (15-17)$$

where β_2 is the first stress parameter in Eq. (15-14).

15.3 Element ATF-MS with Crack Formulated by the Analytical Trial Function Method

An element with crack is shown in Fig. 15.2. The crack surface $\theta = \pi$ and $\theta = -\pi$ are free boundaries. The outer boundary of the element contains n nodes, and there are $2n$ DOFs. The element nodal displacement vector \mathbf{q}^e is

$$\mathbf{q}^e = [u_1 \quad v_1 \quad u_2 \quad v_2 \quad \cdots \quad u_n \quad v_n]^T \quad (15-18)$$

The element stress fields are given by Eq. (15-15), in which \mathcal{S} is a combination of the basic stress analytical solutions at the crack tip of modes I and II, and satisfies the equilibrium differential equations and stress boundary conditions of the crack surface. The stress parameters are

$$\boldsymbol{\beta} = [\beta_1 \quad \beta_2 \quad \cdots \quad \beta_{2M}]^T \quad (15-19)$$

Here, the element stiffness matrix will be derived according to the minimum complementary energy principle.

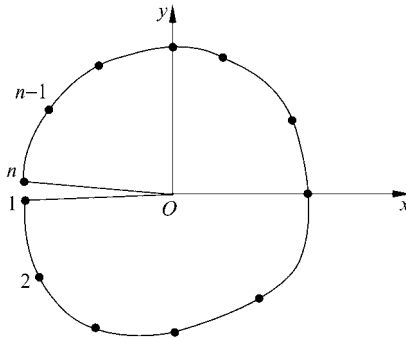


Figure 15.2 An element with crack

The complementary energy functional of the element with crack is

$$\Pi_c = U_c - H \quad (15-20)$$

where U_c is the strain complementary energy of the element; $-H$ is the complementary energy of the boundary displacements \mathbf{q}^e .

The strain complementary energy is

$$U_c = \frac{1}{2} \iint_{\Omega} \boldsymbol{\sigma}^T \mathbf{D}^{-1} \boldsymbol{\sigma} h dA \quad (15-21)$$

where \mathbf{D} is the elastic matrix

$$\mathbf{D}^{-1} = \frac{1}{E'} \begin{bmatrix} 1 & -\mu' & 0 \\ -\mu' & 1 & 0 \\ 0 & 0 & 2(1 + \mu') \end{bmatrix} \quad (15-22)$$

For the plane stress problem

$$E' = E, \quad \mu' = \mu \quad (15-23)$$

and for the plane strain problem

$$E' = E/(1 - \mu^2), \quad \mu' = \mu/(1 - \mu) \quad (15-24)$$

where E is the Young's modulus; μ is the Poisson's ratio.

Substitution of Eq. (15-15) into Eq. (15-21) yields

$$U_c = \frac{1}{2} \boldsymbol{\beta}^T \mathbf{V} \boldsymbol{\beta} \quad (15-25)$$

where

$$\mathbf{V} = \iint_{\Omega} \mathbf{S}^T \mathbf{D}^{-1} \mathbf{S} h dA \quad (15-26)$$

As to the complementary energy of the boundary displacements, we have

$$H = \int_r (T_x \bar{u} + T_y \bar{v}) h ds \quad (15-27)$$

where \bar{u} and \bar{v} are the element boundary displacements; T_x and T_y are the element boundary tractions

$$\begin{Bmatrix} T_x \\ T_y \end{Bmatrix} = \mathbf{L} \mathbf{S} \boldsymbol{\beta} \quad (15-28)$$

When the direction of the boundary outer normal is consistent with r -direction, the direction cosine matrix \mathbf{L} will be

$$\mathbf{L} = \begin{bmatrix} \cos \theta & 0 & -\sin \theta \\ \sin \theta & 0 & \cos \theta \end{bmatrix} \quad (15-29)$$

When an angle γ exists between boundary outer normal and r , \mathbf{L} will be

$$\mathbf{L} = \begin{bmatrix} \cos \theta \cos \gamma & \sin \theta \sin \gamma & -(\sin \theta \cos \gamma + \cos \theta \sin \gamma) \\ \sin \theta \cos \gamma & -\cos \theta \sin \gamma & \cos \theta \cos \gamma - \sin \theta \sin \gamma \end{bmatrix} \quad (15-30)$$

The boundary displacements can be determined by \mathbf{q}^e and its shape function $\bar{\mathbf{N}}$

$$\bar{\mathbf{u}} = \bar{\mathbf{N}} \mathbf{q}^e \quad (15-31)$$

Equation (15-27) can be written as

$$H = \beta^T Hq^e \tag{15-32}$$

where

$$H = \int_r S^T L^T \bar{N} h ds \tag{15-33}$$

Substitution of Eqs. (15-25) and (15-32) into the expression (15-20) of the complementary energy yields

$$\Pi_c = \frac{1}{2} \beta^T V \beta - \beta^T Hq^e \tag{15-34}$$

From the stationary condition of the complementary energy $\delta \Pi_c = 0$, we can obtain

$$\beta = V^{-1} Hq^e \tag{15-35}$$

Finally, the element stiffness matrix can be derived

$$K^e = H^T V^{-1} H \tag{15-36}$$

This element is denoted as ATF-MS.

15.4 Error Analysis of Element ATF-MS with Crack

A cracked plate subjected to tension load is shown in Fig. 15.3. Its stress intensity factor K_I has been calculated by the singular element ATF-MS, and the corresponding analysis of the convergence is also given in reference [2]. The dimensions of the plate $b=2$ and $w=1$; the load intensity at two sides $q=1$; the length of the crack $a=0.5$; the Young's modulus $E=0.21 \times 10^7$; and the Poisson's ratio $\mu=0.3$. A plane strain state is considered for this example.

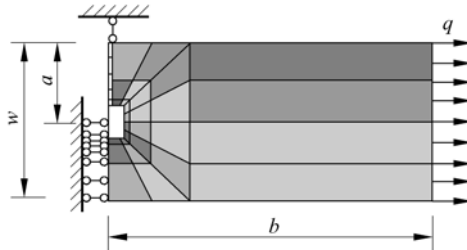


Figure 15.3 The sub-region coupled mesh of a cracked plate subjected to tension load

The mesh used is also plotted in Fig. 15.3: a singular element ATF-MS is located at the tip of the crack; around this singular element, the mesh is composed of layer-by-layer annularly distributed displacement-based elements (isoparametric element Q8), which are denser near the crack and coarser far away from the crack. In this figure, the number of the element layers along the radial direction $S_R = 3$; and the number of the element layers along the circumferential direction $4S_\theta = 8$.

The shape of the singular element ATF-MS is a square, and its half side length is R . The number of the stress terms contained in the basic analytical solutions is M (only the terms of the symmetric stress state are considered).

Here, the influences on the computational errors of the stress intensity factor K_I with variations of the following four parameters

- M —the number of the stress terms used by the singular element
- R —the dimension of the singular element
- $4S_\theta$ —the number of the element layers along the circumferential direction
- S_R —the number of the element layers along the radial direction are studied.

15.4.1 Error Analysis of K_I with Variation of the Number M of Stress Terms ($R = \text{constant}$)

In Fig. 15.4, the longitudinal coordinate e denotes the relative error for the computational results of K_I ; and the horizontal coordinate M denotes the number of the stress terms used by the singular element. Three e - M curves with $\frac{R}{a} = 0.1, 0.3$ and 0.5 , respectively, are plotted. From Fig. 15.4, it can be seen that

- (1) Among the three curves, errors with $\frac{R}{a} = 0.1$ are the smallest.

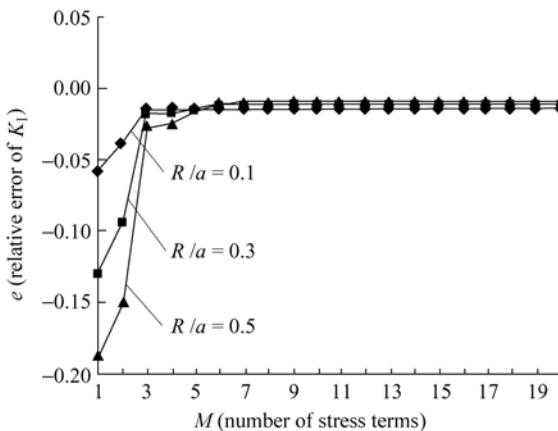


Figure 15.4 e - M curves

(2) With the increasing number M of the stress terms, the computational errors will monotonically decrease. When $M > 4$, the errors are quite small.

15.4.2 Error Analysis of K_I with Variation of the Dimension R of Singular Element ($M = \text{constant}$)

In Fig. 15.5, the longitudinal coordinate e still denotes the relative error for the computational results of K_I ; and the horizontal coordinate $\frac{R}{a}$ denotes the ratio of the dimension R of the singular element to crack length a . Four $e - \frac{R}{a}$ curves with $M = 2, 6, 10$ and 16 , respectively, are plotted. From Fig. 15.5, it can be seen that

(1) among the four curves, errors with $M = 2$ (only the first two stress terms are used) are the highest. With the increasing number M of the stress terms, errors will decrease.

(2) when $M \geq 6$, if the ratio $\frac{R}{a}$ varies within the range $0.03 \sim 0.3$, the computational values will tend to be stable. When $\frac{R}{a} < 0.03$, since the dimension of the singular element is too small, those adjacent displacement-based elements will be distorted, thereby, destabilization may happen in the computational results.

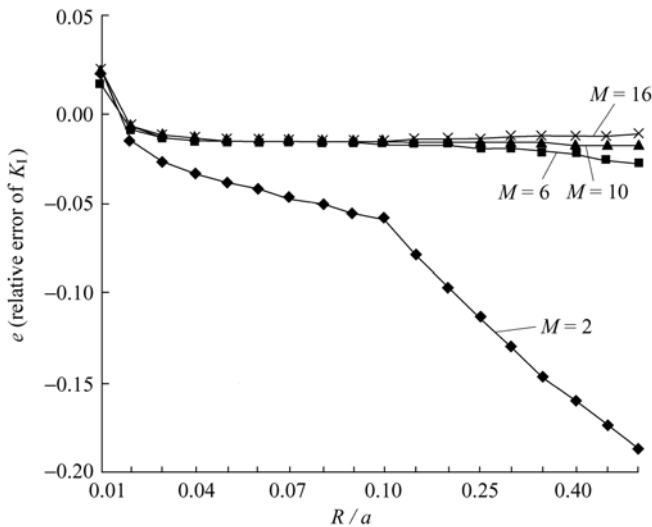


Figure 15.5 $e - \frac{R}{a}$ curves

15.4.3 Error Analysis of K_I with Variation of the Number S_R of Element Layers along the Radial Direction ($4S_\theta = 4$)

In Fig. 15.6, the longitudinal coordinate denotes the computational value of the stress intensity factor K_I ; and the horizontal coordinate denotes the ratio $\frac{R}{a}$. Six curves with $S_R = 1, 2, 3, 4, 6$ and 10 , respectively, are plotted (the number of the element layers along the circumferential direction $4S_\theta = 4$). From Fig. 15.6, it can be seen that

- (1) Among the six curves, errors with $S_R = 1$ are the highest. When S_R increases to 10 , the computational results will be quite close to the exact solutions.
- (2) Since the stress fields near the crack tip vary severely along the radial direction, increase of the number S_R of the element layers along radial direction can effectively improve computational accuracy.

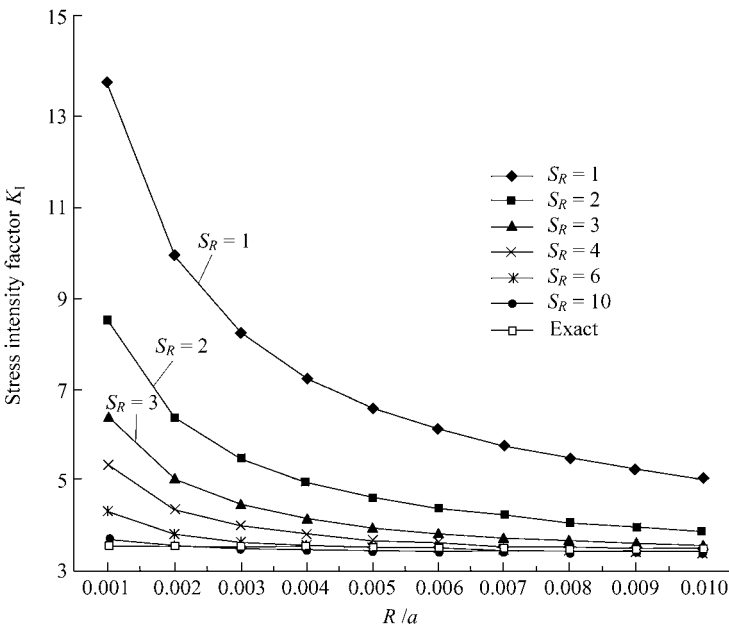


Figure 15.6 Error analysis of K_I with variation of the number S_R of element layers along radial direction

15.4.4 Error Analysis of K_I with Variation of the Number $4S_\theta$ of Element Layers along the Circumferential Direction ($S_R = 1$)

In Fig. 15.7, the longitudinal coordinate denotes the computational value of the

stress intensity factor K_I ; and the horizontal coordinate denotes the ratio $\frac{R}{a}$. Six curves with $S_\theta = 1, 2, 3, 4, 5$ and 6, respectively, are plotted. From Fig. 15.7, it can be seen that by increasing the number $4S_\theta$ of the element layers along the circumferential direction, the precision cannot be improved significantly. This is because the circumferential variations of stress fields near the crack tip are quite gentle.

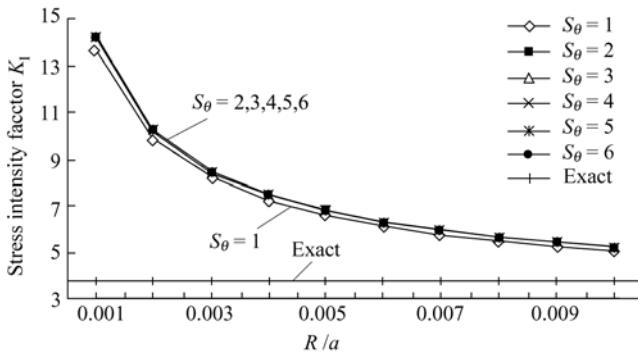


Figure 15.7 Error analysis of K_I with variation of the number $4S_\theta$ of element layers along circumferential direction

15.5 Analysis of Zero Energy Mode in Element and in Structural System

15.5.1 Analysis of Element Zero Energy Mode

Let us consider a plane crack problem. The coupled mesh division shown in Fig. 15.3 is employed for global analysis. Both hybrid singular element and conventional displacement-based element models simultaneously exist in the sub-region mesh, and are coupled with each other.

Assume that the stress expressions (15-15) of the hybrid stress element contains $2M$ stress parameters $\beta_i (i = 1, 2, \dots, 2M)$, and element energy is expressed by Eq. (15-34). Thereby, this element contains $2M$ independent stress (strain) modes, and the energy Π_c corresponding to each mode is nonzero and called as nonzero energy mode.

Assume that there are n nodes on the boundary of the hybrid singular element, so the element possesses $2n$ DOFs. Since there are $2M$ nonzero energy modes, the element has $2n - 2M$ zero energy modes. Among these $2n - 2M$ zero energy

modes, except r rigid body displacements (for plane element, $r=3$), the other zero energy modes are called as spurious zero energy modes.

Let z be the number of the element zero energy modes, and z_1 be the number of the spurious zero energy modes. Then, we have

$$\left. \begin{aligned} z &= 2n - 2M \\ z_1 &= z - r = 2n - 2M - r \end{aligned} \right\} \quad (15-37)$$

From the above equation, it can be seen that by properly increasing the number $2M$ of the stress terms, the number z_1 of the spurious zero energy mode can be reduced, it even becomes negative. (negative z_1 denotes that the number of the stress terms exceeds the lowest number which makes $z_1 = 0$)

If there are no spurious zero energy mode existing in the element, the number $2M$ of the stress terms should be not less than $2n - r$:

$$2M \geq 2n - r \quad (15-38)$$

In order to make further discussions on the element spurious zero energy mode, a brief introduction for the matrix eigenvalue problem is firstly given as follows.

15.5.2 Analysis of the Eigenvalues in Matrix

Let A be a n -order square matrix.

If there is a number λ satisfying

$$Aq = \lambda q \quad (15-39)$$

in which q is a n -order nonzero vector, then, λ is called the eigenvalue (eigenroot) of matrix A ; and q is the eigenvector corresponding to the eigenvalue λ . The eigenvalue λ and its corresponding eigenvector q are called characteristic pair.

The eigenmatrix of matrix A is defined by

$$A - \lambda I = \begin{bmatrix} a_{11} - \lambda & a_{12} & \cdots & a_{1n} \\ a_{21} & a_{22} - \lambda & \cdots & a_{2n} \\ \vdots & \vdots & \vdots & \vdots \\ a_{n1} & a_{n2} & \cdots & a_{nn} - \lambda \end{bmatrix} \quad (15-40)$$

in which I is the n -order identity matrix.

The characteristic equation of matrix A is defined by

$$|A - \lambda I| = 0 \quad (15-41)$$

The left side of the above equation is the determinant of the eigenmatrix, which is called as eigenpolynomial, and denoted by

$$\varphi(\lambda) = |A - \lambda I| \quad (15-42)$$

The n roots $\lambda_1, \lambda_2, \dots, \lambda_n$ of the characteristic equation $\varphi(\lambda) = 0$ are the n eigenvalues of matrix A .

The nonzero solution \mathbf{q} of the homogeneous equation

$$(A - \lambda_i I)\mathbf{q} = \mathbf{0} \quad (15-43)$$

is the eigenvector corresponding to the eigenvalue λ_i of matrix A .

These eigenvalues and eigenvectors possess the following features:

- (1) The eigenvalues of real symmetric matrix are all real number.
- (2) The sum of n eigenvalues of n -order square matrix A equals the trace of A , i.e.,

$$\lambda_1 + \lambda_2 + \dots + \lambda_n = a_{11} + a_{22} + \dots + a_{nn} \quad (15-44)$$

(3) The product of n eigenvalues of n -order square matrix A equals the determinant of A

$$\lambda_1 \lambda_2 \dots \lambda_n = |A| \quad (15-45)$$

Therefore, the necessary and sufficient condition of that matrix is invertible can also be stated as: all eigenvalues of A are nonzero.

(4) If λ_i is a simple root of the characteristic equation, there will be only one linearly independent eigenvector corresponding to λ_i ; If λ_i is a k multiple root of the characteristic equation, there will be k linearly independent eigenvectors corresponding to λ_i .

15.5.3 Analysis of the Eigenvalues in Element Stiffness Matrix

Let \mathbf{K}^e be the element stiffness matrix. Since \mathbf{K}^e is a real symmetric matrix, all eigenvalues of \mathbf{K}^e are real numbers.

The element strain energy U^e is a quadratic expression of the element nodal displacements

$$U^e = \frac{1}{2}(\mathbf{q}^e)^T \mathbf{K}^e \mathbf{q}^e \quad (15-46)$$

where the coefficient matrix \mathbf{K}^e is just the element stiffness matrix.

If \mathbf{q}^e is the eigenvector of \mathbf{K}^e , and corresponding to eigenvalue λ , we have

$$\mathbf{K}^e \mathbf{q}^e = \lambda \mathbf{q}^e \quad (15-47)$$

Substitution of the above equation into Eq. (15-46) yields

$$U^e = \frac{\lambda}{2}(\mathbf{q}^e)^T \mathbf{q}^e \quad (15-48)$$

Since the strain energy U^e is non-negative, we can obtain

$$\lambda \geq 0 \quad (15-49)$$

If $\lambda > 0$, the energy U^e corresponding to the eigenvector \mathbf{q}^e will be greater than zero, i.e., \mathbf{q}^e belongs to the nonzero energy modes.

If $\lambda = 0$, the energy U^e corresponding to the eigenvector \mathbf{q}^e will equal zero, i.e., \mathbf{q}^e belongs to the zero energy modes.

If the zero eigenvalue ($\lambda = 0$) of \mathbf{K}^e is a k multiple root, there will be k linearly independent eigenvectors corresponding to it, therefore, the element possesses k zero energy modes.

From above, it can be seen that, there is a corresponding relationship existing in the analysis of the element zero energy modes and the analysis of the eigenvalues of the element stiffness matrix \mathbf{K}^e :

(1) If the element possesses zero energy mode, the element stiffness matrix will possess zero eigenvalue, and vice versa.

(2) If the element possesses z zero energy modes, the element stiffness matrix will possess zero eigenvalue which is a z multiple root, and vice versa.

(3) Assume that the element possesses r rigid body displacement modes:

$$r = 3 \text{ (2D element)}, \quad r = 6 \text{ (3D element)}, \quad r = 3 \text{ (plate bending element)}$$

then, the element will have r or more zero energy modes; and the element stiffness matrix will possess zero eigenvalue which is a r or more multiple root.

15.5.4 Analysis of the Zero Energy Mode in Structural System

In the previous section, the analysis of the element zero energy mode has been carried out. Now, a further discussion on the zero energy mode in structural system will be given as follows.

In global finite element analysis, the global stiffness matrix \mathbf{K} of the structural system is established by assembling the element stiffness matrix \mathbf{K}^e and introducing the displacement boundary conditions.

In order to ensure that the structural mechanics problem can be solved, the global stiffness matrix should be an invertible one. Thereby, \mathbf{K} should not possess zero eigenvalue, and the structural system should not have zero energy mode, i.e., on the one hand, there is no rigid body displacement mode; on the other hand, there is no spurious zero energy mode either.

As to the first point, if the structural system has enough support conditions which can prevent rigid body displacements, the rigid body displacement modes can be eliminated when the displacement boundary conditions are introduced in the global analysis.

As to the second point, the usual treatment is: it is required that all the element stiffness matrices \mathbf{K}^e should not possess the spurious zero energy modes; and then, the global stiffness matrix \mathbf{K} assembled by these elements will not have the spurious zero energy mode naturally. This is just for the general case. Sometimes the following case may also happen: initially, during the stage of the element analysis, though the spurious zero energy modes happen in very few elements, there are no spurious zero energy modes existing in other elements; after global assembly, these spurious zero energy mode will disappear automatically because they are prevented by constraints, i.e., the structural system after assembly will not have spurious zero energy mode. This case will be discussed as follows.

15.5.5 Theorem for the Analysis of the Spurious Zero Energy Mode in Structural System

Now, let us go back to the plane crack problem, which will be analyzed globally by using the sub-region mixed element system given by Fig. 15.3.

For example, as shown in Fig. 15.3, the mixed mesh, which is composed of hybrid singular and conventional displacement-based elements, is used, and the number $4S_\theta$ is equal to 8, so the number of the nodes in the hybrid singular element is $n = 17$. From the computational results given by Fig. 15.4 and Fig. 15.5, it can be seen that, when the number of stress terms in the hybrid element is $M = 6$, the precisions of the results have already been quite high. Here, according to Eq. (15-37), the number of the spurious zero energy modes in the hybrid element is

$$z_1 = 2n - 2M - r = 34 - 12 - 3 = 19$$

So, it can be seen that, though 19 spurious zero energy modes appear in the individual element, satisfactory results can still be obtained for the structural computations because there is no spurious zero energy mode existing in the structural system.

In the above example, two points can be explained as follows:

(1) The structural system is composed of two parts: the dominant part is the displacement-based element part containing all nodes; and the hybrid element is just an individual element containing partial nodes.

(2) If the dominant part composed of displacement-based elements is geometrically stable, and has no spurious zero energy mode, then, no matter whether the hybrid element possesses spurious zero energy modes, the original system is also geometrically stable, and has no spurious zero energy mode.

These conclusions can be written as the following forms of theorem:

(1) A sub-region mixed element system, which is composed of displacement-based and hybrid elements, is considered. For the global system, the nodal

displacement vector is \mathbf{q} , and the stiffness matrix is \mathbf{K} . For the dominant part composed of displacement-based elements, the nodal displacement vector is still \mathbf{q} , and the stiffness matrix is \mathbf{K}_0 . For the hybrid element, the nodal displacement vector is $\bar{\mathbf{q}}$, and the stiffness matrix is $\bar{\mathbf{K}}$. $\bar{\mathbf{q}}$ is a sub-vector of \mathbf{q}

$$\mathbf{q} = \begin{Bmatrix} \bar{\mathbf{q}} \\ \mathbf{q}^* \end{Bmatrix}$$

According to the assembly rule of the stiffness matrix, we have

$$\mathbf{K} = \mathbf{K}_0 + \begin{bmatrix} \bar{\mathbf{K}} & \mathbf{0} \\ \mathbf{0} & \mathbf{0} \end{bmatrix} \tag{15-50}$$

(2) The singularity theorem of stiffness matrix in the sub-region mixed element system can be stated as follows:

If \mathbf{K}_0 is a nonsingular matrix, then, no matter whether $\bar{\mathbf{K}}$ is singular or not, \mathbf{K} is still a nonsingular matrix.

Proof Since \mathbf{K}_0 is a nonsingular matrix, therefore, for the arbitrary nonzero \mathbf{q} , its strain energy is

$$U_0 = \frac{1}{2} \mathbf{q}^T \mathbf{K}_0 \mathbf{q} > 0 \tag{15-51}$$

No matter whether $\bar{\mathbf{K}}$ is singular or not, for the arbitrary $\bar{\mathbf{q}}$, its strain energy is

$$\bar{U} = \frac{1}{2} \bar{\mathbf{q}}^T \bar{\mathbf{K}} \bar{\mathbf{q}} \geq 0 \tag{15-52}$$

Hence, for the arbitrary nonzero \mathbf{q} , the strain energy of the original system is

$$U = \frac{1}{2} \mathbf{q}^T \mathbf{K} \mathbf{q} = \frac{1}{2} \mathbf{q}^T \mathbf{K}_0 \mathbf{q} + \frac{1}{2} \bar{\mathbf{q}}^T \bar{\mathbf{K}} \bar{\mathbf{q}} > 0 \tag{15-53}$$

Therefore, \mathbf{K} must be a nonsingular matrix. □

(3) Theorem for the analysis of the spurious zero energy mode in the sub-region mixed element system.

The above theorem can also be stated as the theorem for the analysis of the spurious zero energy mode:

If there is no spurious zero energy mode in the dominant part composed of displacement-based elements, then, no matter whether the hybrid element contains spurious zero energy mode or not, the sub-region mixed element system will not contain the spurious zero energy mode.

By the way, here the spurious zero energy mode can exist in the hybrid element, but it is inactive because of the constraints from the dominant part.

15.6 The Basic Analytical Solutions of the Plane Notch Problem

A structure with a notch is shown in Fig. 15.8. The open angle of the notch is α . By employing the stress analysis method proposed by Williams^[3] for the plane notch problem, the analytical solutions for the symmetric and antisymmetric problems can be derived.

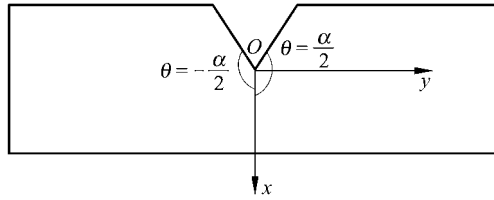


Figure 15.8 A structure with a notch

15.6.1 The Basic Analytical Solutions for Symmetric Problem of Mode I

In polar coordinate system, the symmetric part of the bi-harmonic stress function ϕ is

$$\phi = r^{\lambda+1} [A \cos(\lambda - 1)\theta + B \cos(\lambda + 1)\theta] \quad (15-54)$$

Then, the corresponding stresses are

$$\left. \begin{aligned} \sigma_r &= r^{\lambda-1} (-\lambda) [A(\lambda - 3) \cos(\lambda - 1)\theta + B(\lambda + 1) \cos(\lambda + 1)\theta] \\ \sigma_\theta &= r^{\lambda-1} \lambda(\lambda + 1) [A \cos(\lambda - 1)\theta + B \cos(\lambda + 1)\theta] \\ \tau_{r\theta} &= r^{\lambda-1} \lambda [A(\lambda - 1) \sin(\lambda - 1)\theta + B(\lambda + 1) \sin(\lambda + 1)\theta] \end{aligned} \right\} \quad (15-55)$$

The boundary conditions along the free edges of the notch are

$$\sigma_\theta \Big|_{\theta=\pm\frac{\alpha}{2}} = \tau_{r\theta} \Big|_{\theta=\pm\frac{\alpha}{2}} = 0$$

From the last two expressions in Eq. (15-55), we have

$$A \cos(\lambda - 1) \frac{\alpha}{2} + B \cos(\lambda + 1) \frac{\alpha}{2} = 0 \quad (15-56a)$$

$$A(\lambda - 1) \sin(\lambda - 1) \frac{\alpha}{2} + B(\lambda + 1) \sin(\lambda + 1) \frac{\alpha}{2} = 0 \quad (15-56b)$$

If A and B are not zero at the same time, the determinant of the coefficient matrix should be zero, i.e.,

$$\begin{aligned} |\mathcal{A}| &= (\lambda + 1)\sin(\lambda + 1)\frac{\alpha}{2}\cos(\lambda - 1)\frac{\alpha}{2} - (\lambda - 1)\sin(\lambda - 1)\frac{\alpha}{2}\cos(\lambda + 1)\frac{\alpha}{2} \\ &= (\lambda + 1)[\sin \lambda\alpha + \sin \alpha] - (\lambda - 1)[\sin \lambda\alpha - \sin \alpha] \\ &= 2[\sin \lambda\alpha + \lambda \sin \alpha] = 0 \end{aligned} \quad (15-57)$$

This is the characteristic equation of the symmetric part for the single-material V-notch problem. The eigenroots of the symmetric part can be obtained by solving Eq. (15-57). Here, these eigenroots can be both real and complex numbers. When one eigenroot is a complex number, its conjugated complex number can also satisfy the characteristic equation. So, the complex eigenroots always appear pair-wise in the form of conjugated complex numbers.

Multiply Eqs. (15-56a) and (15-56b) by $\cos\left[(\lambda+1)\frac{\alpha}{2}\right]$ and $\left(\frac{1}{\lambda+1}\right)\sin\left[(\lambda+1)\frac{\alpha}{2}\right]$ respectively, the sum of the results will be

$$A\left\{\cos\left[(\lambda-1)\frac{\alpha}{2}\right]\cos\left[(\lambda+1)\frac{\alpha}{2}\right] + \frac{\lambda-1}{\lambda+1}\sin\left[(\lambda-1)\frac{\alpha}{2}\right]\sin\left[(\lambda+1)\frac{\alpha}{2}\right]\right\} + B = 0$$

i.e.,

$$B = -A\left[\frac{\cos \lambda\alpha + \cos \alpha}{2} + \frac{\lambda-1}{\lambda+1}\left(\frac{\cos \alpha - \cos \lambda\alpha}{2}\right)\right] = -\frac{A}{\lambda+1}[\cos \lambda\alpha + \lambda \cos \alpha]$$

Let $A = 1$, then from Eq. (15-55), we obtain

$$\left\{\begin{array}{l} \sigma_r \\ \sigma_\theta \\ \tau_{r\theta} \end{array}\right\} = \left\{\begin{array}{l} r^{\lambda-1}\lambda[(3-\lambda)\cos(\lambda-1)\theta + (\lambda\cos\alpha + \cos\lambda\alpha)\cos(\lambda+1)\theta] \\ r^{\lambda-1}\lambda[(\lambda+1)\cos(\lambda-1)\theta - (\lambda\cos\alpha + \cos\lambda\alpha)\cos(\lambda+1)\theta] \\ r^{\lambda-1}\lambda[(\lambda-1)\sin(\lambda-1)\theta - (\lambda\cos\alpha + \cos\lambda\alpha)\sin(\lambda+1)\theta] \end{array}\right\} \quad (15-58)$$

15.6.2 The Basic Analytical Solutions for the Antisymmetric Problem of Mode II

In the polar coordinate system, the antisymmetric part of the bi-harmonic stress function which satisfies the compatibility equation $\nabla^4\phi = 0$ can be written as

$$\phi = r^{\lambda+1}[C\sin(\lambda-1)\theta + D\sin(\lambda+1)\theta] \quad (15-59)$$

Similar to the symmetric problem, the characteristic equation with free boundary

can be derived as

$$-\lambda \sin \alpha + \sin \lambda \alpha = 0 \quad (15-60)$$

The basic analytical solutions for the antisymmetric problem of mode II are

$$\begin{Bmatrix} \sigma_r \\ \sigma_\theta \\ \tau_{r\theta} \end{Bmatrix} = \begin{Bmatrix} -r^{\lambda-1} \lambda [(3-\lambda) \sin(\lambda-1)\theta + (\lambda \cos \alpha - \cos \lambda \alpha) \sin(\lambda+1)\theta] \\ -r^{\lambda-1} \lambda [(\lambda+1) \sin(\lambda-1)\theta - (\lambda \cos \alpha - \cos \lambda \alpha) \sin(\lambda+1)\theta] \\ -r^{\lambda-1} \lambda [(1-\lambda) \cos(\lambda-1)\theta + (\lambda \cos \alpha - \cos \lambda \alpha) \cos(\lambda+1)\theta] \end{Bmatrix} \quad (15-61)$$

15.6.3 Construction of Stress Field Subspace

Let λ_n be an arbitrary eigenroot. When λ_n is a complex root, since complex eigenroots always appear pair-wise, thereby, the real and imaginary parts of the stress solutions

$$\operatorname{Re} \begin{Bmatrix} \sigma_r \\ \sigma_\theta \\ \tau_{r\theta} \end{Bmatrix}_{\lambda=\lambda_n} \quad \text{and} \quad \operatorname{Im} \begin{Bmatrix} \sigma_r \\ \sigma_\theta \\ \tau_{r\theta} \end{Bmatrix}_{\lambda=\lambda_n} \quad (15-62)$$

can be treated as two independent stress solutions.

When λ_n is a real root, then the imaginary part will be zero, and only the real part is the nonzero stress solution.

By rationally selecting a set of basic analytical solutions corresponding to low-order eigenroots, a stress field subspace with stress parameters can be obtained and denoted by

$$\begin{Bmatrix} \sigma_r \\ \sigma_\theta \\ \tau_{r\theta} \end{Bmatrix} = \mathbf{S} \begin{Bmatrix} \beta_1 \\ \vdots \\ \beta_{2M} \end{Bmatrix} \quad (15-63)$$

in which \mathbf{S} is determined by Eqs. (15-58), (15-61) and (15-62).

15.6.4 Calculation of the Stress Intensity Factor

The stress intensity factor K_I of mode I is

$$K_I = \sqrt{2\pi} \lim_{r \rightarrow 0} r^{1-\lambda_1} \sigma_\theta |_{\theta=0} = \sqrt{2\pi} \beta_1 \lambda_1 (\lambda_1 + 1 - \lambda_1 \cos \alpha - \cos \lambda_1 \alpha) \quad (15-64)$$

where λ_1 is the minimum positive real root for the symmetric problem of mode I; β_1 is the corresponding stress parameter.

The stress intensity factor K_{II} of mode II is

$$\begin{aligned}
 K_{II} &= \sqrt{2\pi} \lim_{r \rightarrow 0} r^{1-\lambda_2} \tau_{r\theta} \Big|_{\theta=0} \\
 &= \sqrt{2\pi} \beta_2 (-\lambda_2) (1 - \lambda_2 + \lambda_2 \cos \alpha - \cos \lambda_2 \alpha)
 \end{aligned}
 \tag{15-65}$$

where λ_2 is the minimum positive real root for the antisymmetric problem of mode II; β_2 is the corresponding stress parameter.

15.7 Element ATF-VN with Notch Formulated by the Analytical Trial Function Method

As shown in Fig. 15.9, an element with V-notch is considered. The opening angle of the notch is α . The outer circle of the element contains n nodes and $2n$ DOFs. Thus, the element nodal displacement vector is

$$\mathbf{q}^e = [u_1 \quad v_1 \quad u_2 \quad v_2 \quad \cdots \quad u_n \quad v_n]^T$$

Now, the element stiffness matrix will be derived by using the analytical trial function method and the minimum complementary energy principle. This element is denoted as ATF-VN.

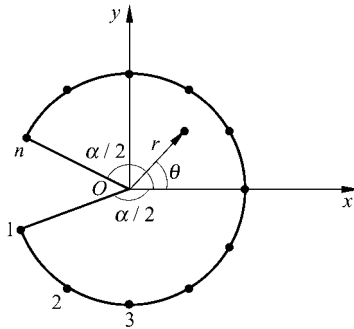


Figure 15.9 An element with V-notch

The derivation procedure is the same as that given in Sect. 15.3, and the basic formulae obtained are also the same. Now, some of them are given as follows.

The element stiffness matrix is still given by Eq. (15-36)

$$\mathbf{K}^e = \mathbf{H}^T \mathbf{V}^{-1} \mathbf{H}$$

in which two matrices \mathbf{V} and \mathbf{H} on the right side are still given by Eqs. (15-26) and (15-33), respectively

$$V = \iint_{\Omega} \mathbf{S}^T \mathbf{D}^{-1} \mathbf{S} h dA$$

$$\mathbf{H} = \int_{\Gamma} \mathbf{S}^T \mathbf{L}^T \bar{\mathbf{N}} h ds$$

Except \mathbf{S} , the definitions of \mathbf{D} , \mathbf{L} , and $\bar{\mathbf{N}}$ are all the same as those given in Sect. 15.3.

Compared with the element with crack given in Sect. 15.3, there are two main differences existing in the element with notch given in this section:

(1) Differences of the stress fields and matrix \mathbf{S}

According to Eq. (15-15) or Eq. (15-63), the stress fields can be expressed as

$$\begin{Bmatrix} \sigma_r \\ \sigma_\theta \\ \tau_{r\theta} \end{Bmatrix} = \mathbf{S} \begin{Bmatrix} \beta_1 \\ \vdots \\ \beta_{2M} \end{Bmatrix}$$

But \mathbf{S} is different from each other: in Sect. 15.3, \mathbf{S} is determined by Eqs. (15-10) and (15-14); in this section, \mathbf{S} is determined by Eqs. (15-58) and (15-61).

(2) Differences of the characteristic equations and eigenroots

In V-notch problem, the opening angle α of the notch is a parameter. The characteristic equations are given by Eqs. (15-57) and (15-60), and can be written as

$$\pm \lambda \sin \alpha + \sin \lambda \alpha = 0$$

The crack problem can be looked upon as a special case of the V-notch problem, in which the parameter α is assigned to be 2π .

In reference [4], there are systematical discussions on the schemes for solving eigenroots of the notch problem. In reference [5], these methods have been improved by proposing the sub-region accelerated Müller method. In Tables 15.1 and 15.2, the values of the real and imaginary parts of the first 7 eigenroot pairs $\lambda_k = \xi_k \pm i\eta_k$ ($k = 1, 2, \dots, 7$) in the notch problem are listed.

Table 15.1 The first 7 eigenroots $\lambda_k = \xi_k \pm i\eta_k$ ($k = 1, 2, \dots, 7$) of the symmetric V-notch problem of mode I

α	ξ_1	η_1	ξ_2	η_2	ξ_3	η_3	ξ_4	η_4
190	0.900 043 76	0	1	0	2.001 795 18	0	2.695 231 53	0
200	0.818 695 81	0	1	0	2.018 264 18	0	2.420 587 07	0
210	0.751 974 51	0	1	0	2.106 286 25	0.096 100 1	3.828 293 71	0.347 176 77
220	0.697 164 94	0	1	0	2.005 648 78	0.198 379 72	3.651 102 30	0.391 981 45

Advanced Finite Element Method in Structural Engineering

(Continued)

α	ξ_1	η_1	ξ_2	η_2	ξ_3	η_3	ξ_4	η_4
230	0.652 269 53	0	1	0	1.915 272 97	0.236 951 87	3.490 348 40	0.410 599 02
240	0.615 731 04	0	1	0	1.833 548 84	0.252 251 27	3.343 717 56	0.414 037 23
250	0.586 278 85	0	1	0	1.759 251 08	0.253 998 99	3.209 376 63	0.407 444 49
260	0.562 839 47	0	1	0	1.691 413 67	0.246 340 64	3.085 831 64	0.393 570 21
270	0.544 483 72	0	1	0	1.629 257 33	0.231 250 53	2.971 843 69	0.373 931 19
280	0.530 395 71	0	1	0	1.572 143 99	0.209 446 39	2.866 373 86	0.349 278 88
290	0.519 854 30	0	1	0	1.519 546 5	0.180 478 02	2.768 545 04	0.319 765 92
300	0.512 221 36	0	1	0	1.471 027 91	0.141 852 90	2.677 615 03	0.284 901 36
310	0.506 932 84	0	1	0	1.426 227 32	0.083 159 46	2.592 958 14	0.243 187 20
320	0.503 490 48	0	1	0	1.302 693 25	0	1.467 008 48	0
330	0.501 453 01	0	1	0	1.202 957 09	0	1.490 377 81	0
340	0.500 426 37	0	1	0	1.125 406 58	0	1.497 613 49	0
350	0.500 052 99	0	1	0	1.058 842 89	0	1.499 727 77	0
α	ξ_5	η_5		ξ_6	η_6	ξ_7	η_7	
190	4.022 680 43	0		4.468 956 72	0	6.142 445 45	0.110 609 04	
200	4.025 002 28	0.243 014 71		5.828 632 84	0.377 126 45	7.631 219 36	0.462 931 49	
210	5.547 288 43	0.459 267 73		7.264 799 21	0.536 558 54	8.981 455 32	0.596 121 47	
220	5.292 797 61	0.494 878 01		6.932 731 97	0.567 288 07	8.571 681 47	0.623 509 63	
230	5.061 211 04	0.507 369 59		6.630 158 89	0.576 050 10	8.198 054 26	0.629 551 95	
240	4.849 458 42	0.506 015 06		6.353 222 50	0.571 559 41	7.855 910 95	0.622 700 58	
250	4.655 052 57	0.495 417 26		6.098 759 71	0.558 220 72	7.541 400 85	0.607 258 88	
260	4.475 934 64	0.478 103 47		5.864 131 58	0.538 470 87	7.251 297 45	0.585 613 03	
270	4.310 377 17	0.455 493 56		5.647 111 62	0.513 683 79	6.982 870 25	0.559 108 24	
280	4.156 917 45	0.428 313 17		5.445 805 98	0.484 565 25	6.733 791 05	0.528 434 74	
290	4.014 309 24	0.396 758 19		5.258 594 12	0.451 315 66	6.502 062 99	0.493 789 48	
300	3.881 487 39	0.360 496 27		5.084 084 09	0.413 644 47	6.285 966 14	0.454 895 93	
310	3.757 542 54	0.318 470 43		4.921 079 46	0.370 618 18	6.084 016 40	0.410 870 72	
320	2.514 054 95	0.190 785 59		3.641 705 67	0.268 252 20	4.768 557 38	0.320 170 77	
330	2.440 491 94	0.114 206 83		3.533 345 48	0.203 710 63	4.625 661 14	0.257 540 31	
340	2.267 186 42	0		2.476 770 05	0	3.431 990 40	0.098 448 11	
350	2.118 822 72	0		2.497 979 92	0	3.181 532 51	0	

Table 15.2 The first 7 eigenroots $\lambda_k = \xi_k \pm i\eta_k$ ($k = 1, 2, \dots, 7$) of the antisymmetric V-notch problem of mode II

α	ξ_1	η_1	ξ_2	η_2	ξ_3	η_3
190	1.798 932 53	0	3.007 825 75	0	3.586 721 26	0
200	1.630 525 00	0	3.122 551 06	0.108 732 10	4.926 986 80	0.319 810 82
210	1.485 811 63	0	2.967 836 19	0.261 186 47	4.688 038 43	0.409 575 49
220	1.359 494 88	0	2.829 075 26	0.316 619 25	4.472 248 09	0.448 844 01
230	1.248 039 54	0	2.703 607 79	0.340 957 34	4.276 106 90	0.463 915 80
240	1.148 912 69	0	2.589 478 97	0.348 374 75	4.096 927 57	0.464 641 40
250	1.060 214 60	0	2.485 167 80	0.344 860 86	3.932 553 70	0.455 814 72
260	0.980 474 87	0	2.389 451 49	0.333 470 69	3.781 211 59	0.440 044 09
270	0.908 529 14	0	2.301 327 00	0.315 836 73	3.641 420 00	0.418 786 68
280	0.843 439 52	0	2.219 960 94	0.292 721 62	3.511 929 49	0.392 780 34
290	0.784 440 51	0	2.144 655 71	0.264 181 64	3.391 679 44	0.362 209 11
300	0.730 900 70	0	2.074 826 15	0.229 425 77	3.279 767 00	0.326 690 28
310	0.682 294 79	0	2.009 983 81	0.186 062 96	3.175 425 46	0.285 026 54
320	0.638 182 43	0	1.949 728 10	0.126 554 45	3.078 011 65	0.234 364 65
330	0.598 191 81	0	1.838 934 04	0	1.948 556 00	0
340	0.562 006 52	0	1.692 249 99	0	1.991 384 81	0
350	0.529 354 71	0	1.588 609 10	0	1.999 106 97	0

α	ξ_4	η_4	ξ_5	η_5	ξ_6	η_6	ξ_7	η_7
190	5.060 479 68	0	5.327 915 57	0	7.090 587 48	0.201 940 45	8.986 626 03	0.306 373 03
200	6.730 024 47	0.423 592 26	8.532 258 54	0.497 160 38	10.333 982 60	0.554 820 34	12.135 360 30	0.602 434 32
210	6.406 179 04	0.500 793 05	8.123 210 11	0.568 017 11	9.839 566 83	0.621 533 63	11.555 479 40	0.666 082 79
220	6.112 922 23	0.533 685 35	7.752 301 03	0.596 947 80	9.390 911 01	0.647 569 48	11.029 023 00	0.689 824 63
230	5.845 854 24	0.544 138 61	7.414 206 64	0.604 260 57	8.981 742 59	0.652 479 25	10.548 754 80	0.692 778 53
240	5.601 514 07	0.541 086 75	7.104 668 57	0.598 518 31	8.606 991 67	0.644 631 07	10.108 784 40	0.683 194 05
250	5.377 078 48	0.529 014 46	6.820 181 00	0.584 068 07	8.262 461 04	0.628 293 97	9.704 217 80	0.665 289 36
260	5.170 199 86	0.510 396 12	6.557 811 90	0.563 318 35	7.944 628 67	0.605 835 93	9.330 939 73	0.641 404 08
270	4.978 902 06	0.486 625 45	6.315 083 20	0.537 627 37	7.650 510 96	0.578 591 12	8.985 458 93	0.612 854 32
280	4.801 507 37	0.458 417 47	6.089 884 17	0.507 692 68	7.377 561 85	0.547 243 11	8.664 792 75	0.580 312 00
290	4.636 582 76	0.425 972 12	5.880 406 25	0.473 713 43	7.123 595 91	0.511 986 21	8.366 378 15	0.543 965 60
300	4.482 899 92	0.388 983 73	5.685 093 59	0.435 407 90	6.886 729 06	0.472 546 80	8.088 002 59	0.503 543 47
310	4.339 406 11	0.346 472 26	5.502 605 95	0.391 872 56	6.665 333 36	0.428 055 52	7.827 750 58	0.458 193 33
320	4.205 205 56	0.296 235 66	5.331 793 33	0.341 129 83	6.458 004 69	0.376 638 90	7.583 964 33	0.406 097 94
330	2.987 004 95	0.166 740 99	4.079 554 65	0.233 016 50	5.171 685 63	0.278 729 57	6.263 546 29	0.314 206 38
340	2.883 885 78	0	2.920 169 71	0	3.961 883 78	0.138 439 15	5.021 511 63	0.191 634 58
350	2.649 698 56	0	2.996 140 98	0	3.714 772 43	0	3.989 019 73	0

15.8 Error Analysis of Element ATF-VN with Notch

15.8.1 Calculation of Stress Intensity Factor K_I of a Specimen with V-Notch Subjected to Unidirection Tension

As an example, a specimen with V-notch subjected to unidirection tension (shown in Fig. 15.10) is considered. The error analysis of the computational results obtained by the element ATF-VN is carried out here. The dimensions of the plate are $b = 1$, $w = 1$ and $a = 0.5$; the load density on the two sides $q = 1$; the opening angle $\alpha = 300^\circ$; the Young's modulus $E = 0.21 \times 10^7$; and the Poisson's ratio $\mu = 0.3$. The reference solution^[6] is $K_I = 3.756$.

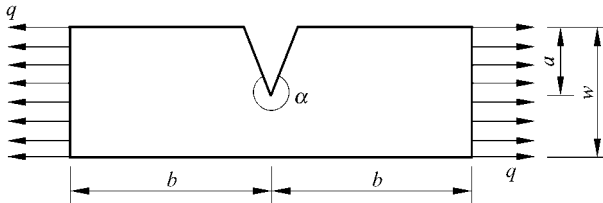


Figure 15.10 A specimen with V-notch subjected to unidirection tension

(1) The error analysis of K_I with variation of the number M of the stress terms (the dimension of the singular element $R = \text{constant}$).

In Fig. 15.11, the longitudinal coordinate e denotes the relative error for the

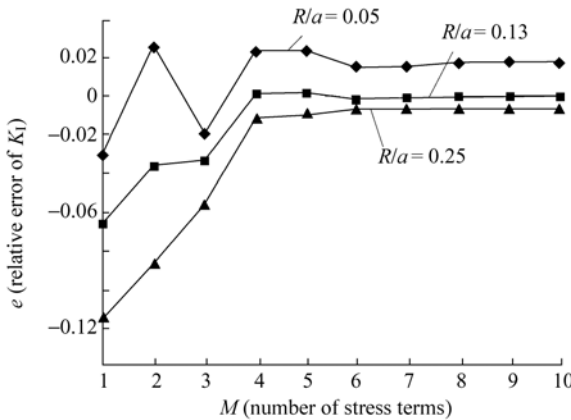


Figure 15.11 e - M curves

computational results of K_I ; and the horizontal coordinate M denotes the number of the stress terms used by the singular element.

Three e - M curves with $\frac{R}{a} = 0.05, 0.13$ and 0.25 are plotted in Fig. 15.11, respectively. These curves show that, with the increase of M , errors will decrease. When M increases to 6, the relative errors will be less than 2%.

This numerical test shows that, when $\frac{R}{a} = 0.1$ and $M=6$, the effect of the global analysis is good.

(2) The error analysis of K_I with variation of the dimension R of the singular element ($M=$ constant)

In Fig. 15.12, the longitudinal coordinate e still denotes the relative error of K_I ; and the horizontal coordinate $\frac{R}{a}$ denotes the ratio of the dimension R of the singular element to notch length a .

In Fig. 15.12(a), five e - $\frac{R}{a}$ curves with the number of the stress terms $M= 1, 2, 3, 4$ and 5 are plotted. Among these five curves, the error is maximum when $M= 1$, and minimum when $M= 5$.

In Fig. 15.12(b), e - $\frac{R}{a}$ curves with the number of the stress terms $M= 6$ to 10 are plotted. From these curves, it can be seen that, error e is insensitive to M ; but the relation between e and $\frac{R}{a}$ is nonlinear; when $\frac{R}{a} = 0.1$, the error is minimum.

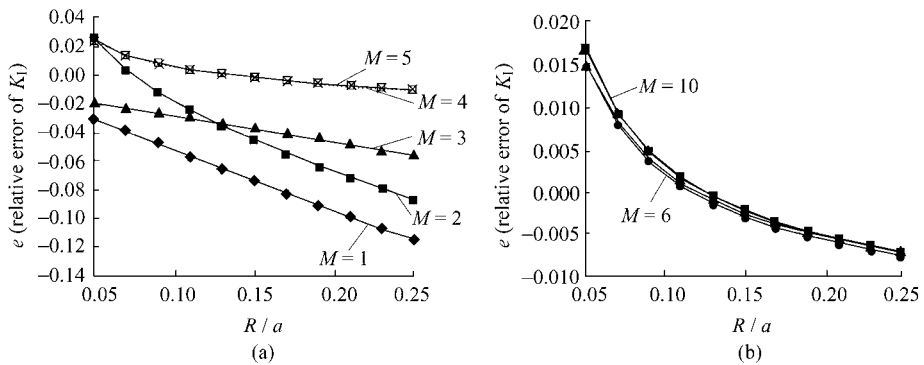


Figure 15.12 e - $\frac{R}{a}$ curves

15.8.2 Calculation of Stress Intensity Factor K_{II} of a Specimen with V-Notch Subjected to Antisymmetric Load

As an example, a specimen with V-notch shown in Fig. 15.13 is considered. The error analysis of K_{II} obtained by the element ATF-VN is carried out.

The dimensions of the specimen are $a = 1$, $w = 3$ and $h = 1$. The Young's modulus $E = 0.21 \times 10^7$; and the Poisson's ratio $\mu = 0.3$. The resultant force $P = 1$. The opening angle α of the notch varies from 360° to 330° .

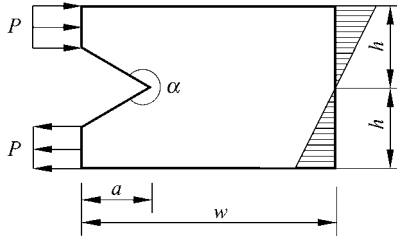


Figure 15.13 A specimen with V-notch subjected to antisymmetric load

The computational results of the stress intensity factor with different number $2M$ of the stress terms are listed in Table 15.3. From the results given by the Table, it can be seen that, when $2M = 12$, the results have already been stable, and the computational errors are less than 1%.

Table 15.3 The stress intensity factor K_{II} with different number of stress terms

Number of stress terms $2M$	360°	350°	340°	330°
2	- 0.000 945 729	- 0.001 327 029	- 0.001 708 115	- 0.001 567 462
4	0.002 090 411	0.419 567 45	0.304 236 10	0.153 866 82
6	0.679 651 54	0.403 623 74	0.281 348 67	0.127 061 63
8	0.447 836 04	0.400 346 10	0.278 282 01	0.123 635 52
10	0.512 325 42	0.398 693 45	0.276 048 56	0.121 872 21
12	0.493 713 40	0.398 760 45	0.276 116 19	0.121 951 93
14	0.493 446 69	0.398 772 48	0.276 129 34	0.121 957 86
16	0.492 738 16	0.398 774 24	0.276 136 54	0.121 974 48
18	0.493 056 95	0.398 778 35	0.276 141 77	0.121 978 14
20	0.493 829 68	0.398 778 33	0.276 141 36	0.121 975 84
Reference [6]	0.500	0.401	0.278	

References

- [1] Williams ML (1957) On the stress distribution at the base of a stationary crack. *Journal of Applied Mechanics* 24: 109 – 114
- [2] Fu XR, Long YQ (2001) Fracture analysis with the sub-region mixed element method. *Gong Cheng Li Xue/Engineering Mechanics* 18(6): 39 – 46 (in Chinese)
- [3] Williams ML (1952) Stress singularities resulting from various boundary conditions in angular corners of plates in extension. *Journal of Applied Mechanics* 14: 526 – 528
- [4] Fan Z, Long YQ (1992) Sub-region mixed finite element analysis of V-notched plates. *International Journal of Fracture* 56: 333 – 344
- [5] Fu XR, Long YQ (2002) Calculation of the eigenvalues—the sub-region accelerated Müller method. In: *Proceedings of the Eleventh National Conference on Structural Engineering (Vol. I)*. China, Changsha, pp226 – 232 (in Chinese)
- [6] Gross B, Mendelson A (1972) Plane elastostatic analysis of V-notched plates. *International Journal of Fracture* 8: 267 – 276

Chapter 16 **Quadrilateral Area Coordinate Systems,** **Part I—Theory and Formulae**

Yu-Qiu Long

Department of Civil Engineering, School of Civil Engineering,
Tsinghua University, Beijing, 100084, China

Song Cen

Department of Engineering Mechanics, School of Aerospace,
Tsinghua University, Beijing, 100084, China

Zhi-Fei Long

School of Mechanics & Civil Engineering, China University of
Mining & Technology, Beijing, 100083, China

Abstract This chapter introduces new concepts for developing the quadrilateral finite element models. Firstly, the quadrilateral area coordinate system (QACM-I) with four coordinate components, which is a generalization of the triangular area coordinate method, is systematically established in detail. Then, on the basis of the QACM-I, another quadrilateral area coordinate system (QACM-II) with only two coordinate components is also proposed. These new coordinate systems provide the theoretical bases for the construction of new quadrilateral element models insensitive to mesh distortion, which will be introduced in Chap. 17.

Keywords quadrilateral element, quadrilateral area coordinate system, coordinate components, QACM-I, QACM-II.

16.1 Introduction

In comparison with the rectangular and triangular elements, the quadrilateral element possesses more flexibility and can be used to model multiform shapes, but its construction procedure is more complicated. The invention of the isoparametric coordinates greatly promotes the development of the quadrilateral elements. At present, the isoparametric coordinate method almost occupies a dominant position in the construction of the quadrilateral elements. But, some

disadvantages still exist in this system:

(1) The relation equations (inverse transformations) in which the isoparametric coordinates (ξ, η) are expressed in terms of the Cartesian coordinates (x, y) are too complicated to use.

(2) The stiffness matrix of the isoparametric element generally cannot be evaluated exactly by numerical integration.

(3) When the shape of an element is distorted, the accuracy of the Serendipity isoparametric element will drop obviously.

How to overcome the above shortcomings of the isoparametric element is an interesting topic which attracted many researchers in the finite element method area for a long time, and is also the background of the developments of the quadrilateral area coordinate method and related quadrilateral elements. It can be seen from this chapter and Chap. 17 that, these new methods are effective tools for eliminating the above disadvantages.

Related new developments were proposed in 1997. The first papers about the QACM-I are references [1–6], and the first papers about the QACM-II are references [7,8].

This chapter will introduce the systematic theories of the quadrilateral area coordinates:

(1) Characteristic parameters for the quadrilateral elements are defined and the degeneration conditions under which a quadrilateral degenerates into a parallelogram (including rectangle) or a trapezoid or a triangle are given;

(2) For the QACM-I, the area coordinates of any point in a quadrilateral are defined, and transformation relations between the area coordinates and the Cartesian or isoparametric coordinates are presented;

(3) For the QACM-I, two identical equations, which the four area coordinate components should satisfy, are given and proved;

(4) Another quadrilateral area coordinate system with only two components (QACM-II) is defined and the transformation relations between the QACM-II and the Cartesian or isoparametric coordinates are presented;

(5) Related differential and integral formulae are given and proved.

This chapter provides a theoretical basis for the construction of new quadrilateral elements in the next chapter. By the combination of the quadrilateral area and the isoparametric coordinates, excellent elements with curved sides can also be derived.

16.2 The Isoparametric Coordinate Method and the Area Coordinate Method

The isoparametric coordinate method^[9,10] has been successfully applied in the construction of the quadrilateral elements. The coordinate transformations between

the isoparametric coordinates (ξ, η) and the Cartesian coordinates (x, y) are

$$\left. \begin{aligned} x &= \frac{1}{4} \sum_{i=1}^4 x_i (1 + \xi_i \xi) (1 + \eta_i \eta) \\ y &= \frac{1}{4} \sum_{i=1}^4 y_i (1 + \xi_i \xi) (1 + \eta_i \eta) \end{aligned} \right\} \quad (16-1)$$

where (x_i, y_i) and (ξ_i, η_i) are the coordinates of node i , respectively. Although the isoparametric coordinates have been broadly applied, there are still some disadvantages which have been mentioned above. Here, some explanations are given:

(1) The inverse transformation of (16-1) is too complicated to use. Reference [11] divided the quadrilateral elements into 6 cases, and derived the corresponding inverse transformation, respectively:

$$\left. \begin{aligned} \xi &= F_1(x, y) \\ \eta &= F_2(x, y) \end{aligned} \right\} \quad (16-2)$$

but $F_1(x, y)$ and $F_2(x, y)$ cannot be expressed by a polynomial in finite terms except for the degenerate case of a parallelogram.

(2) In general, the stiffness matrix of the quadrilateral element constructed by the isoparametric coordinates has to be evaluated by numerical integration instead of exact integration, which leads to the loss of accuracy.

(3) Serendipity isoparametric elements are very sensitive to mesh distortion. Although the shape functions of these elements contain high-order terms of ξ and η , they have only first-order completeness in the Cartesian coordinates x and y . Detailed discussions of this can be found in reference [12], and some convincing numerical examples are also given.

On the other hand, the area coordinate method^[13,14] has been successfully applied in the construction of triangular elements. The coordinate transformation between the triangular area coordinates (L_1, L_2, L_3) and Cartesian coordinates (x, y) is

$$L_i = \frac{1}{2A} (a_i + b_i x + c_i y) \quad (i = 1, 2, 3) \quad (16-3)$$

where a_i, b_i, c_i are constants determined by the nodal coordinates (x_i, y_i) , e.g.

$$a_1 = x_2 y_3 - x_3 y_2, \quad b_1 = y_2 - y_3, \quad c_1 = x_3 - x_2 \quad (16-4)$$

There are only two independent coordinates in L_1, L_2, L_3 which should satisfy the identical equation

$$L_1 + L_2 + L_3 = 1 \quad (16-5)$$

The advantages of the triangular area co-ordinate method are:

- (1) The area coordinate L_i is natural and invariant, that is, when the Cartesian axes rotate, the area coordinate L_i of the given point is invariant.
- (2) The equation of the element boundary line is $L_i = 0$, and therefore the boundary condition is easy to express and be satisfied.
- (3) The inverse transformation of (16-3) is

$$x = \sum_{i=1}^3 L_i x_i, \quad y = \sum_{i=1}^3 L_i y_i \quad (16-6)$$

which is a linear relation, and vice versa.

(4) The stiffness matrix of the triangular element constructed by the area coordinate method can be easily formulated with exact integration instead of numerical integration.

In this chapter, the traditional area coordinate method, which is an efficient tool in the construction of triangular elements, is generalized to formulate the quadrilateral elements. Two characteristic parameters for quadrilateral elements and the general theory of the area coordinates for quadrilateral elements are presented. Thus, it offers a new way to formulate the quadrilateral elements.

16.3 Two Shape Characteristic Parameters of a Quadrilateral

16.3.1 The Definition of Two Shape Characteristic Parameters of a Quadrilateral

Quadrilaterals have various shapes. In references [1] and [3], two dimensionless parameters g_1 and g_2 are defined as the shape characteristic parameters of a quadrilateral (Fig. 16.1(a),(b)):

$$g_1 = \frac{A(\triangle 124)}{A}, \quad g_2 = \frac{A(\triangle 123)}{A} \quad (16-7)$$

where A is the quadrilateral area, and $A(\triangle 124)$ and $A(\triangle 123)$ are triangular areas of $\triangle 124$ and $\triangle 123$, respectively. If we set $g_3 = 1 - g_1$, $g_4 = 1 - g_2$, then from Fig. 16.1 we see that two triangular areas on both sides of the diagonal 24 are $g_1 A$ and $g_3 A$, respectively; while two triangular areas on both sides of the diagonal 13 are $g_2 A$ and $g_4 A$, respectively.

For a convex quadrilateral, the ranges of parameters g_1 and g_2 are taken as

$$0 < g_1 < 1, \quad 0 < g_2 < 1 \quad (16-8)$$

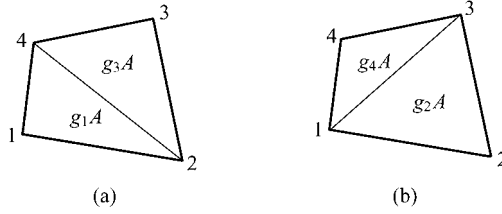


Figure 16.1 Definition of g_1, g_2, g_3 and g_4

from which we have

$$0 < g_3 < 1, \quad 0 < g_4 < 1$$

16.3.2 The Characteristic Conditions for a Quadrilateral to Degenerate into a Parallelogram or a Trapezoid or a Triangle

Special case 1 The characteristic condition under which a quadrilateral degenerates into a parallelogram (including rectangle) is

$$g_1 = g_2 = \frac{1}{2} \tag{16-9}$$

from which we have

$$g_3 = g_4 = \frac{1}{2}$$

Special case 2 The characteristic condition under which a quadrilateral degenerates into a trapezoid is

$$(g_1 - g_2)(g_2 - g_3) = 0 \tag{16-10}$$

which can be resolved into two sub-conditions as follows:

$$g_1 - g_2 = 0 \tag{16-11a}$$

or

$$g_2 - g_3 = 0 \tag{16-11b}$$

Only one of these two sub-conditions needs to be satisfied. They are in correspondence with two degeneration cases respectively as follows:

Condition (16-11a) corresponds to a trapezoid of kind A ($\overline{12//34}$, Fig. 16.2(a)).

Condition (16-11b) corresponds to a trapezoid of kind B ($\overline{23//41}$, Fig. 16.2(b)).

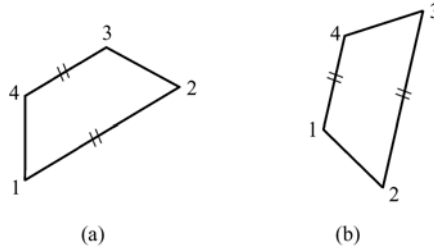


Figure 16.2 Two kinds of trapezoids

(a) Trapezoid of kind $A(1\bar{2} // \bar{3}4)g_1 - g_2 = g_4 - g_3 = 0$; (b) Trapezoid of kind $B(2\bar{3} // \bar{4}1)g_2 - g_3 = g_1 - g_4 = 0$

If both sub-conditions (16-11a,b) are satisfied simultaneously, then the condition (16-9) should be satisfied, which means it degenerates into a parallelogram.

Special case 3 The characteristic condition under which a quadrilateral degenerates into a triangle is

$$g_1 g_2 g_3 g_4 = 0 \tag{16-12}$$

which can be resolved into four sub-conditions as follows:

$$g_1 = 0 \tag{16-13a}$$

or

$$g_2 = 0 \tag{16-13b}$$

or

$$g_3 = 0 \tag{16-13c}$$

or

$$g_4 = 0 \tag{16-13d}$$

If any of the sub-conditions (16-13a,b,c,d) is satisfied, then some three adjacent nodes of the quadrilateral are in line with each other, so the quadrilateral degenerates into one of the four kinds of triangles in Fig. 16.3.

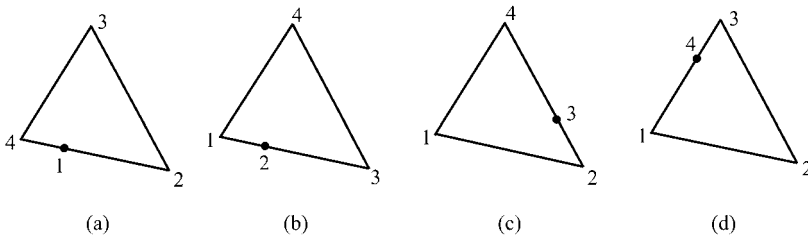


Figure 16.3 Degeneration into four kinds of triangles (some three nodes in line).

(a) $g_1 = 0$ (4,1,2 in line); (b) $g_2 = 0$ (1,2,3 in line); (c) $g_3 = 0$ (2,3,4 in line); (d) $g_4 = 0$ (3,4,1 in line)

If any two adjacent sub-conditions (16-13a,b,c,d) are satisfied simultaneously, then some two adjacent nodes are in coincidence with each other, so the quadrilateral degenerates into one of the four kinds of triangles in Fig. 16.4.

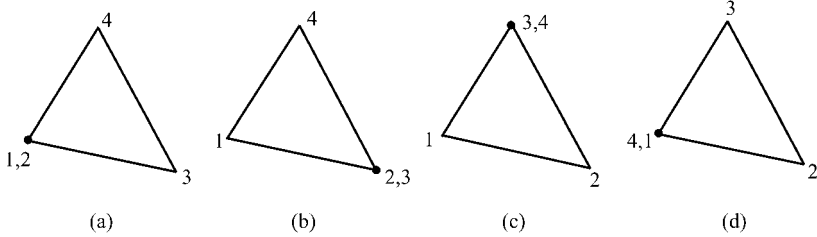


Figure 16.4 Degeneration into four kinds of triangles (some two adjacent nodes in coincidence).

- (a) $g_1 = g_2 = 0$ (1,2 in coincidence);
- (b) $g_2 = g_3 = 0$ (2,3 in coincidence);
- (c) $g_3 = g_4 = 0$ (3,4 in coincidence);
- (d) $g_4 = g_1 = 0$ (4,1 in coincidence)

16.3.3 Two Identical Relations among Nodal Cartesian Coordinates and Parameters g_1 and g_2

The Cartesian coordinates of node i of a quadrilateral are denoted by (x_i, y_i) , $i = 1, 2, 3, 4$. There are two identical relations among (x_i, y_i) and (g_1, g_2) as follows:

$$(1 - g_1) \begin{Bmatrix} x_1 \\ y_1 \end{Bmatrix} - (1 - g_2) \begin{Bmatrix} x_2 \\ y_2 \end{Bmatrix} + g_1 \begin{Bmatrix} x_3 \\ y_3 \end{Bmatrix} - g_2 \begin{Bmatrix} x_4 \\ y_4 \end{Bmatrix} = \begin{Bmatrix} 0 \\ 0 \end{Bmatrix} \quad (16-14)$$

which can also be written as

$$g_3 \begin{Bmatrix} x_1 \\ y_1 \end{Bmatrix} - g_4 \begin{Bmatrix} x_2 \\ y_2 \end{Bmatrix} + g_1 \begin{Bmatrix} x_3 \\ y_3 \end{Bmatrix} - g_2 \begin{Bmatrix} x_4 \\ y_4 \end{Bmatrix} = \begin{Bmatrix} 0 \\ 0 \end{Bmatrix}$$

Proof Point 5, for which the coordinates are assumed to be (x_5, y_5) , is the intersection point of two quadrilateral diagonals 13 and 24 (Fig. 16.5).

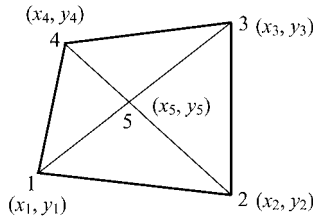


Figure 16.5 Intersection point 5 of diagonals

Firstly, from diagonal 153, we obtain

$$\begin{Bmatrix} x_5 \\ y_5 \end{Bmatrix} = \begin{Bmatrix} x_1 \\ y_1 \end{Bmatrix} + g_1 \begin{Bmatrix} x_3 - x_1 \\ y_3 - y_1 \end{Bmatrix} \quad (16-15)$$

Secondly, from diagonal 254, we obtain

$$\begin{Bmatrix} x_5 \\ y_5 \end{Bmatrix} = \begin{Bmatrix} x_2 \\ y_2 \end{Bmatrix} + g_2 \begin{Bmatrix} x_4 - x_2 \\ y_4 - y_2 \end{Bmatrix} \quad (16-16)$$

From the above equations, Eq. (16-14) can be obtained. \square

16.3.4 The Quadrilateral Determined by Its Base Triangle and Parameters g_1 and g_2

For convenience, we only discuss the case of a convex quadrilateral.

Take the triangle $\triangle 123$ as the base triangle of the quadrilateral (Fig. 16.1(b)). If the base triangle $\triangle 123$ is given, then the coordinate (x_4, y_4) of the fourth node can be determined by g_1 and g_2 as follows:

$$g_2 \begin{Bmatrix} x_4 \\ y_4 \end{Bmatrix} = (1 - g_1) \begin{Bmatrix} x_1 \\ y_1 \end{Bmatrix} - (1 - g_2) \begin{Bmatrix} x_2 \\ y_2 \end{Bmatrix} + g_1 \begin{Bmatrix} x_3 \\ y_3 \end{Bmatrix} \quad (16-17)$$

In fact, Eq. (16-17) can be obtained from Eq. (16-14).

Thus, we can draw a conclusion that a quadrilateral can be determined by the parameters g_1 and g_2 and its base triangle. In other words, if the base triangle is given, the corresponding quadrilateral varies with g_1 and g_2 . Otherwise, if g_1 and g_2 are given, it varies with the base triangle.

It can be proved that the above conclusion still holds if the quadrilateral degenerates into a triangle.

16.4 The Definition of Quadrilateral Area Coordinates (QACM-I)

16.4.1 Definition

In a quadrilateral, the area coordinates (L_1, L_2, L_3, L_4) of any point P are defined as

$$L_i = \frac{A_i}{A} \quad (i = 1, 2, 3, 4) \quad (16-18)$$

where A_1, A_2, A_3, A_4 are the areas of the four triangles formed by point P and two adjacent vertices in the quadrilateral element, respectively (Fig. 16.6).

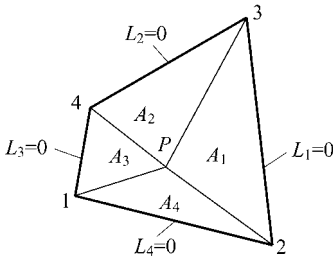


Figure 16.6 The definition of quadrilateral area coordinates

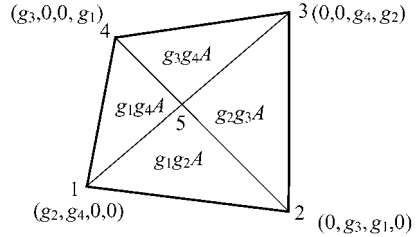


Figure 16.7 Nodal coordinates

Obviously, the equation of every side in a quadrilateral element is

$$L_i = 0 \quad (i = 1, 2, 3, 4) \tag{16-19}$$

The area co-ordinates of the four nodes are (Fig. 16.7):

$$\left. \begin{array}{l} \text{node 1 } (g_2, g_4, 0, 0) \\ \text{node 2 } (0, g_3, g_1, 0) \\ \text{node 3 } (0, 0, g_4, g_2) \\ \text{node 4 } (g_3, 0, 0, g_1) \end{array} \right\} \tag{16-20}$$

The area coordinates of the intersection point 5 of diagonal lines are (Fig. 16.7)

$$(g_2g_3, g_3g_4, g_4g_1, g_1g_2) \tag{16-21}$$

16.4.2 Area Coordinates Expressed by Cartesian Coordinates

The triangle area A_1, A_2, A_3, A_4 in Fig. 16.6 can be obtained by the determinants:

$$\left. \begin{array}{l} A_1 = \frac{1}{2} \begin{vmatrix} 1 & x & y \\ 1 & x_2 & y_2 \\ 1 & x_3 & y_3 \end{vmatrix}, \quad A_2 = \frac{1}{2} \begin{vmatrix} 1 & x & y \\ 1 & x_3 & y_3 \\ 1 & x_4 & y_4 \end{vmatrix} \\ A_3 = \frac{1}{2} \begin{vmatrix} 1 & x & y \\ 1 & x_4 & y_4 \\ 1 & x_1 & y_1 \end{vmatrix}, \quad A_4 = \frac{1}{2} \begin{vmatrix} 1 & x & y \\ 1 & x_1 & y_1 \\ 1 & x_2 & y_2 \end{vmatrix} \end{array} \right\} \tag{16-22}$$

Substituting Eq. (16-22) into Eq. (16-18), we obtain the transformation formula from the Cartesian coordinates to the area coordinates:

$$L_i = \frac{1}{2A}(a_i + b_i x + c_i y) \quad (i = 1, 2, 3, 4) \quad (16-23)$$

in which

$$\begin{aligned} a_i &= x_j y_k - x_k y_j, \quad b_i = y_j - y_k, \quad c_i = x_k - x_j \\ (i &= \overline{1, 2, 3, 4}; \quad j = \overline{2, 3, 4, 1}; \quad k = \overline{3, 4, 1, 2}) \end{aligned} \quad (16-24)$$

The transformation formula (16-23) is linear and similar to formula (16-3).

16.4.3 Two Sets of Equalities about a_i, b_i, c_i

About a_i, b_i and c_i the following two sets of equalities can be obtained:

$$\begin{Bmatrix} \sum_{i=1}^4 a_i \\ \sum_{i=1}^4 b_i \\ \sum_{i=1}^4 c_i \end{Bmatrix} = \begin{Bmatrix} 2A \\ 0 \\ 0 \end{Bmatrix} \quad (16-25)$$

$$g_4 g_1 \begin{Bmatrix} a_1 \\ b_1 \\ c_1 \end{Bmatrix} - g_1 g_2 \begin{Bmatrix} a_2 \\ b_2 \\ c_2 \end{Bmatrix} + g_2 g_3 \begin{Bmatrix} a_3 \\ b_3 \\ c_3 \end{Bmatrix} - g_3 g_4 \begin{Bmatrix} a_4 \\ b_4 \\ c_4 \end{Bmatrix} = \begin{Bmatrix} 0 \\ 0 \\ 0 \end{Bmatrix} \quad (16-26)$$

The proof of formula (16-25) is much easier. The first and second formulas of Eq. (16-26) are proved as follows.

The proof of the second formula of Eq. (16-26):

$$\begin{aligned} \text{LHS} &= g_4 g_1 b_1 - g_1 g_2 b_2 + g_2 g_3 b_3 - g_3 g_4 b_4 \\ &= g_4 g_1 (y_2 - y_3) - g_1 g_2 (y_3 - y_4) + g_2 g_3 (y_4 - y_1) - g_3 g_4 (y_1 - y_2) \\ &= -y_1 g_3 + y_2 g_4 - y_3 g_1 + y_4 g_2 \\ &= 0 \end{aligned} \quad \square$$

Equation (16-14) is quoted in the last step of the above proof, and the proof of the third formula of Eq. (16-26) is similar to this.

The proof of the first formula of Eq. (16-26):

$$\begin{aligned}
 \text{LHS} &= g_4 g_1 a_1 - g_1 g_2 a_2 + g_2 g_3 a_3 - g_3 g_4 a_4 \\
 &= g_4 g_1 (x_2 y_3 - x_3 y_2) - g_1 g_2 (x_3 y_4 - x_4 y_3) + g_2 g_3 (x_4 y_1 - x_1 y_4) - g_3 g_4 (x_1 y_2 - x_2 y_1) \\
 &= -x_1 g_3 (g_2 y_4 + g_4 y_2) + x_2 g_4 (g_3 y_1 + g_1 y_3) - x_3 g_1 (g_4 y_2 + g_2 y_4) + x_4 g_2 (g_1 y_3 + g_3 y_1) \\
 &= (g_2 y_4 + g_4 y_2)(-x_1 g_3 + x_2 g_4 - x_3 g_1 + x_4 g_2) \\
 &= 0
 \end{aligned}$$

□

Equation (16-14) is quoted twice in the last two steps of the above proof.

16.4.4 g_1 and g_2 Expressed by b_i and c_i

From Fig. 16.1(a), we have

$$2Ag_1 = \begin{vmatrix} 1 & x_1 & y_1 \\ 1 & x_2 & y_2 \\ 1 & x_4 & y_4 \end{vmatrix} = \begin{vmatrix} 1 & x_1 & y_1 \\ 0 & c_4 & -b_4 \\ 0 & -c_3 & b_3 \end{vmatrix} = b_3 c_4 - b_4 c_3$$

With cyclic permutation of $g_1 \rightarrow g_2 \rightarrow g_3 \rightarrow g_4 \rightarrow g_1$, we obtain the following formulae:

$$\left. \begin{aligned}
 2Ag_1 &= b_3 c_4 - b_4 c_3 \\
 2Ag_2 &= b_4 c_1 - b_1 c_4 \\
 2Ag_3 &= b_1 c_2 - b_2 c_1 \\
 2Ag_4 &= b_2 c_3 - b_3 c_2
 \end{aligned} \right\} \quad (16-27)$$

which can be used to obtain

$$\left. \begin{aligned}
 2A(g_3 - g_2) &= b_3 c_1 - b_1 c_3 \\
 2A(g_2 - g_1) &= b_2 c_4 - b_4 c_2 \\
 2A &= (b_3 c_4 - b_4 c_3) + (b_1 c_2 - b_2 c_1) = (b_4 c_1 - b_1 c_4) + (b_2 c_3 - b_3 c_2) \\
 &= \frac{1}{2} [(b_1 - b_3)(c_2 - c_4) - (b_2 - b_4)(c_1 - c_3)]
 \end{aligned} \right\} \quad (16-28)$$

16.5 Two Identical Relations Among Area Coordinates (QACM-I)

16.5.1 Two Identical Relations Satisfied by the Area Co-Ordinates (QACM-I)

An arbitrary point in a quadrilateral has two DOFs. Obviously, in the four area

co-ordinates, only two are independent. Namely, there are two identical relations which the four area co-ordinates should satisfy. They are firstly presented and proved in reference [1]:

$$L_1 + L_2 + L_3 + L_4 = 1 \quad (16-29)$$

$$g_4g_1L_1 - g_1g_2L_2 + g_2g_3L_3 - g_3g_4L_4 = 0 \quad (16-30)$$

These two identical relations (16-29) and (16-30), are the fundamental part in the complete definition of the quadrilateral area coordinates. In other words, Eq. (16-18), together with the relations (16-29) and (16-30), constitutes a complete definition of the quadrilateral area coordinate system.

Equation (16-29) holds, obviously, and Eq. (16-30) can be proved as follows.

The proof of Eq. (16-30):

By quoting Eqs. (16-23) and (16-26), Eq. (16-30) can be proved as follows:

$$\begin{aligned} \text{LHS} &= g_4g_1L_1 - g_1g_2L_2 + g_2g_3L_3 - g_3g_4L_4 \\ &= \frac{1}{2A} [g_4g_1(a_1 + b_1x + c_1y) - g_1g_2(a_2 + b_2x + c_2y) + g_2g_3(a_3 + b_3x + c_3y) \\ &\quad - g_3g_4(a_4 + b_4x + c_4y)] \\ &= \frac{1}{2A} \{ [g_4g_1a_1 - g_1g_2a_2 + g_2g_3a_3 - g_3g_4a_4] + x[g_4g_1b_1 - g_1g_2b_2 \\ &\quad + g_2g_3b_3 - g_3g_4b_4] + y[g_4g_1c_1 - g_1g_2c_2 + g_2g_3c_3 - g_3g_4c_4] \} \\ &= 0 \quad \square \end{aligned}$$

Though a definition of the quadrilateral area coordinates similar to Eq. (16-18) has been suggested for constructing several simple contact functions in reference [15], only the establishment of the above identical Eq. (16-30) indicates that the QACM-I can be treated as a complete system.

16.5.2 Use Independent Area Co-Ordinates to Express Others

There are only two independent area coordinates in (L_1, L_2, L_3, L_4) . Independent coordinates can be taken in many ways, but they must be adjacent coordinates, e.g.

$$(L_1, L_2), (L_2, L_3), (L_3, L_4), (L_4, L_1)$$

Otherwise, two opposite coordinates, e.g. (L_1, L_3) or (L_2, L_4) , cannot be taken as independent coordinates. From the rectangle case (a special case of quadrilateral) we can easily understand this conclusion.

Take (L_1, L_2) as independent coordinates:

$$\left. \begin{aligned} L_3 &= g_4 - \frac{g_4}{g_3} L_1 + \frac{g_1 - g_4}{g_3} L_2 \\ L_4 &= g_2 + \frac{g_1 - g_2}{g_3} L_1 - \frac{g_2}{g_3} L_2 \end{aligned} \right\} \quad (16-31)$$

Take (L_2, L_3) as independent coordinates:

$$\left. \begin{aligned} L_4 &= g_1 - \frac{g_1}{g_4} L_2 + \frac{g_2 - g_1}{g_4} L_3 \\ L_1 &= g_3 + \frac{g_2 - g_3}{g_4} L_2 - \frac{g_3}{g_4} L_3 \end{aligned} \right\} \quad (16-32)$$

Take (L_3, L_4) as independent coordinates:

$$\left. \begin{aligned} L_1 &= g_2 - \frac{g_2}{g_1} L_3 + \frac{g_3 - g_2}{g_1} L_4 \\ L_2 &= g_4 + \frac{g_3 - g_4}{g_1} L_3 - \frac{g_4}{g_1} L_4 \end{aligned} \right\} \quad (16-33)$$

Take (L_4, L_1) as independent coordinates:

$$\left. \begin{aligned} L_2 &= g_3 - \frac{g_3}{g_2} L_4 + \frac{g_4 - g_3}{g_2} L_1 \\ L_3 &= g_1 + \frac{g_4 - g_1}{g_2} L_4 - \frac{g_1}{g_2} L_1 \end{aligned} \right\} \quad (16-34)$$

16.6 Transformation Relations Between the Area Coordinate System (QACM-I) and the Cartesian or Isoparametric Coordinate System

16.6.1 Cartesian Coordinates Expressed by the Area Coordinates (QACM-I)

Equation (16-23) is the coordinate transformation formula from Cartesian to area co-ordinates. Now, we derive its inverse formula with which the Cartesian coordinates are expressed by the area coordinates.

Since there are four different ways to take the independent area coordinates: (L_1, L_2) , (L_2, L_3) , (L_3, L_4) , (L_4, L_1) , four inverse transformation formulae can be obtained.

Take (L_1, L_2) as independent coordinates:

$$\left. \begin{aligned} x &= \frac{1}{g_3}(c_2L_1 - c_1L_2) + x_3 \\ y &= \frac{1}{g_3}(-b_2L_1 + b_1L_2) + y_3 \end{aligned} \right\} \quad (16-35)$$

Take (L_2, L_3) as independent coordinates:

$$\left. \begin{aligned} x &= \frac{1}{g_4}(c_3L_2 - c_2L_3) + x_4 \\ y &= \frac{1}{g_4}(-b_3L_2 + b_2L_3) + y_4 \end{aligned} \right\} \quad (16-36)$$

Take (L_3, L_4) as independent coordinates:

$$\left. \begin{aligned} x &= \frac{1}{g_1}(c_4L_3 - c_3L_4) + x_1 \\ y &= \frac{1}{g_1}(-b_4L_3 + b_3L_4) + y_1 \end{aligned} \right\} \quad (16-37)$$

Take (L_4, L_1) as independent coordinates:

$$\left. \begin{aligned} x &= \frac{1}{g_2}(c_1L_4 - c_4L_1) + x_2 \\ y &= \frac{1}{g_2}(-b_1L_4 + b_4L_1) + y_2 \end{aligned} \right\} \quad (16-38)$$

16.6.2 Quadrilateral Area Coordinates (QACM-I) Expressed by the Isoparametric Coordinates

Area coordinates (L_1, L_2, L_3, L_4) can be expressed by the quadrilateral isoparametric coordinates (ξ, η) as follows:

$$\left. \begin{aligned} L_1 &= \frac{1}{4}(1 - \xi)[g_2(1 - \eta) + g_3(1 + \eta)] \\ L_2 &= \frac{1}{4}(1 - \eta)[g_3(1 + \xi) + g_4(1 - \xi)] \\ L_3 &= \frac{1}{4}(1 + \xi)[g_4(1 + \eta) + g_1(1 - \eta)] \\ L_4 &= \frac{1}{4}(1 + \eta)[g_1(1 - \xi) + g_2(1 + \xi)] \end{aligned} \right\} \quad (16-39)$$

It is known that area co-ordinates $L_i (i = 1,2,3,4)$ are the linear functions of the Cartesian coordinates (x, y) . Assume that Z stands for any arbitrary linear function of (x, y) ; then it can be expressed by the quadrilateral isoparametric coordinate (ξ, η) as follows:

$$Z = \frac{1}{4} \sum_{i=1}^4 Z_i (1 + \xi_i \xi) (1 + \eta_i \eta) \tag{16-40}$$

where Z_i, ξ_i, η_i are the values of Z, ξ, η at node i . According to Eq. (16-40) we can obtain Eq. (16-39). Taking the first formula of Eq. (16-39) as an example, Z stands for L_1 . From Eq. (16-20), we get

$$[Z_1 \quad Z_2 \quad Z_3 \quad Z_4] = [g_2 \quad 0 \quad 0 \quad g_3] \tag{16-41}$$

Substituting this into Eq. (16-40), the first formula of Eq. (16-39) can be obtained.

16.7 Differential Formulae (QACM-I)

16.7.1 Transformations of Derivatives (QACM-I)

In a quadrilateral element, any point P has four area coordinate components (L_1, L_2, L_3, L_4) to which the transformation from the Cartesian coordinates (x, y) is given by Eq. (16-23), i.e.,

$$L_i = \frac{1}{2A} (a_i + b_i x + c_i y) \quad (i = 1, 2, 3, 4)$$

From the above equation, the transformation of derivatives of the first and second order in both coordinate systems is presented as follows:

- (1) The transformation of the derivatives of the first order:

$$\begin{Bmatrix} \frac{\partial}{\partial x} \\ \frac{\partial}{\partial y} \end{Bmatrix} = \frac{1}{2A} \begin{bmatrix} b_1 & b_2 & b_3 & b_4 \\ c_1 & c_2 & c_3 & c_4 \end{bmatrix} \boldsymbol{\partial} \tag{16-42}$$

where

$$\boldsymbol{\partial} = \left[\frac{\partial}{\partial L_1} \quad \frac{\partial}{\partial L_2} \quad \frac{\partial}{\partial L_3} \quad \frac{\partial}{\partial L_4} \right]^T \tag{16-43}$$

The direction cosines of the normal vector of each side are:

$$\cos(n_i, x) = -\frac{b_i}{d_i}, \quad \cos(n_i, y) = -\frac{c_i}{d_i} \tag{16-48}$$

The direction cosines of the tangential vector of each side are:

$$\cos(s_i, x) = \frac{c_i}{d_i}, \quad \cos(s_i, y) = -\frac{b_i}{d_i} \tag{16-49}$$

The normal derivative of each side is:

$$\begin{aligned} \frac{\partial}{\partial n_i} &= -\frac{1}{d_i} \left(b_i \frac{\partial}{\partial x} + c_i \frac{\partial}{\partial y} \right) = -\frac{1}{d_i} [b_i \quad c_i] \begin{Bmatrix} \frac{\partial}{\partial x} \\ \frac{\partial}{\partial y} \end{Bmatrix} \\ &= -\frac{1}{2Ad_i} [b_i \quad c_i] \begin{bmatrix} b_1 & b_2 & b_3 & b_4 \\ c_1 & c_2 & c_3 & c_4 \end{bmatrix} \boldsymbol{\theta} \end{aligned} \tag{16-50}$$

The tangential derivative of each side is

$$\begin{aligned} \frac{\partial}{\partial s_i} &= \frac{1}{d_i} \left(c_i \frac{\partial}{\partial x} - b_i \frac{\partial}{\partial y} \right) = \frac{1}{d_i} [c_i \quad -b_i] \begin{Bmatrix} \frac{\partial}{\partial x} \\ \frac{\partial}{\partial y} \end{Bmatrix} \\ &= \frac{1}{2Ad_i} [c_i \quad -b_i] \begin{bmatrix} b_1 & b_2 & b_3 & b_4 \\ c_1 & c_2 & c_3 & c_4 \end{bmatrix} \boldsymbol{\theta} \end{aligned} \tag{16-51}$$

16.8 Integral Formulae (QACM-I)

16.8.1 The Basic Formulae for Area Integrals (QACM-I)

In a quadrilateral element, two equivalent basic integral formulae, which can be applied to evaluate the area integrals for the arbitrary power function $L_1^m L_2^n L_3^p L_4^q$ of the area coordinates, are given as follows:

$$\begin{aligned} \iint_A L_1^m L_2^n L_3^p L_4^q dA &= \frac{m!n!p!q!}{(m+n+p+q+2)!} 2A \\ &\times \left[g_3^{m+n+1} \sum_{k=0}^q \sum_{j=0}^p C_{m+q-k}^m C_{n+p-j}^n C_{k+j}^k g_2^k g_4^j g_1^{p+q-k-j} \right. \\ &\left. + g_1^{p+q+1} \sum_{k=0}^m \sum_{j=0}^n C_{m+q-k}^q C_{n+p-j}^p C_{k+j}^k g_2^k g_4^j g_3^{m+n-k-j} \right] \end{aligned} \tag{A}$$

$$\iint_A L_1^m L_2^n L_3^p L_4^q dA = \frac{m!n!p!q!}{(m+n+p+q+2)!} 2A \times \left[\begin{aligned} &g_4^{n+p+1} \sum_{k=0}^m \sum_{j=0}^q C_{n+m-k}^n C_{p+q-j}^p C_{k+j}^k g_3^k g_1^j g_2^{m+q-k-j} \\ &+ g_2^{m+q+1} \sum_{k=0}^n \sum_{j=0}^p C_{m+n-k}^m C_{q+p-j}^q C_{k+j}^k g_3^k g_1^j g_4^{n+p-k-j} \end{aligned} \right] \quad (B)$$

where
$$C_k^i = \frac{k!}{(k-i)!i!} \quad (16-52)$$

In fact, with the cyclic permutation that we change (m, n, p, q) to (n, p, q, m) and (g_1, g_2, g_3, g_4) to (g_2, g_3, g_4, g_1) in Eq. (A), Eq. (B) can be obtained.

If a quadrilateral element degenerates into a triangular element, e.g. when $g_1 = g_2 = 0$, nodes 1 and 2 become coincident; thus $L_4 = 0, q = 0$, and we substitute them into Eq. (A) or Eq. (B), so that the following famous integral formula for the arbitrary power function of the area coordinates over the triangular element is obtained^[14]:

$$\iint_A L_1^m L_2^n L_3^p dA = \frac{m!n!p!}{(m+n+p+2)!} 2A \quad (16-53)$$

16.8.2 Area Integral Formulae for Lower Power Functions (QACM-I)

For convenience in application, we list the area integral formulae for lower power functions (from first order to third order) as follows according to the basic formulae (A) or (B).

- (1) The first power terms (four in one group)

$$\iint_A \left\{ \begin{matrix} L_1 \\ L_2 \\ L_3 \\ L_4 \end{matrix} \right\} dA = \frac{A}{3} \left\{ \begin{matrix} 1 - g_4 g_1 \\ 1 - g_1 g_2 \\ 1 - g_2 g_3 \\ 1 - g_3 g_4 \end{matrix} \right\} \quad (16-54)$$

- (2) The second power terms (ten in three groups)

$$\iint_A \left\{ \begin{matrix} L_1^2 \\ L_2^2 \\ L_3^2 \\ L_4^2 \end{matrix} \right\} dA = \frac{A}{6} \left\{ \begin{matrix} g_3^2 + g_1 g_2 (g_2 + g_3) \\ g_4^2 + g_2 g_3 (g_3 + g_4) \\ g_1^2 + g_3 g_4 (g_4 + g_1) \\ g_2^2 + g_4 g_1 (g_1 + g_2) \end{matrix} \right\} \quad (16-55)$$

$$\iint_A \begin{Bmatrix} L_1 L_2 \\ L_2 L_3 \\ L_3 L_4 \\ L_4 L_1 \end{Bmatrix} dA = \frac{A}{12} \begin{Bmatrix} g_3 + 2g_4 g_1 g_2 \\ g_4 + 2g_1 g_2 g_3 \\ g_1 + 2g_2 g_3 g_4 \\ g_2 + 2g_3 g_4 g_1 \end{Bmatrix} \tag{16-56}$$

$$\iint_A \begin{Bmatrix} L_1 L_3 \\ L_2 L_4 \end{Bmatrix} dA = \frac{A}{12} \begin{Bmatrix} g_4 - g_1 + 2g_1 g_2 \\ g_1 - g_2 + 2g_2 g_3 \end{Bmatrix} \tag{16-57}$$

(3) The third power terms (20 in five groups)

Considering the above integral formulae (16-54)–(16-57), we find that if the formula in the first line of any group is known, then the others in this group can easily be obtained with the cyclic permutation of $(L_1 \rightarrow L_2 \rightarrow L_3 \rightarrow L_4 \rightarrow L_1$ and $g_1 \rightarrow g_2 \rightarrow g_3 \rightarrow g_4 \rightarrow g_1)$. Thus, only the first formula in each group needs to be listed, for brevity:

$$\iint_A L_1^3 dA = \frac{A}{10} [g_3^3 + g_1 g_2 (g_2^2 + g_2 g_3 + g_3^2)] \tag{16-58}$$

$$\iint_A L_1^2 L_2 dA = \frac{A}{30} [g_3^2 + 2g_1 g_2 g_3 + g_2^2 g_1 (2 + g_1) - 3g_2^3 g_1] \tag{16-59}$$

$$\iint_A L_1^2 L_3 dA = \frac{A}{30} [g_3^2 + g_2 g_3 (1 - 2g_3) + g_2^2 g_1^2] \tag{16-60}$$

$$\iint_A L_1^2 L_4 dA = \frac{A}{30} [3g_1 g_3^2 + g_2 g_3 (g_3^2 + 2g_1^2) + g_1^2 g_2^2] \tag{16-61}$$

$$\iint_A L_1 L_2 L_3 dA = \frac{A}{60} [g_4 - g_1 + 3g_1 g_2 - 2g_1^2 g_2^2] \tag{16-62}$$

16.8.3 The Basic Formulae for Line Integrals (QACM-I)

In a quadrilateral element, the following basic formulae can be used to evaluate the line integral for the arbitrary power function of the area coordinates along each side $L_i = 0$ ($i = 1, 2, 3, 4$):

Along side $12 (L_4 = 0)$

$$\int_0^1 L_1^m L_2^n L_3^p d\bar{s} = \frac{m! n! p!}{(m + n + p + 1)!} g_2^m g_1^p \sum_{k=0}^n g_3^{n-k} g_4^k C_{p+n-k}^p C_{m+k}^m \tag{C1}$$

Along side $\overline{23}(L_1 = 0)$

$$\int_0^1 L_2^p L_3^q L_4^q d\bar{s} = \frac{n!p!q!}{(n+p+q+1)!} g_3^n g_2^q \sum_{k=0}^p g_4^{p-k} g_1^k C_{q+p-k}^q C_{n+k}^n \quad (C2)$$

Along side $\overline{34}(L_2 = 0)$

$$\int_0^1 L_3^p L_4^q L_1^m d\bar{s} = \frac{p!q!m!}{(p+q+m+1)!} g_4^p g_3^m \sum_{k=0}^q g_1^{q-k} g_2^k C_{m+q-k}^m C_{p+k}^p \quad (C3)$$

Along side $\overline{41}(L_3 = 0)$

$$\int_0^1 L_4^q L_1^m L_2^n d\bar{s} = \frac{q!m!n!}{(q+m+n+1)!} g_1^q g_4^n \sum_{k=0}^m g_2^{m-k} g_3^k C_{n+m-k}^n C_{q+k}^q \quad (C4)$$

where \bar{s} is a dimensionless coordinate along side \overline{jk} , and it is 0 at node j and 1 at node k .

In fact, if the cyclic permutation is inserted in Eq. (C1), then Eqs. (C2), (C3) and (C4) can be obtained.

If quadrilateral elements degenerate into triangular elements, e.g. when $g_1 = g_2 = 0$, nodes 1 and 2 become coincident; thus $L_4 = 0$, $q = 0$, we substitute them into Eqs. (C2), (C3) and (C4), so that the following line integral formulae for the arbitrary power function over the triangular element sides are obtained:

$$\left. \begin{aligned} \int_0^1 L_2^n L_3^p d\bar{s} &= \frac{n!p!}{(n+p+1)!} && \text{(along } L_1 = 0) \\ \int_0^1 L_3^p L_1^m d\bar{s} &= \frac{p!m!}{(p+m+1)!} && \text{(along } L_2 = 0) \\ \int_0^1 L_1^m L_2^n d\bar{s} &= \frac{m!n!}{(m+n+1)!} && \text{(along } L_3 = 0) \end{aligned} \right\} \quad (16-63)$$

16.9 The Proof of the Basic Formulae (A) and (B) (QACM-I)

16.9.1 Preparative Formula (D)

$$\int_0^1 (1-t)^i t^j dt = \frac{i!j!}{(i+j+1)!} \quad (D)$$

Proof Using integration by parts

$$\int_0^1 u dv = uv \Big|_0^1 - \int_0^1 v du \quad (16-64)$$

we have

$$\begin{aligned} \text{LHS} &= \frac{1}{j+1} \int_0^1 (1-t)^i dt^{j+1} = \frac{i}{j+1} \int_0^1 (1-t)^{i-1} t^{j+1} dt \\ &= \frac{i!j!}{(i+j)!} \int_0^1 t^{j+i} dt = \frac{i!j!}{(i+j+1)!} = \text{RHS} \quad \square \end{aligned}$$

16.9.2 Preparative Formula (E)

$$\int_0^1 t^m (1-t)^n [\alpha t + \beta(1-t)]^p dt = \frac{m!n!p!}{(m+n+p+1)!} \sum_{k=0}^p \alpha^{p-k} \beta^k C_{m+p-k}^m C_{n+k}^n \quad (\text{E})$$

Proof From formula (D), we can write that

$$\begin{aligned} \text{LHS} &= \int_0^1 t^m (1-t)^n \left[\sum_{k=0}^p \frac{p!}{(p-k)!k!} \alpha^{p-k} \beta^k t^{p-k} (1-t)^k \right] dt \\ &\stackrel{(\text{D})}{=} \sum_{k=0}^p \frac{p!}{(p-k)!k!} \alpha^{p-k} \beta^k \frac{(m+p-k)!(n+k)!}{(m+n+p+1)!} \\ &= \frac{m!n!p!}{(m+n+p+1)!} \sum_{k=0}^p \alpha^{p-k} \beta^k C_{m+p-k}^m C_{n+k}^n = \text{RHS} \quad \square \end{aligned}$$

16.9.3 Subdivision of the Quadrilateral

In order to obtain the basic formula (A), the quadrilateral 1234 is subdivided into two triangles: $\triangle 234$ and $\triangle 124$ (Fig. 16.9). Assume that A , A' and A'' represent the areas of the quadrilateral 1234, $\triangle 234$ and $\triangle 124$, respectively, thus

$$A' = (1 - g_1)A = g_3A \quad (16-65)$$

$$A'' = g_1A \quad (16-66)$$

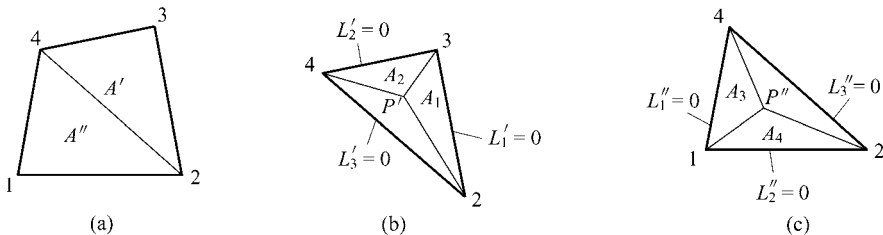


Figure 16.9 Subdivision I of a quadrilateral

Chapter 16 Quadrilateral Area Coordinate Systems, Part I— Theory and Formulae

Since the integral in the basic formula (A) is the integral over the quadrilateral area A (denoted by I), it can be expressed by the sum of the integrals over triangles A' and A'' (denoted by I_1 and I_2).

$$I = \iint_A L_1^m L_2^n L_3^p L_4^q dA = \iint_{A'} L_1^m L_2^n L_3^p L_4^q dA + \iint_{A''} L_1^m L_2^n L_3^p L_4^q dA = I_1 + I_2 \quad (16-67)$$

Consider an arbitrary point P' in $\triangle 234$ (Fig. 16.9(b)). We use two coordinate systems to describe point P' : quadrilateral area coordinates (L_1, L_2, L_3, L_4) and triangular area coordinates (L'_1, L'_2, L'_3) . The relation between these two coordinate systems is:

$$L_1 = g_3 L'_1 \quad (16-68a)$$

$$L_2 = g_3 L'_2 \quad (16-68b)$$

$$L_3 = g_1 L'_2 + g_4 L'_3 \quad (16-68c)$$

$$L_4 = g_1 L'_1 + g_2 L'_3 \quad (16-68d)$$

In fact, the first two formulae (16-68a,b) can be obtained from Eq. (16-65):

$$L_1 = \frac{A_1}{A} = A_1 \left(\frac{g_3}{A'} \right) = g_3 L'_1$$

$$L_2 = \frac{A_2}{A} = A_2 \left(\frac{g_3}{A'} \right) = g_3 L'_2$$

The last two formulae (16-68c,d) can be obtained from (16-31):

$$L_3 = g_4 - \frac{g_4}{g_3} L_1 + \frac{g_1 - g_4}{g_3} L_2 = g_4 - g_4 L'_1 + (g_1 - g_4) L'_2 = g_1 L'_2 + g_4 L'_3$$

$$L_4 = g_2 + \frac{g_1 - g_2}{g_3} L_1 - \frac{g_2}{g_3} L_2 = g_2 + (g_1 - g_2) L'_1 - g_2 L'_2 = g_1 L'_1 + g_2 L'_3$$

Similarly, the relations between these two coordinate systems of any point P'' in $\triangle 124$ are

$$L_3 = g_1 L''_1 \quad (16-69a)$$

$$L_4 = g_1 L''_2 \quad (16-69b)$$

$$L_1 = g_3 L''_2 + g_2 L''_3 \quad (16-69c)$$

$$L_2 = g_3 L''_1 + g_4 L''_3 \quad (16-69d)$$

16.9.4 Area Integral I_1

From the preparative formula (E) and the coordinate transformation (16-68), the area integral I_1 can be evaluated:

$$I_1 = \iint_{A'} L_1^m L_2^n L_3^p L_4^q dA = \frac{m!n!p!q!}{(m+n+p+q+2)!} 2A \times g_3^{m+n+1} \sum_{k=0}^q \sum_{j=0}^p C_{m+q-k}^m C_{n+p-j}^n C_{k+j}^k g_2^k g_4^j g_1^{p+q-k-j} \quad (16-70)$$

Now, we prove it as follows.

First, applying the coordinate transformation (16-68) and the differential area formula $dA = 2Ag_3 dL_1' dL_2'$, we have

$$I_1 = \iint_{A'} g_3^{m+n} L_1^m L_2^n (g_1 L_2' + g_4 L_3')^p (g_1 L_1' + g_2 L_3')^q \cdot 2Ag_3 dL_1' dL_2' \quad (16-71)$$

Second, introducing a new variable $t = \frac{L_2'}{1-L_1'}$, thus

$$I_1 = 2Ag_3^{m+n+1} \int_0^1 \{L_1^m (1-L_1')^{n+p+1} \int_0^1 t^n [g_1 t + g_4 (1-t)]^p \times [g_1 L_1' + g_2 (1-L_1')(1-t)]^q dt\} dL_1' \quad (16-72)$$

Since

$$[g_1 L_1' + g_2 (1-L_1')(1-t)]^q = \sum_{k=0}^q C_q^k g_1^{q-k} g_2^k L_1'^{q-k} (1-L_1')^k (1-t)^k \quad (16-73)$$

substituting it into (16-72), we obtain

$$I_1 = 2Ag_3^{m+n+1} \sum_{k=0}^q C_q^k g_1^{q-k} g_2^k \left(\int_0^1 L_1'^{m+q-k} (1-L_1')^{m+p+k+1} dL_1' \right) \left(\int_0^1 t^n (1-t)^k [g_1 t + g_4 (1-t)]^p dt \right)$$

in which the two integrals can be evaluated by the preparative formulae (D) and (E), and finally Eq. (16-70) is obtained.

16.9.5 Area Integral I_2 and the Derivation of Formula (A)

Similarly, using the coordinate transformation (16-69), we obtain the area integral I_2 as follows:

$$I_2 = \iint_{A'} L_1^m L_2^n L_3^p L_4^q dA = \frac{m!n!p!q!}{(m+n+p+q+2)!} 2A \times g_1^{p+q+1} \sum_{k=0}^m \sum_{j=0}^n C_{m+q-k}^q C_{n+p-j}^p C_{k+j}^k g_2^k g_4^j g_1^{m+n-k-j} \quad (16-74)$$

Superpose I_1 and I_2 obtained from (16-70) and (16-74), thus we can get the expression of area integral I , that is, the basic formula (A).

16.9.6 The Derivation of Formula (B)

The quadrilateral 1234 can be divided into two triangles: $\triangle 123$ and $\triangle 134$ in the way shown in Fig. 16.10. With similar steps, the basic formula (B) for the area integral can be derived.

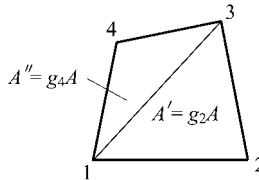


Figure 16.10 Subdivision II of a quadrilateral

16.10 The Proof of the Basic Formulae (C) (QACM-I)

16.10.1 Variation of Area Co-Ordinates (L_1, L_2, L_3, L_4) along Each Side

Define a dimensionless coordinate \bar{s} along side \overline{jk} in the way that it is 0 at node j and 1 at k . Thus, the area coordinate L_i is a linear function of \bar{s} along each side, which are listed in the following table.

$L_i =$	Along line $\overline{12}$ ($L_4 = 0$)	Along line $\overline{23}$ ($L_1 = 0$)	Along line $\overline{34}$ ($L_2 = 0$)	Along line $\overline{41}$ ($L_3 = 0$)
$L_1 =$	$g_2(1-\bar{s})$	0	$g_3\bar{s}$	$g_2\bar{s} + g_3(1-\bar{s})$
$L_2 =$	$g_3\bar{s} + g_4(1-\bar{s})$	$g_3(1-\bar{s})$	0	$g_4\bar{s}$
$L_3 =$	$g_1\bar{s}$	$g_4\bar{s} + g_1(1-\bar{s})$	$g_4(1-\bar{s})$	0
$L_4 =$	0	$g_2\bar{s}$	$g_1\bar{s} + g_2(1-\bar{s})$	$g_1(1-\bar{s})$

(16-75)

16.10.2 The Proof of Formula (C1)

Along side $\overline{12}$ ($L_4 = 0$), the area coordinates L_1, L_2, L_3 are linear functions of \bar{s}

as listed in the first column of the above table. Substitution into the LHS of (C1) yields

$$\begin{aligned}
 \text{LHS} &= g_2^m g_1^p \int_0^1 (1-\bar{s})^m \bar{s}^p [g_3 \bar{s} + g_4 (1-\bar{s})]^n d\bar{s} \\
 &= g_2^m g_1^p \int_0^1 (1-\bar{s})^m \bar{s}^p \left[\sum_{k=0}^n C_n^k g_3^{n-k} \bar{s}^{n-k} g_4^k (1-\bar{s})^k \right] d\bar{s} \\
 &= g_2^m g_1^p \sum_{k=0}^n C_n^k g_3^{n-k} g_4^k \int_0^1 \bar{s}^{p+n-k} (1-\bar{s})^{m+k} d\bar{s} \\
 \underline{\underline{\text{(D)}}} & g_2^m g_1^p \sum_{k=0}^n C_n^k g_3^{n-k} g_4^k \frac{(p+n-k)!(m+k)!}{(m+n+p+1)!} = \text{RHS}
 \end{aligned}$$

So, the formula (C1) holds. The preparative formula (D) is applied in the above steps. Similarly, the other three formulae of equation (C) can be proved.

16.11 The Quadrilateral Area Coordinate System with Two Components (QACM-II)

According to the definition of the QACM-I, this system contains four area coordinate components (L_1, L_2, L_3, L_4), among which two are independent. The existence of the four components must bring distinct complexity to the construction of an element, for example, users may be confused as to how to formulate a complete high order polynomial. And, most formulations expressed by the QACM-I are more complicated than those by the isoparametric coordinates. In view of the shortcomings of the QACM-I, another quadrilateral area coordinate method, denoted as QACM-II, is systematically established in this section. This new QACM-II possesses new physical meanings and contains only two coordinate components. It can not only avoid the defects mentioned above, but also keep the most important advantage of the QACM-I, that is, the linear relationship with the Cartesian coordinates.

Recently the third version of quadrilateral area coordinate method (QACM-III) was developed in reference [16].

16.11.1 The Definition of the New Quadrilateral Area Coordinates Method (QACM-II)

As shown in Fig. 16.11, M_i ($i=1,2,3,4$) are the mid-side points of element sides $\overline{23}$, $\overline{34}$, $\overline{41}$ and $\overline{12}$, respectively. Thus, the position of an arbitrary point P

within the quadrilateral element $\overline{1234}$ can be uniquely specified by the new two-component area coordinates Z_1 and Z_2 (QACM-II), which are defined as:

$$Z_1 = 4 \frac{\Omega_1}{A}, \quad Z_2 = 4 \frac{\Omega_2}{A} \tag{16-76}$$

where A is still the area of the quadrilateral element; Ω_1 and Ω_2 are the *generalized areas* of $\triangle PM_2M_4$ and $\triangle PM_3M_1$, respectively. It must be noted here that the values of *generalized areas* Ω_1 and Ω_2 can be both positive and negative: for $\triangle PM_2M_4$ (or $\triangle PM_3M_1$), if the permutation order of points P , M_2 and M_4 (or P , M_3 and M_1) is anti-clockwise, a positive Ω_1 (or Ω_2) should be taken; otherwise, Ω_1 (or Ω_2) should be negative.

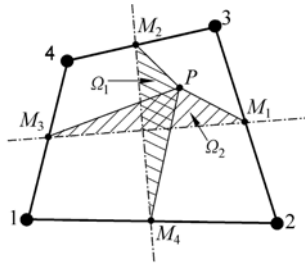


Figure 16.11 Definition of the quadrilateral area coordinates Z_i of QACM-II

Though the QACM-II (Eq.(16-76)) and the QACM-I (Eq. (16-18)) have different physical meanings, it can be proved that they satisfy the following simple linear relations:

$$\left. \begin{aligned} Z_1 &= 2(L_3 - L_1) + (g_2 - g_1) \\ Z_2 &= 2(L_4 - L_2) + (g_3 - g_2) \end{aligned} \right\} \tag{16-77}$$

where g_i ($i=1,2,3,4$) are the shape parameters of the quadrangle and given in Sect. 16.2.

Proof Let (x_i, y_i) ($i=1,2,3,4$) be the Cartesian coordinates of the four corner nodes 1, 2, 3 and 4, respectively; and (x, y) be the Cartesian coordinates of an arbitrary point P within the element. And, from Eq. (16-28), we have

$$\left. \begin{aligned} 2A(g_2 - g_1) &= -b_4c_2 + b_2c_4 \\ 2A(g_3 - g_2) &= b_3c_1 - b_1c_3 \end{aligned} \right\} \tag{16-78}$$

where b_i and c_i ($i=1,2,3,4$) are given by Eq. (16-24). Then, the *generalized areas* of $\triangle PM_2M_4$ and $\triangle PM_3M_1$ in Fig. 16.11 can be obtained as:

$$\Omega_1 = \frac{1}{2} \begin{vmatrix} 1 & x & y \\ 1 & \frac{x_3 + x_4}{2} & \frac{y_3 + y_4}{2} \\ 1 & \frac{x_1 + x_2}{2} & \frac{y_1 + y_2}{2} \end{vmatrix}, \quad \Omega_2 = \frac{1}{2} \begin{vmatrix} 1 & x & y \\ 1 & \frac{x_4 + x_1}{2} & \frac{y_4 + y_1}{2} \\ 1 & \frac{x_2 + x_3}{2} & \frac{y_2 + y_3}{2} \end{vmatrix} \quad (16-79)$$

Substitution of Eqs. (16-24), (16-78) and (16-79) into Eq. (16-76) yields

$$\begin{aligned} 4 \frac{\Omega_1}{A} &= \frac{1}{2} \frac{[(x_3 + x_4)(y_1 + y_2) - (x_1 + x_2)(y_3 + y_4)]}{A} + \frac{x(y_3 + y_4 - y_1 - y_2)}{A} \\ &\quad + \frac{y(x_1 + x_2 - x_3 - x_4)}{A} \\ &= \frac{[(x_4 y_1 - x_1 y_4) + x(y_4 - y_1) + y(x_1 - x_4)]}{A} \\ &\quad - \frac{[(x_2 y_3 - x_3 y_2) + x(y_2 - y_3) + y(x_3 - x_2)]}{A} \\ &\quad + \frac{(x_2 - x_1)(y_3 - y_4) + (x_3 - x_4)(y_1 - y_2)}{2A} \\ &= 2(L_3 - L_1) + \frac{b_2 c_4 - b_4 c_2}{2A} = 2(L_3 - L_1) + (g_2 - g_1) \end{aligned} \quad (16-80a)$$

$$\begin{aligned} 4 \frac{\Omega_2}{A} &= \frac{1}{2} \frac{[(x_4 + x_1)(y_2 + y_3) - (y_4 + y_1)(x_2 + x_3)]}{A} + \frac{x(y_4 + y_1 - y_2 - y_3)}{A} \\ &\quad + \frac{y(x_2 + x_3 - x_4 - x_1)}{A} \\ &= \frac{[(x_1 y_2 - x_2 y_1) + x(y_1 - y_2) + y(x_2 - x_1)]}{A} \\ &\quad - \frac{[(x_3 y_4 - x_4 y_3) + x(y_3 - y_4) + y(x_4 - x_3)]}{A} \\ &\quad + \frac{(x_3 - x_2)(y_4 - y_1) + (x_4 - x_1)(y_2 - y_3)}{2A} \\ &= 2(L_4 - L_2) + \frac{b_3 c_1 - b_1 c_3}{2A} = 2(L_4 - L_2) + (g_3 - g_2) \end{aligned} \quad (16-80b)$$

□

So, according to Eqs. (16-23) and (16-77), the new area coordinates Z_1 and Z_2 will also keep the linear relationship with the Cartesian coordinates (x, y) .

Here, for convenience, two new shape parameters \bar{g}_1 and \bar{g}_2 are defined as:

$$\left. \begin{aligned} \bar{g}_1 &= g_2 - g_1 \\ \bar{g}_2 &= g_3 - g_2 \end{aligned} \right\} \quad (16-81)$$

It can be seen that $\bar{g}_1 = \bar{g}_2 = 0$ for the rectangle cases. Thus, Eq. (16-77) can be rewritten as

$$\left. \begin{aligned} Z_1 &= 2(L_3 - L_1) + \bar{g}_1 \\ Z_2 &= 2(L_4 - L_2) + \bar{g}_2 \end{aligned} \right\} \quad (16-82)$$

And, the new local coordinates of the corner nodes and mid-side points can be written as:

$$\begin{aligned} \text{node1} & \quad (-1 + \bar{g}_2, -1 + \bar{g}_1); & \text{node2} & \quad (1 - \bar{g}_2, -1 - \bar{g}_1) \\ \text{node3} & \quad (1 + \bar{g}_2, 1 + \bar{g}_1); & \text{node4} & \quad (-1 - \bar{g}_2, 1 - \bar{g}_1) \\ M_1 & \quad (1, 0); & M_2 & \quad (0, 1) \\ M_3 & \quad (-1, 0); & M_4 & \quad (0, -1) \end{aligned}$$

It is interesting that the above coordinate values are only small modifications for the isoparametric coordinates.

16.11.2 The Relationship Between the QACM-II and the Cartesian Coordinates

Substitution of Eqs. (16-23) and (16-81) into Eq. (16-82) yields

$$\left. \begin{aligned} Z_1 &= \frac{1}{A}[(a_3 - a_1) + (b_3 - b_1)x + (c_3 - c_1)y] + \bar{g}_1 = \frac{1}{A}[\bar{a}_1 + \bar{b}_1x + \bar{c}_1y] + \bar{g}_1 \\ Z_2 &= \frac{1}{A}[(a_4 - a_2) + (b_4 - b_2)x + (c_4 - c_2)y] + \bar{g}_2 = \frac{1}{A}[\bar{a}_2 + \bar{b}_2x + \bar{c}_2y] + \bar{g}_2 \end{aligned} \right\} \quad (16-83)$$

where

$$\left. \begin{aligned} \bar{a}_1 &= a_3 - a_1, & \bar{b}_1 &= b_3 - b_1, & \bar{c}_1 &= c_3 - c_1 \\ \bar{a}_2 &= a_4 - a_2, & \bar{b}_2 &= b_4 - b_2, & \bar{c}_2 &= c_4 - c_2 \end{aligned} \right\} \quad (16-84)$$

The linear relationship between the QACM-II and the Cartesian coordinates is clearly illustrated.

16.11.3 The Relationship Between the QACM-II and the Isoparametric Coordinates

By substituting the relationship (16-39) of the QACM-I and the isoparametric coordinates and Eq. (16-81) into Eq. (16-82), we have

$$\left. \begin{aligned} Z_1 &= \xi + \bar{g}_2 \xi \eta \\ Z_2 &= \eta + \bar{g}_1 \xi \eta \end{aligned} \right\} \quad (16-85)$$

From Eq. (16-85), it can be seen that the new area coordinates Z_1 and Z_2 will degenerate to be the isoparametric coordinates ξ and η for the rectangular element cases.

16.11.4 Some Discussions on QACM-II for Various Distortion Modes

Some typical shapes of a quadrilateral element and the corresponding shape parameters are summarized as follows:

Parallelogram

$$\bar{g}_1 = \bar{g}_2 = 0 \quad \text{or} \quad g_1 = g_2 = g_3 = g_4 = \frac{1}{2} \quad (16-86)$$

Trapezoid (refer to Fig. 16.12)

$$\bar{g}_1 = 0 \quad \text{or} \quad g_1 = g_2 \quad (\text{for } \overline{12//34}) \quad (16-87a)$$

$$\bar{g}_2 = 0 \quad \text{or} \quad g_2 = g_3 \quad (\text{for } \overline{23//41}) \quad (16-87b)$$

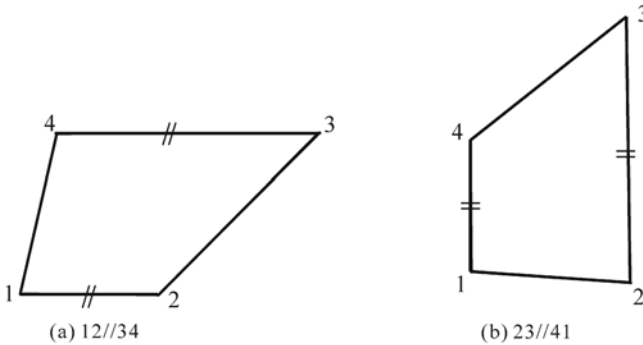


Figure 16.12 Two kinds of trapezoids

Triangular mode I: some three nodes are in line (refer to Fig. 16.13)

$$\left\{ \begin{aligned} \bar{g}_1 &= g_2 \\ \bar{g}_2 &= g_4 \end{aligned} \right\} \quad \text{or} \quad \left\{ \begin{aligned} g_1 &= 0 \\ g_3 &= 1 \end{aligned} \right\} \quad (\text{Fig. 16.13(a): nodes 4, 1, 2 are in line}) \quad (16-88a)$$

$$\left\{ \begin{aligned} \bar{g}_1 &= -g_1 \\ \bar{g}_2 &= g_3 \end{aligned} \right\} \quad \text{or} \quad \left\{ \begin{aligned} g_2 &= 0 \\ g_4 &= 1 \end{aligned} \right\} \quad (\text{Fig. 16.13(b): nodes 1, 2, 3 are in line}) \quad (16-88b)$$

$$\begin{cases} \bar{g}_1 = -g_4 \\ \bar{g}_2 = -g_2 \end{cases} \text{ or } \begin{cases} g_3 = 0 \\ g_1 = 1 \end{cases} \quad (\text{Fig. 16.13(c): nodes 2, 3, 4 are in line}) \quad (16-88c)$$

$$\begin{cases} \bar{g}_1 = g_3 \\ \bar{g}_2 = -g_1 \end{cases} \text{ or } \begin{cases} g_4 = 0 \\ g_2 = 1 \end{cases} \quad (\text{Fig. 16.13(d): nodes 3, 4, 1 are in line}) \quad (16-88d)$$

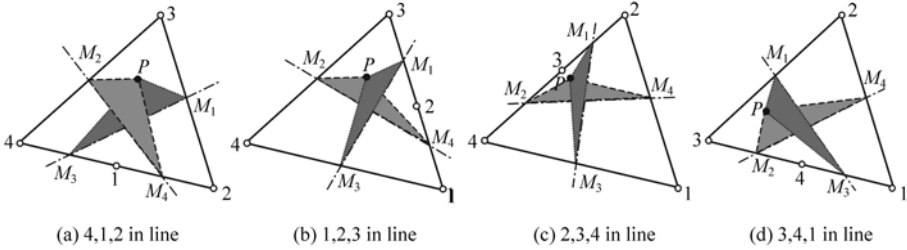


Figure 16.13 Degeneration into triangular mode I: some three nodes are in line

Triangular mode II: some two nodes are in coincidence (refer to Fig. 16.14)

$$\begin{cases} \bar{g}_1 = 0 \\ \bar{g}_2 = 1 \end{cases} \text{ or } \begin{cases} g_1 = g_2 = 0 \\ g_3 = g_4 = 1 \end{cases} \quad (\text{Fig. 16.14(a): nodes 1, 2 are in coincidence}) \quad (16-89a)$$

$$\begin{cases} \bar{g}_1 = -1 \\ \bar{g}_2 = 0 \end{cases} \text{ or } \begin{cases} g_2 = g_3 = 0 \\ g_4 = g_1 = 1 \end{cases} \quad (\text{Fig. 16.14(b): nodes 2, 3 are in coincidence}) \quad (16-89b)$$

$$\begin{cases} \bar{g}_1 = 0 \\ \bar{g}_2 = -1 \end{cases} \text{ or } \begin{cases} g_3 = g_4 = 0 \\ g_1 = g_2 = 1 \end{cases} \quad (\text{Fig. 16.14(c): nodes 3, 4 are in coincidence}) \quad (16-89c)$$

$$\begin{cases} \bar{g}_1 = 1 \\ \bar{g}_2 = 0 \end{cases} \text{ or } \begin{cases} g_4 = g_1 = 0 \\ g_2 = g_3 = 1 \end{cases} \quad (\text{Fig. 16.14(d): nodes 4, 1 are in coincidence}) \quad (16-89d)$$

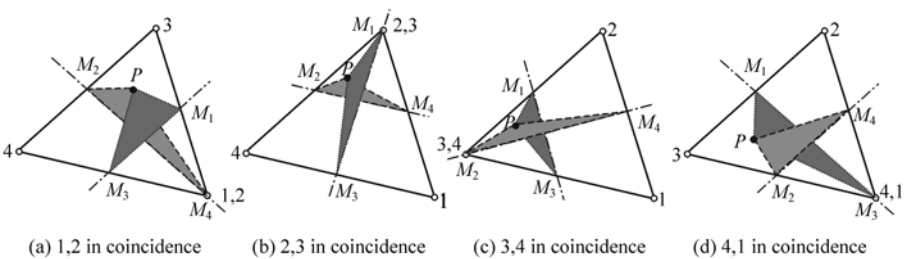


Figure 16.14 Degeneration into triangular mode II: some two nodes are in coincidence

16.11.5 Some Basic Differential Formulae of the QACM-II

(1) The transformation of the derivatives of the first order:

$$\begin{Bmatrix} \frac{\partial}{\partial x} \\ \frac{\partial}{\partial y} \end{Bmatrix} = \frac{1}{A} \begin{bmatrix} \bar{b}_1 & \bar{b}_2 \\ \bar{c}_1 & \bar{c}_2 \end{bmatrix} \begin{Bmatrix} \frac{\partial}{\partial Z_1} \\ \frac{\partial}{\partial Z_2} \end{Bmatrix} \quad (16-90)$$

(2) The transformation of the derivatives of the second order:

$$\begin{Bmatrix} \frac{\partial^2}{\partial x^2} \\ \frac{\partial^2}{\partial y^2} \\ \frac{\partial^2}{\partial x \partial y} \end{Bmatrix} = \frac{1}{A^2} \begin{bmatrix} \bar{b}_1^2 & \bar{b}_2^2 & 2\bar{b}_1\bar{b}_2 \\ \bar{c}_1^2 & \bar{c}_2^2 & 2\bar{c}_1\bar{c}_2 \\ \bar{b}_1\bar{c}_1 & \bar{b}_2\bar{c}_2 & \bar{b}_1\bar{c}_2 + \bar{b}_2\bar{c}_1 \end{bmatrix} \begin{Bmatrix} \frac{\partial^2}{\partial Z_1^2} \\ \frac{\partial^2}{\partial Z_2^2} \\ \frac{\partial^2}{\partial Z_1 \partial Z_2} \end{Bmatrix} \quad (16-91)$$

(3) Normal and tangential derivatives

Assume that n_i and s_i stand for unit vectors oriented in the normal and the tangential direction respectively of the side i in a quadrilateral element (Fig. 16.8). The normal derivative of each side is:

$$\frac{\partial}{\partial n_i} = -\frac{1}{d_i} [b_i \quad c_i] \begin{Bmatrix} \frac{\partial}{\partial x} \\ \frac{\partial}{\partial y} \end{Bmatrix} = -\frac{1}{Ad_i} [b_i \quad c_i] \begin{bmatrix} \bar{b}_1 & \bar{b}_2 \\ \bar{c}_1 & \bar{c}_2 \end{bmatrix} \begin{Bmatrix} \frac{\partial}{\partial Z_1} \\ \frac{\partial}{\partial Z_2} \end{Bmatrix} \quad (16-92)$$

The tangential derivative of each side is:

$$\frac{\partial}{\partial s_i} = \frac{1}{d_i} [c_i \quad -b_i] \begin{Bmatrix} \frac{\partial}{\partial x} \\ \frac{\partial}{\partial y} \end{Bmatrix} = \frac{1}{Ad_i} [c_i \quad -b_i] \begin{bmatrix} \bar{b}_1 & \bar{b}_2 \\ \bar{c}_1 & \bar{c}_2 \end{bmatrix} \begin{Bmatrix} \frac{\partial}{\partial Z_1} \\ \frac{\partial}{\partial Z_2} \end{Bmatrix} \quad (16-93)$$

16.11.6 Some Basic Integration Formulae of the QACM-II

(1) The area integral formulae within a quadrilateral element

The integration formulae for evaluating the area integrals of the arbitrary power function $Z_1^m Z_2^n$ can be written as:

$$\iint_A Z_1^m Z_2^n dA = \frac{A}{4} \sum_{i=0}^m \sum_{j=0}^n C_m^i C_n^j \bar{g}_2^i \bar{g}_1^j P \quad (16-94)$$

where m and n are arbitrary positive integers,

$$P = \frac{[1 - (-1)^M][1 - (-1)^N]}{MN} + \bar{g}_1 \frac{[1 - (-1)^{M+1}][1 - (-1)^N]}{(M + 1)N} + \bar{g}_2 \frac{[1 - (-1)^M][1 - (-1)^{N+1}]}{M(N + 1)} \quad (16-95)$$

with

$$M = m + j + 1, \quad N = n + i + 1 \quad (16-96)$$

Thus, from Eqs. (16-95) and (16-96), we have

$$\left. \begin{aligned} P &= \frac{4}{MN} && \text{(for } M \text{ and } N \text{ are both odd numbers)} \\ P &= 0 && \text{(for } M \text{ and } N \text{ are both even numbers)} \\ P &= \frac{4}{M(N + 1)} \bar{g}_2 && \text{(for } M \text{ is odd, } N \text{ is even)} \\ P &= \frac{4}{(M + 1)N} \bar{g}_1 && \text{(for } M \text{ is even, } N \text{ is odd)} \end{aligned} \right\} \quad (16-97)$$

and C_m^n is defined as

$$C_m^n = \frac{m!}{(m - n)!n!} \quad (16-98)$$

The proof of Eq. (16-94) can be easily performed by using the relationship (16-85) between the QACM-II and the isoparametric coordinates.

Proof of Eq. (16-94)

Substitution of Eq. (16-85) into the left side of Eq. (16-94) yields

$$\iint_A Z_1^m Z_2^n dA = \iint_A (\bar{g}_2 \xi \eta + \xi)^m (\bar{g}_1 \xi \eta + \eta)^n |\mathbf{J}| d\xi d\eta \quad (16-99)$$

where $|\mathbf{J}|$ is the Jacobi determinant; \mathbf{J} is the Jacobi matrix, and it is the same as that of the usual 4-node bilinear isoparametric element Q4:

$$\mathbf{J} = \begin{bmatrix} \frac{\partial N_1^{Q4}}{\partial \xi} & \frac{\partial N_2^{Q4}}{\partial \xi} & \frac{\partial N_3^{Q4}}{\partial \xi} & \frac{\partial N_4^{Q4}}{\partial \xi} \\ \frac{\partial N_1^{Q4}}{\partial \eta} & \frac{\partial N_2^{Q4}}{\partial \eta} & \frac{\partial N_3^{Q4}}{\partial \eta} & \frac{\partial N_4^{Q4}}{\partial \eta} \end{bmatrix} \begin{bmatrix} x_1 & y_1 \\ x_2 & y_2 \\ x_3 & y_3 \\ x_4 & y_4 \end{bmatrix} \quad (16-100)$$

with

$$N_i^{Q4} = \frac{1}{4}(1 + \xi_i \xi)(1 + \eta_i \eta) \quad (i = 1, 2, 3, 4) \quad (16-101)$$

where ξ_i and η_i are the isoparametric coordinates of the four corner nodes. And, from Eqs. (16-25), (16-78) and (16-81), we can obtain:

$$\sum_{i=1}^4 a_i = 2A, \quad b_2 c_4 - b_4 c_2 = 2A \bar{g}_1, \quad b_3 c_1 - b_1 c_3 = 2A \bar{g}_2 \quad (16-102)$$

Then, the Jacobi determinant $|J|$ can be written as:

$$|J| = \frac{1}{8} \sum_{i=1}^4 a_i + \frac{1}{8} (b_2 c_4 - b_4 c_2) \xi + \frac{1}{8} (b_3 c_1 - b_1 c_3) \eta = \frac{A}{4} [1 + \bar{g}_1 \xi + \bar{g}_2 \eta] \quad (16-103)$$

Substitution of Eq. (16-103) into Eq. (16-99) yields

$$\begin{aligned} \iint_A Z_1^m Z_2^n dA &= \frac{A}{4} \iint_A \xi^m \eta^n (1 + \bar{g}_2 \eta)^m (1 + \bar{g}_1 \xi)^n (1 + \bar{g}_1 \xi + \bar{g}_2 \eta) d\xi d\eta \\ &= \frac{A}{4} \iint_A \xi^m \eta^n \sum_{i=0}^m C_m^i \bar{g}_2^i \eta^i \sum_{j=0}^n C_n^j \bar{g}_1^j \xi^j (1 + \bar{g}_1 \xi + \bar{g}_2 \eta) d\xi d\eta \\ &= \frac{A}{4} \sum_{i=0}^m \sum_{j=0}^n C_m^i C_n^j \bar{g}_2^i \bar{g}_1^j \iint_A (\xi^{m+j} \eta^{n+i} + \bar{g}_1 \xi^{m+j+1} \eta^{n+i} + \bar{g}_2 \xi^{m+j} \eta^{n+i+1}) d\xi d\eta \\ &= \frac{A}{4} \sum_{i=0}^m \sum_{j=0}^n C_m^i C_n^j \bar{g}_2^i \bar{g}_1^j P \end{aligned} \quad (16-104)$$

□

(2) Some area integral formulae for lower power functions

For convenience in application, we list the area integral formulae for lower power functions (from first order to fourth order) as follows according to Eq. (16-94):

The first power terms:

$$\iint_A \begin{Bmatrix} Z_1 \\ Z_2 \end{Bmatrix} dA = \frac{A}{3} \begin{Bmatrix} \bar{g}_1 \\ \bar{g}_2 \end{Bmatrix} \quad (16-105)$$

The second power terms:

$$\iint_A \begin{Bmatrix} Z_1^2 \\ Z_2^2 \\ Z_1 Z_2 \end{Bmatrix} dA = \frac{A}{3} \begin{Bmatrix} 1 + \bar{g}_2^2 \\ 1 + \bar{g}_1^2 \\ \bar{g}_1 \bar{g}_2 \end{Bmatrix} \quad (16-106)$$

The third power terms:

$$\iint_A \begin{Bmatrix} Z_1^3 \\ Z_1^2 Z_2 \\ Z_1 Z_2^2 \\ Z_2^3 \end{Bmatrix} dA = \frac{A}{15} \begin{Bmatrix} 3\bar{g}_1(1+\bar{g}_2^2) \\ \bar{g}_2^3 + 2\bar{g}_1^2\bar{g}_2 + 5\bar{g}_2 \\ \bar{g}_1^3 + 2\bar{g}_1\bar{g}_2^2 + 5\bar{g}_1 \\ 3\bar{g}_2(1+\bar{g}_1^2) \end{Bmatrix} \quad (16-107)$$

The fourth power terms:

$$\iint_A \begin{Bmatrix} Z_1^4 \\ Z_1^3 Z_2 \\ Z_1^2 Z_2^2 \\ Z_1 Z_2^3 \\ Z_2^4 \end{Bmatrix} dA = \frac{A}{5} \begin{Bmatrix} \bar{g}_2^4 + \frac{10}{3}\bar{g}_2^2 + 1 \\ \bar{g}_1\bar{g}_2^3 + \frac{7}{3}\bar{g}_1\bar{g}_2 \\ \bar{g}_1^2\bar{g}_2^2 + \bar{g}_1^2 + \bar{g}_2^2 + \frac{5}{9} \\ \bar{g}_1^3\bar{g}_2 + \frac{7}{3}\bar{g}_1\bar{g}_2 \\ \bar{g}_1^4 + \frac{10}{3}\bar{g}_1^2 + 1 \end{Bmatrix} \quad (16-108)$$

(3) Some basic formulae for line integral

In a quadrilateral element, the following basic formulae can be used to evaluate the line integral for the arbitrary power function of QACM-II along each side.

Along side $\bar{23}$

$$\int_0^1 Z_1^m Z_2^n d\bar{s} = \frac{1}{2}(1+\bar{g}_1)^n \sum_{i=0}^m C_m^i g_2^i \frac{1-(-1)^{n+i+1}}{n+i+1} \quad (16-109)$$

Along side $\bar{34}$

$$\int_0^1 Z_1^m Z_2^n d\bar{s} = -\frac{1}{2}(1+\bar{g}_2)^m \sum_{i=0}^n C_n^i g_1^i \frac{1-(-1)^{m+i+1}}{m+i+1} \quad (16-110)$$

Along side $\bar{41}$

$$\int_0^1 Z_1^m Z_2^n d\bar{s} = -\frac{1}{2}(-1)^m(1-\bar{g}_1)^n \sum_{i=0}^m C_m^i g_2^i \frac{1-(-1)^{n+i+1}}{n+i+1} \quad (16-111)$$

Along side $\bar{12}$

$$\int_0^1 Z_1^m Z_2^n d\bar{s} = -\frac{1}{2}(-1)^n(1-\bar{g}_2)^m \sum_{i=0}^n C_n^i g_1^i \frac{1-(-1)^{m+i+1}}{m+i+1} \quad (16-112)$$

where \bar{s} is a dimensionless coordinate along side \bar{jk} ($jk = 23,34,41,12$), it is 0 at node j and 1 at node k .

Proof of Eq. (16-111)

By using Eq. (16-85), Z_1 and Z_2 can be replaced by isoparametric coordinates ξ and η , then

$$\int_0^1 Z_1^m Z_2^n d\bar{s} = \int_0^1 (\xi + \bar{g}_2 \xi \eta)^m (\eta + \bar{g}_1 \xi \eta)^n d\bar{s} \tag{16-113}$$

Along side $\bar{23}$, we have

$$\xi = 1, \quad -1 \leq \eta \leq 1, \quad \bar{s} = \frac{1+\eta}{2} \tag{16-114}$$

Thus, Eq. (16-113) can be rewritten as

$$\begin{aligned} \int_0^1 Z_1^m Z_2^n d\bar{s} &= \frac{1}{2} \int_{-1}^1 (1 + \bar{g}_2 \eta)^m (\eta + \bar{g}_1 \eta)^n d\eta \\ &= \frac{1}{2} (1 + \bar{g}_1)^n \int_{-1}^1 (1 + \bar{g}_2 \eta)^m \eta^n d\eta \\ &= \frac{1}{2} (1 + \bar{g}_1)^n \int_{-1}^1 \eta^n \sum_{i=0}^m C_m^i \bar{g}_2^i \eta^i d\eta \\ &= \frac{1}{2} (1 + \bar{g}_1)^n \int_{-1}^1 \sum_{i=0}^m C_m^i \bar{g}_2^i \eta^{n+i} d\eta \\ &= \frac{1}{2} (1 + \bar{g}_1)^n \sum_{i=0}^m C_m^i \bar{g}_2^i \frac{1 - (-1)^{n+i+1}}{n+i+1} \end{aligned} \tag{16-115}$$

□

The proof procedures of the Eqs. (16-110), (16-111) and (16-112) are similar to the procedure given above.

Thus, a new area coordinate system QACM-II, which only contains two independent components, is successfully established.

References

- [1] Long YQ, Li JX, Long ZF, Cen S (1997) Area-coordinate theory for quadrilateral elements. Gong Cheng Li Xue / Engineering Mechanics 14(3): 1 – 11 (in Chinese)
- [2] Long ZF, Li JX, Cen S, Long YQ (1997) Differential and integral formulas for area coordinates in quadrilateral element. Gong Cheng Li Xue / Engineering Mechanics 14(3): 12 – 22 (in Chinese)
- [3] Long YQ, Li JX, Long ZF, Cen S (1999) Area coordinates used in quadrilateral elements. Communications in Numerical Methods in Engineering 15(8): 533 – 545
- [4] Long ZF, Li JX, Cen S, Long YQ (1999) Some basic formulae for Area coordinates used in quadrilateral elements. Communications in Numerical Methods in Engineering 15(12): 841 – 852

Chapter 16 Quadrilateral Area Coordinate Systems, Part I— Theory and Formulae

- [5] Long YQ, Long ZF, Cen S (1999) Method of area coordinate—from triangular to quadrilateral elements. In: Long YQ (ed) The proceedings of the first international conference on structural engineering (Invited paper). China, KunMing, pp57 – 66
- [6] Long YQ, Long ZF, Cen S (2001) Method of area coordinate—from triangular to quadrilateral elements. *Advances in Structural Engineering* 4(1): 1 – 11
- [7] Chen XM, Cen S, Long YQ, Fu XR (2007) A two-component area coordinate method for quadrilateral elements. *Gong Cheng Li Xue / Engineering Mechanics* 24(Sup. I): 32 – 35 (in Chinese)
- [8] Chen XM, Cen S, Fu XR, Long YQ (2008) A new quadrilateral area coordinate method (QACM-II) for developing quadrilateral finite element models. *International Journal for Numerical Methods in Engineering* 73(13): 1911 – 1941
- [9] Taig IC (1961) Structural analysis by the matrix displacement method. Eng1. Electric Aviation Report No. S017
- [10] Irons BM (1966) Engineering application of numerical integration in stiffness method. *AIAA Journal* 14: 2035 – 2037
- [11] Hua C (1990) An inverse transformation for quadrilateral isoparametric elements: analysis and application. *Finite Elements in Analysis and Design* 7: 159 – 166
- [12] Lee NS, Bathe KJ (1993) Effects of element distortions on the performance of isoparametric elements. *International Journal in Numerical Methods in Engineering* 36: 3553 – 3576
- [13] Murtie JB (1964) Transformation of trilinear and quadriplanar coordinates to and from Cartesian coordinates. *The American Mineralogist* 49(7/8): 926 – 936
- [14] Eisenberg MA, Malvern LE (1973) On finite element integration in natural coordinates. *International Journal in Numerical Methods in Engineering* 7(4): 574 – 575
- [15] Zhong ZH (1993) *Finite element procedures for contact-impact problems*. Oxford University Press, Oxford
- [16] Long YQ, Long ZF, Wang L (2009) The third version of area coordinate systems for quadrilateral elements. *Gong Cheng Li Xue / Engineering Mechanics* 26(2): 1 – 5 (in Chinese)

Chapter 17 **Quadrilateral Area Coordinate Systems, Part II — New Tools for Constructing Quadrilateral Elements**

Song Cen

Department of Engineering Mechanics, School of Aerospace,
Tsinghua University, Beijing, 100084, China

Zhi-Fei Long

School of Mechanics & Civil Engineering, China University of
Mining & Technology, Beijing, 100083, China

Abstract This chapter focuses on the applications of the quadrilateral area coordinate systems discussed in the previous chapter. Here, a series of new quadrilateral elements formulated by the quadrilateral area coordinate methods are introduced in detail. Following the Introduction in Sect. 17.1, the sensitivity analysis of the quadrilateral membrane elements to mesh distortion is discussed in Sect. 17.2. Then, a brief review of the construction of various quadrilateral elements formulated by the quadrilateral area coordinate methods is given in Sect. 17.3. In Sects. 17.4 to 17.7 of this chapter, various quadrilateral membrane elements (4-node element, 4-node element with drilling freedoms, 8-node element) for linear and nonlinear analyses, in which the area coordinate methods are adopted, are introduced in detail. And, in the last three sections (Sects. 17.8 to 17.10), the applications of the area coordinate methods for the quadrilateral thin plate, thick plate and composite laminated plate elements are described, respectively. It is demonstrated that the area coordinate methods are efficient tools for developing simple, effective and reliable serendipity quadrilateral element models.

Keywords quadrilateral element, quadrilateral area coordinate system, generalized conforming, mesh distortion.

17.1 Introduction

For the past years, the isoparametric coordinate method has almost been the unique

tool for constructing arbitrary quadrilateral elements. So, the establishment of the quadrilateral area coordinate theory provides us a new way for related jobs. Especially, some new models formulated by these new tools can still keep high precision in a distorted mesh division, which cannot be easily achieved by the conventional isoparametric elements. At present, some excellent element models, including membrane elements, thin plate elements, thick plate elements and composite laminated plate elements, have already been developed by using the quadrilateral area coordinate method.

Firstly, the sensitivity analysis of the quadrilateral membrane elements to mesh distortion is discussed in Sect. 17.2. It is pointed out that the accuracy of the Serendipity-type elements will drop obviously when the element shapes are distorted. The academic background for the creation of the quadrilateral area coordinate methods is just for overcoming this disadvantage.

Then, a brief review of the finite element models formulated by the quadrilateral area coordinate methods is given in Sect. 17.3.

Various quadrilateral membrane elements formulated by the quadrilateral area coordinate methods are introduced in Sects. 17.4 to 17.7.

Quadrilateral thin plate, thick plate and composite laminated plate elements formulated by the quadrilateral area coordinate methods are described in the last three sections.

17.2 Sensitivity Analysis of Isoparametric Elements to Mesh Distortion

Many finite element models possess high precision in a regular mesh division, but perform badly when the mesh is distorted. So, we say that these elements are sensitive to mesh distortion, which is a fatal disadvantage for applications.

For many years, a great amount of effort has been made by many researchers for developing the elements which are insensitive to mesh distortion. Pian et al.^[1] and Wilson et al.^[2] all discussed this problem, and proposed the hybrid-stress element scheme and the incompatible element scheme, respectively. Though some improvements were obtained, the sensitivity problem to mesh distortion still exists. Xu and Long^[3] adopted the generalized conforming method to develop a quadrilateral membrane element GQ12M8 which is insensitive to mesh distortion. This is a membrane element with drilling freedoms and 8 internal freedoms.

Lee and Bathe^[4] have studied the effects of element distortions on the performance of the isoparametric membrane elements. Isoparametric elements can be classified into two types. One type is named as the Lagrange-type element. The elements which belong to this type usually contain internal nodes, such as the elements Q9 (9 nodes), Q16 (16 nodes) and Q25 (25 nodes). And, the other type is named as the Serendipity-type element. The elements which belong to

this type contain no internal nodes, such as the elements Q8 (8 nodes), Q12 (12 nodes) and Q16 (16 nodes). In reference[4], the sensitivity problem to mesh distortion was tested by systematical numerical examples. It pointed out that the Serendipity family is very sensitive to mesh distortion, and on the contrary, the Lagrange-type elements are quite robust and insensitive to mesh distortion. However, there exist many internal nodes within a Lagrange-type element, which is inconvenient for practical applications.

After the recognition of the above disadvantage of the Serendipity isoparametric elements, many researchers are quite interested in the reason that causes the problem, and hope to find new countermeasures. One of the recent effective strategies is the application of the quadrilateral area coordinate method, a new tool for developing the quadrilateral finite element models. For example, in order to compare with the 8-node Serendipity isoparametric element Q8, reference [5] used the quadrilateral area coordinate method to construct two 8-node elements MQ8-I and MQ8-II. These two new elements exhibit excellent performance in various distorted meshes while the element Q8 is very sensitive to mesh distortion, which shows a striking contrast. On the basis of the comparison between the elements Q8 and MQ8, reference [6] gave systematic discussion on the sensitivity problem to mesh distortion, and proposed related countermeasures which can be stated as follows:

Firstly, the results of a sensitivity test for mesh distortion are given.

As shown in Fig. 17.1, a slender beam under pure bending is divided by two elements. δ is a distortion parameter. The results obtained by the following 4 models are plotted in Fig. 17.2.

Q4: 4-node isoparametric element; Q8: 8-node isoparametric element; MQ8-I and MQ8-II: 8-node elements formulated by the area coordinate method (model I and model II).

It can be seen from Fig. 17.2 that, both the isoparametric elements Q4 and Q8 are very sensitive to mesh distortion while the 8-node elements formulated by the area coordinate method can provide the exact solution when $0 < \delta < 1$.

Secondly, the reason why the Serendipity isoparametric elements Q4, Q8, Q12, ... are sensitive to mesh distortion is analyzed.

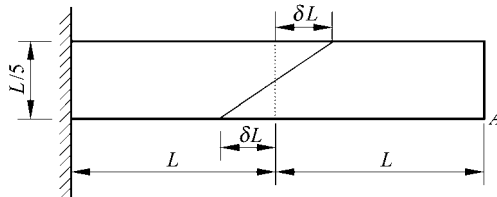


Figure 17.1 Sensitivity test for mesh distortion

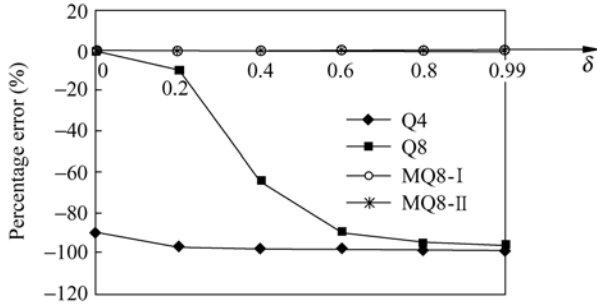


Figure 17.2 Percentage error (%) of the deflection at point *A* in pure bending problem due to mesh distortion

As an example, the displacement polynomial of the element Q12 contains 12 undetermined coefficients (the completeness order for both ξ and η are third order):

$$\begin{aligned}
 u = & \lambda_1 + (\lambda_2\xi + \lambda_3\eta) + (\lambda_4\xi^2 + \lambda_5\xi\eta + \lambda_6\eta^2) \\
 & + (\lambda_7\xi^3 + \lambda_8\xi^2\eta + \lambda_9\xi\eta^2 + \lambda_{10}\eta^3) + (\lambda_{11}\xi^3\eta + \lambda_{12}\xi\eta^3) \quad (17-1)
 \end{aligned}$$

If this polynomial is expressed in terms of the Cartesian coordinates (x, y), then we have:

for regular rectangular element—linear transformation

for distorted quadrilateral element—nonlinear transformation: $x = a_0 + a_1\xi + a_2\eta + a_3\xi\eta$ (bilinear)

The completeness order of the displacement polynomial (17-1) in the Cartesian coordinates (x, y) is:

{ Rectangular element—third order completeness—high precision } sensitive to
 { Distorted element—first order completeness—low precision } mesh distortion

Since there is no $\xi^2\eta^2$ term in Eq. (17-1), x^2 , xy and y^2 terms will disappear when the element is distorted, i.e., only the first order completeness for x and y can be obtained for distorted element.

Finally, conclusion and countermeasure are given as follows.

The accuracy of an element mainly depends on the completeness order for x and y .

Reason which causes the sensitivity problem to mesh distortion—mesh distortion leads to grave consequences that the completeness order for x and y decreases rapidly from third order completeness (in the case of the rectangular element) to first order completeness (in the case of the distorted element).

Countermeasure—the coordinate system which possesses linear relation with (x, y) is preferred during the construction of an element model, for example, if the quadrilateral area coordinate system is used, the completeness order for x and y will not decrease.

17.3 Brief Review of the Finite Element Models Formulated by Quadrilateral Area Coordinate Methods

17.3.1 Some Characteristics and Merits of Universal Area Coordinates (QACM-I)

Both triangular and quadrilateral area coordinates (QACM-I) are two examples that belong to the universal area coordinate method. The former is a special case and a degenerated form of the QACM-I; and the QACM-I is the general form which contains the former. It can be seen that, in fact, the basic formulae of QACM-I are composed of two parts: in the first part are formulae that are newly derived specially for a quadrangle; and in the other part are the generalizations of those which are originally derived for a triangle.

The universal area coordinate system possesses the following characteristics and merits:

- The transformation between the area coordinate system and the Cartesian coordinate system is linear.
(In contrast: the transformation between the isoparametric coordinate system (ξ, η) and the Cartesian coordinate system is nonlinear.)
 - The area coordinate system is a natural coordinate system.
(In contrast: the Cartesian coordinate system is an artificially established system. When the Cartesian axes rotate, the area coordinates of the given point are invariant, while its Cartesian coordinates are not invariant.)
 - Equation of the element boundary line is $L_i = 0$, and therefore the boundary condition is easy to express and be satisfied.
 - Shape functions (or preparatory shape functions) can be written out directly.
- Shape function N_i for 3-node triangular element:

$$\begin{cases} N_1 = L_1 \\ N_2 = L_2 \\ N_3 = L_3 \end{cases} \quad (17-2)$$

Preparatory shape function N_i ($N_i(j) = \delta_{ij}$) for quadrilateral element:

$$\begin{cases} N_1 = \frac{1}{g_2 g_4} L_1 L_2 \\ N_2 = \frac{1}{g_3 g_1} L_2 L_3 \\ N_3 = \frac{1}{g_4 g_2} L_3 L_4 \\ N_4 = \frac{1}{g_1 g_3} L_4 L_1 \end{cases} \quad (17-3)$$

- Stiffness matrix of an element formulated by the area coordinate method can be obtained explicitly.
(Contrast: when the isoparametric coordinates are used, generally, the element stiffness matrix cannot be expressed explicitly, and it is evaluated only by numerical integration.)
- The elements formulated by the area coordinate method are insensitive to mesh distortion.
(Contrast: the serendipity isoparametric elements are very sensitive to mesh distortion.)

17.3.2 New Quadrilateral Elements Formulated by the Area Coordinate Methods

Due to the merits mentioned above, the quadrilateral area coordinate methods (including both QACM-I and QACM-II) have already become new tools for developing the quadrilateral elements. Since 1997, 20 new quadrilateral elements based on the area coordinate method have been proposed in succession by references [5] and [7–18], and they are listed in Table 17.1 (models with symbol* will be introduced in this book).

The 20 quadrilateral elements listed in Table 17.1 can be classified into 7 types:

(1) 4-node membrane elements—4 elements using different shape functions are proposed. Among these models, no. 1, 2 and 4 elements can not only give the exact solutions for pure bending problem by using distorted meshes, but also overcome the trapezoidal locking for the MacNeal thin beam problem, so they possess high computational accuracy and are insensitive to mesh distortion. These three elements will be introduced in Sect. 17.4. And, the performance of the no. 3 element is also better than that of the similar isoparametric model, element QM6^[19]. Furthermore, due to the feature of the quadrilateral area coordinate methods, the analytical element stiffness matrix of the element AGQ6-I (no.1 element) can be formulated, which can improve the computation efficiency. And, in geometrically nonlinear analysis, the element AGQ6-I also exhibits excellent performance, and this will be described in Sect. 17.5. Here, the advantages and potential of the quadrilateral area coordinate methods are fully exhibited.

(2) 4-node membrane elements with drilling degrees of freedom—2 elements, AQ4 θ and AQ4 $\theta\lambda$, are proposed. They will be introduced in Sect. 17.6.

(3) 5, 6, 7 and 8-node membrane elements—8 elements are proposed. No. 13 and 14 elements AQ8 (I and II) will be introduced in Sect. 17.7. When a mesh is distorted, the new element AQ8 can still keep good accuracy, which is obviously better than the conventional 8-node isoparametric element Q8.

Table 17.1 New quadrilateral elements based on the area coordinate method (20 elements)

Problem types	Element names	References
(1) 4-node membrane element	1. *AGQ6-I <ul style="list-style-type: none"> • AGQ6-I with analytical element stiffness matrix • *AGQ6-I for geometrically nonlinear analysis 	2004 [7] 2007 [8] 2008 [9]
	2. *AGQ6-II	2004 [7]
	3. QACM4	2007 [10]
	4. *QACII 6 (by QACM-II)	2008 [11]
(2) 4-node membrane element with drilling degrees of freedom	5. *AQ40	2003 [12]
	6. *AQ40λ	2003 [12]
(3) 5, 6, 7 and 8-node membrane element	7. QACM5 (5-node)	2007 [10]
	8. QACM6 (6-node)	2007 [10]
	9. QACM7 (7-node)	2007 [10]
	10. QACM8 (8-node)	2007 [10]
	11. MQ8-I (8-node)	1998 [6]
	12. MQ8-II (8-node)	1998 [6]
	13. *AQ8-I (8-node)	2000 [13]
	14. *AQ8-II (8-node)	2000 [13]
(4) 4-node axisymmetric element	15. AQACQ6	2007 [14]
	16. AQACQ6M	2007 [14]
(5) 4-node thin plate element	17. ACQ	1997 [15]
	18. *ACGCQ	2000 [16]
(6) 4-node thick plate element	19. *AC-MQ4	2006 [17]
(7) 4-node laminated composite plate element	20. *AC-MQ4-LC	2007 [18]

(4) 4-node axisymmetric elements—2 elements are proposed. Similar to those 4-node membrane elements formulated by the area coordinate method, they also exhibit better performance than the corresponding isoparametric models in distorted meshes.

(5) 4-node thin plate element—2 elements are proposed. Element ACGCQ will be introduced in Sect. 17.8.

(6) 4-node thick plate element—A new thick plate bending element AC-MQ4 is proposed and will be introduced in Sect. 17.9. This element is generalized from the thin plate element ACGCQ by using the rational interpolation technique for shear strain fields which was proposed in reference [20]. When the thickness of a plate becomes small, this element AC-MQ4 will degenerate to be the thin plate element ACGCQ, so no shear locking will happen.

(7) 4-node laminated composite plate element—A new element AC-MQ4-LC is developed by adding bilinear in-plane displacement fields into the formulations of the element AC-MQ4. It will be introduced in Sect. 17.10.

17.4 4-Node Quadrilateral Membrane Elements Formulated by the Area Coordinate Method

There are four 4-node quadrilateral elements, which have been listed in Table 17.1, formulated by the area coordinate methods. They all belong to the generalized conforming element. The differences among these models are that different displacement trial functions and different generalized conforming conditions are employed. Three of these models, the elements AGQ6-I and AGQ6-II^[7], QAC6^[11], exhibit the best performance, and will be introduced in this section. Their construction procedures possess the following characteristics:

(1) The displacement field is expressed with the polynomial in the area coordinates (instead of the isoparametric coordinates). Thus, whether the element is distorted or not, the completeness order of the displacement polynomial in the Cartesian coordinates system (x, y) will not change.

(2) Various generalized conforming conditions are adopted for determining the displacement field, including the nodal version conforming conditions, and integral form conforming conditions of the displacement along the perimeter of the element.

(3) Only the weak patch test, instead of the strict form, is used to assure the convergence of the elements.

(4) The internal DOFs are condensed during the element analysis level. Therefore, the element stiffness matrix is still an 8×8 matrix after condensation.

17.4.1 Formulations of the Element AGQ6-I

1. Element nodal displacement vector \mathbf{q}^e and internal parameter vector $\boldsymbol{\lambda}$

For a 4-node quadrilateral element, the element nodal displacement vector \mathbf{q}^e is composed of the displacement components u and v of the 4 nodes:

$$\mathbf{q}^e = [u_1 \quad v_1 \quad u_2 \quad v_2 \quad u_3 \quad v_3 \quad u_4 \quad v_4]^T \quad (17-4)$$

In addition, the displacement fields u and v are assumed to include two internal parameters, respectively. They form the internal parameter vector $\boldsymbol{\lambda}$

$$\boldsymbol{\lambda} = [\lambda_1 \quad \lambda'_1 \quad \lambda_2 \quad \lambda'_2]^T \quad (17-5)$$

Thus, the displacement fields of the element are composed of two parts and expressed by \mathbf{q}^e and $\boldsymbol{\lambda}$:

$$\begin{Bmatrix} u \\ v \end{Bmatrix} = \begin{Bmatrix} u^0 \\ v^0 \end{Bmatrix} + \begin{Bmatrix} u_\lambda \\ v_\lambda \end{Bmatrix} = \mathbf{N}_q \mathbf{q}^e + \mathbf{N}_\lambda \boldsymbol{\lambda} \quad (17-6)$$

where u^0 and v^0 are the essential displacement fields; u_λ and v_λ are the additional internal displacement fields; N_q is the shape function matrix; and N_λ is the internal parameter shape function matrix;

$$N_q = \begin{bmatrix} N_1^0 & 0 & N_2^0 & 0 & N_3^0 & 0 & N_4^0 & 0 \\ 0 & N_1^0 & 0 & N_2^0 & 0 & N_3^0 & 0 & N_4^0 \end{bmatrix} \tag{17-7}$$

$$N_\lambda = \begin{bmatrix} N_{\lambda 1} & 0 & N_{\lambda 2} & 0 \\ 0 & N_{\lambda 1} & 0 & N_{\lambda 2} \end{bmatrix} \tag{17-8}$$

2. Shape functions N_q

The element displacement fields are expressed with the polynomial in the quadrilateral area coordinates.

The shape functions for u^0 and v^0 have the same forms. So, only the derivation of u^0 is given as follows. Let u^0 be the second-order polynomial in terms of the area coordinates L_1, L_2, L_3, L_4 :

$$u^0 = \alpha_1 + \alpha_2(L_3 - L_1) + \alpha_3(L_4 - L_2) + \alpha_4(L_3 - L_1)(L_4 - L_2) \tag{17-9}$$

In order to determine four constants $\alpha_1, \alpha_2, \alpha_3$ and α_4 , four generalized conforming conditions are introduced:

$$\left. \begin{aligned} \sum_{i=1}^4 (u^0 - \tilde{u})_i &= 0, & \oint_{\partial A^e} l(u^0 - \tilde{u}) ds &= 0 \\ \sum_{i=1}^4 (u^0 - \tilde{u})_i \xi_i \eta_i &= 0, & \oint_{\partial A^e} m(u^0 - \tilde{u}) ds &= 0 \end{aligned} \right\} \tag{17-10}$$

where two conditions are the combination forms of the nodal conforming conditions, and the other two are the integral form conforming conditions along the perimeter ∂A^e of the element; \tilde{u} is the displacement at the element boundary; l and m are the direction cosines of the outer normal along the element boundary.

Then, the shape functions N_i^0 ($i = 1, 2, 3, 4$) can be obtained from the above conforming conditions:

$$N_i^0 = -\frac{1}{2} g_{i+2} + L_i + L_{i+1} + \xi_i \eta_i g_{i+2} P \quad (i = 1, 2, 3, 4) \tag{17-11}$$

where

$$P = \frac{3(L_3 - L_1)(L_4 - L_2) - (g_2 - g_3)(L_3 - L_1) - (g_1 - g_2)(L_4 - L_2) - \frac{1}{2}(g_2 g_4 - g_1 g_3)}{1 + g_1 g_3 + g_2 g_4} \tag{17-12}$$

3. Internal parameter shape functions N_λ

The two shape functions of the internal displacement field u_λ are given by

$$\left. \begin{aligned} N_{\lambda 1} &= L_1 L_3 \\ N_{\lambda 2} &= L_2 L_4 \end{aligned} \right\} \quad (17-13)$$

It can be seen that the nodal values of these two shape functions are both zero. When the element shape degenerates to rectangle, $N_{\lambda i}$ ($i = 1, 2$) will be the same as the internal parameter shape functions of the element Q6 proposed by Wilson et al.^[21].

4. Element stiffness matrix

The element displacement fields are

$$\begin{Bmatrix} u \\ v \end{Bmatrix} = N_q \mathbf{q}^e + N_\lambda \boldsymbol{\lambda} \quad (17-14)$$

It can be shown that such displacement fields are the complete second-order polynomial in terms of the Cartesian coordinates (x, y).

Then, by using the transformation of derivatives of first order, the element strain vector $\boldsymbol{\varepsilon}$ can be obtained:

$$\boldsymbol{\varepsilon} = \mathbf{B}_q \mathbf{q}^e + \mathbf{B}_\lambda \boldsymbol{\lambda} \quad (17-15)$$

with

$$\mathbf{B}_q = [\mathbf{B}_{q1} \quad \mathbf{B}_{q2} \quad \mathbf{B}_{q3} \quad \mathbf{B}_{q4}], \quad \mathbf{B}_{qi} = \begin{bmatrix} \frac{\partial N_i^0}{\partial x} & 0 \\ 0 & \frac{\partial N_i^0}{\partial y} \\ \frac{\partial N_i^0}{\partial y} & \frac{\partial N_i^0}{\partial x} \end{bmatrix} \quad (i = 1, 2, 3, 4)$$

$$\mathbf{B}_\lambda = [\mathbf{B}_{\lambda 1} \quad \mathbf{B}_{\lambda 2}], \quad \mathbf{B}_{\lambda i} = \begin{bmatrix} \frac{\partial N_{\lambda i}}{\partial x} & 0 \\ 0 & \frac{\partial N_{\lambda i}}{\partial y} \\ \frac{\partial N_{\lambda i}}{\partial y} & \frac{\partial N_{\lambda i}}{\partial x} \end{bmatrix} \quad (i = 1, 2)$$

After condensation, the element stiffness matrix of the element can be

expressed by

$$\mathbf{K}^e = \mathbf{K}_{qq} - \mathbf{K}_{\lambda q}^T \mathbf{K}_{\lambda\lambda}^{-1} \mathbf{K}_{\lambda q} \tag{17-16}$$

where

$$\left. \begin{aligned} \mathbf{K}_{qq} &= \iint_{A^e} \mathbf{B}_q^T \mathbf{D} \mathbf{B}_q h dA \\ \mathbf{K}_{\lambda\lambda} &= \iint_{A^e} \mathbf{B}_\lambda^T \mathbf{D} \mathbf{B}_\lambda h dA \\ \mathbf{K}_{\lambda q} &= \iint_{A^e} \mathbf{B}_\lambda^T \mathbf{D} \mathbf{B}_q h dA \end{aligned} \right\} \tag{17-17}$$

in which \mathbf{D} is the elasticity matrix; h is the thickness of element.

17.4.2 Formulations of the Element AGQ6-II

The construction procedure of the element AGQ6-II is similar to that of AGQ6-I. The only difference is that the shape functions N_i^0 are expressed by Eqs. (17-20) and (17-21) instead of Eqs. (17-11) and (17-12). The derivation procedure is given as follows.

The displacement u^0 of the element AGQ6-II is still given by Eq. (17-9). But, the conforming conditions are changed to the following combination conditions at the element nodes:

$$\left. \begin{aligned} \sum_{i=1}^4 (u^0 - \tilde{u})_i &= 0, & \sum_{i=1}^4 (u^0 - \tilde{u})_i \xi_i &= 0 \\ \sum_{i=1}^4 (u^0 - \tilde{u})_i \eta_i &= 0, & \sum_{i=1}^4 (u^0 - \tilde{u})_i \xi_i \eta_i &= 0 \end{aligned} \right\} \tag{17-18}$$

Substitution of Eq. (17-9) into Eq. (17-18) yields:

$$\left. \begin{aligned} \sum_{i=1}^4 u_i &= 4\alpha_1 + 2(g_1 - g_2)\alpha_2 + 2(g_2 - g_3)\alpha_3 + 2(g_2g_4 - g_1g_3)\alpha_4 \\ \sum_{i=1}^4 u_i \xi_i &= 2\alpha_2 \\ \sum_{i=1}^4 u_i \eta_i &= 2\alpha_3 \\ \sum_{i=1}^4 u_i \xi_i \eta_i &= 2(g_3 - g_2)\alpha_2 + 2(g_2 - g_1)\alpha_3 + 2(g_2g_4 + g_1g_3)\alpha_4 \end{aligned} \right\} \tag{17-19}$$

Then, the shape functions of the element AGQ6-II can be obtained:

$$N_i^0 = -\frac{1-g_i}{2} + L_i + L_{i+1} + \xi_i \eta_i (1-g_i) \bar{P} \quad (i = 1,2,3,4) \quad (17-20)$$

where

$$\bar{P} = \frac{1}{g_2 g_4 + g_1 g_3} \left[(L_3 - L_1)(L_4 - L_2) - \frac{1}{2}(g_2 g_4 - g_1 g_3) \right] \quad (17-21)$$

And, other formulations of the element AGQ6-II are the same as those of the element AGQ6-I.

17.4.3 Formulations of the Element QACII6

The construction procedure of the element QACII6 is similar to those of AGQ6-I and AGQ6-II. The main difference is that all formulations are expressed in the QACM-II. The derivation procedure is given as follows.

Equations (17-4) to (17-8) are still adopted. The displacement field u^0 is assumed to be a second order polynomial expressed in Z_1 and Z_2 (QACM-II):

$$u^0 = \alpha_1 + \alpha_2 Z_1 + \alpha_3 Z_2 + \alpha_4 Z_1 Z_2 \quad (17-22)$$

where $\alpha_1, \alpha_2, \alpha_3$ and α_4 are still four unknown constants. In order to determine these four constants, four generalized conforming (point-conforming) conditions are introduced as follows:

$$u^0 \Big|_i = u_i \quad (i = 1,2,3,4) \quad (17-23)$$

After substituting Eq. (17-22) into Eq. (17-23), and replacing Z_1 and Z_2 by their values at four corner nodes, four simultaneous equations can be obtained from Eq. (17-23). Then by solving these equations, we can obtain

$$\begin{aligned} N_i^0 = & \frac{1}{4(1-\bar{g}_1^2 - \bar{g}_2^2)} \left[(1 + \xi_i \bar{g}_1 + \eta_i \bar{g}_2)(1 - \xi_i \bar{g}_1)(1 - \eta_i \bar{g}_2) \right. \\ & + \xi_i (1 + \xi_i \bar{g}_1 - \eta_i \bar{g}_2)(1 - \xi_i \bar{g}_1) Z_1 + \eta_i (1 - \xi_i \bar{g}_1 + \eta_i \bar{g}_2)(1 - \eta_i \bar{g}_2) Z_2 \\ & \left. + \xi_i \eta_i (1 - \xi_i \bar{g}_1 - \eta_i \bar{g}_2) Z_1 Z_2 \right] \quad (i = 1,2,3,4) \end{aligned} \quad (17-24)$$

The internal parameter displacement fields u_λ and v_λ are assumed as follows:

$$\left. \begin{aligned} u_\lambda &= N_{\lambda 1} \lambda_1 + N_{\lambda 2} \lambda_2 \\ v_\lambda &= N_{\lambda 1} \lambda'_1 + N_{\lambda 2} \lambda'_2 \end{aligned} \right\} \quad (17-25)$$

with

$$\left. \begin{aligned} N_{\lambda 1} &= -Z_1^2 + \gamma_1 Z_1 Z_2 + \gamma_2 Z_1 + \gamma_3 Z_2 + \gamma_4 \\ N_{\lambda 2} &= -Z_2^2 + \theta_1 Z_1 Z_2 + \theta_2 Z_1 + \theta_3 Z_2 + \theta_4 \end{aligned} \right\} \quad (17-26)$$

where γ_i and θ_i ($i=1,2,3,4$) are eight unknown constants. The values of each internal parameter displacement field at four corner nodes should be zero. So, we have

$$\left. \begin{aligned} N_{\lambda 1}|_i &= 0 \\ N_{\lambda 2}|_i &= 0 \end{aligned} \right\} \quad (i=1,2,3,4) \quad (17-27)$$

By substituting Eq. (17-26) into Eq. (17-27), the eight unknown constants can be solved out. Finally, we obtain

$$\left. \begin{aligned} N_{\lambda 1} &= -Z_1^2 + \frac{-2\bar{g}_1\bar{g}_2 Z_1 Z_2 + 2\bar{g}_1\bar{g}_2^2 Z_1 + 2(1-\bar{g}_2^2)\bar{g}_2 Z_2 + (1-\bar{g}_1^2 + \bar{g}_2^2)(1-\bar{g}_2^2)}{1-\bar{g}_1^2 - \bar{g}_2^2} \\ N_{\lambda 2} &= -Z_2^2 + \frac{-2\bar{g}_1\bar{g}_2 Z_1 Z_2 + 2(1-\bar{g}_1^2)\bar{g}_1 Z_1 + 2\bar{g}_1^2\bar{g}_2 Z_2 + (1+\bar{g}_1^2 - \bar{g}_2^2)(1-\bar{g}_1^2)}{1-\bar{g}_1^2 - \bar{g}_2^2} \end{aligned} \right\} \quad (17-28)$$

And, other formulations of the element QACII6 are the same as those of the element AGQ6-I.

17.4.4 Numerical Examples

Example 17.1 Cantilever beam divided by five quadrilateral elements (Fig. 17.3).

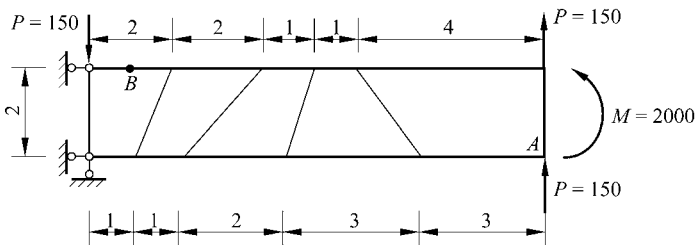


Figure 17.3 Cantilever beam with five irregular elements

The cantilever beam, as shown in Fig. 17.3, is divided by five irregular quadrilateral elements. And, two loading cases are considered: (1) pure bending under moment M ; (2) linear bending under transverse force P . The Young's modulus $E=1500$, Poisson's ratio $\mu=0.25$. The results of the vertical deflection v_A at point A and the stress σ_{xB} at point B are given in Table 17.2.

Compared with the results solved by other element models, it can be seen from

Table 17.2 that the new elements AGQ6-I, AGQ6-II and QACII6 give the best answers. Furthermore, exact solutions can even be obtained by the presented elements for the pure bending case.

Table 17.2 The deflection and stress at selected locations for bending problems of a cantilever beam (Fig. 17.3)

Elements	Load M		Load P	
	v_A	σ_{xB}	v_A	σ_{xB}
Q4	45.7	- 1761	50.7	- 2448
Q6 ^[21]	98.4	- 2428	100.4	- 3354
QC6 ^[22]	96.1	- 2439	98.1	- 3339
NQ6 ^[23]	96.1	- 2439	98.0	- 3294
QM6 ^[19]	96.07	- 2497	97.98	- 3235
P-S ^[1]	96.18	- 3001	98.05	- 3899
QE-2 ^[24]	96.5	- 3004	98.26	- 3906
\bar{B} -Q4E ^[24]	96.5	- 3004	98.26	- 3906
AGQ6-I	100	- 3000	102.0	- 4151
AGQ6-II	100	- 3000	102.7	- 4180
QACII6	100	- 3000	102.7	- 4180
Exact	100	- 3000	102.6	- 4050

Example 17.2 Cook’s skew beam problem (Fig. 17.4).

As shown in Fig. 17.4, a skew cantilever using a 2×2 typical mesh division is subjected to a shear distributed load at the free edge. The results of vertical deflection at point C, the maximum principal stress at point A and the minimum principal stress at point B are listed in Table 17.3. Compared with the other 7 elements, the elements AGQ6-I, AGQ6-II and QAC II 6 exhibit the best convergence.

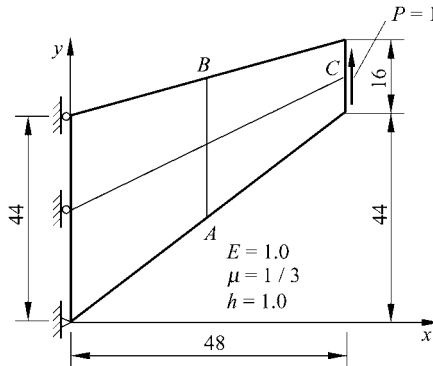


Figure 17.4 Cook’s skew beam problem

Table 17.3 Results for Cook's skew beam problem (Fig. 17.4)

Elements	v _C				σ _{I,max}				σ _{I,min}			
	2 × 2	4 × 4	8 × 8	16 × 16	2 × 2	4 × 4	8 × 8	16 × 16	2 × 2	4 × 4	8 × 8	16 × 16
Q4	11.80	18.29	22.08	23.43	0.1217	0.1873	0.2242	0.2311	-0.0960	-0.1524	-0.1869	-0.1966
Q6 ^[21]	22.94	23.48	23.80	23.91	0.2029	0.2258	0.2334	0.2361	-0.1734	-0.1915	-0.1997	-0.2028
QM6 ^[19]	21.05	23.02			0.1928	0.2243			-0.1580	-0.1856		
HL ^[25]	18.17	22.03	23.39		0.1582	0.1980			-0.1335	-0.1770		
P-S ^[1]	21.13	23.02		23.88	0.1854	0.2241		0.2364				
QE-2 ^[24]	21.35	23.04		23.88	0.1956	0.2261		0.2364				
B-Q4E ^[24]	21.35	23.04		23.88	0.1956	0.2261		0.2364				
AGQ6-I	23.07	23.68	23.87	23.93	0.2023	0.2275	0.2351	0.2365	-0.1758	-0.1972	-0.2016	-0.2033
AGQ6-II	25.92	24.37	24.04	23.97	0.2169	0.2286	0.2352	0.2365	-0.1999	-0.2014	-0.2027	-0.2035
QACII6	25.92	24.37	24.04	23.97	0.2169	0.2286	0.2352	0.2365	-0.1999	-0.2014	-0.2027	-0.2035
Reference Solutions [Ⓢ]	23.96				0.2362				-0.2023			

Ⓢ Results of the element GT9M8^[26] using 64 × 64 mesh.

Example 17.3 MacNeal’s thin cantilever beam with distorted meshes (Fig. 17.5).

Consider the thin beams presented in Fig. 17.5. Three different mesh shapes, rectangular, parallelogram and trapezoidal, are adopted. This example, proposed by MacNeal and Harder^[27], is a famous benchmark for testing the sensitivity to mesh distortion of the 4-node quadrilateral membrane elements. Besides the distortion caused only by the length-width ratio, the composite distortions of parallelogram and trapezoidal shapes together with length-width ratio are also taken into account.

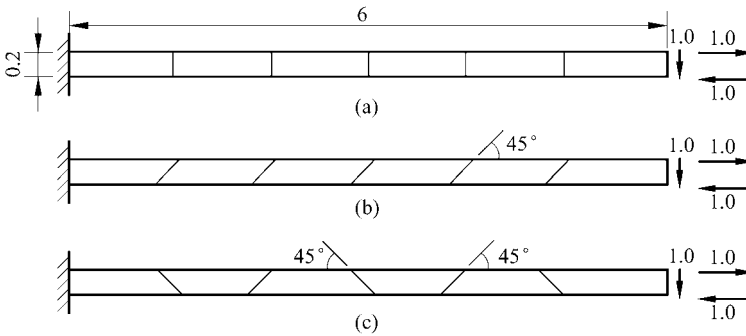


Figure 17.5 MacNeal’s beam
(a) Mesh A; (b) Mesh B; (c) Mesh C

There are two loading cases under consideration: pure bending and transverse linear bending. The Young’s modulus of the beam $E = 10^7$; the Poisson’s ratio $\mu = 0.3$; and the thickness $h = 0.1$.

The results of the tip deflection are shown in Table 17.4. Besides elements AGQ6-I, AGQ6-II and QACII6, the results obtained by the other nine element models are also given for comparison.

From Table 17.4, one can conclude that

(1) It is obvious that the element Q4 suffers from locking problems for all three types of distortion (① length-width ratio distortion, ② parallelogram distortion, ③ trapezoidal distortion) of three different meshes.

(2) The other eight elements can all improve the accuracy more or less.

Firstly, they all exhibit high precision using mesh A, no locking problem happens for the distortion caused by the length-width ratio.

Secondly, although their precisions are also improved using mesh B and mesh C, the locking problems are still not avoided completely, especially for the trapezoidal locking.

(3) The new elements, AGQ6-I, AGQ6-II, and QACII6 possess high accuracy for all three mesh divisions, and are insensitive to three types of distortion. Moreover, they can even produce the exact solutions for the pure bending problem.

Table 17.4 The normalized results of the tip deflection for the MacNeal’s thin beam using different meshes (Fig. 17.5)

Elements	Load P			Load M		
	Mesh A	Mesh B	Mesh C	Mesh A	Mesh B	Mesh C
Q4	0.093	0.035	0.003	0.093	0.031	0.022
QUAD4 ^[27]	0.904	0.080	0.071			
Q6 ^[21]	0.993	0.677	0.106	1.000	0.759	0.093
QM6 ^[19]	0.993	0.623	0.044	1.000	0.722	0.037
P-S ^[1]	0.993	0.798	0.221	1.000	0.852	0.167
RGD20 ^[28]	0.981	0.625	0.047			
PEAS7 ^[29]	0.982	0.795	0.217			
PN340 ^[25]	0.982	0.620	0.065			
ANSYS	0.979	0.624	0.047			
AGQ6-I	0.993	0.994	0.994	1.000	1.000	1.000
AGQ6-II	0.993	0.994	0.994	1.000	1.000	1.000
QACII6	0.993	0.994	0.994	1.000	1.000	1.000
Exact	1.000 ^①			1.000 ^②		

① The standard value is -0.1081 ;

② The standard value is -0.0054 .

Reference [30] has pointed out that if the element can pass the constant strain/stress patch test in a finite size mesh (i.e. the strict patch test), the trapezoidal locking will inevitably appear for the element in the calculation of the MacNeal’s thin beam. One reason that the new elements AGQ6-I, AGQ6-II and QACII6 can successfully avoid trapezoidal locking is that the new tool of the quadrilateral area coordinate systems are used, which can always keep the second-order completeness in the Cartesian coordinates under distortion meshes. Besides, instead of the strict form, only the weak form of patch test is used to assure the convergence of the new elements.

Example 17.4 Cantilever beam divided by two elements containing a parameter of distortion (Fig. 17.6).

The cantilever beam shown in Fig. 17.6 is divided by two elements. The shape of the two elements varies with the distortion parameter e . When $e = 0$, both elements are rectangular. But, with the increase of e , the mesh will be distorted more and more seriously. This is another famous benchmark for testing the sensitivity to the mesh distortion.

For the pure bending problem, the results of the tip deflection v_A at point A are listed in Table 17.5. Besides the elements AGQ6-I, AGQ6-II and QACII6, the solutions obtained by the other five element-models are also given for comparison.

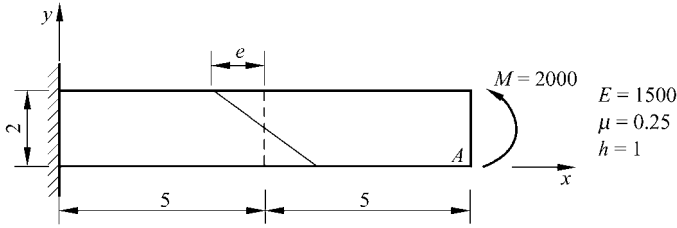


Figure 17.6 Cantilever beam divided by two elements with distortion parameter e

Table 17.5 Results of the tip deflection of a cantilever beam with a distortion parameter e (Fig. 17.6)

e	0	0.5	1	2	3	4	4.9
Q4	28.0	21.0	14.1	9.7	8.3	7.2	6.2
QM6 ^[19]	100	80.9	62.7	54.4	53.6	51.2	46.8
P-S ^[11]	100	81.0	62.9	55.0	54.7	53.1	49.8
QE2 ^[24]	100	81.2	63.4	56.5	57.5	57.9	56.9
\bar{B} -Q4E ^[24]	100	81.2	63.4	56.5	57.5	57.9	56.9
AGQ6-I	100	100	100	100	100	100	100
AGQ6-II	100	100	100	100	100	100	100
QACII6	100	100	100	100	100	100	100
Exact	100	100	100	100	100	100	100

Table 17.5 shows that:

The accuracy of the element Q4 is the poorest. Its relative precision only reaches 28% when $e = 0$.

The accuracies of the elements QM6, P-S, QE2 and \bar{B} -Q4E are better than that of Q4. All these four elements can produce the exact solution when $e = 0$. But, unfortunately, they are still sensitive to the mesh distortion. The relative precision only reaches 63% or so when $e = 1$, and will continue decreasing if e keeps increasing.

But, things become very different for the elements AGQ6-I, AGQ6-II and QAC II 6. All of them can keep providing the exact solutions when e varies from 0 to 5, i.e., they can overcome the trapezoidal locking completely. This shows again the advantages of the quadrilateral area coordinate methods and the weak patch test.

Example 17.5 Weak patch test (Fig. 17.7).

The constant strain/stress weak patch test using irregular mesh is shown in Fig. 17.7. Let Young’s modulus $E = 1000$, Poisson’s ratio $\mu = 0.25$, and thickness of the patch $t = 1$. At first, the patch divided by only three elements, as shown in Fig. 17.7, is considered. Each element is then bisected through the midpoints of the element sides. Thus, each original element is subdivided into four elements.

Repeat this division again and again, the total number of the elements in the refined mesh after each action will be 12, 48, 192, ..., in turn.

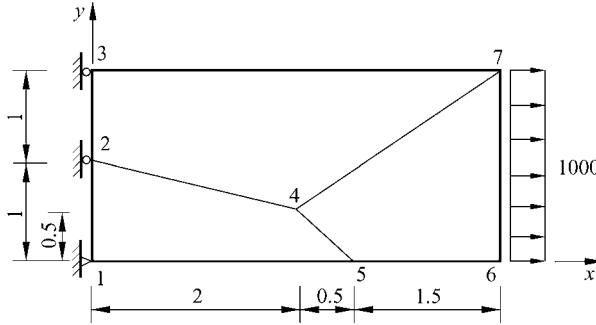


Figure 17.7 Weak patch test

From the results of this problem, it can be seen that the new elements AGQ6-I, AGQ6-II and QACII6 cannot give the exact solutions using the coarse mesh in finite size, i.e., they fail to pass the strict patch test. But, with the subdivision of the mesh, the results obtained by these elements will converge to the exact solutions. Therefore, they pass the weak patch test.

17.4.5 Conclusions

Three 4-node quadrilateral membrane elements, AGQ6-I, AGQ6-II and QACII6, have been developed using the quadrilateral area coordinates and generalized conforming conditions. The formulations of these elements are quite simple and easy to be constructed. And, the potential accuracy and versatility of the said elements have been illustrated using numerical examples, which show that: these new elements can not only produce the exact solutions for the pure bending problems using arbitrary mesh, but also avoid trapezoidal locking of the MacNeal's thin beam with distorted mesh. Compared with other 4-node quadrilateral membrane element models, these new elements exhibit higher precision and are more insensitive to mesh distortion.

Two points are worthy of being pointed out:

(1) This section provides a successful experience for constructing the quadrilateral membrane elements that are insensitive to mesh distortion. For a long time, many researchers have struggled for establishing effective element models that can not only avoid the trapezoidal locking in the MacNeal's thin beam problem, but also ensure the convergence of them. But, after many failed attempts, somebody even suspected that the above two purposes could not be achieved simultaneously. This section negates this suspicion, because it is

obvious that both purposes have been realized by the present elements. The success depends on two keys: the isoparametric coordinates are replaced by the quadrilateral area coordinates; and the strict patch test is replaced by the weak form.

(2) This section also shows the advantages of the quadrilateral area coordinates, especially for their excellent performance that can improve insensitivity of the elements to distorted meshes. This merit has been exhibited in references [5,13] for constructing the 8-node quadrilateral membrane elements, now it is again illustrated here for constructing the 4-node models. Besides, the formulations expressed by the area coordinates are isotropic because the area coordinate system is a natural coordinate system. This is another distinguished characteristic of the area coordinates, which the Cartesian coordinates cannot assure.

17.5 Geometrically Nonlinear Analysis Using Element AGQ6-I

17.5.1 Total Lagrangian Formulation of AGQ6-I

In order to establish the Total Lagrangian (TL) formulation for the element AGQ6-I, the proper strain measure should be the Green's strain:

$$E_{\alpha\beta} = \frac{1}{2}(u_{\alpha,\beta} + u_{\beta,\alpha} + u_{\gamma,\alpha}u_{\gamma,\beta}) \quad (17-29)$$

Where the Green's strain is temporarily written in index tensor form; the indices α , β and γ range from 1 to 2 (so u_1 , u_2 denote u , v in Eq. (17-6), respectively). Substitution of Eq. (17-6) into Eq. (17-29) will lead to quite complicated formulations. In fact, the linear part of the Green's strain plays a dominant role in calculations. Therefore, it is possible to exclude the incompatible displacement from the quadratic displacement term, as in the paper of Wu et al.^[31]:

$$E_{\alpha\beta} = \frac{1}{2}(u_{\alpha,\beta}^0 + u_{\beta,\alpha}^0 + u_{\gamma,\alpha}^0 u_{\gamma,\beta}^0) + \frac{1}{2}(u_{\alpha,\beta}^\lambda + u_{\beta,\alpha}^\lambda) = \frac{1}{2}(u_{\alpha,\beta} + u_{\beta,\alpha} + u_{\gamma,\alpha}^0 u_{\gamma,\beta}^0) \quad (17-30)$$

Based on the above assumption, the Green's strain can be expressed in matrix form:

$$E^e = B_q q^e + B_\lambda \lambda^e + \frac{1}{2} A G q^e \quad (17-31)$$

where

$$\mathbf{G} = [\mathbf{G}_1 \quad \mathbf{G}_2 \quad \mathbf{G}_3 \quad \mathbf{G}_4], \quad \mathbf{G}_i = \begin{bmatrix} \partial N_i^0 / \partial X & 0 \\ 0 & \partial N_i^0 / \partial X \\ \partial N_i^0 / \partial Y & 0 \\ 0 & \partial N_i^0 / \partial Y \end{bmatrix} \quad (i = 1, 2, 3, 4) \quad (17-32)$$

$$\mathbf{A} = \begin{bmatrix} \partial u^0 / \partial X & \partial v^0 / \partial X & 0 & 0 \\ 0 & 0 & \partial u^0 / \partial Y & \partial v^0 / \partial Y \\ \partial u^0 / \partial Y & \partial v^0 / \partial Y & \partial u^0 / \partial X & \partial v^0 / \partial X \end{bmatrix} \quad (17-33)$$

$$\begin{bmatrix} \frac{\partial u^0}{\partial X} & \frac{\partial v^0}{\partial X} & \frac{\partial u^0}{\partial Y} & \frac{\partial v^0}{\partial Y} \end{bmatrix}^T = \mathbf{G} \mathbf{q}^e \quad (17-34)$$

It should be noted that, since the Total Lagrangian form is used, all the derivatives are with respect to the undeformed (or initial) configuration (X, Y) . Here, there is no difference between $\partial/\partial X$ (or $\partial/\partial Y$) and $\partial/\partial x$ (or $\partial/\partial y$).

The condensation of the internal parameter vector $\boldsymbol{\lambda}^e$ can be achieved by using the following stationary condition:

$$\partial U^e / \partial \boldsymbol{\lambda}^e = \mathbf{0} \quad (17-35)$$

in which U^e is the element strain energy. In 2D linear elastic applications U^e can be expressed as follows:

$$U^e = \iint_A \mathbf{E}^{eT} \mathbf{D} \mathbf{E}^e h dA \quad (17-36)$$

Substitution of Eqs. (17-31) and (17-36) into Eq. (17-35) yields:

$$\boldsymbol{\lambda}^e = -\mathbf{R}^{-1} \left(\mathbf{G}_1 + \frac{1}{2} \mathbf{G}_2 \right) \mathbf{q}^e \quad (17-37)$$

with

$$\mathbf{R} = \iint_A \mathbf{B}_\lambda^T \mathbf{D} \mathbf{B}_\lambda h dA, \quad \mathbf{G}_1 = \iint_A \mathbf{B}_\lambda^T \mathbf{D} \mathbf{B}_q h dA, \quad \mathbf{G}_2 = \iint_A \mathbf{B}_\lambda^T \mathbf{D} \mathbf{A} \mathbf{G} h dA \quad (17-38)$$

Thus, the Green's strain vector can be written in the following condensed form:

$$\mathbf{E}^e = (\mathbf{B}_q - \mathbf{B}_\lambda \mathbf{R}^{-1} \mathbf{G}_1) \mathbf{q}^e + \frac{1}{2} (\mathbf{A} \mathbf{G} - \mathbf{B}_\lambda \mathbf{R}^{-1} \mathbf{G}_2) \mathbf{q}^e \quad (17-39)$$

Define the following incremental relation

$$d\mathbf{E} = \mathbf{B}^A d\mathbf{q}^e \quad (17-40)$$

where the matrix \mathbf{B}^A can be evaluated as follows:

$$\mathbf{B}^A = (\mathbf{B}_q - \mathbf{B}_\lambda \mathbf{R}^{-1} \mathbf{G}_1) + (\mathbf{A} \mathbf{G} - \mathbf{B}_\lambda \mathbf{R}^{-1} \mathbf{G}_2) \quad (17-41)$$

The second Piola-Kirchhoff (PK2) stress vector \mathbf{S}^e is calculated by:

$$\mathbf{S}^e = \mathbf{D} \mathbf{E}^e \quad (17-42)$$

with

$$\mathbf{S}^e = [\bar{S}_x \quad \bar{S}_y \quad \bar{S}_{xy}]^T \quad (17-43)$$

So, the internal nodal force vector $\mathbf{f}^{\text{int}^e}$ and the tangent stiffness matrix \mathbf{K}_T^e can be written as follows:

$$\mathbf{f}^{\text{int}^e} = \iint_A (\mathbf{B}^A)^T \mathbf{S}^e h dA \quad (17-44)$$

$$\mathbf{K}_T^e = \mathbf{K}_{\text{mat}}^e + \mathbf{K}_{\text{geo}}^e \quad (17-45)$$

where $\mathbf{K}_{\text{mat}}^e$ is the material tangent stiffness matrix and $\mathbf{K}_{\text{geo}}^e$ is the geometrical tangent stiffness matrix,

$$\mathbf{K}_{\text{mat}}^e = \iint_A (\mathbf{B}^A)^T \mathbf{D} \mathbf{B}^A h dA, \quad \mathbf{K}_{\text{geo}}^e = \iint_A \mathbf{G}^T \mathbf{M} \mathbf{G} h dA - \sum_{i=1}^2 \beta_i \mathbf{H}_i \quad (17-46)$$

$$\left. \begin{aligned} \mathbf{H}_i &= \iint_A \mathbf{G}^T \begin{bmatrix} l_{1i} \mathbf{I} & l_{3i} \mathbf{I} \\ l_{3i} \mathbf{I} & l_{2i} \mathbf{I} \end{bmatrix} \mathbf{G} h dA \quad (i=1,2) \\ \begin{bmatrix} l_{11} & l_{12} \\ l_{21} & l_{22} \\ l_{31} & l_{32} \end{bmatrix} &= \mathbf{D} \mathbf{B}_\lambda, \quad \mathbf{I} = \begin{bmatrix} 1 & 0 \\ 0 & 1 \end{bmatrix} \end{aligned} \right\} \quad (17-47)$$

$$\mathbf{M} = \begin{bmatrix} \bar{S}_x \mathbf{I} & \bar{S}_{xy} \mathbf{I} \\ \bar{S}_{xy} \mathbf{I} & \bar{S}_y \mathbf{I} \end{bmatrix} \quad (17-48)$$

$$[\beta_1 \quad \beta_2]^T = \mathbf{R}^{-1} \iint_A \mathbf{B}_\lambda^T \mathbf{S}^e h dA \quad (17-49)$$

Thus, the Total Lagrangian formulation of AGQ6-I is established. By using Eq. (16-39), all the necessary matrices can be evaluated by the Gauss numerical integration scheme.

17.5.2 Numerical Examples

All examples are selected from the documentation of the FEM software

ABAQUS^[32].

Example 17.6 Deformations of a cantilever beam subjected to a constant tip vertical load P (Fig. 17.8).

As shown in Fig. 17.8, a slender cantilever is subjected to a constant vertical concentrated load $P=269.35\text{N}$ (load direction keeps vertical) at its free tip. The length L , height H and thickness T of the cantilever are as follows: $L=10\text{m}$; $H=147.8\text{mm}$; and $T=100\text{mm}$, so the beam is moderately slender ($L/H\approx 70$). The Young’s modulus $E=100\text{MPa}$; and the Poisson’s ratio $\mu=0$. Bending behavior will be the dominant deformation since axial deformation is insignificant. Two mesh divisions are used: (1) parallelogram (45°) coarse mesh: 1×10 for the 4-node elements and 1×5 for the 8-node elements; and (2) trapezoidal coarse mesh (45°): 1×10 for the 4-node elements and 1×5 for the 8-node elements. The exact solution for the inextensible beam is given in reference [33]. Here, the reference solution is obtained with the 8-node reduced integration isoparametric element in a regular mesh of 1×20 , and is very close to the analytical solution. As shown in Table 17.6, besides the element AGQ6-I, the results by the incompatible isoparametric elements Q6 and QM6, the conventional 4-node isoparametric element Q4, and several ABAQUS elements are all reported for comparison.



Figure 17.8 Slender cantilever subjected to tip vertical load P

Table 17.6 List of quadrilateral element models for comparison

	Element symbols	Features	Number of Gauss integration points
QACM elements (T.L.)	AGQ6-I	4-node, incompatible mode, pass the weak constant strain/stress patch test	3×3
Isoparametric elements (T.L.)	Q4	4-node, standard bilinear isoparametric element	3×3
	Q4-2	as above	2×2
	Q6	4-node, incompatible mode ^[21]	3×3
	Q6-2	as above	2×2
	QM6	4-node, incompatible mode, pass the strict constant strain/stress patch test ^[19]	3×3
	QM6-2	as above	2×2
ABAQUS elements ^[32] (U.L.)	CPS4	4-node, standard, fully integrated	
	CPS4I	4-node, incompatible mode with enhanced assumed strain, pass the strong patch test	
	CPS4R	4-node, standard, reduced-integration, hourglass control	
	CPS8R	8-node, reduced-integration	
	CPS8	8-node, fully integrated	

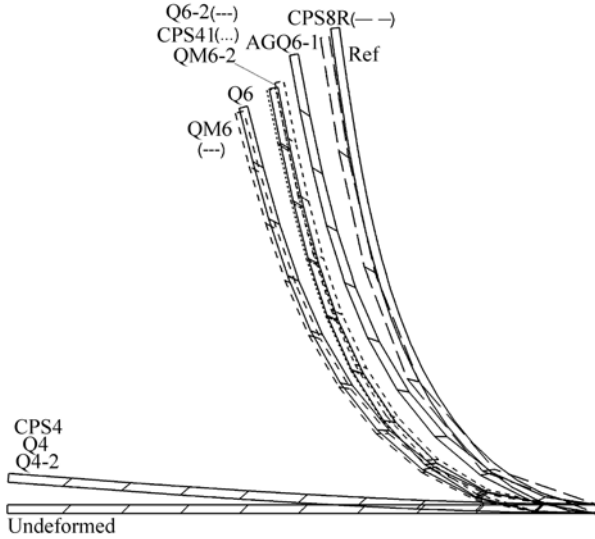


Figure 17.9 Deformations of the beam subjected to constant vertical load P : parallelogram coarse mesh

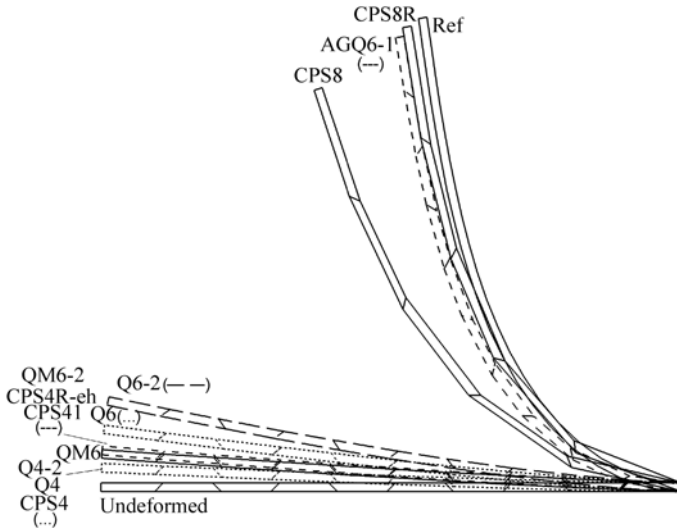


Figure 17.10 Deformations of the beam subjected to constant vertical load P : trapezoidal coarse mesh

The deformations of the beam are plotted in Fig. 17.9 and Fig. 17.10. It can be seen that the element AGQ6-I exhibits obvious advantage when compared with the other 4-node models. Among the results by the 4-node elements, AGQ6-I is the closest one to the solution of the element CPS8R which is recommended by ABAQUS.

Example 17.7 Deformations of a cantilever beam subjected to tip bending moment M (Fig. 17.11).

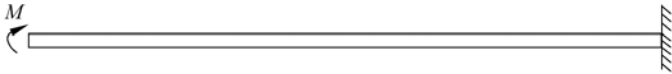


Figure 17.11 Slender cantilever subjected to tip bending moment M

As shown in Fig. 17.11, a slender cantilever is subjected to a bending moment load $M=3384.78\text{N}\cdot\text{m}$ at its free tip. The length L of the beam is 100m. Other dimensions and material constants are the same as those in the previous example. The analytical solution for this problem is $ML/EI=2\pi n$, where I is the section moment of inertia; n is the number of times that the beam will wind around itself. Here $n=2$ is the exact analytical solution. A 1×400 mesh division with the trapezoidal (45°) element shape is adopted. The results by the element AGQ6-1 and some other models are plotted in Fig. 17.12. It is very interesting that the displacement of the beam obtained by the element AGQ6-1 winds exactly two times, while the locking phenomenon happens for the other 4-node elements.

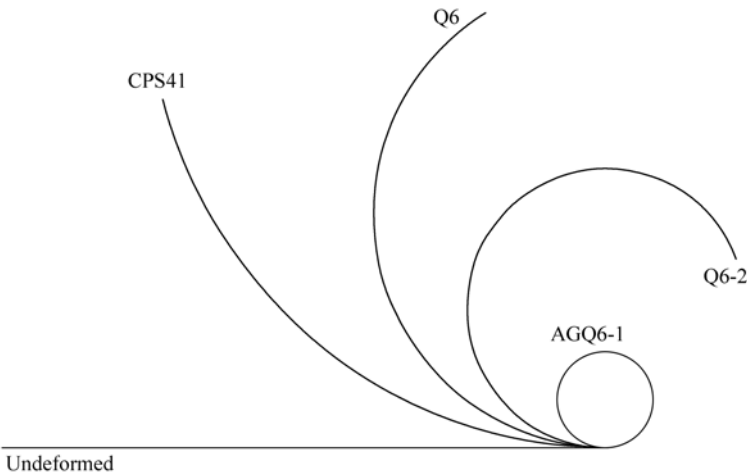


Figure 17.12 Deformations of a slender beam subjected to tip moment load M : trapezoidal mesh 1×400

17.6 Quadrilateral Membrane Elements with Drilling Degrees of Freedom Formulated by the Area Coordinate Method

There are two 4-node quadrilateral elements with drilling degrees of freedom, AQ40 and AQ40 λ , which have been listed in Table 17.1, formulated by the area

coordinate method. They will be introduced in this section. The key points of their construction are as follows:

(1) The element AQ4 θ is derived from the element QACM4^[10] by introducing vertex drilling degrees of freedom $\theta_i (i = 1, 2, 3, 4)$ and their shape functions $N_{u\theta_i}$ and $N_{v\theta_i}$.

(2) The element AQ4 λ is derived from the element AQ4 θ by introducing internal degrees of freedom λ_1, λ'_1 and their shape function N_{λ_1} .

17.6.1 Formulations of the Element AQ4 θ

Consider a 4-node quadrilateral membrane element with vertex drilling degrees of freedom. The element nodal displacement vector can be written as:

$$\mathbf{q}^e = [\mathbf{q}_1^T \quad \mathbf{q}_2^T \quad \mathbf{q}_3^T \quad \mathbf{q}_4^T]^T$$

in which the degrees of freedom for each node are given by

$$\mathbf{q}_i = [u_i \quad v_i \quad \theta_i]^T \quad (i = 1, 2, 3, 4)$$

where u_i and v_i are the nodal translation displacements; θ_i are the additional rigid rotations at vertices.

The element displacement fields are composed of two parts

$$\mathbf{u} = \mathbf{u}^0 + \mathbf{u}^\theta \tag{17-50}$$

The first term on the right side of the above equation represents the displacement fields determined by the nodal translation degrees of freedom; and the second term represents the additional displacement fields caused by the in-plane rigid vertex drilling degrees of freedom.

1. Determination of the displacement fields \mathbf{u}^0

The displacement fields \mathbf{u}^0 are caused by the nodal translation degrees of freedom, and by using the formulations of the element QACM4^[10], they can be expressed in terms of the quadrilateral area coordinates as follows:

$$\left. \begin{aligned} u^0 &= \sum_{i=1}^4 N_i^0 u_i \\ v^0 &= \sum_{i=1}^4 N_i^0 v_i \end{aligned} \right\} \tag{17-51}$$

in which the shape functions N_i^0 are given by

conditions are also used for v_θ):

$$\left. \begin{aligned} \sum_{i=1}^4 (u_\theta^i - \bar{u}_\theta^i) &= 0 \\ \sum_{i=1}^4 \xi_i \eta_i (u_\theta^i - \bar{u}_\theta^i) &= 0 \\ \int_{d_{ij}} (u_\theta - \bar{u}_\theta) d\bar{s} &= 0 \quad (ij = 12, 23, 34, 41) \end{aligned} \right\} \quad (17-56)$$

Substitution of Eq. (17-54) and Eq. (17-55) into the above equation yields

$$\left. \begin{aligned} L\alpha &= Tq^\theta \\ L\beta &= T'q^\theta \end{aligned} \right\} \quad (17-57)$$

From the above equation, we obtain

$$\left. \begin{aligned} \alpha &= L^{-1}Tq^\theta \\ \beta &= L^{-1}T'q^\theta \end{aligned} \right\} \quad (17-58)$$

where

$$L = \begin{bmatrix} 4 & 2(g_1 - g_2) & 2(g_2 - g_3) & 2(g_2g_4 - g_1g_3) & 0 & 0 \\ 0 & 2(g_3 - g_2) & 2(g_2 - g_1) & 2(g_2g_4 + g_1g_3) & 0 & 0 \\ 1 & \frac{g_4 + g_1}{2} & \frac{g_2 - g_3}{2} & \frac{g_2(2g_4 + g_1) - g_3(g_4 + 2g_1)}{6} & 0 & \frac{g_2g_3}{6} \\ 1 & \frac{g_4 - g_3}{2} & \frac{g_1 + g_2}{2} & \frac{g_4(2g_2 + g_1) - g_3(g_2 + 2g_1)}{6} & \frac{g_3g_4}{6} & 0 \\ 1 & \frac{-g_2 - g_3}{2} & \frac{g_1 - g_4}{2} & \frac{g_4(2g_2 + g_3) - g_1(g_2 + 2g_3)}{6} & 0 & \frac{g_1g_4}{6} \\ 1 & \frac{g_1 - g_2}{2} & \frac{-g_3 - g_4}{2} & \frac{g_2(2g_4 + g_3) - g_1(g_4 + 2g_3)}{6} & \frac{g_1g_2}{6} & 0 \end{bmatrix} \quad (17-59)$$

$$T = \frac{1}{12} \begin{bmatrix} 0 & 0 & 0 & 0 \\ 0 & 0 & 0 & 0 \\ 0 & -b_1 & b_1 & 0 \\ 0 & 0 & -b_2 & b_2 \\ b_3 & 0 & 0 & -b_3 \\ -b_4 & b_4 & 0 & 0 \end{bmatrix}, \quad T' = \frac{1}{12} \begin{bmatrix} 0 & 0 & 0 & 0 \\ 0 & 0 & 0 & 0 \\ 0 & -c_1 & c_1 & 0 \\ 0 & 0 & -c_2 & c_2 \\ c_3 & 0 & 0 & -c_3 \\ -c_4 & c_4 & 0 & 0 \end{bmatrix} \quad (17-60)$$

$$\boldsymbol{\alpha} = [\alpha_1 \quad \alpha_2 \quad \alpha_3 \quad \alpha_4 \quad \alpha_5 \quad \alpha_6]^T, \quad \boldsymbol{\beta} = [\beta_1 \quad \beta_2 \quad \beta_3 \quad \beta_4 \quad \beta_5 \quad \beta_6]^T$$

$$\boldsymbol{q}^\theta = [\theta_1 \quad \theta_2 \quad \theta_3 \quad \theta_4]^T$$

Let

$$\left. \begin{aligned} \boldsymbol{G} &= \boldsymbol{L}^{-1} \boldsymbol{T} \\ \boldsymbol{G}' &= \boldsymbol{L}^{-1} \boldsymbol{T}' \end{aligned} \right\} \quad (17-61)$$

then, we have

$$\left. \begin{aligned} \boldsymbol{u}_\theta &= \sum_{i=1}^4 N_{u\theta i} \theta_i \\ \boldsymbol{v}_\theta &= \sum_{i=1}^4 N_{v\theta i} \theta_i \end{aligned} \right\} \quad (17-62)$$

in which the shape functions are

$$\left. \begin{aligned} N_{u\theta i} &= G_{1i} + G_{2i}(L_3 - L_1) + G_{3i}(L_4 - L_2) + G_{4i}(L_3 - L_1)(L_4 - L_2) + G_{5i}L_1L_3 + G_{6i}L_2L_4 \\ N_{v\theta i} &= G'_{1i} + G'_{2i}(L_3 - L_1) + G'_{3i}(L_4 - L_2) + G'_{4i}(L_3 - L_1)(L_4 - L_2) + G'_{5i}L_1L_3 + G'_{6i}L_2L_4 \end{aligned} \right\} \quad (i=1,2,3,4) \quad (17-63)$$

3. Element displacement fields and stiffness matrix

The element displacement fields can be obtained by the superposition of \boldsymbol{u}^0 and \boldsymbol{u}_θ :

$$\boldsymbol{u} = \boldsymbol{u}_0 + \boldsymbol{u}_\theta = \boldsymbol{N} \boldsymbol{q}^e = \sum_{i=1}^4 N_i \boldsymbol{q}_i^e \quad (17-64)$$

where

$$\boldsymbol{N} = [N_1 \quad N_2 \quad N_3 \quad N_4] \quad (17-65)$$

$$N_i = \begin{bmatrix} N_i^0 & 0 & N_{u\theta i} \\ 0 & N_i^0 & N_{v\theta i} \end{bmatrix}$$

And, the element strain fields are

$$\boldsymbol{\varepsilon} = \boldsymbol{B}_q \boldsymbol{q}^e \quad (17-66)$$

where

$$\boldsymbol{B}_q = [B_1 \quad B_2 \quad B_3 \quad B_4]$$

$$\mathbf{B}_i = \begin{bmatrix} \frac{\partial N_i^0}{\partial x} & 0 & \frac{\partial N_{u\theta i}}{\partial x} \\ 0 & \frac{\partial N_i^0}{\partial y} & \frac{\partial N_{v\theta i}}{\partial y} \\ \frac{\partial N_i^0}{\partial y} & \frac{\partial N_i^0}{\partial x} & \frac{\partial N_{u\theta i}}{\partial y} + \frac{\partial N_{v\theta i}}{\partial x} \end{bmatrix} \quad (i = 1, 2, 3, 4) \quad (17-67)$$

Then, the element stiffness matrix of the element AQ40 can be written as

$$\mathbf{K}_{qq} = \iint_{A^e} \mathbf{B}_q^T \mathbf{D} \mathbf{B}_q h dA \quad (17-68)$$

17.6.2 Formulations of the Element AQ40λ

The new element AQ40λ is derived from the element AQ40 by introducing internal degrees of freedom. Firstly, the displacements related to the internal degrees of freedom are assumed to be

$$\left. \begin{aligned} u_\lambda &= \alpha_1 + \alpha_2(L_3 - L_1) + \alpha_3(L_4 - L_2) + \alpha_4 L_1 L_3 + \lambda_1 L_2 L_4 + \lambda_2(L_3 - L_1)(L_4 - L_2) \\ v_\lambda &= \beta_1 + \beta_2(L_3 - L_1) + \beta_3(L_4 - L_2) + \beta_4 L_1 L_3 + \lambda'_1 L_2 L_4 + \lambda'_2(L_3 - L_1)(L_4 - L_2) \end{aligned} \right\} \quad (17-69)$$

Then, four line generalized conforming conditions of zero boundary displacement for u_λ and v_λ are introduced:

$$\int_{d_y} \mathbf{u}_\lambda ds = \mathbf{0} \quad (17-70)$$

Finally, we obtain

$$\left. \begin{aligned} u_\lambda &= \lambda_1 N_{\lambda 1} + \lambda_2 N_{\lambda 2} \\ v_\lambda &= \lambda'_1 N_{\lambda 1} + \lambda'_2 N_{\lambda 2} \end{aligned} \right\} \quad (17-71)$$

where $\lambda_1, \lambda'_1, \lambda_2, \lambda'_2$ are 4 internal parameters; $N_{\lambda 1}$ and $N_{\lambda 2}$ are the shape functions for internal parameters:

$$\left. \begin{aligned} N_{\lambda 1} &= \frac{6g_1 g_2 g_3 g_4 - g_1 g_3 - g_2 g_4}{6(1 - g_1 g_4 - g_2 g_3)} + \frac{g_1 - g_2}{6} (L_3 - L_1) \\ &\quad + \frac{(g_1 - g_4)(g_1 g_4 + g_2 g_3)}{6(1 - g_1 g_4 - g_2 g_3)} (L_4 - L_2) + \frac{g_1 g_4 + g_2 g_3}{1 - g_1 g_4 - g_2 g_3} L_1 L_3 + L_2 L_4 \\ N_{\lambda 2} &= \frac{1}{3} (g_3 - g_2)(L_3 - L_1) - 2(g_1 - g_2)(L_4 - L_2) + (L_3 - L_1)(L_4 - L_2) \end{aligned} \right\} \quad (17-72)$$

Equation (17-71) can be written as

$$\mathbf{u}_\lambda = \mathbf{N}_\lambda \boldsymbol{\lambda} \tag{17-73}$$

where

$$\left. \begin{aligned} \boldsymbol{\lambda} &= [\lambda_1 \quad \lambda'_1 \quad \lambda_2 \quad \lambda'_2]^T \\ \mathbf{N}_\lambda &= \begin{bmatrix} N_{\lambda 1} & 0 & N_{\lambda 2} & 0 \\ 0 & N_{\lambda 1} & 0 & N_{\lambda 2} \end{bmatrix} \end{aligned} \right\} \tag{17-74}$$

From the internal parameter displacements \mathbf{u}_λ , the internal parameter strain can be derived:

$$\boldsymbol{\varepsilon}_\lambda = \mathbf{B}_\lambda \boldsymbol{\lambda} \tag{17-75}$$

After condensation, the stiffness matrix of the element AQ40 λ can be obtained

$$\mathbf{K}^e = \mathbf{K}_{qq} - \mathbf{K}_{\lambda q}^T \mathbf{K}_{\lambda\lambda}^{-1} \mathbf{K}_{\lambda q} \tag{17-76}$$

where

$$\left. \begin{aligned} \mathbf{K}_{qq} &= \iint_{A^e} \mathbf{B}_q^T \mathbf{D} \mathbf{B}_q h dA \\ \mathbf{K}_{\lambda\lambda} &= \iint_{A^e} \mathbf{B}_\lambda^T \mathbf{D} \mathbf{B}_\lambda h dA \\ \mathbf{K}_{\lambda q} &= \iint_{A^e} \mathbf{B}_\lambda^T \mathbf{D} \mathbf{B}_q h dA \end{aligned} \right\} \tag{17-77}$$

17.6.3 Numerical Examples

Example 17.8 Recalculate Example 17.1 by using the elements AQ40 and AQ40 λ .

The results are listed in Table 17.7 (it is a continuous part of Table 17.2).

Table 17.7 Results for a cantilever beam divided by 5 elements (Fig. 17.3)

Elements	Load M		Load P	
	v_A	σ_{xB}	v_A	σ_{xB}
AQ40	97.7	-2947	98.9	-3931
AQ40 λ	100	-2999	101.0	-3907
Exact	100	-3000	102.6	-4050

Example 17.9 Recalculate Example 17.2 by using the elements AQ40 and AQ40 λ .

The results are listed in Table 17.8 (it is a continuous part of Table 17.3).

Table 17.8 Results for Cook’s skew beam problem (Fig. 17.4)

Elements	v_C			σ_{Amax}			σ_{Bmin}		
	2 × 2	4 × 4	8 × 8	2 × 2	4 × 4	8 × 8	2 × 2	4 × 4	8 × 8
AQ40	21.00	23.05	24.28	0.1917	0.2241	0.2377	-0.1877	-0.1939	-0.2060
AQ40λ	22.91	23.66	24.18	0.2498	0.2338	0.2358	-0.1729	-0.1896	-0.2018

Example 17.10 Recalculate Example 17.3 by using the elements AQ40 and AQ40λ.

The results are listed in Table 17.9 (it is a continuous part of Table 17.4).

Table 17.9 Results for MacNeal’s thin beam problem (Fig. 17.5)

Elements	Load P		
	Mesh A	Mesh B	Mesh C
AQ40	0.904	0.906	0.867
AQ40λ	0.993	0.988	0.984

Example 17.11 Recalculate Example 17.4 by using the elements AQ40 and AQ40λ.

The results are listed in Table 17.10 (it is a continuous part of Table 17.5).

Table 17.10 Results of tip deflection for a beam with a distortion parameter e (Fig. 17.6)

e	0	0.5	1	2	3	4	4.9
AQ40	100	99.9	98.9	99.8	102.0	102.2	100.3
AQ40λ	100	100	100	100	100	100	100

From the above numerical examples, it can be seen that the elements AQ40 and AQ40λ possess high accuracy and are quite insensitive to mesh distortion. These two elements and elements AGQ6-I, AGQ6-II and QACII6 presented in Sect. 17.4 are the best 4-node quadrilateral membrane elements. There is a difference among these five elements: elements AQ40 and AQ40λ can pass the strict patch test while AGQ6-I, AGQ6-II and QACII6 can only pass the weak patch test.

17.7 8-Node Quadrilateral Membrane Elements Formulated by the Area Coordinate Method

Four 8-node quadrilateral elements formulated by the area coordinate method, MQ8-I and MQ8-II^[5], AQ8-I and AQ8-II^[13], have already been listed in

Table 17.1. In Sect. 17.2 and Fig. 17.2, a comparison of the elements MQ8-I and MQ8-II with 8-node isoparametric element Q8 is carried out. It can be seen that the accuracy of the elements MQ8-I and MQ8-II is much better than that of the element Q8 when a distorted mesh is used. In this section, the elements AQ8-I and AQ8-II, which are also constructed by the quadrilateral area coordinate method and insensitive to mesh distortion, will be introduced. They are similar to the elements MQ8-I and MQ8-II (only some difference exists in the shape functions).

17.7.1 Preparatory Shape Functions for Corner Nodes

An 8-node quadrilateral plane element is shown in Fig. 17.13.

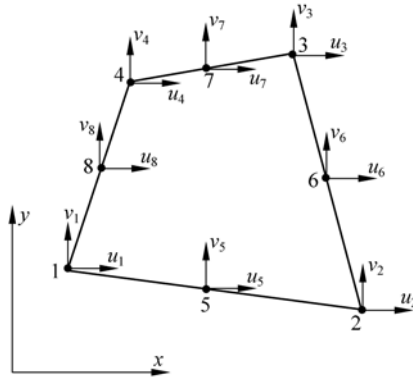


Figure 17.13 An 8-node quadrilateral plane element

Firstly, prescribe a set of shape functions for the four corner nodes 1, 2, 3 and 4:

$$\left. \begin{aligned}
 N_1^0 &= \frac{L_1}{2g_2} \left(1 - \frac{L_4}{g_1} \right) + \frac{L_2}{2g_4} \left(1 - \frac{L_3}{g_1} \right) \\
 N_2^0 &= \frac{L_2}{2g_3} \left(1 - \frac{L_1}{g_2} \right) + \frac{L_3}{2g_1} \left(1 - \frac{L_4}{g_2} \right) \\
 N_3^0 &= \frac{L_3}{2g_4} \left(1 - \frac{L_2}{g_3} \right) + \frac{L_4}{2g_2} \left(1 - \frac{L_1}{g_3} \right) \\
 N_4^0 &= \frac{L_4}{2g_1} \left(1 - \frac{L_3}{g_4} \right) + \frac{L_1}{2g_3} \left(1 - \frac{L_2}{g_4} \right)
 \end{aligned} \right\} \quad (17-78)$$

i.e.,

$$N_i^0 = \frac{L_i}{2g_j} \left(1 - \frac{L_m}{g_i} \right) + \frac{L_j}{2g_m} \left(1 - \frac{L_k}{g_i} \right) \quad (\overline{i, j, k, m} = \overline{1, 2, 3, 4}) \quad (17-79)$$

The above equation can also be written as

$$N_i^0 = \frac{1}{4} \left[1 + \frac{L_i}{g_j} + \frac{L_j}{g_m} - \frac{L_k + L_m}{g_i} + \frac{g_k}{g_0} (g_i L_i L_j - g_j L_j L_k + g_k L_k L_m - g_m L_m L_i) \right] \left. \vphantom{N_i^0} \right\} \\ g_0 = g_1 g_2 g_3 g_4 \quad (17-80)$$

It can be clearly seen that N_i^0 ($i = 1, 2, 3, 4$), which are quadratic, satisfy the following conditions:

$$N_i^0((L_1)_j, (L_2)_j, (L_3)_j, (L_4)_j) = \delta_{ij} = \begin{cases} 1 & (i = j) \\ 0 & (i \neq j) \end{cases} \quad (i, j = 1, 2, 3, 4)$$

But, N_i^0 are not zero at the mid-side nodes 5, 6, 7 and 8. Thus, they cannot be the real shape functions for the corner nodes, and are called the preparatory shape functions for corner nodes.

17.7.2 Shape Functions for Mid-Side Nodes

Secondly, define two sets of shape functions for the mid-side nodes 5, 6, 7, 8 as follows:

(1) For AQ8-I

$$\left. \begin{aligned} N_5 &= \frac{2}{g_1 g_2} L_1 L_3 \left(1 + \frac{2}{g_3 + g_4} L_2 - \frac{2}{g_1 + g_2} L_4 \right) \\ N_6 &= \frac{2}{g_2 g_3} L_2 L_4 \left(1 + \frac{2}{g_4 + g_1} L_3 - \frac{2}{g_2 + g_3} L_1 \right) \\ N_7 &= \frac{2}{g_3 g_4} L_3 L_1 \left(1 + \frac{2}{g_1 + g_2} L_4 - \frac{2}{g_3 + g_4} L_2 \right) \\ N_8 &= \frac{2}{g_4 g_1} L_4 L_2 \left(1 + \frac{2}{g_2 + g_3} L_1 - \frac{2}{g_4 + g_1} L_3 \right) \end{aligned} \right\} \quad (17-81)$$

i.e.,

$$N_{4+i} = \frac{2}{g_i g_j} L_i L_k \left(1 + \frac{2}{g_k + g_m} L_j - \frac{2}{g_i + g_j} L_m \right) \quad (\overline{i, j, k, m} = \overline{1, 2, 3, 4}) \quad (17-82)$$

(2) For AQ8-II

$$\left. \begin{aligned} N_5 &= \frac{4}{g_1 g_2} L_1 L_3 \left(L_2 - L_4 + \frac{g_1 + g_2}{2} \right) \\ N_6 &= \frac{4}{g_2 g_3} L_2 L_4 \left(L_3 - L_1 + \frac{g_2 + g_3}{2} \right) \\ N_7 &= \frac{4}{g_3 g_4} L_3 L_1 \left(L_4 - L_2 + \frac{g_3 + g_4}{2} \right) \\ N_8 &= \frac{4}{g_4 g_1} L_4 L_2 \left(L_1 - L_3 + \frac{g_4 + g_1}{2} \right) \end{aligned} \right\} \quad (17-83)$$

i.e.,

$$N_{4+i} = \frac{4}{g_i g_j} L_i L_k \left(L_j - L_m + \frac{g_i + g_j}{2} \right) \quad (\overline{i, j, k, m} = \overline{1, 2, 3, 4}) \quad (17-84)$$

It can be clearly seen that both sets of shape functions satisfy:

$$N_i((L_1)_j, (L_2)_j, (L_3)_j, (L_4)_j) = \delta_{ij} = \begin{cases} 1 & (i = j) \\ 0 & (i \neq j) \end{cases} \quad (i = 5, 6, 7, 8; \quad j = 1, 2, \dots, 7, 8) \quad (17-85)$$

17.7.3 Shape Functions for Corner Nodes

For corner nodes, the following modified shape functions are employed:

$$\begin{aligned} N_i &= N_i^0 - \left(\frac{1}{2} - \frac{g_i - g_j}{8g_m} \right) N_{4+i} - \frac{g_k(g_j - g_i)}{8g_m g_i} N_{4+j} \\ &\quad + \frac{g_k(g_k - g_m)}{8g_i g_j} N_{4+k} - \left(\frac{1}{2} + \frac{g_m - g_i}{8g_j} \right) N_{4+m} \quad (\overline{i, j, k, m} = \overline{1, 2, 3, 4}) \end{aligned} \quad (17-86)$$

It is obvious that $N_i(i = 1, 2, 3, 4)$ satisfy:

$$N_i((L_1)_j, (L_2)_j, (L_3)_j, (L_4)_j) = \delta_{ij} = \begin{cases} 1 & (i = j) \\ 0 & (i \neq j) \end{cases} \quad (i = 1, 2, 3, 4; \quad j = 1, 2, \dots, 7, 8) \quad (17-87)$$

17.7.4 The Characteristics of the Two New Elements

Equations (17-86) and (17-81) constitute a set of shape functions for the first

8-node quadrilateral element, which is denoted as AQ8-I. And, another set of shape functions can be obtained by combining Eqs. (17-86) and (17-83) for the second element denoted by AQ8-II.

The element displacement fields are

$$u = \sum_{i=1}^8 N_i u_i, \quad v = \sum_{i=1}^8 N_i v_i \quad (17-88)$$

From the above equations, the two new elements possess the following characteristics:

- (1) The displacement fields are cubic both within an element and along the element sides.
- (2) The point conforming condition is satisfied at 8 nodes.
- (3) Since the displacement along each element side is cubic, and satisfies the point conforming condition at 3 points (two end nodes and one mid-side node), it must satisfy the average line conforming condition along this element side.
- (4) The two new elements are both generalized conforming elements.
- (5) When the element degenerates to a rectangular element, the elements AQ8-I and AQ8-II will be the same as those of the Q8 element.

According to the shape functions of the new elements, the element stiffness matrices can be obtained by the conventional procedure.

17.7.5 Numerical Examples

Example 17.12 Pure bending problem of a cantilever beam (Fig. 17.14). The results of displacements and stresses at selected points are calculated by the three meshes plotted in Fig. 17.15.

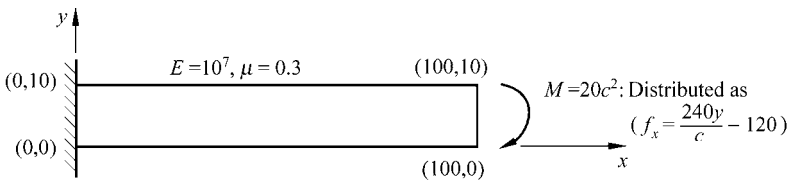


Figure 17.14 Pure bending problem of a cantilever beam

The results obtained by the elements AQ8-I and AQ8-II and other models are listed in Table 17.11. Compared with the Serendipity isoparametric elements Q8 and Q12, the new elements can still keep good accuracy in distorted meshes, but the precisions of the isoparametric elements Q8 and Q12 drop dramatically.

Example 17.13 Linear bending problem of a cantilever beam (Fig. 17.16). Four meshes plotted in Fig. 17.17 are used here.

The results obtained by AQ8-I and AQ8-II are listed in Table 17.12. It is again obvious that the AQ8-I and AQ8-II elements perform better than the Q8 element when irregular meshes are used.

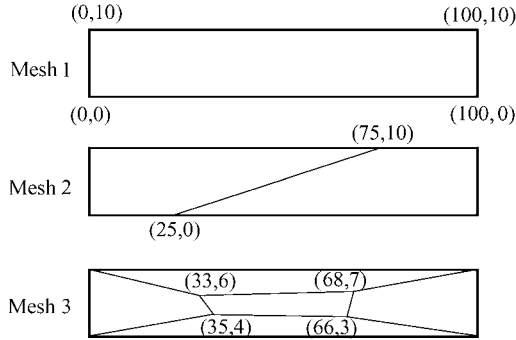


Figure 17.15 Mesh divisions and dimensions for Example 17.12

Table 17.11 Numerical results of the pure bending cantilever beam (Example 17.12)

		Q8	Q12 ^[4]	AQ8-I	AQ8-II	Exact
Mesh 1	$\sigma_x(0, 10)$	120.000	120.0	120.000	120.000	120.0
	$\sigma_x(0, 0)$	- 120.000	- 120.0	- 120.000	- 120.000	- 120.0
	$v(100,0) \times 10^3$	- 12.000	- 12.00	- 12.000	- 12.000	- 12.0
Mesh 2	$\sigma_x(0, 10)$	56.447	125.5	118.222	118.222	120.0
	$\sigma_x(0, 0)$	- 74.863	- 145.5	- 114.667	- 114.667	- 120.0
	$v(100,0) \times 10^3$	- 2.328	- 5.18	- 12.014	- 12.014	- 12.0
Mesh 3	$\sigma_x(0_+, 10)$	13.665	29.4	119.696	119.815	120.0
	$\sigma_x(0, 10_-)$	5.262	14.0	118.887	119.271	120.0
	$\sigma_x(0, 0_+)$	- 5.665	- 13.1	- 119.112	- 119.341	- 120.0
	$\sigma_x(0_+, 0)$	- 14.299	- 28.5	- 119.880	- 119.866	- 120.0
	$v(100,0) \times 10^3$	- 0.477	- 0.69	- 11.997	- 11.997	- 12.0

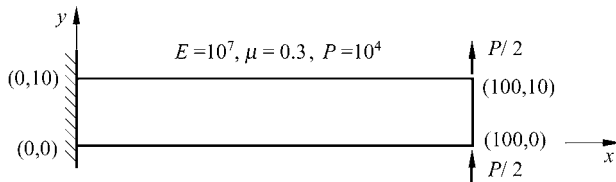


Figure 17.16 Linear bending problem of a cantilever beam

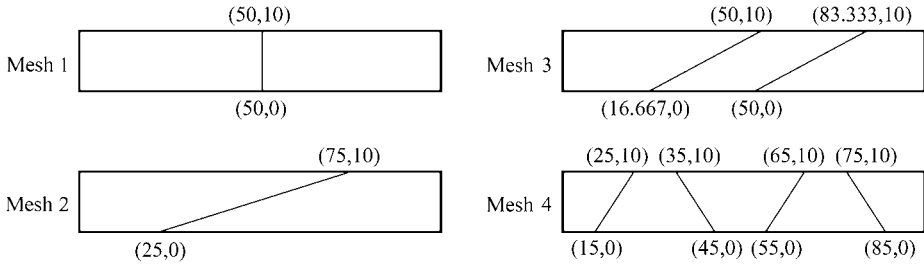


Figure 17.17 Meshes for Example 17.13

Table 17.12 The deflection $v(100,0)$ for the linear bending problem of a cantilever beam (Example 17.13)

	Q8	AQ8-I	AQ8-II	Exact
Mesh 1	3.85	3.85	3.85	4.03
Mesh 2	0.74	3.15	3.15	4.03
Mesh 3	2.00	3.30	3.30	4.03
Mesh 4	3.65	3.99	3.99	4.03

Example 17.14 Sensitivity test for mesh distortion.

Re-perform Examples 17.4 and 17.11 using the mesh shown in Fig. 17.18, where e varies from 0 to $0.99L$. The results obtained by the elements Q4 and Q8 are also explored for comparison.

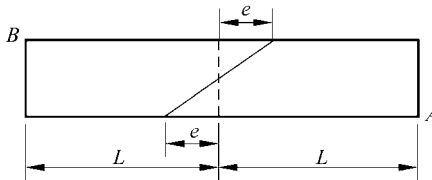


Figure 17.18 Mesh with a distortion parameter a

The curves of the percentage errors of deflection v_A and stress σ_{xB} for the pure bending problem are plotted in Fig. 17.19(a) and (b). It can be seen that, the isoparametric elements Q4 and Q8 are very sensitive to mesh distortion, while the elements AQ8-I and AQ8-II can still give accurate results when the mesh is distorted.

The curves of the percentage errors of deflection v_A for linear bending problem are shown in Fig. 17.20. Again, the precision of the elements AQ8-I and AQ8-II are still much better than those of the elements Q4 and Q8.

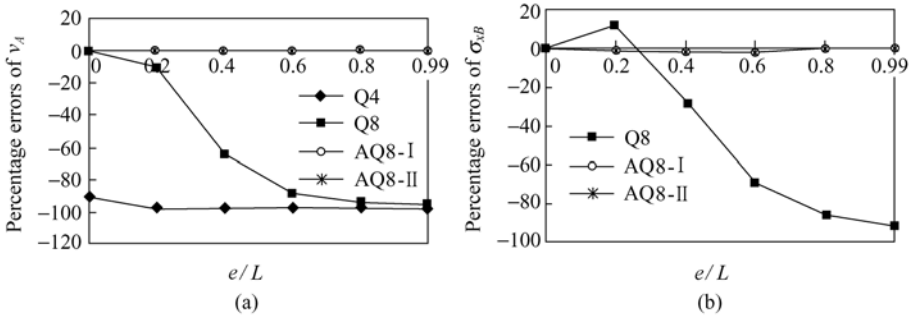


Figure 17.19 Error curves of the results for pure bending problem

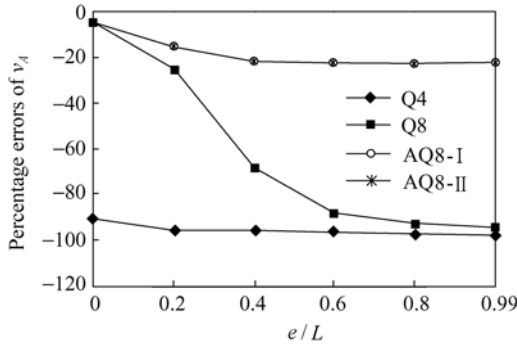


Figure 17.20 Error curves of the results for linear bending problem

17.8 Quadrilateral Thin Plate Element Formulated by the Area Coordinate Method

This section will introduce the quadrilateral thin plate element ACGCQ^[16] formulated by the area coordinate method. This element has 12 degrees of freedom:

$$\mathbf{q}^e = [w_1 \ \psi_{x1} \ \psi_{y1} \ w_2 \ \psi_{x2} \ \psi_{y2} \ w_3 \ \psi_{x3} \ \psi_{y3} \ w_4 \ \psi_{x4} \ \psi_{y4}]^T \quad (17-89)$$

The element deflection field is expressed by a polynomial in terms of the area coordinates. It contains 12 coefficients which are determined by 12 generalized conforming conditions, i.e., 4 nodal conforming conditions for deflection, 4 line conforming conditions for deflection and 4 line conforming conditions for normal rotation. Since the generalized conforming theory and the quadrilateral area coordinate method are employed, this element possesses excellent performance.

17.8.1 Element Deflection Field

The element deflection field consists of two parts:

$$w = w^0 + w^* \quad (17-90)$$

where w^0 is the low-order deflection field, which is related to the nodal displacements w_1, w_2, w_3 and w_4 ; and w^* is the high-order deflection field, which is related to eight unknown coefficients $\lambda_i (i = 1, 2, \dots, 8)$.

Firstly, the low-order deflection field w^0 can be defined as:

$$w^0 = \sum_{i=1}^4 N_i^0 w_i = N^0 \mathbf{q}^e \quad (17-91)$$

where

$$N^0 = [N_1^0 \quad 0 \quad 0 \quad N_2^0 \quad 0 \quad 0 \quad N_3^0 \quad 0 \quad 0 \quad N_4^0 \quad 0 \quad 0] \quad (17-92)$$

N_i^0 is given by Eq. (17-79).

Secondly, the high-order deflection field w^* can be defined as:

$$w^* = \mathbf{F}_\lambda \boldsymbol{\lambda} \quad (17-93)$$

where

$$\mathbf{F}_\lambda = [L_1 L_3 L_2 \quad L_1 L_3 L_4 \quad L_2 L_4 L_1 \quad L_2 L_4 L_3 \quad L_1 L_3 (L_3 - L_1) \quad L_1^2 L_3^2 \quad L_2 L_4 (L_4 - L_2) \quad L_2^2 L_4^2] \quad (17-94)$$

$$\boldsymbol{\lambda} = [\lambda_1 \quad \lambda_2 \quad \lambda_3 \quad \lambda_4 \quad \lambda_5 \quad \lambda_6 \quad \lambda_7 \quad \lambda_8]^T \quad (17-95)$$

The low-order deflection field w^0 in Eq. (17-91) and the total deflection field w in Eq. (17-90) have already satisfied the 4 nodal conforming conditions:

$$(w - \tilde{w})_j = 0 \quad (j = 1, 2, 3, 4 \text{ indicate the node numbers of the element}) \quad (17-96)$$

The eight unknown coefficients λ_i in the total deflection field w are determined by eight generalized conforming conditions, i.e., four line conforming conditions for the deflection w and another four for the normal slope ψ_n as follows:

$$\left. \begin{aligned} \int_{d_{ij}} (w - \tilde{w}) ds &= 0 \\ \int_{d_{ij}} \left(\frac{\partial w}{\partial n} - \tilde{\psi}_n \right) ds &= 0 \end{aligned} \right\} \quad (ij = 12, 23, 34, 41) \quad (17-97)$$

17.8.2 Determination of the Unknown Coefficients λ

Firstly, by substituting Eqs. (17-91) and (17-93) into the first expression of Eq. (17-97) for the deflection w , the coefficients $\lambda_1, \lambda_2, \lambda_3$ and λ_4 in λ can be expressed in terms of $\lambda_5, \lambda_6, \lambda_7, \lambda_8$ and q^e :

$$\lambda' = R\lambda'' + P'q^e \tag{17-98}$$

where

$$\lambda' = [\lambda_1 \ \lambda_2 \ \lambda_3 \ \lambda_4]^T, \quad \lambda'' = [\lambda_5 \ \lambda_6 \ \lambda_7 \ \lambda_8]^T$$

$$R = \begin{bmatrix} \frac{g_2 - g_1}{g_3 + g_4} & -\frac{2}{5} \frac{g_1 g_2}{g_3 + g_4} & 0 & 0 \\ \frac{g_3 - g_4}{g_1 + g_2} & -\frac{2}{5} \frac{g_3 g_4}{g_1 + g_2} & 0 & 0 \\ 0 & 0 & \frac{g_4 - g_1}{g_2 + g_3} & -\frac{2}{5} \frac{g_4 g_1}{g_2 + g_3} \\ 0 & 0 & \frac{g_3 - g_2}{g_4 + g_1} & -\frac{2}{5} \frac{g_2 g_3}{g_4 + g_1} \end{bmatrix} \tag{17-99}$$

$$P' = [P'_1 \ P'_2 \ P'_3 \ P'_4] \tag{17-100}$$

$$P'_1 = \frac{1}{g_0} \begin{bmatrix} \frac{g_3(g_4 - g_3)}{g_3 + g_4} & \frac{c_4 g_3 g_4}{g_3 + g_4} & \frac{-b_4 g_3 g_4}{g_3 + g_4} \\ \frac{g_3(g_2 - g_1)}{g_1 + g_2} & 0 & 0 \\ \frac{g_3(g_2 - g_3)}{g_2 + g_3} & \frac{-c_3 g_2 g_3}{g_2 + g_3} & \frac{b_3 g_2 g_3}{g_2 + g_3} \\ \frac{g_3(g_4 - g_1)}{g_4 + g_1} & 0 & 0 \end{bmatrix}, \quad P'_2 = \frac{1}{g_0} \begin{bmatrix} \frac{g_4(g_3 - g_4)}{g_3 + g_4} & \frac{-c_4 g_3 g_4}{g_3 + g_4} & \frac{b_4 g_3 g_4}{g_3 + g_4} \\ \frac{g_4(g_1 - g_2)}{g_1 + g_2} & 0 & 0 \\ \frac{g_4(g_3 - g_2)}{g_2 + g_3} & 0 & 0 \\ \frac{g_4(g_1 - g_4)}{g_4 + g_1} & \frac{c_1 g_4 g_1}{g_4 + g_1} & \frac{-b_1 g_4 g_1}{g_4 + g_1} \end{bmatrix}$$

$$P'_3 = \frac{1}{g_0} \begin{bmatrix} \frac{g_1(g_4 - g_3)}{g_3 + g_4} & 0 & 0 \\ \frac{g_1(g_2 - g_1)}{g_1 + g_2} & \frac{c_2 g_1 g_2}{g_1 + g_2} & \frac{-b_2 g_1 g_2}{g_1 + g_2} \\ \frac{g_1(g_2 - g_3)}{g_2 + g_3} & 0 & 0 \\ \frac{g_1(g_4 - g_1)}{g_4 + g_1} & \frac{-c_1 g_4 g_1}{g_4 + g_1} & \frac{b_1 g_4 g_1}{g_4 + g_1} \end{bmatrix}, \quad P'_4 = \frac{1}{g_0} \begin{bmatrix} \frac{g_2(g_3 - g_4)}{g_3 + g_4} & 0 & 0 \\ \frac{g_2(g_1 - g_2)}{g_1 + g_2} & \frac{-c_2 g_1 g_2}{g_1 + g_2} & \frac{b_2 g_1 g_2}{g_1 + g_2} \\ \frac{g_2(g_3 - g_2)}{g_2 + g_3} & \frac{c_3 g_2 g_3}{g_2 + g_3} & \frac{-b_3 g_2 g_3}{g_2 + g_3} \\ \frac{g_2(g_1 - g_4)}{g_4 + g_1} & 0 & 0 \end{bmatrix}$$

$$b_i = y_{i+1} - y_{i+2}, \quad c_i = x_{i+2} - x_{i+1} \quad (i = \overline{1,2,3,4}) \quad (17-101)$$

$$g_0 = g_1 g_2 g_3 g_4 \quad (17-102)$$

Secondly, by substituting Eqs. (17-91) and (17-93) into the second expression in Eq. (17-97) for the normal slope ψ_n , and eliminating λ' using Eq. (17-98), we obtain

$$F\lambda'' = Hq^e \quad (17-103)$$

where

$$\left. \begin{aligned} F &= F'' + F'R \\ H &= P - F'P' \end{aligned} \right\} \quad (17-104)$$

and

$$F' = -\frac{1}{12A} \left[\begin{array}{cc} f_{11}g_3(g_4 + 2g_1) & f_{11}g_2(g_1 + 2g_4) \\ f_{22}g_3g_4 & f_{22}[2(g_1 - g_4)(g_1 + g_2) - g_1g_2] \\ f_{33}g_4(g_3 + 2g_2) & f_{33}g_1(g_2 + 2g_3) \\ f_{44}[2(g_3 - g_2)(g_3 + g_4) - g_3g_4] & f_{44}g_1g_2 \\ \\ f_{11}g_2g_3 & f_{11}[2(g_4 - g_3)(g_4 + g_1) - g_4g_1] \\ f_{22}g_3(g_2 + 2g_1) & f_{22}g_4(g_1 + 2g_2) \\ f_{33}[2(g_2 - g_1)(g_2 + g_3) - g_2g_3] & f_{33}g_4g_1 \\ f_{44}g_2(g_3 + 2g_4) & f_{44}g_1(g_4 + 2g_3) \end{array} \right] \quad (17-105)$$

$$F'' = -\frac{1}{12A} \left[\begin{array}{cc} 2f_{11}(g_1^2 + g_4^2 + g_4g_1) & 0 \\ 2f_{22}(g_1 - g_2)(g_2 - g_3) & f_{22}g_3g_4(g_2 - g_3) \\ -2f_{33}(g_2^2 + g_3^2 + g_2g_3) & 0 \\ -2f_{44}(g_3 - g_4)(g_4 - g_1) & f_{44}g_1g_2(g_4 - g_1) \\ \\ -2f_{11}(g_4 - g_1)(g_1 - g_2) & f_{11}g_2g_3(g_1 - g_2) \\ 2f_{22}(g_1^2 + g_2^2 + g_1g_2) & 0 \\ 2f_{33}(g_2 - g_3)(g_3 - g_4) & f_{33}g_4g_1(g_3 - g_4) \\ -2f_{44}(g_3^2 + g_4^2 + g_3g_4) & 0 \end{array} \right] \quad (17-106)$$

$$\mathbf{P} = \frac{1}{4A} \begin{bmatrix} \frac{f_{11}}{g_2} & 0 & 0 & -\frac{1}{g_3} \left(\frac{g_4}{g_2} f_{11} - 2f_{12} \right) & -2Ab_1 & -2Ac_1 \\ \frac{f_{22}}{g_4} & 0 & 0 & \frac{f_{22}}{g_3} & 0 & 0 \\ -\frac{1}{g_4} \left(\frac{g_3}{g_1} f_{33} - 2f_{32} \right) & -2Ab_3 & -2Ac_3 & \frac{f_{33}}{g_1} & 0 & 0 \\ -\frac{1}{g_2} \left(\frac{g_3}{g_1} f_{44} - 2f_{41} \right) & -2Ab_4 & -2Ac_4 & -\frac{1}{g_1} \left(\frac{g_4}{g_2} f_{44} - 2f_{43} \right) & -2Ab_4 & -2Ac_4 \\ \\ -\frac{1}{g_2} \left(\frac{g_1}{g_3} f_{11} - 2f_{14} \right) & -2Ab_1 & -2Ac_1 & \frac{f_{11}}{g_3} & 0 & 0 \\ -\frac{1}{g_4} \left(\frac{g_1}{g_3} f_{22} - 2f_{23} \right) & -2Ab_2 & -2Ac_2 & -\frac{1}{g_3} \left(\frac{g_2}{g_4} f_{22} - 2f_{21} \right) & -2Ab_2 & -2Ac_2 \\ \frac{f_{33}}{g_4} & 0 & 0 & -\frac{1}{g_1} \left(\frac{g_2}{g_4} f_{33} - 2f_{34} \right) & -2Ab_3 & -2Ac_3 \\ \frac{f_{44}}{g_2} & 0 & 0 & \frac{f_{44}}{g_1} & 0 & 0 \end{bmatrix} \quad (17-107)$$

$$f_{ij} = b_i b_j + c_i c_j \quad (i, j = 1, 2, 3, 4) \quad (17-108)$$

Finally, by solving Eq. (17-103), λ'' can be obtained

$$\lambda'' = \mathbf{M}'' \mathbf{q}^e \quad (17-109)$$

where

$$\mathbf{M}'' = \mathbf{F}^{-1} \mathbf{H} \quad (17-110)$$

Substitution of Eq. (17-109) into Eq. (17-98) yields

$$\lambda' = \mathbf{M}' \mathbf{q}^e \quad (17-111)$$

where

$$\mathbf{M}' = \mathbf{P}' + \mathbf{R} \mathbf{M}'' \quad (17-112)$$

17.8.3 Shape Functions and Element Stiffness Matrix

From the above results, the deflection field and its shape functions can be written as:

$$w = w^0 + w^* = Nq^e \quad (17-113)$$

where

$$N = N^0 + F_\lambda M \quad (17-114)$$

$$M = \begin{bmatrix} M' \\ M'' \end{bmatrix} \quad (17-115)$$

The element curvature fields are:

$$\kappa = \begin{Bmatrix} \kappa_x \\ \kappa_y \\ 2\kappa_{xy} \end{Bmatrix} = \begin{bmatrix} -\frac{\partial^2 w}{\partial x^2} & -\frac{\partial^2 w}{\partial y^2} & -2\frac{\partial^2 w}{\partial x \partial y} \end{bmatrix}^T \quad (17-116)$$

Substitution of Eqs. (17-113) and (17-114) into the above equation yields

$$\kappa = B_b q^e \quad (17-117)$$

where B_b is the bending strain matrix,

$$B_b = -\Gamma'' Z \quad (17-118)$$

where

$$\Gamma'' = \frac{1}{4A^2} \begin{bmatrix} b_1^2 & b_2^2 & b_3^2 & b_4^2 & 2b_1b_2 & 2b_2b_3 \\ c_1^2 & c_2^2 & c_3^2 & c_4^2 & 2c_1c_2 & 2c_2c_3 \\ 2b_1c_1 & 2b_2c_2 & 2b_3c_3 & 2b_4c_4 & 2(b_1c_2 + b_2c_1) & 2(b_2c_3 + b_3c_2) \\ 2b_3b_4 & 2b_4b_1 & 2b_1b_3 & 2b_2b_4 & & \\ 2c_3c_4 & 2c_4c_1 & 2c_1c_3 & 2c_2c_4 & & \\ 2(b_3c_4 + b_4c_3) & 2(b_4c_1 + b_1c_4) & 2(b_1c_3 + b_3c_1) & 2(b_2c_4 + b_4c_2) & & \end{bmatrix} \quad (17-119)$$

$$Z = Z^0 + \bar{Z}M \quad (17-120)$$

$$\mathbf{Z}^0 = \frac{1}{4g_0} \begin{bmatrix} 0 & 0 & 0 & 0 & 0 & 0 & 0 & 0 & 0 & 0 & 0 \\ 0 & 0 & 0 & 0 & 0 & 0 & 0 & 0 & 0 & 0 & 0 \\ 0 & 0 & 0 & 0 & 0 & 0 & 0 & 0 & 0 & 0 & 0 \\ 0 & 0 & 0 & 0 & 0 & 0 & 0 & 0 & 0 & 0 & 0 \\ g_1g_3 & 0 & 0 & -g_4g_1 & 0 & 0 & g_1^2 & 0 & 0 & -g_1g_2 & 0 \\ -g_2g_3 & 0 & 0 & g_2g_4 & 0 & 0 & -g_1g_2 & 0 & 0 & g_2^2 & 0 \\ g_3^2 & 0 & 0 & -g_3g_4 & 0 & 0 & g_1g_3 & 0 & 0 & -g_2g_3 & 0 \\ -g_3g_4 & 0 & 0 & g_4^2 & 0 & 0 & -g_4g_1 & 0 & 0 & g_2g_4 & 0 \\ 0 & 0 & 0 & 0 & 0 & 0 & 0 & 0 & 0 & 0 & 0 \\ 0 & 0 & 0 & 0 & 0 & 0 & 0 & 0 & 0 & 0 & 0 \end{bmatrix} \quad (17-121)$$

$$\bar{\mathbf{Z}} = \begin{bmatrix} 0 & 0 & 0 & 0 & -2L_3 & 2L_3^2 & 0 & 0 \\ 0 & 0 & 0 & 0 & 0 & 0 & -2L_4 & 2L_4^2 \\ 0 & 0 & 0 & 0 & 2L_1 & 2L_1^2 & 0 & 0 \\ 0 & 0 & 0 & 0 & 0 & 0 & 2L_2 & 2L_2^2 \\ L_3 & 0 & L_4 & 0 & 0 & 0 & 0 & 0 \\ L_1 & 0 & 0 & L_4 & 0 & 0 & 0 & 0 \\ 0 & L_1 & 0 & L_2 & 0 & 0 & 0 & 0 \\ 0 & L_3 & L_2 & 0 & 0 & 0 & 0 & 0 \\ L_2 & L_4 & 0 & 0 & 2(L_3 - L_1) & 4L_1L_3 & 0 & 0 \\ 0 & 0 & L_1 & L_3 & 0 & 0 & 2(L_4 - L_2) & 4L_2L_4 \end{bmatrix} \quad (17-122)$$

Then, the element stiffness matrix can be written as

$$\mathbf{K}^e = \iint_{A^e} \mathbf{B}_b^T \mathbf{D}_b \mathbf{B}_b dA = \int_{-1}^1 \int_{-1}^1 \mathbf{B}_b^T \mathbf{D}_b \mathbf{B}_b |\mathbf{J}| d\xi d\eta \quad (17-123)$$

where $|\mathbf{J}|$ is the Jacobian determinant; which is the same as that of the 4-node bilinear isoparametric element Q4. Since there is no \mathbf{J}^{-1} (the inverse of the Jacobian matrix \mathbf{J}) existing in strain matrix \mathbf{B}_b , the exact value of \mathbf{K}^e can be obtained when a 3×3 Gauss integration scheme is used.

17.8.4 Numerical Example

Example 17.15 Sensitivity test to mesh distortion.

A clamped square plate subjected to uniformly distributed load q is calculated. The thickness-span ratio of the plate is $h/L = 0.01$. Due to the symmetry, only a quarter of the plate is considered by using the meshes given by Fig. 17.21, in which Δ is a distortion parameter.

The distortion parameter Δ varies from 0 to 2.5. The results of the central deflection w_C computed by element ACGCQ are plotted in Figs. 17.22 and 17.23. And, the results obtained by the elements CRB1, CRB2, S1 in reference [34] and the element DKQ^[35] are also given for comparison.

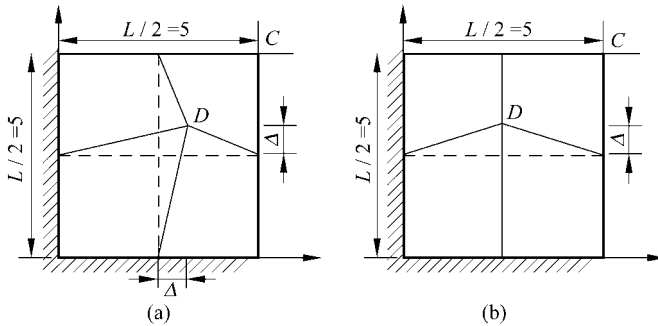


Figure 17.21 Sensitivity test to mesh distortion: mesh for a quarter clamped plate
(a) symmetric distortion 2×2; (b) antisymmetric distortion 2×2

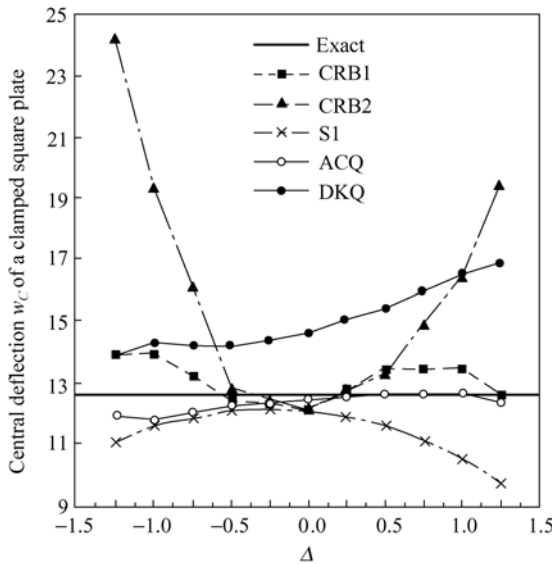


Figure 17.22 Results of the sensitivity test to mesh distortion, symmetric

From Figs. 17.22 and 17.23, it can be seen that the element ACGCQ is robust, it possesses the best accuracy and is very insensitive to mesh distortion. The

advantage of the quadrilateral area coordinate method is exhibited again.

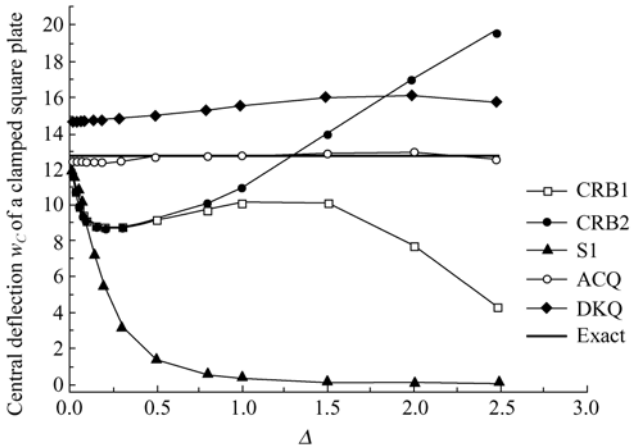


Figure 17.23 Results of the sensitivity test to mesh distortion, antisymmetric

17.9 Quadrilateral Thick Plate Element Formulated by the Area Coordinate Method

In this section, a quadrilateral 12 DOF thin-thick plate bending element AC-MQ4^[17] is constructed by the quadrilateral area coordinate method, rational interpolation scheme for shear strain fields, and generalized conforming theory. When the thickness of the plate approaches to the thin plate limit, this element will degenerate to be the thin plate element ACGCQ.

The main construction steps are as follows: Firstly, based on the Mindlin plate theory, the shear strain and deflection fields are assumed independently, and then, the rotation fields can be derived from such shear strain and deflection fields; Secondly, the shear strain along each element side is determined by Timoshenko's beam theory, and then, the element shear strain fields are obtained by the rational interpolation technique; Thirdly, the deflection field is determined by the nodal conforming conditions for deflections at the corner nodes, and the average line conforming conditions for deflection and normal slope along each element side. This approach has two characteristics: (1) Since the nodal and line generalized conforming conditions are satisfied, convergence can be guaranteed; (2) Since the shear strains degenerate to be zero for the thin plate cases, no shear locking will happen. Numerical examples show that the new element is free of shear locking, insensitive to mesh distortion, and possesses excellent accuracy in the analysis of both thick and thin plates.

17.9.1 Determination of the Element Shear Strain Fields

Consider a thick plate quadrilateral element shown in Fig. 17.24. Its shear strain fields are determined by the following procedure:

Shear strain along each element side → Nodal shear strains → Element shear strain fields

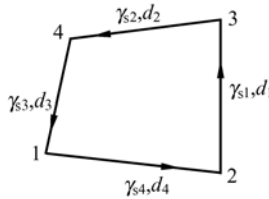


Figure 17.24 The shear strain along each element side

1. Shear strain along each element side

According to the formulae of the thick beam element^[36], the transverse shear strains along the element sides can be obtained as follows:

$$\left. \begin{aligned} \gamma_{s1} &= -\frac{\delta_1}{d_1} \left[2(w_2 - w_3) + (c_1\psi_{x2} - b_1\psi_{y2}) + (c_1\psi_{x3} - b_1\psi_{y3}) \right] \\ \gamma_{s2} &= -\frac{\delta_2}{d_2} \left[2(w_3 - w_4) + (c_2\psi_{x3} - b_2\psi_{y3}) + (c_2\psi_{x4} - b_2\psi_{y4}) \right] \\ \gamma_{s3} &= -\frac{\delta_3}{d_3} \left[2(w_4 - w_1) + (c_3\psi_{x4} - b_3\psi_{y4}) + (c_3\psi_{x1} - b_3\psi_{y1}) \right] \\ \gamma_{s4} &= -\frac{\delta_4}{d_4} \left[2(w_1 - w_2) + (c_4\psi_{x1} - b_4\psi_{y1}) + (c_4\psi_{x2} - b_4\psi_{y2}) \right] \end{aligned} \right\} \quad (17-124)$$

where $\overline{\gamma}_{s1}$, $\overline{\gamma}_{s2}$, $\overline{\gamma}_{s3}$ and $\overline{\gamma}_{s4}$ are the transverse shear strains of the sides $\overline{23}$, $\overline{34}$, $\overline{41}$ and $\overline{12}$, respectively; d_1 , d_2 , d_3 and d_4 are the lengths of the sides $\overline{23}$, $\overline{34}$, $\overline{41}$ and $\overline{12}$, respectively.

$$\begin{aligned} b_1 &= y_2 - y_3, & b_2 &= y_3 - y_4, & b_3 &= y_4 - y_1, & b_4 &= y_1 - y_2 \\ c_1 &= x_3 - x_2, & c_2 &= x_4 - x_3, & c_3 &= x_1 - x_4, & c_4 &= x_2 - x_1 \end{aligned}$$

$$\delta_i = \frac{\left(\frac{h}{d_i}\right)^2}{\frac{5}{6}(1-\mu) + 2\left(\frac{h}{d_i}\right)^2} \quad (i=1,2,3,4) \quad (17-125)$$

where h is the thickness of the plate; μ is the Poisson's ratio. It can be seen that when $h \rightarrow 0$, we have $\delta_i \rightarrow 0$, and then $\gamma_{si} \rightarrow 0$.

Let

$$\gamma_{si}^* = d_i \gamma_{si} \quad (i = 1, 2, 3, 4) \tag{17-126}$$

$$\boldsymbol{\gamma}_s^* = [\gamma_{s1}^* \quad \gamma_{s2}^* \quad \gamma_{s3}^* \quad \gamma_{s4}^*]^T \tag{17-127}$$

Thus, we have

$$\boldsymbol{\gamma}_s^* = \boldsymbol{\Gamma}^* \mathbf{q}^e \tag{17-128}$$

where

$$\boldsymbol{\Gamma}^* = \begin{bmatrix} 0 & 0 & 0 & -2\delta_1 & -c_1\delta_1 & b_1\delta_1 & 2\delta_1 & -c_1\delta_1 & b_1\delta_1 & 0 & 0 & 0 \\ 0 & 0 & 0 & 0 & 0 & 0 & -2\delta_2 & -c_2\delta_2 & b_2\delta_2 & 2\delta_2 & -c_2\delta_2 & b_2\delta_2 \\ 2\delta_3 & -c_3\delta_3 & b_3\delta_3 & 0 & 0 & 0 & 0 & 0 & 0 & -2\delta_3 & -c_3\delta_3 & b_3\delta_3 \\ -2\delta_4 & -c_4\delta_4 & b_4\delta_4 & 2\delta_4 & -c_4\delta_4 & b_4\delta_4 & 0 & 0 & 0 & 0 & 0 & 0 \end{bmatrix} \tag{17-129}$$

2. Nodal shear strains

Following the procedure given by references [20] and [37], the element nodal shear strains γ_{xi} and γ_{yi} ($i = 1, 2, 3, 4$) can be obtained as follows:

$$\left. \begin{aligned} \gamma_{xi} &= \mathbf{X}_s \boldsymbol{\gamma}_s^* \\ \gamma_{yi} &= \mathbf{Y}_s \boldsymbol{\gamma}_s^* \end{aligned} \right\} \tag{17-130}$$

where

$$\boldsymbol{\gamma}_{xi} = [\gamma_{x1} \quad \gamma_{x2} \quad \gamma_{x3} \quad \gamma_{x4}]^T, \quad \boldsymbol{\gamma}_{yi} = [\gamma_{y1} \quad \gamma_{y2} \quad \gamma_{y3} \quad \gamma_{y4}]^T \tag{17-131}$$

$$\mathbf{X}_s = \frac{1}{2A} \begin{bmatrix} 0 & 0 & -\frac{b_4}{g_1} & \frac{b_3}{g_1} \\ \frac{b_4}{g_2} & 0 & 0 & -\frac{b_1}{g_2} \\ -\frac{b_2}{g_3} & \frac{b_1}{g_3} & 0 & 0 \\ 0 & -\frac{b_3}{g_4} & \frac{b_2}{g_4} & 0 \end{bmatrix}, \quad \mathbf{Y}_s = \frac{1}{2A} \begin{bmatrix} 0 & 0 & -\frac{c_4}{g_1} & \frac{c_3}{g_1} \\ \frac{c_4}{g_2} & 0 & 0 & -\frac{c_1}{g_2} \\ -\frac{c_2}{g_3} & \frac{c_1}{g_3} & 0 & 0 \\ 0 & -\frac{c_3}{g_4} & \frac{c_2}{g_4} & 0 \end{bmatrix} \tag{17-132}$$

3. Element shear strain fields

By using the preparatory shape functions N_i^0 given by Eq. (17-79) or Eq. (17-80), the element shear strain fields can be written as

$$\left. \begin{aligned} \gamma_x &= \gamma_{x1}N_1^0 + \gamma_{x2}N_2^0 + \gamma_{x3}N_3^0 + \gamma_{x4}N_4^0 \\ \gamma_y &= \gamma_{y1}N_1^0 + \gamma_{y2}N_2^0 + \gamma_{y3}N_3^0 + \gamma_{y4}N_4^0 \end{aligned} \right\} \quad (17-133)$$

where

$$N_i^0 = \frac{1}{4} \left[1 + \frac{L_i}{g_j} + \frac{L_j}{g_m} - \frac{L_k + L_m}{g_i} + \frac{g_k}{g_0} (g_i L_i L_j - g_j L_j L_k + g_k L_k L_m - g_m L_m L_i) \right] \quad \left. \begin{array}{l} \\ \\ \\ \end{array} \right\} \quad \begin{array}{l} \\ \\ \\ \end{array} \quad (17-134)$$

$(\overline{i, j, k, m} = \overline{1, 2, 3, 4})$

$g_0 = g_1 g_2 g_3 g_4$

Substitution of Eq. (17-130) into Eq. (17-133) yields

$$\boldsymbol{\gamma} = \begin{Bmatrix} \gamma_x \\ \gamma_y \end{Bmatrix} = \begin{bmatrix} N_s^0 \mathbf{X}_s \boldsymbol{\Gamma}^* \\ N_s^0 \mathbf{Y}_s \boldsymbol{\Gamma}^* \end{bmatrix} \mathbf{q}^e = \mathbf{B}_s \mathbf{q}^e \quad (17-135)$$

in which \mathbf{B}_s is the element shear strain matrix,

$$\mathbf{B}_s = \begin{bmatrix} N_s^0 \mathbf{X}_s \boldsymbol{\Gamma}^* \\ N_s^0 \mathbf{Y}_s \boldsymbol{\Gamma}^* \end{bmatrix} \quad (17-136)$$

$$N_s^0 = [N_1^0 \quad N_2^0 \quad N_3^0 \quad N_4^0]$$

17.9.2 Determination of the Element Displacement Fields

The element deflection field w consists of two parts:

$$w = w^0 + w^* \quad (17-137)$$

where w^0 is the low-order deflection field, which is related to the nodal deflections w_1, w_2, w_3 and w_4 ; and w^* is the high-order deflection field, which is related to eight unknown coefficients λ_i ($i=1, 2, 3, \dots, 8$).

Firstly, the low-order deflection field w^0 can be defined as

$$w^0 = \sum_{i=1}^4 N_i^0 w_i = N^0 \mathbf{q}^e \quad (17-138)$$

Advanced Finite Element Method in Structural Engineering

where N_i^0 ($i = 1, 2, 3, 4$) are given by Eq. (17-134).

$$\mathbf{N}^0 = [N_1^0 \quad 0 \quad 0 \quad N_2^0 \quad 0 \quad 0 \quad N_3^0 \quad 0 \quad 0 \quad N_4^0 \quad 0 \quad 0] \quad (17-139)$$

Secondly, the high-order deflection field w^* can be defined as

$$w^* = \mathbf{F}_\lambda \boldsymbol{\lambda} \quad (17-140)$$

where

$$\mathbf{F}_\lambda = [L_1 L_3 L_2 \quad L_1 L_3 L_4 \quad L_2 L_4 L_1 \quad L_2 L_4 L_3 \quad L_1 L_3 (L_3 - L_1) \quad L_1^2 L_3^2 \quad L_2 L_4 (L_4 - L_2) \quad L_2^2 L_4^2] \quad (17-141)$$

$$\boldsymbol{\lambda} = [\lambda_1 \quad \lambda_2 \quad \lambda_3 \quad \lambda_4 \quad \lambda_5 \quad \lambda_6 \quad \lambda_7 \quad \lambda_8]^T \quad (17-142)$$

The element rotation fields can be obtained as follows:

$$\boldsymbol{\psi} = \begin{Bmatrix} \psi_x \\ \psi_y \end{Bmatrix} = \begin{Bmatrix} \frac{\partial w}{\partial x} - \gamma_x \\ \frac{\partial w}{\partial y} - \gamma_y \end{Bmatrix} \quad (17-143)$$

It can be easily proved that the low-order deflection field w^0 in Eq. (17-138) and the total deflection field w in Eq. (17-137) have already satisfied the compatibility conditions at the four nodes, i.e.,

$$(w - \tilde{w})_j = 0 \quad (j = 1, 2, 3, 4 \text{ indicate the node numbers of the element}) \quad (17-144)$$

The eight unknown coefficients λ_i ($i = 1, 2, 3, \dots, 8$) in the total displacement field w are determined by eight generalized conforming conditions, i.e., four average line conforming conditions for the deflection w and another four for the normal slope ψ_n as follows:

$$\int_{di} (w - \tilde{w}) ds = 0 \quad (i = 1, 2, 3, 4) \quad (17-145a)$$

$$\int_{di} (\psi_n - \tilde{\psi}_n) ds = 0 \quad (i = 1, 2, 3, 4) \quad (17-145b)$$

The boundary deflection \tilde{w} along each element side is determined by the formulae of the thick beam element; and the boundary normal slope $\tilde{\psi}_n$ is assumed to be linear along each element side.

By using the eight generalized conforming conditions given by Eq. (17-145), the eight unknown coefficients can be determined as follows:

$$\boldsymbol{\lambda} = \mathbf{M} \mathbf{q}^e \quad (17-146)$$

in which the expression of \mathbf{M} is given in reference [17].

Finally, the element deflection field can be obtained

$$w = w^0 + w^* = \mathbf{N}q^e \tag{17-147}$$

where the shape function matrix \mathbf{N} is given by

$$\mathbf{N} = \mathbf{N}^0 + \mathbf{F}_\lambda \mathbf{M} \tag{17-148}$$

And, the element rotation fields are given by Eq. (17-143). Then the element stiffness matrix can be obtained by conventional procedure. When the thickness of the plate $h \rightarrow 0$, the present element AC-MQ4 will degenerate to be the thin plate element ACGCQ derived in the previous section.

17.9.3 Numerical Example

Example 17.16 Boundary effect problem near the free edges of a plate.

For the boundary conditions along a free edge of plate, the description in the thick plate theory is different from that in the thin plate theory. The former requires that three force boundary conditions must be satisfied, while the latter approximately reduces them to two force boundary conditions. Therefore, difference will exist in the solutions of the two theories near the free edges. That is to say, the solutions of the thick plate theory can reflect the boundary effect (rapid variation of forces near the free edge), but those of the thin plate theory cannot.

Accordingly, the above difference will also exist in the thin plate element and the thick plate element. For studying the boundary effect problem, only the thick plate element can provide rational results.

Figure 17.25 shows a uniformly loaded (load q) square ($h/L = 0.02$) plate with two opposite edges simply supported (hard) and the other two edges free. A 64×64 square mesh was employed for analyzing a quadrant of the plate, and Poisson's ratio $\mu = 0.3$. The results obtained by the present element AC-MQ4 and the element ARS-Q12^[37] are given by Figs. 17.26 through 17.28. And, the series solutions by Kant-Hinton^[38] are also plotted for comparison.

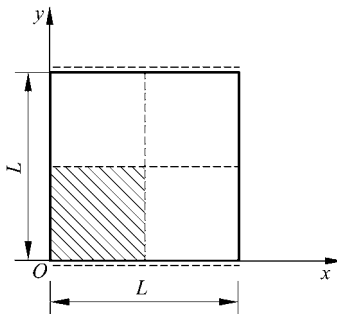


Figure 17.25 Square plate with two opposite edges simply-supported and the other two free

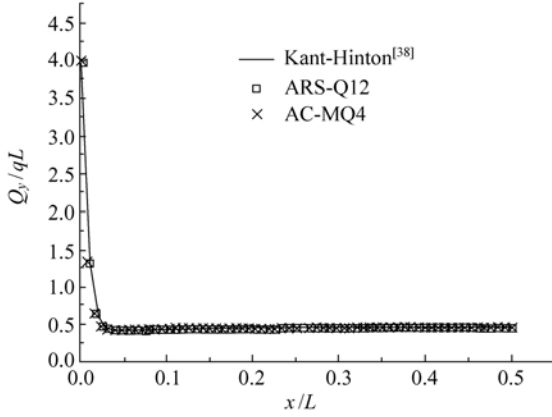


Figure 17.26 Variation of shear force Q_y ($y = 0$)

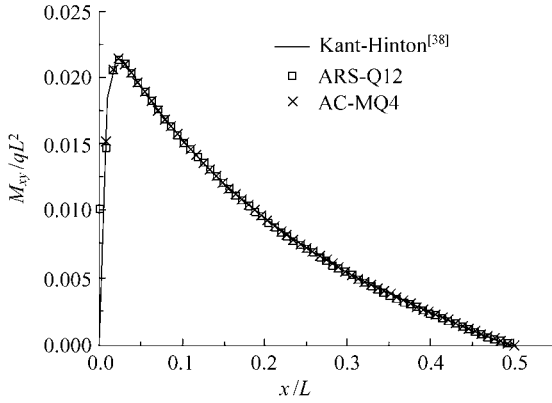


Figure 17.27 Variation of twisting moment M_{xy} ($y = 0$)

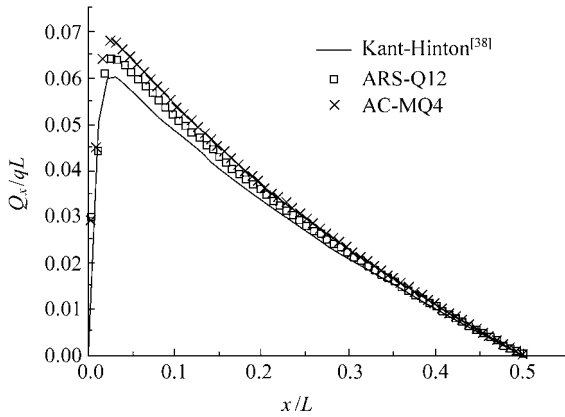


Figure 17.28 Variation of shear force Q_x ($y = 0.5L$)

It is obvious that the shear force and the moment distributions obtained using the two elements AC-MQ4 and ARS-Q12 are in good agreement with those obtained by Kant and Hinton^[38] in the main region and near the edges except for the edge point. The results show that the steep gradient of shear forces and twisting moment at the plate edge can be well represented by the proposed elements.

17.10 Quadrilateral Laminated Composite Plate Element Formulated by the Area Coordinate Method

In the previous section, by introducing the shear strain fields into the thin plate element ACGCQ, the thick plate element AC-MQ4, which is formulated by the area coordinate method, is successfully developed. In reference [18], by adding the bilinear in-plane displacement fields into the element AC-MQ4 (following the procedure of Chap. 9), a quadrilateral 20 DOF plate bending element AC-MQ4-LC for the analysis of arbitrary laminated composite plates is presented. This section will introduce this element.

Consider the laminated composite plate quadrilateral element shown in Fig. 9.3. The element DOFs are defined as follows:

$$\mathbf{q}^e = [u_1 \quad v_1 \quad w_1 \quad \psi_{x1} \quad \psi_{y1} \quad | \quad u_2 \quad v_2 \quad w_2 \quad \psi_{x2} \quad \psi_{y2} \quad | \quad u_3 \quad v_3 \quad w_3 \quad \psi_{x3} \quad \psi_{y3} \quad | \quad u_4 \quad v_4 \quad w_4 \quad \psi_{x4} \quad \psi_{y4}]^T \quad (17-149)$$

Following the procedure given in Sect. 9.3.1, the shear strain matrix can be obtained:

$$\mathbf{B}_s = \begin{bmatrix} N_s^0 \mathbf{X}_s \mathbf{\Gamma}^* \\ N_s^0 \mathbf{Y}_s \mathbf{\Gamma}^* \end{bmatrix} \quad (17-150)$$

where N_s^0 are given by Eqs. (17-136) and (17-134); \mathbf{X}_s and \mathbf{Y}_s are given by Eq. (17-132); and $\mathbf{\Gamma}^*$ is given by Eq. (9-41).

Assume that the in-plane displacement fields of the mid-plane are bilinear fields, i.e., Eq. (9-67), the element in-plane strain matrix can be obtained, see Eqs. (9-68) to (9-71).

The element bending strain matrix can be written as

$$\mathbf{B}_b^c = [\mathbf{B}_{b1}^c \quad \mathbf{B}_{b2}^c \quad \mathbf{B}_{b3}^c \quad \mathbf{B}_{b4}^c] \quad (17-151)$$

$$\mathbf{B}_{bi}^c = \begin{bmatrix} 0 & 0 & B_{b1,3i-2} & B_{b1,3i-1} & B_{b1,3i} \\ 0 & 0 & B_{b2,3i-2} & B_{b2,3i-1} & B_{b2,3i} \\ 0 & 0 & B_{b3,3i-2} & B_{b3,3i-1} & B_{b3,3i} \end{bmatrix} \quad (i = 1,2,3,4) \quad (17-152)$$

where B_{bpq} ($p = 1, 2, 3; q = 1, 2, \dots, 12$) are the components of the bending strain matrix B_b of element AC-MQ4.

Thus, the element stiffness matrix can be obtained according to Eq. (9-77) to Eq. (9-79).

Furthermore, the stress solutions are also improved by the hybrid-enhanced procedure given in Sect. 9.4.

Example 17.17 Recalculate Example 9.1 by using the element AC-MQ4-LC, and the results for the 9-layer (0/90/0/90/0/90/0/90/0) plate are listed in Table 17.13.

Table 17.13 Maximum deflection and stresses in 9-ply (0/90/0/90/0/90/0/90/0) square laminated composite plate (hard simply-supported mode I) subjected to doubly sinusoidal load

h/L	Mesh & models	\tilde{w} $\left(\frac{L}{2}, \frac{L}{2}, 0\right)$	$\tilde{\sigma}_x$ $\left(\frac{L}{2}, \frac{L}{2}, \pm \frac{h}{2}\right)$	$\tilde{\sigma}_y$ $\left(\frac{L}{2}, \frac{L}{2}, \pm \frac{h}{4}\right)$	$\tilde{\tau}_{xy}$ $\left(0, 0, \pm \frac{h}{2}\right)$	$\tilde{\tau}_{xz}$ $\left(0, \frac{L}{2}, 0\right)$	$\tilde{\tau}_{yz}$ $\left(\frac{L}{2}, 0, 0\right)$
0.1	4 × 4	1.515	± 0.526	± 0.460	∓ 0.0212	0.245	0.228
	AC-MQ4-LC 8 × 8	1.520	± 0.521	± 0.456	∓ 0.0214	0.248	0.230
	16 × 16	1.522	± 0.519	± 0.455	∓ 0.0214	0.249	0.231
	DST 10 × 10 ^[39]	1.526	± 0.541	± 0.425		0.219	0.257
	LPL-20β 8 × 8 ^[40]	①	± 0.520	± 0.458	∓ 0.0216	0.248	0.228
	3D elasticity ^[41]	1.512	± 0.551	± 0.477	∓ 0.0233	0.247	0.226
	FSDT	1.522	± 0.519	± 0.454	∓ 0.0215	0.250	0.230
0.02	4 × 4	1.013	± 0.547	± 0.440	∓ 0.0213	0.248	0.212
	AC-MQ4-LC 8 × 8	1.018	± 0.540	± 0.434	∓ 0.0212	0.255	0.218
	16 × 16	1.020	± 0.538	± 0.433	∓ 0.0213	0.257	0.220
	DST 10 × 10 ^[39]	1.020	± 0.522	± 0.447		0.190	0.263
	LPL-20β 8 × 8 ^[40]	①	± 0.540	± 0.434	∓ 0.0214	0.256	0.217
	3D elasticity ^[41]	1.021	± 0.539	± 0.433	∓ 0.0214	0.258	0.219
	FSDT	1.021	± 0.538	± 0.432	∓ 0.0213	0.258	0.219
0.01	4 × 4	1.001	± 0.550	± 0.440	∓ 0.0216	0.248	0.211
	AC-MQ4-LC 8 × 8	1.003	± 0.541	± 0.433	∓ 0.0213	0.254	0.216
	16 × 16	1.005	± 0.539	± 0.432	∓ 0.0213	0.257	0.218
	LPL-20β 8 × 8 ^[40]	①	± 0.541	± 0.433	∓ 0.0214	0.257	0.217
	3D elasticity ^[41]	1.005	± 0.539	± 0.431	∓ 0.0213	0.259	0.219
	FSDT	1.005	± 0.539	± 0.431	∓ 0.0213	0.259	0.219
10 ⁻⁶	4 × 4	1.000	± 0.552	± 0.442	∓ 0.0218	0.250	0.212
	AC-MQ4-LC 8 × 8	1.000	± 0.542	± 0.434	∓ 0.0214	0.257	0.217
	16 × 16	1.000	± 0.540	± 0.432	∓ 0.0213	0.258	0.218
	FSDT	1.000	± 0.539	± 0.431	∓ 0.0213	0.259	0.219

① Reference [40] pointed out that the computational error of the deflection by the element LPL-20β is big, so the results were not given.

Example 17.18 Recalculate Example 9.2 by using the element AC-MQ4-LC, and the results for the 8-layer $[(-45/45)_4]_s$ plate are listed in Table 17.14.

From Tables 17.13 and 17.14, it can be seen that the present element AC-MQ4-LC possesses high accuracy for both displacement and stress solutions. When dealing with single layer isotropic cases, the new laminated element will degenerate into the plate element AC-MQ4 given in the previous section.

Table 17.14 Maximum deflection and stresses in 8-ply $[(-45/45)_4]_s$ square laminated composite plate (hard simply-supported mode II) subjected to doubly sinusoidal load

h/L	Mesh & Models	$w(L/2, L/2) \times 100E_2h^3/L^4q_0$	$\sigma_x(L/2, L/2, h/2) \times h^2/L^2q_0$	$\tau_{xy}(0, 0, -h/2) \times h^2/L^2q_0$	$\tau_{xz}(0, L/2, 0) \times h/Lq_0$
0.1	4 × 4	0.3990	0.1638	0.1350	0.2117
	AC-MQ4-LC 8 × 8	0.4119	0.1499	0.1361	0.2383
	16 × 16	0.4176	0.1459	0.1377	0.2460
	32 × 32	0.4193	0.1448	0.1382	0.2480
	64 × 64	0.4197	0.1446	0.1384	0.2485
	80 × 80	0.4197	0.1445	0.1384	0.2486
	FSDT ^[42]	0.4198	0.1445	0.1384	0.2487
0.05	4 × 4	0.2721	0.1568	0.1438	0.1877
	AC-MQ4-LC 8 × 8	0.2814	0.1489	0.1371	0.2233
	16 × 16	0.2871	0.1458	0.1378	0.2409
	32 × 32	0.2889	0.1448	0.1382	0.2466
	64 × 64	0.2894	0.1446	0.1384	0.2482
	80 × 80	0.2895	0.1445	0.1384	0.2483
	FSDT ^[42]	0.2896	0.1445	0.1384	0.2487
0.01	4 × 4	0.2454	0.1559	0.1657	0.2072
	AC-MQ4-LC 8 × 8	0.2463	0.1472	0.1442	0.2163
	16 × 16	0.2468	0.1451	0.1390	0.2071
	32 × 32	0.2474	0.1447	0.1384	0.2203
	64 × 64	0.2477	0.1446	0.1384	0.2383
	80 × 80	0.2478	0.1445	0.1384	0.2417
	FSDT ^[42]	0.2479	0.1445	0.1384	0.2487

References

- [1] Pian THH, Sumihara R (1984) Rational approach for assumed stress finite elements. International Journal for Numerical Methods in Engineering 20: 1685 – 1695
- [2] Wilson EL, Ibrahimbegovic A (1990) Use of incompatible displacement modes for the calculation of element stiffness or stresses. Finite Elements in Analysis and Design 7: 229 – 241

Advanced Finite Element Method in Structural Engineering

- [3] Xu Y, Long ZF, Long YQ (1998) A generalized conforming quadrilateral membrane element insensitive to geometric distortion. *Advances in Structural Engineering* 1(3): 185 – 191
- [4] Lee NS, Bathe KJ (1993) Effects of element distortions on the performance of isoparametric elements. *International Journal for Numerical Methods in Engineering* 36: 3553 – 3576
- [5] Cen S, Long ZF, Zhang CS (1998) Two eight-node quadrilateral elements constructed by area coordinates. In: *Proceedings of the Seventh National Conference on Structural Engineering (Vol. I)*. China, Shijiazhuang, pp237 – 241 (in Chinese)
- [6] Long YQ, Long ZF, Cen S (2001) Several problems and advances in finite element method. In: *Proceedings of the Tenth National Conference on Structural Engineering (Vol. I)*. China, Nanjing, pp34 – 51 (in Chinese)
- [7] Chen XM, Cen S, Long YQ, Yao ZH (2004) Membrane elements insensitive to distortion using the quadrilateral area coordinate method. *Computers & Structures* 82(1): 35 – 54
- [8] Cen S, Du Y, Chen XM, Fu XR (2007) The analytical element stiffness matrix of a recent 4-node membrane element formulated by the Quadrilateral Area Coordinate method. *Communications in Numerical Methods in Engineering* 23(12): 1095 – 1110
- [9] Du Y, Cen S (2008) Geometrically nonlinear analysis with a 4-node membrane element formulated by the quadrilateral area coordinate method. *Finite Elements in Analysis and Design* 44(8): 427 – 438
- [10] Cen S, Chen XM, Fu XR (2007) Quadrilateral membrane element family formulated by the quadrilateral area coordinate method. *Computer Methods in Applied Mechanics and Engineering* 196(41-44): 4337 – 4353
- [11] Chen XM, Cen S, Fu XR, Long YQ (2008) A new quadrilateral area coordinate method (QACM-II) for developing quadrilateral finite element models. *International Journal for Numerical Methods in Engineering* 73(13): 1911 – 1941
- [12] Chen XM, Long YQ, XU Y (2003) Construction of quadrilateral membrane elements with drilling DOF using area coordinate method. *Gong Cheng Li Xue/Engineering Mechanics* 20(6): 6 – 11 (in Chinese)
- [13] Soh AK, Long YQ, Cen S (2000) Development of eight-node quadrilateral membrane elements using the area coordinates method. *Computational Mechanics* 25(4): 376 – 384
- [14] Guan NX, Cen S, Chen XM (2007) Quadrilateral axisymmetric elements formulated by the area coordinate method. In: Yao ZH, Yuan MW (eds) *Computational Mechanics (Proceedings of the ISCM 2007)*. Tsinghua University Press & Springer, China, Beijing, CD Rom pp1055 – 1059
- [15] Long ZF, Li JX, Cen S, Long YQ (1997) A quadrilateral plate bending element by using area coordinate method. *Gong Cheng Li Xue/Engineering Mechanics* 14(4): 1 – 10 (in Chinese)
- [16] Soh AK, Long ZF, Cen S (2000) Development of a new quadrilateral thin plate element using area coordinates. *Computer Methods in Applied Mechanics and Engineering* 190(8 – 10): 979 – 987
- [17] Cen S, Long YQ, Yao ZH, Chiew SP (2006) Application of the quadrilateral area coordinate method: A new element for Mindlin-Reissner plate. *International Journal for Numerical Methods in Engineering* 66(1): 1 – 45
- [18] Cen S, Fu XR, Long YQ, Li HG, Yao ZH (2007) Application of the quadrilateral area coordinate method: a new element for laminated composite plate bending problems. *Acta Mechanica Sinica* 23(5): 561 – 575

- [19] Taylor RL, Beresford PJ, Wilson EL (1976) A non-conforming element for stress analysis. *International Journal for Numerical Methods in Engineering* 10: 1211 – 1219
- [20] Cen S, Long ZF (1998) A new triangular generalized conforming element for thin-thick plates. *Gong Cheng Li Xue/Engineering Mechanics* 15(1): 10 – 22 (in Chinese)
- [21] Wilson EL, Taylor RL, Doherty WP, Ghabussi T (1973) Incompatible displacement models. In: Fenven ST et al., eds. *Numerical and Computer Methods in Structural Mechanics*. Academic Press, New York, 43 – 57
- [22] Chen WJ, Tang LM (1981) Isoparametric quasi-conforming element. *Journal of Dalian University of Technology* 20(1): 63 – 74 (in Chinese)
- [23] Pian THH, Wu CC (1986) General formulation of incompatible shape function and an incompatible isoparametric element. In: *Proceedings of the Invitational China-American Workshop on FEM*. China, Chengde, pp159 – 165
- [24] Piltner R, Taylor RL (1997) A systematic construction of B-bar functions for linear and nonlinear mixed-enhanced finite elements for plane elasticity problems. *International Journal for Numerical Methods in Engineering* 44: 615 – 639
- [25] Bassayya K, Bhattacharya K, Shrinivasa U (2000) Eight-node brick, PN340, representing constant stress fields exactly. *Computers & Structures* 74: 441 – 460
- [26] Long YQ, Xu Y (1994) Generalized conforming quadrilateral membrane element with vertex rigid rotational freedom. *Computers & Structures* 52(4): 749 – 755
- [27] MacMeal RH, Harder RL (1985) A proposed standard set of problems to test finite element accuracy. *Finite Elements in Analysis and Design* 1(1): 3 – 20
- [28] Chen WJ, Cheung YK (1992) Three dimensional 8-node and 20-node refined hybrid isoparametric elements. *International Journal for Numerical Methods in Engineering* 35: 1871 – 1889
- [29] Andelfinger U, Ramm E (1993) EAS-elements for two-dimensional, three-dimensional, plate and shell structures and their equivalence to HR-elements. *International Journal for Numerical Methods in Engineering* 36: 1311 – 1337
- [30] MacNeal RH (1987) A theorem regarding the locking of tapered four-noded membrane elements. *International Journal for Numerical Methods in Engineering* 24: 1793 – 1799
- [31] Wu CC, Jiao ZP (1993) Geometrically nonlinear analyses for 2-D problems based on the incompatible finite elements with internal parameters. *Acta Mechanica Sinica* 25 (4): 505 – 513 (in Chinese)
- [32] ABAQUS Inc. *ABAQUS Documentation Version 6.5* (2004) ABAQUS Inc., Rawtucket, Rhode Island
- [33] Bisshopp RE, Drucker DC (1945) Large deflection of cantilever beams. *Quarterly of Applied Mathematics* 3(3): 272 – 275
- [34] Weissmen SL, Taylor RL (1990) Resultant fields for mixed plate bending elements. *Computer Methods in Applied Mechanics in Engineering* 79: 321 – 355
- [35] Batoz JL, Tahar MB (1982) Evaluation of a new quadrilateral thin plate bending element. *International Journal for Numerical Methods in Engineering* 18: 1655 – 1677
- [36] Hu HC (1984) *Variational principles of theory of elasticity with applications*. Science Press, Beijing
- [37] Soh AK, Cen S, Long YQ, Long ZF (2001) A new twelve DOF quadrilateral element for analysis of thick and thin plates. *European Journal of Mechanics A/Solids* 20(2): 299 – 326

Advanced Finite Element Method in Structural Engineering

- [38] Kant T, Hinton E (1983) Mindlin plate analysis by the segmentation method. *Journal of Engineering Mechanics, Div. ASCE*, 109: 537 – 556
- [39] Lardeur P, Batoz JL (1989) Composite plate analysis using a new discrete shear triangular finite element. *International Journal for Numerical Methods in Engineering* 27: 343 – 359
- [40] Wu CC, Pian THH (1997) Incompatible numerical analysis and hybrid finite element method. Science Press, Beijing (in Chinese)
- [41] Pagano NJ, Hatfield SJ (1972) Elastic behavior of multilayered bidirectional composites. *AIAA Journal* 10: 931 – 933
- [42] Reddy JN (1997) *Mechanics of laminated composite plates—theory and analysis*. CRC Press, Boca Raton

Chapter 18 Spline Element I—Analysis of High-Rise Building Structures

Yu-Qiu Long

Department of Civil Engineering, School of Civil Engineering,
Tsinghua University, Beijing, 100084, China

Zhong Fan

China Architecture Design and Research Group, Beijing, 100044, China

Abstract This chapter discusses the spline element method, which is the result obtained by the combination of the spline function and the finite element method. Firstly, the characteristics of the spline functions and spline elements are given. Then, the beam and membrane element models constructed by the spline functions are presented. Finally, some applications of these spline elements in the analysis of the shear wall and tube structures are illustrated.

Keywords finite element, spline function, spline element, high-rise building structure.

18.1 Introduction

In the finite element method, a structure will be divided by the elements with piecewise interpolation functions.

The most commonly used piecewise polynomials are Lagrangian interpolations, Hermitian interpolations, spline functions, and so on. Compared with other piecewise polynomials, the spline functions have many advantages. For example, they contain fewer undetermined coefficients; possess high-order continuity; and exhibit high approximate performance. Therefore, the spline function method is increasingly important for various numerical analyses^[1-4].

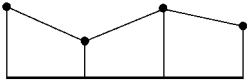
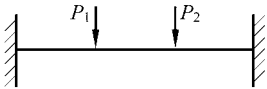
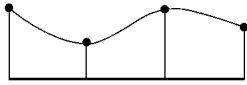
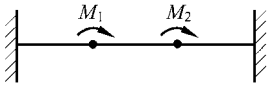
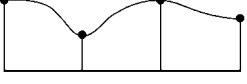

n -order spline function is a piecewise n -order polynomial with C_{n-1} -continuity. The configurations and corresponding mechanics models of linear, quadratic and cubic spline functions are given in Table 18.1.

There are two application patterns of the spline functions in structure analyses. One is the global interpolation scheme, such as the spline variation method and

the spline weighted residual method. The other is the piecewise interpolation scheme, which is called the spline finite element method^[5-9]. The common advantage of these two patterns is that more accurate and smoother solutions can be obtained with fewer degrees of freedom. But, the former is only suitable for domains with regular shapes, while the latter can be conveniently used for structures with complicated geometry.

The spline finite element method is the topic discussed in this and the next chapters.

Table 18.1 Configurations of spline functions and their mechanics models

	Configurations	Mechanics models
Linear spline	 <p>C_0-continuity piecewise fold line</p>	 <p>Displacement curve of a suspended-cable subjected to concentrated loads</p>
Quadratic spline	 <p>C_1-continuity piecewise parabolic curve</p>	 <p>Displacement curve of a beam subjected to concentrated couples</p>
Cubic spline	 <p>C_2-continuity piecewise cubic parabolic curve</p>	 <p>Displacement curve of a beam subjected to concentrated forces</p>

18.2 Spline Beam Elements

Two low-order spline beam elements are introduced in this section. And, the spline thick beam elements considering shear deformation will be given in Sect. 19.2.

18.2.1 Quadratic Spline Beam Element (4 Degrees of Freedom)

A quadratic spline beam element is shown in Fig. 18.1. Its element nodal displacement vector contains 4 degrees of freedom:

$$q^e = [w_1 \quad \theta_1 \quad w_2 \quad \theta_2]^T$$

The element is divided into two segments 13 and 32. Assume that the deflection $w(x)$ is quadratic polynomial within each segment:

$$w(x) = \begin{cases} c_1 + c_2\xi + c_3\xi^2 & \left(0 \leq \xi \leq \frac{1}{2}\right) \\ c_4 + c_5\xi + c_6\xi^2 & \left(\frac{1}{2} \leq \xi \leq 1\right) \end{cases} \quad (18-1)$$

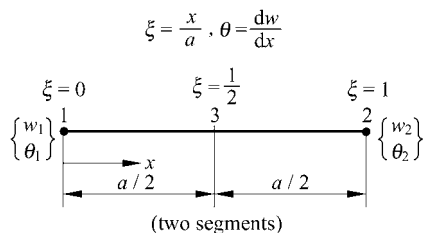


Figure 18.1 Quadratic spline beam element

in which 6 unknown coefficients c_1, \dots, c_6 can be determined by the following 6 conditions

$$\left. \begin{aligned} w|_{\xi=0} = w_1, \quad w|_{\xi=1} = w_2, \quad w|_{\xi=\frac{1}{2}-0} = w|_{\xi=\frac{1}{2}+0} \\ \frac{dw}{dx}|_{\xi=0} = \theta_1, \quad \frac{dw}{dx}|_{\xi=1} = \theta_2, \quad \frac{dw}{dx}|_{\xi=\frac{1}{2}-0} = \frac{dw}{dx}|_{\xi=\frac{1}{2}+0} \end{aligned} \right\} \quad (18-2)$$

Therefore, $w(x)$ can be expressed in terms of 4 shape functions as follows

$$w(x) = N_1^{(0)}(x)w_1 + N_1^{(1)}(x)\theta_1 + N_2^{(0)}(x)w_2 + N_2^{(1)}(x)\theta_2 \quad (18-3)$$

where the shape functions are all quadratic spline functions

$$\left. \begin{aligned} N_1^{(0)}(x) &= \begin{cases} 1 - 2\xi^2 & \left(0 \leq \xi \leq \frac{1}{2}\right) \\ 2(1 - \xi)^2 & \left(\frac{1}{2} \leq \xi \leq 1\right) \end{cases} \\ N_1^{(1)}(x) &= \begin{cases} \frac{a}{2}\xi(2 - 3\xi) & \left(0 \leq \xi \leq \frac{1}{2}\right) \\ \frac{a}{2}(1 - \xi)^2 & \left(\frac{1}{2} \leq \xi \leq 1\right) \end{cases} \\ N_2^{(0)}(x) &= 1 - N_1^{(0)}(x) \\ N_2^{(1)}(x) &= -N_1^{(1)}(a - x) \end{aligned} \right\} \quad (18-4)$$

Finally, the element stiffness matrix can be obtained

$$K^e = \begin{bmatrix} 16 & 8a & -16 & 8a \\ & 5a^2 & -8a & 3a^2 \\ \text{Sym.} & & 16 & -8a \\ & & & 5a^2 \end{bmatrix} \quad (18-5)$$

18.2.2 Cubic Spline Beam Element (6 Degrees of Freedom)

A cubic spline beam element is shown in Fig. 18.2. Its element nodal displacement vector contains 6 degrees of freedom:

$$q^e = [w_1 \quad w_1' \quad w_1'' \quad w_2 \quad w_2' \quad w_2'']^T$$

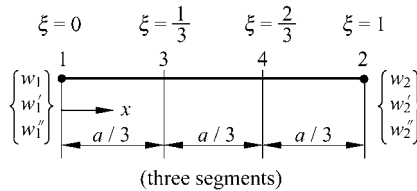


Figure 18.2 Cubic spline beam element

The element is divided into three segments 13, 34 and 42. Assume that the deflection $w(x)$ is cubic polynomial within each segment. It contains 12 unknown coefficients, which can be determined by the boundary conditions at end nodes 1 and 2, and continuous conditions at virtual nodes 3 and 4 of deflection and its first and second order derivatives. Hence, $w(x)$ can be expressed in terms of the 6 shape functions as follows:

$$w(x) = N_1^{(0)}(x)w_1 + N_1^{(1)}(x)w_1' + N_1^{(2)}(x)w_1'' + N_2^{(0)}(x)w_2 + N_2^{(1)}(x)w_2' + N_2^{(2)}(x)w_2'' \quad (18-6)$$

in which the shape functions are all cubic spline functions

$$N_1^{(0)}(x) = \begin{cases} 1 - \frac{9}{2}\xi^3 & \left(0 \leq \xi \leq \frac{1}{3}\right) \\ \frac{1}{6}[5 - 3(3\xi - 1) - 3(3\xi - 1)^2 + 2(3\xi - 1)^3] & \left(\frac{1}{3} \leq \xi \leq \frac{2}{3}\right) \\ \frac{9}{2}(1 - \xi)^3 & \left(\frac{2}{3} \leq \xi \leq 1\right) \end{cases}$$

$$\left. \begin{aligned}
 N_1^{(1)}(x) &= \begin{cases} a\xi(1-3\xi^2) & \left(0 \leq \xi \leq \frac{1}{3}\right) \\
 \frac{a}{18}[4-6(3\xi-1)^2+3(3\xi-1)^3] & \left(\frac{1}{3} \leq \xi \leq \frac{2}{3}\right) \\
 \frac{3}{2}a(1-\xi)^3 & \left(\frac{2}{3} \leq \xi \leq 1\right) \end{cases} \\
 N_1^{(2)}(x) &= \begin{cases} \frac{a^2}{12}\xi^2(6-11\xi) & \left(0 \leq \xi \leq \frac{1}{3}\right) \\
 \frac{a^2}{324}[7+3(3\xi-1)-15(3\xi-1)^2+7(3\xi-1)^3] & \left(\frac{1}{3} \leq \xi \leq \frac{2}{3}\right) \\
 \frac{a^2}{6}(1-\xi)^3 & \left(\frac{2}{3} \leq \xi \leq 1\right) \end{cases} \\
 N_2^{(0)}(x) &= 1 - N_1^{(0)}(x), \quad N_2^{(1)}(x) = -N_1^{(1)}(a-x), \quad N_2^{(2)}(x) = N_1^{(2)}(a-x)
 \end{aligned} \right\} \quad (18-7)$$

Finally, the element stiffness matrix can be obtained

$$\mathbf{K}^e = \frac{EI}{4a^3} \begin{bmatrix} 108 & 54a & 5a^2 & -108 & 54a & -5a^2 \\ & 32a^2 & 3a^3 & -54a & 22a^2 & -2a^3 \\ & & \frac{2}{3}a^4 & -5a^2 & 2a^3 & -\frac{1}{6}a^4 \\ & & & 108 & -54a & 5a^2 \\ \text{Sym.} & & & & 32a^2 & -3a^3 \\ & & & & & \frac{2}{3}a^4 \end{bmatrix} \quad (18-8)$$

18.2.3 Numerical Examples

Example 18.1 A simply-supported beam (span length is L) is subjected to uniformly distributed load q . The flexural rigidity of the beam is EI . The results and errors of the central deflection and moment by the quadratic and cubic spline elements are listed in Tables 18.2 and 18.3.

Table 18.2 Central deflection $w_c / \left(\frac{qL^4}{16EI}\right)$

Number of elements (1/2 beam)	1	2	3	4
Quadratic spline element	0.1979 (5%)	0.2057 (1%)	0.2077 (0.3%)	0.2080 (0.1%)
Cubic spline element	0.2083 (0%)			
Analytical solution	0.2083			

Table 18.3 Central moment $M_c / \left(\frac{qL^2}{8} \right)$

Number of elements (1/2 beam)	1	2
Cubic spline element	1.0186 (2%)	1.0046 (0.5%)
Analytical solution	1.0000	

18.3 Spline Plane Membrane Elements

The spline plane membrane element is introduced as follows. Assume that the shape of the element is rectangle, and bi-quadratic spline functions are used for interpolation^[10].

As shown in Fig. 18.3, a rectangular element is equally divided into 4 sub-regions. And, the coordinates of node ij ($i, j = 1, 2$) are (x_i, y_j) .

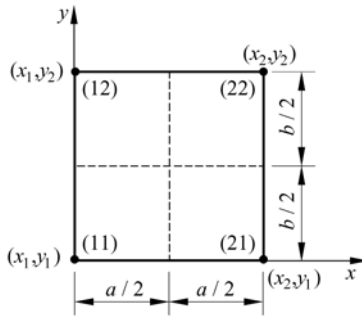


Figure 18.3 Rectangular element (4 sub-regions)

There are 8 degrees of freedom at each node ij

$$\mathbf{q}_{ij} = [u_{ij}^{(00)} \quad u_{ij}^{(10)} \quad u_{ij}^{(01)} \quad u_{ij}^{(11)} \quad \vdots \quad v_{ij}^{(00)} \quad v_{ij}^{(10)} \quad v_{ij}^{(01)} \quad v_{ij}^{(11)}]^T \quad (18-9)$$

where

$$\left. \begin{aligned} u_{ij}^{(00)} &= u|_{(x_i, y_j)}, & u_{ij}^{(10)} &= \frac{\partial u}{\partial x} \Big|_{(x_i, y_j)} \\ u_{ij}^{(01)} &= \frac{\partial u}{\partial y} \Big|_{(x_i, y_j)}, & u_{ij}^{(11)} &= \frac{\partial^2 u}{\partial x \partial y} \Big|_{(x_i, y_j)} \end{aligned} \right\} \quad (18-10)$$

Thus, each element has 32 degrees of freedom

$$\mathbf{q}^e = [\mathbf{q}_{11}^T \quad \mathbf{q}_{21}^T \quad \mathbf{q}_{22}^T \quad \mathbf{q}_{12}^T]^T \quad (18-11)$$

The element displacement fields u and v can be expressed in terms of the nodal displacements as follows:

$$\begin{Bmatrix} u \\ v \end{Bmatrix} = \sum_{i=1}^2 \sum_{j=1}^2 N_{ij} \mathbf{q}_{ij} \tag{18-12}$$

in which the shape functions are all bi-quadratic spline functions

$$N_{ij} = \begin{bmatrix} N_{ij}^{(00)} & N_{ij}^{(10)} & N_{ij}^{(01)} & N_{ij}^{(11)} & 0 & 0 & 0 & 0 \\ 0 & 0 & 0 & 0 & N_{ij}^{(00)} & N_{ij}^{(10)} & N_{ij}^{(01)} & N_{ij}^{(11)} \end{bmatrix} \tag{18-13}$$

$$N_{ij}^{(kl)}(x, y) = N_i^{(k)}(x)N_j^{(l)}(y) \quad (i, j = 1, 2; \quad k, l = 0, 1) \tag{18-14}$$

$N_i^{(k)}(x)$ are the shape functions of the quadratic spline beam element defined in Eq. (18-4), and $N_j^{(l)}(y)$ can be defined similarly.

After the determination of the shape functions, the element stiffness matrix can then be obtained by the conventional procedure. This element is denoted as R-OQQ.

Example 18.2 A simply-supported beam subjected to uniformly distributed load is divided by 6 R-OQQ elements (as shown in Fig. 18.4). The results and comparison of stress $\sigma_x(0, y)$ by the present element and analytical solution are listed in Table 18.4.

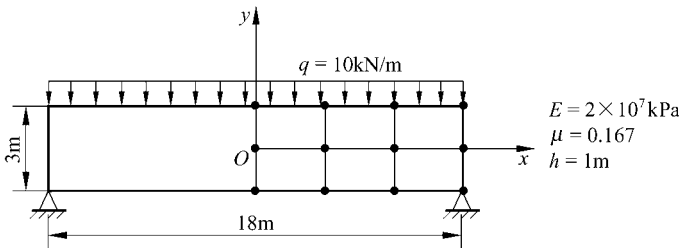


Figure 18.4 A simply-supported beam and mesh division

Table 18.4 Results of stress $\sigma_x(0, y)$

$y(\text{m})$	1.5	1.0	0.5	0	-0.5	-1.0	-1.5
Present element	-273.4	-180.4	-89.8	-0.6	89.6	181.0	273.1
Analytical	-272.0	-179.5	-89.2	0.0	89.2	179.5	272.0

Details about the spline sectorial and triangular elements can be referred to reference [10].

18.4 Analysis of Shear Wall Structures by Spline Elements

Shear wall is one of the important structures popularly used in high-rise buildings.

Ever since finite strip method was proposed by Cheung^[11] for structure analysis, it has been broadly used in computations of high-rise building structures. And, the longitudinal interpolation functions of strip elements also obtain continuous improvements. However, the common characteristic of this kind of method is that the interpolation procedure must be carried out in the whole strip domain, which is only suitable for the structures with regular shapes. Troubles and difficulties often happen when irregular opening hole and boundary shape exist (Fig. 18.5).

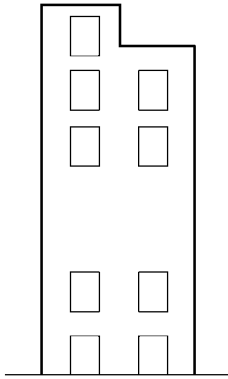


Figure 18.5 Shear wall with opening

Girijavallaham^[12] used conventional triangular and rectangular elements to analyze the coupled shear wall structures, but the density of the mesh is quite high. Recently, the continuity assumption of structure has been widely accepted. So, in the analysis of structures, the discrete connecting beams can be replaced by the equivalent orthotropic plate, which greatly reduces the number of elements. Chan and Cheung^[13] proposed a high-order rectangular element, in which the interpolation polynomials of the element transverse and longitudinal displacements are linear and quintic, respectively. Only a few of such elements are enough for the analysis of the whole structure. However, in general, the numerical instability may occur for high-order polynomial approximation.

In this section, a spline element TB-mn which can be broadly used for the analysis of high-rise building structures will be introduced. The displacement components of this spline element are interpolated locally within an element by using the spline function. Then, according to the characteristics of the high-rise building structures, the orders of spline functions for transverse and longitudinal interpolations are selected properly, so that more accurate results can be obtained

by low-order spline functions and fewer degrees of freedom. Since such spline interpolation is performed only within a local element, just as the conventional displacement-based element, this spline element can easily deal with various structure forms with irregular opening holes and boundary shapes.

18.4.1 Element TB-mn for the Analysis of High-Rise Building Structures^[8-14]

For a plane stress rectangular element for the analysis of high-rise building structures (Fig. 18.6), piecewise spline Hermitian interpolation is used for the transverse displacement u and longitudinal displacement v of the element

$$\begin{Bmatrix} u \\ v \end{Bmatrix} = \sum_{i=1}^2 \sum_{j=1}^2 \sum_{\alpha=0}^{m-1} \sum_{\beta=0}^{n-1} (N_{mn})_{ij}^{\alpha\beta}(x, y) \begin{Bmatrix} u_{ij}^{\alpha\beta} \\ v_{ij}^{\alpha\beta} \end{Bmatrix} \quad (18-15)$$

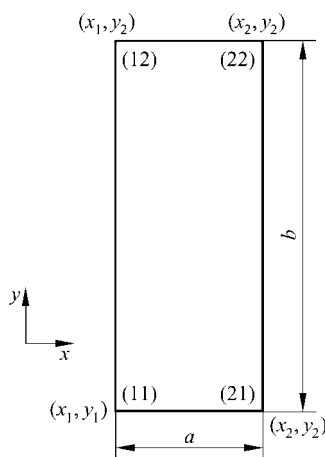


Figure 18.6 Rectangular element

in which m and n are the orders of spline functions; $u_{ij}^{\alpha\beta}$ and $v_{ij}^{\alpha\beta}$ are the values of displacements or their derivatives at element nodes ij ($i, j = 1, 2$)

$$\begin{Bmatrix} u_{ij}^{\alpha\beta} \\ v_{ij}^{\alpha\beta} \end{Bmatrix} = \left. \frac{\partial^\alpha}{\partial x^\alpha} \frac{\partial^\beta}{\partial y^\beta} \begin{Bmatrix} u(x, y) \\ v(x, y) \end{Bmatrix} \right|_{x=x_i, y=y_j} \quad (18-16)$$

The element shape function $(N_{mn})_{ij}^{\alpha\beta}(x, y)$ is composed of two piecewise spline interpolation functions

$$(N_{mn})_{ij}^{\alpha\beta} = (N_m)_i^\alpha(x) (N_n)_j^\beta(y) \quad (18-17)$$

Advanced Finite Element Method in Structural Engineering

where $(N_m)_i^\alpha(x)$ and $(N_n)_j^\beta(y)$ are m and n order spline Hermitian interpolation function, respectively; the expressions of $(N_m)_i^\alpha(x)$ or $(N_n)_j^\beta(y)$ are as follows:

(1) Linear spline interpolation functions ($m = 1$)

$$(N_1)_1^0(x) = 1 - \frac{x+h}{2h} \quad (x \in [-h, h])$$

$$(N_1)_2^0(x) = 1 - (N_1)_1^0(x)$$

(2) Quadratic spline interpolation functions ($m = 2$)

$$(N_2)_1^0(x) = \begin{cases} 1 - \frac{(x+2h)^2}{8h^2} & (x \in [-2h, 0]) \\ \frac{(x-2h)^2}{8h^2} & (x \in [0, 2h]) \end{cases}$$

$$(N_2)_1^1(x) = \begin{cases} (x+2h) - \frac{3(x+2h)^2}{8h} & (x \in [-2h, 0]) \\ \frac{(x-2h)^2}{8h} & (x \in [0, 2h]) \end{cases}$$

$$(N_2)_2^0(x) = 1 - (N_2)_1^0(x), \quad (N_2)_2^1(x) = -(N_2)_1^1(-x)$$

(3) Cubic spline interpolation functions ($m = 3$)

$$(N_3)_1^0(x) = \begin{cases} 1 - \frac{(x+3h)^3}{48h^3} & (x \in [-3h, -h]) \\ \frac{5}{6} - \frac{x+h}{4h} - \frac{(x+h)^2}{8h^2} + \frac{(x+h)^3}{24h^3} & (x \in [-h, h]) \\ -\frac{(x-3h)^3}{48h^3} & (x \in [h, 3h]) \end{cases}$$

$$(N_3)_1^1(x) = \begin{cases} (x+3h) - \frac{(x+3h)^3}{12h^2} & (x \in [-3h, -h]) \\ \frac{4h}{3} - \frac{(x+h)^2}{2h} + \frac{(x+h)^3}{8h^2} & (x \in [-h, h]) \\ -\frac{(x-3h)^3}{24h^2} & (x \in [h, 3h]) \end{cases}$$

$$(N_3)_1^2(x) = \begin{cases} \frac{(x+3h)^2}{2} - \frac{11(x+3h)^3}{72h} & (x \in [-3h, -h]) \\ \frac{7h^2}{9} + \frac{(x+h)h}{6} - \frac{5(x+h)^2}{12} + \frac{7(x+h)^3}{72h} & (x \in [-h, h]) \\ -\frac{(x-3h)^3}{36h} & (x \in [h, 3h]) \end{cases}$$

$$(N_3)_2^0(x) = 1 - (N_3)_1^0(x)$$

$$(N_3)_2^1(x) = -(N_3)_1^1(-x)$$

$$(N_3)_2^2(x) = (N_3)_1^2(-x)$$

In the above expressions, we have $h = \frac{a}{2m}$. And, the interpolation procedure is performed within the range $\left[-\frac{a}{2}, \frac{a}{2}\right]$ (Fig. 18.6).

Similar to the conventional displacement-based element, the displacement interpolation mode of the spline element can also be written in matrix forms

$$\begin{Bmatrix} u \\ v \end{Bmatrix} = N_{mn} \mathbf{q} \quad (18-18)$$

In the analysis of the high-rise building structures, the longitudinal dimensions of the elements are usually much larger than their transverse dimensions. So $m \leq n$ is taken when the piecewise interpolation in an element is considered. The spline element constructed by such interpolation mode is called as TB-mn element. When $m = 1, n = 1$, the element TB-mn will degenerate to be the ordinary bi-linear plane stress rectangular element.

18.4.2 Analysis of Shear Wall Structures by the Element TB-mn

Here, the static and dynamic analyses of the shear wall structures are performed by using the element TB-mn, and several typical examples are given.

For a shear wall with only small opening, the element TB-mn can be used like the usual rectangular element; for a coupled shear wall structure, the wall limbs can be analyzed directly by the element TB-mn; and the connecting beams are equivalently looked upon as orthotropic continuous grids according to the continuity assumption of the structure. The equivalent elastic and shear modulus of the continuous grids are

$$\left. \begin{aligned} \bar{E}_x &= \frac{d}{h} E \\ \bar{E}_y &= 0 \\ \bar{G} &= \frac{d}{h} \frac{E}{(l/d)^2 + 2.4} \end{aligned} \right\} \quad (18-19)$$

in which l and d are the span of the connecting beam and height of beam section, respectively; h is the storey height of the structure.

Example 18.3 Tip displacement of a vertical cantilever beam subjected to horizontal load.

In order to test the performance of the element TB-mn, the tip displacement of a vertical cantilever beam subjected to horizontal force is calculated in this example. Geometries and material properties are given in Fig. 18.7(a). The variations of results of tip displacement with total degrees of freedom are plotted in Fig. 18.7(b). Obviously, the convergence speed of the spline element is much faster than that of the usual rectangular element (TB-11). The results obtained from the element TB-mn by the same mesh are listed in Table 18.5. It can be seen that, when only one element is used, the elements TB-22 and TB-23 already reach good accuracy; even the element TB-12, which has only a few nodal degrees of freedom, can improve the precision greatly.

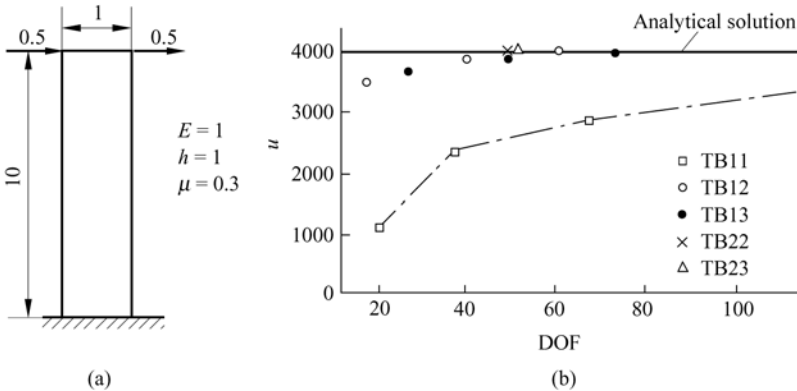


Figure 18.7 Analysis of shear wall structure by element TB-mn

Table 18.5 The tip displacement u of a cantilever beam subjected to horizontal force

Element type	TB-11	TB-12	TB-13	TB-22	TB-23
Nodal degrees of freedom	2	4	6	8	12
Mesh division	1 × 1	102	3452	3649	3724
	1 × 4	1149	3861	3699	4050
Analytical solution	4031				

Example 18.4 Vibration analysis of a cantilever beam.

Dimensions of the cantilever beam are: $h \times b = 1.0\text{cm} \times 0.5\text{cm}$, $l = 10\text{cm}$. Material properties: $E = 2.1 \times 10^5\text{MPa}$, $\mu = 0.3$, and mass density $\rho = 7.8\text{g/cm}^3$. The results of the natural frequency of the cantilever are listed in Table 18.6.

Table 18.6 Natural frequencies of a cantilever beam (10^3rad/s)

Frequency		First-order			Second-order		
Element type		TB-11	TB-12	TB-13	TB-11	TB-12	TB-13
Mesh division	1 × 1		5.778	5.397		48.93	32.81
	1 × 2		5.450	5.336		34.21	32.58
	1 × 4	9.637	5.337		61.62	32.67	
	1 × 8	6.750			41.21		
	1 × 40	5.532			32.97		

Example 18.5 Displacement of a coupled shear wall subjected to horizontal load.

In this example, an 11-storey coupled shear wall structure (Fig. 18.8) is calculated by the element TB-mn (Fig. 18.8). The geometrical and physical parameters are as follows:

$$H = 132\text{ft}^*, \quad W = 18\text{ft}, \quad l = 7\text{ft}, \quad d = 2\text{ft}$$

$$h = 12\text{ft}, \quad E = 0.4 \times 10^5\text{kip/ft}^2, \quad \mu = 0.2, \quad t = 1.0\text{ft}$$

For comparison, the usual rectangular element (TB-11) and spline element are both employed. In order to obtain enough precision, the mesh divided by the usual rectangular elements (contains 572 elements) is quite dense. When the computation is performed by the element TB-mn, a continuity treatment must be used for the connecting beams. The lateral displacement curves of the coupled shear wall are plotted in Fig. 18.8(b). It can be seen that satisfactory results can be obtained by quite sparse mesh when the element TB-mn is used.

Example 18.6 Analysis of the shear wall with local stagger holes at the bottom.

A 6-storey shear wall with local stagger holes at the bottom is shown in Fig. 18.9. Young’s modulus $E = 3.0 \times 10^4\text{MPa}$, Poisson’s ratio $\mu = 1/3$, thickness of the wall is 25cm. The vertical load $q = 100\text{kN/m}$, and horizontal load and other parameters are given in Table 18.7.

For comparison, the results obtained by the usual element and spline element methods are both given. The mesh divided by the usual model, which contains 2192 elements, is quite dense, while only 104 spline elements TB-13 are utilized.

* ft—feet; kip—kilopound. For comparison with results in related references, units of British Imperial system are used here.

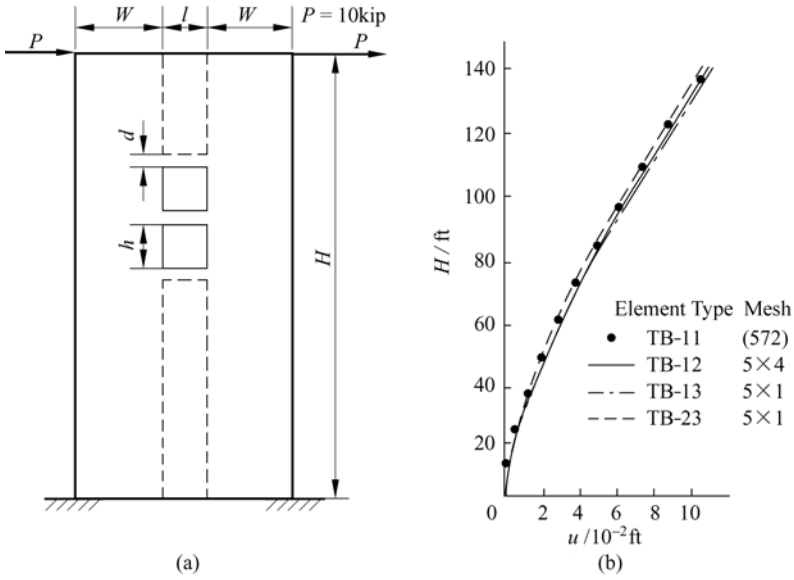


Figure 18.8 Coupled shear wall structure
 (a) Structural geometry; (b) Load-displacement curves

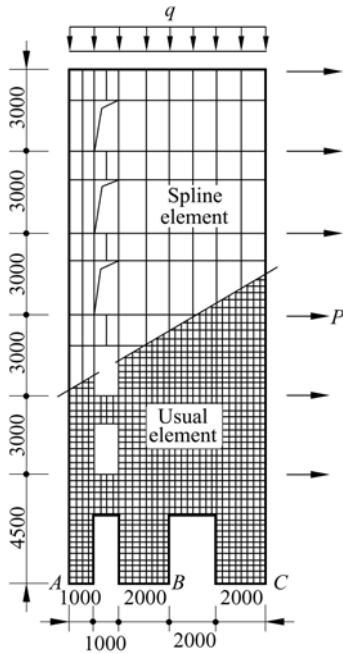


Figure 18.9 Shear wall with local stagger holes at bottom (unit: mm)

From Tables 18.7 and 18.8, it can be seen that, the results of the horizontal displacements of the wall obtained by these two schemes are in good agreement with each other; and, among the computational results of the internal forces at the bottom wall limb, the solutions for the axis forces obtained by the two schemes are in good agreement while the moment solutions have a few differences, however, obvious discrepancies exist in shear force solutions.

Table 18.7 Parameters and horizontal displacements of a shear wall with stagger holes at the bottom

Storey No.		1	2	3	4	5	6
Storey height (m)		4.500	3.000	3.000	3.000	3.000	3.000
Height of connecting beam (m)		1.500	1.000	1.000	1.000	1.000	1.000
Horizontal force P_i (kN)		36.7	61.2	85.7	110.1	134.6	191.0
Horizontal displacement (mm)	Usual element	0.6446	1.015	1.454	1.890	2.227	2.667
	Spline element	0.6633	1.090	1.577	2.048	2.464	2.875

Table 18.8 Results of internal forces at bottom wall limb

Wall limb No.		<i>A</i>	<i>B</i>	<i>C</i>
Moment M (kN · m)	Usual element	45.0	499.0	617.5
	Spline element	60.0	396.8	688.4
Axial force N (kN)	Usual element	1040	3161	3803
	Spline element	775	2946	4248
Shear force (kN)	Usual element	6.4	252.8	365.1
	Spline element	22.8	104.7	489.2

18.5 Analysis of Frame-Tube Structures by Spline Elements

Frame-tube structure or tube structure, which possesses high spatial stiffness and can perform well in earthquake-resistance, is an ideal structural system for the high-rise and super high-rise buildings. To date, great developments have been achieved in the computational theories of the frame-tube structures. Coull and Subedi^[15] proposed an equivalent plane frame method in which the frame-tube structure in a 3D space is simplified as a plane frame, so that the computation cost can be greatly reduced. According to the characteristic of “shear lag” in a rectangular frame-tube structure, Coull and Bose^[16,17] established the corresponding differential equations based on the minimum complementary energy principle. This method is simple, and its accuracy can meet the requirements of design. By assuming that the distribution of the longitudinal stresses along tube section is

piecewise linear, Long et al.^[18] also established the fundamental equations based on the complementary energy principle. This method can produce high precision solutions for internal forces, and can be used for the computation of the tube structures with arbitrary polygonal section.

The following basic assumptions for the tube structures are employed:

(1) For the floor slab, the in-plane stiffness is infinite rigid, and the out-of-plane stiffness is zero;

(2) The bending stresses at the wall panel of the tube structure are ignored.

For the tube structure with a polygonal section, the whole structure is composed of several wall panels. When we analyze each of these wall panels, local coordinates \bar{x}, \bar{y} will be firstly employed. Under this local coordinate system, the element stiffness matrix \bar{K}^e and equivalent nodal load vector \bar{p}^e of the spline element TB-mn can be obtained. When we analyze the whole tube structure, global coordinates x, y, z will be used. By the coordinate transformation formulae, \bar{K}^e and \bar{p}^e , which are established in the local coordinate system, can be transformed into and assembled in the global coordinate system. The procedure is as follows. The transformation between the local and global coordinate systems is shown in Fig. 18.10.

18.5.1 Piecewise Spline Hermitian Interpolation

According to the basic assumptions, the horizontal displacements at the same height of the tube should be the same. Therefore, the horizontal displacement \bar{u} is interpolated only along the longitudinal direction; but the vertical displacement \bar{v} is still interpolated by the spline functions along two directions.

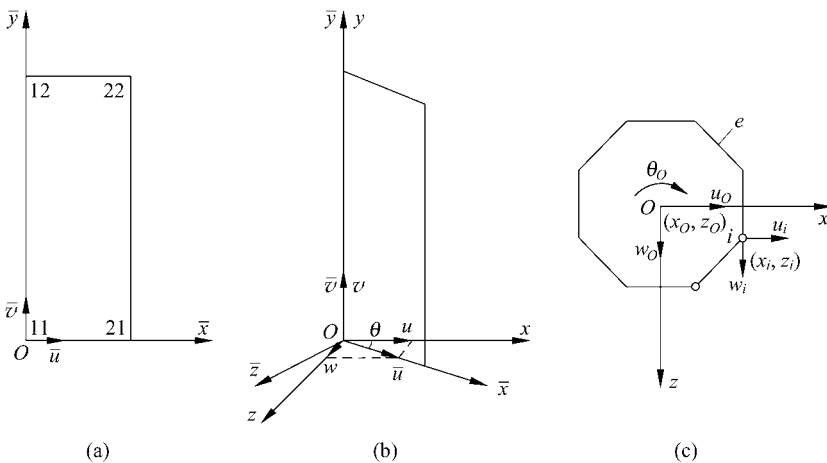


Figure 18.10 Local and global coordinates

(a) Local coordinates; (b) Global coordinates; (c) Coordinate transformation

$$\bar{u} = \sum_{j=1}^2 \sum_{\beta=0}^{n-1} N_{nj}^{\beta}(\bar{y}) \bar{u}_j^{\beta} \quad (18-20)$$

$$\bar{v} = \sum_{i=1}^2 \sum_{j=1}^2 \sum_{\alpha=0}^{m-1} \sum_{\beta=0}^{n-1} N_{mij}^{\alpha\beta}(\bar{x}, \bar{y}) \bar{v}_{ij}^{\alpha\beta} \quad (18-21)$$

In the above equations, \bar{u}_j^{β} and $\bar{v}_{ij}^{\alpha\beta}$ are the nodal values of displacements or their derivatives in the local coordinate system $O\bar{x}\bar{y}$ (Fig. 18.10(a)):

$$\bar{u}_j^{\beta} = \frac{\partial^{\beta}}{\partial \bar{y}^{\beta}} \bar{u}(\bar{y}) \Big|_{\bar{y}=\bar{y}_j} \quad (18-22)$$

$$\bar{v}_{ij}^{\alpha\beta} = \frac{\partial^{\alpha}}{\partial \bar{x}^{\alpha}} \frac{\partial^{\beta}}{\partial \bar{y}^{\beta}} \bar{v}(\bar{x}, \bar{y}) \Big|_{\bar{x}=\bar{x}_i, \bar{y}=\bar{y}_j} \quad (18-23)$$

18.5.2 Coordinate Transformation

The spline interpolations in the local coordinate system have already been finished above. Here they will be transformed into the global coordinate system (Fig. 18.10(b)). The transformations of the displacement components \bar{u} and \bar{v} in the local coordinate system and u, v and w in the global coordinate system are

$$\begin{Bmatrix} u \\ v \\ w \end{Bmatrix} = \begin{bmatrix} \cos \theta & 0 \\ 0 & 1 \\ \sin \theta & 0 \end{bmatrix} \begin{Bmatrix} \bar{u} \\ \bar{v} \end{Bmatrix} \quad (18-24)$$

From this equation, the element stiffness matrix $\bar{\mathbf{K}}^e$ and load vector $\bar{\mathbf{p}}^e$ can be transformed into the global coordinate system

$$\mathbf{K}^e = \mathbf{T} \bar{\mathbf{K}}^e \mathbf{T}^T, \quad \mathbf{p}^e = \mathbf{T} \bar{\mathbf{p}}^e \quad (18-25)$$

in which \mathbf{T} is the coordinate transformation matrix

$$\mathbf{T} = \begin{bmatrix} \mathbf{I}_{d_1 \times d_1} \cos \theta & \mathbf{0} \\ \mathbf{0} & \mathbf{I}_{d_1 \times d_1} \\ \mathbf{I}_{d_1 \times d_1} \sin \theta & \mathbf{0} \end{bmatrix} \quad (18-26)$$

\mathbf{I} is the identity matrix; $d_1 = 2n, d_2 = 4mn$.

Due to the constraint effect of the floor slab, on any section of the tube, the horizontal displacements (u_i, w_i) at node i (i is the transverse node number of element $e, i = 1, 2$) can be expressed in terms of the horizontal displacements and angular displacement (u_0, w_0, θ_0) at a reference point on the same section

(Fig. 18.10(c)):

$$\begin{Bmatrix} u_i \\ w_i \end{Bmatrix} = \begin{bmatrix} 1 & 0 & -(z_i - z_0) \\ 0 & 1 & x_i - x_0 \end{bmatrix} \begin{Bmatrix} u_0 \\ w_0 \\ \theta_0 \end{Bmatrix}$$

Thus, at any height of the tube, there are only three horizontal displacements. Here, the global stiffness matrix and load vector of the tube structure can be written as

$$K = \sum_e HT\bar{K}^e T^T H^T \tag{18-27}$$

$$P = \sum_e HT\bar{p}^e \tag{18-28}$$

In the above equations, H is the transverse constraint matrix

$$H = \begin{bmatrix} I_{d_1 \times d_1} & \mathbf{0} & \mathbf{0} \\ \mathbf{0} & I_{d_2 \times d_2} & \mathbf{0} \\ \mathbf{0} & \mathbf{0} & I_{d_1 \times d_1} \\ A_{d_1 \times d_1} & \mathbf{0} & B_{d_1 \times d_1} \end{bmatrix} \tag{18-29}$$

where A and B are the transformation matrices of the nodal displacements (u_i, w_i) ($i = 1, 2$) and rotation θ_0 at the reference point

$$A = \begin{bmatrix} a_1 I_{n \times n} & \mathbf{0} \\ \mathbf{0} & a_2 I_{n \times n} \end{bmatrix}, \quad B = \begin{bmatrix} b_1 I_{n \times n} & \mathbf{0} \\ \mathbf{0} & b_2 I_{n \times n} \end{bmatrix}$$

$$a_i = -(z_i - z_0), \quad b_i = x_i - x_0 \quad (i = 1, 2) \tag{18-30}$$

Some numerical examples of the tube structures with rectangular and polygonal sections are given as follows.

Example 18.7 Computation of internal forces and displacements of a tube structure with a rectangular section subjected to horizontal load (Fig. 18.11(a),(b)).

The tube structure with a rectangular section is shown in Fig. 18.11(b).

Geometric parameters: $b/c = 1, H/b = 2, 4, 10, h = \text{constant}$; Physical parameters: $E = \text{constant}, \mu = 0.3$.

In this example, the tube structure with a rectangular section is analyzed by the elements TB-12 and TB-13. Due to symmetry, only a quarter of the structure is computed. The results of the displacements and internal forces are listed in Tables 18.9 and 18.10. From Table 18.9, it can be seen that the convergence of displacements by the element TB-mn is very good. Since the spline interpolation orders of the element along two directions are selected rationally, the convergence speed of the displacements is faster with the increase of H/b . The

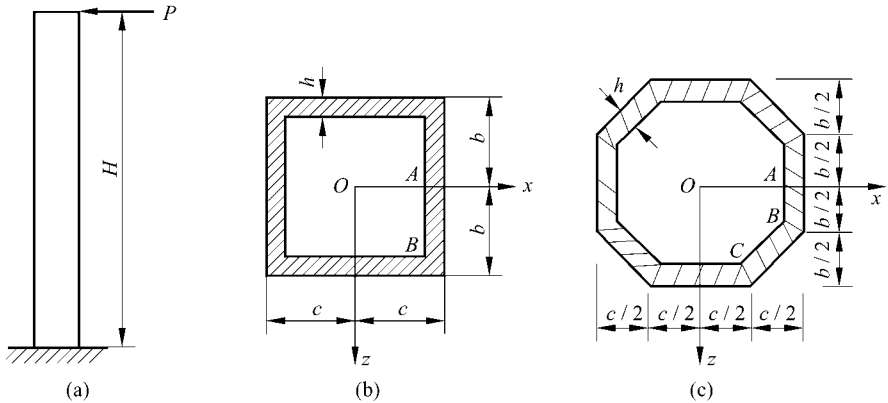


Figure 18.11 Rectangular and polygonal tube structures

Table 18.9 The tip displacement u/u_b ($u_b = \frac{PH^3}{3EI}$) of a tube structure with rectangular section subjected to horizontal concentrated load

Element type		TB-12			TB-13		
H/b		2	4	10	2	4	10
Mesh	1 × 1	3.757	1.625	1.021	3.751	1.637	1.028
	2 × 2	3.856	1.663	1.032	3.856	1.663	1.032
	4 × 2				3.887	1.671	1.033
	4 × 4	3.887	1.671	1.033			
Coull method		3.981	1.741	1.118	3.981	1.741	1.118
Beam theory		1.000	1.000	1.000	1.000	1.000	1.000

Table 18.10 The bottom stress σ_y/σ_b ($\sigma_b = \frac{PH}{I}b$) of a tube structure with rectangular section subjected to horizontal concentrated load

Position		Mid-point A			Corner point B		
H/b		2	4	10	2	4	10
TB-12	1 × 1	0.4011	0.7638	0.9352	1.357	1.135	1.013
	2 × 2	0.5541	0.7813	0.9352	1.658	1.274	1.013
	4 × 4	0.5651	0.7835	0.9216	1.930	1.406	1.111
TB-13	1 × 1	0.3173	0.6724	0.9013	1.410	1.197	1.058
	2 × 1	0.5531	0.7681	0.9236	1.701	1.311	1.081
	2 × 2	0.5643	0.7747	0.9081	1.724	1.352	1.115
	4 × 2	0.5630	0.7794	0.9145	1.976	1.445	1.130
Energy method		0.576	0.787	0.915	1.874	1.438	1.175
Coull method		0.5380	0.7680	0.9070	1.577	1.290	1.116
Beam theory		1.0000	1.0000	1.0000	1.000	1.000	1.000

displacement values of Coull method^[16] given in Table 18.9 are obtained from the force method, so they are larger than the practical displacement values of the structure. Furthermore, with the increase of H/b , the difference of the tip displacements between numerical result and beam theory will reduce gradually. Results of the vertical stress σ_y at the bottom of the tube structure are listed in Table 18.10. It can be seen that, the stress at the mid-point A of the edge is smaller than the stress at the corner point B , which is the so-called “shear lag”. With the increase of H/b , the shear lag effect will weaken. The stress convergence of the spline element is also very good, and is similar to that of the energy method^[18].

Example 18.8 The internal forces and displacements of a tube structure with a polygonal section subjected to horizontal load (Fig. 18.11(a),(c)).

Geometric parameters: $b/c = 1, H/b = 2, 4, 10, h = \text{constant}$; Physical parameters: $E = \text{constant}, \mu = 0.3$. The tube structure with a polygonal section is analyzed by the element TB-13. Numerical solutions of the displacements and stresses are listed in Tables 18.11 and 18.12, respectively, in which the mesh is used for 1/4 of the structure. Satisfactory solutions can be obtained only by a few elements. It can be seen that, the influence of the shear lag effect of the polygonal section tube structure is less than that of the rectangular section tube structure.

Table 18.11 The tip displacement $u/u_b \left(u_b = \frac{PH^3}{3EI} \right)$ of a tube structure with polygonal section

H/b		2	4	10
Mesh	3 × 1	3.142	1.469	1.000
	6 × 1	3.182	1.480	1.001
	6 × 2	3.182	1.480	1.001
	9 × 2	3.190	1.482	1.002
Beam theory		1.000	1.000	1.000

Table 18.12 The bottom stress $\sigma_y/\sigma_b \left(\sigma_b = \frac{PH}{I} b \right)$ of a tube structure with polygonal section

Position		Mid-point A			Corner point B		
H/b		2	4	10	2	4	10
Mesh	3 × 1	0.660	0.855	1.010	1.153	1.062	1.012
	6 × 1	0.761	0.892	0.974	1.313	1.114	1.022
	9 × 1	0.773	0.899	0.975	1.360	1.125	1.023
	6 × 2	0.768	0.880	0.961	1.354	1.156	1.039
	9 × 2	0.771	0.887	0.963	1.426	1.179	1.042
Energy method		0.793	0.897	0.959	1.317	1.159	1.063
Beam theory		1.000	1.000	1.000	1.000	1.000	1.000

(Continued)

Position		Corner point <i>C</i>		
<i>H/b</i>		2	4	10
Mesh	3 × 1	0.502	0.508	0.505
	6 × 1	0.624	0.544	0.510
	9 × 1	0.643	0.551	0.511
	6 × 2	0.646	0.562	0.515
	9 × 2	0.656	0.571	0.518
Energy method		0.651	0.575	0.530
Beam theory		0.500	0.500	0.500

References

- [1] De Boor C (1978) A practical guide to splines. Springer Verlag, New York
- [2] Schumaker LL (1981) Spline function: basic theory. John Wiley and Sons, New York
- [3] Schultz MH (1973) Spline analysis. Prentic-Hall, Englewood Cliff, New Jersey
- [4] Prenter PM (1975) Splines and variational methods. John Wiley and Sons, New York
- [5] Yuan S (1982) Finite element analysis of shell of revolution using cubic B spline. In: Proceeding of International Conference on FEM. China, Shanghai, pp 837 – 840
- [6] Yuan S (1986) Quadratic spline thick/thin plate triangular hybrid elements. In: Proceeding International Conference on Computational Mechanics. Tokyo, pp 1111 – 1116
- [7] Fan Z (1988) Applications of spline elements and sub-region mixed elements in structural engineering [Doctoral Dissertation]. Tsinghua University, Beijing (in Chinese)
- [8] Fan Z, Long YQ (1991) Linear analysis of tall buildings using spline element. Engineering Structure, 13: 27 – 33
- [9] Fan Z, Long YQ (1990) Large deflection and stability analysis by geometrically nonlinear spline element. In: Proceeding of International Conference on Numerical Methods in Engineering, Theory & Applications (Vol. 1). Swansea, UK, pp 414 – 422
- [10] Yuan S (1984) Spline elements in stress analysis [Doctoral Dissertation]. Tsinghua University, Beijing
- [11] Cheung YK (1976) Finite strip method in structural analysis. Bergamon Press, Oxford
- [12] Girijavallaham CV (1969) Analysis of shear wall with opening. Journal of ASCE, STR 10: 2093 – 2102
- [13] Chan HC, Cheung YK (1979) Analysis of shear walls using higher order finite element. Building & Environment, 14: 217 – 244
- [14] Fan Z, Long YQ (1989) Spline thick/thin shell element. In: Proceeding of 2nd East Asia-Pacific Conference on Structural Engineering & Construction. Thailand, Chiang Mai, pp1195 – 1200

Advanced Finite Element Method in Structural Engineering

- [15] Coull A, Subedi NK (1975) Hull-core structures subjected to bending and torsion. In: Proceedings of 9th Congress of International Association for Bridge and Structural Engineering, Preliminary Report, May
- [16] Coull A, Bose B (1975) Simplified analysis of framed-tube structures. Journal of the Structural Division, ASCE, 101(11): 2223 – 2240
- [17] Coull A, Bose B (1976) Torsion of framed-tube structures. Journal of the Structural Division, ASCE 102(12): 2366 – 2370
- [18] Long YQ, Xin KG (1985) Analysis of framed-tube structures of polygonal section by energy method. Journal of Building Structures 6(3): 10 – 16 (in Chinese)

Chapter 19 Spline Element II — Analysis of Plate/Shell Structures

Yu-Qiu Long

Department of Civil Engineering, School of Civil Engineering,
Tsinghua University, Beijing, 100084, China

Si Yuan

Department of Civil Engineering, School of Civil Engineering,
Tsinghua University, Beijing, 100084, China

Abstract This chapter continues focusing on the spline element method. Some applications of the spline elements for thin plate, thin shallow shell, thick-thin plate/shell and geometrically nonlinear problems are discussed in detail.

Keywords finite element, spline function, spline element, plate, shell.

19.1 Spline Elements for Thin Plate Bending

This section will present two rectangular spline elements for the thin plate bending problem^[1].

19.1.1 Bi-Quadratic Rectangular Spline Element (16 DOFs)

The geometries of the bi-quadratic rectangular spline element are still given by Fig. 18.3. There are 4 DOFs at each node ij

$$\mathbf{q}_{ij} = [w_{ij}^{(00)} \quad w_{ij}^{(10)} \quad w_{ij}^{(01)} \quad w_{ij}^{(11)}]^T \quad (19-1)$$

And, each element has 16 DOFs

$$\mathbf{q}^e = [\mathbf{q}_{11}^T \quad \mathbf{q}_{21}^T \quad \mathbf{q}_{22}^T \quad \mathbf{q}_{12}^T]^T \quad (19-2)$$

The element deflection $w(x, y)$ can be expressed in terms of nodal displacements

$$w(x, y) = \sum_{i=1}^2 \sum_{j=1}^2 N_{ij} q_{ij} \tag{19-3}$$

where

$$N_{ij} = [N_{ij}^{(00)} \quad N_{ij}^{(10)} \quad N_{ij}^{(01)} \quad N_{ij}^{(11)}] \tag{19-4}$$

$$N_{ij}^{(kl)} = N_i^{(k)}(x)N_j^{(l)}(y) \quad (i, j = 1,2; k, l = 0,1) \tag{19-5}$$

$N_i^{(k)}(x)$ and $N_j^{(l)}(y)$ are the shape functions of the quadratic spline beam element, and have been given by Eq. (18-4).

Example 19.1 Simply-supported or clamped square plate subjected to uniform load q or central concentrated force P .

The results of the central deflection obtained by the above bi-quadratic spline element and different meshes are listed in Table 19.1.

Table 19.1 Results of the central deflection w_C

Mesh (1/4 plate)	Total DOFs	Uniform load q		Concentrated load P	
		Simply-supported	Clamped	Simply-supported	Clamped
1 × 1	16	0.398	0.099	1.03	0.395
2 × 2	36	0.404	0.120	1.12	0.510
3 × 3	64	0.405	0.123	1.14	0.536
4 × 4	100	0.406	0.125	1.15	0.546
Exact		0.406	0.126	1.16	0.560
Factor		$qL^4/(100D)$		$PL^2/(100D)$	

19.1.2 Bi-Cubic Rectangular Spline Element (36 DOFs)

As shown in Fig. 19.1, a bi-cubic rectangular spline element is divided into nine sub-regions. There are 9 DOFs at each node ij

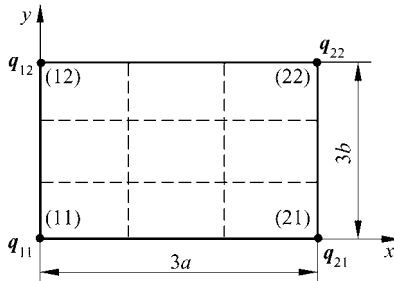


Figure 19.1 Bi-cubic rectangular spline element

$$\mathbf{q}_{ij} = [w_{ij}^{(00)} \quad w_{ij}^{(10)} \quad w_{ij}^{(01)} \quad w_{ij}^{(11)} \quad w_{ij}^{(20)} \quad w_{ij}^{(02)} \quad w_{ij}^{(21)} \quad w_{ij}^{(12)} \quad w_{ij}^{(22)}]^T \quad (19-6)$$

And, each element has 36 DOFs

$$\mathbf{q}^e = [\mathbf{q}_{11}^T \quad \mathbf{q}_{21}^T \quad \mathbf{q}_{22}^T \quad \mathbf{q}_{12}^T]^T \quad (19-7)$$

For each node ij , there are 9 shape functions

$$N_{ij} = [N_{ij}^{(00)} \quad N_{ij}^{(10)} \quad N_{ij}^{(01)} \quad N_{ij}^{(11)} \quad N_{ij}^{(20)} \quad N_{ij}^{(02)} \quad N_{ij}^{(21)} \quad N_{ij}^{(12)} \quad N_{ij}^{(22)}] \quad (19-8)$$

where

$$N_{ij}^{(kl)}(x, y) = N_i^{(k)}(x)N_j^{(l)}(y) \quad (i, j = 1, 2; \quad k, l = 0, 1, 2) \quad (19-9)$$

$N_i^{(k)}(x)$ and $N_j^{(l)}(y)$ are the shape functions of the cubic spline beam element, and have been given by Eq. (18-7).

Example 19.2 Simply-supported or clamped square plate subjected to uniform load q or central concentrated force P .

The above cubic rectangular spline element is used to calculate this example. And for comparison, the results obtained by the rectangular thin plate element ACM and the analytical solutions are also given. (Refer to Table 19.2).

Table 19.2 Central deflection w_C and bending moments M_{xB} , M_{xC} (B is the mid-side point, C is the plate center)

Element type	Mesh (1/4 plate)	Total DOFs	Uniform q				Concentrated force P		
			Clamped		Simply-supported		Clamped		Simply-supported
			w_C	M_{xB}	w_C	M_{xC}	w_C	M_{xB}	w_C
Bi-cubic spline element	1 × 1	36	0.126	-4.69	0.406	4.83	0.554	-0.119	1.15
	2 × 2	81	0.126	-5.01	0.406	4.80	0.559	-0.123	1.16
ACM	6 × 6	147	0.128		0.405		0.571		1.17
Analytical solution			0.126	-5.13	0.406	4.79	0.560	-0.126	1.16
Factor			$qL^4/(100D)$	$qL^2/100$	$qL^4/(100D)$	$qL^2/100$	$PL^2/(100D)$	P	$PL^2/(100D)$

The sectorial and triangular spline elements for the thin plate bending can be found in reference [1].

19.2 Spline Elements for Thick/Thin Beam and Plate

In this section, quadratic and cubic spline thick/thin beam elements are introduced firstly. Then, these beam elements are generalized to establish bi-quadratic and bi-cubic spline thick/thin plate elements^[1].

19.2.1 d -Order Spline Thick/Thin Beam Elements ($d = 2, 3$)

For the spline thin beam elements discussed in Sect. 18.2, the displacement modes of quadratic and cubic spline thin beam elements are given by Eqs. (18-3) and (18-6), respectively. These two displacement modes can be written as

$$w = \sum_{i=1}^2 \sum_{\alpha=0}^{d-1} N_i^\alpha(x) w_i^\alpha \quad (d = 2, 3) \tag{19-10}$$

in which $N_i^{(\alpha)}(x)$ has been simplified as $N_i^\alpha(x)$.

When we construct the thick/thin beam element, the requirements of both thick beam theory and thin beam theory must be considered at the same time:

In the thin beam theory, the rotation of the cross section ψ depends on the deflection w , and $\psi = \frac{dw}{dx}$.

But, in the thick beam theory, w and ψ are two independent displacements, and shear strain $\gamma = \frac{dw}{dx} - \psi$ is generally nonzero.

Here, d -order ($d=2,3$) spline thick/thin beam elements will be developed according to the above requirements.

Firstly, the element DOFs are composed of the following nodal displacements: For the quadratic spline element ($d = 2$), there are 4 DOFs, i.e.,

$$w_i^0, \psi_i^0 \quad (i = 1, 2)$$

For the cubic spline element ($d = 3$), there are 6 DOFs, i.e.,

$$w_i^0, \psi_i^0, \psi_i^1 \quad (i = 1, 2)$$

When the element degenerates to be the thin beam element, the above element DOFs will degenerate to be the DOFs defined in Sect. 18.2.

Secondly, the displacement modes of d -order spline elements are considered. The deflection w is still expressed by the d -order spline functions, and the rotation ψ is expressed by the $d-1$ order spline functions, i.e.,

$$\left. \begin{aligned} w &= \sum_{i=1}^2 N_i^0 w_i^0 + \sum_{i=1}^2 \sum_{\alpha=1}^{d-1} N_i^\alpha \beta_i^\alpha \\ \psi &= D_x N_1^0 \beta_1^0 + \sum_{i=1}^2 \sum_{\alpha=1}^{d-1} D_x N_i^\alpha \psi_i^{\alpha-1} \end{aligned} \right\} \tag{19-11}$$

where $D_x = \frac{d}{dx}$, β_1^0 and $\beta_i^\alpha (i=1, 2; \alpha=1, 2, \dots, d-1)$ are the element internal DOFs which are waiting for being eliminated. It can be noted that ψ should contain a $D_x N_2^0$ term as one of the basis functions, but no matter for $d = 2$ or for

$d = 3$, $D_x N_2^0$ and $D_x N_1^0$ are both linearly dependent ($D_x N_2^0 = -D_x N_1^0$), so only the $D_x N_1^0$ term is reserved in ψ .

After condensation for internal DOFs, the displacement modes of the thick/thin beam element can be obtained

$$w = \sum_{i=1}^2 \left[\bar{N}_i^0 w_i^0 + \sum_{\alpha=1}^{d-1} \bar{N}_i^\alpha \psi_i^{\alpha-1} \right], \quad \psi = \sum_{i=1}^2 \left[\tilde{N}_i^0 w_i^0 + \sum_{\alpha=1}^{d-1} \tilde{N}_i^\alpha \psi_i^{\alpha-1} \right] \quad (19-12)$$

where the shape functions \bar{N}_i^α and \tilde{N}_i^α can be written as:

$d = 2$ (quadratic spline element)

$$\left. \begin{aligned} \bar{N}_i^0 &= N_i^0 + (-1)^i \frac{16\lambda\nu}{a} (N_1^1 + N_2^1) \\ \bar{N}_i^1 &= N_i^1 - 8\lambda\nu (N_1^1 + N_2^1) \\ \tilde{N}_i^0 &= D_x N_i^0 + (-1)^i (16\lambda\nu) D_x N_1^0 \\ \tilde{N}_i^1 &= D_x N_i^1 - 8\lambda\nu a D_x N_1^0 \\ \lambda &= D/(Ca^2), \quad \nu = 1/(1+16\lambda) \end{aligned} \right\} \quad (i = 1, 2) \quad (19-13)$$

$d = 3$ (cubic spline element)

$$\left. \begin{aligned} \bar{N}_i^0 &= N_i^0 + (-1)^i \frac{\lambda\nu}{h} (N_1^1 + N_2^1) \\ \bar{N}_i^1 &= N_i^1 - \frac{3\lambda\nu}{2} (N_1^1 + N_2^1) \\ \bar{N}_i^2 &= N_i^2 + (-1)^i \frac{5\lambda\nu h}{12} (N_1^1 + N_2^1) \\ \tilde{N}_i^0 &= D_x N_i^0 + (-1)^i (3\lambda\nu) D_x N_1^0 \\ \tilde{N}_i^1 &= D_x N_i^1 - \frac{9\lambda\nu h}{2} D_x N_1^0 \\ \tilde{N}_i^2 &= D_x N_i^2 + (-1)^i \frac{5\lambda\nu h^2}{4} D_x N_1^0 \\ \lambda &= D/(Ch^2), \quad h = a/3, \quad \nu = 1/(1+3\lambda) \end{aligned} \right\} \quad (i = 1, 2) \quad (19-14)$$

in which D and C are the bending and shear stiffness, respectively; a is the element length. N_i^α in the above two equations are the shape functions of the spline thin beam element: for the quadratic spline element, N_i^α are defined by Eq. (18-4); for the cubic spline element, N_i^α are defined by Eq. (18-7).

Finally, some features of the displacement modes given by Eq. (19-11) are pointed out as follows:

(1) Within an element, w is expressed by d ($=2,3$)-order spline functions which possess $(d-1)$ -order continuity; ψ is expressed by the derivatives of the d -order spline functions ($(d-1)$ -order spline functions) which possess $(d-2)$ -order continuity.

(2) Between two adjacent elements, w is continuous, but its derivative is generally not; ψ possesses $(d-2)$ -order continuity. When $\lambda=0$ ($C \rightarrow \infty$), $\psi = D_x w$. Thus, w will have $(d-1)$ -order continuity between two adjacent elements, and the element will become a thin beam element with only one independent displacement w , refer to Eq. (19-10).

(3) When $d=2$, the curvature $\kappa = -D_x \psi$ will not be continuous within an element and between two adjacent elements, and bending moments are piecewise constants; When $d=3$, the curvature will be continuous within an element and between two adjacent elements, then, the continuous bending moments can be obtained.

(4) When d is 2 or 3, N_i^α will satisfy the following relation

$$D_x(N_1^1 + N_2^1) - aD_x N_1^0 = 1$$

So, the shear strain $\gamma = D_x w - \psi$ will be a constant within an element, i.e.,

$$\gamma = \begin{cases} \frac{8\lambda\nu}{a} [2(w_2^0 - w_1^0) - a(\psi_1^0 + \psi_2^0)] & (d=2) \\ \frac{\lambda\nu}{h} \left[(w_2^0 - w_1^0) - \frac{3}{2}h(\psi_1^0 + \psi_2^0) + \frac{5h^2}{12}(\psi_2^1 - \psi_1^1) \right] & (d=3) \end{cases}$$

in which λ, ν are defined by Eq. (19-13) or Eq. (19-14). In the above equation, when $C \rightarrow \infty, \gamma \rightarrow 0$.

(5) The numbers of the element DOFs for both thick ($\lambda \neq 0$) and thin ($\lambda = 0$) beams are exactly the same.

19.2.2 Bi- d -Order Spline Thick/Thin Plate Element ($d=2, 3$)

As to plate element, the displacements along x and y directions can be assumed to vary according to Eq. (19-12), i.e., the shape functions can be constructed by pair-wise multiplication of the shape functions given in Eqs. (19-13) and (19-14) for beam element. Thus, the displacement mode of the bi- d -order ($d=2,3$) spline thick/thin plate element can be written as

$$\mathbf{q} = \sum_{i=1}^2 \sum_{j=1}^2 (N_{ij}^{00} w_{ij}^{00} + N_{ij}^{10} \psi_{xij}^{00} + N_{ij}^{01} \psi_{yij}^{00} + N_{ij}^{11} \beta_{ij}^{11} + N_{ij}^{20} \psi_{xij}^{10} + N_{ij}^{02} \psi_{yij}^{01} + N_{ij}^{21} \beta_{ij}^{21} + N_{ij}^{12} \beta_{ij}^{12} + N_{ij}^{22} \beta_{ij}^{22}) \quad (19-15)$$

The above equation is just for the cubic spline element. As to the quadratic spline element, the last five terms should be eliminated. In the above equation, we have

$$\mathbf{q} = \begin{Bmatrix} w \\ \psi_x \\ \psi_y \end{Bmatrix}, \quad \mathbf{N}_{ij}^{\alpha\beta} = \begin{Bmatrix} \bar{N}_i^\alpha(x)\bar{N}_j^\beta(y) \\ \tilde{N}_i^\alpha(x)\bar{N}_j^\beta(y) \\ \bar{N}_i^\alpha(x)\tilde{N}_j^\beta(y) \end{Bmatrix} \begin{pmatrix} i, j = 1, 2 \\ \alpha, \beta = 0, 1, \dots, d-1 \end{pmatrix}$$

\bar{N}_i^α and \tilde{N}_i^α are defined by Eq. (19-13) or Eq. (19-14), in which D and C are the bending stiffness and shear stiffness of the plate, respectively. And, $\beta_{ij}^{\alpha\beta}$ ($\alpha, \beta = 1, 2$) in Eq. (19-15) are generalized nodal displacements, when $C \rightarrow \infty$, we have

$$\psi_x = D_x w, \quad \psi_y = D_y w, \quad \beta_{ij}^{\alpha\beta} = D_x^\alpha D_y^\beta w(x_i, y_i) \quad (i, j = 1, 2; \alpha, \beta = 1, 2, \dots, d) \tag{19-16}$$

as a result of which the thin plate element can be arrived at.

Example 19.3 Simply-supported square plate subjected to uniform load. The Poisson’s ratio $\mu = 0.3$, and let $\bar{\lambda} = D/(CL^2)$.

This example is computed with the quadratic and cubic spline thick/thin plate elements. The results obtained by the quadratic spline element are listed in Tables 19.3a and b, in which the bending moment solutions are the average

Table 19.3a The central deflection $w_C/(qL^4/D)$ of the plate (quadratic spline element)

Mesh for 1/4 plate	Total DOFs	$\bar{\lambda} = 0.000$	$\bar{\lambda} = 0.010$	$\bar{\lambda} = 0.025$	$\bar{\lambda} = 0.050$
1 × 1	16	0.003 98	0.004 75	0.006 04	0.008 31
2 × 2	36	0.004 04	0.004 76	0.005 91	0.007 85
3 × 3	64	0.004 05	0.004 78	0.005 91	0.007 79
4 × 4	100	0.004 06	0.004 79	0.005 91	0.007 77
Analytical solution ^[2]		0.004 06	0.004 80	0.005 91	0.007 76

Table 19.3b The central bending moment $M_{x_C}/(qL^2)$ of the plate (quadratic spline element)

Mesh for 1/4 plate	Total DOFs	$\bar{\lambda} = 0.000$	$\bar{\lambda} = 0.010$	$\bar{\lambda} = 0.025$	$\bar{\lambda} = 0.050$
1 × 1	16	0.0468	0.0523	0.0567	0.0600
2 × 2	36	0.0477	0.0498	0.0502	0.0504
3 × 3	64	0.0478	0.0488	0.0489	0.0489
4 × 4	100	0.0478	0.0484	0.0485	0.0485
Analytical solution ^[2]		0.0479			

values at the nodes. And, results of the cubic spline element are given in Tables 19.4a and b. These results show that for plates with different thickness ($\bar{\lambda}$ is taken different value), both elements can give highly accurate displacements and bending moments. The numbers in the column of $\bar{\lambda} = 0$ are the analytical solutions of the thin plate theory.

Table 19.4a The central deflection $w_C/(qL^4/D)$ of the plate (cubic spline element)

Mesh for 1/4 plate	Total DOFs	$\bar{\lambda} = 0.000$	$\bar{\lambda} = 0.010$	$\bar{\lambda} = 0.025$	$\bar{\lambda} = 0.050$
1 × 1	36	0.004 06	0.004 83	0.006 15	0.008 43
2 × 2	81	0.004 06	0.004 80	0.005 96	0.007 90
3 × 3	144	0.004 06	0.004 80	0.005 93	0.007 81
Analytical solution ^[2]		0.004 06	0.004 80	0.005 91	0.007 76

Table 19.4b The central bending moment $M_{xC}/(qL^2)$ of the plate (cubic spline element)

Mesh for 1/4 plate	Total DOFs	$\bar{\lambda} = 0.000$	$\bar{\lambda} = 0.010$	$\bar{\lambda} = 0.025$	$\bar{\lambda} = 0.050$
1 × 1	36	0.0483	0.0468	0.0451	0.0424
2 × 2	81	0.0480	0.0474	0.0472	0.0471
3 × 3	144	0.0479	0.0477	0.0476	0.0476
Analytical solution ^[2]		0.0479			

19.3 Spline Elements for Shallow Shell

The base plane of the shallow shell is taken as the xOy plane, and the z -axis is normal to the base plane. Equation for the mid-surface of the shallow shell is $z = z(x, y)$. Thus, the initial curvatures of the mid-surface are

$$k_x = \frac{\partial^2 z}{\partial x^2}, \quad k_y = \frac{\partial^2 z}{\partial y^2}, \quad k_{xy} = \frac{\partial^2 z}{\partial x \partial y} \tag{19-17}$$

The tangential displacements of the mid-surface are u and v , and the normal displacement is w . The curvature vector is

$$\boldsymbol{\kappa} = \begin{Bmatrix} \kappa_x \\ \kappa_y \\ 2\kappa_{xy} \end{Bmatrix} = \begin{Bmatrix} -\frac{\partial^2 w}{\partial x^2} \\ -\frac{\partial^2 w}{\partial y^2} \\ -2\frac{\partial^2 w}{\partial x \partial y} \end{Bmatrix} \tag{19-18}$$

And, the strain vector of the mid-surface is

$$\boldsymbol{\varepsilon} = \begin{Bmatrix} \varepsilon_x \\ \varepsilon_y \\ \gamma_{xy} \end{Bmatrix} = \begin{Bmatrix} \frac{\partial u}{\partial x} + k_x w \\ \frac{\partial v}{\partial y} + k_y w \\ \frac{\partial u}{\partial y} + \frac{\partial v}{\partial x} + 2k_{xy} w \end{Bmatrix} \quad (19-19)$$

The projection of the shallow element on the base plane is a rectangle. Let the normal displacement w be bi- d -order ($d = 2,3$) spline, and the tangential displacements u and v be the bi- \bar{d} -order spline ($\bar{d} = 1,2,3$). Then, the displacement mode of the shell element can be written as

$$w = \sum_{i=1}^2 \sum_{\alpha=0}^{d-1} \sum_{j=1}^2 \sum_{\beta=0}^{d-1} N_{ij}^{(\alpha\beta)}(x, y) w_{ij}^{(\alpha\beta)}$$

$$\begin{Bmatrix} u \\ v \end{Bmatrix} = \sum_{i=1}^2 \sum_{\alpha=0}^{\bar{d}-1} \sum_{j=1}^2 \sum_{\beta=0}^{\bar{d}-1} N_{ij}^{(\alpha\beta)}(x, y) \begin{Bmatrix} u_{ij}^{(\alpha\beta)} \\ v_{ij}^{(\alpha\beta)} \end{Bmatrix} \quad (19-20)$$

where

$$N_{ij}^{(\alpha\beta)}(x, y) = N_i^{(\alpha)}(x) N_j^{(\beta)}(y) \quad (19-21)$$

From the different combinations of d and \bar{d} , 6 elements can be obtained^[1], see Table 19.5.

Table 19.5 6 different spline elements for shallow shell

d	\bar{d}	Element symbol	Number of Nodal DOFs	Number of element DOFs
2	1	R-QLL	6	24
	2	R-QQQ	12	48
	3	R-QCC	22	88
3	1	R-CLL	11	44
	2	R-CQQ	17	68
	3	R-CCC	27	108

Example 19.4 Simply-supported elliptic paraboloidal shallow shell with square base plane and subjected to uniform vertical load q . Poisson's ration $\mu = 0.3$.

Equation of the mid-surface is $z = \frac{k}{2}(x^2 + y^2)$, and the side length of the

square base plane is $2a$. Results of the central deflections, bending moments and in-plane forces obtained by three spline elements are listed in Table 19.6.

Table 19.6 Numerical results obtained by 3 different spline elements for shallow shell

	Mesh (1/4 shell)	Total DOFs	w_C	M_{xC}	N_{xC}
R-QQQ	1 × 1	48	4.244	0.6025	− 6.480
	2 × 2	108	4.037	0.2896	− 6.096
	3 × 3	192	4.010	0.2443	− 6.032
	4 × 4	300	4.001	0.2296	− 6.011
R-CQQ	1 × 1	68	3.998	0.1025	− 6.165
	2 × 2	153	3.991	0.1881	− 6.023
	3 × 3	272	3.991	0.2021	− 6.003
R-CCC	1 × 1	108	3.989	0.1275	− 5.874
	2 × 2	243	3.990	0.1884	− 5.963
Analytical solution			3.990	0.2111	− 5.985
Factor			$qa^4/1000D$	$qa^2/100$	qa

19.4 Spline Elements for Thick/Thin Shell

This section will introduce the spline elements for the analysis of both thick and thin shells, which can also be used for thick and thin plates.

The influence of the transverse shear strain should be taken into account in the thick shell element. In order to avoid the shear locking phenomenon, the nodal displacements and transverse shear strains are taken as the independent variables. Since fewer undetermined coefficients and higher continuity exist in the spline functions, a very ideal effect can be achieved if the interpolation functions for the element displacements and transverse shear strains are constructed by the rational selection of the spline functions with different order. Furthermore, since the derivative terms of w at the nodes are replaced by the normal rotations and transverse shear strains of the cross-section, boundary conditions can be introduced easily. The features of this thick shell element are as follows: the interpolations for displacements and transverse shear strains are finished in local element by using the spline functions; each undetermined coefficient represents the nodal value of the element variable or its derivative; higher accurate solutions can be obtained with only low-order spline functions and fewer DOFs.

Two spline element types will be discussed as follows. They are

Rectangular element—suitable for the analysis of the shallow shell with rectangular base;

Sectorial element—suitable for the analysis of the axisymmetric shell.

19.4.1 Rectangular Spline Element for Thick/Thin Shell^{13, 41}

1. The potential energy functional of thick shell

The total potential energy functional of the thick shell can be written as

$$\Pi = \iint_{\Omega} \left(\frac{1}{2} \boldsymbol{\varepsilon}^T \mathbf{D}_p \boldsymbol{\varepsilon} + \frac{1}{2} \boldsymbol{\kappa}^T \mathbf{D}_b \boldsymbol{\kappa} + \frac{1}{2} \boldsymbol{\gamma}^T \mathbf{C} \boldsymbol{\gamma} - qw - q_x u - q_y v \right) dA \quad (19-22)$$

in which $\boldsymbol{\varepsilon}$ is the membrane strain vector in the mid-surface of the shell; $\boldsymbol{\kappa}$ is the curvature vector of the mid-surface:

$$\boldsymbol{\varepsilon} = \begin{Bmatrix} \varepsilon_{xx} \\ \varepsilon_{yy} \\ \varepsilon_{xy} \end{Bmatrix} = \begin{bmatrix} \frac{\partial}{\partial x} & 0 \\ 0 & \frac{\partial}{\partial y} \\ \frac{\partial}{\partial y} & \frac{\partial}{\partial x} \end{bmatrix} \begin{Bmatrix} u \\ v \end{Bmatrix} + \begin{Bmatrix} k_x \\ k_y \\ 2k_{xy} \end{Bmatrix} w = \nabla_{pu} \mathbf{u} + \nabla_{pw} w \quad (19-23)$$

$$\boldsymbol{\kappa} = \begin{Bmatrix} \kappa_x \\ \kappa_y \\ 2\kappa_{xy} \end{Bmatrix} = - \begin{bmatrix} \frac{\partial}{\partial x} & 0 \\ 0 & \frac{\partial}{\partial y} \\ \frac{\partial}{\partial y} & \frac{\partial}{\partial x} \end{bmatrix} \begin{Bmatrix} \psi_x \\ \psi_y \end{Bmatrix} = -\nabla_{p\psi} \boldsymbol{\psi} \quad (19-24)$$

where κ_x , κ_y and κ_{xy} are the initial curvatures of the mid-surface and given by Eq. (19-17); ψ_x and ψ_y are the rotations of the mid-surface. According to the Mindlin assumption, the transverse shear strains $\boldsymbol{\gamma}$, the derivatives of the deflection w and the rotations $\boldsymbol{\psi}$ satisfy the following relation:

$$\boldsymbol{\gamma} = \begin{Bmatrix} \gamma_x \\ \gamma_y \end{Bmatrix} = \begin{Bmatrix} \frac{\partial w}{\partial x} - \psi_x \\ \frac{\partial w}{\partial y} - \psi_y \end{Bmatrix} \quad (19-25)$$

In the variational formulation of the total potential energy functional, the displacements and the transverse shear strains are treated as independent variables, so from Eq. (19-25), the curvatures of the mid-surface $\boldsymbol{\kappa}$ can be expressed in terms of the derivatives of w and $\boldsymbol{\gamma}$.

$$\boldsymbol{\kappa} = - \begin{Bmatrix} \frac{\partial^2}{\partial x^2} \\ \frac{\partial^2}{\partial y^2} \\ 2 \frac{\partial^2}{\partial x \partial y} \end{Bmatrix} w + \begin{Bmatrix} \frac{\partial}{\partial x} & 0 \\ 0 & \frac{\partial}{\partial y} \\ \frac{\partial}{\partial y} & \frac{\partial}{\partial x} \end{Bmatrix} \boldsymbol{\gamma} = \nabla_{bw} w + \nabla_{b\boldsymbol{\gamma}} \boldsymbol{\gamma} \quad (19-26)$$

In the total potential energy functional (19-22), \mathbf{D}_p , \mathbf{D}_b and \mathbf{C} are the membrane, bending and shear stiffness matrices of the shell

$$\mathbf{D}_p = D_p \begin{bmatrix} 1 & \mu & 0 \\ \mu & 1 & 0 \\ 0 & 0 & \frac{1-\mu}{2} \end{bmatrix}, \quad D_p = \frac{Eh}{1-\mu^2} \quad (19-27)$$

$$\mathbf{D}_b = D_b \begin{bmatrix} 1 & \mu & 0 \\ \mu & 1 & 0 \\ 0 & 0 & \frac{1-\mu}{2} \end{bmatrix}, \quad D_b = \frac{Eh^3}{12(1-\mu^2)} \quad (19-28)$$

$$\mathbf{C} = C \begin{bmatrix} 1 & 0 \\ 0 & 1 \end{bmatrix}, \quad C = kGh, \quad G = \frac{E}{2(1+\mu)} \quad (19-29)$$

where E is the Young’s modulus; μ is the Poisson’s ratio; h is the thickness of the shell; k is the section shear coefficient. It can be seen that, in the total potential energy functional, $w \in C_1$, u, v and $\boldsymbol{\gamma} \in C_0$.

2. Rational spline interpolations

Now, the variables w , \mathbf{u} and $\boldsymbol{\gamma}$ of the rectangular element shown in Fig. 19.2 are interpolated, respectively.

Since continuity requirements of \mathbf{u} and $\boldsymbol{\gamma}$ are lower than those of w , the orders of the spline interpolation functions should be selected individually, i.e., both \mathbf{u} and $\boldsymbol{\gamma}$ are one-order lower than w . Here, the following interpolations are used:

$$w = \sum_{i=1}^2 \sum_{j=1}^2 \sum_{\alpha=0}^{d-1} \sum_{\beta=0}^{d-1} N_{ij}^{\alpha\beta}(x, y) w_{ij}^{\alpha\beta} \quad (19-30)$$

$$\mathbf{u} = \begin{Bmatrix} u \\ v \end{Bmatrix} = \sum_{i=1}^2 \sum_{j=1}^2 \sum_{\alpha=0}^{d-2} \sum_{\beta=0}^{d-2} N_{ij}^{\alpha\beta}(x, y) \begin{Bmatrix} u_{ij}^{\alpha\beta} \\ v_{ij}^{\alpha\beta} \end{Bmatrix} \quad (19-31)$$

$$\boldsymbol{\gamma} = \begin{Bmatrix} \gamma_x \\ \gamma_y \end{Bmatrix} = \sum_{i=1}^2 \sum_{j=1}^2 \sum_{\alpha=0}^{d-2} \sum_{\beta=0}^{d-2} N_{ij}^{\alpha\beta}(x, y) \begin{Bmatrix} \gamma_{xij}^{\alpha\beta} \\ \gamma_{yij}^{\alpha\beta} \end{Bmatrix} \quad (19-32)$$

In the above equations, the order of the spline interpolation functions for w is d , while the orders of \mathbf{u} and $\boldsymbol{\gamma}$ are both $d-1$. Usually, $d=2$ or 3 , and corresponding element is quadratic or cubic spline element.

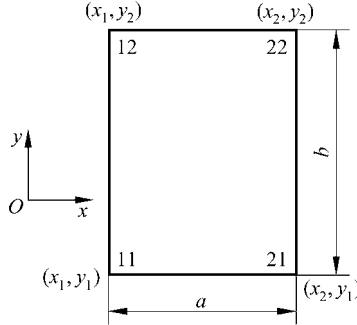


Figure 19.2 Rectangular element

$f_{ij}^{\alpha\beta}$ still represents the derivative value of function f at node ij , i.e.,

$$f_{ij}^{\alpha\beta} = \left. \frac{\partial^\alpha}{\partial x^\alpha} \frac{\partial^\beta}{\partial y^\beta} f(x, y) \right|_{x=x_i, y=y_j} \quad (19-33)$$

where $i, j = 1, 2$ (refer to Fig. 19.2); α and β are the derivative orders with respect to x and y , respectively.

The shape functions $N_{ij}^{\alpha\beta}$ are the product of two spline interpolation functions:

$$N_{ij}^{\alpha\beta}(x, y) = N_i^\alpha(x) N_j^\beta(y) \quad (19-34)$$

The quadratic and cubic spline interpolation functions $N_i^\alpha(x)$ (or $N_j^\beta(y)$) are given by Eqs. (18-4) and (18-7), respectively; and the linear spline interpolation function is

$$\left. \begin{aligned} N_1^0(x) &= 1 - \xi \\ N_2^0(x) &= \xi \end{aligned} \right\} \quad (0 \leq \xi \leq 1) \quad (19-35)$$

In order to deal with boundary conditions conveniently, by using the Eq. (19-25), the following derivative terms of w at nodes can be expressed in terms of rotations $\boldsymbol{\psi}$ and shear strains $\boldsymbol{\gamma}$ at the nodes:

$$\left. \begin{aligned} w_{i,j}^{(\alpha+1)0} &= \psi_{xij}^\alpha + \gamma_{xij}^{\alpha 0} & (\alpha = 0, 1, \dots, d-2) \\ w_{i,j}^{0(\beta+1)} &= \psi_{yij}^\beta + \gamma_{yij}^{0\beta} & (\beta = 0, 1, \dots, d-2) \end{aligned} \right\} \quad (19-36)$$

Therefore, the interpolation formula (19-30) for w can be rewritten as

$$\begin{aligned}
 w = & \sum_{i=1}^2 \sum_{j=1}^2 N_{ij}^{00}(x, y) w_{ij}^{00} + \sum_{i=1}^2 \sum_{j=1}^2 \sum_{\alpha=1}^{d-1} \sum_{\beta=1}^{d-1} N_{ij}^{\alpha\beta}(x, y) w_{ij}^{\alpha\beta} \\
 & + \sum_{i=1}^2 \sum_{j=1}^2 \sum_{\alpha=0}^{d-2} N_{ij}^{(\alpha+1)0}(x, y) (\psi_{xij}^{\alpha} + \gamma_{xij}^{\alpha 0}) + \sum_{i=1}^2 \sum_{j=1}^2 \sum_{\beta=0}^{d-2} N_{ij}^{0(\beta+1)}(x, y) (\psi_{yij}^{\beta} + \gamma_{yij}^{0\beta})
 \end{aligned} \tag{19-37}$$

And, the interpolation formulae (19-37), (19-31) and (19-32) can be written in the following matrix forms

$$\left. \begin{aligned}
 w &= \mathbf{N}_{bw} \bar{\mathbf{w}} + \mathbf{N}_{b\gamma} \bar{\boldsymbol{\gamma}} \\
 \mathbf{u} &= \mathbf{N}_{pu} \bar{\mathbf{u}} \\
 \boldsymbol{\gamma} &= \mathbf{N}_{\gamma} \bar{\boldsymbol{\gamma}}
 \end{aligned} \right\} \tag{19-38}$$

where $\bar{\mathbf{w}}$, $\bar{\mathbf{u}}$ and $\bar{\boldsymbol{\gamma}}$ are the element nodal unknown vectors. Since Eq. (19-36) is used here, the vector $\bar{\mathbf{w}}$ should be

$$\bar{\mathbf{w}} = [\bar{w}_{11}^T \quad \bar{w}_{12}^T \quad \bar{w}_{21}^T \quad \bar{w}_{22}^T]^T \tag{19-39}$$

with

$$\bar{w}_{ij} = [w_{ij}^{00} \quad \psi_{xij}^0 \quad \psi_{yij}^0 \quad w_{ij}^{11} \quad \vdots \quad \psi_{xij}^1 \quad \psi_{yij}^1 \quad w_{ij}^{21} \quad w_{ij}^{12} \quad w_{ij}^{22}]^T \tag{19-40}$$

Equation (19-40) is suitable for cubic spline element. As to the quadratic spline element, only the first four terms will be retained.

Substituting Eq. (19-38) back into Eqs. (19-23) and (19-26), the membrane strain vector $\boldsymbol{\varepsilon}$ and curvature vector $\boldsymbol{\kappa}$ can be written as

$$\begin{aligned}
 \boldsymbol{\varepsilon} &= \nabla_{pu} \mathbf{N}_{pu} \bar{\mathbf{u}} + \nabla_{pw} (\mathbf{N}_{bw} \bar{\mathbf{w}} + \mathbf{N}_{b\gamma} \bar{\boldsymbol{\gamma}}) \\
 &= \mathbf{B}_{pu} \bar{\mathbf{u}} + \mathbf{B}_{pw} \bar{\mathbf{w}} + \mathbf{B}_{p\gamma} \bar{\boldsymbol{\gamma}}
 \end{aligned} \tag{19-41}$$

$$\boldsymbol{\kappa} = \nabla_{bw} (\mathbf{N}_{bw} \bar{\mathbf{w}} + \mathbf{N}_{b\gamma} \bar{\boldsymbol{\gamma}}) + \nabla_{b\gamma} \mathbf{N}_{\gamma} \bar{\boldsymbol{\gamma}} = \mathbf{B}_{bw} \bar{\mathbf{w}} + \mathbf{B}_{b\gamma} \bar{\boldsymbol{\gamma}} \tag{19-42}$$

3. Element stiffness matrix

From the stationary condition of the energy functional, the following equations can be obtained, in which the coefficient matrix is the element stiffness matrix.

$$\begin{bmatrix} \mathbf{K}_{ww} & \mathbf{K}_{wu} & \mathbf{K}_{w\gamma} \\ \mathbf{K}_{uw} & \mathbf{K}_{uu} & \mathbf{K}_{u\gamma} \\ \mathbf{K}_{\gamma w} & \mathbf{K}_{\gamma u} & \mathbf{K}_{\gamma\gamma} \end{bmatrix} \begin{bmatrix} \bar{\mathbf{w}} \\ \bar{\mathbf{u}} \\ \bar{\boldsymbol{\gamma}} \end{bmatrix} = \begin{bmatrix} \mathbf{P}_w \\ \mathbf{P}_u \\ \mathbf{P}_\gamma \end{bmatrix} \tag{19-43}$$

where

$$\begin{aligned}
 \mathbf{K}_{ww} &= \iint_{\Omega^e} (\mathbf{B}_{pw}^T \mathbf{D}_p \mathbf{B}_{pw} + \mathbf{B}_{bw}^T \mathbf{D}_b \mathbf{B}_{bw}) dA \\
 \mathbf{K}_{wu} &= \iint_{\Omega^e} \mathbf{B}_{pw}^T \mathbf{D}_p \mathbf{B}_{pu} dA \\
 \mathbf{K}_{w\gamma} &= \iint_{\Omega^e} (\mathbf{B}_{pw}^T \mathbf{D}_p \mathbf{B}_{p\gamma} + \mathbf{B}_{bw}^T \mathbf{D}_b \mathbf{B}_{b\gamma}) dA \\
 \mathbf{K}_{uu} &= \iint_{\Omega^e} \mathbf{B}_{pu}^T \mathbf{D}_p \mathbf{B}_{pu} dA \\
 \mathbf{K}_{u\gamma} &= \iint_{\Omega^e} \mathbf{B}_{pu}^T \mathbf{D}_p \mathbf{B}_{p\gamma} dA \\
 \mathbf{K}_{\gamma\gamma} &= \iint_{\Omega^e} (\mathbf{B}_{p\gamma}^T \mathbf{D}_p \mathbf{B}_{p\gamma} + \mathbf{B}_{b\gamma}^T \mathbf{D}_b \mathbf{B}_{b\gamma} + \mathbf{N}_\gamma^T \mathbf{C} \mathbf{N}_\gamma) dA \\
 \mathbf{K}_{uw} &= \mathbf{K}_{wu}^T, \quad \mathbf{K}_{\gamma w} = \mathbf{K}_{w\gamma}^T, \quad \mathbf{K}_{\gamma u} = \mathbf{K}_{u\gamma}^T \\
 \mathbf{P}_w &= \iint_{\Omega^e} \mathbf{N}_{bw}^T q dA, \quad \mathbf{P}_u = \iint_{\Omega^e} \mathbf{N}_{pu}^T \begin{Bmatrix} q_x \\ q_y \end{Bmatrix} dA, \quad \mathbf{P}_\gamma = \iint_{\Omega^e} \mathbf{N}_{b\gamma}^T q dA
 \end{aligned}$$

4. Numerical examples

Example 19.5 Internal forces and displacements of simply-supported square plates subjected to uniform load.

In this example, the central deflection w_C and bending moment M_{xC} of simply-supported square plates with different thickness-span ratios are computed by using the quadratic and cubic rectangular spline shell elements ($d = 2, 3$). The results are listed in Tables 19.7 and 19.8. Due to symmetry, only 1/4 of the plate is considered. These results show that, the present spline elements for moderately thick shell possess high precision. When only one cubic element is used, the solutions of deflection w_C and bending moment M_{xC} are very close to the analytical solutions. Even though the quadratic spline element, which has fewer nodal DOFs, is used, the convergence is also quite good.

Table 19.7 The central deflection $w_C E h^3 / q L^4$ of simply-supported square plate subjected to uniform load

Spline order	Mesh	Thickness-span ratio h/L of the square plate				
		0.0001	0.01	0.05	0.10	0.20
$d = 2$	1×1	0.043 46	0.043 49	0.044 00	0.045 47	0.051 41
	2×2	0.044 15	0.044 18	0.044 63	0.046 07	0.051 82
	3×3	0.044 27	0.044 29	0.044 75	0.046 19	0.051 92
	4×4	0.044 31	0.044 33	0.044 79	0.046 23	0.051 97
$d = 3$	1×1	0.044 36	0.044 38	0.044 76	0.046 28	0.052 02
	2×2	0.044 36	0.044 38	0.044 76	0.046 28	0.052 02
Analytical solution ^[5]		0.044 34	0.044 39	0.044 68	0.046 32	0.052 17

Table 19.8 The central bending moment M_{xc} / qL^2 of simply-supported square plate subjected to uniform load

Spline order	Mesh	Thickness-span ratio h/L of the square plate				
		0.0001	0.01	0.05	0.10	0.20
$d = 2$	1×1	0.046 76	0.046 75	0.046 64	0.046 31	0.044 98
	2×2	0.047 66	0.047 66	0.047 64	0.047 57	0.047 34
	3×3	0.047 79	0.047 79	0.047 78	0.047 76	0.047 66
	4×4	0.047 84	0.047 84	0.047 83	0.047 81	0.047 76
$d = 3$	1×1	0.048 35	0.048 35	0.048 35	0.048 37	0.048 43
	2×2	0.048 00	0.048 00	0.048 00	0.048 01	0.048 02
Analytical solution ^[5]		0.047 90				

Example 19.6 Displacements and internal forces of simply-supported double-parabolic shallow shell subjected to uniform load.

The mid-surface equation of the simply-supported (movements along membrane direction are admissible) shallow shell is $z = 0.5k(x^2 + y^2)$, and the shell is subjected to uniform vertical load q (Fig. 19.3). In this example, displacements and internal forces of the double-parabolic shallow shell are computed by using the cubic spline element for moderately thick shell. All results are listed in Table 19.9. From Table 19.9, it can be seen that the displacement w_C possesses faster convergence speed, and the convergence speed of the bending moment M_{xc} is slower.

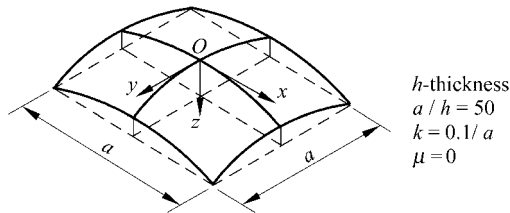


Figure 19.3 Double-parabolic shallow shell

Table 19.9 Results of the double-parabolic shallow shell subjected to uniform load

Mesh	$w_C \left(10^{-4} \frac{qa^4}{D} \right)$	$M_{xc} (10^{-2} qa^2)$	$N_{xc} (qa)$
1×1	0.3996	0.1064	6.123
2×2	0.3990	0.1869	6.020
3×3	0.3990	0.1984	6.000
Reference [1]	0.3990	0.2111	5.985

19.4.2 Sectorial Spline Element for Thick/Thin Axisymmetric Shell³¹

For the analysis of the axisymmetric shell, spherical coordinates r, θ, φ are employed. Then, the membrane strains $\boldsymbol{\varepsilon}$, curvatures $\boldsymbol{\kappa}$ and transverse shear strains $\boldsymbol{\gamma}$ can be expressed in terms of the displacements as follows:

$$\boldsymbol{\varepsilon} = \begin{Bmatrix} \varepsilon_{\varphi\varphi} \\ \varepsilon_{\theta\theta} \\ \varepsilon_{\varphi\theta} \end{Bmatrix} = \begin{bmatrix} \frac{\partial}{\partial s} & 0 & \frac{1}{R} \\ \frac{\cos \varphi}{r} & \frac{1}{r} \frac{\partial}{\partial \theta} & \frac{\sin \varphi}{r} \\ \frac{1}{r} \frac{\partial}{\partial \theta} & r \frac{\partial}{\partial s} \frac{1}{r} & 0 \end{bmatrix} \begin{Bmatrix} u \\ v \\ w \end{Bmatrix} = \nabla_{pu} \mathbf{u} + \nabla_{pw} w \quad (19-44)$$

$$\boldsymbol{\kappa} = \begin{Bmatrix} \kappa_{\varphi} \\ \kappa_{\theta} \\ \kappa_{\varphi\theta} \end{Bmatrix} = \begin{bmatrix} -\frac{\partial}{\partial s} \frac{1}{R} & 0 & \frac{\partial}{\partial s} & 0 \\ -\frac{\cos \varphi}{rR} & -\frac{\sin \varphi}{r^2} \frac{\partial}{\partial \theta} & \frac{\cos \varphi}{r} & \frac{1}{r} \frac{\partial}{\partial \theta} \\ -\frac{2}{rR} \frac{\partial}{\partial \theta} & -2 \sin \varphi \frac{\partial}{\partial s} \frac{1}{r} & 0 & 2 \frac{\partial}{\partial s} \end{bmatrix} \begin{Bmatrix} u \\ v \\ \psi_{\varphi} \\ \psi_{\theta} \end{Bmatrix} = \nabla_{bu} \mathbf{u} + \nabla_{b\psi} \boldsymbol{\psi} \quad (19-45)$$

$$\boldsymbol{\gamma} = \begin{Bmatrix} \gamma_{\varphi} \\ \gamma_{\theta} \end{Bmatrix} = \begin{Bmatrix} \frac{\partial}{\partial s} \\ \frac{\partial}{r \partial \theta} \end{Bmatrix} w - \begin{Bmatrix} \psi_{\varphi} \\ \psi_{\theta} \end{Bmatrix} = \nabla_{\gamma w} w - \boldsymbol{\psi} \quad (19-46)$$

For a sectorial element shown in Fig. 19.4, by imitating the rectangular element, its interpolation formulae of displacements w, u, v and shear strains can be written as

$$\left. \begin{aligned} \mathbf{u} &= \begin{Bmatrix} u \\ v \end{Bmatrix} = \sum_{i=1}^2 \sum_{j=1}^2 \sum_{\alpha=0}^{d-2} \sum_{\beta=0}^{d-2} N_{ij}^{\alpha\beta}(r, \theta) \begin{Bmatrix} u_{ij}^{\alpha\beta} \\ v_{ij}^{\alpha\beta} \end{Bmatrix} \\ w &= \sum_{i=1}^2 \sum_{j=1}^2 \sum_{\alpha=0}^{d-1} \sum_{\beta=0}^{d-1} N_{ij}^{\alpha\beta}(r, \theta) w_{ij}^{\alpha\beta} \\ \boldsymbol{\gamma} &= \begin{Bmatrix} \gamma_{\varphi} \\ \gamma_{\theta} \end{Bmatrix} = \sum_{i=1}^2 \sum_{j=1}^2 \sum_{\alpha=0}^{d-2} \sum_{\beta=0}^{d-2} N_{ij}^{\alpha\beta}(r, \theta) \begin{Bmatrix} \gamma_{\varphi ij}^{\alpha\beta} \\ \gamma_{\theta ij}^{\alpha\beta} \end{Bmatrix} \end{aligned} \right\} \quad (19-47)$$

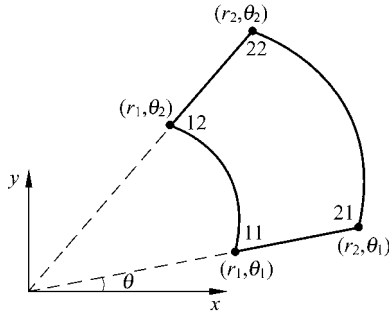


Figure 19.4 Sectorial element

In order to introduce the boundary conditions rationally, the partial derivative terms of the displacement component w at nodes will be replaced by ψ and γ

$$\left. \begin{aligned} w_{ij}^{(\alpha+1)0} &= \psi_{\phi ij}^\alpha + \gamma_{\phi ij}^{\alpha 0} \quad (\alpha = 0, \dots, d-2) \\ w_{ij}^{0(\beta+1)} &= \psi_{\theta ij}^\beta + \gamma_{\theta ij}^{0\beta} \quad (\beta = 0, \dots, d-2) \end{aligned} \right\} \quad (19-48)$$

The other steps are the same as those of the rectangular spline thick shell element, and will not be repeated here.

Example 19.7 Displacements and internal forces of simply-supported circular plate subjected to uniform load.

In this example, the central deflection w_C and bending moment $M_{\phi C}$ of the simply-supported circular plate with different thickness-radius ratios subjected to uniform load are computed by using the sectorial spline element for moderately thick shell. The results are listed in Tables 19.10 and 19.11. Due to symmetry, only one element is used along the hoop direction. It can be seen that excellent convergences of the displacements and internal forces can be obtained from the spline axisymmetric thick shell element.

Table 19.10 The central deflection $w_c D / q R^4$ of simply-supported circular plate subjected to uniform load

Spline order	Number of the elements	The thickness-radius ratio h/R of the circular plate				
		0.0001	0.01	0.05	0.20	0.30
$d = 2$	1	0.061 26	0.061 26	0.061 41	0.064 10	0.067 67
	2	0.063 17	0.063 17	0.063 39	0.066 04	0.069 61
	4	0.063 60	0.063 60	0.063 76	0.066 45	0.070 01
	8	0.063 70	0.063 71	0.063 88	0.066 53	0.070 11
$d = 3$	1	0.063 72	0.063 73	0.063 88	0.066 59	0.070 11
	2	0.063 70	0.063 71	0.063 88	0.066 56	0.070 13
Analytical solution ^[2]		0.063 70	0.063 71	0.063 88	0.066 56	0.070 13

Table 19.11 The bending moment $M_{\phi c} / qR^2$ of simply-supported circular plate subjected to uniform load

Spline order	Number of the elements	The thickness-radius ratio h/R of the circular plate				
		0.0001	0.01	0.05	0.20	0.30
$d = 2$	1	0.1933	0.1933	0.1933	0.1933	0.1933
	2	0.2048	0.2048	0.2048	0.2048	0.2048
	4	0.2063	0.2063	0.2063	0.2063	0.2063
	8	0.2064	0.2064	0.2064	0.2064	0.2064
$d = 3$	1	0.2110	0.2110	0.2110	0.2111	0.2112
	2	0.2074	0.2074	0.2074	0.2075	0.2075
	4	0.2065	0.2065	0.2065	0.2065	0.2066
Analytical solution ^[2]		0.2063				

Example 19.8 Internal forces of a spherical shell subjected to uniform normal load.

Dimensions of the spherical shell and results are given in Fig. 19.5. Due to symmetry, only one cubic spline element for moderately thick shell is used along the hoop direction, and four elements are used along the radial direction. It can be seen that the radial bending moment M_{ϕ} is in exact agreement with the analytical solution^[6], but there is a little difference existing in the hoop membrane force N_{θ} . Reference [7] provides the results obtained by 8 axisymmetric shell elements.

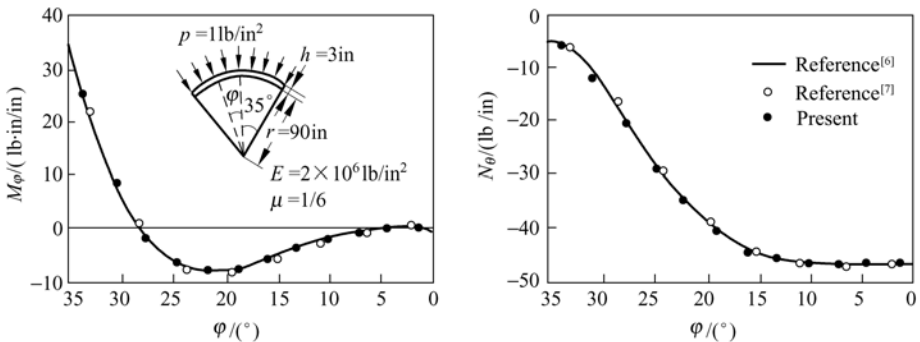


Figure 19.5 Clamped spherical shell

19.5 Spline Elements for Geometrically Nonlinear Analysis^[3-8]

This section will introduce the spline elements for geometrically nonlinear analysis of the shell, which can be used to analyze large deflection problem, determine

critical load, track post-buckling path, and study buckling characters of the plate/shell structure with initial defects.

Two geometrically nonlinear spline elements, rectangular shallow shell element in the Cartesian coordinate system and sectorial axisymmetric shell element in the spherical coordinate system, are discussed as follows.

19.5.1 Rectangular Shallow Shell Element in the Cartesian Coordinate System

As shown in Fig. 19.6, a shallow shell in the Cartesian coordinate system $Oxyz$ is considered. And, the rectangular element shown in Fig. 19.2 is used. The Total Lagrange Formulation of the geometrically nonlinear spline element will be derived from the virtual work principle.

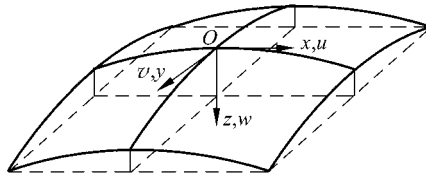


Figure 19.6 Shallow shell in Cartesian coordinate system

1. Nonlinear strain-displacement relation of shell

Here, the von Karman scheme is used. In the coordinate system $Oxyz$, the strain-displacement relation of the shallow shell can be written as

$$\left. \begin{aligned} \varepsilon_{xx} &= \frac{\partial u}{\partial x} + \frac{w}{R_1} + \frac{1}{2} \left(\frac{\partial w}{\partial x} \right)^2 - \zeta \left(\frac{\partial^2 w}{\partial x^2} \right) \\ \varepsilon_{yy} &= \frac{\partial v}{\partial y} + \frac{w}{R_2} + \frac{1}{2} \left(\frac{\partial w}{\partial y} \right)^2 - \zeta \left(\frac{\partial^2 w}{\partial y^2} \right) \\ \varepsilon_{xy} &= \frac{\partial u}{\partial y} + \frac{\partial v}{\partial x} + \frac{\partial w}{\partial x} \frac{\partial w}{\partial y} - \zeta \left(2 \frac{\partial^2 w}{\partial x \partial y} \right) \end{aligned} \right\} \quad (19-49)$$

where R_1 and R_2 are two principal radii of curvature; ζ is the normal coordinate of the shell. The curvatures in the mid-surface of the shallow shell are the same as those in the small deflection theory

$$\kappa_x = -\frac{\partial^2 w}{\partial x^2}, \quad \kappa_y = -\frac{\partial^2 w}{\partial y^2}, \quad 2\kappa_{xy} = -2\frac{\partial^2 w}{\partial x \partial y} \quad (19-50)$$

The above relations can be rewritten as the following matrix forms

$$\boldsymbol{\varepsilon} = \begin{Bmatrix} \boldsymbol{\varepsilon}^p \\ \boldsymbol{\varepsilon}^b \end{Bmatrix} \quad (19-51)$$

in which the superscript p denotes the membrane state; b denotes the bending state.

2. Spline Hermitian interpolation

Spline Hermitian interpolation is employed here for the element displacement components. If m -order spline is used, then, after the assembly of the elements, the interpolation functions will keep C_{m-1} -continuity within the domain. Thus, the displacements can be interpolated by the following equations

$$\left. \begin{aligned} \begin{Bmatrix} u \\ v \end{Bmatrix} &= \sum_{i=1}^2 \sum_{j=1}^2 \sum_{\alpha=0}^{m-1} \sum_{\beta=0}^{m-1} N_{nmij}^{\alpha\beta}(x, y) \begin{Bmatrix} u_{ij}^{\alpha\beta} \\ v_{ij}^{\alpha\beta} \end{Bmatrix} \\ w &= \sum_{i=1}^2 \sum_{j=1}^2 \sum_{\alpha=0}^{n-1} \sum_{\beta=0}^{n-1} N_{nmij}^{\alpha\beta}(x, y) w_{ij}^{\alpha\beta} \end{aligned} \right\} \quad (19-52)$$

where the tangential displacements of the mid-surface u and v are bi- m -order; normal displacement w is bi- n -order. If $m \geq 1$, the membrane forces between elements will be continuous; if $n \geq 2$, the bending moments between elements will be continuous. $u_{ij}^{\alpha\beta}$ (or $v_{ij}^{\alpha\beta}$, $w_{ij}^{\alpha\beta}$) denote the displacement or its derivative at node ij ($i, j = 1, 2$, Fig. 19.2)

$$u_{ij}^{\alpha\beta} = \frac{\partial^\alpha}{\partial x^\alpha} \frac{\partial^\beta}{\partial y^\beta} u(x, y) \Big|_{x=x_i, y=y_j} \quad (19-53)$$

The spline interpolation base function $N_{nmij}^{\alpha\beta}(x, y)$ possesses the following features:

$$\frac{\partial^\alpha}{\partial x^\alpha} \frac{\partial^\beta}{\partial y^\beta} N_{nmij}^{\delta\gamma}(x_k, y_l) = \delta_{ik} \delta_{jl} \delta_{\alpha\delta} \delta_{\beta\gamma} \quad (i, j, k, l = 1, 2; \alpha, \beta, \delta, \gamma = 0, 1, \dots, m-1) \quad (19-54)$$

where δ_{ij} is the Kronecker symbol

$$\delta_{ij} = \begin{cases} 1, & i = j \\ 0, & i \neq j \end{cases}$$

Bi- m -order piecewise spline interpolation base function $N_{nmij}^{\alpha\beta}(x, y)$ is composed of two m -order spline functions

$$N_{mmij}^{\alpha\beta}(x, y) = N_{mi}^{\alpha}(x)N_{mj}^{\beta}(y) \tag{19-55}$$

The quadratic spline function ($m=2$) is defined by Eq. (18.4); the cubic spline function ($m=3$) is defined by Eq. (18.7).

Equation (19-52) can be written as the following matrix form

$$\begin{Bmatrix} u \\ v \\ w \end{Bmatrix} = \begin{bmatrix} N_{mm}^p & \mathbf{0} \\ \mathbf{0} & N_{mm}^b \end{bmatrix} \begin{Bmatrix} \mathbf{q}_u \\ \mathbf{q}_w \end{Bmatrix} = \mathbf{N}\mathbf{q} \tag{19-56}$$

Substitution of Eq. (19-56) into Eq. (19-51) yields

$$\boldsymbol{\varepsilon} = \mathbf{B}_L\mathbf{q} + 0.5\mathbf{B}_{NL}\mathbf{q} \tag{19-57}$$

According to the above interpolation formulae, the element tangential stiffness matrix can be derived. This geometrically nonlinear element is called the rectangular element (NS)_{mm}.

19.5.2 Sectorial Axisymmetric Shell Element in the Spherical Coordinate System

In the large deflection theory of axisymmetric shell, the membrane strains of any point in the mid-surface of the shell are (Fig. 19.7)

$$\left. \begin{aligned} \varepsilon_{\varphi\varphi} &= \frac{\partial u}{\partial s} + \frac{w}{R} + \frac{1}{2} \left(\frac{\partial w}{\partial s} \right)^2 + \zeta \kappa_{\varphi\varphi} \\ \varepsilon_{\theta\theta} &= \frac{1}{R} \frac{\partial v}{\partial \theta} + \frac{w \sin \varphi}{r} + \frac{u \cos \varphi}{r} + \frac{1}{2} \left(\frac{1}{r} \frac{\partial w}{\partial \theta} \right)^2 + \zeta \kappa_{\theta\theta} \\ \varepsilon_{\varphi\theta} &= \frac{1}{r} \frac{\partial u}{\partial \theta} + \frac{\partial v}{\partial s} - \frac{v \cos \varphi}{r} + \frac{\partial w}{\partial s} \frac{1}{r} \frac{\partial w}{\partial \theta} + \zeta \kappa_{\varphi\theta} \end{aligned} \right\} \tag{19-58}$$

And, the curvatures are

$$\left. \begin{aligned} \kappa_{\varphi\varphi} &= \frac{\partial^2 w}{\partial s^2} - \frac{\partial}{\partial s} \left(\frac{u}{R} \right) \\ \kappa_{\theta\theta} &= \frac{\cos \varphi}{r} \left(\frac{\partial w}{\partial s} \right) + \frac{1}{r^2} \frac{\partial^2 w}{\partial \theta^2} - \frac{u \cos \varphi}{rR} - \frac{\sin \varphi}{r^2} \frac{\partial v}{\partial \theta} \\ \kappa_{\varphi\theta} &= \frac{\partial}{\partial s} \left(\frac{1}{r} \frac{\partial w}{\partial \theta} \right) - \frac{1}{rR} \frac{\partial u}{\partial \theta} - \frac{\partial}{\partial s} \left(\frac{v}{r} \right) \sin \varphi \end{aligned} \right\} \tag{19-59}$$

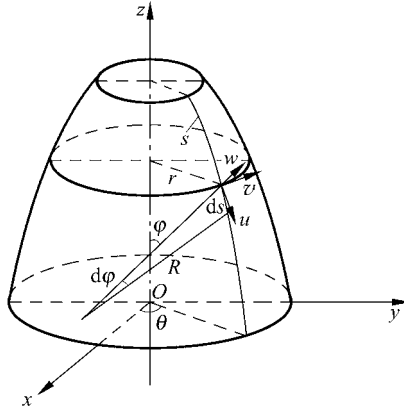


Figure 19.7 Axisymmetric shell in spherical coordinate system

Piecewise spline interpolation is used for the sectorial axisymmetric shell element (Fig. 19.8)

$$\left. \begin{aligned} \begin{Bmatrix} u \\ v \end{Bmatrix} &= \sum_{i=1}^2 \sum_{j=1}^2 \sum_{\alpha=0}^{m-1} \sum_{\beta=0}^{m-1} N_{mij}^{\alpha\beta}(r, \theta) \begin{Bmatrix} u_{ij}^{\alpha\beta} \\ v_{ij}^{\alpha\beta} \end{Bmatrix} \\ w &= \sum_{i=1}^2 \sum_{j=1}^2 \sum_{\alpha=0}^{n-1} \sum_{\beta=0}^{n-1} N_{nij}^{\alpha\beta}(r, \theta) w_{ij}^{\alpha\beta} \end{aligned} \right\} \quad (19-60)$$

Substitution of the above equation into Eqs. (19-58) and (19-59) yields

$$\boldsymbol{\varepsilon} = \mathbf{B}_L \mathbf{q} + 0.5 \mathbf{B}_{NL} \mathbf{q} \quad (19-61)$$

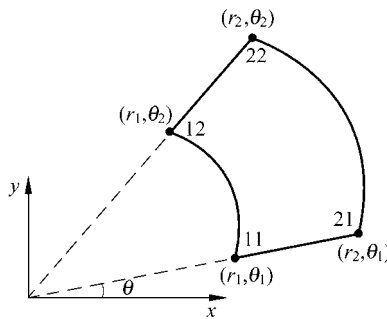


Figure 19.8 Sectorial element

19.5.3 Solution Scheme for Nonlinear Equation Set

Reference [9] gave reviews on the existing solution schemes for the nonlinear

equation set. For weak nonlinear problems, a modified Newton-Raphson method is used here. In order to control iteration times rationally, the load increment will be determined by the nonlinearity of the current equation set. Determining critical load and tracking post-buckling path of structures are difficult points in geometrically nonlinear problems. Here, a fixed arc length method is used to track the post-buckling path when the load reaches extremum and structure becomes unstable. That is to say, when the modified Newton-Raphson method is employed for iteration, the length of the displacement vector is restricted so that the arc length in solution space will keep invariant during the iteration procedure. Since this fixed arc length method cannot give the buckling critical point directly, in order to obtain the correct critical load of the structures, the spline functions will be used for fitting the solution curve near the extremum point. This is because the spline functions possess obvious advantages in computational stability and geometrical approximation. During the iteration, the allowable iteration times are 6 – 8; otherwise, the load increment will be adjusted.

19.5.4 Numerical Examples

Example 19.9 Large deflection analysis of a clamped square plate subjected to uniform load.

The side length of the clamped square plate $2a = 100\text{cm}$, the thickness $h = 0.5\text{cm}$; the Young's modulus $E = 2.05 \times 10^5\text{MPa}$, the Poisson's ratio $\mu = 0.3$.

Due to symmetry, only 1/4 structure is computed by a 4×4 mesh composed of the rectangular element (NS)₂₂. The results are plotted in Fig. 19.9. It can be seen that the results of the present method are in good agreement with the curve of the series solution^[6].

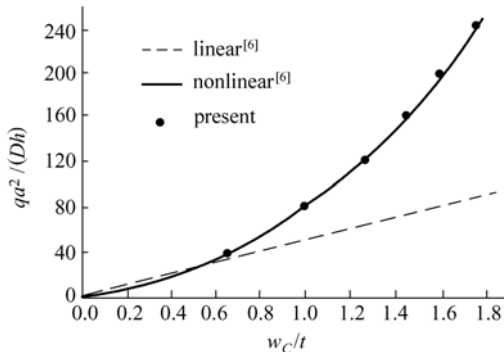


Figure 19.9 Large deflections of clamped plate subjected to uniform load

Example 19.10 Large deflection analysis of the double-parabolic shallow shell.

In this example, the load-displacement curve of the simply-supported double-parabolic shallow shell subjected to central concentrated load is given. Dimensions of the structure and results are all shown in Fig. 19.10.

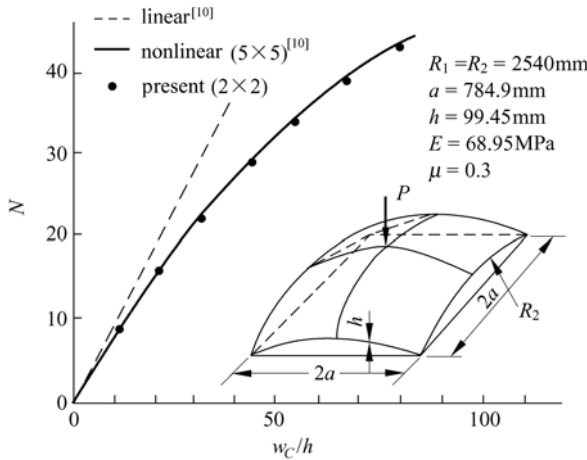


Figure 19.10 The load-displacement curve of double-parabolic shallow shell

Due to symmetry, only 2×2 rectangular elements $(NS)_{33}$ are used for 1/4 of the shell. The results are very close to those obtained in reference [10] using displacement-based elements. But, the number of the displacement-based elements is about six times of that for the spline elements used here.

Example 19.11 Buckling analysis of the spherical shell subjected to uniform outer pressure.

In this example, the buckling problem of the clamped spherical shell subjected to uniform outer pressure (Fig. 19.11(a)) is analyzed. Due to symmetry, only 4 sectorial elements $(NS)_{33}$ are collocated in radius direction. The variation of critical load q_{cr} with parameter $\lambda (\lambda = \sqrt[4]{12(1-\mu^2)}\sqrt{R/h}\beta)$ is plotted in Fig. 19.11(b). When $3.5 < \lambda < 6$, q_{cr} is greatly below the classical value \bar{q}_{cr} ; when $6 < \lambda < 8$, q_{cr} is a little higher than \bar{q}_{cr} ; when $\lambda > 8$, q_{cr} oscillates around \bar{q}_{cr} . The results in this example are in good agreement with those obtained by Budiansky^[11] and Weinitschke^[12]. The load-displacement curves of the spherical shell subjected to uniform outer pressure are given in Figs. 19.11(c),(d): Fig. 19.11(c) is for the case of $\lambda = 5$ which possesses evident extreme point and complete post-buckling curve; Fig. 19.11(d) is corresponding to oblate spherical shell which has no apparent critical point.

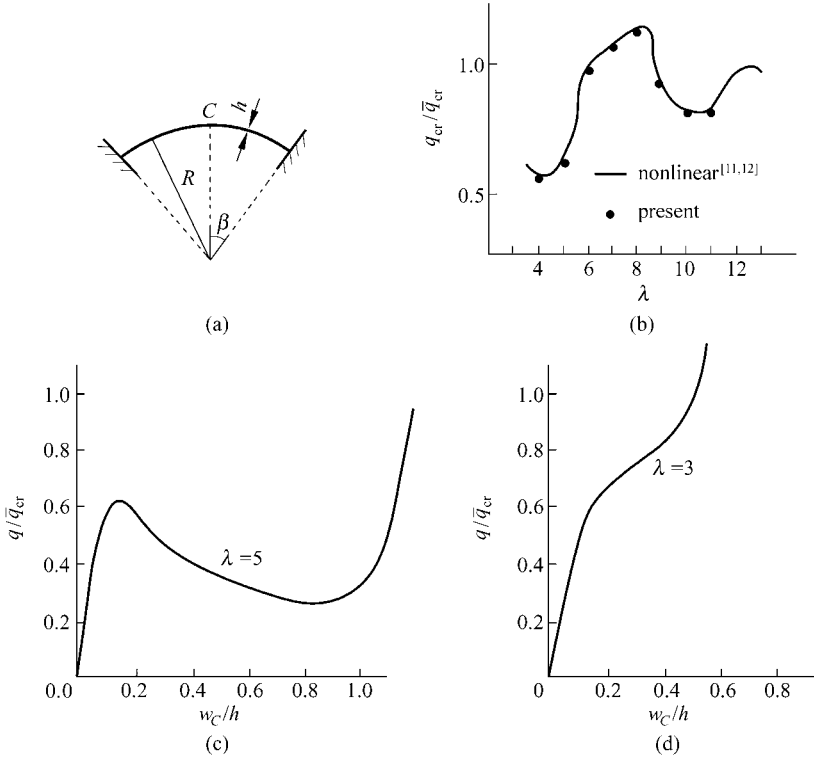


Figure 19.11 Buckling of spherical shell

- (a) clamped spherical shell; (b) critical load of spherical shell under outer pressure;
- (c), (d) load-displacement curve of spherical shell under outer pressure

Example 19.12 Buckling analysis of the circular plate with initial defects.

There are two basic buckling forms for the plate/shell structures: buckling at the bifurcation point and buckling at the extreme point. The former is usually considered within the range of linear elasticity and small displacement, and its critical features are expressed by the linear eigenvalue problem. In practical engineering, initial defects in a structure, caused by manufacture errors, etc., are hard to be avoided. So, the structural state of buckling at the bifurcation point may become that of buckling at the extreme point. In this example, assume that the initial defect is the displacement field caused by uniformly distributed transverse load on the circular plate, in which the initial central deflections w_C^0 are 0.01%, 0.1% and 1% of the thickness, respectively. The radius of the circular plate $a = 20\text{in}$; the thickness $h = 0.2\text{in}$; the Young's modulus $E = 3.0 \times 10^7 \text{psi}$; the Poisson's ratio $\mu = 0.3$. Due to symmetry, only 2 sectorial elements $(NS)_{33}$ are used along the radius direction. The results are shown in Fig. 19.12. It can be seen that the circular plate is very sensitive to initial disturbance. The variation of the load-displacement curve is more and more gentle with the increase of the initial disturbance; on the contrary, the curve varies more severely around the

critical point with the decrease of the initial disturbance. When $w_C^0 = 0.01\%h$, the situation is very close to the case of ideal buckling at the bifurcation point. Giving a tiny initial disturbance to perfect structure is also one of the methods for obtaining the post-buckling path after buckling at the bifurcation point.

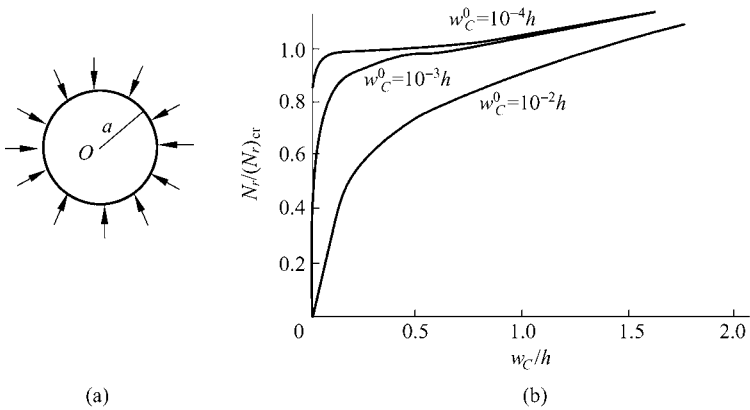


Figure 19.12 Buckling analysis of circular plate with initial defect
 (a) Circular plate subjected to radial pressure; (b) relation between transverse displacement and radial pressure

References

- [1] Yuan S (1984) Spline elements in stress analysis [Doctoral Dissertation]. Tsinghua University, Beijing
- [2] Solid Mechanics Division, Beijing Institute of Mechanics, China Academy of Science (1977) Bending, stability and vibration of sandwich plates. Science Press, Beijing (in Chinese)
- [3] Fan Z (1988) Applications of spline elements and sub-region mixed elements in structural engineering [Doctoral Dissertation]. Tsinghua University, Beijing (in Chinese)
- [4] Fan Z, Long YQ (1989) Spline thick/thin shell element. In: Proceeding of 2nd East Asia-Pacific Conference on Structural Engineering & Construction. Thailand, Chiang Mai, pp 1195 – 1200
- [5] Pryor CWJ, Barker RM, Frederick D (1970) Finite element bending analysis of Reissner plates. Journal of the Engineering Mechanics Division, ASCE, 96(6): 967 – 983
- [6] Timoshenko S, Woinowsky-Krieger S (1959) Theory of plates and shells. McGraw-Hill, New York
- [7] Alexander T (1982) An efficient conforming axisymmetric shell element including transverse shear and rotary inertia. Computers & Structures 15: 567 – 574
- [8] Fan Z, Long YQ (1990) Large deflection and stability analysis by geometrically nonlinear spline element. In: Proceeding of International Conference on Numerical Methods in Engineering, Theory & Applications (Vol. 1). Swansea, UK, pp 414 – 422

Advanced Finite Element Method in Structural Engineering

- [9] Haisler WE, Stricklin J A, Stebbins FJ (1972) Development and evaluation of solution procedures for geometrically nonlinear structural analysis. *AIAA Journal* 10: 264 – 272
- [10] Bathe KJ, Bolourch S (1980) A geometric and material nonlinear plate and shell element. *Computers & Structures* 11: 23 – 48
- [11] Budiansky B (1959) Buckling of clamped shallow spherical shells. In: *Proceeding of IUTAM Symposium on the theory of thin elastic shells*. The Netherlands, Delft, pp 64 – 85
- [12] Weinitschke H (1960) On the stability problem for shallow spherical shells. *Journal of Mathematics and Physics* 38: 208 – 231

Chapter 20 Concluding Remarks

Song Cen

Department of Engineering Mechanics, School of Aerospace,
Tsinghua University, Beijing, 100084, China

Yu-Qiu Long

Department of Civil Engineering, School of Civil Engineering,
Tsinghua University, Beijing, 100084, China

Zhi-Fei Long

School of Mechanics & Civil Engineering, China University of
Mining & Technology, Beijing, 100083, China

Abstract This chapter presents a summary of the contributions of the whole book, including seven new achievements in the finite element method, five new element series with 108 new element models, and new solution strategies for five challenging problems.

Keywords finite element, new achievements, new element series, challenging problems.

20.1 Seven New Achievements in the Finite Element Method

Besides the Introduction and this chapter, this book uses eighteen chapters, three parts to illustrate seven new achievements in the finite element method. The contents of these seven achievements and the corresponding original literatures are listed in Table 20.1.

Table 20.1 Seven new achievements and their original literatures

Name (chapter no.)	New creations	Original literatures
1. Sub-region variational principle (Chap. 2)	1.1 New variational principles based on sub-region interpolation and relaxed continuity conditions at the interfaces are established 1.2 Sub-region mixed energy principle—the theoretical basis of sub-region mixed element method	[1 – 3]

(Continued)

Name (chapter no.)	New creations	Original literatures
	1.3 Sub-region potential energy principle—the theoretical basis of the generalized conforming element 1.4 Sub-region complementary energy principle—the theoretical basis of the stress hybrid element	
2. Variational principle with several adjustable parameters (Chap. 3)	2.1 An optimization space is available for the applications of the variational principles because of the existence of adjustable parameters 2.2 Several patterns of functional transformations are proposed 2.3 Variable-substitution-multiplier method is proposed	[4]
3. Generalized Conforming element (Chaps. 4 – 11)	3.1 Generalized conforming element theory, which can guarantee the convergence of the non-conforming elements, is proposed 3.2 Various new conforming schemes, such as Line conforming, Perimeter conforming, Point-Line-Perimeter conforming, SemiLoof conforming, etc., are proposed 3.3 New rational interpolation scheme for shear strains and mixed assumption method of strains-displacements, which can eliminate shear locking completely, are proposed 3.4 A new hybrid-enhanced procedure, which can improve the accuracy for stress solutions of displacement-based elements, is proposed 3.5 New membrane elements with additional rigid rotation DOFs are developed 3.6 New flat-shell and curved shell elements are constructed	[6]
4. Sub-region mixed element method (Chaps. 12, 13)	4.1 A new mixed finite element method in which a coupling mesh composed of conventional displacement-based and stress-based elements is proposed 4.2 High precision solution methods for crack and notch problems are developed	[7]
5. Analytical trial function method (Chaps. 14, 15)	5.1 A new finite element method, the analytical trial function method, is proposed. It uses the basic analytical solutions as its trial functions which exhibits complementarities of analytical and discrete methods 5.2 High precision solution method is developed for the singular stress problem	[8]
6. Quadrilateral area coordinate method (Chaps. 16, 17)	6.1 Area coordinate method is generalized from triangular elements to quadrilateral elements. Two quadrilateral area coordinate methods (QACM-I and QACM-II) are systematically established 6.2 A new tool for construction of quadrilateral elements is provided. Elements formulated by such tool are more insensitive to mesh distortion than those by the isoparametric coordinate method	[10]
7. Spline element method (Chaps. 18, 19)	7.1 A new method with both merits of high flexibility of finite element method and high smoothing of spline functions is proposed 7.2 New elements for the analysis of plate/shell structures and high-rise buildings are constructed	[11,12]

20.2 Five New Element Series with 108 New Element Models

Brief introduction on the theoretical achievements have been given in Table 20.1. On the basis of these developments, new element models, which possess excellent performance, are successfully developed.

In this book, five new element series with 108 new element models are developed and listed in Table 20.2.

Table 20.2 Five new element series with 108 new element models

New element series		Chapter no.	Number of new element models	Remark	
1	Generalized conforming element series	Thin plate elements Thick and composite plate elements Membrane and shell elements	5,6,7 8,9,10 11	28 11 15	See Table 5.1 See Table 20.3 See Table 20.4
	2 Sub-region mixed element series		12,13	9	See Table 20.5
	3 Analytical trial function element series		q	7	5 generalized conforming elements; 2 singular hybrid elements; See Table 20.6
4 Quadrilateral area coordinate element series		16,17	20	All are generalized conforming elements; See Table 17.1	
5 Spline element series		18,19	18	See Table 20.7	
Total			108 new element models		

Following are the supplementary explanations for the five new element series in Table 20.2.

20.2.1 Generalized Conforming Element Series

Generalized conforming element series are the main part of this book, so eight chapters (Part II, Chaps. 4 – 11) are used to discuss them.

The generalized conforming element series can be divided into three groups: thin plate elements, thick and composite plate elements, membrane/shell elements. Some remarks are given as follows.

1. Generalized conforming thin plate element series

Generalized conforming elements were cradled in the field of the thin plate. The initial generalized conforming elements (elements TGC-9 and RGC-12) are all thin plate bending elements. Therefore, it can be seen that the generalized

conforming element theory can exhibit its advantages most easily in the thin plate problem. This is because the construction of the exactly conforming thin plate element, which belongs to C_1 continuity problems, is a difficult task. But, the generalized conforming element theory can solve this difficulty simply by its own advantages, and both convergence and convenience can be insured. Consequently, it has been paid attention to by some researchers, and successfully generalized to other fields. In general, new theories and methods are firstly born in special areas, and then, are generalized and applied in other areas.

The detailed discussions on generalized conforming thin plate element series can be referred to the content given by Table 5.1. There are 28 element models, which can be classified as five generalized conforming schemes: Line conforming, Line-point conforming, SemiLoof conforming, Perimeter-point conforming and Least square schemes. The wide applicability and the multiplicity of construction schemes are also the features and advantages of the generalized conforming element theory.

2. Generalized conforming thick plate and composite plate element series

The detailed discussions on generalized conforming thick and composite plate element series can be referred to the content given by Table 20.3. There are 11 elements, in which 8 are the thick plate elements, 2 are composite plate elements, and 1 is piezoelectric composite plate element.

Table 20.3 Index of generalized conforming thick and composite plate elements (11 elements)

Symbol of element		Degenerated case	Original reference	Chapter & section no.	
Thick plate element	By assuming (ψ, γ)	1. Triangular element TMT	Thin plate element DKT	[13]	8.5
		2. Quadrilateral element TMQ	Thin plate element DKQ	[14]	8.5
		3. Quadrilateral element ARS-Q12	Thin plate element DKQ	[15]	9.3
	By assuming (w, γ)	4. Triangular element TCGC-T9	Thin plate element GPL-T9	[16]	8.6
		5. Triangular element TSL-T9	Thin plate element LSL-T9	[17]	11.5.3
	From thin plate element to thick plate element	6. Rectangular element LFR1	Thin plate element LR12-2	[18]	8.7
		7. Rectangular element LFR2	Thin plate element ACM	[18]	
		8. Rectangular element GACM	Thin plate element ACM	[19]	
Composite plate element	9. Quadrilateral element TMQ20	Thick plate element TMQ	[20]	9.3	
	10. Quadrilateral element CTMQ20	Thick plate element ARS-Q12	[21]		
Piezoelectric composite plate element	11. Quadrilateral element CTMQE	Composite plate element CTMQ20	[22]	10.3	

During the studies on the generalized conforming thick plate and composite plate elements, developments for two key problems have been achieved:

(1) The shear locking problem—According to the generalized conforming element theory, countermeasures for solving shear locking are proposed. The key point of these countermeasures is the rational interpolation method for shear strains of the thick plates. On the basis of this point, three schemes can be used, such as no. 1–3 elements constructed by assuming (ψ, γ) , no. 4 and 5 elements constructed by assuming (w, γ) , and no. 6–8 elements constructed by the transition from thin plate elements to thick plate elements.

(2) The precisions for stress solutions, including transverse shear stresses at the interfaces of laminated composite plate, are improved—On the basis of the displacement solutions calculated by the generalized conforming elements, a hybrid-enhanced post-processing procedure for stress solutions is used.

3. Generalized conforming membrane and shell element series

Membrane element is the model for plane stress or plane strain problems, and also can be treated as the component of the shell element.

The generalized conforming membrane and shell element series involve 8 membrane elements and 7 shell elements, i.e., totally 15 models. Their detailed information can be found in Table 20.4, in which the membrane elements are classified as elements with or without drilling freedoms, and the shell elements are classified as flat-shell element and shallow shell element.

Table 20.4 Index of generalized conforming membrane and shell elements (15 elements)

Symbol of element	Original reference	Chapter & section no.	Remark
Membrane element	1. Isoparametric element GC-Q6 [23]	11.2	It degenerates to Wilson Q6 element in rectangular case
Membrane element with drilling freedom	2. Rectangular element GR12 [24]	11.3	Without internal parameter
	3. Rectangular element GR12M [24]		With two internal parameters
	4. Quadrilateral element GQ12 [25]	11.3	Without internal parameter
	5. Quadrilateral element GQ12M [25]		With two internal parameters
	6. Triangular element GT9 [26]	11.4	Without internal parameter
	7. Triangular element GT9M [26]		With one internal parameter
8. Triangular element GT9M8 [27]	With eight internal parameters		
Flat-shell element	9. Rectangular element GCR24 [28]	11.5	GCR24 = GR12 + GPL-R12
	10. Triangular element GST18 [29]		GST18 = GT9 + GPL-T9
	11. Triangular element GST18M [29]		GST18M = GT9M8 + GPL-T9
	12. Triangular element GMST18 [17]		GMST18 = GT9 + TSL-T9

(Continued)

Symbol of element		Original reference	Chapter & section no.	Remark
Shallow shell element	13. Rectangular element GC-S20	[30]	11.6	For eliminating membrane locking, generalized conforming conditions between membrane strains and displacements are used
	14. Triangular element SST21	[31]	11.7	For eliminating membrane locking, tangential freedoms at mid-side nodes are introduced
	15. Rectangular element SSR28	[32]	11.9	For eliminating membrane locking, tangential freedoms at mid-side nodes are introduced

During the studies on the generalized conforming membrane and shell elements, developments for three key problems have been achieved:

(1) Rational definition of nodal drilling freedom in membrane element—On the basis of the analysis of the disadvantages existing in two early definitions for nodal rotation freedom, a new more rational definition is proposed.

(2) Double improvements on flat-shell element—Flat-shell element is composed of two parts: membrane element and plate bending element. Here, these two parts are both upgraded: the membrane element part is replaced by the new model with newly defined drilling freedoms, and the plate bending element part is replaced by the generalized conforming element with excellent performance.

(3) Elimination of the membrane locking phenomenon in shallow shell element—By adding the tangential displacement DOFs at the mid-side nodes, the orders of the tangential and normal displacements can match with each other, so that membrane locking will be eliminated.

20.2.2 Sub-Region Mixed Element Series

The sub-region mixed element method is a new finite element method derived from the sub-region mixed variational principle. Its feature is that a coupling mesh composed of conventional displacement-based and singular stress-based elements is used, so that both advantages from the two models can be obtained. It specializes in the analysis of crack and notch problems which contain singular stress points.

This book presents a detailed introduction to the sub-region mixed element method for the analyses of 4 different crack problems and 5 different V-notch

problems. And, the index of the new elements for these 9 problems is given in Table 20.5.

Table 20.5 Index of sub-region mixed elements (9 elements)

Symbol of element		Original reference	Chapter & section no.
Crack problem	1. SRM-C1 2D crack of mode I	[7]	12.3
	2. SRM-C2 2D crack of mixed mode	[33]	12.3
	3. SRM-C3 Crack in thick plate	[34]	12.4
	4. SRM-C4 Surface crack in 3D body	[35]	12.5
Notch problem	5. SRM-V1 Plane V-notch	[36]	13.2
	6. SRM-V2 Bi-material plane notch	[37]	13.3
	7. SRM-V3 Bi-material anti-plane notch	[38]	13.4
	8. SRM-V4 V-notch in thick plate	[39]	13.5
	9. SRM-V5 3D V-notch	[40]	13.6

20.2.3 Analytical Trial Function Element Series

By taking the analytical solutions as trial functions, three developments for the finite element method have been achieved:

(1) For the membrane element, excellent models which can still keep high precision in distorted mesh are successfully constructed.

(2) For the thick plate element, shear locking phenomenon can be eliminated from the outset.

(3) For the crack and notch problems, high precision hybrid elements with singular point are developed.

The index of the new models is given in Table 20.6.

Table 20.6 Index of analytical trial function elements (7 elements)

	Symbol of element	Original reference	Chapter & section no.	Remark
4-node membrane element	1. ATF-Q4a (point conforming)	[41]	14.2	
	2. ATF-Q4b (perimeter-point conforming)			
	3. ATF-Q4θ (with drilling freedoms)			
Thick plate element	4. quadrilateral element ATF-MQ	[42]	14.5	
	5. triangular element GPLM	(this book)	14.6	Generalization of thin plate element GPL
Singular hybrid element	6. ATF-MS (for crack problem)	[43]	15.3	
	7. ATF-VN (for notch problem)	[44]	15.7	

20.2.4 Quadrilateral Area Coordinate Element Series

The establishment of the quadrilateral area coordinate theory provides a new tool for the construction of the quadrilateral element models. Compared with those traditional isoparametric models, the elements formulated by such new tool are more insensitive to various mesh distortions. Up to date, more than 20 models have been developed, including membrane elements, membrane elements with drilling freedoms, thin plate elements, thick plate elements, laminated composite plate element, and so on. The index of these elements can be found in Table 17.1.

20.2.5 Spline Element Series

Spline interpolation—possesses the highest order continuity among the piecewise polynomial with the same order, and the most smoothing curve can be obtained.

Spline element method is a new finite element method which uses spline functions as the interpolation functions in the sub-regions. It possesses high smoothing and precision, which is suitable for complicated structures. This book introduces 18 spline element models, and their detailed information can be referred to Table 20.7. Some materials about triangular, sector and other spline elements can be referred to references [11] and [12].

Table 20.7 Index of spline elements (18 elements)

	Symbol of element	Original reference	Chapter & section no.
Beam element	1. Quadratic spline beam element 2. Cubic spline beam element	[11]	18.2
Membrane element	3. Bi-quadratic spline rectangular element 4. Bi-cubic spline rectangular element	[11]	18.3
Membrane element for high-rise building	5. spline rectangular element TB-12 6. spline rectangular element TB-13 7. spline rectangular element TB-23	[45]	18.4 18.5
Thin plate element	8. quadratic spline rectangular element 9. cubic spline rectangular element	[11]	19.1
Thin-thick plate element	10. quadratic spline rectangular element 11. cubic spline rectangular element	[11]	19.2
Thin shallow shell element	12. spline element R-QQQ 13. spline element R-CQQ 14. spline element R-CCC	[11]	19.3
Thick shallow shell element	15. quadratic spline rectangular element 16. cubic spline rectangular element	[46]	19.4.1
Thick axisymmetric shell element	17. quadratic spline sector element 18. cubic spline sector element	[47]	19.4.2

20.3 New Solution Strategies for Five Challenging Problems

During the developments of many subjects, some plain and simple problems are always encountered and solved firstly, while a few unsolved challenging problems have to be left, even for a long time. The appearance of novel and effective solution strategies for the challenging problems is a symbol of advance in related subjects. For example:

(1) The shear-locking problem in thick plate element and its countermeasures

The shear-locking phenomenon of the thick plate element is caused by false shear strain when analyzing a thin plate. Two effective solution strategies proposed recently are: ① the rational interpolation method for shear strain^[13,16] (1998, locking-free shear strain field is obtained by using the Timoshenko's beam formulae); and ② the analytical trial function method based on the analytical solutions of the thick plate theory^[42].

(2) The sensitivity problem to mesh distortion and its countermeasures

Two effective solution strategies are proposed recently. ① Instead of isoparametric coordinates, the quadrilateral area coordinates are used in the interpolation polynomial of the element displacement field^[48-51]; ② The analytical trial function method is used^[41].

(3) The non-convergence problem of non-conforming elements and its countermeasure

The reason for the appearance of this problem is that the minimum potential energy principle is irrationally used to construct the non-conforming element. The key procedure of the generalized conforming element^[6] is the introduction of the fundamental generalized conforming conditions, which makes the application of the minimum potential energy principle rational, so that the convergence can be ensured.

(4) The accuracy loss problem of stress solutions by displacement-based elements and its countermeasure

The accuracy loss of stress solutions by displacement-based elements is caused by differential operations. Its countermeasure is the hybrid-enhanced post-processing procedure^[21], in which the stresses are computed by using Hellinger-Reissner variational principle, i.e., the differential operations are replaced by a macro method.

(5) The singular stress problem and its countermeasures

In order to improve the computational accuracy near a singular stress point, the analytical solutions with singular terms should be used adequately. Therefore, the effective countermeasures are the sub-region mixed element method^[7] and the analytical trial function method^[8].

References

- [1] Chien WZ (1980) Calculus of variations and finite elements (Vol. I). Science Press, Beijing (in Chinese)
- [2] Long YQ, (1981) Piecewise generalized variational principles in elasticity. Shanghai Mechanics 2(2): 1 – 9. (in Chinese)
- [3] Long YQ, Zhi BC, Yuan S (1982) Sub-region, sub-item and sub-layer generalized variational principles in elasticity. In: He GQ et al (eds) Proceedings of International Conference on FEM. Science Press, Shanghai, pp 607 – 609
- [4] Long YQ (1986) Several patterns of functional transformation and generalized variational principles with several arbitrary parameters. International Journal of Solids and Structures 22(10): 1059 – 1069
- [5] Long YQ, Xin KG (1987) Generalized conforming element. Tumu Gongcheng Xuebao/China Civil Engineering Journal 20(1): 1 – 14 (in Chinese)
- [6] Long YQ, Xin KG (1989) Generalized conforming element for bending and buckling analysis of plates. Finite Elements in Analysis and Design 5: 15 – 30
- [7] Long YQ, Zhi BC, Kuang WQ, Shan J (1982) Sub-region mixed finite element method for the calculation of stress intensity factor. In: He GQ et al (eds) Proceedings of International Conference on FEM. Science Press, Shanghai, pp 738 – 740
- [8] Long YQ, Fu XR (2002) Generalized conforming elements based on analytical trial functions. In: Proceedings of the Eleventh National Conference on Structural Engineering (Vol. I), plenary lecture. China, Changsha, pp28 – 39 (in Chinese)
- [9] Long YQ, Li JX, Long ZF, Cen S (1997) Area-coordinate theory for quadrilateral elements. Gong Cheng Li Xue / Engineering Mechanics 14(3): 1 – 11 (in Chinese)
- [10] Long YQ, Li JX, Long ZF, Cen S (1999) Area coordinates used in quadrilateral elements. Communications in Numerical Methods in Engineering 15(8): 533 – 545
- [11] Yuan S (1984) Spline elements in stress analysis [Doctoral Dissertation]. Tsinghua University, Beijing
- [12] Fan Z (1988) Applications of spline elements and sub-region mixed elements in structural engineering [Doctoral Dissertation]. Tsinghua University, Beijing (in Chinese)
- [13] Cen S, Long ZF (1998) A Mindlin triangular plate element with improved interpolation for the rotation and shear strain fields. Gong Cheng Li Xue/Engineering Mechanics 15(3): 1 – 14 (in Chinese)
- [14] Cen S, Long ZF, Long YQ (1999) A Mindlin quadrilateral plate element with improved interpolation for the rotation and shear strain fields. Gong Cheng Li Xue/Engineering Mechanics 16(4): 1 – 15 (in Chinese)
- [15] Soh AK, Cen S, Long YQ, Long ZF (2001) A new twelve DOF quadrilateral element for analysis of thick and thin plates. European Journal of Mechanics A/Solids 20: 299 – 326
- [16] Cen S, Long ZF (1998) A new triangular generalized conforming element for thin-thick plates. Gong Cheng Li Xue/Engineering Mechanics 15(1): 10 – 22 (in Chinese)
- [17] Chen YL, Cen S, Yao ZH, Long YQ, Long ZF (2003) Development of triangular flat-shell element using a new thin-thick plate bending element based on SemiLoof constraints. Structural Engineering and Mechanics 15(1): 83 – 114
- [18] Long ZF (1992) Locking-free thick plate rectangular element. Gong Cheng Li Xue/Engineering Mechanics 9(1): 88 – 93 (in Chinese)

- [19] Long YQ, Xi F (1992) A universal method for including shear deformation in the thin plate elements. *International Journal for Numerical Methods in Engineering* 34: 171 – 177
- [20] Cen S, Long YQ, Yao ZH (2002) A new element based on the first-order shear deformation theory for the analysis of laminated composite plates. *Gong Cheng Li Xue/Engineering Mechanics* 19(1): 1 – 8 (in Chinese)
- [21] Cen S, Long YQ, Yao ZH (2002) A new hybrid-enhanced displacement-based element for the analysis of laminated composite plates. *Computers & Structures* 80 (9 – 10): 819 – 833
- [22] Cen S, Soh AK, Long YQ, Yao ZH (2002) A new 4-node quadrilateral FE model with variable electrical degrees of freedom for the analysis of piezoelectric laminated composite plates. *Composite Structures* 58(4): 583 – 599
- [23] Long YQ, Huang MF (1988) A generalized conforming isoparametric element. *Applied mathematics and Mechanics (English Edition)* 9(10): 929 – 936
- [24] Xu Y, Long YQ (1993) Generalized conforming rectangular membrane elements with vertex rigid rotational freedom. In: *Proceedings of the Second National Conference on Structural Engineering*, pp199 – 206 (in Chinese)
- [25] Long YQ, Xu Y (1994) Generalized conforming quadrilateral membrane element with vertex rigid rotational freedom. *Computers & Structures* 52(4):749 – 755
- [26] Long YQ, Xu Y (1994) Generalized conforming triangular membrane element with vertex rigid rotational freedom. *Finite Elements in Analysis and Design* 17: 259 – 271
- [27] Xu Y (1994) The generalized conforming approach and the development of the membrane elements with drilling degrees of freedom and thin plate and shell elements [Doctoral Dissertation]. Tsinghua University, Beijing (in Chinese)
- [28] Long YQ, Xu Y (1994) Generalized conforming flat rectangular thin shell element. *Computational Structural Mechanics and Applications* 11(2): 154 – 160 (in Chinese)
- [29] Xu Y, Long YQ, Long ZF (1994) A triangular shell element with drilling freedoms based on generalized compatibility conditions. In: *Proceeding of WCCM III. Japan* pp1234 – 1235
- [30] Long YQ, Zhao JQ (1992) Generalized conforming curved rectangular element for shallow shells. *Gong Cheng Li Xue/Engineering Mechanics* 9(1): 3 – 10 (in Chinese)
- [31] Sun JH (1998) Research on generalized conforming shallow shell element and nonlinear analysis of plate and shell structures [Doctoral Dissertation]. Tsinghua University, Beijing (in Chinese)
- [32] Sun JH, Long ZF, Long YQ, Zhang CS (2001) Geometrically nonlinear stability analysis of shells using generalized conforming shallow shell element. *International Journal of Structural Stability and Dynamics* 1(3): 313 – 332
- [33] Long YQ, Zhao YQ (1985) Calculation of stress intensity factors in plane problems by the sub-region mixed finite element method. *Engineering Software* 7(1): 32 – 35
- [34] Huang MF, Long YQ (1988) Calculation of stress intensity factors of cracked Reissner plates by the sub-region mixed finite element method. *Computers & Structures* 30(4): 837 – 840
- [35] Long YQ, Qian J (1992) Calculation of stress intensity factors for surface cracks in a 3D body by the subregion mixed FEM. *Computers & Structures* 44(1/2): 75 – 78
- [36] Fan Z, Long YQ (1992) Sub-region mixed finite element analysis of V-notched plates. *International Journal of Fracture* 56: 333 – 344

Advanced Finite Element Method in Structural Engineering

- [37] Long YQ, Qian J (1992) Sub-region mixed finite element analysis of V-notches in a bimaterial. In: Zhu DC (ed) *Advances in Engineering Mechanics*. Peking University Press, Beijing, pp54 – 59
- [38] Qian J, Long YQ (1991) Sub region mixed FEM for calculating stress intensity factor of antiplane notch in bi-material. *Computational Structural Mechanics and Applications* 8(3): 325 – 330 (in Chinese)
- [39] Qian J, Long YQ (1992) The expression of stress and strain at the tip of notch in Reissner plate. *Applied mathematics and Mechanics (English Edition)* 13(4): 315 – 324
- [40] Qian J, Long YQ (1994) The expression of stress and strain at the tip of 3-D notch. *Applied mathematics and Mechanics (English Edition)* 15(3): 211 – 221
- [41] Fu XR, Long YQ (2002) Generalized conforming quadrilateral plane elements based on analytical trial functions. *Gong Cheng Li Xue/Engineering Mechanics* 19(4): 12 – 16 (in Chinese)
- [42] Long YQ, Fu XR (2002) Two generalized conforming quadrilateral thick plate elements based on analytical trial functions. *Gong Cheng Li Xue/Engineering Mechanics* 19(3): 10 – 15 (in Chinese)
- [43] Fu XR, Long YQ (2001) Fracture analysis with the sub-region mixed element method. *Gong Cheng Li Xue/Engineering Mechanics* 18(6): 39 – 46 (in Chinese)
- [44] Fu XR (2002) Generalized conforming element method based on the analytical trial functions [Doctoral Dissertation]. Tsinghua University, Beijing (in Chinese)
- [45] Fan Z, Long YQ (1991) Linear analysis of tall buildings using spline element. *Engineering Structure* 13: 27 – 33
- [46] Fan Z, Long YQ (1989) Spline thick/thin shell element. In: *Proceeding of 2nd East Asia-Pacific Conference on Structural Engineering & Construction*. Chiang Mai, Thailand, pp1195 – 1200
- [47] Fan Z, Long YQ (1990) Large deflection and stability analysis by geometrically nonlinear spline element. In: *Proceeding of International Conference on Numerical Methods in Engineering, Theory & Applications (Vol. 1)*. Swansea, UK, pp414 – 422
- [48] Soh AK, Long YQ, Cen S (2000) Development of eight-node quadrilateral membrane elements using the area coordinates method. *Computational Mechanics* 25(4): 376 – 384
- [49] Chen XM, Cen S, Long YQ, Yao ZH (2004) Membrane elements insensitive to distortion using the quadrilateral area coordinate method. *Computers & Structures* 82(1): 35 – 54
- [50] Cen S, Chen XM, Fu XR (2007) Quadrilateral membrane element family formulated by the quadrilateral area coordinate method. *Computer Methods in Applied Mechanics and Engineering* 196(41 – 44): 4337 – 4353
- [51] Chen XM, Cen S, Fu XR, Long YQ (2008) A new quadrilateral area coordinate method (QACM-II) for developing quadrilateral finite element models. *International Journal for Numerical Methods in Engineering* 73(13): 1911 – 1941

Appendix

A The equivalent equation of the functional stationary condition (2-45)

In order to derive the equivalent equation of the stationary condition (2-45), the integration by parts formula (2-53) is used firstly to develop the expression of the functional variation δI_3 .

The area integration terms in δI_3 are

$$\begin{aligned} & \iint_{\Omega_a+\Omega_b} \{ [D(\kappa_x + \mu\kappa_y) - M_x] \delta\kappa_x + [D(\kappa_y + \mu\kappa_x) - M_y] \delta\kappa_y \\ & + 2[D(1-\mu)\kappa_{xy} - M_{xy}] \delta\kappa_{xy} \} dx dy \\ & - \iint_{\Omega_a+\Omega_b} \left[\left(\frac{\partial^2 w}{\partial x^2} + \kappa_x \right) \delta M_x + \left(\frac{\partial^2 w}{\partial y^2} + \kappa_y \right) \delta M_y + 2 \left(\frac{\partial^2 w}{\partial x \partial y} + \kappa_{xy} \right) \delta M_{xy} \right] dx dy \\ & - \iint_{\Omega_a+\Omega_b} \left[\left(\frac{\partial^2 M_x}{\partial x^2} + \frac{\partial^2 M_y}{\partial y^2} + 2 \frac{\partial^2 M_{xy}}{\partial x \partial y} \right) + q \right] \delta w dx dy \end{aligned}$$

The line integration terms in δI_3 are

$$\begin{aligned} & \int_{C_{3a}+C_{3b}} \left(Q_n + \frac{\partial M_{ns}}{\partial s} - \bar{V}_n \right) \delta w ds - \int_{C_{1a}+C_{2a}+C_{1b}+C_{2b}} (w - \bar{w}) \delta \left(Q_n + \frac{\partial M_{ns}}{\partial s} \right) ds \\ & - \int_{C_{2a}+C_{3a}+C_{2b}+C_{3b}} (M_n - \bar{M}_n) \frac{\partial \delta w}{\partial n} ds + \int_{C_{1a}+C_{1b}} \left(\frac{\partial w}{\partial n} - \bar{\psi}_n \right) \delta M_n ds \\ & + \int_{C_{ab}} \left\{ (M_n^{(b)} - M_n^{(a)}) \left(\frac{\partial \delta w}{\partial n} \right)^{(a)} + \left[\left(Q_n + \frac{\partial M_{ns}}{\partial s} \right)^{(b)} + \left(Q_n + \frac{\partial M_{ns}}{\partial s} \right)^{(a)} \right] \delta w^{(a)} \right. \\ & \left. + \left[\left(\frac{\partial w}{\partial n} \right)^{(b)} + \left(\frac{\partial w}{\partial n} \right)^{(a)} \right] \delta M_n^{(b)} - (w^{(b)} - w^{(a)}) \delta \left(Q_n + \frac{\partial M_{ns}}{\partial s} \right)^{(b)} \right\} ds \end{aligned}$$

The corner point and the node terms in δI_3 are

$$\begin{aligned}
 & - \sum_{A_{1a}+A_{1b}} (w - \bar{w}) \Delta \delta M_{ns} + \sum_{A_{2a}+A_{2b}} (\Delta M_{ns} - \bar{R}) \delta w \\
 & - \sum_{J_1} [(w^{(b)} - \bar{w})(\Delta \delta M_{ns})^{(b)} + (w^{(a)} - \bar{w})(\Delta \delta M_{ns})^{(a)}] \\
 & + \sum_{J_2} \{[(\Delta M_{ns})^{(a)} + (\Delta M_{ns})^{(b)} - \bar{R}] \delta w^{(a)} - (w^{(b)} - w^{(a)})(\Delta \delta M_{ns})^{(b)}\}
 \end{aligned}$$

Since the variation of the field variables can be arbitrarily and independently performed, based on the stationary condition (2-45) it can be known that the area integration terms, the line integration terms, the corner point and the node terms in δI_3 should be zero, respectively. From the zero condition of the area integration terms in δI_3 , the field Eq. (2-46) within Ω_a and Ω_b can be derived. From the zero condition of the line integration terms in δI_3 , the boundary condition (2-47) on the boundary lines C_a and C_b and the interface condition (2-48) on the interface C_{ab} can be derived. From the zero conditions of the corner point and the node terms in δI_3 , the corner point condition (2-49) on the boundary line and the node condition (2-50) on the interface can be derived.

B The node conditions derived from the stationary condition (2-77)

Two different node types, J_1 and J_2 , are considered here, respectively. Then, the related node conditions can be derived from the stationary condition (2-77) $\delta \Pi = 0$.

Firstly, consider the node J_1 with supports; the node terms in $\delta \Pi$ related to the node J_1 are composed of the following three terms.

(1) In the potential energy variation $\sum_{e_p} \delta \Pi_p^{(e_p)}$ of all the potential energy elements e_p around the node, the corresponding node term is $\sum_{e_p} (\Delta M_{ns})^{(e_p)} \delta w^{(e_p)}$.

(2) In the complementary energy variation $-\sum_{e_c} \delta \Pi_c^{(e_c)}$ of all the complementary energy elements e_c around the node, the corresponding node term is $-\sum_{e_c} w^{(e_c)} (\Delta \delta M_{ns})^{(e_c)}$.

(3) In δG_1 , the corresponding node terms are

$$- \sum_{e_p} [(w^{(e_p)} - \bar{w})(\Delta \delta M_{ns})^{(e_p)} + (\Delta M_{ns})^{(e_p)} \delta w^{(e_p)}] + \sum_{e_c} \bar{w} (\Delta \delta M_{ns})^{(e_c)}$$

By superposition, the node terms related to the node J_1 in $\delta \Pi$ can be obtained

$$-\sum_e (w^{(e)} - \bar{w})(\Delta\delta M_{ns})^{(e)} \quad (\text{Sum of all elements } e \text{ around the node } J_1)$$

Thereby, from the stationary condition $\delta II = 0$, the interface condition at the node J_1 can be obtained as:

$$w^{(e)} = \bar{w} \quad (e \text{ denotes each element around the node } J_1)$$

Secondly, consider the node J_2 without supports. In δII , the node terms related to the node J_2 are composed of the following three terms.

(1) In the potential variation $\sum_{e_p} \delta II_p^{(e_p)}$ of all the potential energy elements e_p around the node, the corresponding node term is $\sum_{e_p} (\Delta M_{ns})^{(e_p)} \delta w^{(e_p)}$.

(2) In the complementary variation $-\sum_{e_c} \delta II_c^{(e_c)}$ of all the complementary energy elements e_c around the node, the corresponding node term is $-\sum_{e_c} w^{(e_c)} (\Delta\delta M_{ns})^{(e_c)}$.

(3) In δG_2 , the corresponding node terms are

$$\begin{aligned} & \left[\sum_e (\Delta M_{ns})^{(e)} - \bar{R} \right] \delta w^{(a)} + w^{(a)} \sum_e (\Delta\delta M_{ns})^{(e)} \\ & - \sum_{e_p} [w^{(e_p)} (\Delta\delta M_{ns})^{(e_p)} + (\Delta M_{ns})^{(e_p)} \delta w^{(e_p)}] \end{aligned}$$

By superposition, the node terms related to the node J_2 in δII can be obtained

$$\left[\left(\sum_e \Delta M_{ns}^{(e)} - \bar{R} \right) \right] \delta w^{(a)} - \sum_e (w^{(e)} - w^{(a)}) (\Delta\delta M_{ns})^{(e)}$$

Thereby, from the stationary condition $\delta II = 0$, the interface condition at the node J_2 can be obtained as:

$$\sum_e \Delta M_{ns}^{(e)} - \bar{R} = 0 \quad (\text{for the node } J_2)$$

$$w^{(e)} = w^{(a)} \quad (\text{for each element } e \text{ around the node } J_2, e \neq a)$$

C l_{1j} and γ_{1j} in Eq. (13-137)

$$l_{1j} = \frac{c_1 a_{22} - c_2 a_{12}}{a_{11} a_{22} - a_{12} a_{21}}, \quad \gamma_{1j} = \frac{c_2 a_{11} - c_1 a_{21}}{a_{11} a_{22} - a_{12} a_{21}}$$

in which

$$\begin{aligned}
 a_{11} &= \left[-(\lambda_j + 2) + \frac{\lambda_j \mu + 1}{1 - \mu} \right] \cos(\lambda_j + 2) \frac{\alpha}{2} \\
 a_{12} &= \left[-K_{1j} \lambda_j + \frac{\lambda_j \mu + 1}{1 - \mu} \right] \cos \frac{\lambda_j \alpha}{2} \\
 a_{21} &= 2(\lambda_j + 1) \\
 a_{22} &= \lambda_j (1 + K_{1j}) \\
 c_1 &= \left[\frac{\lambda_j \mu + 1}{1 - \mu} \frac{X + G}{(X + G)(\lambda_j + 2) + 2G} - \frac{\mu}{1 - \mu} \right] \cos \frac{\lambda_j \alpha}{2} \\
 c_2 &= \frac{(X + G) \lambda_j}{(X + G)(\lambda_j + 2) + 2G} \sin \frac{\lambda_j \alpha}{2}
 \end{aligned}$$

D s_{1j} and t_{1j} in Eq. (13-144)

$$s_{1j} = \frac{d_1 e_{22} - d_2 e_{12}}{e_{11} e_{22} - e_{12} e_{21}}, \quad t_{1j} = \frac{d_2 e_{11} - d_1 e_{21}}{e_{11} e_{22} - e_{12} e_{21}}$$

in which

$$\begin{aligned}
 e_{11} &= \left[-(\lambda_j + 2) + \frac{\lambda_j \mu + 1}{1 - \mu} \right] \sin \frac{1}{2} (\lambda_j + 2) \alpha \\
 e_{12} &= \left[K_{1j} \lambda_j + \frac{\lambda_j \mu + 1}{1 - \mu} \right] \sin \frac{\lambda_j \alpha}{2} \\
 e_{21} &= 2(\lambda_j + 1) \\
 e_{22} &= \lambda_j (1 + K_{1j}) \\
 d_1 &= \left[\frac{\lambda_j \mu + 1}{1 - \mu} \frac{X + G}{(X + G)(\lambda_j + 2) + 2G} - \frac{\mu}{1 - \mu} \right] \sin \frac{\lambda_j \alpha}{2} \\
 d_2 &= \frac{(X + G) \lambda_j}{(X + G)(\lambda_j + 2) + 2G} \sin \frac{\lambda_j \alpha}{2}
 \end{aligned}$$